STUDIES IN GAS TURBINE PERFORMANCE AND IN COMBUSTION

N.R.L. MACCALLUM

THESIS SUBMITTED FOR THE DEGREE OF

DOCTOR OF SCIENCE

University of Glasgow

Vol. II

March 2000

TEXT CUT OFF IN ORIGINAL

TEXT BOUND INTO THE SPINE

BLANK IN ORIGINAL

A Reprint from *Fuel* Vol. XXXV (April 1956) pp. 169-177

Flame Blow-off from Rectangular Burners

N. R. L. MACCALLUM

BUTTERWORTHS SCIENTIFIC PUBLICATIONS
88 KINGSWAY, LONDON, W.C.2

Flame Blow-off from Rectangular Burners

N. R. L. MACCALLUM

As the literature on flame blow-off from rectangular burners contains discrepancies, the blow-off limits have been obtained for six burners of cross-sectional dimensions ranging from 0·2 cm × 0·3 cm to 5·1 cm × 0·3 cm. Observations of flame lifting from the long side of the burner port have been correlated by the wall velocity gradient calculated at that point, it being assumed that the flow follows the Poiseuille law and that the velocity profile is unaltered by the presence of a flame. Final flame lifting values have also been roughly correlated by the average wall velocity gradient obtained from the pressure drop in the burner channel. This correlation is not limited to laminar flows. The friction coefficients have been measured for the burner channels and, in the laminar flow range, they are found to be inversely proportional to the Reynolds number.

IN THE design of a burner to be used at Glasgow University information was required on the blow-off of laminar pre-mixed flames from rectangular burners.

Prediction of blow-off—It has been shown for circular burners of different diameters that the stability limits can be correlated by the boundary velocity gradient calculated for flow without combustion[1,2]. J. GRUMER, M. E. HARRIS and H. SCHULTZ[3] have investigated blow-off and flash-back in non-circular ports and they conclude that neither the boundary velocity gradient at the centre of one side nor that at a corner, as calculated in the absence of a flame, can be used to correlate the stability limits of non-circular burners. However, Grumer and his associates claim that, in the laminar range, the limits of non-circular channels are correlated with circular channel stability limits by using the appropriate relationships for the friction coefficient λ in the equation:

$$g = \frac{\lambda V \mathcal{R}e}{2\pi d^3} \qquad \ldots.[1]$$

For square channels $\lambda = 75{\cdot}5/\mathcal{R}e^{1{\cdot}11}$ ....[2]

For rectangular channels $\lambda = 161/\mathcal{R}e^{1{\cdot}27}$ ....[3]

where g is the boundary velocity gradient for comparison with circular burner stability data, V the volume flow rate, d the equivalent hydraulic diameter = 4 × area/perimeter and $\mathcal{R}e$ the Reynolds number = $\rho\bar{u}d/\eta$ (ρ = density, $\bar{u}$ = average velocity over channel cross-section and η = absolute viscosity).

An anomaly—Equations 1 and 3 have been used to predict the velocities at which flames will blow off rectangular burners of cross-sectional width 0·32 cm ($\frac{1}{8}$ inch) and cross-sectional lengths varying from 0·2 to 5 cm. The results of these calculations for a 2 per cent butane in air mixture are given in *Table 1*.

These calculations show that the method proposed by Grumer, Harris and Schultz predicts that, for this cross-sectional width, as the cross-sectional length increases beyond 1 cm and tends to infinity the average velocity at blow-off decreases and tends to zero, a result which one would not expect.

Table 1. Blow-off velocities as predicted by the method of Grumer and co-workers*[3]

Burner cross-sectional length cm	0·2	0·3	0·6	1·0	2·0	5·0
Average velocity at blow-off cm/sec	7·9	11·9	17·5	16·8	11·8	4·8

* Rectangular burners of cross-sectional width 0·32 cm; 2 per cent butane–air mixture; critical 'g' from circular burner data 400 sec^{-1} (see Wohl[2])

For a burner of finite cross-sectional width and infinite cross-sectional length, *i.e.* neglecting end effects, one would expect the average velocity at blow-off in laminar flow to be given by:

$$\bar{u} = \tfrac{1}{3}\, bg \qquad \ldots.[4]$$

where b is the half cross-sectional width. For a burner of cross-sectional width 0·32 cm this expression gives an average velocity at blow-off of 21 cm/sec.

Thus the literature appears to be misleading on this subject. In view of this discrepancy a series of experiments has been carried out on the blow-off of butane–air flames from rectangular channels. In the experiments on which the relationships of Grumer, Harris and Schultz are based (equations 1 to 3) the minimum value of the ratio of channel cross-sectional width to cross-sectional length was 0·28. It should be noted that the anomalous behaviour indicated above occurs at values of this ratio which are less than 0·28.

EXPERIMENTAL

Apparatus—Blow-off limits were obtained for burners of the following cross-sectional dimensions: 0·18 cm × 0·33 cm, 0·32 cm × 0·32 cm, 0·63 cm × 0·33 cm, 1·29 cm × 0·33 cm, 2·54 cm × 0·29 cm and 5·08 cm × 0·32 cm. The burners were not water-jacketed, but it is thought that the blow-off limits would not have been appreciably altered by water-jacketing, as it was observed from several tests that a blow-off limit taken immediately after a flame was lighted on a cold burner was in agreement, within experimental error, with the limit taken after the flame had been alight on the burner for some time.

In each burner the approach length was greater than the transition length for a cylindrical channel of similar equivalent hydraulic diameter. A Reynolds number of 2000 was used in the expression[4] giving the transition length X:

$$X = 0{\cdot}065\, d\, \mathcal{R}e \qquad \ldots.[5]$$

The transition length is the length of channel required to change an initially flat velocity profile into one in which the velocity at the centre of the channel is within 1 per cent of the central velocity in Poiseuille flow. Equation 5 has been experimentally confirmed only for flow in cylindrical channels.

The butane and air flows were measured by capillary meters, within an estimated accuracy of 3 per cent.

Flame lifting—The flames did not always lift simultaneously from all parts of the burner port, as can be seen from *Figure 1* showing flames anchored above the 5·08 cm × 0·32 cm burner. At the flow velocity of 290 cm sec the flame lifts first from the centre of the long sides of the burner port (*Figures 1*a, b and c), and at the flow velocity of 27 cm/sec incipient flame lift occurs at the corners of the port (*Figures 1*d and e). The existence of these two forms of

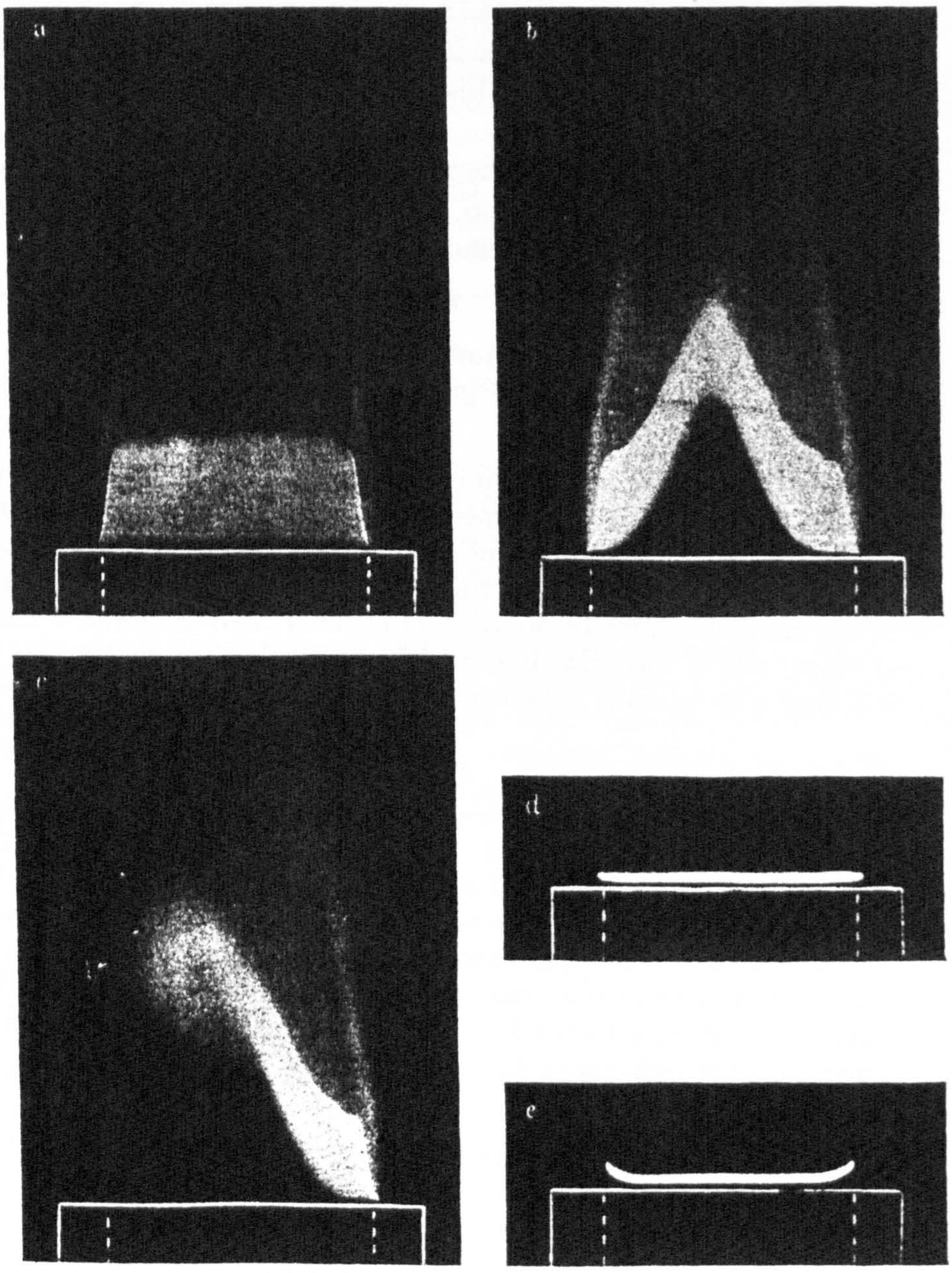

Figure 1. Flames anchored above a 5·08 cm × 0·32 cm burner: butane concentration a *3·96 per cent;* b *3·78 per cent;* c *3·64 per cent (final blow-off at 3·23 per cent);* d *2·33 per cent (final blow-off at 2·16 per cent);* e *2·23 per cent (final blow-off at 2·16 per cent)*

blow-off may be due to the influence of flame thrust on the flow distribution. In Poiseuille flow in the rectangular channel of the burner the wall velocity gradients are lowest at the corners[5]. However when a flame is anchored above the burner the flame pressure will cause a spreading of the flow lines which will increase the velocity gradients at the corners. It is estimated[1] that this spreading of the flow lines is proportional to the term $(S_u \bar{u})^2$, where S_u is the burning velocity. At the conditions corresponding to the flames shown in *Figures 1*a, b and c this term has the value 0·02, and at the conditions corresponding to the flames shown in *Figures 1*d and e the term has the value 0·73. The greater tendency for flow redistribution at the lower velocity may be the cause of the incipient flame lift from the corners of the burner shown in *Figures 1*d and e.

The type of blow-off shown in *Figures 1*a, b and c was only observed with the three largest burners (*viz* those having dimensions 1·29 cm × 0·33 cm, 2·54 cm × 0·29 cm and 5·08 cm × 0·32 cm), and that shown in *Figures 1*d and e was only observed with the 5·08 cm × 0·32 cm burner. In all other cases, the flame lifted from all parts of the burner at the same flow condition.

Flash back—With the larger burners a number of flash-back limits were taken. As these burners were not water-jacketed, however, the results may be of doubtful value, since locally hot walls probably have a greater influence on flash-back than on blow-off.

Pressure drop—In addition to the blow-off and flash-back observations the pressure drop along each of the burner channels was measured over a range of flows.

CORRELATION OF BLOW-OFF RESULTS

Local boundary velocity gradients—As stated earlier, the wall velocity gradient has been used successfully to correlate blow-off limits for circular burners. The applicability of this correlation to rectangular burners has been examined with reference to the lifting of a flame from the centre of the long side of the burner port, using the experimental results described above. In calculating the velocity gradients corresponding to the flows at which the flame lifted it was assumed that Poiseuille flow occurs at the burner port and that the velocity profile is unaltered by the presence of a flame. With these assumptions the velocity u at a point having coordinates (x,y) relative to an origin on the axis is given by[7]:

$$u = -\frac{1}{2\eta}\frac{dp}{dz}\left[(b^2 - y^2) - \frac{32b^2}{\pi^3}\sum_{n=0}^{\infty}\frac{(-1)^{n-1}\cosh\{(2n-1)\pi x/2b\}\cos\{(2n-1)\pi y/2b\}}{(2n-1)^3\cosh\{(2n-1)\pi a/2b\}}\right] \quad \ldots.[6]$$

where $dp\,dz$ is the pressure gradient in the direction of flow, a is the half cross-sectional length and b is the half cross-sectional width.

The average velocity $\bar{u}$ is obtained by integrating the above expression over the cross-sectional area:

$$\bar{u} = \frac{1}{ab} \int_{x=0}^{x=a} \int_{y=0}^{y=b} u \, dx \, dy \qquad \ldots.[7]$$

The wall velocity gradient at the centre of the long side, g_e, is given by:

$$g_e = -\left(\frac{\partial u}{\partial y}\right)_{x=0,\, y=b} \qquad \ldots.[8]$$

Substituting equation 6 in equations 7 and 8 and combining gives:

$$g_e = P\bar{u}b^{-1} \qquad \ldots.[9]$$

$$\text{where } P = \frac{3\left(1 - \frac{8}{\pi^2} \sum_{n=0}^{\infty} (2n+1)^{-2} \operatorname{sech} \frac{(2n+1)\pi a}{2b}\right)}{1 - \frac{192}{\pi^5} \frac{b}{a} \sum_{n=0}^{\infty} (2n+1)^{-5} \tanh \frac{(2n+1)\pi a}{2b}} \qquad \ldots.[10]$$

The series used in equation 10 have been summed by R. W. SMITH, Jr, H. E. EDWARDS and S. R. BRINKLEY, Jr[5] for various values of the ratio b/a. From their results the function P has been calculated and is given in *Table 2*.

Table 2. Values of functions P and Q

b/a	0	0·1	0·2	0·3	0·4	0·5	0·6	0·7	0·8	0·9	1·0
P	3·00	3·20	3·43	3·67	3·88	4·07	4·23	4·38	4·52	4·66	4·80
Q	0·0104	0·0118	0·0131	0·0143	0·0153	0·0161	0·0167	0·0171	0·0174	0·0175	0·0176

Equation 9 is valid only at values of Reynolds number below about 2000, laminar flow in rectangular channels breaking down at that value[6]. Within this range of Reynolds number, equation 9 has been applied to the conditions at which a flame lifted from the centre of the long side of the burner port. The resulting values of the wall velocity gradient at the centre of the long side are plotted on *Figure 2*. The solid curve plotted on *Figure 2* represents the correlation obtained by K. WOHL[2] for blow-off from circular burners. There is seen to be good agreement between the blow-off limits of the various rectangular burners and the blow-off correlation for circular burners, indicating that the wall velocity gradient correlation of flame lift may be extended to the range of rectangular burners tested.

The flash-back limits obtained are also plotted in *Figure 2* where they are compared with the flash-back limits obtained by K. WOHL, N. M. KAPP and C. GAZLEY[1] in a 1·02 cm bore tube. The cause of the wall velocity gradients generally being higher in the rectangular burners than in the circular burner at flash-back may be due to the absence of water jackets from the former.

Velocity gradient in an infinite slit in turbulent flow—In circular burners in which the flow is turbulent the wall velocity gradients at blow-off have been

calculated by K. WOHL, N. M. KAPP and C. GAZLEY[1] and by L. M. BOLLINGER and D. T. WILLIAMS[8] using values of the friction coefficient relevant to turbulent flow. The results obtained are in agreement with the correlation obtained in laminar flow. Treating the 5·08 cm × 0·32 cm burner as a rectangular burner of infinite cross-sectional length and 0·32 cm cross-sectional width enabled the wall velocity gradients at the centre of the long side to

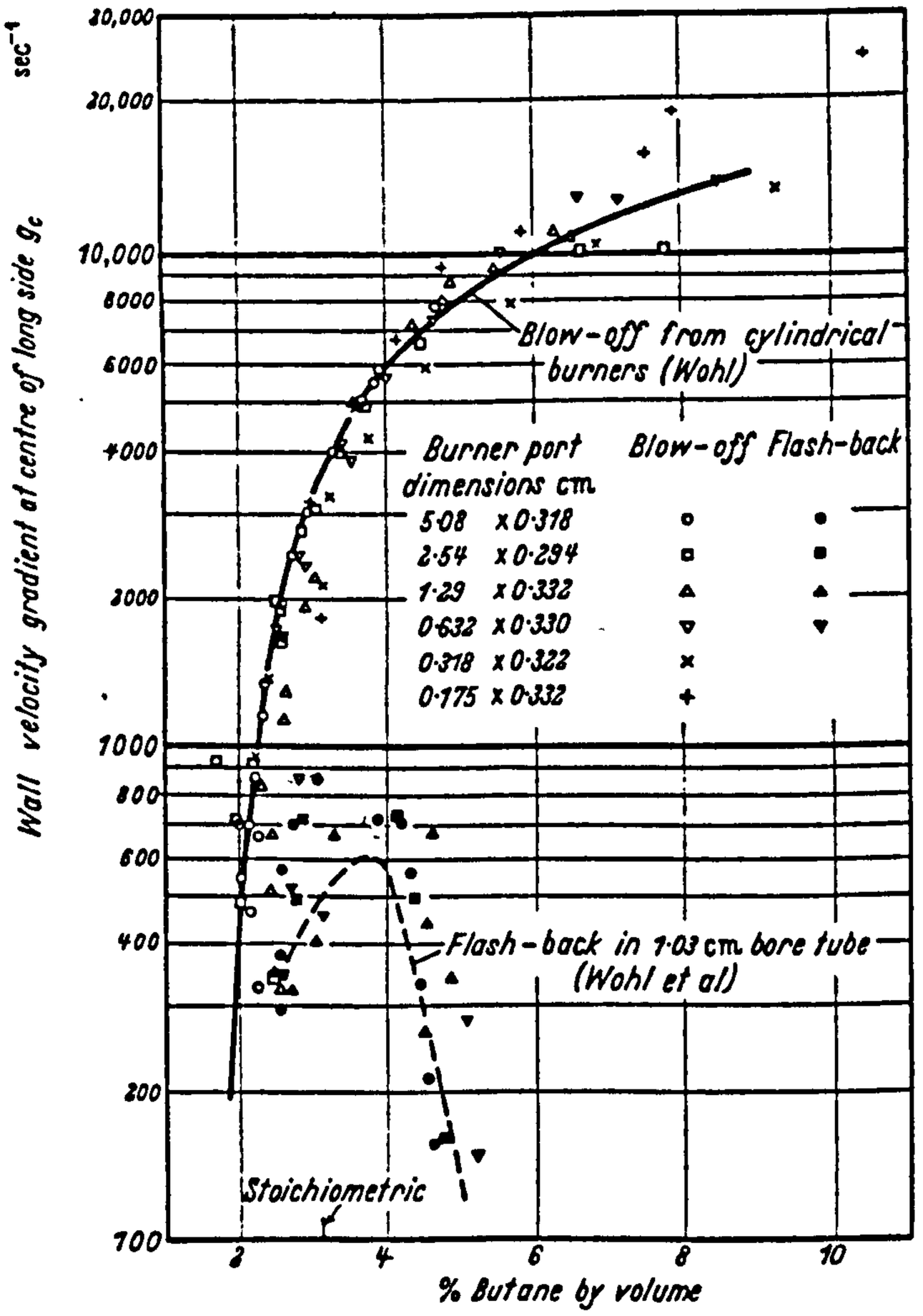

Figure 2. Stability limits of rectangular burners: wall velocity gradient at centre of long side, for flame lifting or flashing back at centre of long side

be calculated for the few blow-off limits in the turbulent range obtained with this burner. The gradients calculated in this way are in good agreement with the correlation obtained from the laminar flow limits of the smaller burners.

Average velocity gradient—The blow-off limits for the rectangular burners have also been correlated in *Figure 3* by the average wall velocity gradient obtained from the pressure drop measurements. The average wall velocity gradient g_{av} is given by:

$$g_{av} = -\frac{1}{\eta_l} \cdot \frac{dp}{dz} \cdot \frac{\text{area}}{\text{perimeter}} \quad \ldots.[11]$$

In this correlation the blow-off limit is taken to be the condition at which the flame finally lifts from the burner port. The blow-off limit for circular burners obtained[2] by Wohl is again drawn. as a solid line, for comparison. This

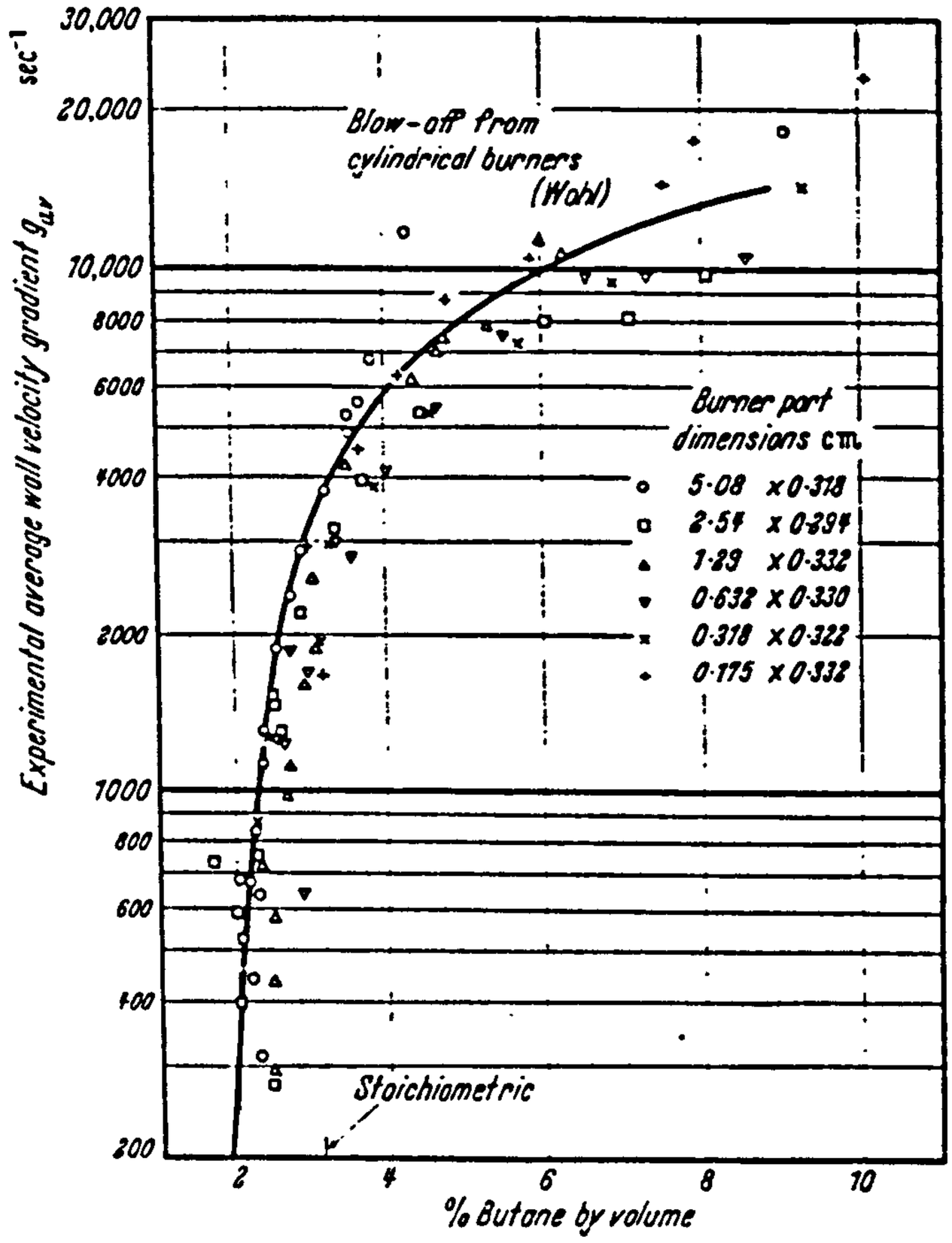

Figure 3. Blow-off from rectangular burners: experimental average wall velocity gradient for final flame lift.

correlation is less satisfactory than that obtained by using equation 9 to calculate the theoretical boundary velocity gradient, but this method of obtaining the average wall velocity gradient from the pressure gradient is applicable to turbulent, as well as to laminar, flows.

CORRELATION OF FRICTION COEFFICIENTS

The friction coefficient λ, as used in this paper, is given by the expression:

$$\frac{dp}{dz} = -\lambda \frac{\rho \bar{u}^2}{2d} \qquad \ldots.[12]$$

where ρ is the density of the fluid.

In steady laminar flow in a rectangular channel the average velocity $\bar{u}$ is given by equation 7 above. Substituting equation 7 in equation 12 leads to:

$$Q\lambda = \mathcal{R}e^{-1} \qquad \ldots.[13]$$

where

$$Q = \frac{(a-b)^2}{96a^2}\left[1 - \frac{192}{\pi^5}\frac{b}{a}\sum_{n=0}^{\infty}(2n+1)^{-5}\tanh\frac{(2n+1)\pi a}{2b}\right] \quad \ldots.[14]$$

Using the arithmetic summations published by Smith and his colleagues[5], values of the function Q have been calculated for various values of the ratio b/a. The results are given in *Table 2.*

Values of the friction coefficients for the rectangular channels were calculated from the pressure drop readings. These values, multiplied by the appropriate value of the function Q, are plotted in *Figure 4.* From this graph it

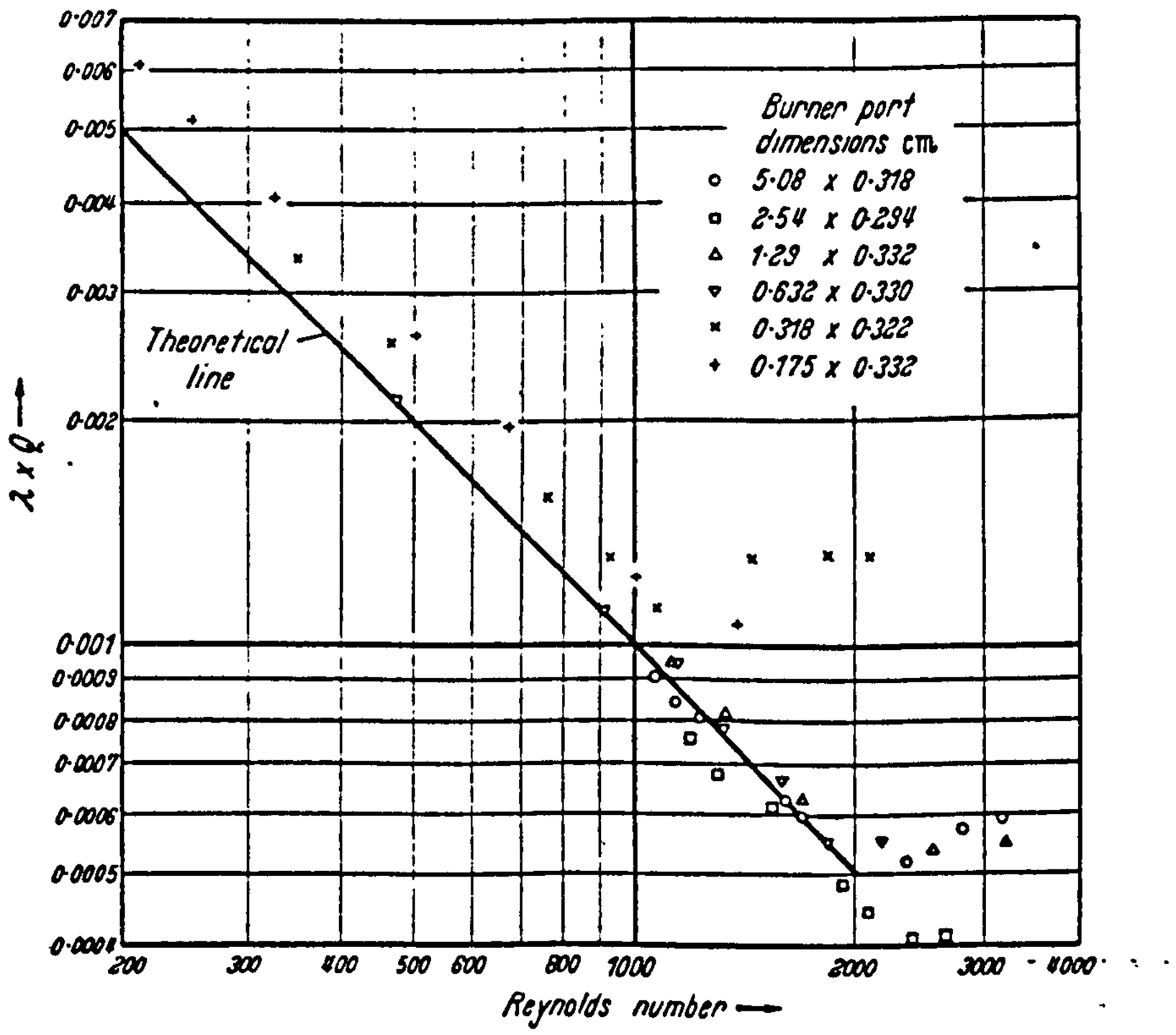

Figure 4. Friction coefficient λ in rectangular channels

is seen that the laminar flow linear relationship between the friction coefficient and Reynolds number breaks down in the four larger channels at a Reynolds number of roughly 2000. However in the two smaller channels the transition from laminar flow appears to begin at a Reynolds number nearer to 1000. For the laminar range points there is considerable scatter about the theoretical line, although for the individual burners the differences between the experimental points and the theoretical values are consistent. It is probable that these consistent discrepancies are partly due to inaccuracies in estimating the mean dimensions of the channel cross-sections. For example an error of 0·01 cm in the measurement of the cross-sectional dimensions of the 0·32 cm × 0·32 cm channel, *i.e.* 3 per cent. can cause a consistent error of 16 per cent in the value of the term $Q\lambda$ calculated from the experimental readings.

Lines drawn through the laminar range experimental points for the various burners would have gradients of 45°, confirming that the friction coefficient for each channel is inversely proportional to the Reynolds number, as indicated in equation 13. This is in disagreement with the conclusions[3] of Grumer, Harris and Schultz who calculated the friction coefficient from flame stability results, using equation 1, and found it to be inversely proportional to a power of the Reynolds number, as shown in equations 2 and 3.

CONCLUSIONS

For the burners tested the following observations were made:

(*1*) Where the Reynolds number is less than 2000 the limits for flame lift from the centre of the long side of the burner port can be correlated by the wall velocity gradient calculated at that point for flow in the absence of a flame.

(*2*) The final flame lift limits can be roughly correlated by the average wall velocity gradient obtained from the measured pressure gradient. This correlation is not limited to flows in which the Reynolds number is less than 2000.

(*3*) The friction coefficient in the burner channel is inversely proportional to the Reynolds number for flows in the laminar region. The constants of proportionality are in fair agreement with those predicted by the laminar flow equations.

That the blow-off limits may be directly correlated by the theoretical wall velocity gradient is in disagreement with the conclusions[3] of Grumer, Harris and Schultz. This disagreement may be due to the use by Grumer and his associates of burners of larger dimensions than those used in the experiments described above. With the larger dimensions the flow velocities at which the Reynolds number is equal to 2000 are lower and at the lower velocities the influence of flame thrust is probably more important. One would expect conclusion 1 above to be valid only when the flow redistribution due to flame thrust is not significant. It should also be noted that the conclusions of Grumer and his colleagues were based largely on flash-back limits, whereas the conclusions given above are drawn only from flame blow-off observations.

The author wishes to thank Professor J. Small and Dr J. Barr of Glasgow University for their encouragement and guidance during the course of the above work.

Department of Mechanical Engineering,
The University, Glasgow

(*Received October 1955*)

REFERENCES

[1] WOHL, K., KAPP, N. M. and GAZLEY, C. *Third Symposium on Combustion, Flame and Explosion Phenomena* p. 3 Williams and Wilkins: Baltimore, 1949
[2] — *Fourth (International) Symposium on Combustion* p. 68 Williams and Wilkins: Baltimore, 1953
[3] GRUMER, J., HARRIS, M. E. and SCHULTZ, H. *ibid* p. 695
[4] PRANDTL, L. and TIETJENS, O. G. *Applied Hydro and Aeromechanics* 1st Edn, p. 22 McGraw-Hill: New York, 1934
[5] SMITH, R. W., Jr. EDWARDS, H. E. and BRINKLEY, S. R., Jr *Rep. Invest. U.S. Bur. Min.* 4885, July, 1952
[6] MCADAMS, W. H. *Heat Transmission* 2nd Edn. p. 124 McGraw-Hill: New York, 1942
[7] CORNISH, R. J. *Proc roy. Soc.* A 120 (1928) 691
[8] BOLLINGER, L. M. and WILLIAMS, D. T. *Tech Notes nat. adv. Comm. Aero., Wash.* No. 1234, 1947

AGARD

MEMORANDUM

Flame Spreading Characteristics in Combustion

N.R.L. Maccallum

DECEMBER, 1955

ADVISORY GROUP FOR AERONAUTICAL RESEARCH AND DEVELOPMENT
PALAIS DE CHAILLOT, PARIS

FLAME SPREADING CHARACTERISTICS IN COMBUSTION

N. R. L. Maccallum

Introduction

In many steady flow combustion systems in which homogeneous mixtures of fuel and air are burned, the flame is anchored on some form of stabiliser such as a bluff body, or a can. Downstream from the stabiliser the flame "spreads" across the main fuel-air mixture. Since flame spreading can take place only if a flame is already successfully stabilised, a discussion of the mechanism of stabilisation is given for each of the flame spreading systems considered.

The study of flame spreading is relevant to the development of high intensity combustion systems.

Flame spreading in laminar flow

An illustration of flame spreading is given by the simple laminar bunsen flame.

Stabilisation.

The anchoring of a bunsen flame has been explained in terms of a balance at one point between the local flow velocity and the burning velocity. At all other points the flow velocity exceeds the burning velocity. The point at which this balance occurs is very close to the stream boundary, and, since the flow velocity at that point is roughly proportional to the boundary velocity gradient, Lewis and von Elbe[1] have proposed that the stability limits of burners of various dimensions may be correlated by the wall velocity gradient. This correlation has been applied very successfully by Lewis and von Elbe themselves, and by Wohl, Kapp and Gazley[2] and others.

Flame spreading.

The shape of the flame front in a bunsen flame has been predicted quite accurately by Lewis and von Elbe[1] simply by assuming that the burning velocity was constant along the whole length of the flame front. The major discrepancies between the theoretical and the observed flame shapes occur at the tip of the flame, and at the flame base. At the flame tip the burning velocity is no longer, in general, constant, due to the influences of heat conduction and diffusion in the vicinity of the curved wave. At the flame base the burning velocity is decreased due to quenching by the burner. Nevertheless, over most of the flame front the burning velocity is, in fact, constant, and in that region the theoretical and experimental flame profiles are in agreement.

Thus, for the simple case of a laminar bunsen burner, it may be predicted with reasonable accuracy whether a flame will be anchored under given flow conditions or not. If the flame is anchored, the shape it assumes may also be predicted, allowance being made for flow redistributions and quenching effects if necessary.

Flame spreading in turbulent flow – Flame stabilisation.

Here again the procedure shall be adopted of considering separately flame stabilisation and flame spreading. It should be noted that, in high velocity systems, there are strong interactions between the flame spreading zone and the flame stabilisation region[3]. Examples of this effect are discussed below in the sections on flame stabilisation.

Flame stabilisation by bluff bodies.

Surveys of the literature on this subject have recently been given by Longwell[4] and Zukoski and Marble.[5].

Various models have been suggested [6, 7,8,9,10] to represent the mechanism of flame anchoring behind bluff bodies such as rods, gutters and discs. Analyses of these models suggest that the group U/D^n will correlate the blow-off results, at any one pressure, as a function of the fuel/air ratio (U is the velocity at blow off, D is the stabiliser dimension. and n is an index). The values of the exponent n which gave the best agreements with the various sets of experimental data varied from 0.45 to 1.0. An explanation of these apparent discrepancies has been given by Zukoski and Marble[5] who have shown that a transition takes place in the wake boundary at a value of the Reynolds Number, based on the stabiliser width, of about 10^4. At that point the wake boundary immediately downstream of the stabiliser, which at lower flows has been laminar, becomes turbulent. Considering only the blow-off results taken at Reynolds Numbers of greater than 10^4 Zukoski and Marble have found all the results, except those of Longwell, Chenevey, Clark and Frost[11] to be correlated by an exponent value of 0.5. Longwell's results, which require an exponent of 1.0, were taken at Reynolds Numbers of the order of 10^6, and it may be that, as Longwell[3] and Zukoski and Marble[5] suggest, in this higher range of Reynolds Number a third regime of wake structure exists.

Spalding[9] suggested from theoretical considerations that the blow-off velocity is proportional to the square of the laminar flame speed. Calculations[12] based on the published blow-off results are seen to be in agreement, in the higher range of Reynolds Number, with this relationship.

De Zubay[7] has found that the blow-off velocity is almost directly proportional to the absolute pressure, as predicted by the theories of Spalding[9], and by the second-order reaction rate theory of Longwell, Frost and Weiss[8].

From the summary given above it is seen that, with the aid of correlations of the type given by Spalding[12], the blow-off velocity, under given conditions of mixture strength, pressure and stabiliser dimension, may be predicted with a fair degree of accuracy.

In the blow-off experiments, which have been referred to above, care was taken to avoid flow and pressure fluctuations. Scurlock[6] has demonstrated that induced turbulence due to, say, a grid in the flow approaching the stabiliser has a deleterious effect on the stability limits. A reduction in the stability limits may also be caused by placing the flameholder in a long parallel walled chamber at a considerable distance from the chamber outlet, so that combustion is almost complete by the time the gases leave the chamber[3,13]. Under these conditions pulsations in the flame front have consistently been observed by Dunlap[14], even at flow velocities of 50ft/sec and less. These reductions in stability limits demonstrate the interaction in high velocity systems between the flame spreading zone and the stability zone.

Flame stabilisation by cans

The stability limits of cans have not been studied as thoroughly as those of simple bluff bodies. Longwell[3] indicates that the blow-out limits at one fuel/air ratio may be correlated by the term A/VP^2 when A is the mass flow rate into the recirculation zone, V is the volume of the recirculation zone and P is the pressure. Other recently published experiments[15] on the stability of a can having a single row of gas inlet holes suggest that the correlating group is $Q/D^{2.4}\ P^{1.5}$ where Q is the mass flow rate through the can inlet holes, and D is the can diameter (all cans were geometrically similar). In comparing these two correlating groups it must be remembered that in one case the mass flow into the recirculation zone was measured, while in the other the measured quantity was the total mass flow rate through the inlet holes.

A can, having three rows of inlet holes, was used as the stabiliser in the pilot of the combustion system shown in Fig. 1. This system was used to study the influence of "flame spreaders" on the overall combustion efficiency. The flame spreaders consisted of a number of flat fingers which were placed across the annular space through which the main fuel-air mixture passed, the roots of the fingers being level with the pilot outlet. It was found that the use of suitable spreaders resulted in considerable improvement in the combustion efficiency performance, details of which are given later. However it was also found that if the number, width and inclination of the fingers, which formed the flame spreader, were increased beyond certain limits, a situation resulted in which combustion was extinguished before the system could be brought to choked tailpipe conditions (the inclination is the angle between the finger and the axis of the duct). Since increases in the number, width and inclination of the fingers of the spreaders leads to more rapid mixing, this would appear to be another example of the interaction of flow fluctuations and combustion stability.

Flame stabilisation by independent pilots

Independent oxygen-hydrogen pilots have been used by Wilkerson and Fenn[16] in studies of the influence of mixing rate on combustion efficiency in ramjets. Here again it is reported[17] that when the mixing rate became excessive combustion was extinguished.

Flame spreading

The process of flame spreading in turbulent flow will now be considered.

Concept of turbulent burning velocity

It has been demonstrated that the concept of a laminar burning velocity proved valuable in the study of flame spreading in a laminar bunsen flame.

Similarly it was thought that a "turbulent" burning velocity would aid the analysis of flames burning in turbulent streams. The first attempt to predict this turbulent burning velocity in terms of the laminar burning velocity and the turbulence characteristics was made by Damkohler[18]. He considered the case where the scale of turbulence is large compared with the flame thickness, which appears to correspond most closely to the situation met in practice, and also the case when the scale is small compared with the flame thickness. For the large scale turbulence it was considered that the turbulence merely caused a wrinkling of the flame front, and assuming that the individual sections of the wrinkled front continue to propagate at the laminar flame speed, Damkohler predicted that the turbulent burning velocity is roughly proportional to the intensity of turbulence. It was assumed for the case of the small scale turbulence that the flame front is not distorted, but that the transport processes within the flame are accelerated. In this way Damkohler obtained –

$$\frac{S_T}{S_L} = \left(\frac{e}{\nu}\right)^{1/2} \qquad \text{Eqn. 1.}$$

where S_T and S_L are the turbulent and laminar burning velocities respectively

e is the eddy diffusivity in the approach stream and ν is the kinematic viscosity.

The concept that a flame in large scale turbulence consists of a rapidly fluctuating laminar flame has also been used by Karlovitz, Denniston and Wells[19] who predicted the turbulent flame speed from the manner in which burning volumes of gas are moved backwards and forwards by the turbulence. Their treatment led to the equations –

$$S_T = S_L + u' \qquad \text{Eqn. 2.}$$

for weak turbulence, $u' \ll S_L$, when u' is the intensity of turbulence

and $S_T = S_L + (2 S_L u')^{1/2}$ Eqn. 3.

for strong turbulence $u' \gg S_L$

Equation 3 was found to fit the experimental values of the turbulent burning velocity of open Bunsen type flames when a turbulence intensity, which was thought to represent the intensity of "flame-generated" turbulence, was used instead of the much smaller intensity of the approach flow turbulence.

This estimation of the intensity of flame generated turbulence represents a considerable advance in the "wrinkled flame front" theories of turbulent flames. However it has been suggested by Longwell, Frost and Weiss[8] that, within a given volume, an insufficient number of laminar flame sheets can be obtained to yield the probable local heat release rates that have been observed in a $1^7/_8$ inch ramjet by Mullen, Fenn and Garmon[20]. This indicates a definite limit to the application of these theories.

An alternative concept of the structure of a turbulent flame has been proposed by Summerfield, Reiter, Kebely and Mascolo[21] who suggest that the flame is a zone of distributed reaction, having smooth spatial variations in the time-average values of temperature and concentration. The transport processes within the combustion zone are controlled by the stream turbulence. On the basis of this model, and by comparison with the laminar flame structure the following "similarity" equation was obtained –

$$\frac{S_T\, d_T}{e} = \frac{S_L\, d_L}{\nu}$$

Eqn. 4.

when d_T and d_L are the thicknesses of the turbulent and laminar flames respectively; other symbols as defined above.

What few experimental data have been obtained are in fair agreement with this equation.

The distributed reaction zone model may prove to be very useful, particularly in the high velocity, high turbulence range of conditions. A difficulty in the application of the theory as it stands is that the left hand side of the above equation contains two terms that are characteristics of the turbulent flame– the burning velocity and the flame thickness.

Flame spreading in ramjets.

Flame spreading in a $1^7/_8$ inch ramjet has been studied by Wilkerson and Fenn[15], the effectiveness of the spreading being represented by the combustion efficiency at the chamber outlet. All the efficiency measurements were taken with choked flow at the burner exit. An independent oxygen-hydrogen pilot was used and it was found that the efficiency with any one geometric system increased considerably when the pilot heat input was increased from 0.5 to 4.5% of the heat release within the chamber (assuming complete combustion). This result cannot be explained by the wrinkled flame front theories of turbulent burning velocity. The distributed reaction zone theory (Equation 4)) cannot yet be applied to these conditions owing to the lack of data on the turbulent flame thickness. A very satisfactory explanation has been given by Wilkerson and Fenn themselves who considered the combustion chamber as a region of homogeneous combustion. The temperature T at a characteristic point in the chamber was assumed to be given by the expression

$$T = Tu + ChK$$

Eqn.5.

when Tu is the temperature of the cold gas, C is a constant, h is the pilot heat input (as a percentage of the total heat release) and K is a factor measuring the rate of mixing of the pilot heat with the main stream. The factor K was determined by observing the temperature distribution with only the hot pilot gases and cold air entering the chamber, the main fuel supply being stopped. Since all measurements were taken using a stoichrometric fuel-air mixture the combustion efficiency, η_c, is assumed to be a function only of the temperature, and is given by –

$$\eta_c = A \exp\left(-\frac{E}{RT}\right)$$

Eqn. 6.

when E is the activation energy.

The constant C in Equation 5 is chosen to fit the experimental results. While Wilkerson and Fenn appreciate that their treatment is over simplified, it nevertheless gives a good correlation of the results.

With the same apparatus Wilkerson and Fenn studied the influence of mixing rate on the combustion efficiency. Different mixing regimes were obtained by placing orifices of diameter ranging from 1½ inch to 1¼ inch in the $1^7/_8$ inch diameter duct carrying the main stream, at a distance of just over 1 inch upstream from the pilot exit. The

mixing factor K was measured for each of the geometries used. With the pilot heat input maintained constant it was found that an increase in the mixing factor K, which was achieved by using a smaller diameter of orifices, was accompanied by an increase in the combustion efficiency. Equations 5 and 6, which had correlated the influence of pilot heat input on the combustion efficiency, were also found to correlate the influence of mixing on the combustion efficiency. These correlations are given in Fig. 2.

The use of devices, such as the orifices used by Wilkerson and Fenn, which increase the mixing simply by imparting general turbulence to the main stream, represents one method of achieving improved flame spreading. In the apparatus shown in Fig. 1 improved flame spreading was achieved by the use of a system of fingers placed across the main stream, the roots of the fingers being level with the pilot exit. It has been shown by gas sampling that mass transfer of pilot gases takes place along the wakes of the fingers, and it appears that when the main fuel supply is introduced these fingers act, at least partially, as flameholders. An example of the influence of the number of fingers and the width of fingers on the overall combustion efficiency is given in Fig. 3. The few tests carried out on the influence of finger inclination indicated that an increase in the inclination leads to a slight improvement in the combustion efficiency performance.

Discussion.

In low speed systems it appears that the flame spreading is controlled by the burning velocity (laminar or turbulent). In the conditions met in a ramjet combustion chamber in which the flow is choked at the tailpipe exit the combustion appears to be more homogeneous and the mixing processes become important. It has been observed that increasing the mixing rate improves the flame spreading, and also that if the mixing rate is increased beyond a certain limit a decrease in the stability, leading to extinction, can occur.

The theoretical analyses of the influence of mixing on the combustion rate which have been made by Berl, Rice and Rosen[22] are relevant to this problem. They have shown that much higher heat release rates can be obtained with optimum mixing, than are obtained with only slight mixing. They have also shown that, when extremely rapid mixing takes place, the time required to burn a given volume of mixture becomes excessive.

Suggestions for Further Research

Since it is seen that mixing has a considerable influence on the combustion rate, future work might fruitfully be directed towards achieving the controlled mixing necessary to give the optimum heat release rate.

It would be useful to know if the finger type flame spreaders, that have been described above, achieve their effect simply by causing general mixing as was the case with the orifices used by Wilkerson and Fenn[15]. An answer to this question might be given by a comparison of the combustion efficiency measurements made with a finger type flame spreader, and with an orifice giving similar values of the pilot heat mixing factor K.

The question of the pressure loss involved in achieving the mixing is also important.

The influence of mixing on the stability of a system has been demonstrated. It is therefore important to develop a piloting unit which will remain stable even when rapid mixing is taking place further downstream. Can-type stabilisers may prove useful in this connection. The influence of heat losses from the stabilising zone, and the ways in which they may be avoided, are important.

The author wishes to thank Professor Small and Dr. Barr of Glasgow University for the guidance and encouragement given by them in the preparation of this review.

References

1. Lewis, B. and von Elbe, G. *"Combustion, Flames and Explosions of Gases"*, Chapter VII Academic Press, New York, 1951.

2. Wohl, K., Kapp N. M., and Gazley C. "The Stability of Open Flames", *Third Symposium of Combustion, Flame and Explosion Phenomena*, p.3, Williams and Wilkins, Baltimore, 1949.

3. Longwell, J. P. "Flame Stabilization and Flame Propagation in Ramjet Combustors", *Combustion Researches and Reviews* 1955, p. 58, AGARD, Butterworths Scientific Publications, London.

4. Longwell, J. P. "Flame Stabilization by Bluff Bodies and Turbulent Flames in Ducts," *Fourth Symposium on Combustion* p. 90, Williams and Wilkins, Baltimore, 1953.

5. Zukoski, E. E. and Marble, F. E. "The Role of Wake Transition in the Process of Flame Stabilization by Bluff Bodies", *Combustion Researches and Reviews 1955*, p. 167, AGARD, Butterworths Scientific Publications, London.

6. Scurlock, A. C. " Flame Stabilization and Propagation in High Velocity Gas Streams", *Meteor Report No. 19*, Cambridge, Mass Inst. Tech. May 1948.

7. DeZubay, E. A. "Characteristics of Disc-controlled Flame", *Aero Digest*, vol. 61, No. 1, p. 54, 1950.

8. Longwell, J. P., Frost, E. E. and Weiss, M. A. "Flame Stability in Bluff Body Recirculation", *Industr. Engng. Chem.*, Vol. 45, p. 1629, 1953.

9. Spalding, D. B. "Theoretical Aspects of Flame Stabilization", *Aircr. Engng.* Vol. 25, p. 264, 1953.

10. Lees, L. "Fluid-mechanical Aspects of Flame Stabilization", J. *Amer. Rocket Soc.*, Vol. 24, p. 234, 1954.

11. Longwell, J. P., Chenevey, J. E., Clark, W. W., and Frost, E. E. "Flame Stabilization by Baffles in a High Velocity Gas Stream", *Third Symposium on Combustion, Flame and Explosion Phenomena*, p. 40, Williams and Wilkins, Baltimore 1949.

12. Spalding, D. B. "Discussion on Technical Combustion Problems", *Selected Combustion Problems*, p. 517, AGARD, Butterworths Scientific Publications, London, 1954.

13. Barrere, M. and Mestre, A. "Stabilization des Flammes par des Obstacles", *ibid*, p. 426.

14. Dunlap, R. A. "Resonance of a Flame in a Parallel-walled Combustion Chamber", *UMM–43 University of Michigan, Aeronautical Research Centre*, March 1950.

15. Probert, R. P. "Application of Research to Gas Turbine Combustion Problems", *Joint Conference on Combustion, Inst. Mech. Engrs. and Amer. Soc. Mech. Engrs.* 1955.

16. Wilkerson, E. C. and Fenn, J. B. "The Effect of Flameholder Geometry on Combustion Efficiency in Ducted Burners", *Fourth Symposium on Combustion*, p. 749, Williams and Wilkins, Baltimore, 1953.

17. Fenn, J. B. Private communication, August 1955.

18. Damkohler, G. "The Effect of Turbulence on the Flame Velocity in Gas Streams", Translated in *NACA Tech. Memo.* 1110, 1947.

19. Karlovitz, B., Denniston, D. W., and Wells, F. E. "Investigation of Turbulent Flames", *J. Chem. Phys.* vol. 19, p. 541, 1951.

20. Mullen, J. W., Fenn, J. B., and Garmon, R. C. "Burners for Supersonic Ramjets", *Ind. Eng. Chem.* vol. 43, p. 195, 1951.

21. Summerfield, M., Reiter, S. H., Kebely, V., and Mascolo, R. W. "The Structure and Propagation Mechanism of Turbulent Flames in High Speed Flow", *J. Amer. Rocket Soc.*, vol. 25, p. 377, 1955.

22. Berl, W. G., Rice, J. L. and Rosen, P. "Flames in Turbulent Streams", *J. Amer. Rocket Soc.*, vol. 25, p. 341, 1955.

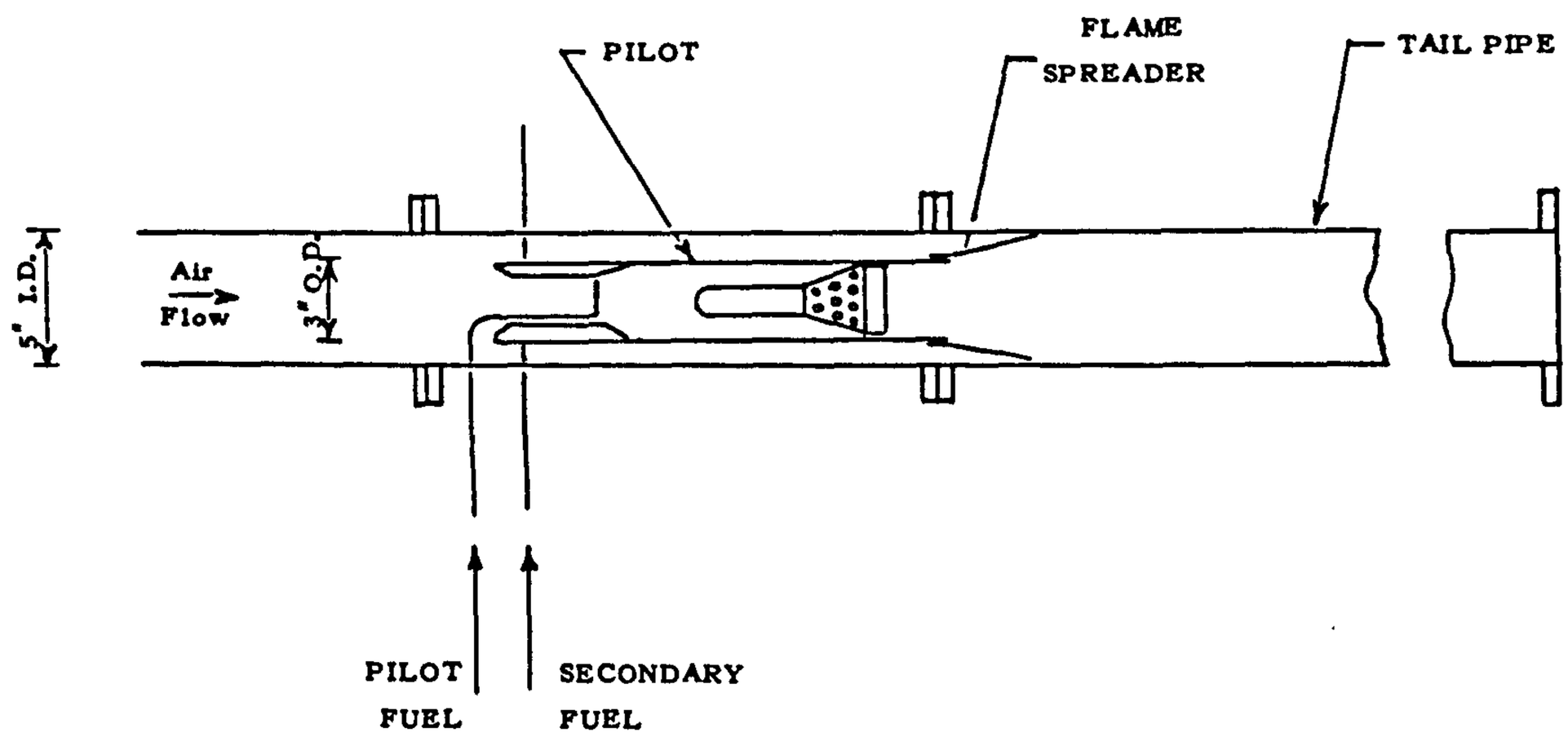

Fig. 1 COMBUSTION SYSTEM USING FLAME SPREADERS

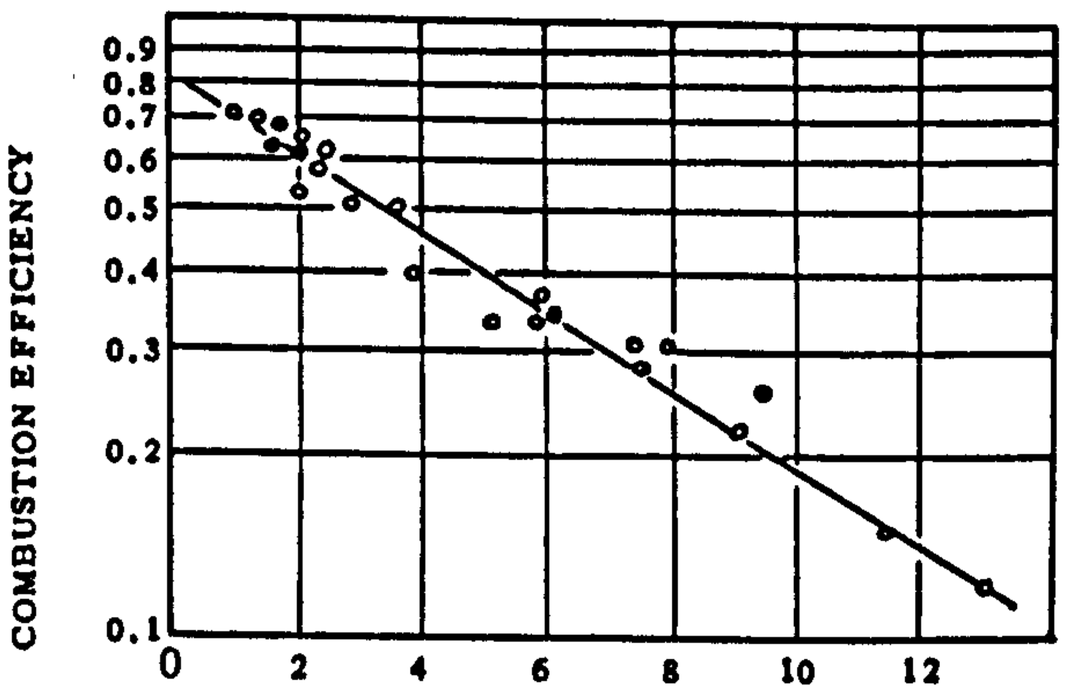

Fig. 2 COMBUSTION EFFICIENCY VARIATION FOR A VARIETY OF PILOT HEATS AND MIXING REGIMES (FROM WILKERSON AND FENN [16])

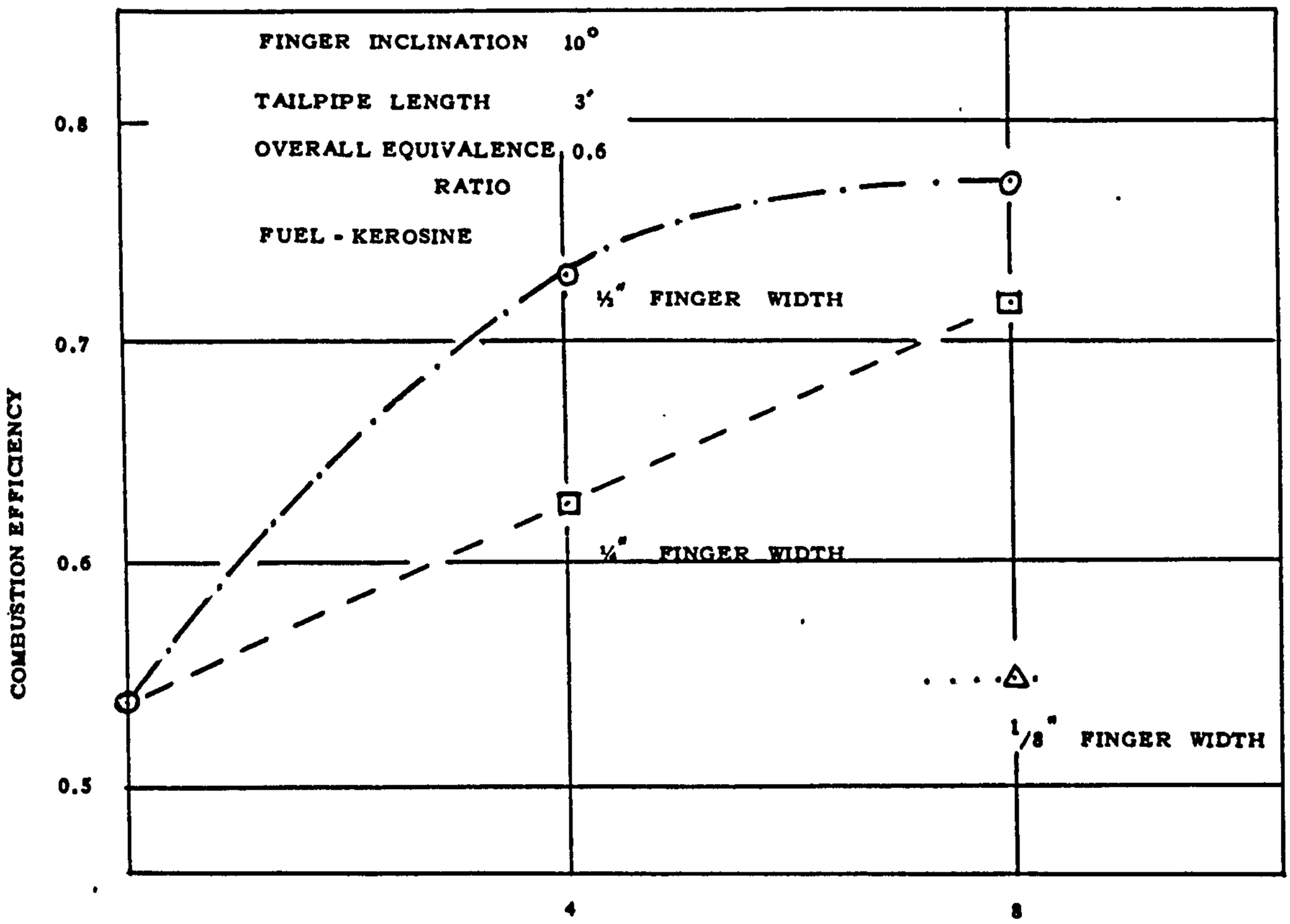

Fig. 3 INFLUENCE OF NUMBER OF FINGERS AND WIDTH OF FINGERS ON OVERALL COMBUSTION EFFICIENCY OF SYSTEM SHOWN IN FIG. 1

Reprinted from the JOURNAL OF THE INSTITUTE OF FUEL, *May*, 1967

M. L. MATHUR, B.E., Ph.D.,* and N. R. L. MACCALLUM, B.Sc., Ph.D.†

Publication 3

Swirling air jets issuing from vane swirlers. Part 1: free jets

Designs of vane swirlers for efficient directing of the air are discussed. A design of 'hubless' swirler is suggested for studying swirling jets. The pressure drop across swirlers and hence the efficiency of the swirl generator is derived from theoretical considerations and is confirmed by experimental results. The pressure drop is proportional to $U_0^2 \tan^2 \theta$ where U_0 is the nozzle velocity and θ is the vane angle. The static pressure on the axis at nozzle exit is found to be proportional to $U_0^2 \tan \theta$ in the case of hubless swirlers. It is shown that a swirling jet experiences a sudden expansion soon after it issues from the nozzle, but after about 2 to 4 d the expansion becomes nearly linear with similar spread angles for jets having varying degrees of swirl. For vane angles of 45° and higher the sub-atmospheric pressure in the central zone of the jet near the nozzle is strong enough to induce recirculation. This recirculation mass flow is roughly proportional to $\tan^2 \theta$. The recirculation results show that $\tan \theta$ itself is a good measure of swirl for jets issuing from vane swirlers.

1. Nomenclature

c_1	constant.
c_2	constant, $c_2 = \frac{k_2}{c_1}$.
d_o	diameter of hubless swirler, in.
d_1, d_2	inner and outer diameters of annular swirler, in.
$(d_2 - d_1)$	equivalent diameter of annular swirler for calculation of Reynolds Number, in.
g	acceleration due to gravity, ft/s².
G_x	axial momentum flux, lb ft/s².
G_ϕ	angular momentum flux, lb ft²/s².
h_f	total pressure drop in a vane swirler, $h_f = (h_{f1} + h_{f2})$, lbf/ft².
h_{f1}	pressure drop for 0° vane, lbf/ft².
h_{f2}	additional pressure drop for increase in vane angle from 0°, lbf/ft².
k	constant, $k = k_1 + k_2 \tan^2 \theta$.
k_1	pressure drop constant for 0° vane angle.
k_2	pressure drop constant for increase in vane angle from 0°.
p	pressure, lbf/ft².
Δp	pressure difference, lbf/ft².
r_1, r_2	inner and outer radii, in.
R	torque mean radius, $R = \frac{1}{3}\left(\frac{d_2^3 - d_1^3}{d_2^2 - d_1^2}\right)$, in.
S	swirl number.
U_0	average nozzle velocity, determined from the total nozzle flow and the cross-sectional flow area of corresponding 0° swirler, ft/s.
U_a	axial component of velocity on jet axis, ft/s.
x	hub ratio $= \frac{d_1}{d_2}$.
θ	swirl vane angle, deg.
ϕ	angle subtended by the vane when viewed in the axial direction, deg.
ρ	jet density, lb/ft³.

2. Introduction

Swirling jets are used in furnaces as a means of controlling the length and stability of the flame. One common method of generating a swirling jet is by employing a vane swirler. This paper describes a study of the design of vane swirlers for the efficient directing of the air. The energy spent in swirl generation and the velocity and static pressure distributions in the jets issuing into the atmosphere are reported, particularly with reference to the central recirculation zone.

3. Review of published work

A bibliographical chart of published work on swirling jets with application to combustion is given in Table 1.

The earliest reference to vane swirlers is given in Watson and Clarke's description[1] of the combustion chambers of the original 'Whittle' engine. Theoretical studies of swirling jets have been made by Loitsyanskii[4] and Gortler[6] but their results are only applicable to fully developed weak swirling jets having no reversal of flow at any point. Experimental studies on swirling jet flames produced by introducing air through tangential ports have been reported by Cude[2,3] who found that the flame length was considerably reduced by swirl. Hottel and Person[5] have studied swirling jets produced by introducing air tangentially into a cylindrical chamber. However, their system did not induce significant amounts of central recirculation and the efficiency and the overall mixing ratio were found to be independent of the ratio of tangential velocity to radial admission velocity (radial admission velocity is proportional to axial velocity). Ullrich[10] has studied annular swirling jets produced by a combination of tangential air inlets and adjustable vanes. He found that swirl introduced instability in the stream, resulting in an unsymmetrical jet. Rose has studied swirling jets generated by a rotating pipe[11] and by a specially designed swirl generator,[12] although in neither case was central recirculation obtained.

Recently Beér and Chigier[15,17] at the International Flame Research Foundation, IJmuiden, have studied swirling jets issuing from a generator having tangential air entries. General velocity profiles, and the form and shape of the central recirculation vortex were obtained. Kerr[22,23,29] and Fraser[22,30] have studied swirling jets issuing from vane swirlers in a boiler furnace and in a model burner respectively. It was found that the angular momentum is conserved along the length of the jet and is equal to the measured torque. Kerr found that his velocity profiles followed the error curve distribution in the fully developed region of the jet, which was the only region investigated. No central recirculation was reported by him. Drake and Hubbard[13,27] have studied the effects of swirl on combustion in the furnace of an experimental water-tube boiler. It was found that an intermediate degree of swirl gave a minimum of unburnt solids in the flue gases.

4. Design of vane swirlers

Many different designs of vane swirlers are used today. Several of these designs only partially deflect the air due to lack of overlap between the adjacent vanes. In the study described here a design for annular swirlers was evolved to give complete deflection of the air, by the provision of adequate overlap. No attempt was made to minimize the pressure loss necessary to generate the swirl.

*Department of Mechanical Engineering, University of Jodhpur (India).
†Department of Mechanical Engineering, University of Glasgow.

TABLE 1 A bibliographical chart of published literature on swirling jets with application to combustion

			Type of swirl generator			Type of jet				
							Model		Enclosed combustion chamber	
Author	Year	Ref. No.	Vane	Tangential entry	Others	Free	Air	Water	Gas Turbine	Boiler
Watson and Clarke	1947	1	*						*	
Cude and Hall	1950	2		*		*				
Cude	1953	3		*						*
Doitsyanskii	1953	4	Mathematical analysis							
Hottel and Person	1953	5	*				*			
Gortler	1954	6	Mathematical analysis							
Clarke	1955	7	*						*	
Poulston and Winter	1956	8	*				*	*		
Winter	1958	9	*					*		
Ullrich	1960	10	Combination of vane and tangential entry			*				
Rose	1962	11		*		*				
Rose	1962	12		*		*				
Drake and Hubbard	1963	13	*							*
Cohen de Lara and Fellous	1963	14	*				*			
Beér and Chigier	1963	15		*		*				*
Cohen de Lara and Fellous	1964	16	*				*			
Chigier and Beér	1964	17		*		*				
Brown and Thring	1964	18	*							*
Beér and Lee	1964	19		*				*		
Livesey and South	1964	20	*			*				
Chigier	1965	21		*		*				
Kerr and Fraser	1965	22	*			*				* cold
Kerr	1965	23	*					*		*
Shao-Lin Lee	1965	24	Mathematical analysis							
Beér	1965	25		*		*				*
Chigier and Chervinsky	1965	26		*		*				
Drake and Hubbard	1966	27	*							*
Patrick	1966	28	General discussion on swirl							

4.1. Annular swirlers

This design is shown in Fig. 1. There are eight vanes, 0·022 in thick. The vanes are symmetrical, and the trailing edges of the vanes do not lie in the plane of the hub exit. The angle subtended by a vane at the axis, when viewed in the axial direction (ϕ), is 75°, giving an overlap of 30° between adjacent vanes. All experimental results reported herein were obtained, unless otherwise stated, from swirlers made to this design.

4.2. Hubless swirlers

For studying swirling jets which are free of hub effect, 'hubless' swirlers were made. The design is developed from the annular swirler design, described above. The vanes are in the shape of segments of a circle, and when assembled in the swirler, all the vanes meet at a point on the axis. In practice it was difficult to manufacture completely accurate hubless swirlers.

5. Swirl number of vane swirlers

The definition of swirl number most commonly accepted is

$$S = \frac{G\phi}{G_x r_2} \quad . \quad . \quad . \quad (1)$$

In the case of vane swirlers equation (1) reduces[22] to

$$S = \frac{R \tan \theta}{r_2} \quad . \quad . \quad . \quad (2)$$

where R, the torque mean radius $= \frac{1}{3}\left(\frac{d_2^3 - d_1^3}{d_2^2 - d_1^2}\right)$

$$= \frac{2 r_2}{3}\left(\frac{1 - z^3}{1 - z^2}\right) \quad (3)$$

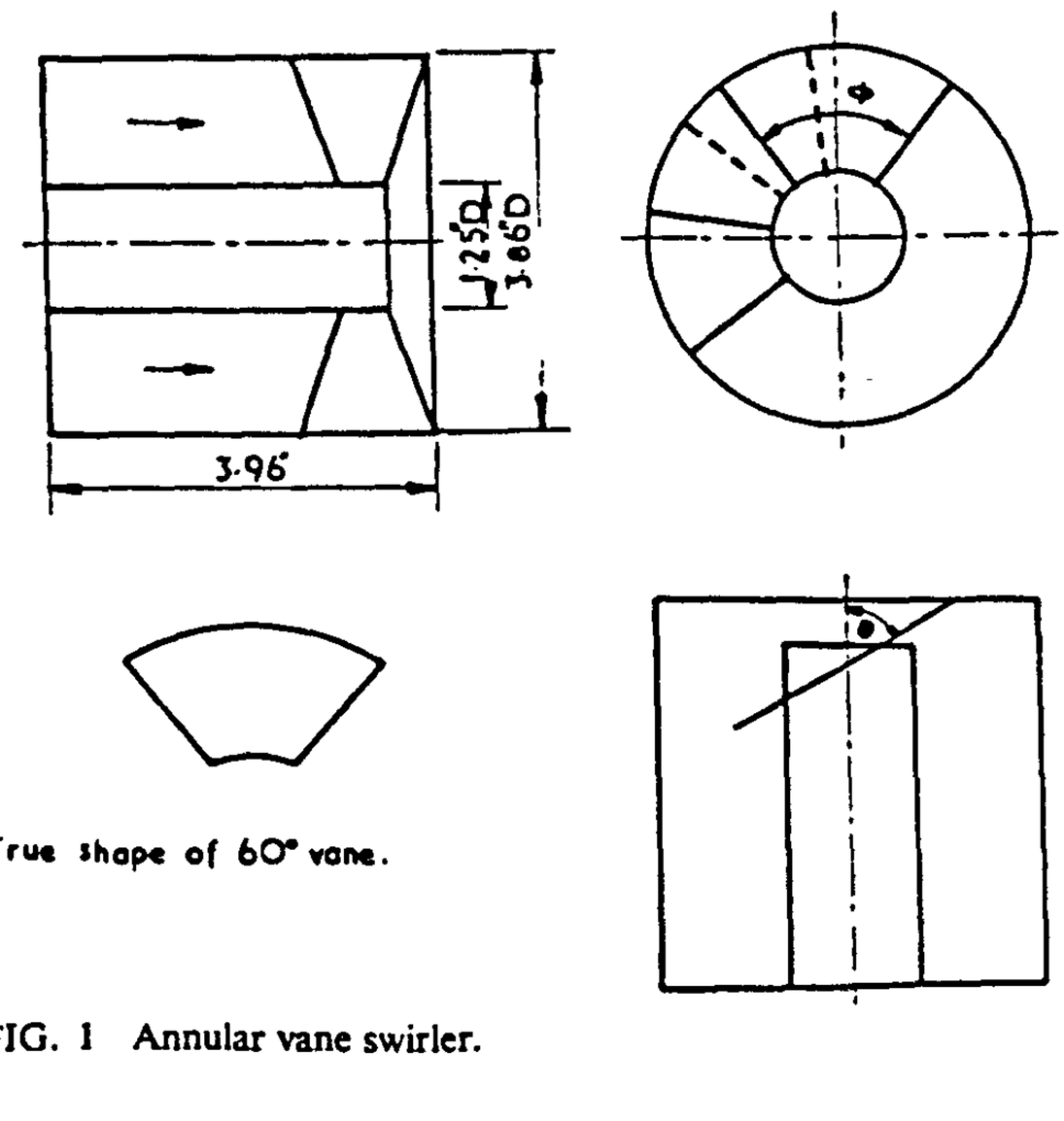

FIG. 1 Annular vane swirler.

TABLE 2 Dimensions and swirl number of swirlers

Swirler	d_2 in	d_1 in	z	Area of flow in²	No. of vanes	Thickness of vanes in	Vane angles	Swirl No. equation (1)
Hubless	0·934	zero	zero	0·602	8	0·022	0°, 15°, 30°, 45°, 60°, 70°, 75°	$0{\cdot}67 \tan\theta$
Annular	3·86	1·25	0·324	10·25	8	0·022	ditto	$0{\cdot}72 \tan\theta$

Thus the swirl number of a hubless swirler

$$= \frac{2}{3} \tan\theta \quad . \quad . \quad . \quad (4)$$

and the swirl number of an annular swirler

$$= \frac{2}{3}\left(\frac{1-z^3}{1-z^2}\right) \tan\theta \quad . \quad . \quad (5)$$

The swirl number of an annular swirler is a function both of the vane angle, θ, and of the hub ratio, z. Comparing swirlers of the same vane angle, annular swirlers having hub ratios in the range 0·2 to 0·5 (the normal practical limits) have swirl numbers ranging from 3 to 17% higher than that of the hubless swirler of the same vane angle. On the other hand, increasing the vane angle from 30° to 60° increases the swirl number by 300%. Thus the effect of hub ratio on swirl number is quite small compared to that of vane angle. Hence for vane swirlers $\tan\theta$ alone may be taken as a measure of the degree of swirl. This approximation has been substantiated by the present study.

The dimensions and swirl numbers of the swirlers studied are given in Table 2.

All swirlers were to Design No. 2 except the annular swirlers having vane angles of 15° and 30°. The designs of these two swirlers were similar to Design No. 2 but did not give the full overlap of 30°. The overlaps in these two cases were −13° and 27° respectively.

6. Theoretical analysis of the pressure drop across vane swirlers

The frictional resistance to fluid flow depends on surface roughness, the area of wetted surface and the density and velocity of the fluid. In the turbulent region the frictional resistance increases approximately with the square of the velocity. The frictional loss for flow through a swirler with axial vanes, i.e. vane angle 0°, may be given by

$$h_{f1} = k_1 \frac{\rho U_0^2}{2g} \quad . \quad . \quad . \quad (6)$$

The value of the constant k_1 depends on surface roughness, wetted area, and the obstruction due to the thickness of the vanes.

If the flow is through a swirler with vanes at an angle, θ, to the axis, additional pressure head is required to increase the velocity from U_0 to $\frac{U_0}{\cos\theta}$. The additional pressure head, h_{f2}, may be given by

$$h_{f2} = k_2 \frac{\rho}{2g}\left(\frac{U_0^2}{\cos^2\theta} - U_0^2\right)$$

$$= k_2 \frac{\rho U_0^2 \tan^2\theta}{2g} \quad . \quad . \quad . \quad (7)$$

where k_2 is a constant.

Factors which affect k_2 are the design and pitch of vanes, and the effectiveness of the vanes in deflecting the air through the passages. The total pressure drop, h_f, is given by

$$h_f = h_{f1} + h_{f2}$$

$$= \frac{\rho U_0^2}{2g}(k_1 + k_2 \tan^2\theta) \quad . \quad . \quad (8)$$

$$= \frac{\rho U_0^2}{2g} k \quad . \quad . \quad . \quad . \quad (9)$$

The term k_1 in equation (8) becomes negligible for vane angles of 45° and higher. The pressure drop is then proportional to the square of the tangent of the vane angle. If all losses are neglected, the theoretical value of k_2 is unity.

If in practice the vanes of a swirler give complete deflection, an efficiency of a swirl generator may be defined as the ratio of the theoretical pressure drop to the actual pressure drop.

i.e. Efficiency of swirl generator

$$= \frac{\text{Theoretical pressure drop}}{\text{Actual pressure drop}}$$

$$\simeq \frac{1}{k_2} \text{ for swirl angles of 45° and above} \quad . \quad (10)$$

7. Experimental work

7.1. Objectives

(*a*) To measure the pressure drop across hubless and annular swirlers in a model burner and compare the results with those predicted by the theoretical analysis.

(*b*) To measure the velocity and static pressure distributions in jets issuing from hubless and annular swirlers in a model burner with special reference to central recirculation.

7.2. Apparatus

The rig consisted of two concentric tubes with metered supplies of air to both the central (primary) and annular (secondary) streams.[31] The primary tube, 1 in inner diameter, 1·188 in outer diameter, was 50 in long. This length is assumed to give a fully developed jet. The secondary tube, 3·86 in inner diameter, was 36 in long. The various hubless and annular swirlers were fitted in turn in the downstream ends of these tubes.

A traversing mechanism positioned the probes which were used to study the jets. The accuracies of locating the probes were ±0·001 in in the horizontal and vertical radial directions and ±0·02 in in the axial direction. The lengths of travel were 12 in in the radial directions and 72 in in the axial direction. A motorized drive was used for the vertical radial travel.

To measure the velocity components in the three-dimensional flow in the swirling jet, a three-dimensional probe, made to the design of Hiett and Powell[32] was used. This probe has the advantage of having only three holes and of being able to measure flows from any direction except parallel to its own axis. Static pressures were measured by a disc static probe to the design of Miller and Comings.[33]

The pressure differences across the probes were measured by an electronic micromanometer of which the output was fed into a potentiometric chart recorder. The components of the electronic micromanometer were maintained at a constant temperature to obtain stability and constant calibration, as described by Kerr.[29] An accuracy of ±0·0005 in water was achieved in the pressure measurements taken in this way. A Casella manometer, having an accuracy of ±0·001 in water, was used to measure the pressure drop across the swirlers.

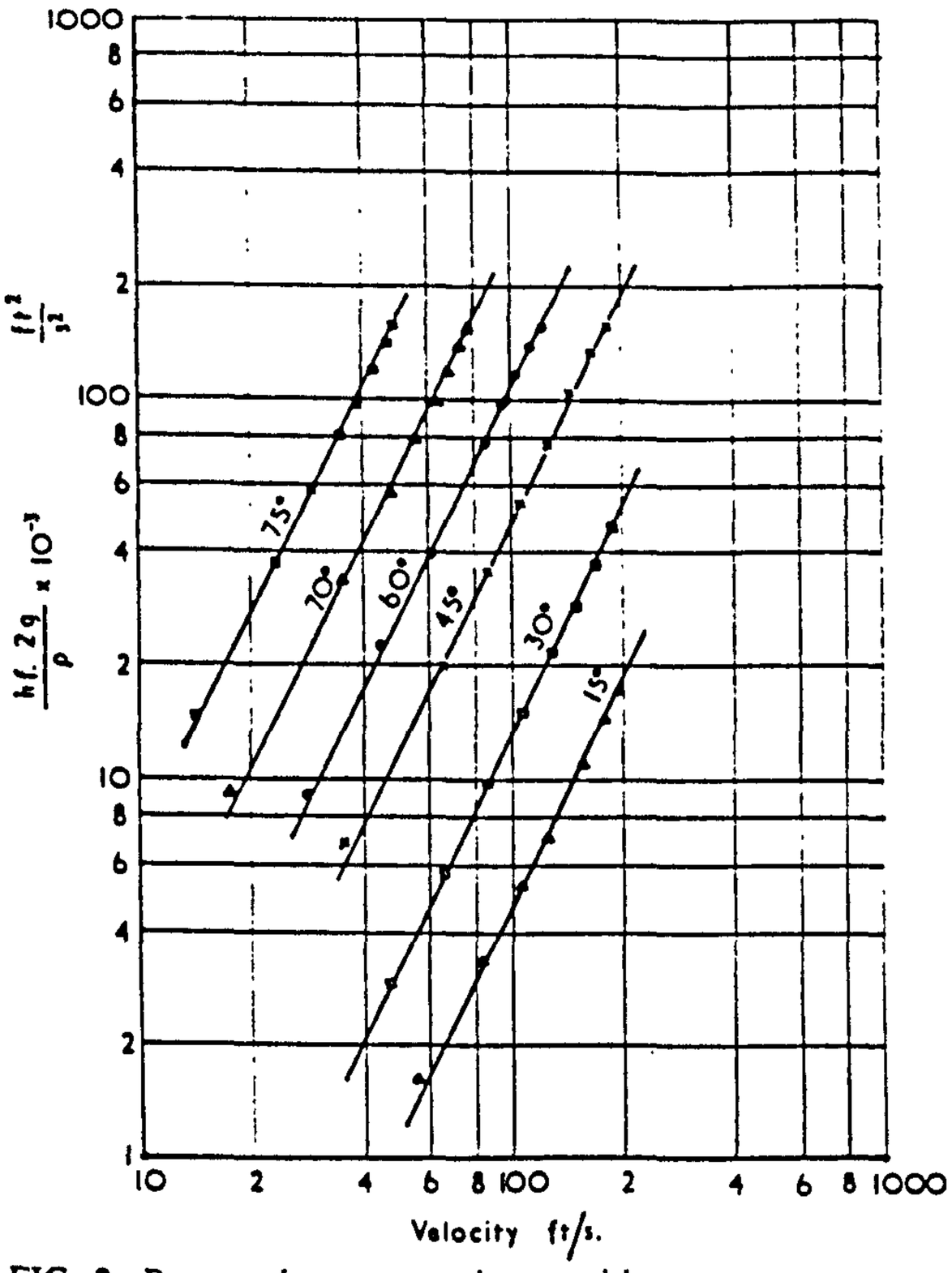

FIG. 2 Pressure drop across primary swirlers.

7.3. Procedure

The exit static pressure and the pressure drop across the hubless swirlers were measured for nozzle velocities (U_0) ranging from 14 to 195 ft/sec (Reynolds Numbers 7×10^3 to $9{\cdot}5 \times 10^4$). Similar readings were taken for the annular swirlers over the nozzle velocity range 12 to 44 ft/sec (Reynolds Numbers $1{\cdot}7 \times 10^4$ to 6×10^5).

The static pressure distributions along the axis and the velocity distributions were measured in the hubless swirling jets for a nozzle velocity of 100 ft/sec and in the annular swirling jets for a nozzle velocity of 39 ft/sec.

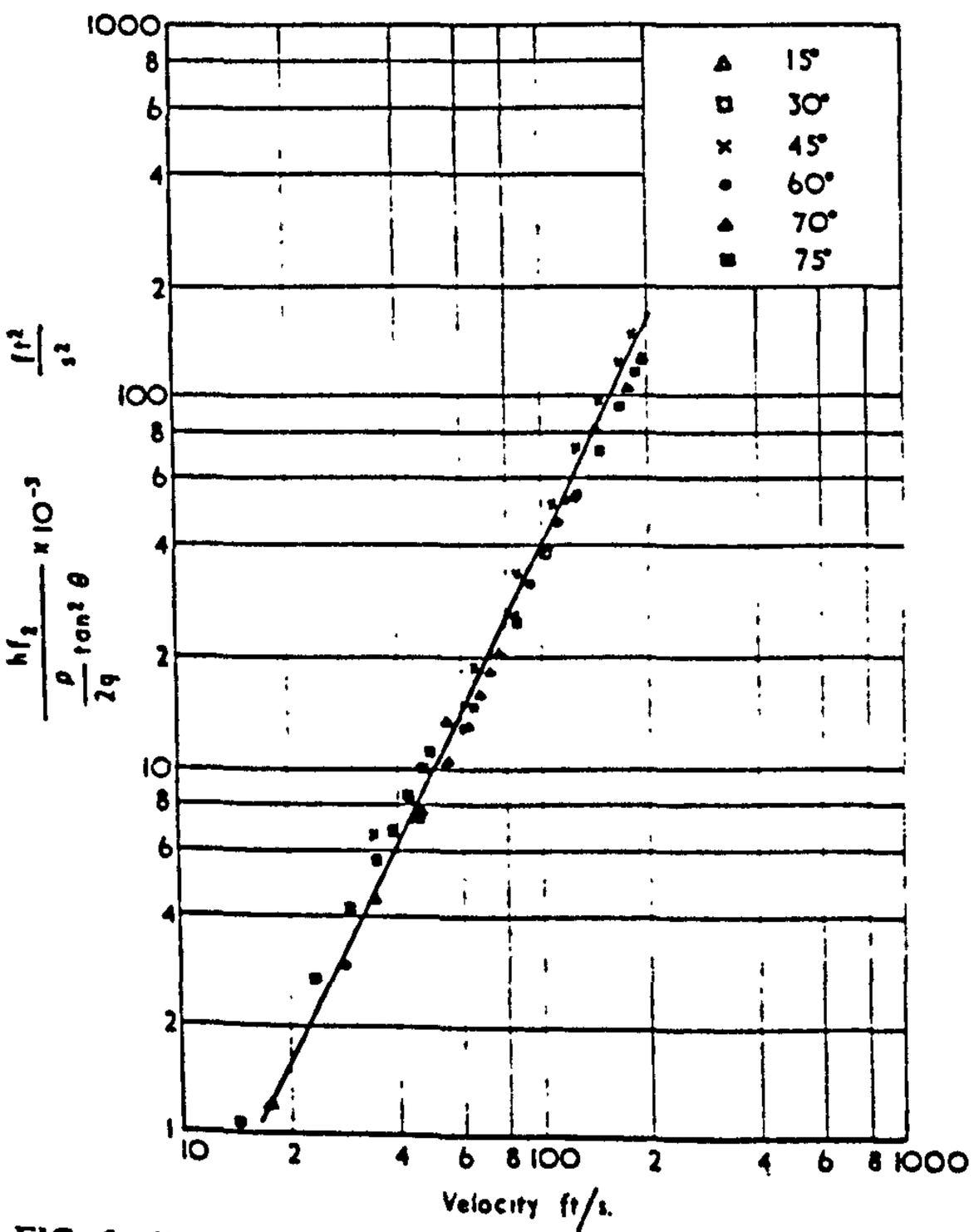

FIG. 3 Pressure drop across primary swirlers.

8. Results and discussion

8.1. Pressure drop across swirlers

The results of the pressure drops across the hubless swirlers are given in Fig. 2. The gradients of the lines on this Figure show that the pressure drop is proportional to the square of the nozzle velocity. If the constant k_1 is determined from the results of the 0° swirler using equations (6), the additional pressure drops, h_{f_2}, due to the inclination of the vanes on the other swirlers may be evaluated. The group ($h_{f_2}/\tan^2\theta$) is plotted against nozzle velocity in Fig. 3. On this plot the results of the various swirlers reduce to a single line, confirming the theoretical analysis (see equations (7) and (8)).

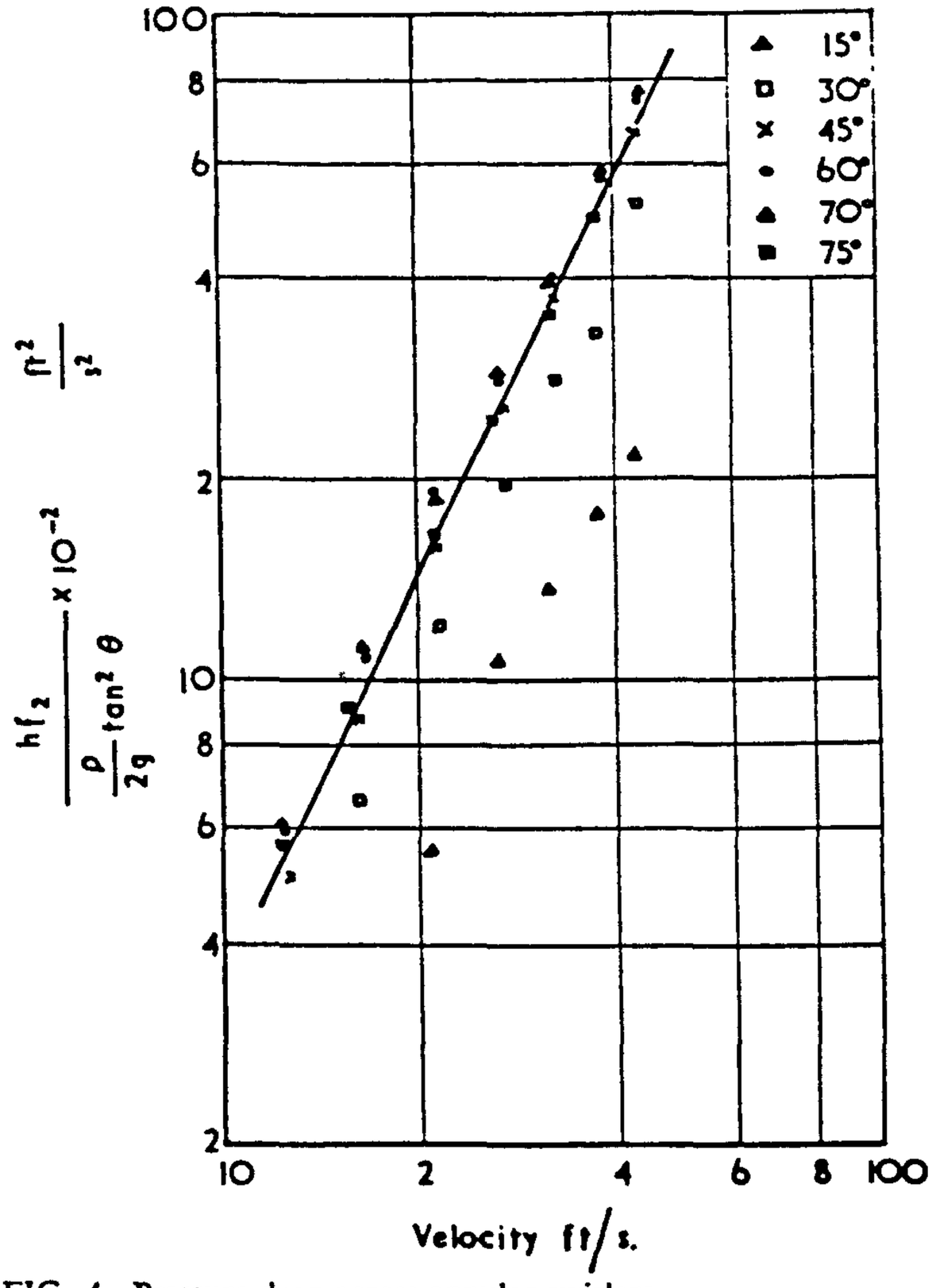

FIG. 4 Pressure drop across annular swirlers.

The pressure drop results obtained with the annular swirlers have been plotted in a similar manner in Fig. 4. In this case the results from all swirlers, except the 15° swirler, correlate satisfactorily. The discrepancy in the results of the 15° swirler is considered to be associated with incomplete deflection of the air due to the negative overlap (−13°) between adjacent vanes.

TABLE 3 Pressure drop across swirlers

Vane angle	Hubless swirlers				Annular swirlers			
	k	k_1	k_2	$\frac{k_1}{k}$	k	k_1	k_2	$\frac{k_1}{k}$
15	0·47	0·219	3·6	0·47	0·18	0·083	1·3	0·46
30°	1·31	,,	3·3	0·17	0·97	,,	2·9	0·085
45°	4·52	,,	4·3	0·05	3·5	,,	3·4	0·024
60°	10·7	,,	3·5	0·02	11·7	,,	3·9	0·007
70°	25·8	,,	3·4	0·009	29·9	,,	4·0	0·003
75°	65	,,	4·6	0·003	49·3	,,	3·5	0·002
Averages			3·78				3·54*	

*Neglecting the results of the 15° swirler.

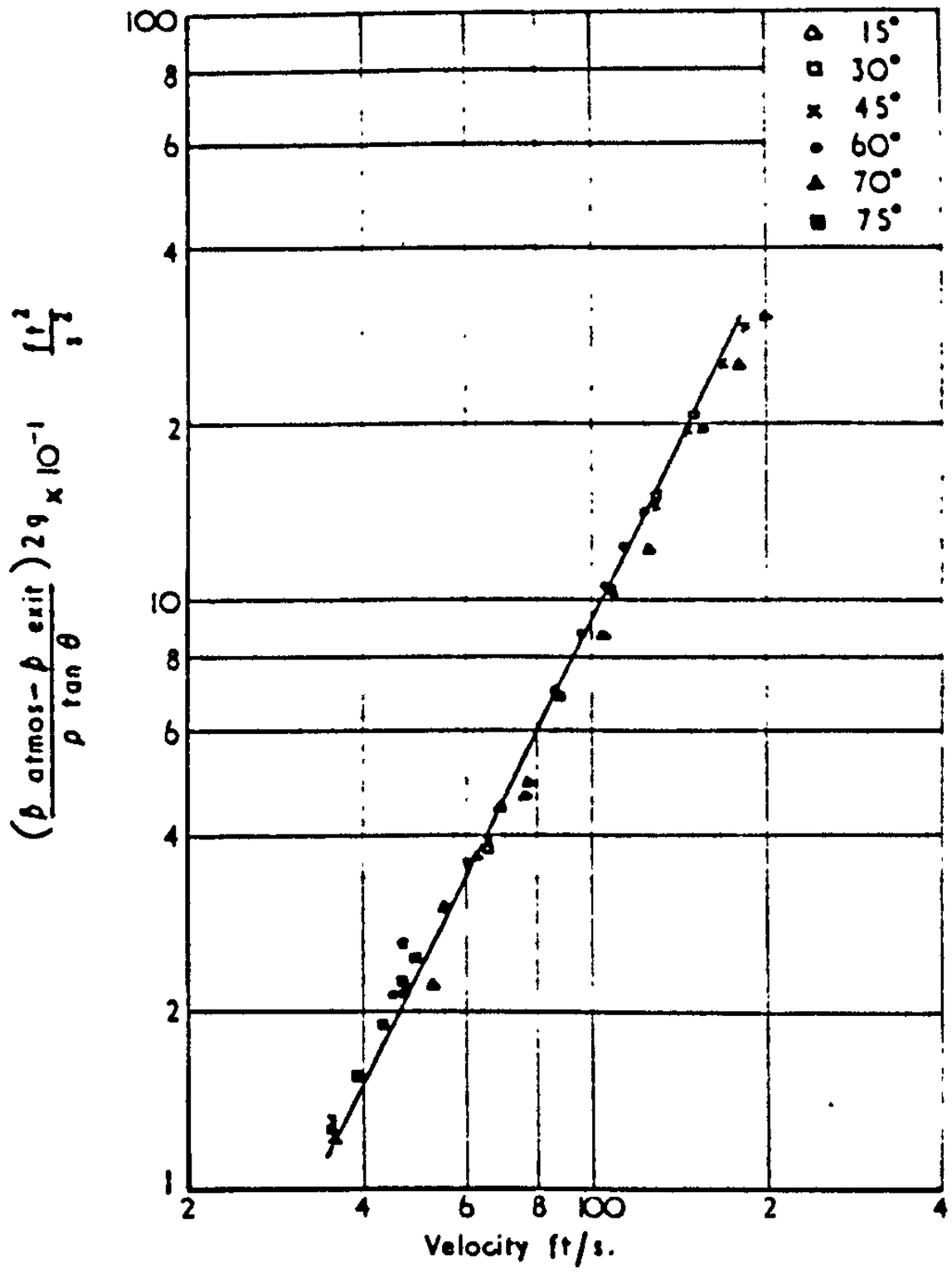

FIG. 5 Exit static pressure on axis in hubless jets.

The values obtained for the constants k, k_1 and k_2 are given in Table 3. On the basis of equation (10) the average value of the efficiency of the swirl generators is 0·27.

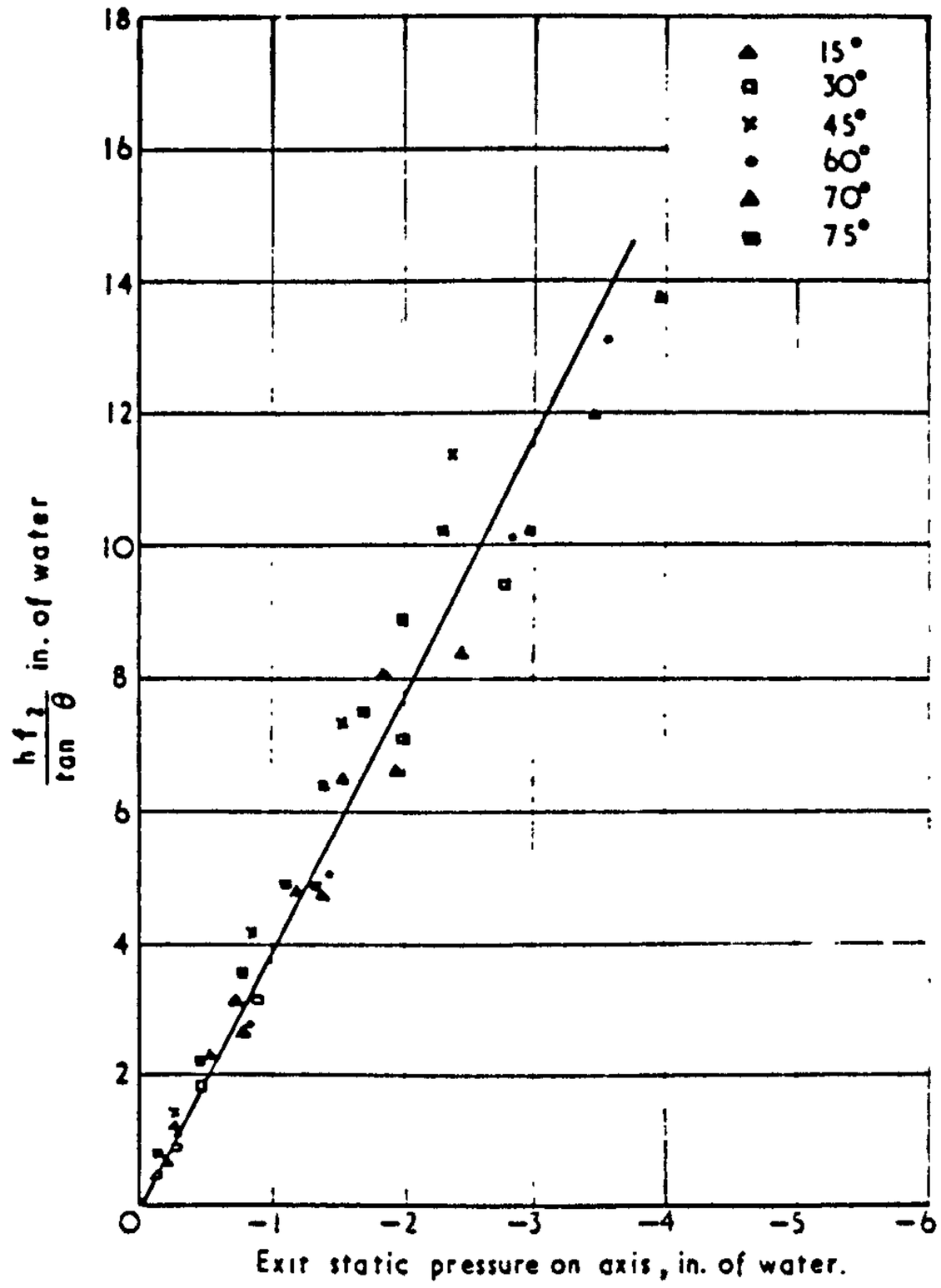

FIG. 6 Pressure drop plotted against exit static pressure on axis in hubless jets.

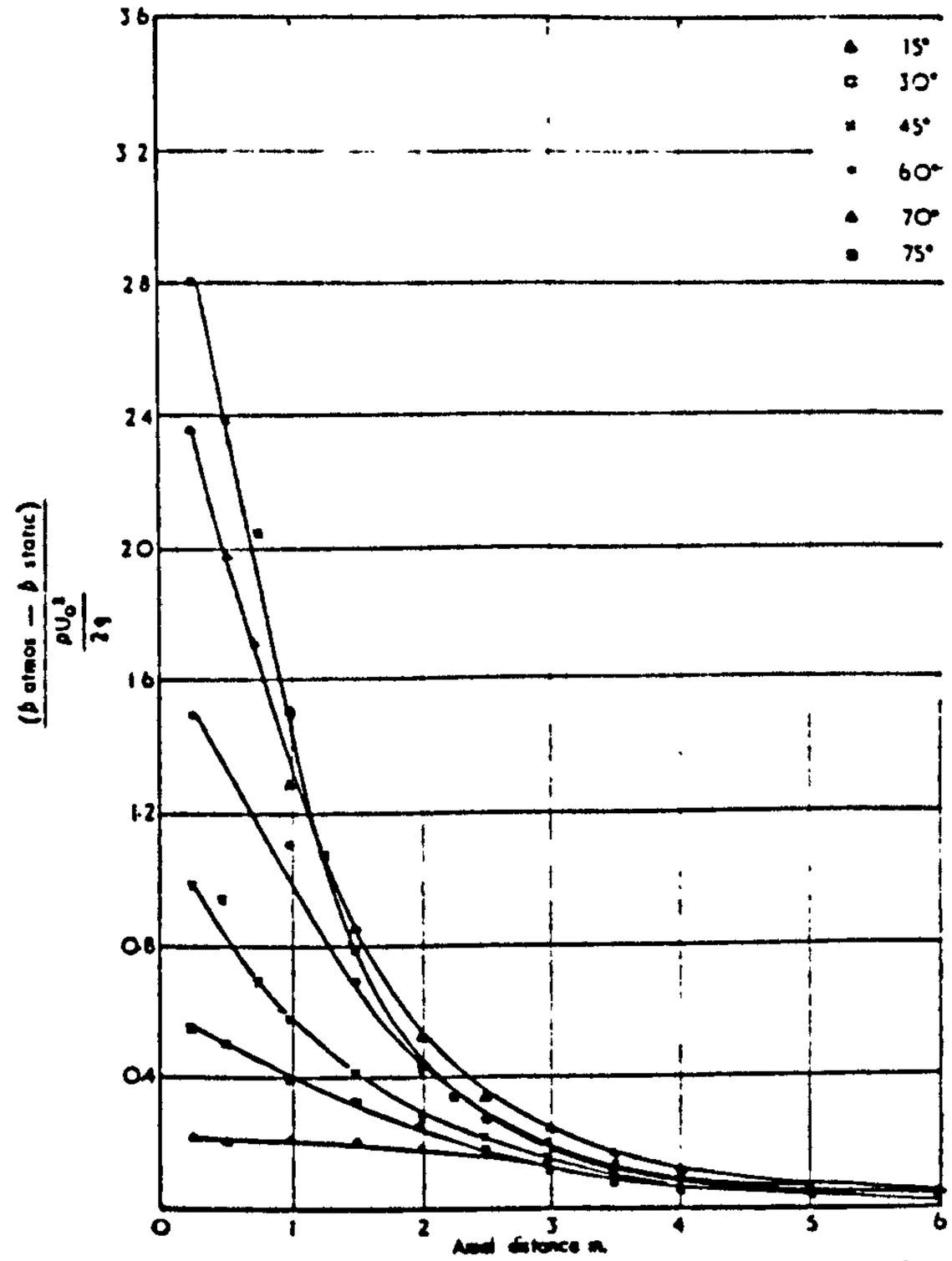

FIG. 7 (*a*) Variation of static pressure along jet axis in hubless jets.

That the values of k_2 for the hubless and annular swirlers are in close agreement indicates that swirlers of different sizes but of similar designs will have similar values of this coefficient k_2. The numerical values of k_2 are high, presumably due to flow disturbance at entry to the swirlers. This loss coefficient could be reduced by efficient design.

The results given above are for simple hubless or annular swirlers but the pressure drop across a complicated composite design of vane swirlers such as

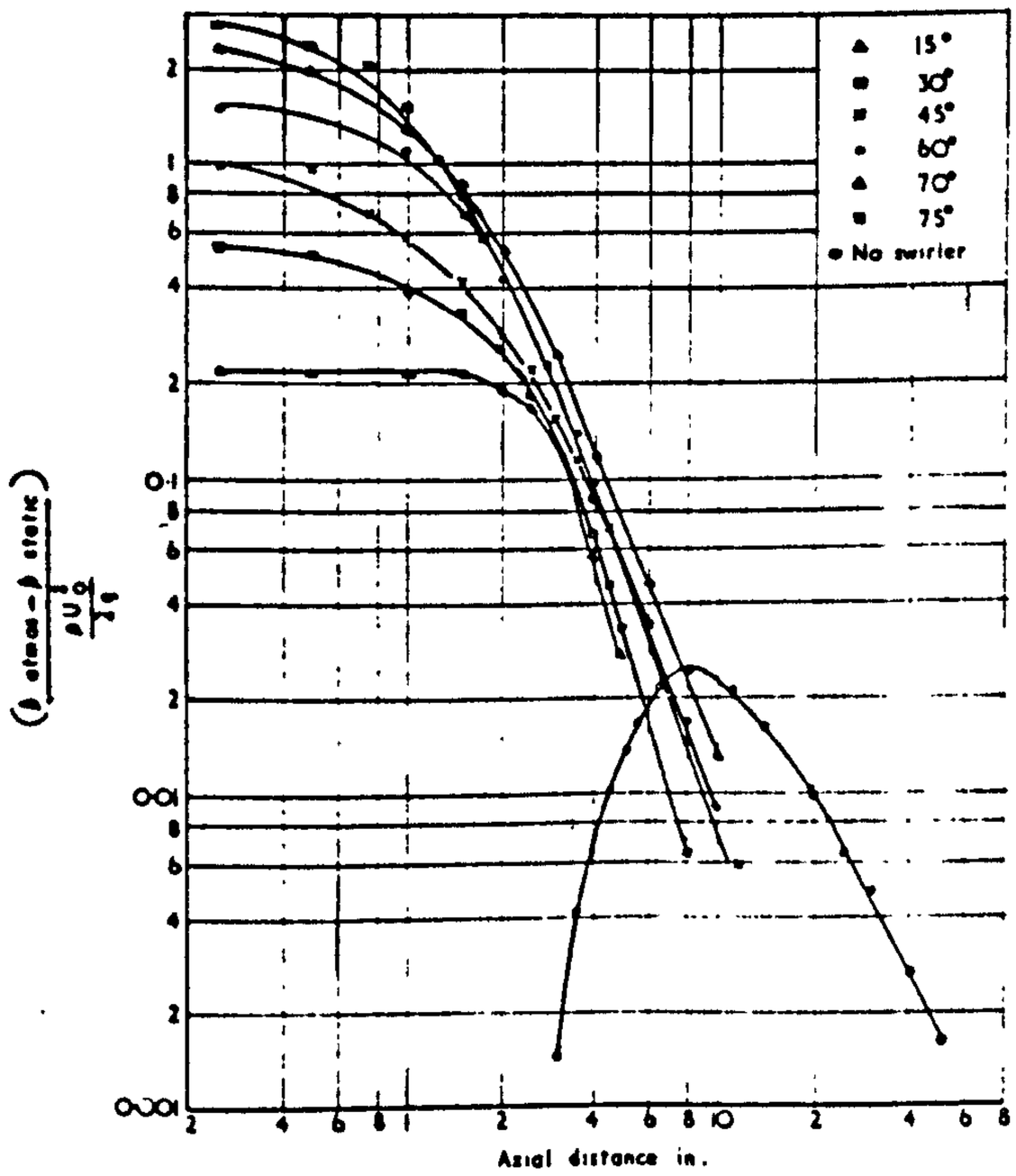

FIG. 7 (*b*) Variation of static pressure along jet axis in hubless jets.

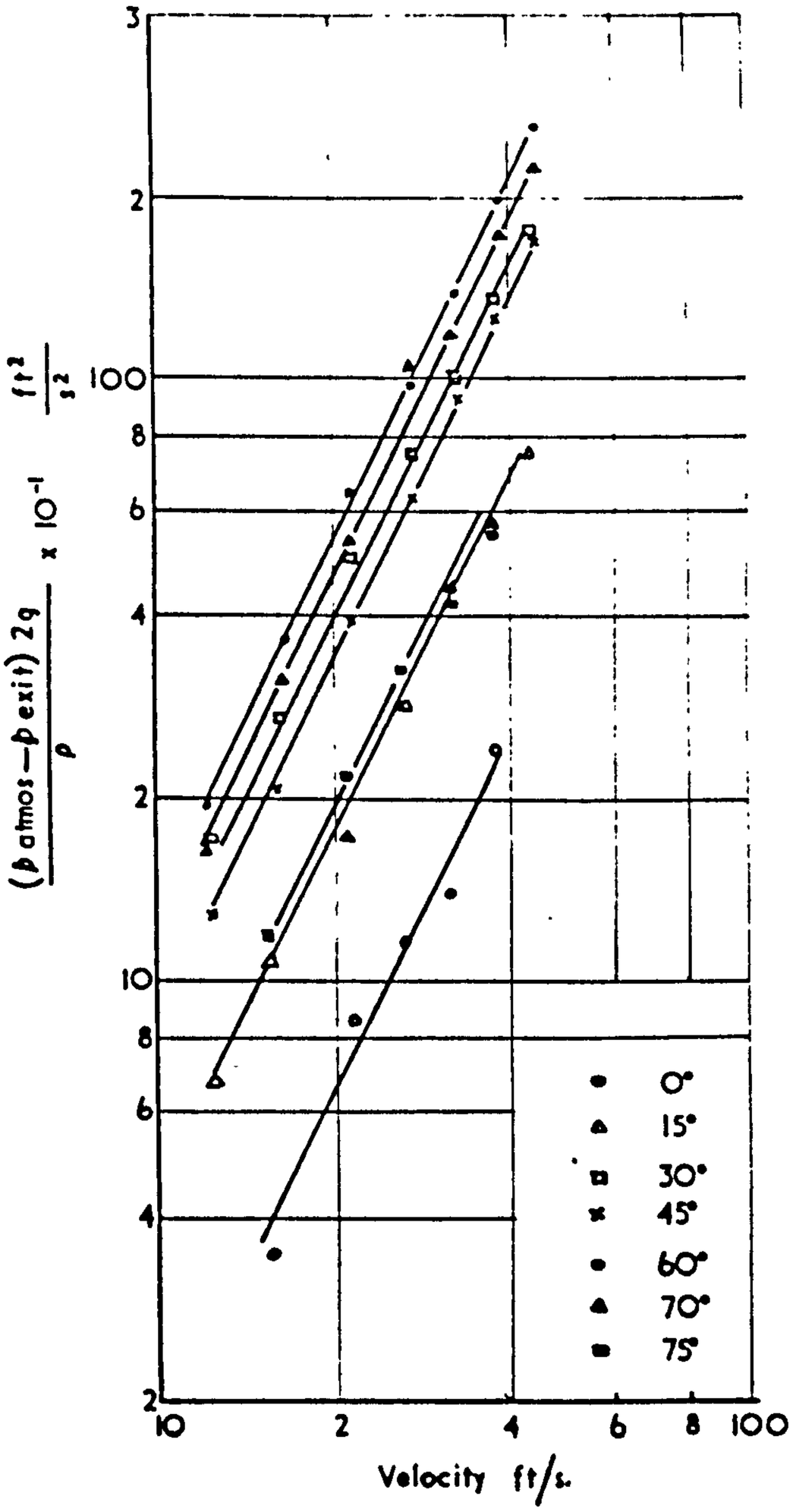

FIG. 8 Exit static pressure on axis in annular jets.

described in reference 22 could also be evaluated in a similar fashion.

A valuable comparison of the efficiencies of different methods of achieving the same degree of swirl could be made by comparing the pressure drops in the swirl generating devices.

8.2. Static pressure on the axis of jets

8.2.1. Hubless swirlers

In jets issuing from the hubless swirlers, the static pressure on the axis of the jet at the swirler exit is sub-atmospheric. The pressure, relative to atmospheric pressure, is found to be proportional to the square of the nozzle velocity and to the tangent of the vane angle (see Fig. 5).

i.e. $$\Delta p = (p_{atmos} - p_{exit}) = c_1 \frac{\rho U_0^2}{2g} \tan\theta \quad . \quad (11)$$

The proportionality with the square of the nozzle velocity is to be expected, but it is not known why the static pressure is proportional to tan θ.

The average value of the constant c_1 is found to be 0·97.

The pressure drop across the swirlers, due to the inclination of the vanes, h_{f2}, has already been found to be proportional to $\tan^2\theta$, and so this pressure drop, h_{f2}, and the exit static pressure, Δp, are related by

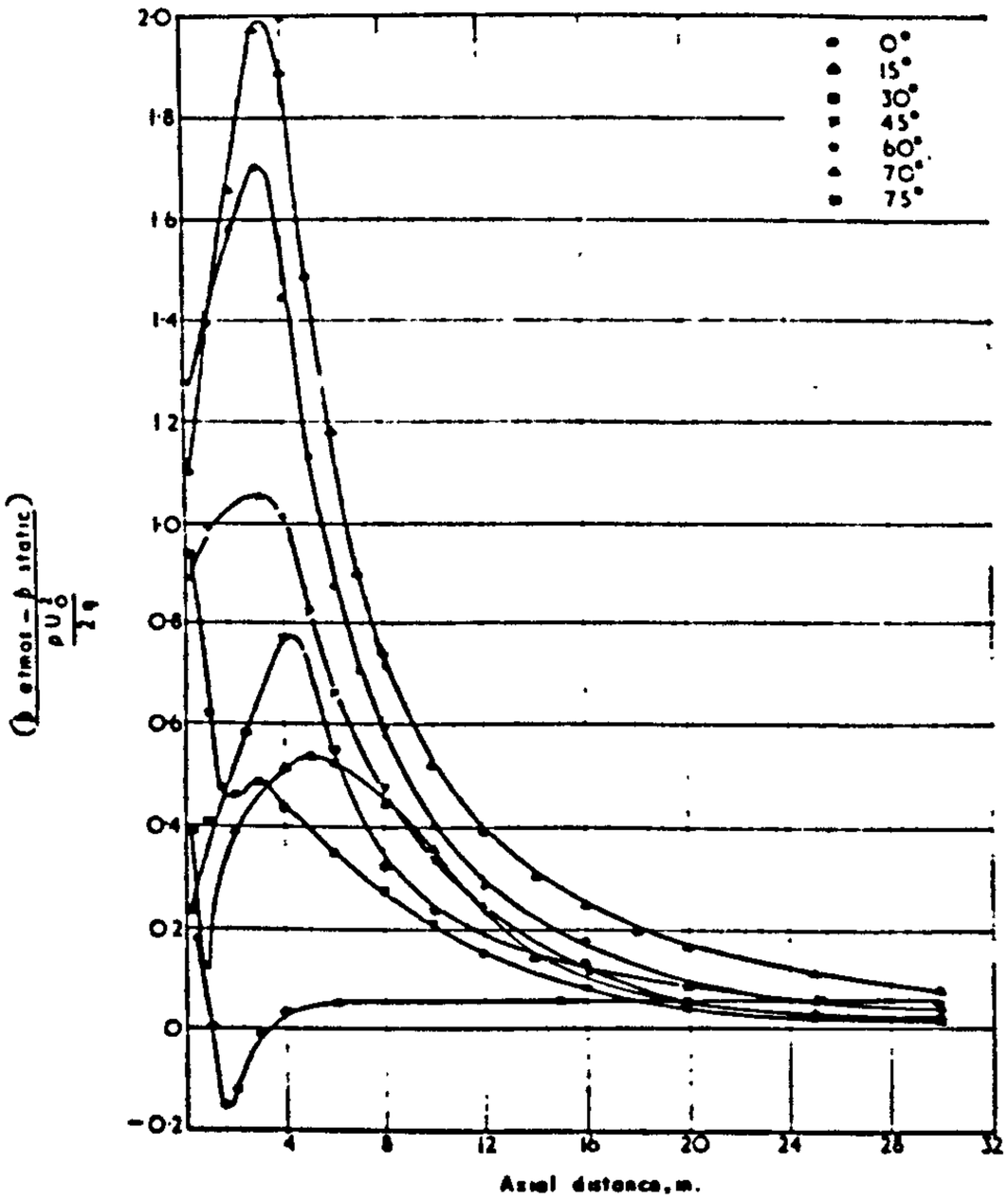

FIG. 9 (*a*) Variation of static pressure along jet axis in annular jets.

$$\frac{h_{f2}}{\Delta p} = \frac{k_2}{c_1} \tan\theta = c_2 \tan\theta \quad . \quad . \quad (12)$$

This relationship is demonstrated in Fig. 6, the average value of constant c_2 being found to be 3·9.

The variation of the static pressure along the axis of the jets is shown in Fig. 7 (*a*) and (*b*). The non-dimensional group $\left(\frac{p_{atmos} - p_{static}}{\frac{\rho U_0^2}{2g}}\right)$ is independent of Reynolds Number.

For comparison with the swirling jets, the static pressure was measured along the axis of an unswirling jet issuing from a nozzle of the same diameter as the swirlers. In this unswirling jet the static pressure at the exit plane is above atmospheric. Moving downstream, the static pressure increases slightly to a maximum at a

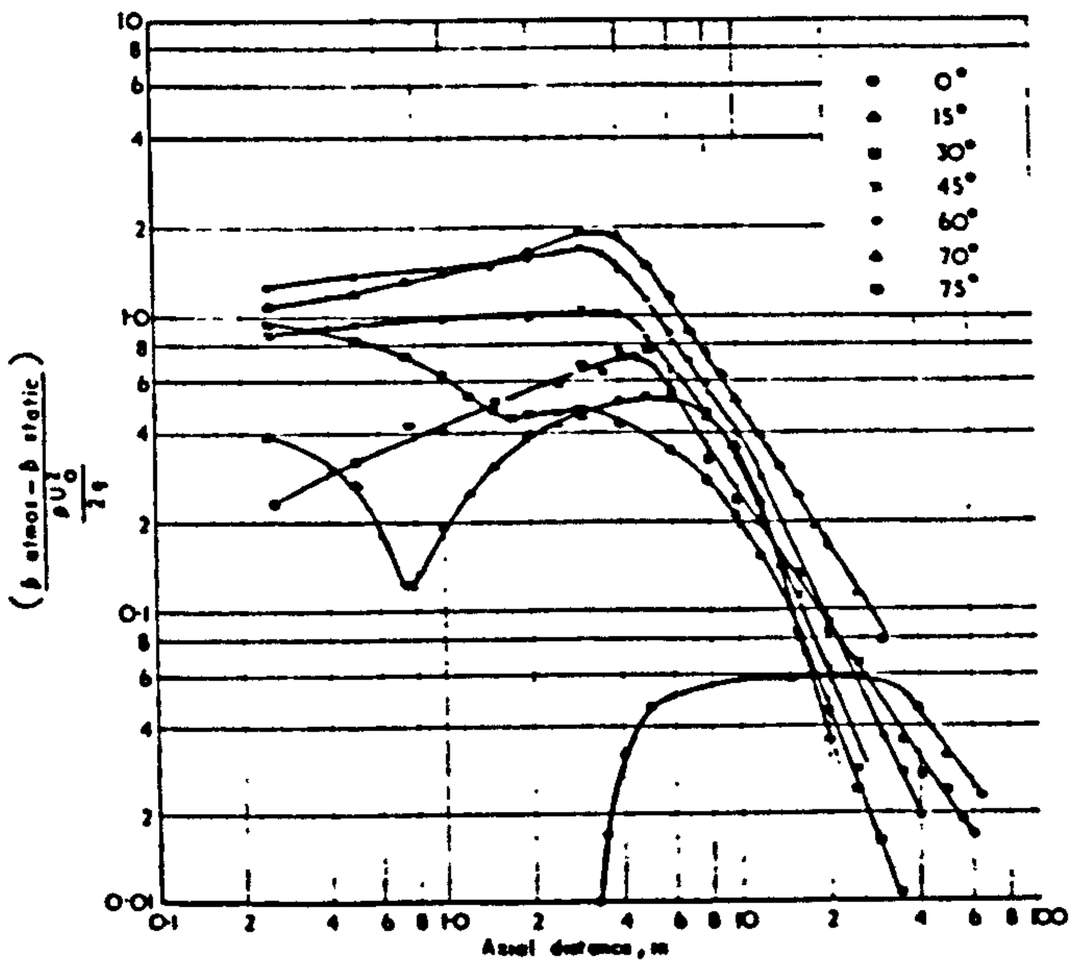

FIG. 9 (*b*) Variation of static pressure along jet axis in annular jets.

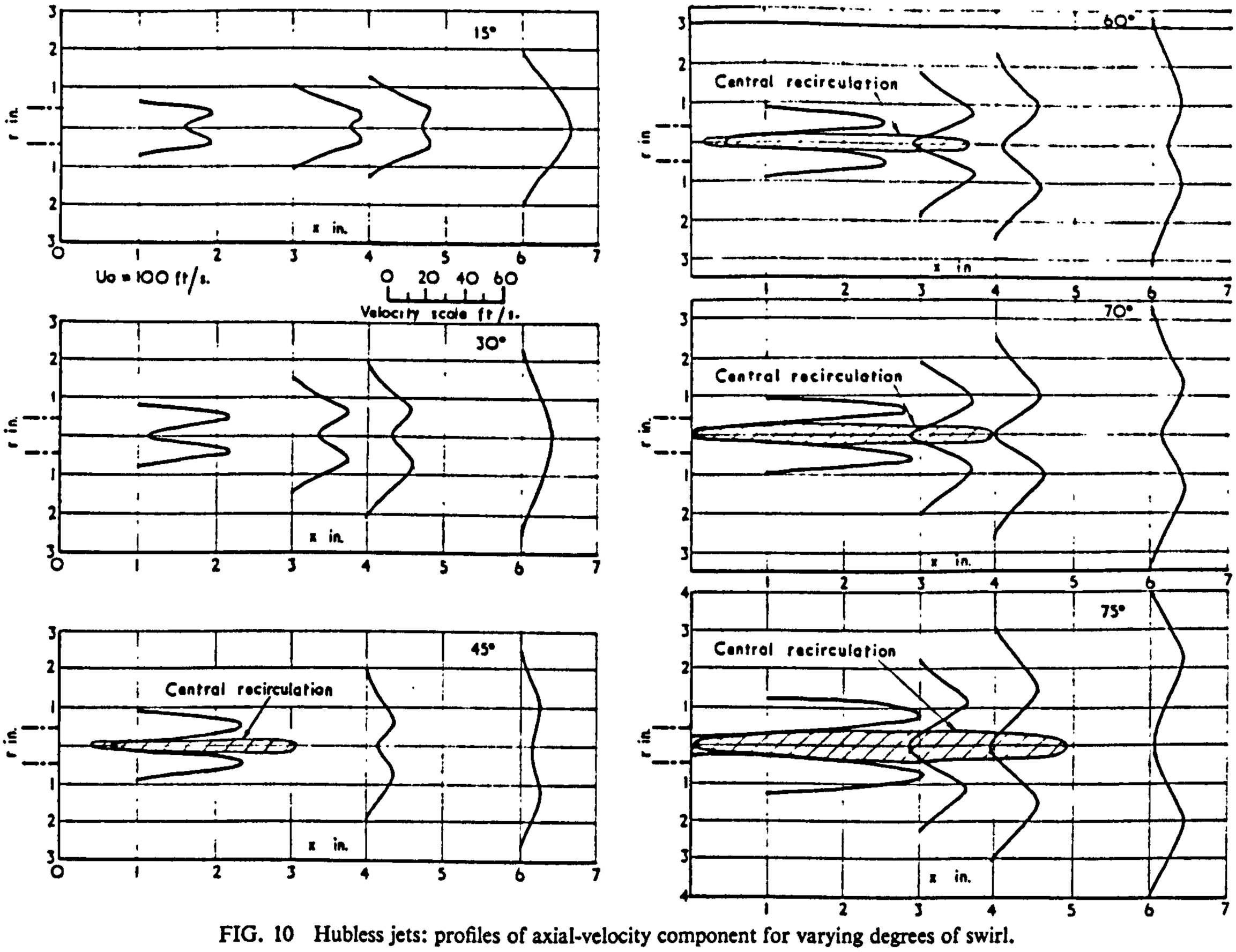

FIG. 10 Hubless jets: profiles of axial-velocity component for varying degrees of swirl.

distance $x/d_o = 0{\cdot}6$. Thereafter the static pressure decreases, equalling atmospheric at $x/d_o = 2{\cdot}6$ and reaching a minimum value at $x/d_o = 8$. At this section the jet is fully developed. Finally the static pressure tends towards atmospheric. In the region beyond about $x/d_o = 20$ this approach is proportional to x^{-2} (see Fig. 7 (*b*)).

In the swirling jets the static pressure on the axis is always sub-atmospheric. The minimum pressure occurs at the swirler exits. On moving downstream from the swirlers the pressure rises towards atmospheric, the approach eventually being proportional to x^{-n}. The value of the index n varied from 3·5 for low-intensity swirl to 2·5 for high-intensity swirl.

8.2.2. Annular swirlers

In jets issuing from annular swirlers the static pressure on the axis of the jet at the swirler exit was sub-atmospheric, and, relative to atmospheric, it was found to be proportional to the square of the nozzle velocity, but not proportional to the tangent of the vane angle, as had been the case with the hubless swirlers. The results are shown in Fig. 8 which illustrates the irregular manner in which static pressure changes with vane angle.

The static pressure distributions along the axis of the swirling jets and also along a corresponding non-swirling jet are shown in Fig. 9 (*a*) and (*b*). The pressure distribution in the non-swirling jet is similar to that described by Chigier and Beér.[34] At the nozzle exit the pressure is sub-atmospheric but on moving downstream the pressure rises rapidly above atmospheric. A maximum pressure is reached at a point, referred to as the 'stagnation point,' where $x/d_2 = 0{\cdot}4$. Thereafter the static pressure falls to below atmospheric pressure. In the swirling jets, those issuing from the 15° and 30° swirlers also show a rapid rise in static pressure immediately downstream of the swirler, although in neither case does the pressure rise to atmospheric. This is then followed by a reduction in pressure to a minimum. Finally the pressure rises, approaching atmospheric asymptotically. In the jets issuing from the swirlers of 45° and higher vane angles there is no initial rise in the static pressure. Instead the pressure falls, reaching a minimum value at a distance about d_2 downstream from the swirler, and thereafter the pressure approaches asymptotically to atmospheric.

It can be seen, on comparing the pressure distributions in the hubless and annular jets, that the behaviour of the hubless jet is simpler and might be mathematically described more easily, which illustrates the usefulness of studying hubless jets.

8.3. Velocity distributions

8.3.1. Axial-velocity distributions

The profiles of the axial component of velocity for jets from hubless and annular swirlers are given in Figs. 10 and 11 respectively. In both the hubless and annular jets the velocity profiles close to the swirler have the shape of double crests separated by a central trough. Within the lengths observed (12 d_o for hubless jets and 7 d_2 for annular jets) the distribution of the axial velocity component does not fit the error curve relationship. (The error curve relationship is applicable to non-swirling jets beyond 8 d, and has also been found in one case to fit swirling jets at distances greater than 12 d.[22])

With vane angles of 45° and greater there is a reverse velocity, i.e. recirculation, in the central zone of the jet near the nozzle. The strength of the recirculation increases

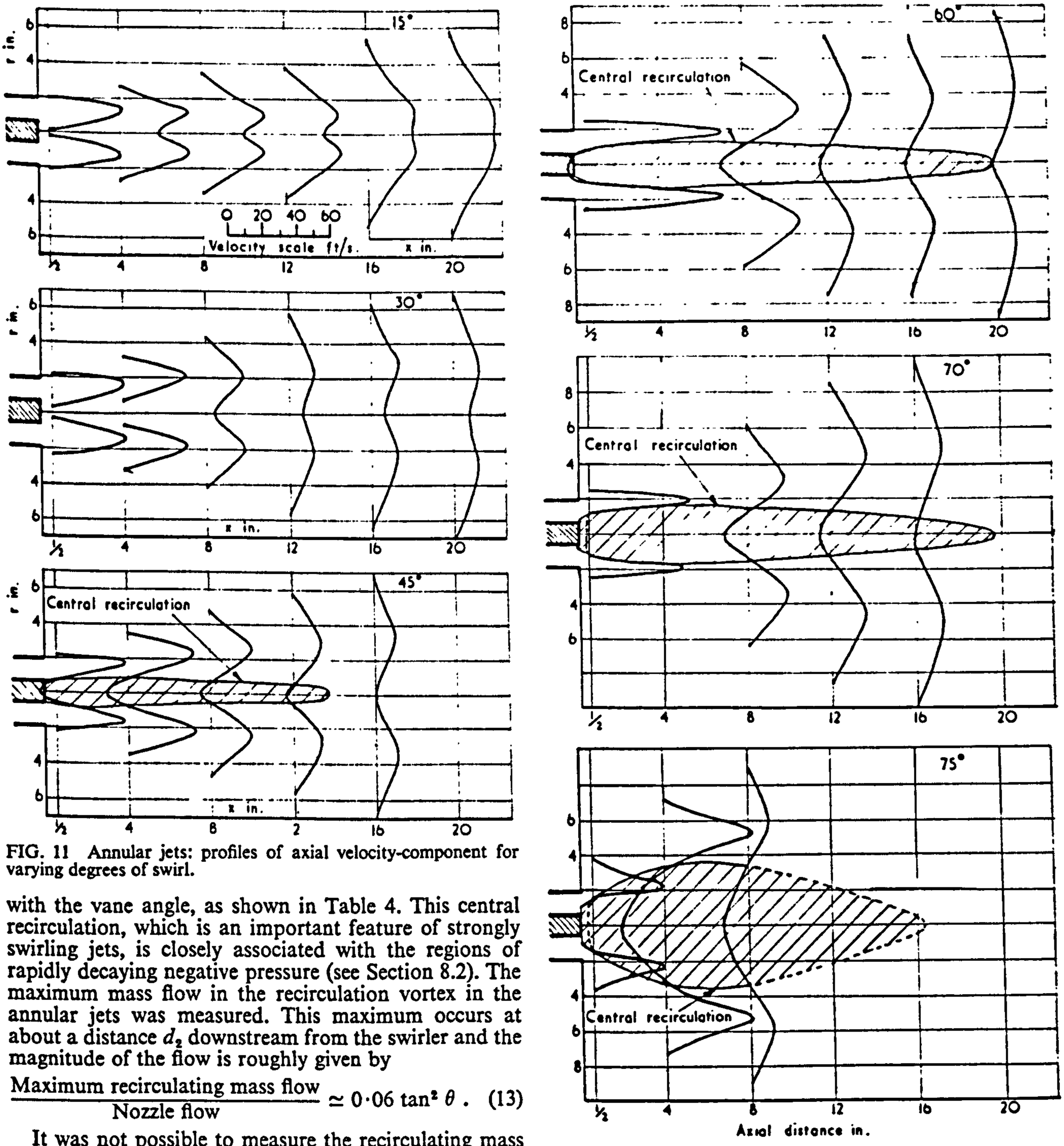

FIG. 11 Annular jets: profiles of axial velocity-component for varying degrees of swirl.

with the vane angle, as shown in Table 4. This central recirculation, which is an important feature of strongly swirling jets, is closely associated with the regions of rapidly decaying negative pressure (see Section 8.2). The maximum mass flow in the recirculation vortex in the annular jets was measured. This maximum occurs at about a distance d_2 downstream from the swirler and the magnitude of the flow is roughly given by

$$\frac{\text{Maximum recirculating mass flow}}{\text{Nozzle flow}} \simeq 0{\cdot}06 \tan^2\theta \,. \quad (13)$$

It was not possible to measure the recirculating mass flows in the hubless jets due to the small cross-sectional area of the vortices.

The results in Table 4 indicate that the limits of recirculation and maximum reverse velocity ratios are generally similar for both hubless and annular swirlers of the same vane angle. This would suggest that the term

TABLE 4 Central recirculation in swirling jets

Vane angle	Jets issuing from hubless swirlers: Limits of recirculation to	from	Max. reverse vel. / Nozzle vel.	Jets issuing from annular swirlers: Limits of recirculation to	from	Max. reverse vel. / Nozzle vel.	Max. reverse flow / Nozzle flow	Max. reverse flow / Nozzle flow × $\tan^2\theta$
15°	Nil		Nil	Negligible				
30°	Nil		Nil	Negligible				
45°	0·3 d_o	3·2 d_o	0·33	Hub	3·7 d_2	0·35	0·039	0·039
60°	0·1 d_o	4 d_o	0·40	Hub	5 d_2	0·77	0·157	0·052
70°	Nozzle exit	4·3 d_o	0·90	Hub	5·2 d_2	0·76	0·434	0·057
75°	Nozzle exit	5 d_o	0·90	Hub	5·2 d_2	0·72	0·84	0·060
Average								0·052

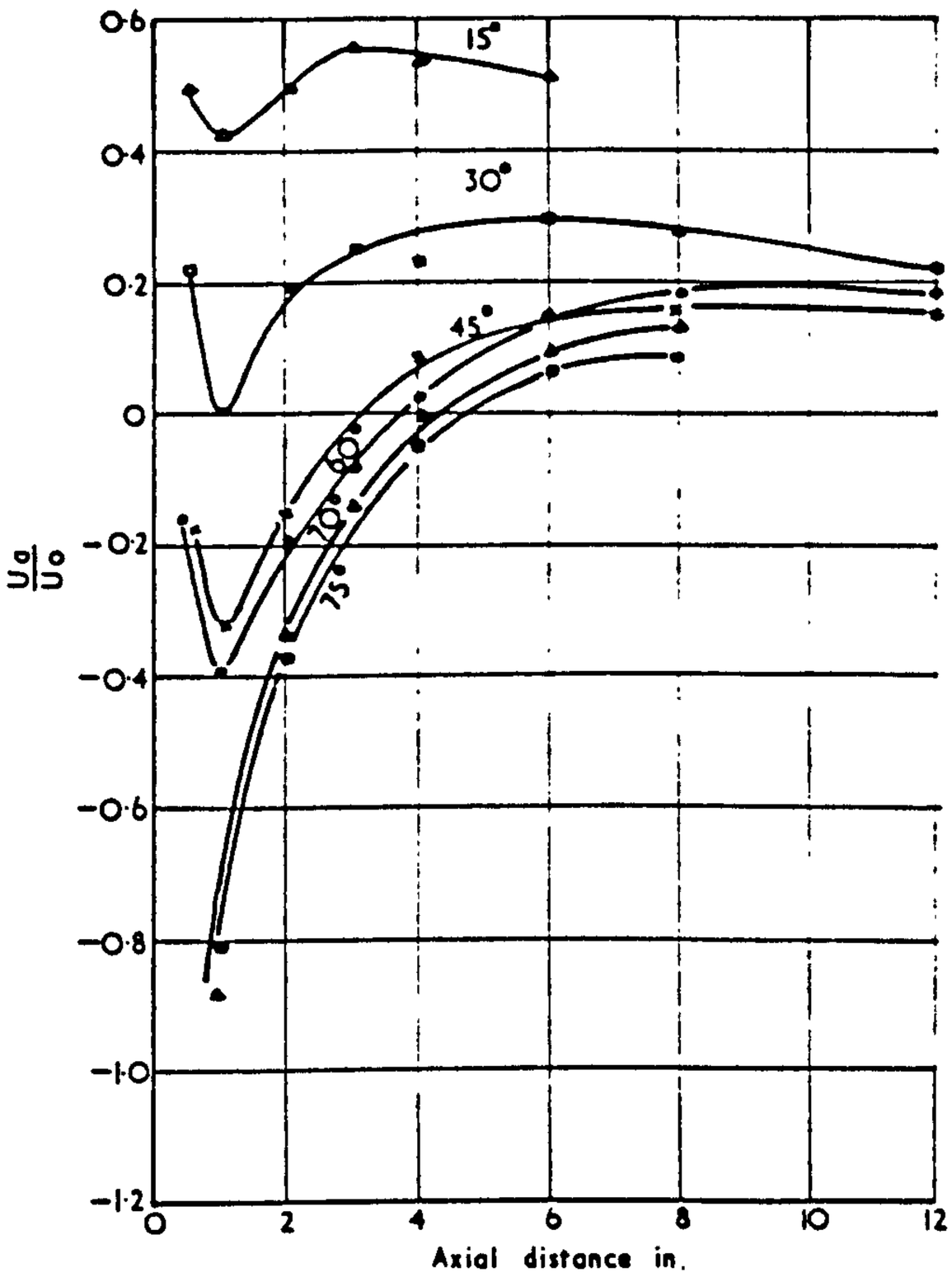

FIG. 12 Hubless jets: decay of axial-velocity along jet axis.

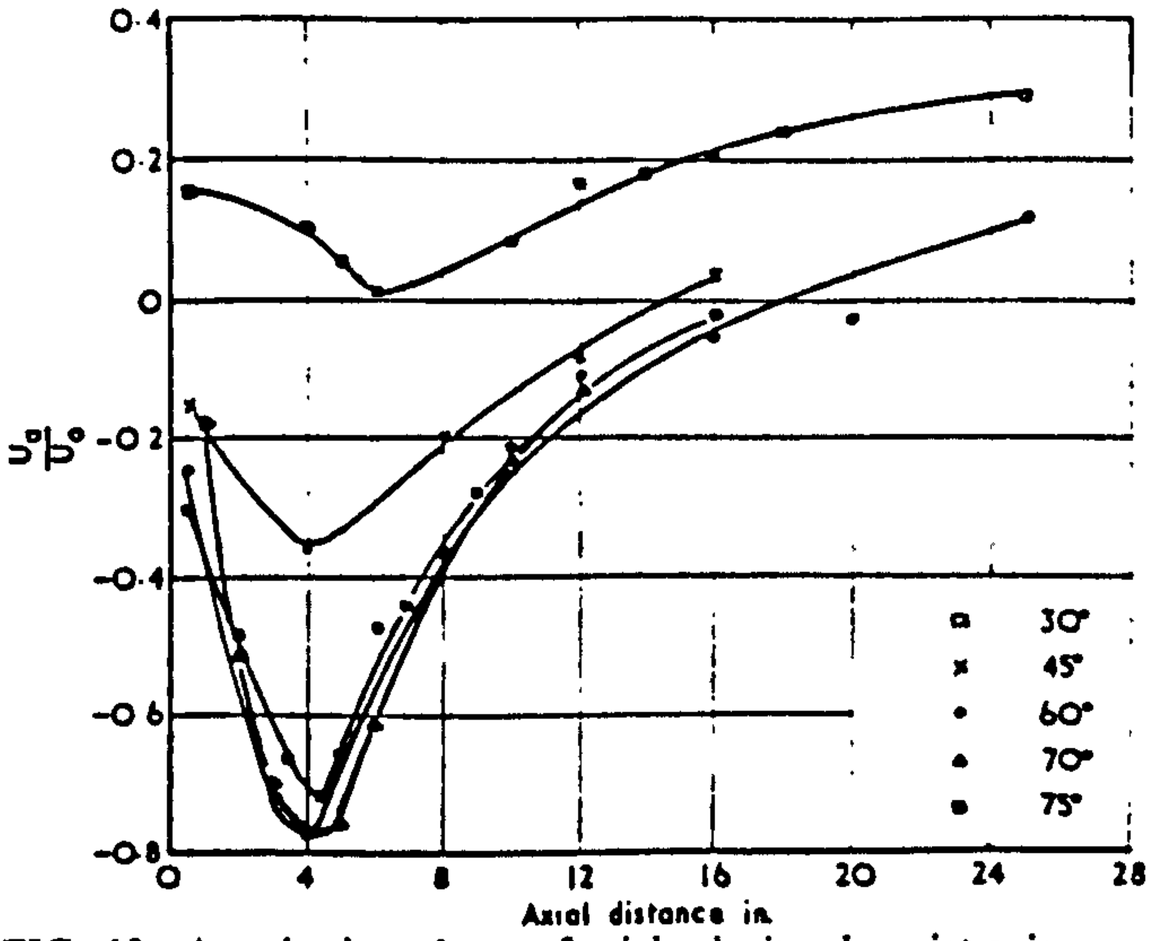

FIG. 13 Annular jets: decay of axial-velocity along jet axis.

$\tan\theta$, instead of $\frac{G\phi}{G_x r_2}$, may be taken as a measure of the degree of swirl for jets issuing from vane swirlers, provided of course that the vanes give sufficient overlap to achieve complete direction.

The variations of the axial component of velocity along the axis of the jets issuing from hubless and annular swirlers are shown in Figs. 12 and 13 respectively. The minimum axial velocity, which as mentioned above, is negative with high degree of swirl, is attained in all cases about one diameter downstream from the swirler. Only in the jets issuing from the 15° and 30° hubless swirlers does the axial velocity component on the axis

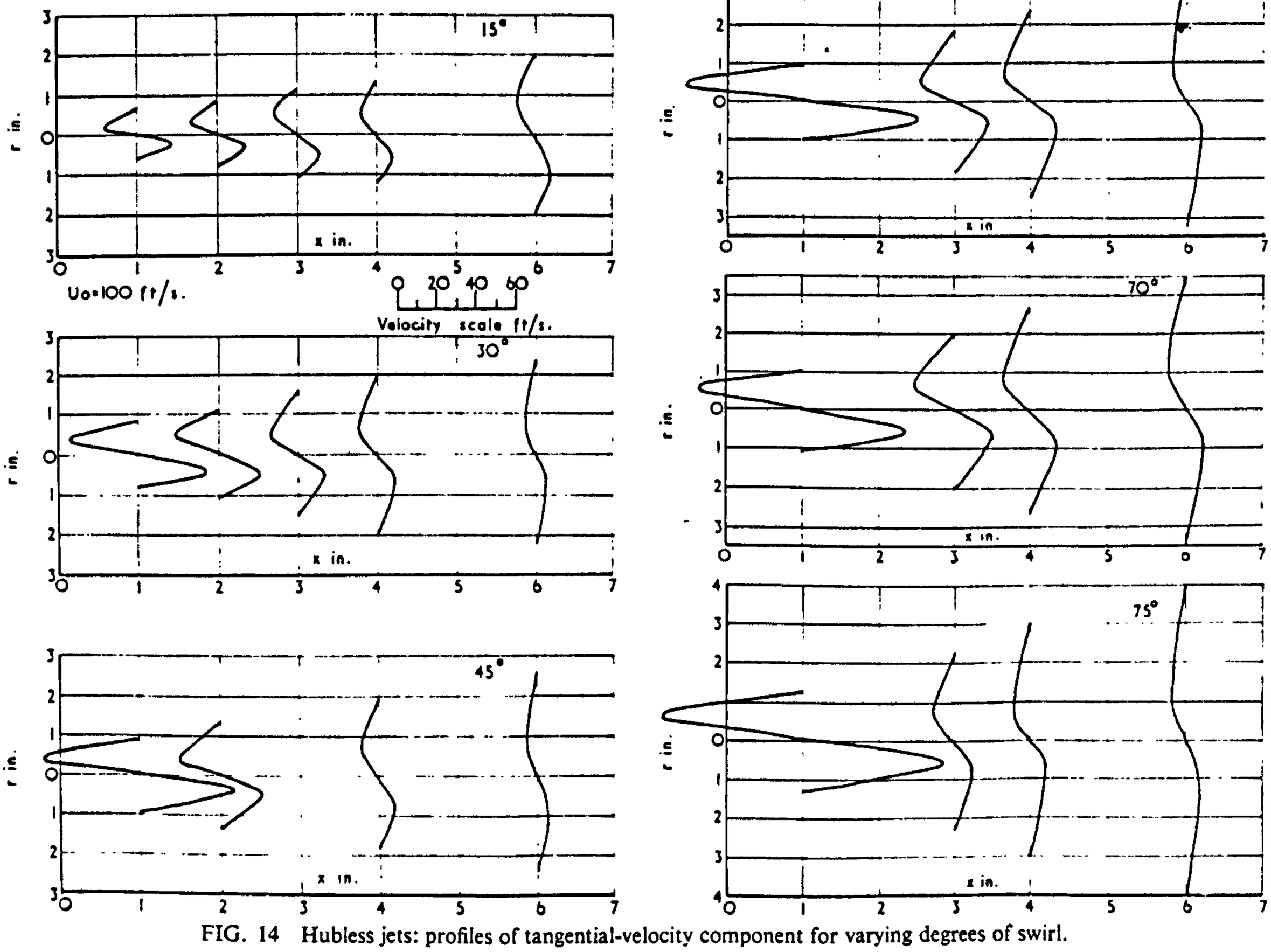

FIG. 14 Hubless jets: profiles of tangential-velocity component for varying degrees of swirl.

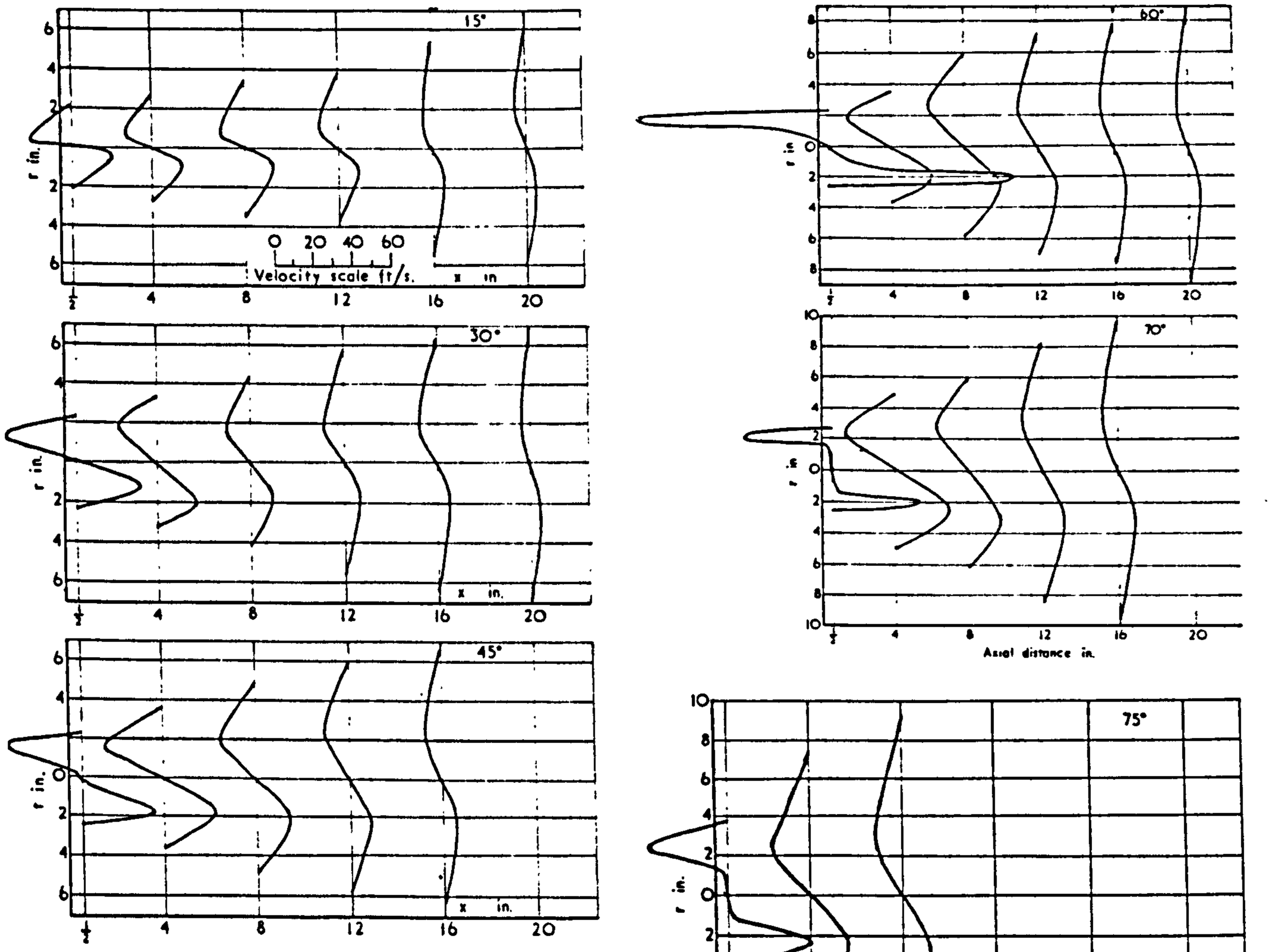

FIG. 15 Annular jets: profiles of tangential-velocity component for varying degrees of swirl.

reach a maximum positive value and then decay within the jet lengths studied.

From the velocity distributions shown in Fig. 10 and 11 it can be seen that the maximum value of the axial component of velocity decays more rapidly as the degree of swirl is increased.

8.3.2. Tangential-velocity distributions

The tangential velocity distributions for jets issuing from hubless and annular swirlers are given in Figs. 14 and 15 respectively. In both types of jets the tangential velocity distributions indicate the jet as being a fixed vortex core surrounded by a free vortex region. The cross-sectional area occupied by the fixed vortex core remains almost constant in the length of the jet, the area being about equal to the swirler exit area.

8.3.3. Variation of jet width along the axis

The width of the jet was found from the axial velocity profiles by assuming the boundary of the jet to be the point where the axial velocity is 10% of the maximum axial velocity in that plane. Jet widths obtained in this manner are plotted in Figs. 16 and 17 for the hubless and annular jets respectively. These results show that a swirling jet, when it emerges from the swirler, initially experiences a rapid rate of expansion, this rate increasing with the swirler vane angle. Further downstream this rate of expansion reduces to a value which is almost independent of the swirler vane angle.

8.4. Combination of hubless and annular swirlers

Many industrial applications employ a combination of two concentric swirlers. It is deduced that in such cases both the inner and outer streams need to be given swirl to achieve significant central recirculation. Satisfactory results should be obtained by using vane angles of 45° for the primary swirler and 45° or higher for the secondary swirler.

9. Conclusions

(1) In the design of vane swirlers for effective directing of the air a positive overlap between adjacent vanes is essential. An overlap of 30° in an eight-vane swirler has been found to be adequate.

(2) The pressure drop across vane swirlers is given by

$$h_f = \frac{\rho U_0^2}{2g}\,(k_1 + k_2 \tan^2\theta).$$

Constant k_1 is negligible for swirlers of vane angles of 45° and higher. Constant $\frac{1}{k_2}$ represents the efficiency of swirl generation. If the value of k_2 is less than unity it indicates that the air is not fully directed.

(3) In hubless jets the static pressure, relative to

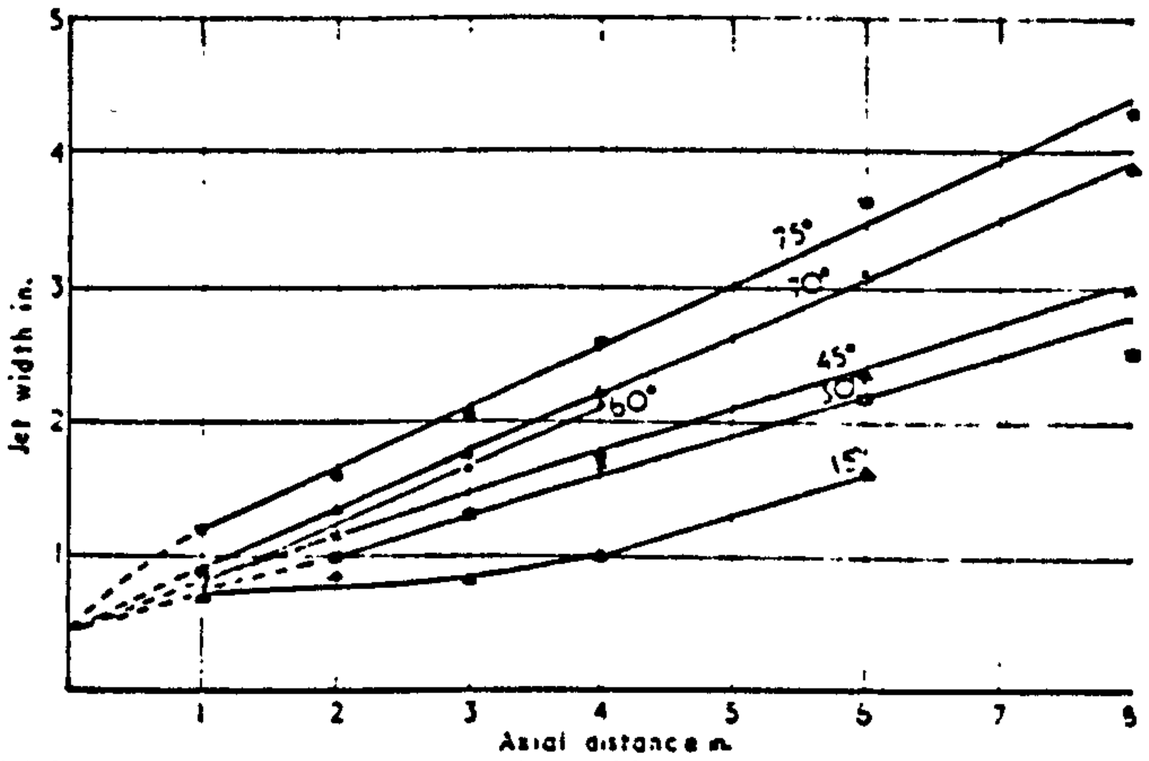

FIG. 16 Hubless jets: variation of jet width along the axis.

atmospheric pressure, at exit from the swirler is proportional to $U_0^2 \tan\theta$. In annular jets the static pressure is proportional to U_0^2 but varies irregularly with θ.

(4) The axial velocity profiles of a swirling jet, within the lengths investigated (7 d_2 for annular and 12 d_0 for hubless swirlers), do not follow the error curve relationship. A swirling jet experiences a sudden expansion soon after it issues from the nozzle—the rate of expansion increasing with degree of swirl. After 2 to 4 d_0 (or d_2) the expansion becomes linear with nearly the same spread angle for jets having varying degrees of swirl.

(5) Central recirculation, extending from 3 to 5 d downstream of the nozzle exit, is an important feature of jets issuing from swirlers of vane angles of 45° and higher. The maximum mass flow in the recirculation vortex, occurring at about one diameter downstream of the nozzle exit, is roughly equal to $0{\cdot}06 \tan^2\theta$ of the nozzle flow.

(6) Tan θ is a good measure of swirl for jets issuing from vane swirlers.

10. Acknowledgments

The authors thank Emeritus Professor James Small, formerly James Watt Professor of Mechanical Engineering, University of Glasgow, for his encouragement and advice. They also thank the members of his staff, particularly Dr. N. M. Kerr and D. Fraser who initiated the study of swirl at the University of Glasgow. M. L. Mathur would like to record his thanks to the Commonwealth Scholarship Commission in the United Kingdom.

11. References

1. WATSON, E. A., and CLARKE, J. S. Combustion and Combustion Equipment for Aero Gas Engines. *J. Inst. Fuel* 1947, (Oct.), **21**, 2 to 34.
2. CUDE, A. L., and HALL, J. R. Tip-Atomising Burners in the O.H. Furnace. *J. Iron Steel Inst.*, 1950 (Aug.), **165** (II), 419 to 429.
3. CUDE, A. L. The length of Oil and Gas Flames. *J. Iron Steel Inst.*, 1953 (Nov.), **175** (III), 304 to 312.
4. LOITSYANSKII, L. G. The Propagation of a Twisted Jet in an Unbound Space Filled with the Same Fluid. *Prikladnaya Matematiza i Mekhanika*, 1953, **17**, 3 to 16.
5. HOTTEL, H. C., and PERSON, R. A. Heterogeneous Combustion of Gases in a Vortex System. Fourth Symposium (International) on Combustion (Williams and Wilkins, Baltimore, 1953).
6. GORTLER, H. Decay of Swirl in an Axially Symmetrical Jet Far from the Orifice. *Revista Matematica Hispano Americana*, 1954, **14** (4 and 5), 143 to 178.
7. CLARKE, J. S. The Relation of Specific Heat Release to Pressure Drop in Aero Gas Turbine Combustion Chambers. A.S.M.E., I.Mech.E. Joint Conference on Combustion, 1955, 354 to 361.
8. POULSTON, B. V., and WINTER, E. F. Techniques for the Study of Air Flow and Fuel Droplet Distribution in Combustion Systems. Sixth Symposium (International) on Combustion (Reinhold Publishing Corporation, New York, 1957).
9. WINTER, E. F. Flow Visualisation Techniques Applied to Combustion Problems. *J. Royal aeronaut. Soc.*, 1958, **62**, 268 to 276.
10. ULLRICH, H. Stromungsvorgänge in Drallbrennern mit regelbarem Drall und bei rotationssymmetrischen Freistrahlen. *Forschung auf dem Gebiete des Ingenieurwesens*, 1960, **26**, 1, 19 to 28.
11. ROSE, W. G. A Swirling Round Turbulent Jet. *J. appl. Mech.*, 1962, **29**, 615 to 625.
12. ROSE, W. G. Generation of a 'Strongly' Swirling Jet. (Report AFOSR 2552 Johns Hopkins University, Dept. Mech. Contract AF 49 (638)—248, Baltimore) 1962, June.
13. DRAKE, P. F., and HUBBARD, E. H. Effect of Swirl on Completeness of Combustion. *J. Inst. Fuel*, 1963 (Sept.), **36**, 389 and 390.
14. COHEN DE LARA, G., and FELLOUS, J. R. Experimental Study in an Isothermal System of Mechanism of Mixing of a Primary Swirling Jet Diffusing in a Cylindrical Chamber with a Uniform Axial Flow of Secondary Air. International Flame Research Foundation, IJmuiden, 1963 (Sept.), Doc. No. Tb–F61/bc/5.
15. BEÉR, J. M., and CHIGIER, N. A. Swirling Jet Flames Issuing from an Annular Burner. 5th Journee d'Etudes sur les Flammes, Paris, 1963, Nov.
16. COHEN DE LARA, G., and FELLOUS, J. R. Experimental Study in an Isothermal Enclosure of the Recirculation Near the Axis of a Swirling Jet Diffusing in a Cylindrical Chamber. International Flame Research Foundation, IJmuiden, 1964, May, Doc. No. Tb–F61/bc/7.
17. CHIGIER, N. A., and BEÉR, J. M. Velocity and Static-Pressure Distributions in Swirling Air Jets Issuing from Annular and Divergent Nozzles. *Trans. A.S.M.E.*, **86**, Series D Jour. Basic Engineering No. 4, Dec. 1964, 788 to 796.
18. BROWN, A. M., and THRING, M. W. The Application of Pressure Jet Burners to Marine Boilers. Tenth Symposium (International) on Combustion, The Combustion Institute, Pittsburgh, 1965.
19. BEÉR, J. M., and LEE, K. B. The Effect of the Residence Time Distribution on the Performance and Efficiency of Combustors. Tenth Symposium (International) on Combustion, The Combustion Institute, Pittsburgh, 1965.
20. LIVESEY, J. L., and SOUTH, R. D. Boiler Air Register Pressure Drop Performance with Particular Reference to Quarl Angle, Swirler Position and Reynolds Number. Manchester University, Report to Admiralty, 1964.
21. CHIGIER, N. A. Flame Stabilization with Swirling Air Jets. *Israel Journal of Technology*, 1965, **3** (1), 31 to 37.
22. KERR, N. M., and FRASER, D. Swirl. Part I: Effect on Axisymmetrical Turbulent Jets. *J. Inst. Fuel*, 1965 (Dec.), **38**, 519 to 526.
23. KERR, N. M. Swirl. Part II: Effect on Flame Performance and the Modelling of Swirling Flames. *J. Inst. Fuel*, 1965 (Dec.), **38**, 527 to 538.
24. SHAO-LIN LEE. Axisymmetrical Turbulent Swirling Jet. *J. appl. Mech.*, 1965 (June), **32**, 258 to 262.

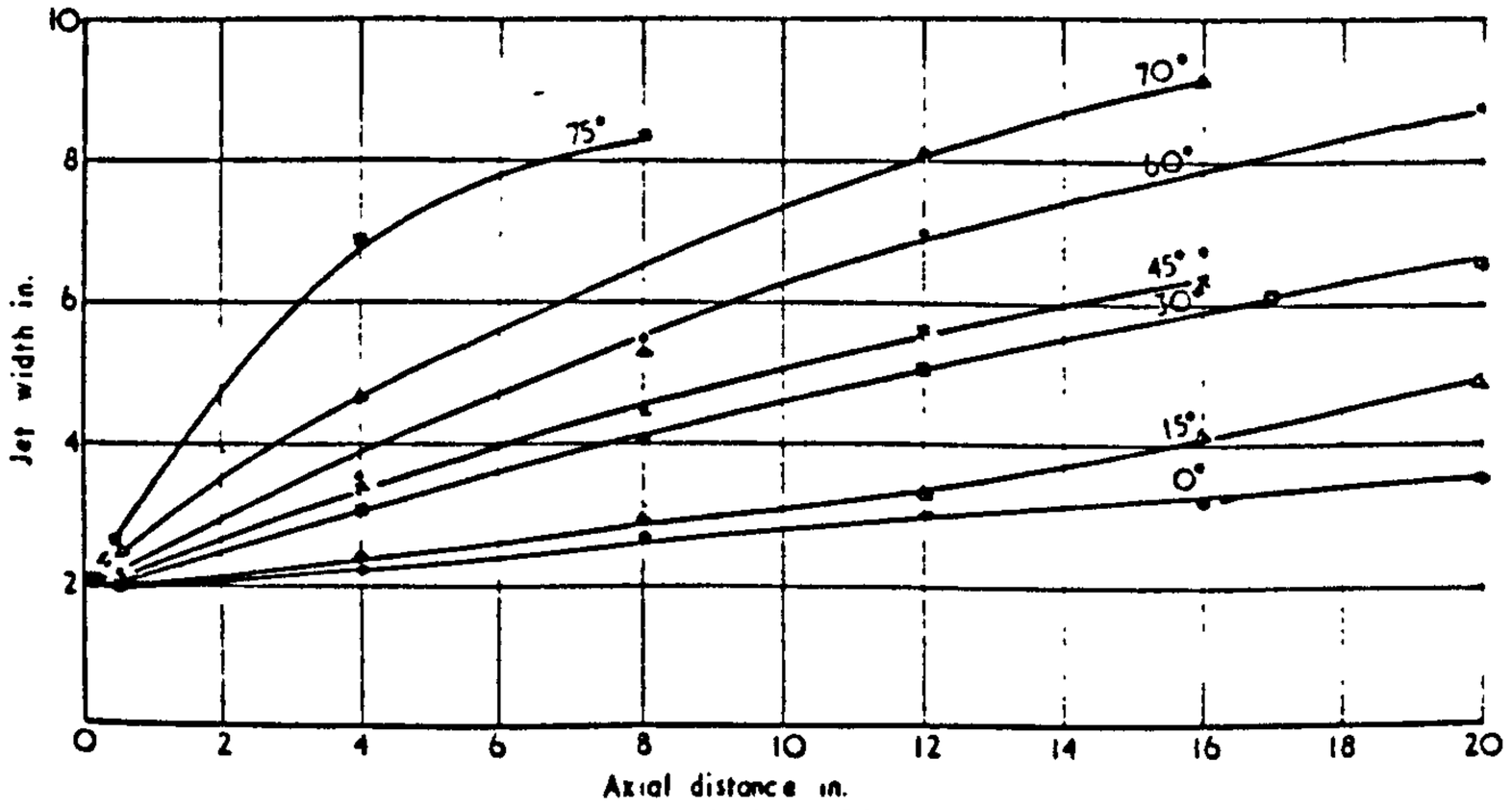

FIG. 17 Annular jets: variation of jet width along the axis.

25. BEÉR, J. M. On the Stability and Combustion Intensity of Pressure-Jet Oil Flames. *Combustion*, 1965 (Aug.) 37, 27 to 34.
26. CHIGIER, N. A., and CHERVINSKY, A. Experimental and Theoretical Study of Turbulent Swirling Jets Issuing from a Round Nozzle. Israel Institute of Technology, TAE Report No. 46, 1965, Nov.
27. DRAKE, P. F., and HUBBARD, E. H. Combustion System Aerodynamics and their Effect on the Burning of Heavy Fuel Oil. *J. Inst. Fuel*, 1966 (March), 39, 98 to 109.
28. PATRICK, M. A. Report of Discussion Group on Swirl. British Flame Research Committee, 1966, Feb.
29. KERR, N. M. An Aerodynamic Study of Swirling Jets and Flames. Ph.D. Thesis, Glasgow University, 1965, May.
30. FRASER, D. Investigation into Swirl in Air Jets. M.Sc. Thesis, Glasgow University, 1964, June.
31. MATHUR, M. L. An Aerodynamic Study of Swirling Jets with Application to Burners. Ph.D. Thesis, Glasgow University, 1966, May.
32. HIETT, G. F., and POWELL, G. E. Three-dimensional Probe for Investigation of Flow Patterns. *Engineer, Lond.*, 1962, 213, 165 to 170.
33. MILLER, D. R., and COMINGS, E. W. Static Pressure Distribution in the Free Turbulent Jet. *J. Fluid Mechanics*, 1957–58, 3, 1 to 16.
34. CHIGIER, N. A., and BEÉR, J. M. The Flow Region near the Nozzle in Double Concentric Jets. International Flame Research Foundation, IJmuiden, 1963, Oct., Doc. No. G02/a/6.

(*Paper received 8th August*, 1966.)

Stephen Austin & Sons Ltd

Reprinted from the JOURNAL OF THE INSTITUTE OF FUEL, June, 1967

M. L. MATHUR, B.E., Ph.D.,* and N. R. L. MACCALLUM, B.Sc., Ph.D.†

Publication 4

Swirling air jets issuing from vane swirlers. Part 2: enclosed jets

Previous work on flow in swirling free jets has been extended by the study of enclosed swirling jets in isothermal air and water models. Profiles of the axial and tangential components of velocity have been obtained in jets issuing from a series of annular swirlers. The maximum and minima of the static pressure at the chamber wall have been related to the jet impingement point and to the positions of the recirculation zones respectively.
Mixing of a swirling primary flow with a surrounding non-swirling secondary flow has been studied. The axial distance required for a given degree of mixing is approximately proportional to $(\tan \theta)^{-0.66}$.
It has been shown that for central recirculation to be established in double concentric jets, swirl must be imparted to both streams. For example, a combination of 45° swirlers in both the inner and outer streams gives satisfactory central recirculation.

1. Nomenclature

d_2 = outer diameter of annular swirler, in.
m_o = nozzle flow, lb/s.
M_{rc} = central recirculation mass flow, lb/s.
M_{rout} = outer recirculation mass flow, lb/s.
U_o = average nozzle velocity, determined from the total nozzle flow and the cross-sectional flow area of corresponding 0° swirler, ft/s.
U_{rc} = central recirculation velocity, ft/s.
l_c = distance to reference concentration on axis, in.
L = half width of the chamber, in.
θ = swirl vane angle, deg.

2. Introduction

Part 1 of this paper[1] described the behaviour of swirling jets issuing from vane swirlers into a free atmosphere. The second part of the programme, reported here, consisted of a study of swirling jets in an air model of a furnace, and in a corresponding water model.

The mixing of a primary swirling air jet, issuing from an annular swirler with helical vanes and diffusing in a cylindrical chamber with a non-swirling secondary air flow, has been studied by Cohen de Lara and Fellous.[2] It was found that the zone of outer recirculation is reduced by the existence of swirl in the primary flow. The same authors have also studied[3] the diffusion of the swirling jet when there is no secondary flow. The central recirculation was found to change irregularly with the degree of swirl over the range tested. However in all cases the position of the maximum reverse flow could be estimated by simple wall pressure measurements. The work of Cohen de Lara and Fellous on helical swirlers issuing into a cylindrical chamber has been extended, as reported in this paper, by studies of jets issuing from constant vane angle swirlers[1] issuing into a model of square cross-section.

3. Objectives

(*a*) To obtain velocity profiles of the jets issuing from vane swirlers in an enclosed air model, and to confirm the general patterns in a water model.

(*b*) To determine the distribution of wall static pressure and to relate this distribution of pressure to the flow pattern.

(*c*) To study the mixing of a primary swirling flow in a surrounding non-swirling secondary flow in the air model, using the nitrous oxide tracer technique.

4. Experimental work—air model

4.1. Apparatus

The air model used in the experiments is shown in Fig. 1. It was a simplified one-fifth-scale model of the furnace of the oil-fired boiler[4] in the Engineering Department, Glasgow University. The model was of square cross-section, the width being 9·6 in. In order to give fully developed jets the length of the model was made 48 in, much greater than the scaled-down furnace length, and a further 72-in long exit pipe was attached to prevent any reversal of flow from the atmosphere into the chamber at high swirl intensities. Two concentric air streams, independently controlled, could enter the air model. The inner stream, equivalent to the primary air in the furnace, entered by a 'hubless' swirler, 0·934 in outer diameter, and the outer stream carrying the secondary air entered by an annular swirler of 3·86 in outer diameter and 1·25 in inner diameter. These dimensions of the primary and secondary swirlers were obtained by scaling from the furnace burner using the Thring-Newby[5] parameter. The swirlers, which had vane angles ranging from 0° to 75°, were the same as those used in Part I[1] of this work.

An arrangement with inner and outer slides was built into one of the side walls of the chamber to enable probes to be inserted and traversed across the jet, a flush and leak-free inner surface still being maintained. Static pressure tappings were provided in one side wall, and in the two end walls.

A three-dimensional probe, of 0·31 in outside diameter, to the design of Hiett and Powell[6] was used for velocity traverses. The probe pressures and wall static pressures were measured by an electronic micromanometer and recorded on a potentiometric recorder to an accuracy of $\pm 0{\cdot}0005$ in H_2O.

4.2. Procedure

Velocity profiles and wall static pressure distributions in the chamber were obtained for jets issuing from annular, i.e. secondary, swirlers having vane angles of 0°, 15°, 30°, 45°, 60°, 70° and 75°, the secondary nozzle velocity being 39 ± 1 ft/s, and there being no primary flow. Similar readings were taken for the jet issuing from the 45° hubless, i.e. primary swirler, there being no secondary flow. For the jets issuing from the remaining primary swirlers (15°, 30°, 60°, 70° and 75°), only the wall static pressures were recorded. For all the primary jets the nozzle velocity was 100 ft/s.

The effect of swirl on the mixing of the primary stream in a non-swirling secondary stream was studied by adding nitrous oxide as a tracer to the primary stream and analysing the samples withdrawn in an Infra-red Gas Analyser. The ratio of the primary nozzle velocity to the secondary nozzle velocity was maintained at 5, typical of the conditions in the original furnace. A primary nozzle velocity of 150 ft/s was used for the 0°, 15°, 30° and 45° primary swirlers, of 100 ft/s for the 60° primary swirler, and of 50 ft/s for the 70° primary swirler, complete traverses being taken in all cases. A few readings, although not sufficient for drawing concentration contours, were also taken with the 75° primary swirler with a primary nozzle velocity of 50 ft/s.

*Department of Mechanical Engineering, University of Jodhpur (India).
†Department of Mechanical Engineering, University of Glasgow.

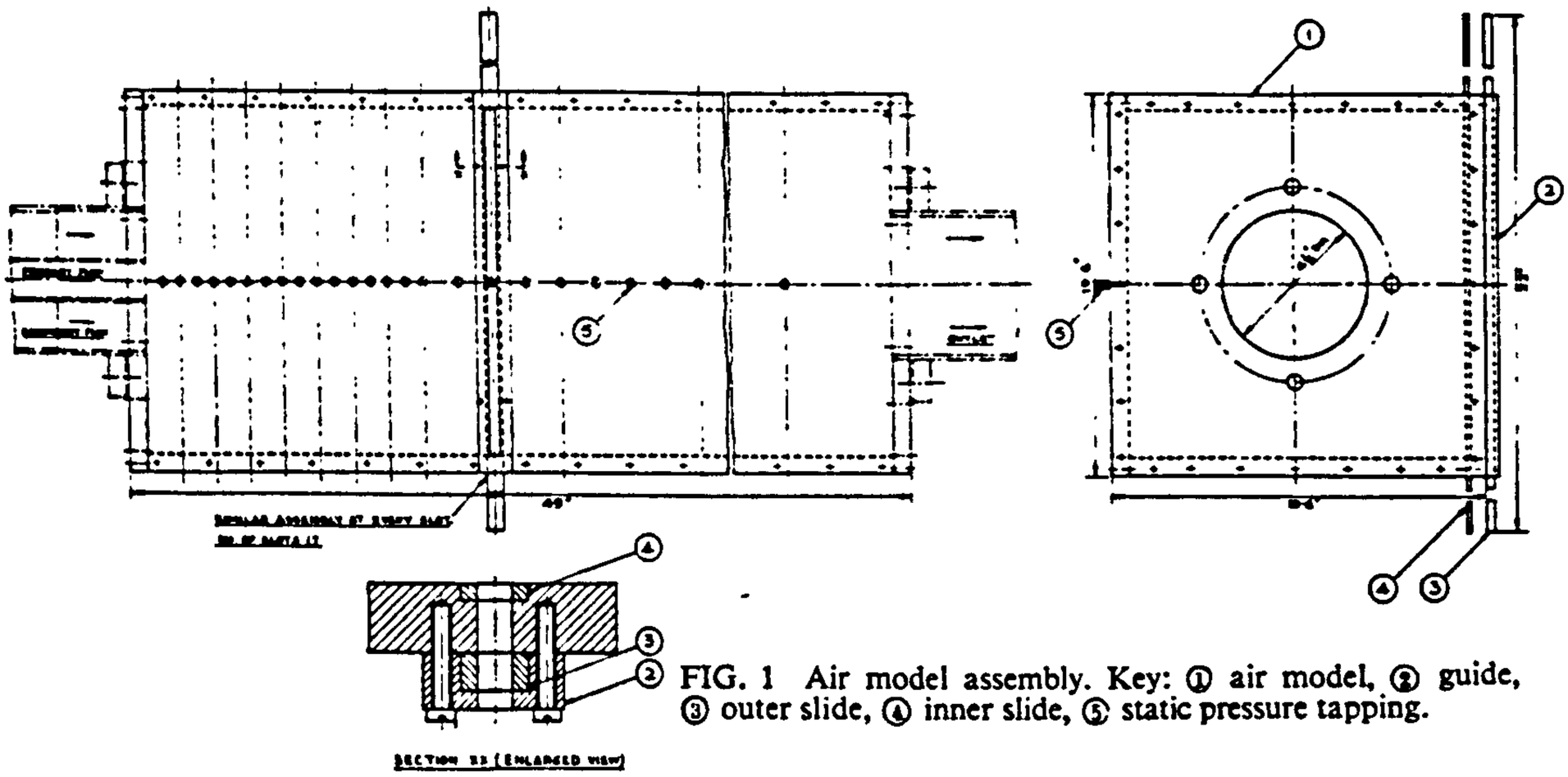

FIG. 1 Air model assembly. Key: ① air model, ② guide, ③ outer slide, ④ inner slide, ⑤ static pressure tapping.

5. Results and discussion—air model

5.1. Secondary swirlers

The profiles of the axial component of velocity in the jets are given in Fig. 2. From these profiles the distances to the point where the jet impinges on the wall, the extents of the recirculation zones, and the recirculation flows have been determined and are given in Table 1.

Within the range of axial distances studied (up to $4d_2$), the axial velocity profiles with the 0° and 15° swirlers are similar to those of free jets,[1] although the jet spread is slightly more rapid. However, it should be noted that all but one of the traverses behind these two swirlers were made in the region before the jet impinges on the walls of the chamber. There is no central recirculation with these two swirlers, except perhaps in a very small zone close to the hub. There are substantial outer recirculation flows—the maximum recirculation mass flows being about 90

TABLE 1 Recirculation velocities and mass flows in enclosed secondary jets

Swirler angle	Axial distance to impingement on wall in	Outer recirculation $\frac{M_{r_{out\ max}}}{M_a}$	Central recirculation Region	$\frac{U_{rc\ max}}{U_o}$	$\frac{M_{rc\ max}}{M_o}$
0°	16 ($4{\cdot}2d_2$)	0·9	Nil	Nil	Nil
15°	9·8 ($2{\cdot}5d_2$)	0·75	Nil	Nil	Nil
30°	4 ($1{\cdot}04d_2$)	Difficult to measure	0·3 in to 13·5 in	0·29 at 6 in	0·36
45°	3·6 ($0{\cdot}93d_2$)	do	Swirler exit to 13·5 in	0·43 at 6·5 in	0·67
60°	3·2 ($0{\cdot}83d_2$)	do	Swirler exit to 13 in	0·50 at 6 in	0·95
70°	<1 (<$0{\cdot}26d_2$)	do	Swirler exit to 8 in on axis: beyond 8 in a forward velocity cone surrounded by a reverse velocity region	0·41 at 3·4 in	1·05
75°	do	do		0·42 at 4·4 in	1·17

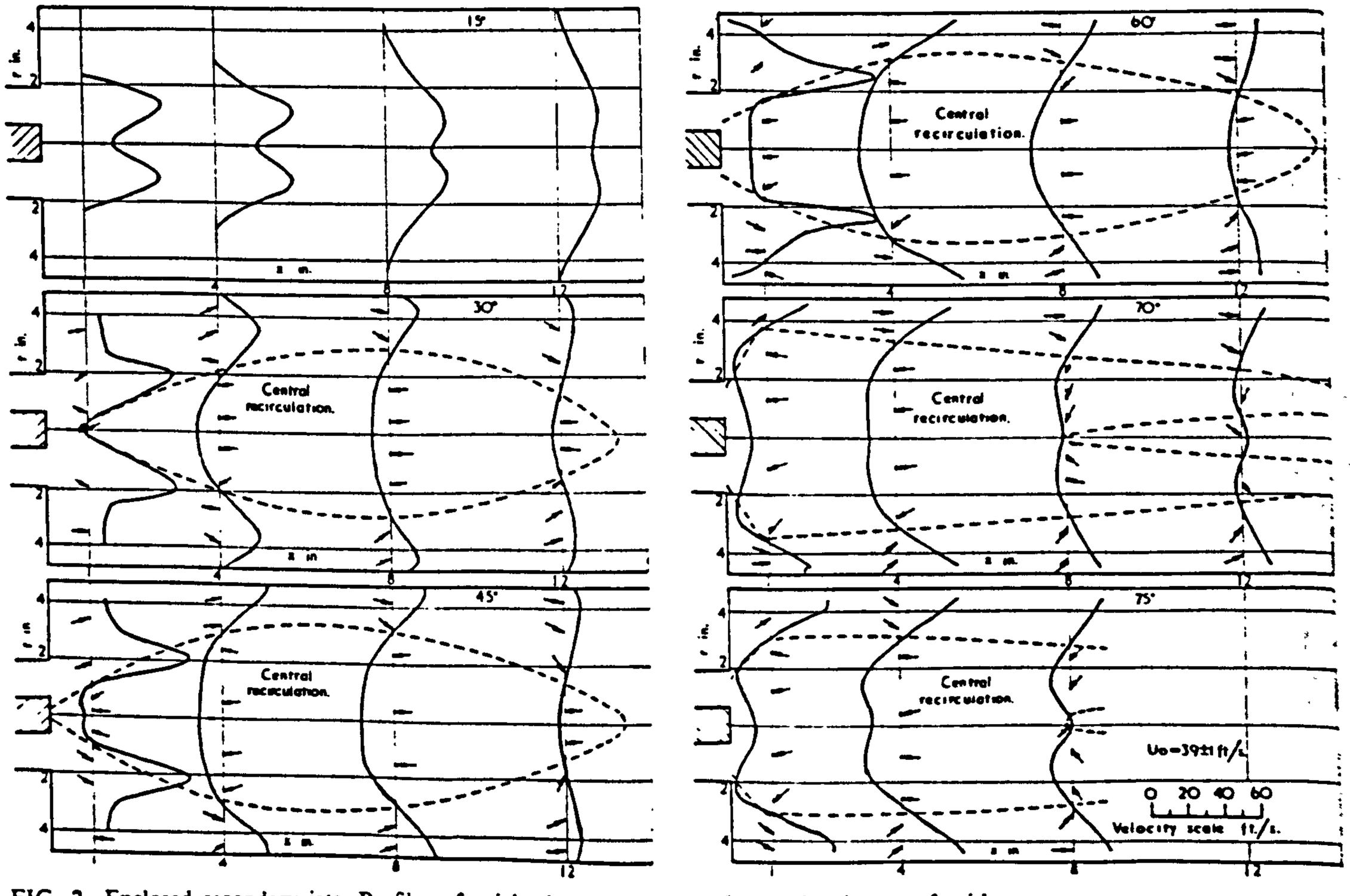

FIG. 2 Enclosed secondary jets. Profiles of axial-velocity component for varying degrees of swirl.

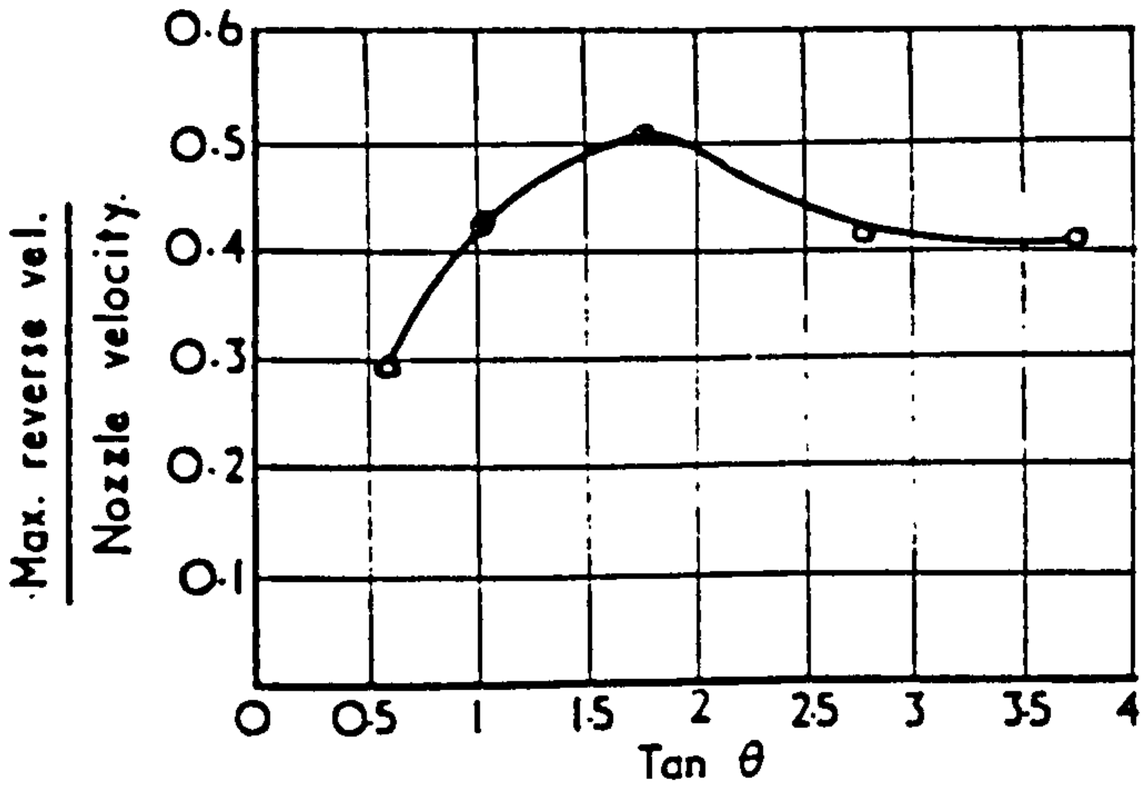

FIG. 3 Maximum reverse velocity on axis in enclosed secondary jets.

and 75% respectively of the nozzle flow for the 0° and 15° swirlers.

When the swirler vane angle increases to 30° and above the initial jet spread is much more rapid than in the corresponding free jets, and the point of impingement on the wall moves progressively much closer to the swirler exit (see Table 1). Correspondingly the length of the outer recirculation vortex reduces. With the 70° and 75° swirlers the jet, as it issues, almost touches the upstream end wall of the chamber. Beyond the point of impingement the velocity profiles in the enclosed model, with their high velocities close to the walls, differ markedly from the corresponding free jet profiles.[1] Central recirculation has become established in the enclosed jet issuing from the 30° swirler and is strengthened with further increase in swirl angle. These central recirculations are much more pronounced than those observed in the corresponding free jets.[1] The more rapid initial spread of the jet in the enclosed model, compared with that of the free jet, is presumably associated with this increase in the central recirculation. At the plane of maximum central recirculation the recirculation 'vortex' occupies between 30 and 50% of the cross-sectional area of the chamber. For the swirlers of vane angles of 60° and greater this central recirculation vortex not only extends upstream to the hub of the swirler, but also slightly 'blocks' the annular flow area at exit from the swirler. The maximum reverse velocity, given in Fig. 3, varies to only a small extent with the degree of swirl. The maximum reverse mass flow, shown in Fig. 4, increases with the degree of swirl, although the increase becomes asymptotic at high degrees of swirl. These maximum reverse flows are different from those observed by Cohen de Lara and Fellous[3] and Brown and Thring.[7] The discrepancy is attributed to the different methods of swirl generation and to the different values of the ratio d_2/L.

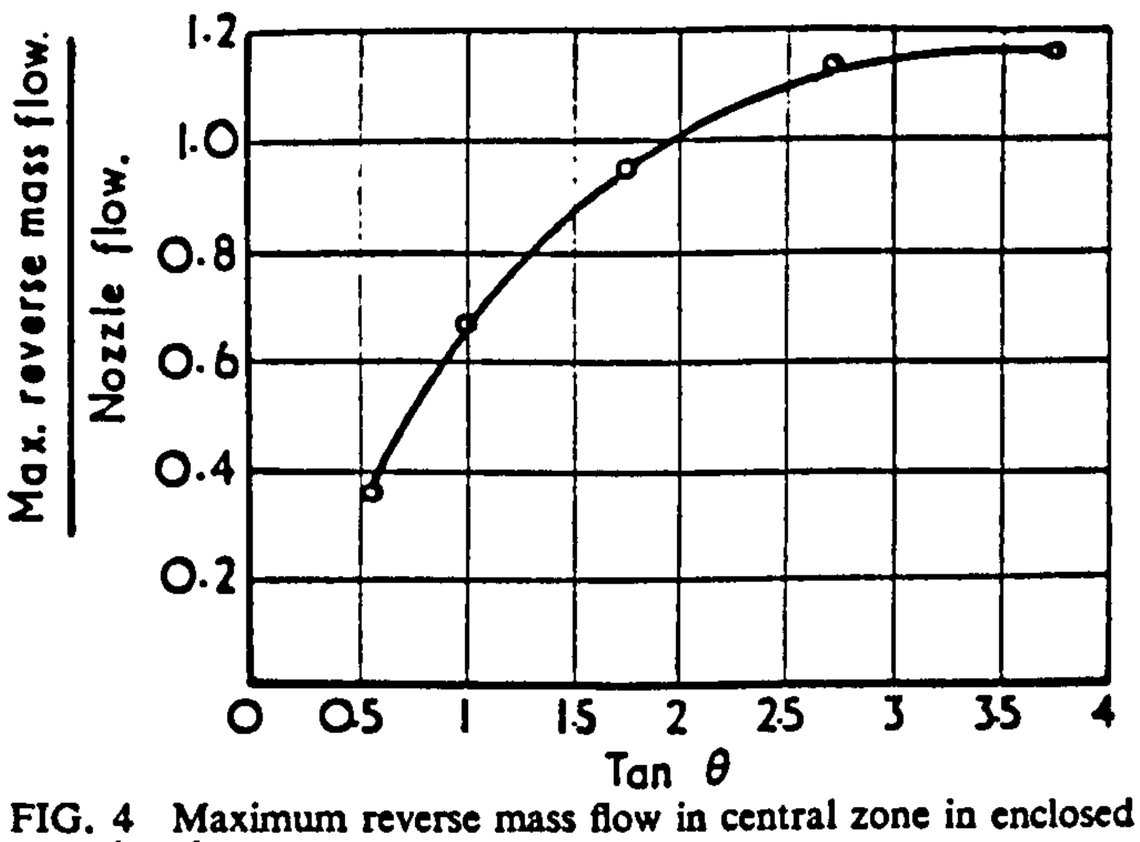

FIG. 4 Maximum reverse mass flow in central zone in enclosed secondary jets.

Profiles of the tangential component of velocity are given in Fig. 5. For the traverses made in the jets which had not yet impinged on the walls, the tangential velocity

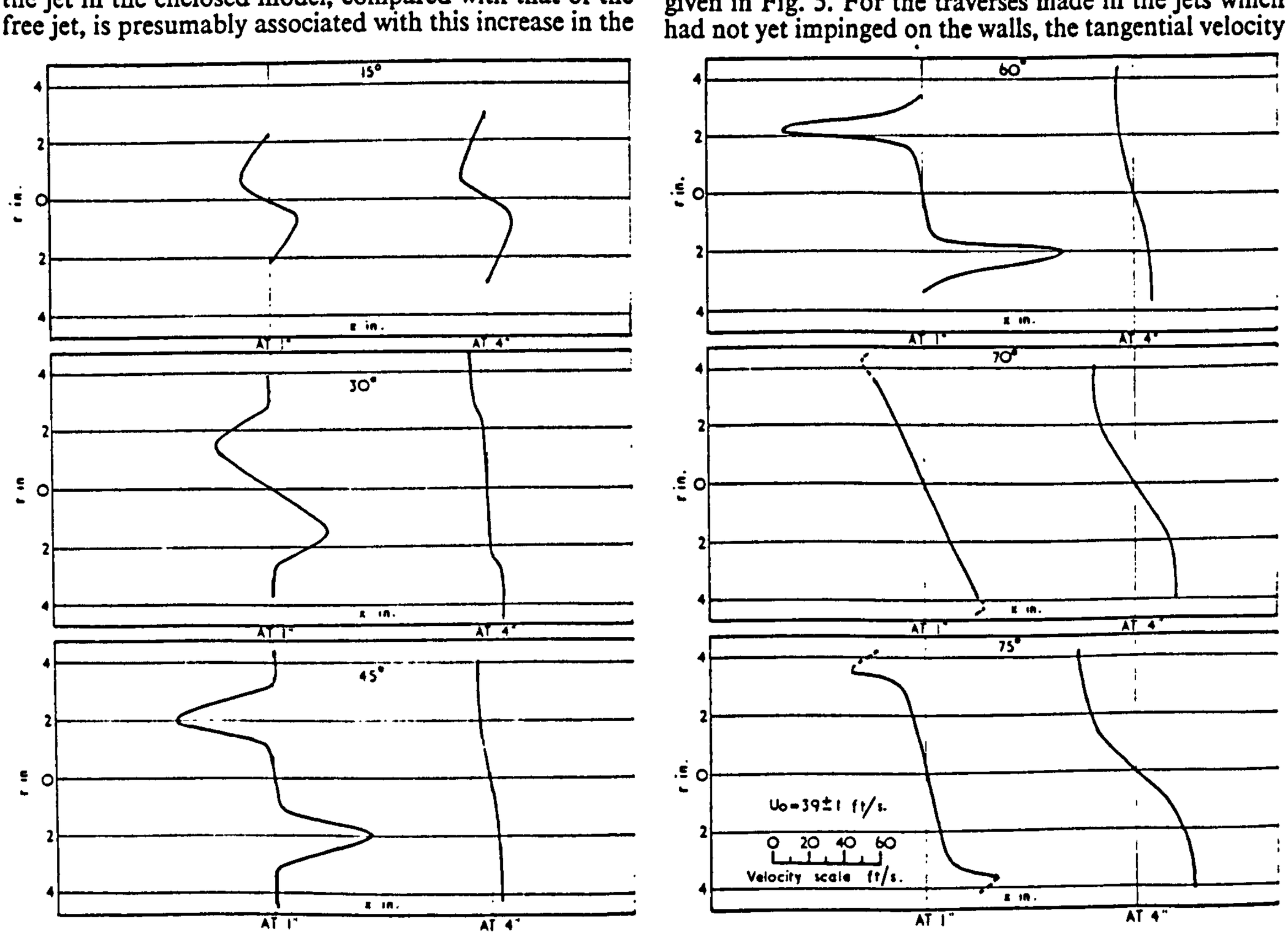

FIG. 5 Enclosed secondary jets. Profiles of tangential-velocity component for varying degrees of swirl.

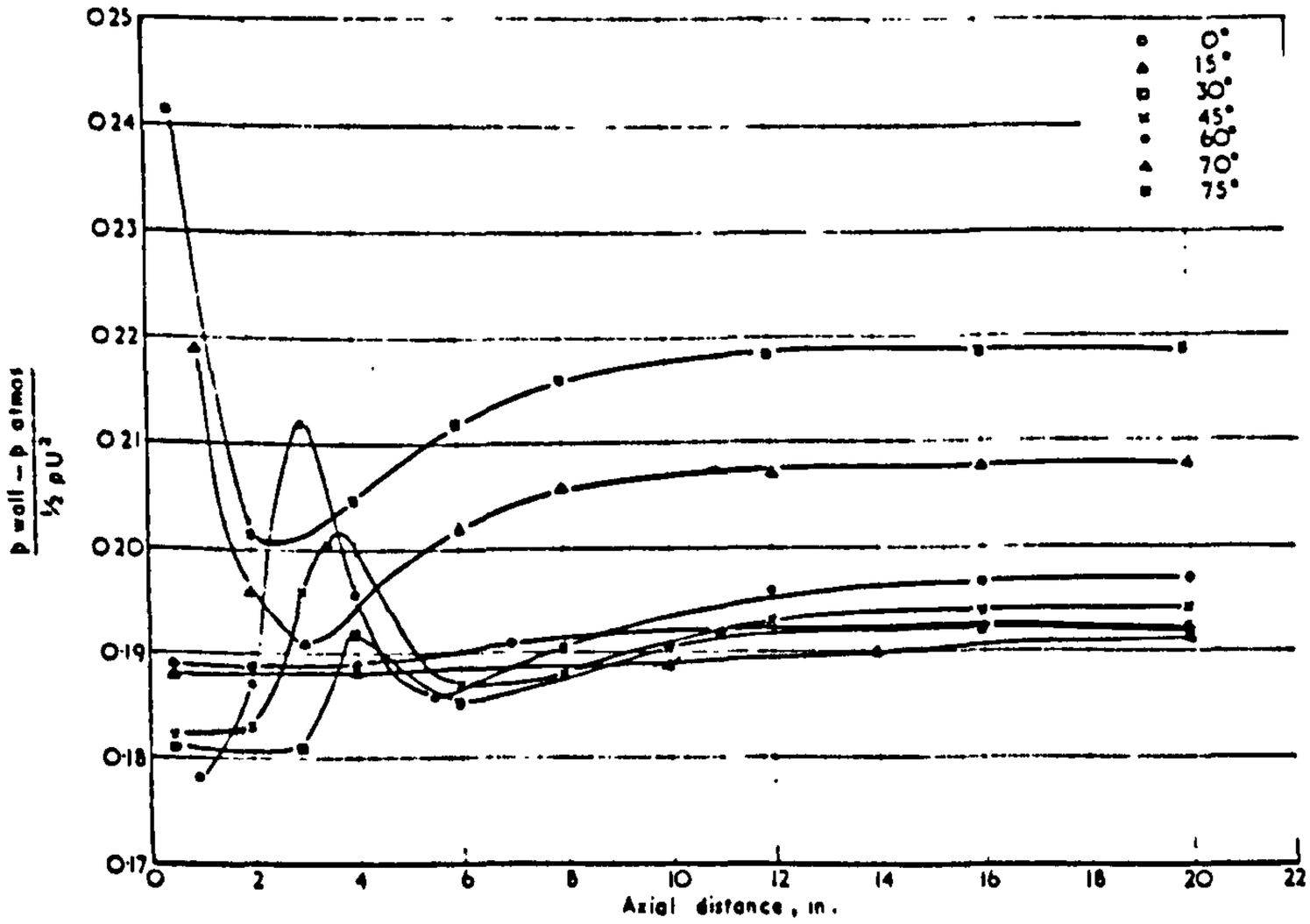

FIG. 6 Wall pressures in enclosed secondary jets.

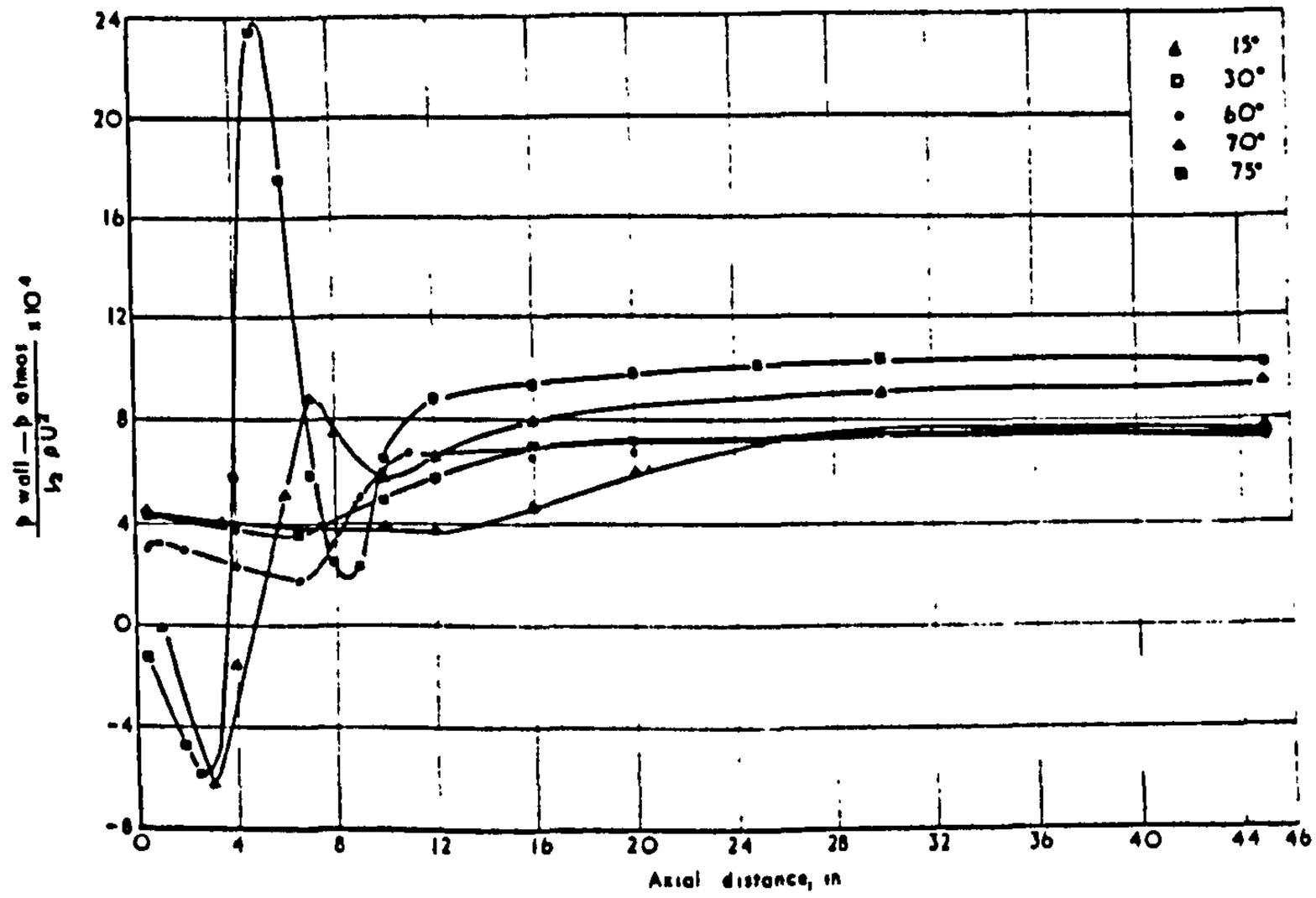

FIG. 7 Wall pressures in enclosed primary jets.

profiles are similar to those obtained in the free jets,[1] i.e. a fixed vortex core surrounded by a free vortex. However, because the rates of spread in this region before impingement in the enclosed jets are more rapid than in the free jet. the reduction in the maximum tangential velocity component on moving downstream is more rapid. After the jets have impinged on the walls the maximum tangential velocities occur close to the wall and the complete flow approximates to a fixed vortex.

As mentioned in Section 4.1. the Thring-Newby parameter was used in scaling the swirler dimensions in the model from the swirler in the furnace. This resulted in the ratio d_2/L in the model being 0·4. while the ratio in the furnace is 0·22. It can be seen from the results described above that. with this very large value of the ratio d_2/L in the model. the proximity of the walls has a significant effect on the flow patterns. The wall effect in the furnace will be less pronounced. due to the lower value of the d_2/L ratio. and thus one would not expect the flow patterns in the furnace to correspond with those observed in the model. This suggests that. in cases where the furnace d_2/L ratio is large. it is not desirable to use the Thring-Newby parameter for scaling. For these cases an alternative method of scaling has been proposed by Robertson.[8]

The wall static pressure distributions are given in Fig. 6. Distinct maxima can be seen in the cases of the 30°, 45° and 60° swirlers. The positions of these maxima are in reasonable agreement with the points of impingement of the jets on the wall predicted from the velocity traverses (see Table 1). This confirms the conclusion of Cohen de Lara and Fellous.[3] For the 0° and 15° swirlers the maximum is too weak to be observed. and for the 70° and 75° swirlers the velocity traverses indicate that the jets strike the wall close to the first pressure tapping.

Downstream from the impingement point a minimum static pressure is observed with the swirlers of vane angles of 30° and more. The position of this minimum agrees fairly closely with the plane of maximum central reverse velocity.

5.2. Primary swirlers

The wall static pressure results are given in Fig. 7. As with the secondary swirling jets, maxima can be seen in the pressure distribution. On the basis of the secondary swirler results. these maxima correspond to the points of

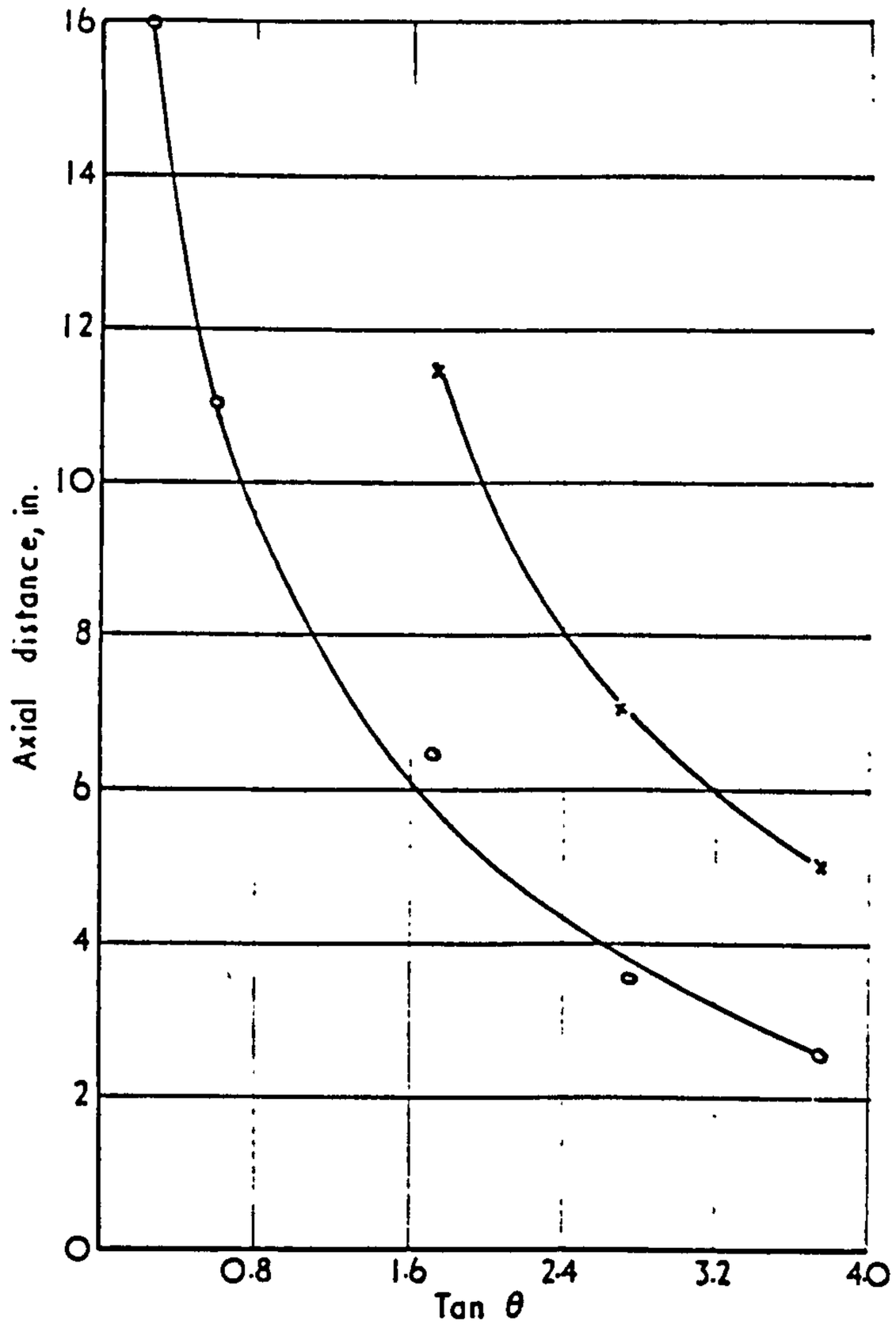

FIG. 8 Enclosed primary jets.
o Centre of outer recirculation.
× Axial distance where jets strike the wall.

impingement of the jets on the wall. Similarly the minima further downstream indicate the positions of the maximum central reverse velocities. Pressure minima can also be seen upstream of the impingement point. As these minima occur roughly midway between the swirler exit and the impingement point, it is deduced that the minima correspond to the centres of the outer recirculation vortices. The positions of the impingement points and outer recirculation centres are given in Fig. 8.

5.3. Mixing of a swirling primary flow in a non-swirling secondary flow

Concentration contours in the double concentric jets for the varying degrees of primary swirl (0° to 70°) are shown in Fig. 9. The reference concentration used is the concentration when the two streams have become fully mixed. The decay of the concentration along the axis is given in Fig. 10. In the absence of swirl there is a 'potential core' along the axis. This core is progressively reduced when swirl is introduced. With the 70° primary swirler the position of the highest concentration is shifted away from the axis.

A logarithmic plot of the axial distance to the point on the axis of reference concentration is given in Fig. 11, to a base of tan θ. These points were obtained by extrapolation from Fig. 10, the result from the 75° swirler being included. The best straight line through the points corresponding to the 15°, 30° and 45° swirlers (all with 150 ft/s nozzle velocity) passes through the remaining points (60°, 70° and 75° swirlers, nozzle velocity 100 or 50 ft/s). From this it is concluded that for swirling jets, as for non-swirling jets, the mixing pattern is independent of nozzle velocity, provided that the velocity ratios are maintained. The linear relationship shown in Fig. 11 has the form

$$l_c = \frac{\text{constant}}{(\tan\theta)^{0.66}}$$

where l_c is the distance along the axis to the point of reference concentration.

In practice the reference concentration is approached asymptotically and it is easier to locate points where the concentration exceeds the reference value by, say, 10%. This practice would be similar to that adopted in defining the boundary of a jet. The points corresponding to a concentration 10% greater than the reference value are also shown in Fig. 11, and they may be joined by a line of similar slope to the line through the reference concentration points.

It can be seen that increasing the degree of swirl greatly reduces the distance to these reference concentration points. These distances in the model to the reference

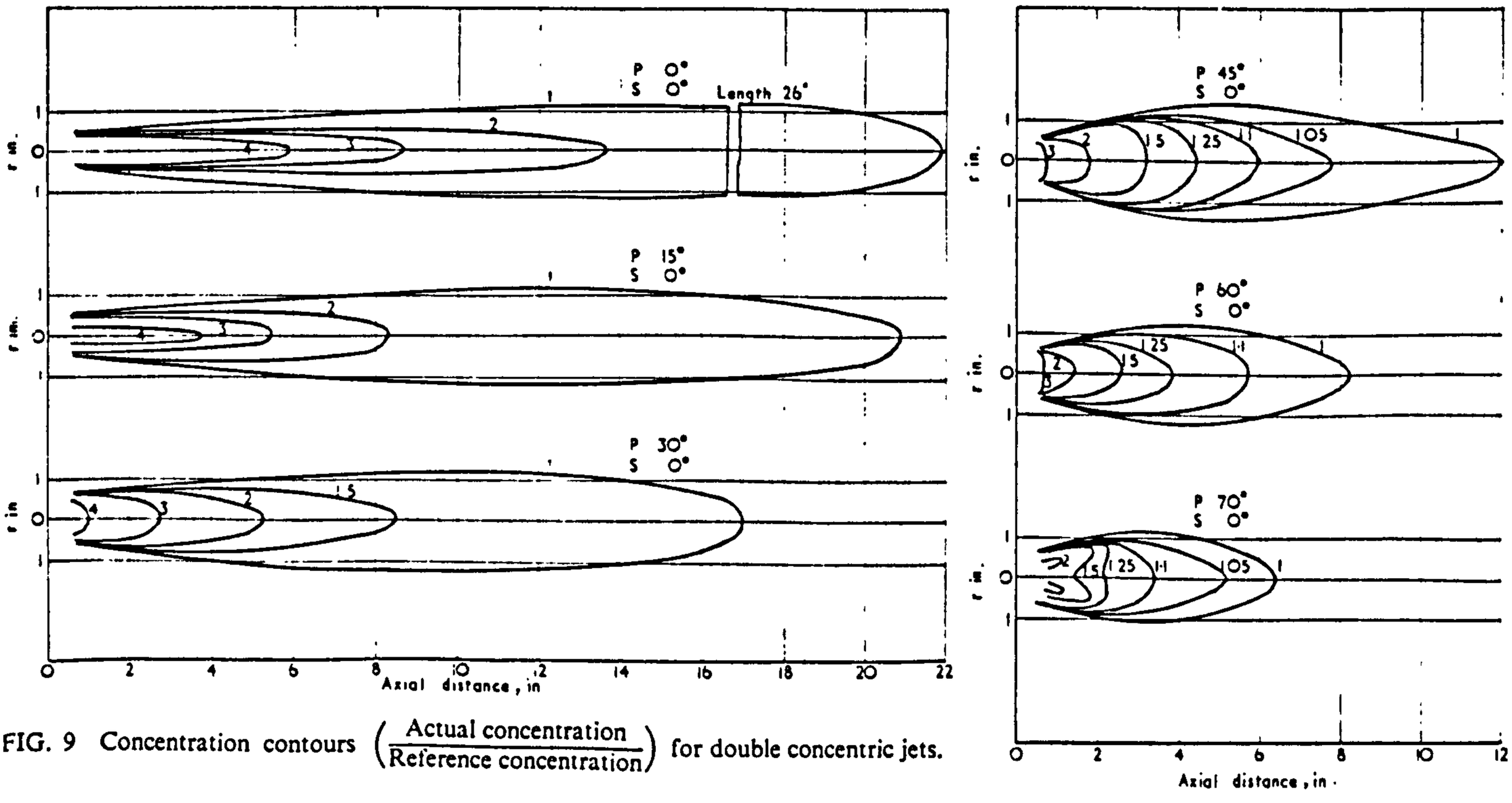

FIG. 9 Concentration contours $\left(\frac{\text{Actual concentration}}{\text{Reference concentration}}\right)$ for double concentric jets.

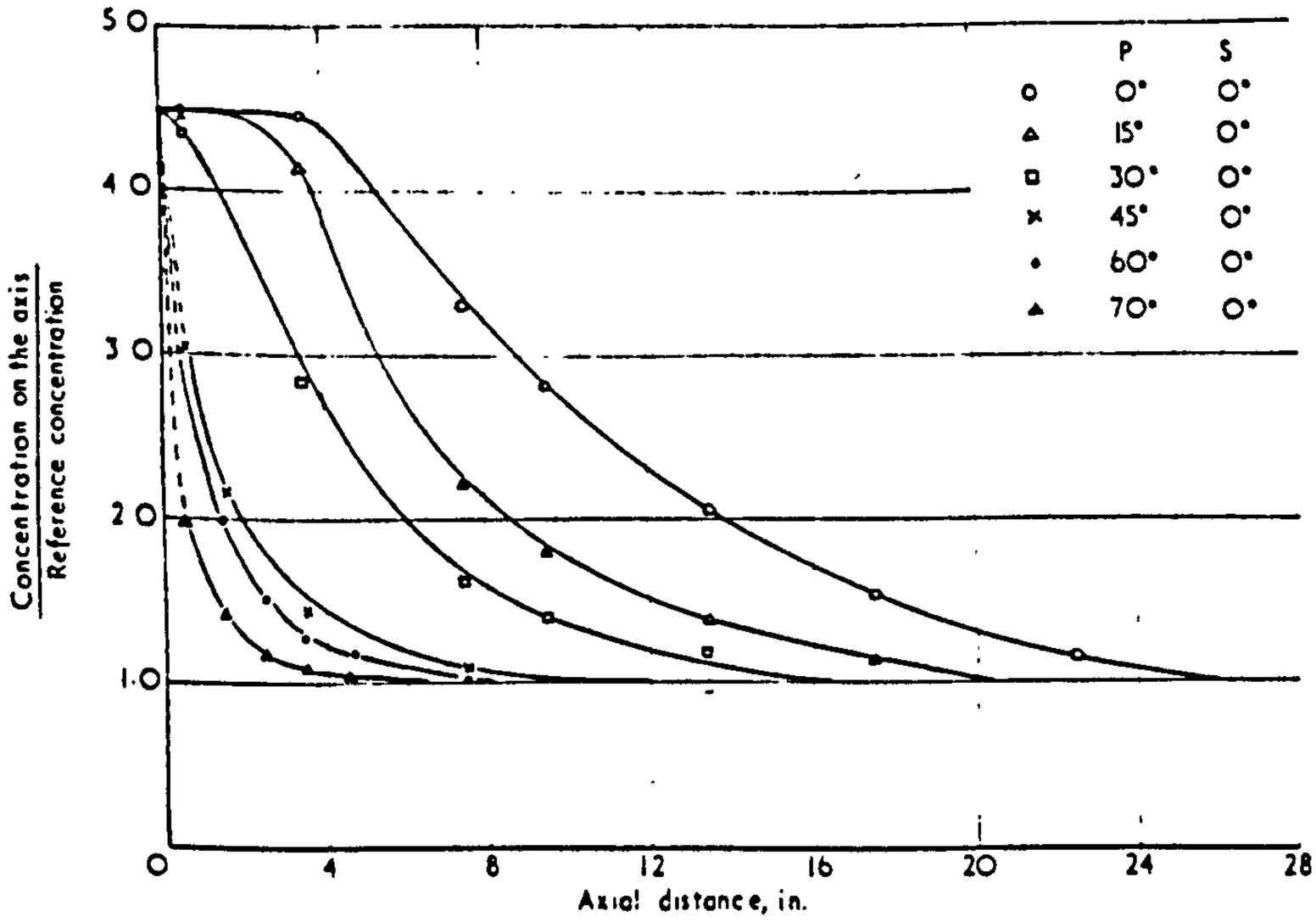

FIG. 10 Decay of concentration along jet axis.

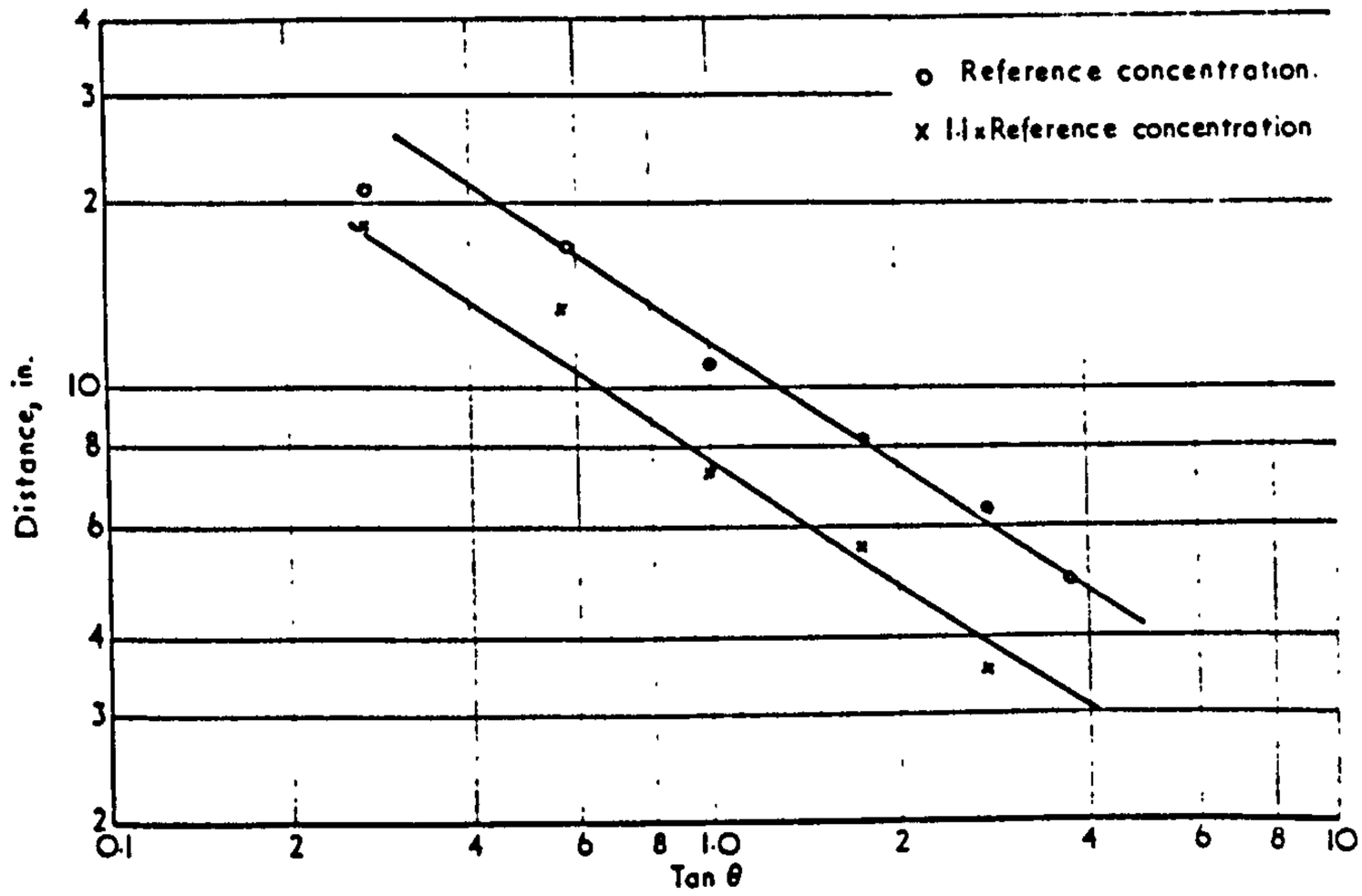

FIG. 11 Distance to reference concentration on axis with varying degrees of swirl.

concentration points are related to the corresponding flame lengths in the furnace. Thus swirl can be used to control the length of a flame in a furnace. However, it should be noted that while a very high degree of swirl will produce a short flame, there may also be incomplete combustion, some fuel escaping from the flame due to the very rapid expansion of the primary jet.

6. Experimental work—water model

6.1. Apparatus

The perspex water model was of 4·2 in square cross-section and 21 in long. These dimensions are 0·44 of the corresponding air model dimensions. It was not possible to manufacture accurate primary swirlers similarly scaled from the air model and so the air model primary swirlers themselves were used in the water model. The secondary swirlers in the water model were made to have a flow area which was nearly $(0{\cdot}44)^2$ of the flow area of the air model secondary swirlers. The value of the ratio d_2/L in the water model almost equalled that in the air model.

6.2. Procedure

Polystyrene particles, on average 0·02 in diameter, were introduced into the water tank upstream of the swirlers. A longitudinal plane through the axis of the swirlers was illuminated by a 2-kW lamp condensed and focused by perspex strip lenses. Photographs of 1/30- or 1/60-second exposure were taken by Ilford HPS (800ASA) film, using a single-lens reflex camera.

When combined flows from the primary and secondary swirlers were being studied, the timing of the exposure could be selected so that the tracers predominated in either the primary or secondary streams.

7. Results and discussion—water model

7.1. Secondary swirlers

Flow patterns were studied in the jets issuing from secondary swirlers in the absence of primary flow. The patterns are similar to those found in the air model. With the 15° swirler there is outer recirculation, but no central recirculation. When the swirler angle is 30° a certain amount of central recirculation can be observed. With the 45° swirler (illustrated in Fig. 12) the central recirculation is firmly established and the outer vortices are considerably reduced. For swirlers of 60° and greater angles the water enters the chamber almost adhering to the end wall. With these swirlers the central recirculation was further increased. In addition a reverse flow was observed along the axis from the chamber exit towards, but not

(a)

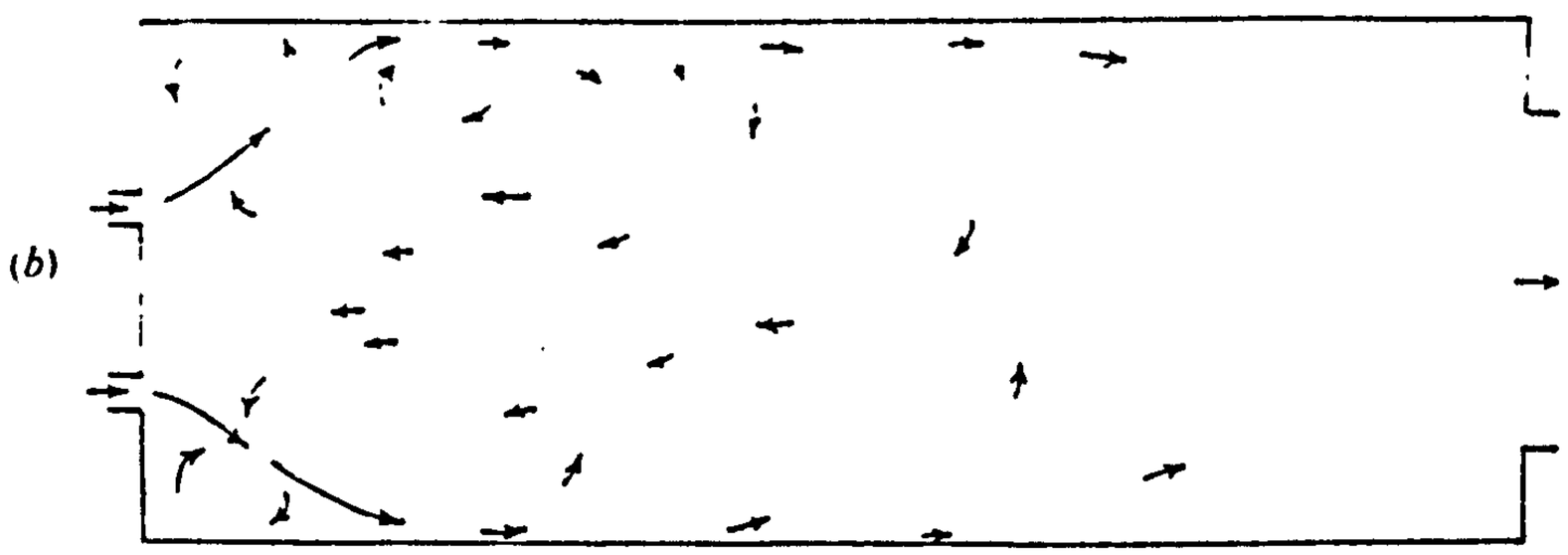

(b)

FIG. 12 Flow pattern in jet issuing from 45° secondary swirler. No primary flow. (*a*) Particle traces, (*b*) Diagram indicating outer and central recirculations.

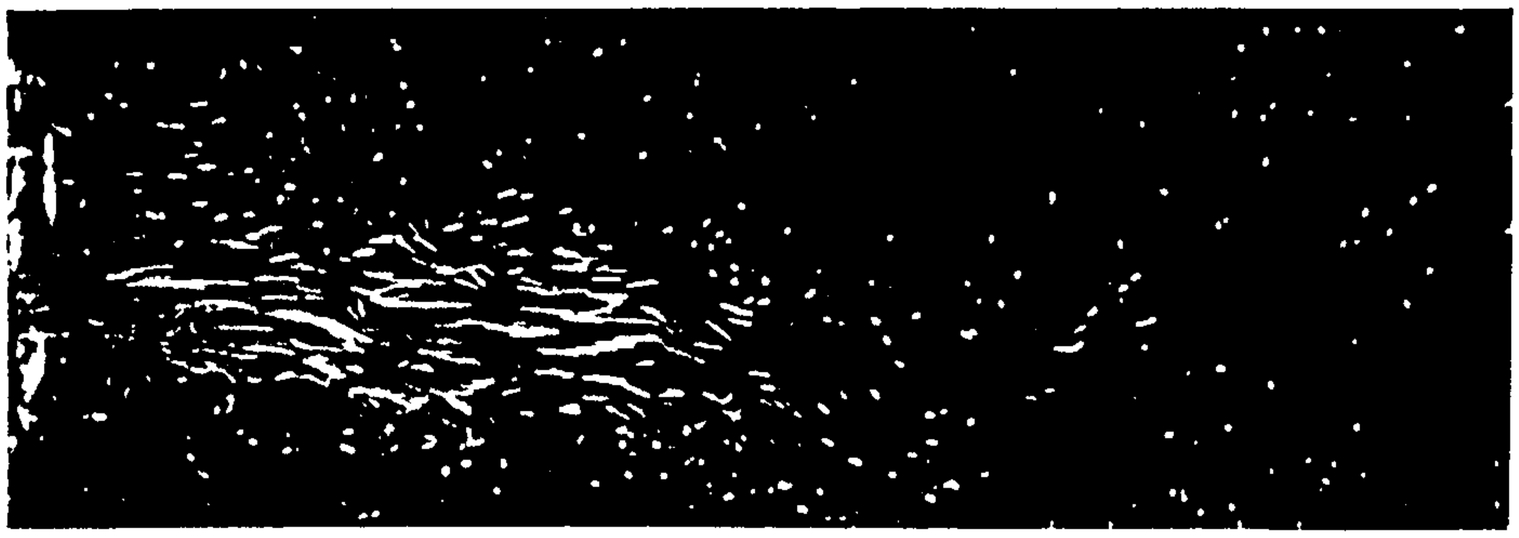

(a)

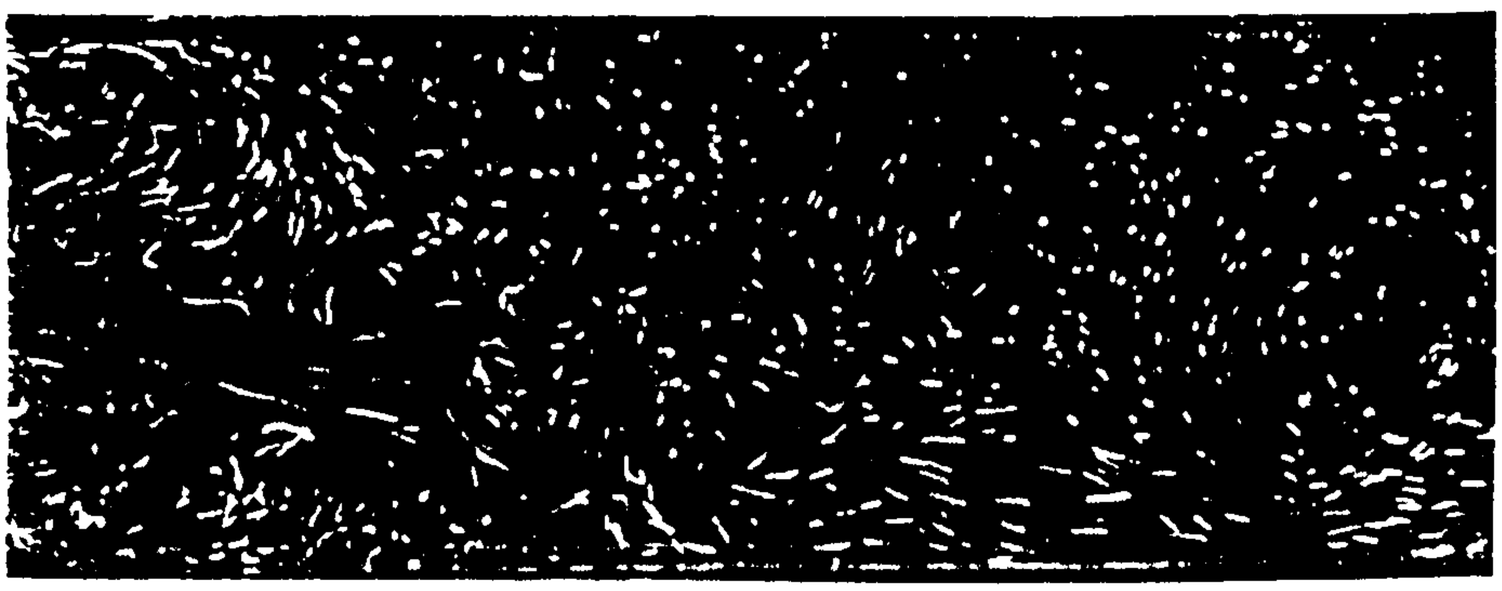

(b)

FIG. 13 Flow pattern in combined jet. 0° primary, 45° secondary swirlers. (*a*) Tracers predominant in primary. (*b*) Tracers predominant in secondary.

quite meeting, the main central recirculation. It is not known if a similar reverse flow occurred in the air model as no traverses were made beyond about 4 d_2 downstream from the swirler.

7.2. Combined jets

Several secondary swirlers were used in conjunction with each primary swirler from 0° to 45° to determine the combination which would give central recirculation. Both the primary and secondary swirlers imparted swirl in the same direction. The nozzle velocity in the primary flow was about five times the secondary nozzle velocity in all cases.

When the primary flow had no swirl, no central recirculation was obtained, even with the highest degrees of secondary swirl—see Fig. 13. When primary swirl was introduced central recirculation became possible—significant central recirculation being obtained with the combination, for example, of 45° primary and 45° secondary swirlers. Alternatively a higher degree of secondary swirl and lower degree of primary swirl (see Fig. 14), or vice versa, gives appreciable central recirculation. This finding confirms the deduction of the previous work[1] that in order to obtain central recirculation in combined jets swirl should be given to both the primary and secondary streams.

8. Conclusions

(1) The initial rates of spread of the jets in the enclosed model are more rapid than those observed in corre-

FIG. 14 Flow pattern in combined jet. 30° primary, 60° secondary swirlers. Tracers predominant in primary.

sponding free jets. The central recirculations. which are established with vane angles of 30° and above. are stronger in the enclosed model than in free jets. Flow patterns were similar in the air and water models.

(2) The velocity profiles before the jet impinges on the wall are similar to those obtained in free jets. but downstream from the impingement point the profiles are completely different.

(3) The maximum in the wall static pressure coincides with the impingement point, and the minima upstream and downstream of this point correspond to the regions of maximum reverse velocity in the outer and central recirculation zones respectively.

(4) The intermixing of double concentric jets is made more rapid by the introduction of swirl. The distance required for a given degree of mixing is related to the degree of swirl. Thus, in a furnace, swirl can play an important part in controlling the length of the flame.

(5) In order to obtain significant central recirculation in double concentric jets it is necessary to give swirl to both streams. For example, a combination of 45° vane angle swirlers in both the inner and outer streams gives satisfactory central recirculation.

9. Acknowledgments

The authors thank Emeritus Professor James Small. formerly James Watt Professor of Mechanical Engineering. University of Glasgow. and members of his staff for their encouragement and advice.

10. References

1. MATHUR, M. L., and MACCALLUM, N. R. L. Swirling Air Jets Issuing From Vane Swirlers. Part 1: Free Jets. *J. Inst. Fuel*, 1967 (May), 39, 214.

2. COHEN DE LARA, G., and FELLOUS, J. R. Experimental Study in an Isothermal System of Mechanism of Mixing of a Primary Swirling Jet Diffusing in a Cylindrical Chamber with a Uniform Axial Flow of Secondary Air. International Flame Research Foundation IJmuiden, 1963, September, Doc. No. Tb-F 61/bc/5.

3. COHEN DE LARA, G., and FELLOUS, J. R. Experimental Study in an Isothermal Enclosure of the Recirculation near the Axis of a Swirling Jet Diffusing in a Cylindrical Chamber. International Flame Research Foundation, IJmuiden, 1964, May, Doc. No. Tb-F 61/bc/7.

4. KERR, N. M. Swirl. Part II: Effect on Flame Performance and the Modelling of Swirling Flames. *J. Inst. Fuel*, 1965 (Dec.), 38, 527 to 538.

5. THRING, M. W., and NEWBY, M. P. Combustion length of Enclosed Turbulent Jet Flames. Fourth Symposium (International) on Combustion. Williams and Wilkins, Baltimore, 1953, 789 to 796.

6. HIETT, G. F., and POWELL, G. E. Three-dimensional Probe for Investigation of Flow Patterns. *The Engineer*, 1962, 213, 165 to 170.

7. BROWN, A. M., and THRING, M. W. The Application of Pressure Jet Burners to Marine Boilers. Tenth Symposium (International) on Combustion, The Combustion Institute, Pittsburgh, 1965.

8. ROBERTSON, A. D. Modification of the Thring-Newby Criterion for Problems where Flow Pattern and Mixing are Equally Important. *J. Inst. Fuel*, 1965 (Nov.), 38, 481 and 482.

(*Paper received* 13*th August*, 1966.)

Stephen Austin & SONS LTD
Oriental and General Printers

FLAME STABILIZATION ON RECTANGULAR BURNERS

RAÚL A. BONILLA H.* AND N. R. L. MACCALLUM†

Disagreement exists between the relationships previously published for correlating the stability limits of rectangular burners in which the flow is fully developed. It is now found that flashback limits in laminar flow can be correlated satisfactorily by the boundary velocity gradient close to the corners of the burner port. The blow-off limits in both laminar and turbulent flow are best correlated by the average velocity gradient around the perimeter of the port. Blow-off limits in laminar flow can also be reasonably correlated by the boundary velocity gradient close to the corners. The velocity gradients are all calculated assuming that the flow is undistorted by the presence of the flame. The correlations are applied to a considerable body of new experimental data and also to the results of the earlier workers.

Introduction

THE correlation of the stability limits of circular burners by means of the wall velocity gradient, as proposed by Lewis and von Elbe[1], has been generally accepted, and its validity has been confirmed for many fuels and oxidants over a wide range of burner diameters. Recently Reed[2, 3] has suggested that a flame blows off due to flame stretch. He proposes the equation

$$g = (0{\cdot}23\,\rho c_p S_u^2/k)\,[1 - (1 - X)^{6{\cdot}4}\,\alpha] \quad [1]$$

which is found to correlate the results of numerous fuels over ranges of pressure, temperature and mixture composition. He shows from equation 1 above that the wall velocity gradient theory is a special case of the flame stretch theory of blow-off. and therefore experimental results quoted in confirmation of the flame stretch theory will also be correlated by the wall velocity gradient. As the object of the work reported here is to compare the stability limits of rectangular burners with those of circular burners, the comparison will be based simply on the critical wall velocity gradient for a particular concentration of a particular fuel.

Burners used in industry are not necessarily circular and consequently attempts have been made to find a wall velocity gradient correlation for burners of non-circular cross section in which the flow is laminar and fully developed. Two of these attempts[4, 6] have yielded different correlations for laminar flow limits in rectangular burners, neither of which fits the other's results. Grumer, Harris and Schultz[4], from stability limits for methane–air mixtures, produced the following equations using the friction coefficient, λ, for relating the stability limits of the rectangular burners with the critical gradients obtained from circular burners

$$g_G = \frac{\lambda V (Re)'}{2\pi d^3} \quad [2]$$

For rectangular channels

$$\lambda = 61{\cdot}4\,(Re)'^{\,1{\cdot}09} \quad [3]$$

For square channels

$$\lambda = 125{\cdot}8\,(Re)'^{\,1{\cdot}24} \quad [4]$$

where g_G is the critical wall velocity gradient for comparison with circular burner data. d is the equivalent diameter = 4 × area/perimeter and $(Re)'$ is the Reynolds number defined by Grumer for his purposes as $4\rho V/\pi\mu d$. The friction coefficient, λ, used by Grumer and as used in this paper is given by

$$\frac{dp}{dZ} = -\lambda\frac{\rho\bar{U}^2}{2d} \quad [5]$$

where $\bar{U}$ is the average velocity and the Z axis lies along the axis of the channel. [The constants used in equations 3 and 4 are those given in a later publication[5].]

Grumer and his colleagues concluded that.

* Escuela Politécnica. Quito. Ecuador.
† Department of Mechanical Engineering. University of Glasgow.

due to flow redistribution when a flame is present. wall velocity gradients calculated for Poiseuille flow in the absence of a flame could not be used for correlation of stability limits.

Later Maccallum°. from measurements with butane–air flames. found that his blow-off results could be correlated by the local wall velocity gradient at the centre of the long side of the port. calculated from undisturbed Poiseuille flow. The wall gradient at the centre of the long side g_c. is given by

$$g_c = P\bar{U}/a \qquad [6]$$

The function P is tabulated by Maccallum[6] from summations published by Smith Jr, Edwards and Brinkley Jr[7]. Maccallum also made some flashback observations, but the gradients at the centre of the long side corresponding to these limits were considerably higher than the critical gradients from circular burner data. Maccallum suggested that this might be due to heating of the walls of the burners which were not water-cooled.

The aim of the work reported here is to present further experimental results using both butane–air and methane–air mixtures and to offer general correlations for flame stability in rectangular burners in which the flow is fully developed. These correlations are applied both to the present results and to the previous results[4, 6].

Experimental

Apparatus

Stability limits of methane–air flames were obtained for burners having the following cross-sectional dimensions: 0·64 cm × 0·58 cm, 1·27 cm × 0·64 cm. 2·55 cm × 0·61 cm, 5·08 cm × 0·65 cm and 1·27 cm × 1·26 cm. The stability limits of butane–air flames were observed with the same burners and also with a burner having a cross section of 2·55 cm × 1·29 cm.

The approach lengths of the burners were, due to manufacturing difficulties, in some cases only about half the transition length, at a Reynolds number of 2000. for a cylindrical channel of similar equivalent hydraulic diameter. The transition length. L. is that required to change an initially flat velocity profile into one in which the velocity at the centre of the channel is within one per cent of the central velocity in Poiseuille flow. and is given by[8]

$$L = 0{\cdot}065\, d(Re) \qquad [7]$$

[The definition of Reynolds number for a rectangular channel used in this equation and subsequently in this paper is given by

$$(Re) = \rho\bar{U}d/\mu$$

This definition differs from that used by Grumer *et al.* in equations 2 to 4.]

That some approach lengths were shorter than the transition length by a factor of about two should only affect the calculations of velocity gradients for stability limits taken when the Reynolds number of the flow in the burner lies between 1000 and 2000. To test if this effect is significant limits were observed for two circular burners of 0·94 cm bore, one being 58 cm long and the other being 90 cm long, the corresponding transition length being 120 cm for a Reynolds number of 2000. No significant effect on the limits was observed and it has therefore been assumed that an approach length of half the transition value produces an exit velocity distribution in which the wall velocity gradients coincide, within experimental error, with those corresponding to fully developed flow.

It has been mentioned above that Maccallum° found, with butane–air mixtures. that the blow-off limits could be correlated by the wall velocity gradient at the centre of the long side. However, at the flashback limits the gradients at the centres of the long side exceeded the corresponding values from circular burner data by a factor of about 1·3 to 1·6. He suggested that if his burners had been water-jacketed some agreement in the flashback limits might have been observed. The effect of water-jacketing was observed in the current series of tests using the 1·27 cm × 1·26 cm burner. It was found that the blow-off limits were not significantly affected and that the volume flows at flashback were reduced by about ten per cent. This effect, while significant, is not sufficient to suggest that flashback may be correlated by the wall velocity gradient at the centre of the long side. All the new results reported here were obtained using water-jacketed burners.

The air and fuel flows were measured by

capillary meters, corrections being made for changes in temperature and pressure. The estimated accuracy of flow measurement is within three per cent.

The fuel used consisted of 97 per cent methane and the remainder inerts.

The butane used had the composition: *n*-butane. 16: isobutane. 34: butene. 32: butadiene. 15: propylene. 3 per cent. with traces of ethane and pentane.

Stability limits

It has been reported[6] that when a flame of high fuel concentration lifts from a rectangular burner of small cross-sectional width/length ratio the flame lifts first from the centre of the long side and finally from the ends. Similar effects were observed in the results reported here although the change in flow conditions from lifting from the middle of the port to final lift was so small as not to be significant. All the limits here correspond to the final flame lift.

On approaching the flashback limits the flame frequently tilted into the burner. Sometimes the flame temporarily completely entered the burner port, only to reappear within a few seconds. These initial transient effects were more noticeable with methane than with butane as the fuel, and they were apparently influenced by draughts. A more repeatable limit was obtained by recording the conditions at which the flame moved at least ten diameters upstream inside the burner, and did not re-emerge. All the flashback limits reported here were recorded in this way.

Correlation of stability limits

The number of limits observed with each burner was considerable. For convenience in correlating the limits of the various burners, interpolated points were selected both for the blow-off and for the flashback limits for each burner.

The first correlating equations applied to the results were equations 2 to 4, due to Grumer *et al.*[4]. The resulting critical gradients, referred to as g_G, are plotted in Figure 1 for the methane–air mixtures. The solid line corresponds to the critical gradients observed using circular burners. It is seen that there is very considerable scatter in the correlation. A similar scatter occurs when the butane–air results are treated in the same manner. The values of the gradient g_G appear to increase as the width length ratio of the burner cross section decreases. A limitation on equations 2 to 4 to exclude such 'slit' burners has already been indicated by Grumer[9].

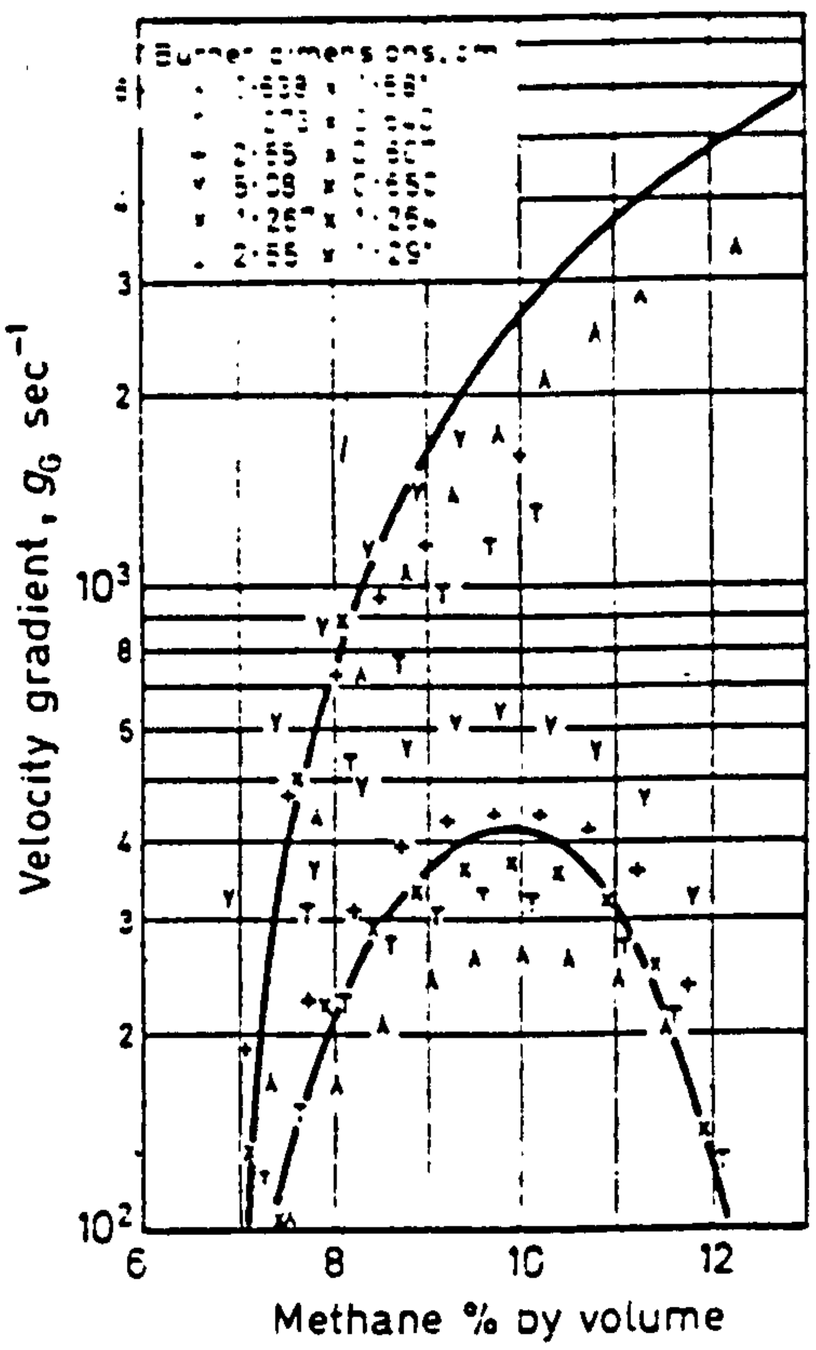

FIGURE 1. Stability limits of rectangular burners: methane–air, gradient g_G

An attempt was next made to correlate the same limits on the basis of the velocity gradient, g_c, at the centre of the long side (equation 6). The blow-off limits with butane appeared to be reasonably correlated, although the methane blow-off limits were clearly not correlated. There was no correlation of the flashback limits with either fuel. The values of g_c at the flashback limits appeared to increase as the burner dimensions increased.

The next attempt at correlation was primarily intended for the flashback results. It has been mentioned earlier that on approaching flashback limits the flame frequently tilted into the burner, entering the port at one corner, or simultaneously at the two corners at one end. Again when the flame finally flashed back it

seemed to advance upstream at the corners. This suggested that it was first near to a corner that the local flame velocity exceeded the local flow velocity. It was decided therefore to evaluate the boundary velocity gradients in the region close to the corner. Smith, Edwards and Brinkley[7] have tabulated values of functions from which the boundary velocity gradient, normal to the wall, can be evaluated at any point around the perimeter of a channel of rectangular cross section. The steps in this evaluation are indicated below.

The boundary velocity gradient normal to the wall at a point on the long side, say, of the port is given by $(dU/dX)_{X=a}$. This gradient is related to gradients on 'reduced' coordinates by

$$\left(\frac{dU}{dX}\right)_{X=a} = \frac{\bar{U}}{a\bar{\omega}}\left(\frac{d\omega}{dx}\right)_{x=1} \qquad [8]$$

where x is the fractional distance X/a, ω is the 'reduced' velocity, and $\bar{\omega}$ is the mean value of the reduced velocity. The function $(d\omega/dx)_{x=1}$ is tabulated as a function of the fractional distance along the long side and of the channel width length ratio. The term $\bar{\omega}$ is tabulated as a function of this latter ratio. Thus having selected the point on the long side of the port, the velocity gradient normal to the wall at that point can be readily evaluated.

It was found for the methane–air flashback results that if a point on the long side at a constant distance of 0·17 cm from the corner of all burners was selected, the boundary velocity gradients at that point normal to the wall gave a rough correlation of the flashback limits with circular burner data. This correlation is shown in Figure 2, the gradient at this point on the long side being referred to as g_s. For the butane–air mixtures, a point at a distance of 0·097 cm from the corner was chosen and the resulting reasonably satisfactory correlation is given in Figure 3. The distances from the

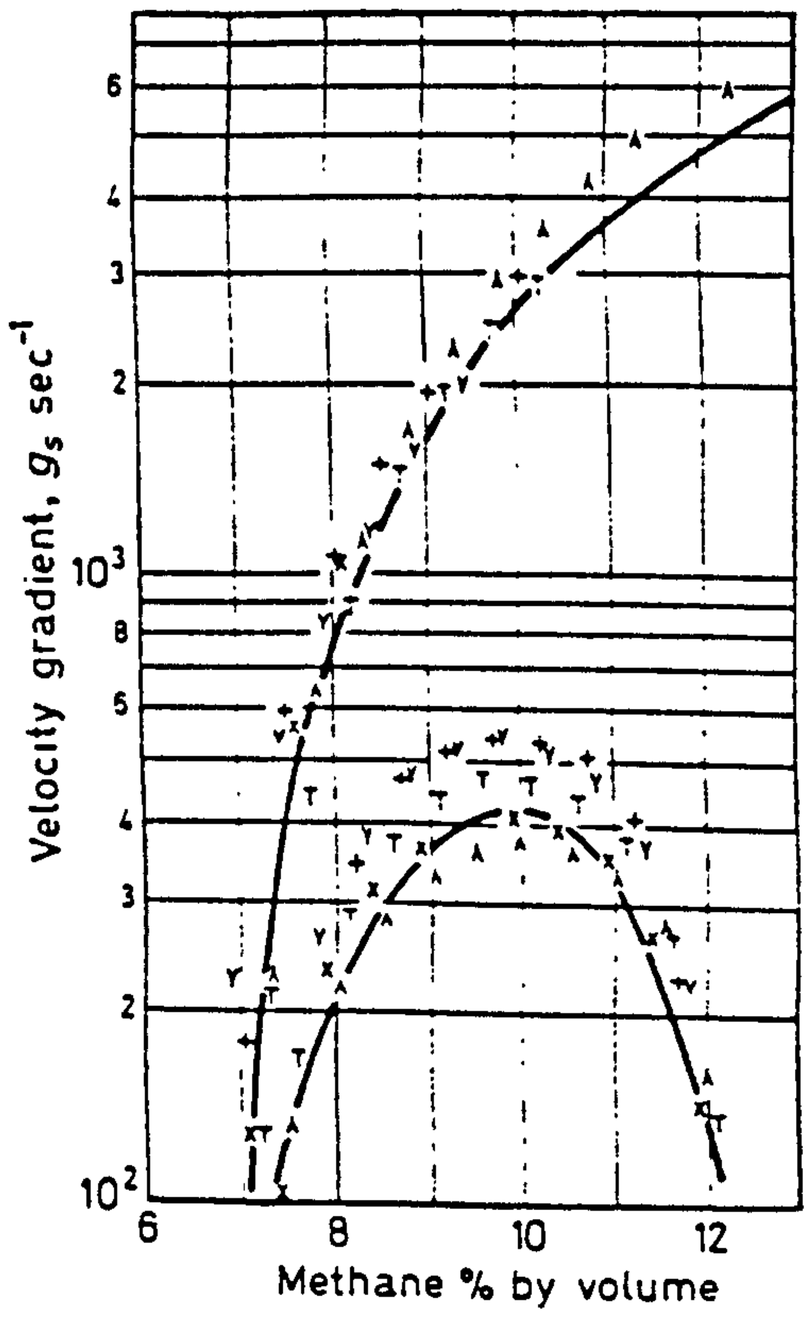

FIGURE 2. Stability limits of rectangular burners: methane–air, gradient g_s

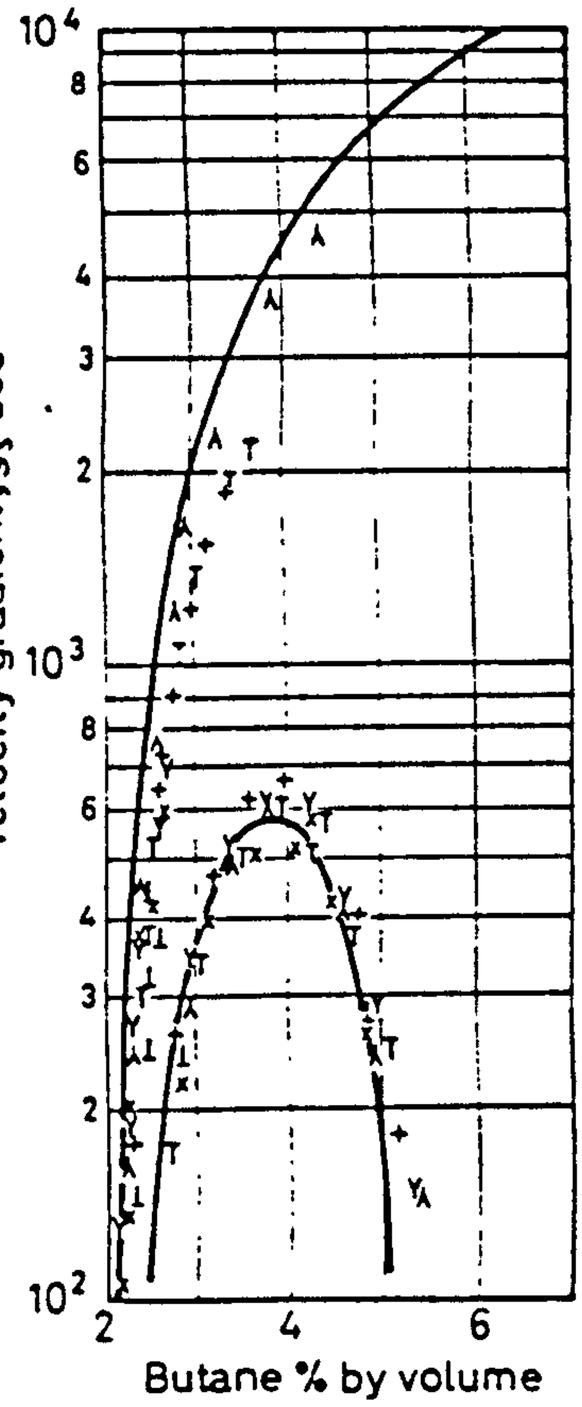

FIGURE 3. Stability limits of rectangular burners: butane–air, gradient g_s

corners were chosen in both cases so that the mean value of the flashback results from the various rectangular burners would coincide

with the critical gradient from circular burner results. It will be noticed that when the gradients at these points on the long side close to the corners are evaluated for the blow-off limits. the various results are grouped together although with methane–air mixtures the gradients are greater than the corresponding circular burner gradients while with the butane–air mixtures the gradients are less than the circular burner gradients.

This method of calculating a wall velocity gradient close to the corner was next refined by evaluating a so-called 'average' gradient in the corner, referred to as g_a. This 'average' gradient is given by

$$g_a = \left\{\left(\frac{dU}{dX}\right)^2_{X=a} + \left(\frac{dU}{dY}\right)^2_{Y=b}\right\}^{\frac{1}{2}} \qquad [9]$$

where b is the half cross-sectional length. The boundary gradients normal to their respective walls, $(dU/dX)_{X=a}$ and $(dU\ dY)_{Y=b}$, are evaluated at equal distances from the corner; again the distances for the methane–air and butane–air mixtures being selected such that the average flashback result of the rectangular burners is in agreement with the circular burner data. The distances were found to be 0·105 cm for methane–air and 0·076 cm for butane–air. The results of evaluating this 'average' gradient in the corner are given in Figure 4 for methane–air mixtures. This correlation is very satisfactory. The correlation is also satisfactory for the butane–air results, but no more satisfactory than the previous correlation (g_s). Comparison of values of the average corner gradient for the blow-off limits shows a fair amount of scatter for both fuel gases, although the mean values are in reasonable agreement with the circular burner gradients.

The distances from the corners at which the velocity gradients are calculated should be related to the quenching distances of the mixtures, though the form of the relationship is not yet known.

From the above it can be seen that two reasonable correlations (g_s and g_a) have been found for the flashback results. For the blow-off limits, the correlation based on g_s is probably the better, though it leaves much to be desired.

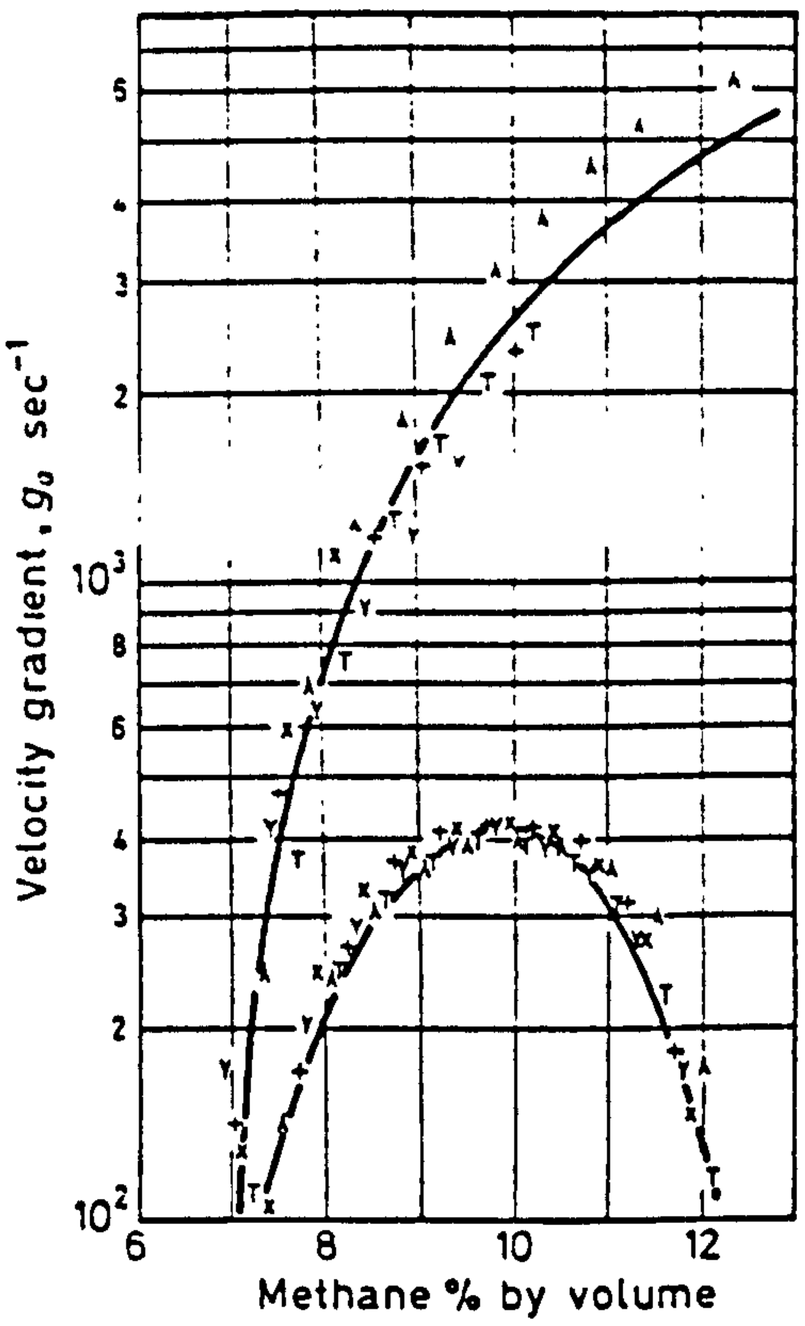

FIGURE 4. Stability limits of rectangular burners: methane–air, gradient g_a

A further correlation has been considered for the blow-off results. The average wall velocity gradients around the perimeter have been evaluated assuming fully developed flow profiles. The average gradient, $g_{av.}$, is given by

$$4(a + b)\, g_{av.}\mu = -4ab\, dp/dZ \qquad [10]$$

Substituting from equation 5 gives

$$g_{av.} = \lambda(Re)\bar{U}/8d \qquad [11]$$

In laminar flow the friction coefficient, λ, in rectangular channels is related[6] to the Reynolds number by

$$Q\lambda = (Re)^{-1} \qquad [12]$$

where Q is a function of the channel cross-sectional width/length ratio and is tabulated[6] from the results given by Smith, Edwards and Brinkley[7].

The average velocity gradients obtained in this way have been used to correlate the blow-off results, the correlation of the butane–air results being shown in Figure 5. This correlation is

96 Proc. Instn. Mech. E. 1969-70, 184, Part 3C (I)

Paper 13

THE PERFORMANCE OF TURBOJET ENGINES DURING THE 'THERMAL SOAK' TRANSIENT

N. R. L. Maccallum*

The changes are considered which might be present within a jet engine during the 'thermal soak' transient to cause the engine's performance to differ from the equilibrium performance. The effects of known values of these changes are given for a simple jet engine over a wide range of engine pressure ratios. Values of these changes are then predicted for a typical engine, and the observed loss in thrust of 1·7 per cent is satisfactorily explained. Two of the major factors giving loss of thrust in the simple jet engine were heat absorption in the turbine metal and heat absorption in the compressor metal. The effects of known values of these two factors on the performance of a typical high by-pass turbofan engine are given. For similar fractional heat absorptions, the losses in thrust of the turbofan engine are roughly double those of the simple jet engine.

INTRODUCTION

AFTER A TURBOJET ENGINE is rapidly accelerated to its maximum speed, a finite time elapses before the various components of the engine attain their equilibrium temperatures. At the commencement of this 'thermal soak' transient the performance of the engine may differ significantly from the equilibrium performance.

In this paper the changes are considered which might be present within the engine during this thermal soak transient. The effects of known values of these changes on the performance of a simple jet engine are given for a wide range of engine pressure ratios. The predictions are then applied to a typical engine and compared with the experimental results. Finally, the effects are evaluated of two of the major factors—heat absorption in the turbine and heat absorption in the compressor—on the performance of a high by-pass turbofan engine.

Notation

A_3 Throat area of high-pressure nozzle guide vanes (simple jet engine).
c_p Specific heat at constant pressure.
f Ratio of rate of heat absorption in metal of element of compressor or turbine to rate of mechanical energy transfer from the fluid in the element.
m Index of non-adiabatic compression or expansion.
$\dot{m}$ Compressor mass flow.
n Index of adiabatic compression or expansion.
P Fluid pressure.
T Fluid temperature.
v Specific volume of fluid.
γ Isentropic index.
η_{pc} Polytropic, or small stage, efficiency of compression.
η_{pt} Polytropic, or small stage, efficiency of expansion.

Prime (') refers to values during the thermal soak transient.

The MS. of this paper was received at the Institution on 1st August 1969 and accepted for publication on 5th September 1969. 33

* *Lecturer, Department of Mechanical Engineering, University of Glasgow, Glasgow, W.2.*

TRANSIENT FACTORS DURING THE THERMAL SOAK

The following transient factors are considered which might cause the performance of a simple jet engine immediately after an acceleration to differ from the equilibrium performance.

(a) Tip clearance changes in the compressor

These are due to differential rates of expansion in the compressor, resulting generally in (1) a reduction in compressor mass flow and (2) a reduction in compressor efficiency. It is estimated from experiment (1)* that a tip clearance change such as to cause a 1 per cent reduction in mass flow will also cause a 1 per cent reduction in compressor efficiency.

(b) Change in throat area of high-pressure nozzle guide vanes

The thermal response of the air-cooled high-pressure nozzle guide vanes of a typical engine of pressure ratio 10

* *References are given in Appendix 13.1.*

has been studied using a simple one-dimensional model. (The results of a test on this engine are given in the next section of this paper.)

For this design it was first predicted that in equilibrium the temperature of the nozzle guide vanes at mid span would be lower than the gas stagnation temperature by 20 per cent of the difference between the gas stagnation temperature and the compressor delivery temperature (assumed to be the high-pressure cooling air temperature). This prediction used standard correlations for the heat transfer from the vanes to the cooling air, and a heat transfer coefficient from the gas to the vanes averaged between Halls' correlation (2) and Hodge's correlation (3). The vane was then treated as having a uniform temperature distribution over its cross-section, but temperature could vary along its length. The transient conditions were simulated by giving a single-step increase to the gas temperature from 730°K (corresponding to ground idling speed) to 1130°K (corresponding to equilibrium at the maximum continuous speed). From observations of fuel flows, temperatures, and pressures during an actual acceleration it is thought that the predicted temperature distribution 8 s after this step increase will roughly correspond to the actual temperature distribution 5 s after the completion of a sudden acceleration. It was found that the average temperature along the span of the vane was within about 25 degK of the equilibrium temperature of 1014°K, and thus further change in throat area due to expansion along the vanes may be ignored. It was not possible, however, to predict the response of the carcase containing the nozzle guide vanes. This, presumably, would have a much slower rate of time response, though the temperature range would be less.

(*c*) *Change in cooling air flows*

Due to differential rates of expansion the effective resistances of the seals which control the cooling flows may alter, allowing the flow rates to alter.

(*d*) *Heat absorption by turbine metal*

During the period that the turbine metal is heating, the gas expansion will be non-adiabatic. A simple method of analysing the effect on performance is given below.

In an adiabatic expansion, the 'small stage' or polytropic efficiency, η_{pt}, relates elemental changes in temperature and pressure:

$$c_p \, dT = \eta_{pt} v \, dP \quad . \quad . \quad . \quad (13.1)$$

This leads to the relation between the index of expansion, n, and the isentropic index, γ:

$$\frac{n-1}{n} = \eta_{pt} \frac{\gamma-1}{\gamma} \quad . \quad . \quad . \quad (13.2)$$

The polytropic efficiency has also been called the path efficiency by Silver (4), who has suggested its applicability to the non-adiabatic situation.

Consider an elemental change in an expansion in which heat is being transferred from the fluid. For this elemental change let the heat transferred from the fluid be the factor, f, of the work transferred from the fluid. Then equation (13.1) becomes:

$$c_p \, dT = (1+f)\eta_{pt} v \, dP \quad . \quad . \quad (13.3)$$

Provided the factor, f, is constant along the turbine, and provided that the fluid properties are uniform over planes through the turbine, then equation (13.3) can be integrated to give the new index of expansion, m:

$$\frac{m-1}{m} = (1+f)\eta_{pt} \frac{\gamma-1}{\gamma} \quad . \quad . \quad (13.4)$$

The above assumptions are made in the analysis given here, and it is also assumed that the small stage efficiency in the non-adiabatic expansion equals the small stage efficiency in the adiabatic expansion.

The above treatment is similar to that already given by Horlock (5).

(*e*) *Heat absorption by compressor metal*

The non-adiabatic flow in the compressor can be analysed in a manner similar to that given for the turbine. In this case the index of compression in the transient conditions, m, is related to the isentropic index by

$$\frac{m-1}{m} = \frac{1+f}{\eta_{pc}} \frac{\gamma-1}{\gamma} \quad . \quad . \quad (13.5)$$

Here again f is the ratio of the heat transferred from the air to the work transferred from the air. Thus for an engine which has accelerated, factor f will be negative for the compressor.

In the thermal soak transient investigated here, in which the engine has already reached its working speed, it is assumed that the aerodynamic patterns of the flows through the compressor and turbine are similar to the equilibrium patterns. Correlations for blade heat transfer coefficients which have been obtained in equilibrium conditions are considered to be applicable to the thermal soak condition. However, it should be noted that, under certain conditions, heat transfer may disturb the aerodynamic flow pattern. It is known (6) (7) that heat transfer causes an earlier transition from a laminar to a turbulent boundary layer in the flow over a heated flat plate. Thus, for example, during and immediately after a rapid deceleration, heat transfer from the compressor blades to the air may cause an earlier separation of the flow. This may be contributory to the greater tendency to stall observed when re-accelerating an engine after a rapid deceleration (8). This effect is being investigated (9).

(*f*) *Heat absorption by combustion chamber metal*

When the engine is governed to run at a constant speed, this heat absorption will only cause a temporary increase in fuel flow, and will not affect the other performance parameters.

(*g*) *Change of final nozzle area*

There are two factors which have opposing effects. Immediately following the acceleration the nozzle dimensions will be smaller than at equilibrium. However, the

heat transfer from the gas may thin the boundary layer so that the effective area is a larger proportion of the geometric area. Thus the net departure from the equilibrium effective area may be small. There is experimental evidence given later suggesting that in one case the change is less than 0·25 per cent.

(*h*) *Clearance changes in turbine*

Due to differential rates of expansion, clearances may differ from their equilibrium values, resulting in changes in turbine efficiency.

The effects of the above factors on the performance parameters of typical simple jet engines have been evaluated. Compressor pressure ratios in the range 5 to 28 have been covered. The engines operated at an air inlet stagnation temperature of 288°K and a turbine inlet stagnation temperature of 1350°K. The polytropic efficiencies of compression and expansion were 0·87 and 0·89, respectively, and the loss in stagnation pressure in the combustion chamber was 6 per cent of the compressor delivery pressure. The rotational speed was held constant during the thermal soak transient (for a multi-spool engine the low-pressure spool speed was held constant), and it was assumed that the high-pressure nozzle guide vanes of the turbine were effectively choked. The effects of known magnitudes of some of the above factors on turbine inlet temperature, turbine outlet temperature, and thrust are given in Figs 13.1, 13.2, and 13.3, respectively. The magnitudes of the transient factors whose effects are illustrated are:

(*a*) (i) Compressor mass flow 0·99 of equilibrium value, i.e. $\dot{m}' = 0{\cdot}99\dot{m}$; (ii) compressor polytropic efficiency $\eta'_{pc} = 0{\cdot}86$ (cf. equilibrium $\eta_{pc} = 0{\cdot}87$).

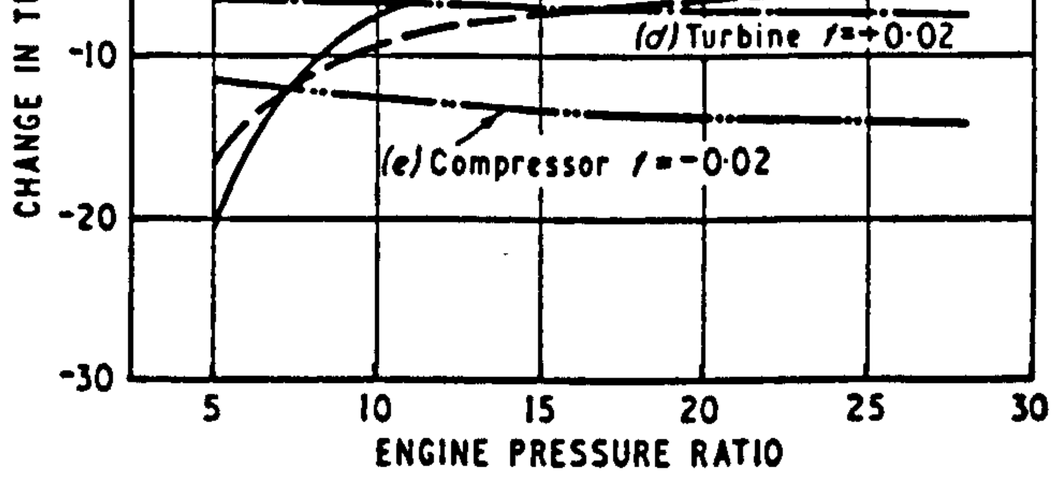

Fig. 13.2. Simple jet engine: effects of changes on turbine outlet temperature

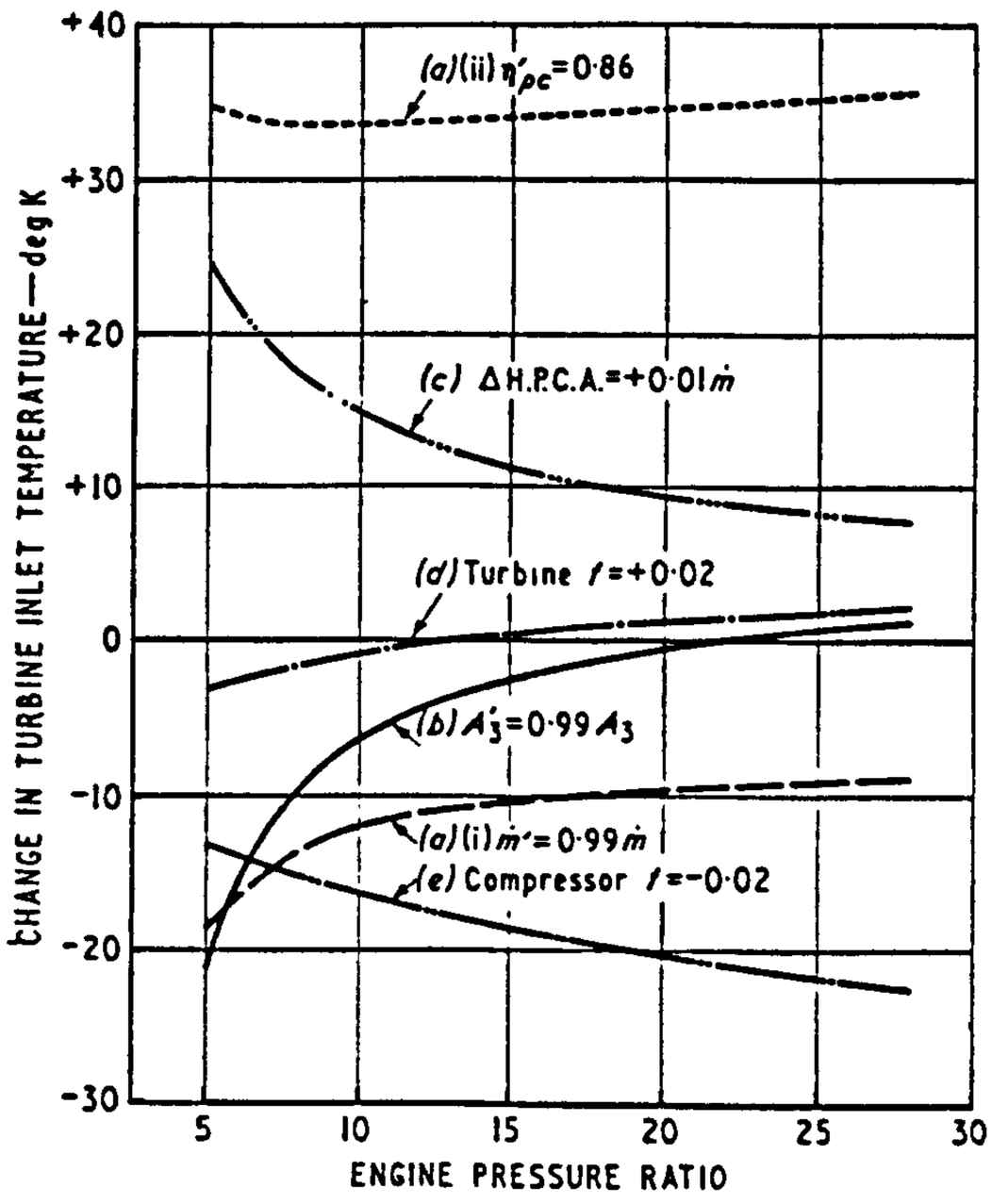

Fig. 13.1. Simple jet engine: effects of changes on turbine inlet temperature

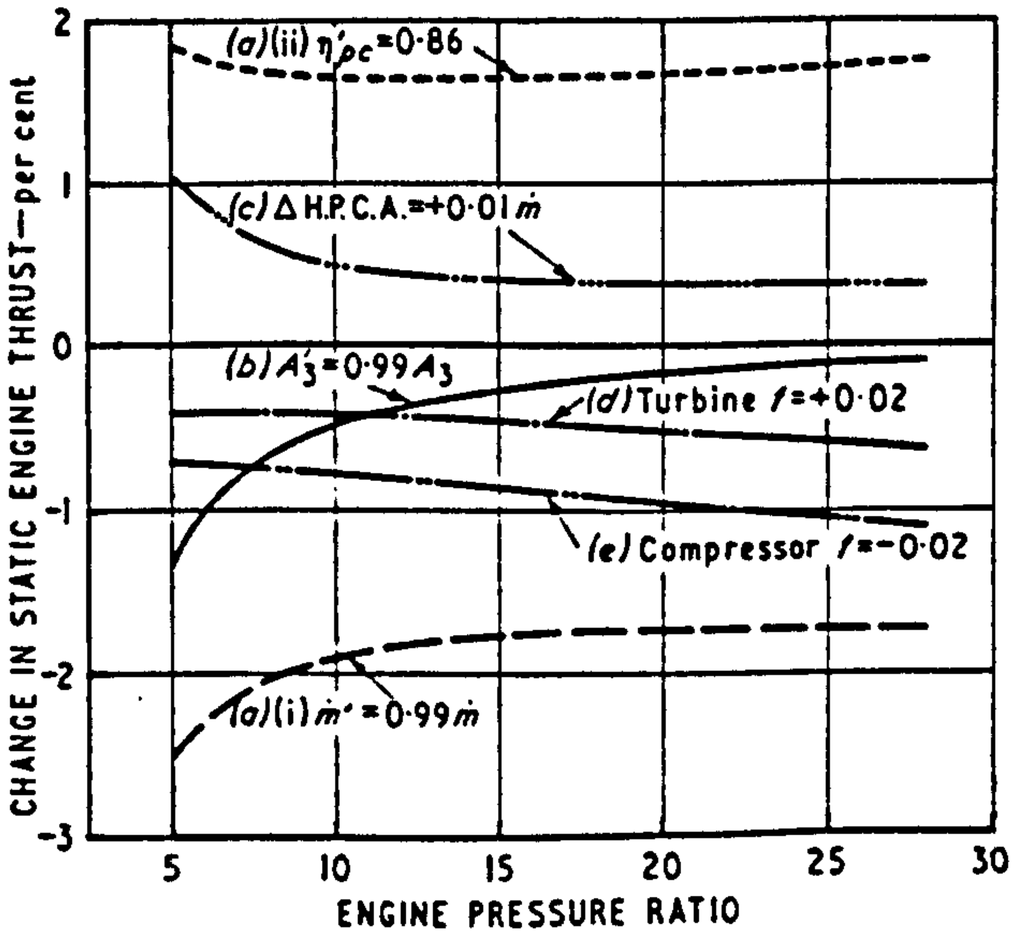

Fig. 13.3. Simple jet engine: effects of changes on static engine thrust

(*b*) High-pressure nozzle guide vane throat area 0·99 of equilibrium value, i.e. $A'_3 = 0{\cdot}99A_3$.

(*c*) Increase in high-pressure cooling air flow by 0·01 of the compressor inlet flow, i.e. Δ(H.P.C.A.) $= +0{\cdot}01\dot{m}$.

(*d*) Heat absorption rate in turbine metal of 0·02 of power transfer from gas, i.e. $f = +0{\cdot}02$.

(*e*) Heat absorption rate in compressor metal of 0·02 of power transfer to air, i.e. $f = -0{\cdot}02$.

The magnitudes of these transient factors have been selected purely arbitrarily at this stage. In a subsequent section of this paper the magnitudes appropriate to a particular jet engine are shown. As the magnitudes of the factors that will be encountered are small, it may be assumed that the performance parameters change linearly.

The graphs corresponding to factors (*a*), (*b*), and (*c*) shown in Figs 13.1, 13.2, and 13.3 are well known, as are the graphs for final nozzle area changes and turbine efficiency changes (omitted from the figures for clarity). The graphs corresponding to factors (*d*) and (*e*) present new information.

It is seen that the turbine inlet temperature is considerably reduced by compressor heat absorption but is almost unaffected by turbine heat absorption. Both turbine outlet temperature and thrust are reduced by heat absorptions in the compressor and in the turbine. The magnitudes of these reductions increase with engine pressure ratio for the same value of the ratio of heat absorption rate to power transfer.

TEST ON A TYPICAL JET ENGINE

A test was carried out on a typical single-spool jet engine of pressure compression ratio 10.

The engine was held at 3000 rev/min (ground idling speed) to allow temperatures to stabilize, and then rapidly accelerated to 7950 rev/min (the maximum continuous speed). The engine speed was thereafter maintained at about 7950 rev/min for 5 min while observations were taken of thrust, jet pipe static pressure, air meter differential, jet pipe temperature, compressor delivery pressure, speed, and air inlet temperature. Readings were taken at 15-s intervals.

It was found that most of the changes in the performance parameters occurred in the first minute. For the purpose of the analysis to be given here, the performance of the engine 5 s after attaining 7950 rev/min (instant 'A' hereafter) will be compared with the performance after a further 60 s have elapsed (instant 'B'). The conditions at the latter point may be regarded for practical purposes as representing equilibrium conditions.

It is assumed that the time lags associated with thrust and pressure measurements are small (say less than 1 s). However, doubt existed about the time lag in the response of the jet pipe thermocouples. At instant 'A' they indicated a temperature of 838°K. Final nozzle mass flow and thrust comparisons with instant 'B' (and equilibrium running) predicted jet pipe temperatures at instant 'A' of 856°K. This figure of 856°K is assumed in this analysis to be representative of the jet pipe temperature at instant 'A'.

The relationship between jet pipe static pressure and thrust observed during the thermal transient was in satisfactory agreement with the relationship subsequently obtained during equilibrium running.

The engine performance figures at instant 'B' and at instant 'A' are given in columns (1) and (10) respectively of Table 13.1.

PREDICTION OF TRANSIENT RESULTS

The transient factors which have previously been described are now applied to the engine which gave the above test results.

Table 13.1. Engine performance figures

	At instant 'B' (i.e. equilibrium)	Effects of changes from equilibrium							Observed differences at 'A' from equilibrium	At instant 'A'
		Air flow $-0{\cdot}4\%$	η_{pc} $-0{\cdot}4\%$	A_3 $-0{\cdot}4\%$	Heat to turbine $f = +0{\cdot}03$	Heat to compressor $f = -0{\cdot}01$	Heat to jet pipe	Sum of predicted changes		
	(1)	(2)	(3)	(4)	(5)	(6)	(7)	(8)	(9)	(10)
Jet pipe temp., °K	868	−3·4	+6·5	−2·6	−10·0	−6·5	−3·0	−19·0	−12	856
Jet pipe static pressure, lbf/in² (gauge)	20·65	−0·25	+0·16	−0·04	−0·17	−0·11	−0·04	−0·45	−0·42	20·23
Thrust, lbf	12 550	−104	+68	−30	−79	−51	−20	−216	−210	12 340
Compressor delivery pressure, lbf/in² (gauge)	127	−0·79	+0·47	+0·39	−0·09	−0·42	−0·03	−0·47	−1	126

(a) Compressor tip clearance

At instant 'A' the compressor mass flow was observed to be 0·4 per cent lower than the equilibrium value at instant 'B'. The departures from equilibrium performance due to this change are given in column (2) of Table 13.1. Assuming a corresponding reduction in compressor efficiency of 0·4 per cent gives the effects listed in column (3) of Table 13.1.

(b) Change in throat area of high-pressure nozzle guide vanes

It has been indicated previously that, for this engine, within 5 s of the completion of the acceleration the temperatures of the aerofoil sections of the nozzle guide vanes are within about 25 degK of the equilibrium values. The effect of the remaining expansion along the vane on the throat area is negligible. However, the carcase containing the nozzle guide vanes will have a much slower thermal response, although the temperature range will be smaller. It is assumed that the temperature of this carcase changes by 200 degK between instants 'A' and 'B', leading to an increase in the throat area of the high-pressure nozzle guide vanes of 0·4 per cent. The effects of this change are given in column (4) of Table 13.1.

(c) Change in cooling air flow

The engine was not instrumented for measurement of the high-pressure cooling air flow. However, the agreement which is presently seen between the sums of the other predicted changes and the observed change in performance suggests that the increase in cooling air flow was small, perhaps 0·2 per cent of the compressor air flow, but the arbitrary assumptions in the predictions must be borne in mind.

(d) Effect of heat absorption by turbine metal

Using the simple one-dimensional model described previously for the nozzle guide vanes, the rates of absorption of heat by the different parts of the turbine have been estimated. Arbitrarily a mass equal to double the root mass has been allocated to each blade (and nozzle guide vane) to make some allowance for the thermal capacity of the parts of the discs and mountings which are in good thermal contact with the blades (and nozzle guide vanes). The results are given in Fig. 13.4, showing the individual absorptions for the high-pressure nozzle guide vanes, for the final stage rotor blades, and for the total turbine. Although a single time constant of 16 s could effectively be applied to the final stage rotor blades, no single constant can be representative of the high-pressure nozzle guide vanes nor of the turbine as a whole.

If it is again assumed that the predicted heat absorption rate in the turbine 8 s after the step increase in temperature corresponds to the absorption rate 5 s after completion of the actual acceleration, then the heat absorption rate in the turbine is about 380 Chu/s, which is 3 per cent of the mechanical energy transfer rate. Making the assumptions previously referred to, the effects of this heat absorption rate of 3 per cent of the work transfer have been evaluated and are given in column (5) of Table 13.1.

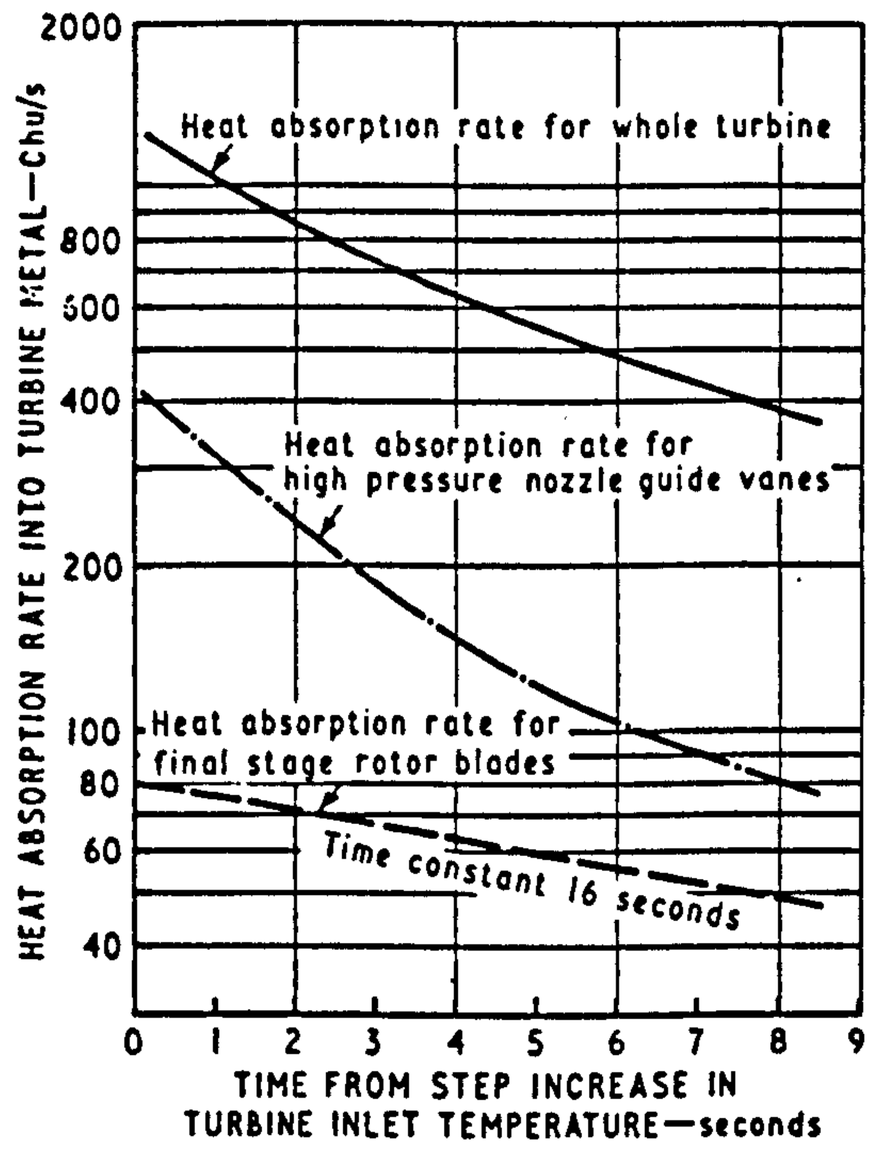

Fig. 13.4. Predicted heat absorption rates in turbine metal following step increase in turbine inlet temperature

(e) Effect of heat absorption by compressor metal

By applying a treatment similar to that described for the turbine it is estimated that 8 s after a step increase in speed from 3000 rev/min to 7950 rev/min (this instant is assumed to correspond to instant 'A'), the heat absorption rate in the compressor is about 130 Chu/s, or 1 per cent of the work transfer rate. In this case, as the rotor blades are held by pins, no additional allowance has been made for the thermal capacities of the disc and carcase metal at the blade mountings. The effects of this heat absorption on engine performance are given in column (6) of Table 13.1.

(f) Effect of heat absorption by combustion chamber metal

As already stated, this only causes a temporary increase in fuel flow, and does not affect the other performance parameters. It was observed during the test that the fuel flow during the 15 s following instant 'A' exceeded the equilibrium fuel flow by about 2 per cent.

(g) Change of final nozzle area

The calculations of final nozzle mass flow and engine thrust which were used to predict the jet pipe temperature at instant 'A' indicated that at instant 'A' the effective area of the final nozzle was at least within 0·25 per cent of the effective area at the end of the transient. Further, the plot of jet pipe static pressure against thrust indicates that

the effective areas are virtually identical. For practical purposes it is concluded that there was no significant change in the effective final nozzle area.

(*h*) *Effect of heat absorption by jet pipe metal*

This was estimated to cause a heat abstraction at instant 'A' of about 130 Chu/s, and the effects of this on the performance are given in column (7) of Table 13.1.

The sums of the above effects (*a*), (*b*), and (*d*) to (*h*) are given in column (8) of Table 13.1 and then compared in column (9) with the observed differences in performance between equilibrium and instant 'A'. (The values of the changes which appear in Table 13.1 are those corresponding to the engine tested, which had a turbine inlet temperature of 1130°K. They do not correspond exactly with the values shown in Figs 13.1, 13.2, and 13.3 for engines having turbine inlet temperatures of 1350°K.) The agreement between the predicted and observed changes is very satisfactory, with the exception of the jet pipe temperature where there is a discrepancy of 7 degK. This cannot be attributed to position error as the 'experimental' temperature at instant 'A' was obtained by comparisons of mass flows and thrusts with equilibrium conditions. It may be that this agreement is as good as can be expected. The compressor delivery pressure was read in the test only to the nearest 1 lbf/in². The agreement between the predicted change of 0·47 lbf/in² and the observed change of 1 lbf/in² is regarded as satisfactory.

The agreements on thrust and jet pipe pressure suggest that there were probably no other factors present which would significantly alter the engine performance. There might have been a slight increase in high-pressure cooling air flow by 0·2 per cent of the total air flow. This would reduce the jet pipe temperature discrepancy from 7 degK to 5 degK and would change the thrust discrepancy from −6 lbf to +10 lbf. There does not appear to have been a significant change in turbine efficiency.

APPLICATION TO HIGH BY-PASS TURBOFAN ENGINES

The two factors which caused the largest deficits in thrust during the thermal soak of the simple jet engine considered above were heat absorption in the turbine metal and heat absorption in the compressor metal.

The effects of these two factors on the performance of turbofan engines of by-pass ratio 6 have been evaluated. As for the simple jet engine calculations, the air inlet stagnation temperature was 288°K, the turbine inlet stagnation temperature was 1350°K, the combustion chamber stagnation pressure loss was 6 per cent of the compressor delivery pressure, and the polytropic efficiencies of compression and expansion were 0·87 and 0·89, respectively. Overall pressure ratios in the range 16 to 28 have been covered and the by-pass pressure was selected in each case to give equal velocities in the by-pass air and turbine exhaust gas exit streams. It was assumed that the

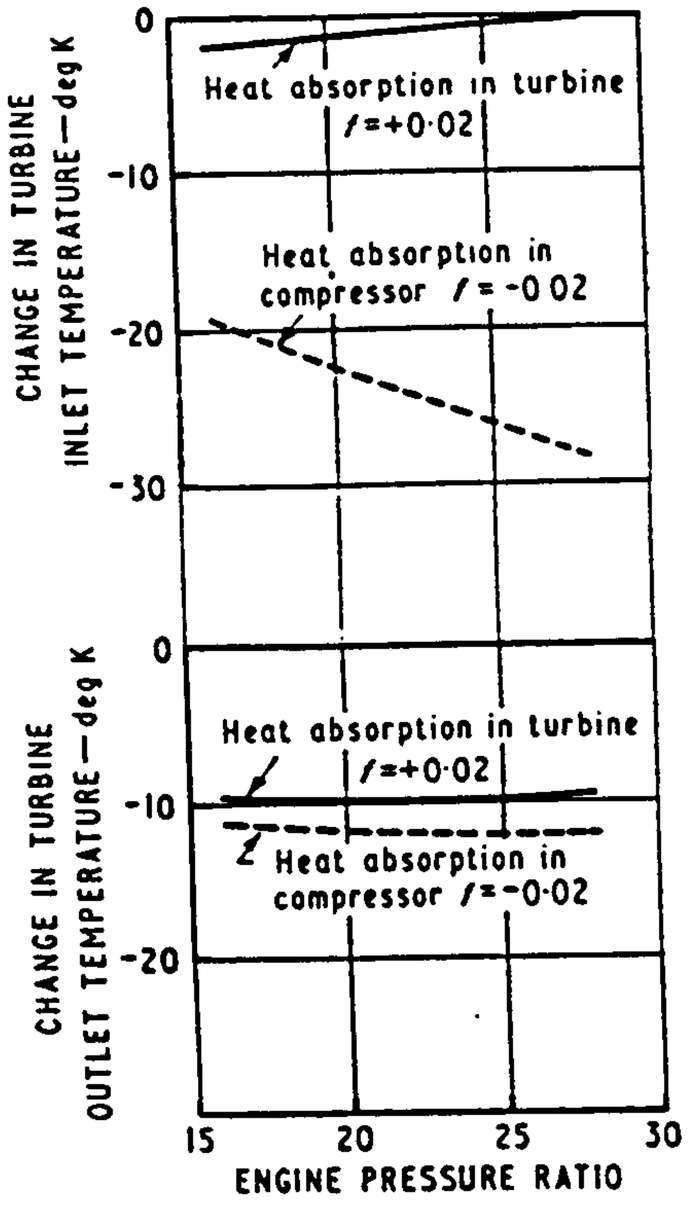

Fig. 13.5. Turbofan engine: effects of turbine and compressor heat absorptions on turbine inlet and outlet temperatures

fan, or compressor for the total air (by-pass air plus 'cycle' air), is on a separate shaft from the 'cycle' air compressor. The rotational speed of the 'cycle' air compressor was held constant during the thermal transient. (For an engine where the 'cycle' air compressor is split, it is assumed that the rotational speed of the first 'cycle' air compressor is held constant.) The rotational speed of the fan, or first compressor, during the transient was then found to be lower than the equilibrium speed. The changes in performance resulting from heat absorption rates in the turbine and in the compressor, in each case of 2 per cent of the power transfer, are given in Figs 13.5 and 13.6.

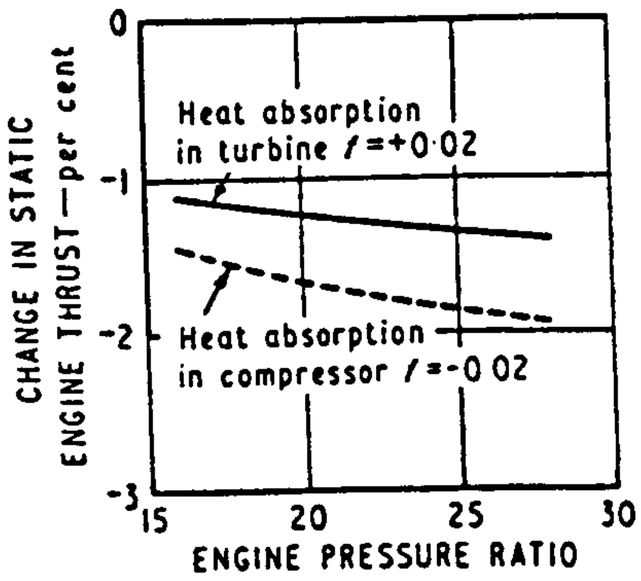

Fig. 13.6. Turbofan engine: effects of turbine and compressor heat absorptions on static engine thrust

It is noted on comparing Fig. 13.5 with Figs 13.1 and 13.2 that the temperature changes in the turbofan engine are similar to those in the simple jet engine. However, comparison of Figs 13.6 and 13.3 shows that for the turbofan engine the reductions in thrust due to heat absorptions are roughly double the corresponding thrust reductions for the simple jet engine. It is thus evident that it is even more desirable for a high by-pass turbofan to use turbines and compressors of low thermal capacity per unit power. The product of thermal capacity and temperature range is a measure of the time integral of the thrust deficit due to heat absorption. The variation of this thrust deficit with time is influenced by the coefficients of heat transfer and the conductivities of the materials.

The reduction in turbine temperatures due to heat absorption in the compressor suggests the possibility of increasing the engine speeds during the transient to give the maximum permissible turbine temperatures.

CONCLUSIONS

A simple jet engine was rapidly accelerated from ground idling speed to its maximum continuous speed. Immediately after completion of the acceleration the engine thrust was lower than the equilibrium thrust by 1·7 per cent (210 lbf). The engine reached equilibrium performance some 60 s after completion of the acceleration. The departures from equilibrium performance which were observed immediately after the acceleration have been satisfactorily accounted for by considering the following factors:

(*a*) Heat absorption in the metal of the turbine (thrust deficit 80 lbf).

(*b*) Heat absorption in the metal of the compressor (thrust deficit 50 lbf).

(*c*) Changes in compressor tip clearances causing a reduction in air flow of 0·4 per cent and an associated reduction in compressor efficiency of 0·4 per cent (combined thrust deficit 36 lbf).

(*d*) High-pressure nozzle guide vane throat area lower than equilibrium value by 0·4 per cent (thrust deficit 30 lbf).

(*e*) Heat absorption in jet pipe metal (thrust deficit 20 lbf).

(*f*) There may also have been an increase in the high-pressure cooling air flow by 0·2 per cent of the compressor flow, giving a thrust increase of 16 lbf.

Graphs have been presented which predict the effects of known rates of heat absorption in the compressor and in the turbine on the performance of simple jet engines over a wide range of pressure ratios.

Similar graphs are presented for a turbofan engine of by-pass ratio 6, showing that the reductions in thrust of the turbofan engine are roughly double those of the simple jet engine, assuming that the rates of heat absorption are the same fractions of the power transfer.

ACKNOWLEDGEMENTS

The author wishes to thank members of the staff of Rolls-Royce Limited for providing information and for their advice; he also wishes to thank Mr A. Sinclair, now a Graduate of Glasgow University, for his assistance and comments.

APPENDIX 13.1

REFERENCES

(1) ROLLS-ROYCE LTD. Unpublished Data, Communication, 1969 (17th February).

(2) HALLS, G. A. 'Air cooling of turbine blades and vanes', Lecture to AGARD, Varenna, Italy 1967 (18th May).

(3) HODGE, R. I. 'A turbine nozzle cascade for cooling studies. Part I', *A.R.C. C.P. No. 492* 1960.

(4) SILVER, R. S. 'Efficiency and losses in expansion and compression processes', *Bull. mech. Engng Educ.* 1967 **6**, 73.

(5) HORLOCK, J. H. *Axial flow turbines* 1966 (Butterworths, London).

(6) LIEPMANN, H. W. and FILA, G. H. 'Investigations of effects of surface temperature and single roughness elements on boundary-layer transition', *N.A.C.A. Rept No. 890* 1947.

(7) HIGGINS, R. W. and PAPPAS, C. C. 'An experimental investigation of the effect of surface heating on boundary-layer transition on a flat plate in supersonic flow', *N.A.C.A. T.N. 2351* 1951.

(8) WARNE, E. H. 'Gas turbine fuel and control systems', *Conf. Technical Advances in Gas Turbine Design, Proc. Instn mech. Engrs* 1968–69 **183** (Pt 3N), 121.

(9) GRANT, A. D. Unpublished work at Glasgow University, 1969.

UNIVERSITY OF GLASGOW

Department of Mechanical Engineering

TURBULENT SWIRLING FLAMES ISSUING FROM VANE SWIRLERS

by

G.G. BAFUWA and N.R.L. MACCALLUM

17th July, 1970

For presentation to 18th Meeting of Aerodynamics Panel, I.F.R.F.

Paris

11th September, 1970

Summary

The aerodynamic characteristics of turbulent swirling flames issuing from annular and hubless swirlers with vane angles of 15°, 30°, 45° and 60° have been investigated. The swirlers were to the same design as those used for previous[1] cold tests. Measurements of the velocity components, static pressure and temperature across and along the jet have been made. The results of the flame tests are compared with those obtained in cold jets. The prediction method of Spalding et al[7] has been used for computing the velocity components in cold and burning jets issuing from a 15° annular swirler.

For annular swirlers with 45° vane angle and over, reverse flow zones were observed as in cold models but the recirculation zone in each case was shorter and wider than that observed in cold tests. The length and width of the recirculation zone also depends on the swirl number. The static pressure remained subatmospheric within the jets for all the swirlers throughout the length investigated. Temperature profiles indicate off-centre maximum values near the swirler exit. The downstream position at which the maximum temperature reaches the axis depends on the swirl number. Within the recirculation zone, temperature gradients are small. Comparisons with cold tests show that the shapes of the axial and tangential velocity profiles are the same in both cases, although the position of maximum reverse velocity is not constant as in cold models. The initial rates of expansion of the swirling flame jets are higher than in cold jets but due to entrainment of ambient fluid the expansion rate drops downstream.

With the hubless swirlers, combustion causes changes in the various profiles similar to those observed with the annular swirlers, expect that the recirculation zones are not shortened.

Table of Contents

1.(a) Nomenclature.

d_o	=	diameter of hubless swirler
d_1, d_2	=	inner and outer diameters of annular swirlers
G_x	=	axial momentum flux
G_θ	=	angular momentum flux
h	=	enthalpy
K	=	reaction rate constant
m	=	mass fraction of chemical species
m_f	=	mixture fraction
p	=	pressure
r	=	radial distance
$\bar{R}$	=	universal gas constant
S	=	swirl number
T	=	temperature
u	=	axial velocity component
v	=	radial velocity component
V_s	=	$u^2 + v^2$
W	=	swirl velocity
x	=	axial distance
z	=	swirler hub ratio = $\frac{d_1}{d_2}$
Γ	=	turbulent exchange coefficient
θ	=	vane angle of swirler
μ	=	viscosity
π	=	product of density and corresponding component of velocity
$\bar{\pi}$	=	vector equivalent of π
ρ	=	density
φ	=	angle subtended by vane when viewed in axial direction or dependent variable
ψ	=	stream function
ω	=	vorticity
STC	=	stoichiometric air/fuel ratio by weight

Subscripts

eff	=	effective value
fu	=	for fuel
max	=	maximum value
max,exit	=	maximum value at exit
ox	=	for oxidant
o	=	for ambient fluid
r	=	in radial direction
x	=	in axial direction
a	=	on the axis

1 (b) List of Figures

2. Introduction

The addition of swirl to the air entering a furnace can be used to control the length and stability of the flame. One common method of generating swirl in the air jet is by means of a vane swirler. A study[1] has previously been made of the performance of vane swirlers and of the aerodynamics of the issuing jets in the absence of combustion. Results were given for air jets issuing into a free atmosphere and into a cold model of a furnace.

This report contains observations of burning swirling jets issuing into a free atmosphere, swirl again being generated by vane swirlers. The results were obtained using both annular and hubless vane swirlers similar to those used in the previous cold study.

Pre-mixed town gas and air was used as the combustible stream.

Observations are reported of the axial and tangential (or swirl) velocities, of the temperatures and of the static pressure in the jet.

3. Design of vane swirlers

3.1 Annular swirlers

The design is shown in Figure 1. The outer and inner diameters of the annular passage are 3.86 in (98.0 mm) and 1.25 in (31.8 mm) respectively. There are eight mild steel symmetrical vanes of thickness 0.032 in (0.813 mm). Swirlers having vanes at inclinations, θ, of 15°, 30°, 45° and 60° to the axis of the flow have been tested. The vane lengths for the 30°, 45° and 60° swirlers are such that when viewed in an axial direction the angle subtended by the vanes at the axis, ϕ, is 75°, thus giving an overlap of 30° between adjacent vanes. With the 15° swirler the overlap was "negative", being -13°.

3.2 Hubless swirlers

"Hubless" swirlers were prepared to a design developed from the annular swirler design. The vanes are in the shape of segments of a circle, and, when assembled in the swirler, all the vanes meet at a point

on the axis. The same vane inclinations of 15°, 30°, 45° and 60° as for the annular swirlers were tested. The overlaps between adjacent are as for the annular swirlers. The swirler diameter, d_o, is 0.93 in (23.7mm).

4. Swirl number

The swirl number used in this paper is defined as

$$S = \frac{2\,G_\phi}{G_x\, d_2} \qquad \ldots.(4.1)$$

where G_ϕ is the axial flux of angular momentum and G_x is the axial flux of axial momentum, ignoring static pressure effects, d_2 is the outer diameter of the swirler.

For annular vane swirlers giving complete deflection equation (4.1) reduces 2,1 to

$$S = \frac{2}{3}\left(\frac{1 - z^3}{1 - z^2}\right) \tan\theta \qquad \ldots.(4.2)$$

The swirlers tested in these experiments had vane angles of 15°, 30°, 45° and 60° and their respective swirl numbers, by equation (4.2) are 0.19, 0.42, 0.72 and 1.25.

For hubless vane swirlers equation (4.1) reduces to

$$S = \frac{2}{3} \tan\theta \qquad \ldots.(4.3)$$

For the 15°, 30°, 45° and 60° hubless swirlers the respective swirl numbers are 0.18, 0.385, 0.67 and 1.16.

5. Experimental work

5.1 Objectives

The object of the experimental work was to obtain results of axial velocity, tangential (or swirl) velocity and static pressure which could be compared with previous results for isothermal jets. Temperature would also be measured.

5.2 Apparatus

A pre-mixed stream of air and town gas was supplied to the test rig which consisted of approach pipes at whose downstream end the various swirlers were fitted. The length of the approach pipe was approximately 10 d_2 for the annular swirlers and 60 d_o for the hubless swirlers.

The mixture issuing from the swirler into the atmosphere was ignited at the swirler exit. It was found that stable flames could be held downstream of the swirler over a wide range of fuel/air ratios. A fuel/air ratio of 0.15 by volume and an average axial nozzle velocity (calculated from mixture flow rate and swirler flow area taking account of vane thickness) of 50 ft/sec (15.2 m/sec) were selected for the experimental observations of the flames issuing from the annular swirlers. For the 15°, 30° and 45° hubless swirlers a fuel/air ratio of 0.20 by volume and an average axial nozzle velocity of 80 ft/sec (24.4 m/sec) were used. For the 60° hubless swirler a stable flame could not be obtained with this mixture and so a fuel/air ratio of 0.25 by volume was selected.

The town gas varied slightly in composition but a typical composition is given in Table 1. For this composition the stoichiometric fuel/air ratio is 0.244 by volume.

The velocity components in the swirling jets were measured by a three hole water-cooled probes to the design of Hiett and Powell[3]. A probe of 0.375 in (9.5 mm) tip diameter was used with the annular swirlers, and of 0.25 in (6.3 mm) tip diameter with the hubless swirlers. Static pressures were measured by a water-cooled disc static probe to the design of Miller and Comings[4]. The pressure differences across the probes were measured by electronic micromanometer[5] to an accuracy of ± 0.0005 in water (± 0.013 mm).

Temperatures were measured by an unshielded Platinum 5% Rhodium/Platinum 20% Rhodium thermocouple (wire diameter 0.01 in (0.25 mm)).

Component	% by volume
H_2	56.1
CO	6.5
CH_4	11.9
C_2H_6	0.6
C_3H_8	3.5
C_4H_{10}	1.8
Unsaturated Hydrocarbon	0.4
CO_2	15.2
H_2	3.6
O_2	0.4

TABLE 1. Composition of coal gas

5.3 Procedure

Pressure and temperature traverses were made in the swirling flames issuing from the swirlers, the gas and air flows being set to give the fuel/air ratios and nozzle velocities listed in paragraph 5.2 above.

6. Results and discussion of aerodynamic tests

6.1 Axial velocity distribution

The distributions of the axial component of velocity for the annular swirler studies are presented in Figure 2a - d and for the hubless swirlers in Figure 3a,b. With the exception of the 15° hubless swirler, the profiles close to the swirler exit show two crests representing the off-axis maximum velocities together with a central trough representing the minimum (sometimes reverse) velocity. As the flow proceeds downstream the maximum velocity tends towards the axis, the position at which it reaches the axis depending on the swirl number. For example Figure 2a shows that

the maximum velocity for the 15° annular swirler has reached the axis at 1.0 d_2 from the inlet whereas annular swirlers of higher vane angles have off-centre maximum velocities throughout the axial distance investigated. For the 15° hubless swirler the maximum axial velocity is observed at the axis at the traversing plane nearest to the swirler exit at 1.0 d_o from swirler exit. This jet resembles most closely an unswirled jet issuing from a pipe.

Central reverse flows were observed with the 45° and 60° annular swirlers and with the 30°, 45° and 60° hubless swirlers. The width and length of the recirculating zone increases with swirl number.

The rates of decay of the axial velocity along the axis, plotted as a ratio of the maximum axial velocity at the swirler exit, are shown in Figure 2e for the annular swirlers and Figure 3c for the hubless swirlers. For the hubless swirlers the maximum axial velocity at the plane one diameter downstream from the swirler is taken as the reference. The positions of maximum reverse velocity for the 45° and 60° annular swirlers are 0.5 d_2 and 1.5 d_2 respectively, and for the 30°, 45° and 60° hubless swirlers the positions are at approximately 1.0 d_o, 1.5 d_o and 2.0 d_o respectively. For annular and hubless swirlers of 30° and over the axial velocity on the axis reduces immediately downstream of the swirler after which the velocity increases. The subsequent increase in the axial velocity is associated with the movement of the position of maximum axial velocity at any cross-sectional plane towards the axis as the fluid moves downstream.

The profiles of the rates of decay of the maximum axial velocity, as a ratio of the maximum axial velocity at the swirler exit, are given in Figure 2f for the annular swirlers and Figure 3d for the hubless swirlers. Between exit and about 2.5 diameters no generalisation of the shape can be made, presumably due to the effects of high temperature and hence density gradients. Downstream of this region the rate of decay of the maximum axial velocity increases with swirl number.

6.2 Swirl velocity distribution

The swirl velocities are shown in Figures 4a-d for the annular swirlers and Figures 5a,b for the hubless swirlers. Beyond about 2.5 diameters the profiles of the swirl velocity indicate a central forced vortex core surrounded by an annular free vortex region. Closer to the swirler and at the higher swirl numbers the profile is distorted from the forced/free vortex pattern, the distortions becoming more severe as the swirler is approached. The distortion of the inlet profile due to changes in swirl number has been reported[6] in isothermal air jets and when the added complexity of combustion is present, the distortion can be expected to be more severe.

Where reverse flows are obtained, it is seen that within the reverse flow zones the swirl velocities are low, although within a short radial distance outside the reverse flow boundary the swirl velocity increases rapidly to its maximum value.

Figure 4e shows the variation of the ratio of maximum swirl velocity at a plane to the value at exit from the annular swirlers and Figure 5c gives the corresponding decay for the flame jets issuing from the hubless swirlers. In the region from about 1 diameter downstream the decay rate increases with the degree of swirl. It seems possible that at some distance downstream of the range of measurements the maximum swirl velocity will be independent of swirl. The region where this might occur however is not usually of great interest.

6.3 Static pressure distribution

The results for the annular swirlers are given in Figures 6a-d and for the hubless swirlers in Figures 7a,b. The static pressures are subatmospheric at the swirler exits and remain so throughout the lengths investigated for all swirlers. Close to the swirler exit the profiles show an off-centre maximum subatmospheric value and a minimum subatmospheric value on the axis. Moving downstream from the exit, the radial position of the maximum subatmospheric pressure may move outwards before tending towards the axis (45° and 60° swirlers, annular and hubless), or it may

approach the axis without first diverging (15°, annular and hubless). The 30° annular swirler followed the latter pattern while the 30° hubless swirler adopted the former pattern. The axial position where the maximum subatmospheric pressure reaches the axis depends on the swirl number. As swirl increases the position first moves away from the swirler and then appears to move back towards the swirler for the highest degree of swirl. For the 45° annular swirler which position occurs at about 2 d_2 downstream, while for the 45° hubless swirler the position is about 5 to 6 d_o downstream.

The rates of decay of the maximum subatmospheric pressure and of the pressure on the axis along the jet are shown in Figures 6e,f for the annular swirlers and Figures 7c,d for the hubless swirlers. In each case the rate of decay increases with the degree of swirl.

The positions of the maximum subatmospheric pressures on the axis in the 45° and 60° annular swirlers correspond with the positions of maximum reverse velocity (these were the only annular swirlers which produced significant recirculation).

For the annular swirlers, the positions of maximum reverse velocity with the 45° and 60° swirlers correspond with the positions of maximum subatmospheric pressure on the axis. For the hubless swirlers the experimental evidence is less definite - accurate velocity and pressure measurements in the recirculation region were very difficult.

6.4 Temperature distribution

As shown in Figures 8a-d and 9a,b the maximum temperature position near the swirler exit moves away from the axis with both the annular and hubless swirlers as the swirl number increases. For swirlers of vane angles higher than 15°, the spread of the jet causes a corresponding increase in the radial position of the peak temperature until the axial temperature is sufficiently high when the profiles become flat near the axis. Further downstream, the maximum temperature is recorded on the axis.

In Figures 8e and 8f are shown, for the annular swirlers, the variation of temperature rise on the axis and the peak temperature rise along the jet as ratios of the maximum flame temperature rise respectively. For the 15° and 30° swirlers, the temperatures on the axis increase in the region close to the exit before dropping off further downstream but the 30° and 60° swirlers show a continuous decrease. The distance downstream of the position of maximum temperature rise is greater for smaller swirl numbers. This indicates that as the swirl number increases the position of complete combustion moves towards the swirler thus confirming the shortening of the flame as the swirl number increases.

The variations of the temperature rise along the jets issuing from the hubless swirlers follow trends similar to those for the annular swirlers described above, though the reduction in temperature is less rapid at corresponding distances downstream.

7. Comparison of results with cold jets

It is interesting to compare the results with those observed in cold free jets issuing from similar vane swirlers[1]. Due to the difficulties in making accurate observations in the small diameter jets issuing from the hubless swirlers the comparison is drawn principally on the results obtained with the annular swirlers.

7.1 Annular swirlers

7.1.1 Axial-velocity distribution

Double humped distributions of the axial component of velocity are observed in both burning and cold jets close to the swirler. However, the trough in velocity at the axis disappears within a shorter distance in the burning jets. For example, with the 15° swirler the trough disappears at an axial distance of one diameter while in the cold jet the trough persists to an axial distance of at least 4 diameters.

The maximum axial velocity in the burning jets rises initially to roughly double (not constant, diminishes as swirl increases) the maximum axial velocity in the corresponding cold jets. The fractional decays in

the maximum axial velocity downstream from about one diameter are similar in both the burning and cold jets, the decay becoming more rapid as the swirl vane angle increases.

In both burning and cold jets, increasing the swirl results in the establishment of central recirculation zones. However, the critical degree of swirl required in burning jets is slightly higher. At corresponding degrees of swirl the central recirculation zones are shorter and wider. This widening is to be expected due to the density change resulting from combustion. The extents of the recirculations in the burning and cold jets are given in Table 2. The table also shows the magnitudes and locations of the maximum reverse velocities and maximum reverse mass flows. It is seen that the magnitudes of the reverse mass flows in the burning jets are much lower than in the corresponding cold jets. In the cold jets the ratio of the maximum reverse flow to the nozzle flow had been found to be roughly proportional to $\tan^2\theta$. However in the burning jets the maximum reverse flow varies even more rapidly with swirl.

The position of the maximum reverse velocity in the burning jet appears to move downstream from 0.5 d_2 to 1.5 d_2 as the vane angle is increased from 45° to 60°, whereas in the cold jet the position was independent of swirl vane angle, occurring at one diameter.

7.1.2 Tangential-velocity distributions

In both the burning and cold jets the rate of decay of the tangential component of velocity increases as the swirl vane angle increases, the decays in the hot jets being slightly more rapid.

7.1.3 Variations of jet width

The jet width is defined here by the line where the axial component of velocity is 10% of the maximum axial component of velocity at that plane.

In cold jets it was observed that there was an initial very rapid opening out of the jet. This initial rate of expansion increased with swirl vane angle. After the initial rapid opening the expansion rate reduced to a value which was almost constant and independent of vane angle.

TABLE 2. Central Recirculations in Burning and Cold Swirling Jets - Annular Swirlers.

Swirler Vane Angle	Jet	Downstream limit of recirculating zone	Width of recirculating zone	Max. reverse vel. / Nozzle vel.	Position of max. reverse vel.	Max. reverse flow / Nozzle flow	Position of max. reverse flow	Max. reverse flow / Nozzle flow x $\tan^2\theta$
15°	Burning) Cold)	Negligible						
30°	Burning) Cold)	Negligible						
45°	Burning	2.0 d_2	0.83 d_2	0.5	0.5 d_2	0.005	1.0 d_2	0.005
	Cold	3.7 d_2	0.51 d_2	0.35	1.0 d_2	~~0.001~~ 0.04	1.0 d_2	0.04
60°	Burning	3.0 d_2	1.8 d_2	0.7	1.5 d_2	0.06	1.5 d_2	0.02
	Cold	5.0 d_2	0.65 d_2	0.77	1.0 d_2	0.16	1.0 d_2	0.05

In the burning jets the initial spread for a given swirler is even more rapid than for the cold jets. Thereafter the rate of expansion drops (Figure 10). At the higher degrees of swirl the rate of expansion drops to a value which is less than the expansion rate of the cold jet. Thus ultimately, burning and cold jets will have the same widths. With the 60° swirler (illustrated in Figure 11) it would appear from extrapolation that the widths of the hot and cold jets will be equal at a downstream distance of roughly 8 d_2. At lower degrees of swirl the plane where the burning and cold jet widths merge will be much further downstream.

The initial widening of the burning jet relative to the cold jet is due to the density change resulting from combustion. It might be expected that the development in the early stages will be rather similar to the development in a cold jet, issuing from the same vane swirler, which has already opened out to a flow area to accommodate the density ratio due to combustion, namely 5.4. Thus for the 60° swirler (Figure 10) the plane in the cold jet one diameter downstream from the swirler exit might correspond to the commencement of the burning jet. It can be seen that widths of the burning jet in the region from say 0.5 d_2 to 4 d_2 correspond roughly with the widths of the cold jet in the region from 1.5 d_2 to 5 d_2. Beyond about 4 d_2 in this burning jet the density change due to combustion is effectively reduced by the entrainment of the cold air, and the jet width becomes diminishingly greater than the width of the cold jet at the same axial distance. The recirculation zone is seen to be shortened by combustion but with this 60° swirler the shortening is greater, by a factor of 2, than the suggested displacement of one diameter required to make the early stages of the outer boundaries similar for the burning and cold jets.

7.1.4 Exoerimental swirl numbers

Integrations of the momentum flux profiles indicate that the tangential momentum fluxes in the burning jets are about double the tangential momentum fluxes observed in cold jets with the same feed velocity. The axial momentum fluxes (ignoring the static pressure terms) are also considerably increased. These increases are associated with the higher pressure required of the gas/air supply system to overcome the effective "flame" pressure. This flame pressure is significant in spite of the burning jet being unenclosed.

The static pressure term which should be included in the axial momentum flux can amount to up to 70% (60° Swirler) of the "velocity" term and therefore should be included in the definition of swirl number.

7.2 Hubless Swirlers

The effects of combustion on the distributions of axial velocity, swirl velocity and pressure in jets issuing from hubless vane swirlers are similar to those noted above in jets issuing from annular vane swirlers, with the notable exception that the recirculation zone does not appear to be shortened. Due to difficulties in measuring velocities in the small diameter recirculation zones it is not possible however to be explicit about the positions of the maximum reverse velocities and flows in the zone.

8. Prediction of flow distribution

The theoretical analysis discussed below is based on the finite difference prediction method formulated by Spalding et al. The prediction method will therefore not be discussed fully but further information about the derivation and simplification can be obtained from references 7 and 8.

Defining vorticity as

$$\omega = \frac{\partial v}{\partial x} - \frac{\partial u}{\partial r} \qquad \ldots.(8.1)$$

and stream function as

$$r \rho u = r \pi_x = \frac{\partial \psi}{\partial r} \qquad \ldots.(8.2a)$$

$$r \rho v = r \pi_r = - \frac{\partial \psi}{\partial x} \qquad \ldots.(8.2b)$$

second order partial differential equations of the elliptic type can be written for vorticity, stream function, swirl velocity, W, and when there is combustion, similar equations can be written for fuel mass fraction, enthalpy and mixture fraction defined as

$$m_f = \text{mixture fraction} = \left(m_{fu} - \frac{m_{ox}}{STC} \right) \qquad \ldots(8.3)$$

These equations are derived from considerations of the conservation of chemical species, momentum in the x, r and θ directions, and mass. The general form of the elliptic equation is

$$a \bar{\pi} \cdot \text{grad } \varphi = \text{Div } \left[b \text{ Grad } (C\varphi) \right] + d. \qquad \ldots.(8.4)$$

where the coefficients a, b, c and d for each dependent variable are shown in Table 3.

By dividing the flow field into a number of control volumes and integrating the above equations over each control volume taking account of the direction of flow, finite difference forms of the equations were obtained. For the solution of the finite difference equations, a multi-purpose computer program was written by Spalding et al and this

TABLE 3 Relations for a, b, c, d of equation 8.4.

φ	a	b	c	d
$\frac{\omega}{r}$	1	1	μ_{eff}	$\frac{1}{r}\left[2\,\mu_{eff}\,\frac{\partial}{\partial r}\left(\frac{\omega}{r}\right) - \text{Grad}\left(\frac{V_s^2}{2}\right) \cdot \text{Iso}\,\rho + \frac{\partial}{\partial x}\left(\frac{\rho W^2}{r}\right)\right]$
ψ	0	$\frac{1}{r^2}$	1	$\rho\left(\frac{\omega}{r}\right) - \frac{1}{r^2\rho}\left[v\,\frac{\partial \rho}{\partial x} - u\,\frac{\partial \rho}{\partial r}\right]$
W	1	μ_{eff}	1	$-\frac{V_\theta}{r}\left[\pi_r + \frac{\mu_{eff}}{r} + \frac{\partial\,\mu_{eff}}{\partial r}\right]$
m_{fu}	1	$\Gamma_{fu,eff}$	1	$-K\,m_{fu}\,m_{ox}\,\rho^2\,\sqrt{T}\,e^{-\frac{E}{\bar{R}T}}$
h	1	Γ_{eff}	1	0
$\dot{m}_f$	1	Γ_{eff}	1	0

programme can be modified for the analysis of various flow conditions, e.g. [8]. This programme was modified for the present computation and for processing in a KDF9 and in a UNIVAC 1108 computer.

8.1 Details of Computation

The equations for vorticity, stream function, swirl velocity, fuel mass fraction and enthalpy were considered with a 16 x 14 non-uniform grid system. The inlet profiles of the vorticity, stream function and swirl velocity were derived from the assumed distribution of the axial components. The swirl velocity was calculated from the equation

$$w = u \tan \theta \qquad \ldots(8.5)$$

The distribution of the enthalpy was taken as uniform at the ~~exit~~ inlet and, for the present analysis, arbitrary values of the distribution of fuel mass fraction were specified. The analysis has been carried for an annular swirler having a vane angle of 15°. A similar analysis has been carried out for a cold jet issuing from a 45° annular swirler but the results are not shown because of limitation of space. The specification of the axial velocity components at inlet gives a triangular profile with a maximum value of 80 ft/sec at the mid-point of the annular flow section. The computation was stopped when the fractional difference between two successive iterations is 0.005.

The boundary conditions are shown in Figures 12 (a) and (b)

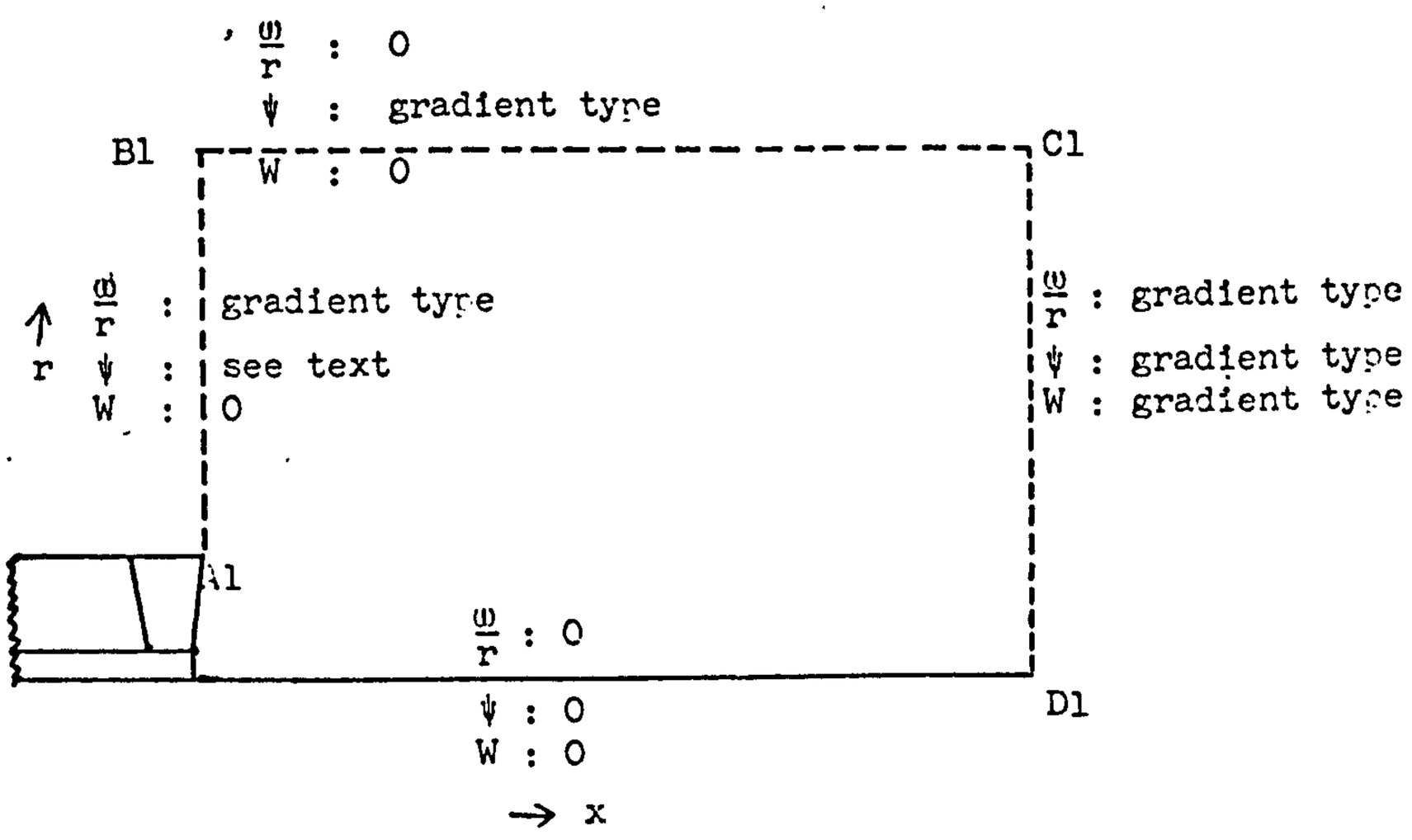

Fig. 12a Boundary conditions for isothermal free swirling flow.

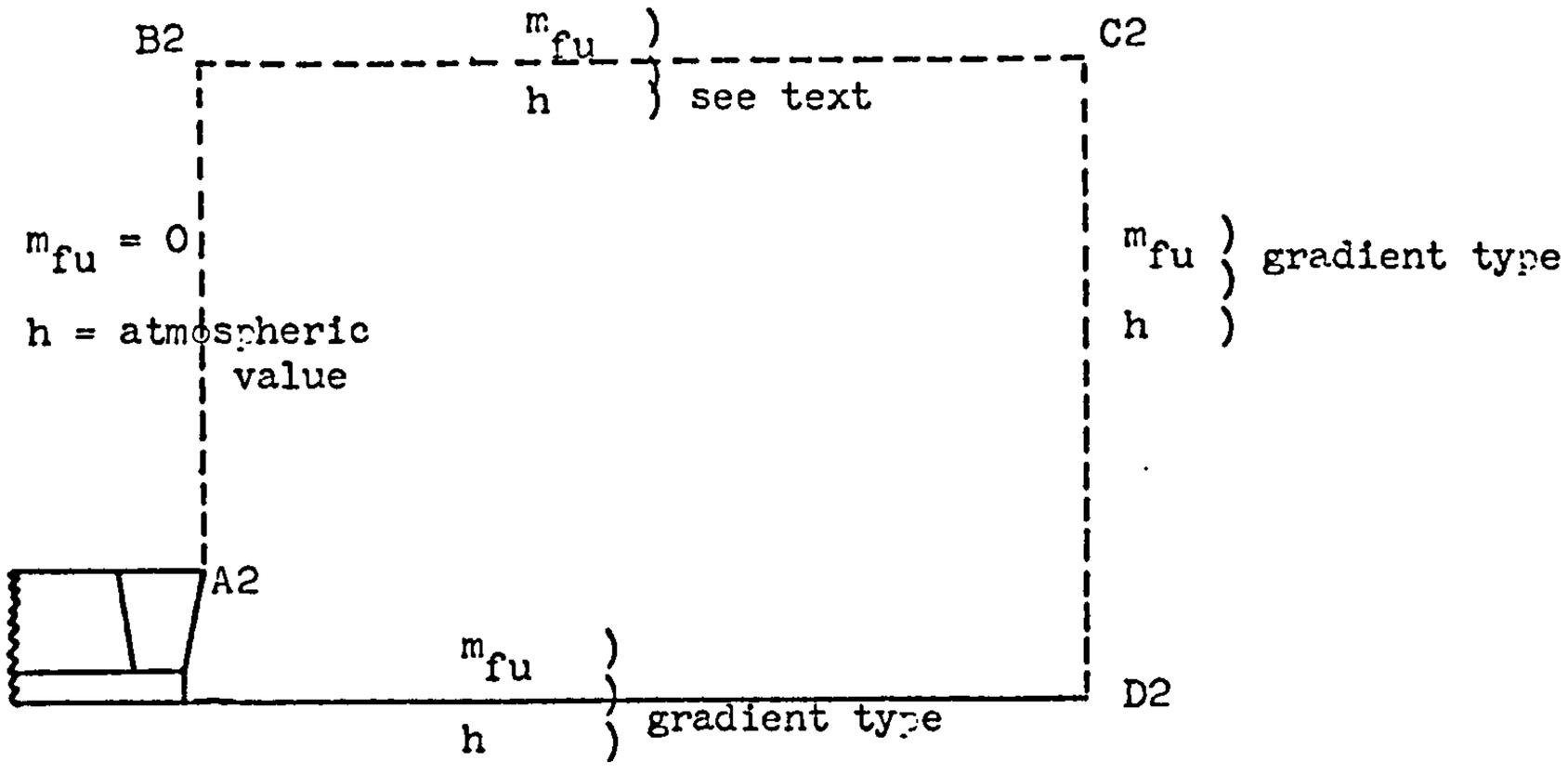

Fig. 12b Boundary conditions for combustion variables.

At the boundary B2, C2, the gradient type of boundary conditions was used except at the first few grid points where atmospheric values were taken.

8.2 Results

The predicted cold results for the 15° annular swirler are shown in Figure 13 (a) and (b). The results are compared with the experimental results in (1). It will be seen that the predictions show the general features, e.g. free and forced vortex regions, in a swirling jet and also compares favourably with experimental results.

Using the assumptions discussed in Section 8.1, the predicted results for the burning jet (f/a 0.24 by volume) are shown in Figures 14 (a) - (c). Work is continuing on the computational procedure for burning jets.

9. Conclusions

When combustion takes place in a swirling flow, the general shapes of the profiles of the aerodynamic variables remain similar to those for a cold flow although there are significant differences between the rates of change of the variables along and across the flow field, as a result of the density gradients. For both cold and burning swirling flows, the rate of change of the variables is strongly dependent on the swirl number.

For swirlers with vane angles of 45° and over, recirculation zones were observed, as in the cold jets (recirculation was also observed with the 30° hubless swirler). With the annular swirlers the recirculation zones were shorter and wider than those observed in the cold jets, while with the hubless swirlers the recirculation zones were of similar length but wider. In annular swirlers the position of the maximum reverse velocity, which was found to be constant for all swirlers with recirculation zones in cold flow, depends on the swirl number. It moves downstream as the reverse flow zone gets wider and longer with increasing swirl number.

The initial rate of expansion of a burning jet is higher than for a cold jet. The rate of expansion is slowed down further downstream by the entrainment of ambient field and at a position far away from the swirler exit, the width of a burning and cold jet can be expected to correspond. This position will depend on the swirl number and it can be expected to increase with reduction in swirl number since rate of entrainment increases with swirl number.

As the swirl number increases, the position of the maximum flame temperature from the swirler exit decreases and there is a shortening of the length of the flame.

The prediction method indicates the general pattern of the profiles in a swirling flow. The results however depend strongly on the velocity distribution and the boundary conditions.

10. Acknowledgements.

The authors wish to thank Professor R.S. Silver for his advice and encouragement. The contribution of all those connected with the construction of the test rig is gratefully acknowledged. G.G. Bafuwa expresses his gratitude to the Commonwealth Scholarship Commission in the United Kingdom.

11. References

1. MATHUR, M.L. and MACCALLUM, N.R.L., Swirling air jets issuing from vane swirlers. Pt. 1: Free Jets. J. Inst. Fuel, May 1967, 40, 214 to 225.

2. KERR, N.M. and FRASER, D., Swirl. Pt. 1: Effect on axisymmetrical turbulent jets. J. Inst. Fuel, Dec. 1965, 38, 519 to 526.

3. HIETT, G.F. and POWELL, G.E. Three dimensional probe for investigation of flow patterns. The Engineer, 1962, 213, 165 to 170.

4. MILLER, D.R. and COMINGS E.W. Static pressure distribution in free turbulent jets. J. Fluid Mechanics, 1957-58, 3, 1 to 16.

5. KERR, N.M. An aerodynamic study of swirling jets and flames. Ph.D. Thesis, Glasgow University, May 1965.

6. CHIGIER, N.A. and BEER, J.M. Velocity and static pressure distribution in swirling air jets issuing from annular and divergent nozzles. International Flame Research Foundation, Doc. no. K20/A/12, Nov. 1963.

7. GOSMAN, A.D., PUN, W.M., RUNCHAL, A.K., SPALDING, D.B., WOLFSHTEIN, M.W., Heat and Mass transfer in recirculating flows. Imperial College of Sc. and Techn. London, SC/R/3, Oct. 1968.

8. ODLOZINSKI, G. A procedure for predicting the distribution of velocity and temperature distribution in a flame stabilized behind a bluff-body. Imperial College of Sc. and Techn. London EF/R/G/2, Oct. 1968.

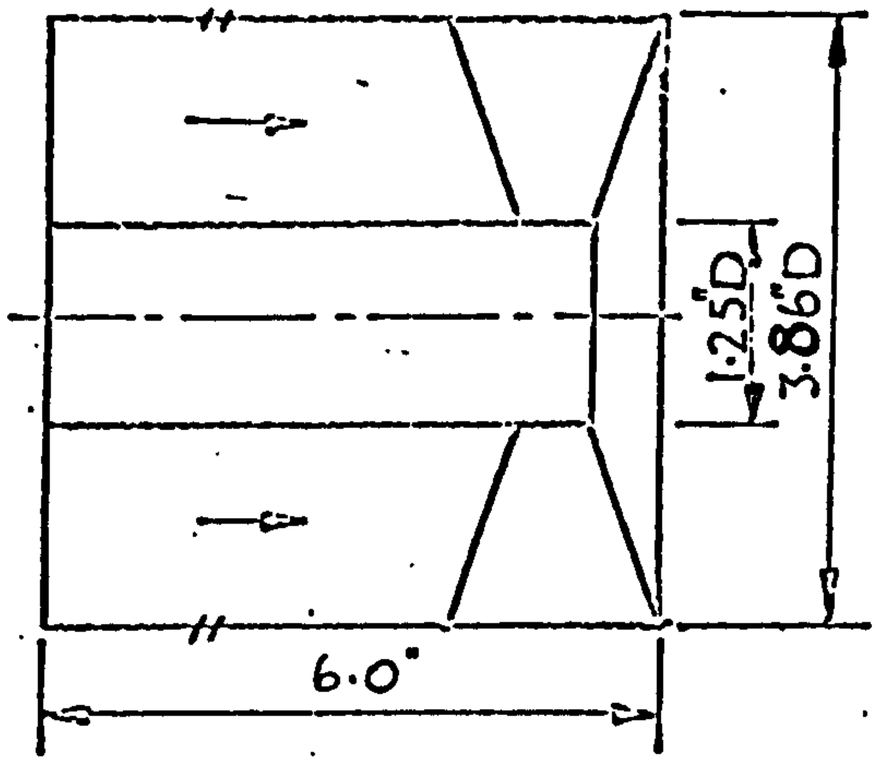

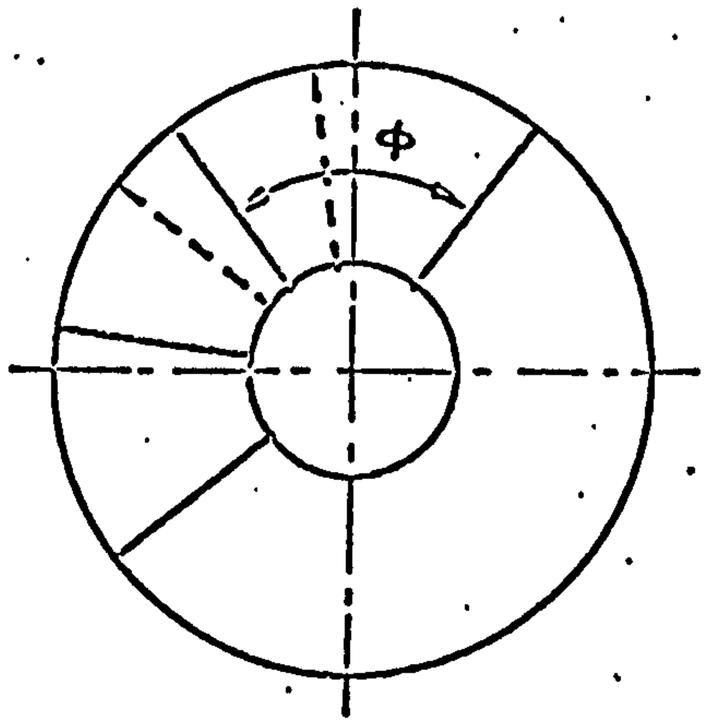

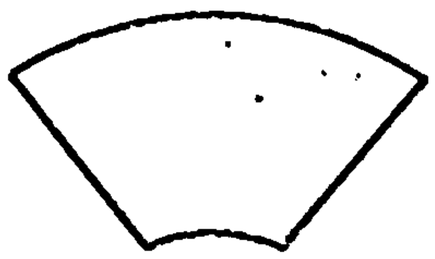

True shape of 60° vane.

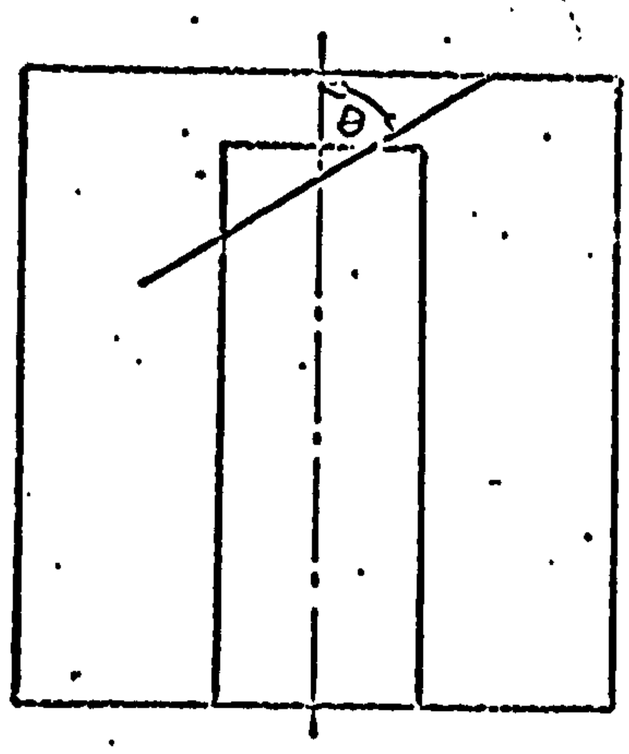

FIGURE 1 Annular Vane Swirler

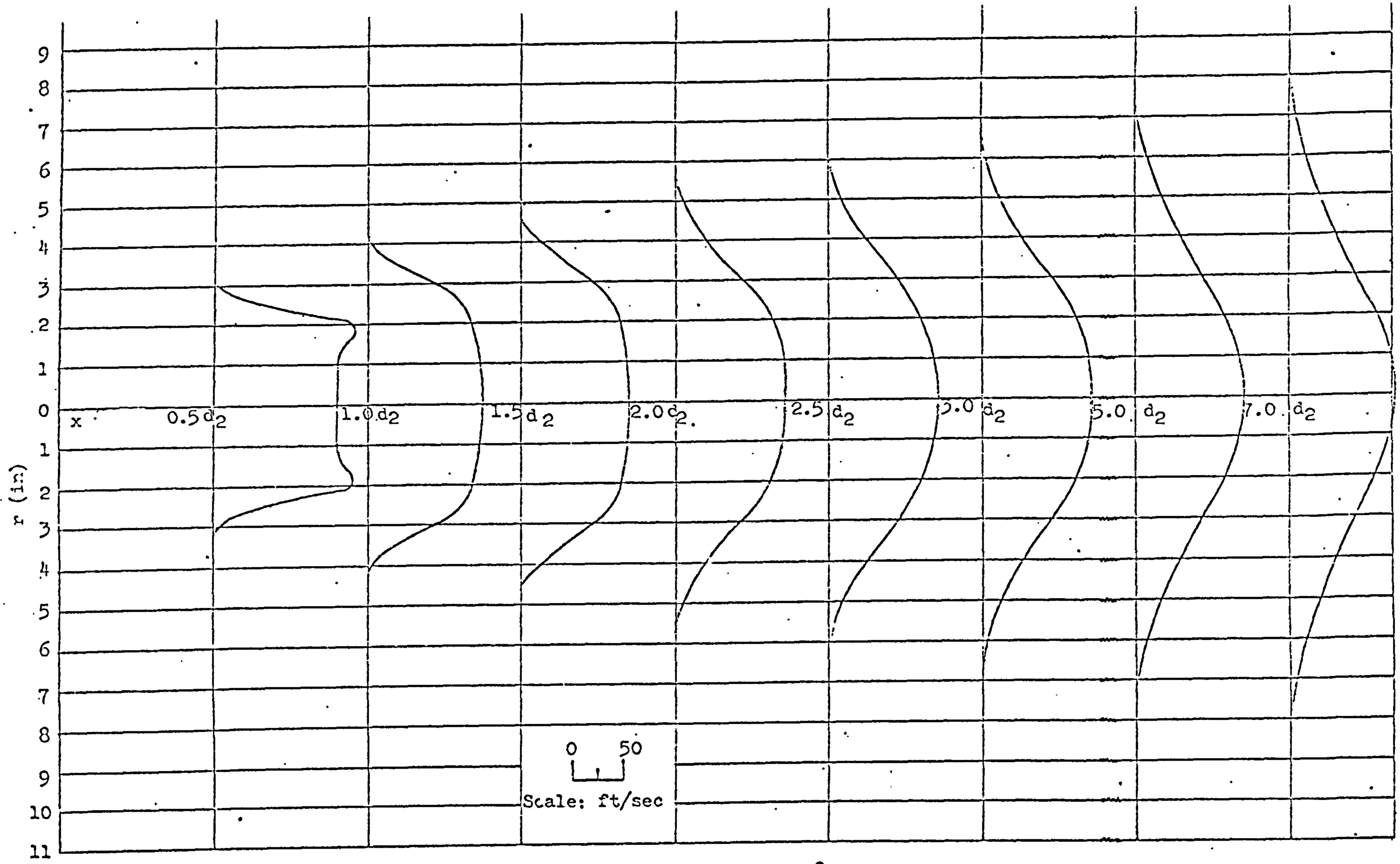

FIGURE 22 Radial distribution of axial velocity for 15° Annular Swirler

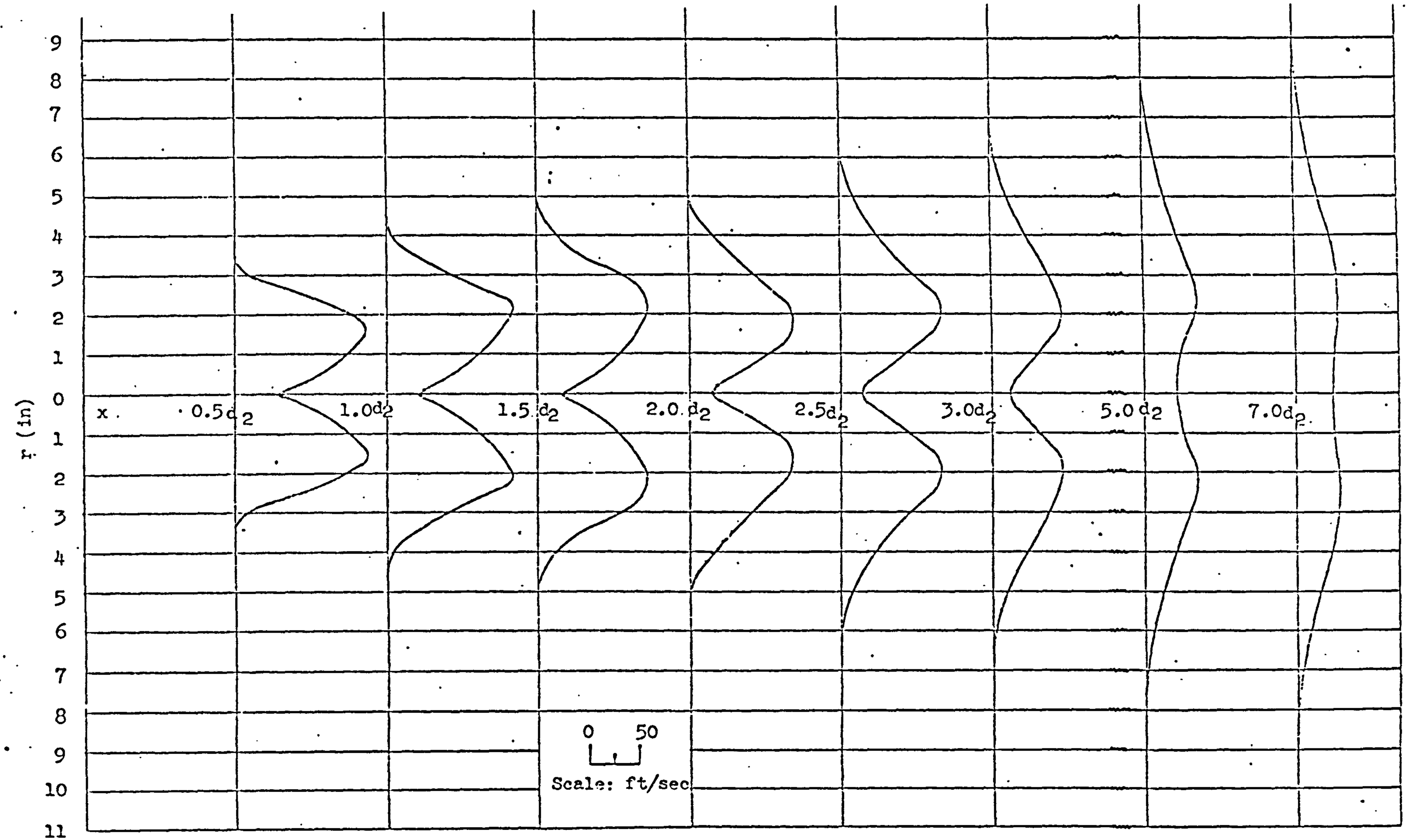

FIGURE 2b Radial distribution of axial velocity for 30° Annular Swirler

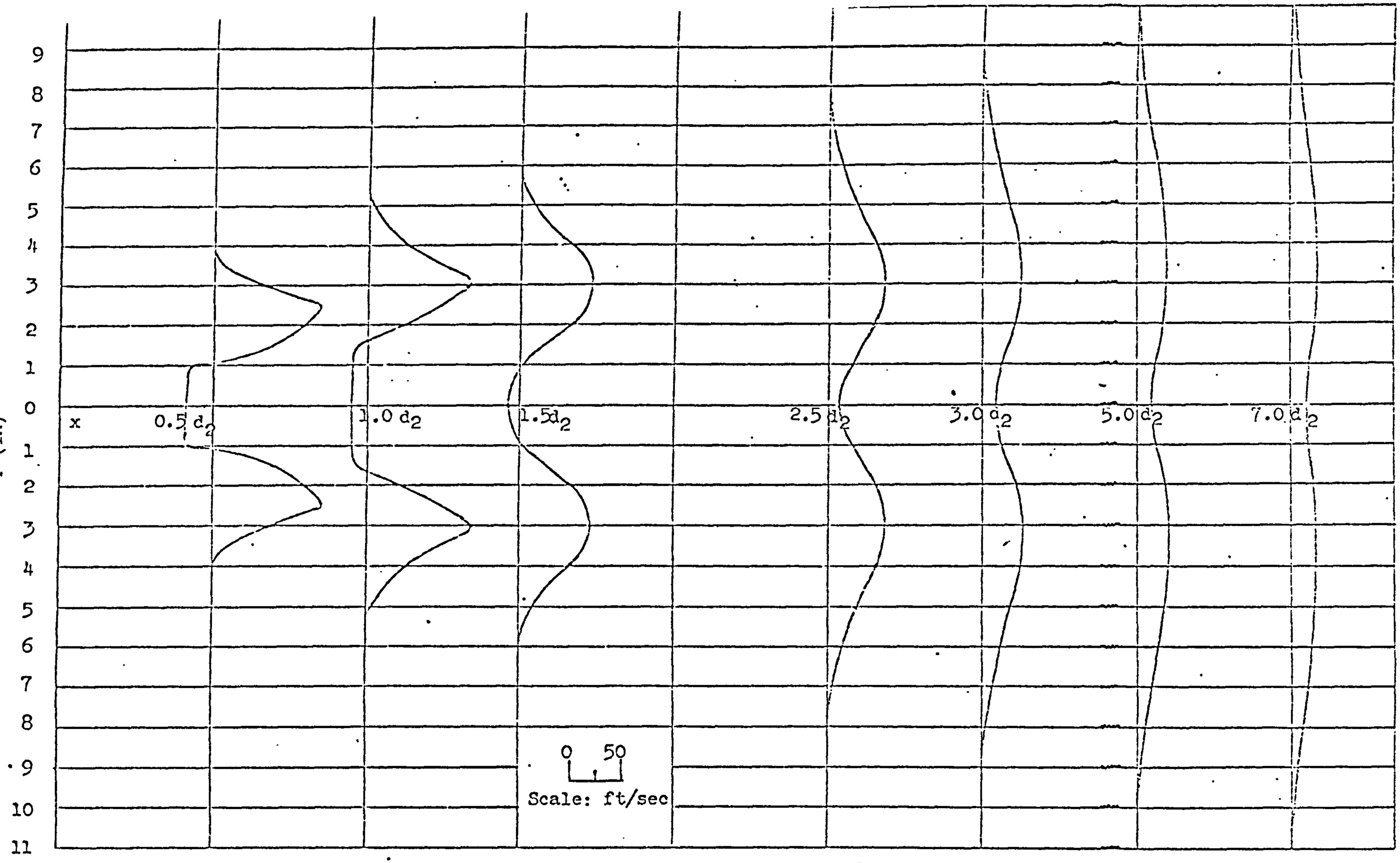

FIGURE 2c Radial distribution of axial velocity for 45° Annular Swirler

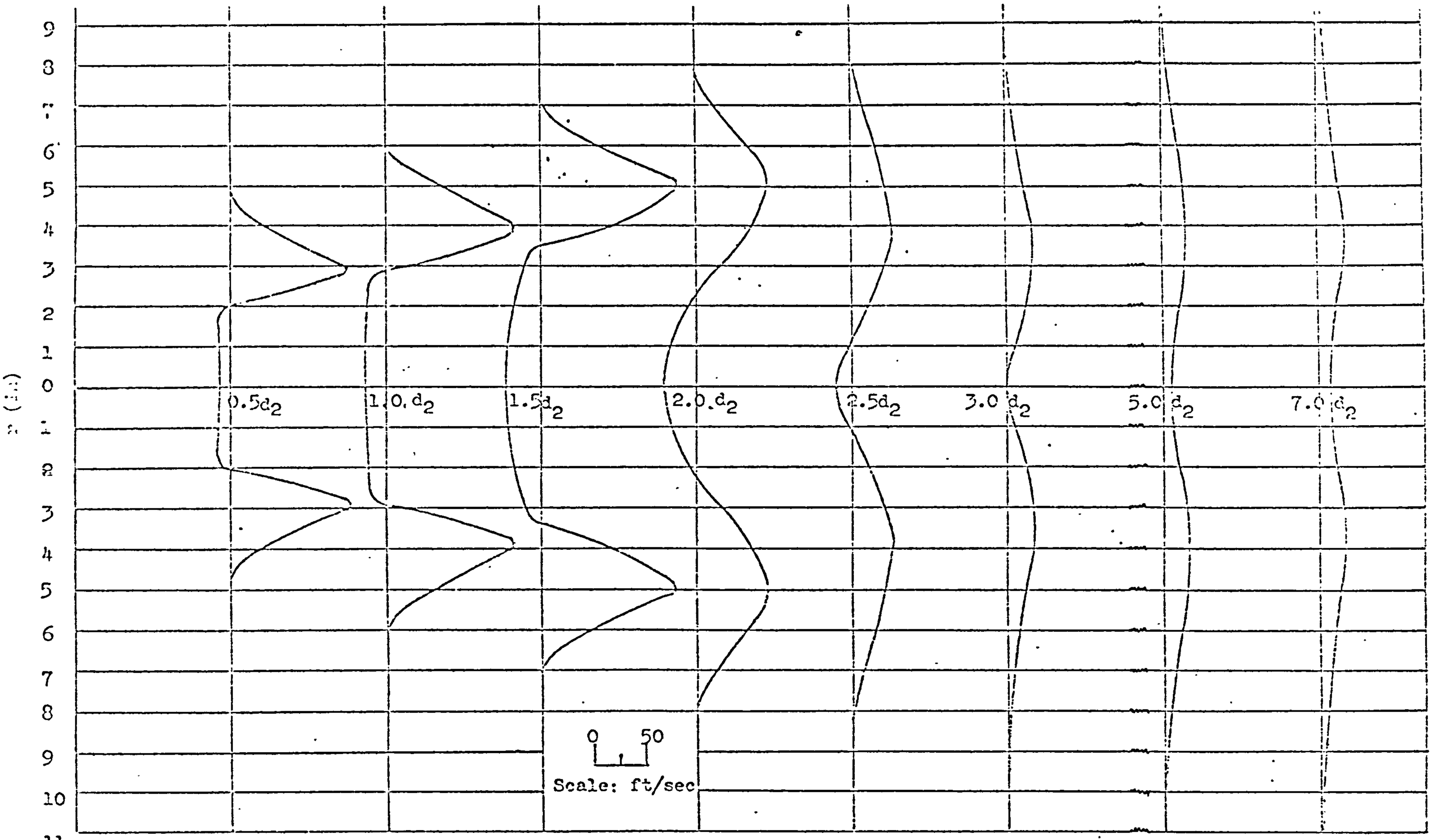

FIGURE 2d Radial distribution of axial velocity for 60° Annular Swirler

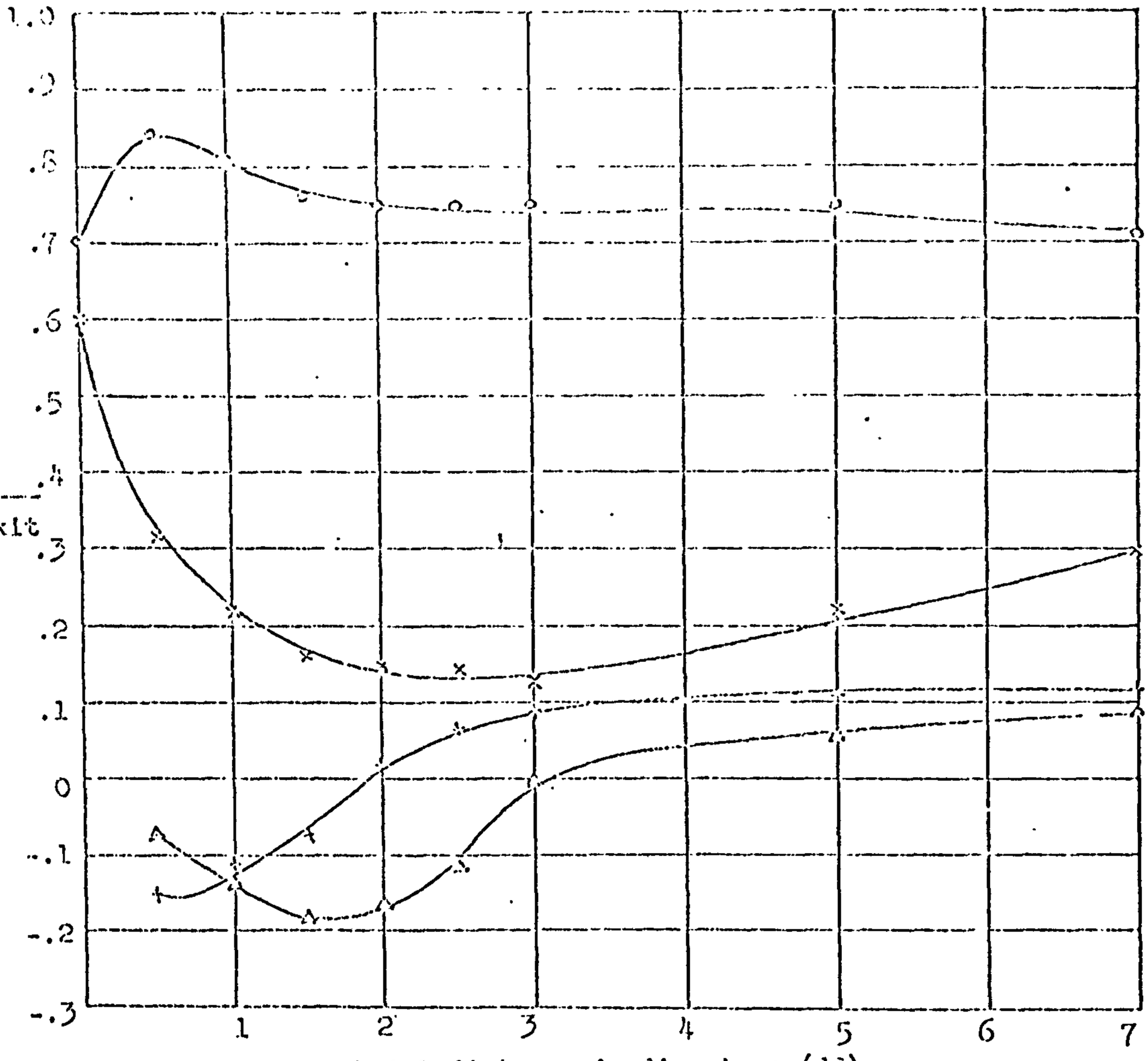

FIGURE 2e Annular Swirlers: Decay of axial velocity along jet axis

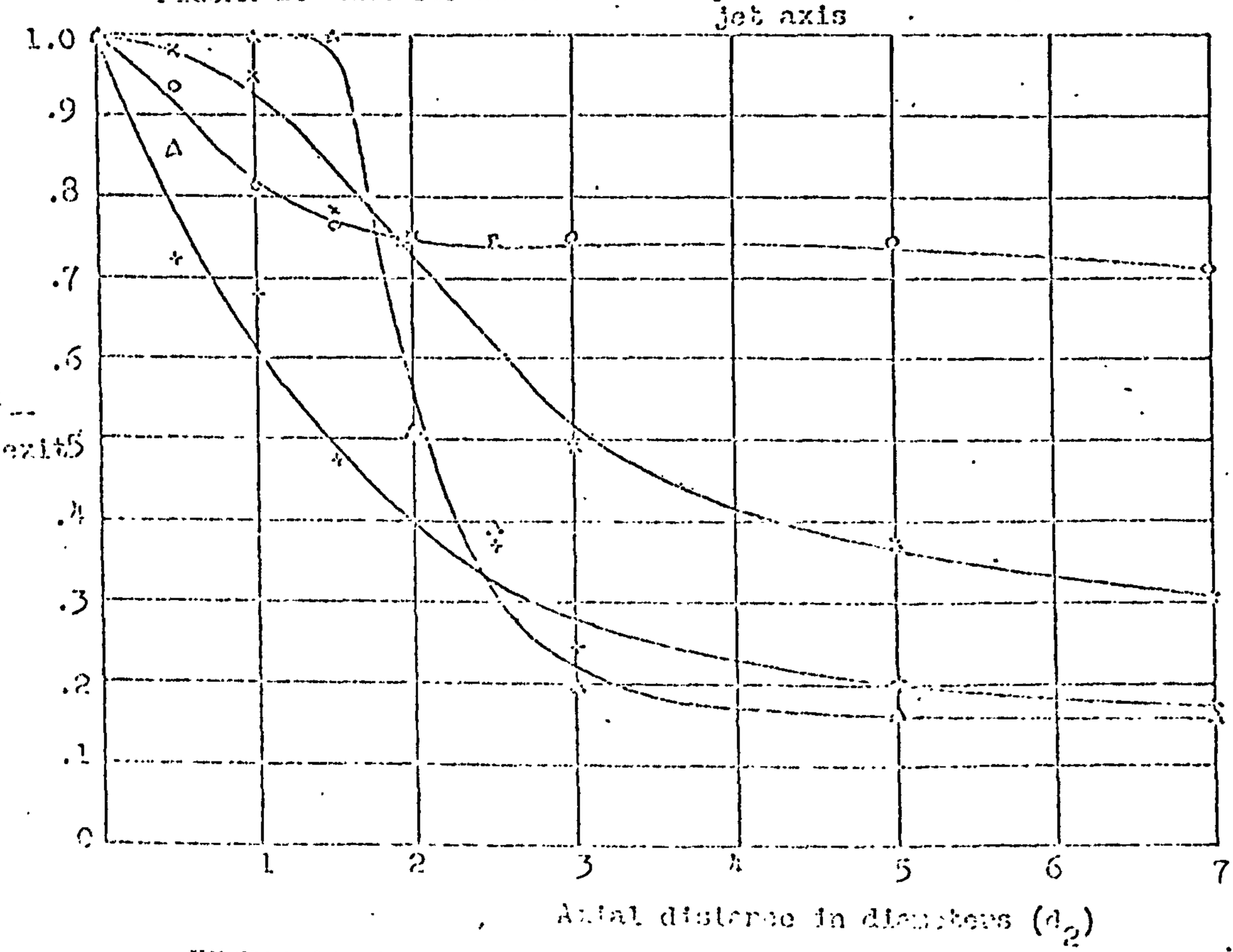

FIGURE 2f Annular Swirlers: Decay of maximum axial velocity along the je

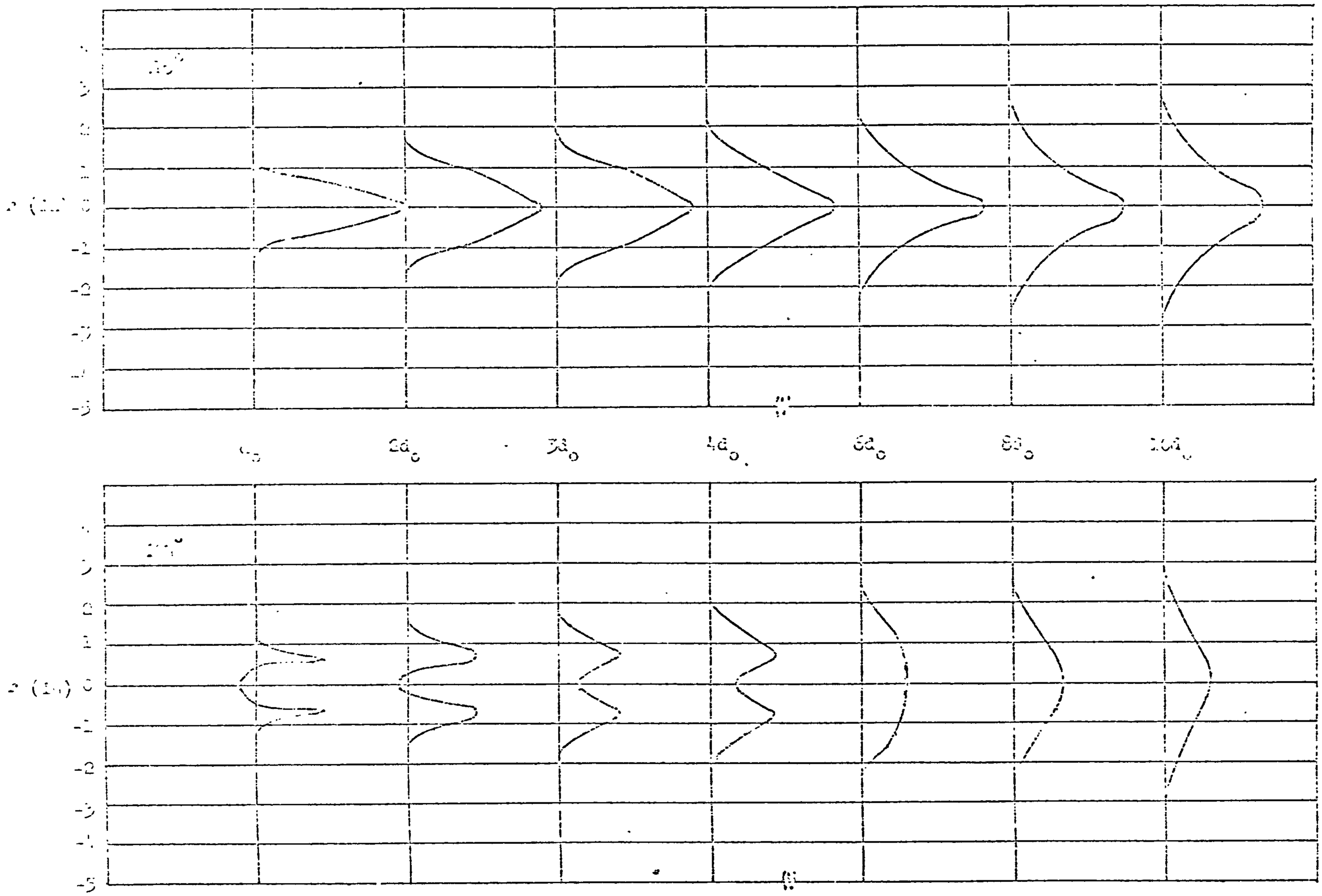

FIGURE 3a Radial distribution of axial velocity for 15° and 30° Hubless Swirlers

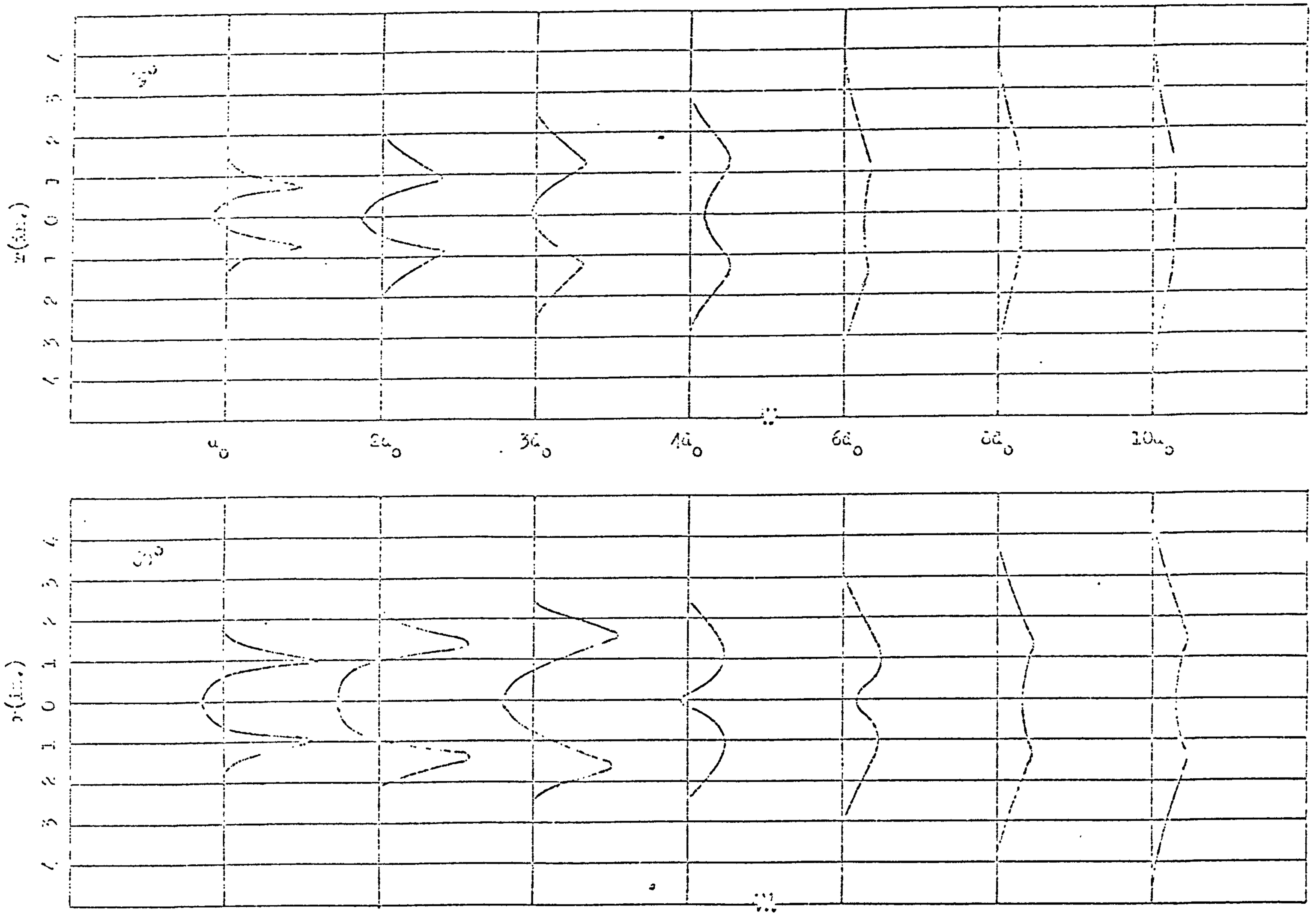

Figure 5c. Radial distribution of axial velocity for 45° and 60° Bubless Swirlers

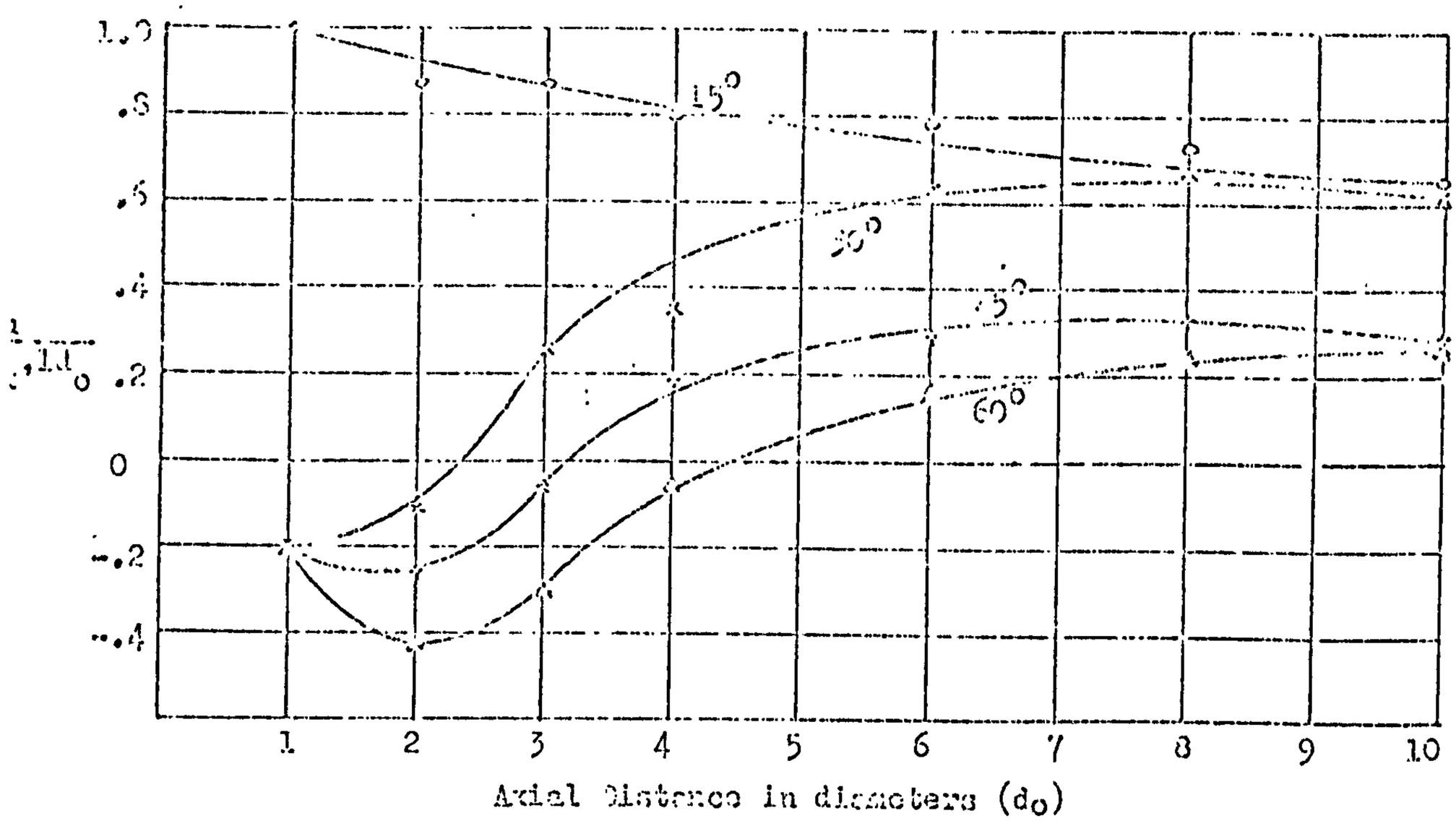

Figure 3c. Hubless Swirlers: Decay of axial velocity along the jet axis

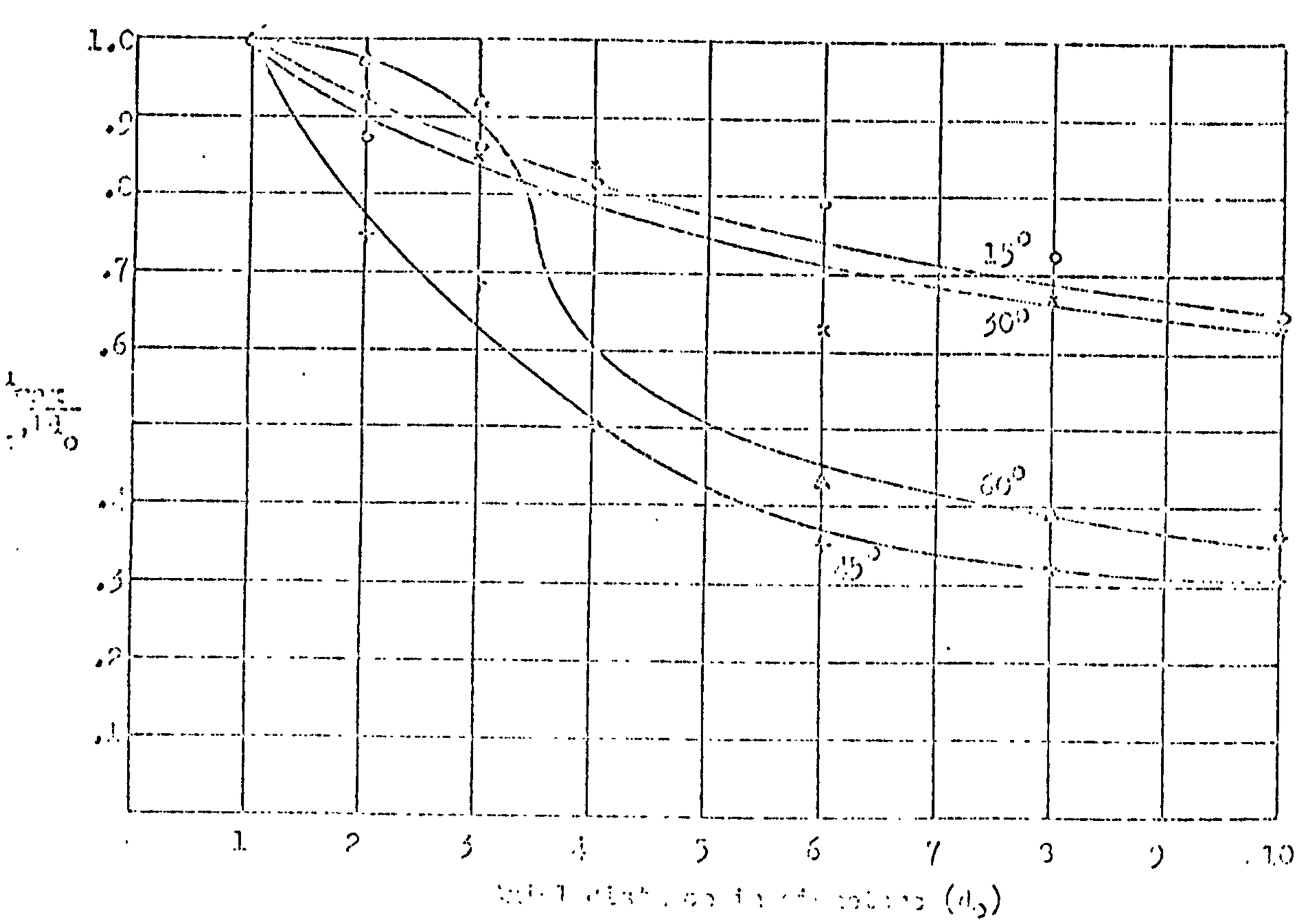

Figure 3d. [illegible]

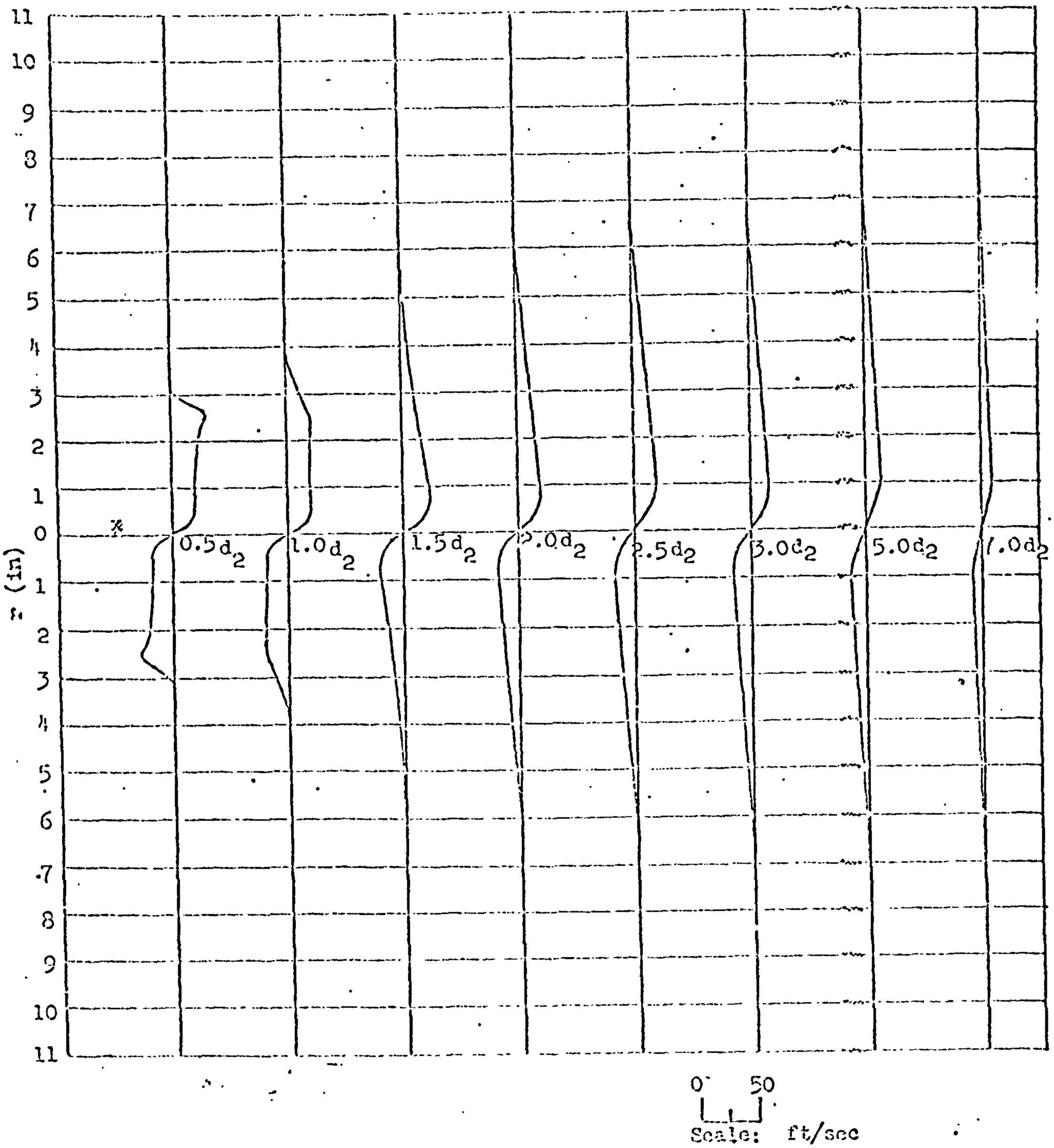

FIGURE 4: Radial distribution of swirl velocity for 15° inlet Guide

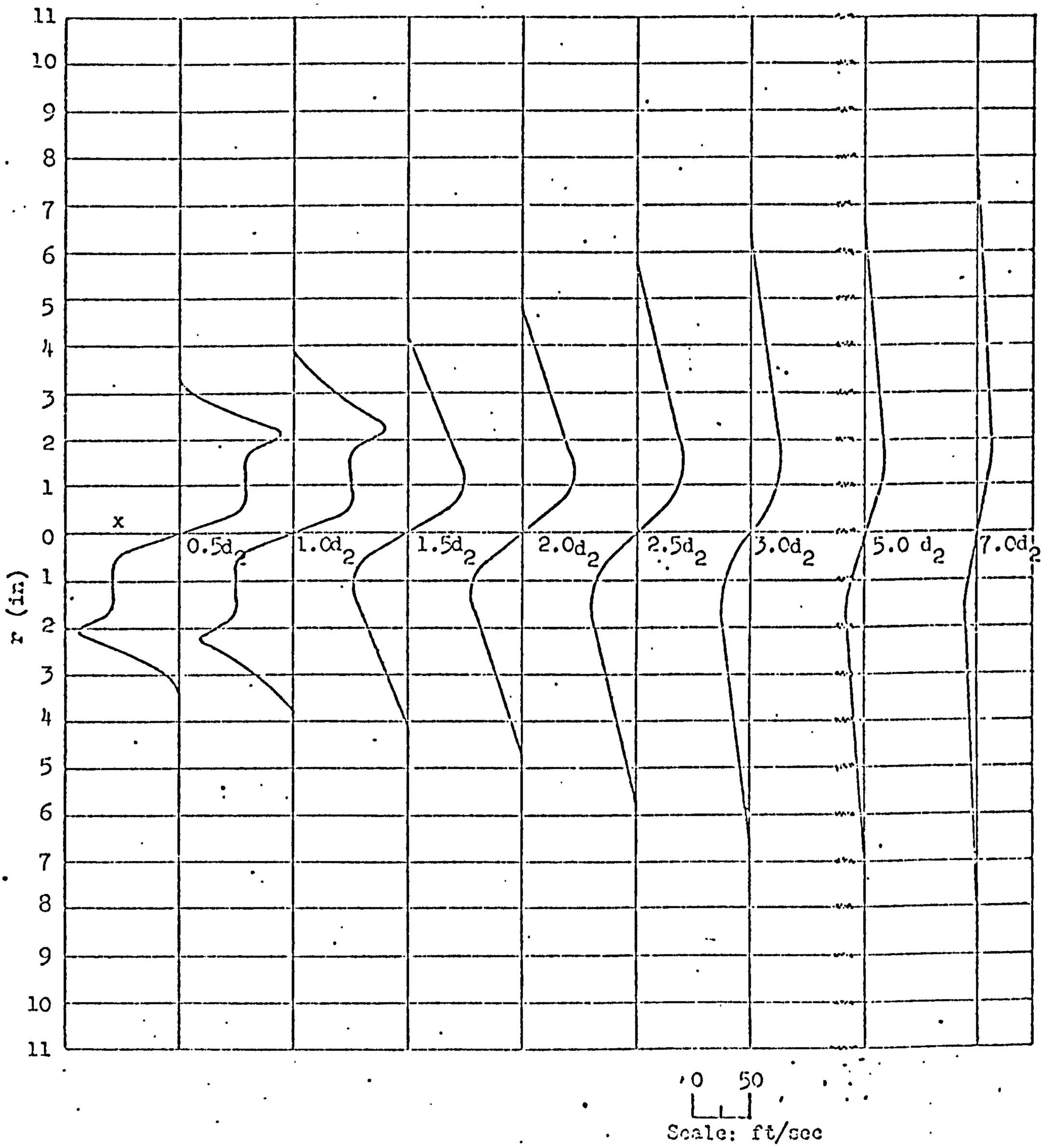

FIGURE 4b Radial distribution of swirl velocity for 30° Annular Swirler

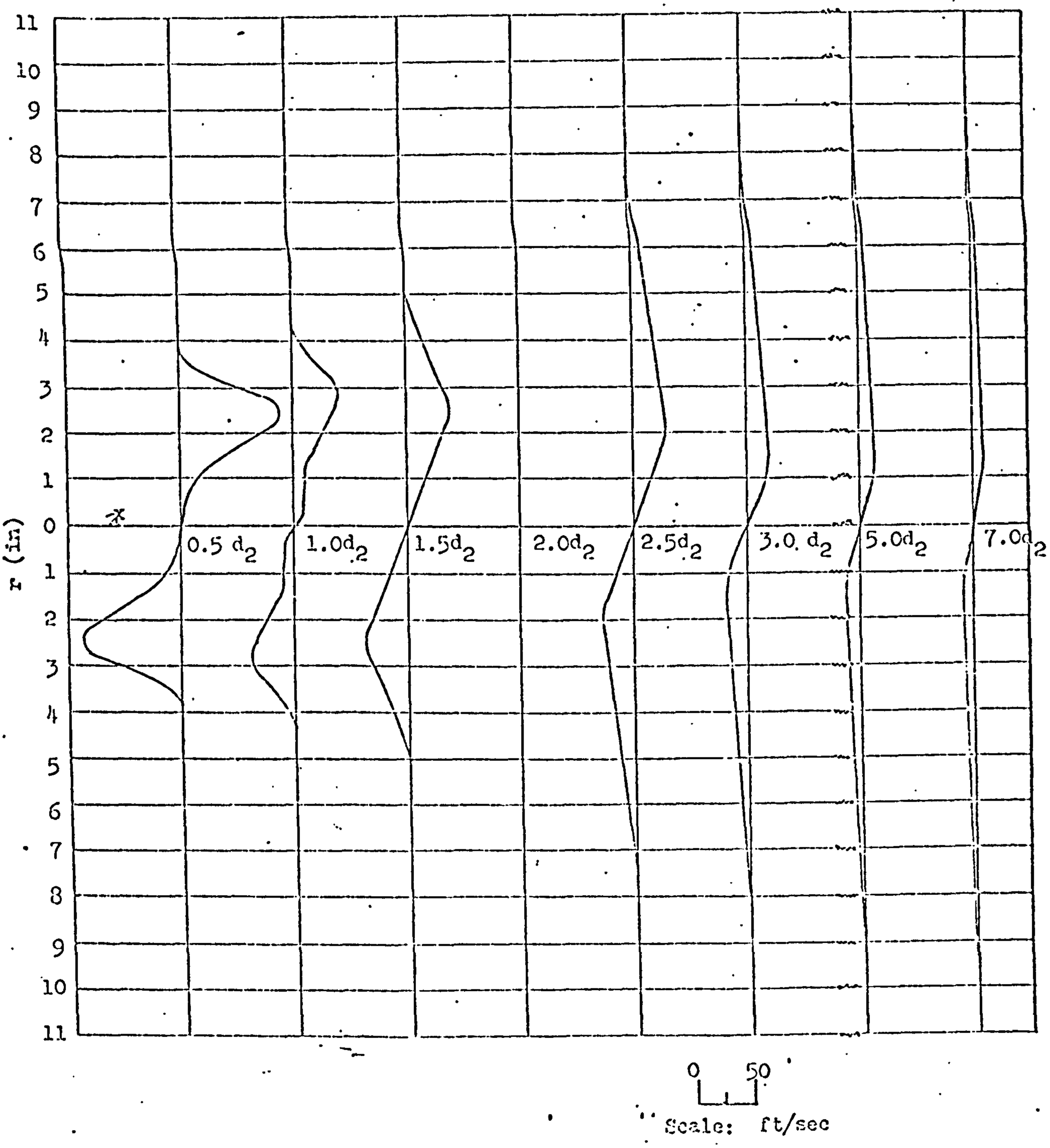

FIGURE 4c Radial distribution of swirl velocity for 45° Annular Swirler

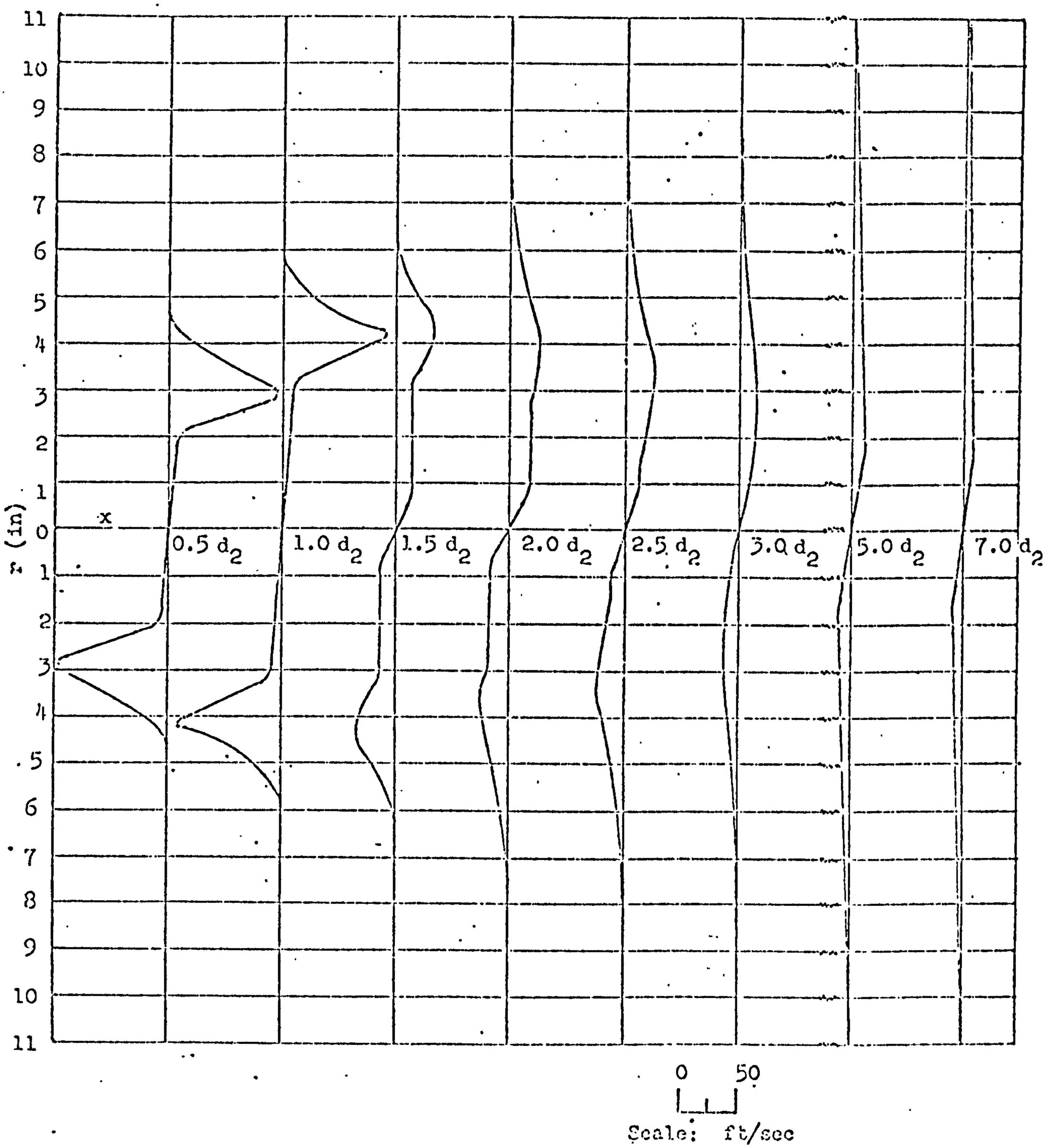

FIGURE 4d Radial distribution of swirl velocity for 60° Annular Swirler

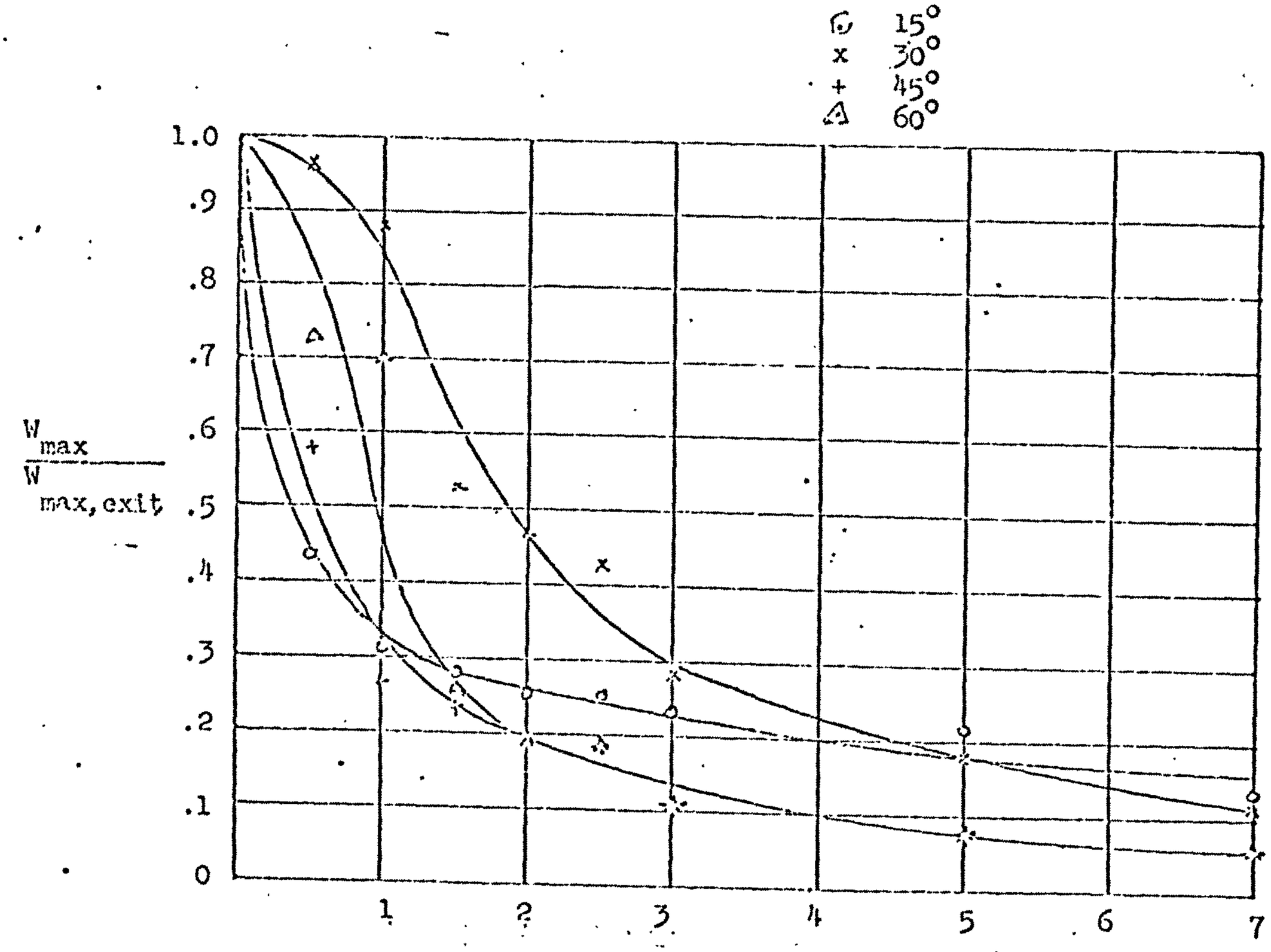

Figure No. Annular swirlers: Decay of maximum axial velocity along the jet.

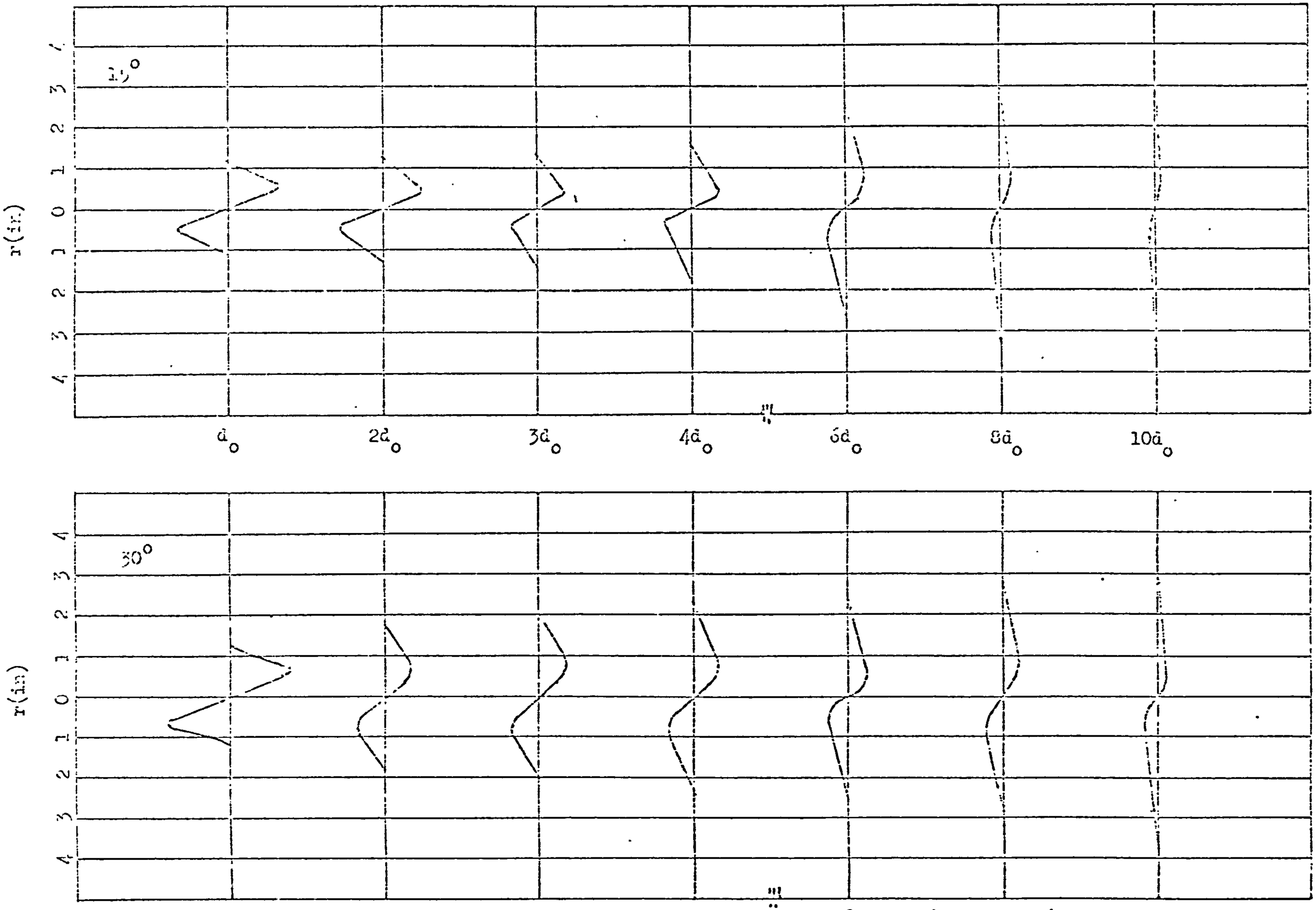

Figure 5a. Radial distribution of swirl velocity for 15° and 30° Hubless Swirlers

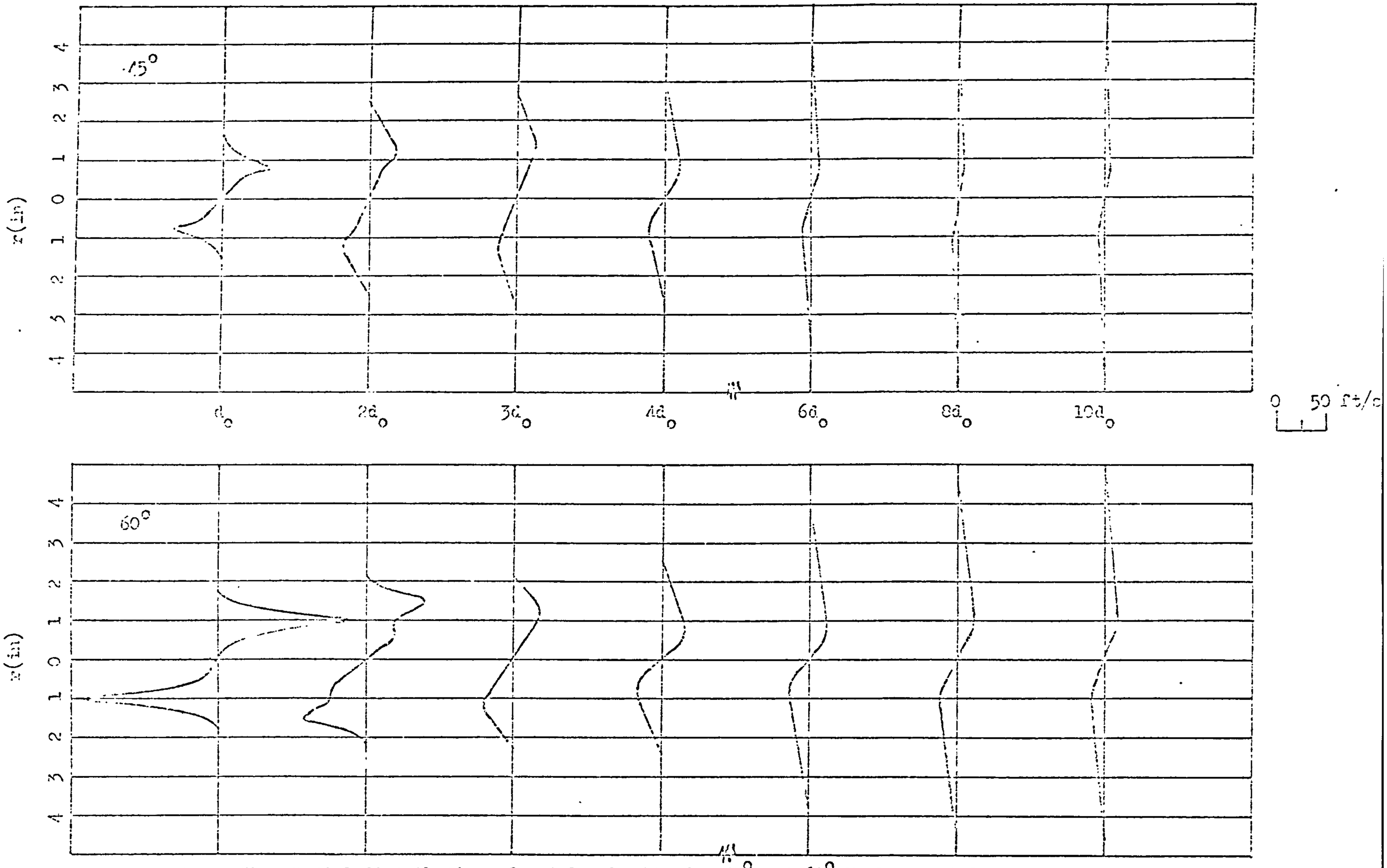

Figure 5b. Radial distribution of swirl velocity for 45° and 60° Hubless Swirlers

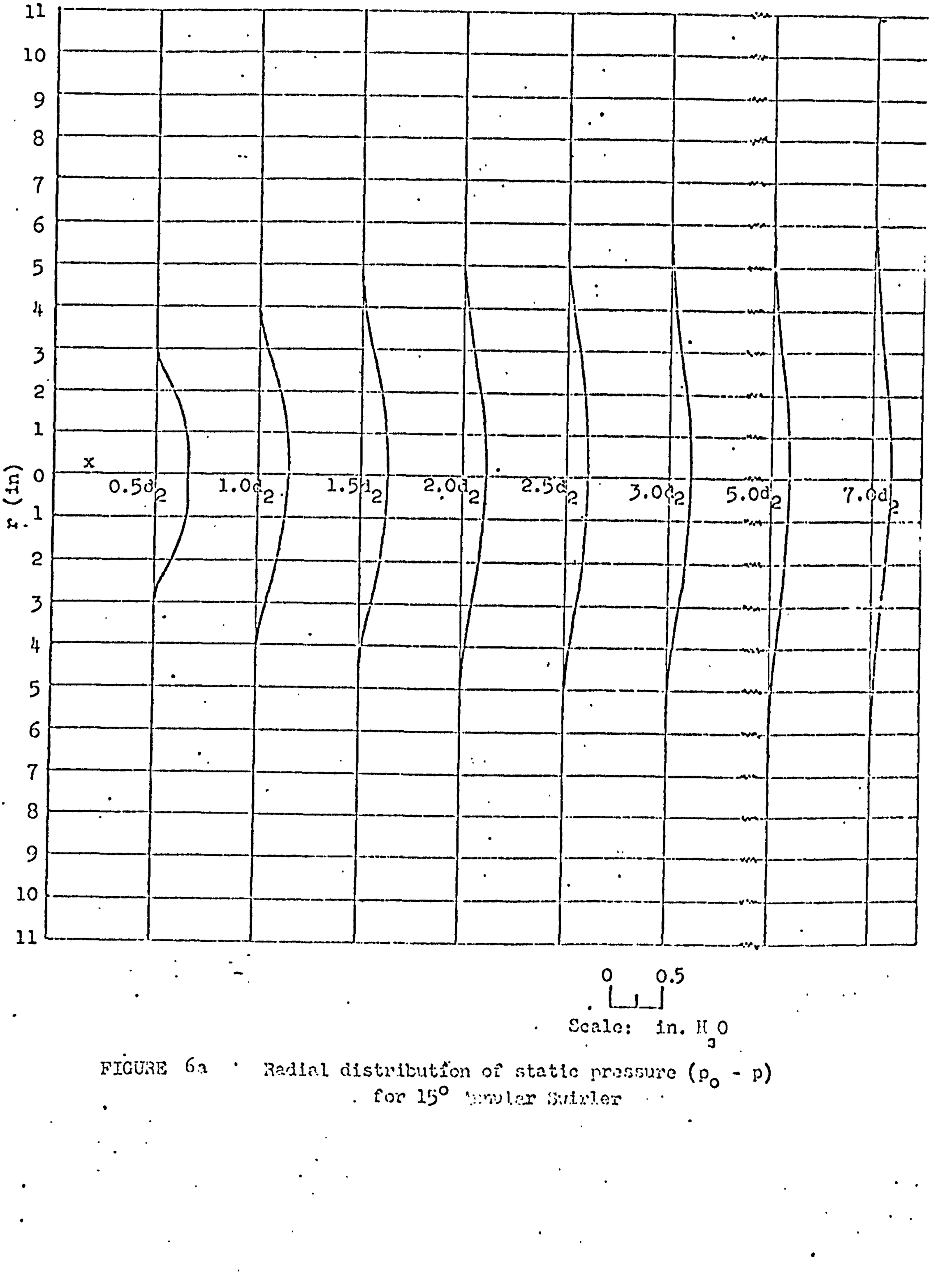

FIGURE 6a Radial distribution of static pressure ($p_o - p$) for 15° Annular Swirler

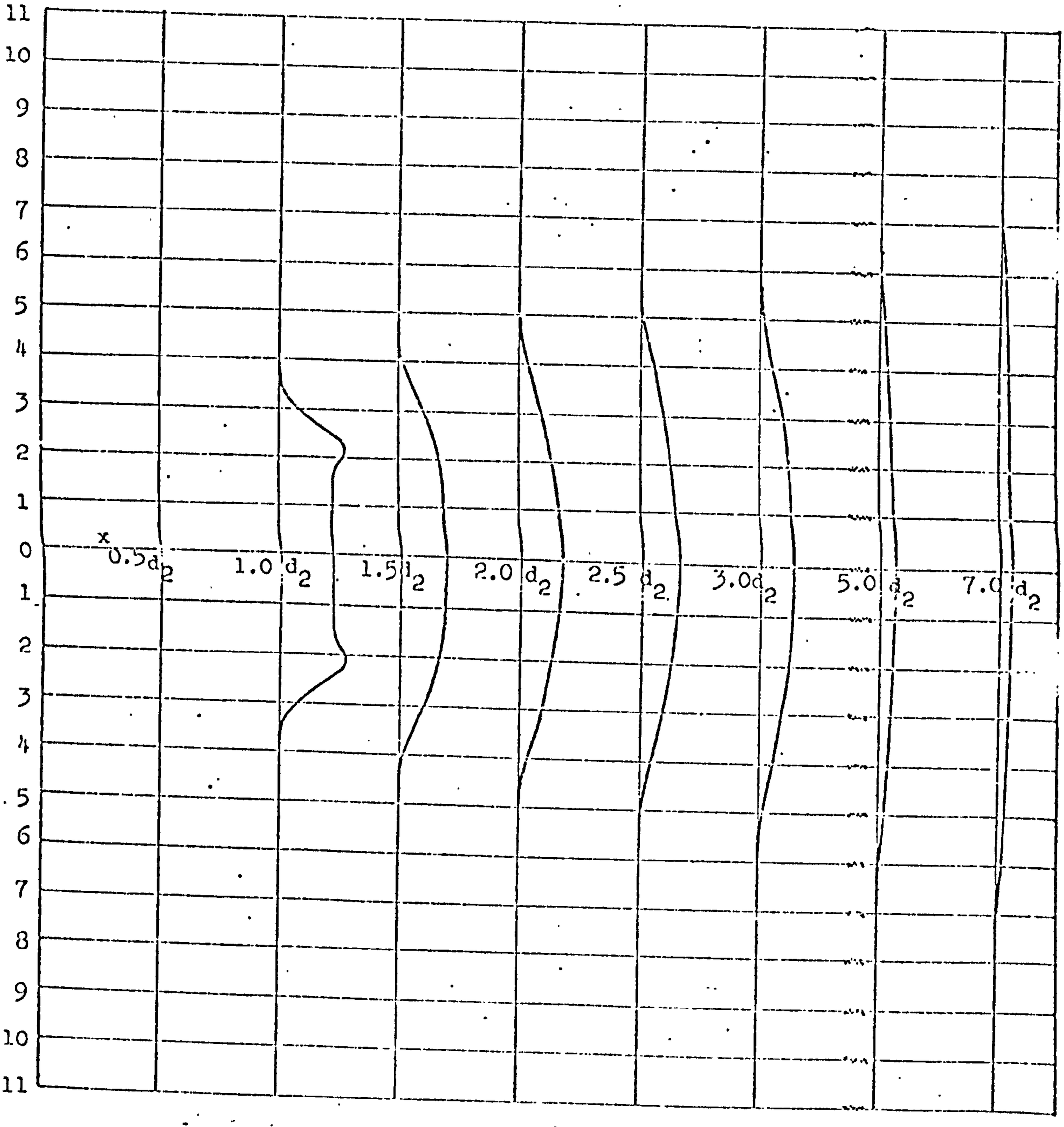

FIGURE 6b Radial distribution of static pressure ($p_o - p$) for 30° Annular Orifice

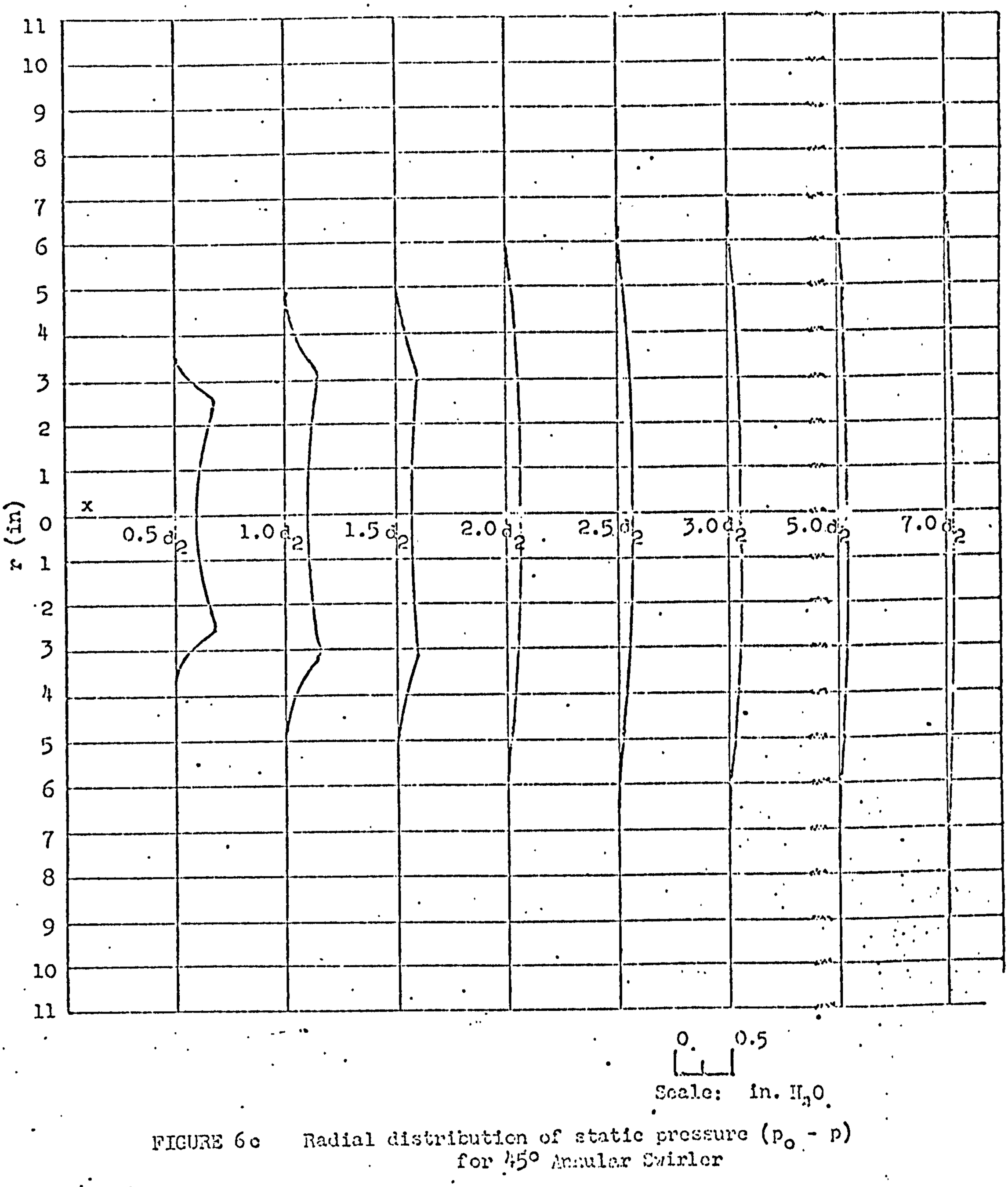

FIGURE 6c Radial distribution of static pressure ($p_o - p$) for 45° Annular Swirler

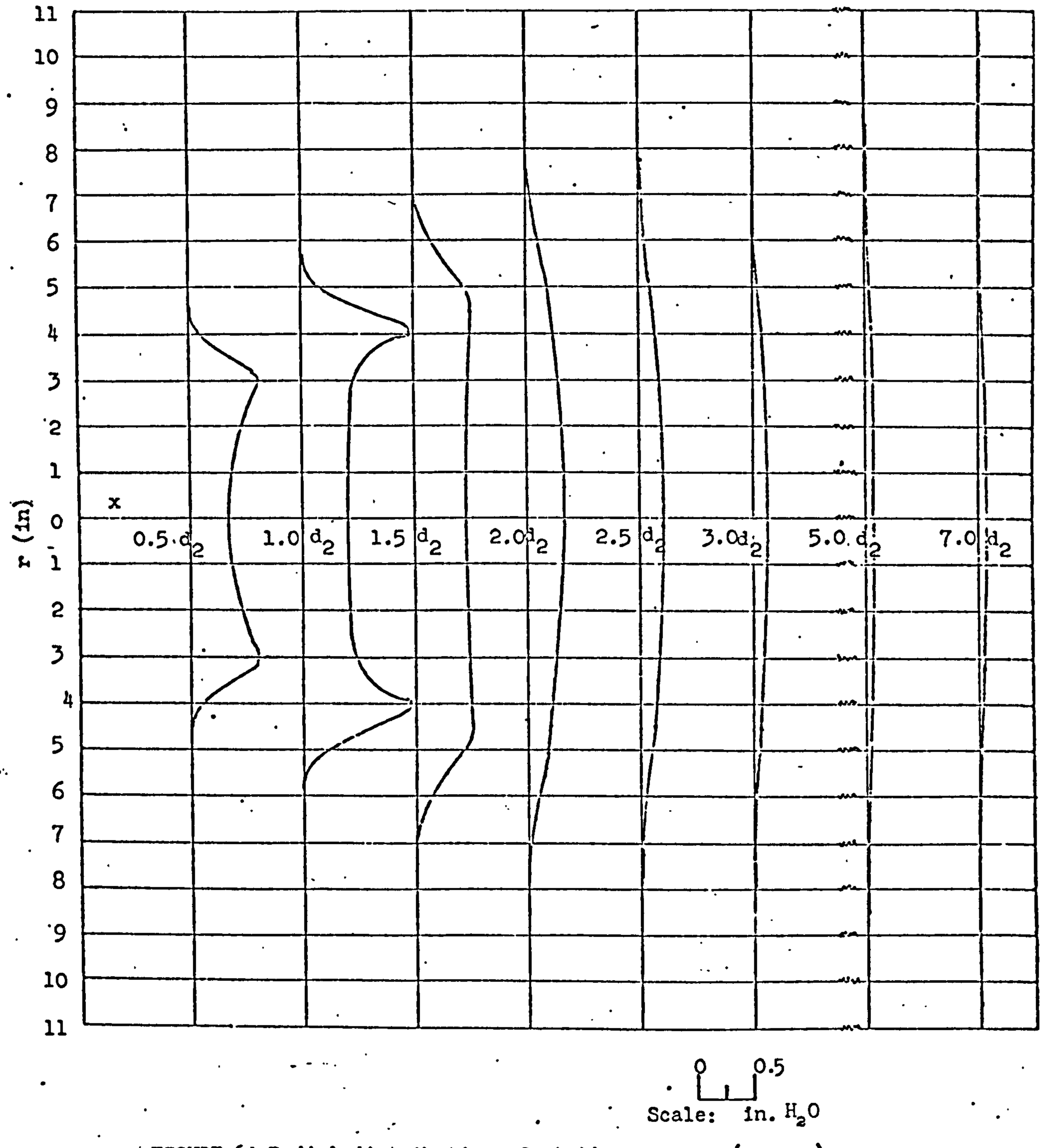

FIGURE 6d Radial distribution of static pressure (p_o - p) for 60° Annular Swirler

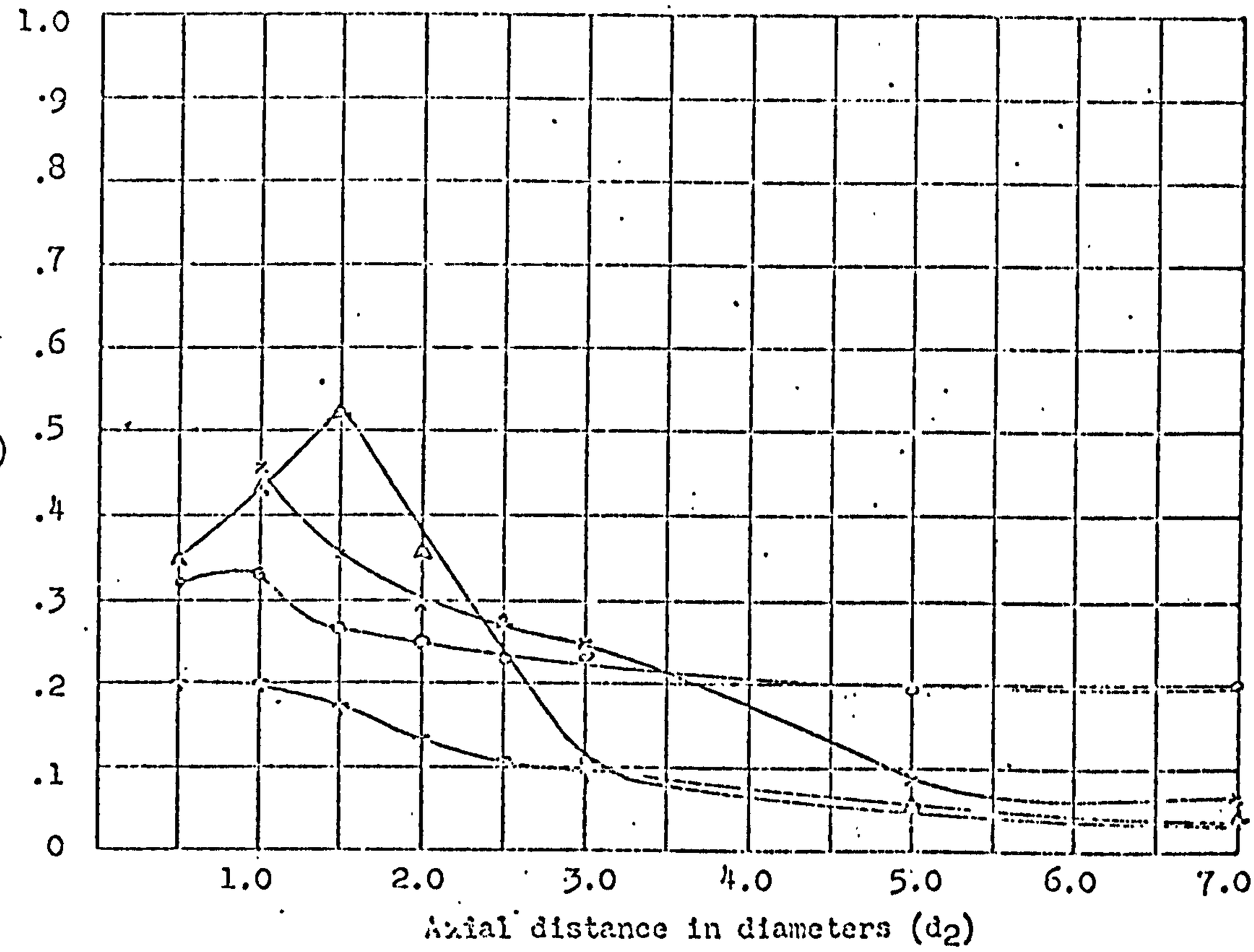

FIGURE 6e Annular Swirlers: Decay of static pressure along the jet axis

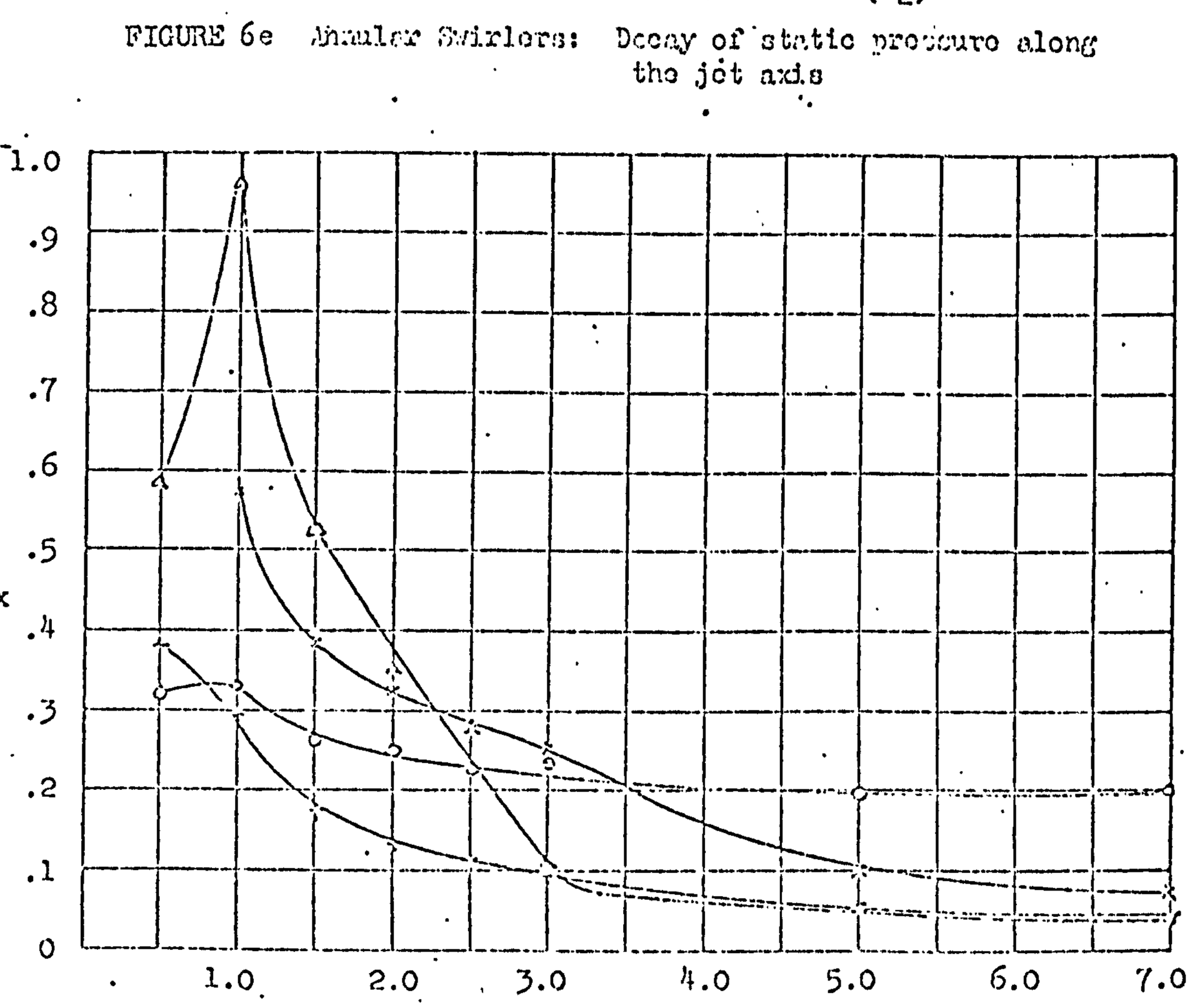

FIGURE 6f Annular Swirlers: Decay of maximum static pressure along the jet

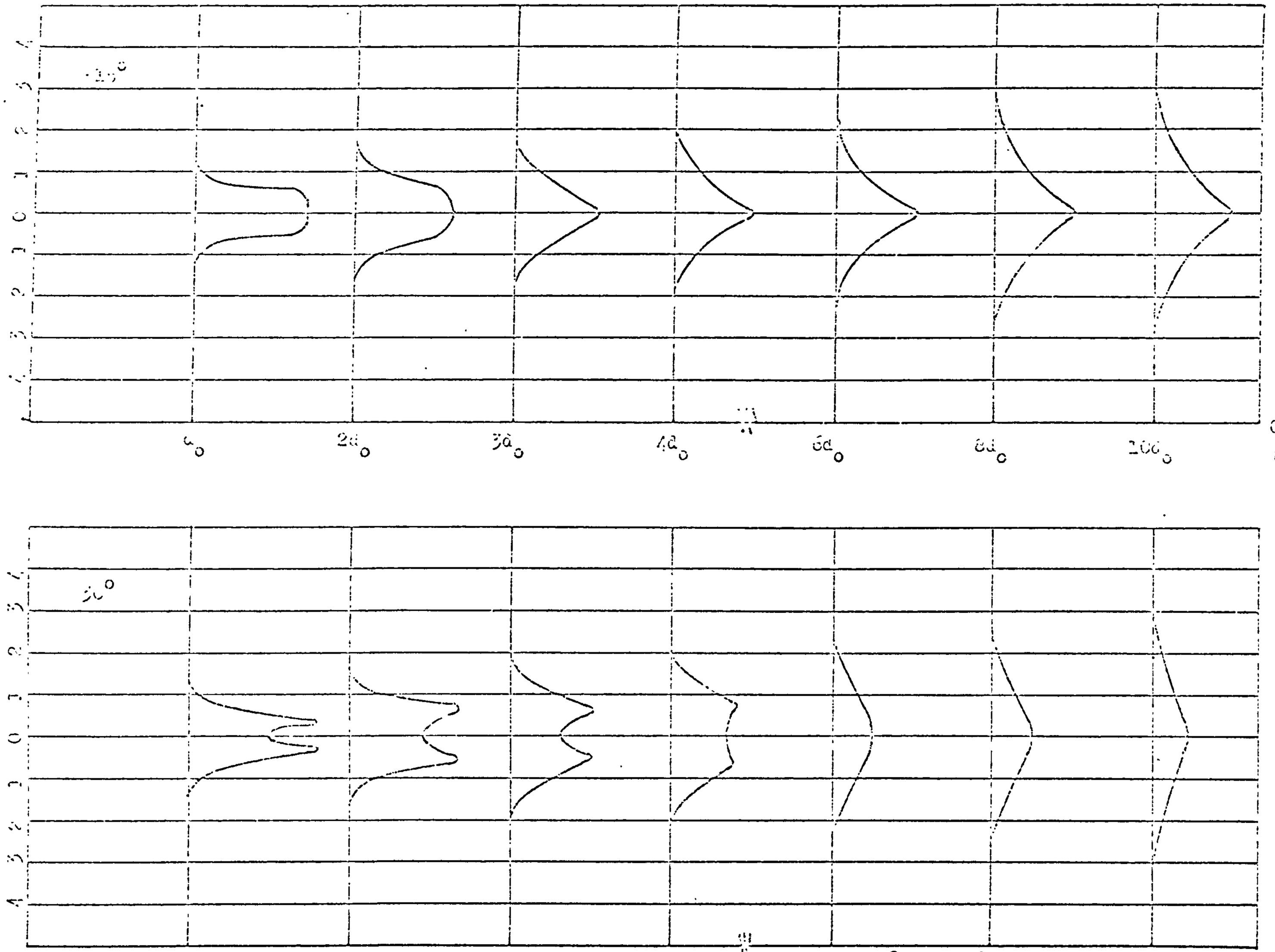

Figure 7a Radial distribution of static pressure (p_o-p) for 15° and 30° Lubless Swirlers

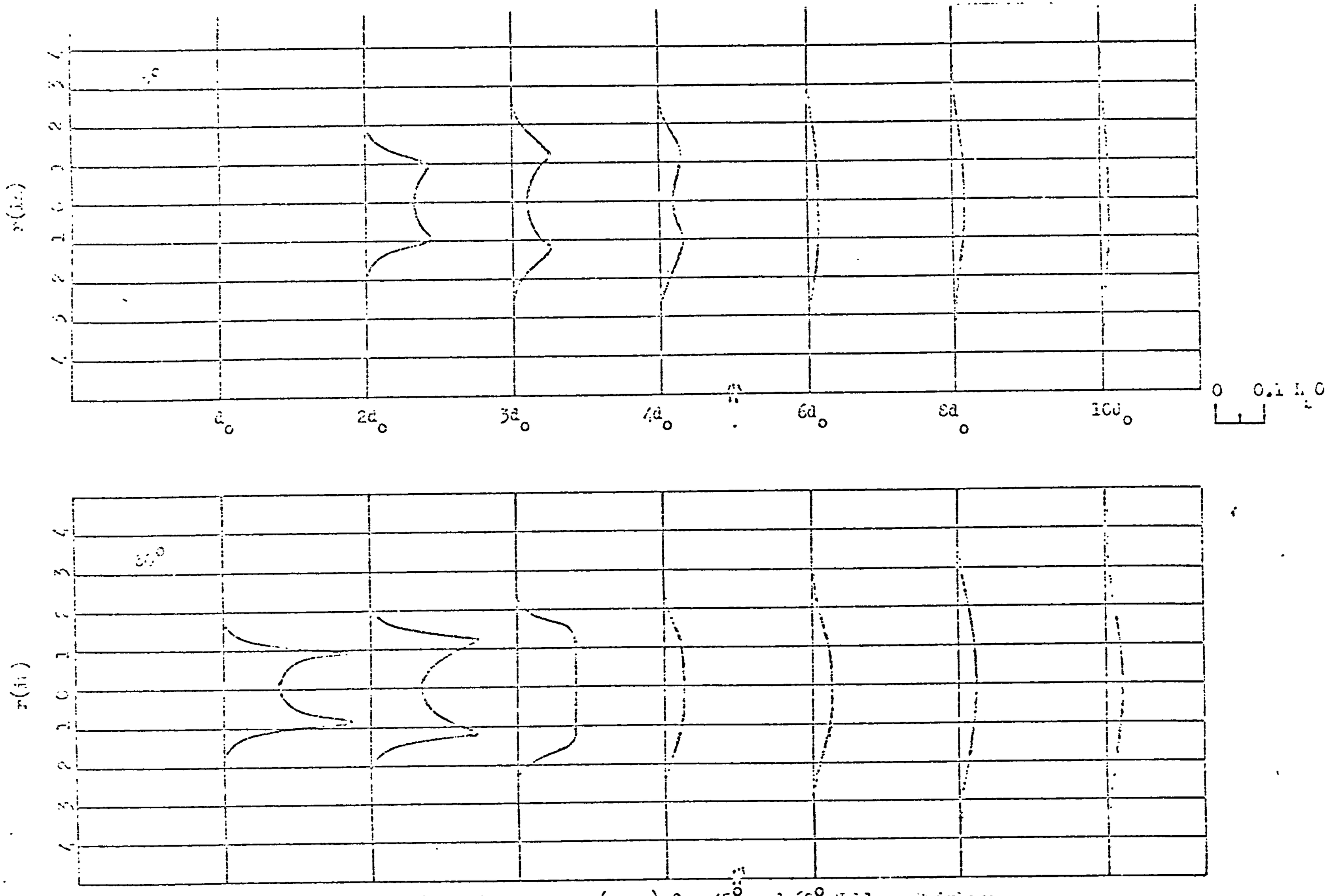

Figure 7b Radial distribution of static pressure (p_o-p) for 45° and 60° Hubless Swirlers

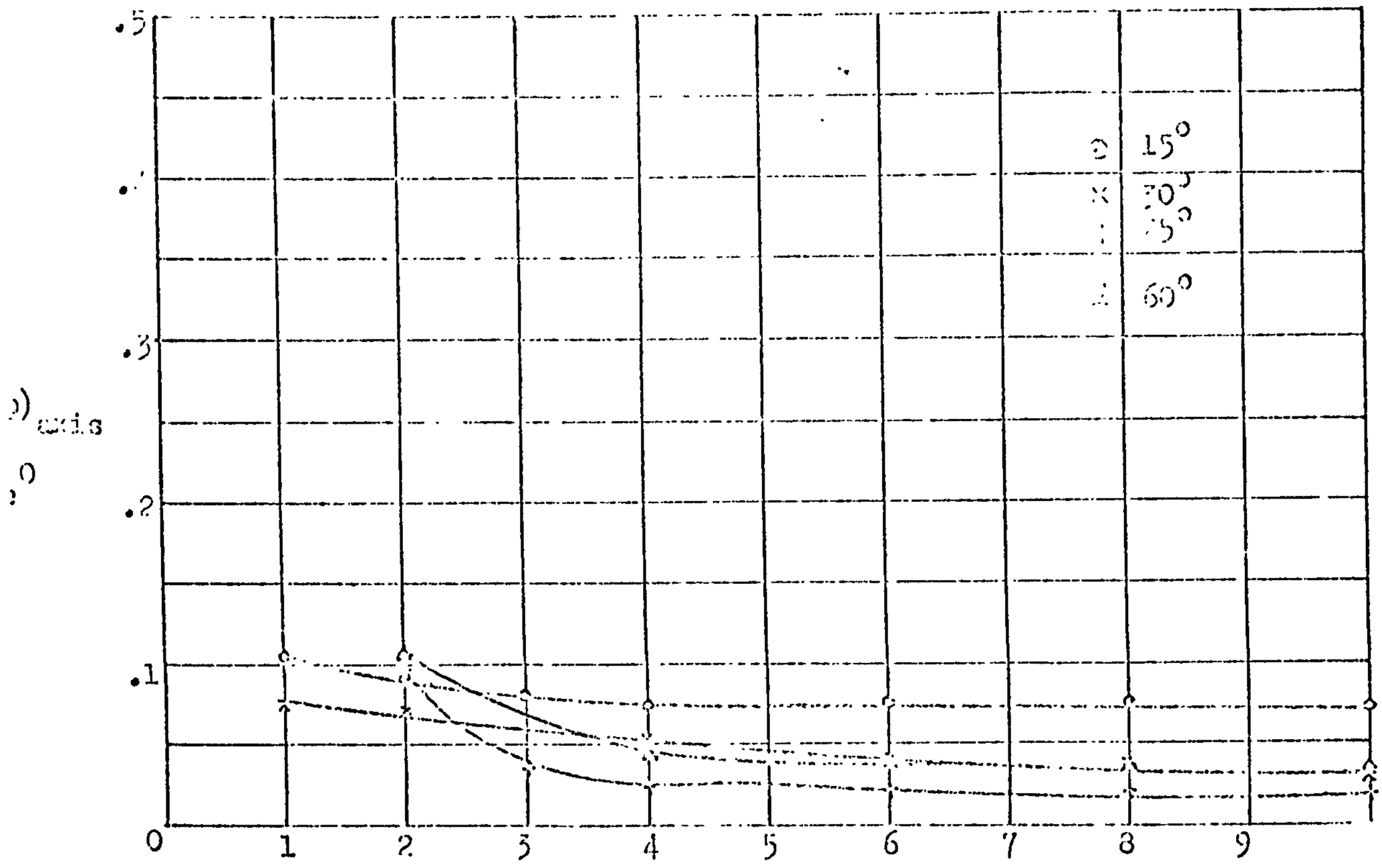

Axial distance in diameters (d_o)

Figure 7c Subsonic Jet: Decay of static pressure along the jet axis

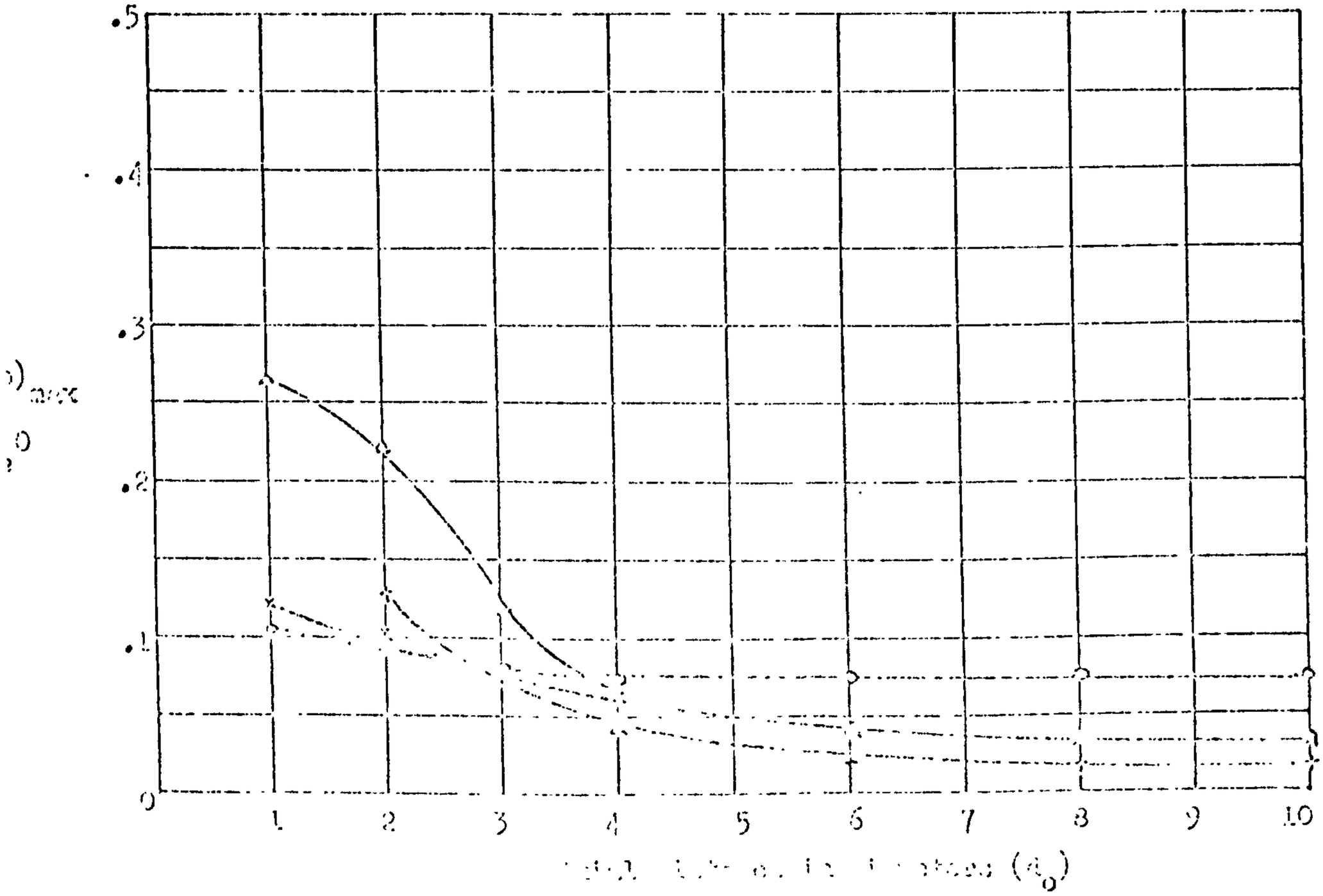

Axial distance in diameters (d_o)

Figure 7d Subsonic Jet: Decay of maximum static pressure along the jet

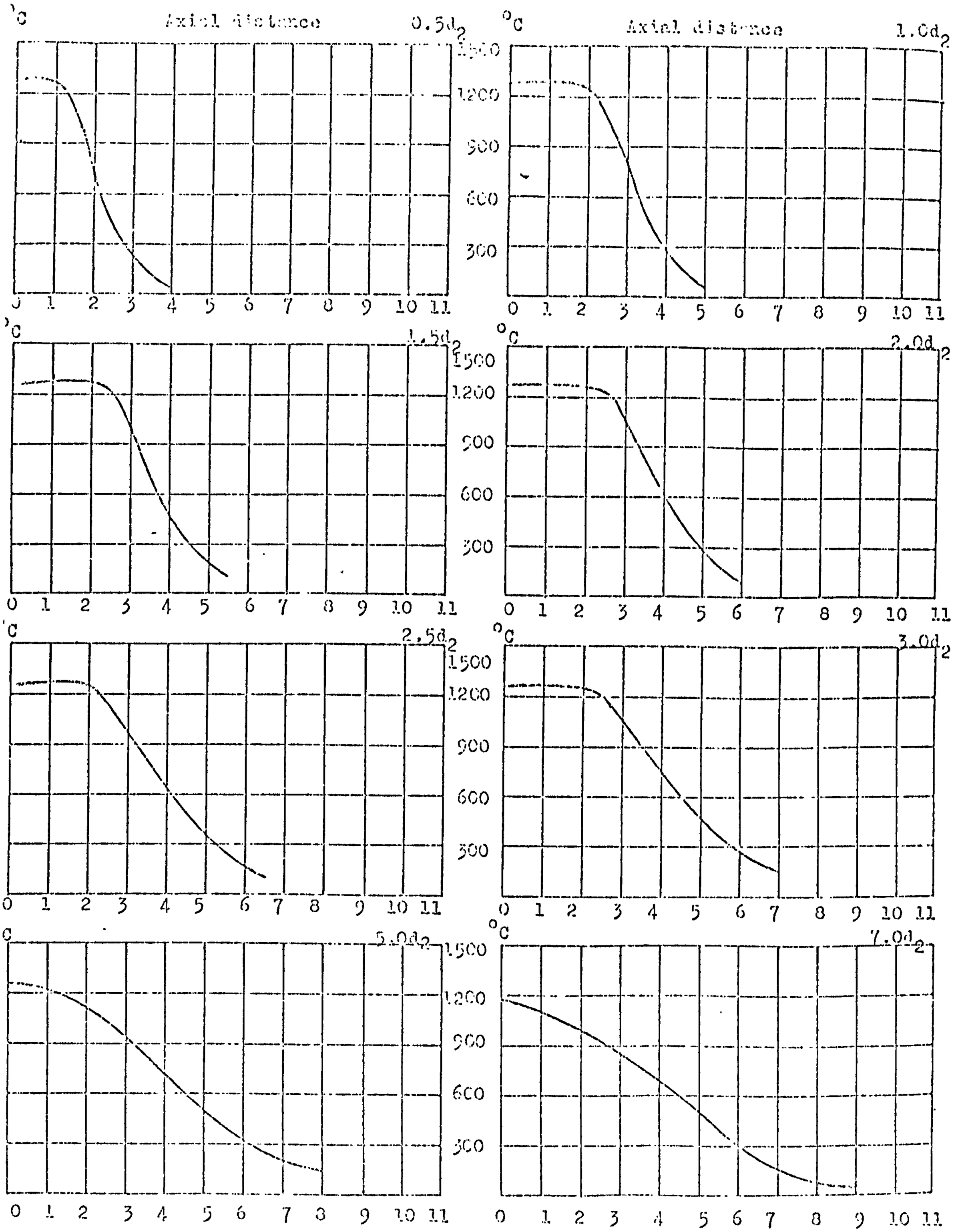

Figure 8a Temperature Distribution for 15° Annular Swirler.

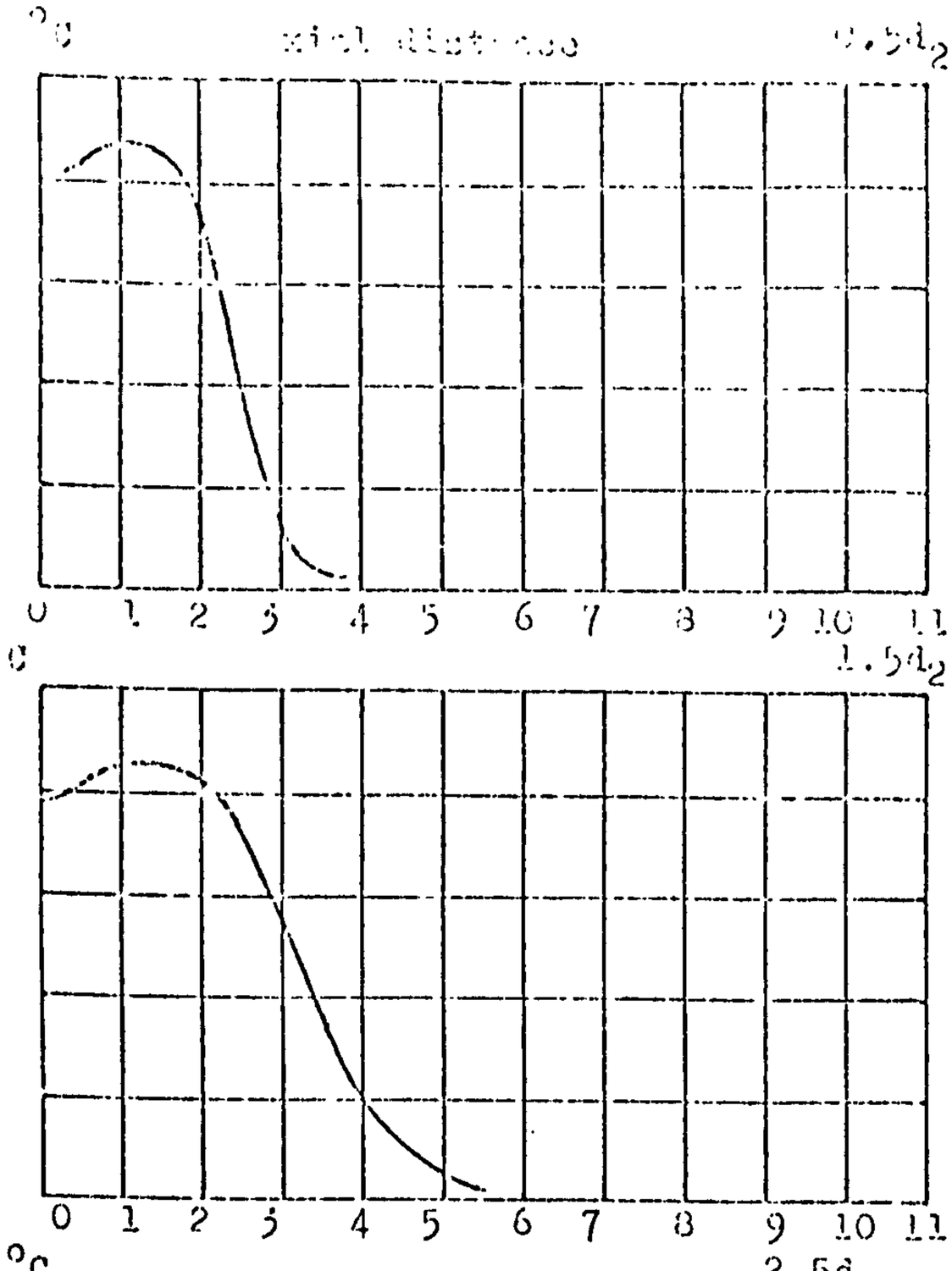

Radial Distance (in)

Radial Distance (in)

Fig. 9 Temperature Distribution for 30° Included Wedge.

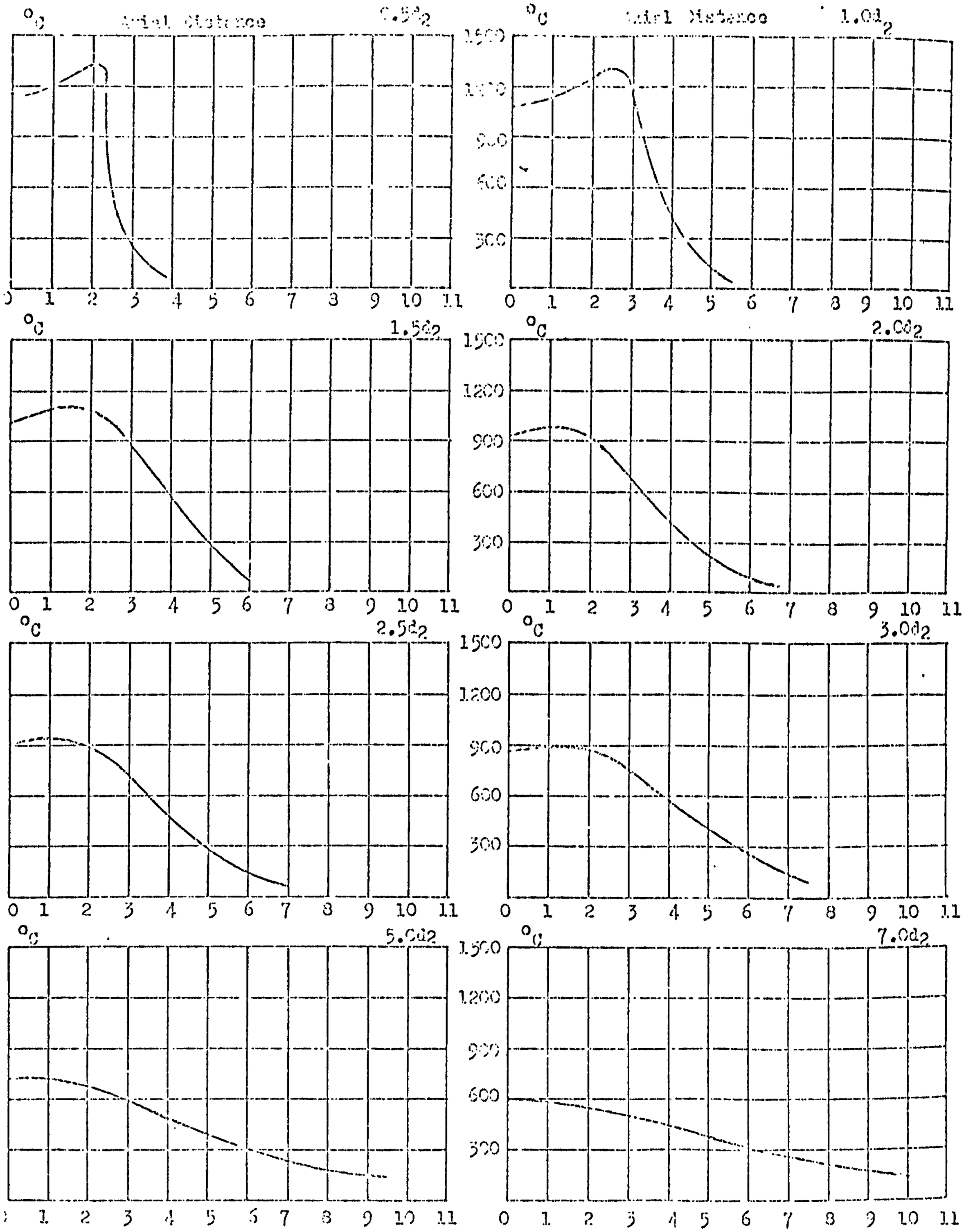

Figure 6. Temperature Distribution for 45° Annular Cooler

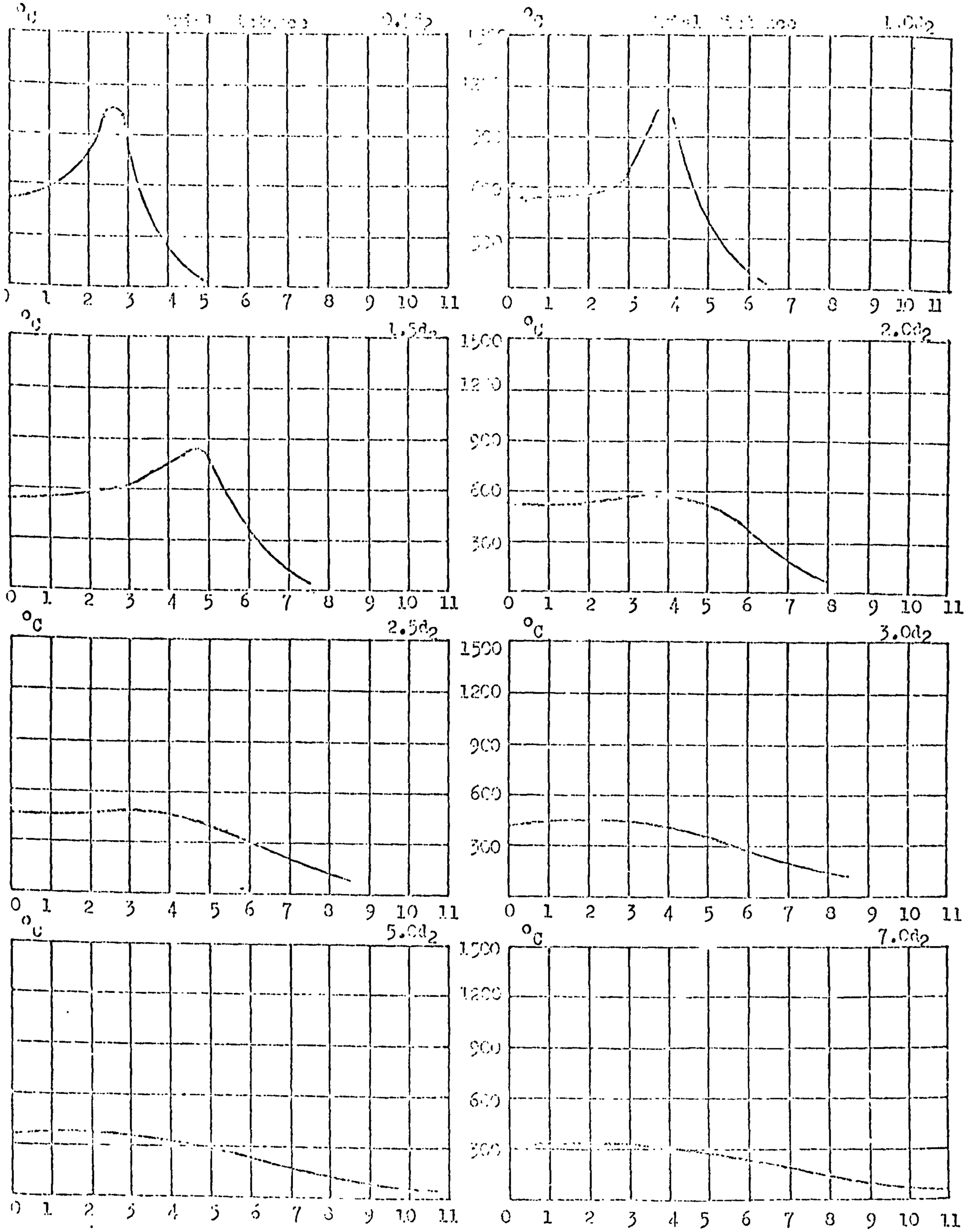

Figure 24 Temperature Distribution for 30° Annular Nozzles.

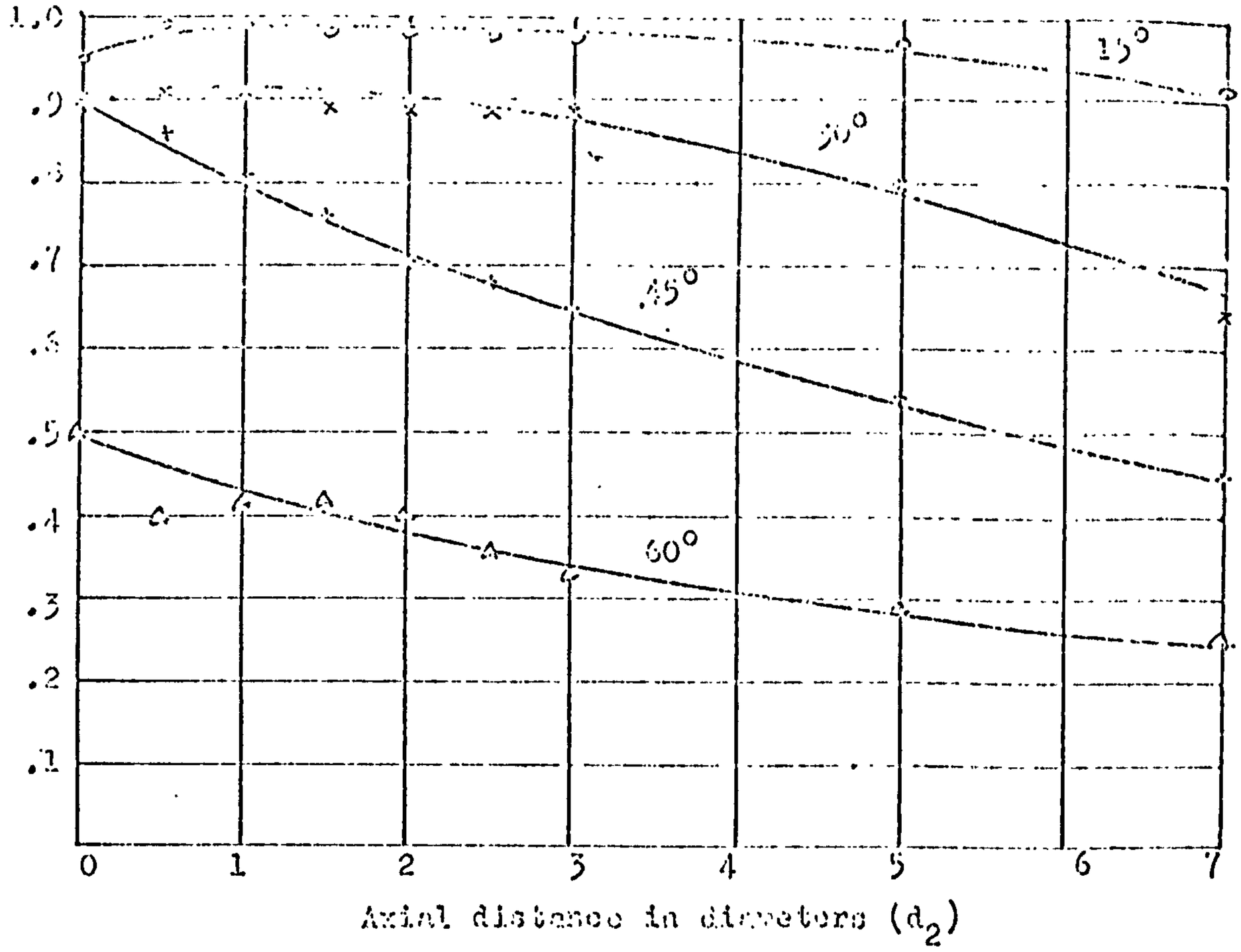

Figure 8. Annular Swirlers: Variation of temperature rise along the jet axis.

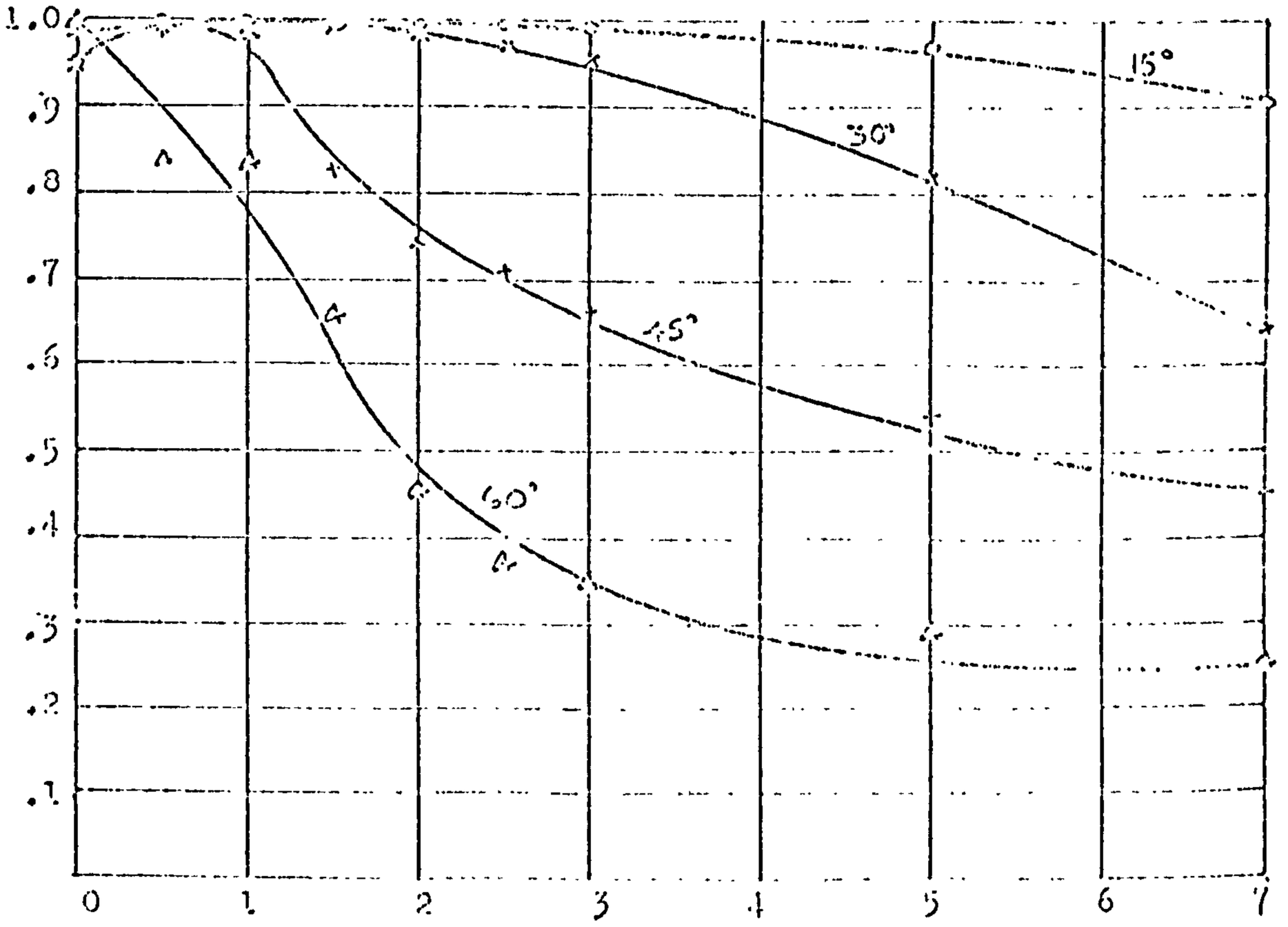

Figure 9. Annular Swirlers: Variation of maximum temperature rise along the jet.

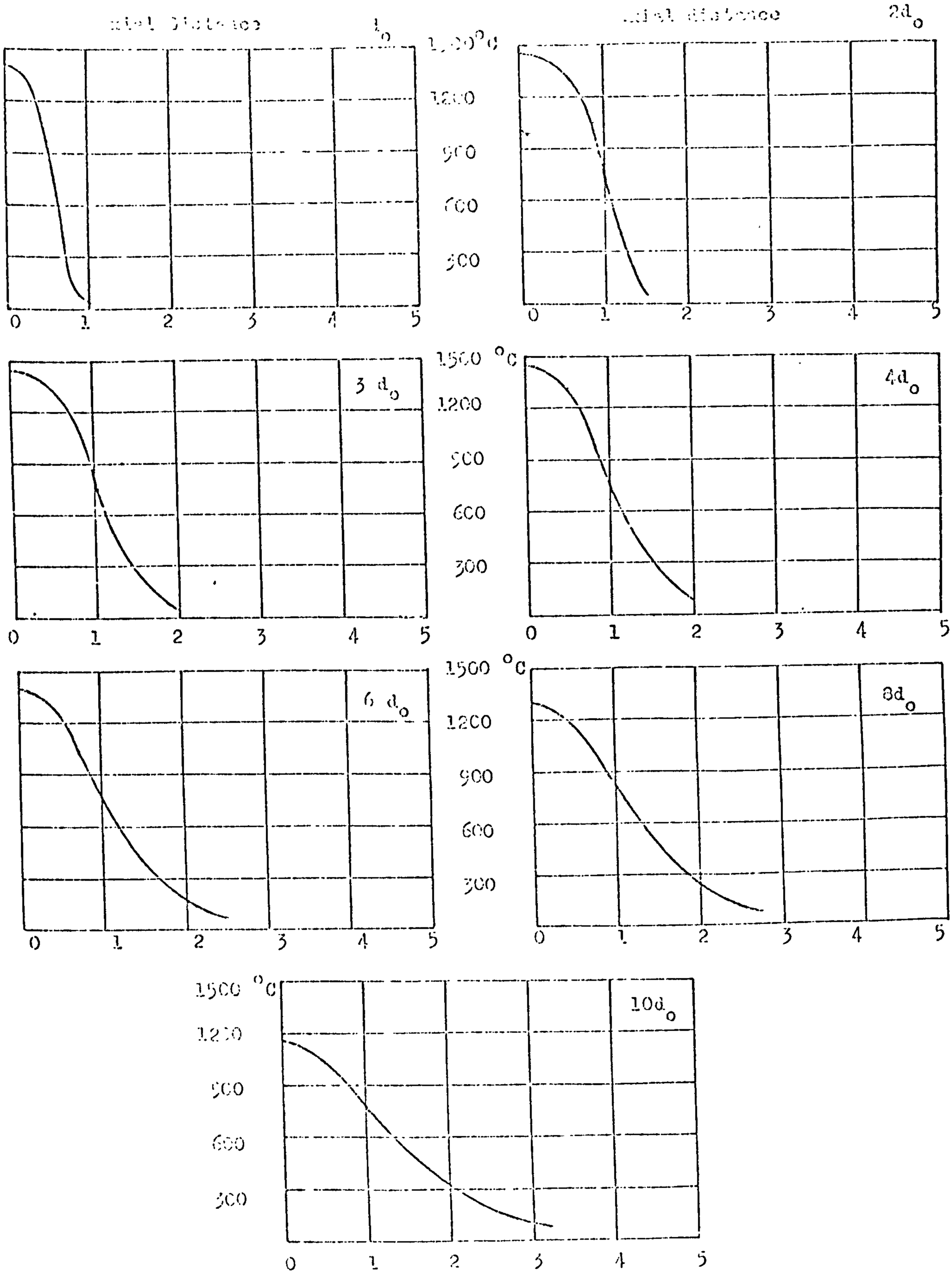

Figure 9: Temperature Distribution for 15° Hubless Deflector

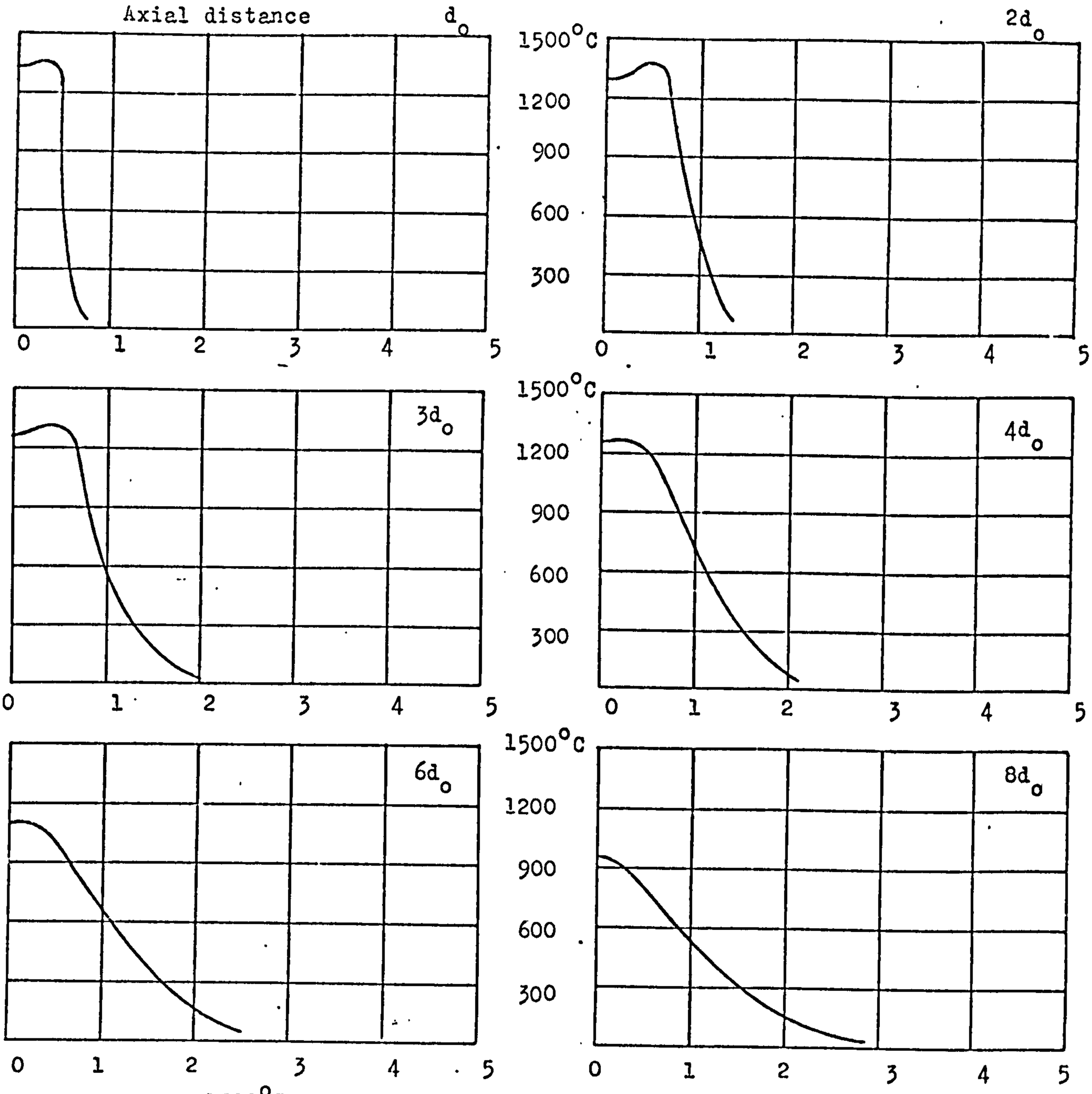

Figure 9b Temperature distribution for 30° Hubless Swirler.

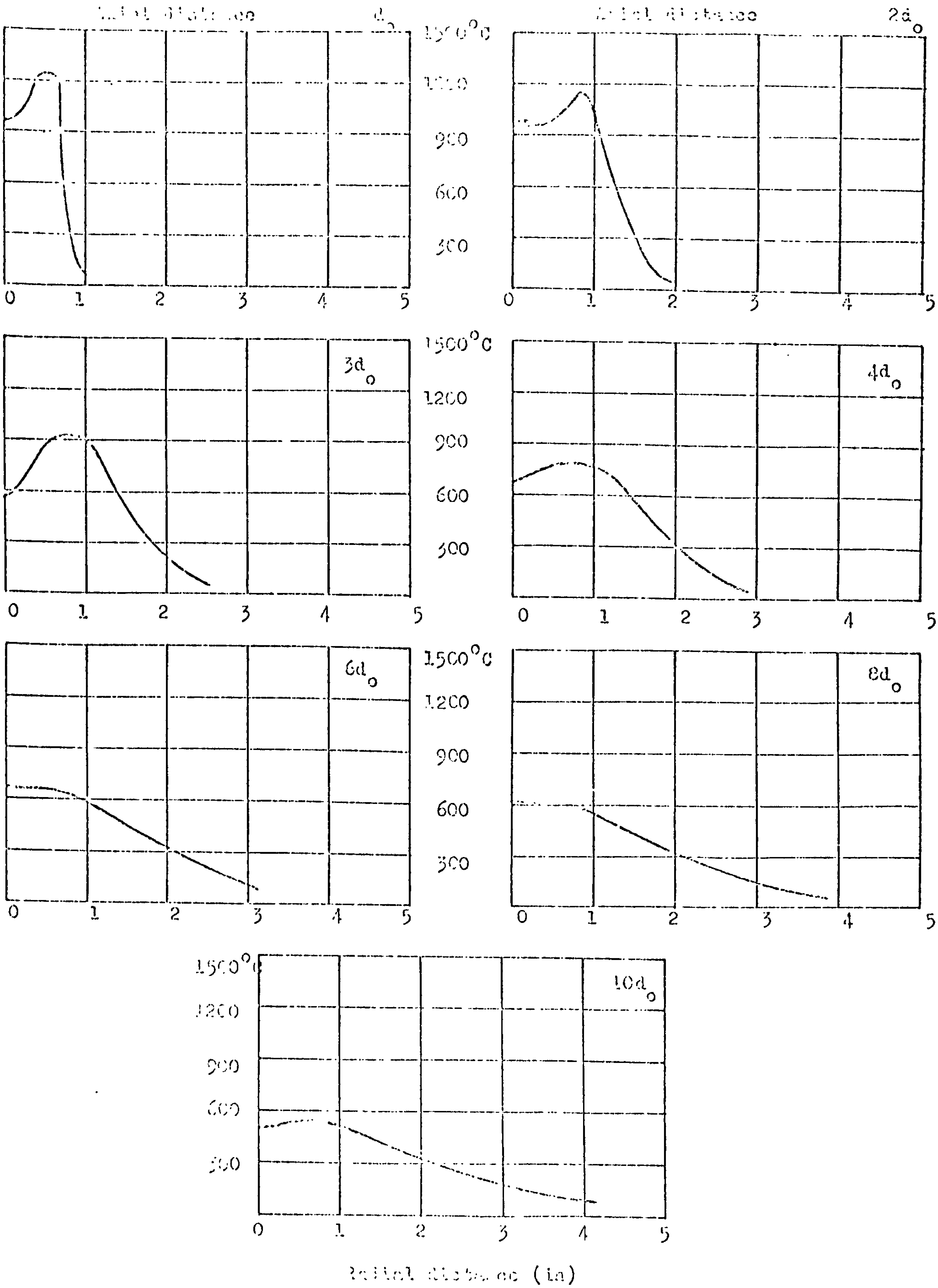

Figure 9c Temperature distribution for 45° [illegible] Swirler.

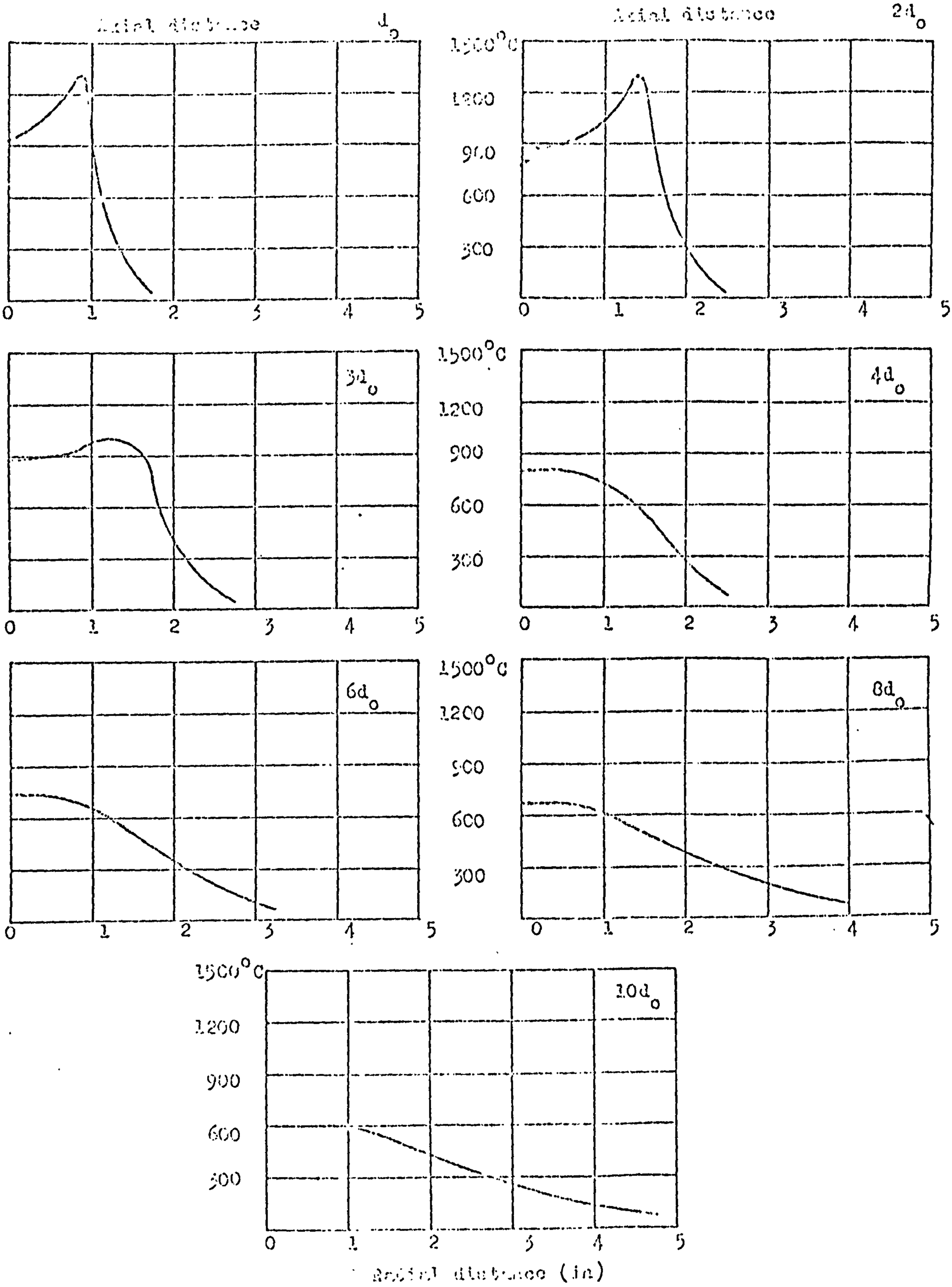

Figure 9d Temperature distribution for 60° dribbles twirler

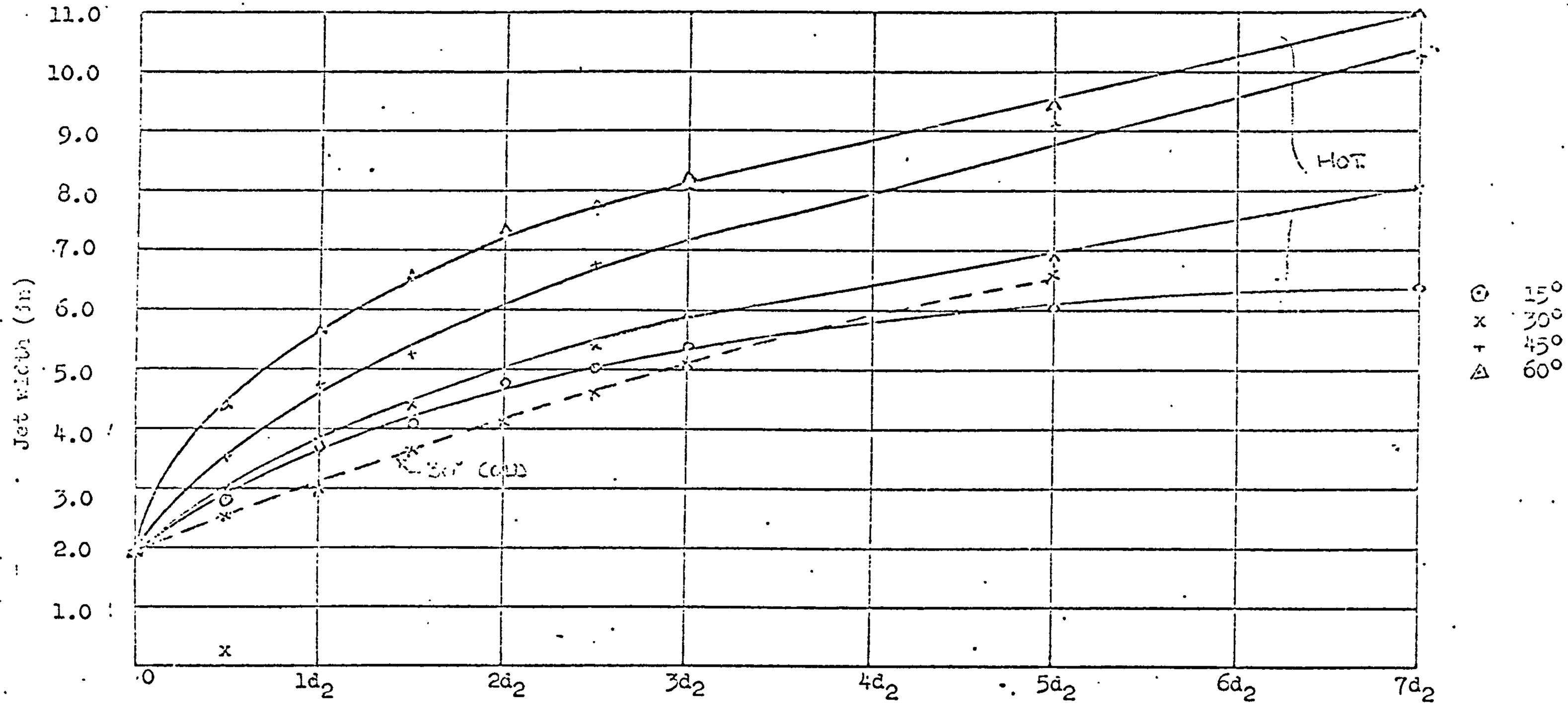

FIGURE 10 Annular Swirlers: Variation of jet width

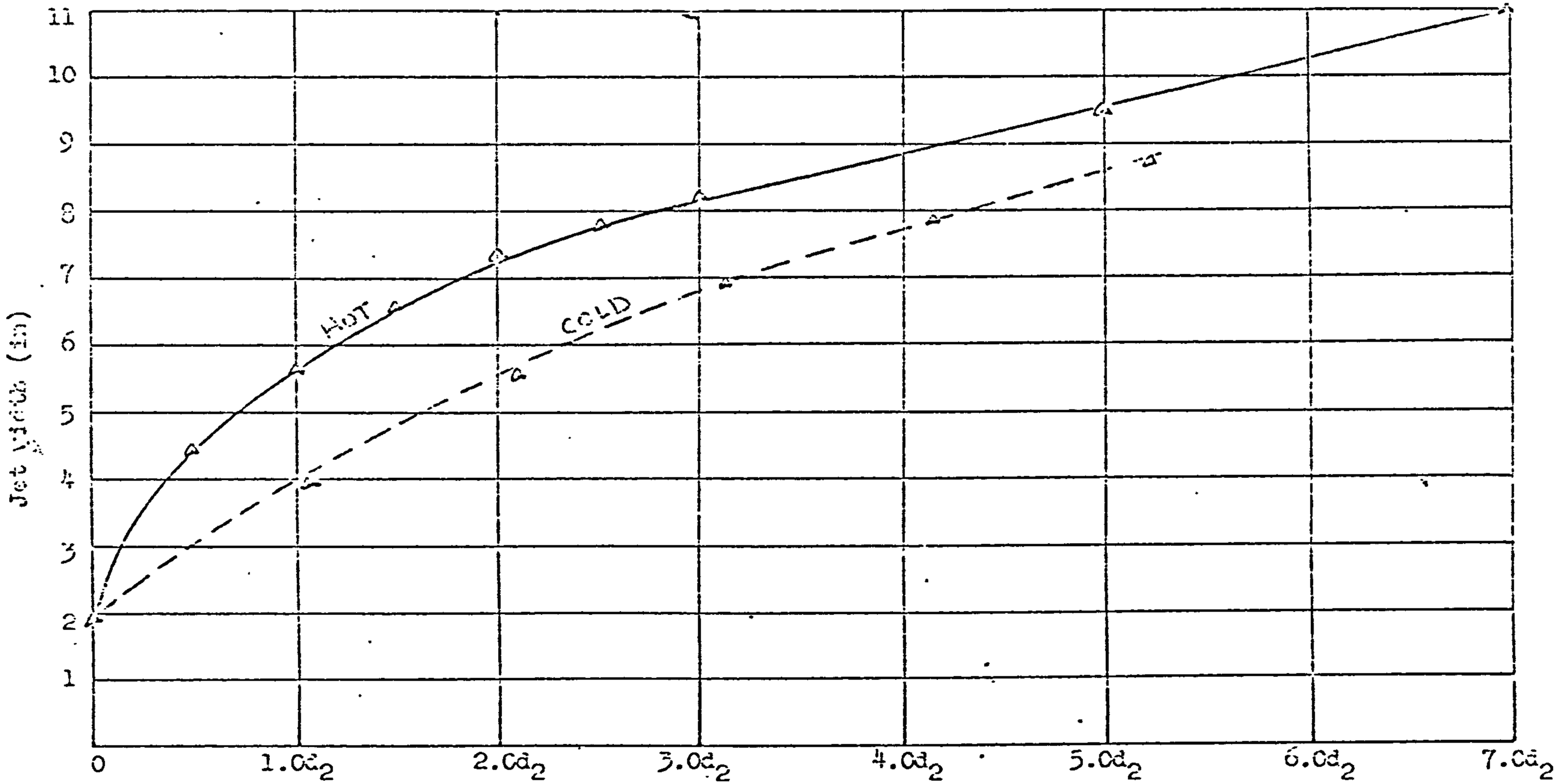

FIGURE 11 Comparison of cold and hot jet widths: 60° Annular Swirler

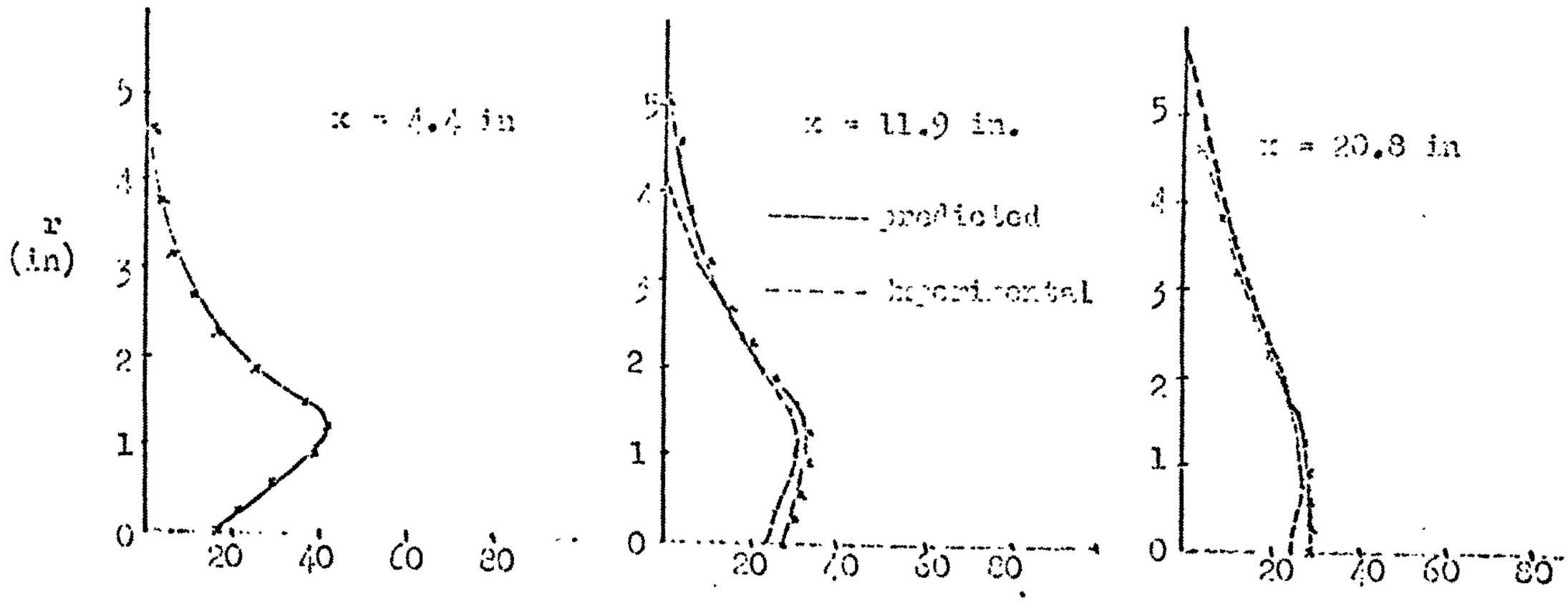

Figures 13a Predicted radial distribution of axial velocity in isothermal jet from 15° Annular Swirler

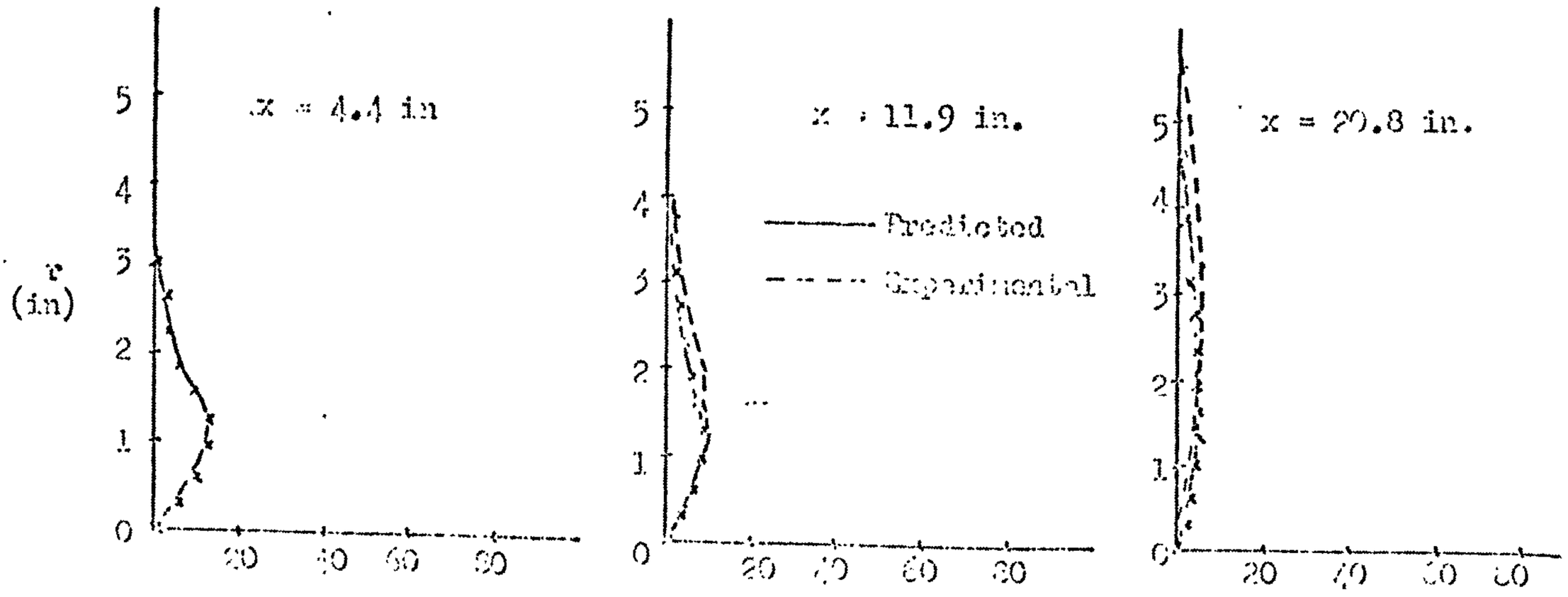

Figure 13b Predicted radial distribution of axial velocity in isothermal jet from 15° Annular Swirler

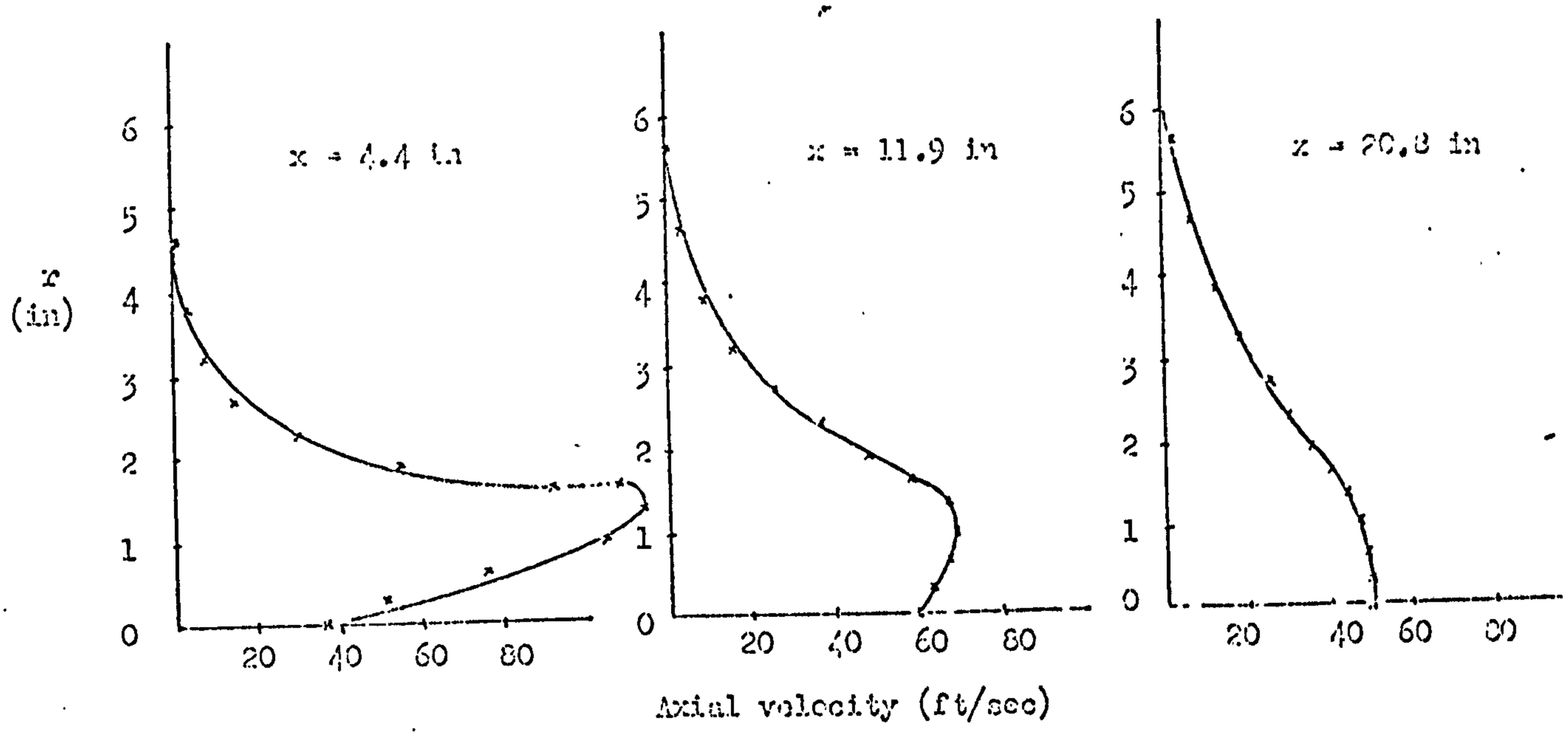

Figure 14a Predicted radial distribution of axial velocity in burning jet (f/a 0.24) from 15° Annular Swirler

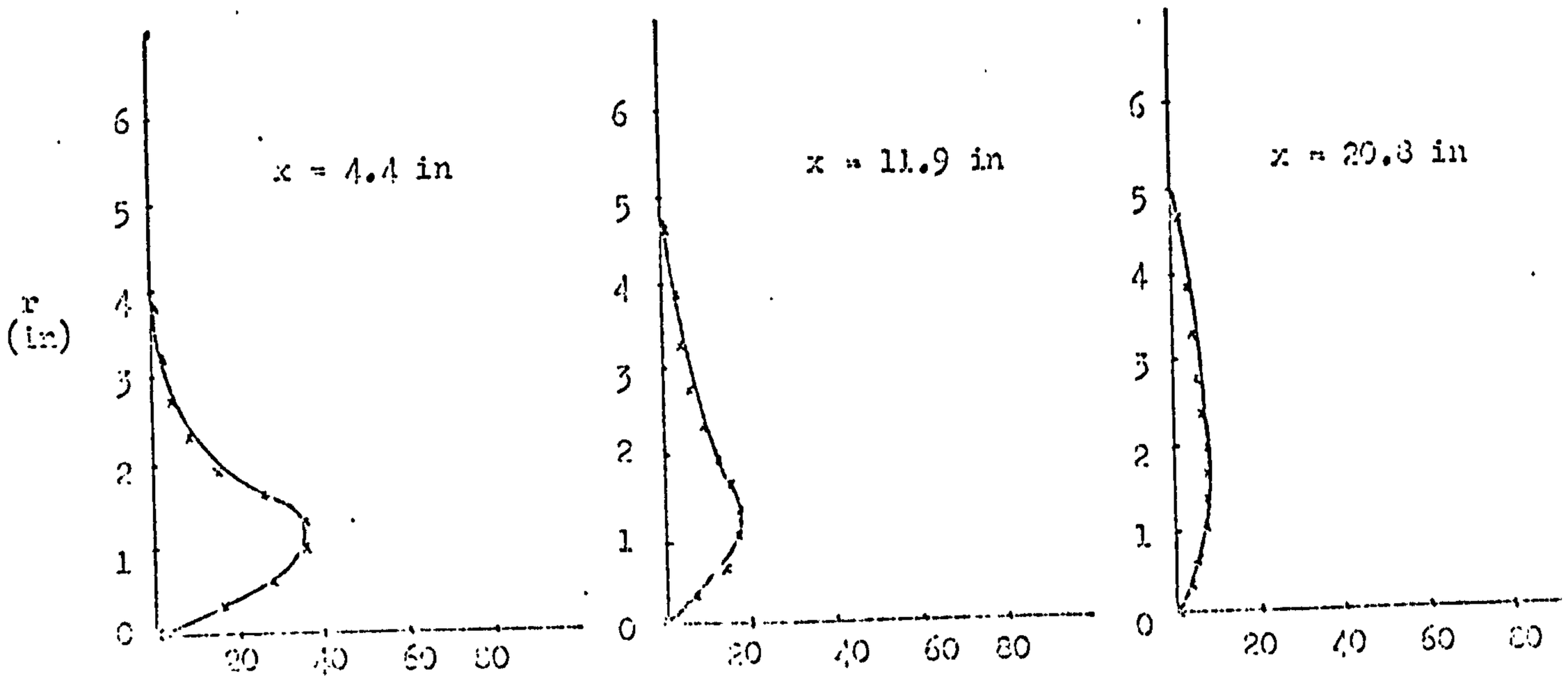

Figure 14b Predicted radial distribution of axial velocity in burning jet (f/a 0.24) from 15° Annular Swirler

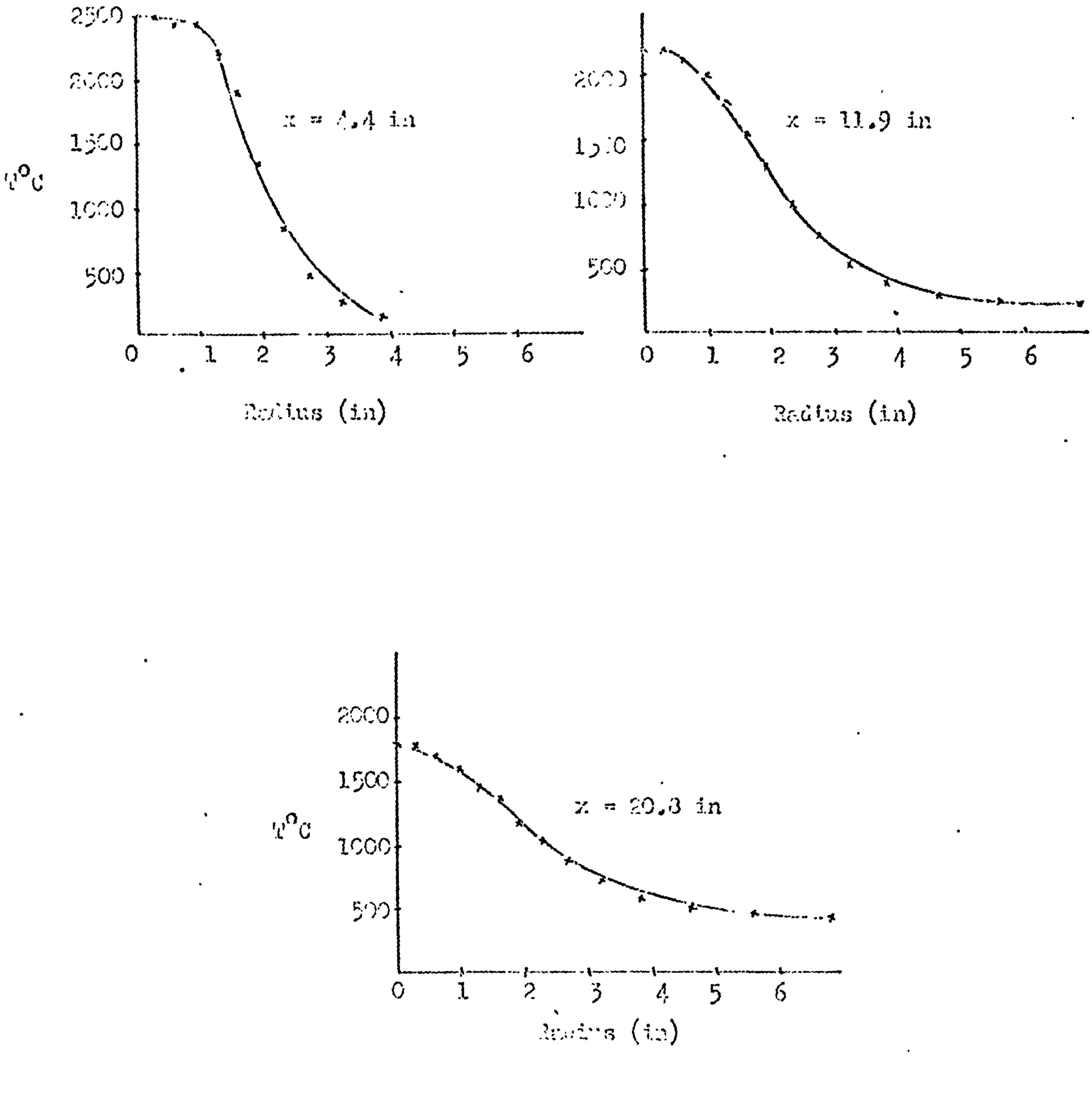

Figure 14c Predicted radial distribution of temperature in burning jet (r/e 0.26) for 15° annular burner

 Instn. Mech. E., 1974, (Conf. Pub 36, 1973)

C36/73

EFFECT OF 'BULK' HEAT TRANSFERS IN AIRCRAFT GAS TURBINES ON COMPRESSOR SURGE MARGINS

N. R. L. MACCALLUM*

During transients of gas turbines, bulk heat transfers take place in the compressors and turbines to, or from, the air or gas streams. The effects these have on the compressor surge lines and on the steady-running conditions have been investigated theoretically for four typical transients of a twin-spool bypass engine. The two most serious situations found occur in the low-pressure (LP) compressor during an altitude deceleration and in the high-pressure (HP) compressor when attempting an acceleration immediately following a rapid deceleration. In these two cases the appropriate surge margins are reduced by 18 and 35 per cent respectively.

1 INTRODUCTION

The behaviour of gas turbines during and immediately following accelerations or decelerations is of great interest. Methods have been developed for predicting the dynamic response during these transients (1), (2)†. These methods have used the characteristics of the components (compressors and turbines) observed under steady-running conditions. However, it is known that the behaviour of a gas turbine during, for example, an acceleration depends on the state of the engine immediately before the acceleration is commenced. In one case (3) it is reported that the allowable increase in fuel flow without causing compressor surge when accelerating an engine is approximately halved if the engine is 'hot' following a previous rapid deceleration, as compared with an engine that is starting from 'cold'. Thus there must on some occasions be considerable departures of components from their equilibrium characteristics.

Four possible causes of these departures from equilibrium are given below.

(1) The stability of the boundary layers on the aerofoils in the compressors and turbines may be altered by heat transfer from the air or gas to the blades during an acceleration and by heat transfer from the blades to the air or gas during a deceleration.

(2) The above mentioned heat transfers which occur in the compressors may alter the compressor characteristics because of the resulting density changes in the air.

(3) The non-adiabatic nature of the compressions and expansions may cause the engine working line to be displaced.

(4) Tip and axial clearances in the compressors and turbines may be significantly different from equilibrium values due to the markedly different response rates of blades, discs and outer casings to changes in air or gas temperature. For example, in transients at sea level the aerofoils of compressor blades typically have time constants in the range 0·5–10 s, turbine blades in the range 2–16 s, while a turbine disc may have a time constant of 40 s. If clearances are increased during a transient this lowers the component efficiency and, for a compressor, decreases the mass flow delivery.

A study of the first factor listed above, the effect of heat transfer on boundary layer stability, is reported separately by Grant (4).

This paper presents the results of a theoretical investigation of the second and third factors—the effects of 'bulk' heat transfers on compressor characteristics and on the working line of the engine. The fourth factor can only be investigated with reference to particular designs, and in some cases this has been done.

1.1 Notation

A	Effective throat area of turbine nozzle guide vanes.
C_D	Coefficient of discharge of non-adiabatic nozzle, defined by ratio of actual mass flow to mass flow through adiabatic nozzle of same geometric size and at same inlet conditions and exit pressure.
F	Ratio of heat transfer to fluid in an element of a compressor or turbine to work transfer from the fluid in the same element.
HP	High pressure.
LP	Low pressure.
m	Index of non-adiabatic compression or expansion.
N_A	Non-dimensional compressor speed at condition A, a non-adiabatic surge point.
N_B	Non-dimensional compressor speed corresponding to point B on the adiabatic surge line, point B being such that the density ratio across

The MS. of this paper was received at the Institution on 6th June 1972 and accepted for publication on 2nd October 1972. 33

* *Senior Lecturer, Department of Mechanical engineering, University of Glasgow G12 8QQ.*

† *References are given in Appendix 36.1.*

the compressor is the same as at the non-adiabatic surge point A.

P Stagnation pressure.

R_{SB} Compressor pressure ratio at adiabatic surge point B.

R'_{SA} Compressor pressure ratio at the non-adiabatic surge point A.

R_W Compressor pressure ratio in adiabatic steady-running.

r Pressure ratio across a nozzle.

γ Isentropic index.

η_{pc} Polytropic, or small stage efficiency of compression.

η_{pt} Polytropic, or small stage efficiency of expansion.

Station numbering

1. LP compressor inlet
2. HP compressor inlet
3. HP compressor delivery
4. HP turbine inlet
5. LP turbine inlet

2 EFFECT OF BULK HEAT TRANSFER ON COMPRESSOR CHARACTERISTICS

The engine investigated in the work here reported is a twin-spool axial flow bypass engine of compression ratio 20.

Firstly the magnitudes of the heat transfers were assessed. This was done by representing the blades of the compressors as isolated aerofoils and the platforms were regarded as being flat surfaces with fins (5). To make some allowance for the disc or casing in thermal contact with the blade platform, the platform masses were increased by 50 per cent. Typically the time constants for the response of the aerofoils are shorter than those for the 'finned' platforms by a factor of about 6. The heat-transfer coefficients used for the pressure surfaces of the aerofoils were taken as being as on a flat plate with a turbulent boundary layer from the leading edge. For the suction surfaces the heat transfer coefficients were taken as the arithmetic mean of completely laminar and completely turbulent boundary layers on a flat plate. It is interesting to note that the average coefficients for the aerofoils in the compressor obtained in this way are within about 5 per cent of the coefficients that are obtained if the correlation given by Halls (6) for turbine blades is applied to the compressor blades.

Four typical transients have been studied.

(1) Acceleration at sea level from ground idle speed to maximum speed.

(2) Deceleration at 12 200 m altitude (40 000 ft). 0·61 Mach number from maximum speed to flight idle speed.

(3) Deceleration at sea level over the same non-dimensional speed range as in transient (2).

(4) Deceleration at sea level from maximum speed to ground idle speed.

All the transients were virtually completed, so far as speed was concerned, in 10 s.

2.1 Acceleration

In the acceleration (1) the temperature reduction in the LP compressor below the adiabatic compressor exit temperature is small and never exceeds about 3 deg K. The effect of the resulting density change on the LP compressor characteristics is negligible. In the HP compressor the temperature reduction due to heat transfer is more marked. being as high as 18 deg K summed along the compressor, midway through the acceleration. The work input increases during the acceleration, and the heat transfer, expressed as a fraction of the instantaneous work transfer has a numerical maximum of 0·07 after 3·6 s of the acceleration. Figure 36.1 shows the temperature reduction due to heat transfer and the ratio of this heat transfer to the work transfer during the acceleration. It was decided to investigate the conditions of the compressor after 3·6 s of the acceleration, because it is at this instant that the fractional heat transfer, F, is at its numerical maximum. At this instant the temperature reduction due to heat transfer is 15 deg K.

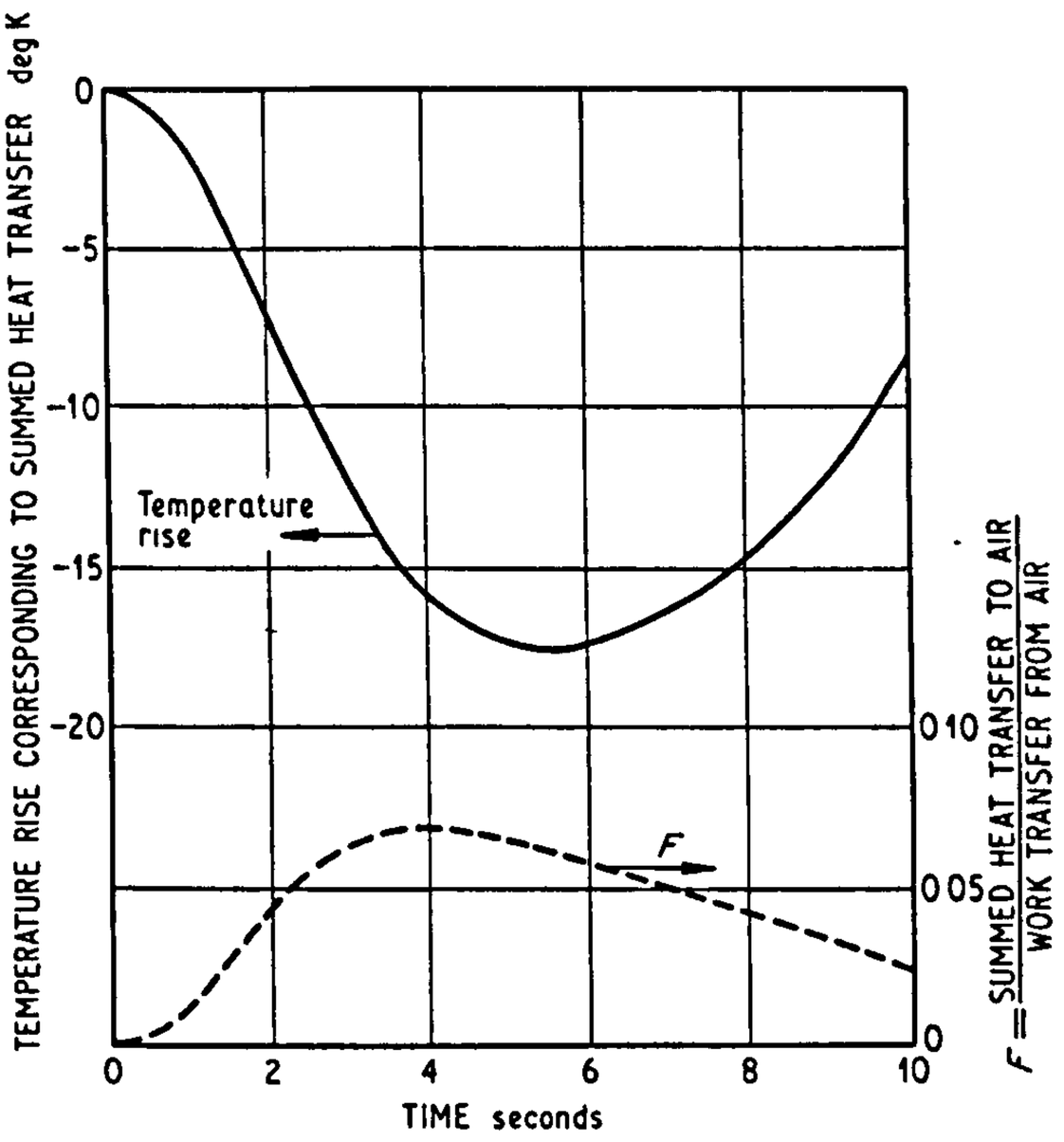

Fig. 36.1 Heat transfer in HP compressor during a sea level acceleration (transient (1))

The effect of the heat transfer on the compressor characteristics was predicted by adapting the simple stage-stacking method which had been used by Huppert and Benser for an adiabatic compressor (7). For simplicity, the 12-stage HP compressor was divided into four groups of three stages and individual stage characteristics assumed for each of the groups. The characteristics, in the form of pressure rise coefficients and efficiencies to a base of flow coefficient, were taken to be similar to those of Huppert and Benser, and of performance such as to satisfy the design pressure ratio and surge margin at the maximum speed. It was assumed that the stall experienced in all stages was of the root-to-tip type as all the stages in the HP compressor are of high hub-tip ratio. Using this method the adiabatic characteristic was predicted corresponding to the non-dimensional speed observed at 3·6 s in the acceleration. It was found that the predicted characteristic differed somewhat from that observed in tests of the complete compressor. To allow subsequent comparisons of the movements of surge lines and working lines, it was decided to

adjust the predicted characteristic to agree with the observed overall characteristic. This adjusted characteristic, and the associated surge line, are shown as solid lines on Fig. 36.2. The effect of heat transfer, in this case from the air, was then allowed for by inserting the temperature changes due to heat transfer between the stages in the stacking calculation. This result, scaled in the same manner as for the adiabatic prediction, and the associated surge line are shown as dotted lines on Fig. 36.2. It is seen that the pressure ratio at the surge point is increased from 4·60 to 4·70, but the movement of the surge line itself is negligible. The stacking calculations indicate that at this speed the surge in both the adiabatic and non-adiabatic cases is due to stall in the 7–9th stages. The effect of the heat transfer is equivalent to a movement of the constant non-dimensional speed line, in the direction anticipated in that heat transfer in an acceleration lowers the temperatures, compared to the adiabatic values, at the various stages along the compressor and therefore raises the 'effective' non-dimensional speed.

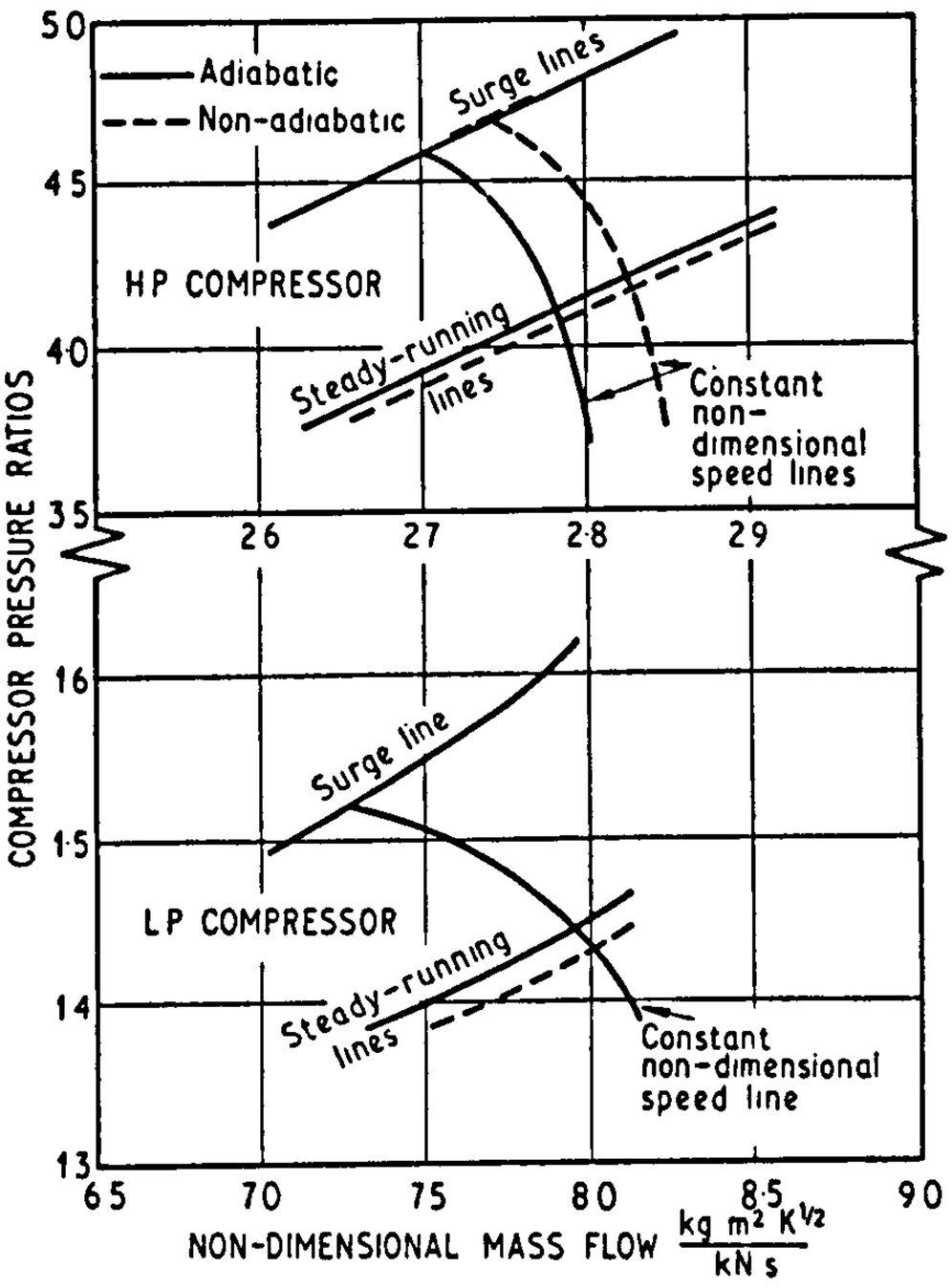

Fig. 36.2 Effects of heat transfer on surge and steady-running lines at 3·6 s in sea level acceleration (1)

2.2 Decelerations

Calculations similar to those described above for acceleration (1) were carried out for three decelerations (2)–(4). As in the acceleration, the temperature changes in the LP compressor due to heat transfer are small, never exceeding about 4 or 5 deg K. The temperature changes in the HP compressor due to heat transfer are much more significant, having maximum values of 22, 11 and 23 deg K respectively in the three decelerations. Fig 36.3 gives the temperature changes due to heat transfer during the altitude deceleration (2). The thermal effects in the sea level deceleration over the same non-dimensional speed range (3) are roughly one half to one third of those observed in the altitude deceleration. This is due to the much higher air mass flow rates through the compressor at sea level. In the sea level

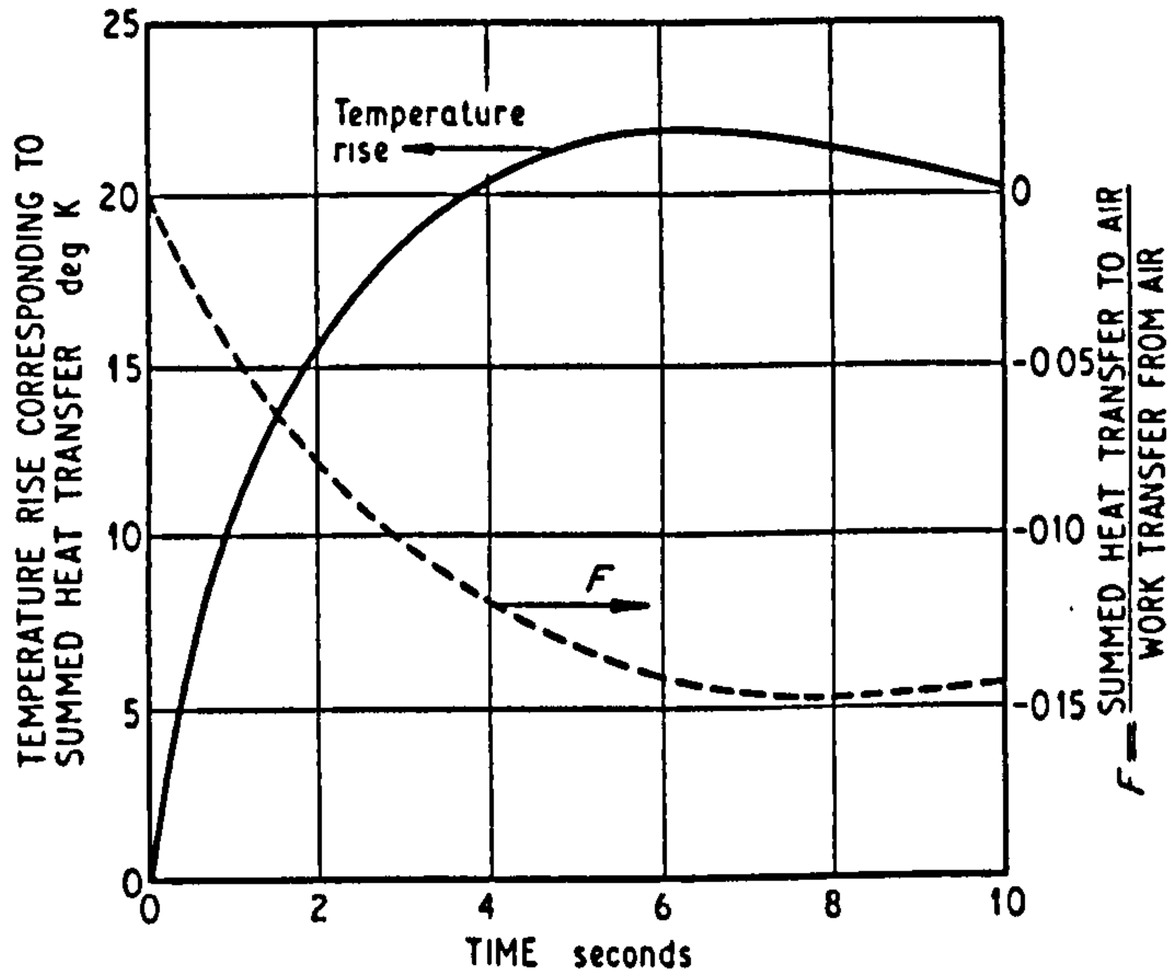

Fig. 36.3 Heat transfer in HP compressor during a deceleration at 12 200 m (40 000 ft) altitude 0·61 Mach number (transient (2))

deceleration to the ground idle speed (4) the thermal effects are similar to those observed in the altitude deceleration. Since in these decelerations the thermal effects are close to, or at, their maximum values at the ends of the deceleration, the conditions of the compressor at these end conditions were investigated.

The effects of heat transfer on the surge line were determined by the method described previously. As before, the predicted characteristics were scaled so that the adiabatic predictions agreed with overall test results. It was found that the surge point at the speed corresponding to the end of each of the decelerations is associated with stall in the first stage of the compressor. Heat transfer causes a

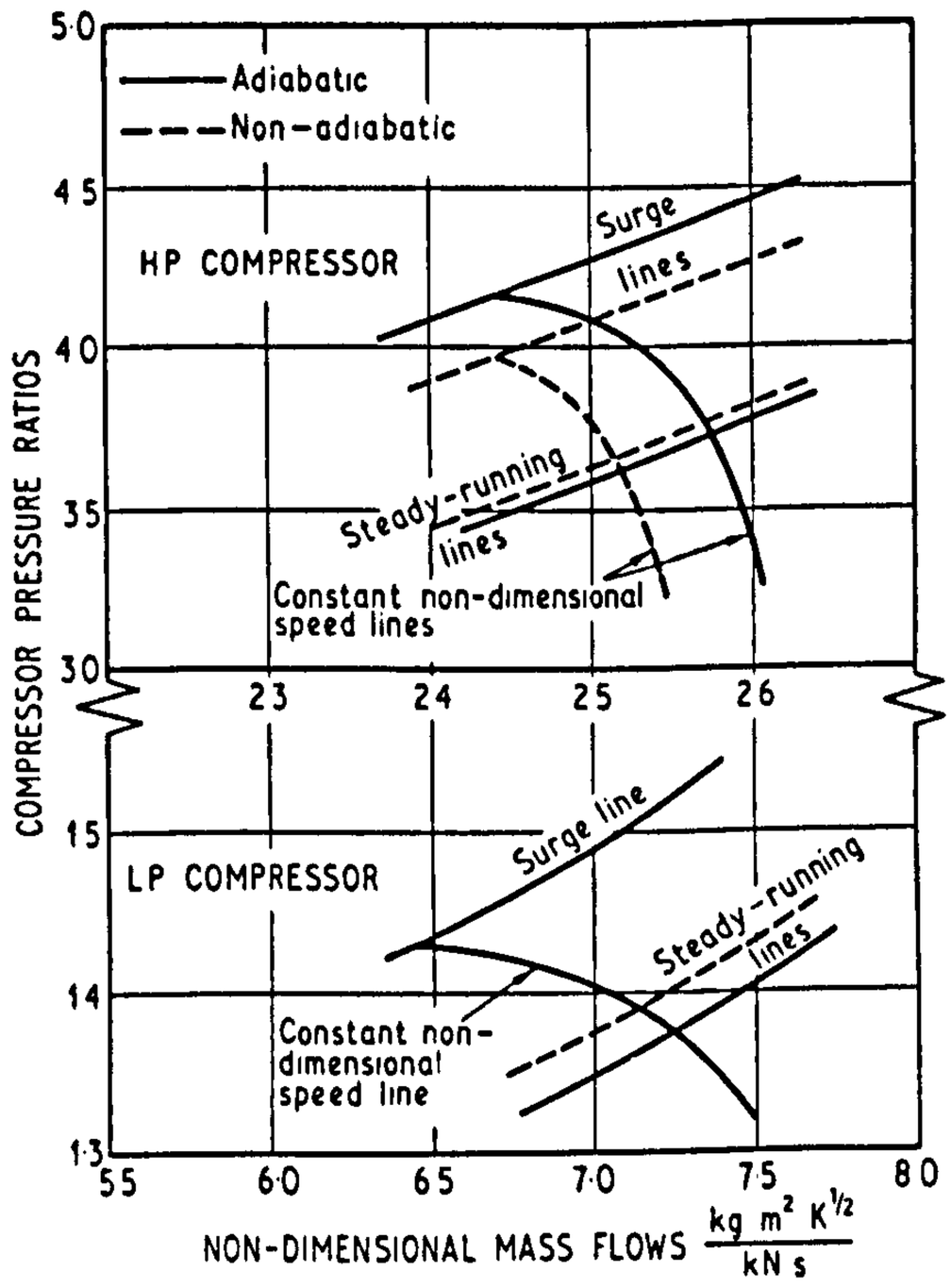

Fig. 36.4 Effects of heat transfer on surge and steady-running lines at end of altitude deceleration (2)

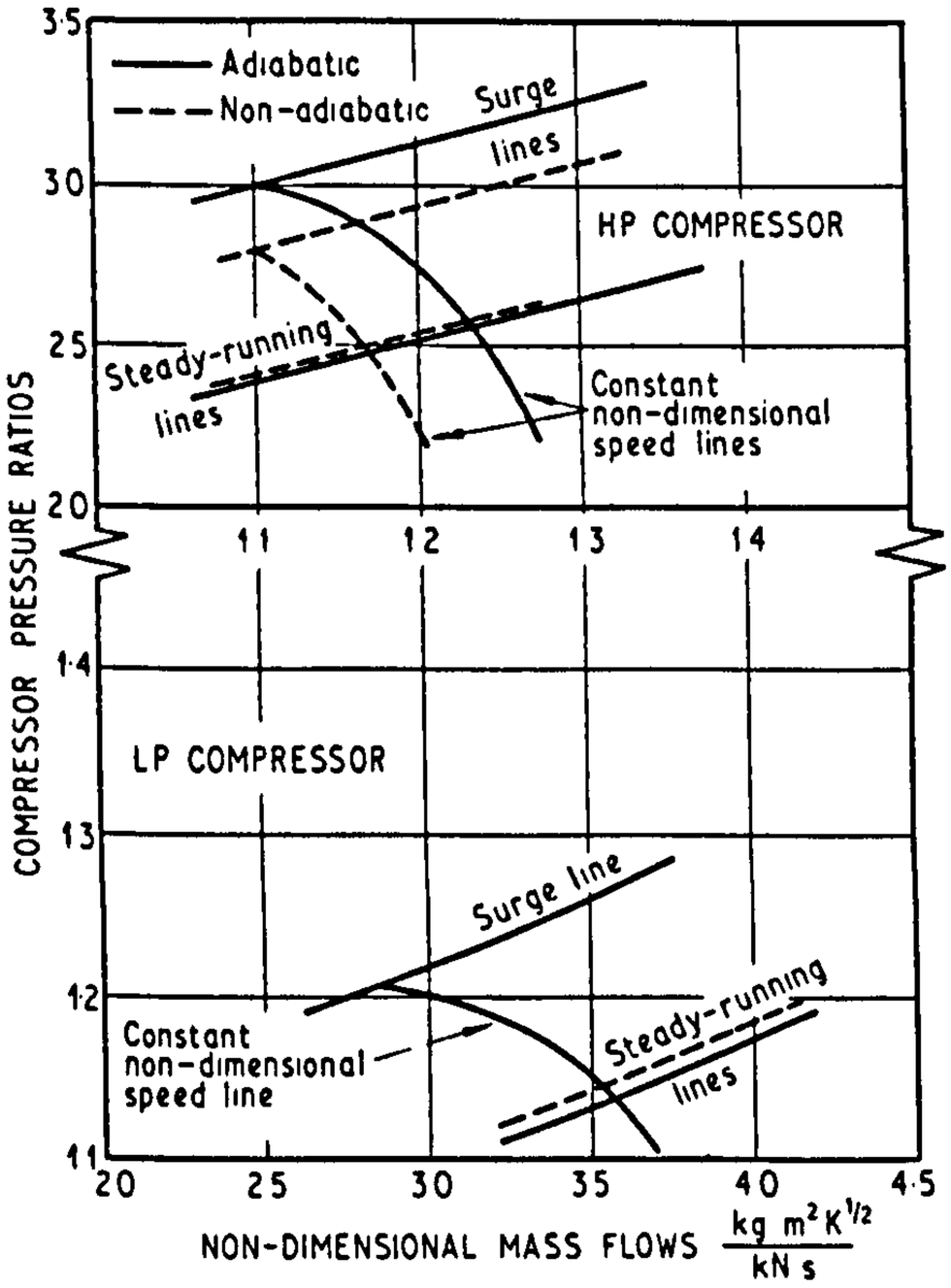

Fig. 36.5 Effects of heat transfer on surge and steady-running lines at end of sea level deceleration to ground idle speed (4)

reduction in the 'effective' non-dimensional speed. But as first stage stall controls surge, according to the stage characteristics adopted, then the surge point is moved considerably from the adiabatic surge line, as shown in Figs. 36.4 and 36.5 for the altitude deceleration (2) and for the sea level deceleration to ground idle speed (4) respectively. The other deceleration (3), is not shown, the deterioration in this case being about one third of that in deceleration (2).

Heat transfer has a slight effect on the location of stall in the compressor. During the decelerations, the heat transfer to the air tended to move the stall further forward in the machine to a position corresponding to stall at a lower rotational speed. However, the effect was fairly small and in none of the transients considered was the stall position moved from one group of three stages to the next, and of course at the ends of the decelerations, stall in the adiabatic case was already in the first stage.

2.3 Comparison with other predictions.

A helpful analysis of the effects of heat transfer on the surge line has been made by Barnes (8). His method applies to the situation where the mass flow rate at surge at a particular speed is the same in both the adiabatic and non-adiabatic cases. This therefore limits the application to the lower speed region where surge is associated with first stage stall. For this condition he shows that the pressure ratios for the non-adiabatic surge, R'_{SA}, at speed N_A is given by

$$\frac{R'_{SA}-1}{R_{SB}-1}=\left(\frac{N_A}{N_B}\right)^2 \qquad \ldots(1)$$

where R_{SB} is the pressure ratio at the adiabatic surge point giving the same density ratio across the machine as occurs in the non-adiabatic case, and N_B is the speed corresponding to this point.

The results of this prediction for the surge points at the conclusions of the two decelerations (2) and (4) are in close agreement with the predictions of the stacking method. These surge conditions, as mentioned, are associated with first stage stall. Unfortunately, Barnes' method cannot be applied when surge is associated with stall towards the rear stages of the compressor, as was the situation at 3·6 s of acceleration (1). Also, Barnes' method requires knowledge of the density ratio in the non-adiabatic case.

3 EFFECT OF BULK HEAT TRANSFER ON STEADY RUNNING WORKING LINES

Surge margin can be expressed by the difference between the surge pressure ratio and the pressure ratio of the steady-running working line at that particular mass flow rate. A study has therefore been made of the effects of the heat transfers in transients on the steady-running working line of the same twin-spool bypass engine. Bulk heat transfers have two effects in this context; compressions and expansions are non-adiabatic and the effective areas of the throats of the nozzle guide vanes are altered.

It has been shown (9) that in non-adiabatic expansions, if the ratio, F, of the heat transfer to the fluid to the work transfer from the fluid is constant along the turbine then

$$\frac{m-1}{m}=(1-F)\eta_{pt}\frac{\gamma-1}{\gamma} \qquad \ldots(2)$$

The corresponding equation for compressions is

$$\frac{m-1}{m}=\frac{(1-F)}{\eta_{pc}}\frac{\gamma-1}{\gamma} \qquad \ldots(3)$$

In (9), which dealt only with heat absorptions, a factor f was used, defined by the ratio of the heat transfer from the fluid to the work transfer from the fluid. The sign given to heat transfer was the opposite to the normal thermodynamic convention. In the work reported here, the ratio F follows the normal convention.

Using the revised finned blade model (5) the heat transfers in the two compressors and two turbines were determined during the four transients (1)-(4). The heat transfer coefficients used for the compressors were obtained as described previously and for the turbines, Halls correlation was used (6). It was found that, at any instant, the factor F varied considerably within the individual components. For example, after 3 s of acceleration (1), the average value of F for stages 1-3 of the HP compressor is 0·030 while it is 0·103 for stages 10-12. At the end of the acceleration the F values are more uniform, being 0·025 and 0·039 respectively at these locations. In spite of this variation, it is considered that the error resulting from using an averaged F for a component is small and averaged values have been used in this work.

The magnitudes and effects of the bulk heat transfers in the compression and expansion processes at 3·6 s of acceleration (1) and at the conclusions of decelerations (2) and (4) are shown in Table 1. The heat transfers are very considerable, when compared with the work transfers, particularly in the turbines.

Heat transfers during the transients may also affect the effective flow controlling areas at the nozzle guide vane throats in the HP and LP turbines. This effect is in the

opposite direction to the uncompleted thermal expansion. For example, at the end of the altitude deceleration (2) the temperature of the aerofoils of the first set of HP nozzle guide vanes is some 100 deg K above the equilibrium value. This corresponds to a linear contraction still to be completed of 0·14 per cent, and a probable throat area reduction of 0·4 per cent. However, the heat transfer to the gases in these nozzle guide vanes raises the gas stagnation temperature by 10·7 deg K. This causes a reduction in the 'coefficient of discharge' of the nozzles. Watson (10) has investigated this effect, both theoretically and experimentally. His one-dimensional theory predicts the coefficient of discharge, C_D, of a non-adiabatic nozzle, ignoring friction, to be given by

$$C_D = r^{\left(\frac{1}{m}-\frac{1}{\gamma}\right)}\left[\frac{1-r^{\frac{m-1}{m}}}{(1-F)(1-r^{\frac{\gamma-1}{\gamma}})}\right]^{\frac{1}{2}} \quad \ldots(4)$$

where r is the ratio of the downstream static pressure to the upstream stagnation pressure and C_D is defined by the ratio of the mass flow in the non-adiabatic nozzle to the mass flow in an adiabatic nozzle of the same geometric size and at the same inlet conditions and exit pressure. For the case at the end of the altitude deceleration the above expression gives a C_D of 0·989. Combining this reduction with the higher geometric area indicates an effective area at the end of the deceleration of 0·993 of the equilibrium effective area.

The expression given in equation (4) for the C_D in a non-adiabatic nozzle is based on a one-dimensional analysis. A more recent investigation of flow in non-adiabatic nozzles also uses a one-dimensional theory (11). However, preliminary boundary layer calculations allowing for changes in displacement thickness due to heat transfer, after the method of Harris and Luxton (12), and assuming a one-dimensional flow outwith the boundary layer, indicate that the reduction in C_D due to heat transfer should be about 0·015 for the condition at the end of the altitude deceleration. It was decided to adopt these predictions which considered boundary layer behaviour rather than use the simple one-dimensional theory of equation (4). On this basis, the effective area of the first set of HP nozzle guide vanes at the end of the altitude deceleration is 0·988 of the equilibrium value. The HP and LP nozzle guide vanes were treated in this way for all the transients, and the effects on the steady-running pressure ratios are shown in Table 1.

The summation of the effects of the non-adiabatic compressions and expansions and of the effective area changes on the steady-running line are indicated by the dotted lines on Figs. 36.2, 36.4 and 36.5, corresponding to the three transients (1), (2) and (4) respectively. Equilibrium steady-running lines are indicated by the solid lines.

4 DISCUSSION OF PREDICTIONS

There must be some reservations about the accuracy of the results owing to the approximations that were required in the stacking procedure and in the calculations for simulating the steady running of the engine. Nevertheless, the general effects must be valid and these are discussed below.

Heat transfer causes only slight changes in the surge line and constant speed lines of the LP compressor. The changes are probably small enough to be ignored. However, significant changes occur in the characteristics of the HP compressor. In the low speed range where surge is associated with first stage stall, the surge line is depressed by heat transfer from the blades etc. to the air. At the conclusion of the altitude deceleration the deterioration is worth about 29 per cent of the margin between the equilibrium surge and working lines. The corresponding reduction at the end of the sea level deceleration to ground idle speed is 30 per cent. When accelerating an initially cold engine there will be corresponding beneficial displacements of the surge line at the low speed end.

At higher rotational speeds, compressor surge is associated with stall in stages nearer the exit of the compressor. In these circumstances, there does not seem to be a significant displacement of the surge line due to heat transfer, only a movement of the constant speed line to a

Table 1. Effects of changes in components on steady-running compressor pressure ratios

	3·6 s in acceleration (1)			End of deceleration (2)			End of deceleration (4)		
	F	δRW		F	δRW		F	δRW	
		LP Comp	HP Comp		LP Comp	HP Comp		LP Comp	HP Comp
Heat transfer in LP compressor	+0·03	−0·003	0·000	−0·13	+0·007	0·000	−0·30	+0·003	0·000
Heat transfer in HP compressor	+0·07	−0·003	−0·050	−0·14	+0·007	+0·065	−0·19	+0·003	+0·020
Heat transfer in HP turbine	−0·15	−0·005	+0·030	+0·23	+0·007	−0·030	+0·26	+0·002	−0·030
Heat transfer in LP turbine	−0·50	−0·009	+0·020	+0·32	+0·005	−0·015	+0·29	0·000	0·000
Effect due to δA_4		0·000	−0·030		0·000	+0·040		0·000	+0·020
Effect due to δA_5		0·000	0·000		0·000	0·000		+0·002	0·000
$\Sigma\, \delta RW$		−0·020	−0·030		+0·026	+0·040		+0·010	+0·010
RW		1·446	4·10		1·378	3·73		1·138	2·56
R'_W		1·426	4·07		1·404	3·79		1·148	2·57

position of higher effective speed during an acceleration and of lower effective speed during a deceleration.

As to the effects on the steady-running line, the effects on the line in the LP compressor due to the transfers in the various components are additive. The steady-running line is lowered when heat transfer is from the air or gas, as in an acceleration, and raised in the conditions corresponding to a deceleration. At the conclusion of the altitude deceleration (2) the raising of the steady-running line due to heat transfers reduces the surge margin by 18 per cent. At the conclusion of the sea level deceleration (4) the reduction in surge margin is 8 per cent. This reduction can be serious during a deceleration in that the trajectory in the LP compressor during a deceleration is raised above the steady-running line. The altitude deceleration is seen to be the one more prone to surge the LP compressor.

The steady-running line in the HP compressor is, as expected, unaffected by heat transfer in the LP compressor. It is only affected by heat transfer in the LP turbine when the LP turbine is unchoked. Under these conditions, heat transfer alters the pressure ratio across the turbine and hence the effective flow capacity of the turbine. The summed effects of the heat transfers in the two turbines almost exactly cancel the effect of the heat transfer in the HP compressor, with little resulting net effect on the steady-running line. However, the position of the steady-running line is seen to be very sensitive to changes in the flow capacity of the HP turbine. For example, the suggested reduction in the flow capacity of 1·2 per cent at the end of the altitude deceleration (2) causes an increase in the steady-running pressure ratio of 0·04 which reduces the surge margin by just under 6 per cent. When these changes are coupled with the changes in the surge line due to heat transfer there is a reduction in the surge margin of 35 per cent at the conclusion of the altitude deceleration (2) and of 32 per cent at the conclusion of the sea level deceleration to the ground idle speed (4). There is an increase in the surge margin of 4 per cent at 3·6 s in the sea level acceleration (1). The reductions in surge margins in the HP compressor during decelerations are probably unimportant during the decelerations themselves since the HP compressor decelerates away from surge, but will be important if an acceleration is attempted immediately following the deceleration.

The above predictions for the changes in the steady-running points due to heat transfer may not be exactly the same as those observed during transients, as the pressure ratios and component efficiencies at the transient points differ from the steady-running values. However, the predictions given above are helpful in that they give magnitudes of the effects that may be encountered.

5 CONCLUSIONS

The magnitudes of the heat transfers in typical transients in a twin-spool bypass engine have been assessed. These heat transfers in the various components can be quite considerable, rising to 0·3–0·5 of the work transfers in turbines and to 0·15–0·20 of the work transfers in compressors.

The effects of the heat transfers in the LP compressor on the compressor characteristics are small. In the HP compressor the effects are more marked. One effect in the HP compressor is to move the effective non-dimensional speed. The other effect, which is on the surge line, depends on where the stall causing surge occurs in the HP compressor. If it is first stage stall, then the surge point comes at the same mass flow rate as in the adiabatic case, but at the new 'effective' speed. However, if the stall causing surge occurs near the rear of the compressor then the surge point may lie very close to the adiabatic surge line, and there is only the change in effective speed.

The effects of heat transfers on the steady-running lines in the compressors have also been assessed. Heat transfers not only cause the compressions and expansions to be non-adiabatic but they also affect critical flow areas such as at the nozzle guide vanes in the HP and LP turbines. The steady-running line in the HP compressor is particularly sensitive to changes in the effective capacity of the HP nozzle guide vanes. The relationship between heat transfer and the effective capacity of the nozzle guide vanes was estimated from preliminary boundary layer calculations. Further work is required in this direction.

When the effects on the surge line and on the steady-running line are combined, the most serious situations appear to arise in the LP compressor during an altitude deceleration (18 per cent reduction in surge margin) and in the HP compressor when attempting an acceleration immediately following a rapid deceleration (35 per cent reduction in surge margin). The situation in the LP compressor during the deceleration could be improved by using a variable area final nozzle with the nozzle area reduced during deceleration.

The effects of heat transfer have been assessed only at the steady-running conditions corresponding to instants during or at the ends of transients. It is now proposed that these effects be included in transient programmes such as those of Saravanamuttoo and Fawke (1), (2).

6 ACKNOWLEDGEMENTS

The author wishes to thank the staff of Rolls-Royce (1971) Limited both for providing engine test data and for their advice and comments. He also wishes to thank Professor R. S. Silver, and colleagues, at the University of Glasgow for their encouragement and advice, and Mr O. Skyllingstad, now a Graduate of the University of Glasgow, for his assistance and comments.

APPENDIX 36.1

References

(1) Saravanamuttoo, H. I. H. and Fawke, A. J. 'Simulation of gas turbine dynamic performance', ASME paper No. 70-GT-23.
(2) Fawke, A. J. and Saravanamuttoo, H. I. H. 'Experimental investigation of methods for improving the dynamic response of a twin-spool turbojet engine', *J. Engng Pwr., Trans. Am. Soc. mech. Engrs* 1971 93, 418–24.
(3) Warne, E. H. 'Gas turbine fuel and control systems', *Proc. Instn mech. Engrs* 1968–69 183 (Pt 3N), 121–127.
(4) Grant, A. D. 'The effect of heat transfer on boundary layer stability in axial flow compressors'. Paper to this Conference.
(5) Maccallum, N. R. L. 'Models for the representation of rotary machine blades during temperature transients', Mechanical Engineering Department Report, University of Glasgow, 1971, (September).
(6) Halls, G. A. 'Air cooling of turbine blades and vanes', Lecture to AGARD, Varenna, Italy, 1967.
(7) Huppert, M. C. and Benser, W. A. 'Some stall and surge phenomena in axial flow compressors', *J. Aeronaut. Sci.* 1953 20, 835–45.
(8) Barnes, J. F. Private Communication, 1970 (April).

(9) Maccallum, N. R. L. 'The performance of turbojet engines during the "thermal soak" transient', *Proc. Instn mech. Engrs* 1969–70 184 (Pt 3G(II)), 23–29.
(10) Watson, W. G. 'One-dimensional expansion of a compressible fluid in a convergent nozzle with heat flow and friction', Ph.D. Thesis, University of Glasgow, 1956.
(11) Chen, W. W. L., Vachon, R. I. and Dyer, D. F. 'Quasi-steady compressible flow with heat transfer in accelerating nozzles and ducts', *J. Spacecraft Rockets* 1969 6, 308–311.
(12) Harris, H. D. and Luxton, R. E. 'Calculation of heat transfer coefficients in cooled turbine cascades', *Aeronaut. Q.* 1966. 17, 253–268.

COMBUSTION INSTITUTE - 1ST EUROPEAN SYMPOSIUM

SEPTEMBER 1973

FLAME STABILIZATION IN SWIRLING JETS

by

G.G. Bafuwa and N.R.L. Maccallum
Department of Mechanical Engineering
The University, Glasgow.

22nd March, 1973

FLAME STABILIZATION IN SWIRLING JETS

by

G.G. Bafuwa* and N.R.L. Maccallum**
* Department of Mechanical Engineering, Ahmadu Bello University, Zaria, Nigeria.
** Department of Mechanical Engineering, The University of Glasgow, Glasgow, Scotland.

Introduction

Vane swirlers are commonly used for generating swirl in air (and gas) jets entering furnaces. If the swirl is sufficiently strong, a central recirculation zone may be established. This report describes a study of the mechanism of flame stabilization by this central recirculation zone in pre-mixed town gas - air jets. A means of correlating the stability limits is proposed.

Apparatus

The swirlers used were of "hubless" design (1), 23.7 mm diameter, having vanes at angles of 30°, 45° or 60° to the axis of the jet (a vane angle of 15° was insufficient to establish a swirl controlled central recirculation zone). The pre-mixed town gas-air jets issued from these swirlers into free air.

The town gas had the following typical volumetric composition:- H_2, 0.56; CO, 0.06; CH_4, 0.12; C_2H_6, 0.01; C_3H_8, 0.04; C_4H_{10}, 0.02; CO_2, 0.15; N_2, 0.04.

Results

The central recirculation zone controlled only the weak stability limits. The stability of the rich flames depended on secondary combustion with entrained air. For this investigation of the role of the central recirculation zone, only the weak limits were relevant.

One of the authors (G.G.B.) acknowledges the financial support of the Commonwealth Scholarship Commission, and the other (N.R.L.M.) acknowledges the financial support of the Science Research Council.

Flame stabilization

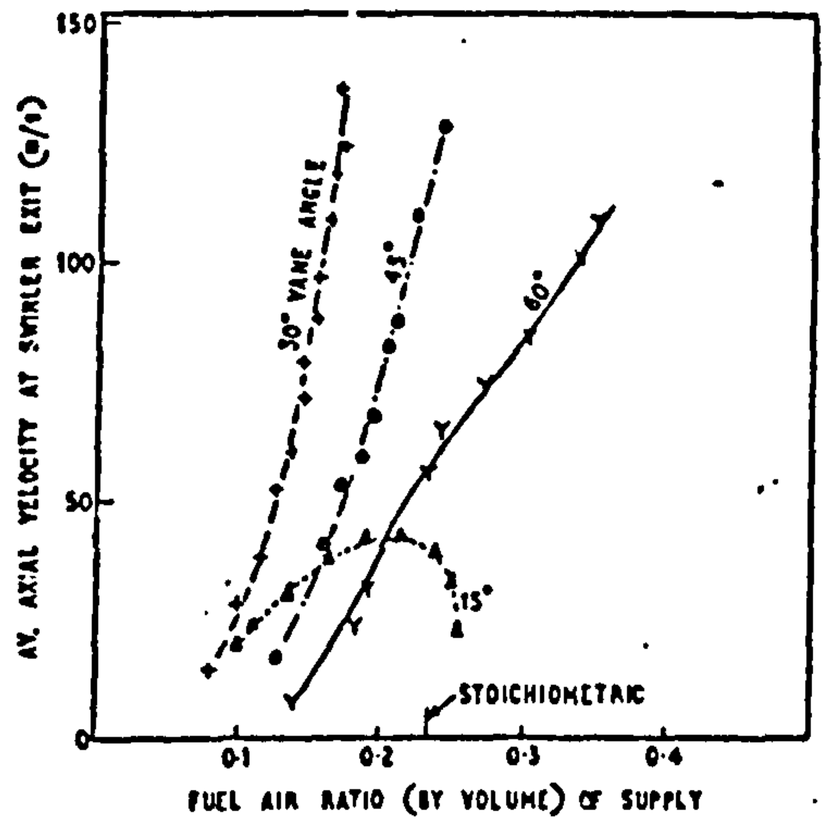

Fig.1. Weak Stability Limits

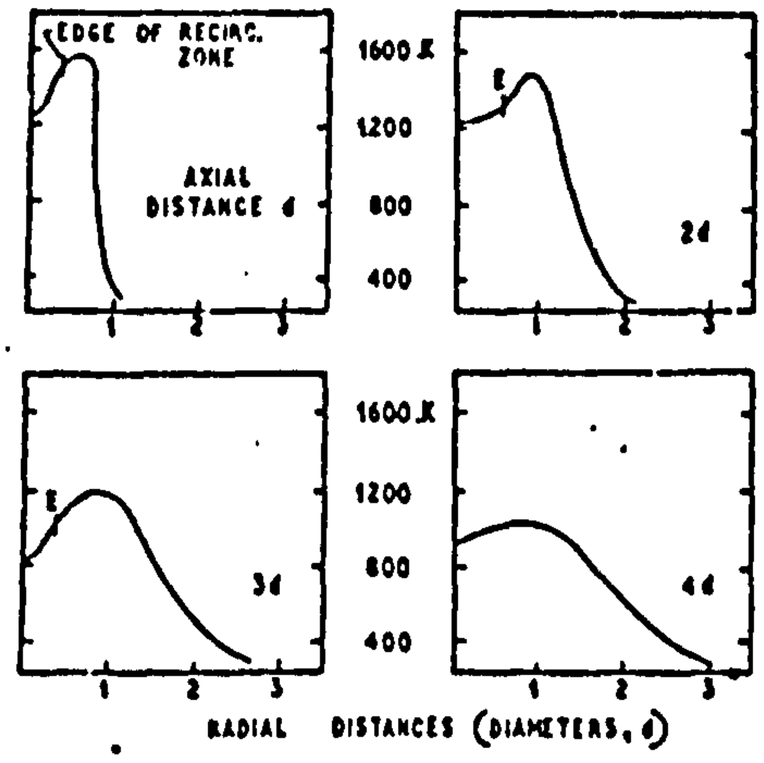

Fig.2. Temperature Distⁿ. 45° Swirler, 0.2 F/A

Fig. 1 shows these weak limits for the 30°, 45° and 60° swirlers, the axial component of velocity being plotted against the fuel/air ratio in the issuing jet. For interest, the stability limits of the 15° swirler are also shown - this swirler could not create a central recirculation zone.

Theories of Bluff Body Flame Stabilization

Various satisfactory models have been proposed for flame stabilization in the recirculation zones behind bluff bodies. For example Zukoski and Marble (2) have shown the importance of the time, τ, that an element of fresh charge is in contact with the hot recirculation zone. This time is taken as the length of the recirculation zone, L, divided by the stream velocity, U_{max}. This time was found, for a given fuel/air ratio, to be substantially independent of the variables of flame holder shape and size. These results for time τ have been interpreted by Lewis and von Elbe (3) in terms of flame stretch by arguing that during the time in which the mass element sweeps along the recirculation zone, a wave element advances with the burning velocity, S_u, from the anchoring point, which is adjacent to the bluff body, a distance, y, across the stream to meet the element which just touches the end of the wake. Then

$$\tau = \frac{L}{U_{max}} = \frac{y}{S_u} \qquad (1)$$

The test for stability is the stretch of the flame front when this element is "on its own" at the downstream

end of the recirculation zone. If the stretch parameter, K, equal to $(\eta_o/U)(dU/dy)$, exceeds a critical value of about unity, extinction occurs.. This development by Lewis and von Elbe partially explains the variation of τ with fuel/air ratio.

An entirely different mechanism for flame stabilization in recirculation zones has been given by Spalding (4). Several models were considered, typically based on the ignition of the fresh charge by the recirculating flow, the rate of reaction in the mixture of fresh charge and recirculating products being assumed to follow a simple bi-molecular equation. A diagram of this model is given in Fig. 3 and stable combustion is illustrated in Fig. 4.

The predictions of the above mentioned models have been found to be compatible with the observed stability limits when the recirculation zone contains only burning charge or products of combustion.

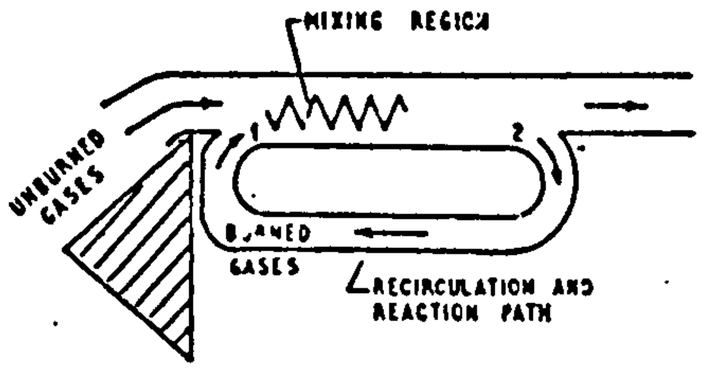

Fig.3. Flame Stabilization by Recirculation (From Spalding (4))

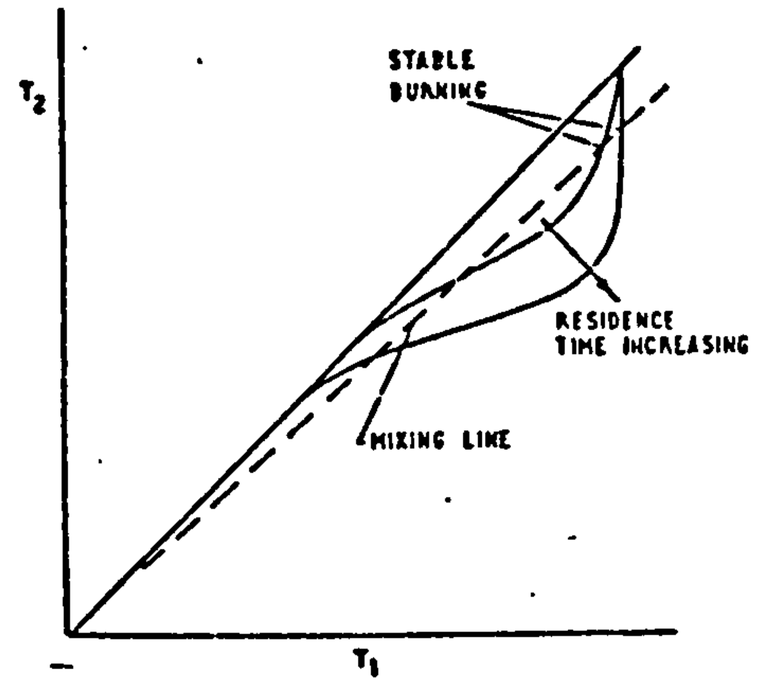

Fig.4. Mixing and Reaction Relations

Comparison of Results with predictions of Bluff Body Models

An initial application of "contact time" (2) predicts that, since increasing the vane angle from 30° to 60° (for example) lengthened the recirculation by about 70% (5), there should be a corresponding increase in blow-off velocity. The opposite effect is observed (Fig. 1).

Flame stabilization

The explanation is considered to lie in the effect of the externally entrained air on the central recirculation zone. Typical temperature traverses across the recirculation zone of the 45° swirler are shown in Fig. 2 (5). The temperatures in the recirculation zone, where reaction is virtually complete, are considerably less than the adiabatic flame temperature, and less than where the fresh charge is burning. This is due to the gas feeding the recirculating zone being diluted by ambient air - an effect which increases with swirl.

Recognition of this dilution effect suggests that the blow-off velocities should be plotted against the corresponding temperatures where combustion is initiated at the edge of the recirculation zone. The axial components of the blow-off velocities are plotted in Fig. 5(a) and the absolute components in Fig. 5(b). These results support this type of correlation; that using the absolute velocity being the better. The mass ratios of entrained air to total gases in the recirculation zone were found to be 0.26, 0.40 and 0.53 for the 30°, 45° and 60° swirlers respectively.

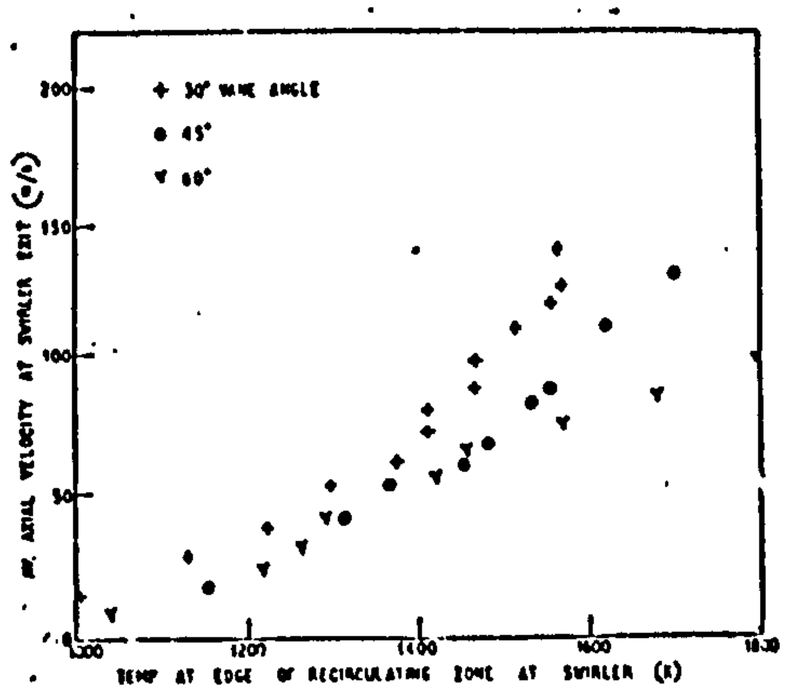

Fig.5(a) Weak Stability Limits

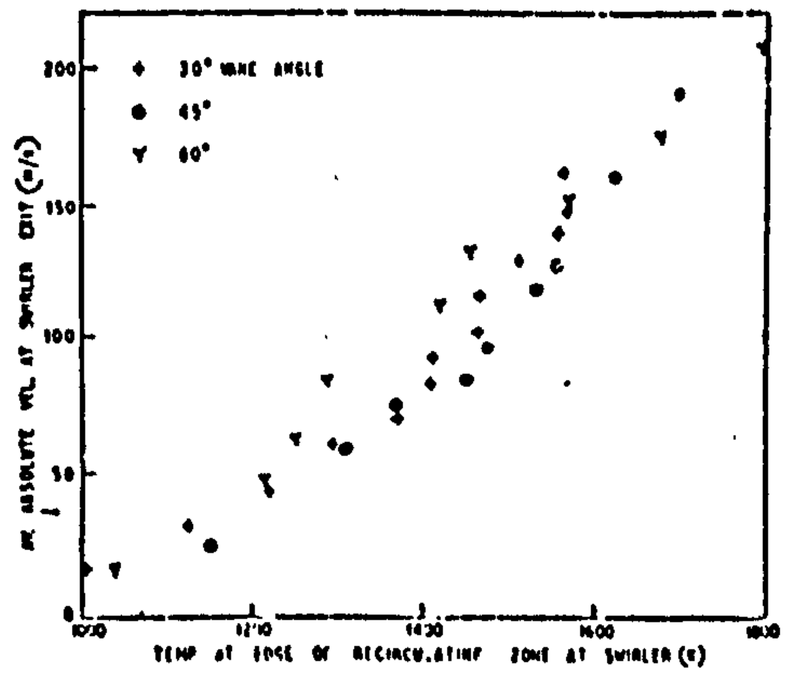

Fig.5(b) Weak Stability Limits.

Accepting this dilution effect, can the above mentioned models be suitably adjusted? In its simple form the contact time model cannot be altered. In the flame stretch theory (3), S_u in Eqn.(1) and the flame thickness, η_o, in the stretch factor can be taken at the fuel/air ratio corresponding to the recirculation zone. Comparing the two extreme swirlers (30° and 60°), at a temperature,

the axial velocity for the 60° swirler is about 10% lower and length L is about 70% greater. Eqn. (1) then gives y_{60} almost double y_{30}. The velocity gradients at the "break points" are about 20% lower for the 60° swirler (5), hence K_{60} is about 0.4 K_{30} instead of being the same.

The effect of entrainment is perhaps most easily understood using Spalding's model (4). A simple adaption of this is to draw the reaction curves (Fig. 4) appropriate to the fuel/air ratio of the diluted stream after entraining the ambient air. It is plausible that raising the degree of swirl increases the diluting effect to such an extent that the values of T_1, at a flow velocity, are effectively unaltered at the blow-off limits although the approach fuel/air ratios are much higher.

Application to Flames in Furnaces

In swirling furnace flames, the central recirculation zones will entrain considerable quantities of the externally recirculated gases. In this case the external gases will be hot products of combustion. If these have not been cooled by the furnace walls, etc., then the effective fuel/air ratio for stabilization in the recirculation zone will be the same as in the approach stream. However if some cooling has occurred, correction for the effective fuel/air ratio will be necessary. A limited number of stability limits (6) taken in hot and cold furnaces agree with this form of correction.

Conclusions

The stabilization of flames in the central recirculation zones of swirling free jets is very much influenced by entrainment of ambient air into the central zone. This entrainment increases with degree of swirl and amounts to just over 50% of the recirculating flow for the 60° vane swirler.

The weak stability limits can be correlated reasonably by plotting the absolute component of velocity leaving the swirler against the temperature at the edge of the recirculating zone nearest to the swirler. The results are explained more readily by the Spalding model (4) than by flame stretch.

References

1. Mathur, M.L. and Maccallum, N.R.L., "Swirling air jets issuing from vane swirlers". J. Inst. Fuel 40, p.214 (1967).

2. Zukoski, E.E. and Marble, F.E., AGARD "Combustion Researches and Reviews". Butterworth, London, 1955, p.167; Gas Dynamics Symposium on Aerothermochemistry, 1955, Northwestern University, 1956, p.205.

3. Lewis, B. and von Elbe, G. "The concept of flame stretch". Z. Phys. Chem. 37, p.287. (1963).

4. Spalding, D.B., "Theoretical aspects of flame stabilization", Aircr. Engng. 25, p.264 (1953).

5. Bafuwa, G.G. and Maccallum, N.R.L., "Turbulent swirling flames issuing from vane swirlers", 18th Meeting Aerodynamics Panel, IFRF, Paris, 1970, DOC No. G02/CA/5.

6. Beltagui, S.A., Unpublished Work, Glasgow University, 1972.

COMBUSTION INSTITUTE - 1ST EUROPEAN SYMPOSIUM

SEPTEMBER 1973

VANE-SWIRLED FLAMES IN FURNACES

by

S.A. Beltagui* and N.R.L. Maccallum**

*British Steel Corporation, Swinden Laboratories, Rotherham.
**Department of Mechanical Engineering, University of Glasgow.

Department of Mechanical Engineering,
University of Glasgow.

26th February, 1975

VANE-SWIRLED FLAMES IN FURNACES

by
S.A. Beltagui* and N.R.L. Maccallum**
*British Steel Corporation, Swinden Laboratories, Rotherham
**Department of Mechanical Engineering, University of Glasgow

Introduction

If the flow entering a furnace is given swirl, the resulting flow within the furnace can be greatly altered. Addition of a small amount of swirl accelerates the spread of the jet, while still maintaining forward velocities on the jet axis. If the swirl is sufficiently increased, a central recirculation zone (C.R.Z.) is established. This paper presents the results of the continuation of a previous study (1) of the flows issuing from a range of vane swirlers.

Apparatus

Swirlers: of hubless and annular design (2), vanes at 15°, 22°, 30°, 45° and 60° to jet axis: diameters; hubless, 93 mm; annular, 98 mm outer, 32 mm hub.

Furnaces: firebrick, 0.46 m i.d. (D/d = 5), 1.4 m length; cement, 0.225 m i.d. (D/d = 2.5), 0.9 m length.

Combustible: premixed town gas-air, fuel/air ratio generally 0.125 by volume (3).

There was no quarl, and the exit from the swirler was in the plane of the inner surface of the furnace end-wall. The instrumentation was as used previously (1). Tests were performed in both burning and isothermal conditions.

Results

Some of the aerodynamic results obtained with the D/d = 5 furnace have been reported previously (1). The other results, and those in the D/d = 2.5 furnace are given in reference (3). A wide variety of flow types was observed, ranging from the very weak swirl case in which there is no significant trough in velocity at the axis (referred to as Type A) to those with a strongly established C.R.Z. (Type D). In Type B flow there is a trough in velocity at the axis, but no reverse flow. A regime in which there is a weak central reverse flow (mass flow $<$ 0.1 of the burner flow) is called a Type C flow.

The type of flow adopted depends primarily on the swirler vane angle and on the density ratio resulting from combustion. For example, in isothermal flow, transition from B to C Type flow occurs at a vane angle of about 22°, whereas under combustion conditions ($\rho_u/\rho_b = 5$) the vane angle for transition is about 30°. The effect of relative furnace size is not

The authors wish to acknowledge the financial support of the Science Research Council.

great in the range observed, although the smaller relative furnace size tends to give transitions at slightly lower vane angles.

Correlation of Results

A correlation of these transitions is desirable. The applicability of the commonly used Swirl Number $S = T/(G_t d)$ has been examined. Experimental values of the momentum fluxes in the two furnaces (typical results shown in Figs. 1 and 2 from (4)) have been compared with those predicted from the simple analysis of Kerr and Fraser (5)

$$T = \frac{\pi}{12} \rho_u U^2 d^3 \frac{(1 - z^3)}{(1 - z^2)^{3/2}} \tan \theta \qquad (1)$$

and

$$G_t = \frac{\pi}{4} d^2 \rho_u U^2 \qquad (2)$$

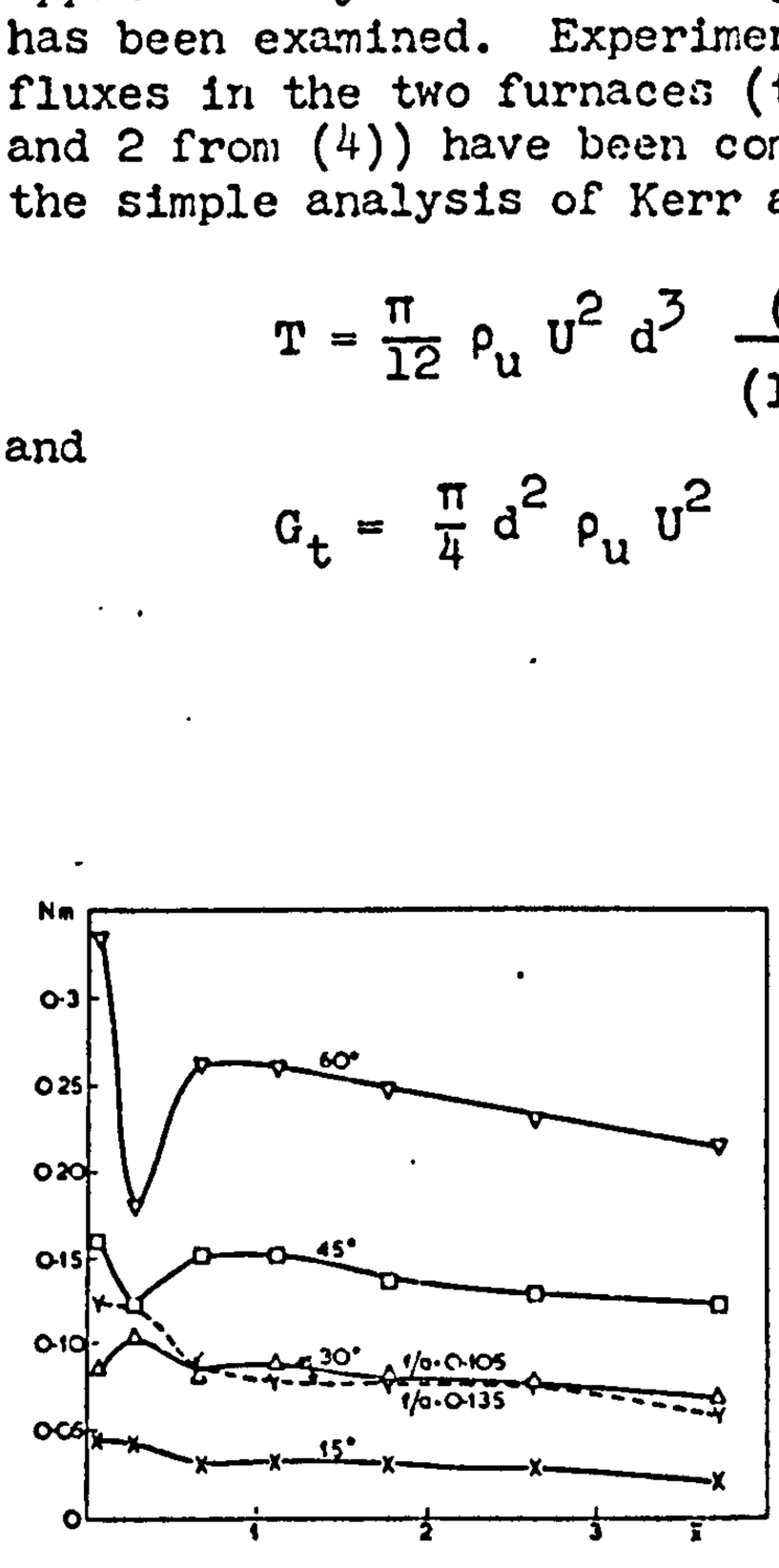

Fig 1. Axial flux of tangential momenta
Hubless swirler flames in D/d = 2·5 furnace

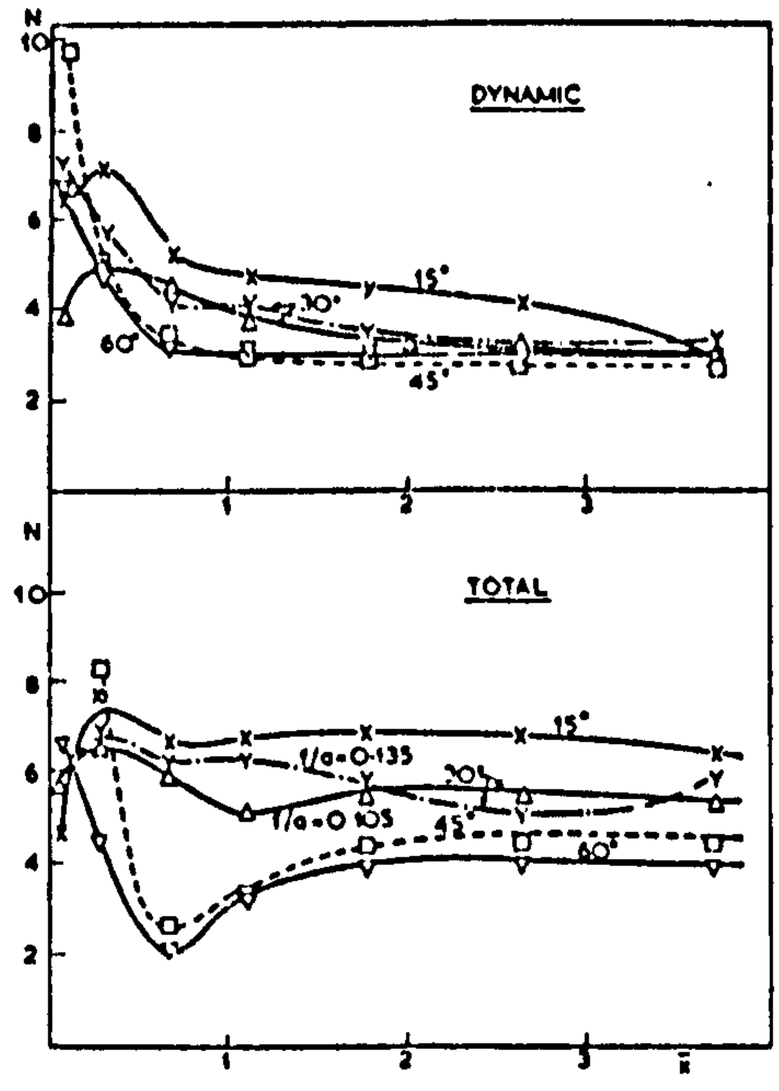

Fig.2. Axial momentum fluxes
Hubless swirler flames in D/d = 2·5 furnace

The experimental values of the tangential momentum fluxes in the developed flow beyond the CRZ (where present) are considerably higher than the prediction of Eqn. (1), the ratios to the predicted value being 2.2 and 1.7 for isothermal flows in the D/d = 2.5 and 5 furnaces, and 3.0 and 2.0 for the

corresponding burning jets. Experimental values of total axial momentum flux require a definition of reference static pressure. Several have been proposed (5). The one selected here is the pressure at the centre of the peripheral recirculation zones in the unswirled isothermal flow in that furnace. Here again the total axial momentum fluxes observed in the developed flows differ from the prediction of Eqn. (2), the ratios to the prediction being 2.1 and 0.85 for isothermal conditions in the D/d = 2.5 and 5 furnaces, and 3.5 and 1.1 for the corresponding burning conditions. While there is scatter, it is clear that the observed fluxes in the developed flows (where the fluxes are more nearly conserved) differ from the simple predictions, being influenced both by combustion and D/d ratio. Consequently the correlation between flow types has been sought in terms of experimental fluxes rather than predicted values. In view of the uncertainty regarding the reference pressure required to define the total experimental axial momentum flux, for simplicity this flux has been based solely on the axial velocity component. The dynamic component is shown in the upper portion of Fig. 2. Regarding the linear dimension required in the Swirl Number, it is seen that (a) the same swirler can give different velocity patterns as the relative furnace size is changed and (b) the dimensions of the C.R.Z., when established, are primarily functions of D, and not of d. Thus the new definition of the experimental Swirl Number is

$$S^* = T/(G_d D) \qquad (3)$$

This parameter, S*, has given a very satisfactory correlation between flow types (Fig. 3). The transitions from flow types A to B, B to C and C to D occur at values of S* of 0.08, 0.11 and 0.18 respectively. Further, for the same swirler, in say isothermal flow, the S* values are very similar in the two relative furnace sizes. A corresponding result holds for burning flows having the same fuel/air ratio.

There is a change in the slopes of both the isothermal and burning correlations at a vane angle of about 30°. In the burning case this corresponds to the transition to a C.R.Z.

The displacement of the correlation for the burning jets from the isothermal correlation is a function of fuel/air ratio, as discussed below.

Prediction of Swirl Number S* - Use for Design

The S* - θ relations (Fig. 3) required extensive experimentation. Satisfactory prediction of these relations has not yet been made, although it is helpful to note that S* is very nearly proportional to tan θ, particularly for Type D flows. If the isothermal correlation is established, a

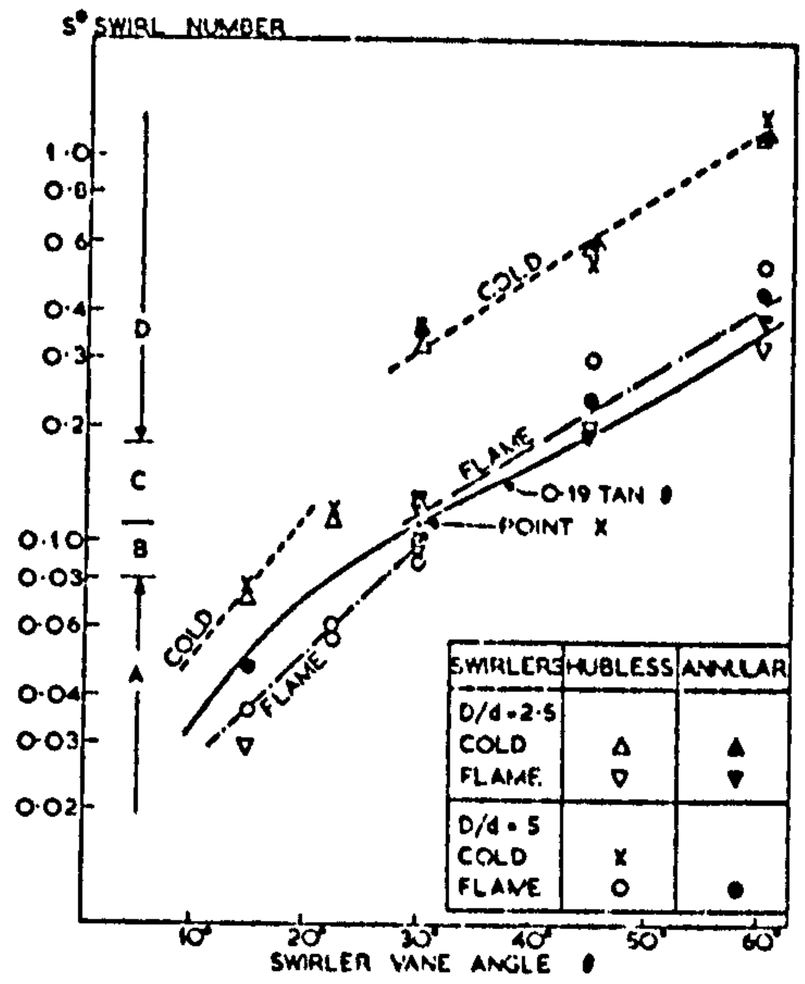

Fig. 3. Swirl number relation to input conditions and flow types

method is outlined below for prediction of the burning correlation.

Let the pressure drop required for the density change in the furnace be F_1 times that for one-dimensional flow. When combustion occurs let us assume the dynamic component of the axial momentum flux is increased due to this pressure change acting across the front face of the furnace. Assuming, further, that the isothermal dynamic axial momentum flux is a fraction, F_2, of that given by Eqn. (2), the dynamic axial momentum flux in the burning case is

$$G_{db} = F_2 \frac{\pi}{4} d^2 \rho_u U^2 + F_1 \frac{\pi}{4} D^2 \rho_u U^2 \left(\frac{d}{D}\right)^4 \left(\frac{\rho_u}{\rho_b} - 1\right) \qquad (4)$$

The tangential momentum fluxes are slightly increased by combustion, as discussed above. Letting the ratios of these tangential fluxes, burning to isothermal, be F_3, then the Swirl Number ratio for a particular swirler is

$$\frac{S_b^*}{S_i^*} = \frac{F_2 F_3}{F_2 + F_1 \left(\frac{d}{D}\right)^2 \left[\left(\frac{\rho_u}{\rho_b}\right) - 1\right]} \qquad (5)$$

F_3 is almost independent of (D/d) and a mean value of 1.3 is reasonable. F_2 is markedly influenced by (D/d) and has

values of 0.51 and 0.16 for the (D/d) values of 2.5 and 5 respectively. Using these values for F_2 and F_3, it is found that a value of 2.1 for F_1 fits both sets of furnace results (premixed gas-air flames). With other forms of firing, F_1 and F_3 may be altered. The changes in F_3 will probably be small enough to ignore. F_1 will probably be reduced if combustion is slower, but should not drop below unity.

When using vane swirlers similar to those tested here, the isothermal correlation given in Fig. 3 can be used, and modified for combustion using Eqn. (5).

For other designs of vane swirlers, the isothermal correlation can be established in a model (use (D/d) values in the range 2.5 to 5). Alternatively, the burning correlation can be established by using the sharp discontinuity that exists in the variation with θ of the minimum static pressure on the axis. This discontinuity is the transition from flow Type B to C and corresponds to the value 0.11 for S*, locating the equivalent of point x on Fig. 3. The proportionality with tan θ allows an approximate correlation to be drawn. The burning tests used to find the discontinuity in axis pressure may be carried out on a model.

Conclusions

The flow types resulting from vane-generated swirl are correlated by an experimental Swirl Number, S*. The isothermal S* - θ relation for the present design of swirlers has been established and an expression has been developed for giving the burning relationships. Methods requiring much less experimentation are suggested for establishing the corresponding relationships for other designs.

References

1. BELTAGUI, S.A. and MACCALLUM, N.R.L. "Aerodynamics of swirling flames - Vane generated type". 1st European Symp. on Combustion, 1973.
2. MATHUR, M.L. and MACCALLUM, N.R.L. "Swirling air jets issuing from vane swirlers". J. Inst. Fuel 40, p.214 (1967).
3. BELTAGUI, S.A. and MACCALLUM, N.R.L. "Aerodynamics of vane-swirled flames in furnaces". Mech. Eng. Report, Glasgow University, 1974.
4. BELTAGUI, S.A. and MACCALLUM, N.R.L. "The modelling of vane-swirled flames in furnaces". Mech. Eng. Report, Glasgow University, 1974.
5. KERR, N.M. and FRASER, D.A. "Swirl. Part I: Effect on axisymmetrical turbulent jets". J. Inst. Fuel 38, p.519 (1965).

Nomenclature

d	swirler diameter
D	furnace diameter
F_1, F_2, F_3	factors defined in text
G	axial momentum flux
S	swirl number $T/(G_t d)$
S*	swirl number $T/(G_d D)$
T	tangential momentum flux
U	av. axial velocity approaching swirler
$\bar{x}$	(axial distance/D)
z	hub diameter ratio
θ	vane angle to axis
ρ	density

Subscripts

b	burned	i	isothermal	u	unburned
d	dynamic	t	total		

COMBUSTION INSTITUTE - 2ND EUPOPEAN SYMPOSIUM

SEPTEMBER 1975

VANE-SWIRLED FLAMES IN FURNACES

by

S.A. Beltagui* and N.R.L. Maccallum**

*British Steel Corporation, Swinden Laboratories, Rotherham.
**Department of Mechanical Engineering, University of Glasgow.

Presented at Combustion Institute 2nd European Symposium, Orleans
September 1975.

Department of Mechanical Engineering,
University of Glasgow.

26th February, 1975

VANE-SWIRLED FLAMES IN FURNACES

by
S.A. Beltagui* and N.R.L. Maccallum**
*British Steel Corporation, Swinden Laboratories, Rotherham
**Department of Mechanical Engineering, University of Glasgow

Introduction

If the flow entering a furnace is given swirl, the resulting flow within the furnace can be greatly altered. Addition of a small amount of swirl accelerates the spread of the jet, while still maintaining forward velocities on the jet axis. If the swirl is sufficiently increased, a central recirculation zone (C.R.Z.) is established. This paper presents the results of the continuation of a previous study (1) of the flows issuing from a range of vane swirlers.

Apparatus

Swirlers: of hubless and annular design (2), vanes at 15°, 22°, 30°, 45° and 60° to jet axis: diameters; hubless, 93 mm; annular, 98 mm outer, 32 mm hub.

Furnaces: firebrick, 0.46 m i.d. (D/d = 5), 1.4 m length; cement, 0.225 m i.d. (D/d = 2.5), 0.9 m length.

Combustible: premixed town gas-air, fuel/air ratio generally 0.125 by volume (3).

There was no quarl, and the exit from the swirler was in the plane of the inner surface of the furnace end-wall. The instrumentation was as used previously (1). Tests were performed in both burning and isothermal conditions.

Results

Some of the aerodynamic results obtained with the D/d = 5 furnace have been reported previously (1). The other results, and those in the D/d = 2.5 furnace are given in reference (3). A wide variety of flow types was observed, ranging from the very weak swirl case in which there is no significant trough in velocity at the axis (referred to as Type A) to those with a strongly established C.R.Z. (Type D). In Type B flow there is a trough in velocity at the axis, but no reverse flow. A regime in which there is a weak central reverse flow (mass flow $<$ 0.1 of the burner flow) is called a Type C flow.

The type of flow adopted depends primarily on the swirler vane angle and on the density ratio resulting from combustion. For example, in isothermal flow, transition from B to C Type flow occurs at a vane angle of about 22°, whereas under combustion conditions ($\rho_w/\rho_b = 5$) the vane angle for transition is about 30°. The effect of relative furnace size is not

The authors wish to acknowledge the financial support of the Science Research Council.

great in the range observed, although the smaller relative furnace size tends to give transitions at slightly lower vane angles.

Correlation of Results

A correlation of these transitions is desirable. The applicability of the commonly used Swirl Number $S = T/(G_t d)$ has been examined. Experimental values of the momentum fluxes in the two furnaces (typical results shown in Figs. 1 and 2 from (4)) have been compared with those predicted from the simple analysis of Kerr and Fraser (5)

$$T = \frac{\pi}{12} \rho_u U^2 d^3 \frac{(1 - z^3)}{(1 - z^2)^{3/2}} \tan \theta \qquad (1)$$

and

$$G_t = \frac{\pi}{4} d^2 \rho_u U^2 \qquad (2)$$

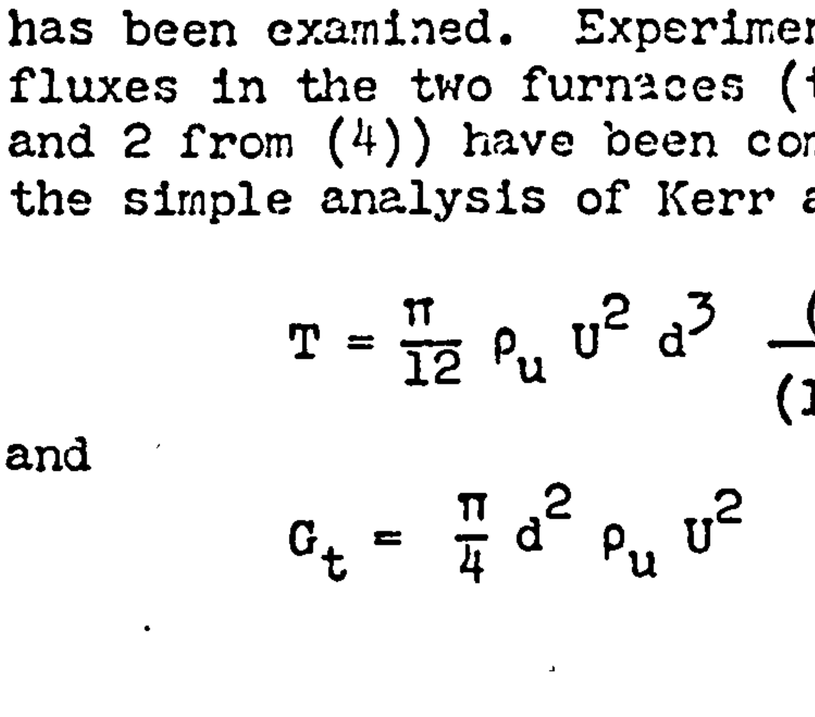

Fig. 1. Axial flux of tangential momenta Hubless swirler flames in D/d = 2·5 furnace

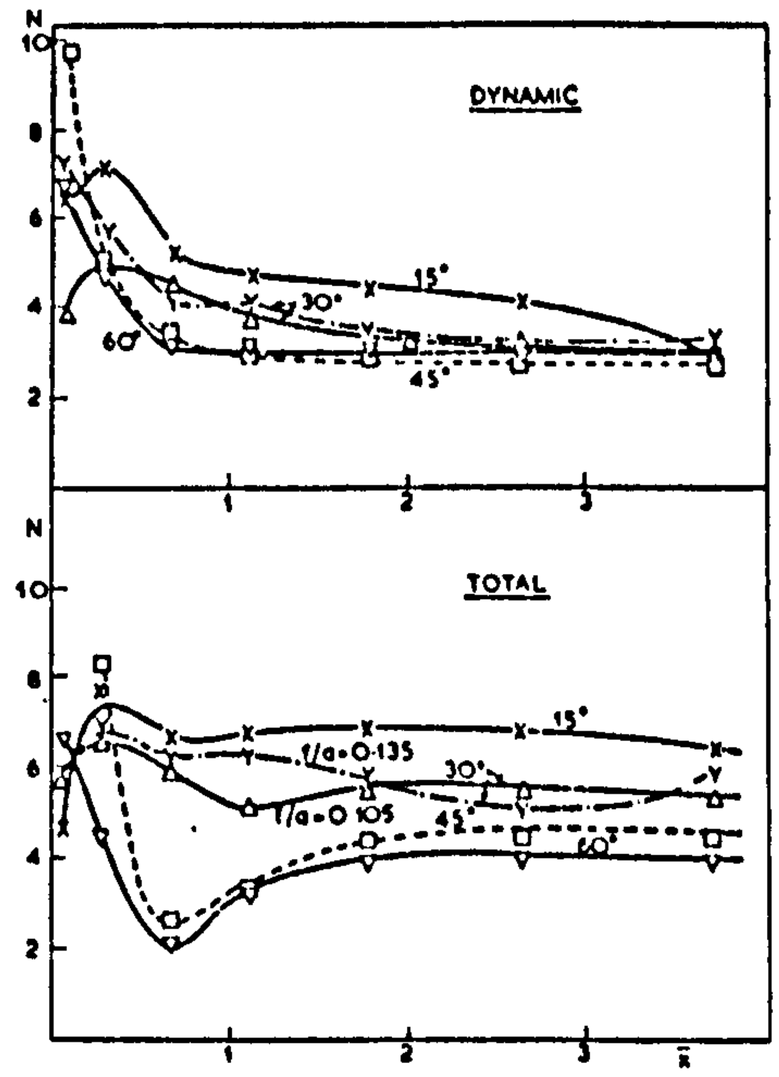

Fig. 2 Axial momentum fluxes Hubless swirler flames in D/d = 2·5 furnace

The experimental values of the tangential momentum fluxes in the developed flow beyond the CRZ (where present) are considerably higher than the prediction of Eqn. (1), the ratios to the predicted value being 2.2 and 1.7 for isothermal flows in the D/d = 2.5 and 5 furnaces, and 3.0 and 2.0 for the

corresponding burning jets. Experimental values of total axial momentum flux require a definition of reference static pressure. Several have been proposed (5). The one selected here is the pressure at the centre of the peripheral recirculation zones in the unswirled isothermal flow in that furnace. Here again the total axial momentum fluxes observed in the developed flows differ from the prediction of Eqn. (2), the ratios to the prediction being 2.1 and 0.85 for isothermal conditions in the D/d = 2.5 and 5 furnaces, and 3.5 and 1.1 for the corresponding burning conditions. While there is scatter, it is clear that the observed fluxes in the developed flows (where the fluxes are more nearly conserved) differ from the simple predictions, being influenced both by combustion and D/d ratio. Consequently the correlation between flow types has been sought in terms of experimental fluxes rather than predicted values. In view of the uncertainty regarding the reference pressure required to define the total experimental axial momentum flux, for simplicity this flux has been based solely on the axial velocity component. The dynamic component is shown in the upper portion of Fig. 2. Regarding the linear dimension required in the Swirl Number, it is seen that (a) the same swirler can give different velocity patterns as the relative furnace size is changed and (b) the dimensions of the C.R.Z., when established, are primarily functions of D, and not of d. Thus the new definition of the experimental Swirl Number is

$$S^* = T/(G_d D) \qquad (3)$$

This parameter, S*, has given a very satisfactory correlation between flow types (Fig. 3). The transitions from flow types A to B, B to C and C to D occur at values of S* of 0.08, 0.11 and 0.18 respectively. Further, for the same swirler, in say isothermal flow, the S* values are very similar in the two relative furnace sizes. A corresponding result holds for burning flows having the same fuel/air ratio.

There is a change in the slopes of both the isothermal and burning correlations at a vane angle of about 30°. In the burning case this corresponds to the transition to a C.R.Z.

The displacement of the correlation for the burning jets from the isothermal correlation is a function of fuel/air ratio, as discussed below.

Prediction of Swirl Number S* - Use for Design

The S* - θ relations (Fig. 3) required extensive experimentation. Satisfactory prediction of these relations has not yet been made, although it is helpful to note that S* is very nearly proportional to tan θ, particularly for Type D flows. If the isothermal correlation is established, a

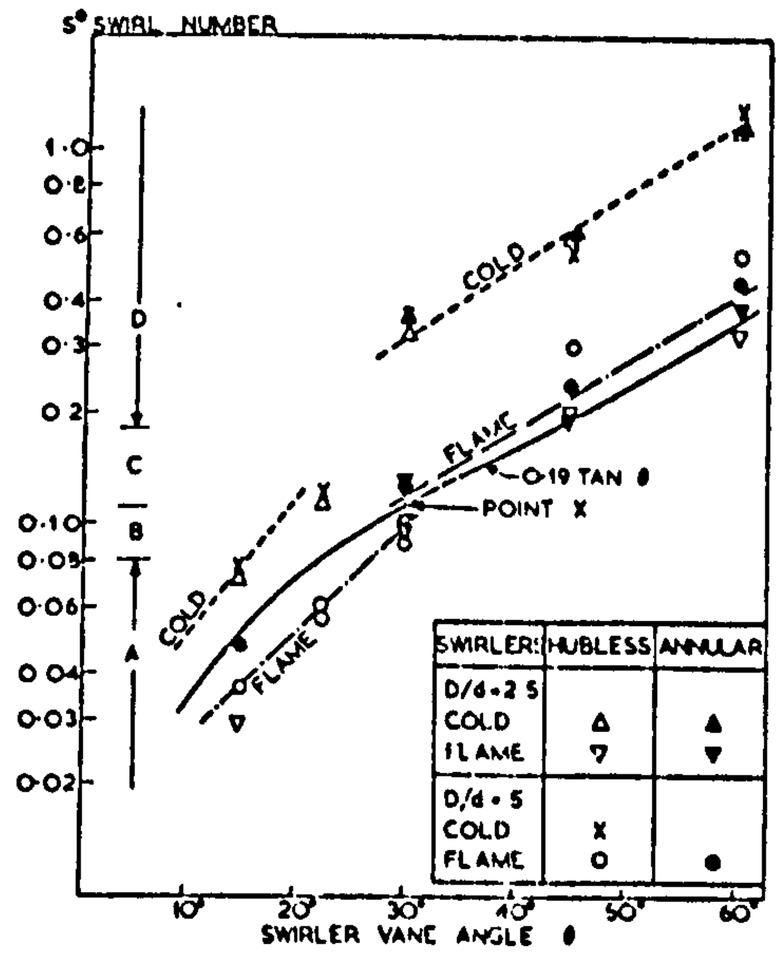

Fig.3. Swirl number relation to input conditions and flow types

method is outlined below for prediction of the burning correlation.

Let the pressure drop required for the density change in the furnace be F_1 times that for one-dimensional flow. When combustion occurs let us assume the dynamic component of the axial momentum flux is increased due to this pressure change acting across the front face of the furnace. Assuming, further, that the isothermal dynamic axial momentum flux is a fraction, F_2, of that given by Eqn. (2), the dynamic axial momentum flux in the burning case is

$$G_{db} = F_2 \frac{\pi}{4} d^2 \rho_u U^2 + F_1 \frac{\pi}{4} D^2 \rho_u U^2 \left(\frac{d}{D}\right)^4 \left(\frac{\rho_u}{\rho_b} - 1\right) \qquad (4)$$

The tangential momentum fluxes are slightly increased by combustion, as discussed above. Letting the ratios of these tangential fluxes, burning to isothermal, be F_3, then the Swirl Number ratio for a particular swirler is

$$\frac{S_b^*}{S_i^*} = \frac{F_2 F_3}{F_2 + F_1 \left(\frac{d}{D}\right)^2 \left[\left(\frac{\rho_u}{\rho_b}\right) - 1\right]} \qquad (5)$$

F_3 is almost independent of (D/d) and a mean value of 1.3 is reasonable. F_2 is markedly influenced by (D/d) and has

values of 0.51 and 0.16 for the (D/d) values of 2.5 and 5 respectively. Using these values for F_2 and F_3, it is found that a value of 2.1 for F_1 fits both sets of furnace results (premixed gas-air flames). With other forms of firing, F_1 and F_3 may be altered. The changes in F_3 will probably be small enough to ignore. F_1 will probably be reduced if combustion is slower, but should not drop below unity.

When using vane swirlers similar to those tested here, the isothermal correlation given in Fig. 3 can be used, and modified for combustion using Eqn. (5).

For other designs of vane swirlers, the isothermal correlation can be established in a model (use (D/d) values in the range 2.5 to 5). Alternatively, the burning correlation can be established by using the sharp discontinuity that exists in the variation with θ of the minimum static pressure on the axis. This discontinuity is the transition from flow Type B to C and corresponds to the value 0.11 for S*, locating the equivalent of point x on Fig. 3. The proportionality with tan θ allows an approximate correlation to be drawn. The burning tests used to find the discontinuity in axis pressure may be carried out on a model.

Conclusions

The flow types resulting from vane-generated swirl are correlated by an experimental Swirl Number, S*. The isothermal S* - θ relation for the present design of swirlers has been established and an expression has been developed for giving the burning relationships. Methods requiring much less experimentation are suggested for establishing the corresponding relationships for other designs.

References

1. BELTAGUI, S.A. and MACCALLUM, N.R.L. "Aerodynamics of swirling flames - Vane generated type". 1st European Symp. on Combustion, 1973.
2. MATHUR, M.L. and MACCALLUM, N.R.L. "Swirling air jets issuing from vane swirlers". J. Inst. Fuel 40, p.214 (1967).
3. BELTAGUI, S.A. and MACCALLUM, N.R.L. "Aerodynamics of vane-swirled flames in furnaces". Mech. Eng. Report, Glasgow University, 1974.
4. BELTAGUI, S.A. and MACCALLUM, N.R.L. "The modelling of vane-swirled flames in furnaces". Mech. Eng. Report, Glasgow University, 1974.
5. KERR, N.M. and FRASER, D.A. "Swirl. Part I: Effect on axisymmetrical turbulent jets". J. Inst. Fuel 38, p.519 (1965).

Nomenclature

d swirler diameter
D furnace diameter
F_1, F_2, F_3 factors defined in text
G axial momentum flux
S swirl number $T/(G_t d)$
S* swirl number $T/(G_d D)$
T tangential momentum flux
U av. axial velocity approaching swirler
$\bar{x}$ (axial distance/D)
z hub diameter ratio
θ vane angle to axis
ρ density

Subscripts

b burned
d dynamic
i isothermal
t total
u unburned

Publication 13

an ASME publication

$3.00 PER COPY
$1.50 TO ASME MEMBERS

Models for the Representation of Turbomachine Blades During Temperature Transients

N. R. L. MACCALLUM

Senior Lecturer,
Department of Mechanical Engineering,
University of Glasgow,
Glasgow, Scotland

When the operating conditions of turbomachinery are changed, as when a gas turbine is accelerated, heat is transferred from or to the various components of the machine. One of the significant heat transfers is with the blading. Several simple models for the blade and platform arrangement are compared. Satisfactory representation is obtained from a simple eight-element Finite Difference Model and from a Revised Fin Model. Computer running times are similar, but the latter allows more convenient hand calculations and is more suitable when predicting the thermal response of casings or disks to which the blades are attached.

Contributed by the Gas Turbine Division of The American Society of Mechanical Engineers for presentation at the Gas Turbine and Fluids Engineering Conference, New Orleans, La., March 21-25, 1976. Manuscript received at ASME Headquarters December 11, 1975.

Copies will be available until December 1, 1976.

Models for the Representation of Turbomachine Blades During Temperature Transients

N. R. L. MACCALLUM

INTRODUCTION

When the air or gas temperatures change in turbomachinery, as in a gas turbine when it changes speed, transient heat transfers take place to, or from, the blades until they and their attachments reach their new equilibrium temperatures. The heat-transfer rate can have important influences on the behavior of the machine. For example, the heat-transfer rate to, or from the stator blade platforms in an axial-flow compressor has a large influence on the temperature response of the outer casing, whose thermal expansion or contraction directly affects the blade tip clearances. This could be a contributory factor in causing the thrust transient of a typical turbojet engine to lag appreciably behind the speed transient (1).[1] Further, heat transfer to, or from the blade aerofoils can affect the stability of the boundary layer flow (2) and the compressor surge margins (3)—a 30 percent reduction in surge margin has been predicted when attempting a re-acceleration at altitude of a "hot" engine.

The heat-transfer rate during and following a transient depends on the heat-transfer coefficients and on the blade geometry. This paper compares simple geometric models for the blade and platform arrangement used in axial-flow machines. The models are compared on accuracy, computing time, simplicity of geometry and suitability for use alongside models representing other components. Satisfactory models will enable the prediction of the heat-transfer rates and of the blade and platform temperatures during and following the transient, for known heat-transfer coefficients.

MODELS FOR UNCOOLED BLADES

A typical blade in an axial-flow machine consists of a thin aerofoil attached to a platform. Integral with the platforms of rotor blades are the mountings, e.g., fir trees or pin joints. The mass of the material used in the platform-mounting arrangement may be of the same order as the mass of the aerofoil.

Predictions of heat-transfer rates and blade temperatures depend both on the values of the heat-transfer coefficients used in the calculations, and on the model adopted to represent the blade. In view of the uncertainties in the predictions of heat-transfer coefficients, it is considered that a simple model which is reasonably accurate is adequate at this stage.

[1] Underlined numbers in parentheses designate References at end of paper.

NOMENCLATURE

A = surface area, except A_{xa} which is cross-sectional area of aerofoil, m^2
c = specific heat, J/kg K
h = average heat-transfer coefficient, W/m^2K
k = thermal conductivity, w/m K
m = mass, kg
Nu = Nusselt number
P = perimeter for convective heat transfer, m
Q = heat-transfer rate, w
Re = Reynolds number
T = temperature, deg K
x = distance along aerofoil from platform, m
τ = time constant, sec

Subscripts

a = aerofoil
b = used in steady-state mean blade temperature
c = cooling air
f = "fin"
g = gas or air
p = platform
t = total
x = used in A_{xa} which is cross-sectional area of aerofoil

Table 1 Dimensions of Blades

Blade	Aerofoil mass, kg	Aerofoil surface area, m^2	Platform mass, kg	Platform surface area, m^2	Specific heat, kJ/kg K
L.P. Comp. 2 Rot	0.145	0.031	0.164	0.0024	0.92
H.P. Comp. 11 Rot	0.0031	0.00094	0.0052	0.00024	0.52
H.P. Turb. 2 Rot	0.035	0.0037	0.023	0.00032	0.54

Finite Difference Model (F.D. Model)

An obvious method is that using finite difference methods (4) on a model which consists of an aerofoil divided along its length into equal elements, each spanning the aerofoil cross section. A single comparatively large element represents the platform and root attachment. Such a model was used in the analysis described in Reference (1). Any variation in temperature across the chord of the blade is ignored. The accuracy of the model can be improved, within the limitations of the foregoing assumption, by increasing the number of elements into which the blade is divided. This has been investigated by varying the number of elements in the range from 8 to 128. Slight errors resulted from using fewer than 16 elements, as is seen later, but increasing the number of elements above 32 was found to be unnecessary.

This 32-element representation has been used for several blades in the compressors and turbines of a typical two-spool turbojet engine. Three blades have been selected for this paper as indicating the range of conditions that can be experienced, these blades being the 2nd Row Rotor Blade in the Low-Pressure Compressor, the 11th Row Rotor Blade in the High-Pressure compressor, and the 2nd Row Rotor Blade in the High-Pressure Turbine. These blades are referred to as Blade A, Blade B, and Blade C, respectively. The masses and surface areas of these blades are listed in Table 1.

The response of Blade A to a step change from idling speed to maximum continuous speed conditions is given by the solid lines in Fig. 1 (while a step change is not a practical situation, the response can indicate any dominant time constants). The response is represented by the heat-transfer rate, the fractional change still to occur in the platform temperature, appropriately called "Incompletion Ratio" by Dusinberre (4) and the fractional change still to occur in the aerofoil temperature (taken at mid-blade height). The average coefficient of heat transfer over the aerofoil was assumed to be given by the expression given by Halls (5)

$$Nu = 0.235\, Re^{0.64} \qquad (1)$$

This correlation was derived for turbine rotor blades and is not strictly applicable to compressor blades. However, as this paper is concerned with comparing one model with another, this correlation has been used for both turbine and compressor blades. The coefficients of heat transfer to the platform surfaces will be much higher than for undisturbed flow through the annular ducts forming the compressor and turbine. This is due to the large changes in the tangential velocities of the platforms in moving from a stator passage to a rotor passage and back to a stator passage, etc. For simplicity, since we are comparing models, it has been assumed that the coefficient of heat transfer to a platform is the same as that to the aerofoil of the same blade.

It is to be noted from Fig. 1 that both the aerofoil and the platform temperatures show virtually exponential approaches (with, of course, different time constants) to their new equilibrium values. The heat-transfer rate shows a decay characterized by two time constants, the larger time constant (which dominates the transfer from 40 sec onward) being almost identical to the time constant for the platform temperature. This behavior suggests that an alternative to the Finite Difference Model might be to represent the complete blade by the sum of an aerofoil and a

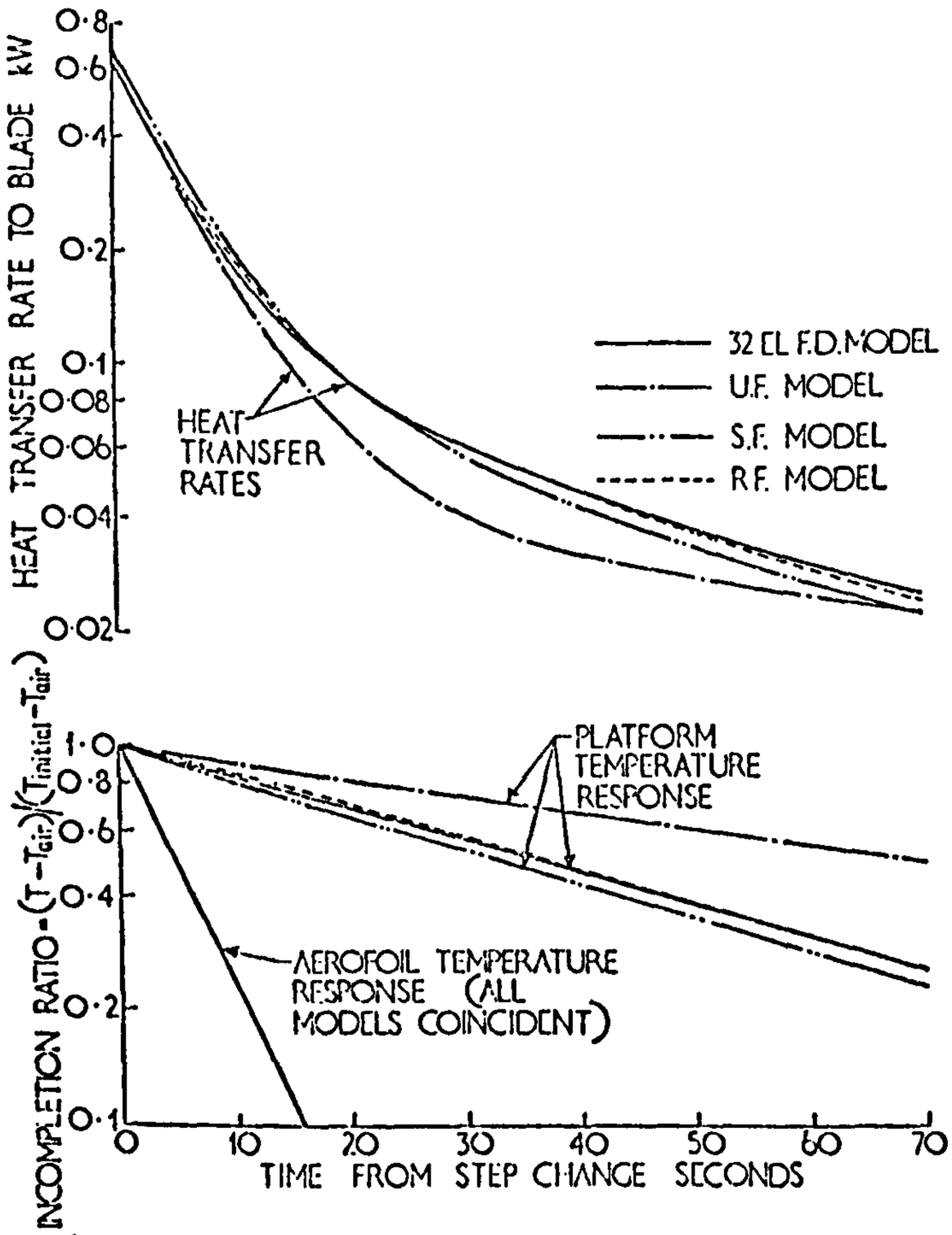

Fig. 1 Predicted response of L.P. compressor 2nd row rotor blade to a step change—idling speed to maximum continuous speed

platform, each with its own heat-transfer area per unit mass, and, hence, its own time constant. Three models of this type are considered in the following paragraphs. The predictions of these models are compared with those of the 32-element Finite Difference Model, which is taken as reference.

Unfinned Model (U.F. Model)

The blade is regarded in this model as being represented by the sum of two separate masses—the aerofoil mass and the platform mass. For the platform, the appropriate heat-transfer area is the platform surface area.

The total heat-transfer rate from the blade at any instant is given by

$$Q_t = h_a A_a (T_a - T_g) + h_p A_p (T_p - T_g) \qquad (2)$$

The time constants for the two components are given by

$$\tau_a = \frac{m_a c}{h_a A_a} \qquad (3)$$

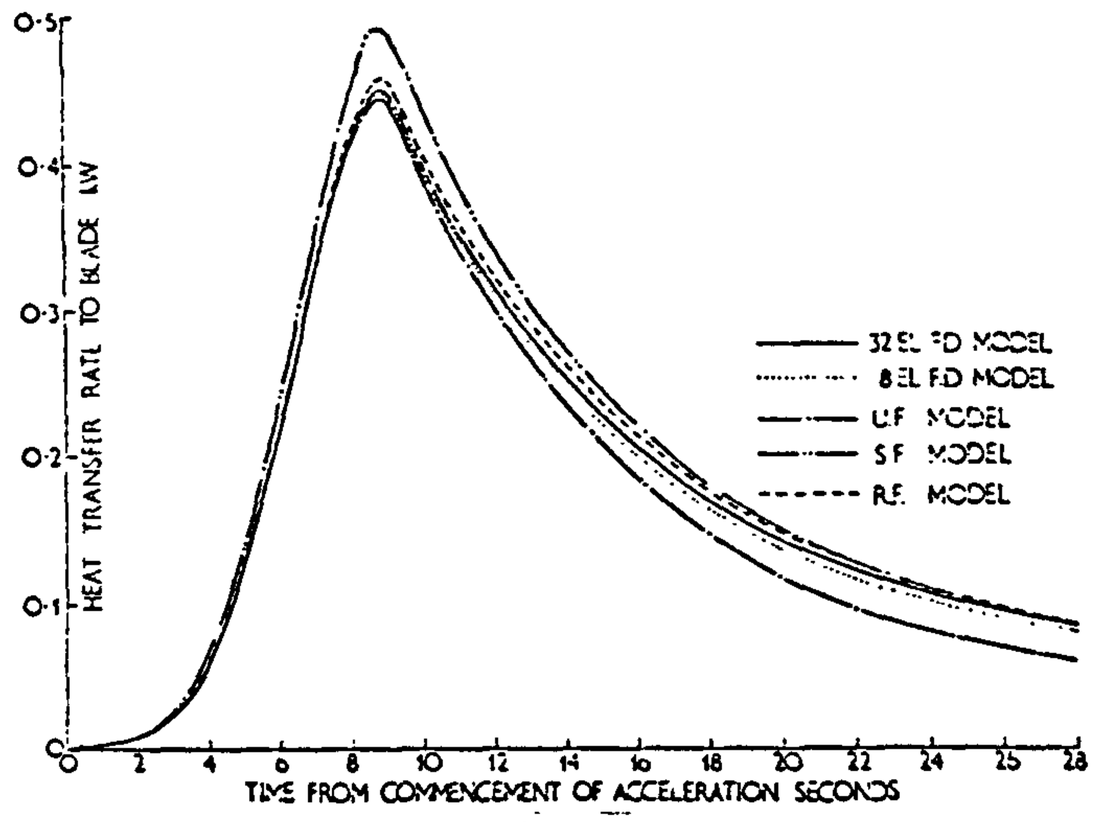

Fig. 2 Predicted heat-transfer rate to L.P. compressor 2nd row rotor blade during and following an acceleration

$$\tau_p = \frac{m_p c}{h_p A_p} \qquad (4)$$

The predictions of this model for Blade A are shown by the single chain-dotted lines in Fig. 1. Although the prediction of aerofoil temperature agrees exactly with that given by the F.D. Model, the predictions are otherwise far from satisfactory. Obviously, some allowance must be made for the ability of the aerofoil to act as a fin attached to the platform. This is investigated in the next models.

Simple Finned Model (S.F. Model)

The blade is represented by the sum of the aerofoil and the "finned" platform.

For the "finned" platform, the thermal capacity of the fin is ignored, and it is assumed that the fin is completely effective from the commencement of the transient. This is an approximation because the fin only has effect after the fin temperatures have moved from the initial value toward the new air or gas temperature. The considerable lengths of the aerofoils, compared to their thicknesses, and the high heat-transfer coefficients, allow the fins to be regarded as of "infinite" length.

For an infinite fin, the steady-state temperature distribution along the fin is given by [see standard texts such as Reference (6)]

$$(T - T_g) = (T_p - T_g) \exp\left[-x \left(\frac{h_a P_a}{k A_{xa}}\right)^{\frac{1}{2}}\right] \qquad (5)$$

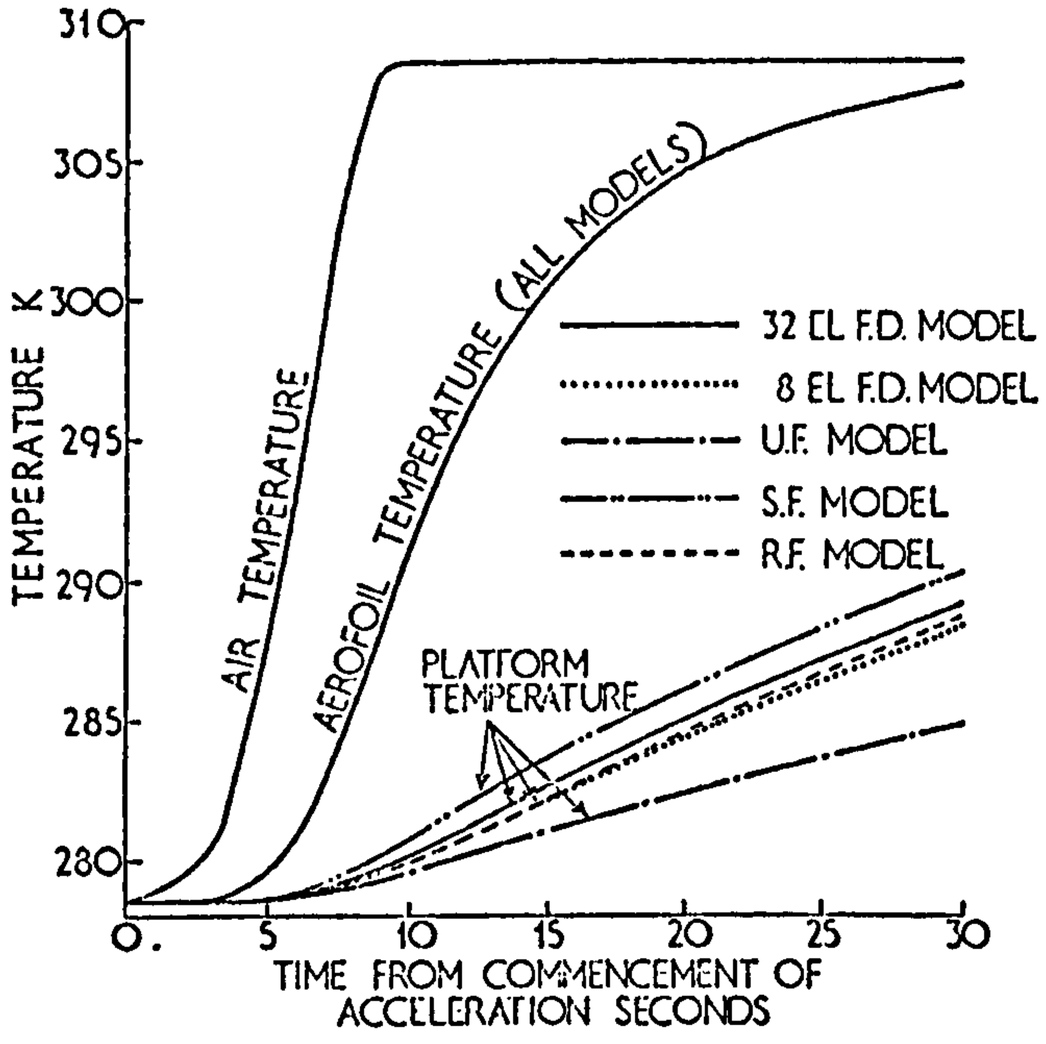

Fig. 3 Predicted temperatures of L.P. compressor 2nd row rotor blade during and following an acceleration

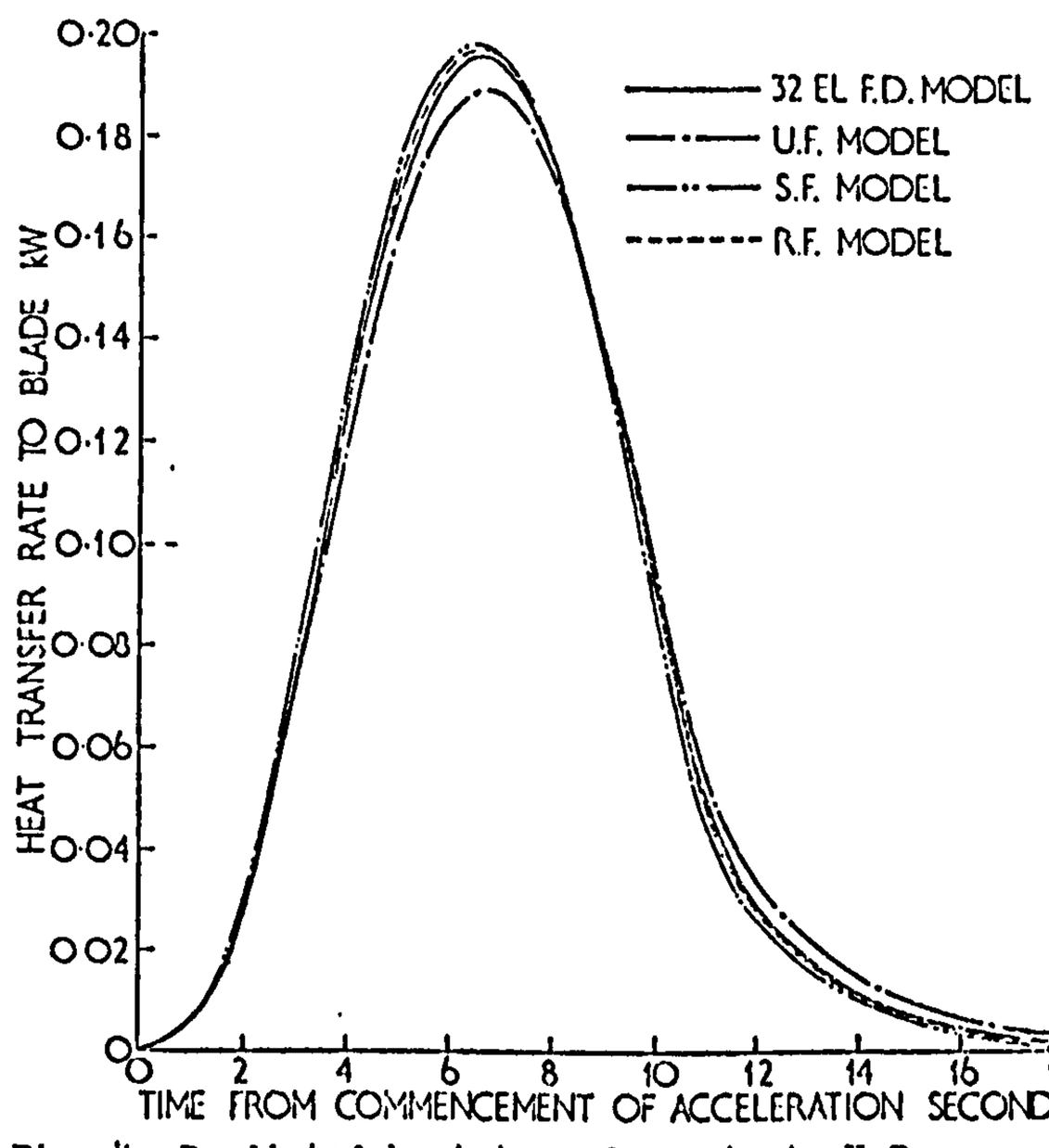

Fig. 4 Predicted heat-transfer rate to H.P. compressor 11th row rotor blade during and following an acceleration

The heat conducted by the fin from the platform is given by

$$-k A_{xa} \left(\frac{dT}{dy}\right)_{x=0} = k A_{xa} (T_p - T_g) \left(\frac{h_a P_a}{k A_{xa}}\right)^{\frac{1}{2}} \qquad (6)$$

The total heat-transfer rate from the platform at any instant is given by

$$Q_p = (T_p - T_g)\left(h_p A_p + k A_{xa} \left(\frac{h_a P_a}{k A_{xa}}\right)^{\frac{1}{2}}\right) \qquad (7)$$

The time constant for the finned platform is given by

$$\tau_p = \frac{m_p c}{h_p A_p \left(1 + \left(\frac{k A_{xa} h_a P_a}{h_p^2 A_p^2}\right)^{\frac{1}{2}}\right)} \qquad (8)$$

The predictions of this Simple Finned Model (S.F. Model) for Blade A are shown by the double chain-dotted lines in Fig. 1. The predictions of this Model are better than those of the U.F. Model, but they still have some unsatisfactory features. A major one is the erroneously high predicted heat-transfer rate at the commencement of the transient. This error in the S.F. Model is due to the assumption that the fin is effective immediately after the transient commences. An improvement to overcome this weakness in the Model is given in the Revised Finned Model which is now discussed.

Revised Finned Model (R.F. Model)

This Model is developed from the S.F. Model by including a factor to bring the "effectiveness" of the fin from zero at the commencement of the transient to the value indicated by equation (6) at some later time. This factor is required because initially the fin cannot be conducting heat from, or to, the platform as all the fin material is at the platform temperature. Thus, a factor for multiplying the second term in the brackets on the right-hand side of equation (7) might be

$$\left(1 - \frac{T_f - T_g}{T_p - T_g}\right)$$

where T_f is a "fin" temperature. One would expect this "fin" temperature to move exponentially from its initial value to the new air or gas temperature, and it can be argued that the time constant for this change will be the same as the time constant for the aerofoils themselves. In that case, the

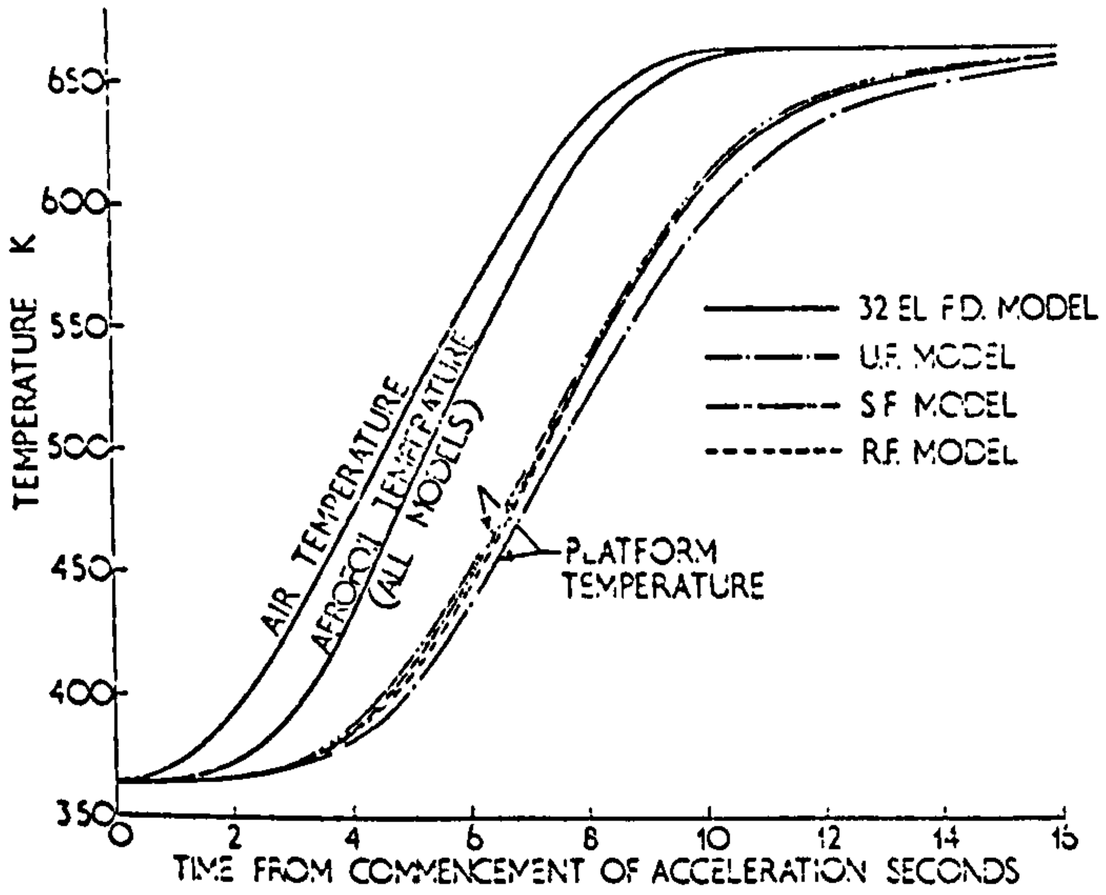

Fig. 5 Predicted temperatures of H.P. compressor 11th row rotor blade during and following an acceleration

fin temperature, T_f, is the same as the aerofoil temperature, T_a. The revised form of equation (7) then becomes

$$Q_p = (T_p - T_g)\left(h_p A_p + \left(1 - \frac{T_a - T_g}{T_p - T_g}\right) k A_{xa} \left(\frac{h_a P_a}{k A_{xa}}\right)^{\frac{1}{2}}\right) \quad (9)$$

The same multiplying factor is applied to the second term in the brackets in the denominator of equation (8) to give the "time constant" for the response at that instant. This "time constant" will not be constant even with steady ambient conditions until this mulitplying factor becomes virtually unity.

The "time constant" equation is

$$\tau_p = \frac{m_p c}{h_p A_p \left(1 + \left(1 - \frac{T_a - T_g}{T_p - T_g}\right)\left(\frac{k A_{xa} h_a P_a}{h_p^2 A_p^2}\right)^{\frac{1}{2}}\right)} \quad (10)$$

The predictions of this Revised Finned Model (R.F. Model) for Blade A are shown by the dashed lines in Fig. 1. For most of the range plotted, the predictions of temperatures and heat-transfer rates are undistinguishable, on the logarithmic plot used, from those of the F.D. Model (taken as the reference Model). The discrepancies in the temperature responses of the aerofoil and platform never exceed 2 percent. For the heat-transfer rate, the predictions of the R.F. Model are high by up to 4 percent during the period 5 to 15 sec and low after about 40 sec. By 70 sec, the predictions are low by about 5 percent.

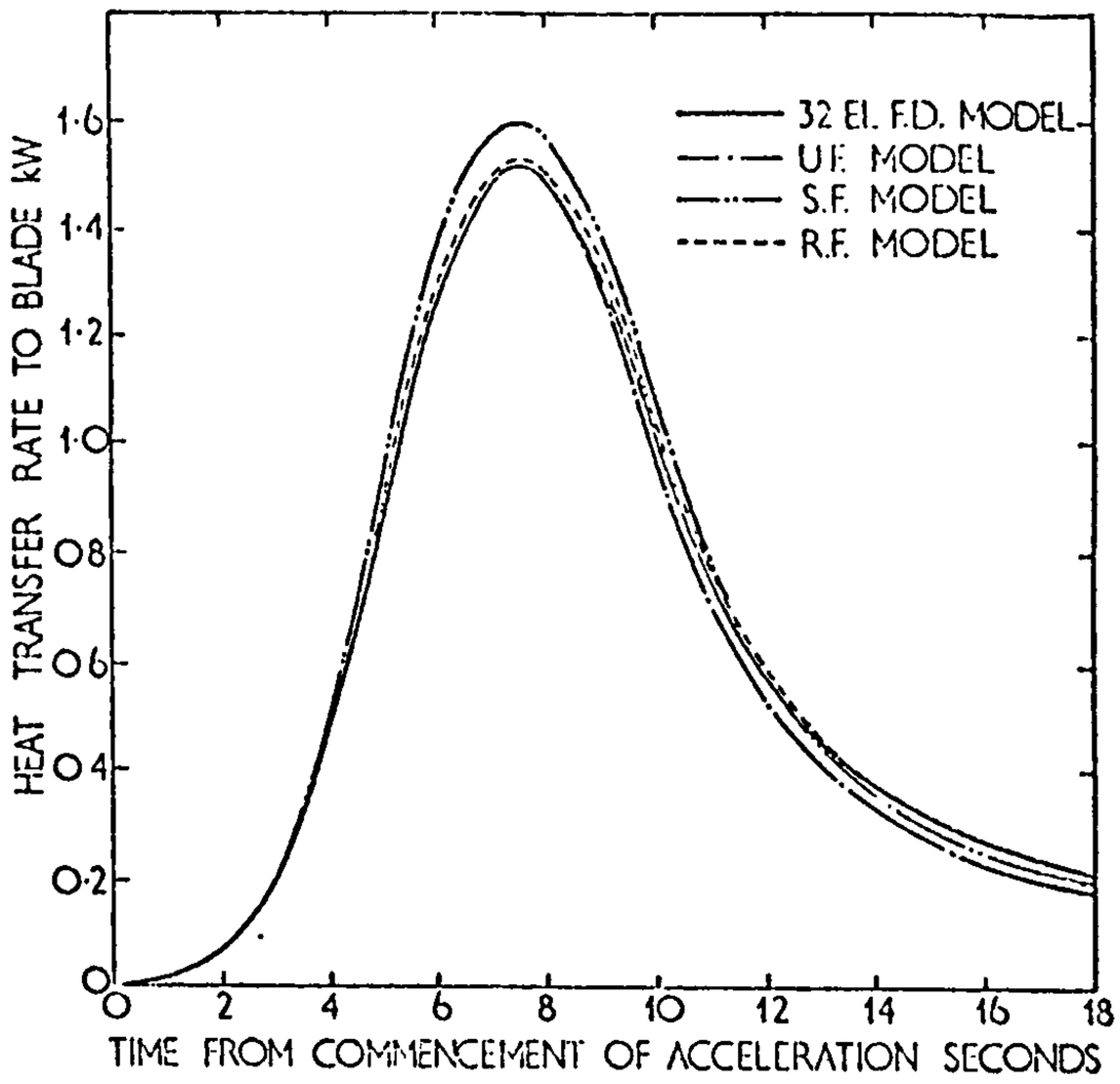

Fig. 6 Predicted heat-transfer rate to H.P. turbine 2nd row rotor blade during and following an acceleration

It can be seen that this R.F. Model gives a simulation which is completely adequate for practical purposes.

Application of Models to Uncooled Blades During Accelerations

In practice, the flow conditions around blades do not undergo step changes. A typical acceleration from idling speed to the maximum speed may last 10 sec. For these accelerations, it is important to know how reliable the predictions of the models described in the foregoing are. The Finite Difference Model having 32 elements is again taken as giving the true response.

The results for the predicted heat-transfer rates and temperatures for Blade A during and following a typical acceleration are given in Figs. 2 and 3, respectively. Conditions during the acceleration were represented by the method of successive intervals. The corresponding predictions for Blade B are given in Figs. 4 and 5 and for Blade C in Figs. 6 and 7.

The predicted heat-transfer rates based on the U.F. Model and on the S.F. Model are surprisingly good for Blade B. The predictions are less satisfactory for Blade A, because the effect of the fin is more significant for Blade A (where it accounts for up to 50 percent of the heat to the platform) than for Blade B (less than 16 percent of heat to platform). When the fin has small

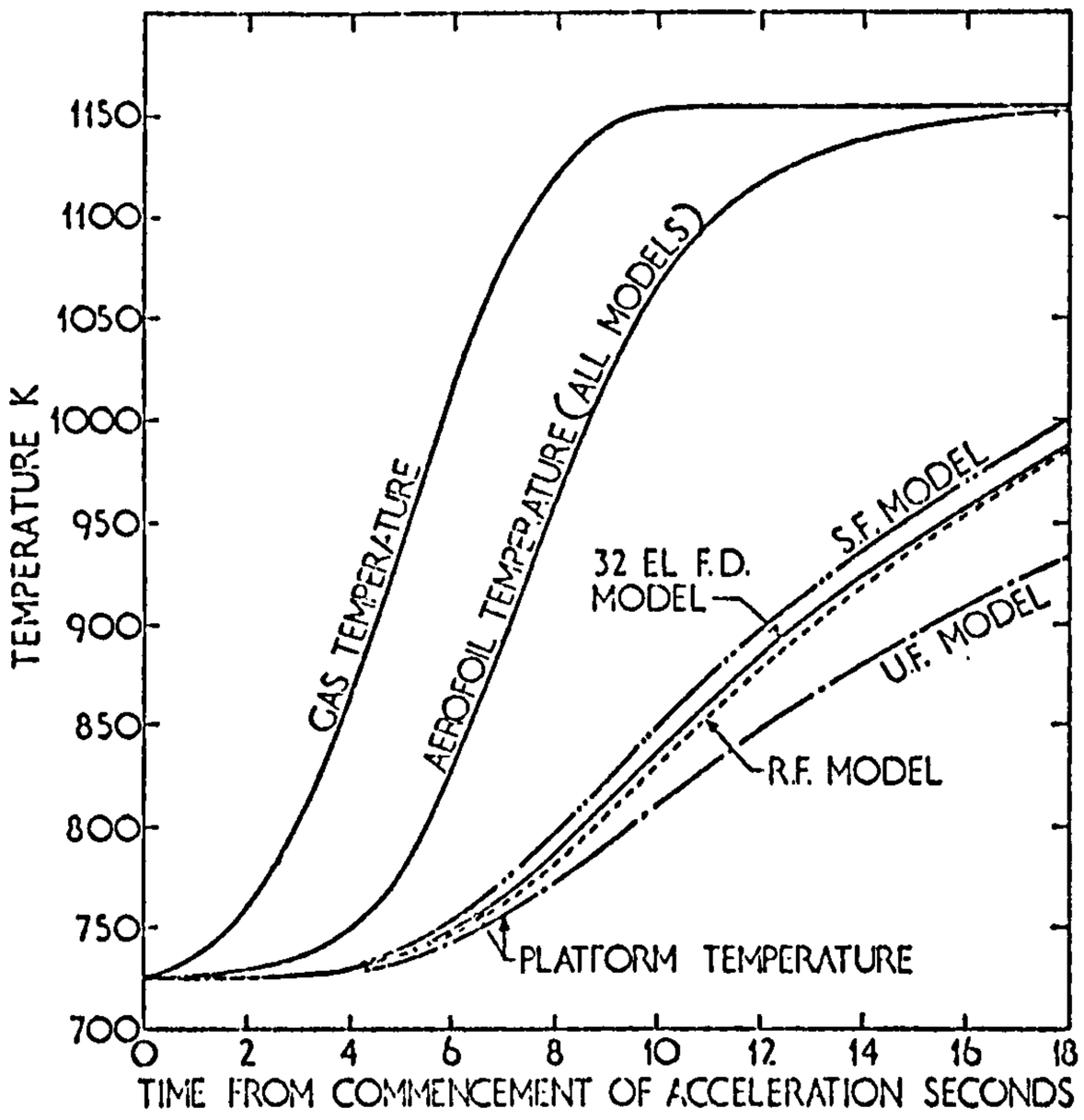

Fig. 7 Predicted temperatures of H.P. turbine 2nd row rotor blade during and following an acceleration

effect, these two Models give similar predictions. Also, since these Models represent the two extremes, their predictions are close to the true response. For Blade C, the fin has an effect intermediate between those for Blades A and B.

The predicted heat-transfer rates given by the R.F. Model lie between those of the U.F. Model and the S.F. Model and are, therefore, in very good agreement with the true behavior. Any discrepancy never exceeds 4 percent until well after the completion of the acceleration, by which time the heat-transfer rates have reduced to less than 15 percent of their peak values.

The temperatures of the platform and aerofoil given by the R.F. Model are also in very good agreement with the expected values. The predicted platform temperatures given by the U.F. Model and the S.F. Model show significant discrepancies. A slower response is predicted by the U.F. Model and the S.F. Model predicts a faster response.

ASSESSMENT OF MODELS

It can be seen that the Revised Finned Model is significantly better than either the Unfinned or Simple Finned Models. The program running times are virtually the same for all three, and each requires the storage of only two temperatures for each blade (an aerofoil temperature and a platform temperature).

The question now arises whether this R.F. Model possesses any advantages over a Finite Difference Model. The 32-element F.D. Model requires storage for 33 elements per blade. This can be reduced to 17 by assuming that conduction along the aerofoil is insignificant beyond mid-blade height. The program running time for this simplified F.D. Model is almost double that for the R.F. Model. Running time and storage for the R.F. Model can be further reduced by reducing the number of elements in the Model. It is important to know to what extent this can be done without significant error. This has been investigated, and it is considered that the number of elements per aerofoil can be reduced to 8 without the errors becoming excessive. The predictions of this 8-element F.D. Model are shown for only one of the cases considered—the acceleration transient for Blade A (Figs. 2 and 3). The corresponding results for the other cases have not been plotted to avoid obscuring the Figures. From Fig. 2, it can be seen that within the time range plotted (0 to 28 sec) the 8-element F.D. Model and the R.F. Model are roughly comparable in accuracy of heat-transfer rate predictions. In the first 10 sec of the transient, the predictions of the 8-element F.D. Model lie within 1 percent of the expected rates, after which time the predictions become progressively low—at 28 sec the prediction is low by 5 percent. For the R.F. Model, the predictions are high by amounts of less than 2.5 percent during the first 10 sec. In the next 10 sec, during which time the rates are decaying, the predictions are high by amounts up to 4 percent and finally high by 2.5 percent at 28 sec. The predictions of platform temperature by the R.F. Model are better than those by the 8-element F.D. Model.

Comparisons between the R.F. Model and the 8-element F.D. Model for other blades are similar.

The program running times for the two models are similar, but the 8-element F.D. Model requires more storage, although this is hardly significant with present facilities.

The R.F. Model possesses the advantage that analytic expressions are available [equations (9) and (10)] for the heat transfer to the blade platforms. This is important when one considers how the blade is mounted in the machine. It has been assumed in using the Models described in the foregoing that the entire platform mass is at a uniform temperature and that the platform is insulated from the part of the machine (e.g., turbine disk or outer casing) on which it is mounted. This will not be the case in practice.

For example, much of the heat transferred to, or from, the outer casing of a compressor following a transient is transferred through the stator blade platform mountings. (The other major thermal path is by convection to the surfaces adjacent to the rotor blades.) There will be contact resistances in the conduction path between the platforms and the outer casings. In analyzing the behavior of this system, it will be much simpler if an expression can be written down for the heat transfer to the platform, and this can readily be done using equations (9) and (10). The problem can, of course, be solved by finite difference methods, but this will be less convenient to arrange due to the long time constant of the outer casing and the shortness of the time intervals required to avoid instability in the numerical solution of the finite difference equations for the blade Model. It is considered that for this application, the Revised Finned Model for the blade has an advantage over the Finite Difference Model.

MODELS FOR COOLED BLADES

The models described in the foregoing can be applied to cooled blades, provided the temperature differences and time constants used are as follows. The gas temperature, T_g, in equations (2), (5), (6), (7), (9), and (10) should be replaced by the steady-state mean blade temperature, T_{b_c}, corresponding to the gas and cooling-air temperatures applying at that instant. The group ($h_a A_a$) appearing in equations (2) and (3) should be replaced by ($h_a A_a + h_c A_c$). The group ($h_a P_a$) appearing in equations (5) to (10) should be replaced by ($h_a P_a + h_c P_c$).

By the foregoing alterations, the thermal response of the cooled aerofoil can be well simulated. The representation of the platform is less accurate, but errors should not be serious.

CONCLUSIONS

Adequate representation of a blade in a typical axial-flow turbomachine is provided by either a Finite Difference Model in which the aerofoil length into 8 elements, or by a Revised Finned Model. Simpler Finned and Unfinned Models are almost as satisfactory in cases where the aerofoil cross-sectional area is small compared to the platform area. On the basis of these Models, satisfactorily accurate values of heat-transfer rates and blade temperatures can be predicted, provided the values of heat-transfer coefficients are known.

Program running times for all the Models are similar. The Finned Models possess the advantage that expressions can be written down for the heat transfer to, or from the platforms. This will be helpful when studying the temperature responses of the disks or casings to which the blades are attached. The Finned Models allow convenient hand calculations of blade response for simplified transients.

ACKNOWLEDGMENTS

The author wishes to thank members of staff of Rolls-Royce (1971) Limited for engine data. He also wishes to thank them, and colleagues at the University of Glasgow for advice and comments.

REFERENCES

1 Maccallum, N. R. L., "The Performance of Turbojet Engines during the Thermal Soak Transient," Proceedings of the Institution of Mechanical Engines, Vol. 184, Part 3G (II), 1969-1970, pp. 23-29.

2 Grant, A. D., "Effect of Heat Transfer on Boundary Layer Stability in Axial Flow Compressors," Heat and Fluid Flow in Steam and Gas Turbine Plant, Institution of Mechanical Engineers, London, 1974, pp. 252-258.

3 Maccallum, N. R. L., "The Effect of Bulk Heat Transfers in Aircraft Gas Turbines on Compressor Surge Margins," Ibid., pp. 94-100.

4 Dusinberre, G. M., Heat Transfer Calculations by Finite Differences, 1st ed., International Textbook Company, Scranton, Pa., 1961.

5 Halls, G. A., "Air Cooling of Turbine Blades and Vanes," Advisory Group for Aeronautical Research and Development, Meeting at Varenna, Italy, May 18, 1967.

6 Ede, E. J., An Introduction to Heat Transfer Principles and Calculations, 1st edition, Pergamon, Oxford, 1967.

Reprinted from the JOURNAL OF THE INSTITUTE OF FUEL, *December, 1976.*

Publication 15

S A BELTAGUI BSc PhD* and N R L MACCALLUM BSc PhD†

Aerodynamics of vane-swirled flames in furnaces

Selected results are presented of a series of aerodynamic measurements of isothermal and burning swirling flows in two furnaces. Annular and hubless vane swirlers having vane angles in the range 15°–60° were tested. The two furnaces had diameter ratios, compared with the swirler, of 2.5 and 5. The parameters measured were the three components of velocity, static pressure, temperature and carbon dioxide concentration. Distinctive flow patterns were observed. These flow types have been classified into types A, B, C and D. The transitions from one flow type to the next, due to change in vane angle, have been found to be correlated by a new swirl number, $S^* = T/(G_d D)$. This correlation covers the two furnace sizes and both the isothermal and burning swirling flows

1. Nomenclature

D	diameter of furnace
d	diameter of hubless swirler, diameter of equivalent hubless swirler to have same flow area as annular swirler
f/a	fuel/air ratio by volume
G_d	dynamic component of axial momentum flux, $\int 2\pi r \rho u^2 dr$
$\dot{m}$	mass flow rate
p	static pressure
r	radius
S^*	swirl number defined by $\frac{T}{G_d D}$
T	axial flux of tangential momentum, $\int 2\pi r^2 \rho u w dr$
U	average axial velocity leaving swirler, based on cross-sectional area of swirler ignoring vane thickness
u, v, w	velocity components in the axial, radial and tangential directions
x	axial distance
x_i	distance to point of impingement of jet on furnace wall
ρ	density
ρ_u	density of unburned mixture
ΔT	temperature rise
ΔT_a	temperature rise when complete adiabatic combustion

2. Introduction

Swirl produces notable effects on flames, generally making them shorter and highly stable over a wide range of air and fuel flows. One common method of generating a swirling jet is to employ a vane swirler. The authors in this paper present the results of an aerodynamic study of the application of vane-generated swirl to premixed town gas-air flames in two furnaces.

3. Experimental work

3.1. Variables investigated

(1) Degree of swirl: vane angles of 0°, 15°, 22°, 30°, 45° and 60° to the axial direction.

(2) Swirler geometry: hubless and annular swirlers.

(3) Furnace confinement: furnace diameter/burner diameter ratios of 2.5 and 5.0.

(4) Reynolds number: for one geometry the values of 7.5×10^5 and 10.2×10^5 were used. For all other tests the value was 9×10^5 (based on swirler diameter and axial velocity leaving swirler).

(5) Flow with combustion, as compared with isothermal flow.

(6) Fuel/air ratio, particularly when swirl is near the critical value and a change in fuel/air ratio may just create a central recirculation zone, or just suppress it.

3.2. Apparatus

Six hubless vane swirlers were made to the design of Mathur and Maccallum,[1] having the vane angles listed in section 3.1. The swirler diameter was 93 mm. The vanes (eight in each swirler) were made of stainless steel, 1.6 mm thick. The 30°, 45° and 60° swirlers had an angular overlap, when viewed along the axis, of 30° between adjacent vanes. Because it was necessary for practical reasons to keep the vanes a reasonable length, the overlaps of the other swirlers were reduced from this ideal value, being 15° for the 22° swirler and 0° for the 15° swirler. Five annular swirlers were made, having the same vane angles as the hubless ones but omitting the 22° angle. The outer and hub diameters of the annular swirlers were 98 and 32 mm respectively. The annular swirlers had the same exit cross-sectional areas as the hubless ones.

*Formerly British Steel Corporation, Swinden Laboratories, Rotherham; now Department of Mechanical Engineering, Faculty of Engineering, University of Alexandria, Egypt.
†Department of Mechanical Engineering, University of Glasgow.

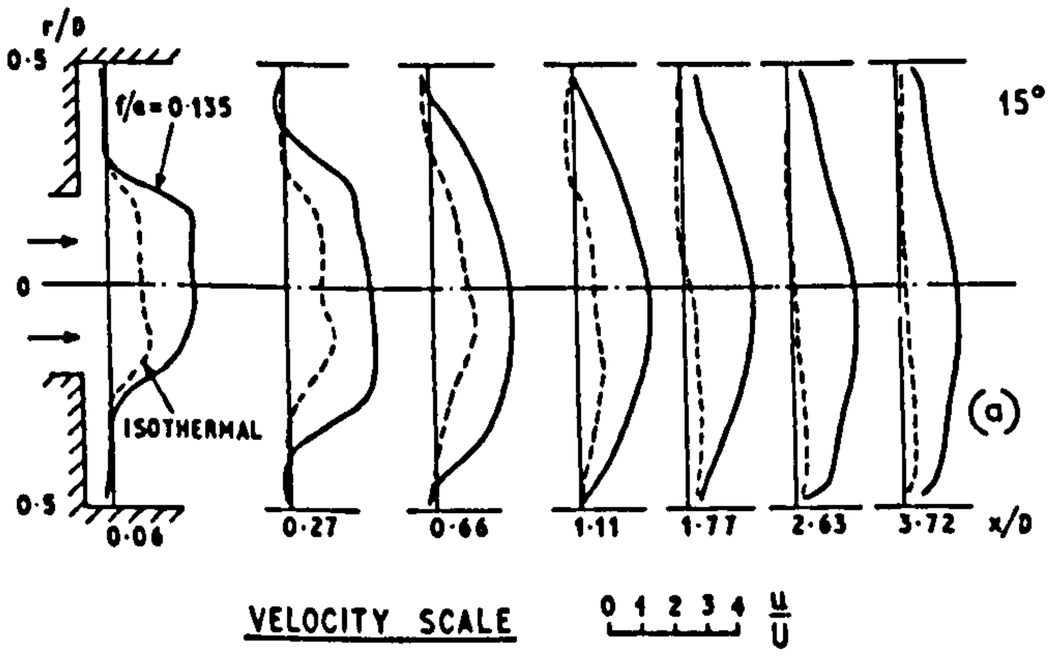

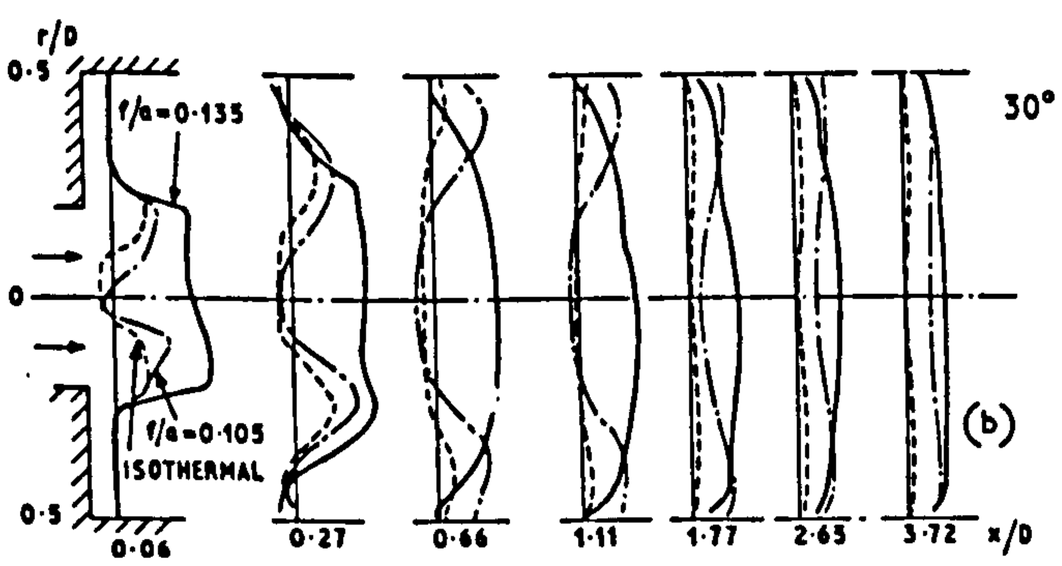

FIG. 1a, b Axial velocity distributions. Hubless swirlers. D/d = *2.5 furnace*

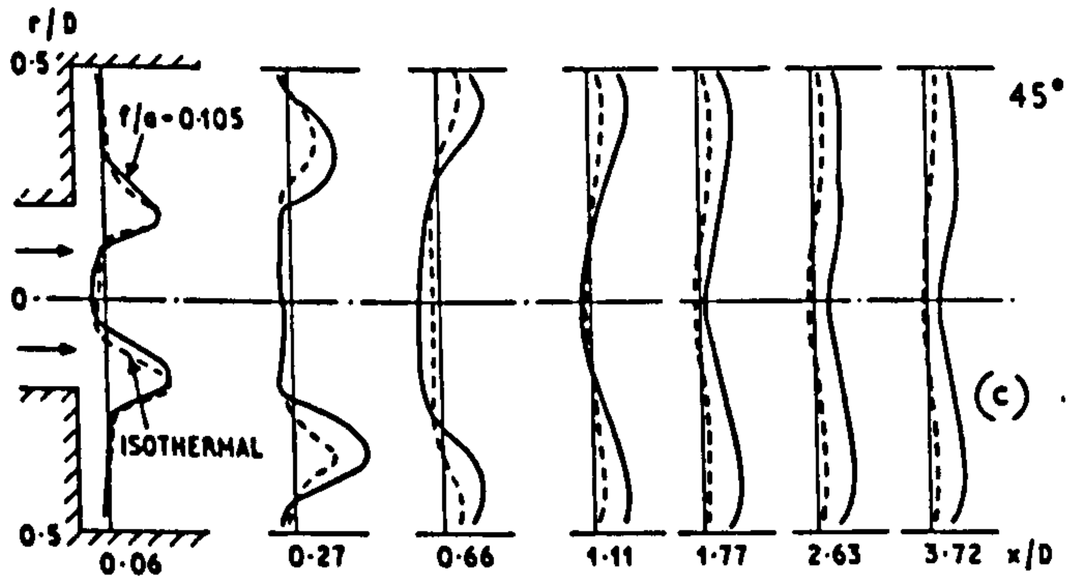

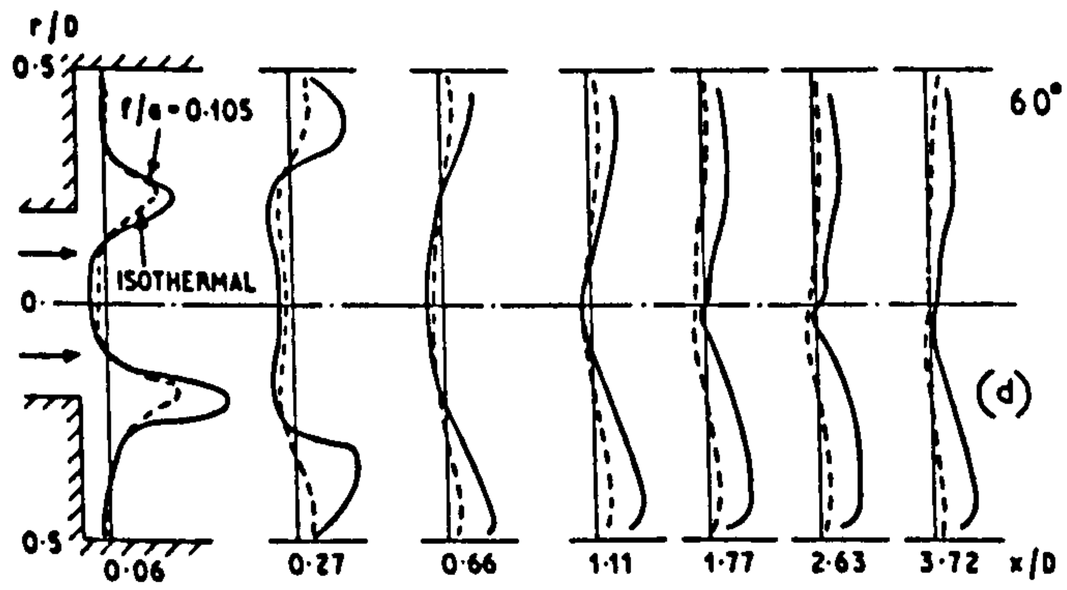

FIG. 1c, d Axial velocity distributions. Hubless swirlers. D/d = *2.5 furnace*

Furnaces of 460 mm inside diameter and 1.4 m length and 225 mm inside diameter and 0.9 m length were built; side-arch fire bricks were used for the former and fire bricks cast from heat-resisting cement for the other furnace. There was no quarl and the exit from the swirler was in the plane of the inner surface of the end wall of the furnace.

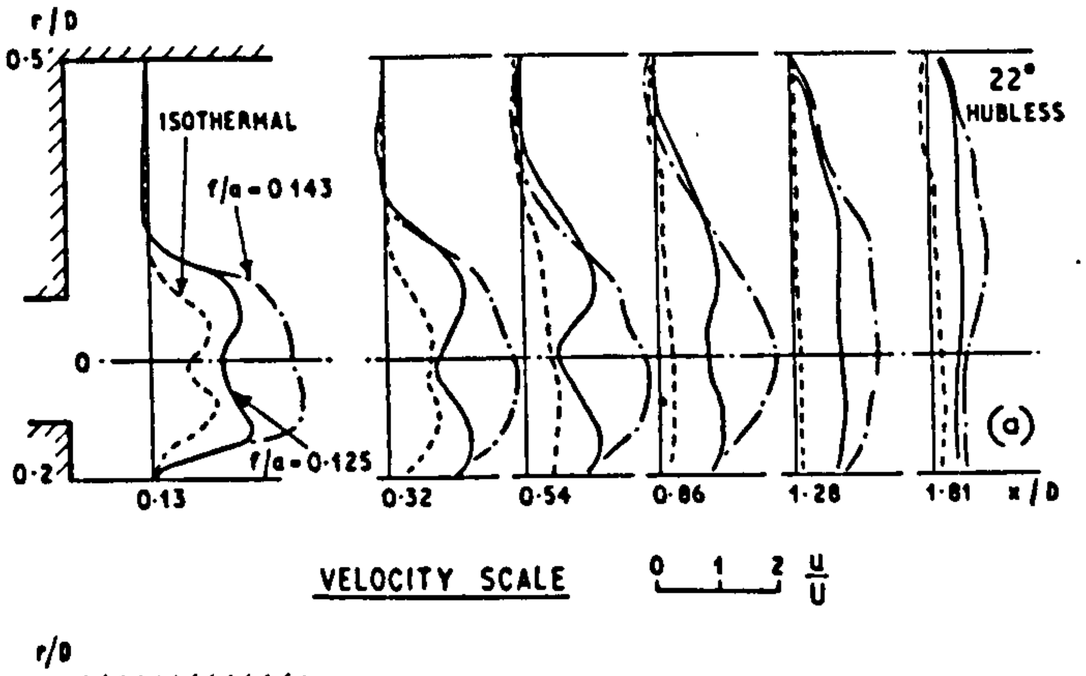

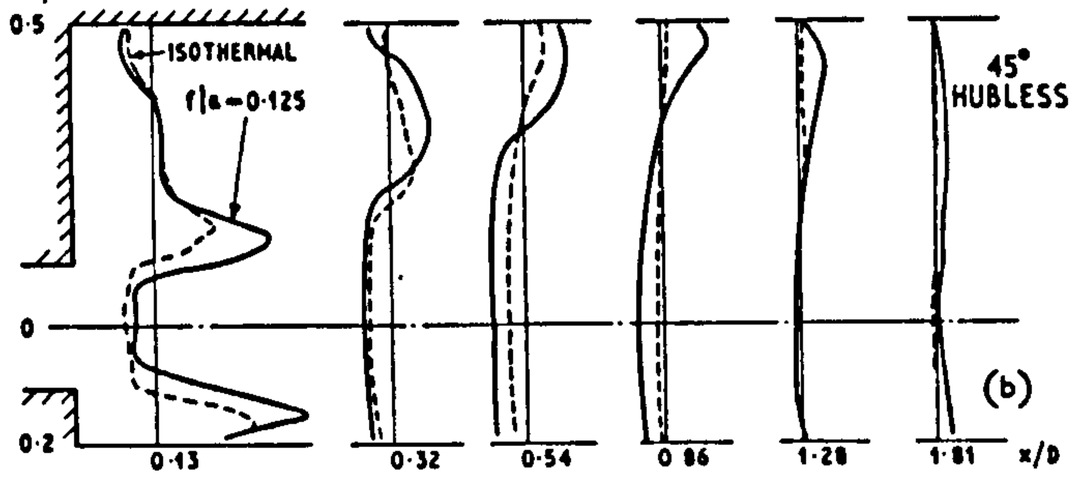

FIG. 2a, b Axial velocity distributions. Hubless swirlers. D/d = *5.0 furnace*

TABLE 1 Composition of town gas

Constituent	% by volume
H_2	48.2
CH_4	29.4
C_2H_6	0.8
C_3H_8	0.1
C_4H_{10}	0.1
CO	1.3
CO_2	11.1
O_2	1.8
N_2	7.2

The air and town gas flows were metered by sharp-edged orifice plates. The gas and air streams were mixed well upstream of the swirler, so that a homogeneous flow entered the furnace. A typical composition of the town gas is given in Table 1.

3.3. Observations

The flow parameters measured were the three components of the time-averaged velocity, the local static pressure, the temperature and the carbon dioxide concentration. The velocity measurements were made by means of a water-cooled three-hole probe to the design of Hiett and Powell.[2] The outside diameter of the probe tip was 6.35 mm. This probe was also calibrated for measurements of static pressure. These were generally satisfactory provided the flow vector was not principally in a radial direction. In the locations where this occurred, a disc probe to the design of Miller and Commings[3] was used. Temperatures were measured by a Pt 5% Rh–Pt 20% Rh thermocouple. The carbon dioxide analysis was performed by an infra-red gas analyser.

Because of the limitations of the probe materials, and the difficulties in cooling them, fuel/air ratios were

TABLE 2 Characteristic dimensions, swirl numbers and flow types

Swirler vane angle deg.	Swirler type H—hubless A—annular	D/d	Flow state I—isothermal B—burning (f/a)	Swirl number S^*	Flow type	Impingement length x_i/D	CRZ Length/D	CRZ Max diameter/D	CRZ Max $\frac{u_{rev}}{U}$	CRZ Max $\frac{\dot{m}_{rev}}{\dot{m}_{swirl}}$
15	H	2.5	I	0.074	A	asym.	—	—	—	—
22	H	2.5	I	0.120	C	1.2	0.44	0.15	0.36	0.044
30	H	2.5	I	0.329	D	0.54	1.5	0.57	0.35	0.27
45	H	2.5	I	0.582	D	0.45	→	0.67	0.37	0.29
60	H	2.5	I	1.159	D	0.20	→	0.65	0.37	0.80
30	A	2.5	I	0.364	D	0.66	1.85	0.26	0.39	0.09
45	A	2.5	I	0.572	D	0.48	→	0.62	0.28	0.29
60	A	2.5	I	1.149	D	0.27	→	0.61	0.50	0.47
15	H	5	I	0.079	A	asym.	—	—	—	—
22	H	5	I	0.119	B	1.2	—	—	—	—
30	H	5	I	0.363	D	0.82	→	0.63	0.20	1.13
45	H	5	I	0.553	D	0.44	→	0.70	0.38	1.8
60	H	5	I	1.250	D	0.12	→	0.70	0.34	2.6
15	H	2.5	B	0.030	A	1.2	—	—	—	—
30	H	2.5	B (0.135)	0.095	B	0.80	—	—	—	—
30	H	2.5	B (0.105)	0.103	C	0.52	1.0	0.41	0.48	0.06
45	H	2.5	B	0.198	D	0.42	1.0	0.56	0.59	0.24
60	H	2.5	B	0.324	D	0.22	1.6	0.56	0.65	0.19
30	A	2.5	B (0.135)	0.137	C	0.61	0.85	0.15	0.42	0.01
30	A	2.5	B (0.105)	0.119	C	0.56	1.35	0.41	0.46	0.07
45	A	2.5	B	0.194	D	0.47	1.63	0.53	0.47	0.15
60	A	2.5	B	0.382	D	0.28	1.80	0.57	0.58	0.25
0	H	5	B	0.000	A	>1.8	—	—	—	—
15	H	5	B	0.037	A	>1.8	—	—	—	—
22	H	5	B (0.143)	0.059	A	1.2	—	—	—	—
22	H	5	B (0.125)	0.054	B	1.1	—	—	—	—
30	H	5	B	0.088	B	1.1	—	—	—	—
45	H	5	B	0.302	D	0.45	1.50	0.71	0.53	0.59
60	H	5	B	0.520	D	0.18	1.83	0.71	0.55	0.75
0	A	5	B	0.000	A	>1.8	—	—	—	—
15	A	5	B	0.047	A	1.6	—	—	—	—
30	A	5	B	0.106	B	1.2	—	—	—	—
45	A	5	B	0.233	D	0.47	1.72	0.63	0.45	0.49
60	A	5	B	0.436	D	0.36	1.72	0.70	0.56	0.81

generally kept to about 0.125 by volume (stoichiometric, 0.24). With the smaller furnace, oscillations were sometimes encountered when the fuel/air ratio was 0.125. It was found that these oscillations could be avoided by altering the fuel/air ratio. Consequently the following fuel/air ratios were used with the smaller furnace: 15° swirler, 0.135; 45° and 60° swirlers, 0.105; 30° swirler, both 0.105 and 0.135.

4. Results and discussion

4.1. Flow regimes

There are significant differences between the forms of the flow patterns obtained in the various systems. To assist the study of these patterns, the flows have been classified into four categories: A, B, C and D.

Flows classified as type A are those in which the maximum forward axial velocities are always close to the centre of the jet. This type of flow is obtained when there is no swirl, or very weak swirl. The jets, both isothermal and burning, issuing from the 0° and 15° swirlers, annular and hubless, in both furnaces are of this type (eg Fig. 1*a*).

The opposite extreme of flow pattern, type D, occurs when there is a well-established CRZ (central recirculation zone). An arbitrary minimum value of 0.1 for the ratio of the maximum reverse mass flow in the CRZ to the burner mass flow has been selected to characterize this flow type.

Flows such as these were obtained with both annular and hubless 45° and 60° swirlers in both isothermal and burning conditions in both furnaces (eg Figs. 1*c*, 1*d*, 2*b*). The isothermal flows from both 30° swirlers in both furnaces were also of this type, but not the corresponding burning flows. The axial velocity profiles of the flows, isothermal and burning at two fuel/air ratios, with the

FIG. 3a, b Decay of maximum axial velocity along the furnace. Hubless swirler flames

30° hubless swirler in the $D/d = 2.5$ furnace are shown in Fig. 1*b*. The burning jet, at the fuel/air ratio of 0.105, represents type C flow. There is a CRZ, but the maximum reverse mass flow in it is less than 0.1 of the burner mass flow. An increase of the fuel/air ratio to 0.135 causes disappearance of the CRZ, though troughs remain in the axial velocity distribution around the axis near the burner. This pattern is referred to as type B, the distinction between it and type C being that there is no CRZ.

The distinction between type B and type A flows is not definite. The division adopted is that type B flows must show, near the burner, a double-crested axial velocity distribution with a minimum on the centre line.

It has been found that in the two furnaces the transitions from one flow type to the next, in both isothermal and burning conditions, are correlated by a swirl number S^* defined by

$$S^* = \frac{T}{G_d D} \quad . \quad . \quad . \quad . \quad . \quad . \quad (1)$$

where T is the experimentally measured tangential momentum flux, G_d is the experimentally measured dynamic component of the axial momentum flux and D is the furnace diameter. The transitions from flow types A to B, B to C, and C to D occur at values of S^* of 0.08, 0.11 and 0.18 respectively. The use of the swirl number S^* is discussed more fully in reference 4.

4.2. Axial velocity distributions

The general effect of combustion, when compared with the isothermal situation, is to increase the axial components of velocity, as expected. Also, sometimes the flow regime is altered, as described above.

Axial velocity distributions for a selection of the combinations of swirlers and furnaces are given in Figs. 1 and 2; a few results have previously been reported in reference 5, they are reported more extensively than here in reference 6 and fully in reference 7. The results obtained using the annular swirlers have not been illustrated here. These results were generally very similar to those from the corresponding hubless swirlers. Full traverses from one side of the furnace to the other were possible in the smaller furnace. In the larger one it was possible to traverse only from one side to a fractional radius of about 0.4 on the other side. The authors comment on those jets which appeared asymmetric in section 4.10.

Increasing the degree of swirl, by increasing the vane angle, accelerates the spread of the jet. A measure of the jet spread is given by the distance to the point of impingement of the jet on the furnace walls (defined by the intersection of the zero axial velocity contour with the wall). Values of the impingement distances x_i, normalized by dividing by the furnace diameter D, are given in Table 2. The factors which influence the spread of the jet are discussed in section 4.9.

At high degrees of swirl a CRZ is established. The maximum dimensions of these CRZ's and the maximum reverse velocities and mass flow rates in them are given in Table 2. For the well-established type D flows, several conclusions can be drawn. The maximum diameter of the CRZ is uninfluenced by further increases in swirl once the CRZ is well established. The maximum diameter is primarily controlled by the furnace diameter. Its fractional width is only slightly altered by changes in the diameter ratio (D/d); it is reduced from 0.7 to 0.64 for the isothermal jets when (D/d) is reduced from 5.0 to 2.5. Combustion has little effect on the maximum diameter in the larger furnace, but narrows the zone by about 12% in the smaller furnace.

The maximum length of the CRZ is not significantly altered by the degree of swirl. The length, when normalized by dividing by the furnace diameter D, is slightly reduced when (D/d) is reduced from 5.0 to 2.5. Combustion causes appreciable shortening.

The maximum reverse velocity as a fraction of the swirler exit velocity is independent of (D/d) change. It increases only slightly with swirl, and increases noticeably when combustion occurs. This increase is however less than the relative density change, and so the maximum reverse mass flows are reduced by combustion. Swirl increases the maximum reverse mass flows. Increase of the ratio (D/d) increases the maximum reverse mass flow (expressed as a fraction of the swirler mass flow).

Although combustion, when compared with the isothermal situation (an extreme fuel/air ratio change), causes little alteration to flow patterns of established type D flows, comparatively small changes in fuel/air ratio can cause considerable alterations in the patterns when the swirl number S^* is near the critical value of 0.11. For example, consider the previously mentioned case of the 30° hubless swirler in the $D/d = 2.5$ furnace (Fig. 1*b*). Increasing the fuel/air ratio by 30% from 0.105 suppressed the CRZ and changed the flow pattern from type C to type B. The explanation for this is discussed in reference 4.

Decays of the maximum forward axial components of

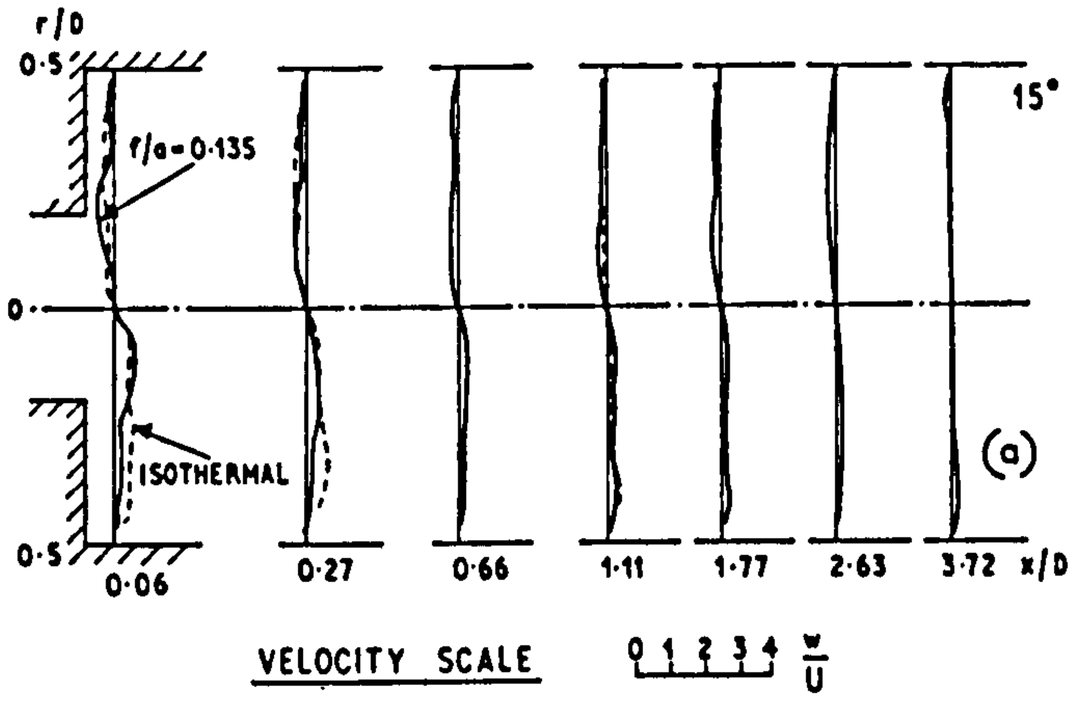

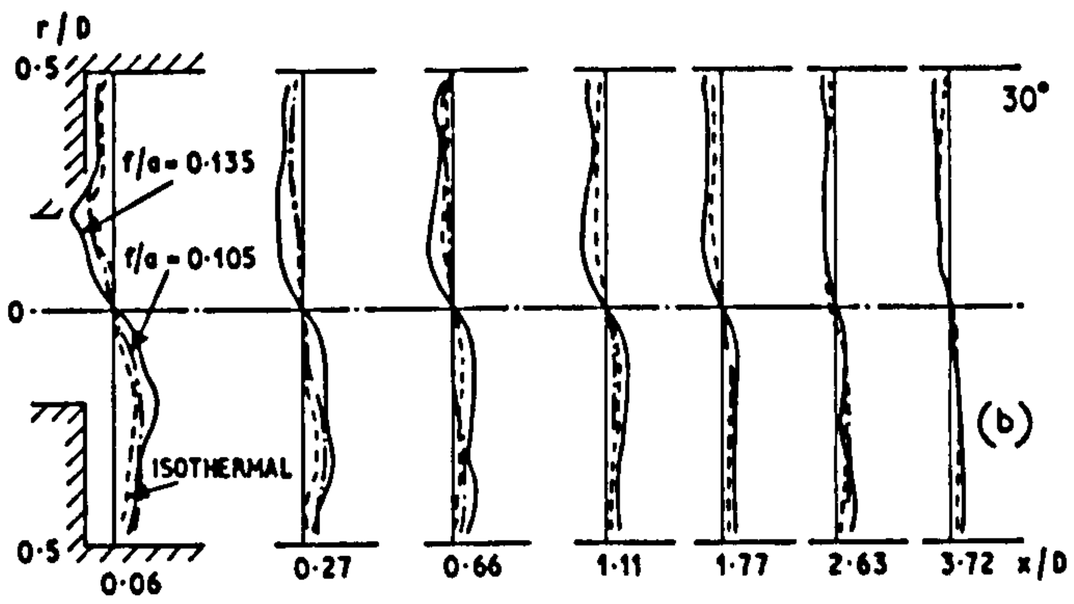

FIG. 4a, b Tangential velocity distributions. Hubless swirlers. D/d = *2.5 furnace*

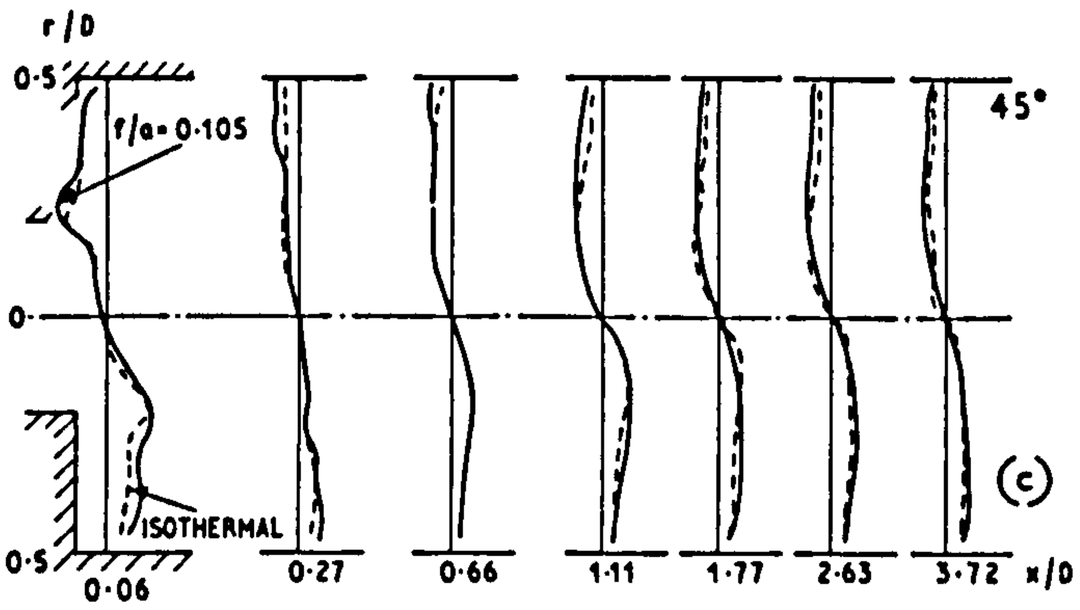

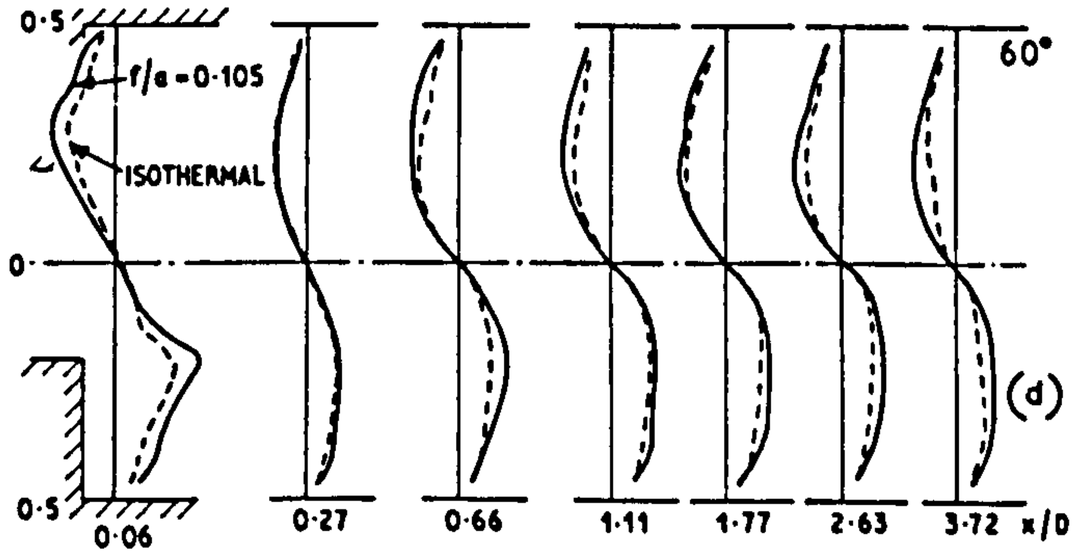

FIG. 4c, d Tangential velocity distributions. Hubless swirlers. D/d = *2.5 furnace*

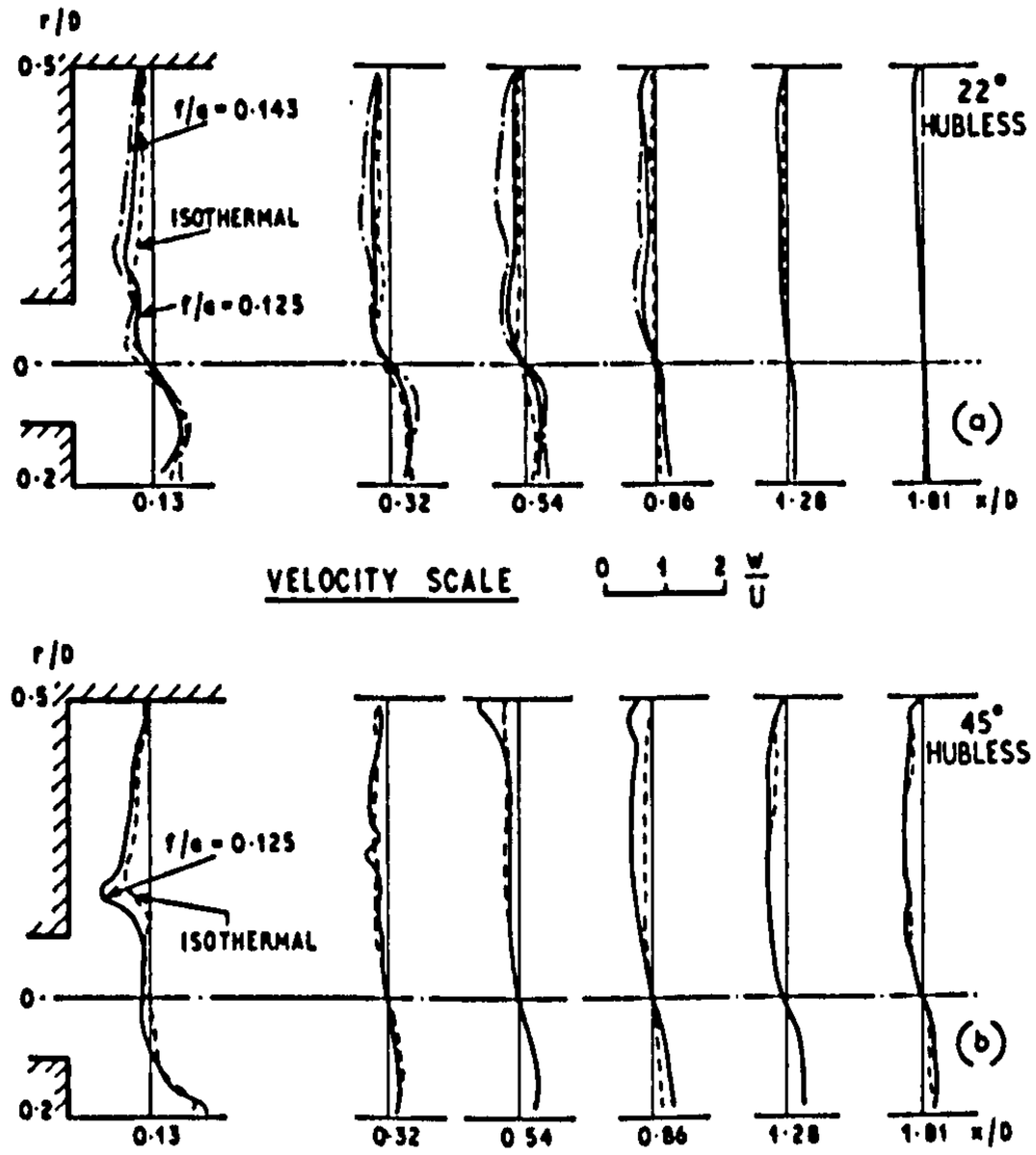

FIG. 5a, b Tangential velocity distributions. Hubless swirlers. D/d = *5.0 furnace*

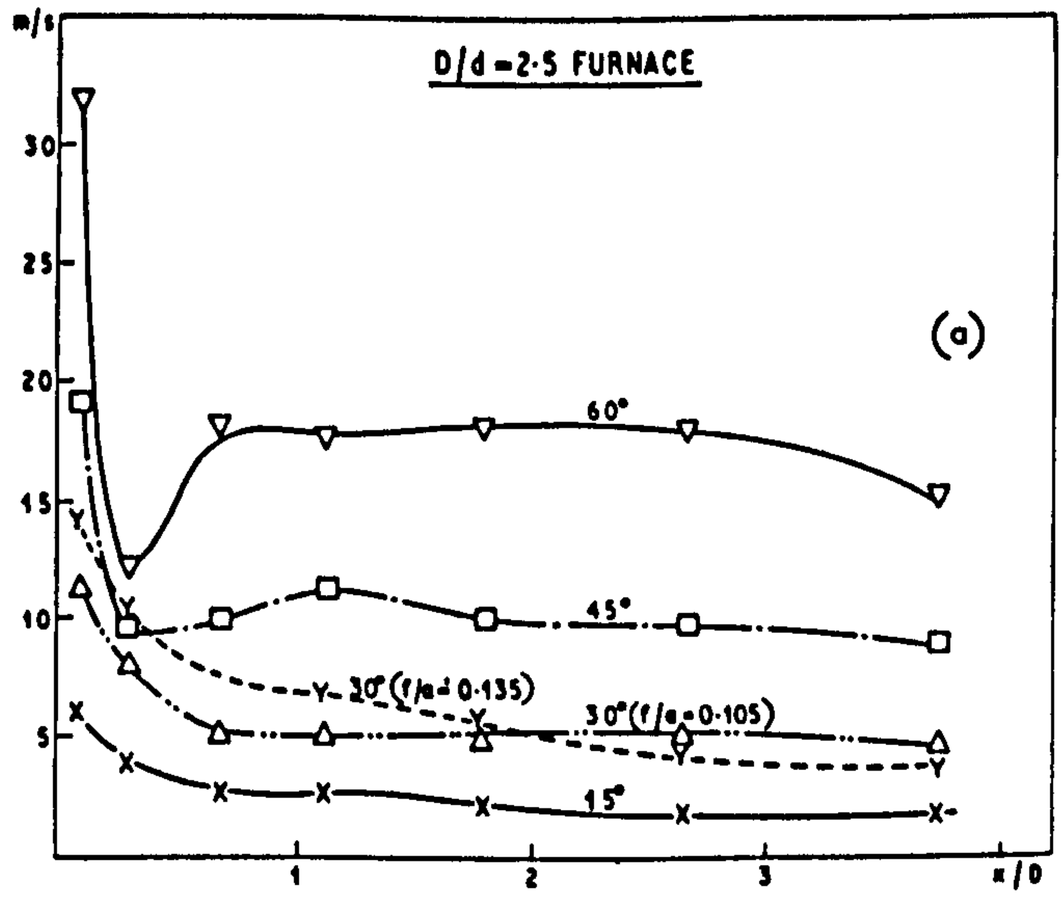

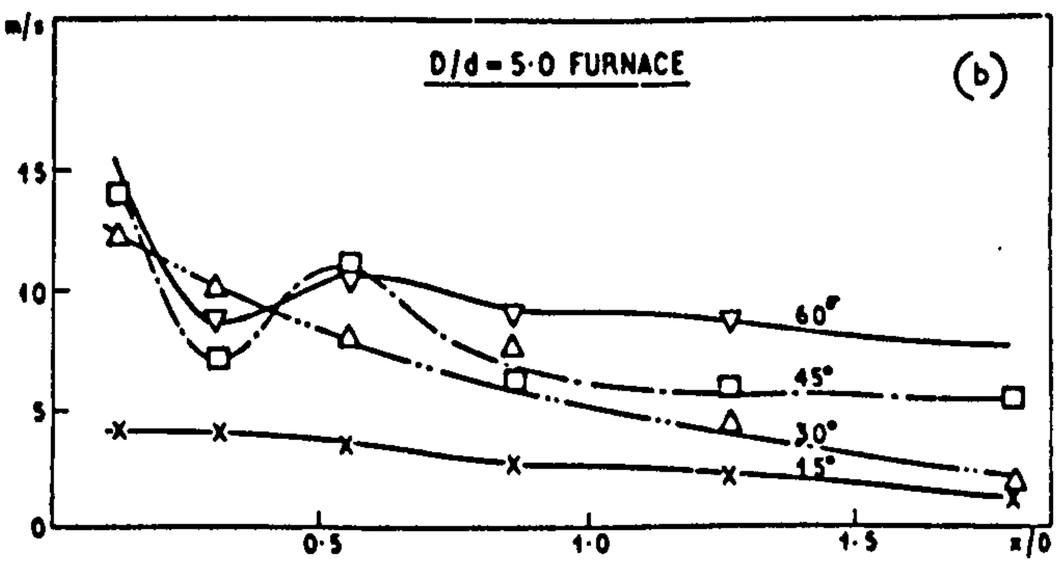

FIG. 6a, b Decay of maximum tangential velocity along the furnace. Hubless swirler flames

velocity in the burning jets in the two furnaces are given in Figs. 3*a* and 3*b*. The corresponding results for the isothermal jets are not illustrated, but are included in this discussion. For type A flows there is little or no decay up to the impingement point, and thereafter a steady decay. Flow types B and C show a more rapid decay up to some distance, beyond which there is little decay. The region where the initial decay ceases is moved forward in

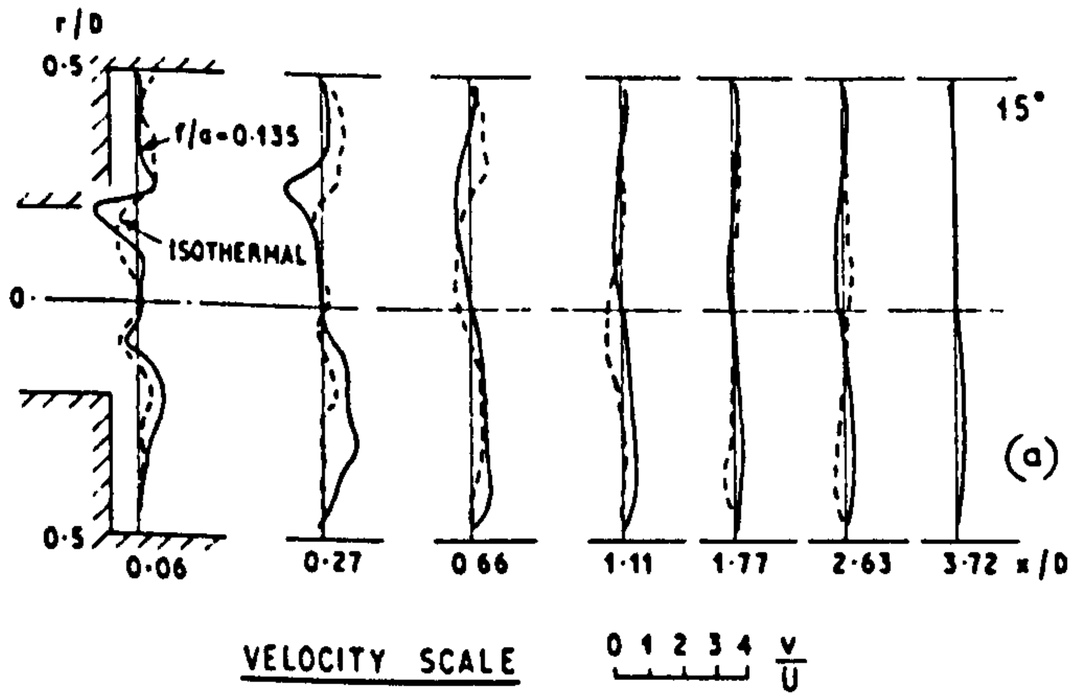

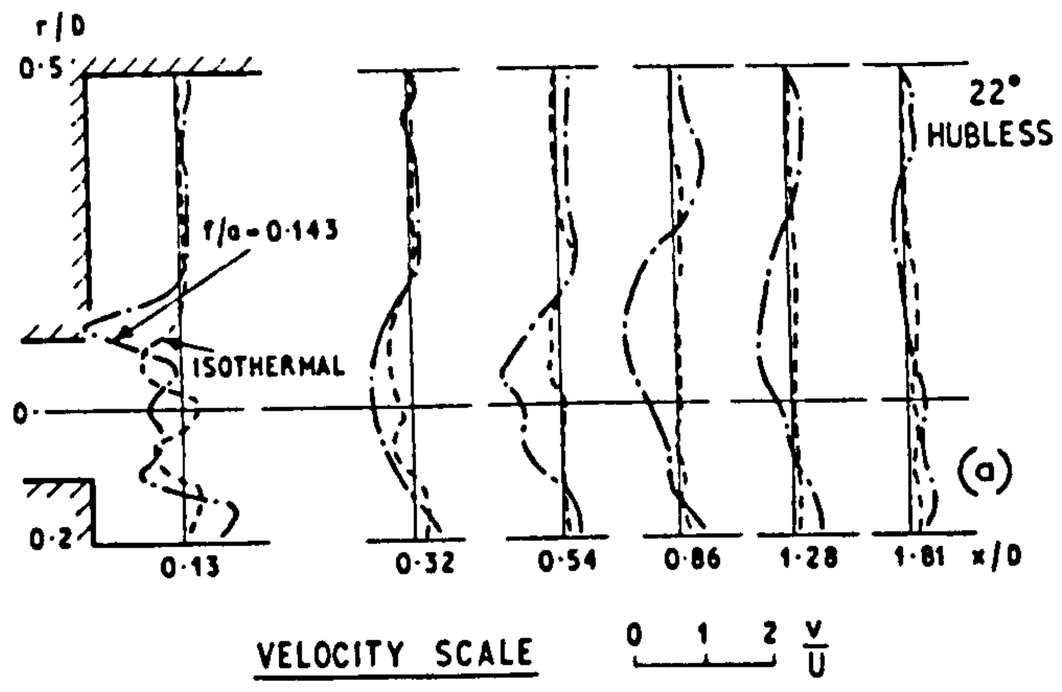

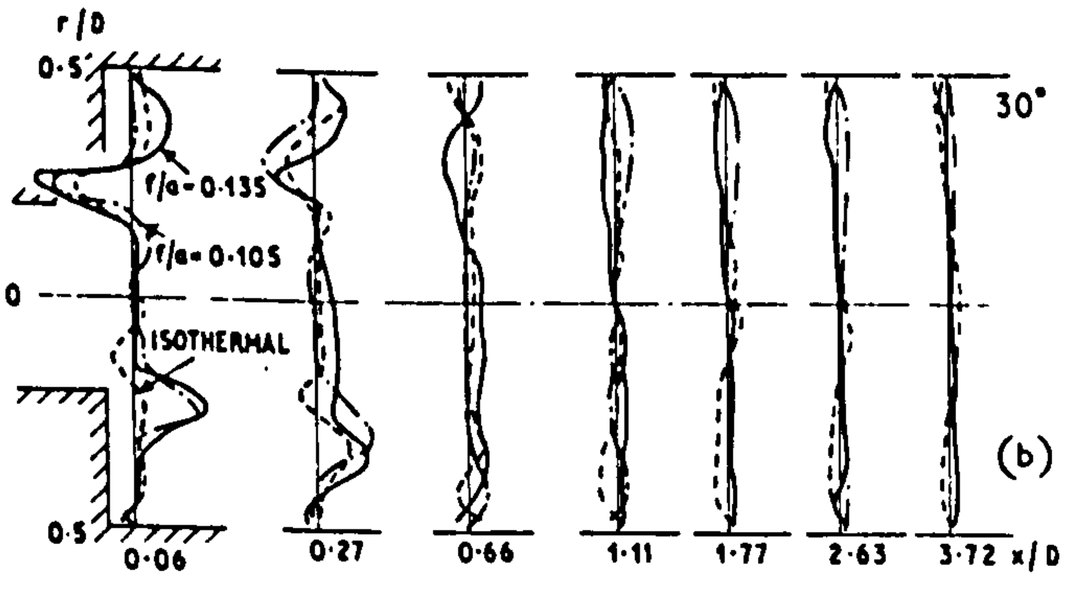

FIG. 7a, b Radial velocity distributions. Hubless swirlers.
D/d = 2.5 furnace

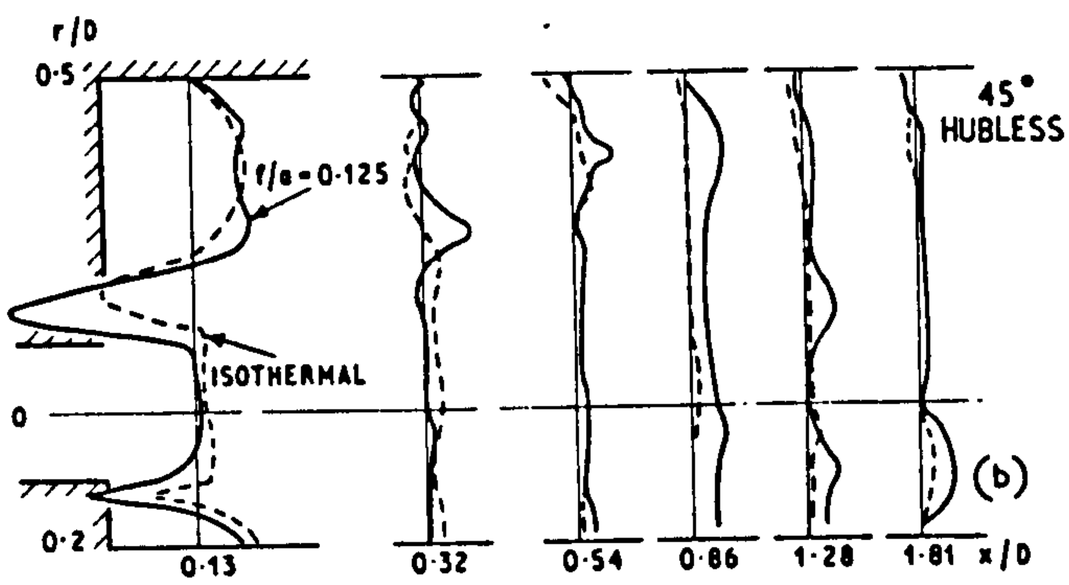

FIG. 8a, b Radial velocity distributions. Hubless swirlers.
D/d = 5.0 furnace

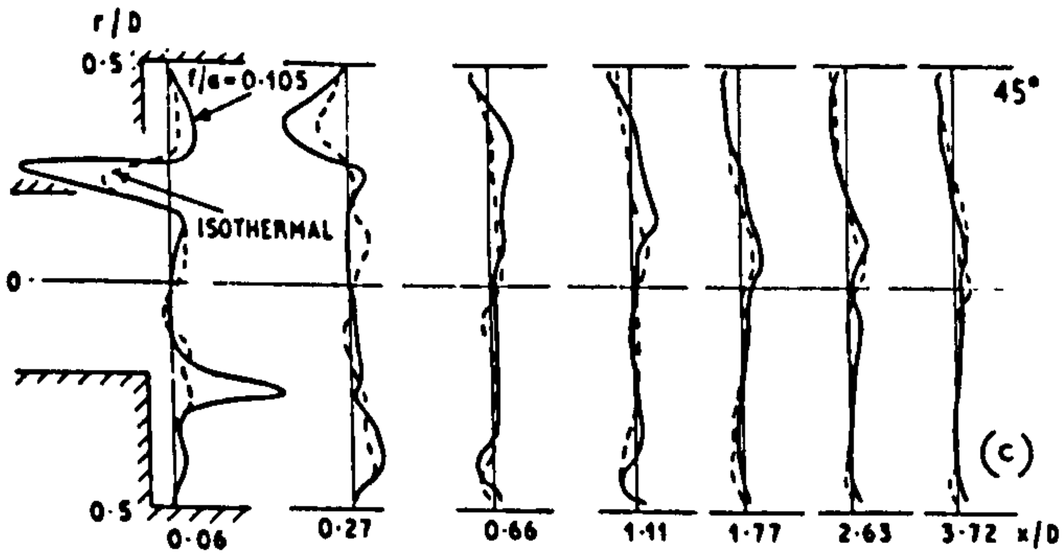

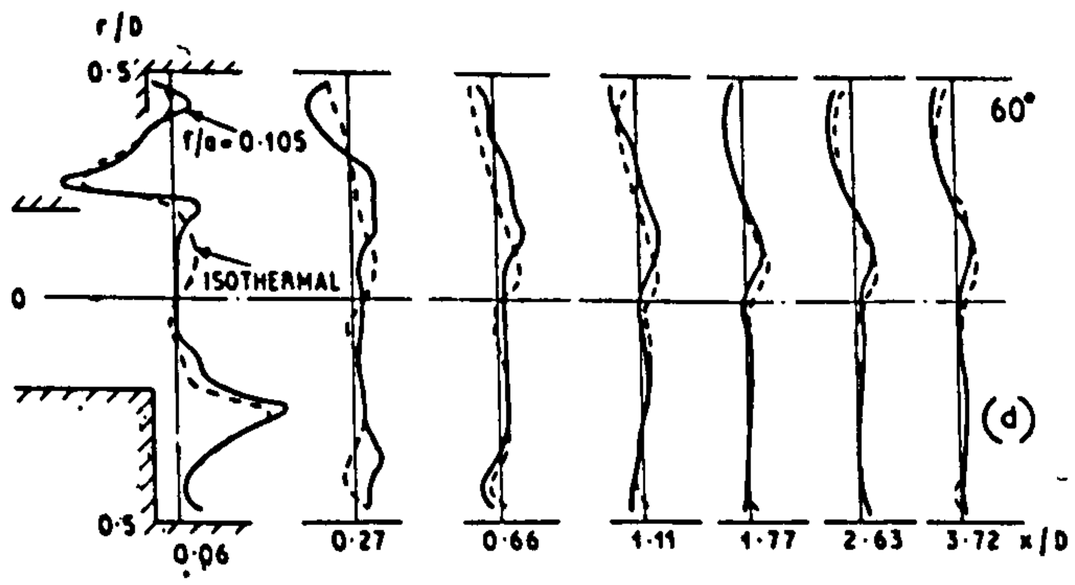

FIG. 7c, d Radial velocity distributions. Hubless swirlers.
D/d = 2.5 furnace

the furnace as swirl increases. In type D flows, the decays in the isothermal jets are similar to those in types B and C, but with even more rapid decays which end at an axial distance of about 1*D*. Some burning jets show similar decays, while others differ. One such differing case is that of the 45° swirlers in the $D/d = 2.5$ furnace. Here an increase in the maximum axial velocity is observed in the first 0.5*D*, followed by a decay. The increase in the first section is consistent with the continuity equation. Density in the forward flow is reducing owing to reaction. Also, the forward mass flow is increasing owing to entrainment from the central and peripheral recirculation zones (PRZ), while the net flow area between the PRZ and the CRZ is decreasing.

4.3. Tangential velocity distributions

Tangential components are generally only slightly increased by combustion. Tangential velocity distributions for the selected cases are shown in Figs. 4 and 5.

For flows of types C and D (ie with a CRZ) the position of the maximum tangential velocity moves rapidly towards the walls (as for the maximum axial velocities) and then a distribution takes place in such a way that there is a considerable annular area over which the tangential velocity components are almost uniform. The tangential velocities in the CRZ and in the PRZ are small. For type A and B flows the tangential velocity spreads less rapidly, without the maximum occurring near the wall.

The decays of the maximum tangential velocities are shown in Figs. 6*a* and 6*b*. Flows of types A and B show an initial steady decay to some value which is maintained thereafter. The end of the decay occurs after about 1*D*. Type C flows follow the same pattern with a more rapid initial decay and a higher ultimate value. Some type D flows indicate an increase in the maximum tangential velocity after the initial very rapid decay. Thereafter there is a slow decay to the value which is maintained to the furnace exit. Part of this apparent increase in tangential velocity could be due to the higher turbulence in the reaction zone, causing the probe to indicate, from the

(*continued on p 189*)

observed time-mean pressure values, values of average velocity components which are erroneously high.[7]

4.4. Radial velocity distributions

These distributions for the same selection of geometries are shown in Figs. 7 and 8. The sign convention used is that in the upper half of any diagram positive values correspond to inward radial velocity components. In the lower half of the diagram the convention is reversed. Thus for a perfectly symmetric jet the distributions should be diagonally symmetric. Frequently the apparent distributions are not of this form, sometimes because the jets at low degrees of swirl tended to be asymmetric, and sometimes because of experimental error in recording

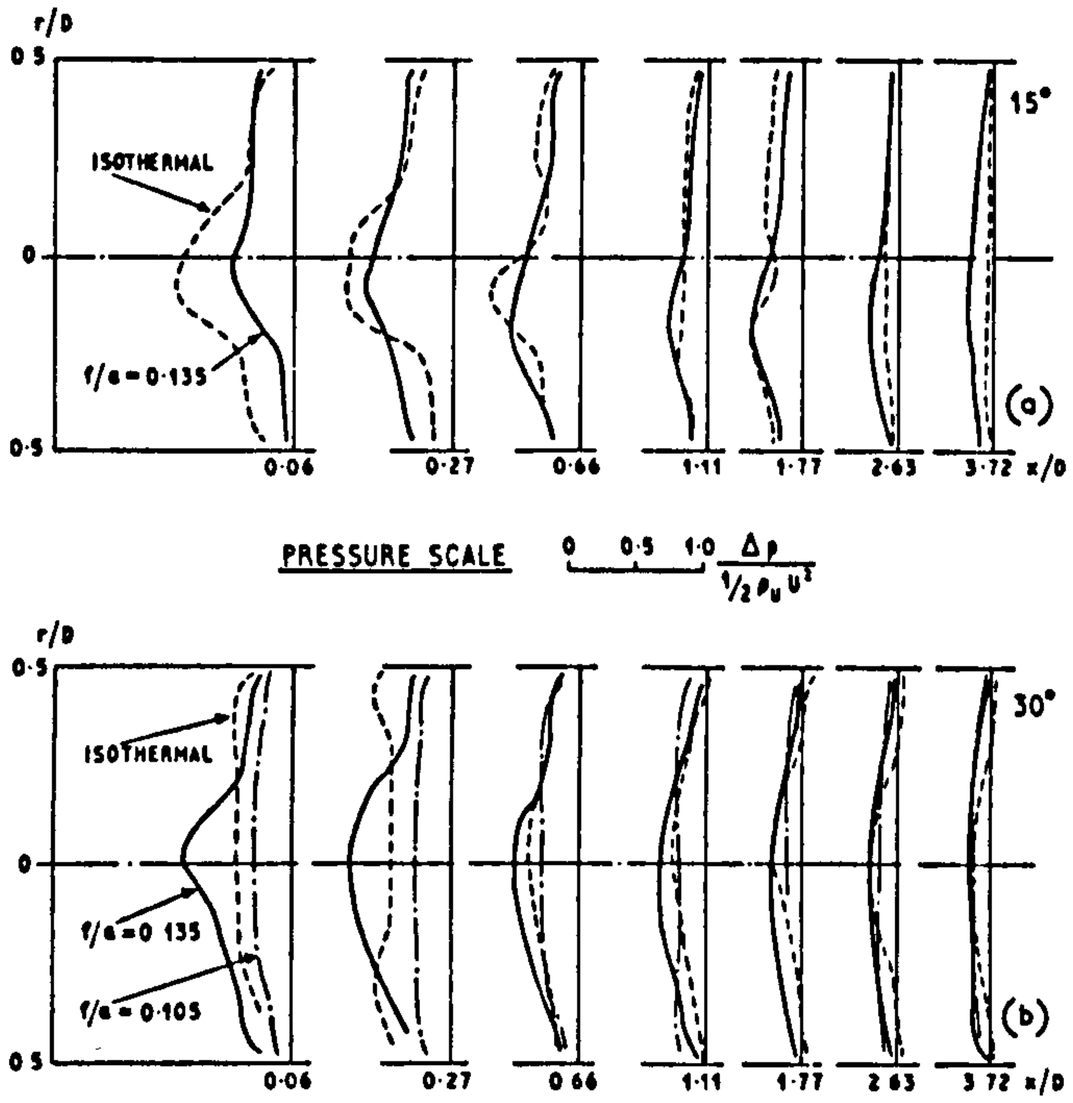

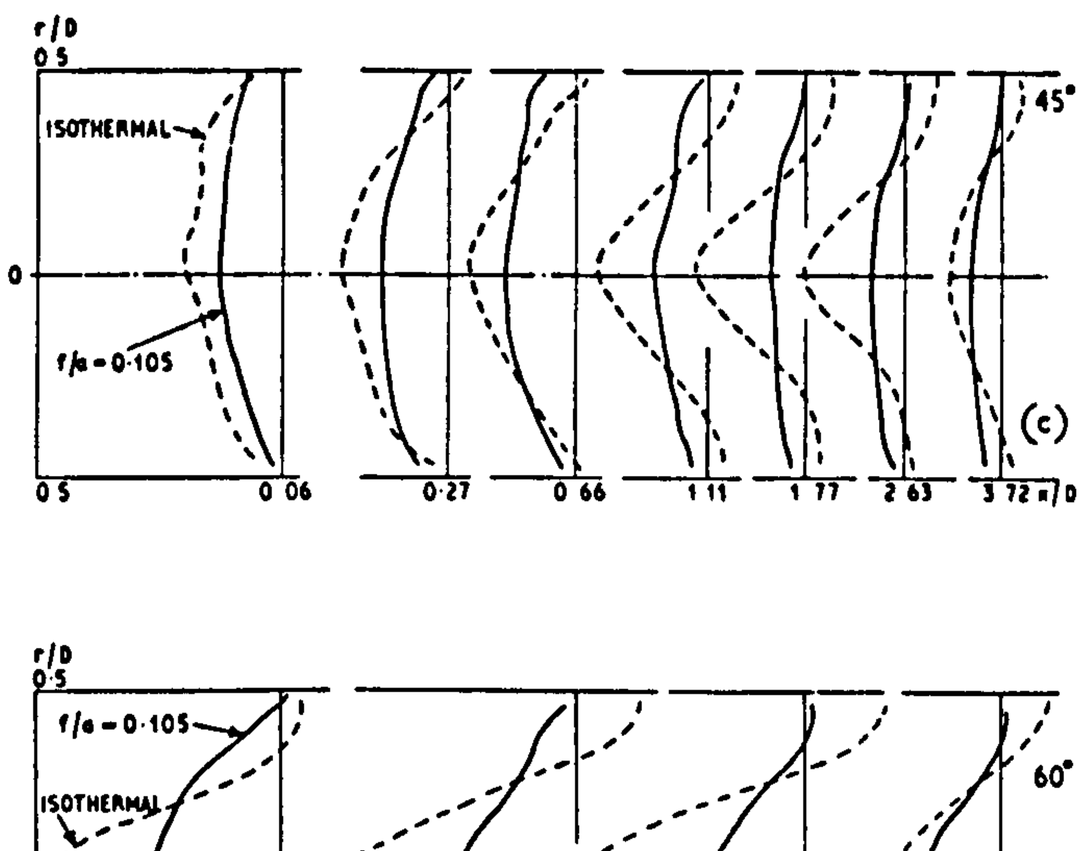

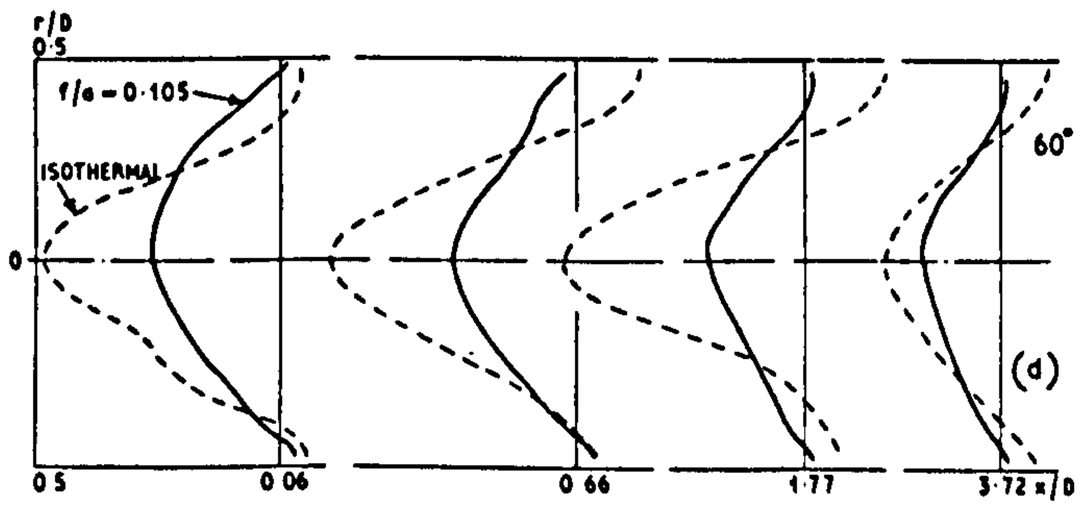

FIG. 9c, d Static pressure distributions. Hubless swirlers. D/d = 2.5 furnace

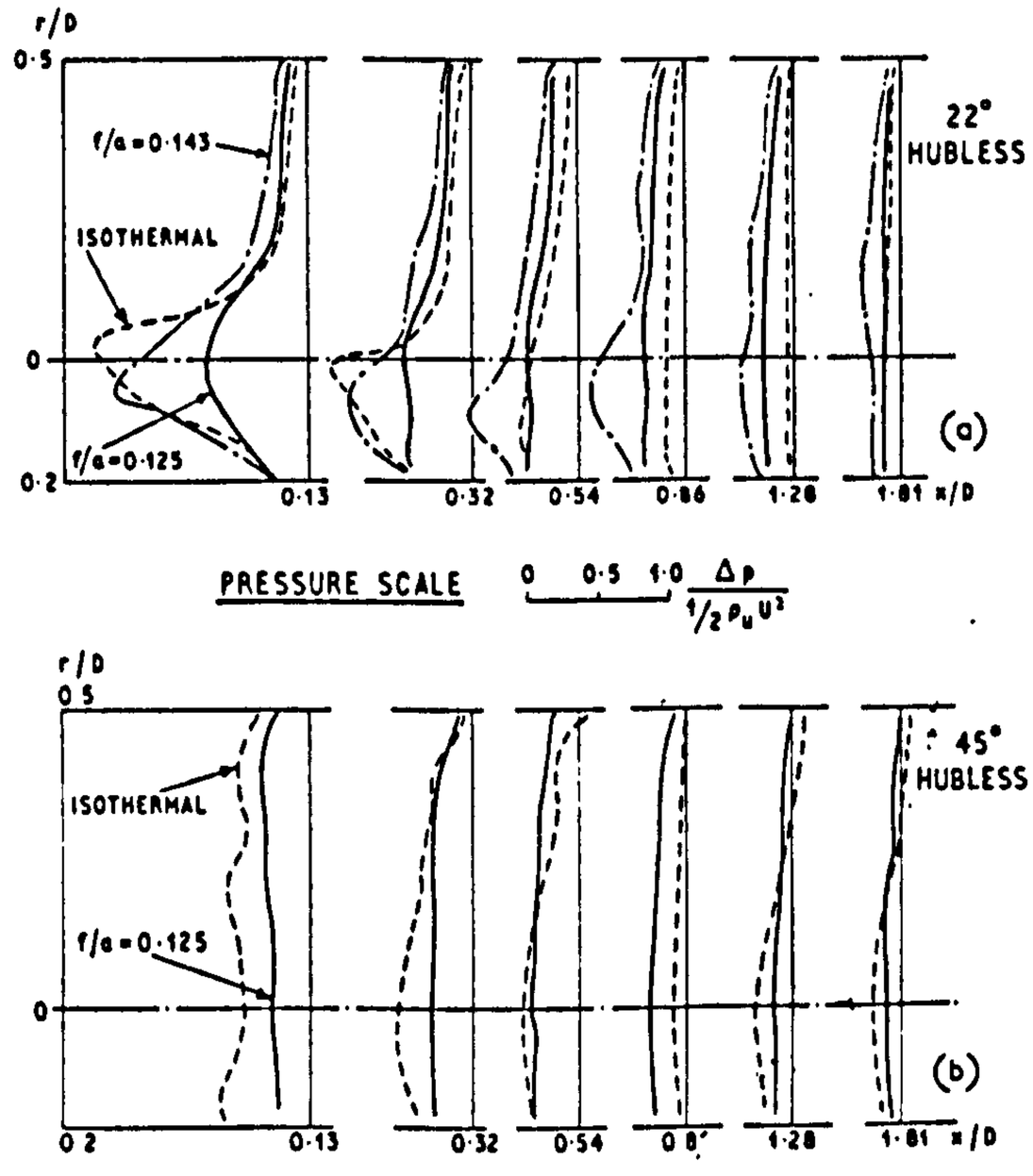

FIG. 10a, b Static pressure distributions. Hubless swirlers. D/d = 5.0 furnace

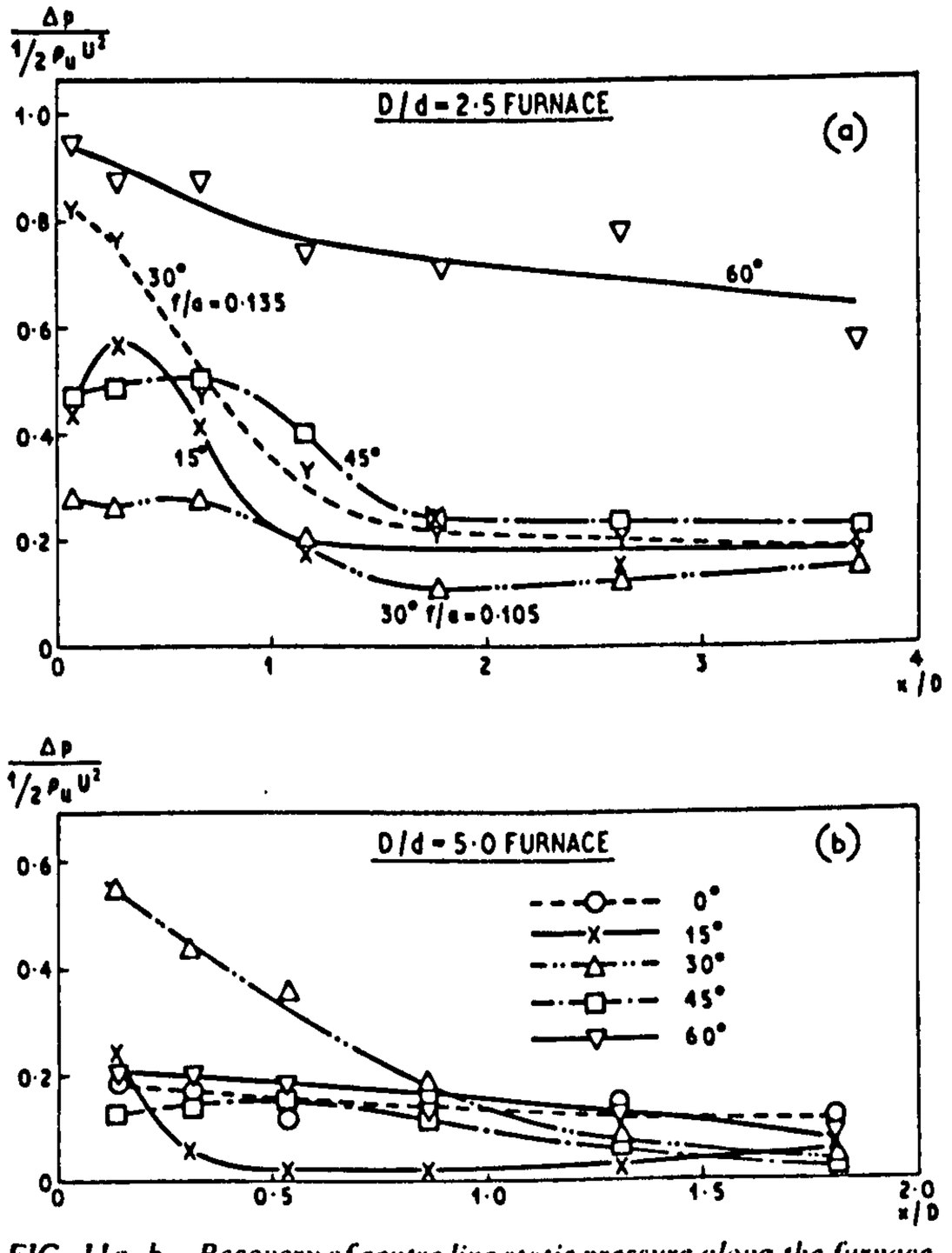

FIG. 11a, b Recovery of centre line static pressure along the furnace. Hubless swirler flames

the radial component. The probe readings are liable to be in error in regions where the flow has a high radial component but a low axial component.

The distributions show that, close to the swirlers, the radial components are of the same order as the axial

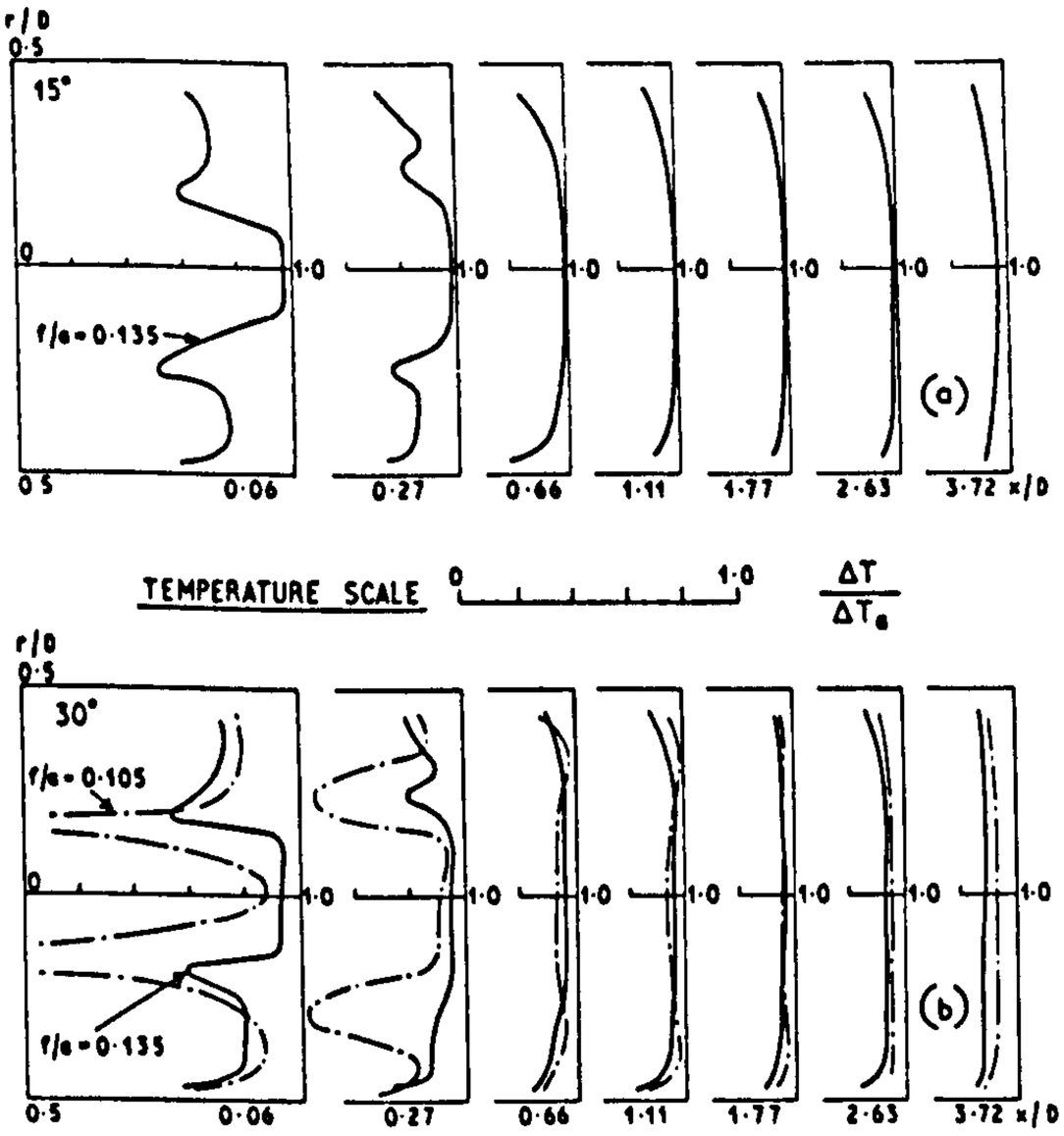

FIG. 12a, b Temperature rise. Hubless swirlers. D/d = *2.5 furnace*

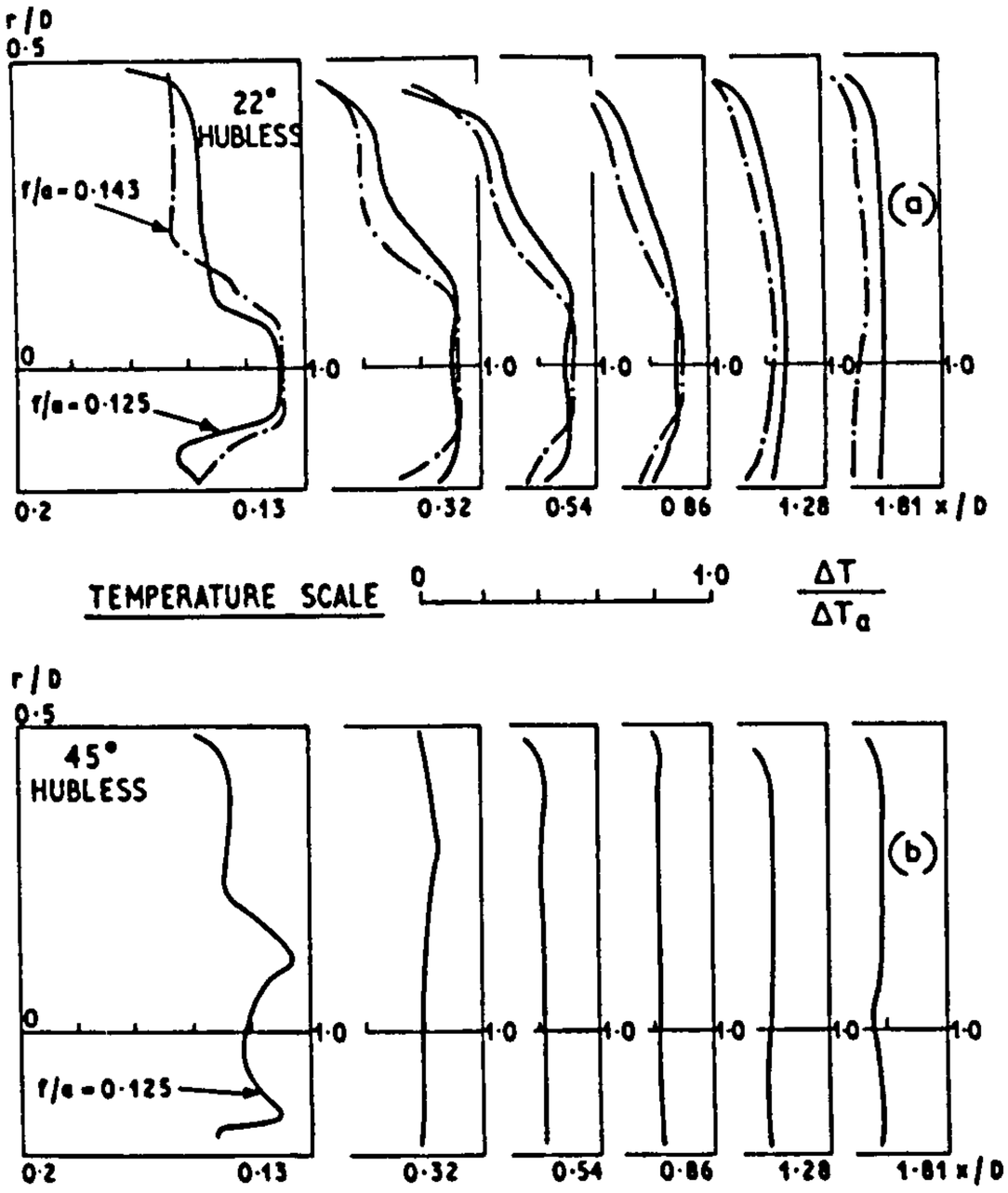

FIG. 13a, b Temperature rise. Hubless swirlers. D/d = *5.0 furnace*

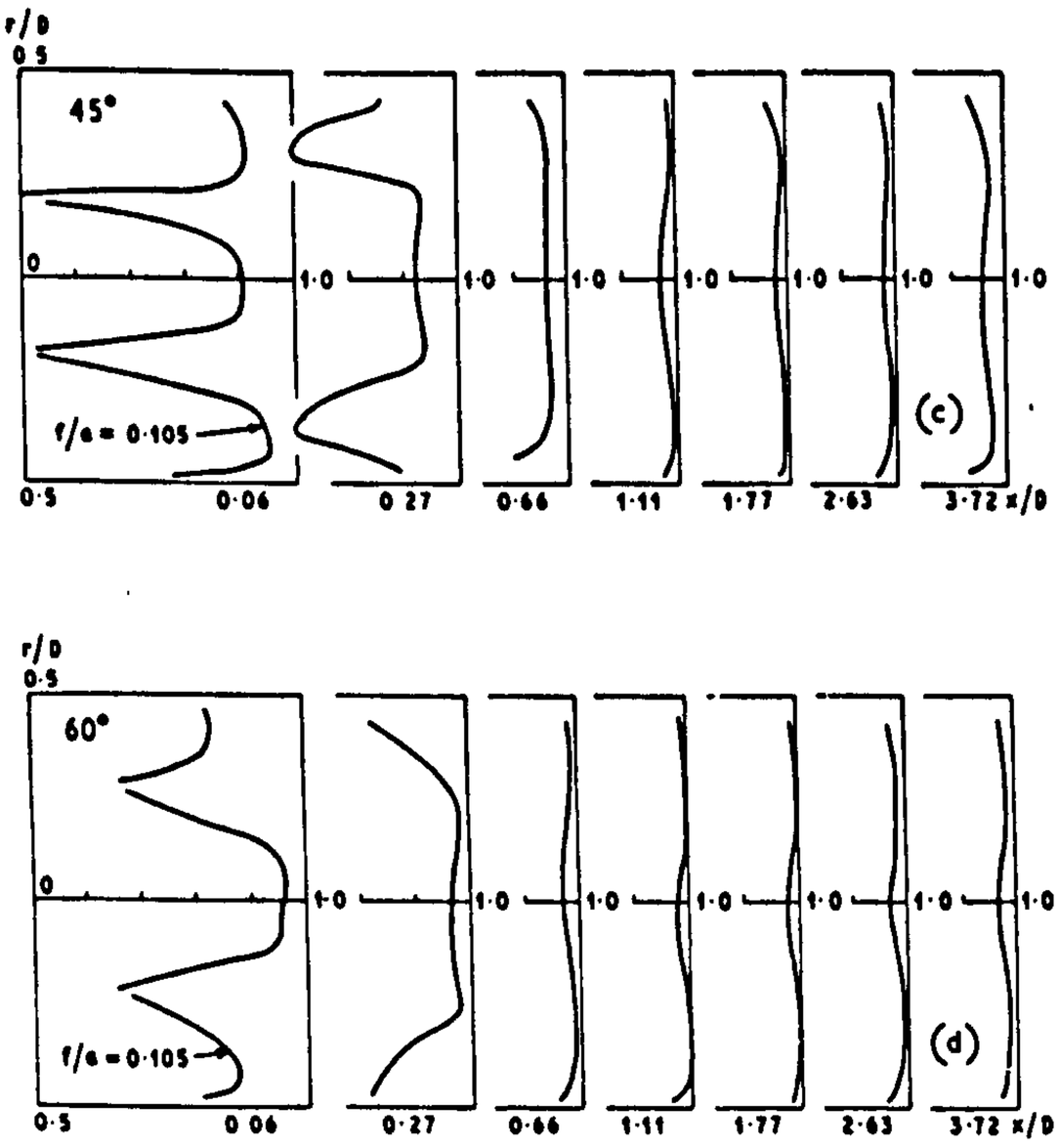

FIG. 12c, d Temperature rise. Hubless swirlers. D/d = *2.5 furnace*

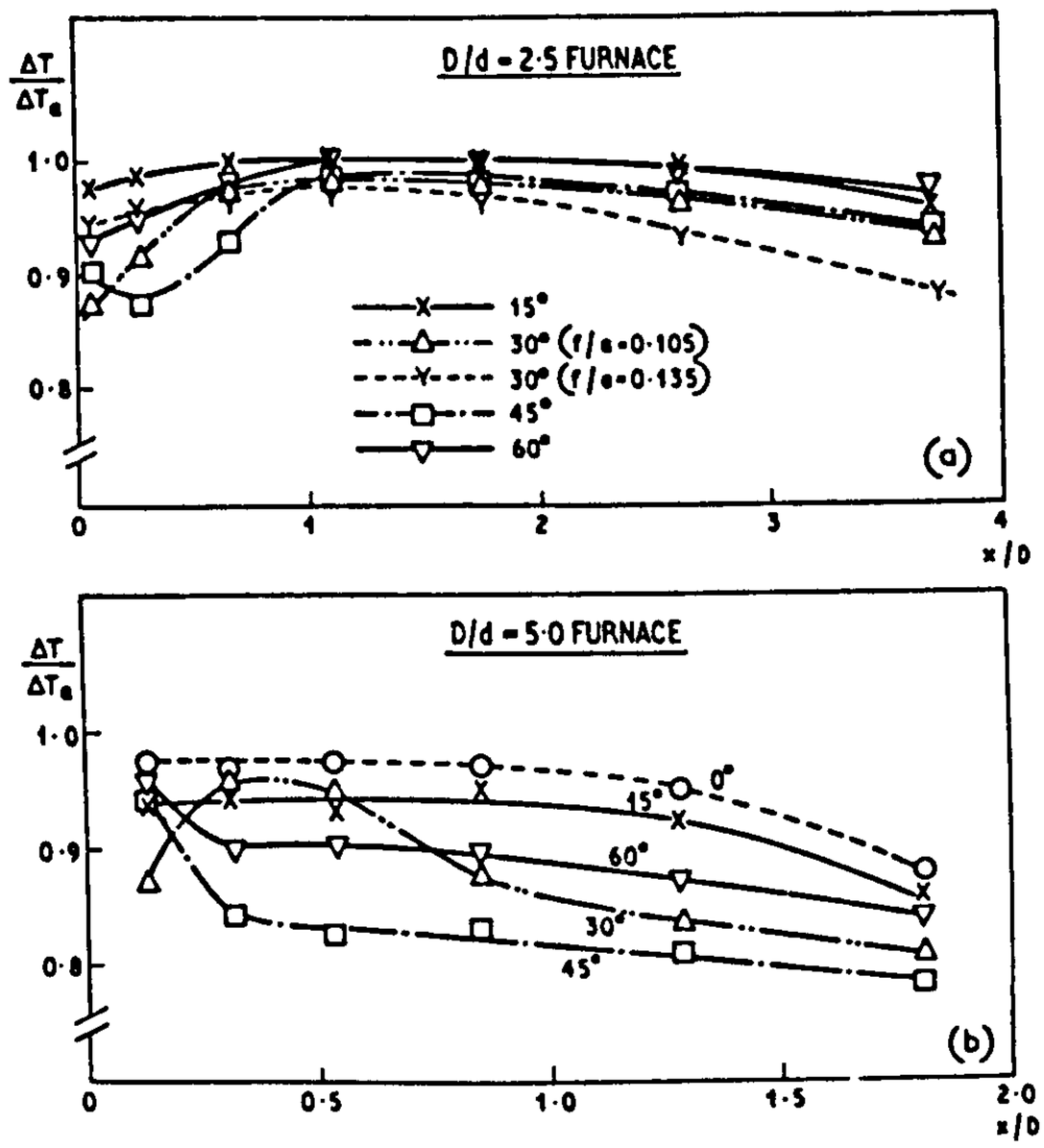

FIG. 14a, b Maximum temperature rise along the furnace. Hubless swirlers

components. The radial values drop rapidly and at axial distances greater than about 1*D* they are very small. Combustion tends to increase the magnitudes of the radial velocities in the early stages, but has little effect thereafter.

4.5. Static pressure distributions

These are given in Figs. 9 and 10. The pressures in the flow are generally sub-atmospheric, rising to about or just above atmospheric at the walls. Combustion always brings the static pressure closer to atmospheric.

Pressures across the CRZ and across the PRZ are essentially uniform. There are high pressure gradients in the regions of high velocity.

The effect of increasing swirl from a type A flow is to lower progressively the centre line pressure close to the swirler. This increases the adverse pressure gradient

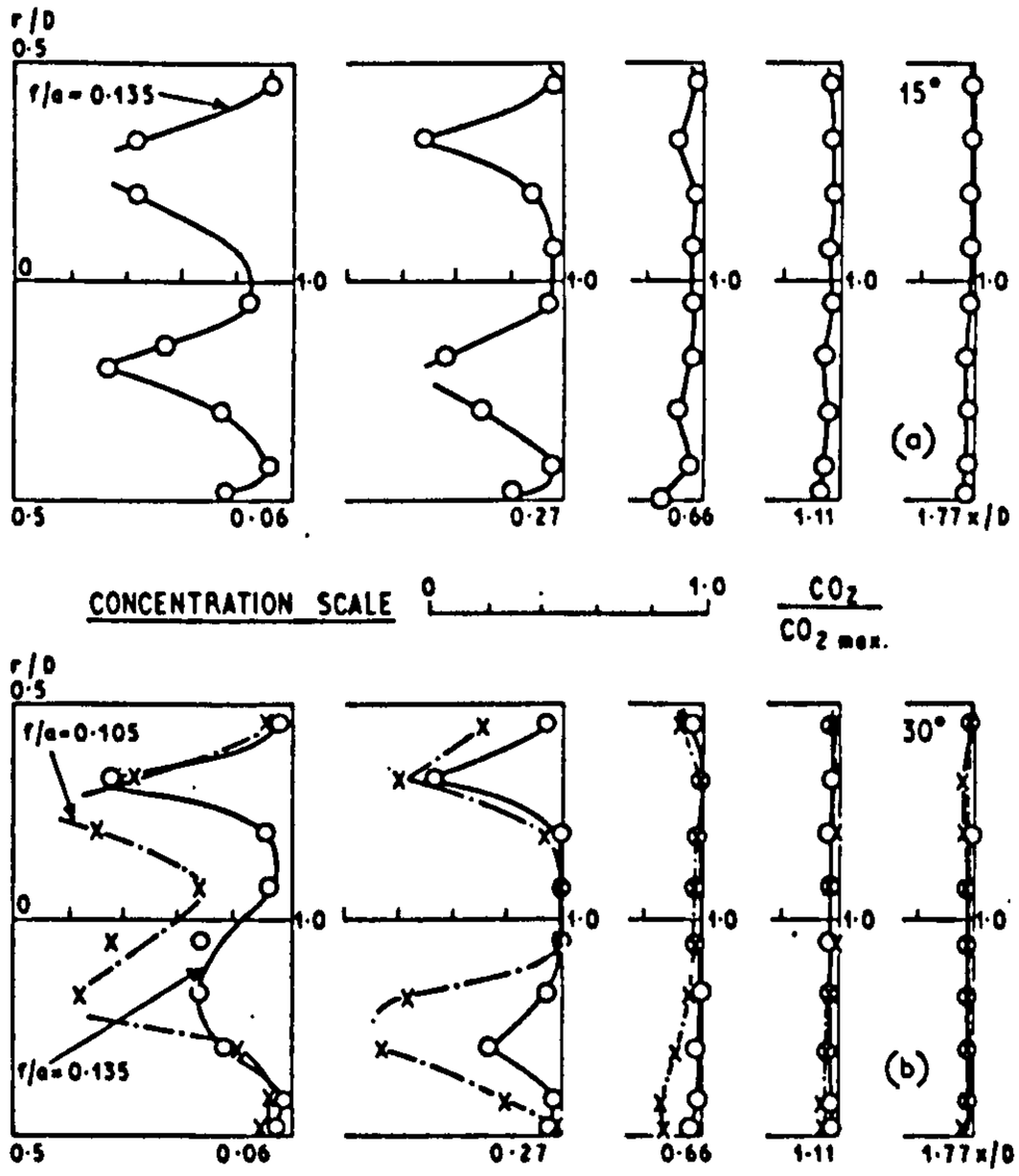

FIG. 15a, b CO_2 concentrations. Hubless swirlers. D/d = 2.5 furnace

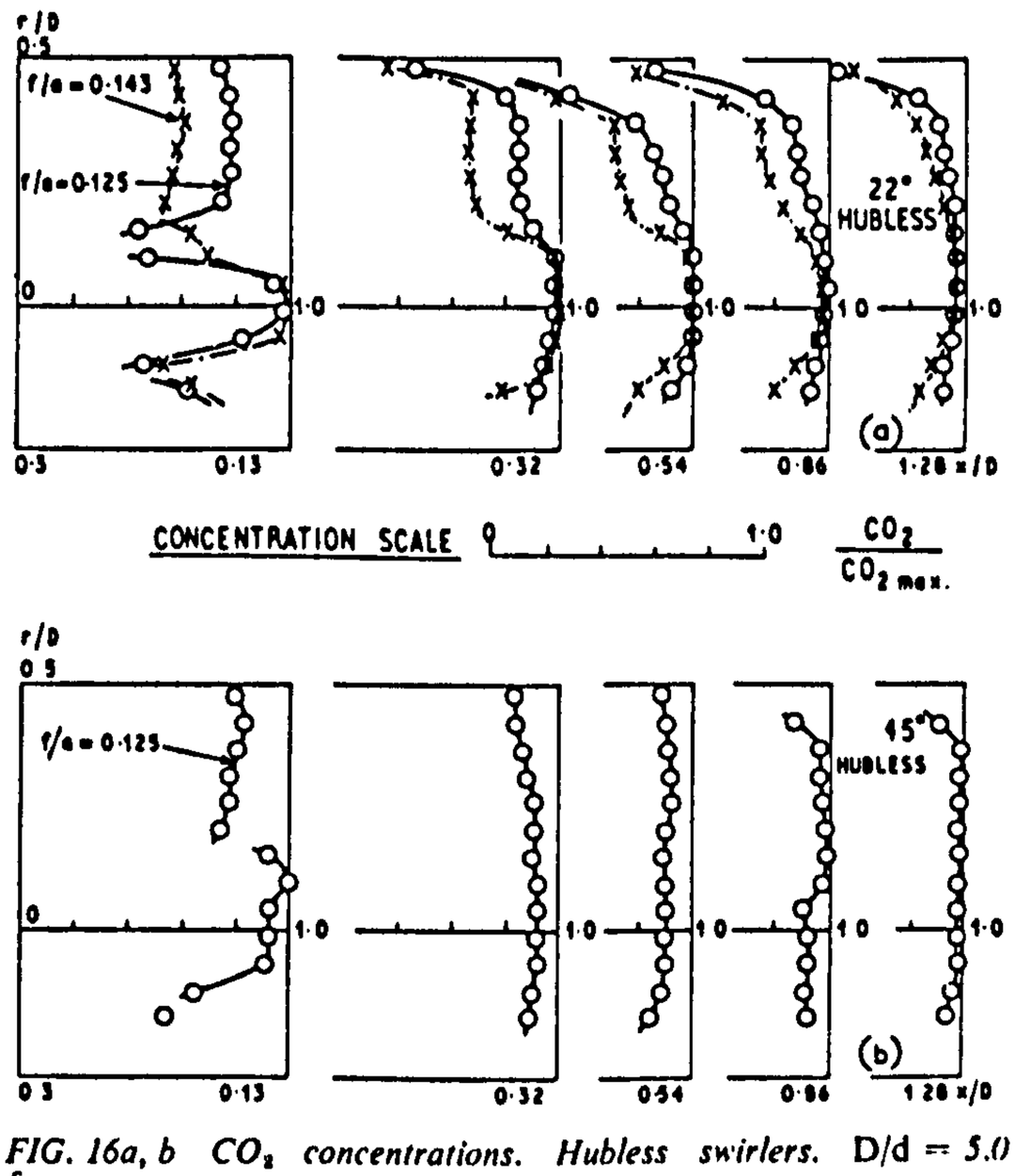

FIG. 16a, b CO_2 concentrations. Hubless swirlers. D/d = 5.0 furnace

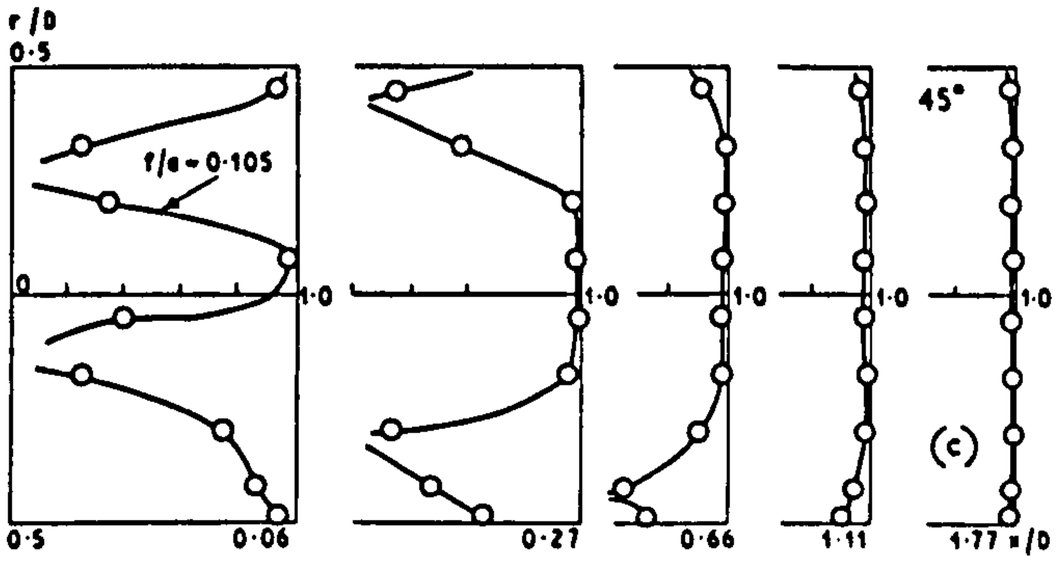

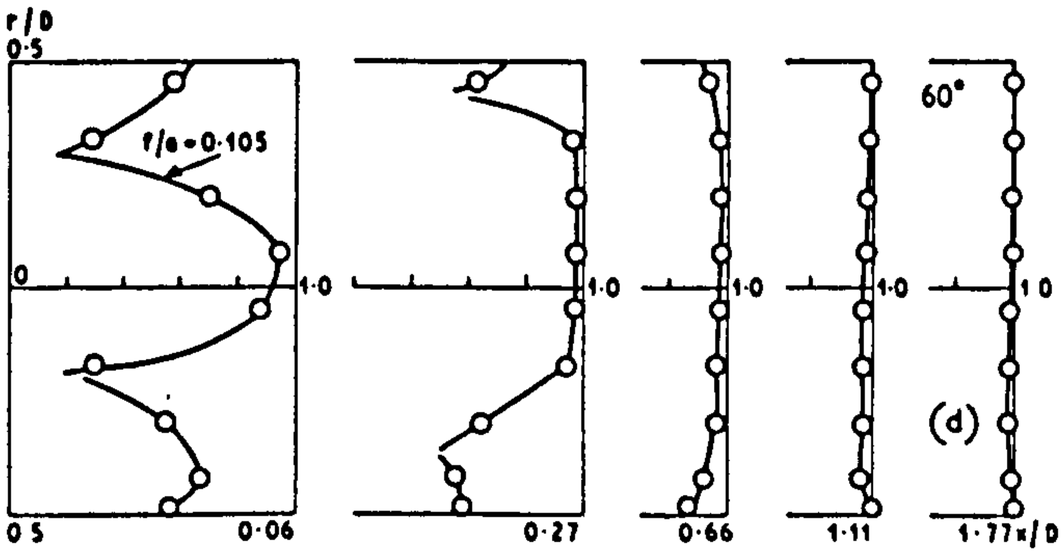

FIG. 15c, d CO_2 concentrations. Hubless swirlers. D/d = 2.5 furnace

along the axis, until it is too great to be sustained by the shear forces. The flow on the centre line then reverses, the CRZ appears, and the centre line pressure near the swirler rises markedly. This process is shown in Fig. 11. For example, for the smaller furnace, with the 30° swirler, at a fuel/air ratio of 0.135, there is no CRZ. At a fuel/air ratio of 0.105, with the same swirler, a CRZ exists and the centre line pressure close to the swirler moves much closer to atmospheric.

4.6. Temperature distributions

Typical temperature distributions are given in Figs. 12 and 13. The variations in maximum temperatures are shown in Fig. 14.

For flows of types A and B, combustion starts from the centre line, in the velocity trough due to the hub (if present) or due to the meeting of the vanes on the axis. Peak temperatures are recorded on the centre line. As swirl is increased the peak becomes wider. At higher swirl, when a CRZ exists, the initial temperatures are lower and reach their maximum values further down the furnace. When the CRZ exists in the $D/d = 2.5$ furnace, the peak temperatures at a plane lie just inside the CRZ. This is slightly different from the observations in corresponding open flames[8] where the peak temperatures lay just outside the CRZ. The difference may be caused by the open flames entraining ambient air[9] into the CRZ, which lowers the temperature, whereas enclosed flames entrain gases from the PRZ, which are comparatively hot. The corresponding temperature distributions in the $D/d = 5$ furnace apparently represent an intermediate condition.

With type C and D flames, a uniform temperature across the furnace is reached in a shorter distance than with the less swirled flames.

4.7. Carbon dioxide concentration distributions

These are shown in Figs. 15 and 16, as fractions of the CO_2 concentrations for complete combustion. They are probably of most interest near the swirler where they

confirm the locations of reaction indicated from the temperature distributions.

4.8. Effect of Reynolds number

The effect of Reynolds number change was studied for one arrangement: 45° hubless swirler in furnace having $D/d = 5$, for isothermal flow. The Reynolds number, based on the average axial component of velocity leaving the swirler, on the unburned density and on the swirler diameter, was changed from 7.5×10^5 to 10.2×10^5. No significant changes were observed in the non-dimensionalized velocity profiles or pressure distribution.

4.9. Comparisons of jet spreads

4.9.1. Effect of swirl

Jet spreads, as defined by the zero axial velocity contours, are shown in Fig. 17 for some selected cases in the two furnaces. Increasing the swirler vane angle increases the rates of spreads of the jets.

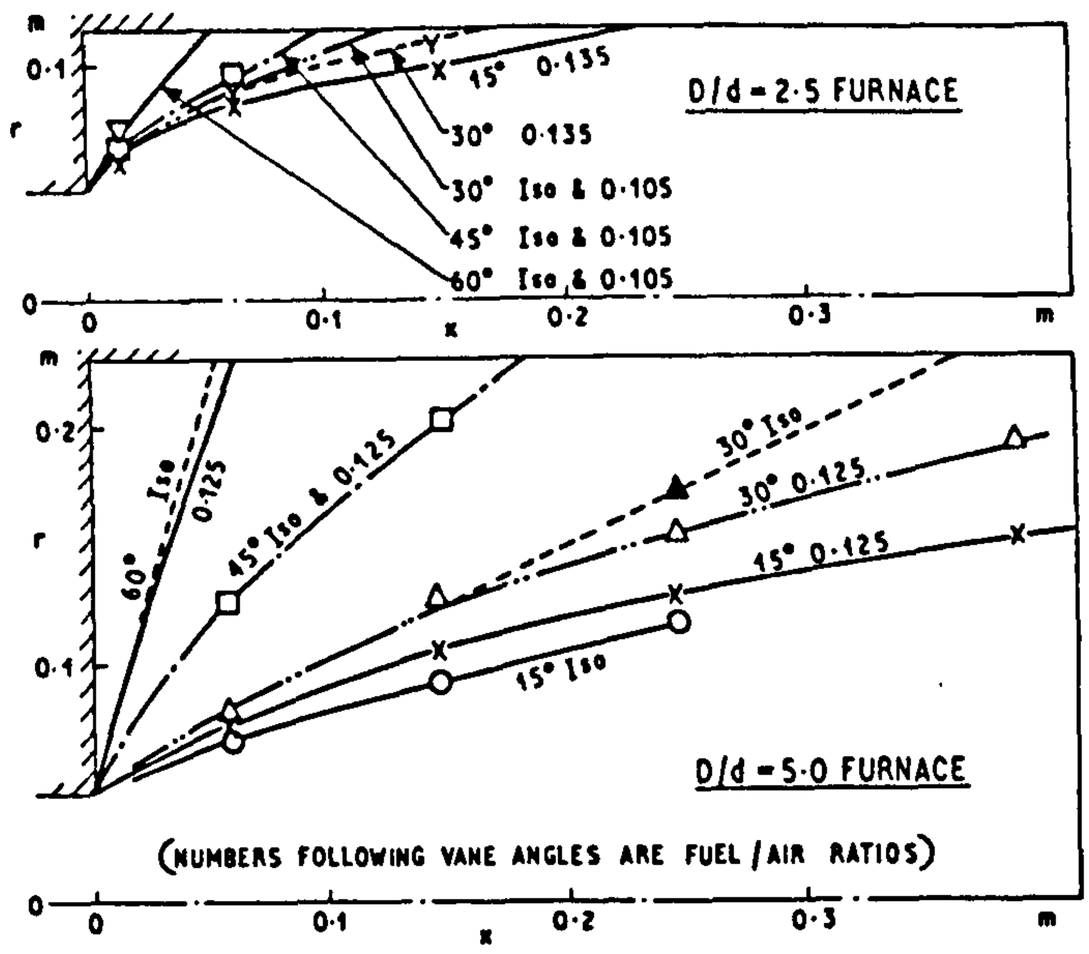

FIG. 17 Jet spread. Hubless swirlers

4.9.2. Effect of confinement

Confinement has been found to cause a rapid increase in the spreading rate of cold swirling jets.[1]

Free burning swirling jets expand more rapidly than isothermal jets.[8] The effect of confinement on the spread is less noticeable in the burning case. The expansions in the smaller furnace ($D/d = 2.5$) have to be compared with the early stages of the free burning jets where the spreads are rapid. In this case there is little effect on spread, particularly at the higher degrees of swirl. However, at the free jet diameters corresponding to the larger furnace ($D/d = 5$) the free jet expansion is less rapid. The confinement by this furnace maintains a more rapid spread.

On comparing the two furnaces, the lengths to impingement divided by the appropriate furnace diameter are very similar for a given swirler (see Table 2).

4.9.3. Effect of combustion

Useful comparisons can be made when there is no flow pattern change due to combustion.

For flow types C and D there is little change in spread due to combustion. The only noticeable effect occurs with the 60° swirler where the isothermal jet spread is slightly faster, impingement distances, which are already very short, being reduced by about 15% in the larger furnace.

For flows types A and B, combustion increases the rate of jet spread.

4.9.4. Effect of hub

The effect in the smaller furnace is not noticeable.

In the larger furnace ($D/d = 5$), the spreads of the jets from the annular swirlers are slightly less rapid than from the hubless ones when flow is of type D, ie strong CRZ. For other flow types the effect of the hub is to make the spreads slightly faster.

4.9.5. Summary of effects

For systems with established CRZs, for practical purposes the spread of the confined jets (measured by x_i/D) is controlled by the vane angle of the swirler, for values of confinement diameter ratio D/d in the range 2.5 to 5. The effects of combustion, of a hub and of the value of D/d in this range appear to be second order.

It should be noted that the presence of combustion in these cases can alter the swirl number S^* by a factor of about 3 for the same swirler vane angle. Thus spread cannot be related to this swirl number.

For flow patterns types A and B, combustion and confinement both cause a noticeable increase in the rate of jet spread.

4.10. Flow asymmetry

Several of the jets, particularly those with low degrees of swirl and in the larger furnace, developed into asymmetric flows. One example, that of the isothermal flow from the 15° swirler in the $D/d = 2.5$ furnace, is shown in Fig. 1*a*. In this case the jet attaches itself to one side of the furnace at an axial distance of about $1.5D$.

Jet asymmetry can have three causes:

(*a*) constructional asymmetries which bias the jet direction,

(*b*) coanda effect,

and (*c*) vortices which are established between the main forward flow and the recirculation zones.[10] These vortices precess either on the axis of the jet or on an axis inclined to the jet. In the latter case the jet appears asymmetric. This effect is diminished by combustion.

It is worth noting that the asymmetry observed in the furnaces at low degrees of swirl was indeed reduced when combustion took place, suggesting that the precessing vortex cores might be contributing to the jet asymmetry.

5. Conclusions

(1) Swirl can bring about significant changes in the flow and combustion patterns of premixed flames in furnaces. If swirl is sufficiently strong, a central recirculation zone (CRZ) is established. The flow conditions under which the CRZ appears in the two furnaces tested, with both

isothermal and burning jets, have been correlated by a swirl number S^* based on the furnace, and not the swirler, diameter. The critical value of S^* for the establishment of the CRZ is 0.11. Wide ranges of S^*, and of flow patterns, can be obtained with the same vane swirler, using different fuel/air ratios. Thus swirler vane angle alone is insufficient to define the flow type.

(2) When a CRZ is well established, its maximum diameter is primarily a function of the furnace diameter (about $0.65D$), and is only slightly altered by further increases in swirl, by combustion or by (D/d) ratio change. The CRZ length also is proportional to the furnace diameter but is somewhat reduced by combustion.

(3) For flows with a well-established CRZ, the spread of the jet up to the impingement point is a function of the swirler vane angle. Combustion and (D/d) ratio have little effect. This spread is not correlated by the swirl number S^*.

(4) The presence of a central hub in the swirler, of diameter 0.33 of the swirler outer diameter, had little effect on the flow and combustion patterns.

6. Acknowledgments

The authors wish to thank Prof R S Silver, and colleagues on his staff, for their encouragement and advice. They also wish to thank the Science Research Council for financial support.

7. References

1. MATHUR M L and MACCALLUM N R L. Swirling air jets issuing from vane swirlers. Part 1: Free jets. Part 2: Enclosed jets. *J Inst Fuel*, 1967 (May, June), **40**, 214–224 and 238–245.
2. HIETT G F and POWELL G E. Three-dimensional probe for investigation of flow patterns. *Engineer, Lond*, 1962, **213**, 165–170.
3. MILLER D R and COMINGS E W. Static pressure distribution in the free turbulent jet. *J Fluid Mechanics*, 1957–58, **3**, 1–16.
4. BELTAGUI S A and MACCALLUM N R L. The modelling of vane-swirled flames in furnaces. *J Inst Fuel*, 1976 (Dec), **49**, 193–200.
5. BELTAGUI S A and MACCALLUM N R L. Aerodynamics of swirling flames—vane-generated type. Combustion Institute, First European Symposium, Sheffield, 1973.
6. BELTAGUI S A and MACCALLUM N R L. The aerodynamics and modelling of vane-swirled premixed flames in furnaces. Int Flame Res Foundn Doc no F21/CA/14, 1st Joint Aerodynamics and Heat Transfer Panel Meeting, Toulouse, Nov 1975.
7. BELTAGUI S A. Aerodynamics and modelling of vane-swirled flames in furnaces. PhD Thesis, Glasgow University, May 1974.
8. BAFUWA G G and MACCALLUM N R L. Turbulent swirling flames issuing from vane swirlers. Int Flame Res Foundn Doc no GO2/ca/3, 18th Aerodynamics Panel Meeting, Paris, Sept 1970.
9. BAFUWA G G and MACCALLUM N R L. Flame stabilization in swirling jets. Combustion Institute, First European Symposium, Sheffield, 1973.
10. SYRED N and BEÉR J M. Effect of combustion upon precessing vortex cores generated by swirl combustors. 14th Symposium (Intn) on Combustion, Combustion Institute, Pittsburgh, 1973.

(Paper received 12 May 1975)

Printed in England by Stephen Austin and Sons Ltd., Hertford.

Reprinted from the JOURNAL OF THE INSTITUTE OF FUEL, *December, 1976.*

S A BELTAGUI BSc PhD* and N R L MACCALLUM BSc PhD†

The modelling of vane-swirled flames in furnaces

Comparisons are made of the fluxes of tangential and axial momentum in burning and isothermal jets issuing from vane swirlers into two furnace sizes. These and other experimental results indicate limitations on the use of the previously adopted swirl number. A new swirl number S^* is suggested which is based on the experimentally measured momentum fluxes and on the furnace diameter D. This swirl number is valuable in classifying the flow patterns, correlating combustion effects and relative furnace size. When vane swirlers which are similar to those reported are to be used, their performance, in respect of flow type, velocity profiles, mixing and jet spread, can be predicted with reasonable accuracy from the correlations provided. When other vane swirlers are to be used, suitable model tests are suggested

1. Nomenclature

d diameter of hubless swirler; equivalent diameter of annular swirler $d_2(1 - z^2)^{\frac{1}{2}}$

d_1, d_2 hub, outer diameters of annular swirler

D diameter of furnace

F_1 factor on pressure drop required for combustion $F_1\Delta p$

F_2 factor on isothermal dynamic axial momentum compared with equation (3)

F_3 ratio of burning tangential momentum flux to isothermal tangential momentum flux

G axial momentum flux

$\dot{m}$ mass flow rate

p pressure

Δp pressure drop required for combustion, assuming one-dimensional flow

r radius

S swirl number defined by $\frac{T}{G_t d}$

S^* swirl number defined by $\frac{T}{G_d D}$

T axial flux of tangential momentum $\int 2\pi r^2 \rho u w dr$

u local axial component of velocity in furnace

U average axial component of velocity leaving swirler, based on cross-sectional area of swirler ignoring vane thickness

w local tangential component of velocity in furnace

$\bar{x}$ axial distance in units of furnace diameter

z hub ratio of annular swirler $\frac{d_1}{d_2}$

ρ density

θ swirler vane angle to axial direction

(*continued on p 194*)

*Formerly British Steel Corporation, Swinden Laboratories, Rotherham; now Department of Mechanical Engineering, Faculty of Engineering, University of Alexandria, Egypt.
†Department of Mechanical Engineering, University of Glasgow.

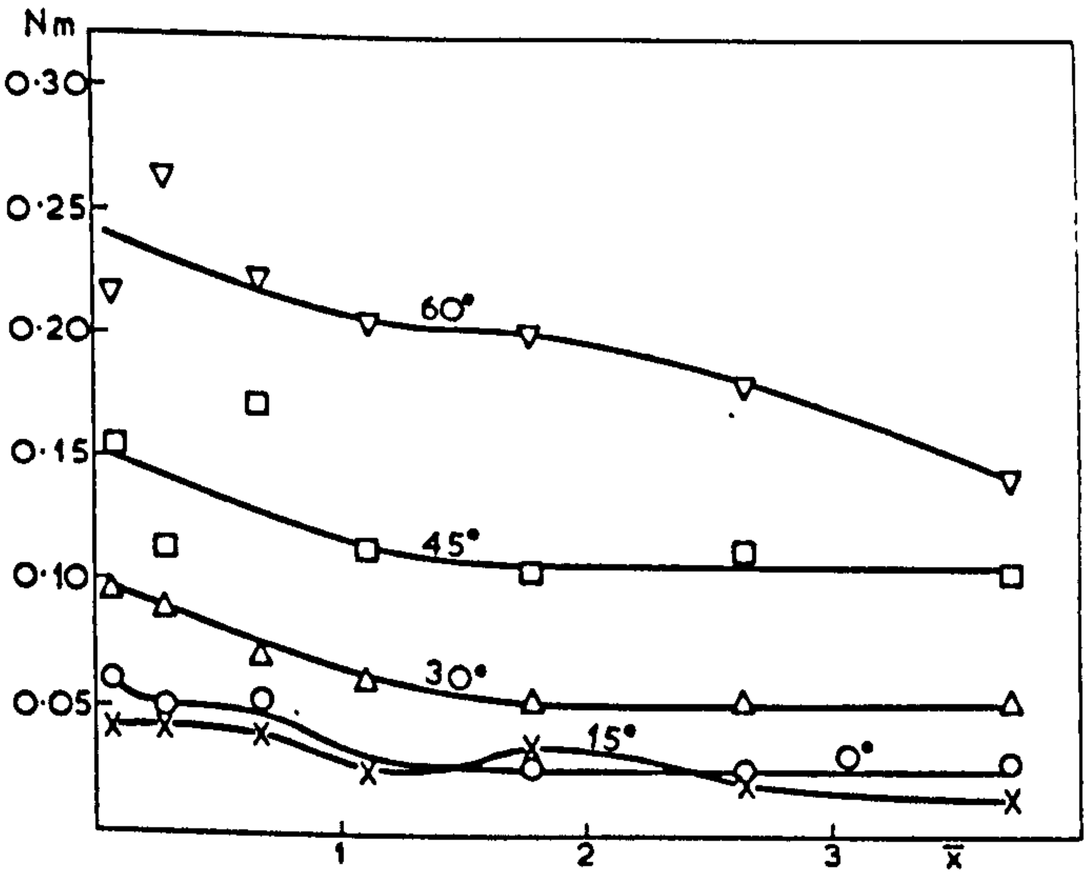

FIG. 1 Axial flux of tangential momenta. Hubless swirlers cold flow in D/d = *2.5 furnace*

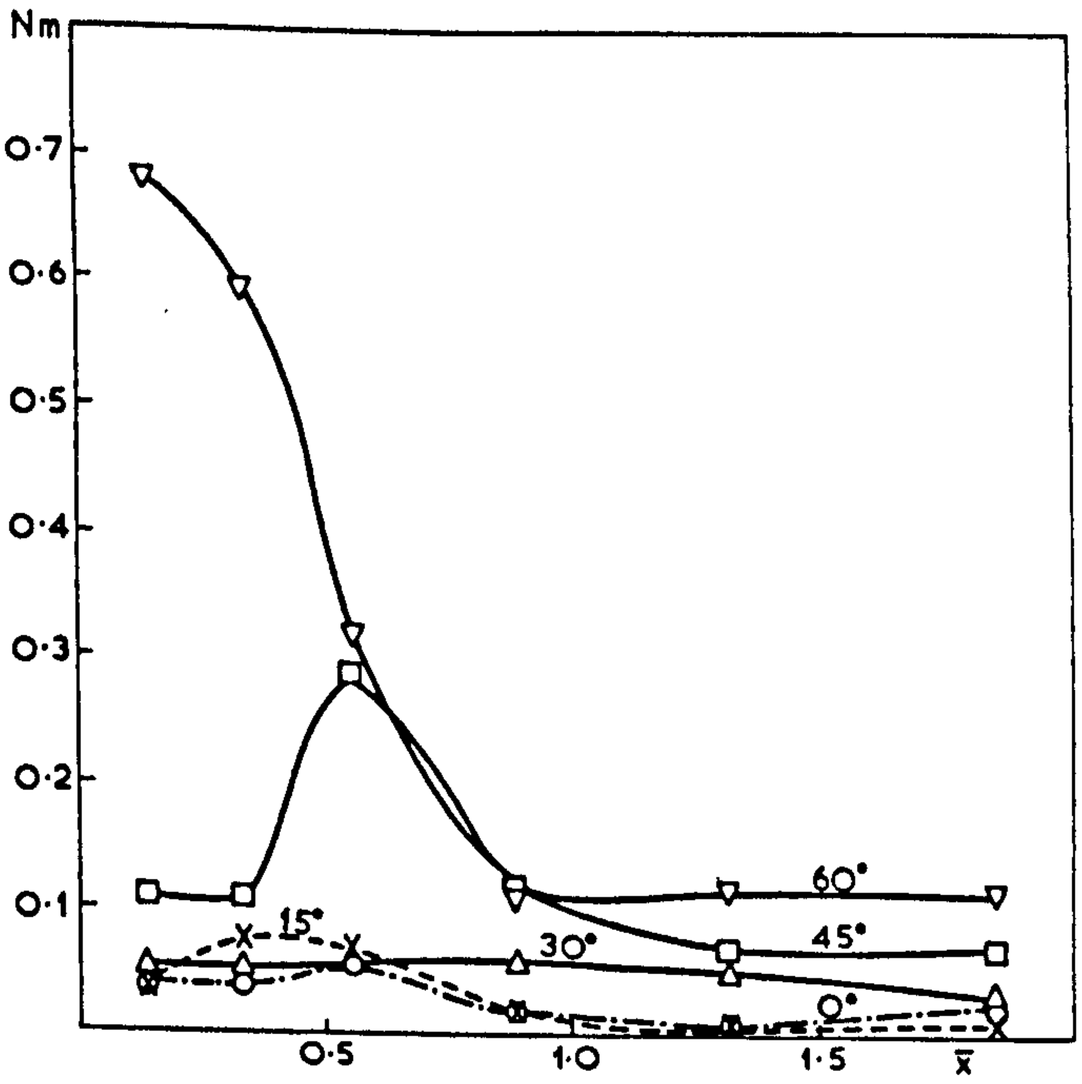

FIG. 2 Axial flux of tangential momenta. Hubless swirlers cold flow in D/d = *5.0 furnace*

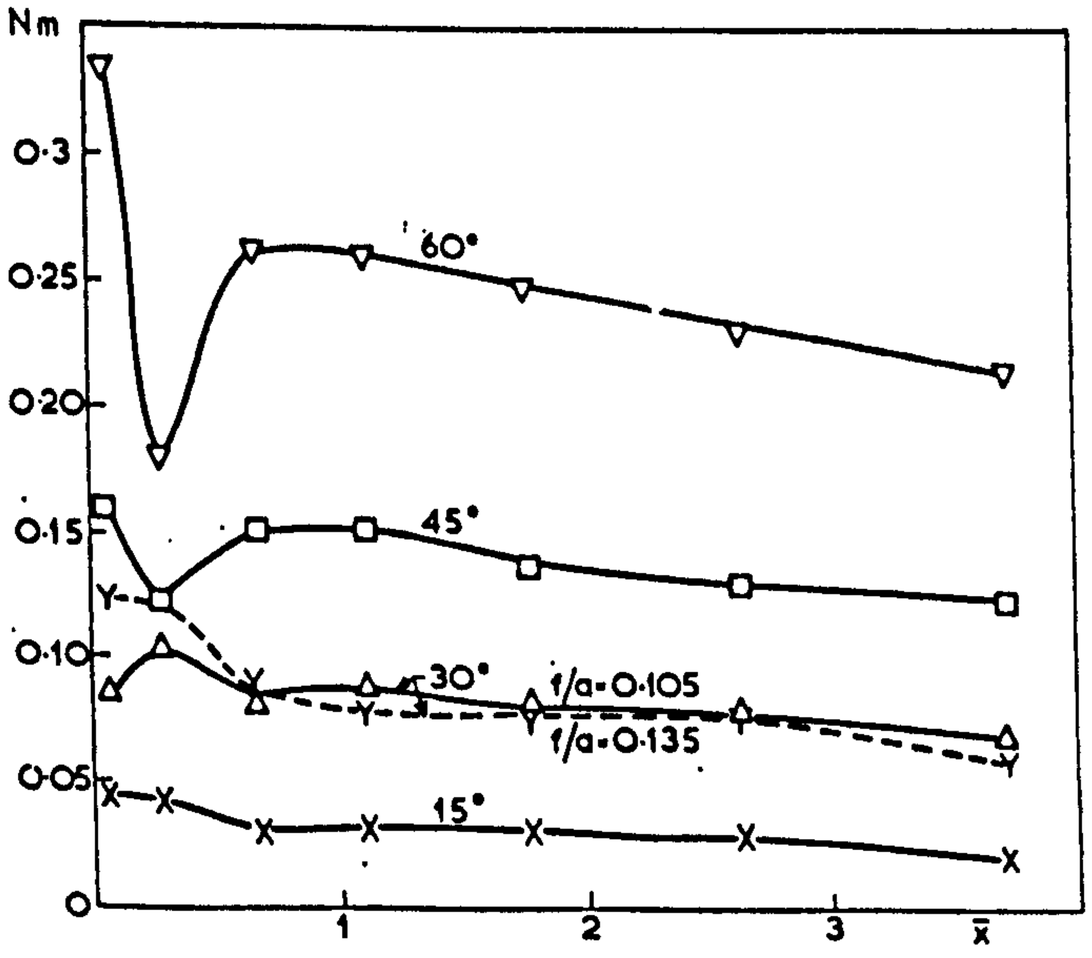

FIG. 3 Axial flux of tangential momenta. Hubless swirler flames in D/d = *2.5 furnace*

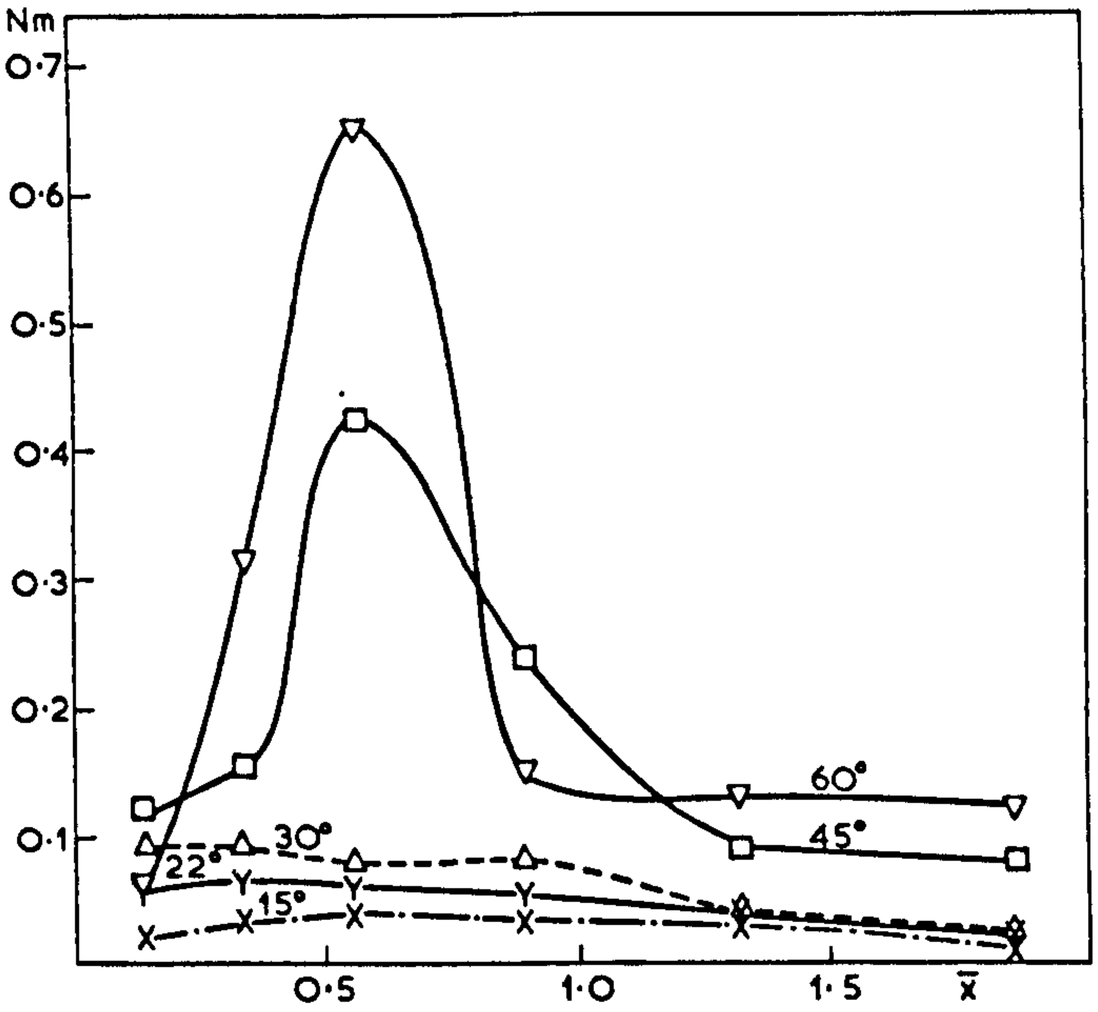

FIG. 4 Axial flux of tangential momenta. Hubless swirler flames in D/d = *5.0 furnace*

Subscripts

a	ambient
b	burning
d	dynamic
i	isothermal
m	model
p	prototype
ref	reference
rev	reverse
sw	swirler
t	total
u	unburned

2. Introduction

Swirl is frequently used in furnaces to obtain suitable flow patterns. A common method of giving swirl to the flow is by the use of vane swirlers. The aerodynamic behaviour of jets issuing from vane swirlers has been studied at Glasgow University under a range of conditions: isothermal jets, open[1,2] and enclosed [3,4,5] and premixed burning jets, open [6,7] and enclosed.[4,5,8] With the exception of the first tests,[1] all the swirlers were of similar designs.[2] The object of the authors in this paper is to compare the results of these tests and to provide correlations from which subsequent designers will be able to select the swirlers necessary to achieve the flow patterns required, or, where correlations are incomplete, directions for equivalent model testing.

3. Momentum fluxes

A quantitative measure of swirl is required. The accepted measures are based on the fluxes of tangential and axial momentum. It is informative to compare the momentum fluxes which have been obtained by integrating the traverses made in the tests mentioned in section 2.

3.1. Tangential momentum flux

The results of integrations of the traverses[4,5] made in isothermal flows in furnaces having furnace diameter to

burner diameter ratios of 2.5 and 5 are given in Figs. 1 and 2 respectively. In both cases the swirlers were of hubless design. The corresponding results under burning conditions (premixed town gas-air) are given in Figs. 3 and 4 respectively. The fuel/air ratio was 0.125 by volume (stoichiometric 0.24) in the $D/d = 5$ furnace and varied between 0.105 and 0.135 in the $D/d = 2.5$ furnace.

There is some scatter, particularly in the early part of the flow and in the $D/d = 5$ furnace where velocities are lower and more difficult to measure. However, it can be seen that beyond the central recirculation zone (CRZ), which extends to about 1.5 furnace diameters, the momenta become more uniform. The tangential momentum values increase with swirl. It is also to be noted that the tangential momenta are higher in the burning jets. Comparing sections downstream of the CRZ, they are higher by between 20 and 40%.

These values can also be compared with those predicted in the simple analysis of Kerr and Fraser,[1] who assumed a uniform velocity distribution at the swirler exit plane and that all the fluid left at the swirler vane angle. This led to the expression

$$T = \frac{\pi}{12}\rho_u U^2 d^3 \frac{(1 - z^3)}{(1 - z^2)^{\frac{1}{2}}} \tan\theta \quad . \quad . \quad . \quad (1)$$

for the tangential momentum flux. All the observed tangential momentum fluxes are higher than those predicted by equation (1). The ratios of observed to predicted fluxes are approximately 2.2 and 1.7 for the isothermal jets in the $D/d = 2.5$ and 5 furnaces respectively, and 3.0 and 2.0 respectively for the corresponding burning jets. Corresponding ratios for isothermal[2] and burning[7] free jets are 2.0 and 3.2 respectively. The only explanation that can be offered for the observed values being above those predicted is that the velocity distribution leaving the swirler is not uniform, and there is a higher axial component of velocity at the larger swirler radii, and consequently a larger tangential momentum is imparted. This effect is more marked when the ratio (D/d) is reduced, and when combustion is taking place. The observed fluxes, for a given furnace and isothermal/combustion state, are proportional to tan θ, as predicted by equation (1).

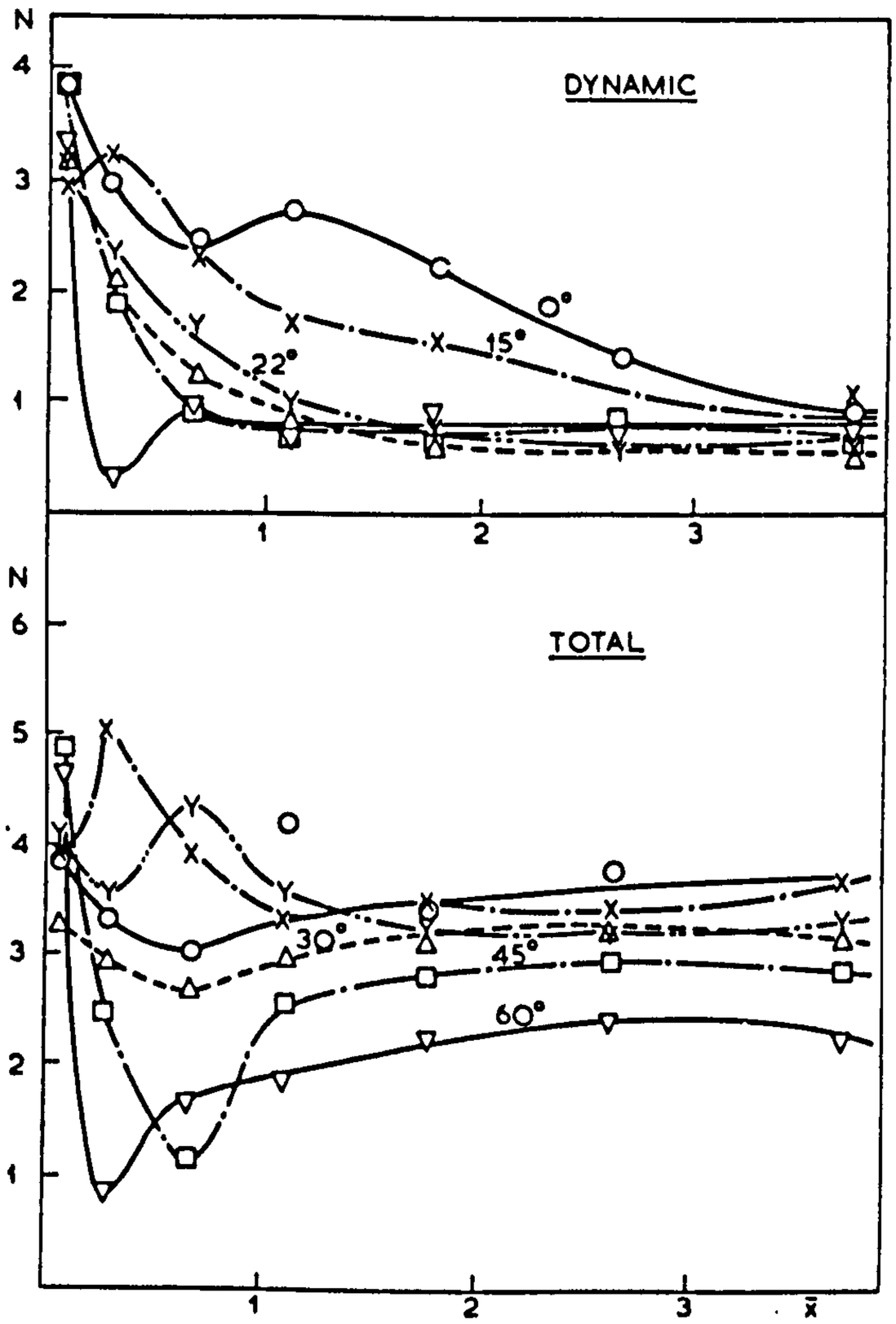

FIG. 5 Axial momentum fluxes. Hubless swirlers cold flow in D/d = *2.5 furnace*

3.2. Axial momentum flux

The total axial momentum flux across a plane is given by

$$G_t = 2\pi \int_0^{D/2} [\rho u^2 + (p - p_{ref})]\, r\, dr \quad . \quad . \quad (2)$$

The flux contains two terms: the dynamic term and the static pressure term. The dynamic term G_d is obtained readily by integration of the group (ρu^2). To evaluate the static pressure term, a reference pressure p_{ref} must be selected. The following alternatives for p_{ref} have been considered:

(*a*) The atmospheric pressure outside the furnace. An objection to this is that the general static pressure level within the furnace varies with the flow and with the chimney suction.

(*b*) The wall static pressure at the exit section of the furnace. This again was variable and affected by the flow currents at this section.

(*c*) The static pressure at the centre of the peripheral, or external, recirculation zone (PRZ) for each case. An objection is that this value is affected by swirl since the tangential velocities do not vanish in the PRZ. Also the value is influenced by the jet spread rate.

(*d*) The static pressure at the centre of the PRZ for the non-swirled cold flow in the furnace under test. This reference pressure has been selected as it avoids the objections mentioned in (*c*). Consequently the net value of the static pressure term in the axial momentum flux will show the effects of swirl and of combustion in the same confinement.

The axial momentum fluxes are given in Figs. 5–8, these results corresponding to the tangential momentum fluxes shown in Figs. 1–4. For the axial momenta, the dynamic term is plotted in the upper part, and the total momentum (p_{ref} as in (*d*) above) in the lower part of each figure. In each case, after fluctuating values in the early part of the flow, the total momentum flux steadies and is conserved. The dynamic term decays to a value which becomes more constant at axial distances greater than about 1.5D.

Comparing the values which obtain after the initial variations, the dynamic term becomes smaller as swirl increases, and also decreases as the diameter ratio (D/d) is increased. When combustion is taking place the dynamic term is about four times as great as for the isothermal flow. In the $D/d = 2.5$ furnace the total momentum fluxes are lowered by increasing the swirl, the negative component due to the pressure depression at

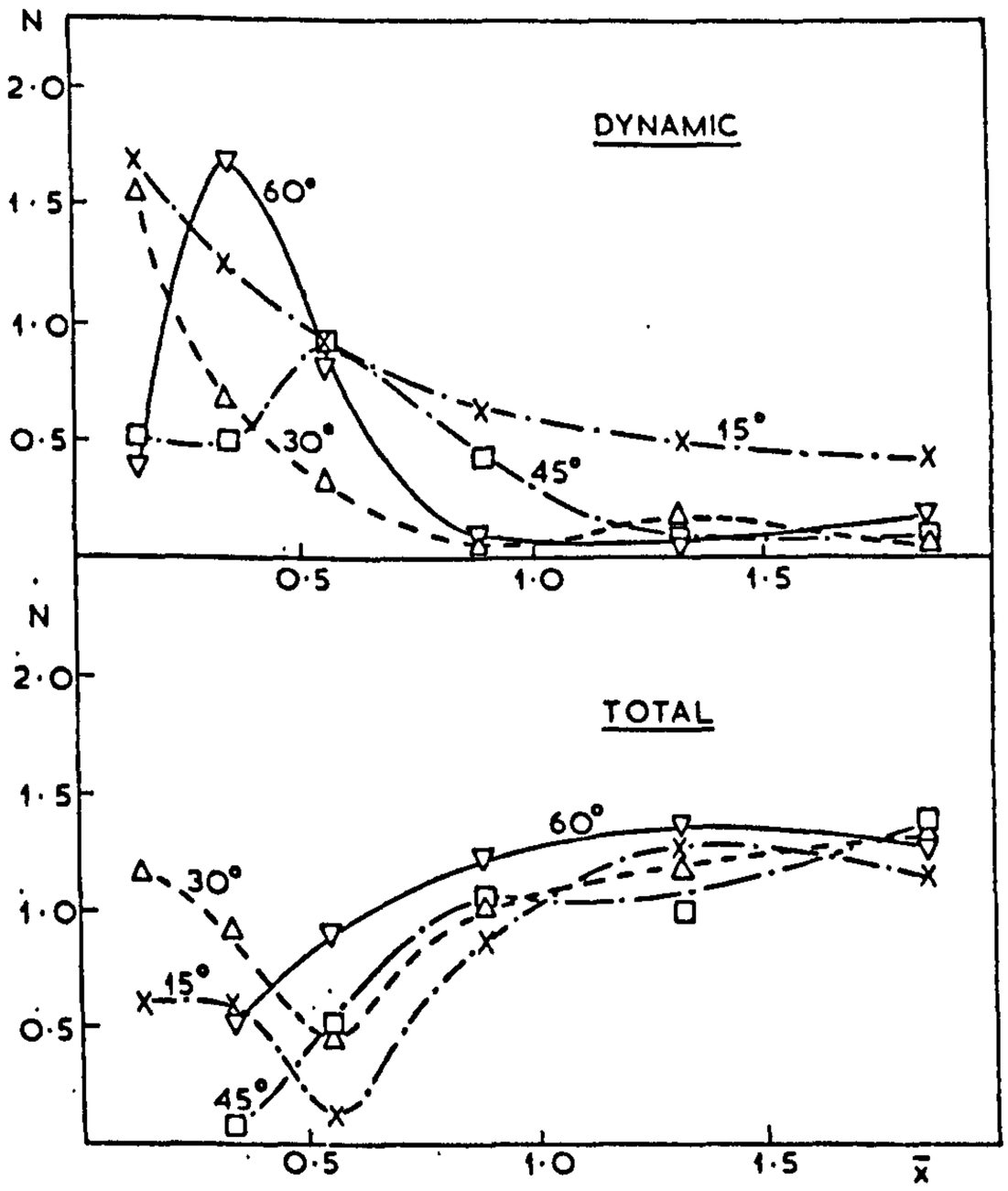

FIG. 6 Axial momentum fluxes. Hubless swirlers cold flow in D/d = *5.0 furnace*

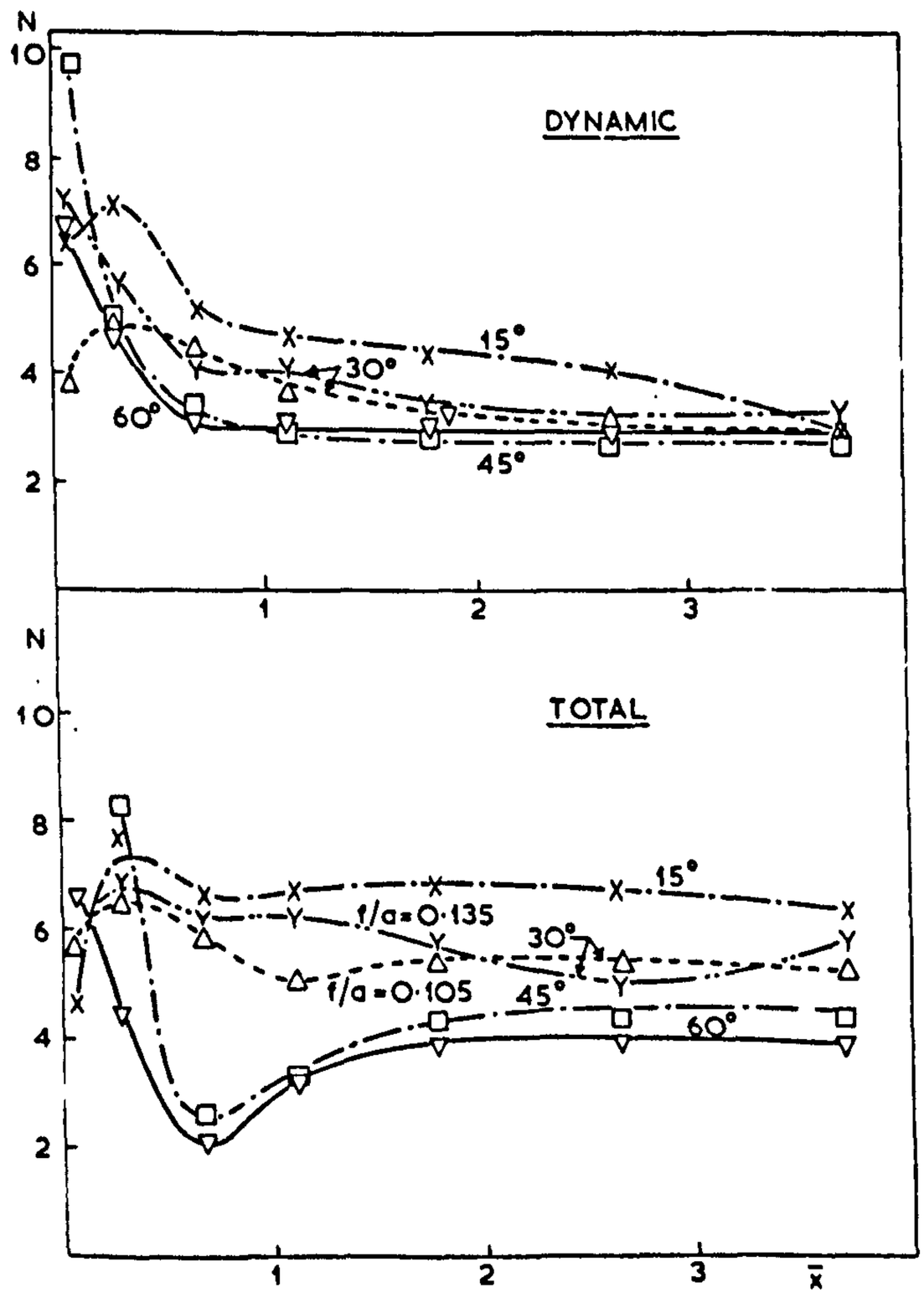

FIG. 7 Axial momentum fluxes. Hubless swirler flames in D/d = *2.5 furnace*

the centre of the jet having an increasing effect. In the $D/d = 5$ furnace the total axial momentum flux is almost

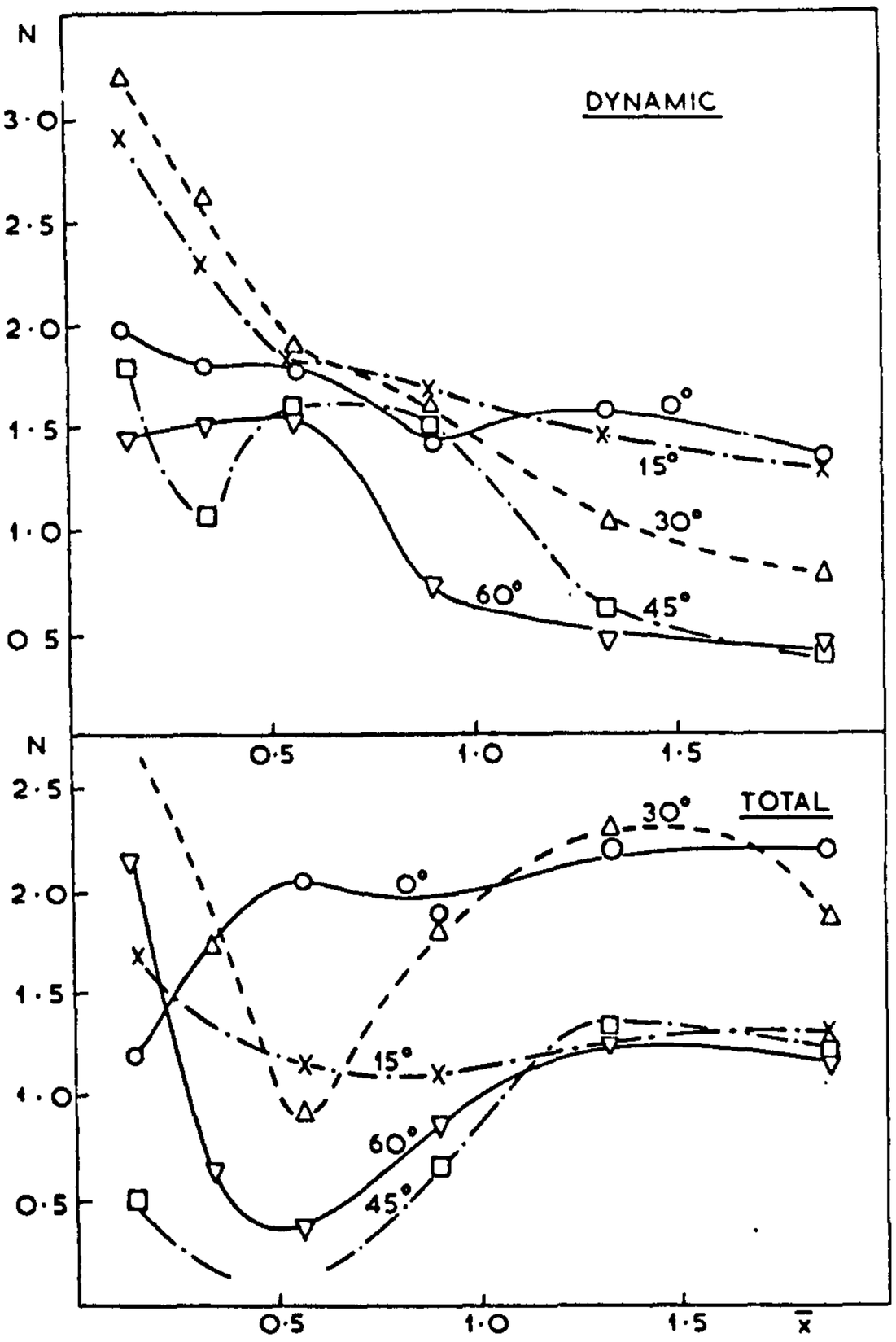

FIG. 8 Axial momentum fluxes. Hubless swirler flames in D/d = *5.0 furnace*

independent of swirl in the isothermal flow but apparently varies when combustion occurs. Part of this inconsistency may be due to experimental error in determining these fluxes in a highly turbulent stream moving at comparatively low velocity (in the $D/d = 5$ furnace).

Again, it is instructive to compare the observed axial momentum fluxes with those predicted from Kerr and Fraser's[1] expression

$$G = \frac{\pi}{4} d^2 \rho_u U^2 \quad . \quad . \quad . \quad . \quad . \quad (3)$$

Kerr and Fraser did not mention the pressure term when writing the above expression, but by assuming the pressure is uniform across the swirler exit and equal to the reference pressure, the expression can be interpreted as meaning the total axial momentum flux.

The ratios of the measured total axial momentum fluxes (p_{ref} as in (d) above) in the developed flows to that given by equation (3) are, when averaged, 2.1 and 0.85 for the isothermal jets in the $D/d = 2.5$ and 5 furnaces respectively, and 3.5 and 1.1 respectively for the corresponding burning jets. It is difficult to explain how the observed total momentum fluxes in the isothermal cases can exceed the prediction of equation (3), other than to point out that these fluxes were determined using an arbitrary assumption for the reference pressure. Equation (3) contains only a dynamic term, and it has been helpful to compare the observed dynamic contributions to the axial momentum flux with equation (3). The

resulting ratios are 0.51 and 0.16 for the isothermal jets in the $D/d = 2.5$ and 5 furnaces respectively, and 2.2 and 0.6 for the corresponding burning jets. The reason of course for the dynamic terms being lower in the larger furnace is that the jet has a greater expansion, and hence lower axial velocities, in the larger furnace.

4. Swirl number

4.1. Previous definitions

A widely accepted definition has been[9]

$$S = \frac{T}{G_t d} \quad . \quad . \quad . \quad . \quad . \quad . \quad . \quad (4)$$

where the linear dimension is the diameter d of the swirler.

Kerr and Fraser,[1] using equations (1) and (3) and the associated assumptions (section 3), obtained

$$S = \tfrac{1}{3} \frac{(1 - z^3)}{(1 - z^2)^{\frac{1}{2}}} \tan \theta \quad . \quad . \quad . \quad . \quad (5)$$

However, the following considerations must be taken into account.

(1) The velocity profiles and pressure distribution at the swirler exit are not uniform.

(2) The increase in the axial momentum flux, observed above, as the result of the higher static pressure required when combustion occurs, was not considered in equation (3). Differences in the velocity profiles can also be observed when combustion occurs.

(3) The same swirler can give different velocity profiles as the confinement is changed.

Because of factors (2) and (3) the tangential momentum flux is changed both by combustion and confinement, as described in section 3.1.

(4) The dimensions of the CRZ, when established by the swirl, are primarily functions of the furnace diameter D rather than of the swirler diameter d.

4.2. New measure of swirl: swirl number S^*

In this new definition of a swirl number, the furnace diameter D is adopted as the linear measure appearing in the denominator. This follows from the suggestion first made by Kerr[10] for the similarity of swirling flows in furnaces. The suggestion is supported by some of the points listed above, particularly (3) and (4). For the fluxes T and G, which appear in the swirl number, the experimentally measured fluxes in the developed flows, described in section 3, are used. The choice of axial momentum flux presents some problems, partly owing to the choice of reference pressure from which the static pressure term can be calculated. It has been found that the most useful choice has been to omit the static pressure term and base the axial momentum flux solely on the dynamic term. Thus the definition of the new swirl number is

$$S^* = \frac{T}{G_d D} \quad . \quad . \quad . \quad . \quad . \quad . \quad (6)$$

The above pairing of interpretations of axial momentum flux and of diameter is the only one which has correlated the transitions of flow types.

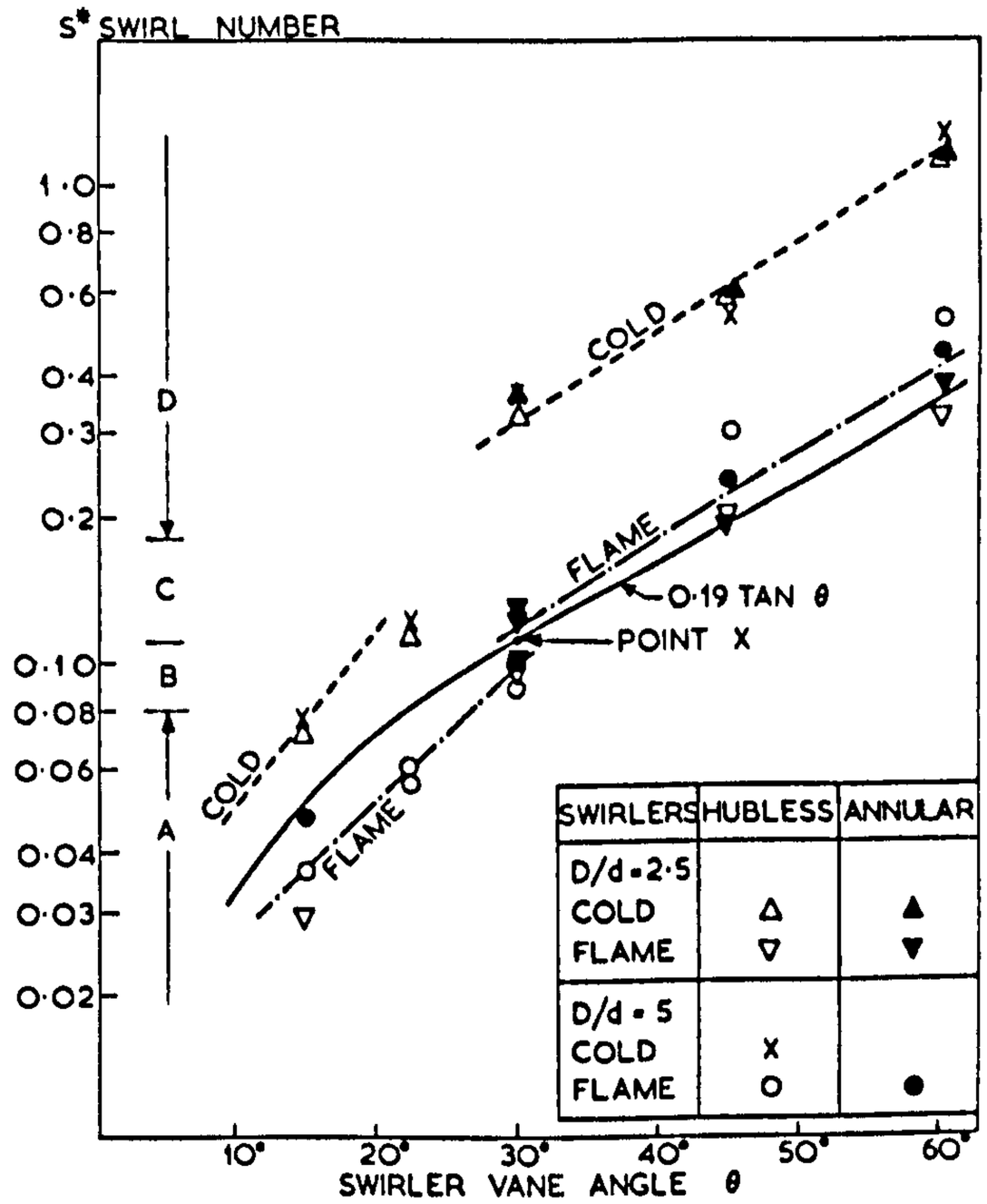

FIG. 9 Swirl number relation to input conditions and flow types

5. Modelling for flow patterns—use of S^*

The swirling flow results discussed in this paper have been divided into four classifications.[5] A type A flow had axial velocity profiles very similar to those of an unswirled jet. A flow in which there was a well-established CRZ was classified as type D. The intermediate flow conditions were described as types C or B depending on whether there was a flow reversal on the axis, or not. It is found that for the tests reported above, transition from one flow type to the next occurs at the same value of S^*, irrespective of the furnace/swirler diameter ratio D/d and irrespective of whether the jet is burning or isothermal. The transitions from types A to B, from B to C and from C to D occur at values of S^* of 0.08, 0.11 and 0.18 respectively. A further important feature is that for the same swirler, in say isothermal flow, the S^* values are very similar for the two values of the ratio D/d (ie 2.5 and 5). A similar result is obtained for the burning flows having the same fuel/air ratio. The only slight apparent departure from this is at vane angles close to that giving the critical S^* value of 0.11. Under these conditions the lower value of the D/d ratio tends to give the higher value of S^* and a greater tendency towards a CRZ. The results are illustrated in Fig. 9.

It is noted that there is a change in the slopes of both isothermal and burning correlations at a vane angle of about 30°. In the burning case this corresponds with the establishment of central reverse flows.

The displacement of the correlation for the burning jets from the isothermal correlation is a function of the fuel/air ratio. This relation is discussed in section 6.

It is found that the velocity profiles in the furnaces downstream from the maximum width of the CRZ (ie at axial distances greater than $1D$) are similar at the same values of S^*, profiles being compared at similar values of the ratio of axial distance to furnace diameter. Thus this

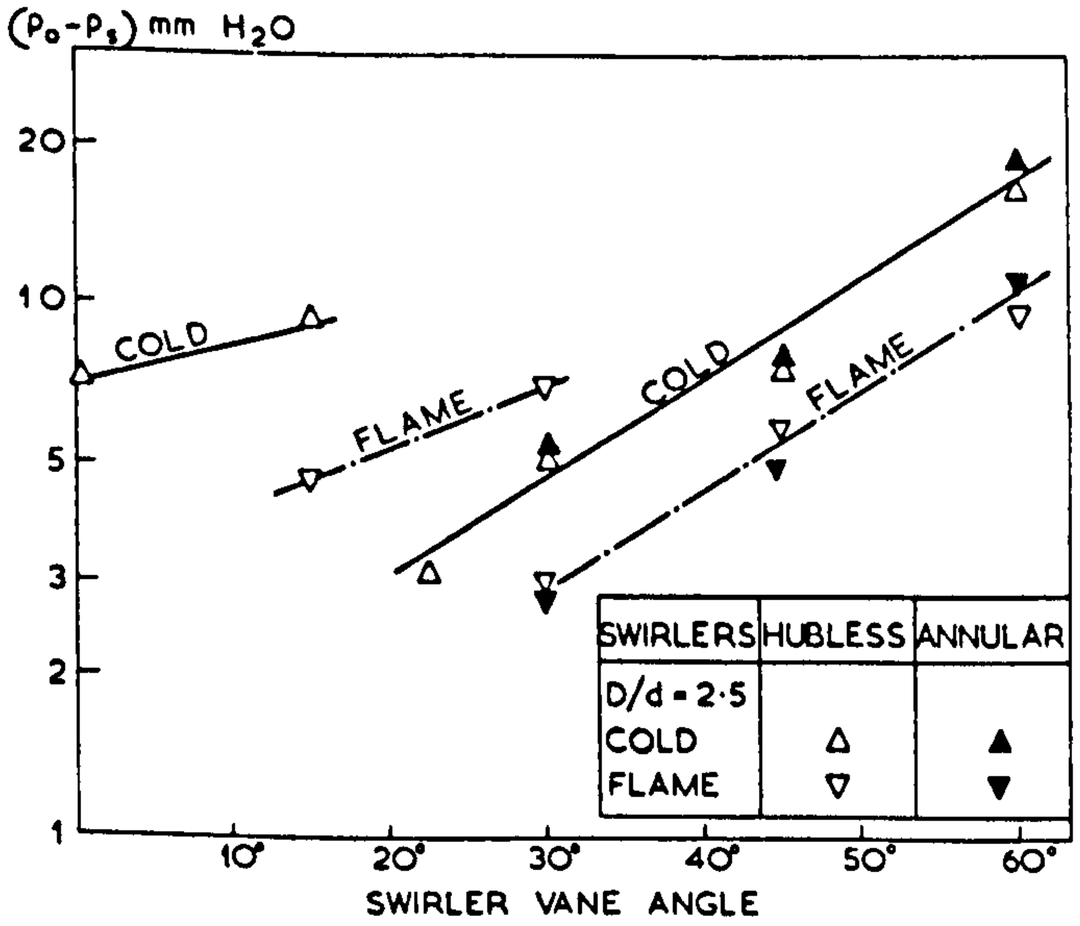

FIG. 10 Variation of the minimum static pressure at the centre line with swirler vane angle

swirl number can be used as a modelling parameter both for the prediction of the type of CRZ and for the flow pattern which develops beyond its maximum width.

6. Prediction of swirl number S^*

The relations between S^* and swirler vane angle shown in Fig. 9 depend on extensive experimental measurements. It would be very desirable if these relations could be predicted. This has not yet been found possible, although it is helpful to note that S^* is very nearly proportional to $\tan\theta$, particularly for type D flows, as shown in Fig. 9. A method is given below whereby once the isothermal correlation is established, the correlation for the burning condition can be predicted.

Assuming one-dimensional flow within the furnace, the pressure drop required for the density change is given by

$$\Delta p = \rho_u U^2 \left(\frac{d}{D}\right)^4 \left(\left(\frac{\rho_u}{\rho_b}\right) - 1\right) \quad . \quad . \quad . \quad (7)$$

As the actual flow is not one-dimensional, the actual pressure drop will be a factor F_1 times Δp. When combustion occurs let us assume that the dynamic component of the axial momentum flux is raised because this pressure change ($F_1 \Delta p$) acts across the front face of the furnace cross-section. Assuming, further, that the isothermal dynamic axial momentum flux is a fraction F_2 of that given by equation (3), the dynamic axial momentum flux in the burning case is given by

$$G_{ab} = F_2 \frac{\pi}{4} d^2 \rho_u U^2 + F_1 \frac{\pi}{4} D^2 \rho_u U^2 \left(\frac{d}{D}\right)^4 \left(\frac{\rho_u}{\rho_b} - 1\right) \quad (8)$$

The ratio of the dynamic axial momentum fluxes in the burning and isothermal cases is given by

$$\frac{G_{ab}}{G_{is}} = \frac{F_2 + F_1 \left(\frac{d}{D}\right)^2 \left(\frac{\rho_u}{\rho_b} - 1\right)}{F_2} \quad . \quad . \quad . \quad (9)$$

The tangential momentum fluxes are slightly increased by combustion, as seen in section 3.1. Letting the ratio of these fluxes, burning to isothermal be factor F_3, then the swirl number ratio, for a particular swirler, becomes

$$\frac{S_b^*}{S_i^*} = \frac{F_2 F_3}{F_2 + F_1 \left(\frac{d}{D}\right)^2 \left(\frac{\rho_u}{\rho_b} - 1\right)} \quad . \quad . \quad . \quad (10)$$

The factor F_3 is almost independent of the (D/d) ratio. Its values are 1.4 and 1.2 for the (D/d) values of 2.5 and 5 respectively. It is reasonable to adopt a mean value of 1.3 within this range of relative furnace sizes. The factor F_2 is markedly influenced by the ratio (D/d) and has values of 0.51 and 0.16 for the (D/d) values of 2.5 and 5 respectively (section 3.2). Using these values for F_2 and value 1.3 for F_3, it is found that an F_1 value of 2.1 fits both sets of furnace results reported here. The present results have been obtained with premixed gas-air flames. With other forms of firing, factors F_1 and F_3 may be altered. The changes in F_3 will probably be small enough to be ignored. Factor F_1 may be reduced if combustion is slower, but presumably will not drop below unity.

For design purposes, when using vane swirlers similar those tested here, it is suggested that the isothermal correlation for $S^* - \theta$ given in Fig. 9 be used, and modified when combustion occurs by equation (10).

For other designs of vane swirlers, the isothermal S^*—vane angle correlation can be established from integrations of velocity traverses in a model. The swirler diameter in the model can have any value provided the (D/d) ratios in the prototype and model lie in the range reported here (2.5 to 5). An alternative method of establishing the burning relationship is to make use of the discontinuity at the flow transition from type B to C that occurs in the variation of minimum static pressure on the axis with vane angle. These correlations for the burning and isothermal flows in the $D/d = 2.5$ furnace are shown in Fig. 10. As mentioned earlier, this transition point for the burning case approximately represents the lower swirl limit of the portion of the $S^* - \theta$ correlation which is proportional to $\tan\theta$. Thus the vane angle corresponding to type B to C transition at that fuel/air ratio can be established from burning model tests (D/d ratio in the present range). This angle corresponds to the value of 0.11 for S^*, locating the equivalent of point X on Fig. 9. The position of the correlation for burning type D flows at that fuel/air ratio can be estimated using the proportionality with $\tan\theta$. The corresponding isothermal correlation can be drawn using equation (10).

7. Modelling for mixing

Where the intended prototype is to have a central recirculating flow, it is suggested that a good measure of the equivalence of the flows in the isothermal model and in the prototype is given by the respective ratios of the maximum reverse mass flows in the CRZ to the swirler mass flow. Ideally these ratios should be equal.

This mass flow ratio has been determined for the results discussed here and is plotted in Fig. 11 against the swirl number S^*, and in Fig. 12 against the vane angle. Before discussing these results, the difficulty of measuring the reverse mass flow rates must be emphasized, particularly for the $D/d = 5$ furnace where the average velocities are lower. Referring to Fig. 11, it is seen that for the $D/d = 2.5$ furnace, S^* correlates the burning and isothermal maximum reverse mass flow ratios. The correlation is not valid in the $D/d = 5$

furnace. However it would appear that this correlation can usefully be used in the range for D/d values of, say, 2.5 to 3.5. Comparison of the maximum reverse mass flow ratios with the swirler vane angle θ (Fig. 12) shows that, at a given value of θ, the reverse mass flow ratios, burning, in the $D/d = 5$ furnace are similar to those in isothermal flow in the $D/d = 2.5$ furnace. The $D/d = 2.5$ furnace in isothermal flow represents the isothermal model, scaled according to Thring-Newby,[11] of the burning flow in the $D/d = 5$ furnace. Thus a second method of achieving equivalent mixing is to use an isothermal model in which the swirler diameter is scaled according to Thring-Newby and to use the same vane angle.

8. Modelling for jet spread

The jet spread results from these tests have been discussed in reference 5. The principal conclusion reported there was that, for flows with central recirculation (ie types C and D) the jet spread is a function only of the swirler vane angle.

9. Use for design

If vane swirlers are selected which are similar to those used in the work reported here, then the information provided here and in reference 5 should provide satisfactory predictions of the jet spread, of the flow type, of the velocity profiles and of the maximum reverse mass flows in the CRZ (if present).

If another design of vane swirler is used, an isothermal model will give helpful predictions of the behaviour in the prototype, although not all features can be found from a single model. For example, where the prototype flow is to be of type D, the relationship between S^* and vane angle (or equivalent measure) for the burning conditions must first be estimated as outlined in section 6. A suitable prototype vane angle can then be selected. If then it is required to predict the impingement point and mixing patterns, these can be found using an isothermal model having the same swirler vane angle as in the prototype and with the swirler diameter scaled according to Thring-Newby

$$\frac{(d/D)_m}{(d/D)_p} = \left(\frac{\rho_u}{\rho_b}\right)^{\frac{1}{4}} \quad . \quad . \quad . \quad . \quad . \quad (11)$$

The swirl number S^* in the model will be higher than in the prototype by a factor depending on the furnace fuel/air ratio (eg a factor of about 3 in the present work); consequently the velocity profiles downstream from the maximum CRZ width will not correspond.

Should it be necessary to predict the velocity profiles in this downstream region, the vane angle should be reduced in the model until the values of S^* in model and prototype are equal (see section 6). If the (D/d) ratios in the model and prototype are the same and in the approximate range 2.5–3.5, then the model test will give the CRZ mixing in addition to the downstream velocity profiles.

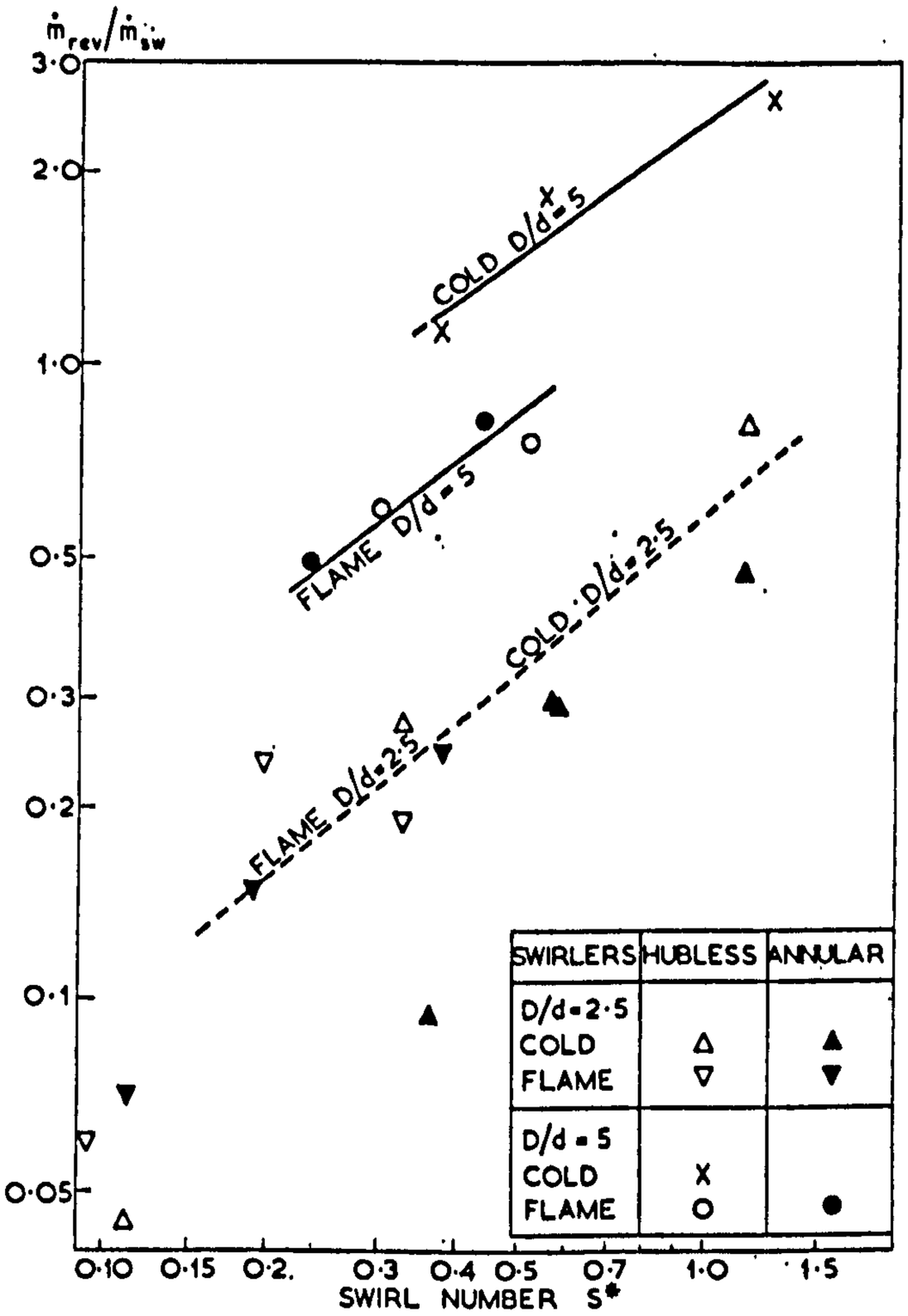

*FIG. 11 Maximum reverse mass flow in CRZ; variation with swirl number S**

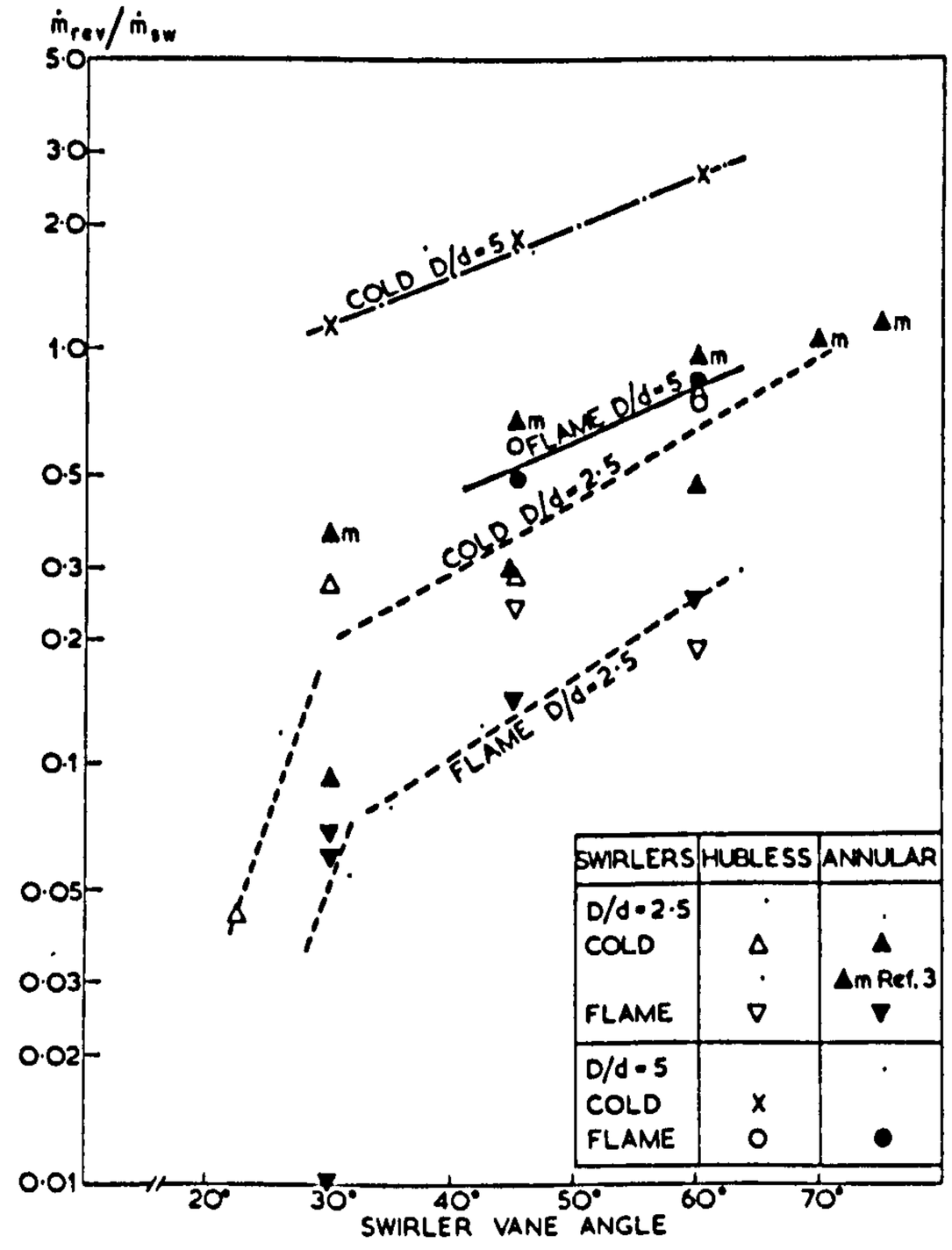

FIG. 12 Maximum reverse mass flow in CRZ; variation with swirler vane angle

10. Acknowledgments

The authors wish to thank Prof R S Silver, and colleagues on his staff, for their encouragement and advice. They

also wish to thank the Science Research Council for financial support.

11. References

1. KERR N M and FRASER D. Swirl. Part I: Effect on axisymmetrical turbulent jets. *J Inst Fuel*, 1965 (Dec), 38, 519–526.
2. MATHUR M L and MACCALLUM N R L. Swirling air jets issuing from vane swirlers. Part 1: Free jets. *J Inst Fuel*, 1967 (May), 40, 214–225.
3. MATHUR M L and MACCALLUM N R L. Swirling air jets issuing from vane swirlers. Part 2: Enclosed jets. *J Inst Fuel*, 1967 (June), 40, 238–245.
4. BELTAGUI S A. Aerodynamics and modelling of vane-swirled flames in furnaces. PhD Thesis, Glasgow University, May 1974.
5. BELTAGUI S A and MACCALLUM N R L. Aerodynamics of vane-swirled flames in furnaces. *J Inst Fuel*, 1976 (Dec), 49, 183–193.
6. BAFUWA G G. Characteristics of swirling flames issuing from vane swirlers. PhD Thesis, Glasgow University, Aug 1970.
7. BAFUWA G G and MACCALLUM N R L. Turbulent swirling flames issuing from vane swirlers. Int Flame Res Found Doc no GO2/ca/3, 18th Aerodyn Pan Mtg, Paris, Sept 1970.
8. BELTAGUI S A and MACCALLUM N R L. Aerodynamics of swirling flames—vane generated type. Combustion Institute, First European Symposium, Sheffield, 1973.
9. BEÉR J M and CHIGIER N A. Combustion aerodynamics. Applied Science Publishers, London, 1972.
10. KERR N M. Swirl. Part II: Effect on flame performance and the modelling of swirling flames. *J Inst Fuel*, 1965 (Dec), 38, 527–538.
11. THRING M W and NEWBY M P. Combustion length of enclosed turbulent jet flames. Fourth Symposium (Inter) on Combustion, Williams and Wilkins, Baltimore, 1953, 789–796.

(Paper received 12 May 1976)

Printed in England by Stephen Austin and Sons Ltd., Hertford.

LAND SEA AIR SPACE

SOCIETY OF AUTOMOTIVE ENGINEERS, INC.
400 Commonwealth Drive, Warrendale, Pa. 15096

The Effect of Boundary Layer Changes Due to Transient Heat Transfer on the Performance of an Axial-Flow Air Compressor

N. R. L. Maccallum
Dept. of Mechanical Engrg., Univ. of Glasglow (Scotland)
A. D. Grant
Dept. of Mechanical Engrg., Univ. of Strathclyde (Scotland)

Society of Automotive Engineers

International Automotive Engineering
Congress and Exposition
Cobo Hall, Detroit
February 28 - March 4, 1977

770284

770284

The Effect of Boundary Layer Changes Due to Transient Heat Transfer on the Performance of an Axial-Flow Air Compressor

N. R. L. Maccallum
Dept. of Mechanical Engrg., Univ. of Glasgow (Scotland)
A. D. Grant
Dept. of Mechanical Engrg., Univ. of Strathclyde (Scotland)

INTRODUCTION

The transient behaviour of aircraft gas turbines is of great interest. Much attention is given to the avoidance of surge in the compressor(s). One particularly taxing transient appears to be a rapid throttling back, followed by an acceleration while the engine is still hot. In one case (1)* the allowable increase in fuel flow without causing surge is only about half of that when the engine is starting from "cold". Four possible causes for this reduction have been suggested (2). One is that at the beginning of such an acceleration, the blades in the compressor(s) are at temperatures higher than that of the air passing over them, the resulting heat transfer possibly causing changes in the growth of the boundary layer. An earlier separation, and a reduction in flow deflection have been noted in both experimental and theoretical studies of flow over a hot convex surface (3).

In the present work, the results of this investigation on single surfaces are incorporated in an exploratory method for predicting the characteristics of a multi-stage axial-flow compressor. The method is illustrated by applying it to the conditions in a compressor at the end of a rapid deceleration at 12,200 m altitude (40,000 ft) from maximum speed to flight idle speed, prior to a possible acceleration. The compressor selected is the 12-stage High Pressure (H. P.) compressor of a typical twin-spool axial-flow bypass engine of compression ratio 20.

Surge in an axial-flow compressor, such as considered here, is influenced by three-dimensional effects. Ideally, some form of prediction method

* Numbers in parentheses designate References at end of paper.

ABSTRACT

During transient operation of a gas turbine there are significant heat transfers between the fluid stream and the blades of the compressor and turbine. At the end of a rapid deceleration from maximum speed to idling speed, heat transfer to the compressor blade boundary layers may cause sufficient disturbance to delay any immediate re-acceleration. As a first estimate in one severe case - at altitude in an aircraft engine of compression ratio 20 - the surge margin prior to the re-acceleration is reduced by about 40% due to boundary layer effects, and by a further 25% due to "bulk" heat transfer.

based on blade-element data, with radial integration, followed by axial stacking, should be used. Such a procedure is very complex, and some of the necessary data are as yet incomplete. In the present exploratory calculation, it has therefore been decided to simplify the calculations by adopting a two-dimensional procedure based on the mean blade height. The aim of the study is of course to predict the change in the characteristics of the real, three-dimensional compressor due to heat transfer. It is considered that a reasonable first estimate of this effect will be given by the differences between the two sets of characteristics of the compressor, as predicted by the two-dimensional method without, and with heat transfer.

PREDICTION METHOD - ADIABATIC FLOW

The object of the investigation reported in this paper is a prediction of the changes in compressor characteristics brought about by heat transfer. Consequently the aim of the work described in this section was the development of a method of predicting the characteristics, in adiabatic flow, which gives results in reasonable agreement with experiment and which gives a realistic representation of stall and the source of surge. It was not considered necessary that the predictions should be in exact agreement with experiment.

The method developed involves row by row calculations, at the mean blade height, based on two-dimensional cascade data, represented by plots of designed deflection, ϵ^*, versus design exit angle, $\alpha_2{}^*$, and of the ratio ϵ/ϵ^* and of the profile drag coefficient, C_{dp}, versus the group $(i - i^*)/\epsilon^*$. These relationships are taken from Figs. 8 and 9 of Reference (4). The second of these relationships is reproduced to give the adiabatic correlations shown in Fig. 1 of this paper.

In the method developed here, the flow is compressible, Mach Number effects (5) are allowed for and the calculation procedure accounts for variation of axial velocity within the row in so far as it affects the exit velocity triangle and the energy transfer. The effect of axial velocity change on the deviation (6) is not included. In justification of the use of calculations at the mean blade height, this is considered reasonable (4), (7) for hub/tip radius ratios greater than 0.6. In the present work they are in the range 0.61 to 0.91.

DEFINITION OF SURGE LINE - Knowledge ot the position of the surge line is essential for deciding what engine acceleration schedules may be allowed. For the present work it is therefore required that a prediction be made of the onset of surge. One possible approach is to draw the surge line through the peak-pressure-ratio points of the performance map (7). An alternative approach is offered by Gray (8) who indicates that in the surging cycle, stall progresses through all stages.

At high rotational speeds the rear stages of the compressor tend to stall first. This can trigger stall in adjacent stages. The triggering advances rapidly through the machine until all stages are stalled and the compressor surges. Thus one criterion used here is that if a stage at the rear of the compressor stalls, then this represents the onset of surge. The quantitative definition of the stalling of a blade row used here is the same as that for cascades (9), viz. that the profile drag coefficient rises to double its minimum value. This occurs when the numerical value of the group $(i - i^*)/\epsilon^*$ reaches 0.4.

At low rotational speeds, stall first occurs in the early rows of the compressor, rotating stall cells being established. These can exist without causing surge. However, if the exit flow is sufficiently throttled the stall cells spread and surge occurs. On Gray's hypothesis, the stall cell zones must have extended along the length of the compressor.

In the same paper Gray proposes the model that, when the stable rotating stall exists there are two types of flow regime in the annulus. In one section there are the stall zones which have zero net throughflow, and in the other, covering the remainder of the annulus, there is normal unstalled flow. An attempt has been made to incorporate this model in the present production method. However, arbitrary assumptions have had to be made

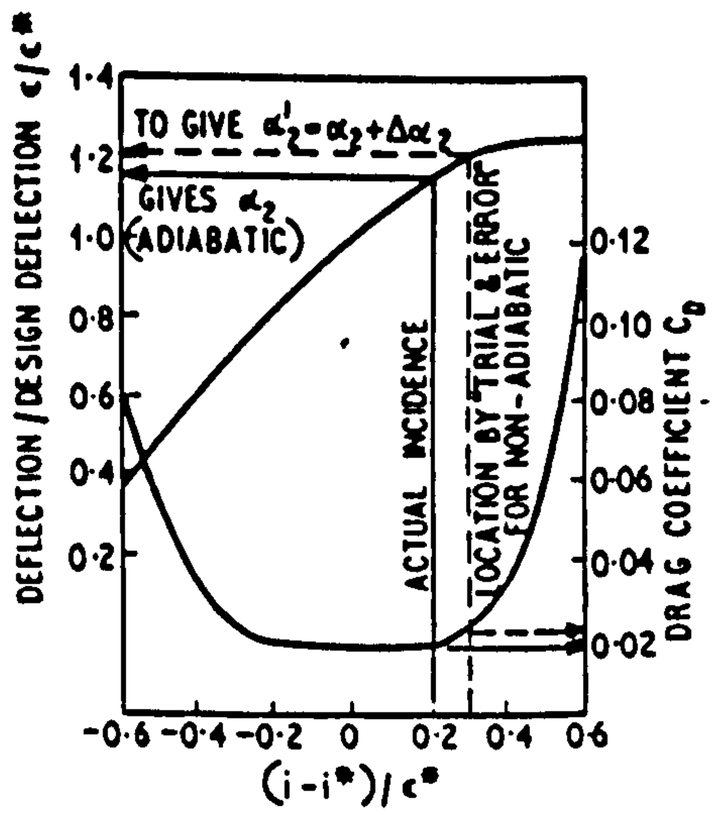

Fig. 1 - Howell and Bonham's correlation (4) for deflection and drag coefficient at other than design incidence in adiabatic flow - and assumed non-adiabatic behaviour

as to the average losses in a row operating under these conditions. Further, it has been assumed that the flow returns immediately to the normal pattern at the first row at which the average value of incidence is insufficient to cause stall. The low speed surge criterion adopted here is that surge occurs when at least three of the early stages have stall zones, the calculation procedure having been based on the above assumption, or when the overall pressure rise - mass flow characteristic has a positive slope, whichever occurs first.

APPLICATION OF METHOD - The method has been applied to the 12-stage H.P. compressor previously mentioned. The data required for the program are the absolute air inlet angle approaching the first row of rotor blades, the blade inlet angles and the design incidences and deflections for all rows of rotor and stator blades. Other geometric parameters of blade height, blade row mean diameter, mean blade spacing and mean chord are also needed. The fractional bleed, which occurs after the 6th stage stator blades is also required, as are appropriate values of the work-done factor. In the program, efficiencies are calculated using profile drag, annulus drag and secondary loss values based on cascade results (9). In the compressor the efficiencies are lower, and arbitrary factors have been introduced to make this adjustment.

The predictions of the program, and the results of rig tests are compared in Fig. 2 for values of 9.33 and 9.77 of the speed parameter ($n/\sqrt{T}$). These speeds are adjacent to the flight idling speed value of 9.63. The row efficiencies used were scaled from those calculated from cascade data to make the overall efficiency conform with that observed in the rig tests. This required lowering the efficiencies by 17% and 1% respectively for the two speeds of 9.33 and 9.77. Work-done factors were selected which gave satisfactory placings of the predicted constant-speed lines relative to the mass flow rate. The factors selected were in the ranges 0.78 to 0.70 and 0.86 to 0.76 respectively for the two speeds. Surge line location was as described earlier. At these speeds the onset of surge is associated with stall zones originating in the early blade rows.

Using the adjusting factors as described above, the predictions of the shapes of the constant-speed lines and of the position of the surge line represent a reasonable match with the experimental results.

EFFECT OF HEAT TRANSFER ON BOUNDARY LAYER DEVELOPMENT

It was now necessary to examine the effects of heat transfer from the metal surfaces on the flow of air through the compressor. Heat transfer produces a reduction in air density, which makes itself felt in two distinct ways. Firstly, there is a general reduction in the density of the air leaving the compressor, a "bulk" effect which may in itself cause a significant drop in performance (2). Secondly, there is the more localised effect on the boundary layers which develop on the annulus walls

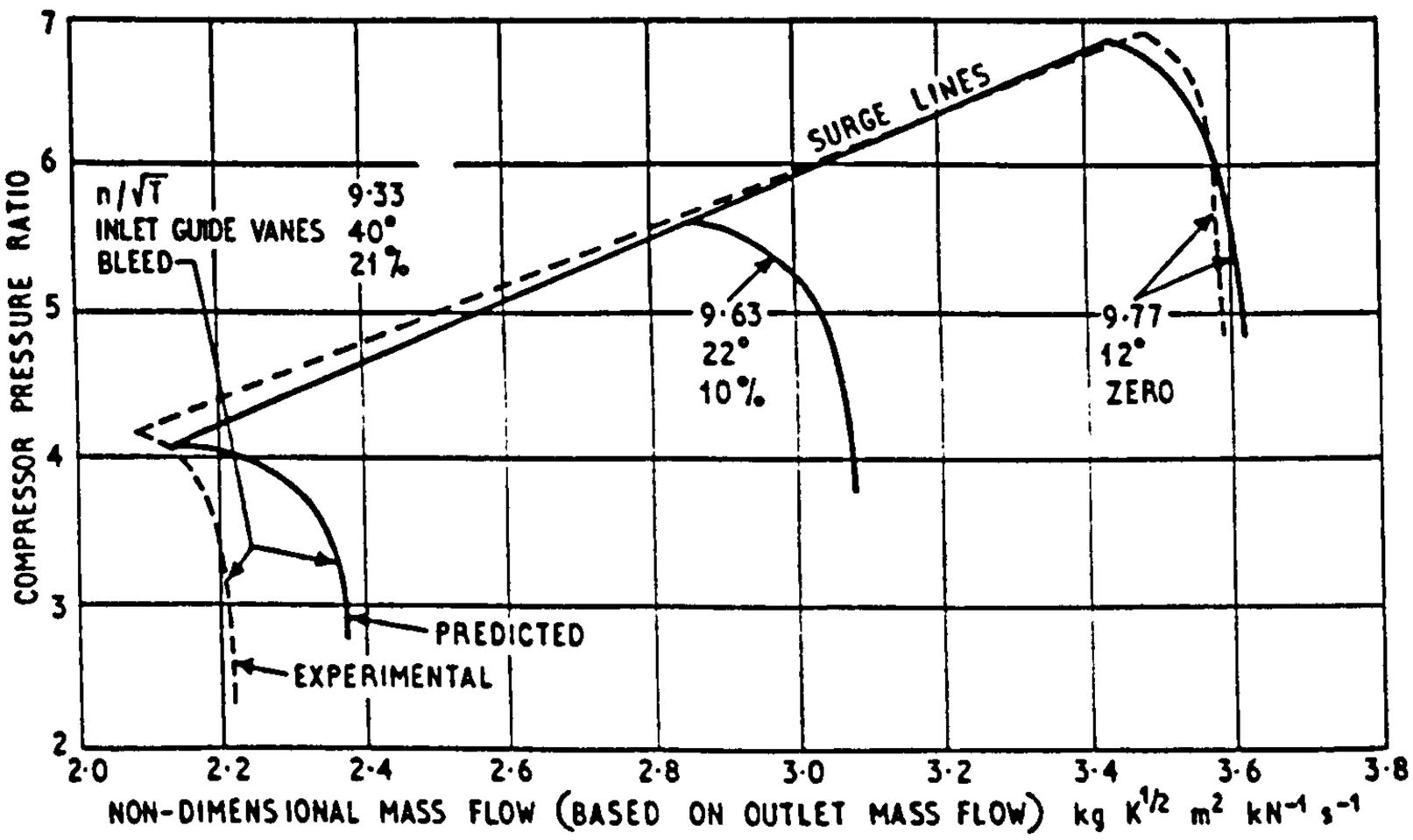

Fig. 2 - Predicted and experimental characteristics of H.P. compressor in vicinity of flight idling speed

and blade surfaces, which will be considered here in some detail.

In general terms, heat transfer from a wall to a boundary layer increases the rate at which the layer develops, by the influence of local density reduction on the momentum integral equation. The effect is made more severe by the presence of an adverse pressure gradient. Transition from laminar to turbulent flow in the boundary layer is also influenced by heating, with the transition region moving upstream and reducing in length. Finally, in cases where the boundary layer separates, it has been observed that heat transfer will generally accelerate the process (10).

Turning now to the case of the axial compressor, it seems probable that the annulus boundary layers will be thickened slightly, creating extra losses due to blockage. Similar thickening will occur in the layers on the blading, but here the effect is complicated by pressure gradients. On the pressure surfaces of the blades, the boundary layers will be thin, and because of the concavity of the surface, there will be a tendency for the hot air near the surface to move towards the edge of the boundary layer. This produces a circulatory effect (Taylor-Görtler vortices may be present even during adiabatic conditions, and heating will strengthen them) which prevents the build-up of a region of low-density air. It is thus anticipated that the development of these pressure surface boundary layers is not significantly influenced by heat transfer.

On the suction surfaces of the blades, however, conditions are different, in that there is a strong adverse pressure gradient and that the convex surface will prevent recirculation of the hot air. The boundary layer would be expected to thicken appreciably. Consequently, the wake developed behind each blade would be thicker, resulting in an increase in losses due to profile drag. There is a further complication in the disparity of effects between suction and pressure surfaces: the angular stream deflection produced by the blades may be reduced, as will be seen later.

In order to examine the development of blade boundary layers, a computer prediction method was employed. In the method, laminar boundary layer growth is predicted by the theory of Luxton and Young (11). The possibility of the development of a separation bubble, with subsequent turbulent reattachment, is considered as an alternative to straight-forward transition of the attached boundary layer. Calculation of turbulent boundary layer development is based upon the entrainment theory of Head (12), as modified for compressible flow by Green (13). Allowance for longitudinal surface curvature is made by means of modifications to the momentum integral equation, as suggested by Patel (14). It was assumed here that static pressure variations normal to the surface were negligible, across the thickness of the boundary layer.

The method has been tested by one of the present authors (3), (10) by comparing its predictions with the observed movements of the separation point on a heated convex - plate simulation. Typical results are shown in Fig. 3. There is good agreement between the predicted and observed movements.

The prediction method has been applied to aerofoils and conditions typical of axial-flow compressor practice. Blade configurations and pressure distributions were chosen from data supplied by Rhoden (15) and Masek and Norbury (16). Three incident angles were examined for each blade, one representing typical operating incidences, and the other two being respectively favourable and unfavourable. Nine sets of calculations were made under adiabatic conditions, and then repeated with the blade surface temperature at 30 deg K above that of the air stream.

It was found that the region of most rapid boundary layer growth was on the suction surface near the trailing edge of each blade, the layer there being fully turbulent. Upstream, in the laminar and transition regions, the layers were thin and the predicted effect of heat transfer was small. Attention was then centred on the turbulent boundary layer, and particularly on the development of δ^*, the displacement thickness, which measures the

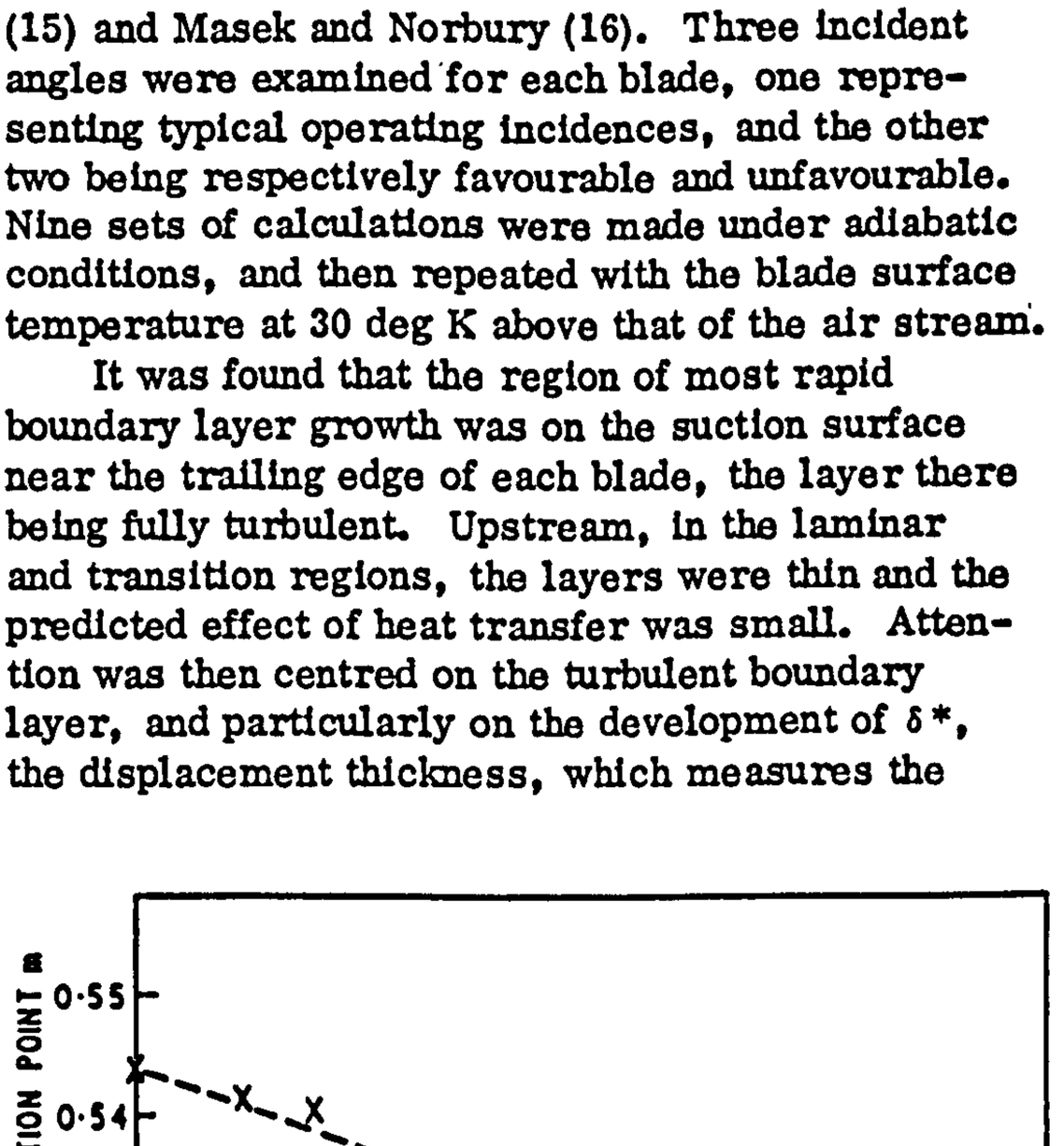

Fig. 3 - Separation point movement due to heat transfer - curved wall, low speed flow - Ref. (10)

effective blockage produced by boundary layer growth.

In all cases, the effect of heat transfer was to increase the displacement thickness of the turbulent boundary layer. This was most pronounced in the cases where separation took place; in the majority of these, the heat transfer was predicted to cause a small upstream movement of the separation point. Fig. 4 shows the effect of heating on displacement thickness in two typical cases, one involving turbulent separation and one where attached flow is maintained throughout.

The above comments applied only to the suction surface boundary layers. In contrast, those on the pressure surfaces were largely insensitive to heat transfer from the wall, and were in any case much thinner overall than their counterparts. The likely consequences for the wake formed behind a hot blade are illustrated in Fig. 5. The wake component from the pressure surface boundary layer is substantially independent of heat transfer, and so its thickness and angle of departure from the blade trailing edge will not change with blade temperature. However, the more rapid growth of the suction surface boundary layer on a "hot" blade will result in a change in its angle of departure compared with the adiabatic case; this change, exaggerated for clarity, is shown as ($2\Delta\alpha_2$) in Fig. 5. For the subsequent development of the wake behind the "hot" blade, one component of which is undeviated and the other deflected through the angle ($2\Delta\alpha_2$), it is suggested that it adopts the direction shown in the Figure, making an angle of approximately $\Delta\alpha_2$ with its direction in adiabatic conditions. Thus the overall result of heat transfer from the blade to the boundary layer is the formation of a thicker wake, and a reduction in the effective deflection produced by the blade, by an angle $\Delta\alpha_2$.

The value of $\Delta\alpha_2$ will of course depend upon blade and stream temperatures. The predictions discussed here were all made for a rise in blade temperature from 270 K to 300 K and at the compressor inlet density. The results must be viewed in this context. It would appear that $\Delta\alpha_2$ is also strongly influenced by conditions in the suction surface boundary layer, namely whether or not it is turbulent and whether or not it has separated. Finally, there appears to be an appreciable dependence upon blade configuration, as evidenced by the considerable scatter in Fig. 6 where $\Delta\alpha_2/\epsilon^*$ is plotted against the group $(i - i^*)/\epsilon^*$.

A relationship between these two quantities was required from this graph for incorporation into subsequent calculations. The following linear relation was adopted

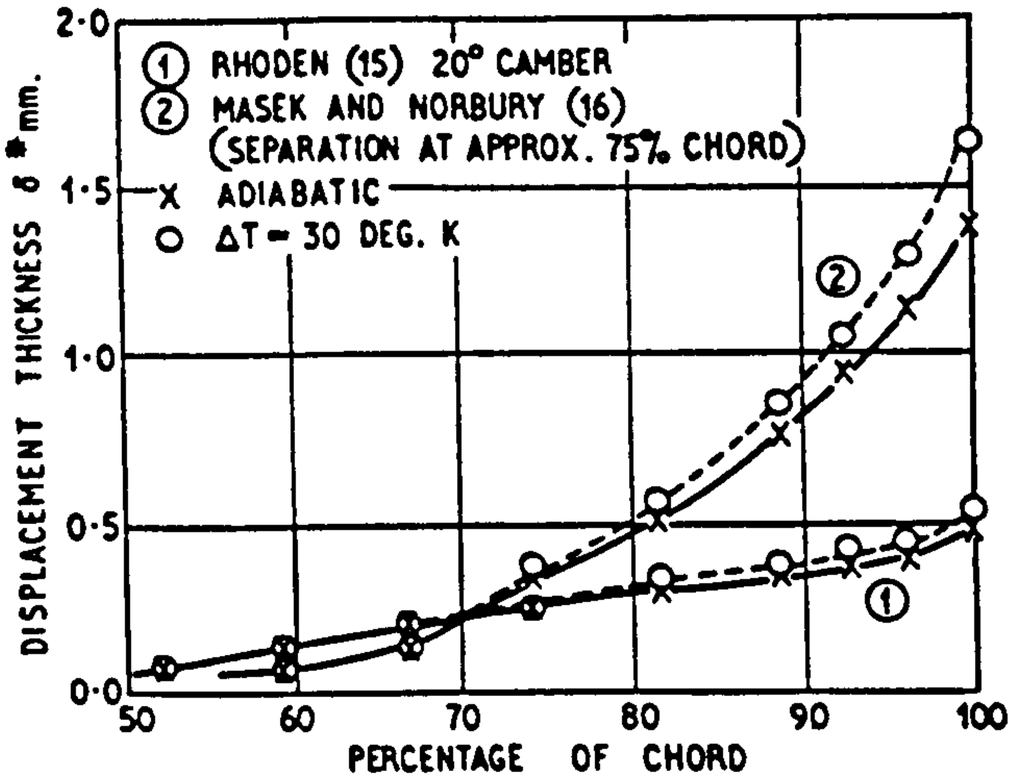

Fig. 4 - The effect of heat transfer on boundary layer growth on aerofoil suction surfaces

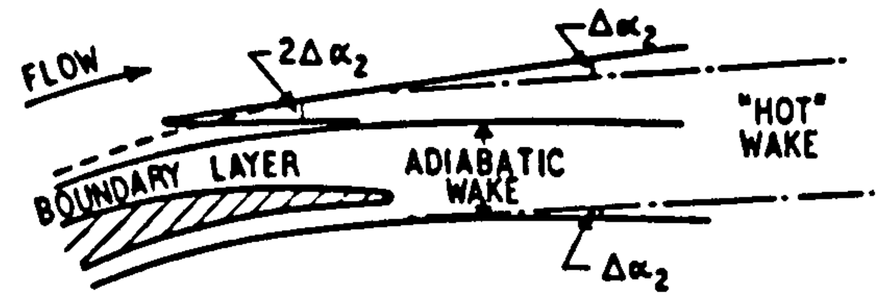

Fig. 5 - The effect of heat transfer on wake development

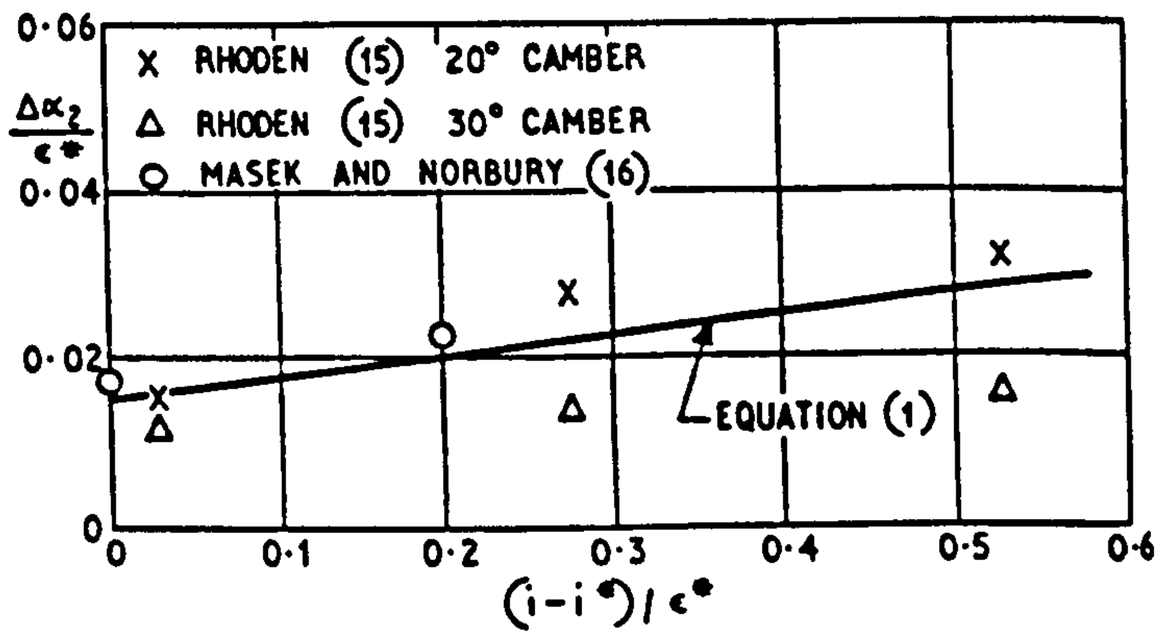

Fig. 6 - Wake deflection as a function of incidence conditions for $\Delta T = 30$ deg K

$$\frac{\Delta\alpha_2}{\epsilon^*} = \Delta T\,(0.0005 + 0.00084\,\frac{i - i^*}{\epsilon^*})$$

This is illustrated in Fig. 6. Because of the scatter in the predictions, this approach cannot be regarded as very satisfactory, but was considered acceptable for a first investigation. It is assumed in the relationship that the effect of heat transfer varies linearly with ΔT, the excess blade temperature,

which is justified by earlier experimental findings (10).

A final set of predictions was made for the conditions corresponding to the later stages of the compressor. The effect of the increased air density was to increase the inertia of the flow, reducing boundary layer thickness and delaying separation. But once separation had occurred the rate of growth of the displacement thickness was increased. There was some variation in the new values of the change of deflection, depending on the original position of the separation point, but in no case was there a reduction in $\Delta\alpha_2$. In order to avoid overestimating the effect, it was decided to use throughout the relation developed for the inlet flow conditions (equation (1)). It should be emphasised that this is not regarded as a definitive statement. Further investigation is required.

PREDICTION METHOD - NON-ADIABATIC FLOW

The reduction in deflection due to heat transfer, described above, was incorporated in the prediction method used for adiabatic flow. There is another effect which must be considered. For a given incidence angle, the profile drag will be increased if the deflection is reduced, because losses are closely related to the width of the wake, which is closely related to the deviation. To quantify this effect for inclusion in the prediction method, it has been assumed that the profile drag coefficient in the non-adiabatic case equals the profile drag coefficient observed in adiabatic flow when the air exit angle is the same as that occurring in the non-adiabatic case. This assumption is illustrated by the dashed lines on Fig. 1.

These two effects due to boundary layer changes have been incorporated in the prediction method. The further effect due to density changes resulting from "bulk" heat transfers to the air has also been included. Results are discussed below.

RESULTS

The prediction methods have been applied to the conditions in the H.P. compressor of the engine previously mentioned, at the conclusion of a rapid deceleration from maximum speed to the flight idling speed, at flight Mach number of 0.61 at 12,200 m altitude (40,000 ft). This type of transient had previously been found to show the greatest effects of "bulk" heat transfers (2).

The predicted constant-speed characteristics, both in the adiabatic and non-adiabatic cases, show distinct maximum pressure-ratio values as the mass flow is reduced. The predicted surge lines are drawn through these maxima. In the computational model used, only the first row of rotor blades was showing stall cells at these "surge" conditions.

The results are shown in Fig. 7. The predicted adiabatic surge and speed characteristics are shown by solid lines. When the boundary layer effects resulting from heat transfer are taken into account the corresponding characteristics are shown by dashed lines. It is noted that the surge condition occurs at virtually the same mass flow as in the adiabatic case.

The engine working line is included in Fig. 7 and it is seen that the surge margin, at a mass flow rate, is reduced due to these boundary layer changes by about 40%. The temperature differences between the aerofoils of the blades and the air stream ranged from 29 deg K to 15 deg K. These temperature differences had been predicted using models described by Maccallum (17).

It is worth noting that the reduction in pressure rise achieved by the compressor when the heated boundary layer effects are present is due to two factors - a reduction in small-stage efficiency, associated with the broader blade wakes, and a reduction in flow deflection in passing through a blade row.

Inclusion of bulk heat transfer effects (2) in addition to boundary layer changes leads to the result shown by the chain-dotted lines in Fig. 7. Bulk heat transfers cause a loss in surge margin of about 25%, in addition to that due to boundary layer changes.

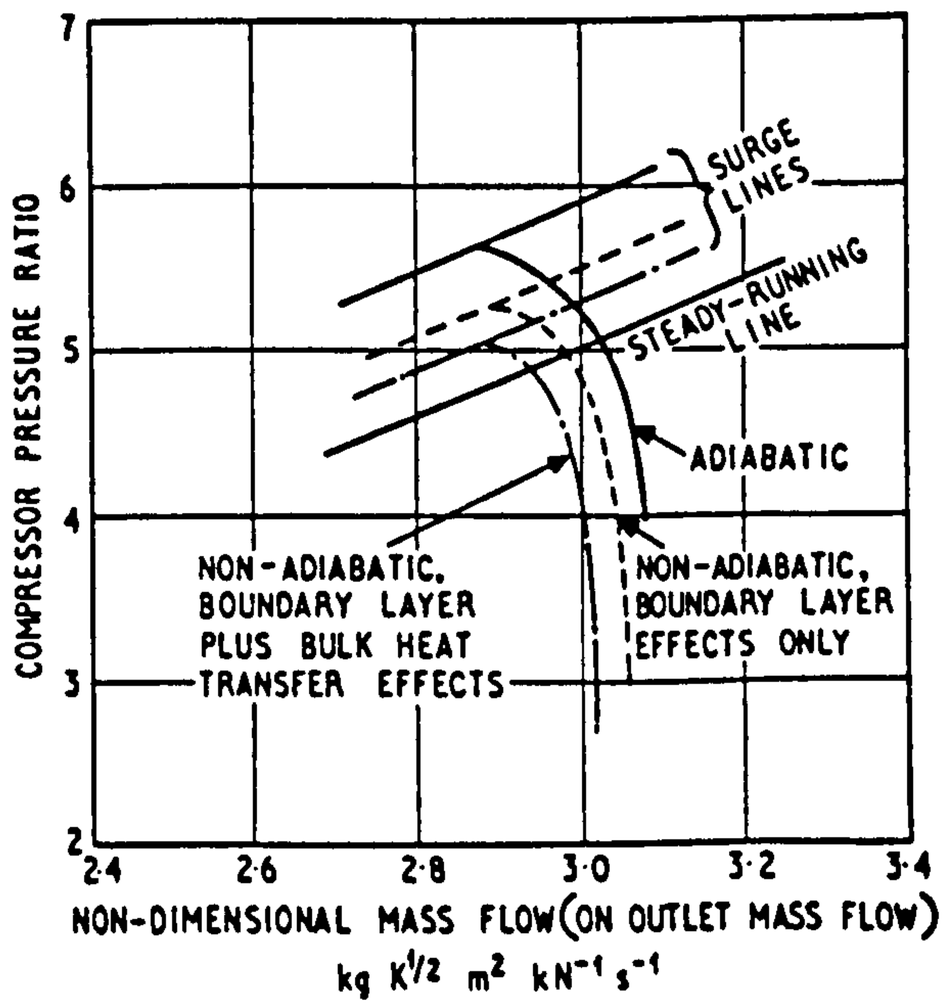

Fig. 7 - Predicted effects on H.P. compressor characteristics at end of altitude deceleration

CONCLUSIONS

A method has been developed for predicting the effects of boundary layer changes due to heat transfer on the characteristics of an axial-flow compressor. When applied to a severe transient of an aircraft engine - a rapid deceleration at altitude to the flight idling speed prior to an acceleration - there is apparently a marked reduction in surge margin. The reduction is estimated to be about 40%. There is estimated to be a further reduction of about 25% due to the "bulk" heat transfers causing density changes.

Several assumptions were made in the course of the investigation. These were made so that the order of the effects on compressor performance could be assessed. It is contended that this investigation shows that these effects are appreciable, and that this problem merits further investigation to clarify some of the assumptions.

ACKNOWLEDGMENTS

The authors wish to thank staff of Rolls-Royce (1971) Limited both for providing engine test data and for their advice and comments. They also wish to thank Mr. B. S. McLean and Mr. A. H. R. Hunter, now Graduates of the University of Glasgow for their assistance.

NOMENCLATURE

C_{dp}	=	profile drag coefficient
i, i^*	=	incidence, design incidence angles
i'	=	incidence angle, under adiabatic flow, to give same exit angle as occurs in non-adiabatic case
n	=	rotational frequency, s^{-1}
T	=	stagnation temperature at inlet, K
ΔT	=	difference between blade aerofoil temperature and adiabatic wall temperature, deg K
α_2, α_{2*}	=	exit, design exit angles (wake angles)
$\Delta\alpha_2$	=	change in the wake angle due to heat transfer
δ^*	=	boundary layer displacement thickness, mm
ϵ, ϵ^*	=	deflection, design deflection

REFERENCES

1. E. H. Warne, "Gas turbine fuel and control systems", Proc. Instn. mech. Engrs. 1968-69, 183 (Pt 3N), 121-27.

2. N. R. L. Maccallum, "Effect of bulk heat transfers in aircraft gas turbines on compressor surge margine", Heat and Fluid Flow in Steam and Gas Turbine Plant, Instn. mech. Engrs., London, 1974, 94-100.

3. A. D. Grant, "The effect of heat transfer on boundary layer stability in axial flow compressors", ibid, 252-258.

4. A. R. Howell and R. P. Bonham, "Overall and stage characteristics of axial-flow compressors", Proc. Instn. mech. Engrs, 1950, 163, 235-248.

5. A. R. Howell, "The present basis of axial flow compressor design. Part I. Cascade theory and performance", Aeronaut. Res. Counc. Rep. Memo. 2095, 1942.

6. D. Pollard and J. P. Gostelow, "Some experiments at low speed on compressor cascades". J. Engng. Pwr., Trans. Am. Soc. mech. Engrs. 1967 (July,) 427-436.

7. W. H. Robbins and J.F. Dugan Jr., "Prediction of off-design performance of multistage compressors". Ch.X. Aerodynamic design of axial-flow compressors, N.A.S.A.-S.P. 36, 1965.

8. S. Gray, "Stage matching, stall, and surge in multi-stage axial flow compressors", Proc. Instn. mech. Engrs. 1969-70, 184 (Pt. 3G(II)), 49-56.

9. A. R. Howell, "Fluid dynamics of axial compressors", Proc. Instn. mech. Engrs., 1946, 153, 441-452.

10. A. D. Grant, "The effect of heat transfer on boundary layer stability", Ph.D. Thesis, University of Glasgow, 1973.

11. R. E. Luxton and A. D. Young, "A generalised method for the calculation of the laminar compressible boundary layer with heat transfer and non-uniform pressure distribution". Aeronaut. Res. Counc. Rep. Memo. 3233, 1960.

12. M. R. Head, Entrainment in the turbulent boundary layer", ibid, 3152, 1960.

13. J. E. Green, "The prediction of the turbulent boundary layer development in compressible flow", J. Fluid Mech. 1968, 31, 753-778.

14. V. C. Patel, "The effects of curvature on the turbulent boundary layer", Aeronaut. Res. Counc. Rep. Memo. 3599, 1969.

15. H. G. Rhoden, "Effects of Reynolds Number on the flow of air through a cascade of compressor blades", ibid, 2919, 1956.

16. Z. Masek and J. F. Norbury, "Low-speed performance of a compressor cascade designed for

prescribed velocity distribution and tested with variable axial velocity ratio". Heat and Fluid Flow in Steam and Gas Turbine Plant, Instn. mech. Engrs., London, 1974, 224-236.

17. N. R. L. Maccallum, "Models for the representation of turbomachine blades during temperature transients", ASME Paper 76-GT-23.

Publication 18
77-GT-87

an ASME publication

The Effect of a Transversely Injected Stream on the Flow Through Turbine Cascades: Part I—Flow Effects

K. D. SHRIVASTAVA

Professor,
Department of Mechanical Engineering,
M.A. College of Technology,
Bhopal, India

N. R. L. MacCALLUM

Senior Lecturer,
Department of Mechanical Engineering,
University of Glasgow,
Glasgow, Scotland

A study has been made of the flow-through turbine cascade when a transverse flow is injected into the main flow immediately in front of the cascade. A separation bubble was observed on the end-wall immediately behind the injection slot. At the suction surface end of this bubble a vortex moved into the main flow and continued downstream through, and beyond, the cascade. The effects of the separation bubble and of the vortex were observed in measurements of pressure around the blade surfaces, in boundary layer transverses on the end-wall, and in total head and directional transverses across the cascade exit.

Contributed by the Gas Turbine Division of The American Society of Mechanical Engineers for presentation at the Gas Turbine Conference & Products Show, Philadelphia, PA, March 27-31, 1977. Manuscript received at ASME Headquarters December 22, 1976.

Copies will be available until December 1, 1977.

The Effect of a Transversely Injected Stream on the Flow Through Turbine Cascades: Part I—Flow Effects

K. D. SHRIVASTAVA

N. R. L. MacCALLUM

NOMENCLATURE

- a = distance along chord from leading edge of blade
- A = a parameter, defined by equation (4)
- b = injection jet width
- c = chord
- C_p = pressure coefficient, defined by $(p - p_1)/(p_{o1} - p_1)$
- d = distance along blade pitch from one mid-passage line to next, in direction of blade suction surface
- $\dot{m}$ = mass flow rate
- n = index to fit power law equation (1)
- p = pressure
- Q = ratio of maximum velocity of injected jet to velocity of main approach flow
- s = blade pitch
- u,w = velocity components in boundary layer parallel and normal to the local main velocity, U
- U = velocity of main flow outside the boundary layer
- y = distance from end-wall carrying the injection slot
- α = main fluid angle, measured from axial direction
- γ = stagger angle
- δ = thickness of skewed boundary layer, defined by point where layer begins to skew
- ε = w/u
- θ = angle between injected jet and cascade end-wall

Subscripts

- o = stagnation
- w = end-wall
- 1 = inlet to cascade
- 2 = outlet from cascade
- app = approach
- ave = average
- inj = injected
- max = maximum

INTRODUCTION

In a typical gas turbine, small airflows are extracted from the main flow to cool various components of the turbine, e.g., blades, nozzle guide vanes, and disks. After they have fulfilled their function, these cooling flows are returned to the main flow in the turbine. The cooling air from the blades and vanes usually returns via holes in the blade surfaces. The disk cooling air returns by entering the main flow transversely between blade rows. It has been observed that these transversely injected flows can cause appreciable alteration in the performance characteristics of the turbine. This has been most noticeable in multi-spool engines where the matching of the turbines is upset.

This paper describes an experimental investigation of the aerodynamic effects of injecting air transversely in front of a two-dimensional cascade of turbine nozzle guide vanes.

APPARATUS AND TEST PROCEDURE

Apparatus

This consisted of a cascade of five blades (four passages) of 129-mm (5.07-in.) chord, 381-mm (15.0 in.) height, at 88-mm (3.5-in.) pitch having profiles typical of an intermediate or low pressure row of nozzle guide vanes. The blade length was sufficient to ensure that secondary flows did not affect the flow at the mid-blade height.

The cascade was placed in the suction to a variable speed fan.

Typically, the flow velocity at exit from the cascade was 27 m/sec (90 ft/sec) corresponding to a blade Reynolds Number, based on this exit velocity of 2.5×10^5.

The main airflow to the cascade entered through a contraction of area ratio 8.3. Wire grids were placed in this contraction to give a turbulence level of 1.5 percent at the cascade inlet. This turbulence level ensured that the operating Reynolds Number was well above the critical.

The slot through which the transverse flow was injected was placed across one end-wall, immediately in front of the leading edges of the cascade blades. The end-wall boundary layer in the main flow approaching this slot was sucked away some 180 mm (7 in.) upstream of the slot.

The cascade and injection parameters were as follows: (a) stagger angle, 45 deg; (b) main fluid inlet angle, 15 deg; (c) width of injected jet, 9.1 mm (0.36 in.); (d) angle of injected flow to cascade end-wall, 90 deg; and (e) ratios of injected velocity to main approach flow velocity, 0.0, 0.5, 1.0, and 1.5. At the maximum injection rate, the transversely injected mass flow was 3.6 percent of the main approach flow. The injected flow was at the same temperature as the main flow.

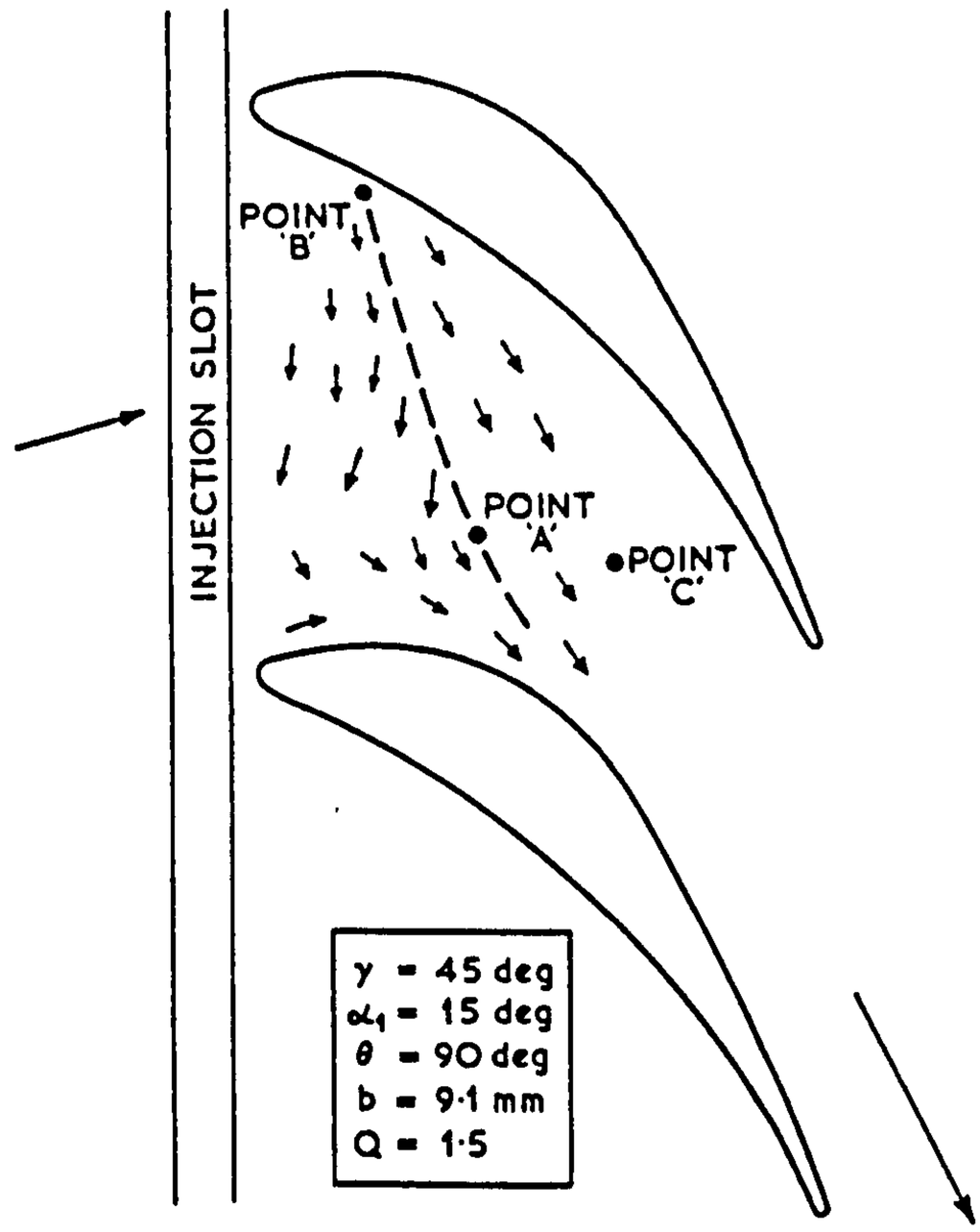

Fig. 1 Velocity directions on end-wall behind injection slot

Test Procedure

The angles of the exit side-walls, relative to the cascade, were adjusted until there was a symmetric velocity distribution across the exit flow. The fan speed was then adjusted to give an approach velocity of 13.6 m/sec (45 ft/sec), and the following observations were made:

1 Total head pressure distribution and flow direction in the end-wall boundary layer behind the injection slot at point C (Fig. 1), i.e., midway between blades and at an axial chord distance of 0.64
2 Pressure distribution around the suction and pressure surfaces of the middle blade in the cascade, over a range of blade heights
3 Total head pressure distribution and flow direction across a traversing plane 200 mm (7.9 in.) downstream in the flow direction of the cascade exit. This corresponded to an axial downstream distance of 88 mm (0.92 axial chord).

The flow was also visualized, mainly using short lengths of thread, particular attention being given to the region immediately downstream of the injection slot.

RESULTS

Qualitative Effects -- Flow Visualization

When the additional flow was injected transversely across the main flow, a separation bubble was formed on the cascade end-wall immediately behind the injection slot. This creation of a separation bubble has, of course, been widely studied in situations where there is no cascade (1, 2).[1] In much of that work, the pressure gradient along the flow was effectively zero. In the presence of a positive pressure gradient, the bubble length increased (2). In the work reported here, the bubble lengths were much shorter than those obtained in streaming flow (no pressure gradient). This is attributed to the combination of the negative pressure gradient and the presence of secondary flows (1) in the cascade.

An illustration of the bubble size is given in Fig. 1 which gives the flow directions, as indicated by threads, on the end-wall surface immediately behind the injection slot. In this case, the injected jet had a velocity

[1] Underlined numbers in parentheses designate References at end of paper.

1.5 times the main flow velocity. The reattachment boundary at the downstream end of the separation bubble is indicated by line AE. The average length of the bubble, in the flow direction, is about 0.25 chord. It is to be noted that there are considerable velocity components along the bubble, parallel to the inlet plane of the cascade, the direction being toward the suction surfaces of the blades. This is in keeping with the observation of Blair (3) that the effectiveness of an end-wall cooling film, injected at 30 deg to the main flow, is much greater nearer the suction surfaces due to the coolant being swept by secondary flows across the channel toward the suction surface.

In other flow visualization studies, using liquid films which dry on the surfaces, and from surveys using threads, it was seen that a vortex appears near the end of the separation bubble close to the blade suction surface, i.e., in the vicinity of point A in Fig. 1. This vortex lifts a short distance away from the end-wall and then tends to adopt the mean flow direction through the cascade passage. This vortex is almost certainly associated with the increased secondary flows outside the end-wall boundary layer which are observed at point C (in Fig. 1) when the transverse flow is introduced (discussed in the following). The vortex continues through the passage and persists well downstream of the cascade exit. This can be seen in the exit traverse (Fig. 11) discussed later.

End-Wall Secondary Flows within the Passage

The distributions of velocity and flow direction in the boundary layer, and adjacent main flow, at point C (Fig. 1) are given in Fig. 2.

For the case of no injection, the skewing of the boundary layer is typical of that on the end-walls of cascades, as studied by others. For example, Mager (4) has proposed that the components of velocity in the boundary layer are given by

$$\frac{u}{U} = \left(\frac{y}{\delta}\right)^{\frac{1}{n}} \qquad (1)$$

and

$$\frac{w}{U} = \varepsilon_w \left(\frac{y}{\delta}\right)^{\frac{1}{n}} \left(1 - \frac{y}{\delta}\right)^2 \qquad (2)$$

Subsequently, Johnston (5) has introduced the

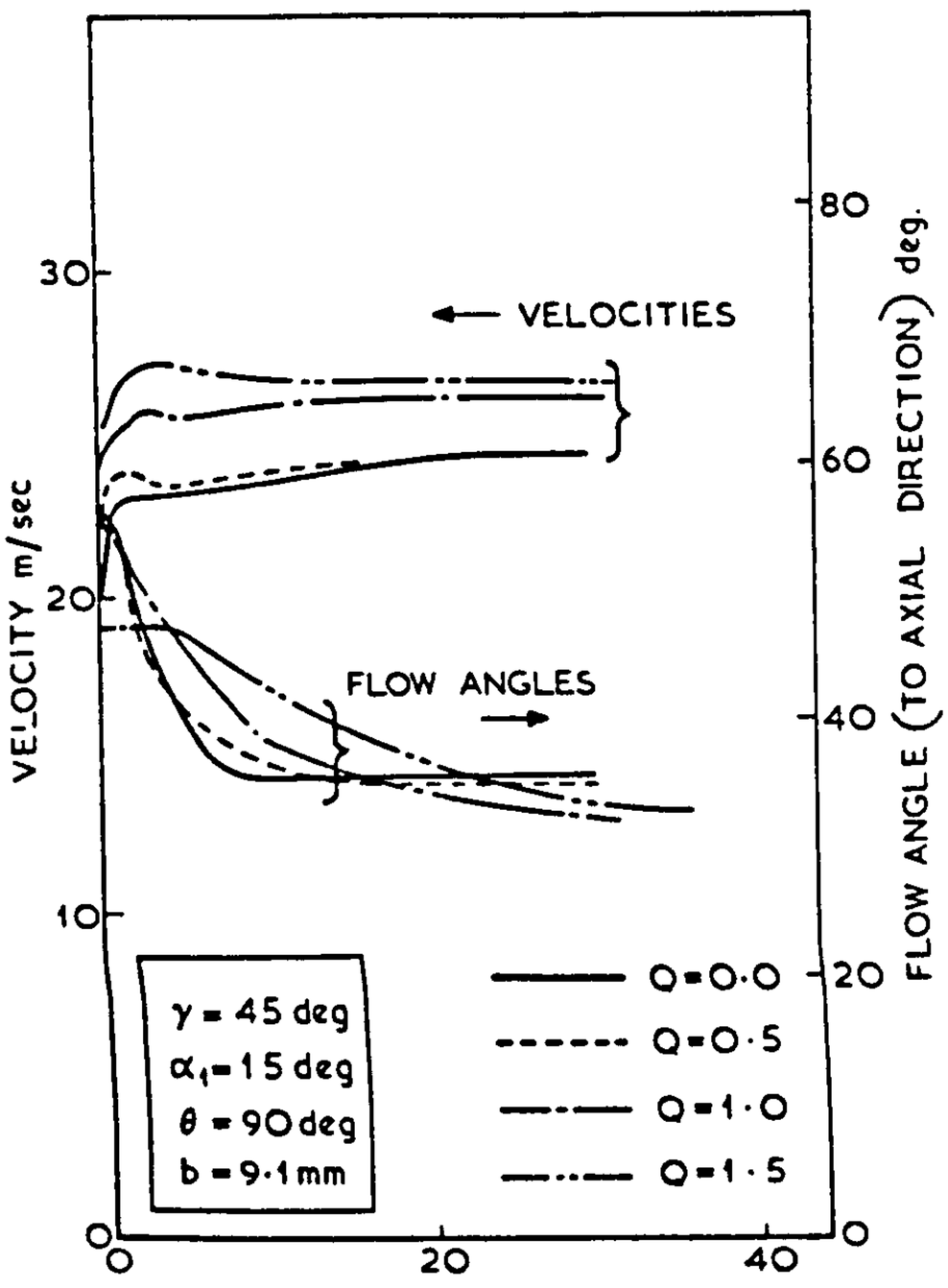

Fig. 2 Effects of transverse injection on velocities and directions in boundary layer on cascade end-wall (Point C)

concept of the inner and outer layers, and, according to his model, the cross-flow velocities in the inner layer are given by

$$\frac{w}{U} = \varepsilon_w \frac{u}{U} \qquad (3)$$

and in the outer layer by

$$\frac{w}{U} = A\left(1 - \frac{u}{U}\right) \qquad (4)$$

The parameter, A, is given by

$$A = -2\,U^2 \int_{\alpha_1}^{\alpha} \frac{d\alpha}{U^2} \qquad (5)$$

The components of velocity in the skewed boundary, observed in the present work with no injection, are shown on a Polar Plot in Fig. 3. The boundary-layer thickness was defined by the point where, on approaching the end-wall, the

fluid flow began to skew (ε). A value of 19 for the index n in equation (1) was found to fit the experimental data. This value is considerably higher than the values of about 7 to 9 usually observed in the absence of pressure gradients. The change to 19 is attributed to the negative pressure gradient.

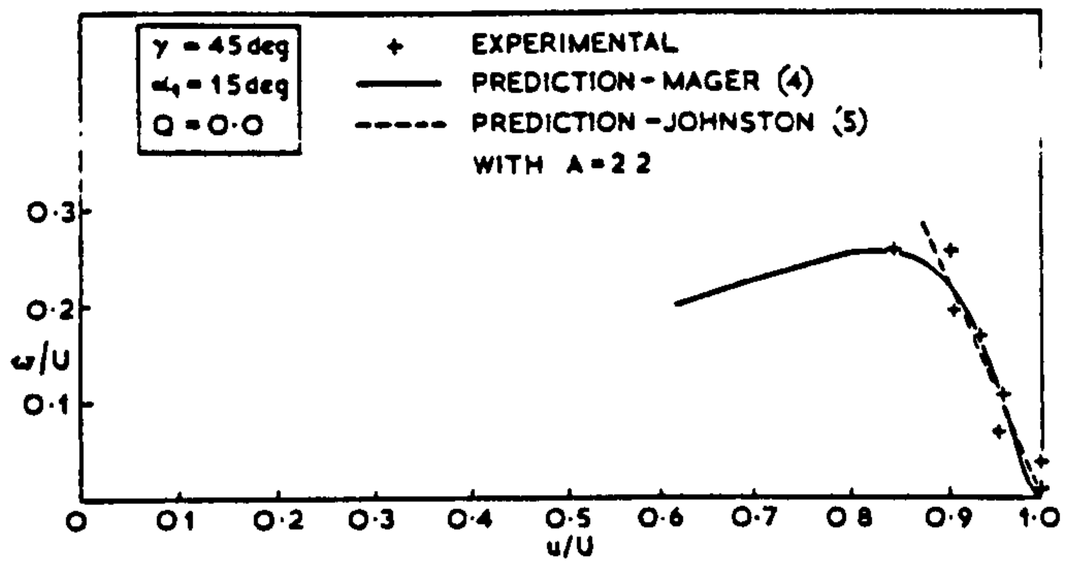

Fig. 3 Polar plot of velocity components in boundary layer on channel end-wall (Point C) -- no injection

Using n = 19 in equations (1) and (2) gave the predictions from Mager's model shown in Fig. 3.

According to Johnston's model, it appears that all the experimental points are in the outer layer where the secondary components of velocity are given by equation (4). The value of A in this equation to give the best fit is 2.2. This does not compare well with the value of 3.9 predicted by equation (5). It has, however, been shown by Horlock (7) that equation (5) is limited to unconfined flows and will tend to be in error in the bounded flow in a blade channel.

The predictions of the two models (with the exception of the prediction of A) are very similar and in close agreement, allowing for experimental error, with the observed results. While it is realized that there are shortcomings in these simple models, e.g., in the use of a power law in equation (1), it is important to note that in this turbine cascade, these simple models give realistic predictions.

When the transverse flow is introduced, there is a considerable change in the boundary-layer flow at point C. In the extreme case of maximum injection (Q = 1.5), the boundary layer itself is no longer skewed, but there is considerable change of direction in the main flow outside the boundary layer. This change of direction in the main flow occurs in the region which is influenced by the vortex emanating from around point A (Fig. 1), discussed in the previous section. If one assumes that a measure of this skewing in the main flow near the end-wall is given by the change in angle in the flow at the position corresponding to the edge of the boundary layer (as defined in the foregoing) when there was no injection, then this measure, ϕ, has values of 3.5, 9, and 12 deg for values of the injection parameter, Q, of 0.5, 1.0, and 1.5, respectively.

At the intermediate transverse injection rates (Q = 0.5 and 1.0), there is some skewing within the end-wall boundary layer.

For the case where Q = 1.5 and the boundary layer is virtually two-dimensional, the velocity distribution in the layer is fitted reasonably well by a power law using n = 22 [equation (1)], which is very close to the value of 19 observed in the skewed boundary when there is no transverse injection.

Pressure Distributions on Blade Surface

At mid-blade height, the pressure distribution is virtually unaffected by the transverse injection, except that it increases the main flow velocity in the region not disturbed by the jet.

At blade heights close to the end-wall behind the injection slot, alterations due to the transverse flow are observed. The results are illustrated in Figs. 4 to 7 for the four distances from the end-wall -- y/c = 0.025, 0.075, 0.20, and 1.48 (mid-blade height), respectively.

Closest to the end-wall and at the highest injection rate, the pressure on the suction surface is affected for about 40 percent of the chord, and for about 15 percent chord on the pressure surface. The separation bubble connects suction and pressure surfaces on the opposite faces of the channel and tends to equalize the pressures. The length in which the pressure distribution is thus affected are in agreement with the lengths of the separation bubble observed in the flow visualization studies (Fig. 1).

It is also noted that the pressure distribution on the suction surface downstream from the separation bubble is also affected. For example, at y/c = 0.20 (Fig. 6), the pressure in this region first reduces as transverse injection is introduced, and then when the injection rate is a maximum, it rises again at positions between about 50 and 80 percent chord. It is considered that this is due to the development of the vortex, emanating from point A

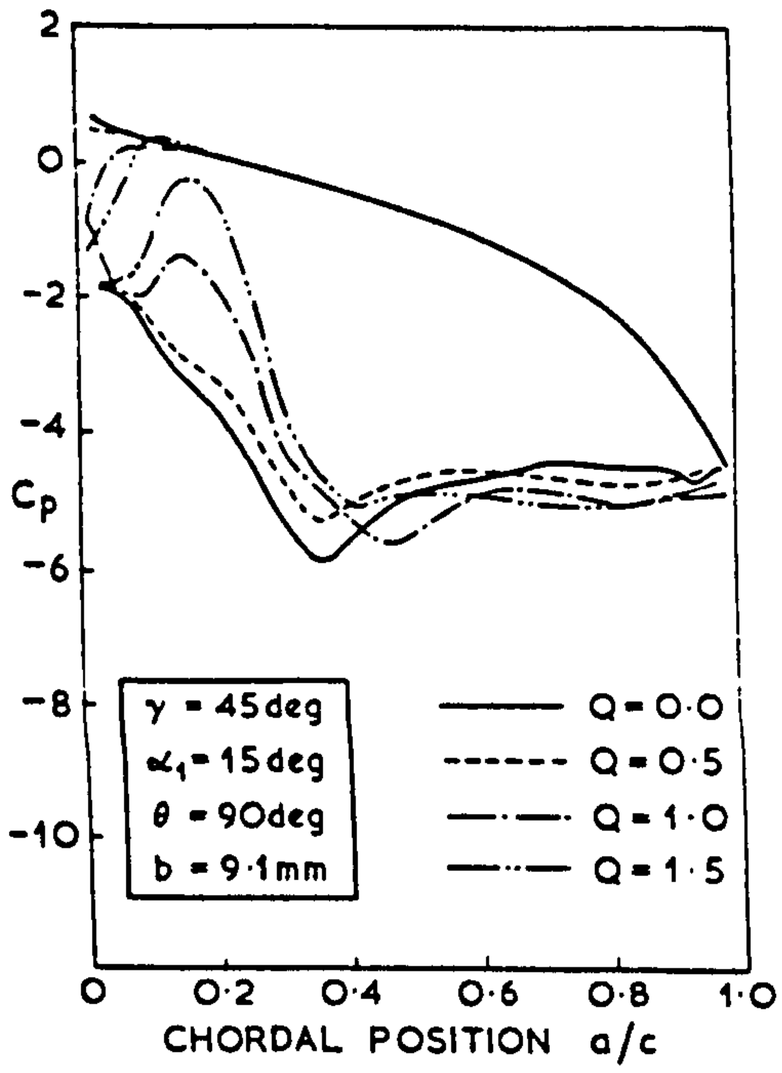

Fig. 4 Pressure distribution around blade at y/c = 0.025

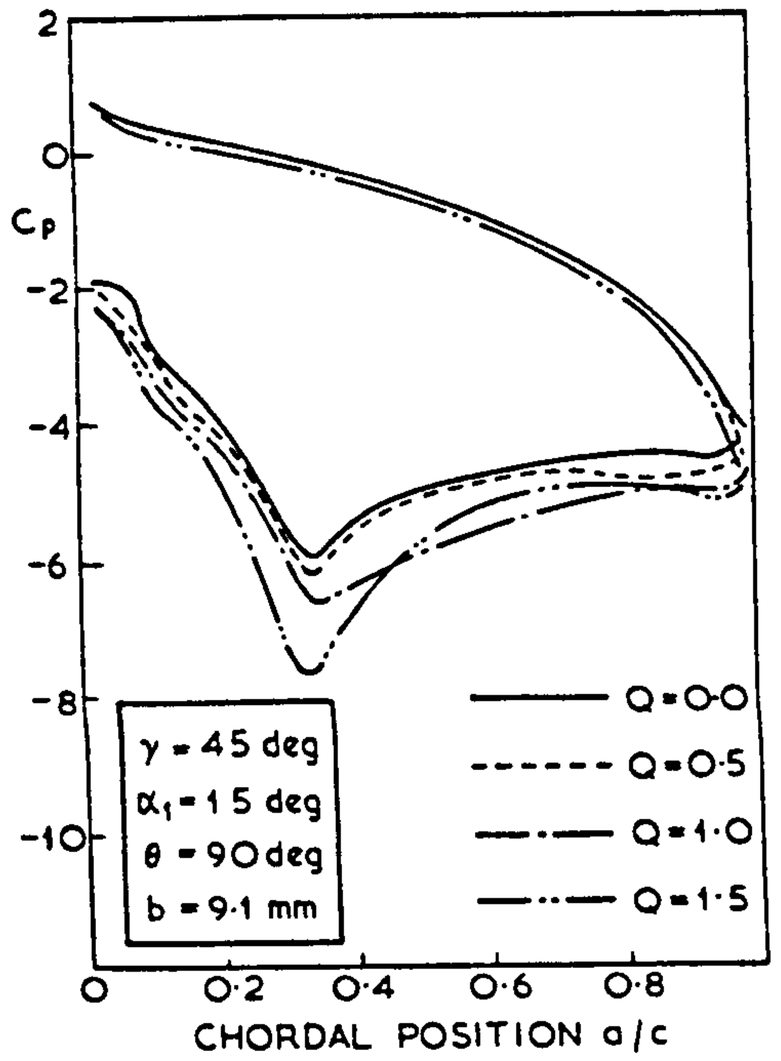

Fig. 6 Pressure distribution around blade at y/c = 0.20

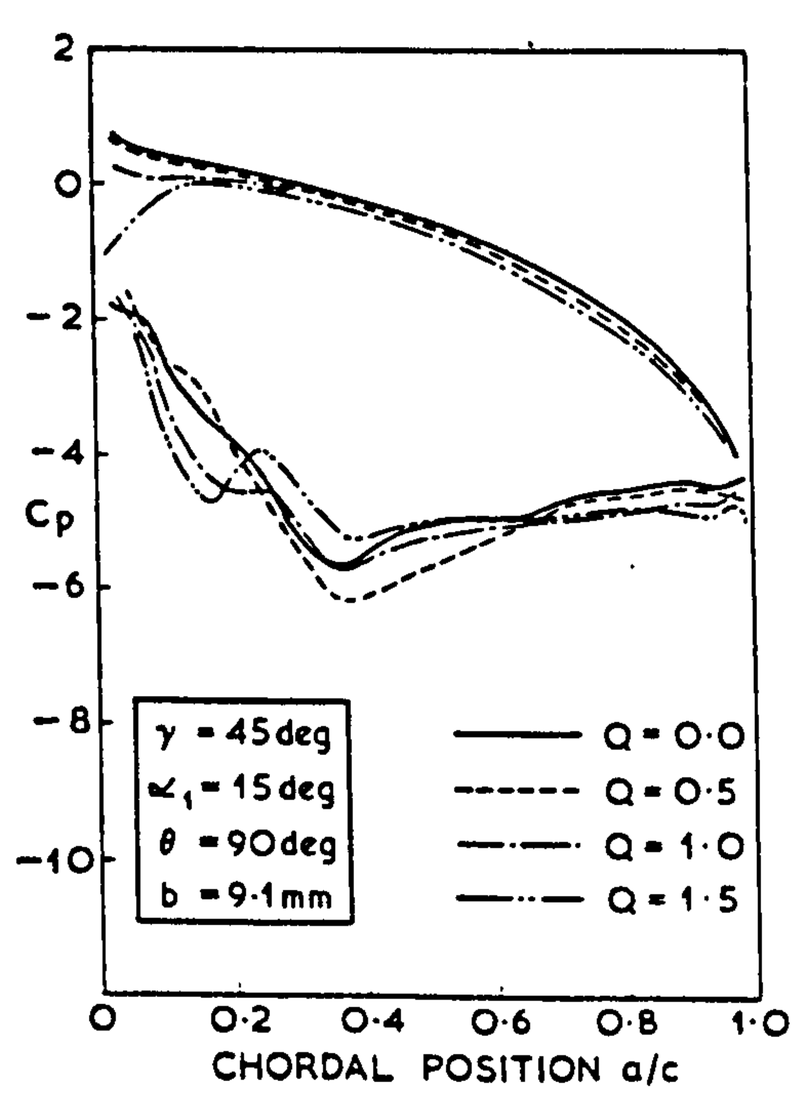

Fig. 5 Pressure distribution around blade at y/c = 0.075

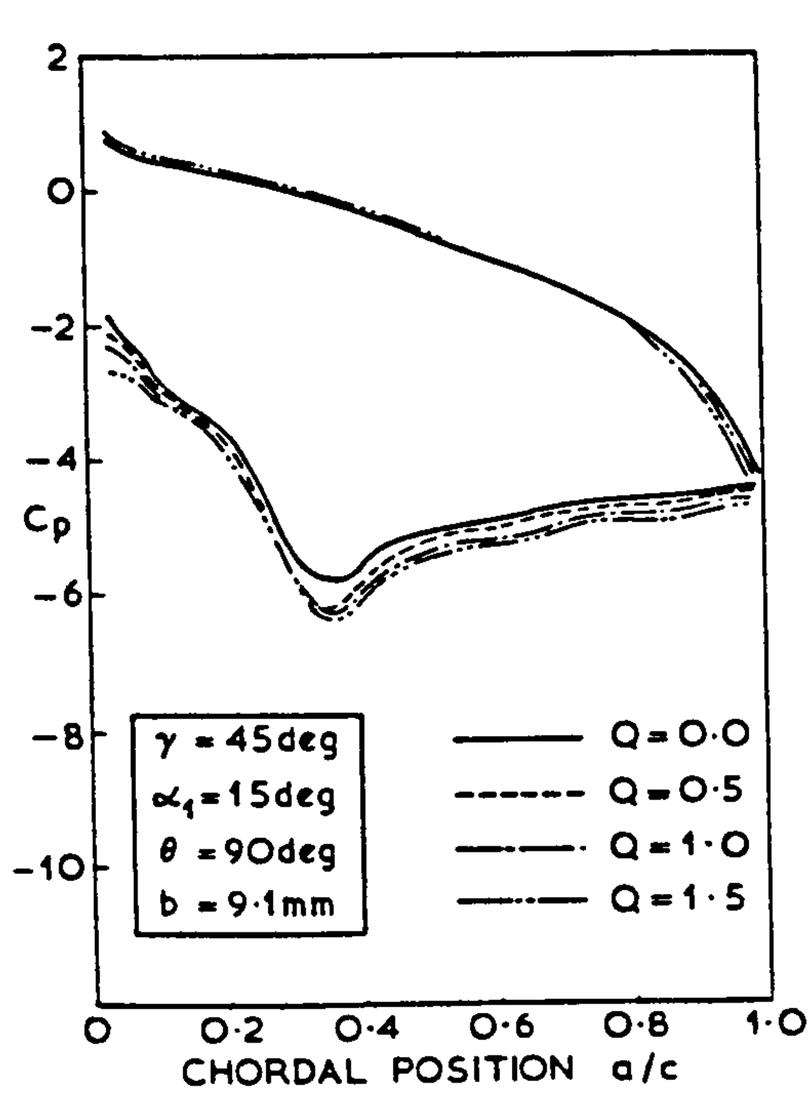

Fig. 7 Pressure distribution around blade at y/c = 1.48

(Fig. 1), which sweeps downstream close to the suction surface.

Exit Traverse

Velocity Distributions. The velocity distributions in the main flow direction across the cascade exit traverse plane have been determined from the total head measurements. The distributions with no transverse injection and with maximum injection are shown in Figs. 8 and 9, respectively, these depicting the distributions when viewed in the downstream direction.

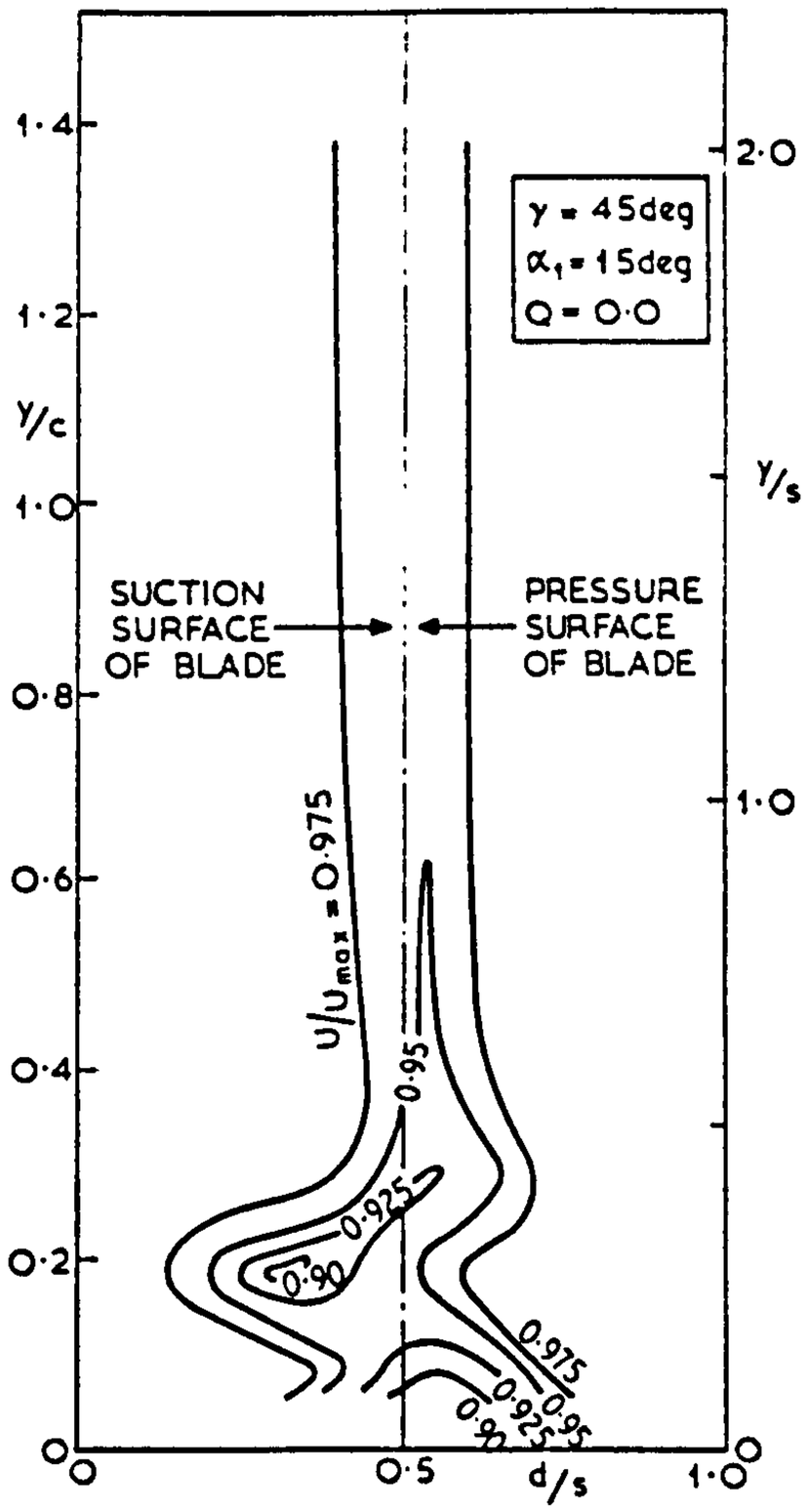

Fig. 8 Velocity contours at outlet traverse plane -- no transverse injection

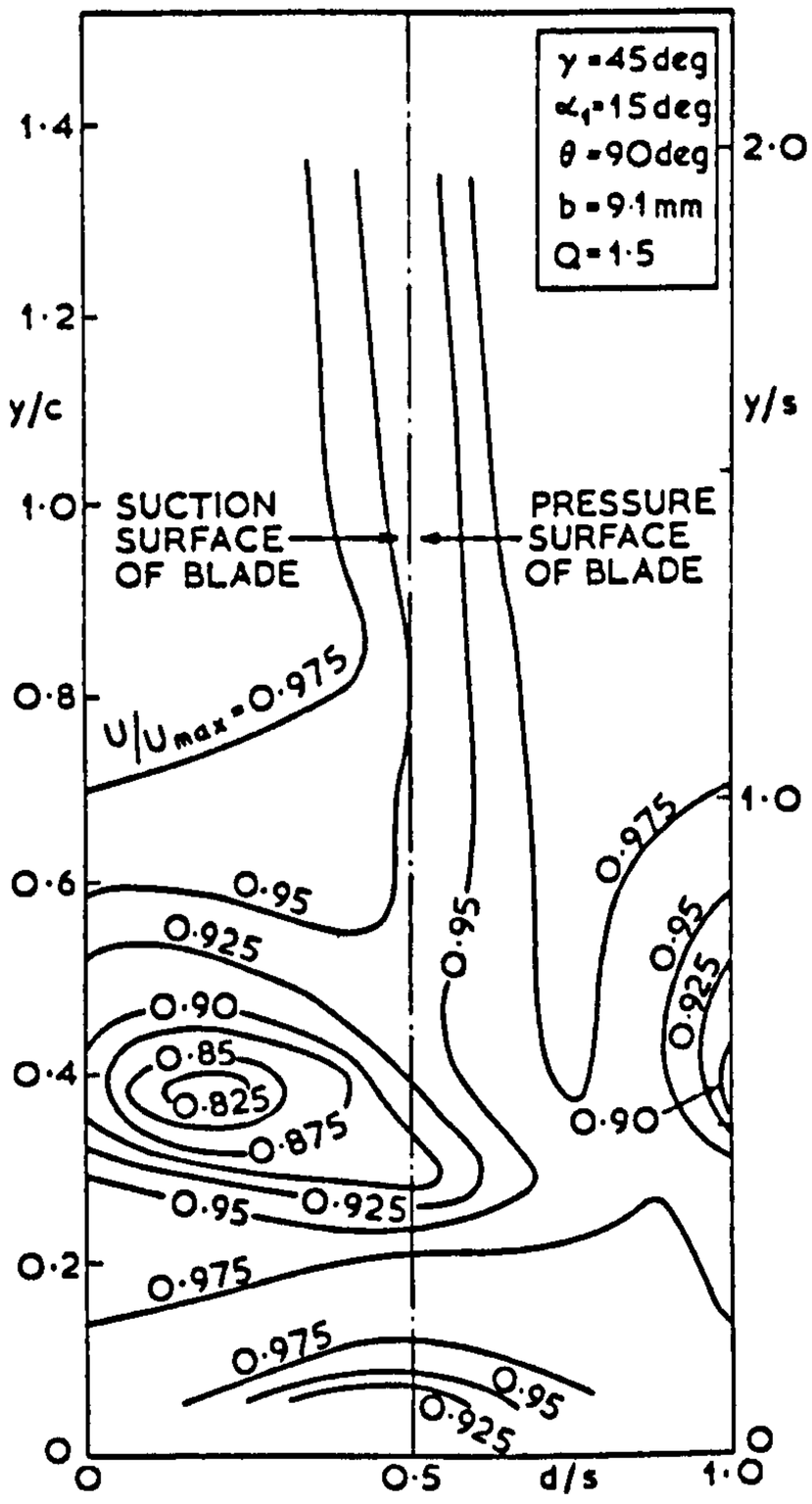

Fig. 9 Velocity contours at outlet traverse plane -- with transverse injection

Transverse injection has the effect of creating a significant trough in the exit velocity distribution at a height of about 0.38 chord above the end-wall from which the transverse flow is introduced. The minimum velocity in this trough is about 0.82 of the mid-passage velocity at the mid-blade height. The trough does not lie directly in the wake of the blade, but between the suction surface and the mid-passage, being rather nearer the latter. This trough in forward velocities coincides with the center of the exit vortex indicated in the angular deviation traverses at the same plane and discussed in the next section. At mid-blade height, the wake behind the blade is slightly increased by transverse injection.

The results when lower injection velocities are used lie intermediate between the two cases illustrated in Figs. 8 and 9. Integrated results (as integrated total head losses) from all four tests are discussed later.

Angular Deviations. Distributions of angular deviations are given in Figs. 10 and 11 for the cases with no transverse injection and with the maximum transverse injection, respectively. For the case without transverse injection, there is only significant deviation (say greater than 3 deg) close to the end-wall of the cascade. Here the deviation is positive. This is in agreement with established results. When the transverse injection is introduced, there are strong positive deviations at blade heights in the range 0.1 to 0.3 chord, and strong negative deviations at heights of around 0.5 chord. These deviations are greatest downstream of the flow between the suction surface and the mid-channel. These deviations and the change of deviation across the pitch at the height of 0.38 chord indicates the presence of a vortex centered near point D in Fig. 11. The vortex as viewed in this figure, which is looking downstream, is rotating in a counter-clockwise direction; i.e., at the side of the vortex nearest the suction surface it is moving away from the end-wall. It is important to note that point D coincides with the trough in the forward velocity distribution (Fig. 9). This vortex is the con-

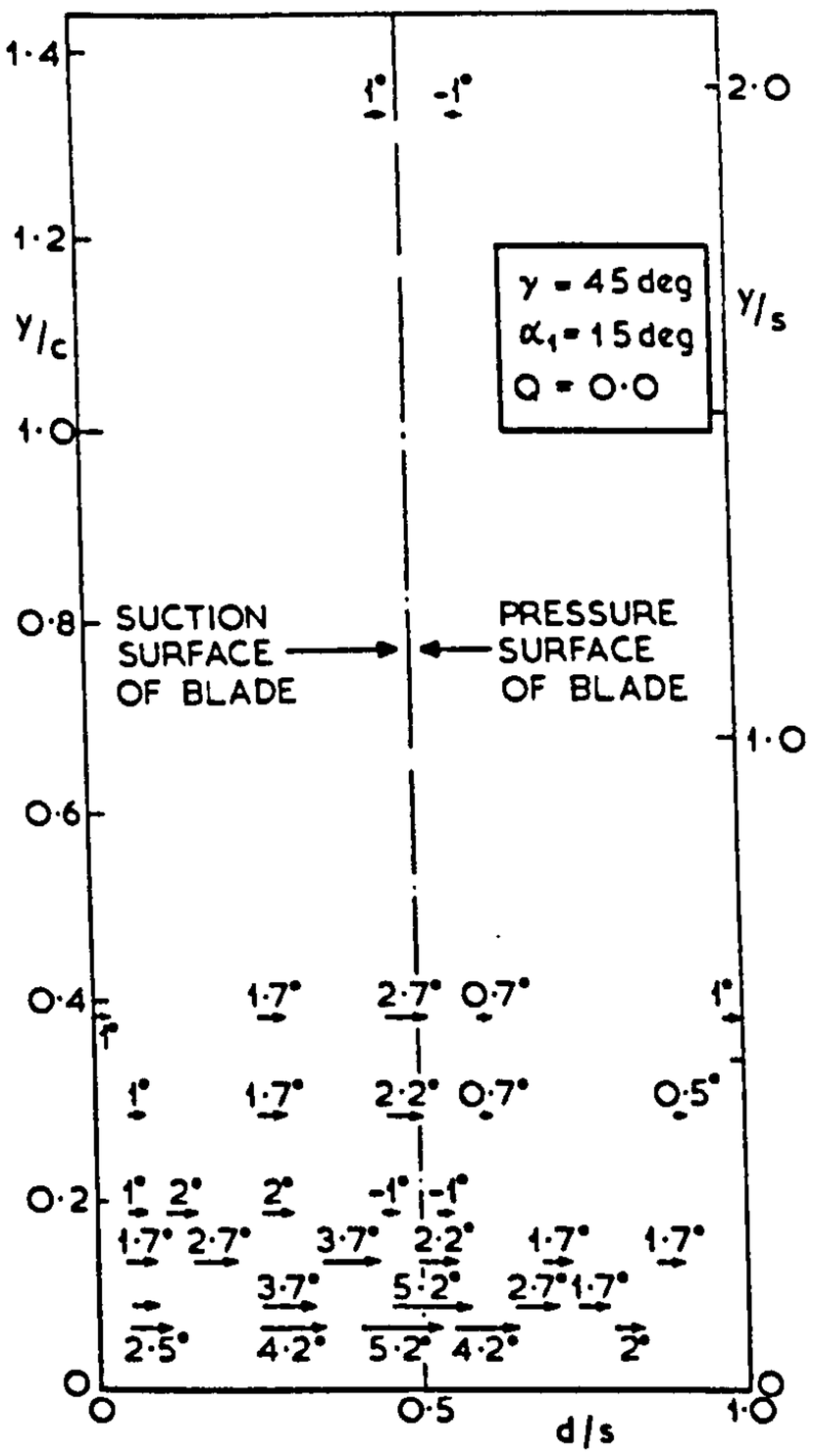

Fig. 10 Deviations at outlet traverse plane -- no transverse injection (location of measurement is tail of arrow)

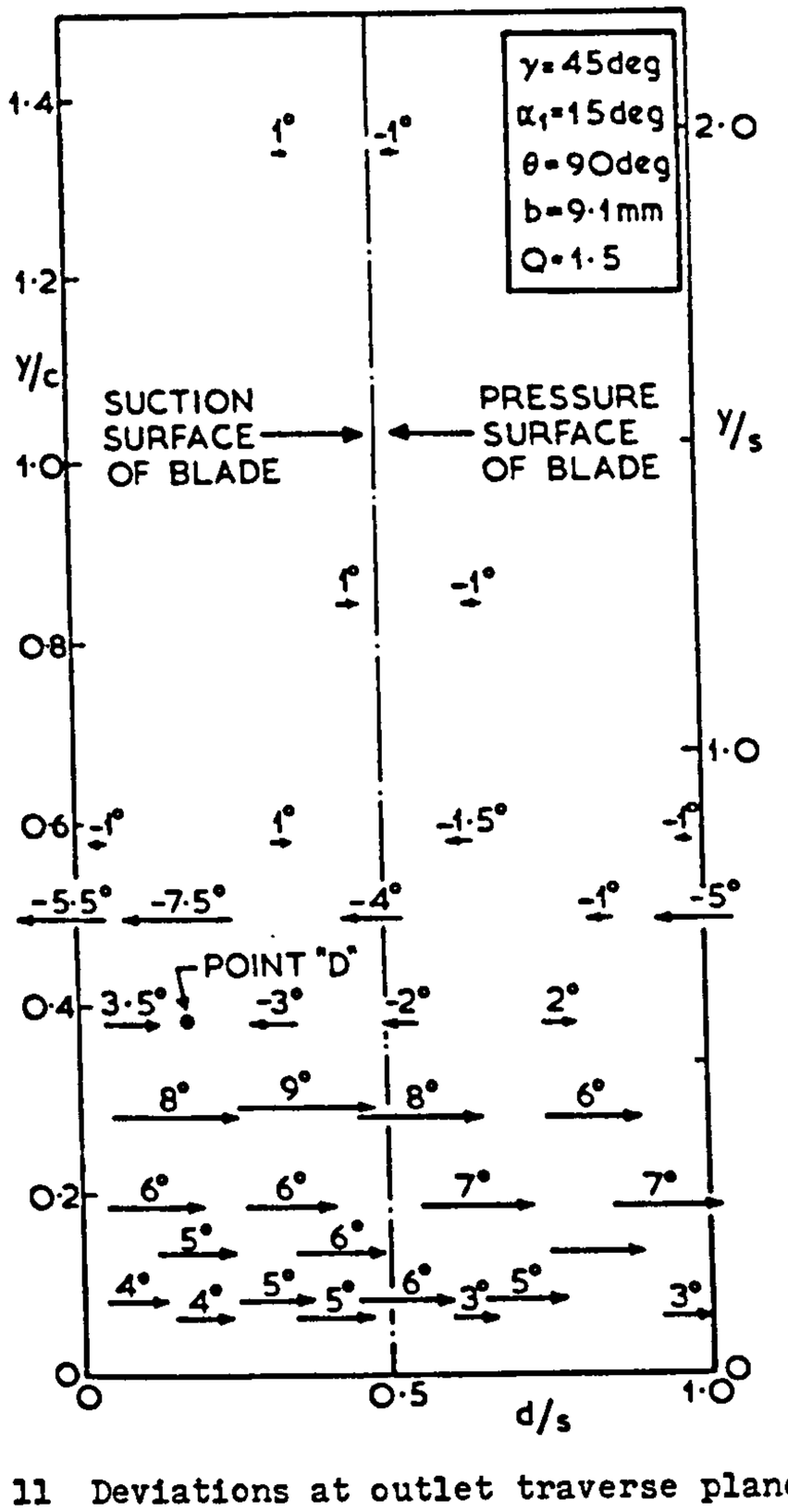

Fig. 11 Deviations at outlet traverse plane -- with transverse injection (location of measurement is tail of arrow)

tinuation of the vortex observed in the flow visualization studies which left the separation bubble in the region of point A (Fig. 1).

Integrated Stagnation Pressure Losses. To provide numerical comparisons, some form of mean values across a pitch at the various blade heights are required for the parameters of stagnation pressure loss and deviation. If sufficient points are taken, it is considered (8) that suitable averages are obtained simply by taking arithmetic mean values.

The results, thus averaged, are given in Fig. 12. The peak losses in stagnation pressure, at the various injection rates, occur at the heights along the blade where the variation in outlet angle is most influenced by the exit vortex.

The only hitherto published experimental work on the effects of transverse flows on cascade performance that has been traced is that by Deich, et al. (9). Their cascade was of impulse blading design, and their results are shown in Fig. 13 compared with the extreme injection rate results of the present work. Both sets of results are of the same form. Furthermore, the losses of Deich et al., and also those of the present work, when integrated along the blade height, are in good agreement with a one-dimensional theory given in another paper by the present authors (10).

Integrated Deviations. The deviations, integrated in the pitch direction, are shown in Fig. 14.

When transverse injection is taking place, there is positive deviation near to the end-wall. This average deviation first increases and then decreases, almost linearly, as distance from the end-wall increases. A maximum negative deviation is observed, after which the mean flow angle rises toward the value in the main stream which has been unaffected by the injec-

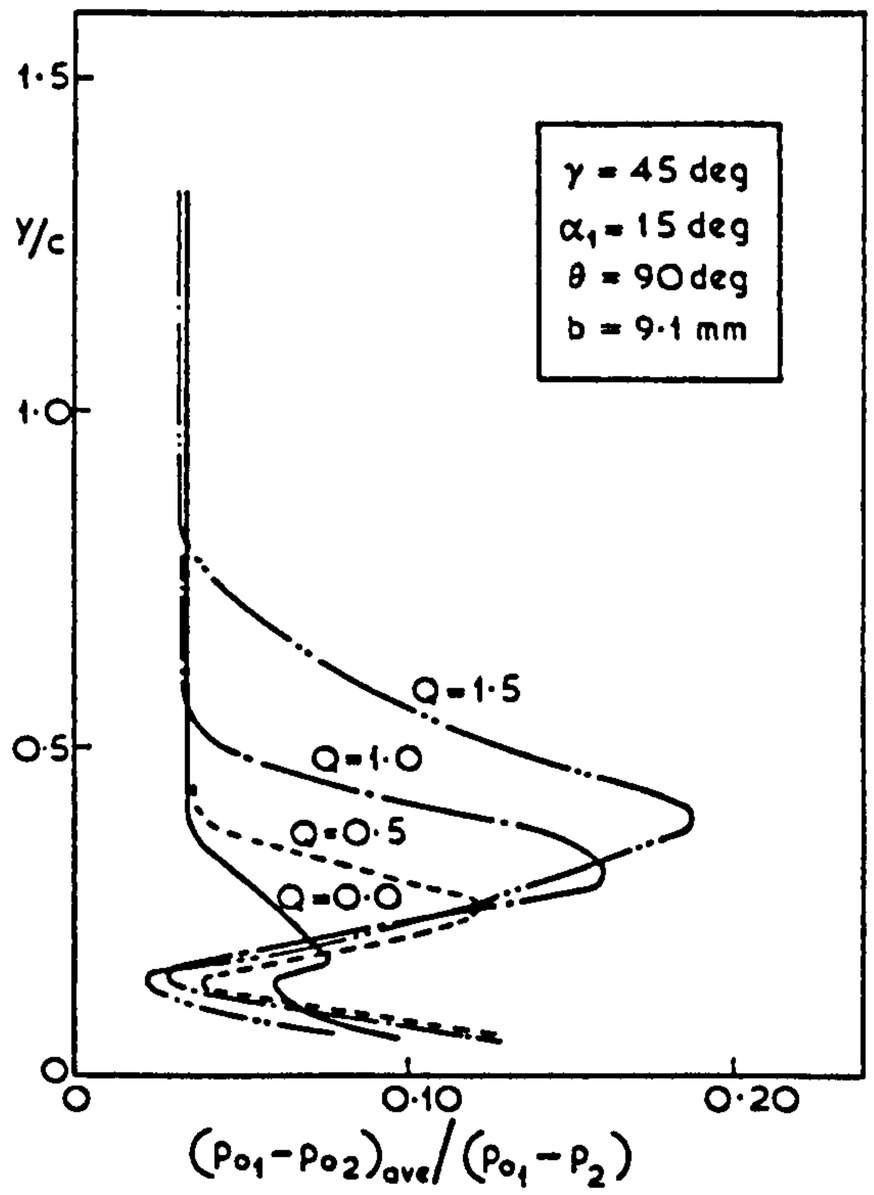

Fig. 12 Integrated stagnation pressure losses -- effect of transverse jet velocity

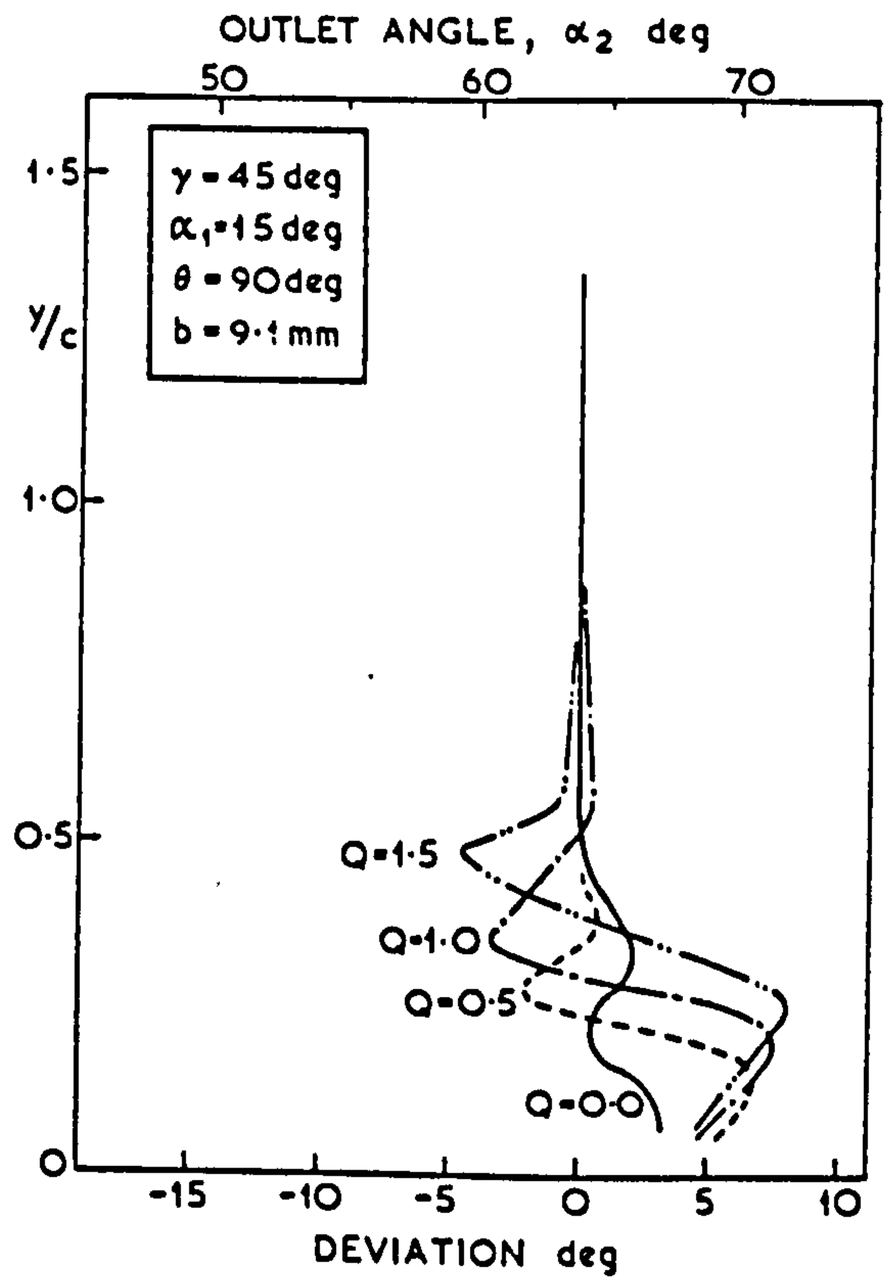

Fig. 14 Integrated deviations -- effect of transverse jet velocity

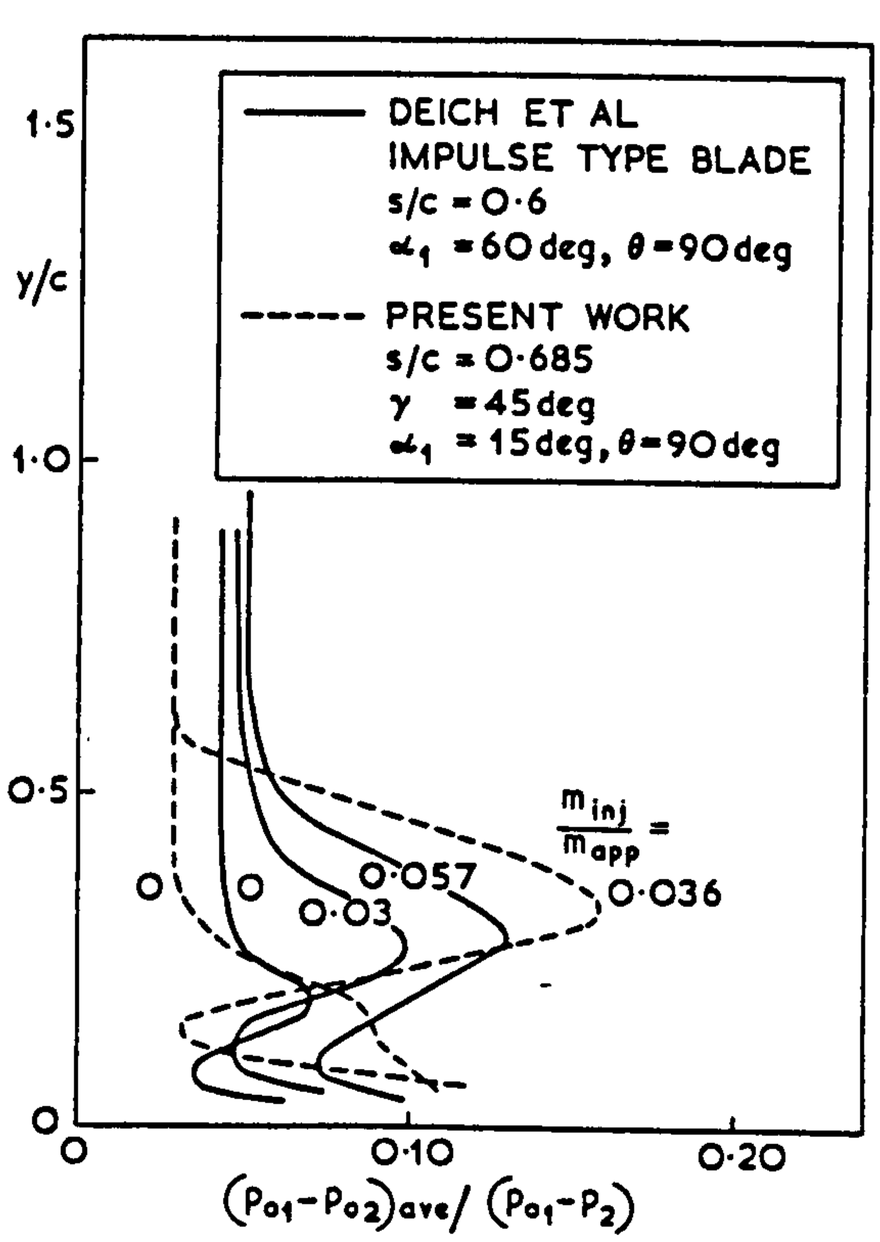

Fig. 13 Integrated stagnation pressure losses -- comparison of Deich et al. (9) and present work

tion. The mid-point between the maximum positive and maximum negative deviations represents the height of the center of the exit vortex, i.e., the height of points such as point D in Fig. 11.

CONCLUSIONS

Increasing the transverse jet velocity causes increasing disturbance to the flow within the cascade and in the exit flow. The disturbance is observed in the following effects:

1 A separation bubble appears on the cascade end-wall immediately behind the injection slot. This extends at the maximum in the present work to about 40 percent chord on the suction surface, and to about 15 percent chord on the pressure surface.

2 More pronounced secondary flows are set up within the passages of the cascade out with the boundary layer on the end-wall behind the injection slot.

3 The pressure distributions on the blades are disturbed in the vicinity of the separation bubble and of the vortex which leaves from it. The changes are such as to reduce lift.

4 A vortex-like flow appears at the suction surface end of the separation bubble and moves downstream with the main flow at a short distance from the end-wall. This vortex persists in the exit flow, causing local deviations, in the present work of up to 8 deg. The core of the vortex passes between the mid-channel and the suction surface. The direction of the vortex is away from the end-wall at the side nearest the suction surface. Associated with the vortex is a trough in the forward velocity, at worst in this cascade the velocity in the trough dropping to some 82 percent of the adjacent plateau velocities.

A subsequent paper (10) gives graphical and numerical comparisons of the effects of the parameters of injection jet velocity, jet width, jet inclination, main flow approach angle, and cascade stagger angle. In that paper, the losses of stagnation pressure across the cascade and the changes in flow capacity are compared with the predictions of a very simple one-dimensional theory.

ACKNOWLEDGMENTS

The authors wish to thank Professor R. S. Silver for his encouragement. They wish to thank the staff of Rolls-Royce (1971) Ltd. for stimulating comments. One (K.D.S.) wishes to thank the Commonwealth Scholarship Commission and the Leche Trust for grants. Both authors wish to thank the Science Research Council for financial support.

REFERENCES

1 Bourque, C., and Newman, B. G., "Reattachment of a Two-Dimensional Incompressible Jet to an Adjacent Flate Plate," The Aeronautical Quarterly, Vol. 11, 1960, pp. 201-232.

2 Wygnanski, I., and Newman, B. G., "The Reattachment of an Inclined Two-Dimensional Jet to a Flat Surface in Streaming Flow," Canadian Aeronautics and Space Institute Transactions, Vol. 1, 1968, pp. 3-8.

3 Blair, M. F., "An Experimental Study of Heat Transfer and Film Cooling on Large-Scale Turbine Endwall," ASME Paper No. 74-GT-33.

4 Mager, A., "Generalization of Boundary-Layer Momentum-Integral Equations to Three-Dimensional Flows including those of Rotating System," NACA Report No. 1067, 1952.

5 Johnston, J. P., "On the Three-Dimensional Turbulent Boundary Layer Generated by Secondary Flow," Journal of Basic Engineering, Vol. 82, 1960, pp. 233-248.

6 Mager, A., Mahoney, J. J., and Budinger, R. E., "Discussion of Boundary Layer Characteristics near the Wall of an Axial Flow Compressor," NACA Report No. 1085, 1952.

7 Horlock, J. H., "Cross Flows in Bounded Three-Dimensional Turbulent Boundary Layers," Journal of Mechanical Engineering Science, Vol. 15, 1973, pp. 274-284.

8 Ikue, T., Inoue, M., and Kuromaru, M., "Research on Two-Dimensional Retarded Cascade. Part II," Bulletin of the Japan Society of Mechanical Engineers, Vol. 15, No. 84, 1972, p. 713.

9 Deich, M. E., et al., "Influence of the Pattern of Leakage of the Medium through the Root Clearance on the Stage Efficiency," Thermal Engineering, Vol. 19, No. 6, 1972, pp. 113-116.

10 Shrivastava, K. D., and Maccallum, N. R. L., "The Effect of a Transversely Injected Stream on the Flow through Turbine Cascades: Part II -- Performance Changes."

Publication 19

77-GT-88

an ASME publication

$3.00 PER COPY
$1.50 TO ASME MEMBERS

The Effect of a Transversely Injected Stream on the Flow Through Turbine Cascades: Part II—Performance Changes

K. D. SHRIVASTAVA

Professor,
Department of Mechanical Engineering,
M.A. College of Technology,
Bhopal, India

N. R. L. MacCALLUM

Senior Lecturer,
Department of Mechanical Engineering,
University of Glasgow,
Glasgow, Scotland

This paper reports the changes in the performance of three turbine cascades when a transverse flow is injected from an end-wall into the main flow immediately in front of the cascade. The cascades used the same blade profiles, but set at stagger angles of 35, 40, and 45 deg. The effects of the following other variables were also investigated—main flow inlet angle, injection jet inclination to main flow, injection jet velocity, and jet width. The performance changes were assessed by measurements of averaged stagnation pressure losses, reductions in flow capacities, measurements of secondary flows within the channel, and measurements of the exit vortex.

Contributed by the Gas Turbine Division of The American Society of Mechanical Engineers for presentation at the Gas Turbine Conference & Products Show, Philadelphia, PA, March 27-31, 1977. Manuscript received at ASME Headquarters December 22, 1976.

Copies will be available until December 1, 1977.

THE AMERICAN SOCIETY OF MECHANICAL ENGINEERS, UNITED ENGINEERING CENTER, 345 EAST 47th STREET, NEW YORK, N.Y. 10017

The Effect of a Transversely Injected Stream on the Flow Through Turbine Cascades: Part II—Performance Changes

K. D. SHRIVASTAVA N. R. L. MacCALLUM

NOMENCLATURE

b = injection jet width
c = chord
d = distance along blade pitch from one mid-passage line to next, in direction of blade suction surface
D = measure of strength of exit vortex, defined by $(\Delta\alpha^*)(\Delta y^*/c)$
E = measure of kinetic energy of tangential components in exit vortex, defined by $(\Delta\alpha^*)^2(\Delta y^*/c)^2$
f = ratio of cascade exit mass flow to mass flow of main approach stream
F = measure of angular momentum of exit vortex, defined by $(\Delta\alpha^*)(\Delta y^*/c)^3$
k = ratio of specific heats
$\dot{m}$ = main approach mass flow rate
M = Mach number
p = pressure
Q = ratio of maximum velocity of injected jet to velocity of main approach flow
s = blade pitch
T = temperature
U = velocity of main flow outside the boundary layer
y = distance from end-wall carrying the injection slot
α = main fluid angle, measured from axial direction
γ = stagger angle
η = nozzle efficiency
θ = angle between injected jet and cascade end-wall
ρ = density
ϕ = change in angle of flow at the position of the outer edge of the end-wall boundary layer when there was no injection

Subscripts

o = stagnation
1,2 = inlet to, outlet from cascade
d = datum, i.e., with no injection
ave = average
max = maximum
ref = reference

Superscripts

' = after mixing
* = over range of maximum angular effects (integrated over pitch) of exit vortex

INTRODUCTION

When a flow is injected transversely into the main flow entering a row of turbine blades or nozzle guide vanes, as when disk cooling air in a gas turbine is returned, several significant effects in the flow are observed (1).[1] A separation bubble is formed on the end-wall of the blade passage immediately behind the injection slot. Near the blade suction surface end of this bubble, a vortex moves into the main flow and continues downstream through, and beyond, the blade row. The object of the present work was to study the effects on the performance of typical cascades of turbine blades of the variables of injection velocity, injection jet width, injection inclination to the main flow, main flow inlet angle, and cascade stagger angle. The performance parameters considered were the magnitudes of the secondary flows on the channel end-walls, the pressure distributions on the blade surfaces, the losses in stagnation pressure and efficiency of the cascades, the effective flow capacities of the cascades and the strengths of the exit vortices.

VARIABLES EXAMINED

The apparatus, which was based on a cascade of typical turbine nozzle guide vanes, was the same as that previously described (1), with the additional features that the main flow inlet angle,

[1] Underlined numbers in parentheses designate References at end of paper.

the cascade stagger angle, and the inclination and width of the injected flow to the main flow could all be varied. The aspect ratio of the cascade was 3.0. Typically, the approach velocity of the main flow was 13.6 m/sec, giving an exit velocity of about 27 m/sec. The injected flow was at the same temperature as the main flow. The combinations of variables examined are listed in Table 1. The instrumentation for examining the flow was as described in Reference (1), there being pressure measurements on the suction and pressure surfaces of the mid-blade of the cascade, velocity traverses (magnitude and direction) within the cascade passage near the end-wall behind the injection slot (mid-way between the blades and at an axial chord of 0.64), and exit traverses for velocity and direction at an axial distance downstream from the cascade of 0.92 axial chord.

Table 1 Combinations of Variables Tested

Stagger Angle γ deg	Inlet Angle α_1 deg	Injection Angle θ deg	Jet Width b mm	Jet velocity / Main velocity Q
45	15	90	9.1	1.5
				1.0
				0.5
				0.0
			5.6	1.5
				0.5
			2.4	1.5
				0.5
		60	9.1	1.5
	0	90	9.1	1.5
				0.0
	30			1.5
				0.0
40	15			1.5
				0.0
35				1.5
				0.0

RESULTS AND DISCUSSION

Only a selection of the results are illustrated in this paper, but the conclusions drawn are based on all the results.

The exit plane velocity distributions for the cases without injection and with maximum injection jet velocity (Q = 1.5) and width (b = 9.1 mm) and at the inclination (θ) of 90 deg have been given in Figs. 8 and 9, respectively, of Reference (1). The effect of reducing the inclination of the jet is seen in Fig. 1 of the present paper. These tests had been carried out with a main flow inlet angle of 15 deg. The effects of the transverse injection when the main flow inlet angle is 30 deg are seen by comparing Figs. 2 and 3 (Q = 0.0 and 1.5, respectively), and the effects at a different stagger angle (γ = 35 deg c.f. 45 deg) are seen by comparing Figs. 4 and 5.

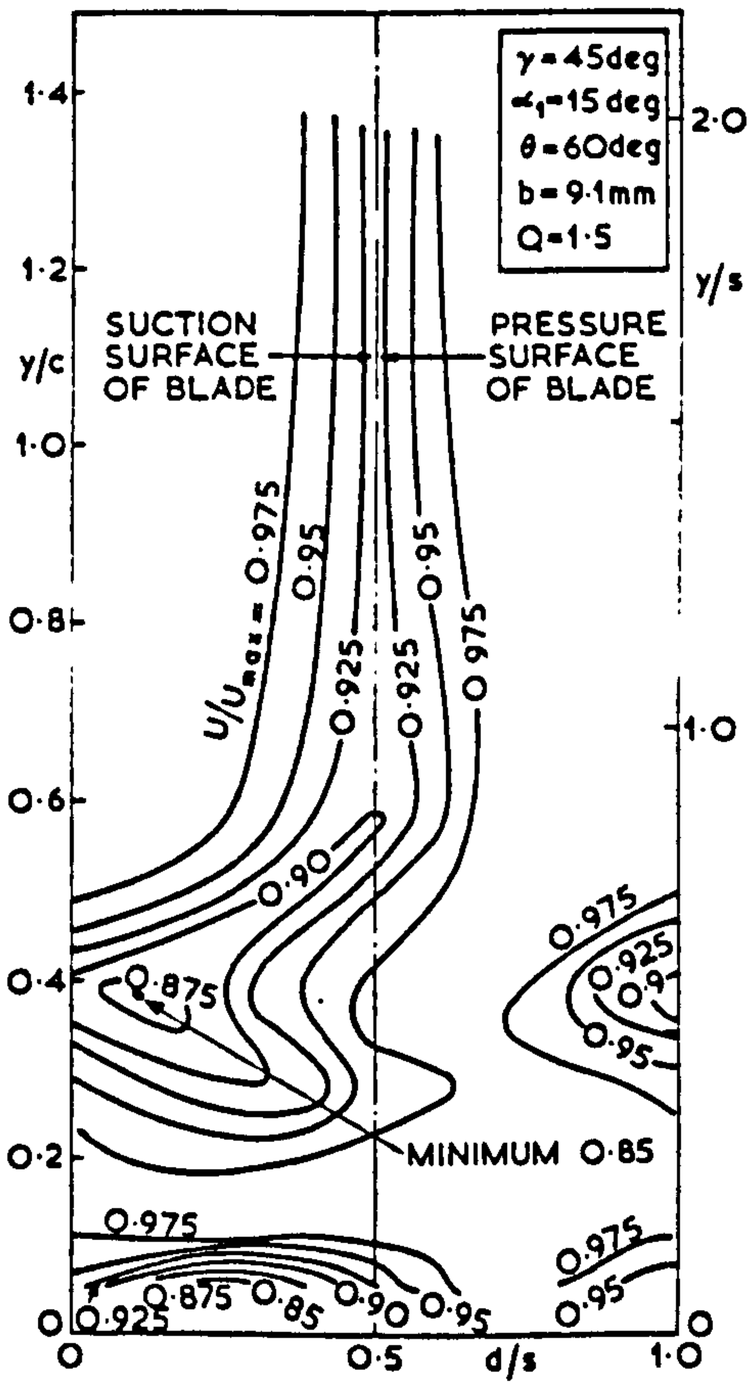

Fig. 1 Velocity contours at outlet traverse plane—injection at 60 deg

The effects of varying the injection jet width and inclination on the pitch-integrated stagnation pressure losses and pitch-integrated deviations at exit are shown in Figs. 6 and 9, respectively, the corresponding results at the different inlet angle of 30 deg are shown in Figs. 7 and 10, and those at the different stagger angle of 35 deg are shown in Figs. 8 and 11. The effects of varying the injection jet velocity at the maximum jet width, in the present apparatus, have been shown in Figs. 12 and 14 of Reference (1). Equivalent results by Deich et al. (2) are also shown in Fig. 13 of Reference (1).

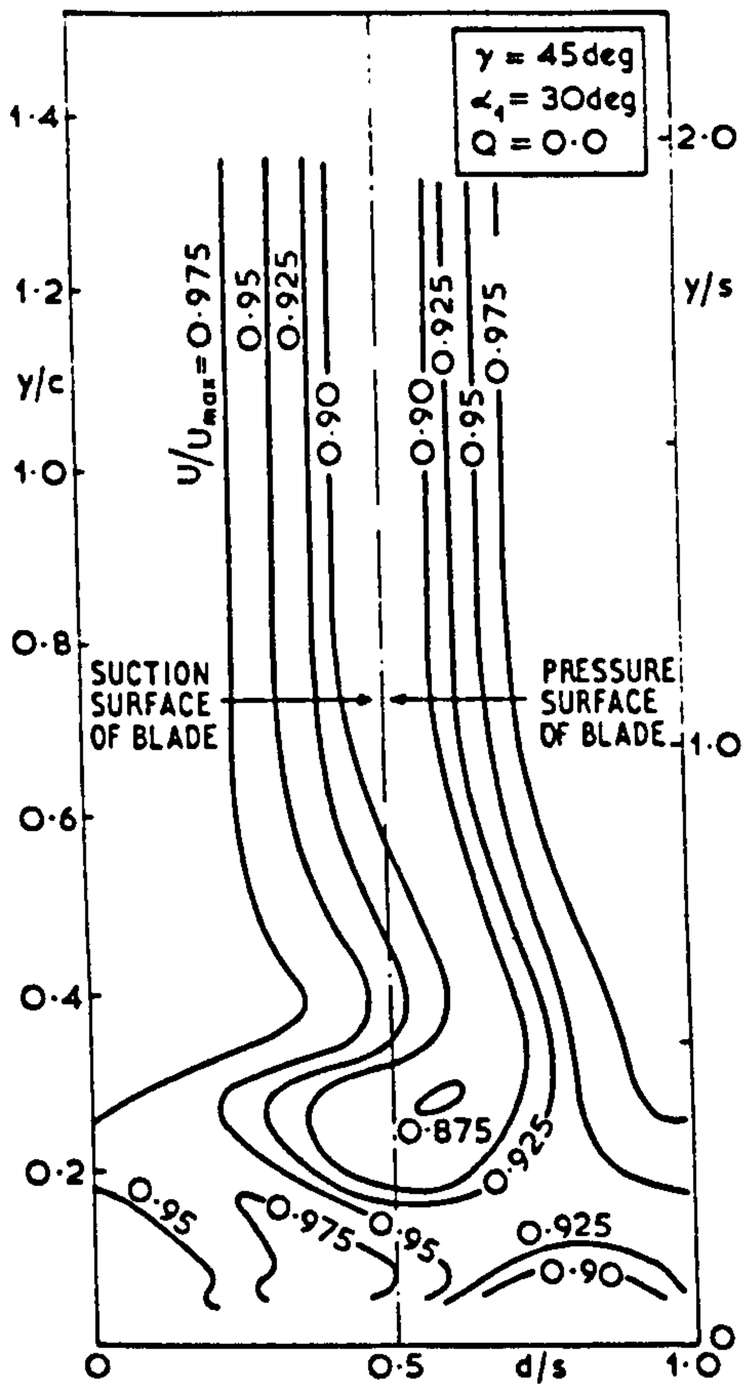

Fig. 2 Velocity contours at outlet traverse plane—main flow inlet angle 30 deg, no transverse injection

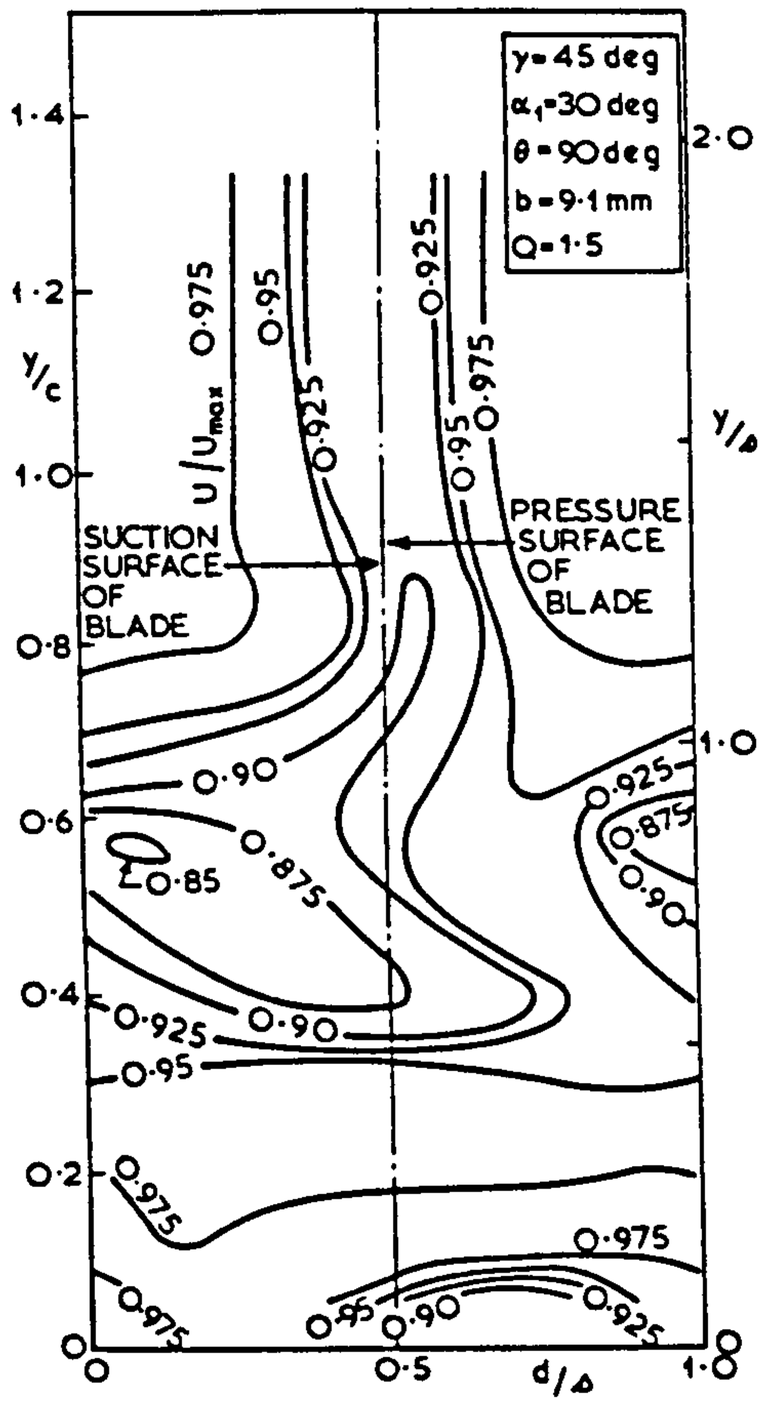

Fig. 3 Velocity contours at outlet traverse plane—main flow inlet angle 30 deg, with transverse injection

It has been found that when transverse injection is introduced, the end-wall boundary within the channel becomes less skewed and may even appear two-dimensional (1). However, there is appreciable skewing in the flow outwith the boundary layer. The measure that has been adopted of this secondary flow in the main stream is the change in the angle of the flow at the position of the outer edge of the end-wall boundary layer when there had been no injection. This parameter, ϕ, is listed in Table 2 for the various arrangements tested.

Table 2 Comparisons of End-Wall Skewing Parameter, ϕ, and of "Strengths" of Exit Vortex

Cascade and Jet Parameters				End-wall skewing Parameter	Exit Vortex Parameters		
γ deg	α_1 deg	Q	θ deg	ϕ deg	D/D_{ref}	E/E_{ref}	F/F_{ref}
45	15	1.5	90	12	1.0	1.0	1.0
		1.0		9	0.59	0.35	0.28
		0.5		3.7	0.46	0.21	0.19
	30	1.5		21	1.39	1.94	2.42
	0			6.9	0.53	0.28	0.26
40	15			12	1.18	1.40	1.91
35				16	1.75	3.03	5.2
45			60	4.5	0.67	0.44	0.49

The reference values (D_{ref} etc) are the values of the parameters obtained with the reference geometry (γ = 45 deg, α_1 = 15 deg, θ = 90 deg) and with Q = 1.5.

For all the above cases, the injected jet width, b, was 9.1 mm.

Effects of Test Variables

In general, it is found that if a variable is altered in a manner to increase, say, the separation bubble size, then more pronounced secondary flows within the passage are observed adjacent to the end-wall behind the injection slot, the area of the blade surfaces over which the pressure distribution is affected is increased, the strength of the vortex in the exit flow is increased, its location moves further away from

the end-wall, and the trough in the forward velocity in the center of the vortex becomes more pronounced. All the foregoing effects are implied when, in the discussion which follows, a change in a variable is said to cause a "deterioration" in the flow.

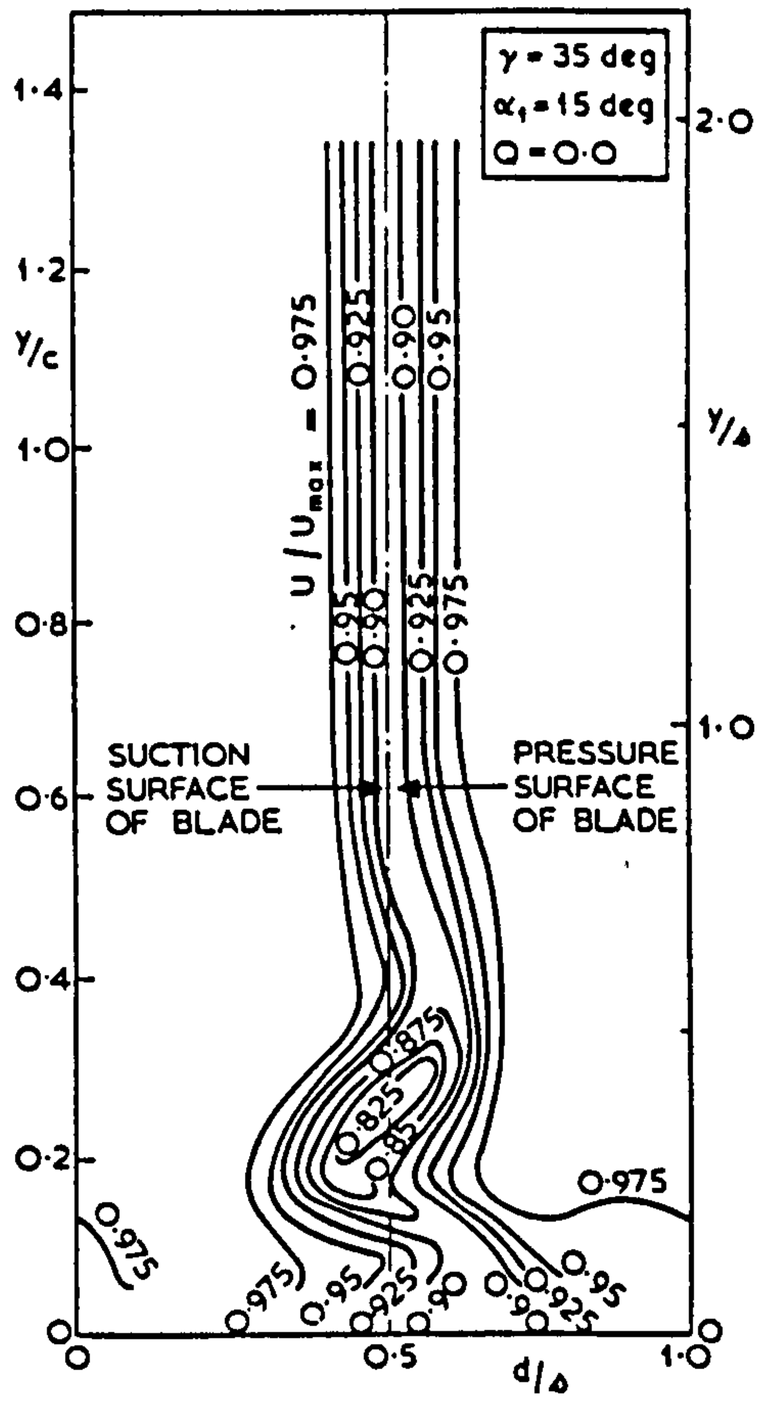

Fig. 4 Velocity contours at outlet traverse plane—stagger angle 35 deg, no transverse injection

The flow in the cascade deteriorates as the velocity of the transverse jet increases and as the width of the jet increases. The deteriorations, within the accuracy of the tests, may be taken as linear with these variables. Thus, the deterioration is proportional to the volume flow (or mass flow) rate of the injected jet.

Reducing the inclination of the injected jet to the main flow lessens the deterioration, although not, perhaps, to the extent suggested by the simple theory discussed in the following sections.

Increase of the main flow inlet angle, with a consequent increased turning angle within the cascade, is accompanied by a more significant deterioration of the flow under transverse injection conditions.

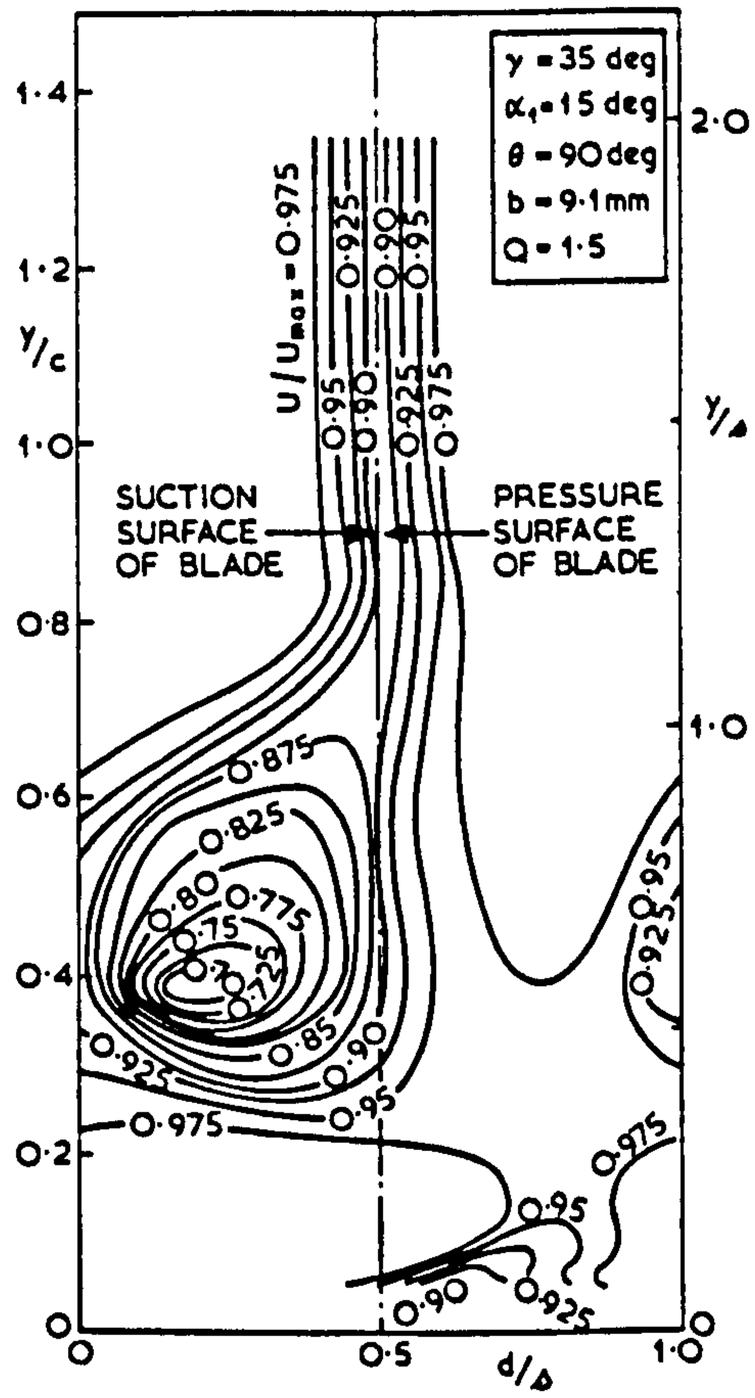

Fig. 5 Velocity contours at outlet traverse plane—stagger angle 35 deg, with transverse injection

When the stagger angle of the cascade is reduced to 40 deg and then 35 deg, the effect of transverse injection is to cause progressively more marked deteriorations in the flow.

Stagnation Pressure Losses—Comparison with One-Dimensional Theory

A simple one-dimensional theory is given in the Appendix which relates the losses in stagnation pressure and the changes in flow capacity of the cascade to the parameters defining the transversely injected flow. The treatment given in the Appendix is for incompressible flow (valid for the present work) and includes the inclination of the jet to the main flow as a variable. A compressible flow treatment, but restricted to injection at 90 deg only, has been given by Barnes and Fray (3).

In both these theories, the effect of the cascade is ignored and the main flow is assumed to maintain its direction without change of cross-sectional area during mixing.

The loss in stagnation pressure, predicted by the incompressible theory, is,

$$-\Delta p_o = \tfrac{1}{2} \rho U_1^2 \left[(f^2 - 1) - 2 (f - 1) Q \cos\theta \cos\alpha_1 \right] \qquad (1)$$

The corresponding results from the compressible flow analysis (3), with $\theta = 90$ deg, is

$$\frac{p_o - p_o'}{p_o} = -\frac{\Delta p_c}{p_o} = k M^2 \left[f \left(\frac{T_o'}{T_o} \right)^{\frac{1}{2}} - 1 \right] \qquad (2)$$

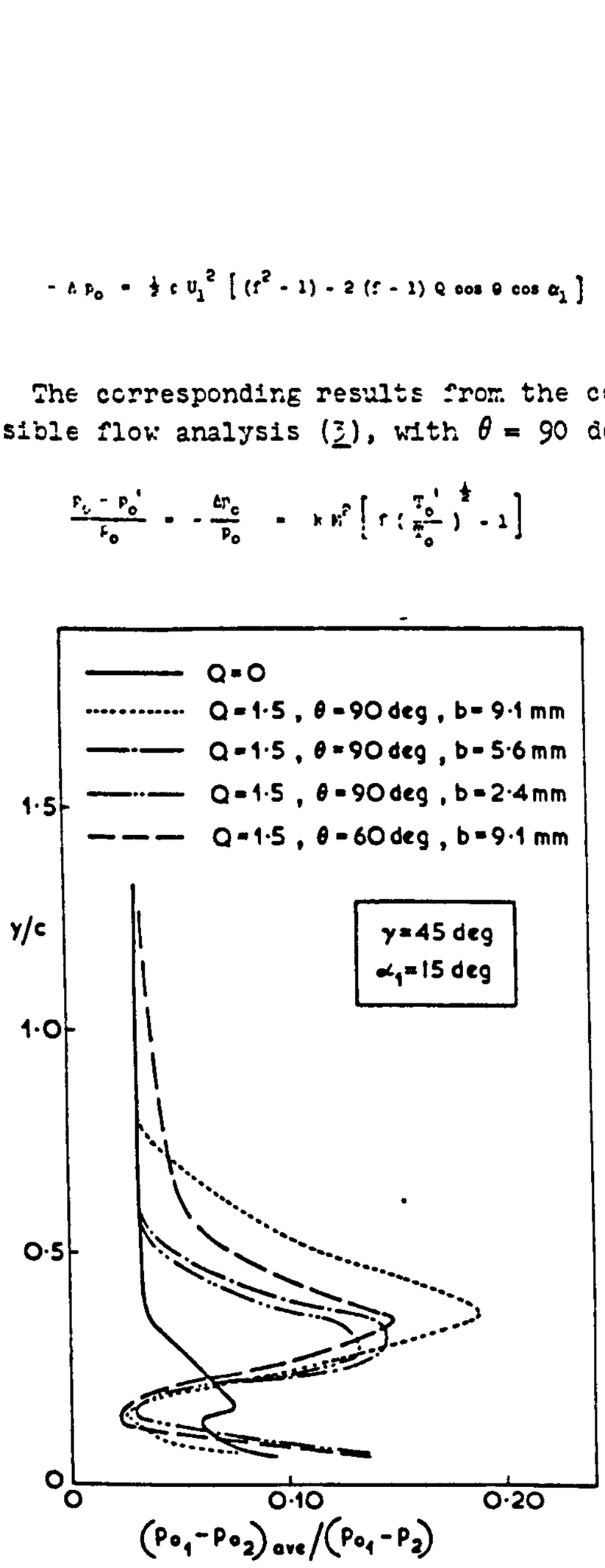

Fig. 6 Integrated stagnation pressure losses— effects of jet width and jet inclination

Equation (2), with T_o and T_o' equal, and for incompressible flow, reduces to equation (1) for the case of $\theta = 90$ deg. It is to be noted that for this case of $\theta = 90$ deg, the loss in stagnation pressure is a function only of the ratio of the injected mass flow to the main approach flow ($f - 1$) and of the inlet velocity head. The predicted loss is independent of cascade parameters such as aspect ratio.

The results of the comparison are given in Fig. 12, where the observed losses in stagnation pressure are plotted to a base of the losses predicted by equation (1). The observed losses were obtained by comparing integrations across the exit traverse plant with and without injection. Allowing for the inevitable error arising from comparing two similar values of averaged losses (the largest observed increase in losses amounted

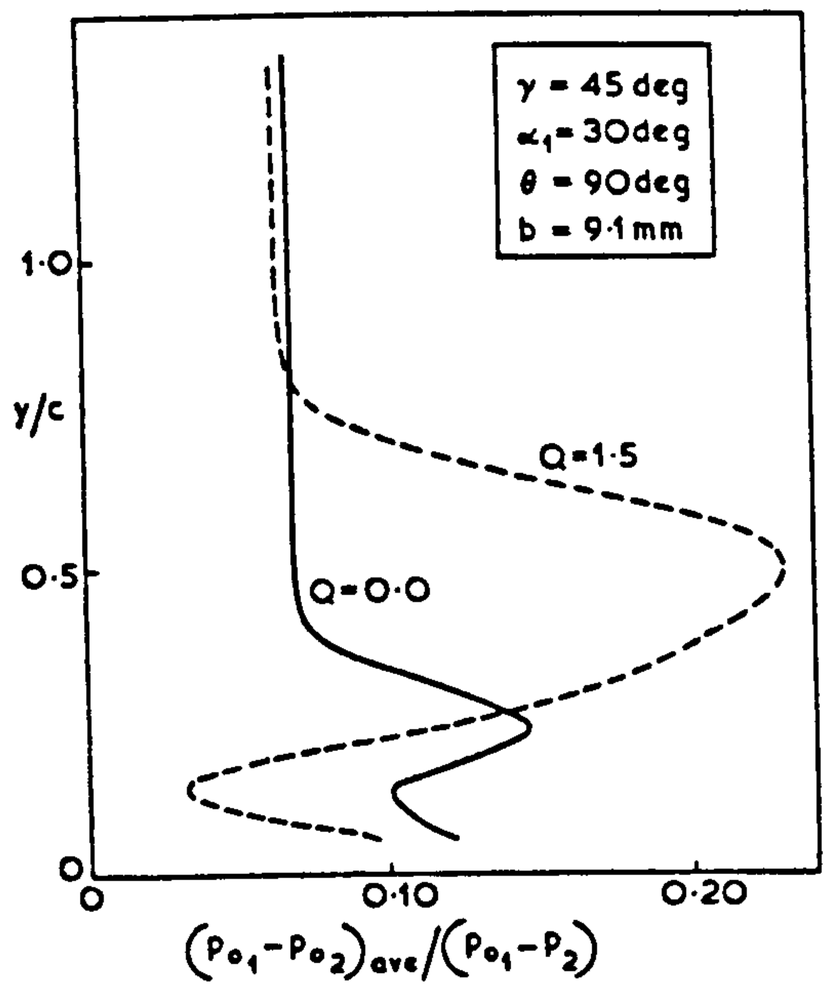

Fig. 7 Integrated stagnation pressure losses for main flow inlet angle of 30 deg

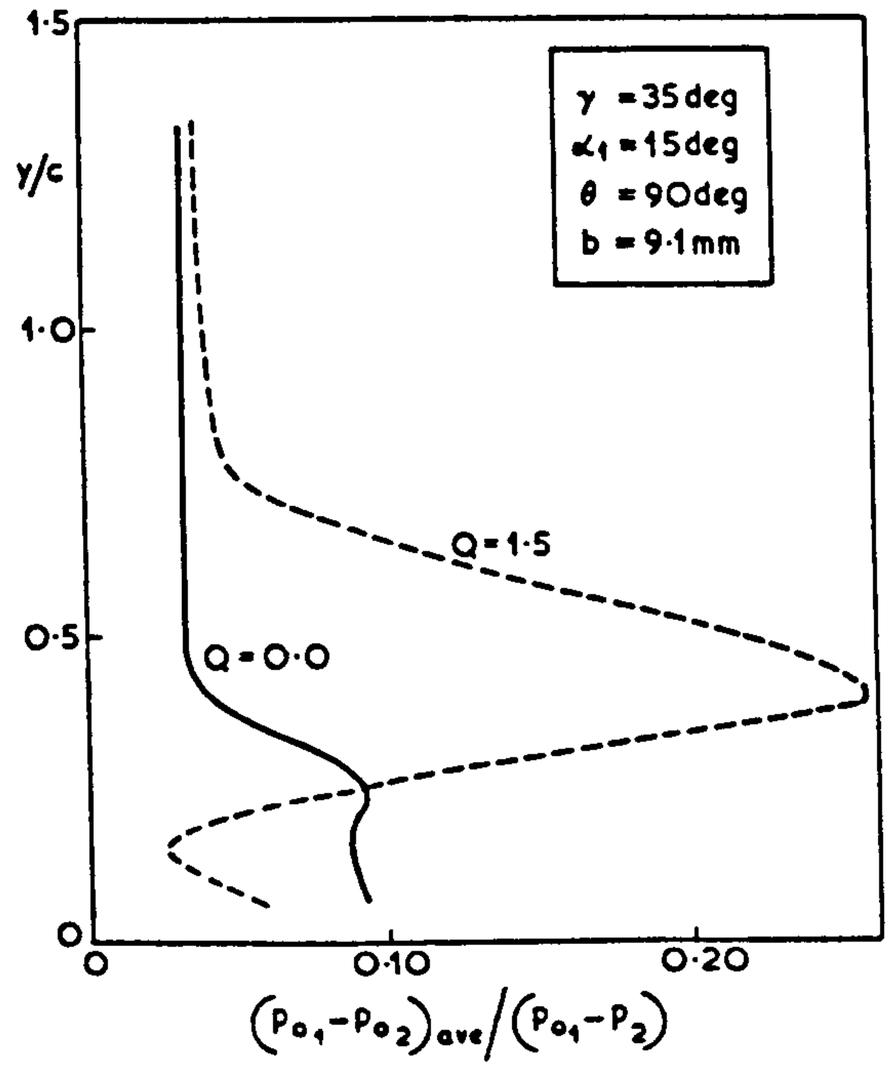

Fig. 8 Integrated stagnation pressure losses for cascade stagger angle of 35 deg

to 30 percent of the datum losses), the agreement is very good for the cases where $\theta = 90$ deg. The experimental losses where $\theta = 60$ deg are lower than for the $\theta = 90$ deg case, but the reduction is not as large as the 70 percent predicted by equation (1).

The simple theory has also been applied to the arrangement tested by Deich et al. (2), and

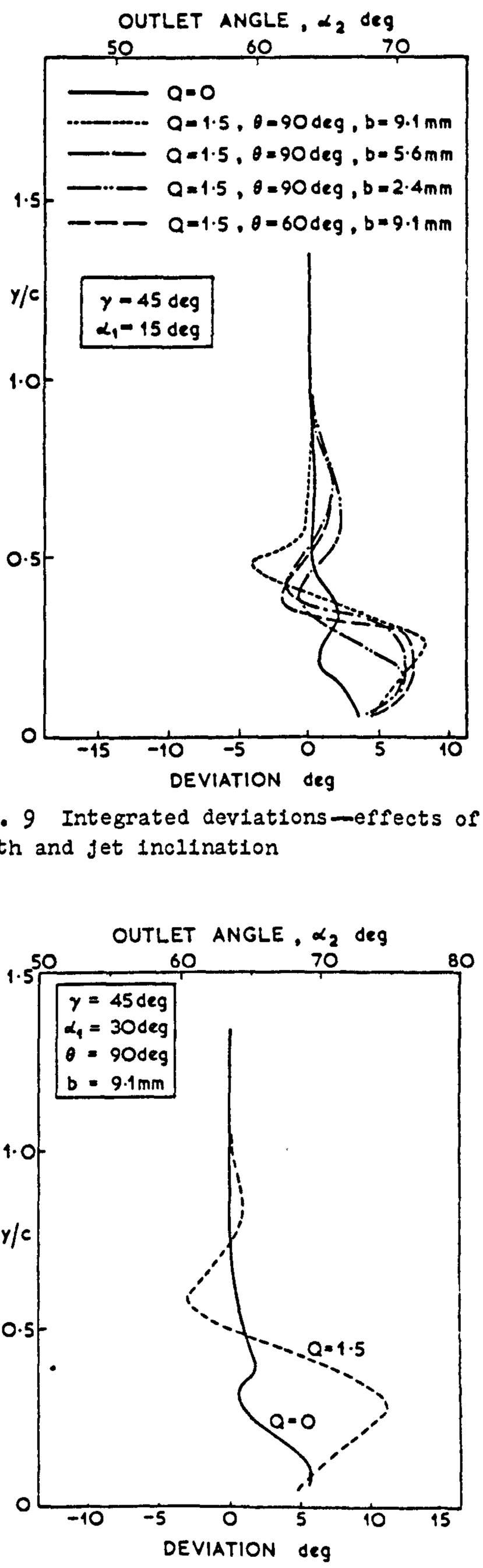

Fig. 9 Integrated deviations—effects of jet width and jet inclination

Fig. 10 Integrated deviations for main flow inlet angle of 30 deg

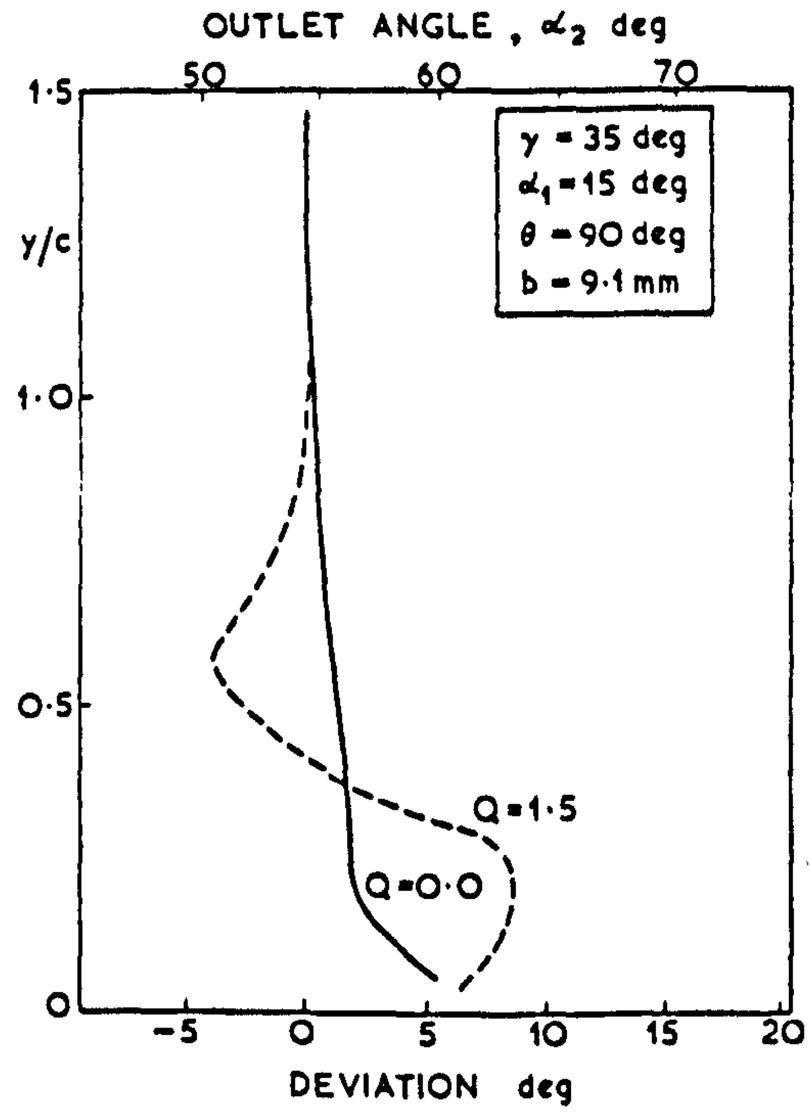

Fig. 11 Integrated deviations for cascade stagger angle of 35 deg

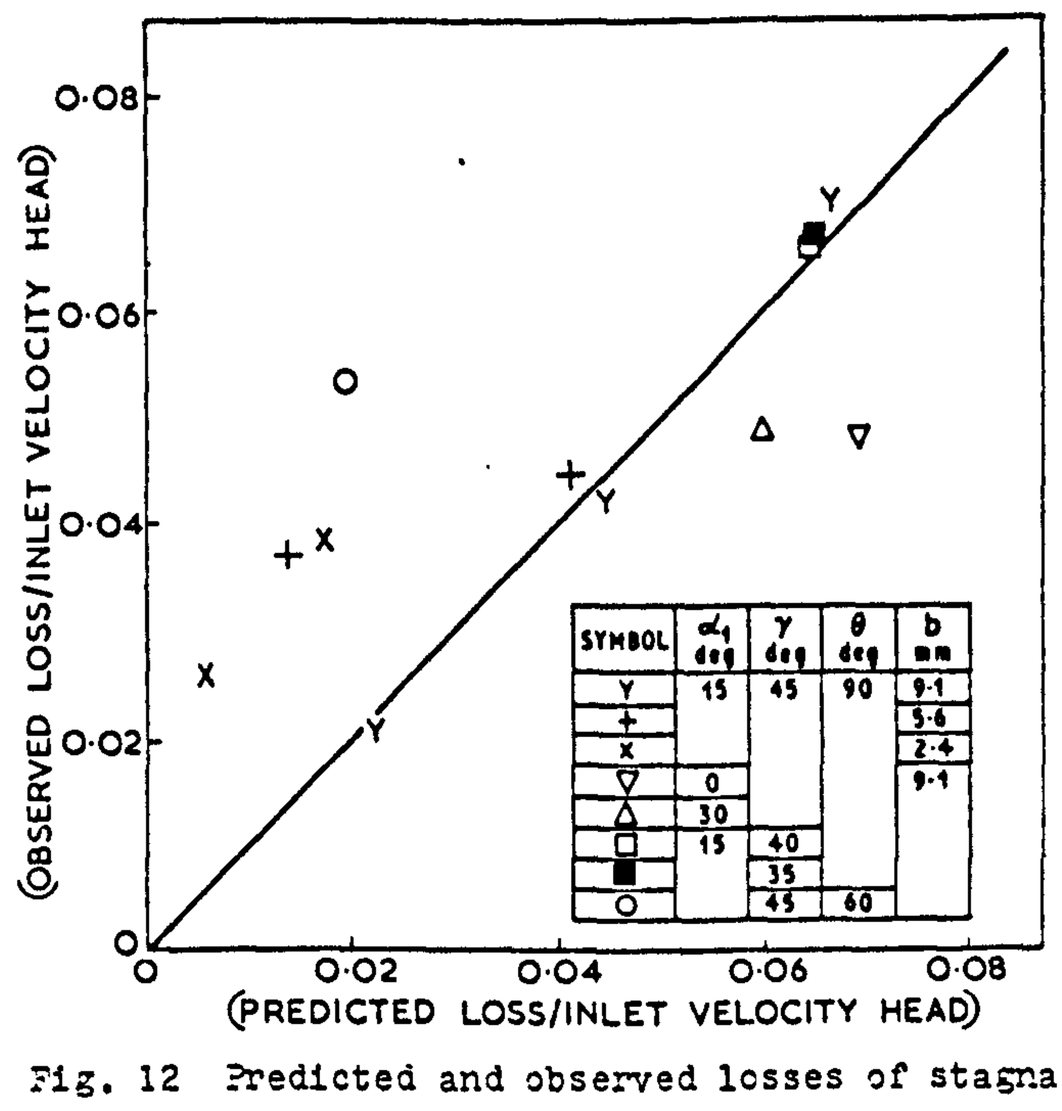

Fig. 12 Predicted and observed losses of stagnation pressure—effect of transverse injection

here too, good agreement was obtained between the predicted and observed losses.

It is valuable to express the increase in losses in terms of a reduction in nozzle guide vane efficiency. The nozzle efficiency is taken for this incompressible flow case as

$$\eta = 1 - \frac{p_{o_1} - p_{o_2}}{p_{o_1} - p_2} \qquad (3)$$

On this basis, the efficiency of the nozzle in the present work when $\gamma = 45$ deg and $\alpha_1 = 15$ deg and without transverse injection is measured as 0.958. When the transverse flow is introduced at 90 deg at the maximum velocity ($Q = 1.5$) and maximum jet width ($b = 9.1$ mm), the observed nozzle efficiency drops to 0.948. (Under these conditions, the injected flow was 3.6 percent of the approach flow.)

Cascade Flow Capacity—Comparison with One-Dimensional Theory

For the same approach mass flow in the main stream, the cascade exit static pressure has to be lowered when the transverse flow is introduced by an amount given by (see Appendix)

$$-\Delta p_2 = \tfrac{1}{2}\rho U_1^2 \left[(f^2 - 1) - 2(f - 1) Q \cos\theta \cos\alpha_1 \right] + (f^2 - 1)(p_{o_1} - p_{2d}) \qquad (4)$$

This reduction in the exit static pressure for the same main flow is a measure of the lowering of the flow capacity of the cascade, when expressed in terms of the main flow as a function of the cascade pressure drop.

The results of the present tests are compared with the predictions of equation (4) in Fig. 13. There is good agreement for all cases, including that with injection at 60 deg. The dominant term on the right side of equation (4) is the second term, this being about 80 to 85 percent of the total predicted reduction in static pressure.

For the case of maximum injection (3.6 percent) at 90 deg, the observed required reduction in exit static pressure for the same main flow is 6.8 percent of the original cascade pressure drop. Thus, the reduction in flow capacity for an unchanged pressure drop is 3.4 percent, reckoned on the main approach flow. The prediction of equation (4) is slightly greater than this—a 4.2 percent reduction.

Exit Vortex—Quantitative Comparisons

Pronounced vortices have been observed in the cascade exit flow. When a vortex exists in a flow approaching a row of blades, then this vortex appears to maintain its existence and "bounces off" the blades, causing local flow distortion and separation (4, 5). These effects have apparently only been observed qualitatively. It is likely that if vortices such as those observed in the present work are created at some intermediate row of blades in a turbine, then they may cause significant disturbances in the subsequent blade rows in the machine.

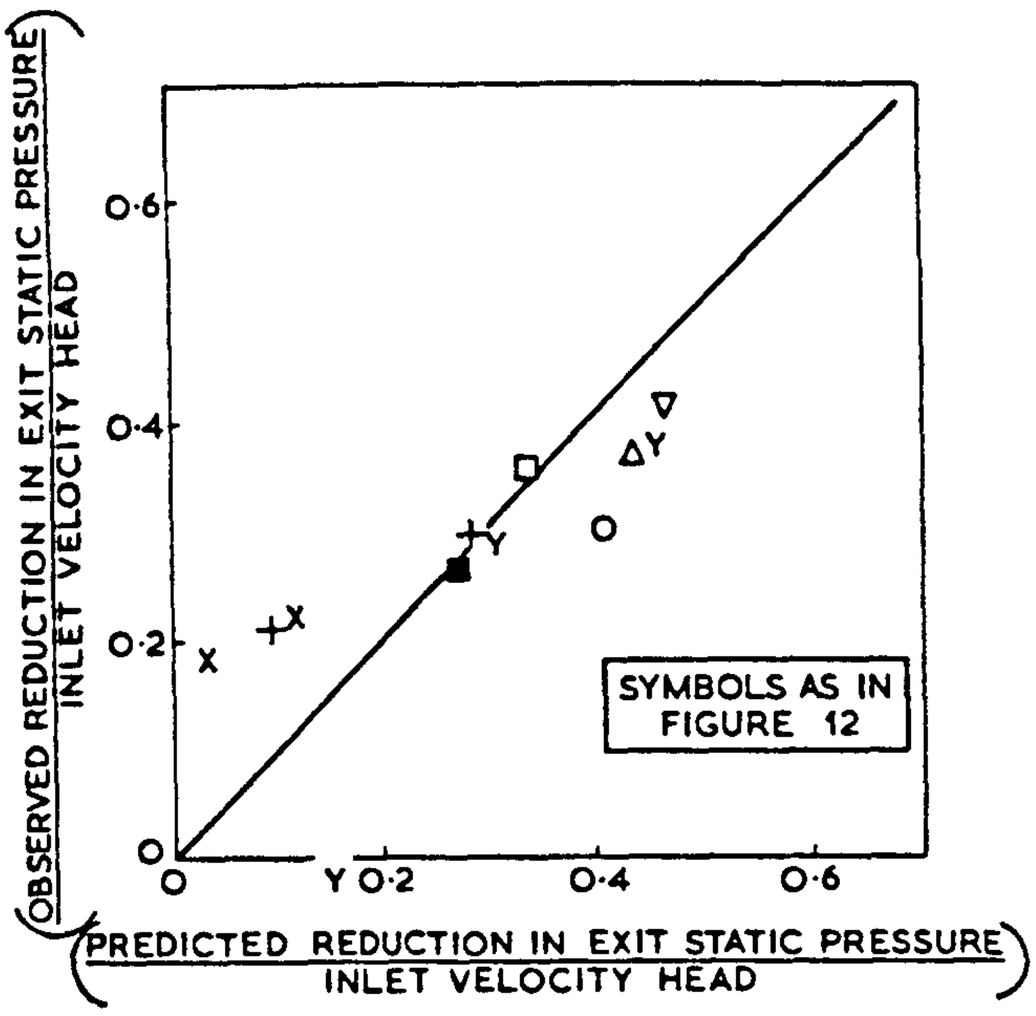

Fig. 13 Predicted and observed changes in downstream static pressure—effect of transverse injection

It is desirable to have some quantitative indication of the effects of the test variables on the "potential" of the vortex for disturbing subsequent flows. Three possible measures for this "potential" are suggested here—the circulation, the kinetic energy of the tangential velocity components in the vortex, and the angular momentum of the vortex. If the vortex is assumed to be in solid body rotation, bounded in diameter by the positions of maximum pitch-integrated positive and negative deviations, then three parameters, D, E, and F, which are proportional to the foregoing measures, respectively, are defined by

$$D = (\Delta\alpha^\circ)(\Delta V^\circ/c) \qquad (5)$$

$$E = (\Delta\alpha^\circ)^2(\Delta V^\circ/c)^2 \qquad (6)$$

$$F = (\Delta\alpha^2)(\Delta^\circ/c)^3 \qquad (7)$$

The results of applying these equations are shown in Table 2 where the values of D, E, and F for various arrangements are compared with Reference Values, these being for the cascade having $\gamma = 45$ deg, $\alpha = 15$ deg with injection at 90 deg at the maximum rate ($Q = 1.5$, $b = 9.1$ mm).

The cases where there was no transverse injection have been omitted, as under these conditions there were no clearly defined exit vortices of size comparable to those observed when there was transverse injection.

As can be seen, parameter D increases almost linearly with jet velocity. Parameters E and F increase more rapidly. The exit vortex is strengthened when the main flow inlet angle is increased to 30 deg, and very markedly increased when the stagger is reduced. Reducing the inclination of the transverse jet to 60 deg roughly halves the strength of the vortex. The changes are in reasonable quantitative agreement with the changes in the end-wall skewing parameter, ϕ.

CONCLUSIONS

The cascade variables of inlet angle and stagger angle affect the disturbance, as described in Reference (1), caused by transverse injection. Increasing the inlet angle slightly increases the disturbance, while reducing the stagger angle produces a more marked increase in disturbance.

Variation of the injected jet variables of velocity and jet width indicates that the extent of the deterioration of the flow resulting from injection is almost proportional to the injected mass flow.

Reducing the inclination of the injected jet from 90 to 60 deg roughly halves the disturbance.

For the cascade itself, the changes in efficiency and in flow capacity are in close agreement with a simple one-dimensional theory. In a typical case, injection at 90 deg of a flow amounting to 3.6 percent of the main approach flow causes a reduction in nozzle efficiency of 1 percent and a reduction in the flow capacity (expressed in terms of the main approach flow) of 4 percent.

It is likely that the strong exit vortex, which is present in the flow leaving the cascade, will cause a deterioration in the flow through subsequent blade rows in the turbine. No quantitative data are yet known on the extent of this effect.

APPENDIX

ONE-DIMENSIONAL THEORY FOR LOSSES IN STAGNATION PRESSURE AND FLOW CAPACITY

The theory given in the following is an extension to that of Barnes and Fray (3) in that angles of injection other than 90 deg and main flow inlet angles of other than zero deg are included. It is more restrictive in that it is limited to incompressible, uniform temperature flow.

It is assumed that the mixing takes place extremely rapidly and is completed before the flow enters the cascade. Thus, it is assumed that the main flow retains its approach direction during the mixing.

Momentum balance between the planes before injection and after mixing gives (Fig. 14)

$$p_2 - p' = \rho U_1^2 \left[(f^2 - 1) - (f - 1) Q \cos\theta \cos\alpha_1 \right] \qquad (8)$$

The loss in stagnation pressure between these planes is then

$$-\Delta p_0 = \tfrac{1}{2} \rho U_1^2 \left[(f^2 - 1) - 2 (f - 1) Q \cos\theta \cos\alpha_1 \right] \qquad (1)$$

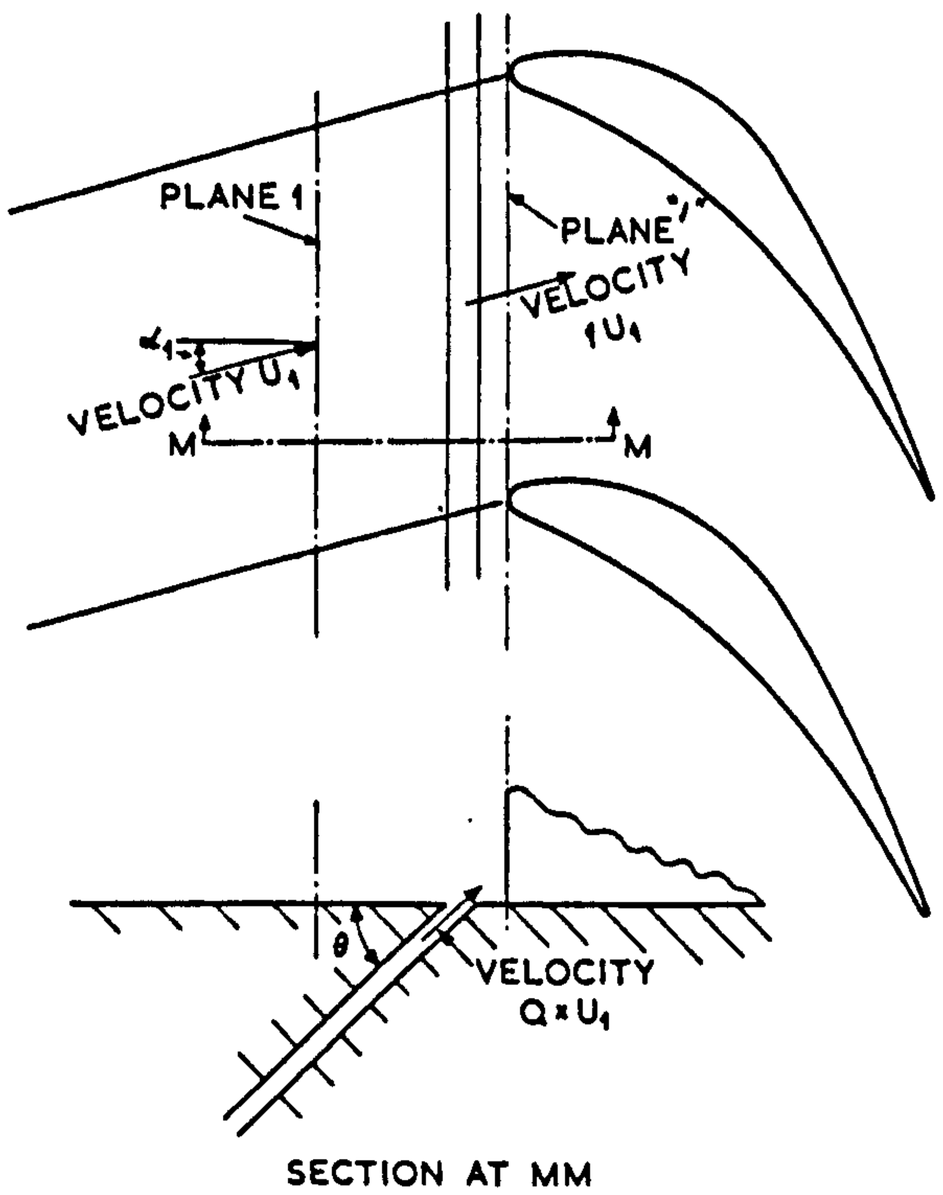

Fig. 14 Model for one-dimensional mixing

The loss of flow capacity in the cascade can be expressed in terms of the reduction in approach main flow for the same pressure drop across the cascade from inlet stagnation to outlet static conditions. It can also be expressed, for this non-choked cascade, in terms of the reduction in exit static pressure for the same main approach flow. The exit static pressure has to

be lower due to two effects: (a) there is the loss in stagnation pressure due to injection, given by equation (1); and (b) the cascade threat has to accommodate the total flow, and this will require an increased pressure drop. Summing these effects gives

$$-\Delta p_2 = \tfrac{1}{2}\rho U_1^2\left[(r^2-1) - 2(r-1)Q\cos\theta\cos\alpha_1\right] + (r^2-1)(p_{o_1} - p_{2d}) \quad (4)$$

The foregoing expression provided a useful comparison of flow capacities in the present work. The corresponding expression giving the flow capacity changes in terms of main approach flow changes for the same cascade pressure ratio (or drop) is

$$-\frac{\Delta\dot{m}}{\dot{m}} = \tfrac{1}{2}\left(-\frac{\Delta p_2}{p_{o_1} - p_{2d}}\right) \quad (9)$$

the term $(-\Delta p_2)$ having been obtained using equation (4).

ACKNOWLEDGMENTS

The authors wish to thank Professor R. S. Silver for his encouragement. They wish to thank staff of Rolls-Royce (1971) Ltd. for stimulating comments. One (K.D.S.) wishes to thank the Commonwealth Scholarship Commission and the Leche Trust for grants. Both authors wish to thank the Science Research Council for financial support.

REFERENCES

1 Shrivastava, K. D., and Maccallum, N. R. L., "The Effect of a Transversely Injected Stream on the Flow Through Turbine Cascades: Part I—Flow Effects," ASME Paper No. 77-GT-87.

2 Deich, M. E., et al., "Influence of the Pattern of Leakage of the Medium Through the Root Clearance on the Stage Efficiency," Thermal Engineering, Vol. 19, No. 6, 1972, pp. 113-116.

3 Barnes, J. R., and Fray, D. E., "An Experimental High Temperature Turbine, Part II. The Effects of Cooling on the Aerodynamic Performance," Aeronautical Research Council R&M. No. 3405, 1965.

4 Herzig, H. Z., Hansen, A. G., and Costello, G. R., "A Visualization Study of Secondary Flows in Cascades," NACA Report No. 1163, 1954.

5 Hansen, A. G., and Herzig, H. Z., "Secondary Flows and Three-Dimensional Boundary Layer Effects," NASA S.P. 36, 1965, pp. 385-411.

LAND SEA AIR SPACE

SOCIETY OF AUTOMOTIVE ENGINEERS, INC.
400 Commonwealth Drive, Warrendale, Pa. 15096

Transient Expansion of the Components of an Air Seal on a Gas Turbine Disc

N. R. L. Maccallum
Dept. of Mechanical Engrg.,
Univ. of Glasgow (Scotland)

Society of Automotive Engineers

Aerospace Meeting
Airport Sheraton Inn, Los Angeles
November 14-17, 1977

770974

770974

Transient Expansion of the Components of an Air Seal on a Gas Turbine Disc

N. R. L. Maccallum
Dept. of Mechanical Engrg.,
Univ. of Glasgow (Scotland)

WHEN A GAS TURBINE has its speed suddenly changed, some time may elapse between the turbine reaching its new speed and the performance stabilising. The progress of the turbine towards its stabilised performance, after reaching its new speed, can be called the "thermal soak" transient (1)*. Factors which influence this transient are (i) non-adiabatic compressions and expansions (ii) altered blade tip clearances due to differential rates of expansions (iii) altered seal clearances due to differential rates of expansion (iv) altered critical flow areas e.g. at nozzle guide vanes. This paper describes a theoretical investigation of one of these factors - the expansions of the components of an air seal on a turbine disc during and following an acceleration from Ground Idling Speed to Maximum Speed, and the contractions during and following a deceleration back to the Idling Speed. The gas turbine investigated is a typical two-spool by-pass jet engine.

DESCRIPTION OF SEAL

The Seal is illustrated in Fig. 1. The Seal is formed between the tips of four fins which are integral with the Turbine Disc (of the No. 1 High Pressure Turbine) and a Stationary Ring mounted on the partition wall, A. High Pressure Cooling Air (taken from the delivery of the High Pressure Compressor) is supplied to the left side of the Seal (as viewed in Fig. 1). The purpose of the Seal is to allow a small, controlled flow of this Cooling Air to pass through Zone B, cooling the face of the Turbine Disc and then leaving through the gap between the downstream edge of the platforms of the first set of High Pressure Nozzle Guide Vanes (H.P.1 N.G.V's) and the front edge of the platforms of the first set of High Pressure Blades (H.P.1 blades). The outward flow of

* Numbers in parentheses designate References at end of paper.

ABSTRACT

Using simple finite-difference models with appropriate boundary conditions, methods have been developed for predicting the movements of the critical components of an air seal on the face of the first High Pressure Turbine Disc of a typical two-spool Gas Turbine. The methods have been applied to two testing transients - the acceleration and the deceleration between the Ground Idling and Maximum Speeds. In the acceleration, seal openings of double the equilibrium value are predicted to persist for 30 s after completion of the speed transient.

cooling air prevents the ingress of hot turbine gases.

At Maximum Speed the radial clearance between the tips of the fins mounted on the Turbine Disc and the inner surface of the Stationary Ring should be between 0.13 mm and 0.23 mm.

The Turbine Disc material is Incoloy 901, chosen for creep strength properties, while the Stationary Ring is made from a Martensitic Stainless Steel.

The radial expansions of the Fins on the Disc and of the Stationary Ring from cold, stationary, to equilibrium at the Maximum Speed are given in Table 1.

Using the results given in Table 1, the cold radial clearance is then (0.18 + 1.37 - 0.82), i.e. 0.73 mm.

MODEL FOR TURBINE DISC

The transient temperature response of the Disc has been predicted by a simple finite-difference method using nodal resistance networks. The geometry of the disc has been approximately represented by the model shown in Fig. 2, the model consisting of 20 equal radial increments, each annular ring so formed being divided in the axial direction into 10 elements.

The Boundary conditions at the various faces are discussed below.

BOUNDARY CONDITION: DISC FACE 1 - The mechanism of heat transfer to this Face can be considered to be that to a rotating disc adjacent to a stationary surface (wall A), the outer periphery of the system being shrouded with a small clearance (between the platforms of the N.G.V's and Blades) and with an outward flow of coolant air. The heat transfer and/or drag characteristics of this and other systems having some similarities to it have been studied by several workers (2) -

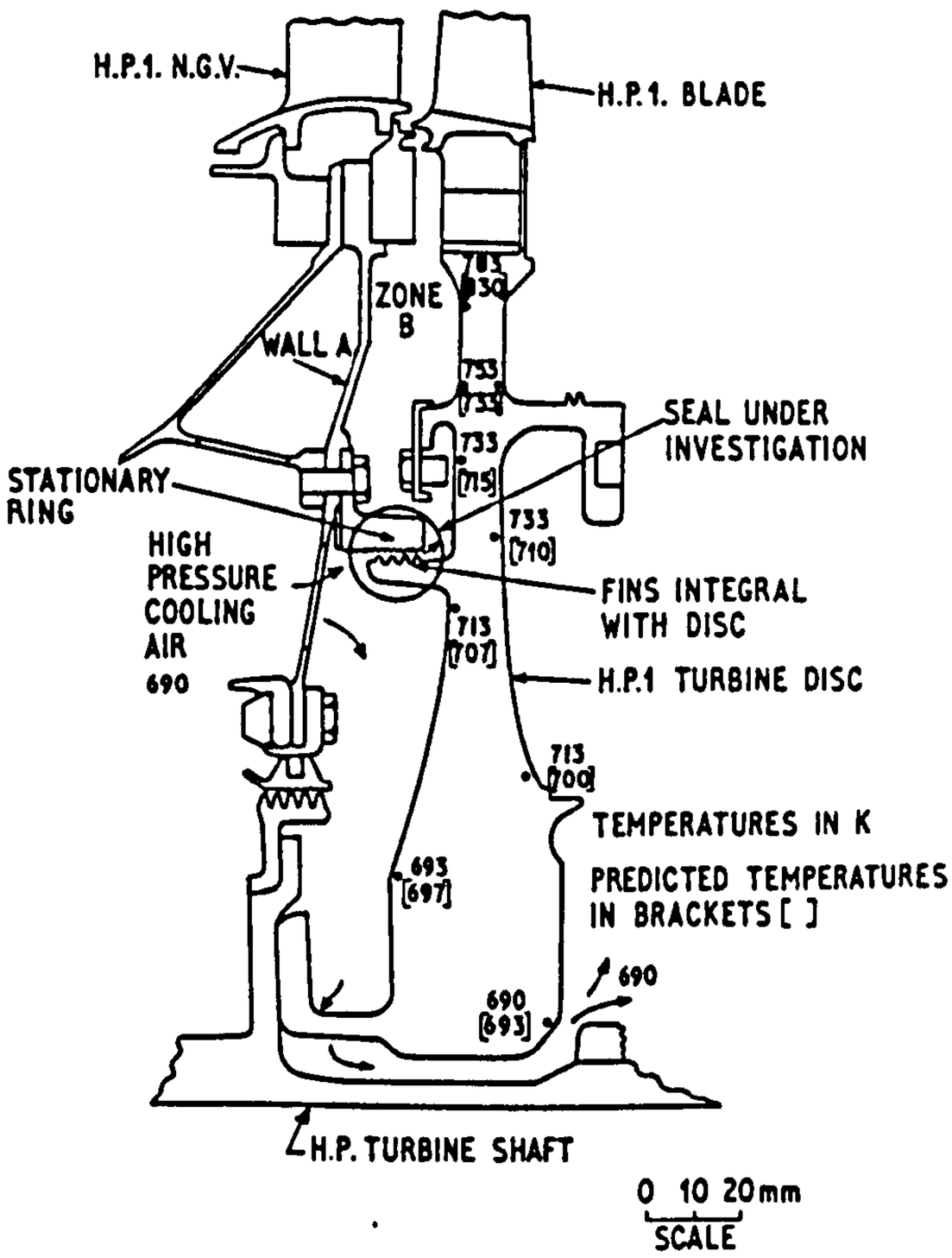

Fig. 1 - Seal on H.P.1 turbine disc and equilibrium turbine disc temperatures - predicted and from thermal point test - turbine inlet temperature 1365 K

Table 1 - Expansions, Cold to Equilibrium at Maximum Speed

	Turbine Disc	Stationary Ring
Av. Temperature at maximum speed, K	706	737
Material	Incoloy 901	Stainless Steel
Av. linear coefficient of thermal expansion	14.47×10^{-6}	11.05×10^{-6}
Radial expansion at seal due to temperature increase - cold to maximum speed, mm	1.14	0.82
Radial expansion at seal due to centrifugal effect at maximum speed (214 rev/s), mm	0.23	-
Total radial expansion, mm	1.37	0.82

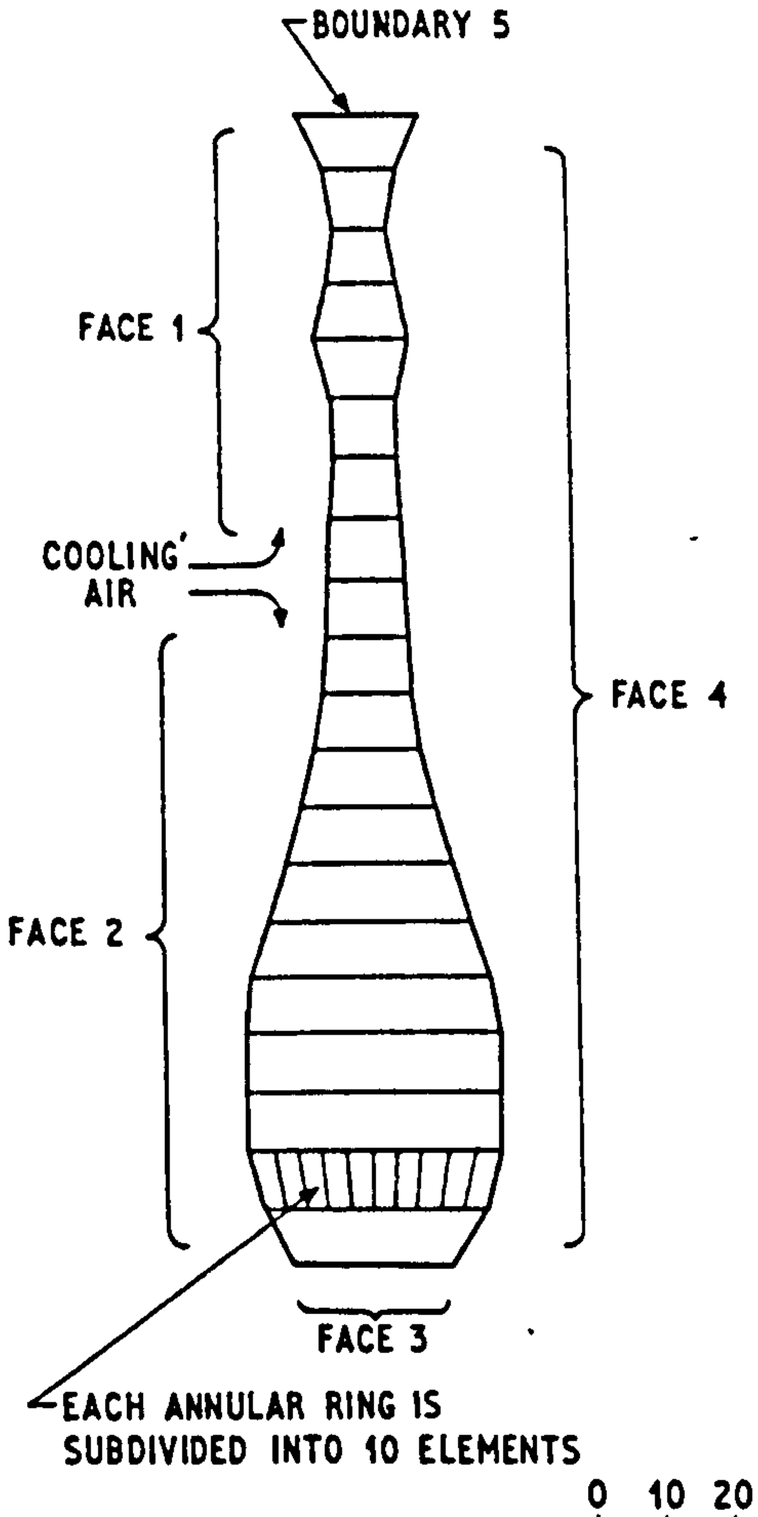

Fig. 2 - Simplified model to represent turbine disc

(6). It was decided to base the heat transfer expressions to be used in the present work on experimentally derived correlations. Unfortunately in none of the above listed cases did the experimental conditions correspond with those in the situation being examined. The major difference was in rotational Reynolds Number (Re) - in the present case it being 12×10^6 whereas the highest value used in the experiments (2), (3) was 4×10^6. However these results can be extrapolated with some confidence due to the close relationship between the results for these shrouded discs and those for free rotating discs. Consequently the correlations used in the present work are those for free rotating discs, modified for the effects of stator wall, shroud and cooling air flow.

The local Nusselt Number on a free rotating disc at Re values approaching 10^6 agrees experimentally (7) with

$$Nu_r = 0.0195 (Re_r)^{0.8} \qquad (1)$$

Drag predictions and experiments, coupled with Reynolds Analogy, (8) indicate that in the range $10^6 \leqslant Re \leqslant 10^7$ the average Nusselt Number on the free disc should be proportional to $(Re)^{0.8}$, so one would expect equation (1) to be reasonably satisfactory up to Re value of 12×10^6. The effects of the adjacent stator wall, of the shroud and of the coolant flow on the drag moment of the disc face have been investigated by Bayley and Owen (2) at Re values up to 4×10^6. At Re of 4×10^6, with the value of gap ratio, G, of 0.074 (the present case), with the value of shroud clearance ratio, G_c, of 0.003 (the present case) and with a value of coolant mass flow coefficient, C_w, of 2.4×10^4 (scaled in proportion to Re from the present case at equilibrium), the drag coefficient is about 30% higher than that of a free disc. This result is not greatly influenced by changes in mass flow or in shroud clearance ratio - doubling the mass flow increases the drag by about 10% while doubling the shroud clearance reduces it by about 5%. In the extrapolation of the 30% increase (c.f. free disc) to the Re value of 12×10^6, it is possible that this excess should be reduced. On the other hand, as seen later, the cooling air flows during the transients being studied are frequently considerably higher than the equilibrium values, which would tend to increase the excess. Consequently it has been assumed that the ratio of the shrouded disc drag to the free disc drag is 1.3 at the operating value of Re - 12×10^6. Assuming that there is a similar increase in Nusselt Number, the local Nusselt Number on Face 1 is given by

$$Nu_r = 0.0253 (Re_r)^{0.8} \qquad (2)$$

It is important to compare this prediction, based on drag moment coefficients, with any other available predictions. For the present case at maximum speed, equation (2) integrated over Face 1 gives a value of 10,700 for the average Nusselt Number. The average value over the same face predicted from the heat transfer correlation of Kapinos (3) is 8680. In this calculation it was assumed that Kapinos's expression could be used, without serious error, up to the value of 12×10^6 for Re, which is beyond the limit of 4×10^6 for Re, to which it had been established. One explanation for the discrepancy between Kapinos's prediction and that of equation (2) is that Kapinos's systems had not been shrouded. The presence of the shroud is seen to increase the drag moment, typically by 15% (2). Allowance for this would place the two predictions in close agreement. No comparisons other than that with Kapinos have been made as the Re

values used in the tests of other workers were 5×10^5 or less.

In the calculation procedure adopted, allowance is made for the change in temperature of the cooling air as it moves outwards over Face 1. Heat is transferred between the air and both the Disc and the wall A. It is assumed that the total heat transfer to/from this air is 1.5 times that transferred from/to the Disc (the values of this factor 1.5 and of other similar factors are not critical to the results). The effective temperature of the air for heat transfer with the disc is taken as the static temperature plus the dynamic temperature ($\omega^2 r^2/2 c_p$).

BOUNDARY CONDITION: DISC FACE 2 - In this case the coolant flows inwardly. The drag moment coefficients, and average Nusselt Numbers for inward flow appear to be lower than those for outward flows (4),(5). The comparisons are only available at comparatively low values of Reynolds Number. Comparing drag moment coefficients (on different rigs, (4), c.f. (2)) at Re of 5×10^5 suggests that the value for inward flow is about 0.75 of that for outward flow. At the lower value of 2.06×10^5 for Re, the average Nusselt Number for inward flow is about 0.6 of the value for the outward flow (5). In view of the apparent reduction in the difference between the inward and outward flow results as Reynolds Number increases, it is assumed that at Re values of about 10^7, applying to Face 2, the ratio of Nusselt Numbers might be much closer to unity, say 0.9. This assumption has been used in the present work.

BOUNDARY CONDITION: DISC FACE 3 - This face is the outer wall of an annular passage through which passes the air for cooling the remainder of the H.P. Turbine and the L.P. Turbine. The standard equation for forced convection in developed pipe flow has been used

$$\frac{hd}{k} = 0.023 \left(\frac{Wd}{A\mu}\right)^{0.8} (Pr)^{0.4} \qquad (3)$$

In determining the change in temperature of the cooling air, it is assumed that the heat transferred to/from the cooling air is 3 times that transferred from/to the Disc at Face 3 (the factor 3 is possibly an overestimate, but reducing it to 2 has only a slight effect on the predictions).

BOUNDARY CONDITION: DISC FACE 4 - The air which cools Face 4 is surrounded by walls (H.P.1 and H.P.2 Turbine Discs) rotating at H.P. Shaft Speed. There are two extremes for the regime of this air flow. At one extreme the air rotates with the adjacent Turbine Discs at the H.P. Shaft Speed, in which case the heat transfer can be regarded as being by natural convection in a high gravity field, the gravitational acceleration being

$$g = \omega^2 r \qquad (4)$$

The natural convection correlation is

$$Nu_r = 0.12 (Gr \times Pr)^{0.33} \qquad (5)$$

At the other extreme, the core flow of the air can be assumed initially to have no angular momentum, and the heat transfer mechanism is as for Face 1, the local Nusselt Number being given by equation (2). At a typical radius on Face 4, the local Nusselt Number predicted from equation (5) is about 0.5 of that predicted from equation (2). Some indication of the nature of the actual flow in this case is given by comparison with the flow between discs and stationary walls. Bayley and Owen (6) indicate that at a gap ratio of 0.03 the flow in the core is essentially radial. At lower values of gap ratio it is mixed. In the engine case being considered the equivalent gap ratio is about 0.08, although there is no stationary wall to inhibit rotational motion. Thus the flow will probably more nearly approximate to the mechanism having little angular momentum. For the present work, heat transfer at Face 4 has been assumed to be given by equation (2), but with the constant reduced by 20% to make some allowance for development of angular momentum.

It is assumed that the heat transferred to/from the air is 2 times that given from/to the H.P.1 Disc.

BOUNDARY CONDITION: DISC FACE 5 - This boundary is in contact with the platforms of the H.P.1 Blades. This surface will be at a temperature somewhere between that of the average metal temperature of the blade (1177 K at Maximum Speed) and that of the entering cooling air (737 K at Maximum Speed). A value 20% from the average metal temperature to the cooling air temperature has been used in the present work. The resulting expansion is not greatly sensitive to this factor - a change to 40% only alters the expansion at 30 s after commencing an acceleration by 0.6% of the total expansion over the transient.

COMPARISON OF PREDICTIONS WITH EQUILIBRIUM TEMPERATURES - A set of observed equilibrium H.P.1 Turbine Disc temperatures (at 1365 K Turbine Inlet temperature) is shown in Fig. 1.

The cooling air used for the Disc is drawn from the High Pressure (H.P.) Compressor

delivery and then passes adjacent to a wall separating it from the Low Pressure (L.P.) Cooling Air before reaching the Turbine Disc. Prediction of the heat transfer from the H.P. Cooling Air is difficult. To obtain satisfactory agreement between prediction and experiment on the equilibrium temperatures of the bulk of the Disc, it appears that the H.P. Cooling Air must be cooled by about 25 deg C by heat transfer to the L.P. Cooling Air. This deduction has been adopted to give the predicted equilibrium Disc temperatures (bracketed) shown in Fig. 1. The observed increase in temperature with radius is satisfactorily predicted.

MODEL FOR STATIONARY RING

The Stationary Ring and the simplified model used to represent it are shown in Fig. 3. The Boundary conditions are discussed below.

BOUNDARY CONDITION: STATIONARY RING FACE 1 - There is no high velocity over Face 1 and so the heat transfer coefficient has been based on natural convection correlations, increased by an assumed 50% as an allowance for local flows. This arbitrary assumption is not critical as the heat transferred across Face 1 is only a small fraction of the heat transferred to the Ring.

BOUNDARY CONDITION: STATIONARY RING FACE 3 - This is the serrated face opposite the tips of the four Fins carried by the Turbine Disc. This face experiences very high velocities. One possible basis of heat transfer prediction is relative to the correlation for fully developed, enclosed flow (equation (3)). On the one hand the local coefficients will tend to be higher than corresponding to this correlation as the flow profiles are more nearly those at entry sections. On the other hand the regions of this face which are not directly opposite the tips of the fins will experience lower coefficients. As a first estimate it has been assumed that the developed, enclosed flow correlation may be used. It will be seen from typical temperature distributions in this Ring (Fig. 6) that the temperature at this face comes very quickly to near to the temperature of the adjacent air and the heating of the Ring through this face tends to be limited by the conductivity of the Ring material, rather than by the local convective heat transfer coefficient.

BOUNDARY CONDITION: STATIONARY RING FACE 4 - This face is part of the stationary partition A (Fig. 1) which forms one wall of Zone B, the facing wall on that zone being the Turbine Disc. The local coefficient of heat transfer on Face 4 is some function of the local coefficient on the adjacent face of the Turbine Disc. It has been seen (9) that the Drag Moment Coefficient on the stator wall at the relevant gap ratio varies from about 0.35 to about 0.55 of the Drag Moment Coefficient on the Rotor Disc over a range of inward coolant air flows, somewhat lower than in the present work, and at a lower rotational Reynolds Number. It has been assumed here that the heat transfer coefficient on this Face 4 is 0.55 of the local value on the adjacent Turbine Disc face. This assumption is only an approximation, particularly for the section of Face 4 which is normal to the Disc face, rather than facing it.

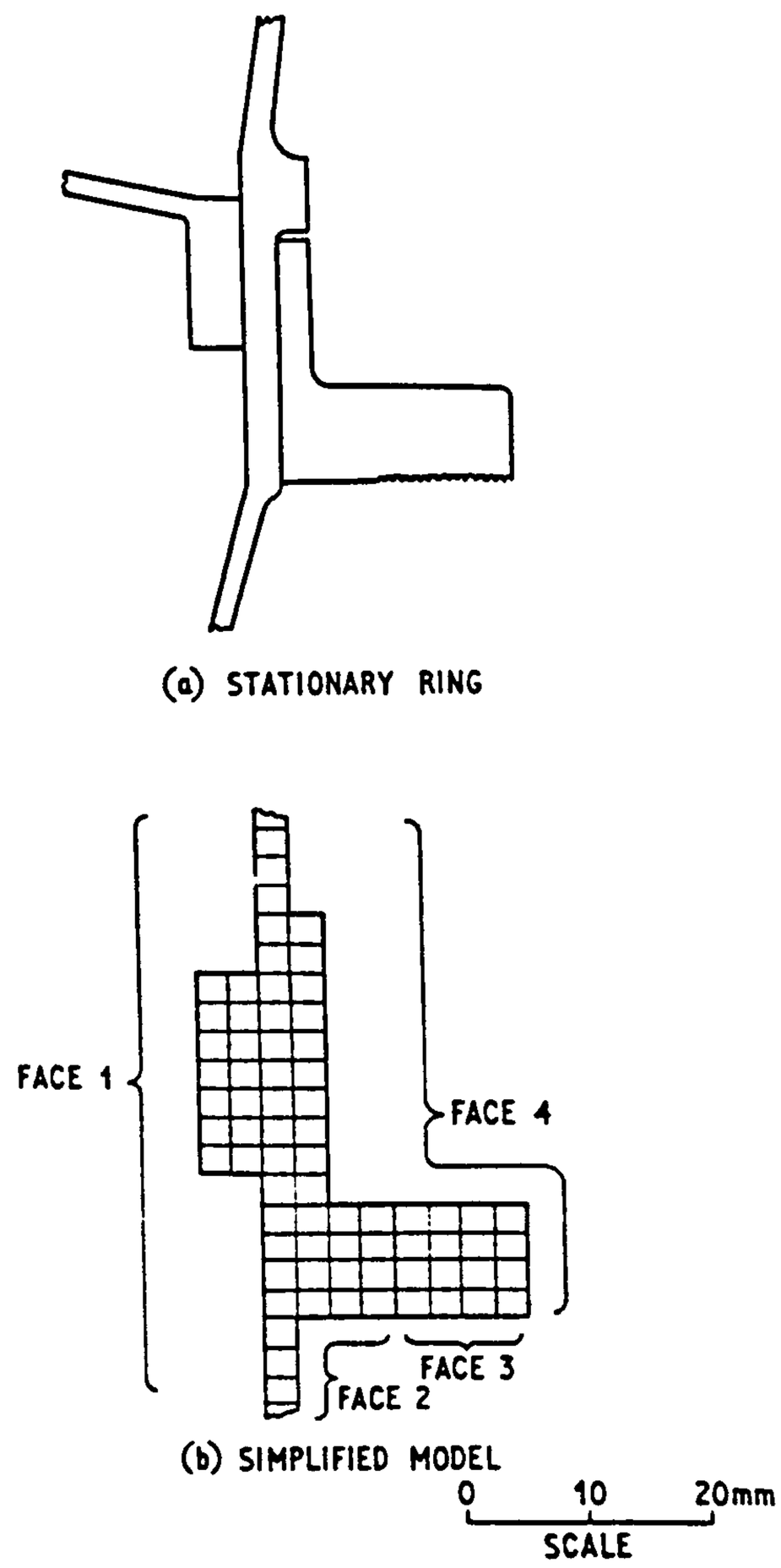

(a) STATIONARY RING

(b) SIMPLIFIED MODEL

Fig. 3 - Stationary ring and simplified model

BOUNDARY CONDITION: STATIONARY RING FACE 2 - This face is in a zone similar to Face 4, in that it is in proximity to the rotating Turbine Disc. It has been assumed here also that the local heat transfer coefficient is 0.55 or the local value on the adjacent Turbine Disc.

PREDICTED MOVEMENTS

As indicated earlier, the mean radial clearance at the Seal when at equilibrium at the maximum speed is 0.18 mm, and the corresponding cold radial clearance is 0.73 mm. It is therefore to be expected that the transients in which large seal clearances occur will be those which involve large speed changes. It will be seen later that the thermal response of the Turbine Disc is less rapid than that of the Stationary Ring. Hence larger Seal openings will be observed in accelerations, and there will be some tendency towards smaller openings in decelerations. A larger Seal opening allows an excessive consumption of cooling air, which causes a deterioration in the engine performance, as discussed later.

It was therefore decided that the most relevant and testing transients in which to investigate the responses of the seal components would be an acceleration from Ground Idling Speed to the Maximum Speed and a deceleration over the reversed speed range.

ACCELERATION - The speed transient is completed in under 10 s, but when the techniques described above are applied it is found that the thermal responses are much less rapid, for example the Turbine Disc response is found to be represented by a two time-constant system, the dominant time constant being 60 s. The dominant time-constant for the Stationary Ring is 17 s.

The results of the predictions of the movements of the inner surface of the Stationary Ring, and of the tips of the fins integral with the Turbine Disc are shown in Fig. 4. The most probable movements of these components are shown by the solid lines, and heat transfer coefficient being as defined earlier. An indication of the effects of changes in these coefficients is given by the dashed lines which represent coefficients lowered by 25% for the Stationary Ring and raised by 25% for the Turbine Disc. The results incorporate the expansion due to centrifugal effects and also the thermal strain deflection due to the fins on the Turbine Disc heating more

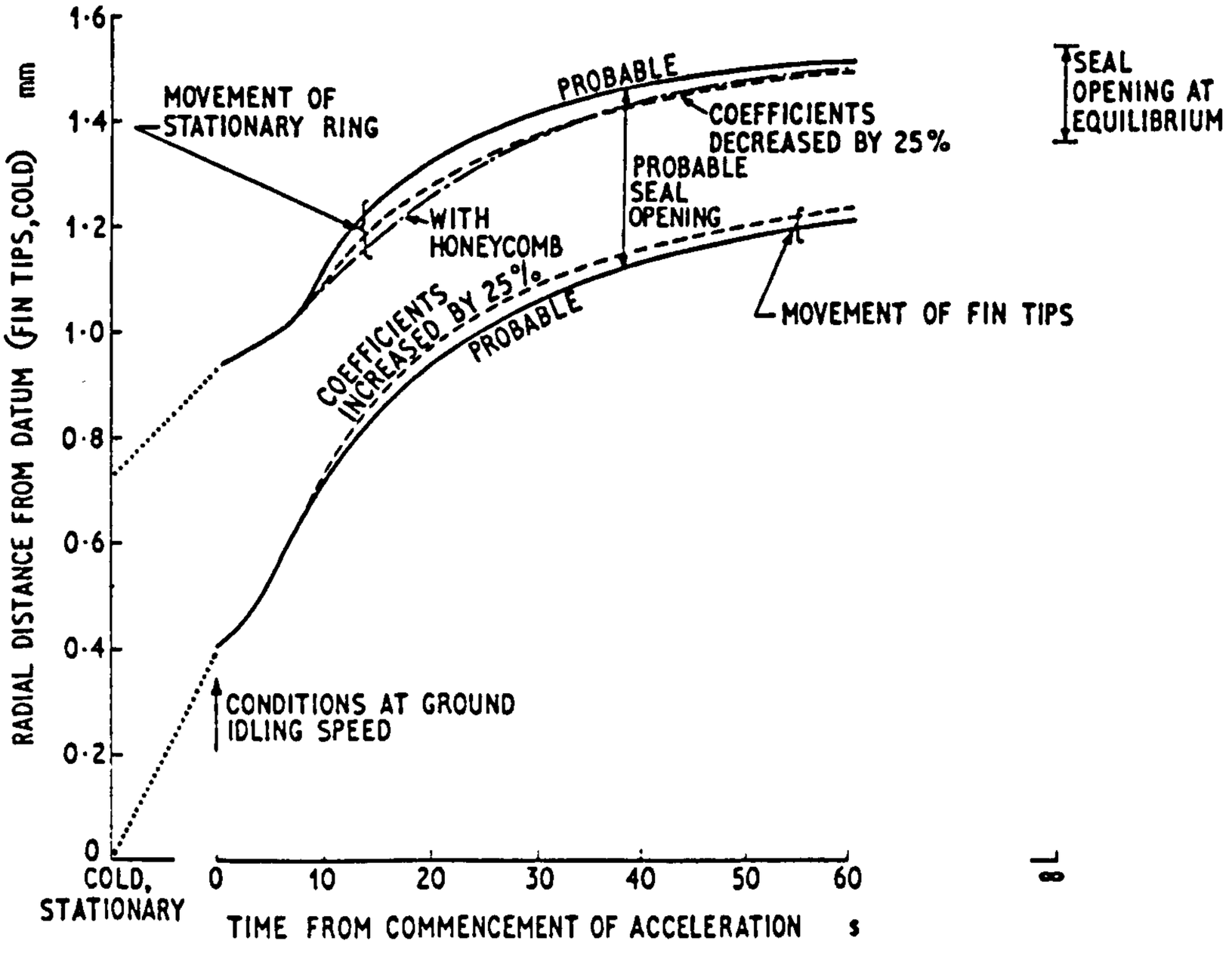

Fig. 4 - Predicted movements of seal components during and following an acceleration from ground idling to maximum speed

rapidly than the Disc itself. This latter effect is most marked between 10 s and 30 s after starting the acceleration. The maximum deflection of the fins relative to the Disc occurs at about 20 s, and is about 0.025 mm, at a time when the seal opening is about 0.40 mm.

It is worth noting that during the transient, the major portion of the heat that is received by the Turbine Disc is supplied by the "cooling" air, and not by conduction from the Turbine Blades.

From Fig. 4, on the basis of the probable expansions, the seal clearance when the speed transient has been completed is about 2.3 times the equilibrium value, and remains at least double the equilibrium value for a further 30 s.

The thermal response of the Stationary Ring is more rapid than that of the Turbine Disc. At an instant 20 s after commencing the acceleration the Disc has achieved 45% of its thermal growth while the Stationary Ring's fractional growth is 64%.

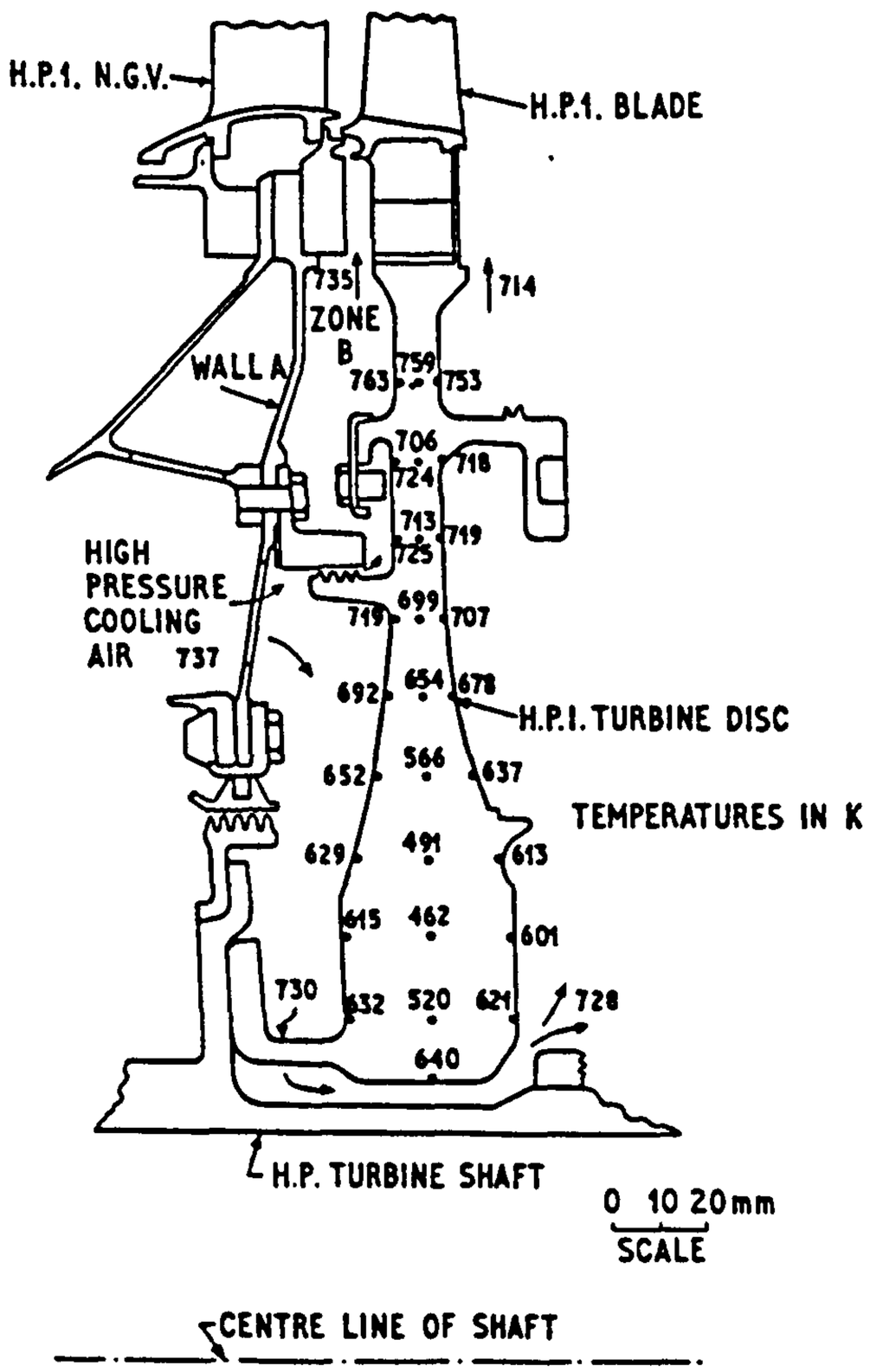

Fig. 5 - Predicted temperatures in turbine disc 30 s after commencement of acceleration

The techniques described can also predict the transient temperature distribution within the components. The results at 30 s after commencing the acceleration are given in Figs. 5 and 6. In the Turbine Disc, particularly in the more massive section near the shaft, there are seen to be considerable temperature gradients, both in the radial and axial directions.

DECELERATION - In this case again, the speed transient for the change from Maximum to Ground Idling Speeds is completed in less than 10 s. The thermal responses of the Seal's components are much less rapid, even when compared to their responses to the acceleration. This reduction in response is due to the lower heat transfer coefficients at the Ground Idling Speed, as compared to the Maximum Speed, resulting from the lower densities and lower rotational speed. The responses of both the Disc and of the Stationary Ring are more closely approximated by single time-constant systems than had been the case following the acceleration. The dominant time-constants are 89 s and 45 s for the Turbine Disc and Stationary Ring respectively.

The predicted movements at the Seal are shown in Fig. 7. The most probable movements are indicated by the solid lines. If the coefficients to the Disc are increased by 25%, and those to the Stationary Ring are lowered by 25%, then the revised predictions are as indicated by the dashed lines.

Although the thermal response of the Stationary Ring is more rapid, the seal

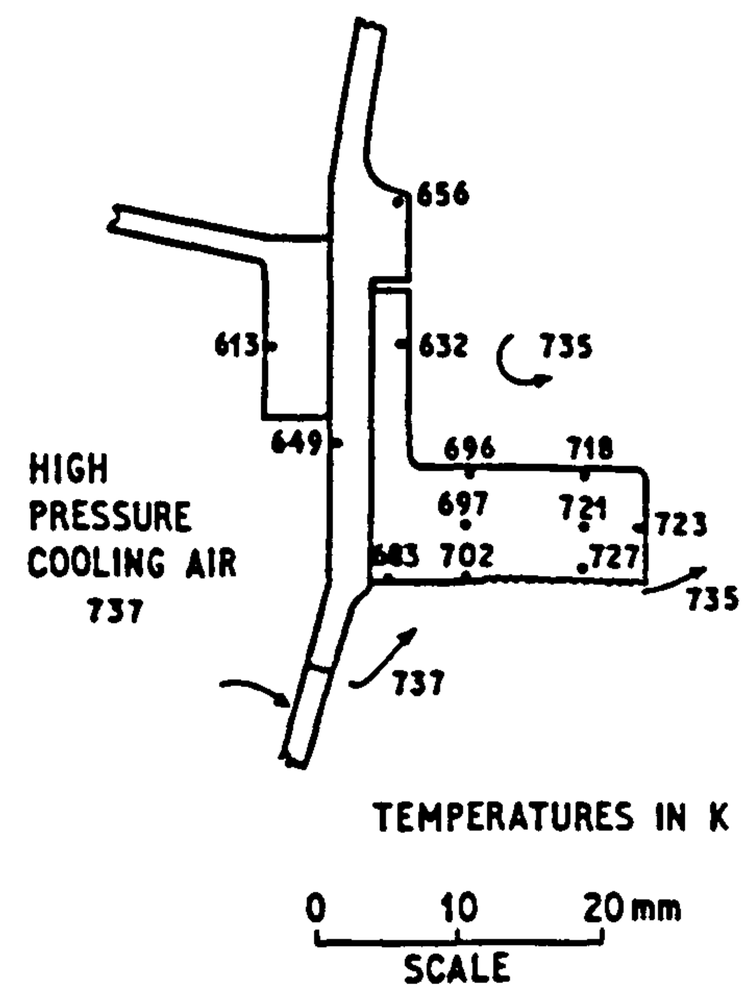

Fig. 6 - Predicted temperatures in stationary ring 30 s after commencement of acceleration

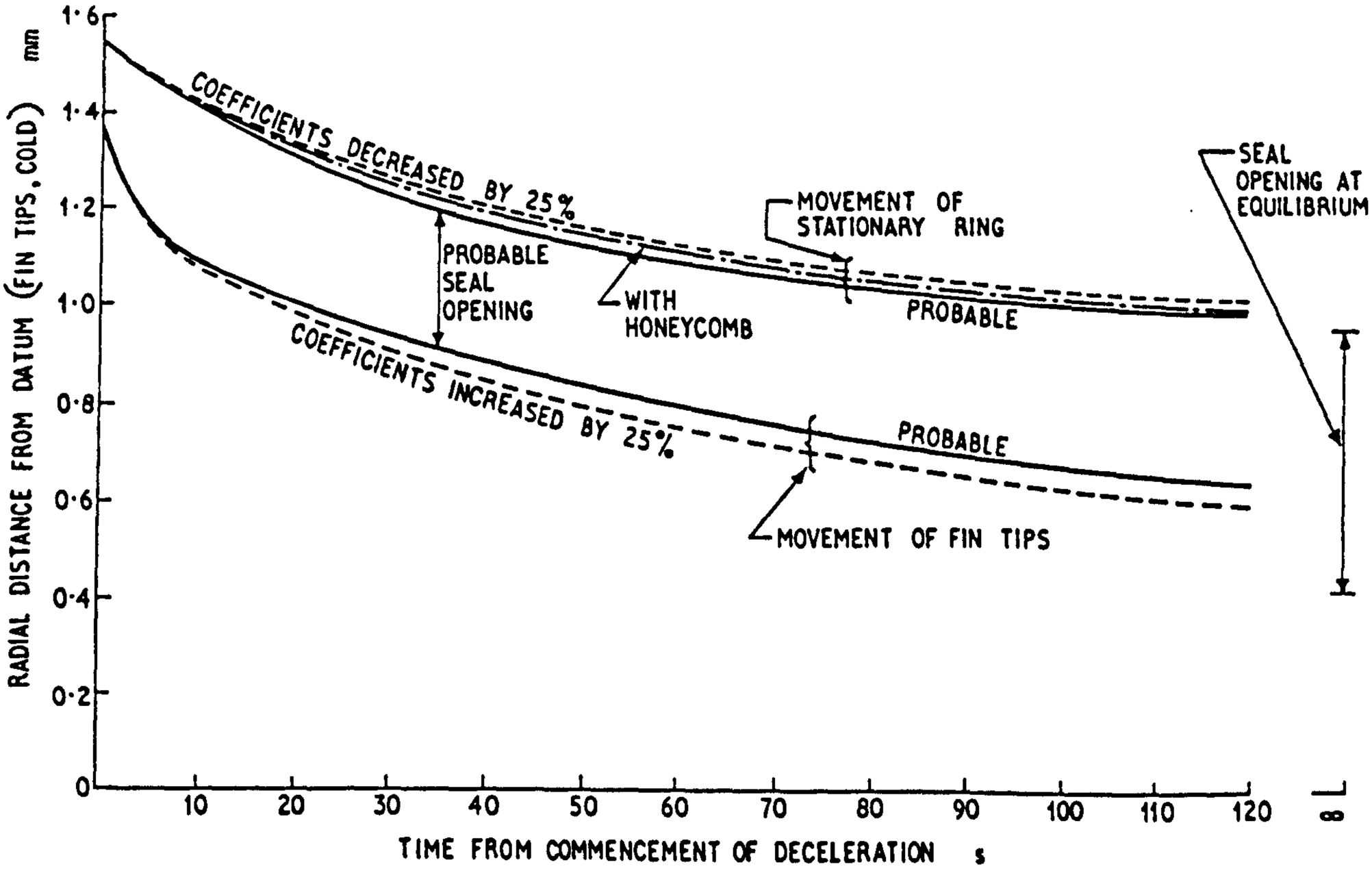

Fig. 7 - Predicted movements of seal components during and following a deceleration from maximum to ground idling speed

clearance does not noticeably decrease, but rather increases, because (a) the Disc loses its centrifugal expansion within the 10 s of the speed transient, and (b) the Disc material has a higher coefficient of thermal expansion and therefore has to achieve a greater thermal contraction.

During and following the deceleration the temperature distributions within the Disc are more uniform than following the acceleration. A typical distribution, 30 s after commencing the deceleration, is given in Fig. 8. The local temperature gradients are about 40% of those that existed 30 s after commencing the acceleration (Fig. 5).

EFFECT OF INCREASING NUMBER OF ELEMENTS IN MODEL - The adequacy of the model used for the Turbine Disc was tested by increasing the number of elements in the axial direction from 10 to 14, the number of radial divisions being kept at 20. The change in the average Disc temperature was typically just under 1 deg K, which is equivalent to a change in the Seal Clearance of less than 1% of its equilibrium value at the maximum speed, i.e. less than 0.002 mm. This change is considered to be insignificant, and so the 10 x 20 element model can be regarded as adequate.

EFFECTS ON ENGINE PERFORMANCE

The flow of cooling air through Zone B (Fig. 1) during the first 30 or so seconds of the thermal soak transient following the acceleration will be about double the equilibrium value. This excessive flow reduces the quantity of air to provide the gases to pass through the H.P.1 Nozzle Guide Vanes. Although this particular excessive cooling air flow is returned to the main-stream immediately after the H.P.1 N.G.V's, it will be deficient in momentum in the main flow direction. There will be a reduction in the power output from the H.P.1 Turbine. An investigation has been made (10) of the losses arising from the transverse injection of an air flow such as this immediately in front of a blade cascade. The loss in stagnation pressure in the immediately following cascade was found to agree with the simple theory proposed by Barnes and Fray (11). In addition, vortices were seen to be generated, being initiated in the separation bubbles formed by the transverse injection

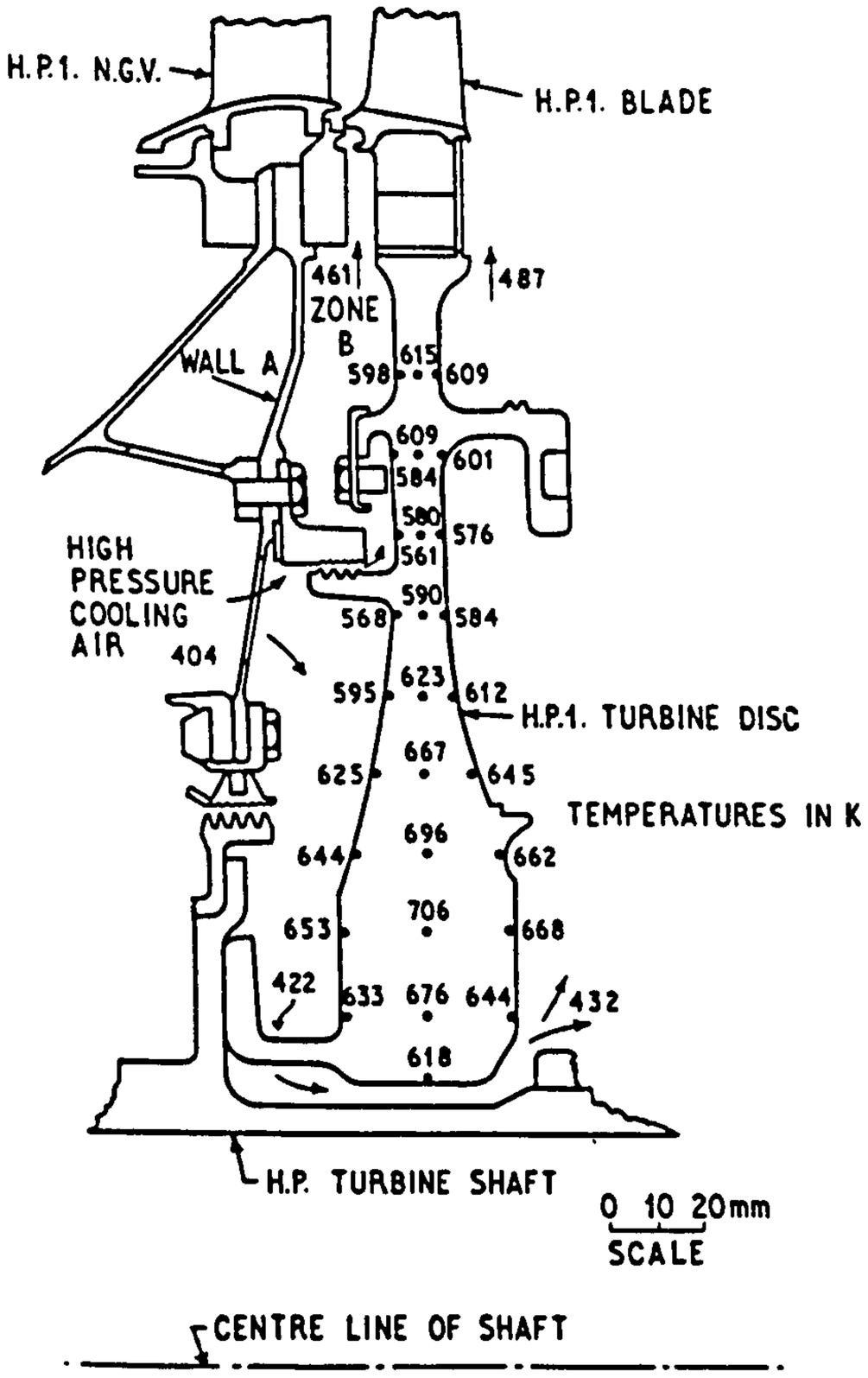

Fig. 8 - Predicted temperatures in turbine disc 30 s after commencement of deceleration

on the cascade end walls. These vortices may persist into further blade rows in the machine, causing further losses. Investigation is continuing on this problem.

The responses to the deceleration are less critical, provided that mechanical contact between the opposing faces is avoided. This condition is satisfied in the present case.

POSSIBLE METHODS OF IMPROVING RESPONSE

The problem of the large clearance during and following the acceleration could be reduced if the coefficients of expansion of the two materials for the Turbine Disc and the Stationary Ring were more similar. If a stainless steel, similar to that for the Stationary Ring, were used for the Disc, following the acceleration the excess clearance above the steady-running value would be reduced by about one third. However a penalty would be incurred in creep strength.

Alternatively the Seal could be designed to operate at a smaller radius on the disc, so reducing the transient opening.

Another alternative, using essentially the original design, is to replace the face of the Stationary Ring immediately opposite the fin tips by a honeycomb mesh, of poor thermal conductivity, and in poor thermal contact with the body of the Stationary Ring. This would tend to restrict the heat flow into the Ring from this Zone of high heat transfer coefficients. The honeycomb mesh should be adequate for sealing purposes. The predicted expansion following the acceleration, for such an arrangement, is shown by the chain-dotted line on Fig. 4 (to be compared with the solid line curve for datum). The improvement is small, but helpful, reducing the excess clearance above the steady-running value by about 20% at 30 s after starting the acceleration. The predicted movement following the deceleration is similarly indicated in Fig. 7. The effect of the honeycomb in this latter transient is less than in the acceleration, due to the greater reduction in heat transfer coefficient at Face 3 than at the other Faces when operating at Idling Speed as compared with Maximum Speed.

CONCLUSIONS

Very simple finite-difference models, with appropriate boundary conditions, have been used to predict the expansions and contractions during transients of the components of an Air Seal on a Turbine Disc of a Gas Turbine. The finite-difference models need not be very sophisticated, as the most critical factors are the specifications of the heat transfer coefficients at the various boundaries.

The predictions of the Turbine Disc model for the steady state are in reasonable agreement with thermal paint results.

The most severe transient is an acceleration from Ground Idling Speed to Maximum Speed. Although the speed transient is completed in 10 s, the predicted seal opening, and resultant cooling air flow is at least double the equilibrium value for a further 30 s. Modifications to the design offering some improvements have been suggested.

Transient temperature distributions within the components can easily be obtained.

NOMENCLATURE

A = flow cross-sectional area

c_p = fluid specific heat at constant pressure

C_w = coolant mass flow coefficient ($= W/\mu r_o$)

d = equivalent diameter of flow cross-section ($= 4A/p$)

g = acceleration due to local gravity

G = gap ratio ($= s/r_o$)

G_c = shroud clearance ratio ($= s_c/r_o$)

Gr = Grashof Number ($= \ell^3 \theta \alpha \rho^2 g/\mu^2$)

h = local heat transfer coefficient

k = fluid thermal conductivity

ℓ = typical linear dimension

Nu_r = local Nusselt Number ($= hr/k$)

p = perimeter of flow cross-section

Pr = Prandtl Number ($= \mu c_p/k$)

r, r_o = local radius, outer radius of disc

Re = rotational Reynolds Number ($= \rho \omega r_o^2/\mu$)

Re_r = local rotational Reynolds Number ($= \rho \omega r^2/\mu$)

s = axial clearance between stator and rotor

s_c = axial clearance between shroud and rotor

W = local coolant mass flow rate

α = fluid bulk coefficient of thermal expansion

μ = fluid viscosity

ρ = fluid density

θ = temperature difference

ω = angular velocity of rotating disc

ACKNOWLEDGEMENTS

The author wishes to thank the staff of Rolls-Royce (1971) Ltd. for their co-operation and stimulation and for providing necessary data on engine design and materials. He wishes to thank colleagues at the University of Glasgow for their advice and comments.

REFERENCES

1. N.R.L. Maccallum, "The performance of turbojet engines during the thermal soak transient", Proc. Instn. mech. Engrs. 1969-70, 184 (Pt. 3G(II)), 23-29.

2. F.J. Bayley and J.M. Owen, "The fluid dynamics of a shrouded disc system with a radial outflow of coolant", J. Engng. Pwr., Trans. Am. Soc. mech. Engrs. Series A, 1970, 92, 335-341.

3. V.M. Kapinos, "Heat transfer from a disc rotating in a housing with a radial flow of coolant", J. Engng. Phys. 1965, 8, 35-38.

4. D.E. Metzger and J.W. Mitchell, "Heat transfer from a shrouded rotating disc with film cooling", J. Heat Transfer, Trans. Am. Soc. mech. Engrs., Series C, 1966, 88, 140-146.

5. D.E. Metzger, "Heat transfer and pumping on a rotating disc with freely induced and forced cooling", J. Engng. Pwr., Trans. Am. Soc. mech. Engrs. Series A, 1970, 92, 342-348.

6. F.J. Bayley and J.M. Owen, "Flow between a rotating and a stationary disc", Aeronaut. Q., 1969, 20, 333-354.

7. E.C. Cobb and O.A. Saunders, "Heat transfer from a rotating disc", Proc. Roy. Soc. Series A, 1956, 236, 343-351.

8. L.A. Dorfman, "Hydrodynamic resistance and heat loss of rotating solids", 1963 (Oliver and Boyd, Edinburgh).

9. F.J. Bayley and L. Conway, "Fluid friction and leakage between a stationary and rotating disc", J. mech. Engng. Sci., 1964, 6, 164-172.

10. K.D. Shrivastava and N.R.L. Maccallum, "The effect of a transversely injected steam on the flow through turbine cascades: Part I - Flow effects and Part II - Performance changes", ASME Papers Nos. 77-GT-87 and 77-GT-88.

11. J.F. Barnes and D.E. Fray, "An experimental high-temperature turbine. Part II. The effects of cooling on the aerodynamic performance", Aeronaut. Res. Counc. Rep. Memo. 3405, 1965.

Society of Automotive Engineers, Inc.
400 COMMONWEALTH DRIVE, WARRENDALE, PA 15096

12 page booklet.

Printed in U.S.A.

Publication 21
Paper No. 78-GT-24

an ASME publication

PRICE AT WEMBLEY 1.00£

B. A. Aburwin
Research Student

N. R. L. Maccallum
Senior Lecturer

Department of Mechanical Engineering,
University of Glasgow,
Glasgow, Scotland

The Effect of a Transversely Injected Stream on the Flow Through Turbine Cascades: Part III—Influence of Aspect Ratio

An experimental investigation has been made of the effect of a transversely injected stream on the flow through turbine cascades similar to those in which previous studies [1, 2][1] had been made, but having aspect ratios of 1.5 and 1.0 compared to the previous value of 3.0. New instrumentation includes a five-hole probe. The average losses in stagnation pressure and the changes in flow capacity remain in agreement with one-dimensional theory. The exit vortex is moved towards the end-wall as aspect ratio is reduced. The strength of the vortex is diminished when the aspect ratio is reduced from 3.0 to 1.5, but there is little change for the further reduction of aspect ratio.

Introduction

When an additional flow is injected transversely into the main flow entering a row of turbine blades or nozzle guide vanes, as when disk cooling air in a gas turbine is returned, several significant effects in the flow are observed [1]. These effects include the formation of a separation bubble on the passage end-wall immediately behind the injection slot, and the appearance of a vortex starting near the suction side and moving into the main flow from this bubble and continuing in the flow leaving the blade row. The experimentally observed influences of main flow inlet angle, blade stagger angle, injection slot width and injection velocity on the performance changes resulting from transverse injection for a typical blade row have been reported [2]. In that work the aspect ratio of the blade cascade had been 3.0, that being sufficient to ensure that secondary flows did not influence conditions at the mid-blade height. The present paper reports the performance changes that have been observed experimentally when the aspect ratio is reduced to 1.5 and 1.0.

Apparatus and Test Procedure

Apparatus. This consisted of a cascade of five blades (four passages) of 129 mm (5.07 in.) chord at 88 mm (3.5 in.) pitch, having profiles [1] typical of an intermediate or low pressure row of nozzle guide vanes. These blades were the same as those used in the previous studies [1, 2], and coordinates of the profile are given in Table 1. The blade height in the tunnel was 381 mm (15.0 in.), which provided the aspect ratio of 3.0. The lower values of aspect ratio were obtained by inserting an additional partition wall inside the tunnel, parallel with the end-wall in which the injection slot was positioned. This partition wall extended in the upstream direction into the approach contraction, and in the downstream direction it continued to 4.5 axial chord beyond the exit traverse plane.

The cascade was placed in the suction to a variable speed fan.

Typically, the average flow velocity at exit from the cascade was 27 m/s (90 ft/s) corresponding to a blade Reynolds Number, based on this exit velocity, of 2.5×10^5.

Wire grids in the approach contraction gave a turbulence level of 1.5 percent at the cascade inlet. This turbulence level ensured that the Reynolds Number was well above the critical.

The slot through which the transverse flow was injected was placed across one end-wall, immediately in front of the leading edges of the blades. The end-wall boundary layer in the main flow approaching this slot was sucked away some 180 mm (7 in.) upstream of the slot.

The cascade parameters used in these tests were: stagger angle, 45 deg; main fluid inlet angle, 15 deg; angle of injected flow to cascade end-wall, 90 deg. The ratio of the injected jet velocity to the main approach flow velocity was generally 1.5 or 0.0, with one additional test being made with the velocity ratio of 1.0. (The injection velocity ratio of 1.5 is higher than normally encountered in practice, however the present results may be linearly interpolated, since the effects of injection are proportional to injection velocity [1]). The width of the injection slot was adjusted as the aspect ratio was changed, to maintain the ratio of injected mass flow to main mass flow at 0.035 when the injected velocity ratio was 1.5. To achieve the zero injection ve-

[1] Numbers in brackets designate References at end of paper.

Contributed by The Gas Turbine Division for presentation at the Gas Turbine Conference, London, England, April 9–13, 1978, of THE AMERICAN SOCIETY OF MECHANICAL ENGINEERS. Manuscript received at ASME Headquarters December 14, 1977. Paper No. 78-GT-24.
Copies will be available until December 1978.

Table 1 Coordinates of blade profile—45 deg stagger angle

x/c	0.0	0.047	0.156	0.272	0.373	0.450	0.512	0.574	0.629	0.691
z/c pressure	0.0	0.025	0.080	0.156	0.238	0.315	0.388	0.474	0.564	0.697
z/c suction	0.0	−0.016	−0.021	0.008	0.070	0.159	0.272	0.398	0.522	0.684

locity, the injection slot was sealed with tape.

The injected flow was at the same temperature as the main flow.

The plenum chamber supplying the injection slot was designed to insure uniform stagnation pressure across the length of the slot. The chamber provided a contraction of area ratio not less than 15 leading into the slot, and this gave a slot coefficient of discharge of 0.97. However there will be some variation in static pressure in the main flow field outside the slot, across the span of a blade passage. Consequently there may be some variation in local injection velocity across a passage span. A hot-wire anemometer was therefore provided for traversing along the slot to measure the local velocities in the injection jet.

Test Procedure. With the aspect ratio set at 3.0, the angles of the exit side-walls were adjusted, relative to the cascade, until there was a symmetric velocity distribution across the exit flow. This setting also satisifed symmetry of the exit flow when the aspect ratio was reduced to 1.5. However a slight discrepancy appeared when the aspect ratio was further reduced to 1.0. In order to simplify the comparison of the results, it was decided to maintain the same wall positions, although at the expense of this slightly incorrect alignment at the lowest aspect ratio.

With this side-wall setting, and with the partition placed to give the required aspect ratio, the fan speed was then adjusted to give an approach velocity into the test portion of the cascade of 13.6 m/s (45 ft/s). The following observations were made:

1 Pressure distribution around the suction and pressure surfaces of the middle blade of the cascade, over a range of blade heights;

2 Total head pressure distribution, and flow directions and velocities, using a five-hole spherical probe (8 mm diameter) across a traversing plane 200 mm (7.9 in.) downstream in the flow direction from the cascade exit. This corresponded to an axial downstream distance of 88 mm (0.92 axial chord). The use of the five-hole probe in place of the three-hole probe used in the earlier work allowed measurement to be made of the velocity components parallel to the blade height direction;

3 Rotational speed of a "vorticity meter" traversing across the same plane as used for the exit velocities, etc. The vorticity meter had four vanes, three mm high, carried on a spindle rotating in galvanometer bearings. The speed was measured by stroboscope.

Results and Discussion

In the results presented here, when injection was taking place the injection velocity ratio compared to the main approach flow velocity was generally 1.5, and the injected mass flow was 0.035 of the main flow. Some additional results at the intermediate injection velocity ratio of 1.0 (and injection mass flow ratio of 0.023) are shown in Figs. 6(b), 7, 8, and 9(b).

Variation of Jet Velocity Along Injection Slot. The manner in which the Injection Jet velocity varies along the length of the slot is shown in Fig. 1. There is an above-average flow from the portion of slot adjacent to the suction surface of the blade, whereas the flow is below average in front of the pressure surface. The amounts by which these maximum and minimum velocities depart from the mean velocity are not great, being about 12 percent.

Pressure Distributions on Blade Surface. The pressure distributions at four blade heights for the case with aspect ratio of 1.0 are shown in Fig. 2 (a)–(d). The pressure distributions at the blade mid-height ($y/c = 0.48$) are unaffected by the transverse injection, except that the pressures are changed to match the higher total mass flow now passing through the blade channels. The pressure distributions at the lower blade heights of $y/c = 0.2$ and $y/c = 0.075$ follow the same pattern. It is only at the blade height closest to the injection end-wall that significant changes are observed. It is seen that a separation bubble exists on the end-wall behind the injection slot, and extending to about 0.1 chord adjacent to the pressure surface and to about 0.35 chord adjacent to the suction surface. This bubble is similar to that observed previously [1] at the aspect ratio of 3.0. The extent of the separation bubble, at the height of y/c of 0.025, is slightly reduced from that observed with the aspect ratio of 3.0. Also, with the aspect ratio of 3.0, the bubble had risen to a y/c value of at least 0.075 above the end-wall. However at the aspect ratio of 1.0, no trace of the bubble is observed at the y/c value of 0.075.

These effects of aspect ratio on the height of the separation bubble are to be expected, i.e., the bubble is "squeezed" downwards as the aspect ratio is lowered. However the length of the separation bubble on the end-wall seems not to be significantly altered.

Exit Velocity Distributions.

Main Velocity Component. Contours of the main velocity component are shown in Figs. 3 and 4 for the aspect ratios of 1.5 and

Nomenclature

a = distance along chord from leading edge of blade
c = chord
C_p = pressure coefficient, defined by $(p - p_1)/(p_{0_1} - p_1)$
d = distance along blade pitch from one mid-passage line to next, in direction of suction surface
D = measure of strength of exit vortex, defined by $(\Delta\alpha^*)\,(\Delta y^*/c)$
E = measure of kinetic energy of tangential components in exit vortex, defined by $(\Delta\alpha^*)^2\,(\Delta y^*/c)^2$
f = ratio of cascade exit mass flow to mass flow of main approach stream
F = measure of angular momentum of exit vortex, defined by $(\Delta\alpha^*)\,(\Delta y^*/c)^3$
p = pressure
Q = ratio of maximum velocity of injected jet to velocity of main approach flow
s = blade pitch
U = velocity in main flow direction
v = velocity
y = distance from end-wall carrying injection slot
α = main flow angle, measured from axial direction
η = nozzle efficiency
θ = angle between injected jet and cascade end-wall
ρ = density

Subscripts

0 = stagnation
1, 2 = inlet to, outlet from cascade
∞ = mainstream
ave = average
d = datum, i.e. with no injection
inj = injection
max = maximum
ref = reference
s = secondary

Superscript

* = range of pitch-integrated exit vortex

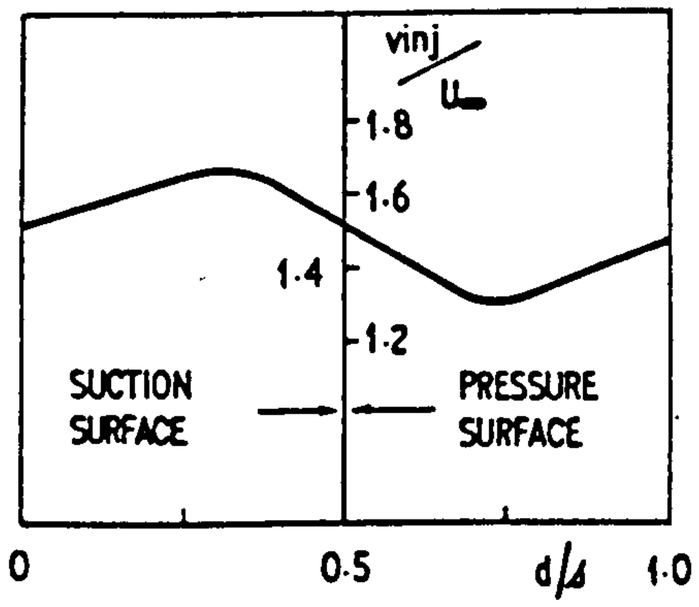

Fig. 1 Span-wise variation of jet velocity

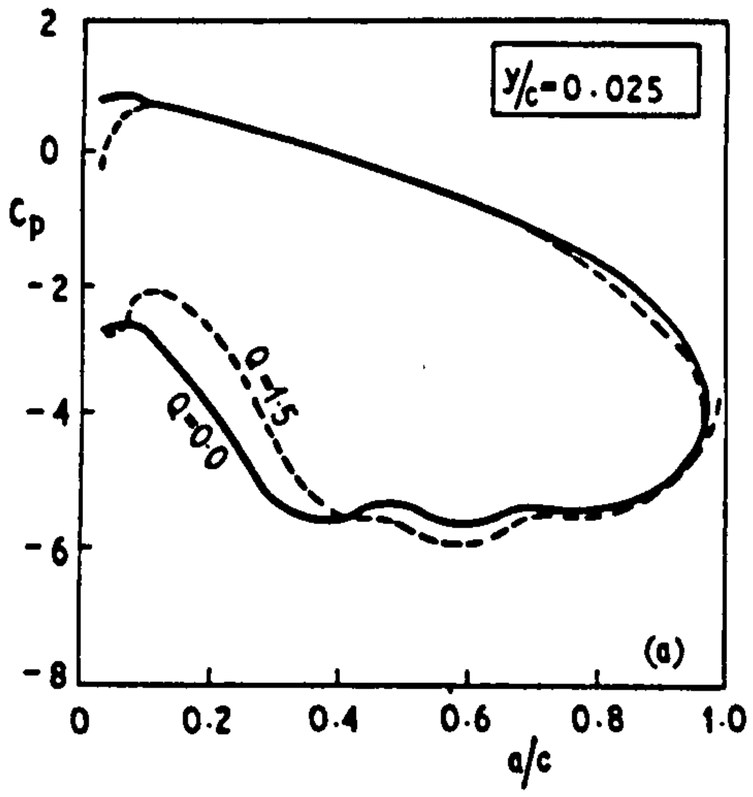

Fig. 2(a)

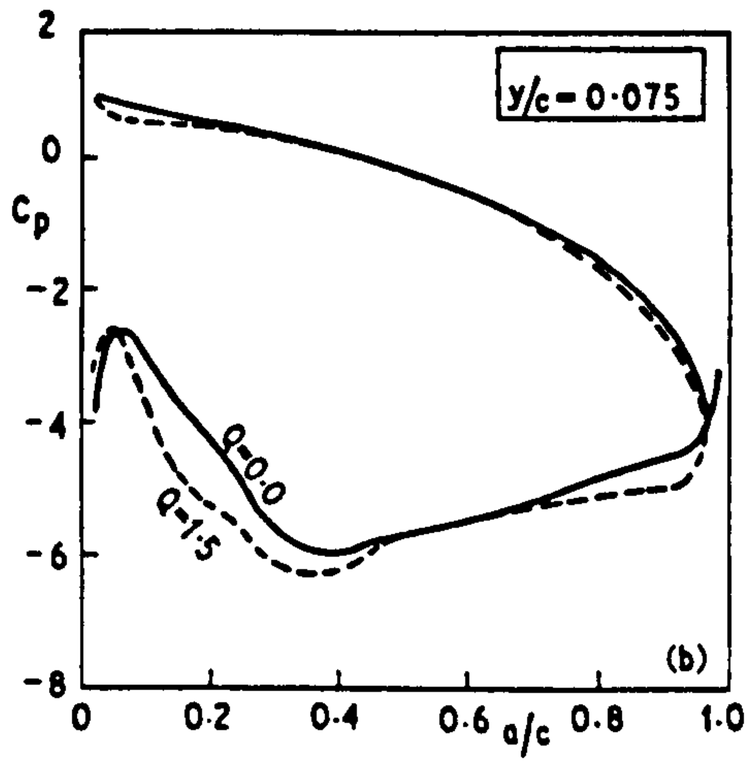

Fig. 2(b)

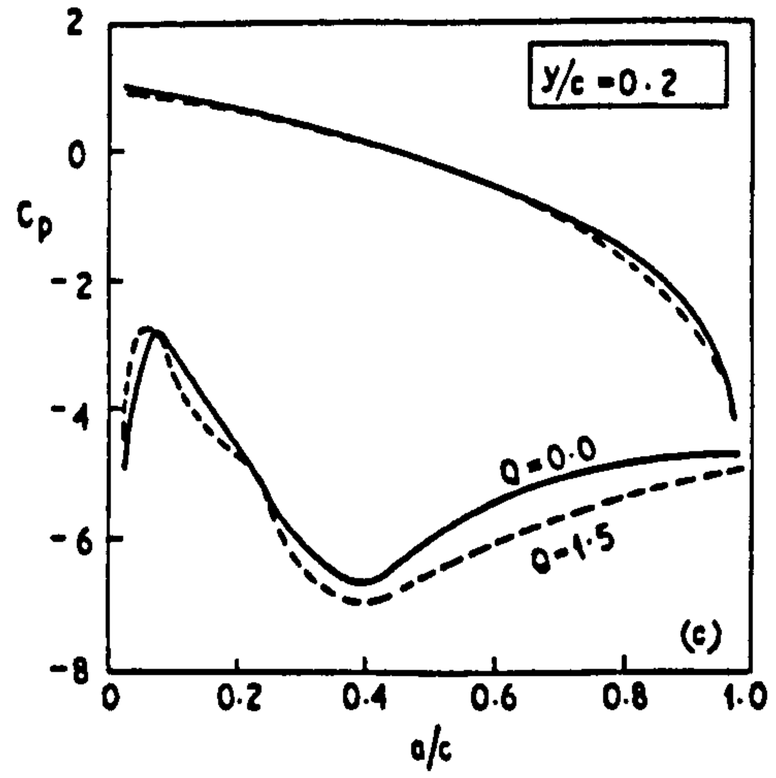

Fig. 2(c)

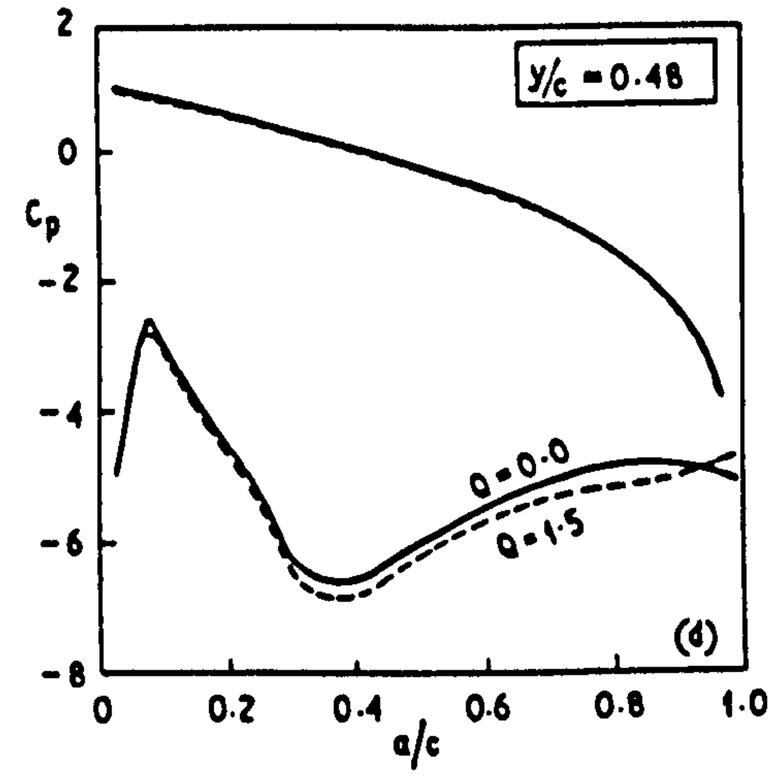

Fig. 2(d)

Fig. 2 Pressure distribution around blade—aspect ratio 1.0

1.0, respectively. The contours are drawn for the region up to the blade mid-height, as this is the region primarily influenced by the injection. The transverse injection has the effect of creating troughs in the exit flow pattern, in the same manner as had been previously observed [1] at the higher aspect ratio of 3.0. The troughs coincide with the centers of the exit vortices observed in the secondary flows, discussed later. The magnitudes of the velocity depressions in these troughs are virtually uninfluenced by aspect ratio, the velocities at the centers of the troughs, compared to the mid-passage velocity at the blade mid-height, being 0.82, 0.80, and 0.80 for the aspect ratios 3.0, 1.5, and 1.0, respectively. As the aspect ratio is reduced, these troughs are moved towards the injection end-wall, but at a diminishing rate.

At the lowest aspect ratio tested (i.e., 1.0), the disturbance to the velocity distribution, resulting from transverse injection, extends virtually to the blade mid-height.

Secondary Flow Velocity Components. The five-hole probe used in the exit traverses enabled both components of the secondary velocity to be measured. When there is no injection, the secondary velocities are comparatively small—for the aspect ratio of 1.0 the highest amounted to 0.06 of the maximum main velocity component at the exit plane (Fig. 5(a)). When transverse injection is introduced, a strong vortex is seen (Fig. 5(b)) and the secondary velocities around this vortex rise to about 0.11 of the maximum main velocity component. This vortex, in the case illustrated, is centered around a point at about $y/c = 0.27$ and downstream from between the mid-channel and the suction surface of the blade. The location of this vortex was confirmed by the vorticity meter, which showed its highest rotational speed in this position.

Integrated Stagnation Pressure Losses. To provide numerical comparisons, the stagnation pressure losses have been averaged across a pitch.

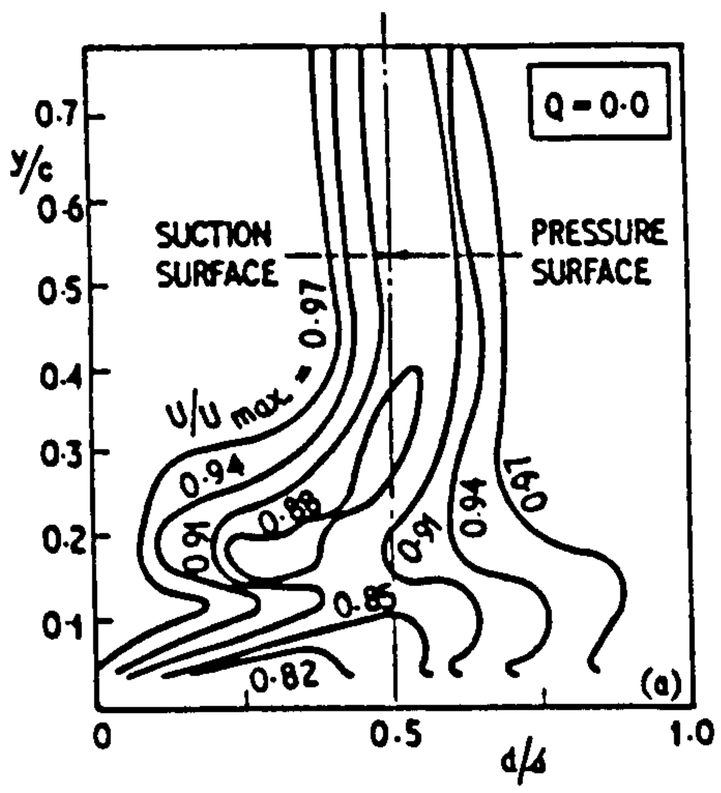

Fig. 3(a)

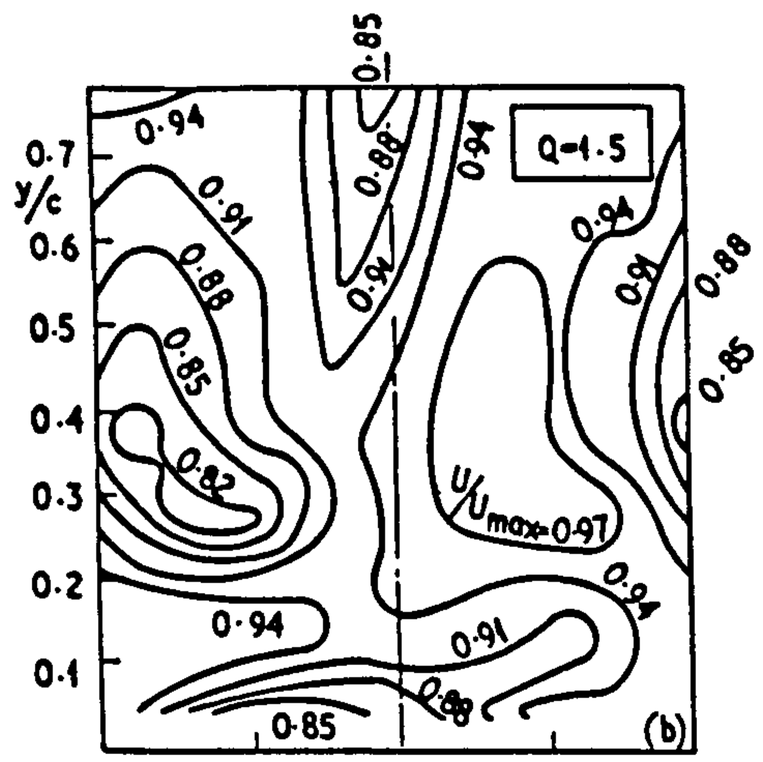

Fig. 3(b)

Fig. 3 Velocity contours at outlet traverse plane—aspect ratio 1.5

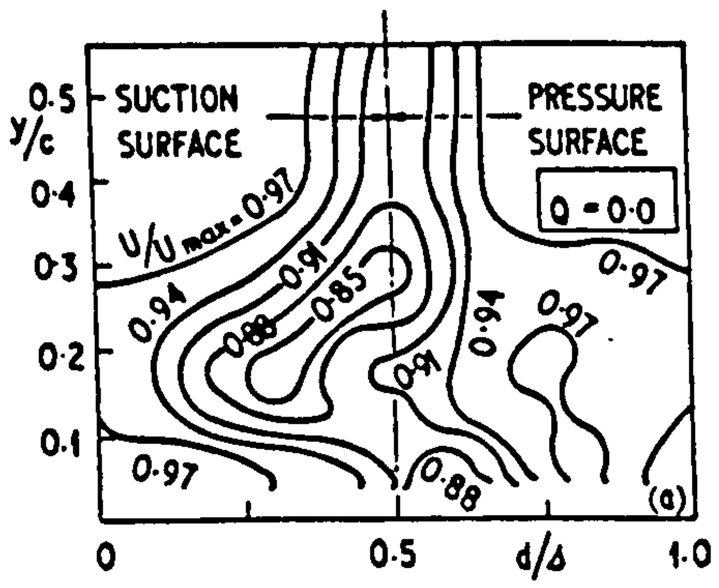

Fig. 4(a)

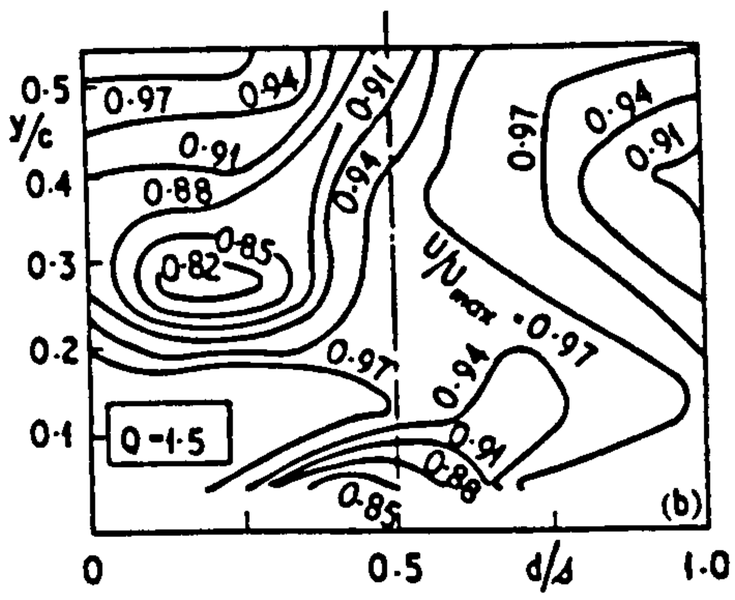

Fig. 4(b)

Fig. 4 Velocity contours at outlet traverse plane—aspect ratio 1.0

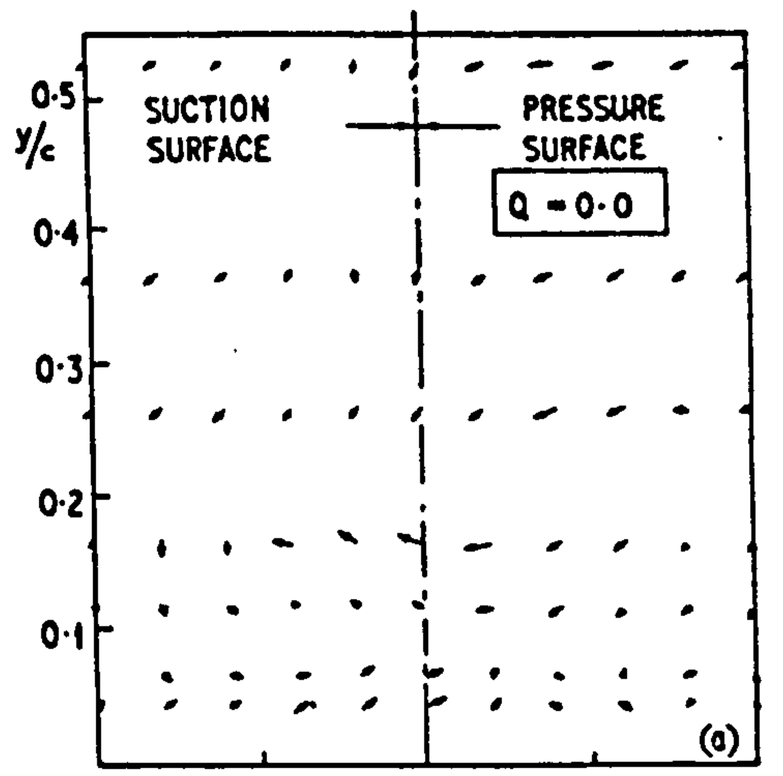

Fig. 5(a)

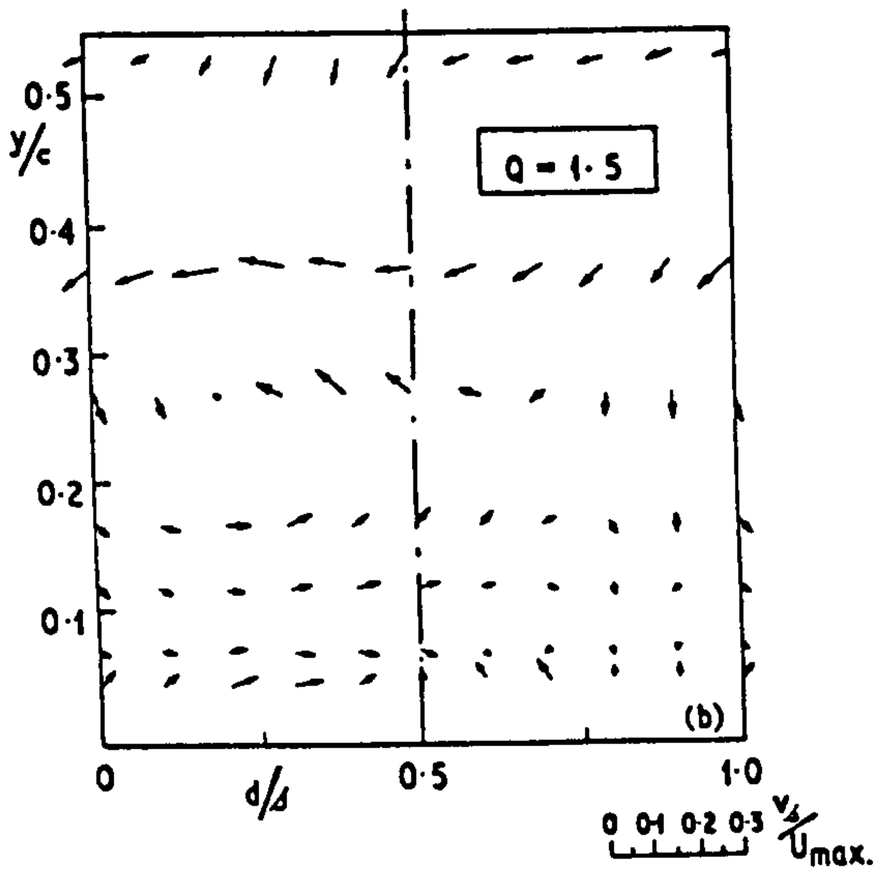

Fig. 5(b)

Fig. 5 Secondary velocities at outlet traverse plane—aspect ratio 1.0

The results, with and without injection, are shown in Figs. 6(a), (b), and (c), respectively, for the three aspect ratios.

When there was no injection, provided the aspect ratio was at least 1.5, the distribution of losses was reasonably symmetric about the blade mid-height. However, at the aspect ratio of 1.0 the losses appear

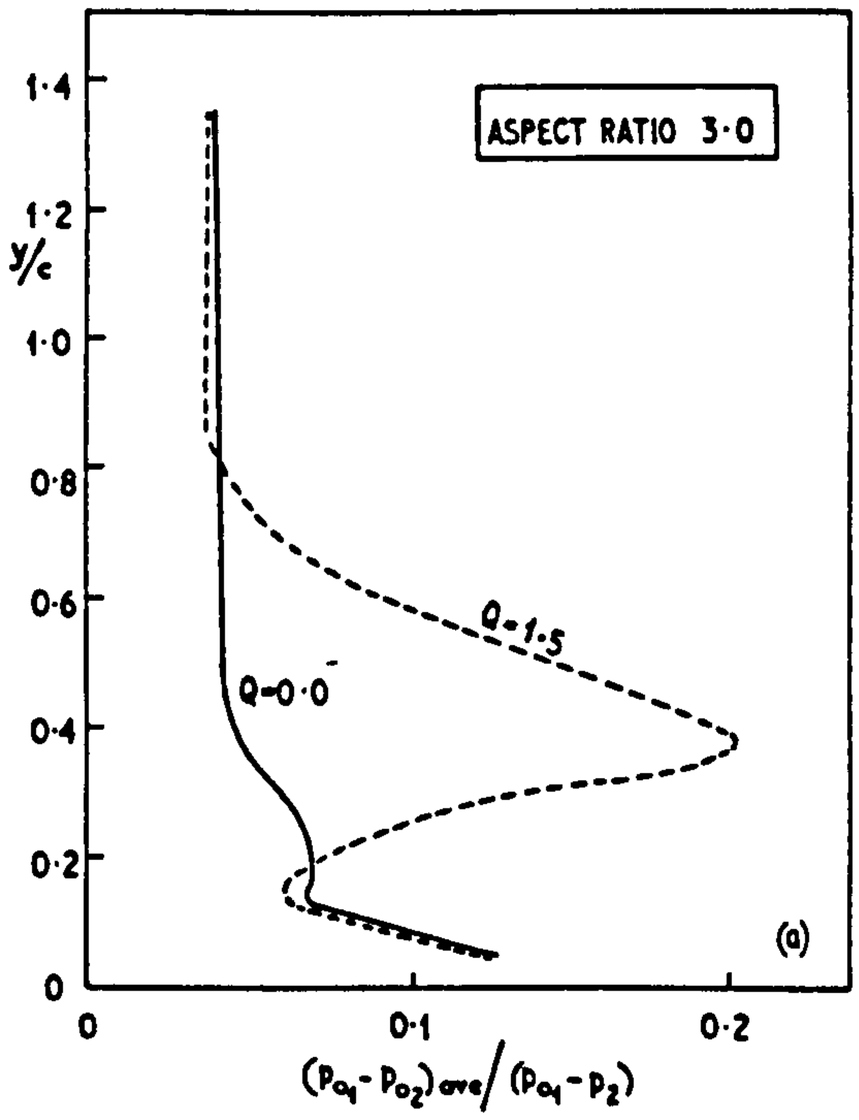

Fig. 6(a)

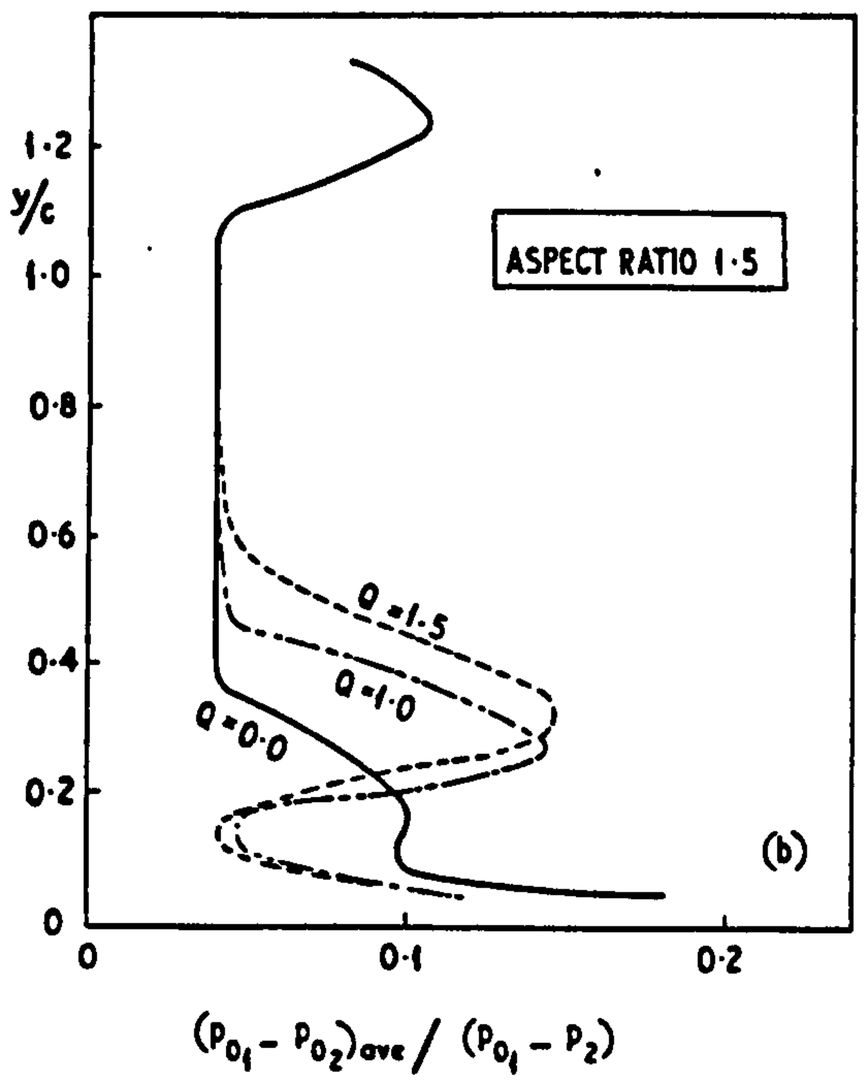

Fig. 6(b)

to be significantly higher near the end-wall which does not carry the injection slot. The only explanations that can be offered are (1) that this end-wall would have a thicker boundary layer at inlet to the cascade, as there was no boundary layer removal, and (2) the end-wall has a slot at the exit plane to allow traversing by the probes. These factors may become more significant as the aspect ratio is reduced. The forms of these integrated losses, when there is no injection, are of the customary patterns which result from the blade profile losses (uniform over the blade height), the boundary layers on the end-walls and the corner vortices (e.g. [3]). The profile loss is, as expected, unaffected by aspect ratio. The secondary and end-wall losses are approximately similar for aspect ratios of 3.0 and 1.5, but of course in the latter case they represent double the loss when averaged over the blade height. The asymmetry when the aspect ratio is 1.0 makes comparisons difficult.

When the transverse injection is introduced, the adjacent corner vortices are displaced and dominated by the vortex originating in the vicinity of the separation bubble and continuing in the exit flow, as discussed in the previous sections. The integrated pressure loss profiles show a peak adjacent to the eye of this vortex. When the aspect ratio is 1.0, injection appears to reduce the secondary losses associated with the corner vortices on the end-wall opposite to that carrying the injection slot.

To assist comparisons of performance, spanwise averages of these pitch-averaged pressure losses have been made, and these are discussed in the next section.

Overall Average Stagnation Pressure Losses. Overall average stagnation pressure losses have been obtained. From these, nozzle efficiencies have been calculated, according to the relation for incompressible flow

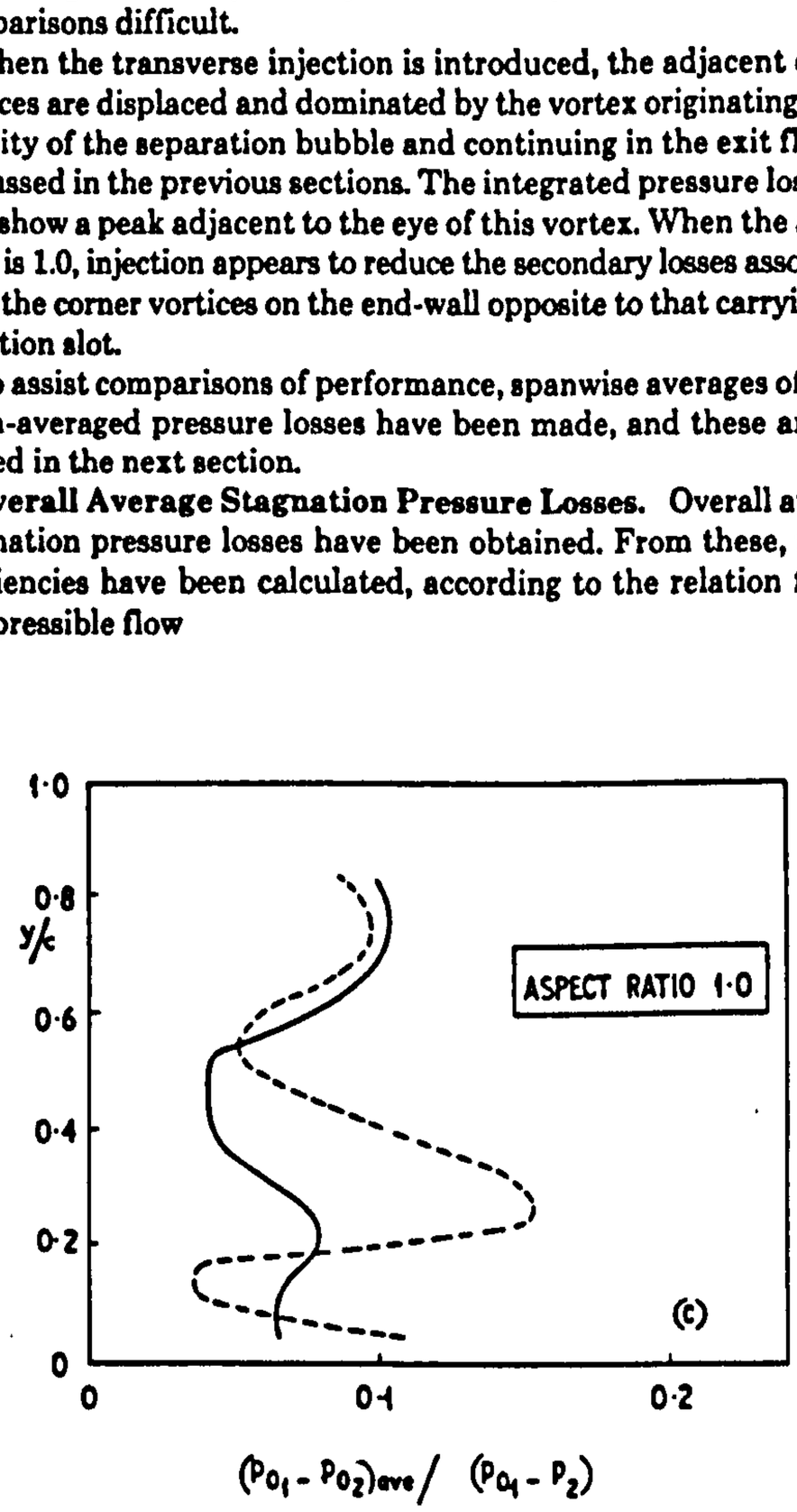

Fig. 6(c)

Fig. 6 Integrated stagnation pressure losses

Table 2 Nozzle efficiencies and "strengths" of exit vortex

Aspect Ratio	Inject. Veloc. Ratio Q	Inject. Mass Ratio	Nozzle Effy. η	Exit Vortex Parameters D/D_{ref}	E/E_{ref}	F/F_{ref}
3.0	0.0	0.0	0.947	0.39	0.15	0.29
	1.5	0.035	0.936	1.00	1.00	1.00
1.5	0.0	0.0	0.929	0.16	0.03	0.05
	1.0	0.023	0.925	0.44	0.19	0.15
	1.5	0.035	0.923	0.56	0.36	0.44
1.0	0.0	0.0	0.930	0.20	0.04	0.09
	1.5	0.035	0.915	0.64	0.41	0.58

The reference values (D_{ref} etc) are the values of the parameters obtained with aspect ratio of 3.0 and $Q = 1.5$.

$$\eta = 1 - \frac{p_{0_1} - p_{0_2}}{p_{0_1} - p_2} \quad (1)$$

The results are given in Table 2. The efficiencies, when there is no injection, decrease as aspect ratio diminishes, chord of course remaining constant, in a manner similar to that generally observed (e.g. [4]). When injection is introduced, there is a reduction in efficiency which appears almost constant for a given mass injection ratio, although it is possible that the reduction will be more marked if the aspect ratio is reduced below 1.0. In the range of aspect ratios from 3.0 to about 1.0, transverse injection at a mass ratio of 0.035 causes a loss in efficiency of about one percent.

The losses in stagnation pressure have also been compared with those predicted by a simple one-dimensional theory [5, 2]. In [2] the predicted loss had been shown to be

$$\Delta p_0 = \tfrac{1}{2}\rho U_1^2[(f^2 - 1) - 2(f - 1)Q \cos\theta \cos\alpha_1] \quad (2)$$

The comparison between observed and predicted losses is given in Fig. 7. Some results from the previous work [2] at aspect ratio 3.0 have been included. The agreement is reasonable for aspect ratios 3.0 and 1.5. The observed loss becomes somewhat above the predicted loss when the aspect ratio is 1.0.

The one-dimensional theory has also been used as a basis of comparison for changes in flow capacity expressed by reductions in exit static pressure for the same main approach mass flow. The predicted reduction in exit static pressure is given by [2]:

$$-\Delta p_2 = \tfrac{1}{2}\rho U_1^2[(f^2 - 1) - 2(f - 1)Q \cos\theta \cos\alpha_1] + (f^2 - 1)(p_{0_1} - p_{2d}) \quad (3)$$

The comparison between observation and prediction is given in Fig. 8, again including previous results. Agreement again is reasonable.

Integrated Deviations. Pitch-integrated deviations are given in Figs. 9(a) to (c). The range of integrated deviations when transverse injection is taking place is somewhat reduced from about 10 deg to about 7 deg when the aspect ratio is lowered from 3.0 to 1.5. The further lowering of aspect ratio to 1.0 has little effect.

The much increased variation in deviation resulting from transverse injection is indicative of the presence of the exit vortex. In the earlier work [2] an attempt had been made to quantify this exit vortex by defining parameters D, E, and F which were proportional, respectively, to the circulation, to the kinetic energy of the tangential velocity components in the vortex, and to the angular momentum of the vortex, if the vortex were assumed to be a rotating solid body bounded in diameter by the positions of maximum pitch-integrated positive and negative deviations. The parameters are given by

$$D = (\Delta\alpha^*)(\Delta y^*/c) \quad (4)$$

$$E = (\Delta\alpha^*)^2(\Delta y^*/c)^2 \quad (5)$$

$$F = (\Delta\alpha^*)(\Delta y^*/c)^3 \quad (6)$$

These measures of the exit vortex have been applied in the present work, and the results are included in Table 2, where the values at as-

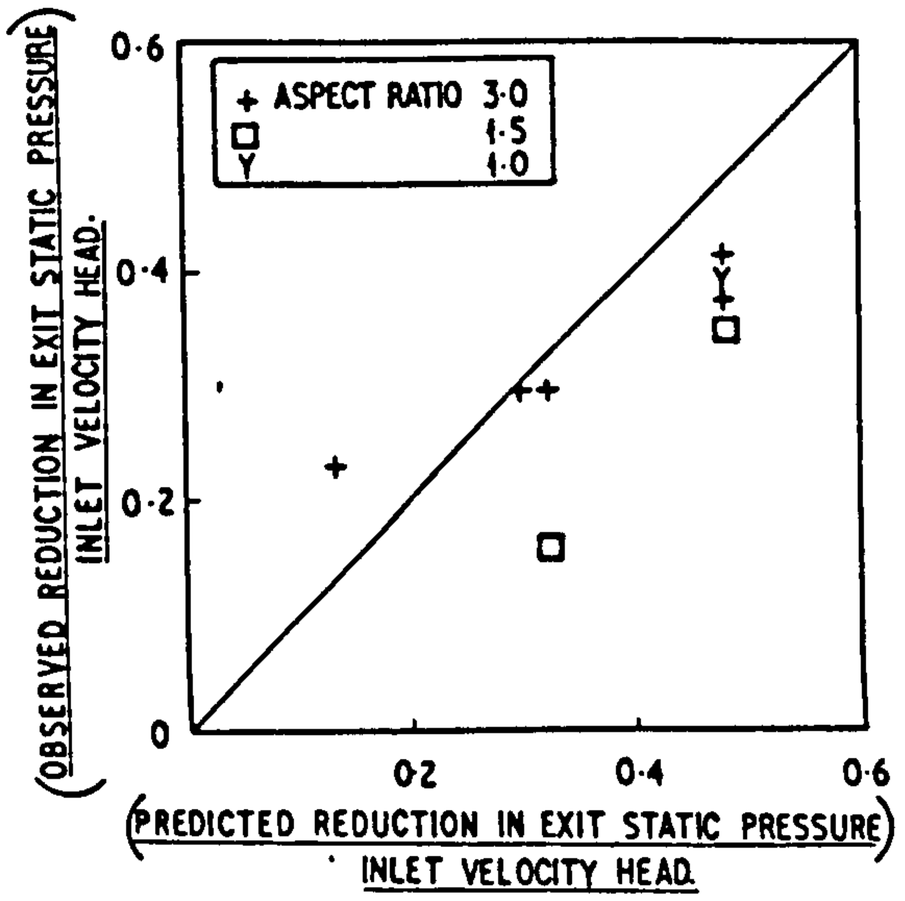

Fig. 8 Predicted and observed changes in downstream static pressure

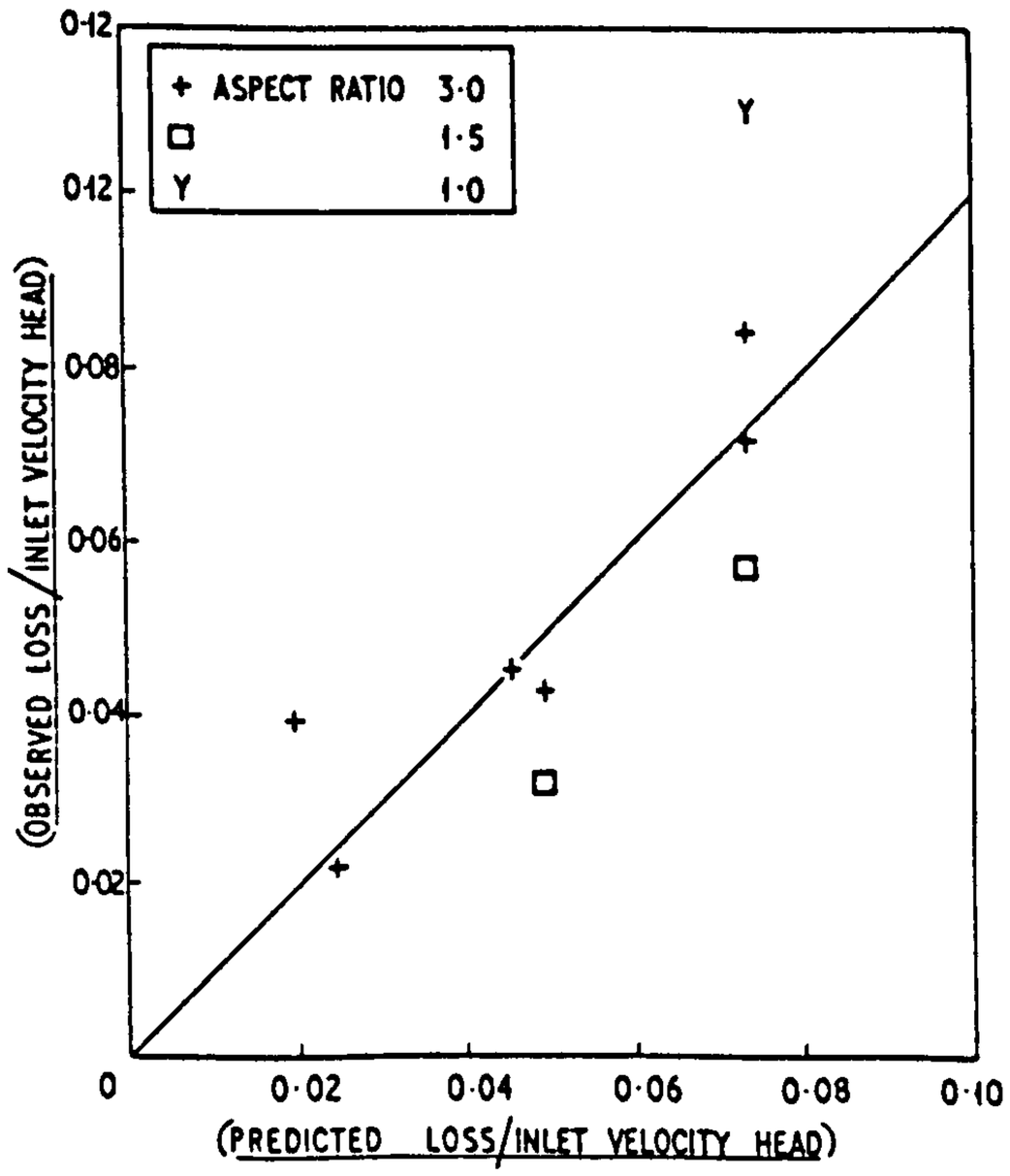

Fig. 7 Predicted and observed losses of stagnation pressure

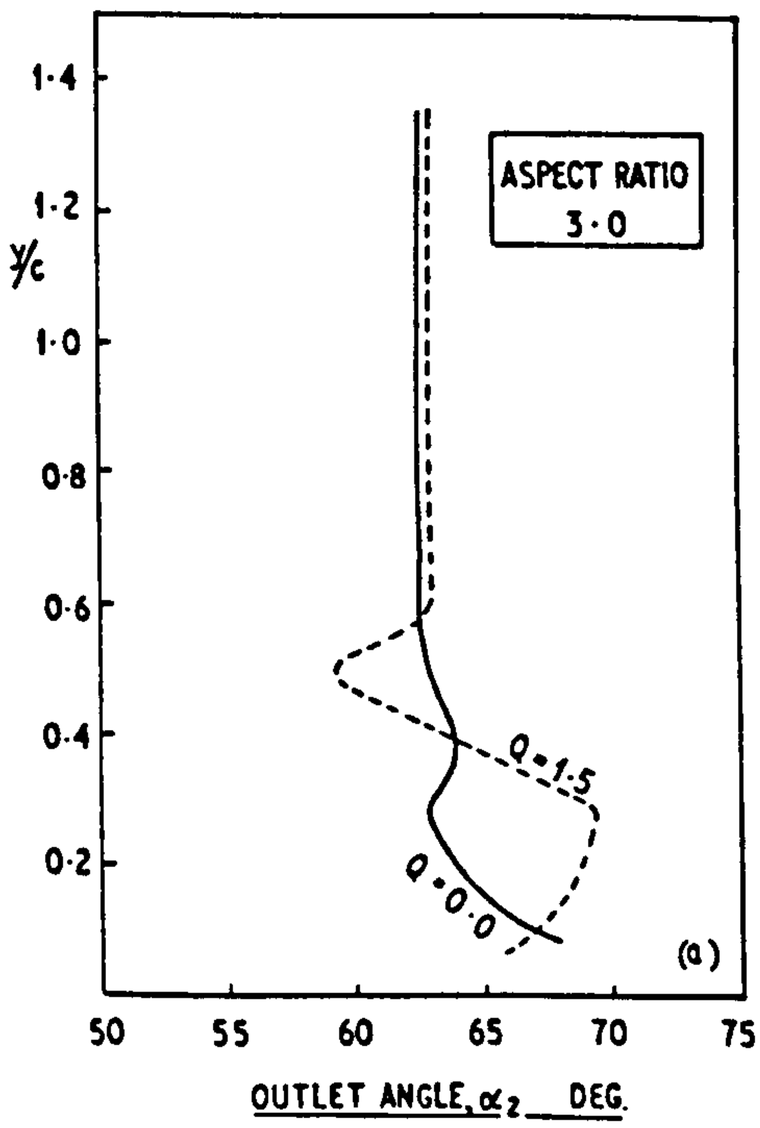

Fig. 9(a)

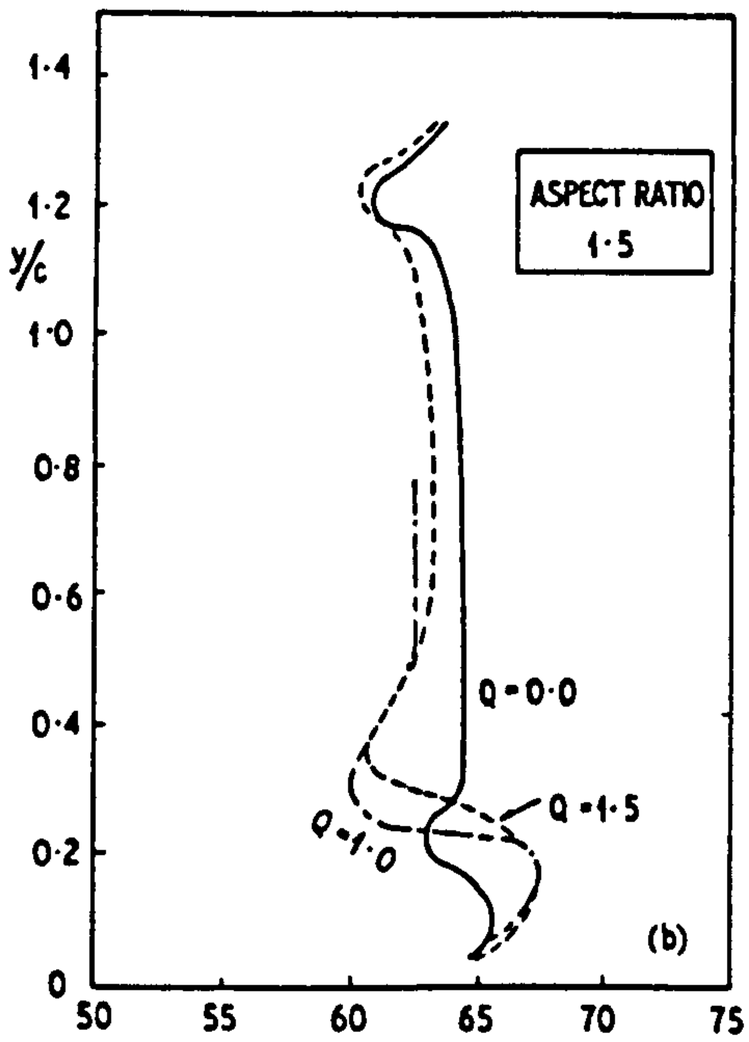

Fig. 9(b)

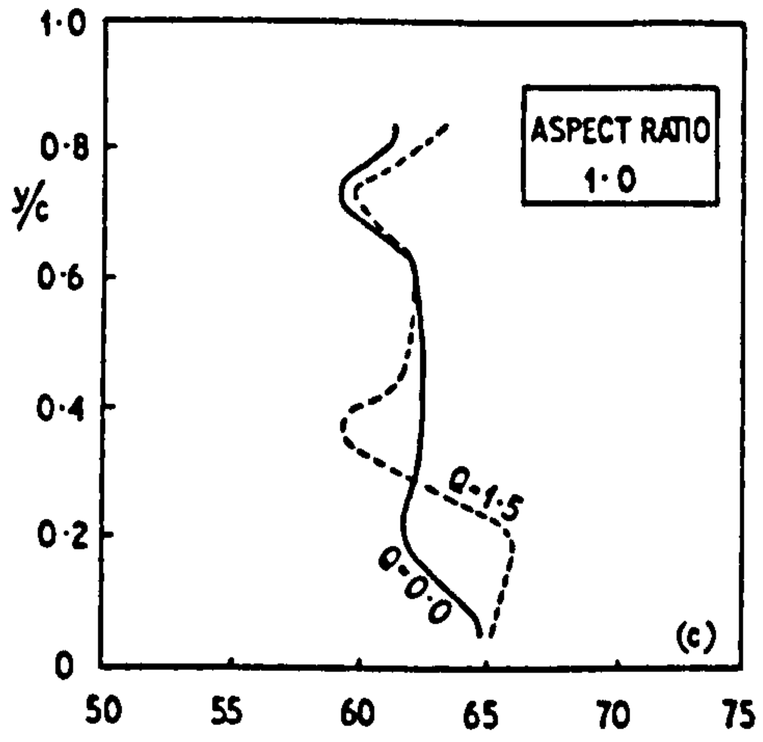

Fig. 9(c)

Fig. 9 Integrated deviations

pect ratios 1.5 and 1.0 are compared with those at aspect ratio 3.0, and injection mass ratio 0.035, which is taken as reference. There is inevitably experimental error in the results obtained, but it appears that reducing the aspect ratio has reduced the strength of the exit vortex. However it might be that at the lower aspect ratios, between 1.5 and 1.0, this reduction has ended.

Conclusions

The following effects from transverse injection occur as the aspect ratio is reduced (at constant chord):

1 The height of the separation bubble on the end-wall behind the injection slot is reduced, but the extent of the bubble along the end-wall is only slightly diminished;

2 The stagnation pressure losses (and nozzle efficiency reductions) remain approximately constant and in agreement with a one-dimensional theory, except when the aspect ratio drops to around 1.0 where there may be a tendency for losses to increase;

3 Flow capacity reductions remain constant and in agreement with the one-dimensional theory;

4 The position of the exit vortex is moved towards the end-wall as aspect ratio is reduced, the range of movement being from y/c = 0.38 to y/c = 0.27 as aspect ratio is reduced from 3.0 to 1.0

5 The strength of the exit vortex, as indicated by circulation, or rotational kinetic energy, or rotational momentum, is reduced by lowering the aspect ratio from 3.0 to 1.5, but the further reduction to 1.0 produced little change.

Acknowledgments

The authors wish to thank Professor R. S. Silver for his encouragement, the staff of Rolls-Royce Ltd. for stimulating comments, and the Science Research Council for financial support.

References

1 Shrivastava, K. D., and Maccallum, N. R. L., "The Effect of a Transversely Injected Stream on the Flow Through Turbine Cascades: Part I—Flow Effects," ASME Paper No. 77-GT-87.

2 Shrivastava, K. D., and Maccallum, N. R. L., "The Effect of a Transversely Injected Stream on the Flow Through Turbine Cascades: Part II—Performance Changes," ASME Paper No. 77-GT-88.

3 Dunham, J., "A Review of Cascade Data on Secondary Losses in Turbines," Journal of Mechanical Engineering Science, Vol. 12, No. 1, 1970, pp. 48–59.

4 Ainley, D. G., and Mathieson, G. C. R., "An Examination of the Flow and Pressure Losses in Blade Rows of Axial-Flow Turbines," Aeronautical Research Council R & M No. 2891, 1955.

5 Barnes, J. F., and Fray, D. E., "An Experimental High Temperature Turbine: Part II—The Effects of Cooling on the Aerodynamic Performance," Aeronautical Research Council R & M No. 3405, 1965.

Printed in U. S. A.

Publication 22

79-GT-18

ted in U.S.A.

an ASME publication

$3.00 PER COPY
$1.50 TO ASME MEMBERS

Vortex Effects Resulting from Transverse Injection in Turbine Cascades, and Attempts at Their Reduction

B. A. ABURWIN

Research Student

N. R. L. MACCALLUM

Senior Lecturer

Dept. of Mechanical Engineering,
University of Glasgow,
Glasgow, Scotland

A preliminary experimental investigation has been made of the effects of vortices in the approach stream on turbine blade row performance. The vortex regime has been simulated by stationary vortex generators. The net pressure losses within the following blade row were reduced by 23 and 12 percent when the vortex generators were placed in line, respectively, with the mid-passages and with the leading edges. Further, the discrete inlet vortices had virtually disappeared at the exit plane. In addition, methods have been tested for reducing the exit vortex, particularly when enhanced by transverse injection. The most effective scheme examined was a fence location on the suction surface near the endwall. However, there is a pressure loss penalty.

Contributed by the Gas Turbine Division of The American Society of Mechanical Engineers for presentation at the Gas Turbine Conference & Exhibit & Solar Energy Conference, San Diego, Calif., March 12-15, 1979. Manuscript received at ASME Headquarters December 8, 1978.

Copies will be available until December 1, 1979.

THE AMERICAN SOCIETY OF MECHANICAL ENGINEERS, UNITED ENGINEERING CENTER, 345 EAST 47th STREET, NEW YORK, N.Y. 10017

Vortex Effects Resulting from Transverse Injection in Turbine Cascades, and Attempts at Their Reduction

B. A. ABURWIN N. R. L. MACCALLUM

NOMENCLATURE

c = chord
d = distance along blade pitch from one mid-passage line to next, in direction of suction surface
D = measure of strength of exit vortex, defined by $(\Delta\alpha^*)(\Delta y^*/c)$
E = measure of kinetic energy of tangential components in exit vortex, defined by $(\Delta\alpha^*)^2(\Delta y^*/c)^2$
F = measure of angular momentum of exit vortex, defined by $(\Delta\alpha^*)(\Delta y^*/c)^3$
p = pressure
Q = ratio of maximum velocity of injected jet to velocity of main approach flow
s = blade pitch
U = velocity in main flow direction
v = velocity
x = distance in axial direction from leading edge
y = distance from end-wall carrying injection slot
z = distance along pitch direction from leading edge
α = main flow angle, measured from axial direction
ρ = density

Subscripts

o = stagnation
1, 2 = inlet to, outlet from cascade
amb = ambient
ave = average
s = secondary

Superscript

* = range of pitch-integrated exit vortex

INTRODUCTION

When an additional flow is injected transversely into the main flow entering a row of turbine blades, as when disk cooling air in a gas turbine is returned, several significant effects in the main flow are observed (1).[1] One of these effects is the strengthening of the secondary vortex in the flow leaving the blade, or nozzle guide vane row. The influences of injection and cascade variables on the strength of this exit vortex have been studied in straight cascades (2, 3) and in an annular cascade (4).

The present work had two aims. The first

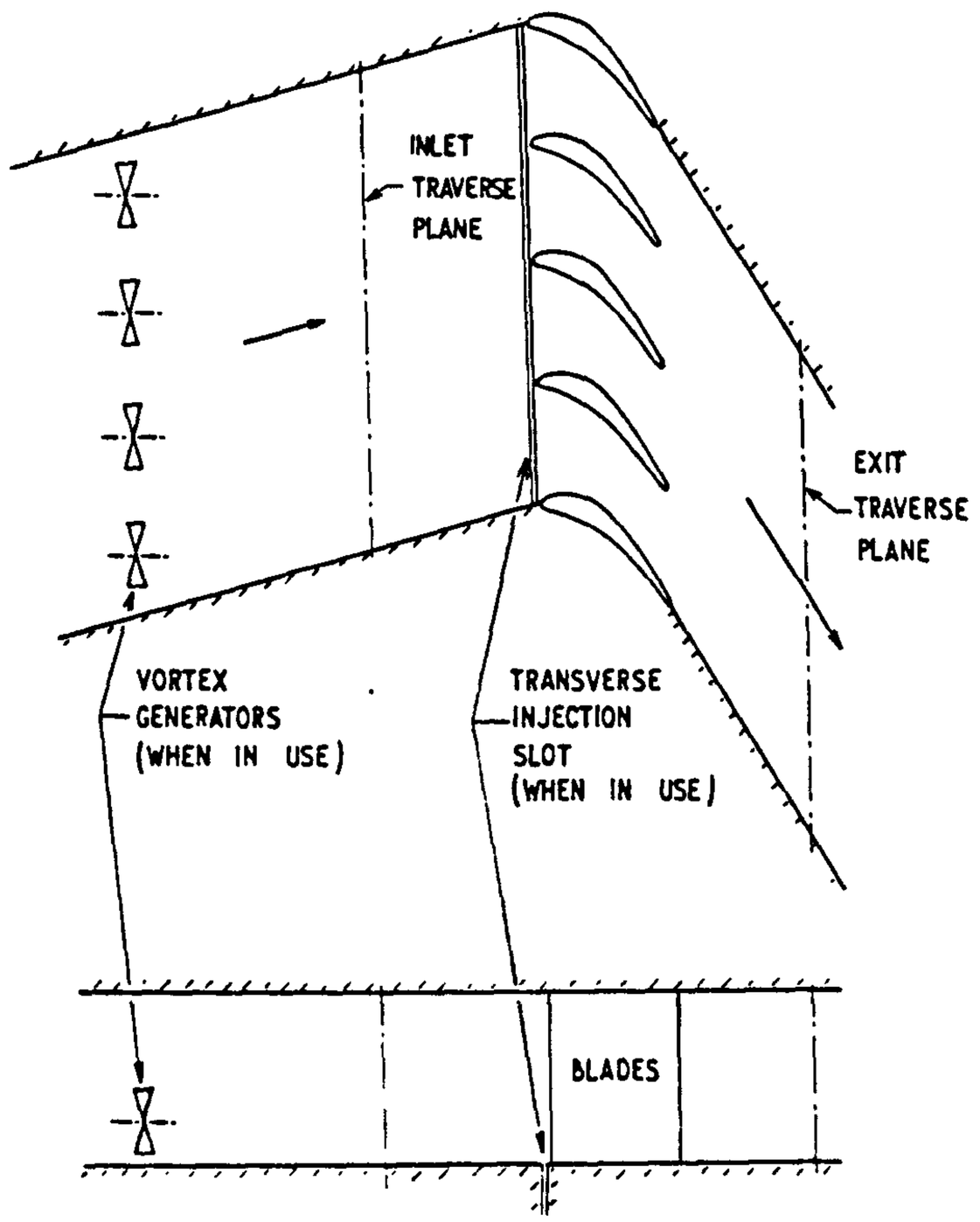

Fig. 1 Test cascade

[1] Underlined numbers in parentheses designate References at end of paper.

Table 1 Coordinates of Blade Profile -- 40-Deg Stagger Angle

pressure surface	x/c	0.0	0.049	0.162	0.285	0.392	0.476	0.542	0.613	0.676	0.749
	z/c	0.0	0.021	0.066	0.172	0.265	0.275	0.32	0.324	.327	.283
suction surface	x/c	0.0	.045	0.151	0.272	0.376	0.461	0.537	0.61	0.672	0.728
	z/c	0.0	-0.022	-0.035	-0.016	0.035	0.119	0.226	0.346	0.465	0.615

was to investigate the effect of the exit vortex leaving one row of blades on the performance of the next row. The second aim was to study methods of reducing the strength of the exit vortex. These investigations are discussed in turn in this paper, and the major conclusions are brought together in the final section.

APPARATUS

This consisted of a cascade of five blades (four passages) having a chord of 129 mm (5.07 in.), of aspect ratio 1.0, set at a stagger angle of 40 deg and at a pitch of 88 mm (3.5 in.). The cascade, which had been used in previous related experiments (1-3), is illustrated in Fig. 1, and the coordinates of the blade profile are given in Table 1. The cascade was placed in the suction to a variable speed fan. Typically, the flow velocity at exit from the cascade was 23 m/s (75 ft/s), corresponding to a Reynolds Number, based on the exit velocity and chord, of 2.2×10^5.

The main airflow to the cascade entered through a contraction of area ratio 8.3. Wire grids were placed in this contraction to give a turbulence level, when there were no vortex generators present, of 1.5 percent at inlet to the cascade. The inlet to the cascade was set to give an air angle of 15 deg to the axial direction.

When transverse injection was required, this was made through a slot 3.0 mm wide, running across one end-wall immediately in front of the cascade, as illustrated in Fig. 1. In the present work, the injected air was directed at right angles to the main air flow. The injected flow and the main flow were at the same temperature. When not required, the injection slot was taped over.

Performance of the cascade was established by traversing the flows at inlet and outlet. The inlet traverse plane was at an axial distance of 1.3 axial chord upstream from the blade leading edge, and the downstream plane was at an axial distance of 1.0 axial chord from the trailing edge. The instrument used for measuring the flow velocity, direction and pressure was a five-hole spherical probe of 8-mm dia. This instrument was checked satisfactorily in these flows against a three-hole probe of 2.7-mm dia. Estimated accuracy of the five-hole probe is ± 0.5 m/sec in velocity components and ± 0.5 deg in direction.

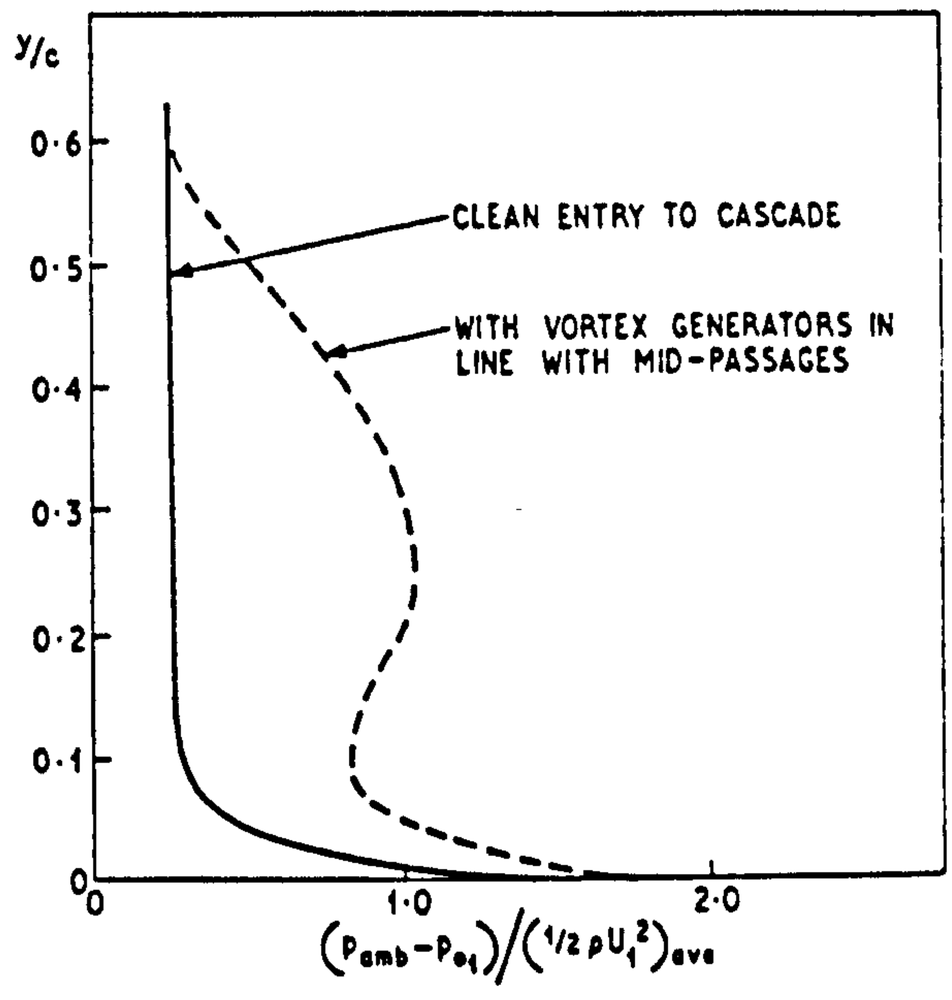

Fig. 2 Inlet pressure loss distributions - without and with vortex generators

The central blade in the cascade was provided with pressure tappings from which the pressure distributions could be observed, over a range of blade heights.

EFFECT OF VORTICES IN FLOW ENTERING A BLADE ROW

As described earlier, there are secondary vortices in the flow leaving a turbine blade row, and these are considerably enhanced if a flow is injected transversely into the main flow entering that blade row. In many turbines, the flow leaving this row of blades then enters a subsequent row.

The aim of the tests reported here was to simulate this series of vortices leaving the first row, and study their effect on the second row. For this work, the second row was represented by the straight cascade described in the previous section, and the vortices in the cascade entry flow were formed by introducing a series of vortex generators. In the real turbine the vortices move periodically across the entry to the passages, from the pressure to the suction surfaces. As time-mean instrumentation was to be used to measure the flow velocity and direction and the pressure at outlet from the

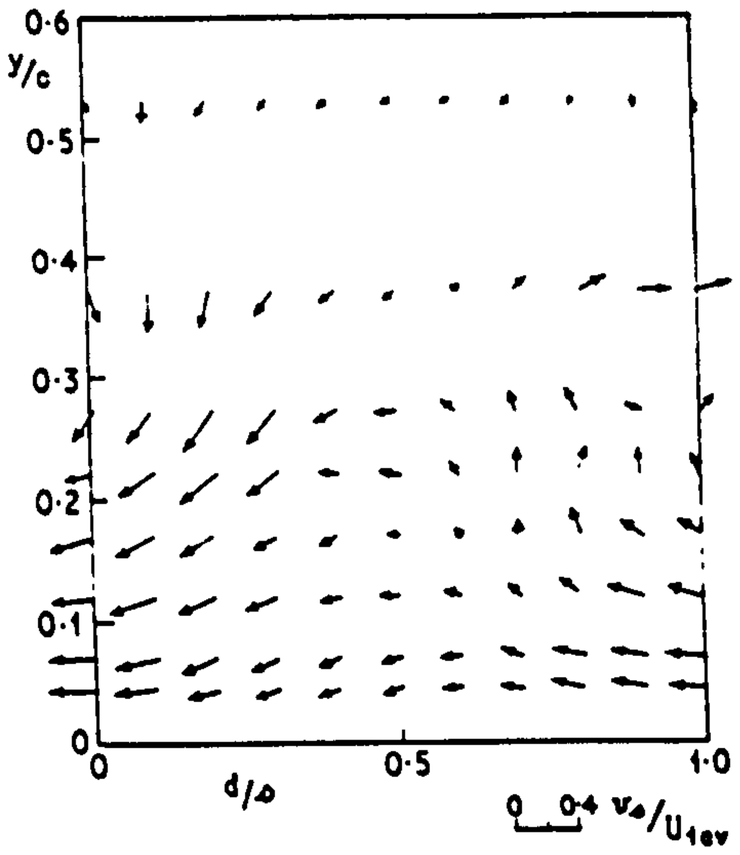

Fig. 3 Secondary velocities at inlet to cascade - vortex generators in line with mid-passages

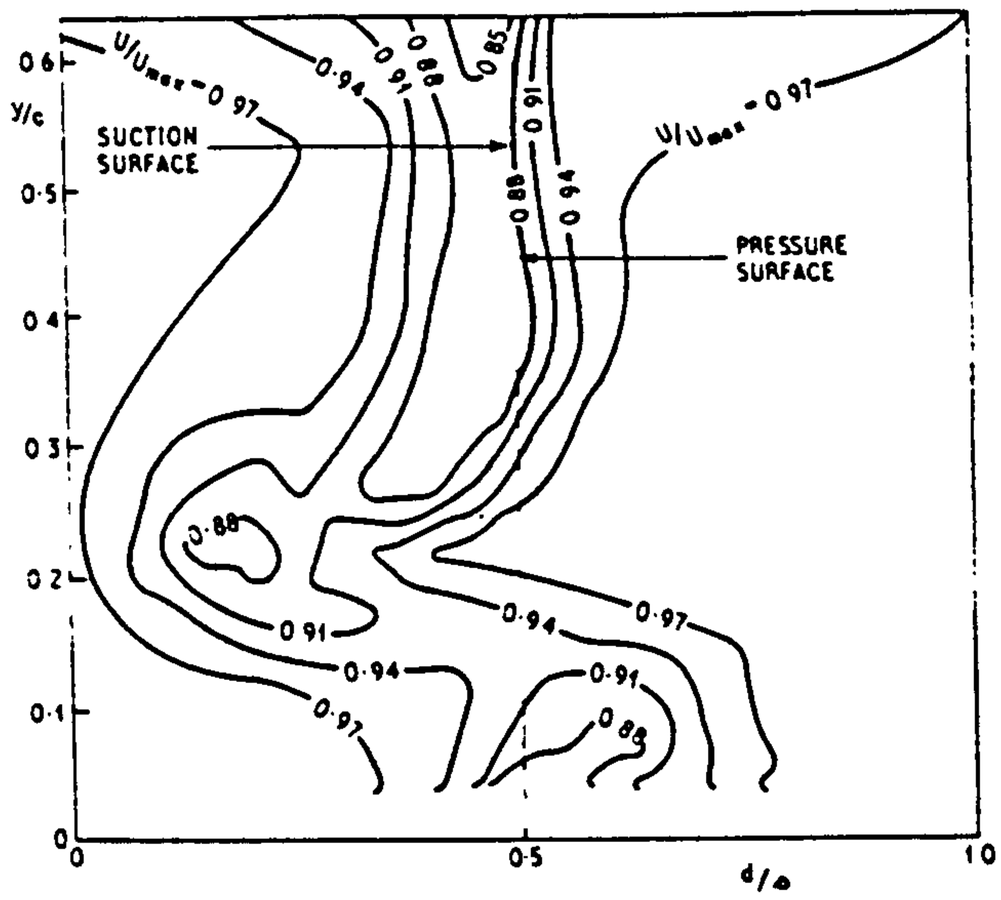

Fig. 5 Velocity contours at outlet traverse plane - clean entry to cascade

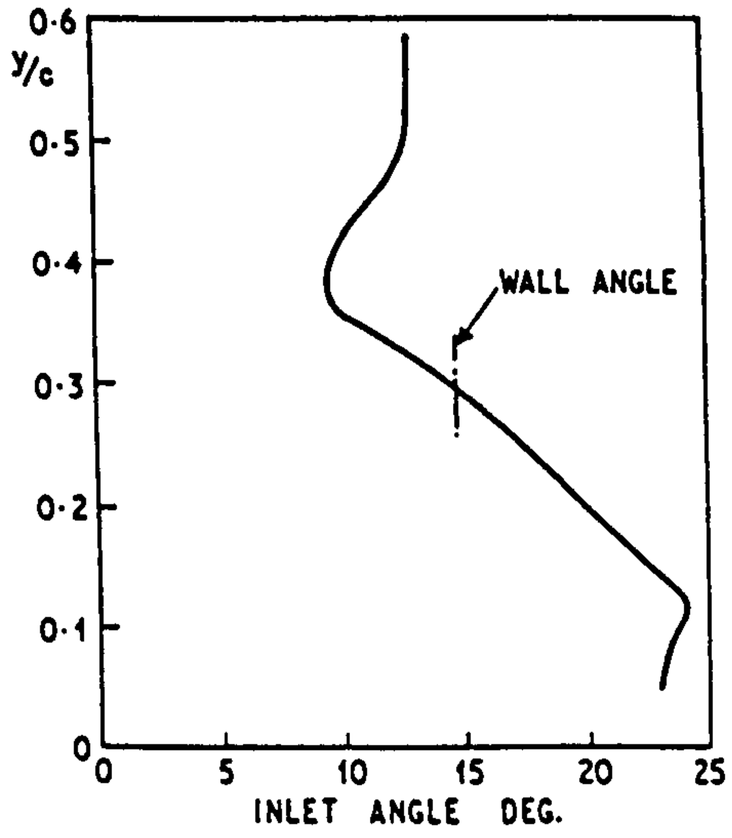

Fig. 4 Integrated inlet angles - vortex generators in line with mid-passages

test cascade, it was decided that for this initial study, the vortex generators should be kept stationary relative to the cascade. Tests would be carried out with generators in different positions relative to the cascade. This use of stationary generators, while not truly representative, should give helpful indications of the effects of these vortices. The design of the entry section to the cascade is greatly simplified by this procedure.

Vortex Generators

The vortex generators were prepared from thin metal disks, 51-mm dia, cut to make eight vanes, and the vanes twisted to 45 deg to the axis of the disk, the direction of twisting being such as to simulate the exit vortex; i.e., the flow at the side of the vortex nearest the end-wall is twisted toward the suction surface of the passage from which it is leaving. This means that when the vortex enters the next row of blades, the flow at the side of the vortex nearest to the end-wall is twisted toward the pressure surface of this new row.

The vortex generators were mounted, as illustrated in Fig. 1, with their axes at a height of 33 mm (0.26 chord) from one end-wall and at an axial distance of 300 mm (3.1 axial chord) in front of the cascade. The axes of the generators were parallel to the axial flow direction. This positioning of the generators produced vortices which corresponded with the slightly asymmetric exit vortices to be simulated (1).

In the first series of tests using the vortex generators, the generators were placed as illustrated in Fig. 1, in the lines leading to the mid-passage positions. In the second test, the generators were placed in line with the leading edges of the blades. In both cases, therefore, the pitch between the generators was the same as the pitch of the blades in the cascade.

Test Procedure

For these tests, no transverse injection was used and the injection slot was taped over, as was the boundary layer suction slot.

With the entry to the cascade in the

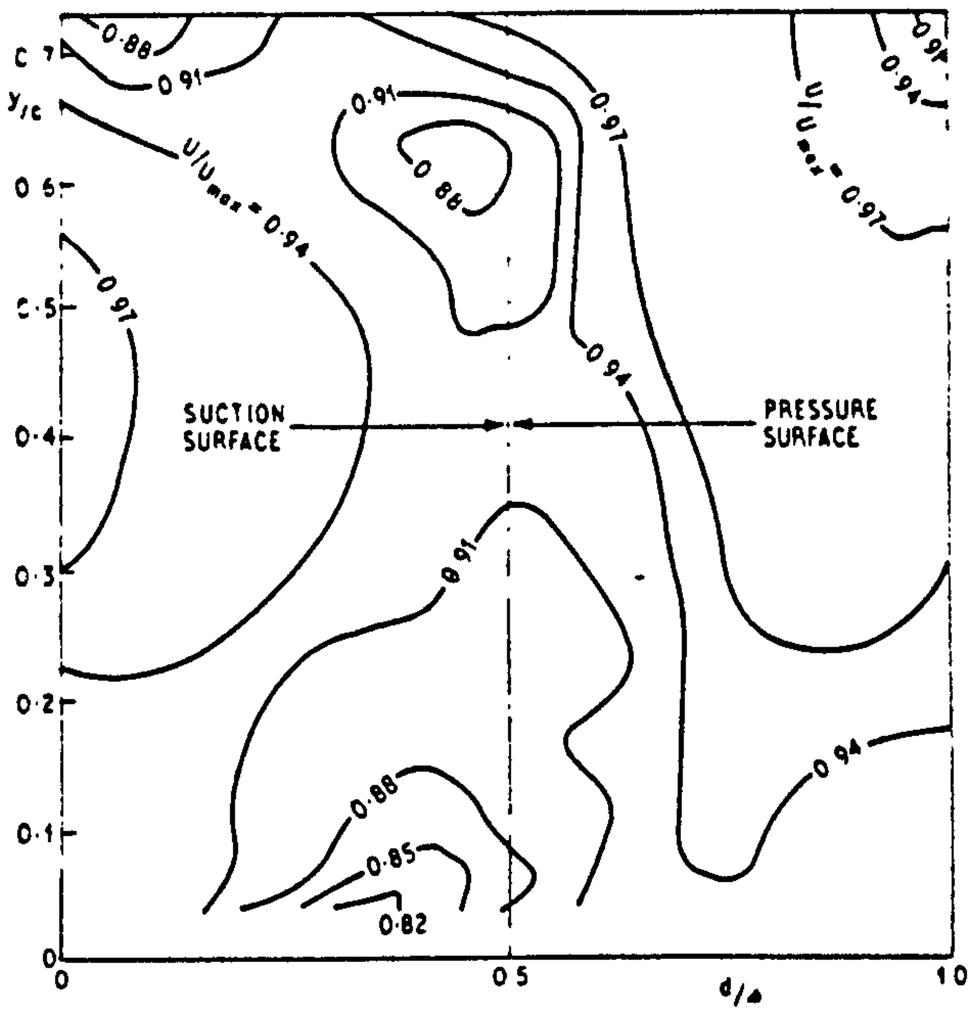

Fig. 6 Velocity contours at outlet traverse plane - vortex generators in entry in line with mid-passages

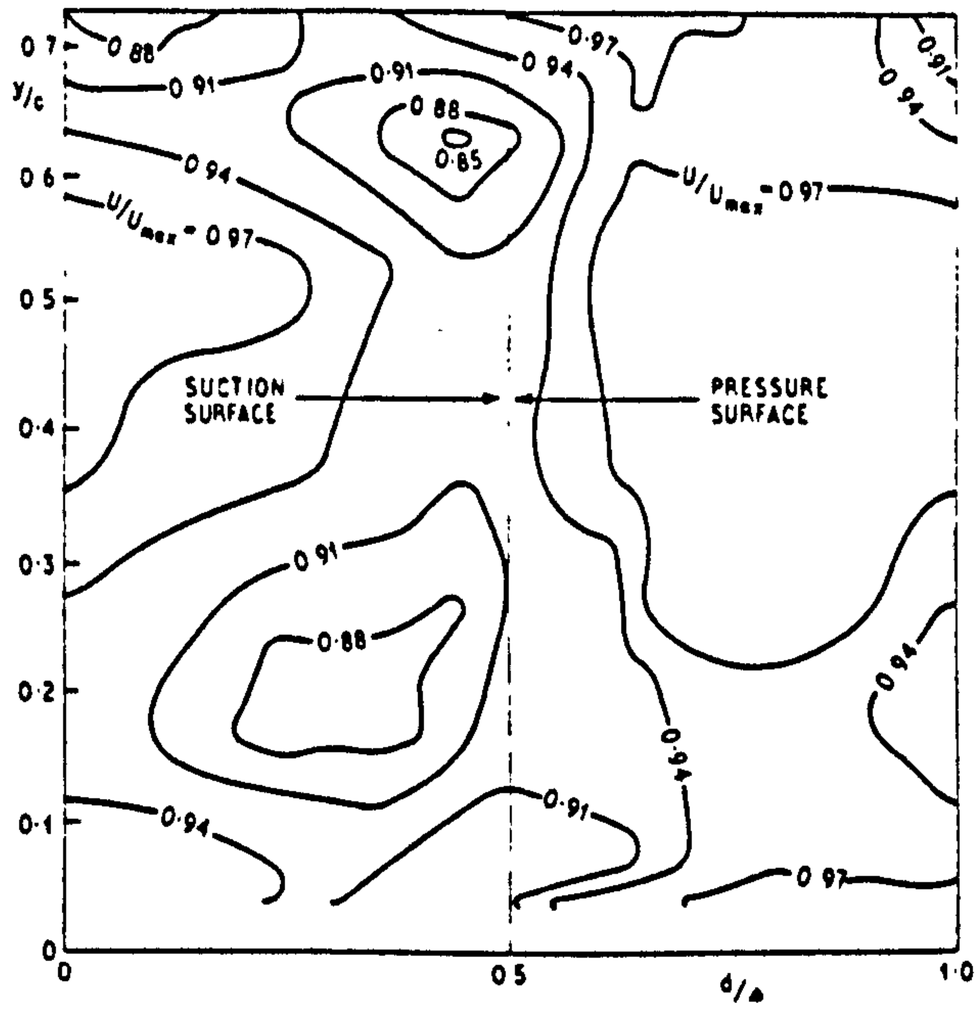

Fig. 7 Velocity contours at outlet traverse plane - vortex generators in entry in line with leading edges

"clean" state, i.e., with no vortex generators introduced, the angles of the exit side-walls were adjusted, relative to the cascade, until there was a symmetric velocity distribution across the exit flow. This occurred when the exit side-walls were at 59.5 deg to the axial direction. The performance of the cascade was then established by traversing the flows at inlet and outlet. Pressure distributions around the blade surfaces were also recorded.

Vortex generators were then introduced, as described in the previous section, and the above series of readings repeated.

Results and Discussion

Inlet Velocity Distributions. The pitch-integrated inlet pressure loss distributions, relative to atmospheric pressure, are shown in Fig. 2, over 60 percent of the blade span, starting from the end-wall on which the vortex generators are mounted.

When there are no vortex generators the losses are very uniform, and small, being due to the inlet system, including turbulence grids.

The introduction of the vortex generators produces, as intended, vortex motion and the secondary flow components are illustrated in Fig. 3; in this case, the generators are situated in line with the mid-passage positions. The blockage of the vortex generator leads to a reduction in forward velocity downstream from the generator, and this is indicated by the pitch-integrated loss distribution shown in Fig. 2. The peak of this pressure loss associated with the vortex occurs at a blade span value of about 0.24 for y/c, which compares with the span position of the generators of 0.26 for y/c. Pitch-integrated inlet angles are shown in Fig. 4.

Strengths of Inlet Vortices. It is necessary to compare the strengths of these vortices produced by the vortex generators with the strengths of the vortices which are introduced into blade passage exit flows as a result of transverse injection. Three simple parameters have been used to quantify the strengths of these exit vortices (2). These parameters, D, E, and F, are proportional to the circulation, to the kinetic energy of the tangential components velocity components in the vortex, and to the angular momentum of the vortex, respectively, if the vortex is assumed to be a rotating solid body bounded in diameter by the positions of maximum pitch-integrated positive and negative deviation. The parameters are given by

$$D = (\Delta\alpha^*)\ (\Delta y^*/c) \qquad (1)$$

$$E = (\Delta\alpha^*)^2\ (\Delta y^*/c)^2 \qquad (2)$$

$$F = (\Delta\alpha^*)\ (\Delta y^*/c)^3 \qquad (3)$$

For a typical case with transverse injection

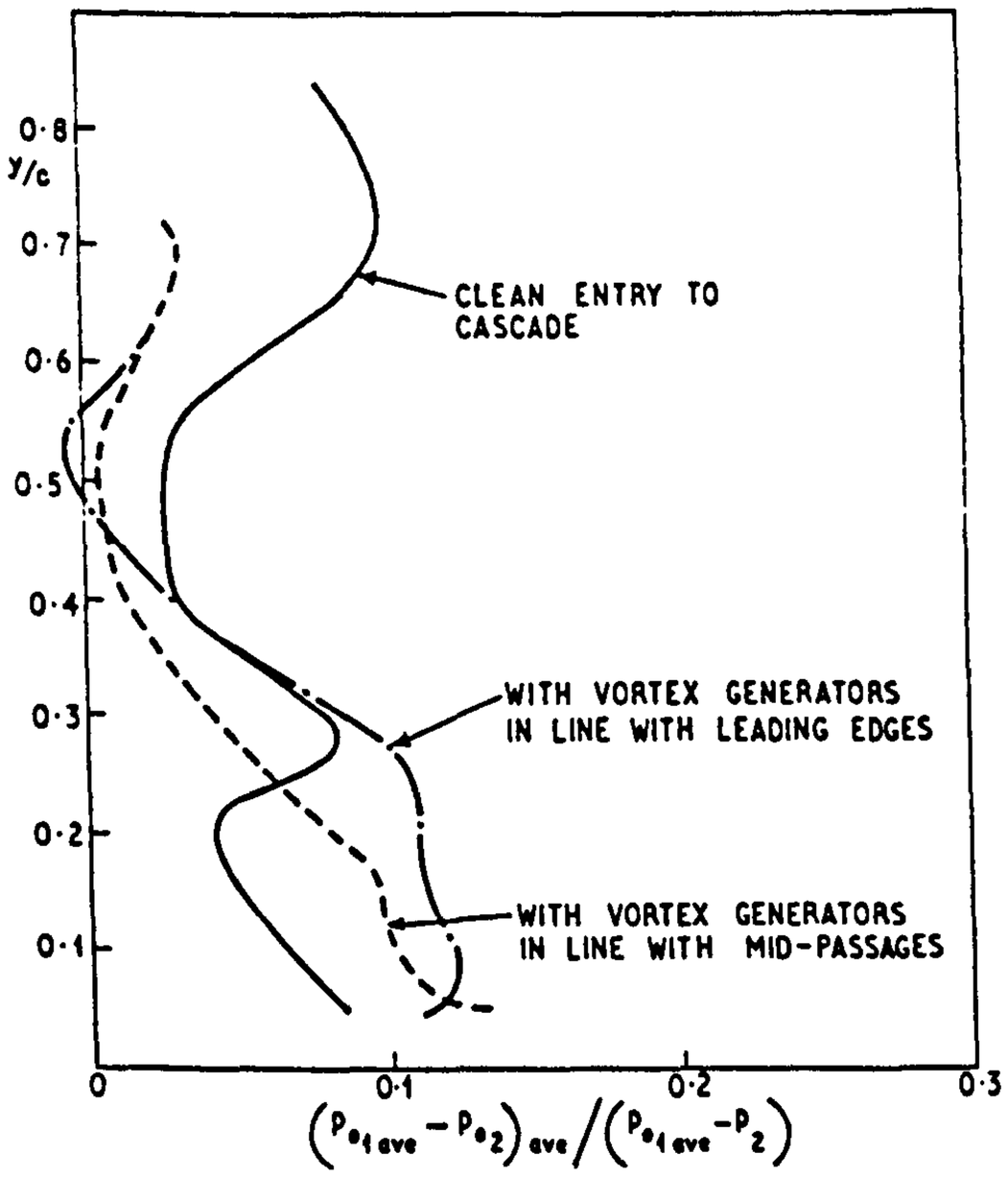

Fig. 8 Integrated stagnation pressure losses across cascade for entry flows without and with vortices

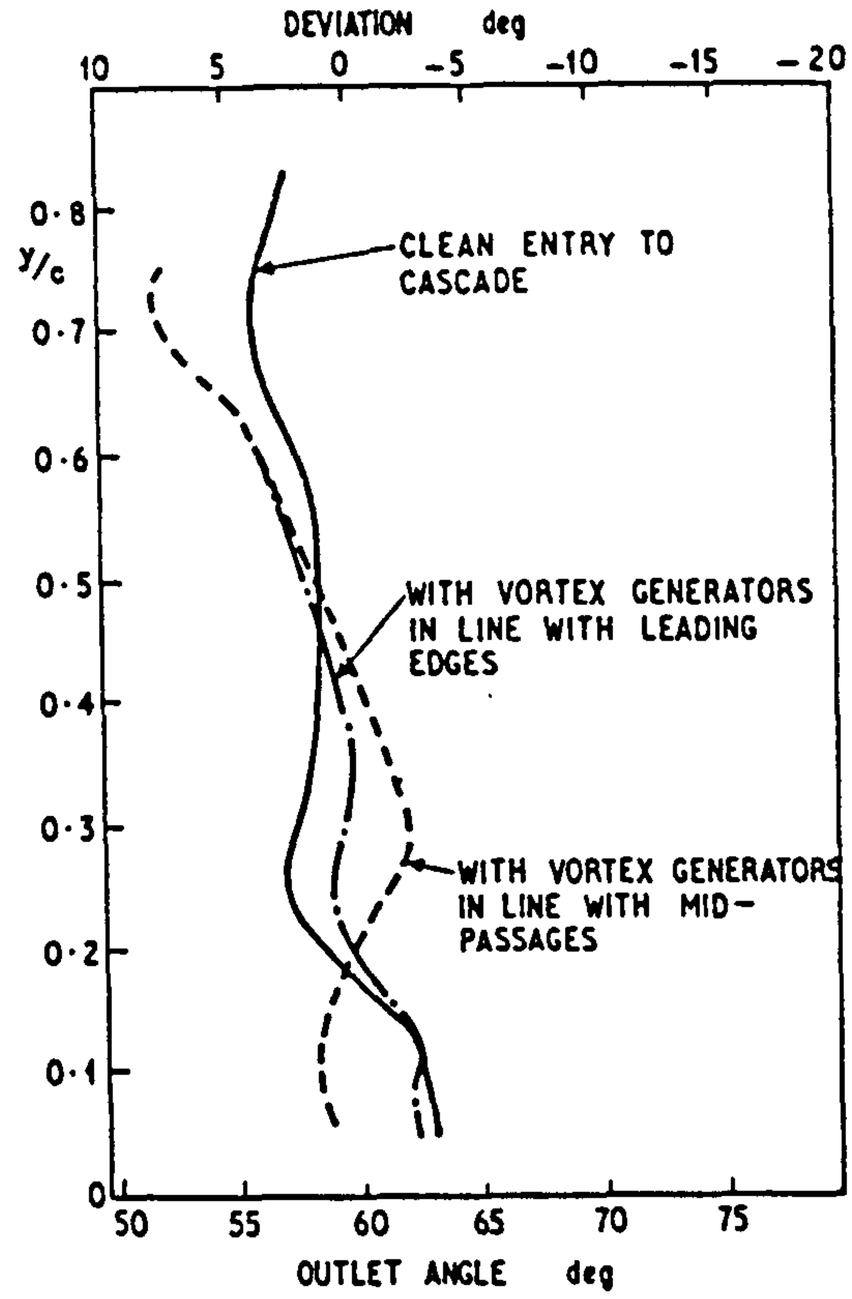

Fig. 9 Integrated outlet angles for entry flows without and with vortices

(3) -- aspect ratio 1.0, stagger angle 45 deg, inlet angle 15 deg, mass injection ratio 0.036 -- the values of the parameters, D, E, and F, for the exit vortices are 1.4, 2.0, and 0.062, respectively. When the flow is considered relative to the next row of blades, these parameters will be somewhat changed due to the change in ($\Delta\alpha^*$) as predicted from the velocity triangles. Typically, the value of ($\Delta\alpha^*$) might be increased by 50 percent; thus, the values of D, E, and F with reference to the next row of blades might become 2.1, 4.5, and 0.093, respectively.

When the same technique is applied to the vortices produced by the generators in the entry section of the present apparatus, the values of the parameters, D, E, and F, are 3.6, 13, and 0.22, respectively.

Thus, the generators being used are creating vortices which are, say, twice as strong as those resulting from the typical transverse injection case referred to (3). As it had been found that the strength of the exit vortex resulting from transverse injection is roughly proportional to the mass injection ratio, it was decided to continue with the present vortex generators, and the results obtained can be scaled linearly to correspond to the appropriate exit vortex strength.

Outlet Velocity Distributions and Losses. Outlet velocity distributions are shown in Figs. 5, 6, and 7 for the cases of "clean" entry to cascade, vortex generators in line with mid-passages and vortex generators in line with blades, respectively.

The major point to note is that, while with the clean entry to the cascade the wake trough drops to about 0.86 of the plateau velocity, when the vortices are introduced in the inlet flow, the blade wake trough is less marked and for a considerable proportion of the span, the velocity in the wake does not drop lower than 0.9 of the maximum velocity. The velocity gradients are, in general, weaker when inlet vortices are present.

The losses in stagnation pressure, relative to the average inlet stagnation pressure, have been integrated across the pitch, and are shown in Fig. 8 as loss coefficients. These coefficients have been based on the average, rather than the maximum inlet stagnation pressure due to the large change introduced by the vortex generators in the inlet stagnation pressure distribution (Fig. 2). The average kinetic energy associated with the rotating motion in the inlet vortices is very small, less than

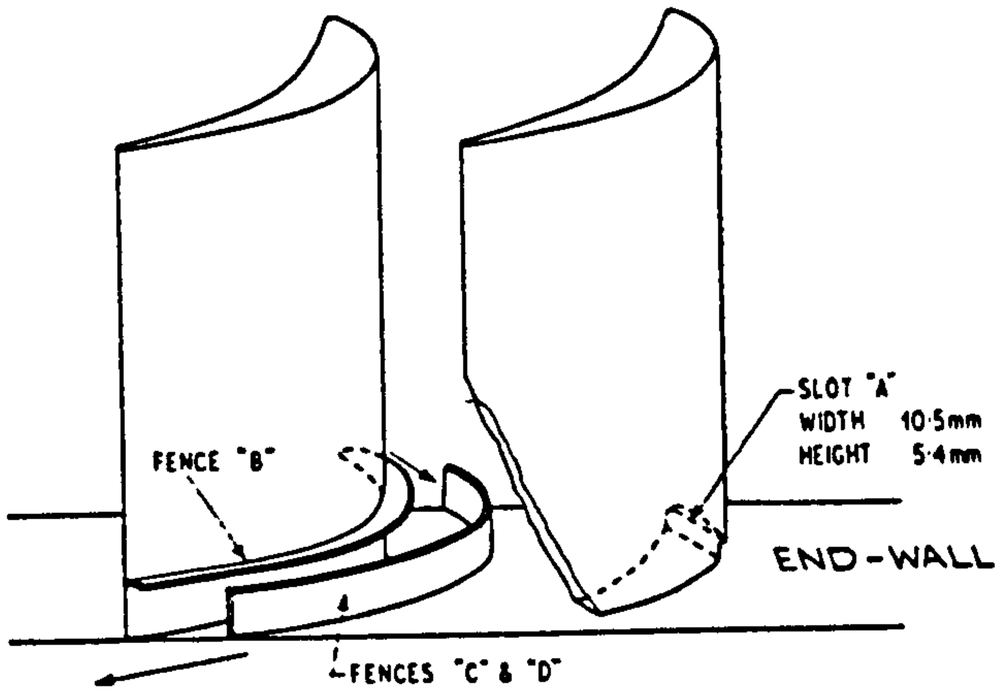

Fig. 10 Schemes for exit vortex reduction

0.1 percent of the kinetic energy of the cascade exit flow, so its contribution as an energy or velocity head input is negligible. Span-wise integration of the loss coefficients, up to a y/c value of 0.75 gives a value for the average loss coefficient of 0.064 for the "clean" inlet condition and values of 0.049 and 0.056 for the cases where there are inlet vortices, in line, respectively, with the mid-passage and with the

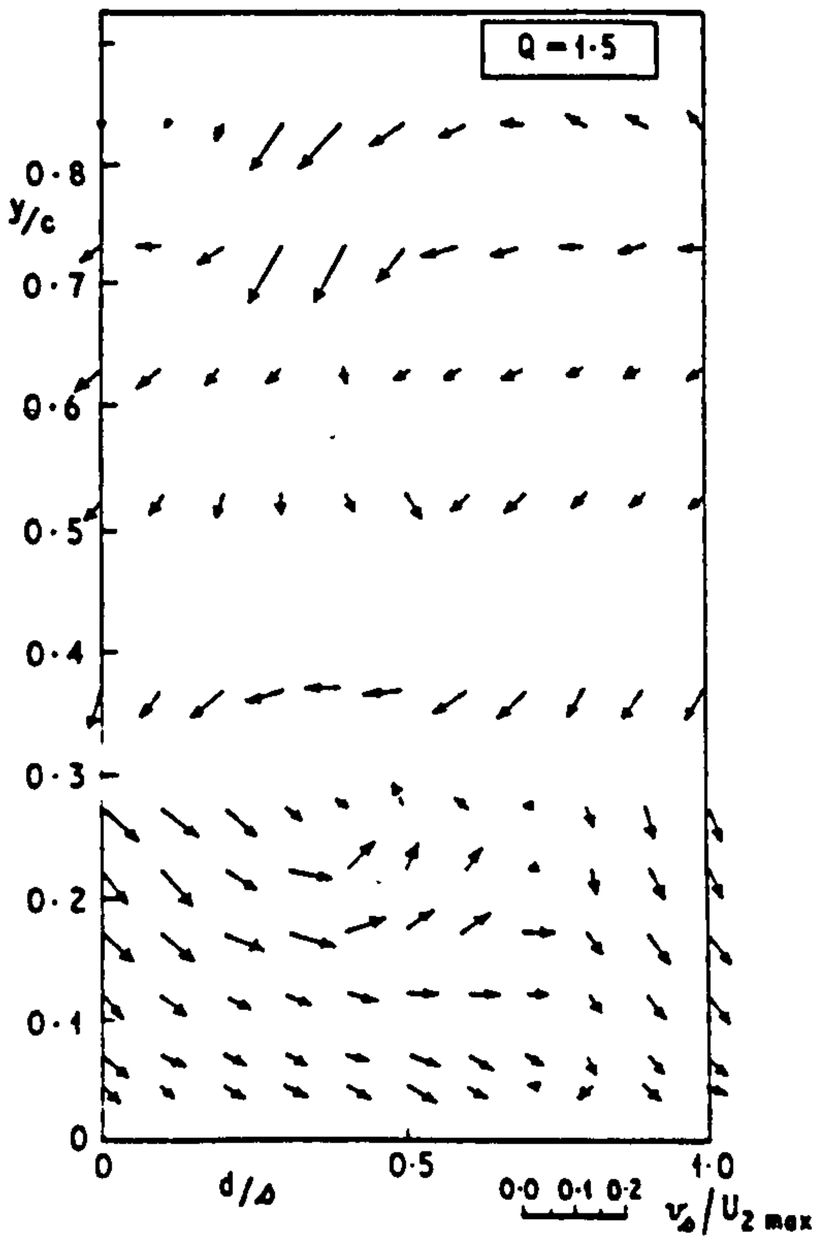

Fig. 11 Secondary velocities at outlet traverse plane - with transverse injection - basic cascade

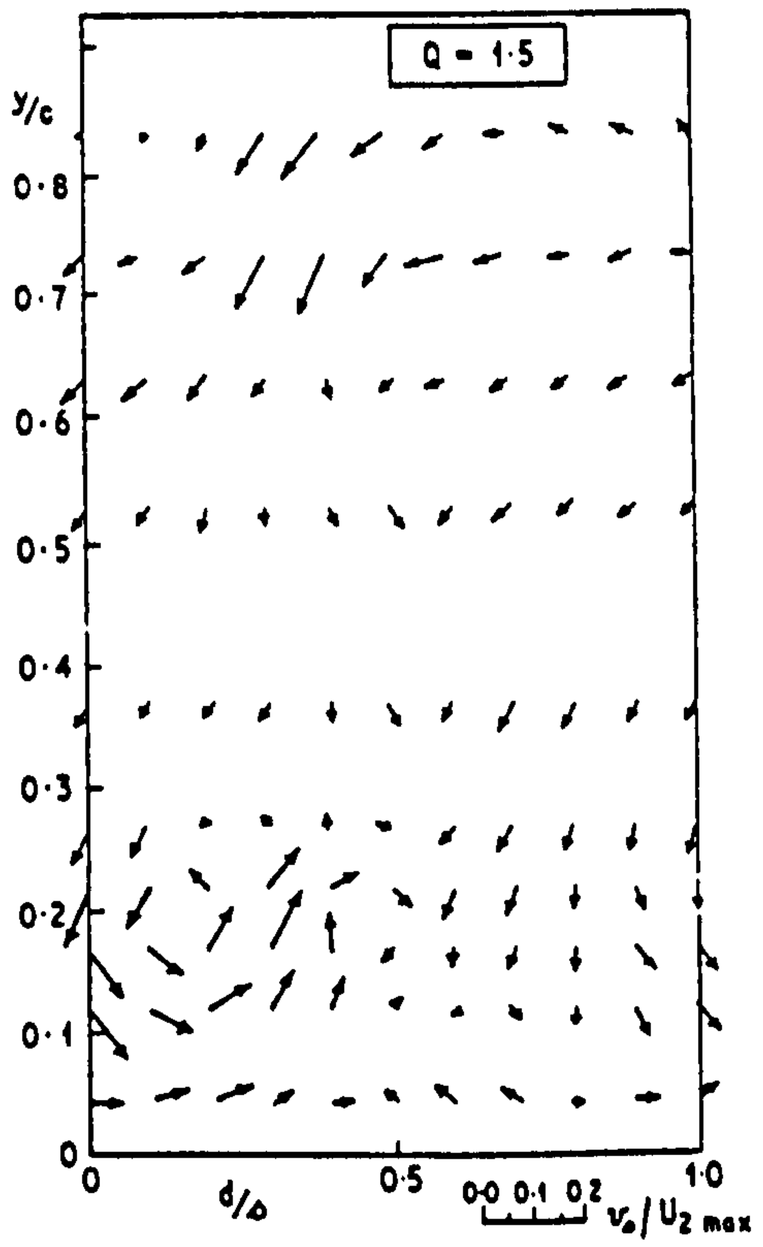

Fig. 12 Secondary velocities at outlet traverse plane - with transverse injection - with thick end-wall fence "C"

blades. At first sight, this reduction in losses when inlet vortices are present is somewhat surprising. However, this finding is consistent with the lower velocity gradients present in the exit flow and, hence, less severe dissipation regions.

On examining the secondary velocity components in the exit flow in the region up to y/c = 0.6, when the inlet flow to the cascade is "clean" the highest local secondary velocity amounts to 12 percent of the maximum main flow velocity. When the vortices are introduced into the inlet flow the highest local secondary velocities are between 9 and 10 percent of the maximum main flow velocity. It is important to note that the pronounced vortex, which had existed in the inlet flow, appears to have been dissipated in passing through the blade channel.

The pressure distributions around the blade showed no discontinuities when vortices were introduced, and the changes which were observed were in line with the altered overall loss of the cascade.

The manner in which the pitch-integrated deviations in the exit flow are influenced by inlet vortices is indicated in Fig. 9. Unfortunately, these pitch-integrated curves con-

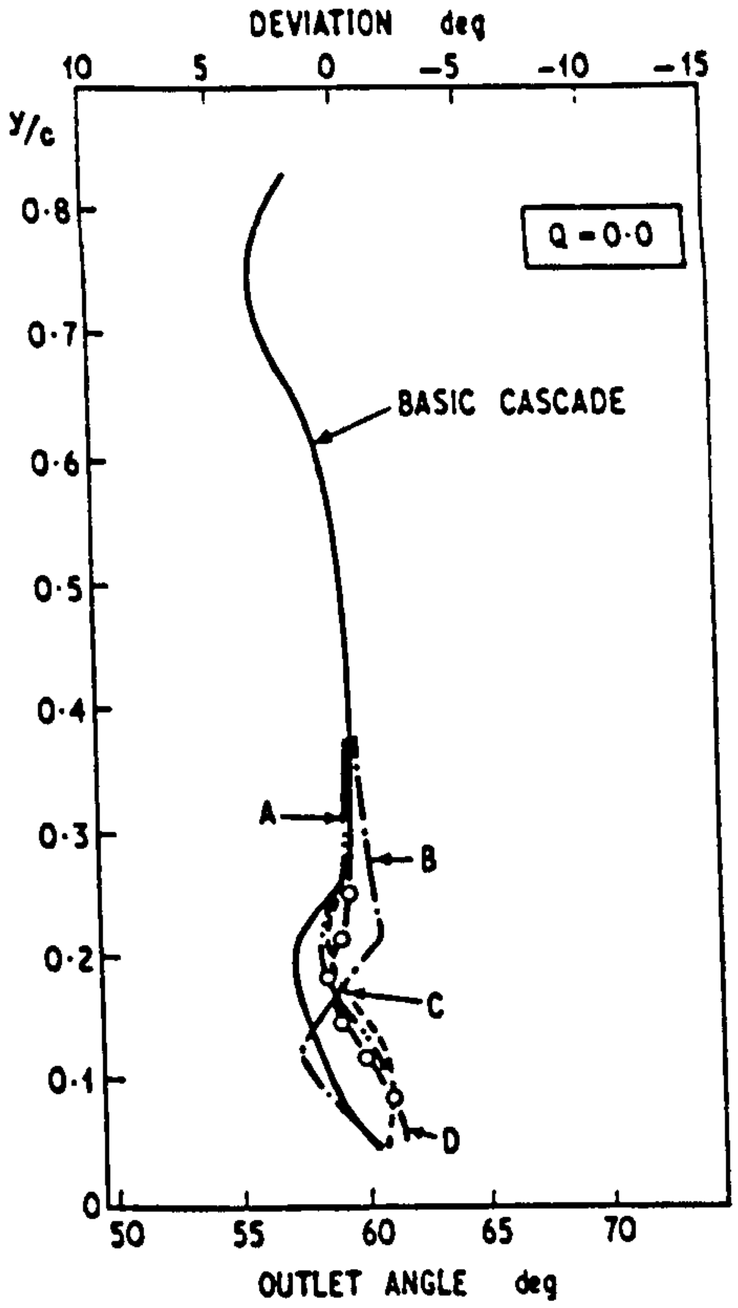

Fig. 13 Integrated outlet angles for various vortex reducing schemes - no transverse injection

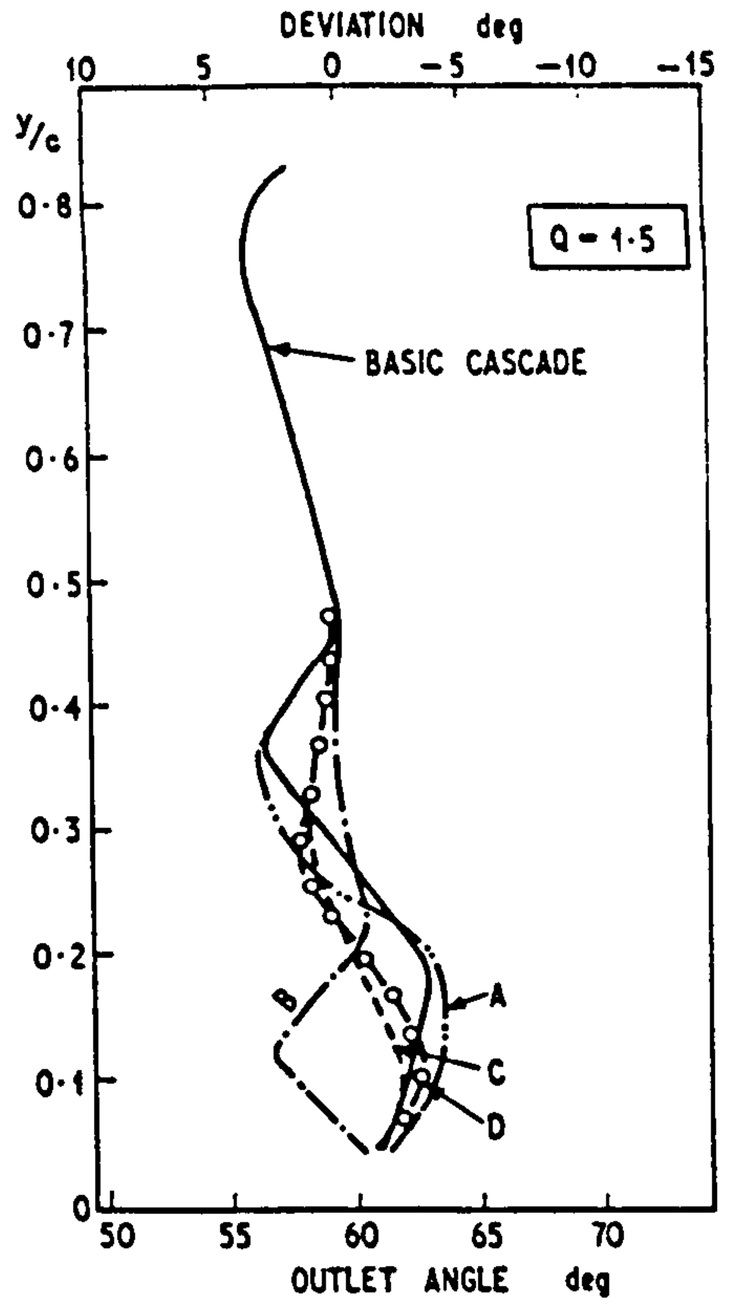

Fig. 14 Integrated outlet angles for various vortex reducing schemes - with transverse injection

ceal the reduction in secondary velocities when vortices are introduced. It should also be noted, however, that when there are vortices in the inlet flow, frequently the highest secondary velocities are in directions which are not parallel to the end-wall, and, therefore, they will not show up in plots of deviations.

The improvement in the secondary flows resulting from the inlet vortices is probably associated with the direction of rotation of the inlet vortex. As stated previously, this direction is such that the side of the vortex nearest to the adjacent end-wall is twisted toward the pressure surface of the blades which the flow is entering. The higher turning angle obtained in the passage in the flow nearest the end-wall brings the end-wall flow out at an angle nearer to the main flow, rather than over-turning it.

REDUCTION OF STRENGTH OF VORTICES RESULTING FROM TRANSVERSE INJECTION

An investigation has been made of several possible methods of reducing the strength of the vortices in the flow leaving a turbine blade row which result from transverse injection in front of that blade row.

Devices Examined

Two different techniques have been considered. The first was an attempt to counter the motion from the pressure to the suction surface which had been observed within the separation bubble on the end-wall immediately downstream of the slot from which the transverse jet emerged (1). It appeared that the exit vortex originated from near the suction surface end of this separation bubble. If the mass flow, and hence momentum, within the bubble toward the suction surface could be reduced, then the exit vortex might be weakened. The method used was to cut a slot through the blade adjacent to the end-wall, as illustrated (Scheme A) in Fig. 10. The slot runs from a position of high pressure on the pressure surface side to a position of lower pressure on the suction side. It will, therefore, carry fluid into the separation bubble with a momentum to oppose the previously observed flow within the bubble. The dimensions of the slot are given in Fig. 10.

The second technique was to employ boundary layer fences, as described by Prumper (2), on the suction surface of the blades near the end-wall from which the transverse jet is injected

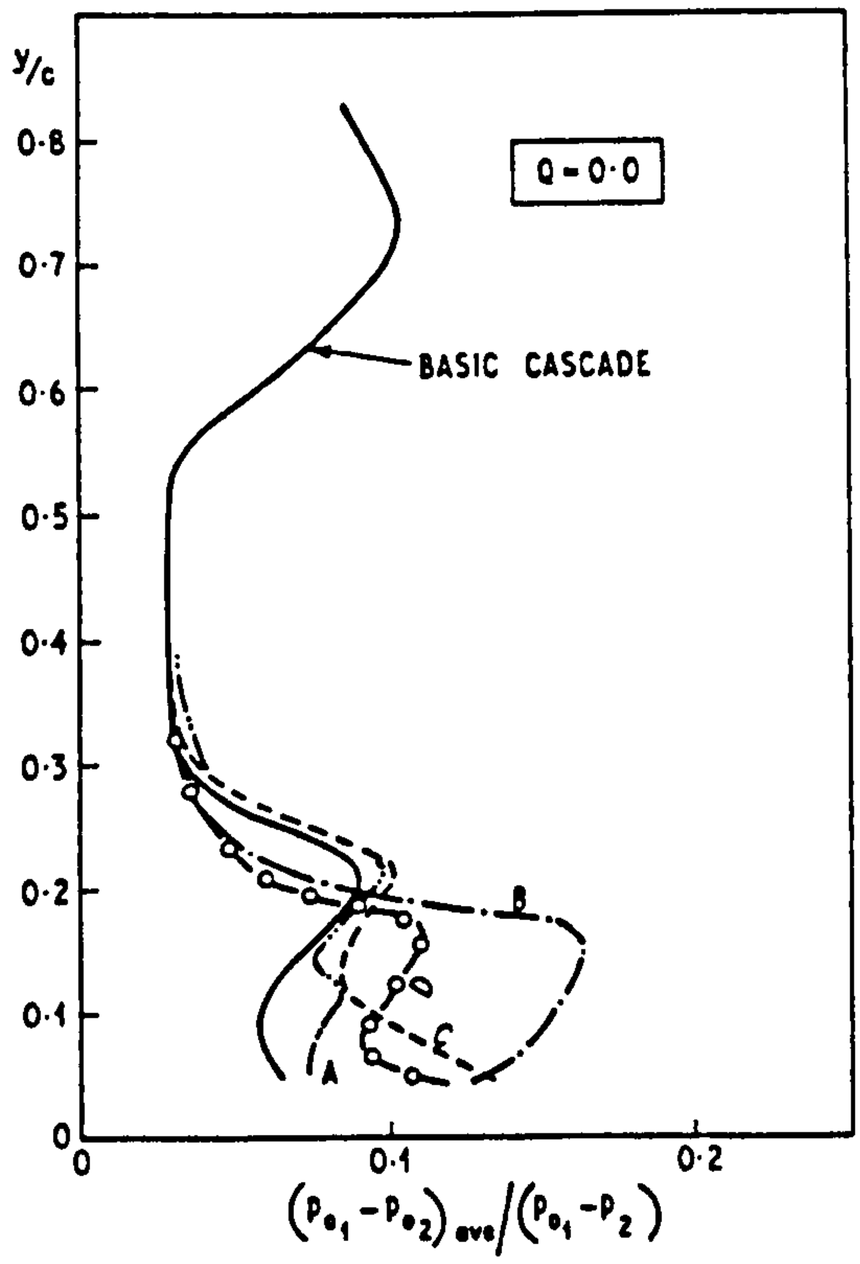

Fig. 15 Integrated stagnation pressure losses for various vortex reducing schemes - no transverse injection

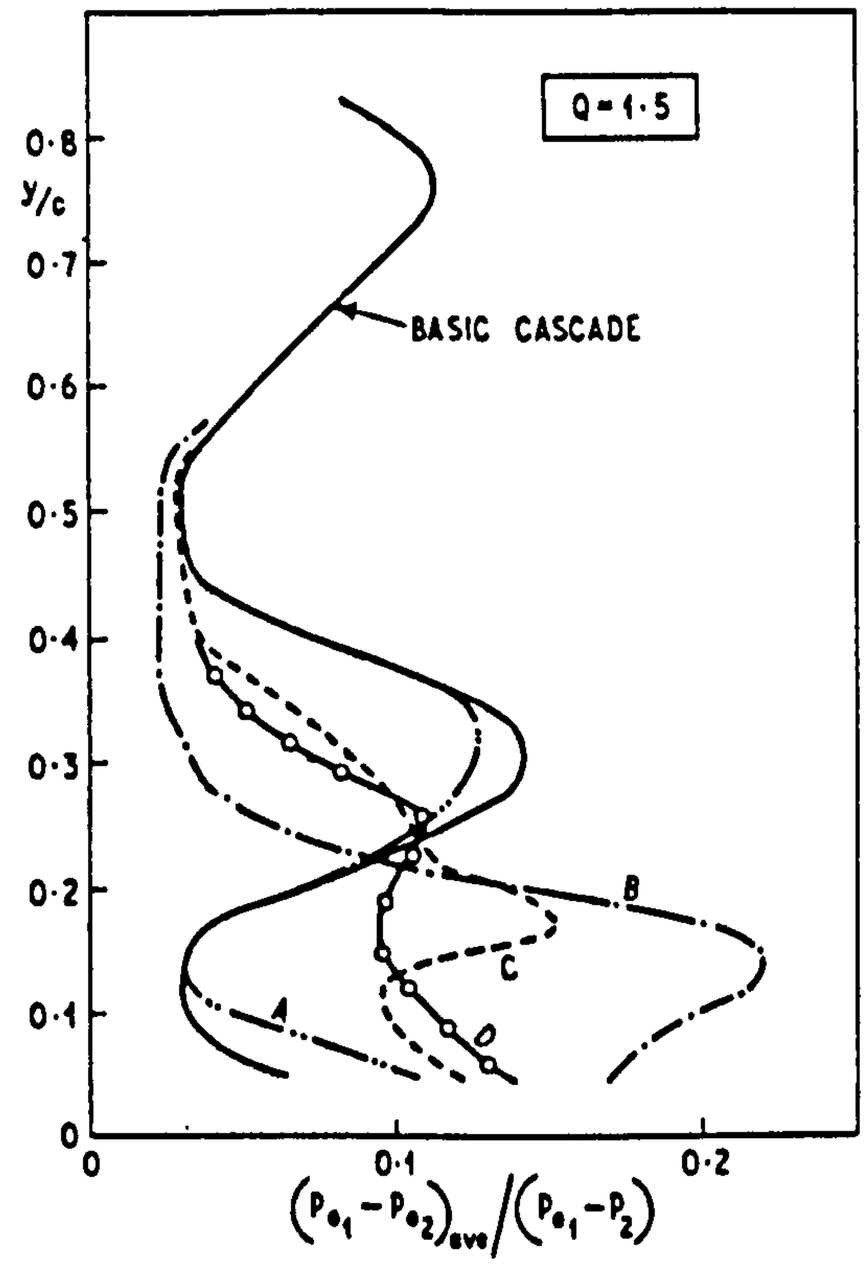

Fig. 16 Integrated stagnation pressure losses for various vortex reducing schemes - with transverse injection

(Scheme B), and on the end-wall itself parallel to the suction surfaces (Schemes C and D). Fence B runs the full length of the suction surface at a distance of 15.9 mm above the end-wall and extends 7 mm out from the suction surface. The thickness of the fence is 0.33 mm. Fences C and D stand 13.5 mm out from the end-wall, have the same profile as the suction surface, and are positioned throughout their lengths at 0.33 blade pitch from the suction surface. Fence C is 1.6 mm thick (the "thick" fence) while Fence D is 0.46 mm thick (the "thin"fence).

Test Procedure

The turbine cascade employed was the same as that used for the investigation described in the earlier part of this paper on the effect of vortices in the flow entering a cascade, i.e., the leading particulars were: stagger angle, 40 deg; inlet angle, 15 deg; aspect ratio, 1.0. When transverse injection was introduced, the velocity of the jet was 1.5 times, the velocity of the main approach flow and the injection slot width was such that the ratio of injected mass flow to main mass flow was 0.036. When no transverse flow was required, the injection slot was taped over. The boundary layer on the end-wall carrying the injection slot was sucked away 180 mm in front of the slot.

Results and Discussion

As the primary aim of the various devices was to reduce the exit vortex resulting from transverse injection, the exit velocity patterns under conditions of transverse injection are first considered, particularly with reference to the secondary velocity components.

With the basic cascade, transverse injection led to the significant vortex in the exit flow illustrated in Fig. 11. The introduction of Scheme A (slot through blade) made little difference to this pattern. The fences on the end-wall (Schemes C and D) led to a slightly reduced vortex closer to the end-wall, and a smaller vortex alongside, in counter rotation. This is illustrated in Fig. 12. The device which was most successful in reducing the exit vortex was the fence on the blade suction surface (Scheme B). In order to give a numerical comparison between the flows with the various Schemes, the extremes of local deviations immediately above and below the apparent eye of the vortex have been examined. With the basic cascade, the range of local deviations is just over 10 deg, while with Scheme B, it is about 5 deg. Schemes A, C, and D indicate correspond-

Table 2 Pressure Loss Coefficients for Various "Vortex Reducing" Schemes

Geometry	$\bar{\omega}_{p_{o1} - p_{o2}}$ ave	$\bar{\omega}_{p_{o1} - p_2}$
	No transverse injection	Injection mass ratio = 1.03%
Basic Cascade	0.061	0.075
Scheme A - slot through blade	0.068	0.078
Scheme B - fence on suction surface	0.077	0.085
Scheme C - thick end-wall fence	0.080	0.083
Scheme D - thin end-wall fence	0.068	0.079

ing deviation ranges of about 11, 9, and 6.5 deg, respectively.

Pitch-integrated deviations are shown in Figs. 13 and 14 for cases without and with transverse injection. Due to the creation by the fences of other, smaller vortices, it is not meaningful to apply equations (1) to (3) to these pitch-integrated deviations. However, the curves do give some indication of the variation of directions in the exit flow. On this basis, Scheme B (fence on suction surface) is seen to be about the best of the alternatives, when transverse injection is taking place.

However, the changes in pressure loss coefficients resulting from using the various devices must also be examined. The pitch-integrated loss coefficients are shown in Figs. 15 and 16 for the situations without and with transverse injection. To assist in the comparison of the loss coefficients, the pitch-integrated coefficients have been averaged over the blade span up to $y/c = 0.8$. The results are given in Table 2. For the cases without transverse injection, all Schemes adopted lead to higher pressure losses, the greatest increase being with Scheme C (thick fence on end-wall) while the smallest increase is with Scheme A (slot through blade). When transverse injection is present, all Schemes except Scheme A lead to increased losses, when compared to the basic cascade, Scheme B being the worst. With Scheme A, the losses are virtually unchanged. Thus, in no case has there been a reduction in losses in the present work, although Fences of types B, C, and D have been reported as giving reduced losses elsewhere (5). The explanation for this

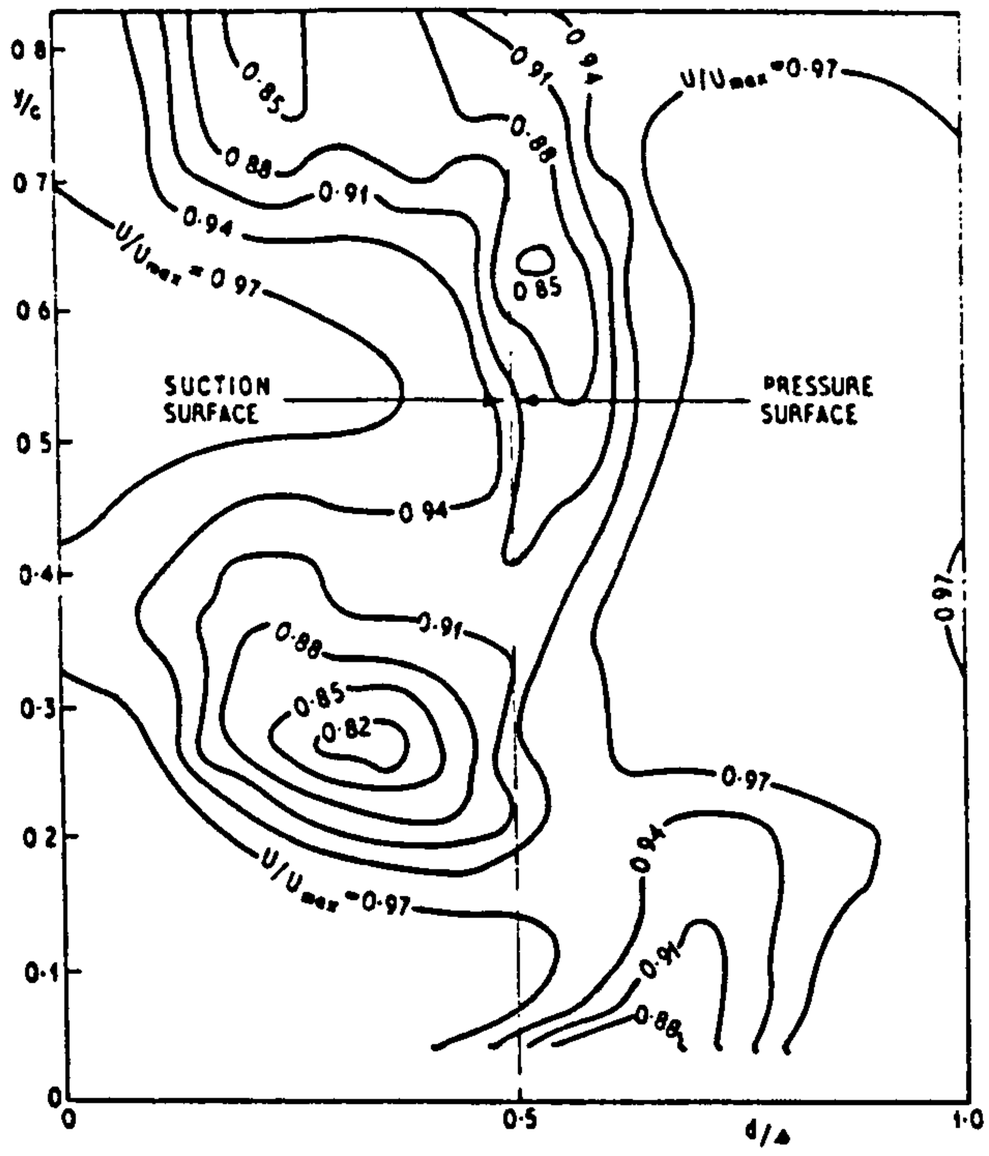

Fig. 17 Velocity contours at outlet traverse plane - with transverse injection - basic cascade

discrepancy may lie in the very low aspect ratio (0.25) used in Reference (5), which causes the two end-wall secondary flows to interact.

Further insight into the effect of the various Schemes on pressure losses can be gained by looking at the exit main flow velocity distributions. Only two of these velocity distributions are presented here -- that for the basic cascade in Fig. 17 and that with Scheme D (thin fence on end-wall) in Fig. 18. In both cases, transverse injection is taking place. The pronounced trough associated with the exit vortex from the basic cascade is considerably diminished by the fence.

CONCLUSIONS

When there are vortices adjacent to an end-wall in the flow approaching a cascade of turbine blades, the vortices having the direction of rotation toward the pressure surface for the fluid on the side of the vortex nearest the end-wall -- as results from transverse injection in front of the previous row of blades -- then, from these initial studies, there appears to be a reduction in the pressure loss in the row of blades being considered. The vortices themselves virtually disappear as the flow passes through the blade channels. These findings require further testing to provide confirma-

tion, particularly as in this simulation the vortex generators were stationary relative to the cascade that the flow was entering.

The vortex which results from transverse injection can be reduced. Of the devices tested for achieving this, the most effective was a boundary layer fence on the suction surface of the blade, near to the end-wall. However, a significant penalty in pressure loss is incurred. Devices which have lower pressure loss penalties are less effective in vortex reduction. In view of the conclusion given in the preceding paragraph, it may not be desirable to reduce the vortex which results from transverse injection.

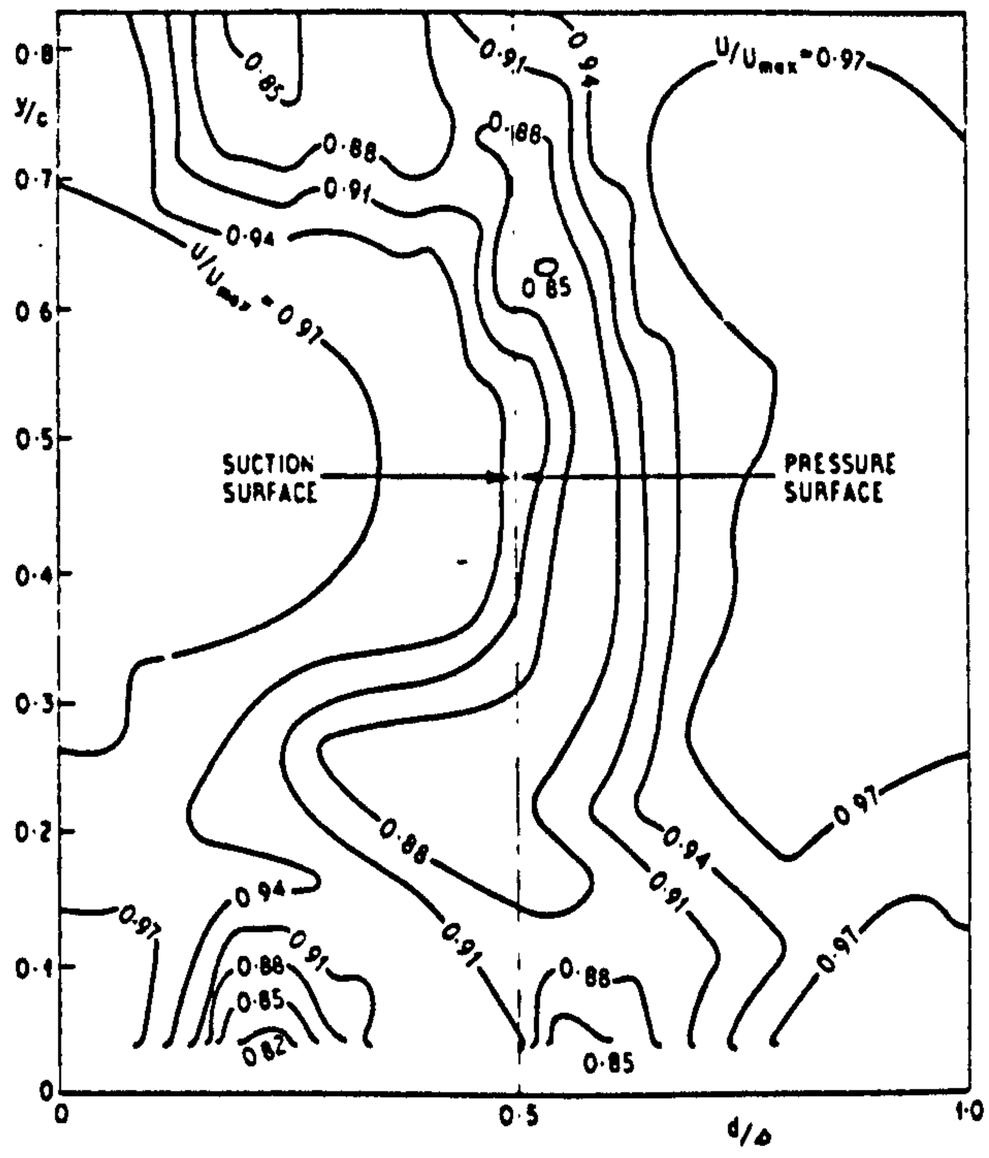

Fig. 18 Velocity contours at outlet traverse plane - with transverse injection - with thin end-wall fence "D"

ACKNOWLEDGMENTS

The authors wish to thank Professor E. S. Silver for his encouragement, staff of Rolls-Royce Ltd., for stimulating comments, and the Science Research Council for financial support.

REFERENCES

1 Shrivastava, K. D., and Maccallum, N. R. L., "The Effect of a Transversely Injected Stream on the Flow Through Turbine Cascades: Part I -- Flow Effects," ASME Paper No. 77-GT-87.

2 Shrivastava, K. D., and Maccallum, N. R. L., "The Effect of a Transversely Injected Stream on the Flow Through Turbine Cascades: Part II -- Performance Changes," ASME Paper No. 77-GT-88.

3 Aburwin, B. A., and Maccallum, N. R. L., "The Effect of a Transversely Injected Stream on the Flow Through Turbine Cascades: Part III -- Influence of Aspect Rates," ASME Paper No. 78-GT-24. To be published in Journal of Engineering for Power.

4 Bindon, J. P., Aburwin, B. A., and Maccallum, N. R. L., "Comparison of Transverse Injection Effects in Annular and in Straight Turbine Cascades," Paper offered to ASME Gas Turbine Conference, 1979.

5 Prumper, H., "Application of Boundary Layer Fences in Turbomachinery," Paper II-3 in AGARDograph 164, 1972, pp. 311-331.

ted in U.S.A.

79-GT-17

an ASME publication

$3.00 PER COPY
$1.50 TO ASME MEMBERS

Comparison of Transverse Injection Effects in Annular and in Straight Turbine Cascades

J. P. BINDON

Senior Lecturer,
Dept. of Mechanical Engineering,
University of Natal,
Durban, South Africa

B. A. ABURWIN

Research Student

N. R. L. MACCALLUM

Senior Lecturer

Dept. of Mechanical Engineering,
University of Glasgow,
Glasgow, Scotland

An experimental investigation has been made of the effects of transverse injection from the hub in front of the blades of an annular cascade. The hub end-wall boundary layer could be skewed, by rotating the nose cone. The data on transverse injection effects in straight cascades was extended to provide comparisons with the annular cascade results. Similar effects were observed in the two types of cascades, the principal effects being the creation of a separation bubble on the hub end-wall behind the injection slot, and the strengthening of the passage vortex, which is lifted away from the hub end-wall.

Contributed by the Gas Turbine Division of The American Society of Mechanical Engineers for presentation at the Gas Turbine Conference & Exhibit & Solar Energy Conference, San Diego, Calif., March 12-15, 1979. Manuscript received at ASME Headquarters December 8, 1978.

Copies will be available until until December 1, 1979.

Comparison of Transverse Injection Effects in Annular and in Straight Turbine Cascades

J. P. BINDON B. A. ABURWIN N. R. L. MACCALLUM

NOMENCLATURE

c = chord
C = flow velocity
d = distance along blade pitch from one mid-passage line to next, in direction of suction surface
D = measure of strength of exit vortex, defined by $(\Delta\alpha^*)(\Delta y^*/c)$
E = measure of kinetic energy of tangential components in exit vortex, defined by $(\Delta\alpha^*)^2(\Delta y^*/c)^2$
f = ratio of cascade exit mass flow to mass flow of main approach stream
F = measure of angular momentum of exit vortex, defined by $(\Delta\alpha^*)(\Delta y^*/c)^3$
ζ = ratio of maximum velocity of injected jet to velocity of main approach flow
s = blade pitch
U = hub peripheral speed
x = distance in axial direction from leading edge
y = distance from end-wall carrying injection slot
z = distance along pitch direction from leading edge
α = main flow angle, measured from axial direction
η = nozzle efficiency
θ = angle between injected jet and cascade end-wall
ρ = density

Subscripts

o = stagnation
1,2 = inlet to, outlet from cascade
ave = average

Superscript

* = range of pitch-integrated exit vortex

INTRODUCTION

In a typical gas turbine, small airflows are extracted from the main flow to cool various components of the turbine, e.g., blades, nozzle guide vanes, and disks. After they have fulfilled their function, these cooling flows are returned to the main flow in the turbine. The cooling air from the blades and vanes usually returns via holes in the blade surfaces. The disk cooling air returns by entering the main flow transversely from between blade rows. The effect of such a transversely injected stream on the flow through the immediately following row of blades has been studied where the following row is a straight cascade (1-3).[1] Interactions with the secondary flows were observed. Of course, in practice the row will be an annular cascade, rotating or stationary. When the annular cascade is stationary, as when it represents a row of nozzle guide vanes, the basic secondary flows are somewhat modified and there is an inward radial flow in the wakes of the blades (4, 5). For a moving annular row, i.e., a row of turbine blades, there is an outward radial secondary flow (6). The present paper reports on a study of the effects of transverse injection in a stationary annular cascade. The cascade had the additional facility of being able to give skew to the hub end-wall boundary layer, as it approached the injection slot and the cascade. Comparisons are made with the effects in straight cascades.

APPARATUS AND TEST PROCEDURE

Annular Cascade

The annular cascade of stationary nozzle guide vanes was designed and built by Sjolander (7). It is described by him, and also by Bindon (8) who added to the rig the facility to skew the hub end-wall boundary layer by rotating the hub ahead of the cascade.

[1] Underlined numbers in parentheses designate References at end of paper.

Table 1 Coordinates of Blade Profiles

Annular Cascade - [illegible] deg stagger angle									
x/c	0.0	[illegible]	[illegible]	[illegible]	[illegible]	[illegible]	[illegible]	[illegible]	[illegible]
z/c pressure	0.0	[illegible]	0.002	0.122	[illegible]	[illegible]	[illegible]	[illegible]	[illegible]
z/c suction	0.0	-0.026	-0.027	-0.011	0.042	0.116	0.221	0.341	[illegible]

Straight Cascade - [illegible] deg stagger angle									
x/c	0.0	[illegible]	[illegible]	[illegible]	[illegible]	[illegible]	[illegible]	[illegible]	[illegible]
z/c pressure	0.0	0.025	0.080	0.156	0.238	[illegible]	[illegible]	0.474	0.564	0.697
z/c suction	0.0	-0.016	-0.021	0.008	0.070	0.159	0.272	0.398	0.522	0.684

The blades are of T6 profile, on a parabolic camber line, with a blade outlet angle of 50 deg. Coordinates of the blade profile are given in Table 1. Leading dimensions are: chord, 76.2 mm (3 in.); blade height, 50.8 mm (2 in.); thus aspect ratio, 0.667; cascade diameter at mean blade height, 0.356 m (14 in.). There are 16 blades, giving a pitch at the mean blade height of 69.8 mm and of 60 mm at the hub. The main airflow through the cascade was supplied from an axial compressor via a settling chamber fitted with screens. The flow entered the cascade axially, as illustrated in Fig. 1, and left with a direction at 45 deg to the axial. The Reynolds Number, based on the cascade exit velocity, was 2.5×10^5. The nose cone, which formed the inner end-wall of the approach annulus, extended 0.4 m upstream of the cascade, parallel to the axis of the cascade. This nose cone could be rotated in the direction across a blade passage from the pressure to the suction surfaces to simulate the skewing which occurs in a turbomachine. In the present work, this hub in the approach was either stationary, or was rotated with a surface speed equal to the axial air velocity at inlet to the cascade.

A small air flow could be injected transversely into the main stream from the circumferential gap between the nose cone and the front edge of the hub of the cascade. The width of this gap was chosen to give a ratio of injected mass flow to main mass flow of 0.024 when the injected stream velocity was 1.5 times the main flow velocity. The inclination of the jet to the main flow was 83 deg. The flow from the slot was uniform from channel to channel. When no injected flow was required, the pipe supplying this injection slot was blanked off.

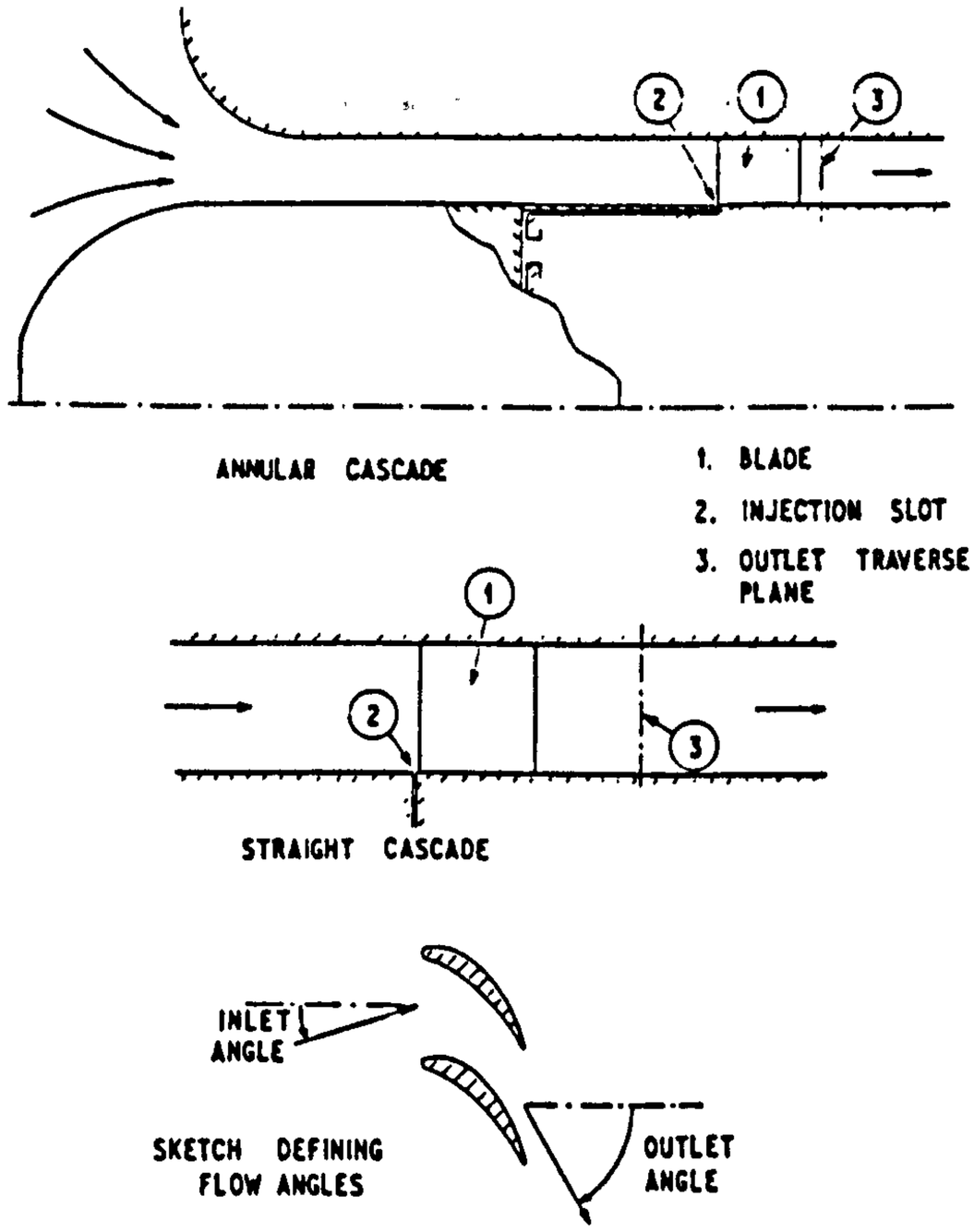

Fig. 1 Test cascades

Flow visualization studies were made on the hub end-wall. It was found that drops of a mixture of titanium oxide and light engine oil provided a helpful picture of the end-wall flow.

The boundary layer on the hub end-wall, behind the injection slot, was traversed for total head and for direction at various locations in the blade passage. Also, traverses were made of the exit flow, at an axial distance of 0.25 axial chord from the blade outlet. The exit traverses extended from the hub end-wall to a distance from the hub of 0.7 of the blade height. A three-hole 90-deg cobra probe, of head dimensions 1.9 x 0.64 mm, was used for all traverses.

Straight Cascade

The cascade is the same as that used in previous studies (1-3). The blades are on an approximately parabolic camber line, of 129-mm (5.07-in.) chord, and 88-mm (3.5-in.) pitch, and set at a stagger angle of 45 deg. Blade profile coordinates are given in Table 1. A movable partition wall had been inserted in the tunnel parallel to and opposite the end-wall in which the injection slot was positioned. This adjustable partition wall allows the aspect ratio

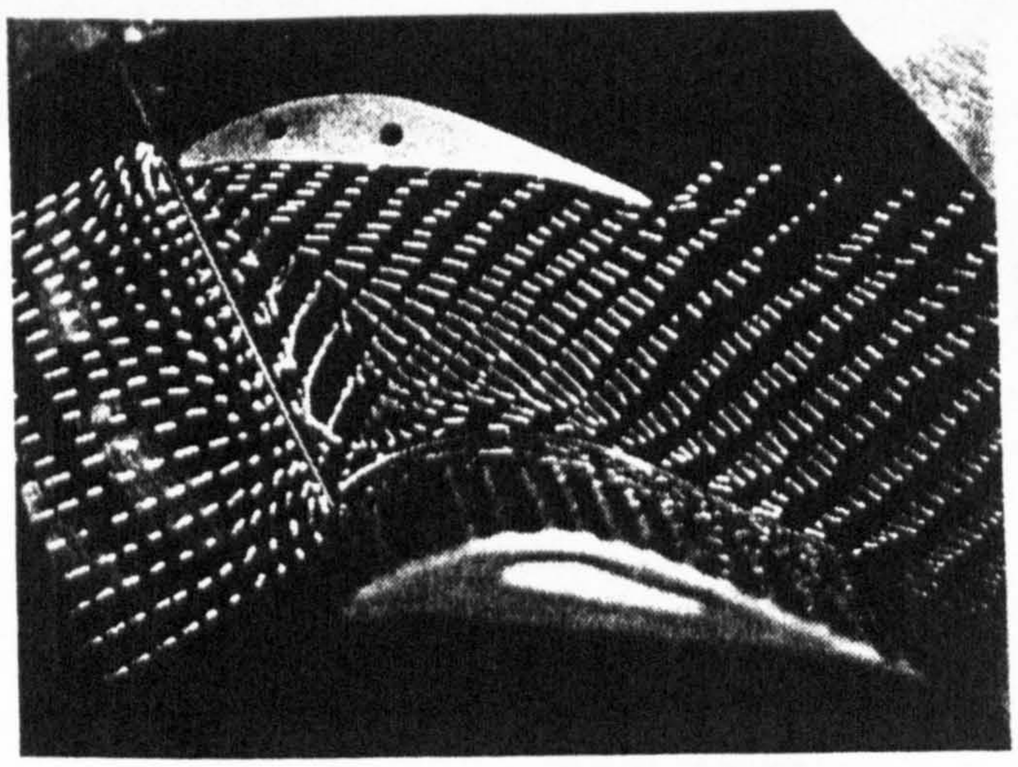

Fig. 2 Visualization of hub end-wall flows, Q = 1.5, U/C_1 = 0.0

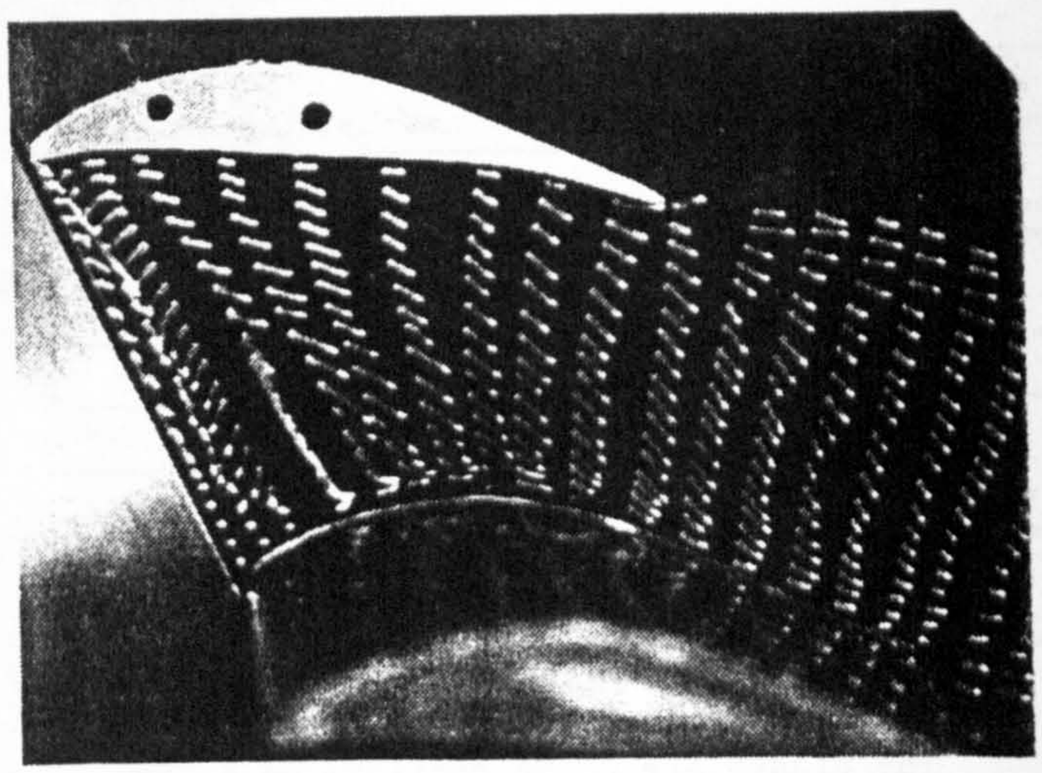

Fig. 3 Visualization of hub end-wall flows, Q = 1.5, U/C_1 = 1.0

of the cascade to be reduced from the value of 3.0 when there is no partition wall. In previous investigations (3), the aspect ratio had been reduced to 1.5 and 1.0. To allow a closer similarity to the annular cascade being tested, the aspect ratio of this straight cascade was further reduced to 0.8 for the present work. The injection slot, which was in the lower end-wall immediately in front of the leading edges of the blades, was of a width such that the injected mass flow was 0.024 of the main mass flow when the injected stream velocity was 1.5 times the main flow approach velocity; these ratios are identical to the ratios in the annular cascade tests. The injected stream enters at 90 deg to the end-wall and, hence, to the main flow direction. When the injected stream is not required, the injection slot is taped over.

The boundary layer on the end-wall in which the injection slot is placed was sucked away 180 mm upstream of the slot.

The cascade was placed in the suction to a variable speed fan. The flow entering the cascade was directed at 15 deg to the axial. At the cascade exit, the side-walls were adjusted in angle, relative to the cascade, until there was a symmetric velocity distribution across the exit flow. This occurred when the walls were at 65 deg to the axial. This angle is slightly greater than the value of 63 deg required for the earlier investigations at aspect ratios of 3.0 and 1.5. A fan speed was used such that the Reynolds Number, based on the cascade exit velocity, was 2.5×10^5. Turbulence grids in the contraction leading to the cascade gave a turbulence intensity of 1.5 percent at the cascade.

Total head pressure distributions, flow directions, and velocities were measured 200 mm downstream in the flow direction from the cascade exit. The instrument used was a five-hole spherical probe of 8-mm dia. This allowed measurement of components of velocity normal to the end-wall, which proved helpful in studying exit vortices. The five-hole probe was checked satisfactorily in these flows against a three-hole probe of 2.7-mm dia.

In both the annular and straight cascades, the injected flow was at the same temperature as the main flow.

RESULTS AND DISCUSSION

The results of corresponding tests in the two cascades are described below. Before making comparisons, the differences between the cascades should be summarized. The inlet angles (to the axial direction) are 0 and 15 deg, respectively, for the annular and straight cascades. The blades have different profiles, and the average flow angles (relative to the axial) at exit are -5 and 65 deg, respectively. The annular cascade has no boundary layer suction from the end-wall through which the transverse injection takes place. However, tests on the straight cascade, in the absence of end-wall boundary layer suction, indicate that changes due to this are only second-order.

Flow Visualization on Hub End-Wall

Traces of hub end-wall flows in the annular cascade, as indicated by titanium oxide-

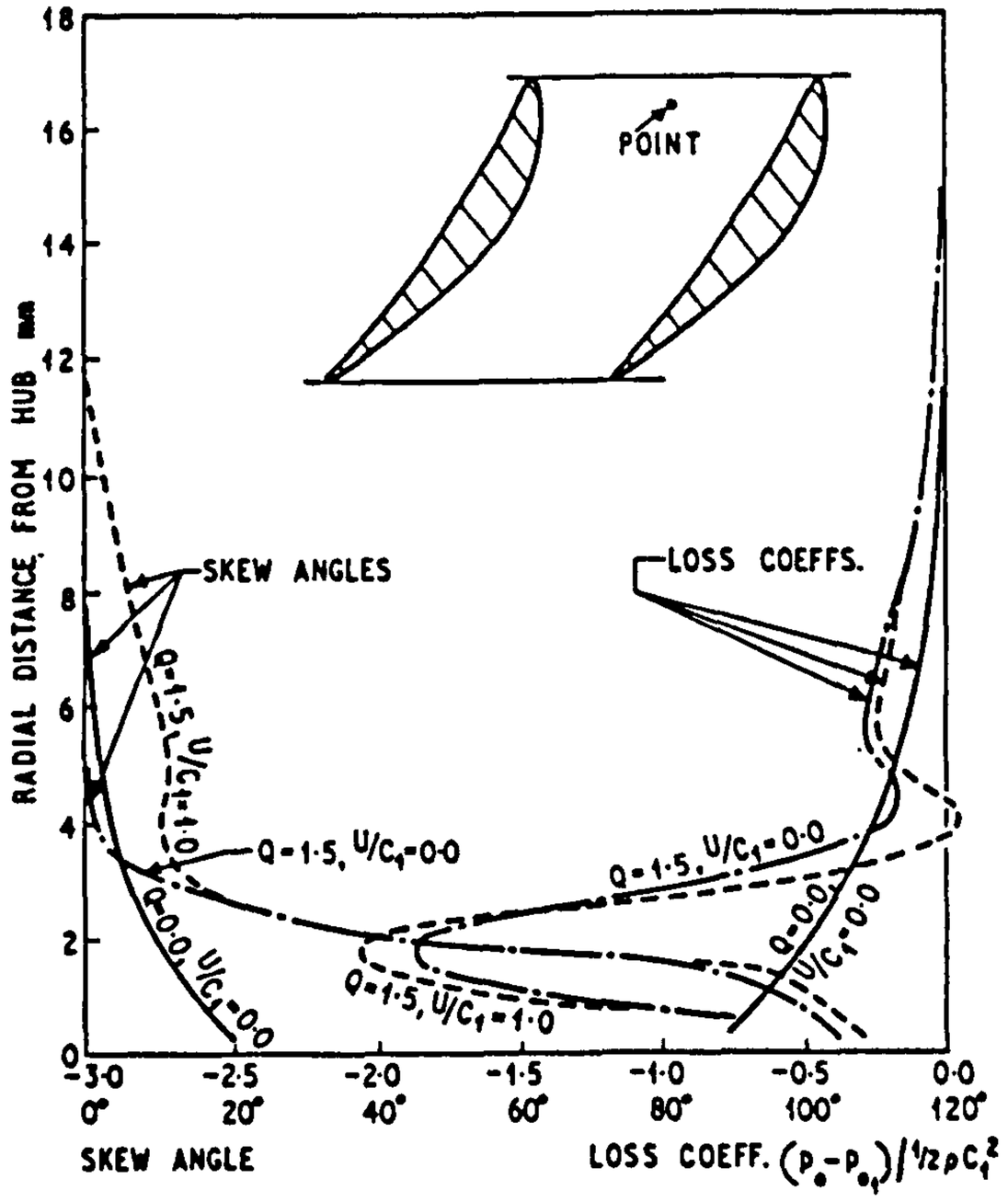

Fig. 4 Hub end-wall boundary layer profiles at 10 percent axial chord in mid-passage

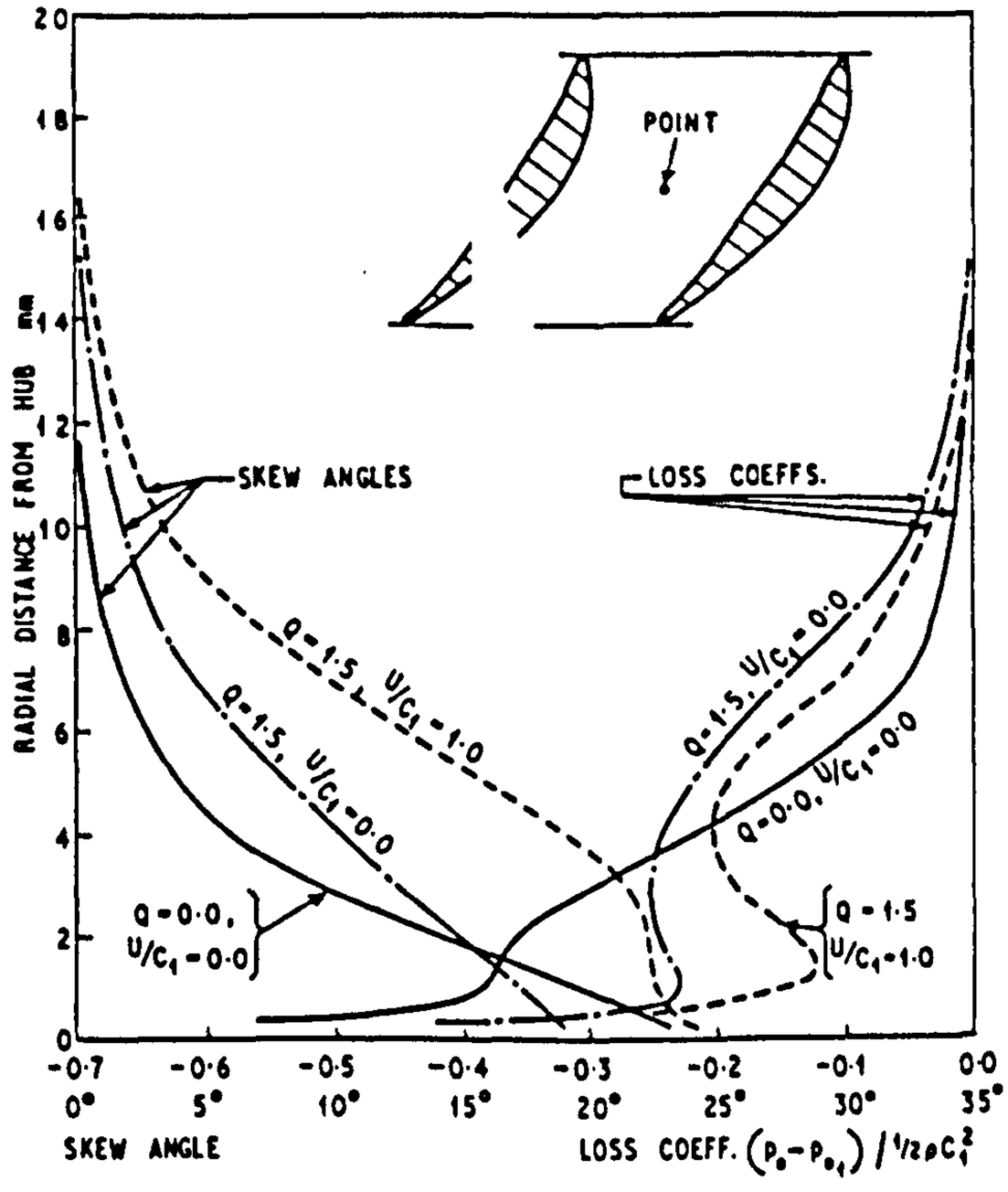

Fig. 5 Hub end-wall boundary layer profiles at 50 percent axial chord in mid-passage

oil drops, are shown in Figs. 2 and 3. In both cases, there is transverse injection from the slot between the nose cone and the hub end-wall. In Fig. 2, the nose cone is stationary, and in Fig. 3 the nose is being rotated with a surface speed equal to the axial velocity of the approaching main flow. The separation bubble previously observed in straight cascades (1) is again seen in both cases, and the position of the reattachment line is similar, extending from about 0.1 axial chord on the pressure side to about 0.3 axial chord on the suction side. Within the separation bubble itself, there is a considerable component of velocity from the pressure to the suction surface, and a rotation of the bubble about this axis of transverse movement. Little difference is made to the separation bubble when the approaching end-wall boundary layer is skewed, but downstream of the reattachment line, there is indication of a slightly more skewed end-wall flow.

These observations of the effects of transverse injection in the annular cascade are in general agreement with those described in straight cascades.

Boundary Layer Traverses on Hub End-Wall

The results of the traverses in the annular cascade at a point at 10 percent axial chord on the mid-passage line are shown in Fig. 4. This location is within the separation bubble that is present when there is transverse injection. The existence of the separation bubble is clearly indicated by the plots of skew angle, when with injection the skew rises to more than 100 deg from the mainstream flow, i.e. the local flow is moving back upstream. The height of the bubble is about 6 percent of the blade height, or 4 percent of the chord. Approach end-wall skewing has no effect in this region, but above the bubble, it increases the skew. Apparent losses in total pressure are also shown in this figure. The readings are of questionable significance when the probe is within the separation bubble, due to the swirling, turbulent nature of the flow. Outside the separation bubble, and when there is no transverse injection, the results are as to be expected.

Similar transverses at another point on the mid-passage line, but further downstream -- at 50 percent axial chord -- are shown in Fig. 5. This position is well clear of the separation

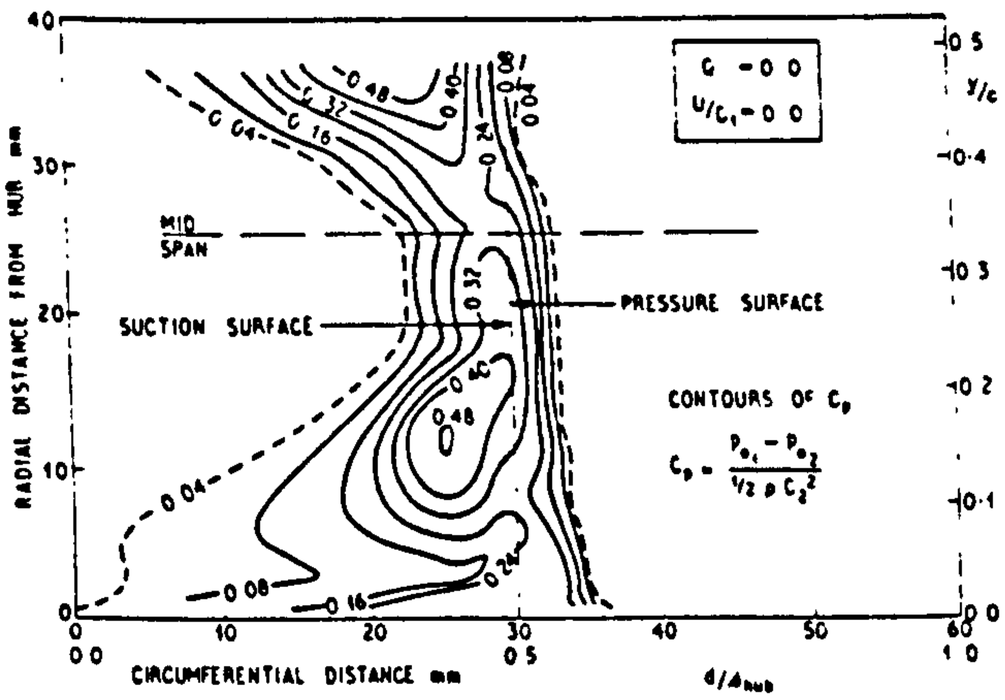

Fig. 6 Loss contours at exit from annular cascade - no transverse injection, non-skewed hub approach boundary layer

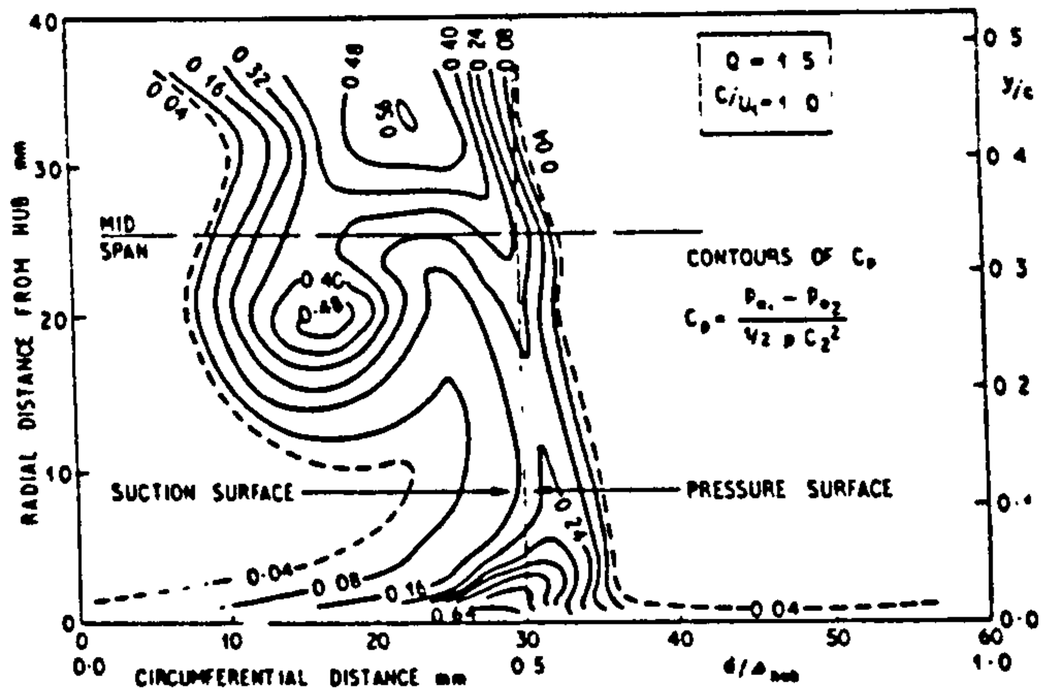

Fig. 8 Loss contours at exit from annular cascade - with transverse injection, skewed hub approach boundary layer

bubble on the end-wall, and the flow is securely reattached. The effect of injection, with no skewing of the approach end-wall boundary layer, is to reduce slightly skew immediately adjacent to the end-wall, but further from the wall, say at distances of 4 to 2[illegible] percent of blade height, the skew is increased. When skew is given to approach end-wall boundary layer, in addition to the transverse injection, then there is a further increase in the skewing of the boundary layer at this location on the passage end-wall.

Summarizing, the effect of transverse injection in an annular cascade on the end-wall boundary layer is similar to that previously reported in straight cascades (1).

Pressure Loss Distributions at Outlet

Pressure loss distributions at the outlet traverse planes are shown in Figs. 6, 7, and 8, respectively, for the annular cascade when there was no injection and no skewing of the approach end-wall boundary layer, for injection but no skewing, and, finally, injection and skewing. Circumferential distances are mapped as straight lines on these figures, and the length of the base-line represents the blade pitch at the hub. The results for the straight cascade are shown in Figs. 9 and 10, without and with transverse injection, respectively. To assist comparisons, the losses from the two different cascades are normalized against the outlet velocity head. However, there are other differences: in the straight cascade, the traverses are made much further from the blade exit, and the blades are of different profiles.

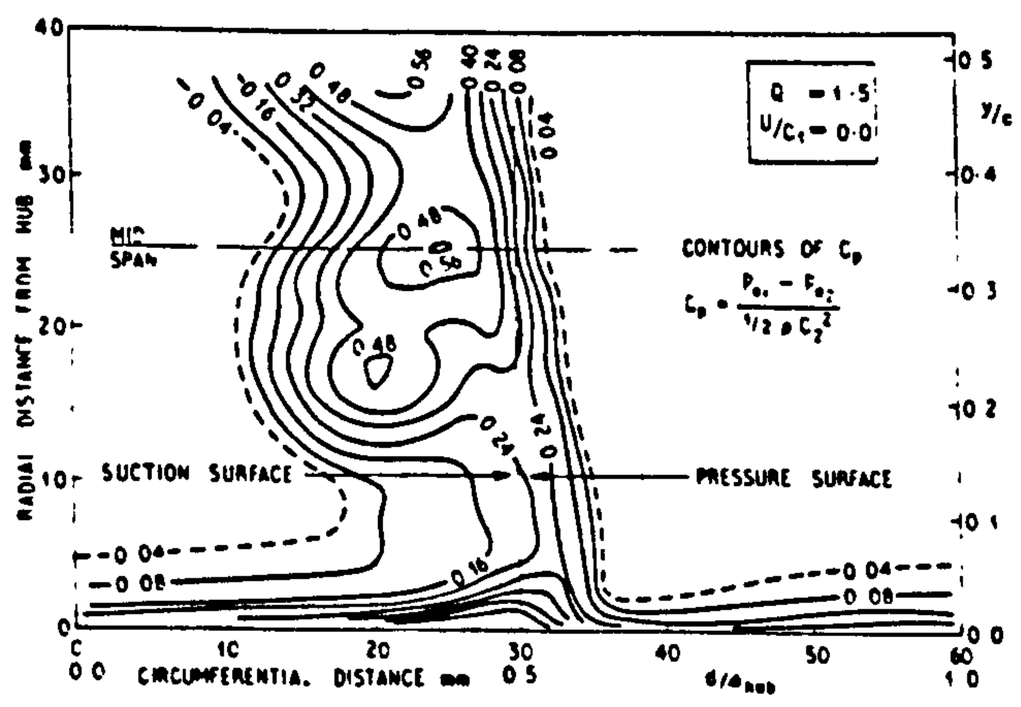

Fig. 7 Loss contours at exit from annular cascade - with transverse injection, non-skewed hub approach boundary layer

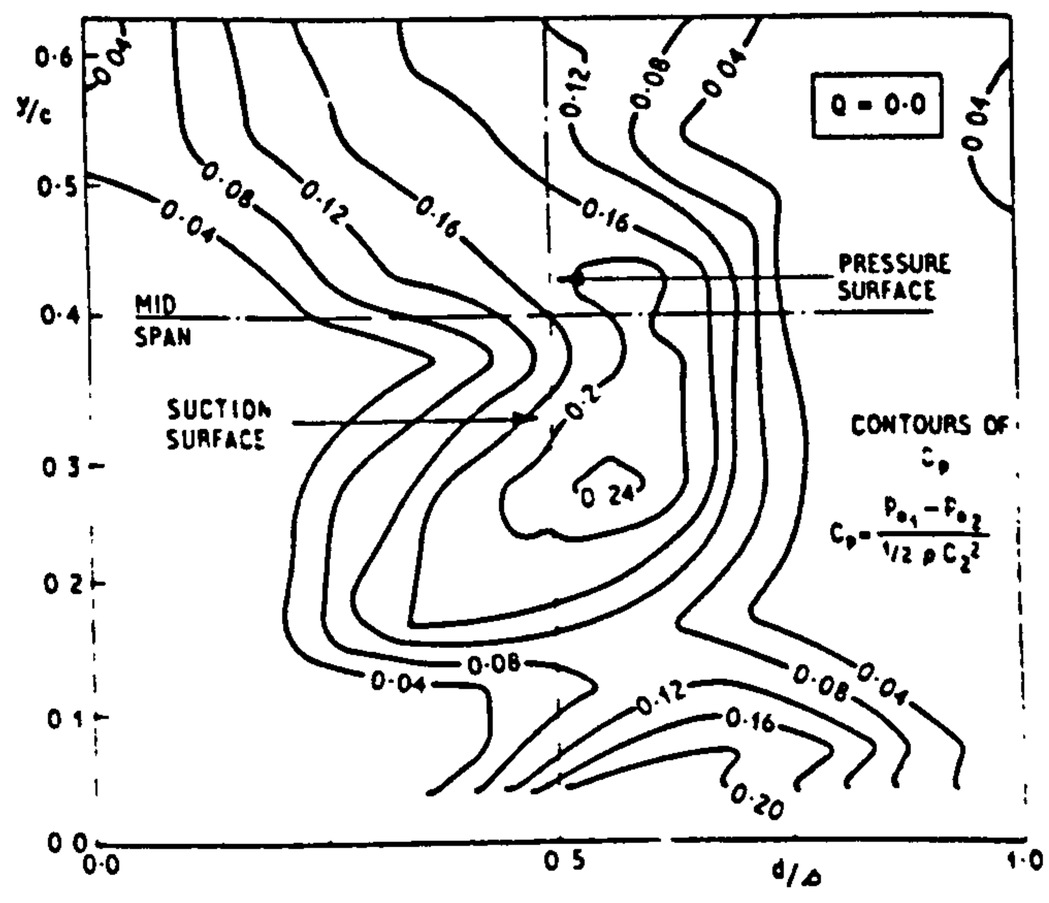

Fig. 9 Loss contours at exit from straight cascade - no transverse injection

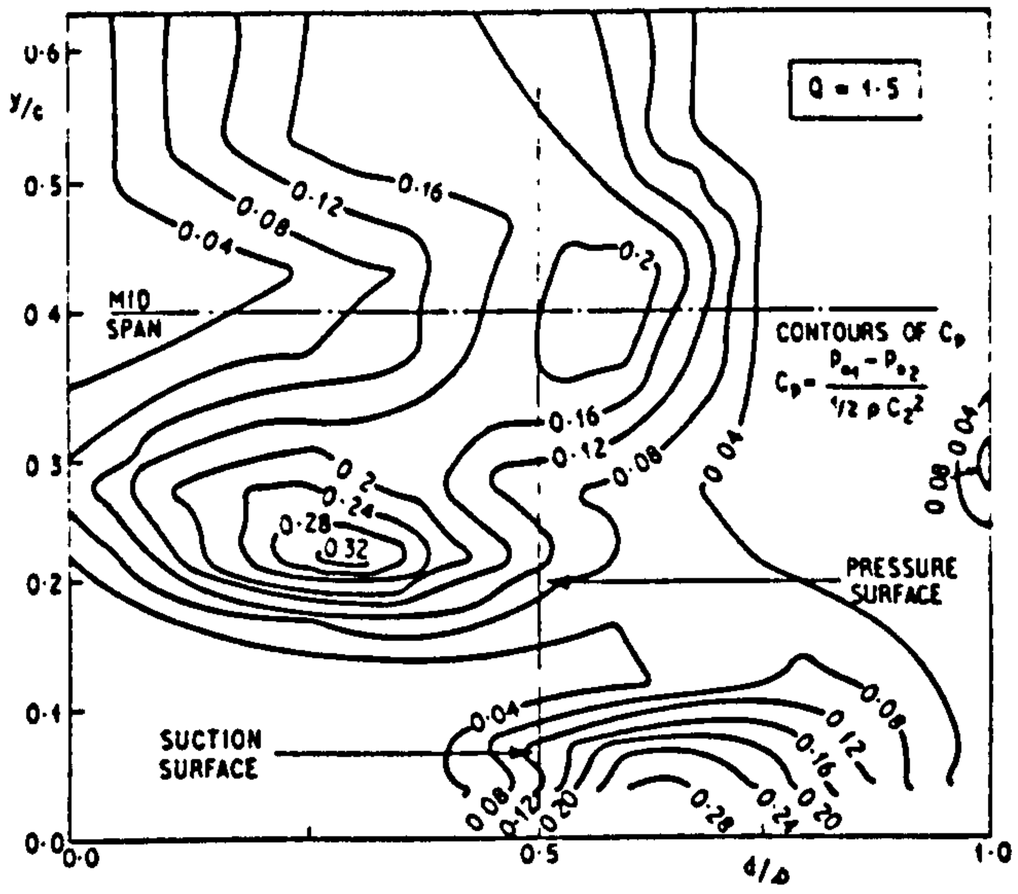

Fig. 10 Loss contours at exit from straight cascade - with transverse injection

Nonetheless, one can make reasonable deductions as to the effects of transverse in injection in each cascade.

In the straight cascade, transverse injection causes a high loss region in the wake to be intensified and displaced away from the suction surface and toward the end-wall. This zone of low forward velocity has been identified as being a vortex (1), the side nearest to the end-wall rotating toward the suction surface. This result with an aspect ratio of 0.8 is in line with the observations at higher aspect ratios, and confirming that the location of the vortex moves progressively but slowly toward the end-wall as aspect ratio is lowered -- now being at y/c = 0.23 c.f. at y/c = 0.27 when aspect ratio was 1.0.

In the annular cascade, without skewing the approaching hub boundary layer (Figs. 6 and 7), transverse injection causes similar effects -- a region of high loss appears in the channel flow, from adjacent to the suction-surface, and separated from the end-wall loss regions. Transverse injection lifts the high loss core away from the end-wall and injection plus skewing lifts it even further. The lifting effect of injection is unexpected since, as will be seen later, the overall losses are increased by injection and the radial pressure gradient could be expected to move the lower velocity region toward the hub. The trough in forward velocity is seen from the detailed deviation traverses to be a vortex. The magnitude of the maximum loss in this region is not greatly different from the maximum wake loss when there was

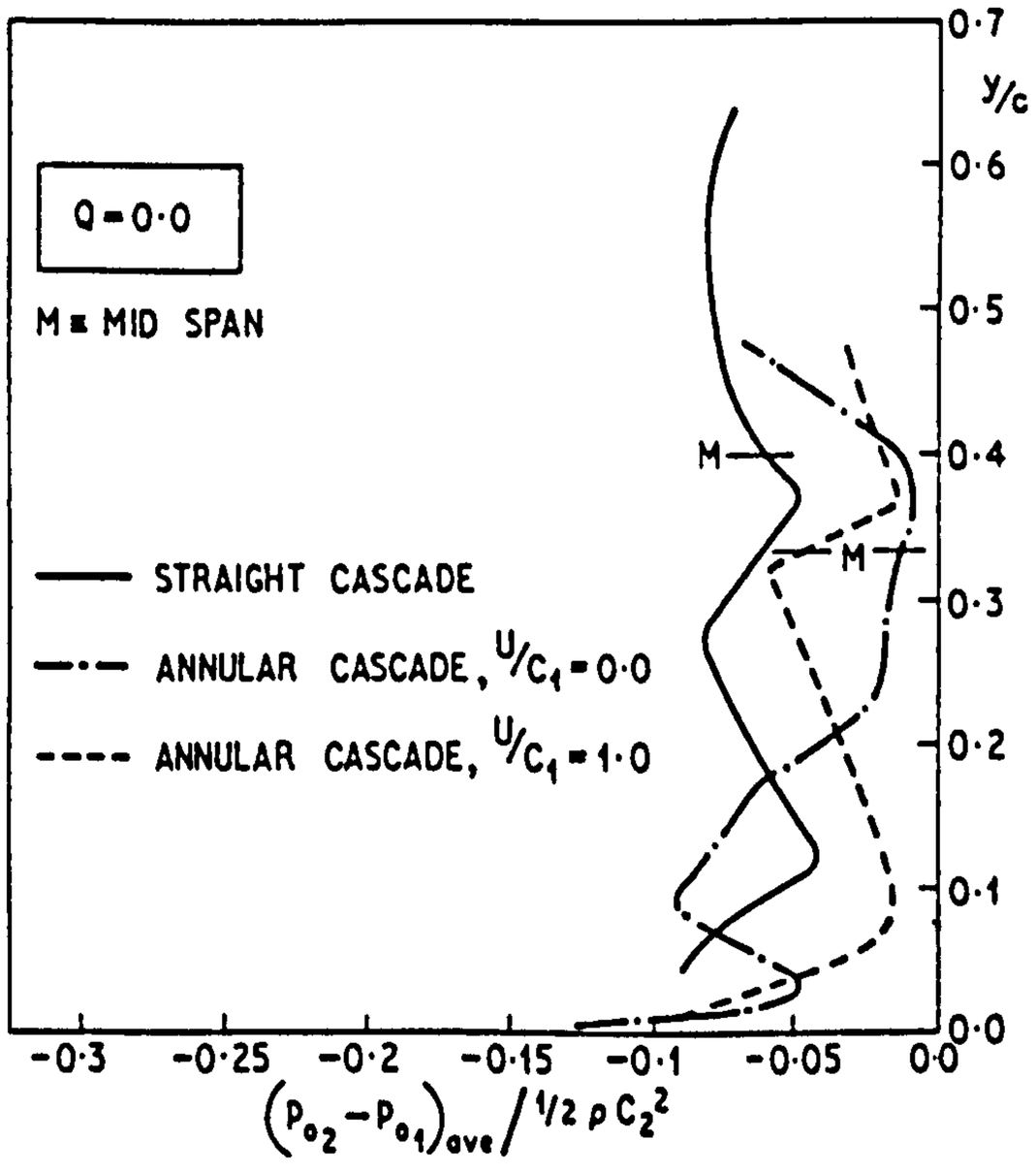

Fig. 11 Integrated stagnation pressure losses - no transverse injection

no transverse injection.

When the approach hub boundary layer to the annular cascade is skewed, the losses at the hub end-wall are somewhat distributed along the blade wake by the lifting of the passage vortex. This result is not shown here but is given in Reference (8) and discussed in detail. When transverse injection is added this vortex region in the passage is enhanced.

Integrated Stagnation Pressure Losses

Pitch integration of the stagnation pressure loss distributions shown in Figs. 6 to 10 leads to the results shown in Fig. 11 when there is no injection, and in Fig. 12 for the cases where injection is taking place. Both area averaging and mass averaging methods were used, with little discrepancy. Where numerical comparisons are made, as when studying the effect of transverse injection on nozzle efficiency, consistent averaging techniques were adopted. In all cases, the effect of transverse injection is seen to form a high loss zone which is well separated from the hub end-wall boundary layer.

Overall Average Stagnation Pressure Losses

To provide numerical comparisons of performance changes, the pitch-integrated pressure

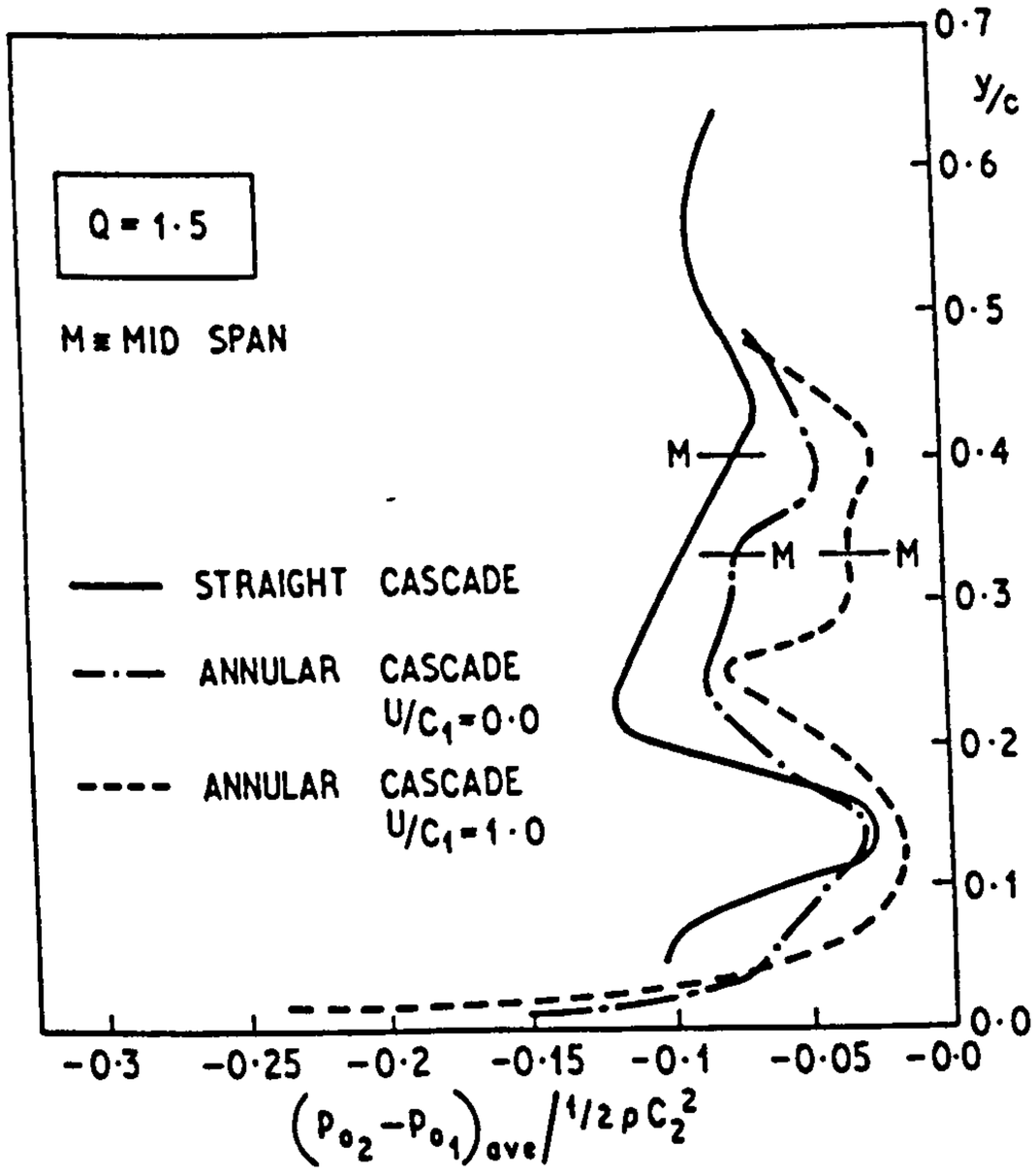

Fig. 12 Integrated stagnation pressure losses - with transverse injection

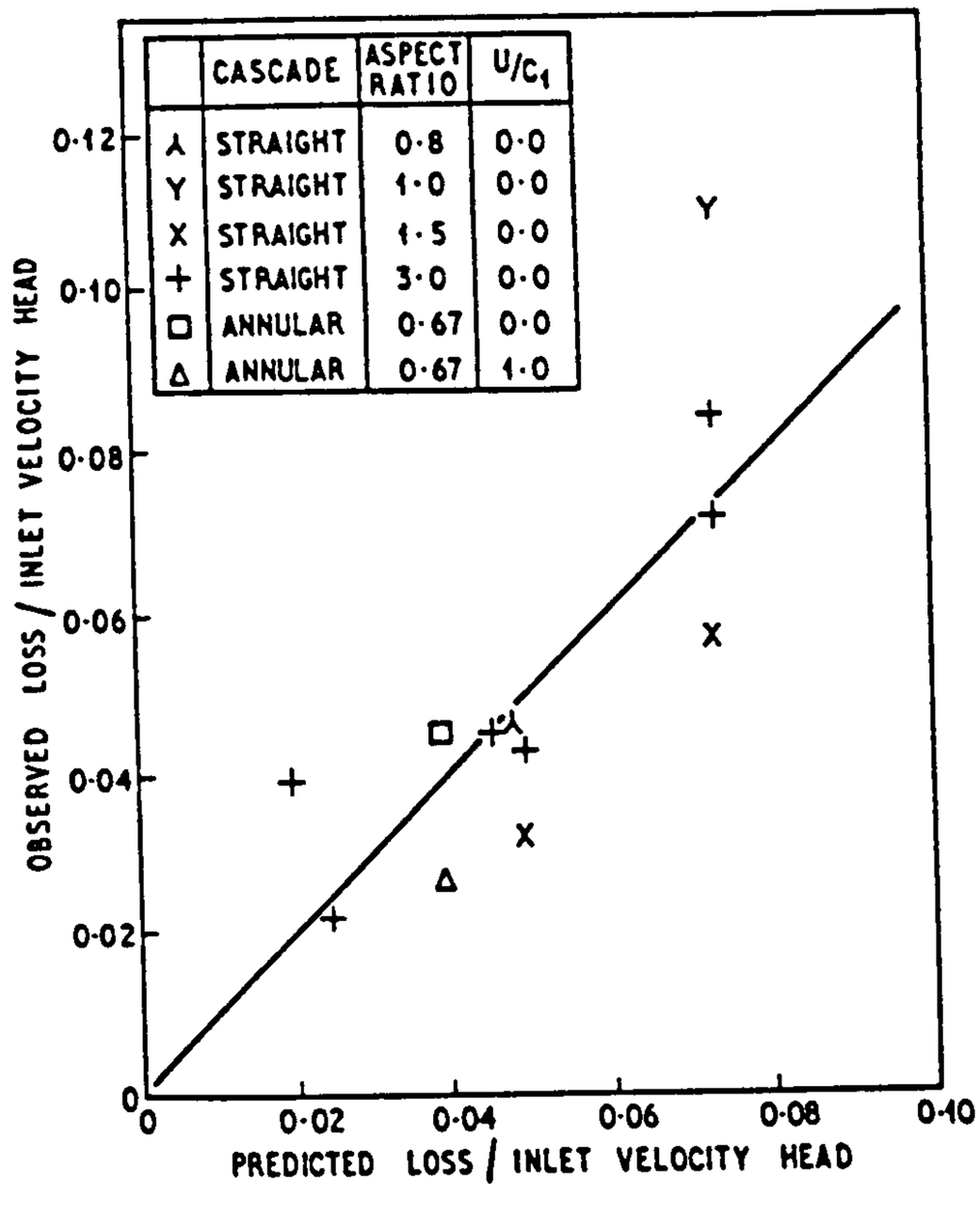

Fig. 13 Predicted and observed losses of stagnation pressure

loss curves were averaged along the span of the blades. It had not been possible to extend the total pressure traverses to the outer annular wall due to the goose-necking of the cobra probe and of the five-hole probe. Thus, information was restricted to 70 percent of the blade height in the annular cascade and to 80 percent of the blade height in the straight cascade. The assumption adopted for the remaining portion, which is adjacent to the end-wall opposite to the end-wall from which the transverse injection is made, was that the loss distribution was the same as that at the other end of the blade, when there was no injection, and that this distribution was not affected by transverse injection. On this basis, nozzle efficiencies have been determined from the relation

$$\eta = 1 - \frac{(p_{o_1} - p_{o_2})_{ave}}{(p_{o_2} - p_2)_{ave}} \qquad (1)$$

This relation is not quite the same as that used in earlier work (3), but in the form shown here, it provides a convenient indication of efficiency and of efficiency change, particularly in the annular cascade. The results are given in Table 2. The effects of transverse injection on nozzle efficiency are apparently greater in the annular cascade, but this effect is explained below as being a function of the lower exit angle of the annular cascade.

The changes in the averaged losses in stagnation pressure have also been compared with the predictions of a simple one-dimensional theory (9, 2). In Reference (2), the predicted loss had been shown to be

$$\Delta P_c = \tfrac{1}{2}\rho\, C_1^2 \left[(f^2 - 1) - 2\,(f - 1)\, Q \cos\theta \cos\alpha_1\right] \qquad (2)$$

The comparison between observed and predicted

Table 2 Nozzle Efficiencies and "Strengths" of Exit Vortex

Cascade	Aspect Ratio	U/C1	Inject. Mass Ratio	Nozzle Effy. η	Exit Vortex Parameters		
Straight	0.8	0.0	0.0	0.92[illegible]	0.62	0.[illegible]	0.01[illegible]
Straight	0.8	0.0	0.02[illegible]	0.91[illegible]	1.1[illegible]	1.[illegible]	0.0[illegible]
Annular	0.6[illegible]	0.0	0.0	0.9[illegible]	1.6[illegible]	2.[illegible]	0.05[illegible]
Annular	0.6[illegible]	0.0	0.02[illegible]	0.94[illegible]	[illegible]	2[illegible]	[illegible]
Annular	0.6[illegible]	1.0	0.0	0.9[illegible]	[illegible]	1[illegible]	0.2[illegible]
Annular	0.6[illegible]	1.0	0.02[illegible]	0.9[illegible]	[illegible]	2[illegible]	[illegible]

(Authors: Binder, Aburwir & Marcillac)

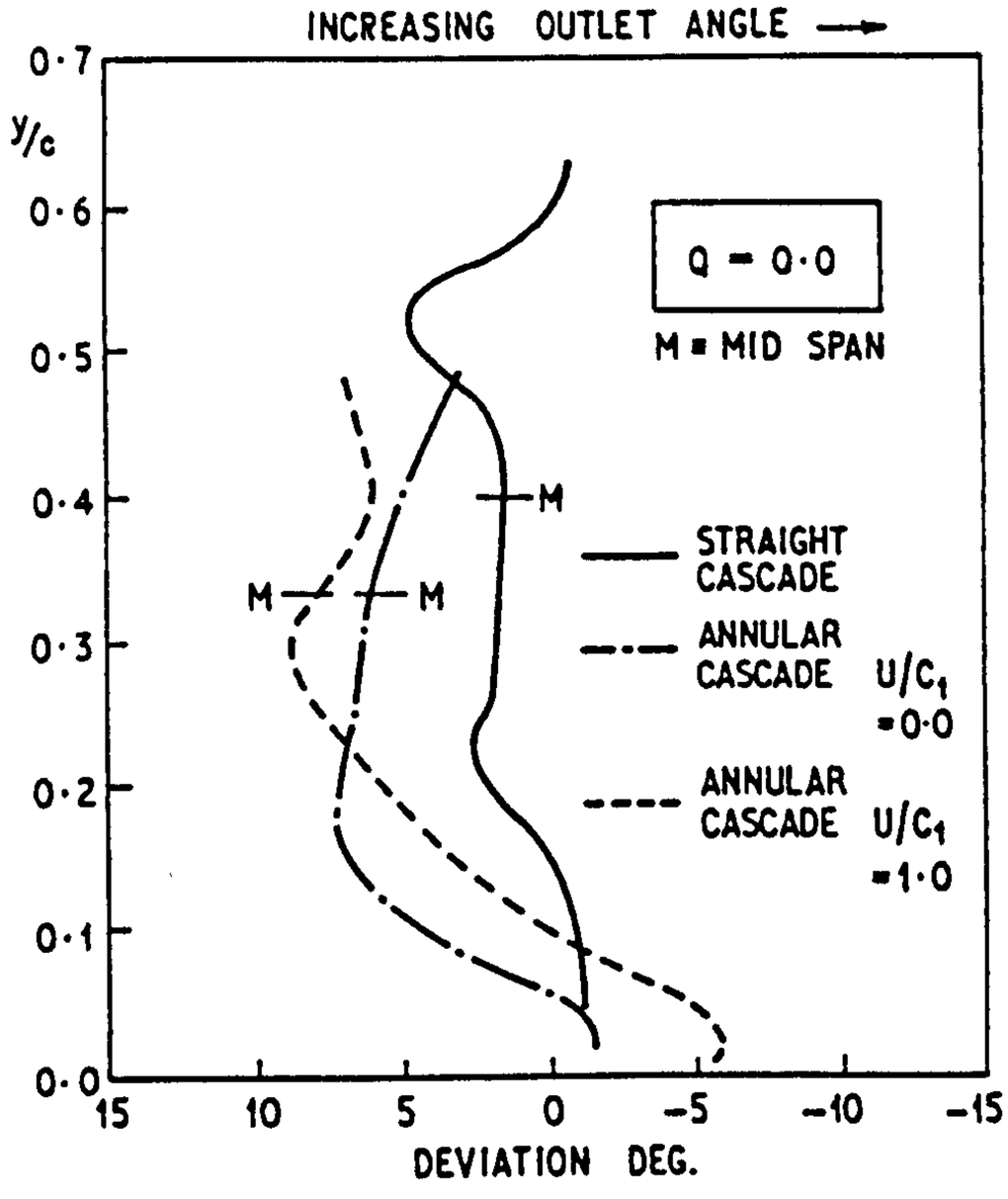

Fig. 14 Integrated deviations - no transverse injection

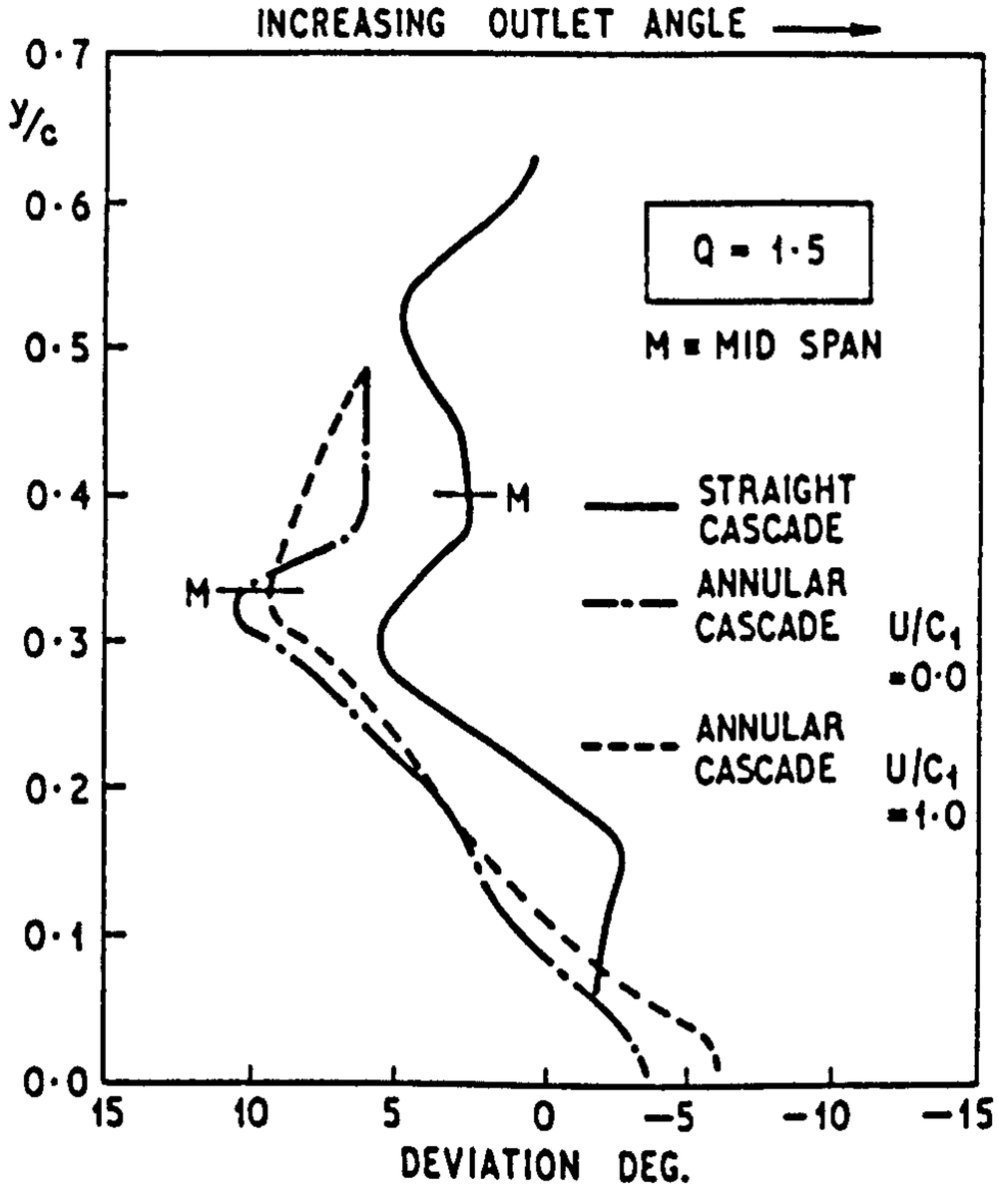

Fig. 15 Integrated deviations - with transverse injection

increase in losses is given in Fig. 13 results at other aspect ratios in the straight cascade (3) also being shown. Agreement is fairly good for the present work.

Equation (2) also explains why the efficiency reductions associated with transverse injection are greater in the nozzles used in the annular cascade than in those used in the straight cascade. From the equation, the loss in stagnation pressure is proportional to the velocity head at inlet to the cascade. The change in efficiency is equal to the loss in stagnation pressure divided by the exit velocity head. Thus, predicted change in efficiency, for a given mass injection ratio, is proportional to inlet velocity head divided by exit velocity head. Blades with higher exit angles (from the axial direction) will, therefore, show lower efficiency reductions.

Integrated Deviations

Pitch-integrated deviations are given in Figs. 14 and 15. When there is no transverse injection (Fig. 14), the exit flow in the annular cascade shows considerable change in angle close to the hub, particularly when the hub boundary layer approaching the cascade is skewed. These changes in average angle are made even larger when transverse injection is introduced.

In the more highly distorted flow that exists when transverse injection is taking place, the effect of skewing the approaching hub boundary layer is less marked. This is to be expected, as the transverse stream as it enters causes considerable disturbance to the skewed boundary layer and, of course, lifts it off the end-wall for a short distance.

In the straight cascade, the flow direction had been much more uniform when there was no transverse injection, but the introduction of the transverse stream caused considerable deviations, associated with the strong exit vortex previously described (1).

In earlier work (2), an attempt had been made to quantify this exit vortex by defining parameters D, E, and F which were proportional, respectively, to the circulation, to the kinetic energy of the tangential velocity components, and to the angular momentum of the vortex, if the vortex were assumed to be a rotating solid body bounded in diameter by the positions of maximum pitch-integrated positive and negative deviations. The parameters are given by

$$D = (\Delta\alpha^*)\ (\Delta y^*/c) \qquad (3)$$

$$E = (\Delta\alpha^*)^2\ (\Delta y^*/c)^2 \qquad (4)$$

$$F = (\Delta\alpha^*)\ (\Delta y^*/c)^3 \qquad (5)$$

These measures of the exit vortex have been applied in the present work and the results are shown in Table 2. In all cases, transverse injection has increased these measures, and it would appear that the increases in the annular cascade, whether with or without approach end-wall skew, are greater than those in the straight cascade.

CONCLUSIONS

Transverse injection from the hub end-wall in front of an annular cascade produces effects similar to those previously observed in straight cascades, viz. a separation bubble is formed on the hub end-wall immediately behind the injection slot, within the bubble there is movement toward the suction surface, and a strong vortex develops in the exit flow.

The changes in stagnation pressure loss and in efficiency are in reasonable agreement with the simple one-dimensional theory which had previously been found applicable to results from straight cascades.

Skewing the hub boundary layer as it approached the annular cascade, there being no transverse injection, had been found to have considerable effect on the secondary flows (8). This effect of introducing skewing is less marked when transverse injection is taking place.

ACKNOWLEDGMENTS

The authors wish to thank Carleton University, Ottawa, Canada for experimental facilities and to thank the National Research Council of Canada, the South African Council for Scientific and Industrial Research, the University of Natal, and the Science Research Council (U.K.) for financial support. They also wish to thank Professor R. S. Silver, University of Glasgow, for his encouragement and to thank the Staff of Rolls-Royce Ltd. for stimulating comments.

REFERENCES

1 Shrivastava, K. D., and Maccallum, N. R. L., "The Effect of a Transversely Injected Stream on the Flow through Turbine Cascades: Part I -- Flow Effects," ASME Paper No. 77-GT-87.

2 Shrivastava, K. D., and Maccallum, N. R. L., "The Effect of a Transversely Injected Stream on the Flow through Turbine Cascades: Part II -- Performance Changes," ASME Paper No. 77-GT-88.

3 Aburwin, B. A., and Maccallum, N. R. L., "The Effect of a Transversely Injected Stream on the Flow through Turbine Cascades: Part III -- Influence of Aspect Ratio," ASME Paper No. 78-GT-24. To be published in Journal of Engineering for Power.

4 Rohlik, H. E., Kofskey, M. G., Allen, H. W., and Herzig, H. Z., "Secondary Flows and Boundary Layer Accumulations in Turbine Nozzles," NACA Report 1168, 1954.

5 Kofskey, M. G., and Allen, H. W., "Smoke Study of Nozzle Secondary Flows in a Low-Speed Turbine," NACA TN 3260, 1954.

6 Lakshminarayana, B., and Horlock, J. H., "Review: Secondary Flows and Losses in Cascades and Axial-Flow Turbomachines," International Journal of Mechanical Sciences, Vol. 5, 1963, pp. 287-307.

7 Sjolander, S. A., "The End-wall Boundary Layer in an Annular Cascade of Turbine Nozzle Guide Vanes," Technical Report No. ME/A 75-4, Carleton University, Ottawa, 1975.

8 Bindon, J. P., "The Effect of Hub Inlet Boundary Layer Skewing on the End-wall Shear Flow and Outlet Flow Patterns in an Annular Turbine Cascade," Paper offered to ASME Gas Turbine Conference, 1979.

9 Barnes, J. F., and Fray, D. E., "An Experimental High Temperature Turbine: Part II -- The Effects of Cooling on the Aerodynamic Performance," Aeronautical Research Council R & M. No. 3405, 1965.

Publication 24

ted in U.S.A.

79-GT-143

an ASME publication

$3.00 PER COPY
$1.50 TO ASME MEMBERS

Thermal Influences in Gas Turbine Transients — Effects of Changes in Compressor Characteristics

N. R. L. MACCALLUM

Senior Lecturer,
Dept. of Mechanical Engineering,
University of Glasgow,
Glasgow, Scotland

During transients of axial-flow gas turbines, the characteristics of the compressor are altered. The changes in these characteristics (excluding surge line changes) have been related to transient heat transfer parameters, and these relations have been incorporated in a program for predicting the transient response of a single-shaft aero gas turbine. The effect of the change in compressor characteristics has been examined in accelerations using two alternative acceleration fuel schedules. When the fuel is scheduled on compressor delivery pressure alone, there is no increase in predicted acceleration times. When the fuel is scheduled on shaft speed alone, the predicted acceleration times are increased by about 5 to 6 percent.

Contributed by the Gas Turbine Division of The American Society of Mechanical Engineers for presentation at the Gas Turbine Conference & Exhibit & Solar Energy Conference, San Diego, Calif., March 12-15, 1979. Manuscript received at ASME Headquarters December 26, 1978.
Copies will be available until December 1, 1979.

THE AMERICAN SOCIETY OF MECHANICAL ENGINEERS, UNITED ENGINEERING CENTER, 345 EAST 47th STREET, NEW YORK, N.Y. 10017

Thermal Influences in Gas Turbine Transients — Effects of Changes in Compressor Characteristics

N. R. L. MACCALLUM

ABSTRACT

During transients of axial-flow gas turbines, the characteristics of the compressor are altered. The changes in these characteristics (excluding surge line changes) have been related to transient heat transfer parameters, and these relations have been incorporated in a program for predicting the transient response of a single-shaft aero gas turbine. The effect of the change in compressor characteristics has been examined in accelerations using two alternative acceleration fuel schedules. When the fuel is scheduled on compressor delivery pressure alone, there is no increase in predicted acceleration times. When the fuel is scheduled on shaft speed alone, the predicted acceleration times are increased by about 5 to 6 per cent.

NOMENCLATURE

A = flow area
c = chord
c_p = specific heat at constant pressure
F = ratio of heat transfer to fluid to work transfer from fluid in an element of a compressor or turbine
h = heat transfer coefficient
k = thermal conductivity of fluid
ℓ = distance from leading edge
m = index of non-adiabatic compression or expansion
M = mass flow rate of fluid
N = rotational speed of shaft
P = pressure
Pr = Prandtl Number
Q = heat flux to fluid in compressor or turbine
T = temperature
y = blade height
γ = isentropic index
η = small-stage, or polytropic efficiency
μ = viscosity

Subscripts

1,2 = inlet to, outlet from compressor
ave = average
lam = laminar
th = throat
turb = turbulent

INTRODUCTION

It is important that reliable methods are developed for the prediction of the transient behaviour of gas turbines. For example, one wants to be able to predict the speed response and the thrust response of an aero gas turbine when a given acceleration fuel schedule is applied.

The earliest programs for the prediction of the transient performance used equilibrium characteristics for the components, and ignored heat transfer effects. However these simple programs seriously underpredicted the times required for the speed and thrust responses - Thomson (1)[1] quotes underpredictions of 20 to 30 per cent for acceleration times.

The discrepancies between these simple predictions and the observed acceleration times have been attributed to one or more of the following factors:

(a) heat absorptions in the compressor(s) and turbine(s)

[1] Underlined numbers in brackets designate references at end of paper.

(b) heat absorption in the combustion chamber metal
(c) incorrect tip clearances in compressor(s) and turbine(s) during transient
(d) incorrect seal clearances during transient
(e) lag in combustion process.

Fawke and Saravanamuttoo (2), after making reasonable simplifying assumptions, have included factor (a). Thomson (1) makes an estimate of the fuel flow equivalent to the difference between the increased fuel flow and the observed increases in kinetic energy and exhaust energy flux. This is then deducted from the fuel flow in the acceleration schedule used in the prediction program. Thomson also indicates methods of predicting heat transfer to combustion chambers, tip clearance changes and combustion lag - factors (b), (c) and (e). Maccallum (3) has illustrated how seal clearance changes in transients may be predicted. Excessive openings of critical seals may cause significant increases in cooling air flows, which will result in proportionately less gas passing through the higher pressure stages of the turbine. Also, the effects of these flows, if they return to the main flow in the turbine, may have to be considered (4) to (8).

One factor which has not previously been considered is:

(f) the change in the compressor characteristic due to the transient heat transfer.

A theoretical investigation of this aspect is reported in the present paper. In addition, there is an assessment of the heat transfer correlations, and of the simplifying geometric assumptions that have previously been used.

HEAT TRANSFER IN COMPRESSORS AND TURBINES

Heat Transfer Correlations

For flows in compressors and turbines, Fawke and Saravanamuttoo (2) have used the Colburn Equation

$$\frac{hy}{k} = 0.023 \left(\frac{My}{A\mu}\right)^{0.8} (Pr)^{0.4} \qquad (1)$$

This equation is valid for developed flow. However the flow over the aerofoil of a blade in a compressor or turbine will be far from developed. A new boundary layer has to be started at the leading edge of each blade. Consequently it might be more reasonable, say for the compressor, to use the flat plate correlations for developing laminar and turbulent layers. Thus for a laminar layer of length l, the average heat transfer coefficient is given by

$$h_{lam} = 0.664\ k\ (Pr)^{0.333} \left(\frac{M}{A\mu l}\right)^{0.5} \qquad (2)$$

and for a turbulent boundary layer

$$h_{turb} = 0.037 \left(\frac{M}{A}\right) c_p \left(\frac{Ml}{A\mu}\right)^{-0.2} (Pr)^{-0.667} \qquad (3)$$

In a compressor, it might be assumed that the boundary layer on the pressure surface was turbulent throughout its length, while that on the suction surface was initially laminar, becoming turbulent. An average heat transfer coefficient might then be given by

$$h_{ave} = 0.25\ h_{lam} + 0.75\ h_{turb} \qquad (4)$$

Comparing the predictions of equations (1) and (4) indicates that the values of coefficient given by equation (1) are typically at least 30 per cent lower than those given by equation (4).

The above expressions have ignored the influence of turbulence in the main flow. Turbulence intensities are known to be high (5 to 10 per cent). Two recent studies on typical turbine (not compressor) blades show that such levels increase the average heat transfer coefficient. Brown and Burton (9) indicate a 60 per cent increase in average heat transfer coefficient for an increase in turbulence intensity from 1.8 to 8.6 per cent (intensity defined by root mean square of fluctuations, normalised by free stream velocity). Bayley and Milligan (10) show increases of similar nature but depending on the frequency of the turbulence fluctuations. The range of increase in coefficients was from 20 per cent to 160 per cent for turbulence intensities varying between 14 and 46 per cent. It is suggested therefore that a reasonable practice to adopt in calculating heat transfer coefficients in a compressor is to use equation (4) with the coefficient increased by 60 per cent. This practice has been adopted in the present work.

For turbines, fortunately there is more experimental data available giving average coefficients on blades. For example Halls (11) quotes

$$\frac{hc}{k} = 0.235 \left(\frac{Mc}{A_{th}\mu}\right)^{0.64} \qquad (5)$$

It is suggested that where experimental correlations of this nature are available, these should be used. In the present work, heat transfer coefficients were calculated from the above equation. It is interesting to note that the predictions of equation (4), when applied to typical turbine blades, give coefficients which have to be increased by about 80 per cent to bring them into line with the experimental correlation of equation (5). This magnitude of increase provides support for the increase of 60 per cent recommended for the compressor.

Representation of Blades during Temperature Transients

Several models have been suggested (12) for representation of blades during temperature transients. Each of these is adequate for speed transients, and so it is recommended that nothing more sophisticated than a simple "unfinned" model is required, in which the aerofoils and platforms are represented by separate plates of equivalent total surface areas and thermal capacities. To make some allowance for the thermal contact between platforms and the devices on which they are mounted - disks or casings - in the present work the platform thermal capacities have been increased by 50 per cent.

CHANGES IN COMPRESSOR CHARACTERISTICS DUE TO HEAT TRANSFER

Having established heat transfer rates, two effects are now examined. The first results from changes in the development of the boundary layers on the aerofoils, particularly on the suction surfaces. The second is due simply to the alteration in density of the air at a plane, resulting from the heat transfer from, or to, the air in the section of the compressor up to that plane. This results in an alteration in the local ratio of axial velocity to blade speed.

Effect of heat transfer on Boundary Layers

In general terms, heat transfer from a wall to a boundary layer increases the rate at which the layer develops. The effect is more severe in the presence of an adverse pressure gradient. The transition region is moved upstream and, in cases where the boundary layer separates, heat transfer generally accelerates the process (13, 14). This advancement of the separation point was observed experimentally, and was also predicted by a procedure based on a modified momentum integral equation.

These findings have been applied (15) to the flow in an axial air compressor. It is suggested there that heat transfer from the blades to the air has little effect on the development of the layer on the pressure surfaces. However on the suction surfaces the prediction method shows under certain conditions a significant increase in the displacement thickness in the vicinity of the trailing edge when the heat transfer is to the air. This is illustrated qualitatively in Fig. 1. In this case the angle of departure of the flow on the suction surface will be increased (angles measured from the axial direction) due to the more rapid displacement thickness development. It was

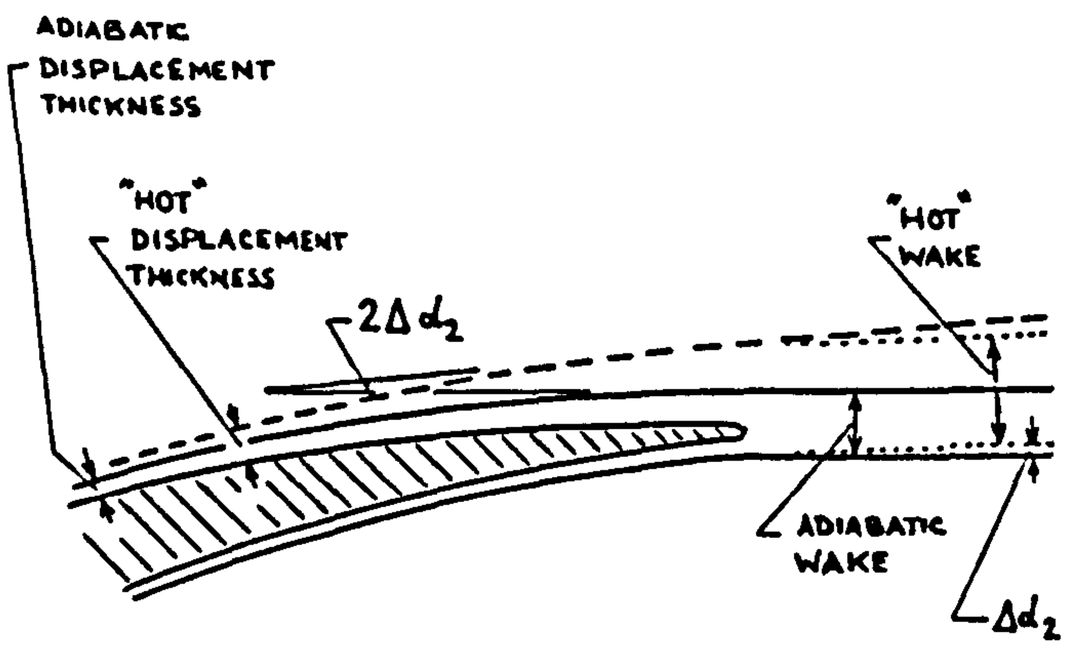

Fig. 1 The effect of heat transfer from a "hot" compressor blade on boundary layer development (Ref.15)

then assumed that the averaged increase in the leaving angle from a "hot" blade will be one half of the increase in the inclination of the line through the boundary of the displacement thickness on the suction surface. Thus for a "hot" blade there will be a reduced deflection across the blade row. If the blade is "cold" there is the possibility of increased deflection. These changes are predicted to take place only if the flow is near to separating, i.e. when there is significant positive incidence. In reference (15) these effects were incorporated in a program for predicting the compressor characteristics. This program also assumed that the wake losses in a non-adiabatic situation corresponded to the losses in the adiabatic case where the incidence to a blade row produced the same average leaving angle as in the non-adiabatic case. It was predicted that these boundary layer changes cause the constant speed pressure characteristics of the compressor to be displaced, and also cause movement of the surge line.

Effect of density change due to heat transfer

This density change due to heat transfer alters the ratio of axial velocity to blade speed, and hence alters the working points of the stages. The effect this has on the compressor constant speed pressure characteristics and surge line has been predicted in references (16) and (15).

Changes in Compressor Characteristics

In the present work, a sixteen-stage axial flow compressor of a single-shaft aero gas turbine, of maximum pressure ratio 9.5, was selected for studying these effects.

The thermal response of the compressor to an acceleration was first predicted, each blade row of the compressor being treated individually. The temperature differences between the air and the aerofoil surfaces, and the heat fluxes, were then included in the program for predicting the performance of the compressor. Predicted characteristics are shown on Figs. 2, 3 and 4 for the conditions existing during the acceleration when the compressor is at 85, 90 and 95 per cent respectively of the maximum speed. The predicted characteristics in which both boundary layer changes and density changes due to heat transfer are accounted for are represented by chain dotted lines. The corresponding characteristics when only the boundary layer changes are allowed for are indicated by the dashed lines and the adiabatic characteristics are shown by the solid lines. It is seen that in all cases there is a shift of the speed line, the major contributor to this displacement being the density change resulting from heat transfer. The predicted adiabatic surge line is shown, as are the predicted surge terminations of the non-adiabatic characteristics - in the present work the definition adopted for the location of the surge position is the point where the pressure characteristic has a maximum.

Predicted characteristics at speeds of 85 and 90 per cent during decelerations from 100 per cent speed are also shown on Figs. 2 and 3.

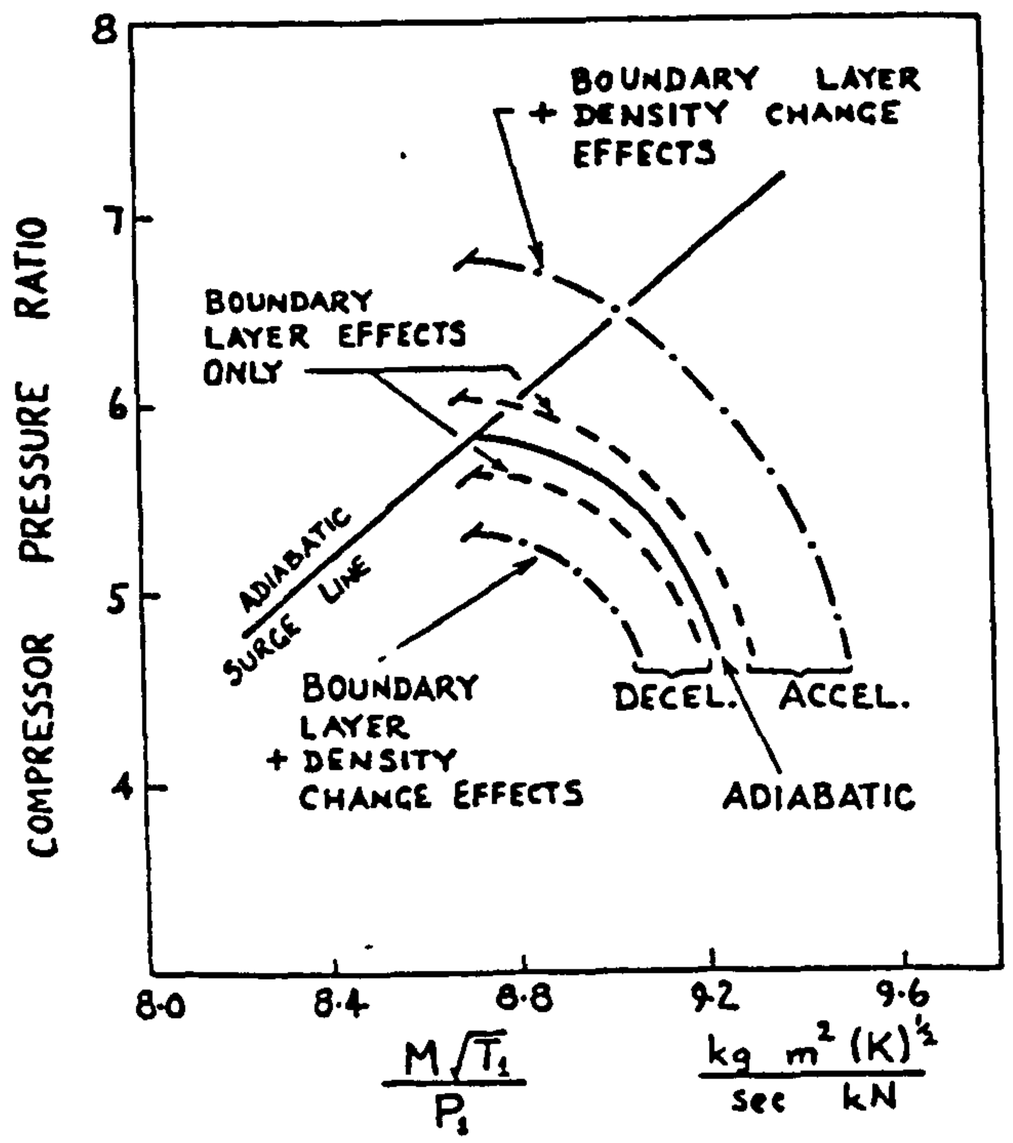

Fig. 2 Predicted effects of heat transfer on compressor characteristics during acceleration and deceleration at sea level - $N/\sqrt{T_1}$ = 0.85 x take-off $N/\sqrt{T_1}$

The movements of the surge lines are important, and one case has been discussed in some detail in

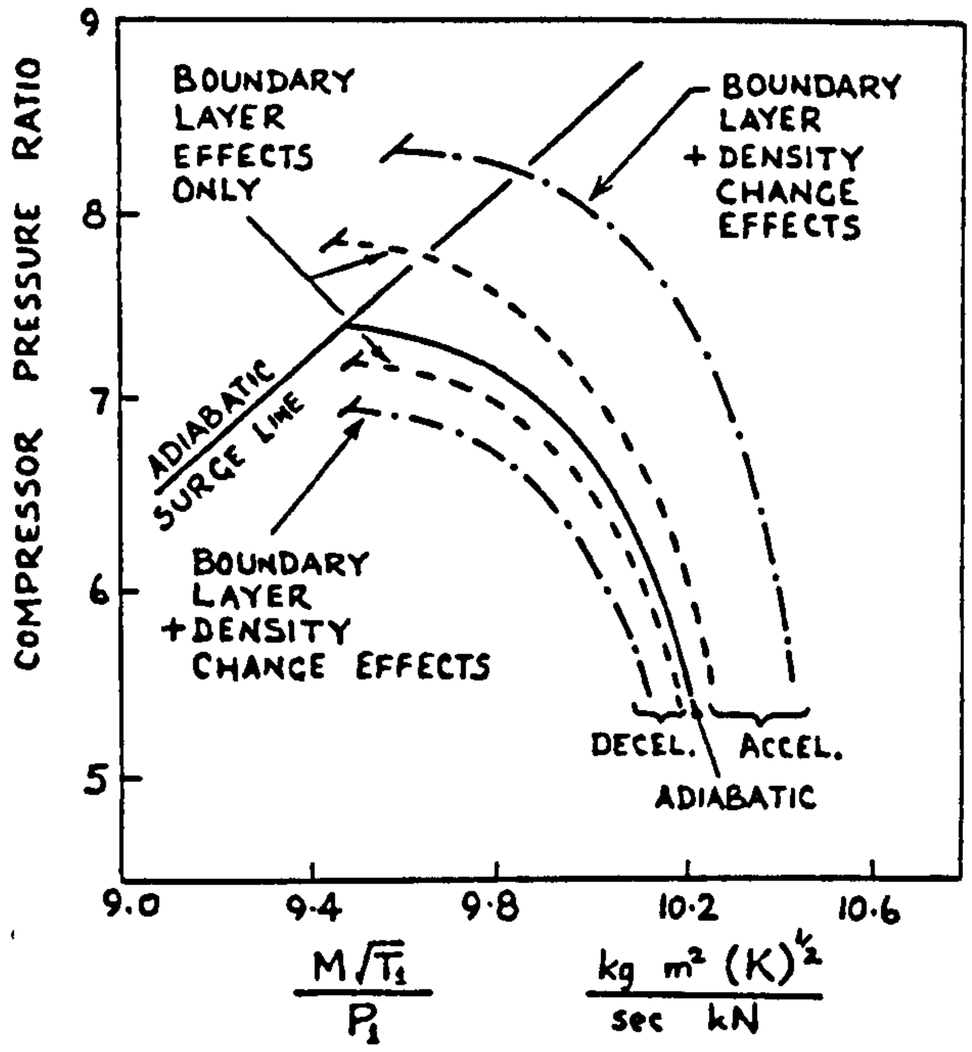

Fig. 3 Predicted effects of heat transfer on compressor characteristics during acceleration and deceleration at sea level – $N/\sqrt{T_1}$ = 0.90 x take-off $N/\sqrt{T_1}$

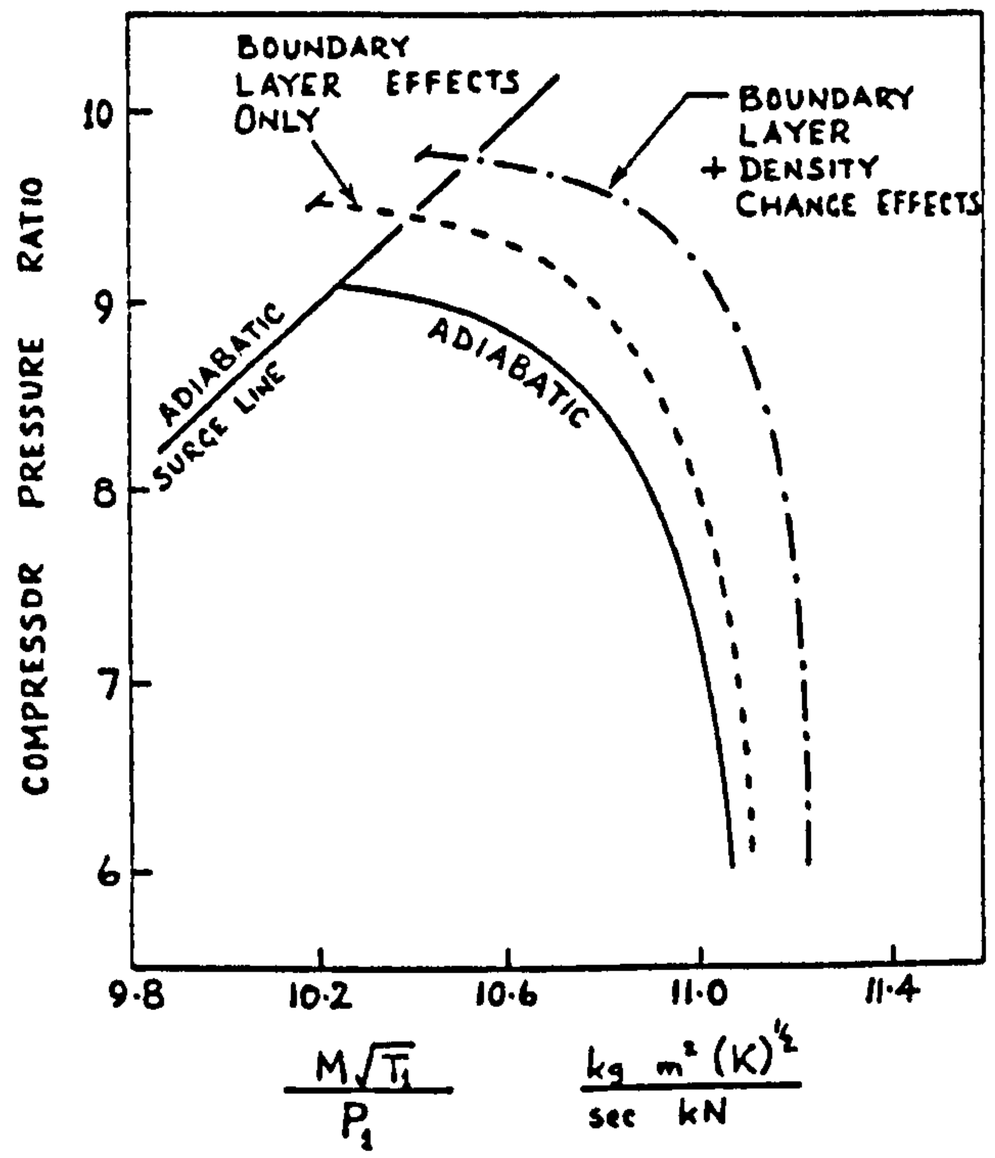

Fig. 4 Predicted effects of heat transfer on compressor characteristics during an acceleration at sea level – $N/\sqrt{T_1}$ = 0.95 x take-off $N/\sqrt{T_1}$

reference (15). In the present paper this is not discussed further, apart from stating that during an acceleration of a "cold" engine the surge line is beneficially moved by the heat transfer. During a deceleration, deterioration of the surge line is predicted.

The movement of the constant speed line is important to the present investigation of transient response. Examination of the results shown in Figs. 2 to 4 suggests that the transient characteristics may be regarded as being similar to the equilibrium characteristics when the compressor is running adiabatically at a speed different by, say, ΔN from the actual speed, N, of the compressor. Thus the "aerodynamic" or effective speed of the compressor is (N + ΔN). The correlation of these "speed changes" with relevant transient parameters is discussed below.

RELATION OF CHANGES IN CONSTANT SPEED CHARACTERISTICS TO TRANSIENT PARAMETERS

The changes due to the two effects - boundary layer and density changes - are considered separately.

Firstly, estimates were made of the changes in effective compressor speed, ΔN, corresponding to the displacements of the constant speed characteristics shown in Figs. 2, 3 and 4 due to the boundary layer effects. Grant (13) has shown that, for a given air temperature, changes in boundary layer development - for example movement of the separation point - are proportional to the temperature difference between the surface and the air. Therefore the changes in speed, ΔN, found above have been plotted, in normalised form, against this temperature difference, normalised by the average temperature in the compressor. These results are shown in Fig. 5. The correlation is not good, but bearing in mind that the movements due to boundary layer effects are small,

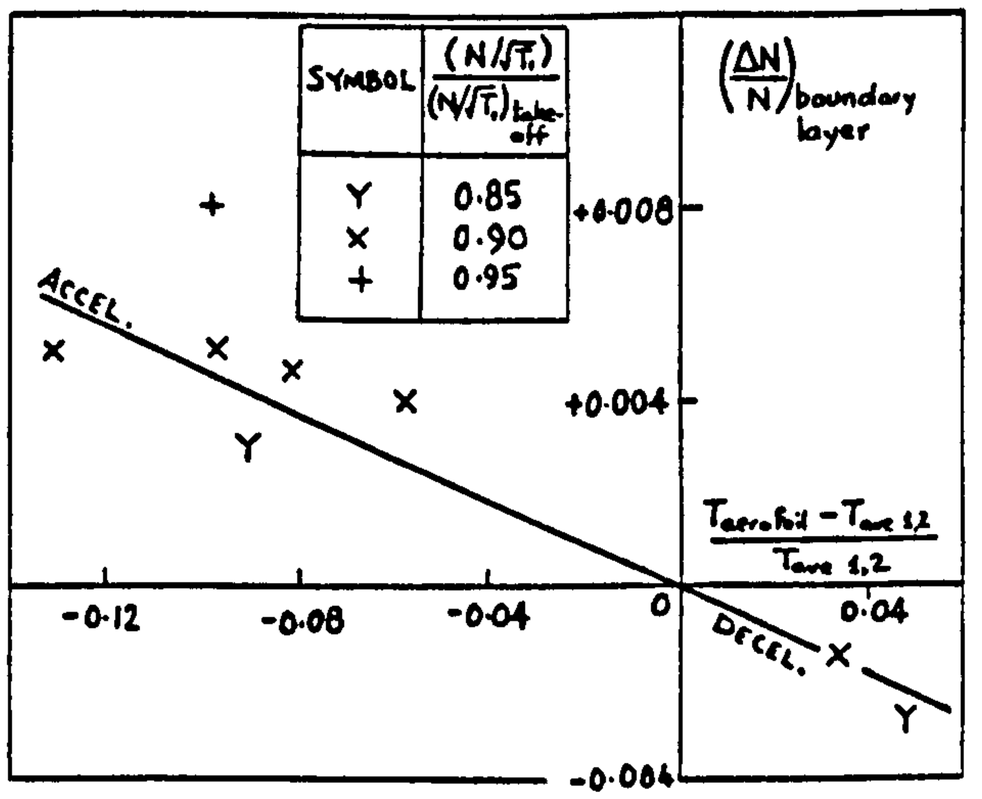

Fig. 5 Predicted changes in "effective" speed of compressor during transients due to boundary layer effects

the following relation, illustrated by the solid line on Fig. 5 was adopted –

$$\left(\frac{\Delta N}{N}\right)_{\text{boundary layer}} = -0.055\left(\frac{T_{\text{aerofoil}} - T_{\text{air}}}{T_{\text{ave 1,2}}}\right) \quad (6)$$

In a similar manner, estimates were made of the changes in effective compressor speed due to the density changes resulting from heat transfer. These are plotted on Fig. 6 against the heat flux per unit mass of air. A much better correlation is found for these changes, represented by the expression

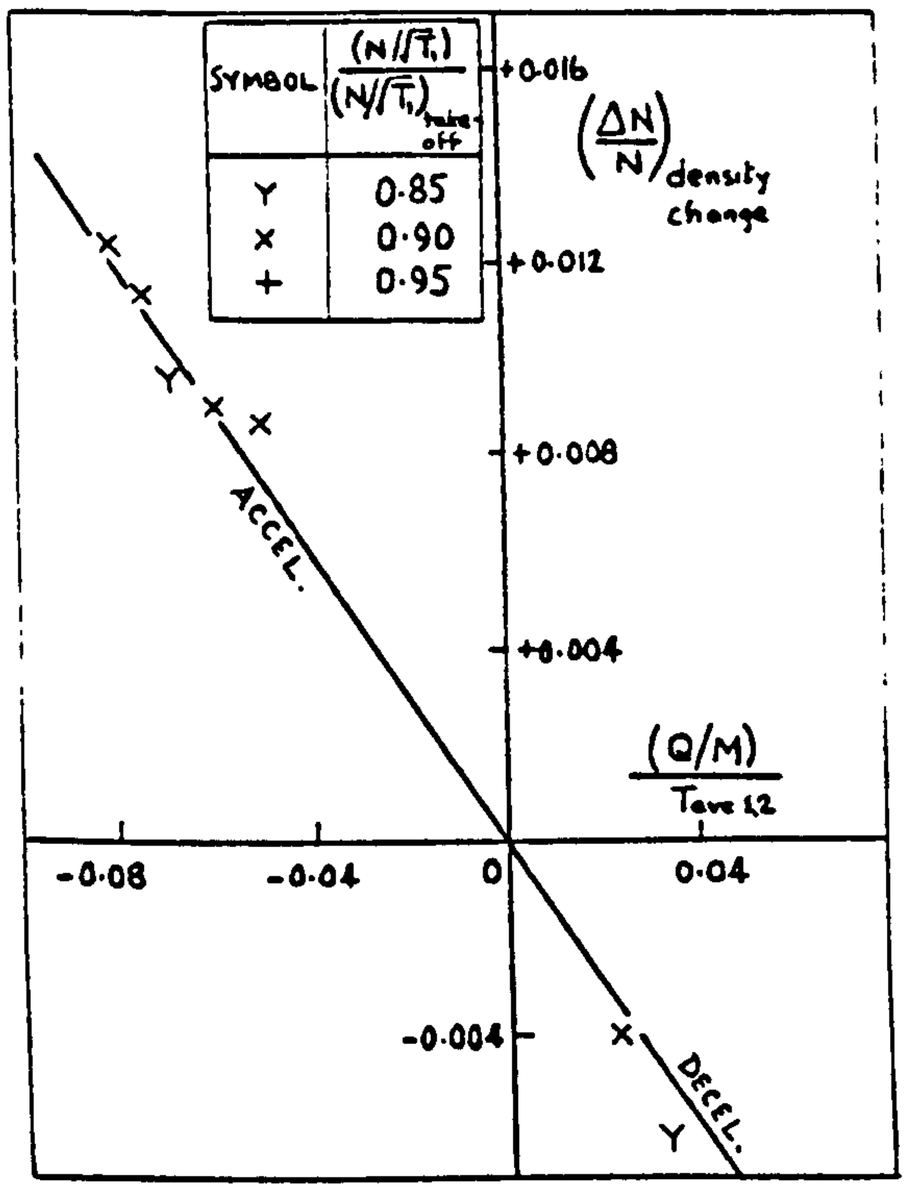

Fig. 6 Predicted changes in "effective" speed of compressor during transients due to density change resulting from heat transfer.

$$\left(\frac{\Delta N}{N}\right)_{\text{density change}} = -0.15 \left(\frac{Q}{M}\right) \frac{1}{T_{\text{ave 1,2}}} \qquad (7)$$

These expressions have been incorporated in the gas turbine transient program discussed later.

NON-ADIABATIC COMPRESSIONS AND EXPANSIONS

If the ratio, F, of the heat transfer to the air to the work transfer from the air in an element of a compressor remains constant along the compressor, then it has been shown (17) that the index of the actual compression path, m, is related to the isentropic index by

$$\frac{m-1}{m} = (1-F)\frac{\eta(\gamma-1)}{\gamma} \qquad (8)$$

The corresponding relation for turbines is

$$\frac{m-1}{m} = (1-F)\,\eta\,\frac{\gamma-1}{\gamma} \qquad (9)$$

This simple analysis has been included in the gas turbine transient program discussed later. The analysis produces results virtually identical to those given by the method adopted by Thomson (1).

SIMPLIFIED THERMAL REPRESENTATION OF COMPRESSORS AND TURBINES

Ideally, in temperature transients, each row of blades in the compressor, or turbine, should be treated separately as blade dimensions vary from row to row. However this greatly complicates the inclusion of thermal effects in gas turbine transient programs. It would be much more satisfactory if an adequate representation could be provided by a single representative row of blades, or failing this, say two or four representative rows. The row, or rows would have the appropriate total surface areas of aerofoils and platforms, and the appropriate thermal capacities. The accuracy of some form of simplified representation has been assessed in the present work by considering the acceleration of the sixteen-stage axial compressor previously discussed. The predicted total fluxes of heat, per unit mass of air, to the metal of the compressor are compared on Fig. 7 for the three cases of complete row by row representation, representation by four characteristic rows and representation by a single characteristic row. The four-row model is very satisfactory, discrepancies being typically less than 3 per cent. The single row representation is less accurate however and heat transfer rates are overpredicted, particularly during the last 2 seconds of the speed transient, when the discrepancies range from 10 to 15 per cent.

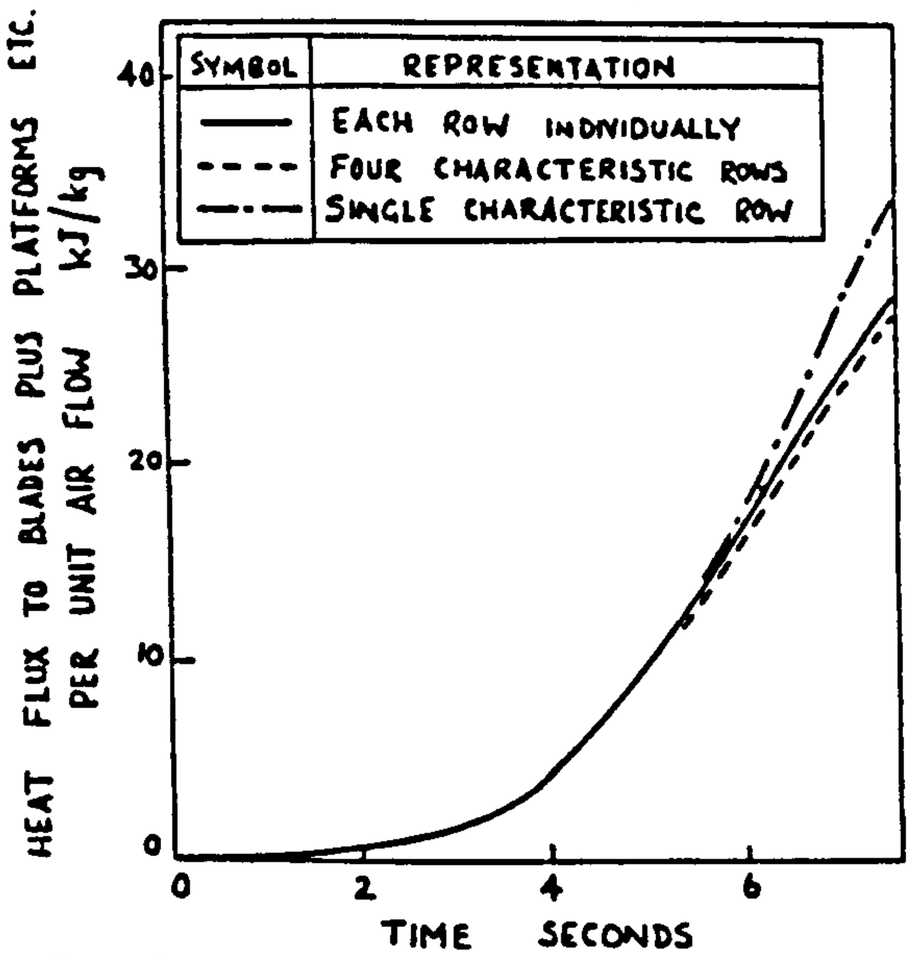

Fig. 7 Validity of simplified representation of a sixteen-stage axial compressor in a temperature transient - predicted thermal response to an acceleration at sea level.

In view however of the other uncertainties in the inclusion of heat transfer in gas turbine transient prediction procedures, it is considered that the single blade row representation is adequate for most purposes. The transient program used below utilises single-row representation.

PREDICTED EFFECTS OF HEAT TRANSFER IN GAS TURBINE TRANSIENT RESPONSES.

A program was prepared for predicting the transient response of a single-spool aero gas turbine engine. The engine used the sixteen-stage axial compressor whose transient characteristics have been analysed in the previous paragraphs.

The speed transient program incorporated the facilities discussed above for including non-adiabatic compressions and expansions and also allowed for the displacement of the constant speed lines on the compressor's characteristics. Single-row representation was used for calculating the heat transfer rates in the compressor and turbine.

The transient response has been calculated for accelerations at sea level using two alternative acceleration fuel schedules.

In the first the fuel flow is a function of the compressor delivery pressure, as illustrated in Fig. 8,

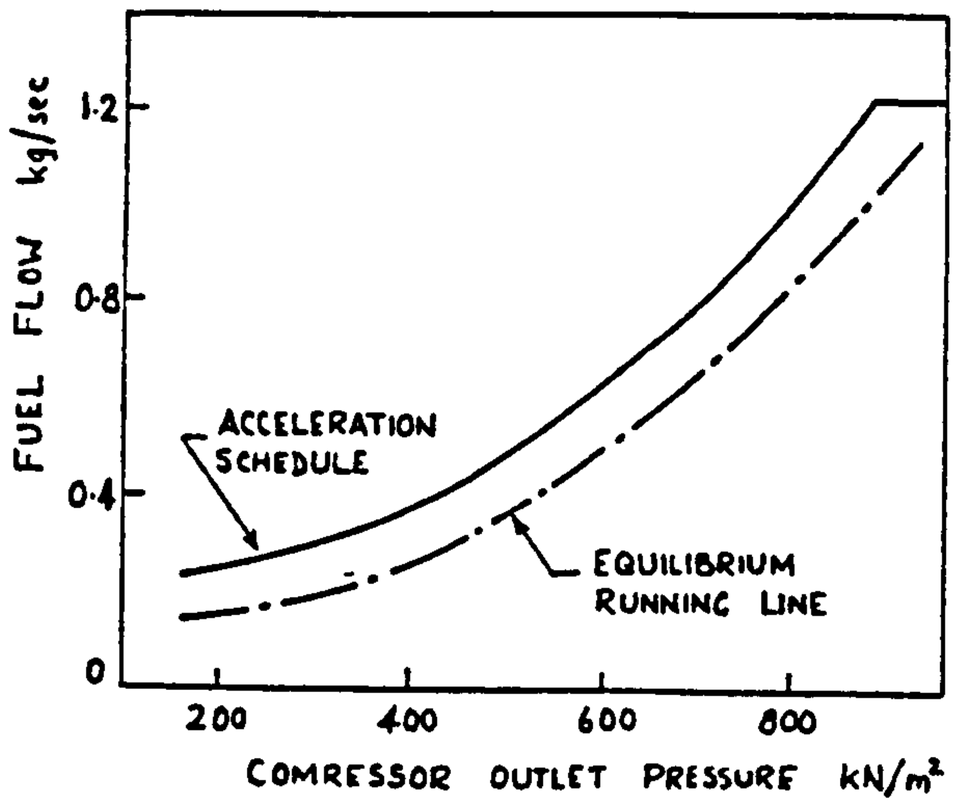

Fig. 8 Acceleration fuel schedule "A" - function of compressor outlet pressure.

and in the second the fuel flow is a function of the engine shaft-speed as given in Fig. 9.

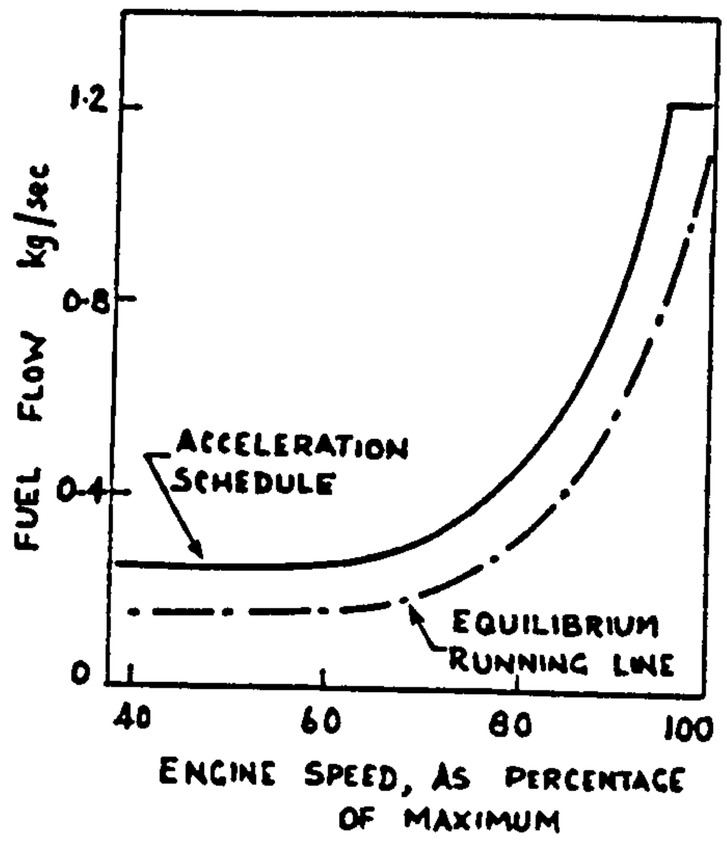

Fig. 9 Acceleration fuel flow schedule "B" - function of engine speed, for acceleration at sea level.

The predicted responses to the acceleration fuel schedule based on pressure are given in Fig. 10. Two starting speeds are considered - 30 per cent and 50 per cent of maximum speed. Fig. 10 shows the predicted responses for the following assumed situations:

(a) adiabatic compression and expansion,
(b) with heat transfer to compressor, but ignoring movement of characteristic,

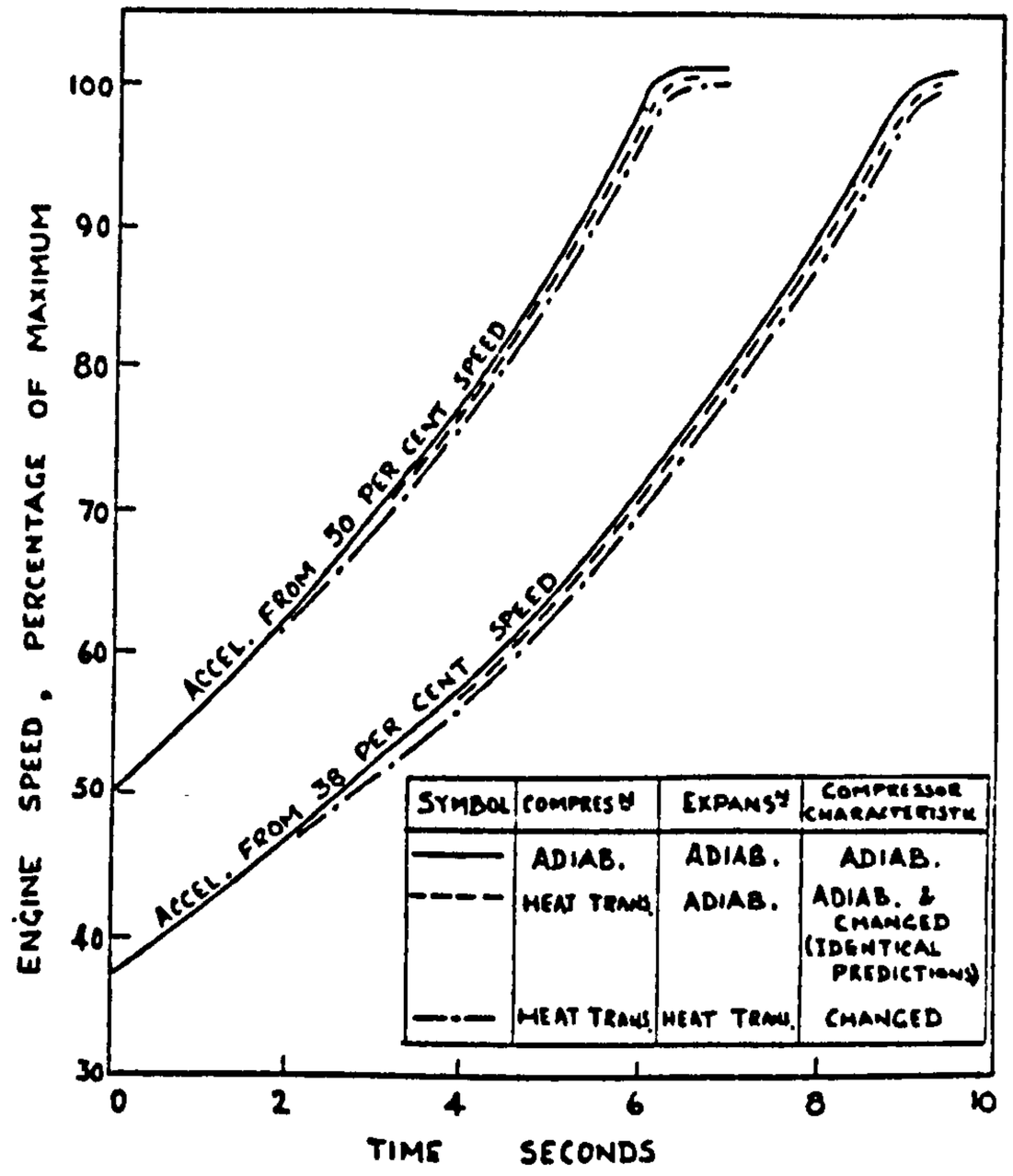

Fig. 10 Predicted accelerations at sea level using fuel schedule "A" - function of compressor outlet pressure.

(c) with heat transfer to compressor, and including movement of characteristic,
(d) with heat transfer to compressor and to turbine, and movement of compressor characteristic accounted for.

The results show that the inclusion of heat transfer causes a slight lengthening of the predicted acceleration times, but this amounts to only about 5 per cent. Inclusion of the change in compressor characteristics produces no alteration in the predicted acceleration times.

The predicted responses to the acceleration fuel schedule based on shaft speed are given in Fig. 11. Inclusion of heat transfer in the compressor and turbine again leads to an increase in the predicted acceleration times, though the change is only about 3 to 4 per cent. However there is a significant change when the alteration in compressor characteristics is introduced. This increases the predicted acceleration times by about a further 5 to 6 per cent.

The magnitudes of the changes in predicted acceleration times due to the inclusion of heat transfer in the compressor and turbine (but ignoring compressor characteristic change) are similar to those reported by Fawke and Saravanamuttoo [2]

CONCLUSIONS

Transient heat transfers alter the characteristics of axial flow compressors. The changes in characteristics can be approximated by using the concept of changes in effective speed, and these changes can be correlated to heat transfer parameters.

The techniques have been applied to a single-shaft aero gas turbine. When the gas turbine uses an acceleration fuel schedule which is a function solely of compressor delivery pressure, inclusion of the

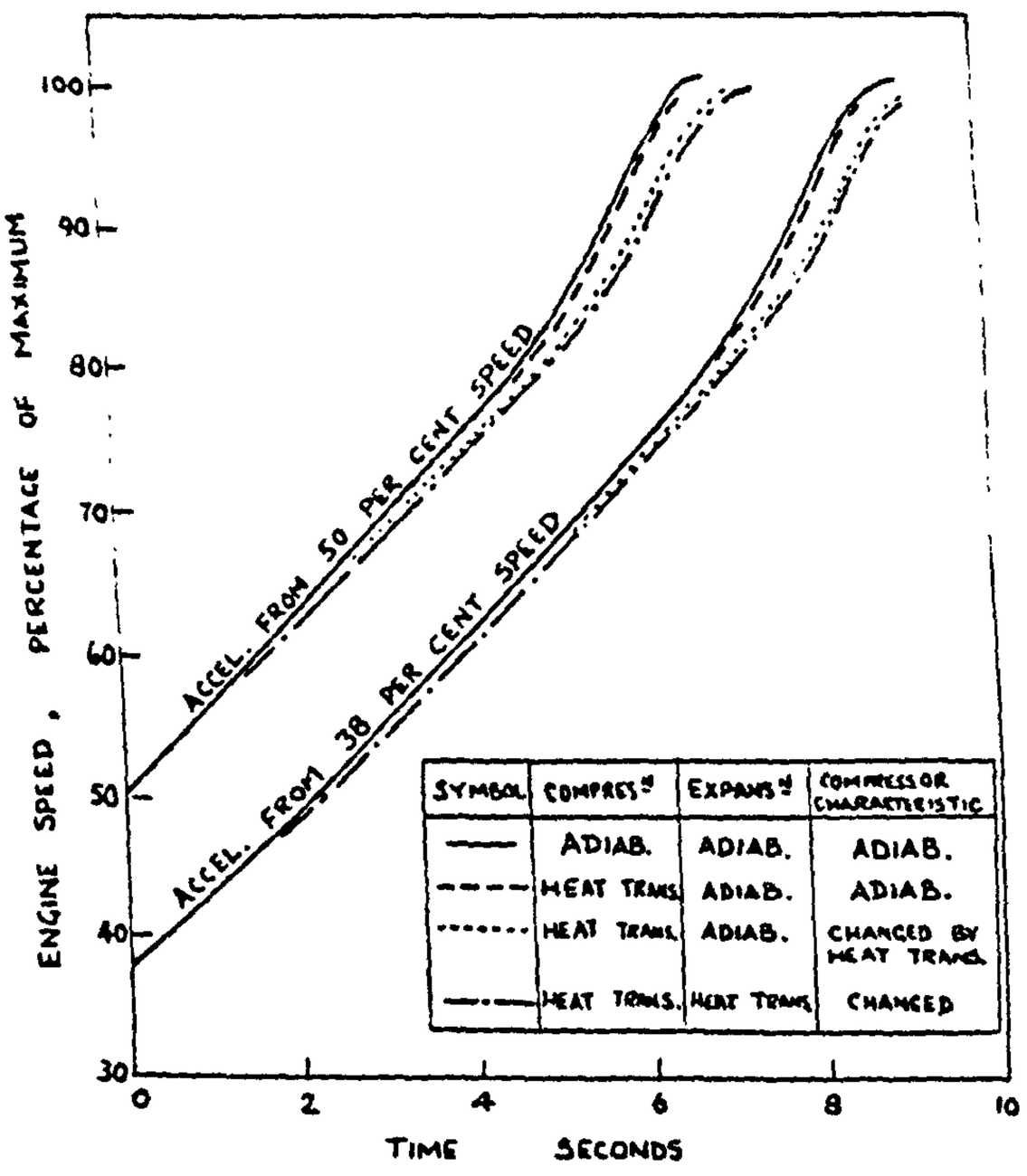

Fig. 11 Predicted accelerations at sea level using fuel schedule "B" - function of engine speed.

compressor characteristic alteration in the engine transient program produces no change in the predicted acceleration times. However when the gas turbine uses an acceleration fuel schedule which is a function solely of shaft speed, the predicted acceleration times are lengthened by 5 to 6 per cent by allowing for the change in the compressor characteristics. In a deceleration, with the fuel scheduled on the shaft speed, the predicted deceleration time would be extended.

Heat transfer correlations have been compared and recommendations are made.

Simplified thermal representations of a compressor have been assessed, and a single-blade representation is adequate for most purposes.

ACKNOWLEDGEMENTS

The author wishes to thank the staff of Rolls-Royce Limited for their helpful comments. He also wishes to thank Professor R.S. Silver, and colleagues at the University of Glasgow for their encouragement and advice.

REFERENCES

1 Thomson, B., "Basic Transient Effects of Aero Gas Turbines," AGARD Conference Proceedings 151, Dec. 1975.

2 Fawke, A.J., and Saravanamuttoo, H.I.H., "Digital Computer Simulation of the Dynamic Response of a Twin-Speed Turbofan with Mixed Exhausts, "Aeronautical Journal, Vol. 77, Sept. 1973, pp. 471-478.

3 Maccallum, N.R.L., "Transient Expansion of the Components of an Air Seal on a Gas Turbine Disc," SAE Paper 770974, 1977.

4,5 Shrivastava, K.D., and Maccallum, N.R.L., "The Effect of a Transversely Injected Stream on the Flow Through Turbine Cascades: Part I - Flow Effects, and Part II - Performance Changes," ASME Papers Nos. 77-GT-47 and 77-GT-88.

6 Aburwin, B.A., and Maccallum, N.R.L., "The Effect of a Transversely Injected Stream on the Flow Through Turbine Cascades: Part III - Influence of Aspect Ratio," to be published in Journal of Engineering for Power.

7 Bindon, J.P., Aburwin, B.A., and Maccallum, N.R.L., "Comparison of Transverse Injection Effects in Annular and in Straight Turbine Cascades", Paper to ASME Gas Turbine Conference, 1979.

8 Aburwin, B.A., and Maccallum, N.R.L., "Vortex Effects resulting from Transverse Injection in Turbine Cascades, and attempts at their Reduction," Paper to ASME Gas Turbine Conference, 1979

9 Brown, A., and Burton, R.C., "The Effects of Free-Stream Turbulence Intensity and Velocity Distribution on Heat Transfer to Curved Surfaces," ASME Paper No. 77-GT-48.

10 Bayley, F.J., and Milligan, R.W., "The Effect of Free-Stream Turbulence upon Heat Transfer to Turbine Blading," AGARD, Propulsion and Energetics Panel Meeting, Ankara, September, 1977.

11 Halls, G.A., "Air Cooling of Turbine Blades and Vanes," Lecture to AGARD, Varenna, Italy, May 1967.

12 Maccallum, N.R.L., "Models for the Representation of Turbomachine Blades during Temperature Transients," ASME Paper No. 76-GT-23.

13 Grant, A.D., The Effect of Heat Transfer on Boundary Layer Stability, Ph.D. Thesis, University of Glasgow, 1973.

14 Grant, A.D., "The Effect of Heat Transfer on Boundary Layer Stability in Axial Flow Compressors," Heat and Fluid Flow in Steam and Gas Turbine Plant, Instn. mech. Engrs., London, 1974, pp 252-258.

15 Maccallum, N.R.L., and Grant, A.D., "The Effect of Boundary Layer Changes due to Transient Heat Transfer on the Performance of an Axial Flow Air Compressor," SAE Paper 770284, 1977

16 Maccallum N.R.L., "Effects of 'Bulk' Heat Transfers in Aircraft Gas Turbines on Compressor Surge Margins," Heat and Fluid Flow in Steam and Gas Turbine Plant, Instn. mech. Engrs, London, 1974, pp. 94-100.

17 Maccallum, N.R.L., "The Performance of Turbo-Jet Engines during the 'Thermal Soak' Transient," Proceedings of the Instn. mech. Engrs, London, Vol. 184, Part 3G(II), 1969, pp. 23-29

Publication 25

81-GT-21

AN ASME PUBLICATION
$4.00 per copy $2.00 to ASME Members

THE AMERICAN SOCIETY OF MECHANICAL ENGINEERS
345 E 47 St., New York, N.Y. 10017

Further Studies of the Influence of Thermal Effects on the Predicted Acceleration of Gas Turbines

N. R. L. MacCallum
University of Glasgow,
Glasgow, Scotland

A previous study has investigated the effect of changes in compressor characteristics, due to transient heat transfers, on the predicted accelerations of a single-spool aero gas turbine of pressure ratio 9.5. In the present paper the analysis is extended to a two-spool bypass engine of pressure ratio 21. The increases in the predicted acceleration times of this engine, due to the inclusion of heat absorption and compressor characteristic change, are more marked than with the lower pressure ratio engine, depending on the fuel schedule used. The effects of changes in component efficiencies on predicted acceleration have also been studied. Again, the higher pressure ratio engine shows the greater influence. Compared with thermal absorptions, it is likely that component efficiency changes have as much, if not more effect on predicted accelerations.

ABSTRACT

A previous study has investigated the effect of changes in compressor characteristics, due to transient heat transfers, on the predicted accelerations of a single-spool aero gas turbine of pressure ratio 9.5. In the present paper the analysis is extended to a two-spool bypass engine of pressure ratio 21. The increases in the predicted acceleration times of this engine, due to the inclusion of heat absorption and compressor characteristic change, are more marked than with the lower pressure ratio engine, depending on the fuel schedule used.

The effects of changes in component efficiencies on predicted acceleration have also been studied. Again, the higher pressure ratio engine shows the greater influence. Compared with thermal absorptions, it is likely that component efficiency changes have as much, if not more effect on predicted accelerations.

NOMENCLATURE

$\dot{f}$ = fuel flow
F = ratio of heat transfer to fluid to work transfer from fluid in an element of a compressor or turbine
c_p = specific heat at constant pressure
$\dot{m}$ = mass flow rate of fluid
N = rotational speed of shaft
P = pressure
Q = heat flux to fluid in compressor or turbine
T = temperature

Subscripts
1,2 = inlet to, outlet from compressor (L.P.)
3 = outlet from H.P. compressor in 2-spool engine

INTRODUCTION

It is important that reliable methods are developed for the prediction of the transient behaviour of gas turbines. For example, accurate predictions are required for the thrust response and speed response of an aero gas turbine when a given acceleration fuel schedule is used.

The earliest programs for the prediction of the transient performance used equilibrium characteristics for the components, and ignored heat transfer effects. However these simple programs seriously underpredicted the times required for the speed and thrust responses - Thomson (1)[1] quotes underpredictions of 20 to 30 per cent for acceleration times.

The discrepancies between these simple predictions and the observed acceleration times have been attributed to one or more of the following factors:

(a) heat absorptions in the compressor(s) and turbine(s)
(b) heat absorption in the combustion chamber metal
(c) incorrect tip clearances in compressor(s) and turbine(s) during transient
(d) change in compressor(s) characteristics due to transient heat transfer
(e) incorrect seal clearances during transient
(f) packing lags
(g) lag in the combustion process

The heat absorptions in factor (a) have been included by Fawke and Saravanamuttoo (2), after making reasonable assumptions to simplify the problem. A different method of dealing with this factor was adopted by Thomson (1), who estimated the difference

1 Underlined numbers in brackets designate references at end of paper.

Contributed by the Gas Turbine Division of THE AMERICAN SOCIETY OF MECHANICAL ENGINEERS for presentation at the Gas Turbine Conference & Products Show, March 9-12, 1981, Houston, Texas. Manuscript received at ASME Headquarters December 4, 1980.
Copies will be available until December 1, 1981.

between the increased fuel flow energy input and the observed increases in kinetic energy and exhaust energy flux. This difference was then deducted from the fuel flow in the engine's acceleration schedule to give the "effective" fuel flow for the transient prediction. Thomson also indicated methods of predicting heat transfer to combustion chambers, and of predicting tip clearance changes and packing and combustion lags - factors (b), (c), (f) and (g) above. Maccallum (3) has illustrated how seal clearance changes may be predicted. Excessive openings of critical seals will cause increases of cooling air flows which will reduce the amount of gas passing through the higher pressure stages of the turbine.

The factor (d) - changes in compressor characteristics due to transient heat transfer - has been studied (4) with reference to a single-spool aero gas turbine of pressure ratio 9.5. There it was seen that the predicted acceleration time was increased by 5 to 6 per cent due to compressor characteristic changes if the accelerating fuel flow is scheduled on engine shaft speed alone. However if the fuel flow is scheduled on compressor delivery pressure there is no effect on the prediction of acceleration times. For both types of schedule, allowance for heat absorptions in the compressor and turbine caused increases of about 4 to 5 per cent in the predicted acceleration times.

In the work reported in this paper, the effects of changes in component efficiency, and of component mass flow capacity, on predicted acceleration times are given for the same single-spool gas turbine. The analysis is then extended to a two-spool bypass engine where the influences of heat absorptions, compressor characteristic changes and component efficiency changes on predicted acceleration times are considered, two alternative accelerating fuel schedules being used.

SINGLE-SPOOL ENGINE

A study has previously been made (4) of the effects of factors (a) and (d) on the predicted acceleration times of a single-spool aero gas turbine of maximum pressure ratio 9.5. The calculation procedure adopted was described in reference (4). Allowance was made both for the non-adiabatic compression in the compressor and for the non-adiabatic expansion in the turbine. The method adopted involved the instantaneous calculations in both components of the ratio, F, of the heat transfer to the air/gas in an element of the component to the work transfer from the air/gas in the same element. It was assumed that at any instant the value of this ratio, F, was constant along the component, which allowed integration along the component. Having accepted this approximation, it was then possible, without significant error (4), to simplify the representation of the thermal response of the compressor or turbine by the use of a single characteristic size of blade plus platform and shroud. The results obtained by this procedure were similar to those given by the method developed by Bauerfeind (5), and subsequently used by Thomson (1). The additional effect studied in reference (4) was the effect of the change in compressor characteristics due to heat transfer - factor (d). Two mechanisms have been described whereby transient heat transfer can alter the characteristics. The first mechanism is by a change in the development of the boundary layer on the suction surfaces of the blade aerofoils. If the heat transfer is from the blade to the air, as during and following a deceleration, then the boundary layer on the suction surface thickens more rapidly, and deflection of the air flow is reduced, and a wider wake, with increased losses, results. For the single-spool compressor, of maximum compression ratio 9.5, used for this analysis in reference (4), the change in "effective" speed was related to the "mean" temperature difference between the aerofoils and the air by the equation

$$\left(\frac{\Delta N}{N}\right)_{\text{boundary layer}} = -0.055\,\frac{(T_{\text{aerofoil}} - T_{\text{ave 1,2}})}{T_{\text{ave 1,2}}} \qquad (1)$$

The second mechanism for altering the compressor characteristics is due to the change in the density of the air, after a given stage, due solely to the transient heat transfer. This change in density disturbs the matching of the subsequent rows in the compressor. For the single-spool compressor analysed in reference (4) the resulting change in effective speed was correlated by

$$\left(\frac{\Delta N}{N}\right)_{\text{density change}} = -0.15\,\frac{Q}{\dot{m}c_p T_{\text{ave 1,2}}} \qquad (2)$$

Influence of predicted heat transfers on acceleration times

The results of including heat transfers in the compressor and turbine, and of including compressor characteristic change, in the calculation of the response of a single-spool engine have been reported in reference (4) and the principal results are summarised here. The engine maximum pressure ratio was 9.5. Accelerations at sea level were studied using two alternative fuel schedules. In the first schedule the accelerating fuel flow was a function of compressor delivery pressure alone, and in the second it was a function of engine shaft speed alone. Allowance for heat absorptions in the compressor and in the turbine slowed the predicted accelerations for both accelerating fuel schedules, times being increased by about 5 per cent with the "pressure" fuel schedule, and by about 4 per cent with the "speed" fuel schedule. Compressor characteristic change had no influence on the predicted acceleration when the pressure fuel schedule was used, but it slowed the acceleration by about 5 per cent when the accelerating fuel flow was scheduled on shaft speed.

Influence of component efficiency changes on acceleration times

It is very likely that the efficiencies of the compressor and of the turbine during a speed transient will differ from the equilibrium values corresponding to that instantaneous shaft speed, inlet temperature, and component pressure ratio. A study has therefore been made of the sensitivity of the predicted acceleration times of the single-spool engine described in the preceding paragraph to changes in compressor efficiency and turbine efficiency. The results of 2 per cent reduction in component efficiencies when using the accelerating fuel flow scheduled on pressure are given in Fig. 1. The predicted acceleration times are increased by about 8 per cent for this reduction in compressor efficiency, and by about 15 per cent for the corresponding reduction in turbine efficiency. The corresponding results for the case where the accelerating fuel flow is scheduled on engine shaft speed are shown in Fig. 2, where the increases in accelerating times are slightly greater, being about 11 per cent and about 17 per cent for the 2 per cent reductions

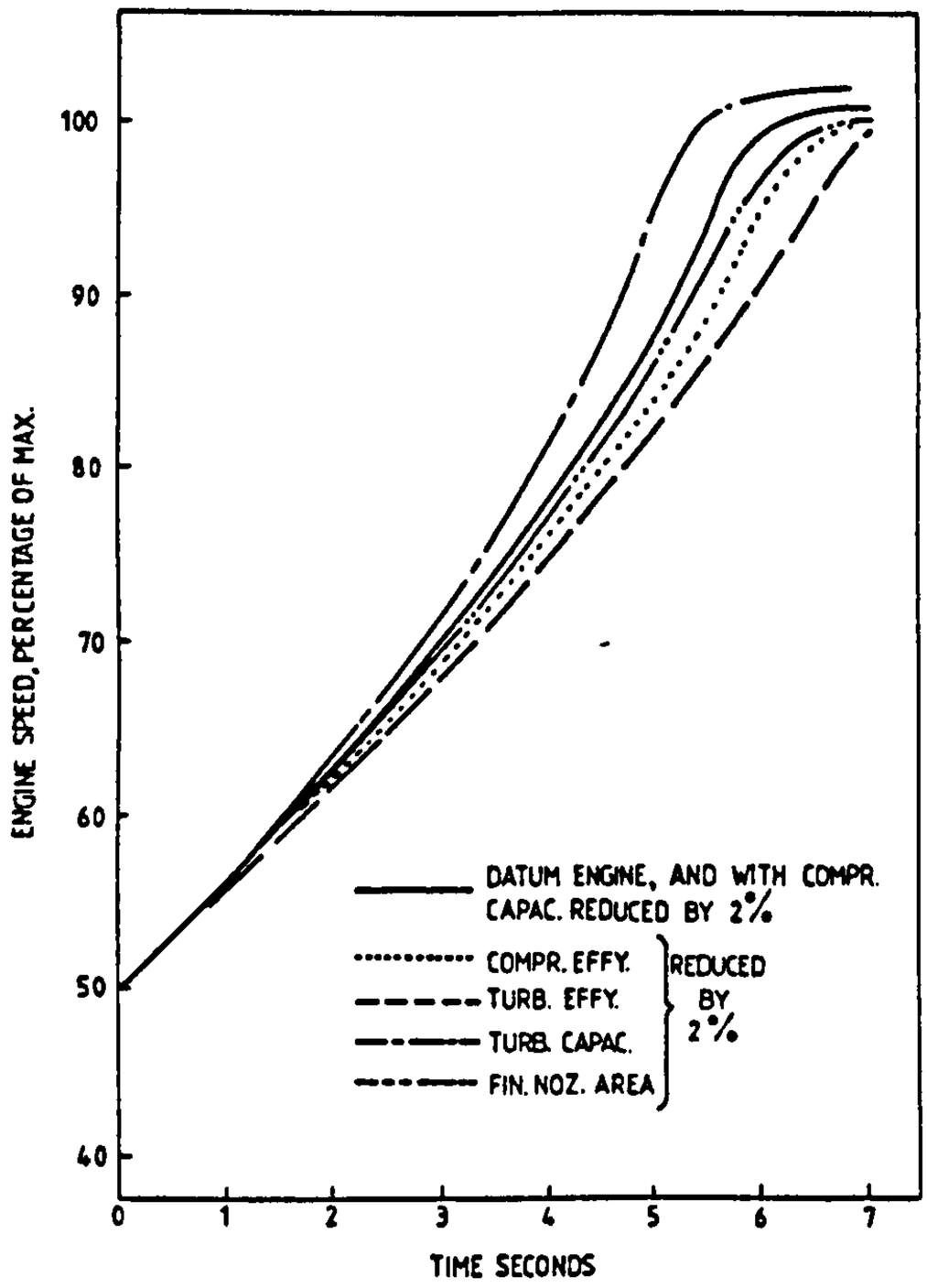

Fig. 1 Effect of changes on predicted accelerations - single-spool engine using fuel flow scheduled as function of compressor delivery pressure.

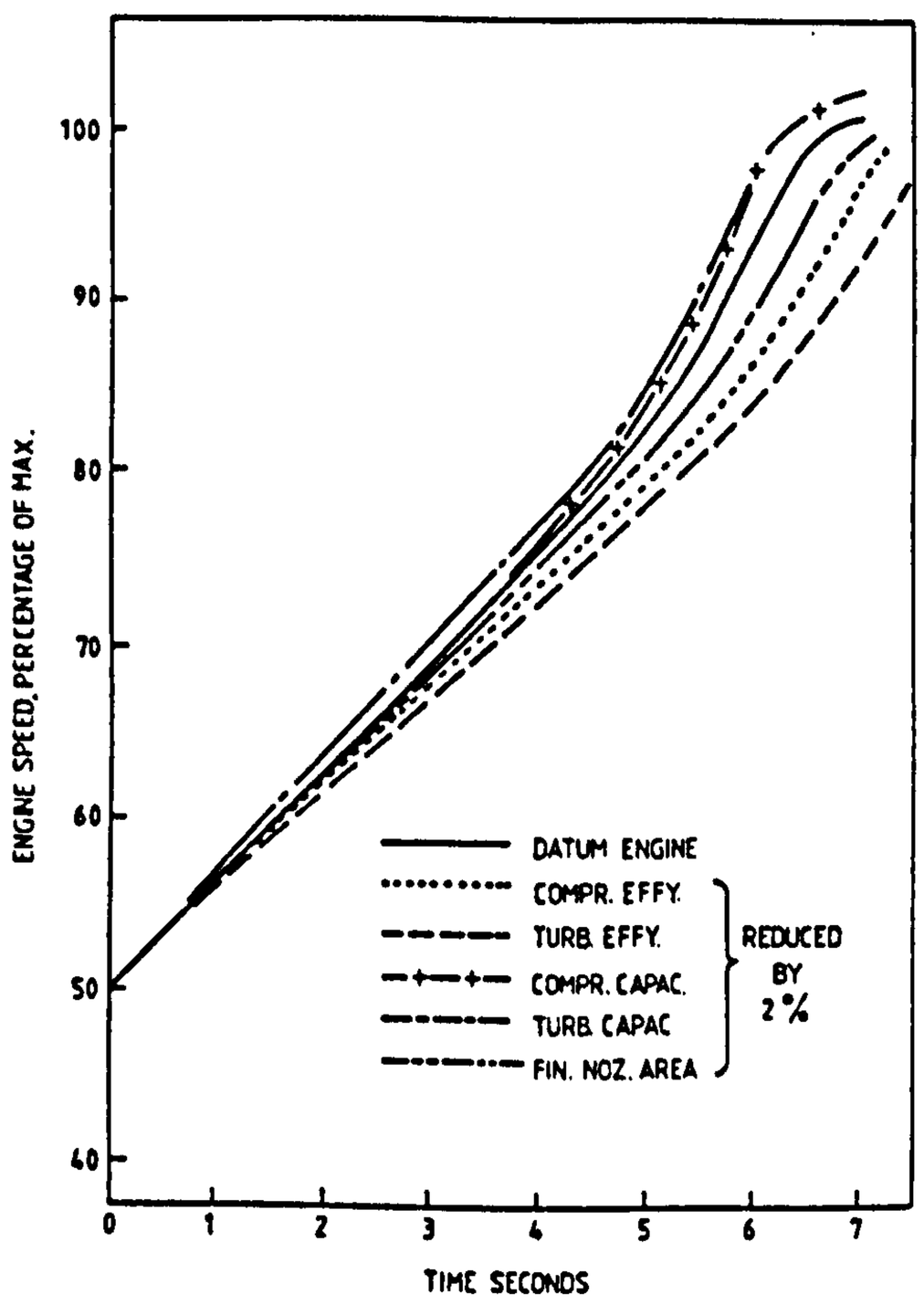

Fig. 2 Effect of changes on predicted accelerations - single-spool engine using fuel scheduled as function of engine speed.

in compressor efficiency and in turbine efficiency respectively.

Comparing the effects on predicted acceleration times of the inclusion of heat transfer processes with the effects of component efficiency changes, inclusion of heat transfer is equivalent, when using the pressure fuel schedule, either to a reduction in compressor efficiency of about 1.2 per cent, or to a reduction in turbine efficiency of about 0.7 per cent. When the accelerating fuel flow is scheduled on the shaft speed, the inclusion of heat transfer is equivalent either to a reduction of about 1.6 per cent in compressor efficiency, or to a reduction of about 1.0 per cent in turbine efficiency.

It should be noted that a reduction in compressor efficiency is usually due to an increase in tip clearance. Associated with this increased tip clearance, there is also a reduction in the mass flow delivered by the compressor at that particular non-dimensional rotational speed and pressure ratio. As a working guide, it is estimated (6) that when clearance changes etc. cause a reduction in compressor efficiency of 1 per cent, there is an associated loss of 1 per cent in the mass flow capacity of the compressor. The effect of a reduction in the compressor flow capacity on the predicted acceleration times is discussed in the next section.

Influence of changes in flow capacities and nozzle area on acceleration times

As described above, it is possible for the flow capacity of a compressor to differ during a transient, from the corresponding steady-running value. Also, during transients, the effective flow areas of the turbine's nozzle guide vanes, and of the final nozzle, may differ from their steady-running values. The effects of 2 per cent reductions in the flow capacity of the compressor and also of 2 per cent reductions in the effective throat areas of the nozzle guide vanes and of the final nozzle have been studied with reference to the predicted acceleration times of the single-spool engine used as an illustration above. The results are shown in Fig. 1 for the case where the accelerating fuel flow is scheduled on the compressor delivery pressure, and in Fig. 2 for the case of the accelerating fuel flow scheduled on the shaft speed.

The reduction of the compressor flow capacity has no effect on the acceleration time when the fuel schedule based on the compressor delivery pressure is used. When the accelerating fuel schedule based on the shaft speed is used, the time for an acceleration is reduced by about 4 per cent by the 2 per cent reduction in compressor flow capacity. This is to be expected as the shaft speed will be higher for a particular inlet air mass flow, allowing a higher fuel flow and higher fuel/air ratio. Of course the trajectory of the acceleration on the compressor characteristic will be nearer to the surge line. When the compressor performance changes of efficiency reduction and mass flow reduction are coupled together by the working rule suggested in reference (6), namely equal incremental fractional changes in both parameters, then for the 2 per cent reduction the acceleration times are increased by about 8 per cent when the pressure schedule is used, and increased by about 7 per cent when the shaft speed schedule is used.

The reduction of the turbine nozzle guide vane effective flow area leads to faster accelerations with both types of accelerating fuel schedule. The schedule based on compressor delivery pressure shows the greater change - accelerating times being reduced by about 10 per cent due to the 2 per cent reduction in guide vane flow area. With the fuel flow scheduled on the shaft speed, acceleration times are reduced by about 4 per cent.

The effect of reducing the final nozzle effective flow area by 2 per cent is to increase acceleration times by about 6 per cent for both fuel schedules.

TWO-SPOOL BYPASS ENGINE

The analysis described above has been extended to the case of a two-spool bypass engine having a mixed exhaust. The engine was of overall maximum pressure ratio 21, the corresponding pressure ratio of the high pressure compressor being 7.6. The bypass ratio at the maximum conditions was 0.58. The engine was of similar thrust to the single-spool engine chosen as an example in the first analysis.

In considering the heat transfer effects in the compressors, allowance was made, as previously, both for the non-adiabatic compressions and for the alteration in the compressor characteristics. For the L.P. (low pressure) compressor, the change in effective speed due to boundary layer effects was given by

$$\left(\frac{\Delta N}{N}\right)_{\text{boundary layer}} = -0.10\,\frac{(T_{\text{aerofoil}} - T_{\text{ave 1,2}})}{T_{\text{ave 1,2}}} \qquad (3)$$

The alteration in effective speed due to density change resulting from heat transfer was given by

$$\left(\frac{\Delta N}{N}\right)_{\text{density change}} = -0.10\,\frac{Q}{\dot{m}c_p\,T_{\text{ave 1,2}}} \qquad (4)$$

For the H.P. (high pressure) compressor the corresponding relations were found to be

$$\left(\frac{\Delta N}{N}\right)_{\text{boundary layer}} = -0.15\,\frac{(T_{\text{aerofoil}} - T_{\text{ave 2,3}})}{T_{\text{ave 2,3}}} \qquad (5)$$

and

$$\left(\frac{\Delta N}{N}\right)_{\text{density change}} = -0.15\,\frac{Q}{\dot{m}c_p\,T_{\text{ave 2,3}}} \qquad (6)$$

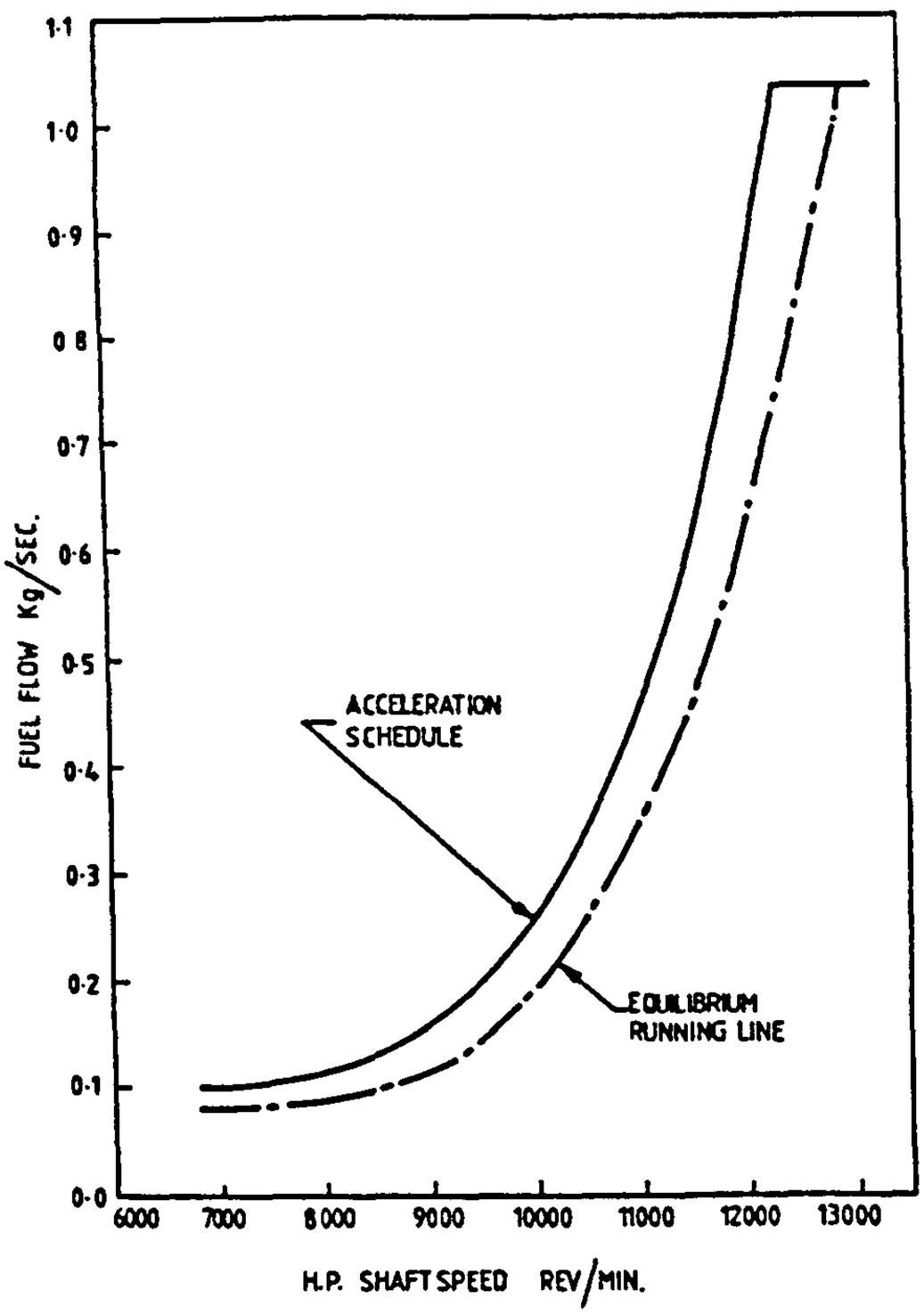

Fig. 3 Two-spool bypass engine - fuel flow scheduled as function of H.P. shaft speed.

<u>Influence of predicted heat transfers on acceleration times</u>

The effects of heat transfers on the predicted acceleration times have been obtained for sea level accelerations on two alternative accelerating fuel flow schedules. In the first schedule the fuel flow was made a function of the H.P. shaft speed. This accelerating fuel flow schedule is shown on Fig. 3 where it can be compared with the equilibrium fuel flow. In the second schedule used, the fuel flow divided by the product of the H.P. shaft speed and the H.P. compressor inlet pressure was made a function of the H.P. compressor pressure ratio. This schedule, and the equilibrium relationship are illustrated in Fig. 4.

The effects of heat transfers in the L.P. and H.P. compressors, including characteristic changes where appropriate, and of heat transfers in the H.P. and L.P. turbines have been studied individually. The procedures adopted were similar to those used with the single-spool engine. The influences of heat transfers in the two compressors are illustrated in

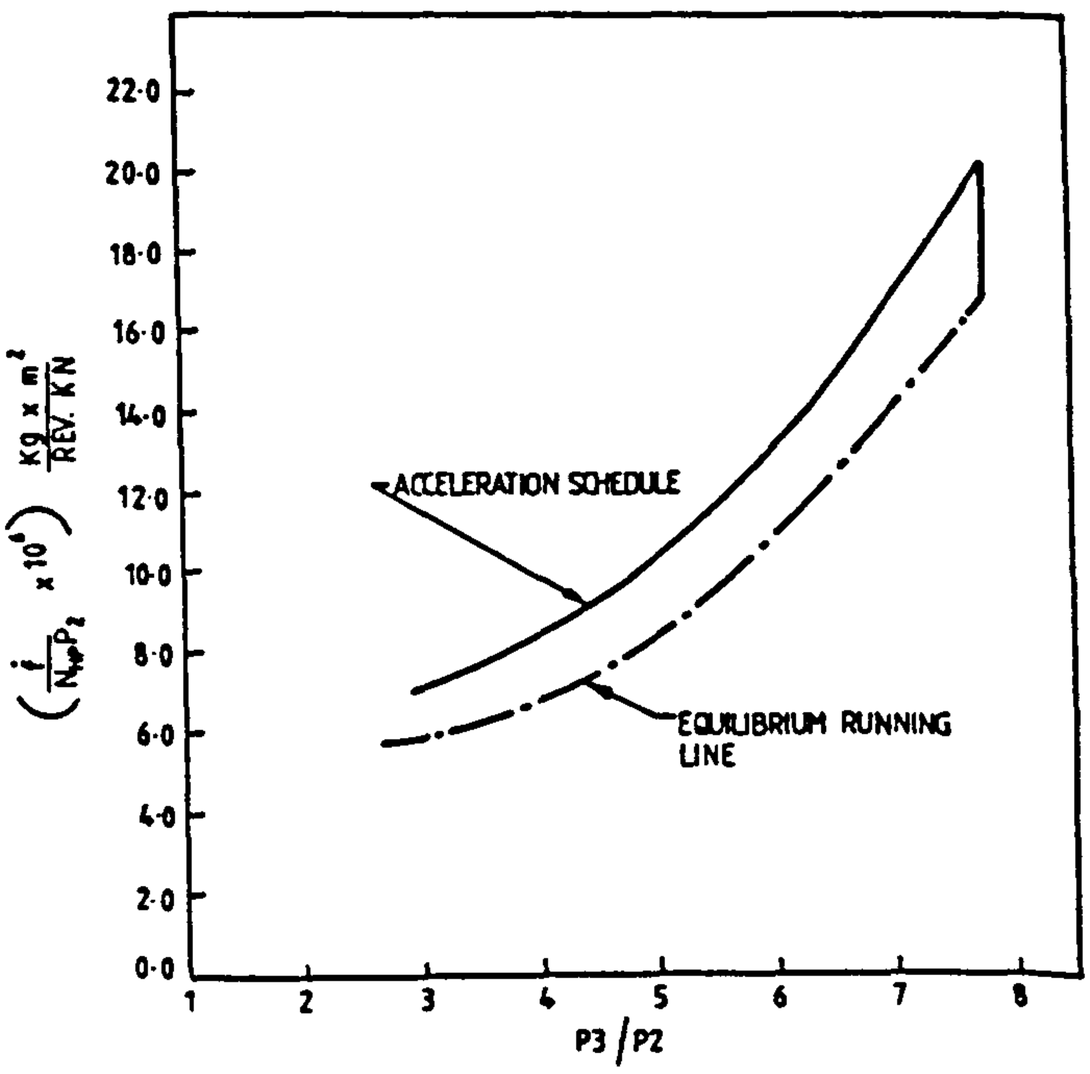

Fig. 4 Two-spool bypass engine - fuel flow group scheduled as function of H.P. compressor pressure ratio.

Fig. 5 for the case of accelerations on the H.P. shaft speed fuel schedule, and in Fig. 6 for the schedule using the fuel flow group as a function of H.P. compressor pressure ratio. With both schedules, the effect of changes in the characteristics of the L.P. compressor was negligible, and can therefore be ignored. Allowance for heat transfer in the L.P. compressor increased acceleration times (averaged for the two shafts) by about 2 per cent when the fuel was scheduled on H.P. shaft speed, and decreased the acceleration times by slightly smaller amounts when the fuel flow group was scheduled on H.P. compressor pressure ratio. Allowance for heat transfer plus characteristic change in the H.P. compressor showed an increase of about 6 per cent in the predicted acceleration time when the fuel flow is scheduled on H.P. shaft speed, and an increase of about 2.5 per cent when the fuel flow group is scheduled on the H.P. compressor pressure ratio. The case where the fuel flow is scheduled on the H.P. shaft speed is very sensitive to the changes in the characteristics of the H.P. compressor which lead to changes in effective speed, hence the large increase in predicted acceleration times.

With regard to heat transfers in the turbines, whose effects on predicted acceleration times are shown in Figs. 5 and 6 for the two fuel schedules, the heat transfer in the L.P. turbine has negligible effect. The heat transfer in the H.P. turbine does have a noticeable effect, increasing the acceleration times for both fuel flow schedules by about 5 per cent.

When all these heat transfer effects are included the acceleration time when using the H.P. shaft speed fuel schedule is increased by about 13 per cent, as indicated in Fig. 5. With the fuel flow group scheduled on the H.P. compressor pressure ratio, the inclusion of all the heat transfer effects increases the predicted acceleration time by about 6 per cent, as shown in Fig. 6.

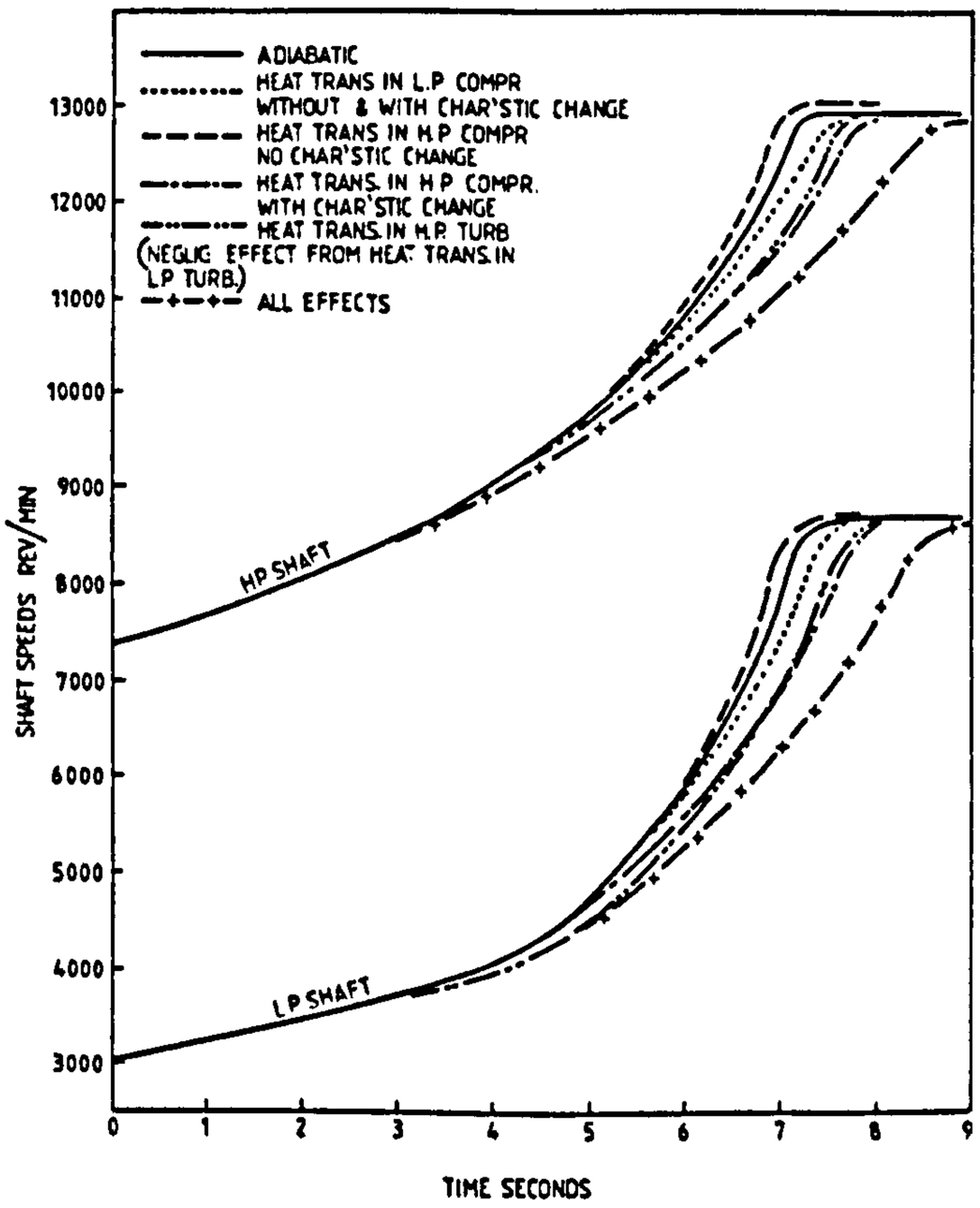

Fig. 5. Effect of heat transfers on predicted accelerations - two-spool bypass engine using fuel scheduled as function of H.P. shaft speed.

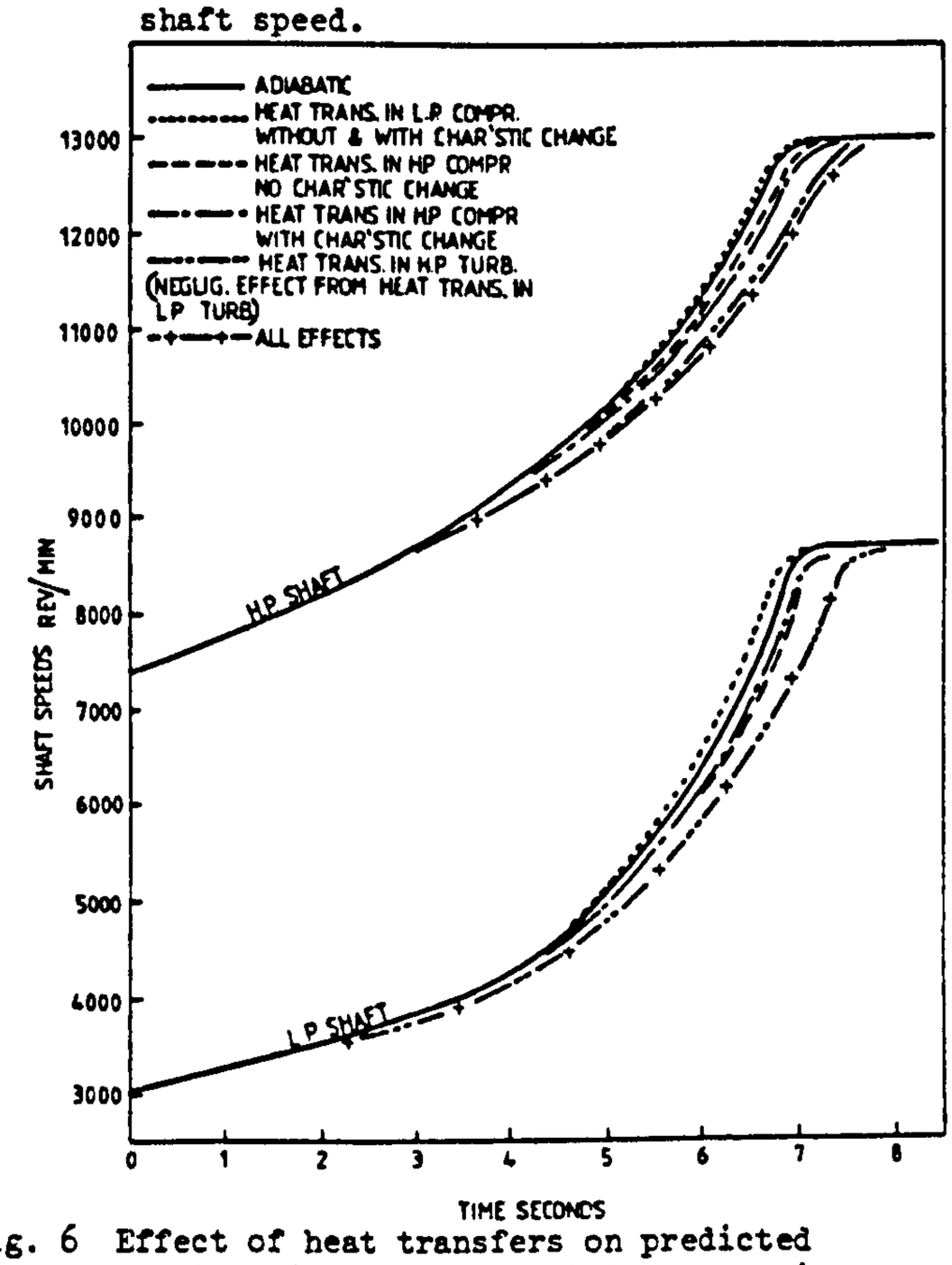

Fig. 6 Effect of heat transfers on predicted accelerations - two-spool bypass engine using fuel flow group scheduled as function of H.P. compressor pressure ratio.

Influence of component efficiency changes on acceleration times

For this engine also, a study has been made of the sensitivity of the predicted acceleration times to changes in the efficiencies of the compressors and turbines.

The results of 2 per cent reductions in component efficiencies when using the accelerating fuel flow scheduled on the H.P. shaft speed are shown in Fig. 7. The changes in L.P. compressor efficiency and L.P. turbine efficiency have very little effect. Reductions in the efficiencies of the H.P. components have marked effect, there being increases in acceleration times of 27 and 40 per cent respectively for the reductions in H.P. compressor and H.P. turbine efficiencies. The corresponding effects when the accelerating fuel flow group is scheduled on the H.P. compressor pressure ratio are shown in Fig. 8. In this case, changes in efficiency of the components on the L.P. shaft have a slight effect, the acceleration times being increased by between 1 and 2 per cent by reductions in efficiency of 2 per cent in either the L.P. compressor or the L.P. turbine. The reductions in acceleration rates due to lowered efficiencies in the H.P. shaft components are again considerable, though not as great as with the first accelerating fuel schedule. Reductions of 2 per cent in the H.P. compressor and H.P. turbine efficiency increase the acceleration times by 20 and 34 per cent respectively.

If the summed influences of thermal absorptions and compressor characteristic change, as discussed earlier, are compared with these effects, the combined

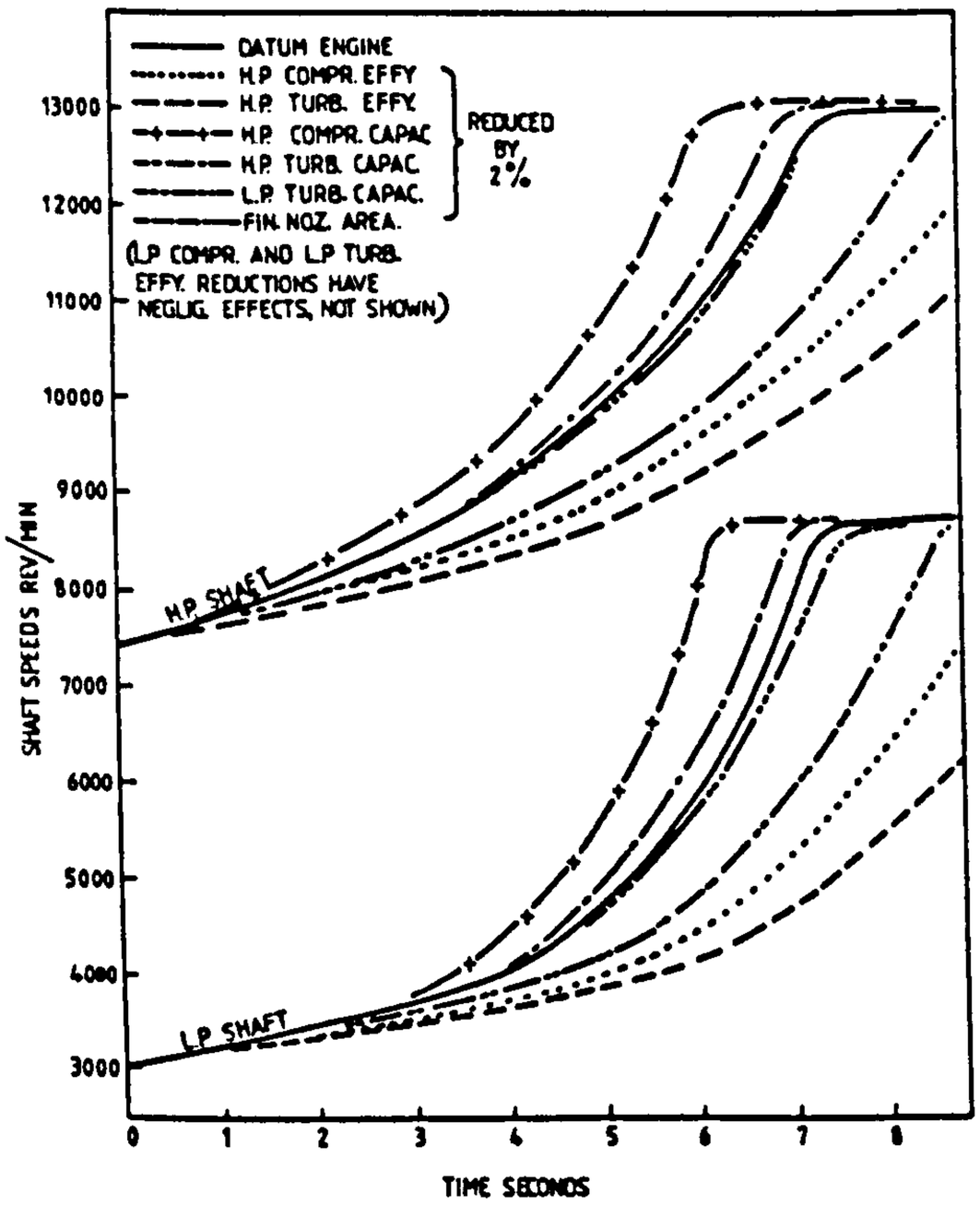

Fig. 7 Effect of changes on predicted accelerations - two-spool bypass engine using fuel flow scheduled as function of H.P. shaft speed.

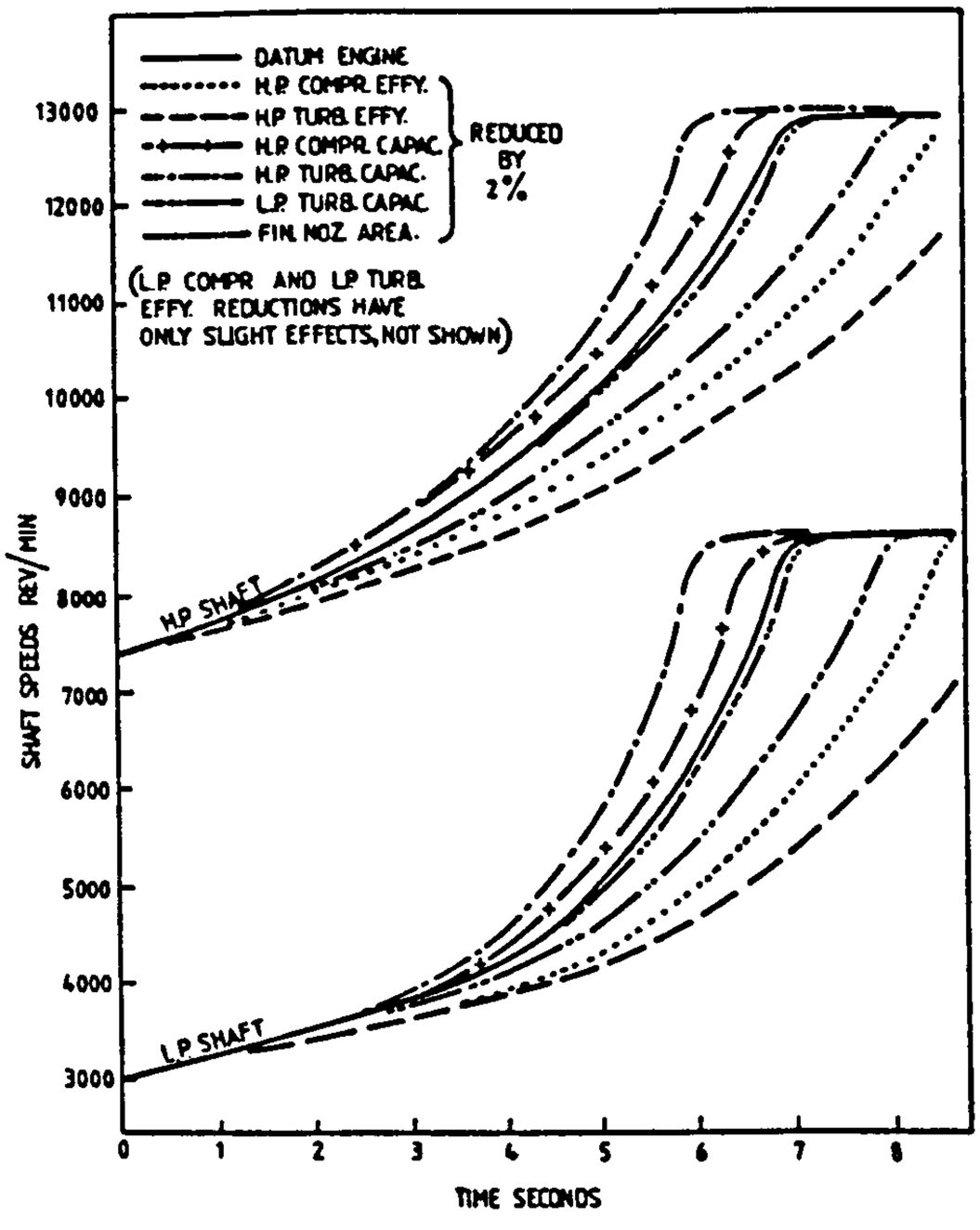

Fig. 8 Effect of changes on predicted accelerations - two-spool bypass engine using fuel flow group scheduled as function of H.P. compressor pressure ratio.

thermal effects are equivalent, when using the fuel schedule based on H.P. shaft speed, either to a reduction in H.P. turbine efficiency of 0.7 per cent or a reduction in H.P. compressor efficiency, without accompanying loss of mass flow, of 1 per cent. If there is a loss in compressor mass flow capacity, as discussed previously, then the reduction in H.P. compressor efficiency would have to be about 2 per cent to give a reduction in acceleration rate equivalent to that due to the thermal effects. When the fuel schedule based on H.P. compressor pressure ratio is used, the equivalent reductions in component efficiency are - 0.4 per cent for the H.P. turbine and 0.7 per cent and 1.0 per cent respectively for the H.P. compressor without and with associated mass flow reductions.

Influence of changes in flow capacities and nozzle area on acceleration times

The effects on acceleration times of reductions in the flow capacities of the two compressors, of reductions in the effective flow areas of the nozzle guide vanes of the two turbines, and of a reduction in the flow area of the final nozzle have been studied.

Change in the flow capacity of the L.P. compressor had negligible effect. The change in the flow capacity of the H.P. compressor produced significantly faster accelerations. When the accelerating fuel flow was scheduled on the H.P. shaft speed, a 2 per cent reduction in the H.P. compressor capacity reduced the acceleration time by about 14 per cent (Fig. 7). With the alternative fuel schedule (fuel flow group being a function of H.P. compressor pressure ratio) the reduction in acceleration time was less marked - about 5 per cent (Fig. 8). These faster accelerations are to be expected, as, with the first fuel schedule, the H.P. shaft speed has to be higher to accommodate a particular non-dimensional mass flow at inlet to the H.P. compressor. The fuel flow is of course directly a function of this shaft speed, and is very sensitive to it, see Fig. 3. With the second fuel schedule, the dominant factor is that the fuel flow is proportional to the H.P. shaft speed, if we assume the H.P. compressor inlet pressure and pressure ratio are the same. The higher H.P. shaft speed required leads to a higher fuel flow for essentially the same air flow, hence a faster acceleration.

When the effective throat area of the guide vanes of the H.P. turbine is reduced by 2 per cent, faster accelerations are predicted with both fuel schedules (Figs. 7 and 8), the reductions in acceleration times being 4 and 12 per cent respectively for the two schedules. The reason for the second schedule showing such a marked change is that the fuel flow in this schedule is very much influenced by the H.P. compressor pressure ratio, which rises markedly when the throat area of the H.P. turbine is reduced.

Reduction of the effective throat area of the L.P. turbine leads to very much slower accelerations. This is because the matching of the engine is altered to lower the H.P. shaft speed relative to the L.P. shaft, and to lower the pressure ratio across the H.P. compressor. Thus the predicted increases in the acceleration times for a 2 per cent reduction in L.P. turbine effective throat area are 17 and 12 per cent for the fuel schedules based on H.P. shaft speed and on H.P. compressor pressure ratio respectively.

Change in the final nozzle area produces very little difference in the acceleration times. With both fuel schedules, a reduction of 2 per cent in the area leads to an increase of just over 1 per cent in the acceleration times.

COMPARISONS BETWEEN ENGINES

The results described in the previous sections provide the possibility of some comparisons between the two engines considered. The overall pressure ratios are 9.5 for the single-spool engine and 21 for the two-spool bypass engine.

Comparison of thermal effects on predicted acceleration times

If we compare the predicted acceleration times for the two engines when the accelerating fuel flow schedule is based on the speed of the compressor (or H.P. compressor), it is seen that when all the thermal effects are included the predicted acceleration times are increased by about 9 and 13 per cent for the single-spool and two-spool engines respectively.

The other fuel schedules used with the two engines are not exactly equivalent in that with the single-spool engine the fuel flow is a function of the compressor delivery pressure (or pressure ratio for sea level accelerations), whereas with the two-spool engine it is the fuel flow divided by the product of the H.P. shaft speed and H.P. compressor inlet pressure which is the function of the H.P. compressor pressure ratio. However the dominant influence in both schedules is the compressor pressure ratio, and on this basis some comparisons can be made. With these schedules, inclusion of all the thermal effects increases the acceleration times by about 5 and 6 per cent respectively for the single and two-spool engines respectively.

Summarising these results, the higher pressure ratio two-spool engine is more influenced by thermal effects - a result which is to be expected. However the increase is not great when the more practical fuel schedules based on the compressor pressure ratio are used. The larger effects when the fuel flows are scheduled on the compressor (H.P.) shaft speed are very much due to the increased "effective" speeds of the compressors resulting from the transient heat transfers.

Comparison of effects of component efficiency and area changes

The effects on predicted accelerations of 2 per cent reductions in compressor efficiency in the two-spool engine are just about double the effects in the single-spool engine. This result is not seriously influenced by the fuel schedule used.

Similarly, when the turbine efficiencies are lowered by 2 per cent the increases in acceleration times with the two-spool engine are about double the increases with the single-spool engine.

Changes in the effective throat area of the turbine (H.P.) produce similar changes in the predicted acceleration times of the two engines when results with fuel schedules based on compressor (H.P.) pressure ratio are compared, and when results using schedules based on compressor (H.P.) shaft speed are compared. The former fuel schedules are the more sensitive to the throat area changes.

Change of the final nozzle area of the two-spool bypass, mixed exhaust engine had very little effect on predicted acceleration times, whereas a 2 per cent area reduction with the single-spool engine is predicted to increase the acceleration time by 6 per cent.

LIKELY RANGE OF COMPONENT EFFICIENCY CHANGES AND AREA CHANGES

As it has been seen that predicted acceleration times are very sensitive to changes in component efficiency, it would be valuable to know the likely amounts by which component efficiencies during a transient could differ from corresponding steady running values. Such experimental data are scarce. Thomson (1) has indicated, for a typical two-spool bypass engine, reductions of up to 2 per cent in the H.P. compressor efficiency and of up to 1.5 per cent in the H.P. turbine efficiency. Maccallum (7) has estimated an average reduction of 1 per cent in compressor efficiency for the single-spool engine used as an example in the first part of this paper, but no change in turbine efficiency.

Changes in effective control areas are difficult to forecast. One estimate for the two-spool bypass engine used in the present study is that the effective throat area of the H.P. turbine is increased by about 0.9 per cent during an acceleration (8).

If it is assumed that the following departures from equilibrium performance are likely to occur during an acceleration of the two-spool bypass engine - H.P. compressor efficiency and mass flow reduction 1 per cent, H.P. turbine efficiency reduction 0.5 per cent and H.P. turbine effective throat area increased by 0.5 per cent - then the resulting predicted acceleration times are increased by about 18 per cent for both the fuel schedules considered. Alongside these, the increases in predicted acceleration times due to heat absorptions and changes in characteristics were 13 and 6 per cent respectively for the "speed" and "pressure ratio" fuel schedules respectively.

CONCLUSIONS

Transient heat transfers affect the predictions of the acceleration times of gas turbines. The predictions are also affected by departures in component efficiencies from the expected values. The effects of these factors on the predicted acceleration times depend on the engine and the accelerating fuel schedule used. The higher the pressure ratio of the engine the more pronounced are these effects.

For a two-spool bypass engine of maximum pressure ratio 21, when a fuel schedule based on H.P. compressor speed is used, inclusion of heat absorptions in the components, and associated changes in compressor characteristics, increases the predicted times for an acceleration at sea level by about 13 per cent. If the accelerating fuel schedule is based on H.P. compressor pressure ratio, the predicted times are increased by about 6 per cent. The predictions of acceleration times are very sensitive to alterations in component efficiencies, and increases in predicted acceleration of the same magnitudes as those resulting from thermal absorptions etc., quoted above, would have followed from reductions in H.P. turbine efficiency of 0.7 per cent or 0.4 per cent respectively for the two fuel schedules.

One estimate has been made of the likely changes in component efficiencies and control areas for the previously mentioned two-spool bypass engine, and this suggests, for these effects alone, increases of 18 percent in the acceleration times for both the fuel schedules considered. Coupled with the heat absorption effects and changes in the compressors' mass flow characteristics this then gives increases in the predicted acceleration times of about 30 percent and 24 percent, respectively, for the two fuel schedules.

The sensitivity of the predictions to component efficiency change indicates that more accurate data is required on component efficiencies in transients.

ACKNOWLEDGEMENT

The author wishes to thank staff of Rolls-Royce Limited, and colleagues at the University of Glasgow for their valuable comments and encouragement.

REFERENCES

1 Thomson, B., "Basic Transient Effects of Aero Gas Turbines", AGARD Conference Proceedings 151, Feb 1975.
2 Fawke, A.J., and Saravanamuttoo, H.I.H., "Digital Computer Simulation of the Dynamic Response of a Twin-Spool Turbofan with Mixed Exhausts, "Aeronautical Journal Vol 77, September 1973, pp 471-478.
3. Maccallum, N.R.L.,"Transient Expansion of the Components of an Air Seal on a Gas Turbine Disc," SAE Paper 770974, 1977.
4. Maccallum, N.R.L., "Thermal Influences in Gas Turbine Transients - Effects of Changes in Compressor Characteristics," ASME Paper 79-GT-143, 1979.
5. Bauerfeind, K., Doctoral thesis, Technical University of Munich, 1968.
6. Rolls-Royce Limited, Unpublished Data Communication, Feb 1969.
7. Maccallum, N.R.L., "A Study of the Predicted Acceleration Times of an Avon RA29 Jet Engine", University of Glasgow Mechanical Engineering Department Report, April 1979
8 Maccallum, N.R.L., "Effects of 'Bulk' Heat Transfers in Aircraft Gas Turbines on Compressor Surge Margins", Heat and Fluid Flow in Steam and Gas Turbine Plant, Instn. Mech Engrs, London, 1974, pp 94-100.

AGARD

ADVISORY GROUP FOR AEROSPACE RESEARCH & DEVELOPMENT

7 RUE ANCELLE 92200 NEUILLY SUR SEINE FRANCE

Paper Reprinted from
Conference Proceedings No. 324

ENGINE HANDLING

NORTH ATLANTIC TREATY ORGANIZATION

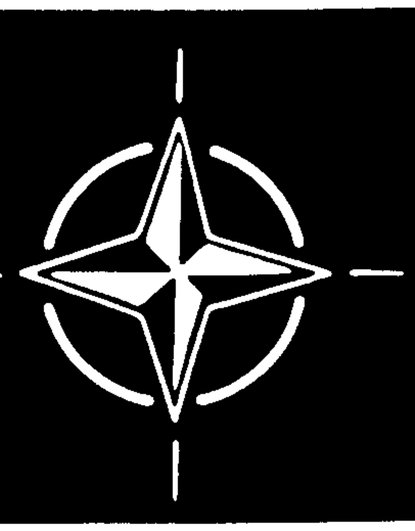

AXIAL COMPRESSOR CHARACTERISTICS DURING TRANSIENTS

N.R.L. MACCALLUM

Reader

Department of Mechanical Engineering
University of Glasgow
GLASGOW G12 8QQ

SUMMARY

The anticipated effects of heat transfer on the characteristics of an axial-flow air compressor have been estimated using two different prediction methods. The second method, which incorporates end-wall boundary layers, predicted somewhat smaller changes of characteristics than those indicated by the earlier method. As the second method uses a model of the flow which is probably more realistic, for the present it is considered that its predictions on heat transfer effects on characteristics are more accurate. In an altitude deceleration of a typical 12-stage compressor it is therefore estimated that surge margins might be reduced by about 20 or 25%. In a sea-level acceleration there are similar increases in surge margins, as compared to adiabatic characteristics.

Decreasing the stagger angle increases slightly the susceptibility to characteristics being altered due to heat transfer effects in transients.

List of symbols

c_p	specific heat at constant pressure
C_h	enthalpy-equivalent static-pressure-rise coefficient
e	deflection
g	staggered spacing between blades
h	annulus height
i	incidence
$\dot{m}$	mass flow rate
N	rotational speed
Q	heat flux to air in compressor
T,ΔT	temperature, temperature difference
α	air angle
δ	displacement thickness
ε	tip clearance
ν	kinematic viscosity
λ	fractional effective area
$\Delta\phi$	change in angle of projected displacement thickness line

Subscripts		Superscript	
ht	heat transfer	*	design
∞	core		
2	exit		

1. INTRODUCTION

The behaviour of aircraft gas turbines during rapid accelerations and decelerations is of considerable interest. It is important that these transients can be carried out rapidly, without any malfunctioning of the engine - in particular without encountering a serious stall or surge in the compressor(s).

It appears that the steady-running characteristics of the engine and its components are not always applicable in transients. For example it has been found that the margin of compressor pressure ratio available between the working line and the surge line (the surge margin) is influenced by the immediately preceding history of the engine - in one case Warne (Ref. 1) reported that the "overfuelling margin" for an acceleration was halved if the engine had immediately previously been allowed to "soak" at a high speed.

The purpose of the present paper is to consider the factors arising in transients which might affect the performance characteristics of axial-flow air compressors. The magnitudes of these factors are estimated, and the factors are incorporated in two alternative procedures for predicting the performance of the compressors, the influence of these factors on the compressors' characteristics thus being indicated.

2. PREDICTION METHODS - ADIABATIC FLOW

The flow in an axial-flow air compressor, particularly as surge is approached, is influenced by three-dimensional effects. Ideally, the prediction method used should be based on blade-element data, with radial integration, followed by axial stacking. Such

a procedure is complex, and some of the information required is as yet incomplete. In the present work, which is regarded as exploratory rather than definitive, a simple two-dimensional procedure has been adopted, using calculations at the pitch-line and modified in two different ways. The modification used in the first method allows the possibility of the existence of stall cells. In the second method the modification takes account of the growth of the end-wall boundary layers on the casing and hub of the annular flow passage. These methods are now described, referred to as Methods 1 and 2 respectively.

2.1 METHOD 1: PITCH-LINE WITH STALL CELLS

This method has been used by Maccallum and Grant (Ref. 2) and is described in fuller detail in that paper. Briefly, the method uses row by row calculations at the mean blade height, based on the two-dimensional cascade data published in Ref. 3. The flow is compressible and Mach Number effects (Ref. 4) are allowed for. Axial velocity variation within a row is incorporated into the exit velocity triangles and energy transfer calculations, although its effect on deviation (Ref. 5) is not included.

When the incidence of the flow into a particular row becomes too great, it is assumed that a stall cell is then formed in part of the annular area, and in the remaining area normal flow is restored. The quantitative definition adopted for this stalling of a blade row is that the profile drag coefficient rises to double its minimum value, and this occurs when the numerical value of the dimensionless relative incidence group $(i-i^*)/e^*$ reaches 0.4. When the flow through a particular row is reduced below that giving this stalling value of the incidence group, it is assumed that the flow redistributes itself in the annulus so that part of the annulus operates with a flow giving exactly this stalling value of the incidence group, and the remainder of the annulus is occupied by a stall cell with no significant flow.

Inherent in this type of pitch-line prediction method is the need to insert a work-done factor to account for the reduced energy transfer resulting from the development of the axial velocity profiles. Alternatively a blockage factor can be used. In the present study, work-done factors were used.

The application of this prediction method is illustrated later in Section 4.1.

2.2 METHOD 2: PITCH-LINE WITH END-WALL BOUNDARY LAYER

It has been found by Koch (Ref. 6) that the limiting pressure rise potential of axial-flow compressor stages can be correlated with the peak pressure recovery data (Ref. 7) of two-dimensional diffusers having a 9% blockage in the inlet flow profile. In this correlation, illustrated in Fig. 1, a parameter representing the stalling effective static pressure rise is plotted against the ratio of the diffusion length to the exit width (staggered) of the diffusion passages. The parameter representing the stalling effective pressure rise of a stage is based on the static pressure rise coefficient, C_h, normalised by the pitch-line free stream dynamic head. This coefficient is adjusted for tip clearance, axial spacing, Reynolds Number and for an "effective dynamic pressure factor" to account for the proneness to stall of low stagger stages.

As the flow through a stage is throttled so that the limiting, or stalling, pressure rise condition referred to above is approached, the end-wall boundary layers thicken, as shown by Smith (Ref. 8). The effective area ratio, at which the stalling pressure rise occurred was found to be a function of the tip clearance, staggered gap and blade height (Ref. 6)

$$\lambda = 1 - (0.34 + 2\,\overline{\epsilon/g}\,)\,(\overline{g/h}) \qquad (1)$$

At lower pressure loadings the end-wall boundary layers are thinner and the effective area ratio is higher. The relationship is complex and is illustrated in Fig. 2 by plots, given by Smith (Ref. 8), of the normalised displacement thickness of the casing boundary layer as a function of the loading and of the tip clearance.

This data of Smith's on the relationship between the displacement thicknesses and the pressure loading allows a means of calculating the blockage factor for loadings lower than the limiting value. This, combined with the stalling pressure rise factors provided by Koch (Ref. 6), was the basis of the second prediction method used in the present work. The flow is assumed to be concentrated in the central core of the annulus with blocked regions of thicknesses equal to the displacement thicknesses adjacent to the casing and hub walls. For the flow in the core, it is assumed that the two-dimensional procedure described in Section 2.1 above can be used. In a typical calculation procedure for a stage, first the limiting pressure rise is determined from Koch's correlation, the flow velocities used in the denominator of the pressure rise coefficient being those corresponding to the core flow when the boundary layer blockages are those occurring at the stalling pressure condition (Eqn. (1)). A test blockage is then tried, giving core velocities, and angles through the stage. The pressure rise predicted from the two-dimensional procedures is then compared with the limiting, or stalling, value. The ratio of these two pressure rises then gives displacement thicknesses from Fig. 2, and its equivalent at the hub, which give a new blockage for that stage. This procedure is repeated until convergence is obtained. This calculation is carried out through all stages of the compressor in succession.

The loss in efficiency to be expected from the effects of blockage has been incorporated using the results of Smith (Ref. 8) who found, on average, that the "tangential force thickness" was about half the displacement thickness i.e. the reduction in torque due to the low mass flow in the boundary layer was only half the reduction there should have been had the blockage area been passing no flow at all.

Koch's correlation was developed essentially for low speed compressors. For high speed compressors Koch found the stalling pressure rises of the stages tended to fall below the correlation. To allow for this effect a factor was introduced into the present prediction program to scale down the correlation values of limiting pressure rise.

The use of this second prediction method is illustrated later in Section 4.2.

3. EFFECTS IN TRANSIENTS - GENERAL DESCRIPTION

Several effects occur in transient operations of gas turbines which can alter the characteristics of the compressor. These have been listed for an axial-flow compressor (Ref. 9) and partially studied (Ref. 9,2). These effects are now reviewed.

3.1 DENSITY CHANGES RESULTING FROM HEAT TRANSFER

During an acceleration of an initially "cold" engine, there will be heat transfer from the air as it passes through the compressor to the blades, platforms and casings. This will make the air more dense, and will lower the axial component of velocity at a particular stage in the compressor as compared to the steady-running state at that particular non-dimensional rotational speed, based on inlet temperature. This alters the stage matching. Similar effects, but opposite in direction, occur during decelerations.

The temperature distributions shown by Smith (Ref. 8) for a 12-stage compressor, under steady-running conditions, indicate that the energy dissipated into heat due to losses adjacent to the end-walls tends to remain within the end-wall boundary layers. Consequently it appears that heat transfers to, or from, platforms and casings will have little influence on the temperature, hence density, of the flow at the pitch-line. However the heat transfers to, or from, the aerofoils of the blades will immediately influence pitch-line density. Thus the procedure that has been adopted in the pitch-line calculations described in Methods 1 and 2 in the previous section is that only the heat transfers to, or from, the aerofoils of the blades alter the density as compared to adiabatic running.

3.2 BOUNDARY LAYER DEVELOPMENT ON BLADE AEROFOILS

It has been shown (Ref. 10) that the separation from a convex curved surface in an adverse pressure gradient can occur earlier if the surface is at a temperature above the temperature of the flowing air. These results, on a large curved surface, have been used to validate a prediction method which has subsequently been applied to flows over typical compressor blades (Ref. 2). For conditions when the flow on the suction surface of the blade is near to separation, if the blade is then made hot, compared to the air, the displacement thickness increases much more rapidly near the trailing edge. There is no significant effect on the pressure surface. The behaviour of the boundary layers is shown qualitatively in Fig. 3. If the projected suction surface displacement thickness line with the hot blade is compared with the corresponding adiabatic line, it has been moved through an angle $\Delta\phi$. Since the boundary layer on the pressure surface has not been affected, it has been assumed that the flow leaving the blade is, on average, displaced through an angle $\Delta\phi/2$. Thus the flow through the compressor blading of that row receives a reduced deflection. The correlation found in Ref. 2 for this reduced deflection, or increased exit angle, $\Delta\alpha_2$ is

$$\Delta\alpha_2/e^* = \Delta T(0.0005 + 0.00084(i-i^*)/e^*) \qquad (2)$$

It is also likely that the wake from the hot blade will be wider, and there will be higher profile drag losses associated with this. The assumption has been made (Ref. 2) that the drag coefficient is that corresponding to the pseudo incidence angle which would give the "revised" exit angle.

3.3 BOUNDARY LAYERS ON END-WALLS

The effect of heat transfer on the thickness of the boundary layers on the end-walls, and hence on the blockage, is uncertain. One simple approximation is to assume that the effect is similar to the effect on the thickness of turbulent boundary layers on flat plates (Ref. 11).

$$\delta_{ht}/\delta = (\nu_{wall}/\nu_{\infty})^{0.2} \qquad (3)$$

This assumption has been used in Method 2, described in Section 2.2.

3.4 TIP CLEARANCE CHANGES

Due to the different rates of response of discs, blades and casing to temperature changes resulting from pressure ratio changes, tip clearances will differ from those occurring in steady running. These clearance changes will alter efficiencies and hence characteristics. The changes in tip clearances can be fed directly as input into prediction Method 2. Prediction Method 1 requires this information expressed as changes in efficiency.

Tip clearance changes in transients, and their relation to efficiency changes are considered in Paper 17 to this meeting (Ref. 12)

4. PREDICTIONS IN TRANSIENTS

The effects during transients of the factors of density change due to heat transfer, boundary layer development on the aerofoils and end-wall boundary layer development have been considered with application to the 12-stage axial flow H.P. compressor of a two-spool by-pass engine having mixed exhausts and of overall compression ratio 20. However the effects on the characteristics resulting from tip clearance changes (Section 3.4) have not been included.

The method of calculating the average heat transfer coefficient over the blades has been described previously (Ref. 2). Briefly, a weighted average coefficient between that for a laminar boundary layer and that for a turbulent boundary layer starting on a flat plate has been used, increased by 50% as an approximate allowance for the high turbulence levels occurring in compressors.

4.1 PREDICTIONS BY METHOD 1: PITCH-LINE WITH STALL CELLS

This method has previously been applied to the conditions occurring in the compressor at the end of a rapid acceleration at 12,200 m altitude (40,000 ft.) from maximum speed to the flight idle speed. It had been found, for a range of engines, that an immediate re-acceleration of the engine from the flight idle condition represented a severe test of the engine's ability to avoid surge - hence the interest in this transient.

The results are shown in Fig. 4, the adiabatic constant speed characteristic being represented by the solid line. In order to obtain satisfactory agreement between the adiabatic predictions and rig results, work-done factors in the range 0.81 to 0.71 and an efficiency factor of 0.92 were used. The prediction of where surge will occur on this constant speed characteristic is not easy. Some workers (e.g. Ref. 13) have suggested the maximum pressure-ratio point, while others (e.g. Ref. 14) have suggested an averaged stage loading. In the present work, for the adiabatic characteristic, the maximum pressure-ratio point has been used. For the non-adiabatic situations, the point has been selected where the group of four stages most heavily loaded have an average axial velocity to blade speed ratio equal to that in the same group of four stages when at "surge" on the adiabatic characteristic. Thus the characteristics shown in Fig. 4 were obtained. This method predicts very considerable reductions in surge margin, reduced by between 50 and 60% due to the combined effects of density change caused by heat-transfer and aerofoil boundary layer changes, each of these individually causing a reduction of 25 to 30%.

It was explained in Section 3.1 that it has been assumed that only the heat transferred from the aerofoils contributed to a density change of the air at the pitch-line. This represente about one third of the total amount of the heat being transferred from the complete compressor. The remaining heat, from platforms and casings, is regarded as being held in the end-wall boundary layer flows.

It has been suggested (Ref. 15) that the movements of the constant-speed characteristics are equivalent to the compressor operating at a new "effective" speed. Correlations for these changes have been given for a 16-stage compressor of a single-spool engine (Ref. 15) and for the 12-stage compressor being studied in the present work (Ref. 16). The latter correlations for this compressor are

$$(\Delta N/N)_{\text{boundary layer}} = -0.15 \frac{\Delta T_{ave}}{T_{air,\ ave}} \qquad (4)$$

and

$$(\Delta N/N)_{\text{density change}} = -0.15 \frac{Q}{T_{air,\ ave}} \qquad (5)$$

4.2 PREDICTIONS BY METHOD 2: PITCH-LINE WITH END-WALL BOUNDARY LAYER

This Method has been applied to the transient condition described above.

In order to line up the prediction of the adiabatic characteristics, work-done factors in the range 0.78 to 0.72, a factor on efficiency of 0.95 and a factor of 0.70 on the correlation of Koch (Ref. 6) were used. The adiabatic surge point was taken as the point of maximum pressure ratio, and for the non-adiabatic cases it was the condition giving the same averaged axial velocity to blade speed ratio as at adiabatic surge for the group of four most heavily loaded stages - i.e. the same criteria as used in Section 4.1. The results are shown in Fig. 5.

It is seen that this method predicts a less severe reduction in surge margin, and a

somewhat reduced change in effective speed than had been predicted by Method 1. Part of the reason for the reduced effects is that, considering the effects on the boundary layer on the aerofoil suction surface, with this end-wall program which incorporates blockage, the indicences to the blades in the core flow are reduced, and the flow on the suction surface is less liable to separate - consequently the effects of heat transfer from the blade are less noticeable.

This Method has been applied to an instant during a sea-level acceleration of the same engine, and the results are shown in Fig. 6. Movements of the constant speed line and an improvement in the surge margin, as compared to adiabatic, are predicted.

It is thought that the predictions of this Method 2 will be more accurate than the predictions of Method 1, due to the better flow description used.

5. INFLUENCE OF STAGGER ANGLE ON SUSCEPTIBILITY TO HEAT TRANSFER EFFECTS

Using Method 2, the susceptibility to heat transfer effects has been studied for a compressor having altered stagger angles. The compressor essentially had the geometry of the compressor considered in Section 4, but with stagger angles decreased by 3^{o} throughout and then increased by 3^{o} throughout compared to the orginal. The predicted changes in characteristics at the conclusion of the altitude deceleration are shown in Figs. 7 and 8 respectively. It appears that the changes occurring when the stagger angles are increased by 3^{o} are similar to those in the reference compressor. When the stagger angles are reduced by 3^{o} the effects of heat transfer are slightly more marked than in the reference case.

6. CONCLUSIONS

Compressor characteristics are altered during transients due to the effects of heat transfer.

Of the two prediction methods used, it is considered that the results from Method 2, which incorporates end-wall boundary layers, are more accurate. This method indicates reductions in surge margins of 20 to 25% in altitude decelerations, and increases of similar magnitudes in accelerations.

Movement of constant speed lines can be quantified in terms of "effective" speeds.

7. REFERENCES

Ref. 1 Warne, E.H., "Gas turbine fuel and control systems", Proc. Instn. Mech. Engrs., 1968-69, 183 (Pt 3N), 121-27.

Ref. 2 Maccallum, N.R.L. and Grant, A.D., "The effect of boundary layer changes due to transient heat transfer on the performance of an axial-flow air compressor", SAE Paper 770284, 1977.

Ref. 3 Howell, A.R. and Bonham, R.P., "Overall and stage characteristics of axial-flow compressors", Proc. Instn. Mech. Engrs. 1950, 163. 235-248.

Ref. 4 Howell, A.R., "The present basis of axial flow compressor design. Part I. Cascade theory and performance", Aeronaut Res. Counc. Rep. Memo 2095, 1942.

Ref. 5 Pollard, D. and Gostelow, J.P., "Some experiments at low speed on compressor cascades", J. Engng. Pwr. Trans. Am. Soc. Mech. Engrs. 1967 (July) 89, 427-36.

Ref. 6 Koch. C.C., "Stalling pressure rise capability of axial flow compressor stages", Am. Soc. Mech. Engrs. Paper No. 81-GT-3, 1981.

Ref. 7 Sovran, G and Klomp, E.D., "Experimentally determined optimum geometries for rectilinear diffusers with rectangular, conical or annular cross section", Fluid Mechanics of Internal Flow, Elsevier Publishing, Amsterdam, Netherlands, 1967, 270-319.

Ref. 8 Smith, L.H. Jr., "Casing boundary layers in multistage axial-flow compressors", Flow Research on Blading, ed. L.S. Dzung, Elsevier Publishing, Amsterdam, Netherlands, 1970, 275-304.

Ref. 9 Maccallum, N.R.L., "Effect of bulk heat transfer in aircraft gas turbines on compressor surge margins", Heat and Fluid Flow in Steam and Gas Turbine Plant, Inst. Mech. Engrs., London, 1974, 94-100.

Ref. 10 Grant, A.D., "The effect of heat transfer on boundary layer stability", Ph.D. Thesis, University of Glasgow, 1973.

Ref. 11 Krieth, F., "Principles of Heat Transfer", 2nd Ed., International Textbook Company, Scranton, 1965, 316.

Ref. 12 Pilidis, P. and Maccallum, N.R.L., "Models for predicting tip clearance changes in gas turbines", AGARD Propulsion and Energetics Panel Meeting, Agios Andreas, 1982, Paper 17.

Ref. 13 Robbins, W.H. and Dugan, J.F. Jr., "Prediction of off-design performance of multi-stage compressors", NASA - S.P.36, 1965.

Ref. 14. Howell, A.R. and Calvert, W.J., "A new stage stacking technique for axial-flow air compressor performance prediction", J. Engng. Pwr., Trans. Am. Soc. Mech. Engrs., 1978, 100, 698-703.

Ref. 15 Maccallum, N.R.L., "Thermal influences in gas turbine transients - effects of changes in compressor characteristics", Am. Soc. Mech. Engrs. Paper No. 79-GT-143, 1979.

Ref. 16 Maccallum, N.R.L. "Further studies of the influence of thermal effects on the predicted acceleration of gas turbines", Am. Soc. Mech. Engrs. Paper No. 81-GT-21, 1981.

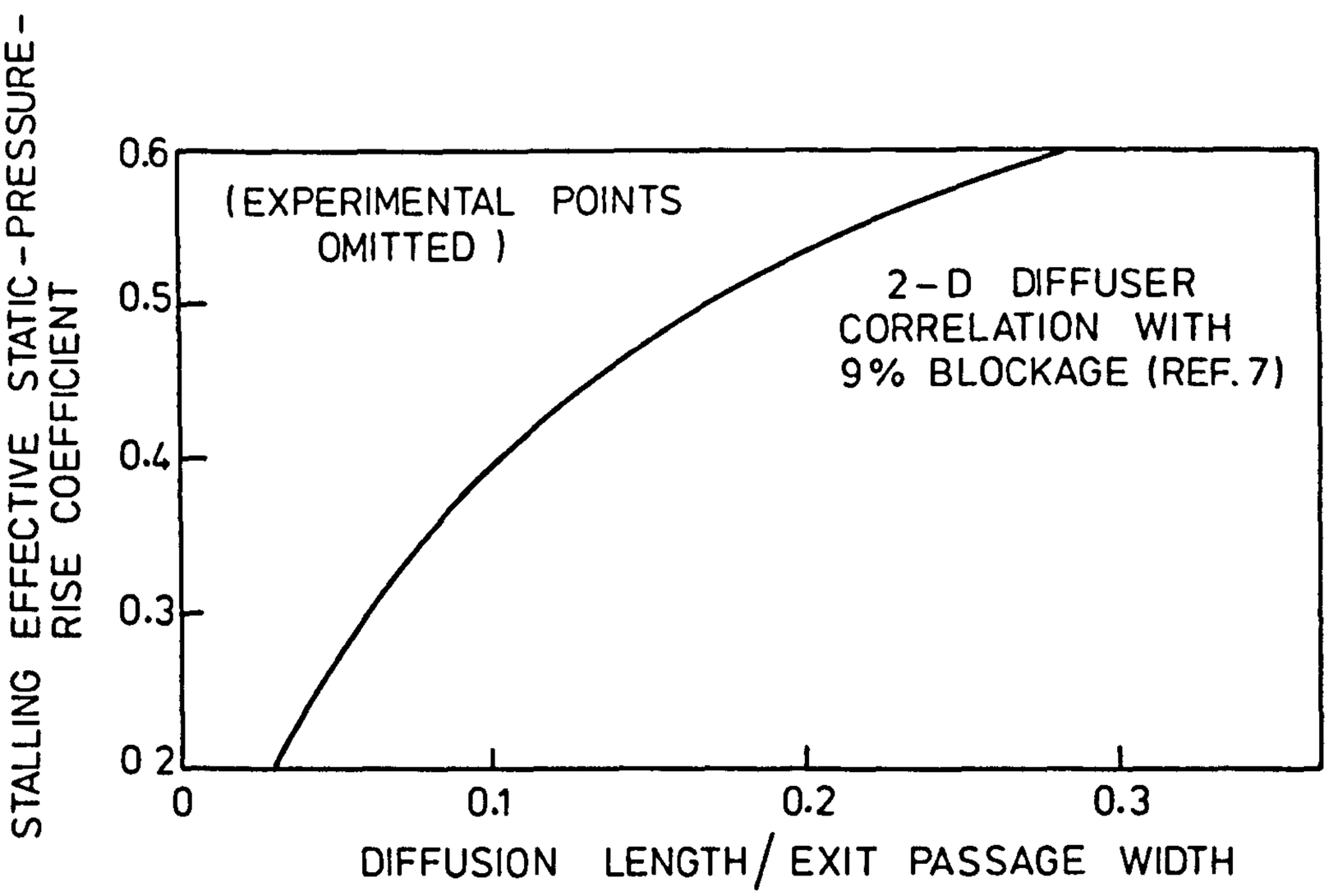

FIG. 1 CORRELATION OF STALLING EFFECTIVE STATIC PRESSURE RISE COEFFICIENTS (REF. 6)

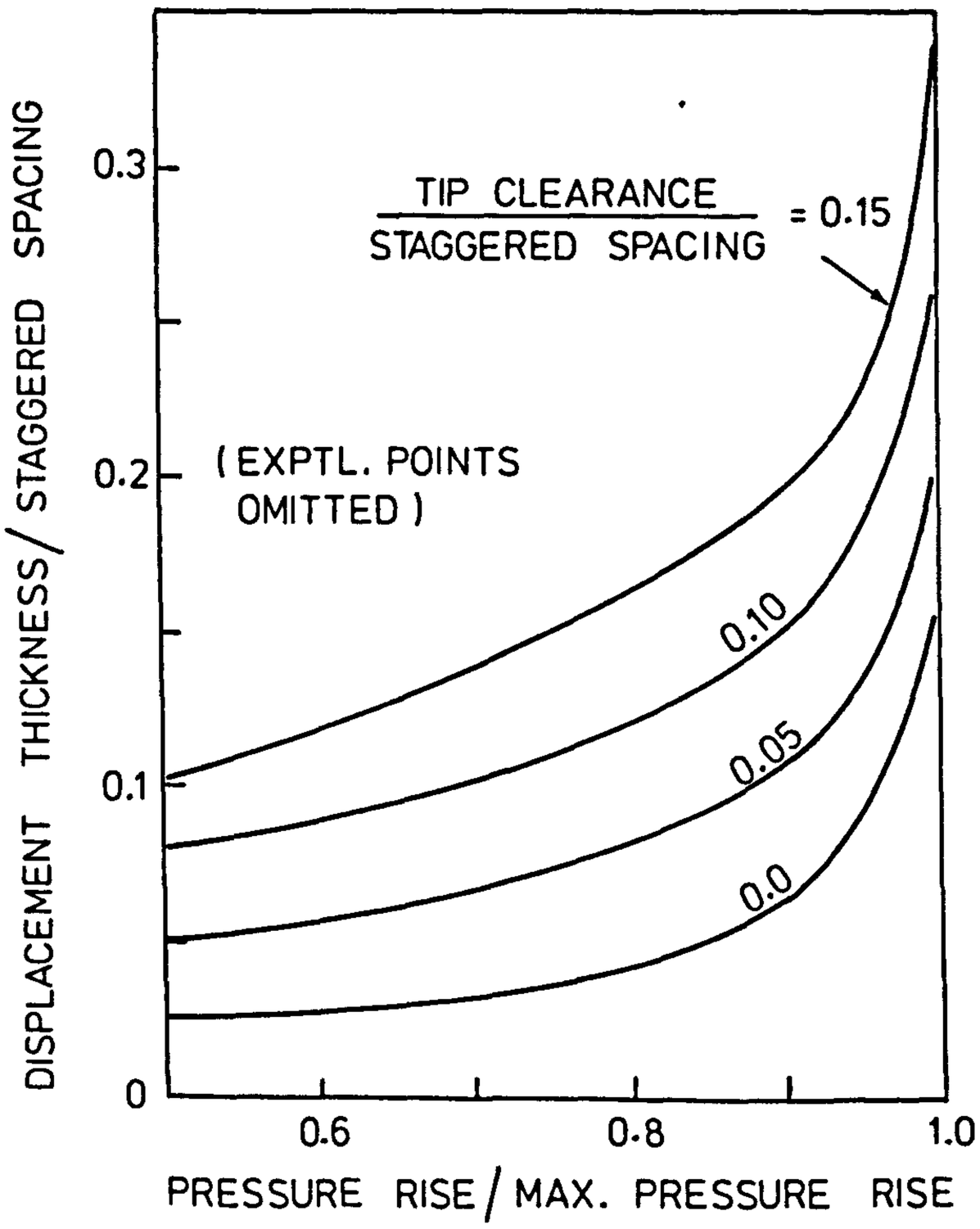

FIG. 2 DISPLACEMENT THICKNESS OF CASING BOUNDARY LAYERS (REF. 8)

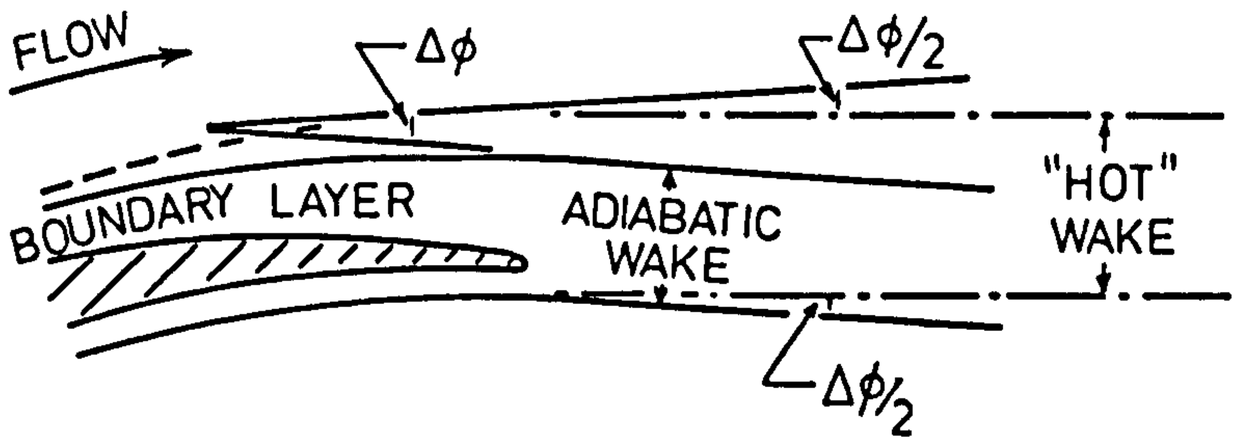

FIG.3 THE EFFECT OF HEAT TRANSFER ON WAKE DEVELOPMENT (REF. 2)

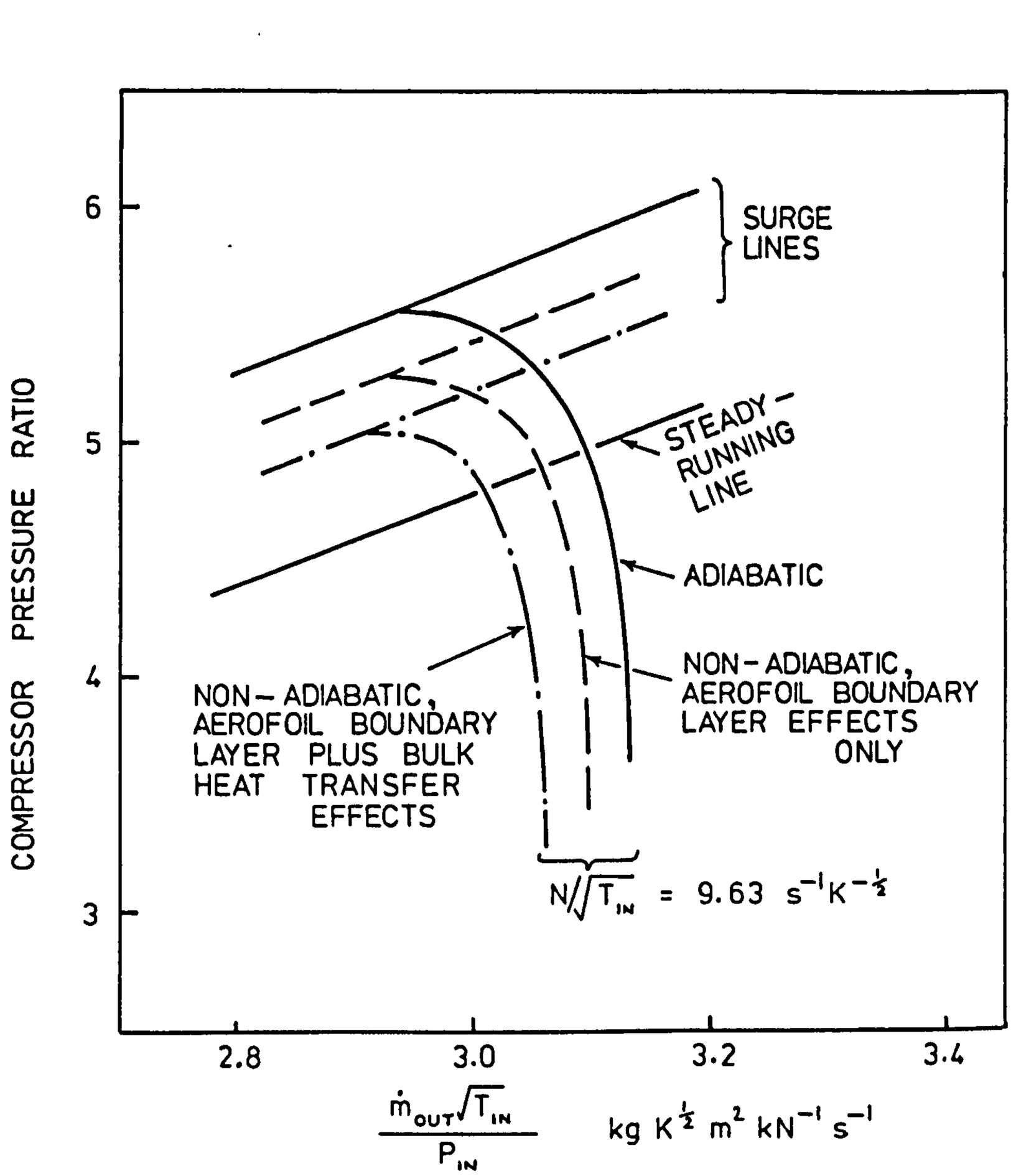

FIG.4 EFFECTS PREDICTED BY METHOD 1 ON H.P. COMPRESSOR CHARACTERISTICS AT END OF ALTITUDE DECELERATION

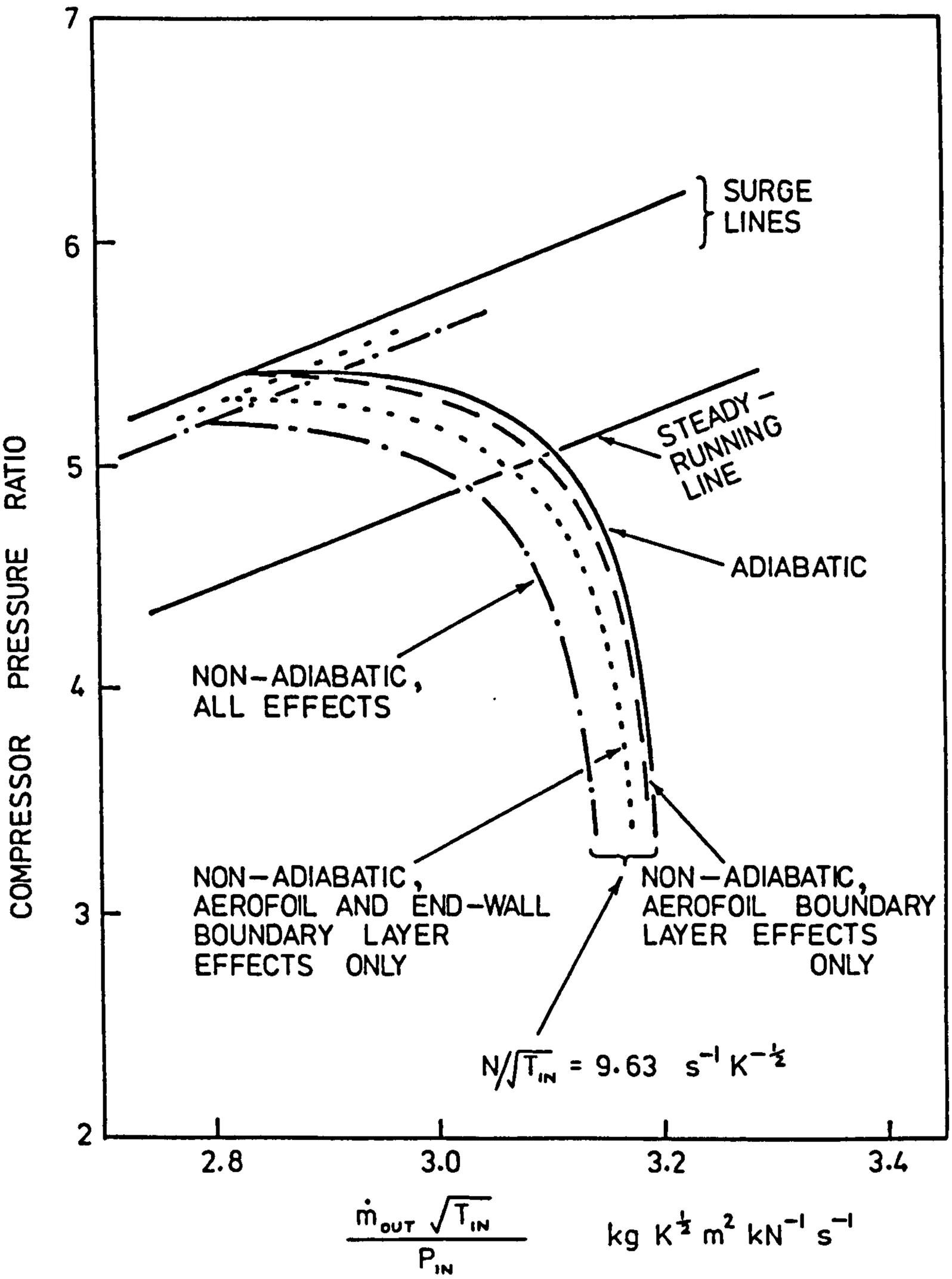

FIG.5 EFFECTS PREDICTED BY METHOD 2 ON H.P. COMPRESSOR CHARACTERISTICS AT END OF ALTITUDE DECELERATION

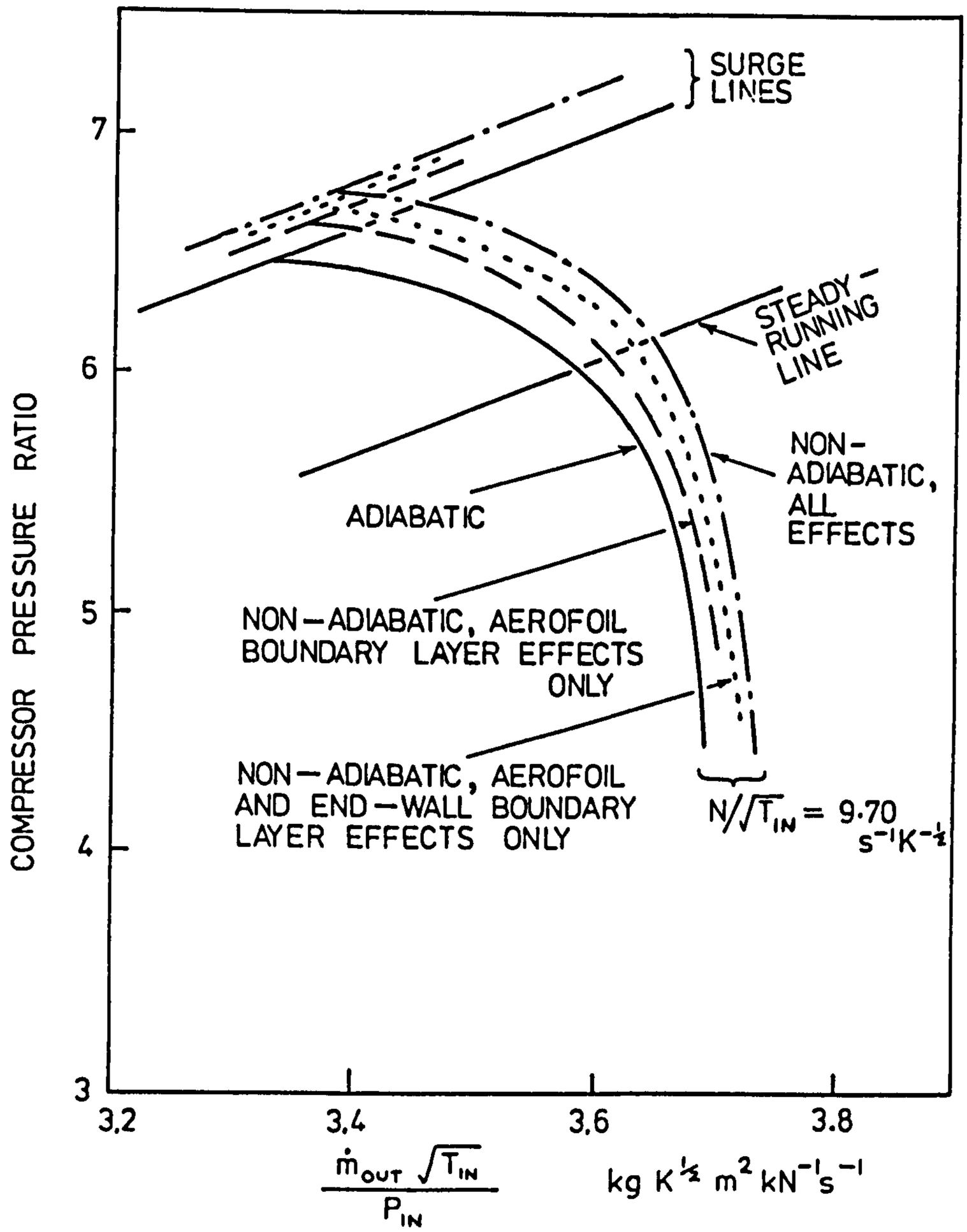

FIG. 6 EFFECTS PREDICTED BY METHOD 2 ON H.P COMPRESSOR CHARACTERISTICS AT 6 SEC. IN SEA-LEVEL ACCELERATION

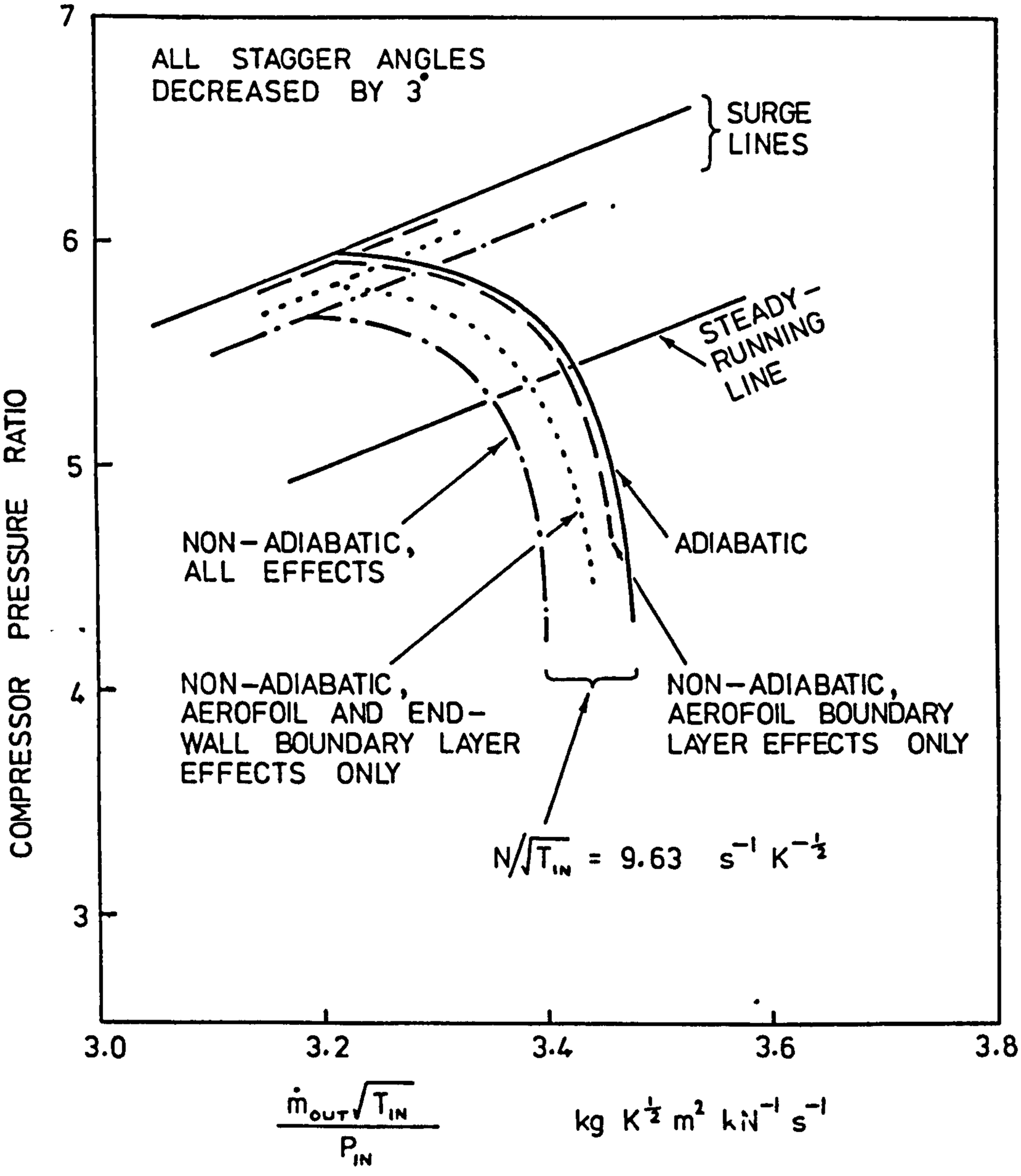

FIG.7 EFFECTS PREDICTED BY METHOD 2 ON H.P. COMPRESSOR CHARACTERISTICS AT END OF ALTITUDE DECELERATION – ALL STAGGER ANGLES DECREASED BY 3°

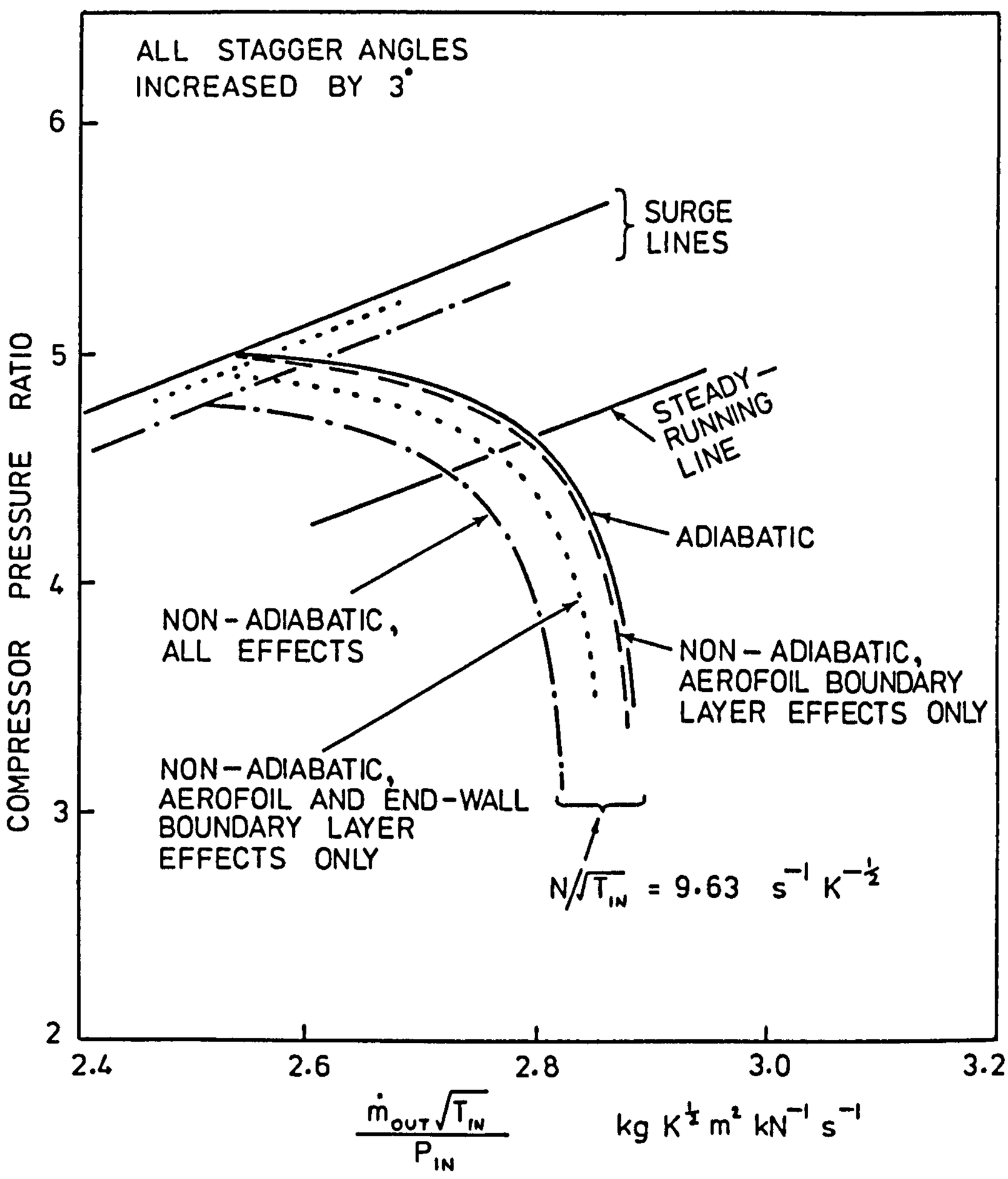

FIG. 8 EFFECTS PREDICTED BY METHOD 2 ON H.P. COMPRESSOR CHARACTERISTICS AT END OF ALTITUDE DECELERATION — ALL STAGGER ANGLES INCREASED BY 3°

DISCUSSION

D.K. Hennecke, Ge.

The heat transfer in a compressor during an acceleration or deceleration is transient. Therefore, I would like to know if the compressor characteristics you have calculated are valid for one instant in time.

Author's Reply

The compressor characteristics shown are in each case valid only for one instant in a particular transient.

J. Hourmouziadis, Ge.

MTU has had some experience with surging compressors during transients, however we were not able to identify any heat transfer effects. What is your estimate of the relationship in magnitude between such effects and those of changing clearances at the blade tip?

Author's Reply

The heat transfer effects must exist and the predictions in the paper indicate they are not insignificant. I would estimate that the changes in characteristics due to heat transfer effects might approach in magnitude the changes due to tip clearances.

P.F. Neal, UK

In your work on the effect of heat transfer on surge margin you have shown a significant effect with measurements at steady conditions. Dr Hennecke has already asked about the transient heat transfer effects on surge but have you done any work on the difference in surge margin between say a cold accel and a hot reslam considering the dynamic effect that any mass that is accelerated when its density reduces basically produces an oscillatory (or unstable) motion?

Author's Reply

I have not considered the dynamic effect in accelerating a flow that you describe. The present method does predict that the surge margin when accelerating a hot engine will be less than when accelerating a cold engine from the same initial speed. The effect you mention could accentuate this reduction.

K. Bauerfeind, Ge.

From some work carried out at MTU in the late 60's we found an additional effect, i.e. a change of the efficiency due to what one could term "interstage cooling" during an accel with a compressor. Could you comment on the magnitude of this effect?

Author's Reply

The procedures described in the present paper recognise this effect. It has been assumed that the small-stage efficiencies of the steps between the interstage coolings are the same as they would have been in adiabatic flow at the same values of the stage axial velocity ratios and stage pressure ratios. The method is described in Reference 9.

In the H.P. Compressor considered in the present paper, during a sea level acceleration the sum of the interstage cooling effects, i.e. the temperature drop due to heat transfer, peaks at about 7 per cent of the temperature rise due to compression. This effect gives beneficial reductions in the powers absorbed by the compressors. However, there is a detrimental loss due to transient heat transfers in the turbines during the acceleration which more than balances the benefit in the compressors, and predicted accelerations are slowed 5 to 6 per cent when these effects are taken into account (Refs. 15, 16).

Publication 27

AGARD

ADVISORY GROUP FOR AEROSPACE RESEARCH & DEVELOPMENT

7 RUE ANCELLE 92200 NEUILLY SUR SEINE FRANCE

Paper Reprinted from
Conference Proceedings No. 324

ENGINE HANDLING

NORTH ATLANTIC TREATY ORGANIZATION

MODELS FOR PREDICTING TIP CLEARANCE CHANGES IN GAS TURBINES

P. Pilidis and N.R.L. Maccallum

Research Student Reader

Department of Mechanical Engineering
University of Glasgow
Glasgow G12 8QQ

SUMMARY

Clearances at compressor and turbine blade tips and seals alter during and following transients. These changes affect the performance of the components of the engine.

In the present paper a model has been developed to predict these clearance changes. The model divides the stage into the casing, blade and disc sections, the disc being split into three elements. A simplified version has been produced for inclusion in engine transient performance programs.

As an illustration the models have been applied to the H.P. Compressor of a two-spool by-pass engine, and to two seals controlling bleed and cooling flows. The results indicate that the effect of compressor blade tip clearance is small. More significant are the effects of the seal clearance changes.

List of Symbols

D	Diameter
Gr	Grashof Number
L	axial length of stage
Nu	Nusselt Number
Pr	Prandtl Number
Re	Reynolds Number

Subscripts

av	average
i	hub of blade
o	casing
r	at a radius

1. INTRODUCTION

It is desirable to develop accurate methods for predicting the transient behaviour of gas turbines. For example, reliable predictions are needed for the speed response and thrust response of an aero gas turbine when a given acceleration fuel schedule is applied.

The earliest programs for the prediction of the transient behaviour used equilibrium characteristics for the components, and ignored heat transfer effects. However these simple procedures had weaknesses, for example they seriously underestimated the times required for the speed and thrust responses - Thomson (Ref. 1) quotes underpredictions of 20 to 30% for acceleration times.

The influences of the direct heat transfer effects on these predictions of responses have subsequently been studied for a typical single-spool (Ref. 2) and a typical two-spool by-pass engine (Ref. 3). Alterations in tip clearances cause changes in component efficiencies. This can be regarded as an indirect effect of heat transfer, although tip clearances are also influenced by centrifugal and pressure effects. It has been shown (Ref. 3) that predicted acceleration rates are very sensitive to changes in component efficiency - a loss of 1% in H.P. turbine efficiency increases the time for acceleration of a typical two-spool by-pass engine by 17%. A further indirect effect of heat transfer is the response of seals which control cooling air flows. It is therefore appropriate to consider whether engine transient programs should include allowance both for the direct heat transfer effects (Ref. 2) and for the indirect effects of tip clearance and seal response.

The object of the present paper is to find models from which tip clearance, and hence efficiency, changes can be predicted, and also models for seal clearance changes. The aim is to incorporate these models, if required, in the engine transient programs. The models can of course be used to predict the transients most likely to cause "rubs", thereby assisting design.

2. PROCEDURE FOR ESTIMATION OF BLADE TIP CLEARANCE EFFECT

The H.P. Compressor of a typical two-spool by-pass engine, of overall compression ratio 20 and having mixed exhausts, has been selected to demonstrate how the representation of a multi-stage turbomachine can be simplified, still retaining reasonable accuracy.

2.1 MODEL FOR BLADE TIP MOVEMENT

The movement of the blade tip depends on the responses of the disc and of the blade. Studies using the finite element program of Ref. 4 have indicated that the complex shape of the disc can be broken down into three components - a thick hub portion, a thin diaphragm and an outer section or rim (Fig. 1). With regard to transient heat transfers to, or from, these disc elements, some faces are rotating adjacent to stationary faces while other faces form walls of what are effectively rotating chambers. For rotating faces adjacent to stationary faces, the correlation used is (Ref. 5) -

$$Nu_r = 0.0253(Re_r)^{0.8} \quad (1)$$

For rotating faces which form walls of rotating chambers the heat transfer mechanism is effectively natural convection in a high gravity field, the value of the gravitational acceleration being a function of both the local radius and the rotational speed and the correlation is -

$$Nu_r = 0.12(Gr.Pr)^{0.33} \quad (2)$$

For heat transfer to turbine blades, a suitable correlation is that given by Halls (Ref. 6) -

$$Nu_{av} = 0.235(Re)^{0.64} \quad (3)$$

For compressor blades, one approach has been to adopt a weighted average between laminar and turbulent boundary layers developing on flat plates (Ref. 7). The results of this method have been found to be within 5% of the results obtained by applying Hall's turbine correlation to the compressor blades. Therefore for convenience in the present work, which is intended to produce a model applicable to both compressor and turbine tip movements, Hall's correlation has been used for all blades.

Centrifugal effects have also been accounted for. The centrifugal growth for the simplified "three element" disc was calculated ensuring continuity of radius dimension at the interfaces between the elements and a multiplying factor of 1.3 was introduced to line up with growths calculated by finite element analysis.

Disc distortion in the angular direction during acceleration has been calculated, but the resulting radial movement is found to be negligible.

2.2 MODEL FOR CASING MOVEMENT

The casing structure of the H.P. Compressor is subjected to internal pressure from the core air and to external pressure from the by-pass air, and also exchanges heat with these two air flows. In order to estimate the heat transfer coefficient at the internal surface of the casing, one approach is to regard this as a cylinder in which a smaller cylindrical shape is rotating, the heat transfer coefficient in this case being given by (Ref. 8) -

$$Nu = 0.015(1 + 2.3(D_o-D_i)/L)(D_o/D_i)^{0.45}\ (Re)^{0.8}\ (Pr)^{0.33} \quad (4)$$

In applying the above equation to the present work, the linear axial dimension, L, used was the axial length of the blade pair, it being assumed that the end-wall boundary layer is effectively restarted at each blade pair. For the outer surface of the casing, the expression for a developing turbulent boundary layer on a flat plate was used.

2.3 CLEARANCE MOVEMENTS

The methods described in the preceding sections have been used to predict the clearance movements during and following an acceleration for each of the 12 stages of the H.P. Compressor of the two-spool by-pass engine previously referred to. The engine was stationary, at sea level, and the speed transient was completed in 11 seconds. The predicted results for stages 1, 5 and 11 are shown in Figs. 2, 3 and 4 respectively. In each there is a rapid reduction in tip clearance during the speed transient, due to centrifugal growth and comparatively rapid thermal growth of the blades. The pressure movement of the casing is small, amounting to about 1% of the blade tip movement. The thermal response of the casing is less rapid than that of the blades. Much of this takes place after the speed transient is completed. Finally the disc thermal response is achieved, which may take up to 360 s or longer for completion. To indicate the relative rates of the thermal responses of the various components, the time constants for Stage 5 at three instants in the transient are given in Table 1.

Time in transient	2s	6s	10s
Disc hub	108s	66s	37s
Disc diaphragm	38s	17.8s	9.6s
Disc outer section	12.7s	9.0s	5.5s
Blade	2.3s	1.6s	1.0s
Casing	10.4s	7.6s	4.8s

Table 1. Stage 5: Time Constants during Acceleration

2.4 EQUIVALENT STAGE AND EFFICIENCY CHANGES

It would be excessively cumbersome to have to include each individual blade row of each compressor and turbine into the transient program for the engine. The use of single "equivalent" stages would be highly desirable. A single equivalent stage can give satisfactory heat transfer rates (Ref. 2). A single equivalent stage has been developed, based on the averaged dimensions of the 12 stages and using averaged properties of specific heat and thermal expansion coefficient, to represent tip clearance and associated efficiency changes. (Ref. 9).

The efficiency changes, relative to zero tip clearances, have been calculated during the acceleration transient using the efficiency alterations in each of the 12 stages calculated individually. The results are shown in Fig. 5. The efficiency changes predicted using the single equivalent stage were next calculated, and are also shown in Fig. 5. It is seen that the efficiency changes predicted by the equivalent method are in satisfactory agreement with the calculation based on all 12 stages, discrepancies never exceeding 0.7% of efficiency.

A further simplification has been introduced to reduce the property data required. The simplification involves the continuity of radius at the interfaces between the elements forming the disc, the movement of the outer edge of the platform being taken as the sum of the relative radial growths across the three elements. The efficiency changes predicted with this simplified analysis are shown by the solid line on Fig. 5. There is satisfactory agreement between these predictions and those based on the 12 stages. This simplified model has been used in the engine transient program and sample results are discussed in the next paragraph.

2.5 EFFECTS OF EFFICIENCY CHANGES IN ACCELERATIONS

The methods described above have been used to illustrate the effect of accounting for efficiency changes resulting from tip clearance alterations on predictions of acceleration rates. The transient considered was a sea-level acceleration of the two-spool by-pass engine previously considered. The effects in the H.P. Compressor only are illustrated here. At each time increment in the transient the tip clearance was determined and hence the efficiency change relative to zero tip clearance. The tip clearance for steady running at that speed and flow condition was also determined, and the corresponding efficiency change from zero clearance. Thus the alteration in compressor efficiency at each time increment during the transient as compared to the equivalent steady running condition was found. These alterations in compressor efficiency are shown in Fig. 6, where it is seen that the changes are very small, less than 0.15%, and generally beneficial. The reason for the smallness of the effect is that the partially incomplete expansion of the disc is compensated by the partially incomplete expansion of the casing.

The effect of these alterations in compressor efficiency on the predicted acceleration rate has been estimated using the engine transient program, and has been found to be very small, indeed too small to be illustrated.

3. PROCEDURE FOR ESTIMATION OF SEAL CLEARANCE MOVEMENTS

The methods and model used for tip clearance can be adapted for making estimates of seal clearance movements during transients. In the engine considered in the present study, two relevant seals are the H.P. Compressor 12th Stage Outer Seal and the H.P Cooling Air Seal on the H.P.1 Turbine Disc.

3.1 H.P. COMPRESSOR 12th STAGE OUTER SEAL

The movements of this seal have been studied by Lim (Ref. 10) using finite difference methods. The predictions of Lim and of the present much simpler method are compared on Fig. 7. The agreement is sufficiently close to allow the present models to be used for seal clearance predictions during transients. It is seen that during most of the acceleration speed transient, seal clearances exceed their maximum speed stabilised values by up to 30%.

3.2 H.P. COOLING AIR SEAL ON H.P.1 TURBINE DISC

The movements of this seal have been studied previously by finite difference methods (Ref. 5). The seal clearances during the acceleration speed transient exceed the maximum speed stabilised values by more than 100%. (Ref. 8)

3.3 EFFECTS OF SEAL CLEARANCE MOVEMENTS IN ACCELERATIONS

In the early programs for predicting the acceleration or deceleration rates of gas turbines it would probably be assumed that cooling and bleed air flows remained a constant fraction of the core air flow during the transient. However it has been illustrated above that seal clearances during the speed change period of a typical acceleration can be very much higher than the maximum speed stabilised or "design" clearances. Consequently these cooling and bleed flows, expressed as fractions, will exceed the "design" fractions.

Allowance for the movements of the H.P. Compressor 12th Stage Outer Seal and of the H.P. Cooling Air Seal on the H.P.1 Turbine Disc have been included in the engine transient program, and the results, for the sea-level acceleration, are illustrated in Fig. 9. The predicted acceleration rate is slowed by about 5% due to inclusion of these effects.

4. CONCLUSIONS

A simple model can be used to predict tip clearances of individual stages during a transient. An equivalent stage can be developed which will give an "averaged" tip clearance from which efficiency changes of the component - e.g. the compressor - can be calculated. During an acceleration of a typical two-spool engine, in the H.P. Compressor, the tip clearance changes, and efficiency alterations, as compared to steady running, are small and tend to be favourable.

The techniques for tip clearance prediction can be applied to seals. Some seals are seen to have large clearances during accelerations. Allowance for this makes predicted acceleration rates significantly slower than if this effect had been ignored.

REFERENCES

Ref. 1 Thomson, B. "Basic Transient Effects of Aero Gas Turbines" AGARD Conf. Proc. 151, Feb 1975.

Ref. 2 Maccallum, N.R.L. Thermal Influences in Gas Turbine Transients - Effects of Changes in Compressor Characteristics. ASME Paper 79-GT-143, 1979.

Ref. 3 Maccallum, N.R.L. Further Studies of the Influence of Thermal Effects on the Predicted Accelerations of Gas Turbines. ASME Paper 81-GT-21, 1981.

Ref. 4 Neilson, W. The Finite Element Method in Transient Heat Conduction. Final Year Project, University of Glasgow, April 1973.

Ref. 5 Maccallum, N.R.L. Transient Expansion of the Components of an Air Seal on a Gas Turbine Disc. S.A.E. Paper 770974, 1977.

Ref. 6 Hall, G.A. Air Cooling of Turbine Blades and Vanes. Lecture to AGARD, Varenna, Italy, 1967.

Ref. 7 Maccallum, N.R.L. Effect of Bulk Heat Transfer in Aircraft Gas Turbines on Compressor Surge Margins. Heat and Fluid Flow in Steam and Gas Turbine Plant. Inst. Mech. Engrs., London 1974, 94-100.

Ref. 8 Tachibana, F. and Fukui, S. Convective Heat Transfer of the Rotational and Axial Flow between Concentric Cylinders. Bull. of Japanese Soc. M.E., vol. 7, no. 26, 1964.

Ref. 9 Lakshminarayana, B. Methods of Predicting the Tip Clearance Effects in Axial Flow TurboMachinery. Transactions of the ASME, Journal of Basic Engineering, vol. 92, Sept. 1970.

Ref. 10 Lim, T.J. An Investigation into the Seal Clearance and Temperature Response during Transient of the Stage 12th H.P. Compressor of a Twin Spool By-Pass Jet Engine. Final Year Project, University of Glasgow, 1980.

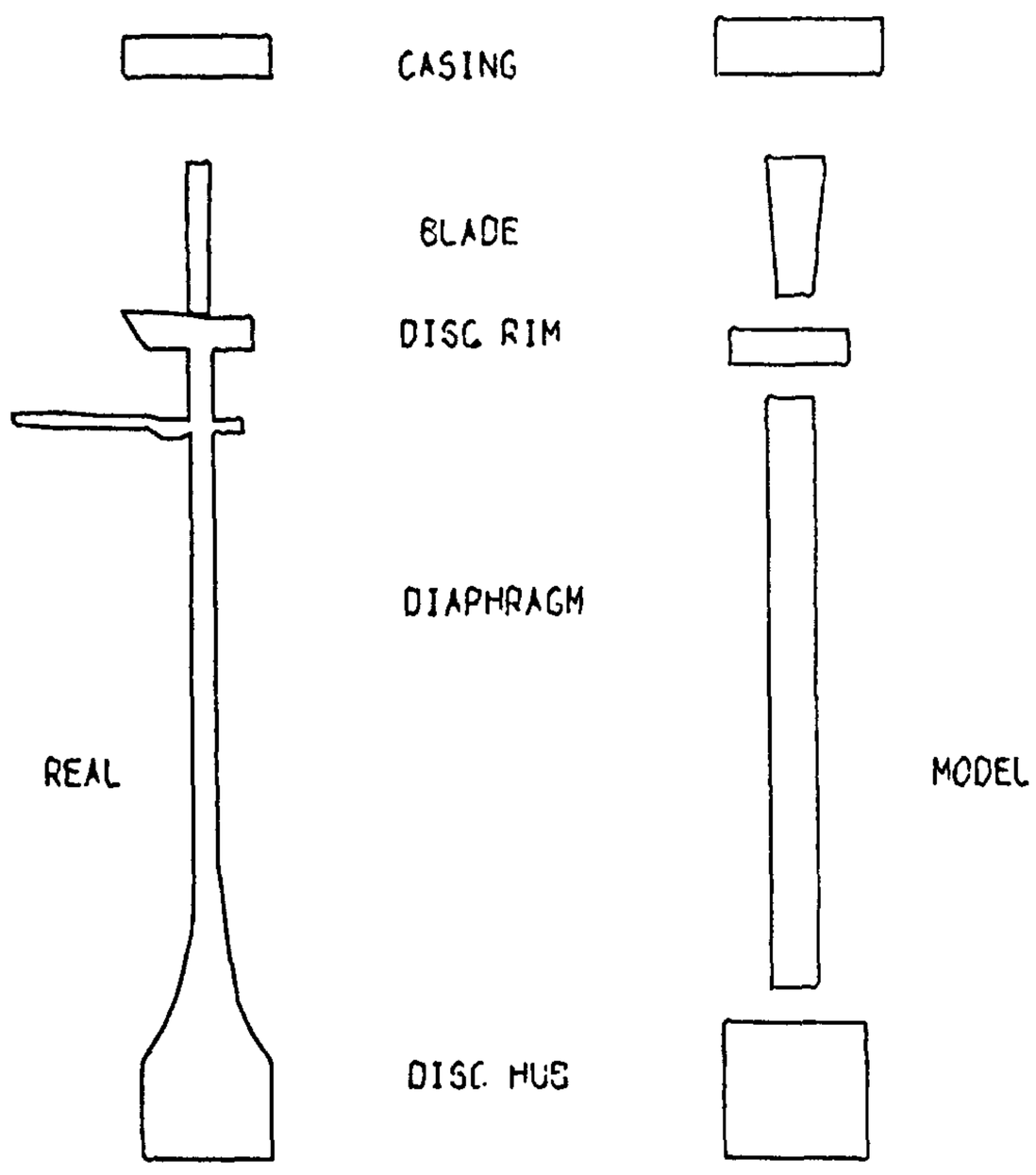

FIG. 1

REPRESENTATION OF A TYPICAL STAGE.

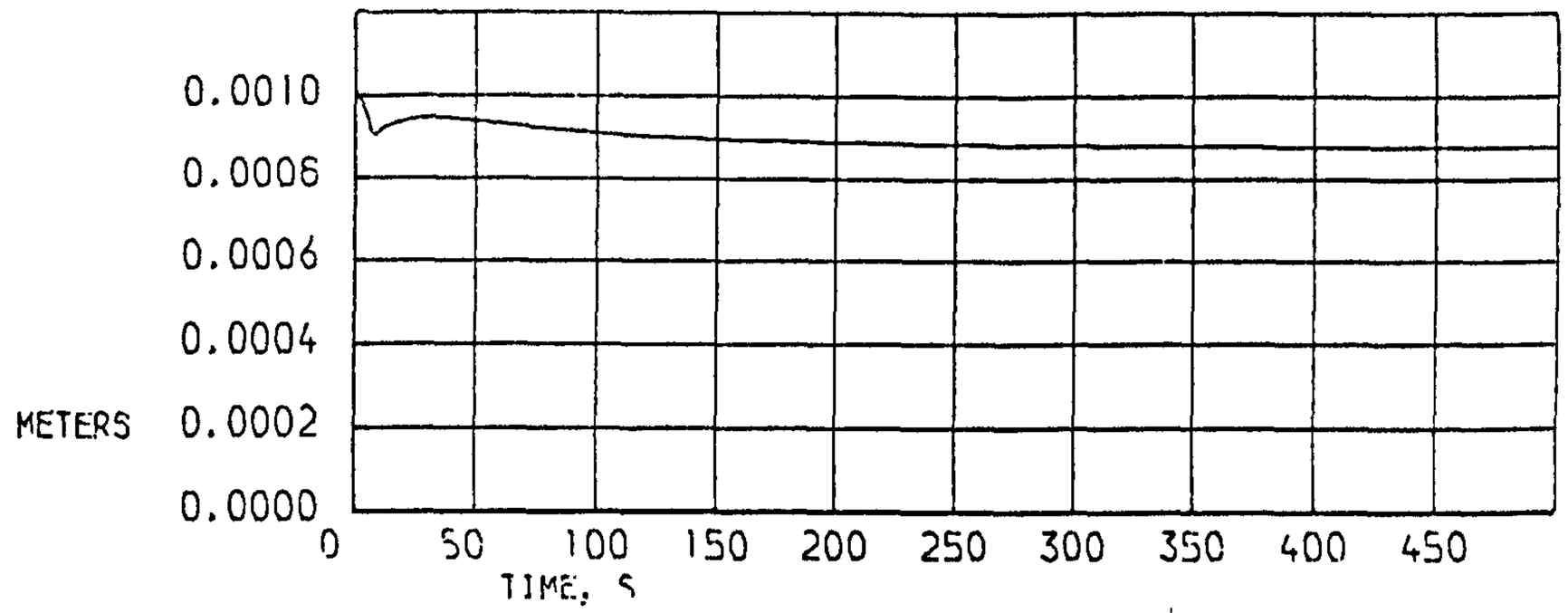

FIG. 2 STAGE 1

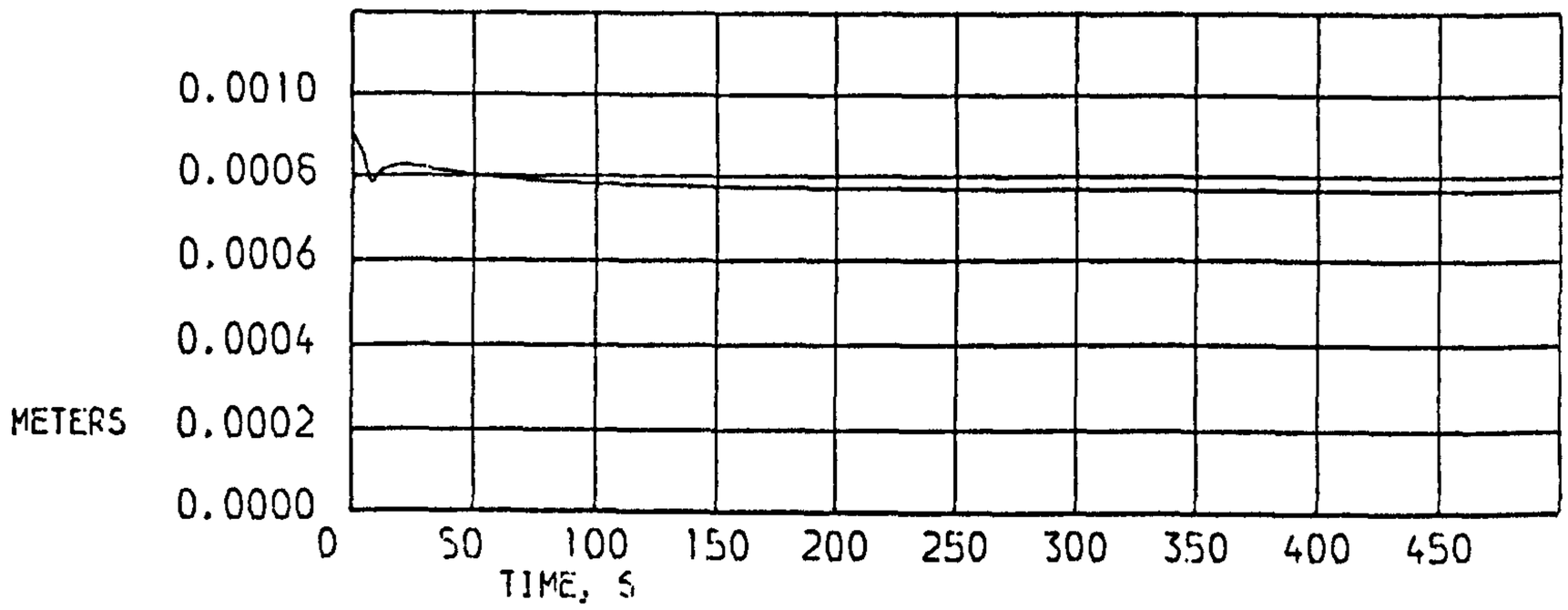

FIG. 3 STAGE 5

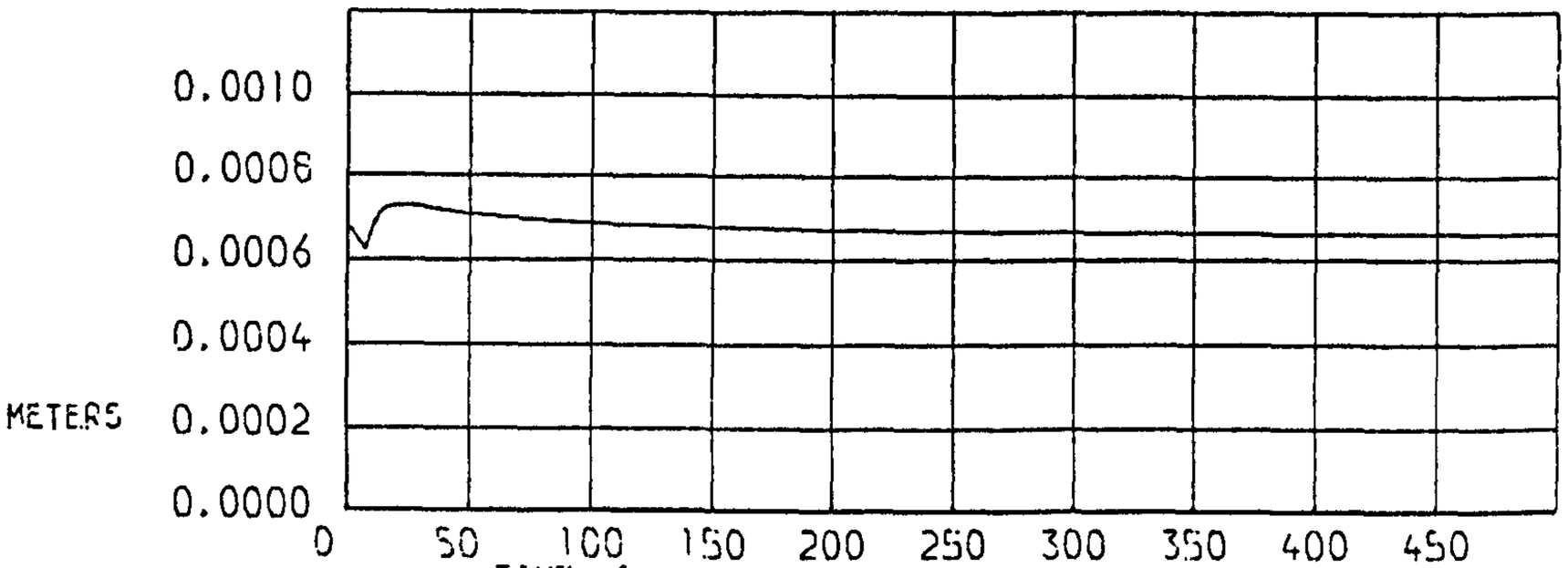

FIG. 4 STAGE 11

PREDICTED TIP CLEARANCES DURING AND FOLLOWING SEA LEVEL ACCELERATION.

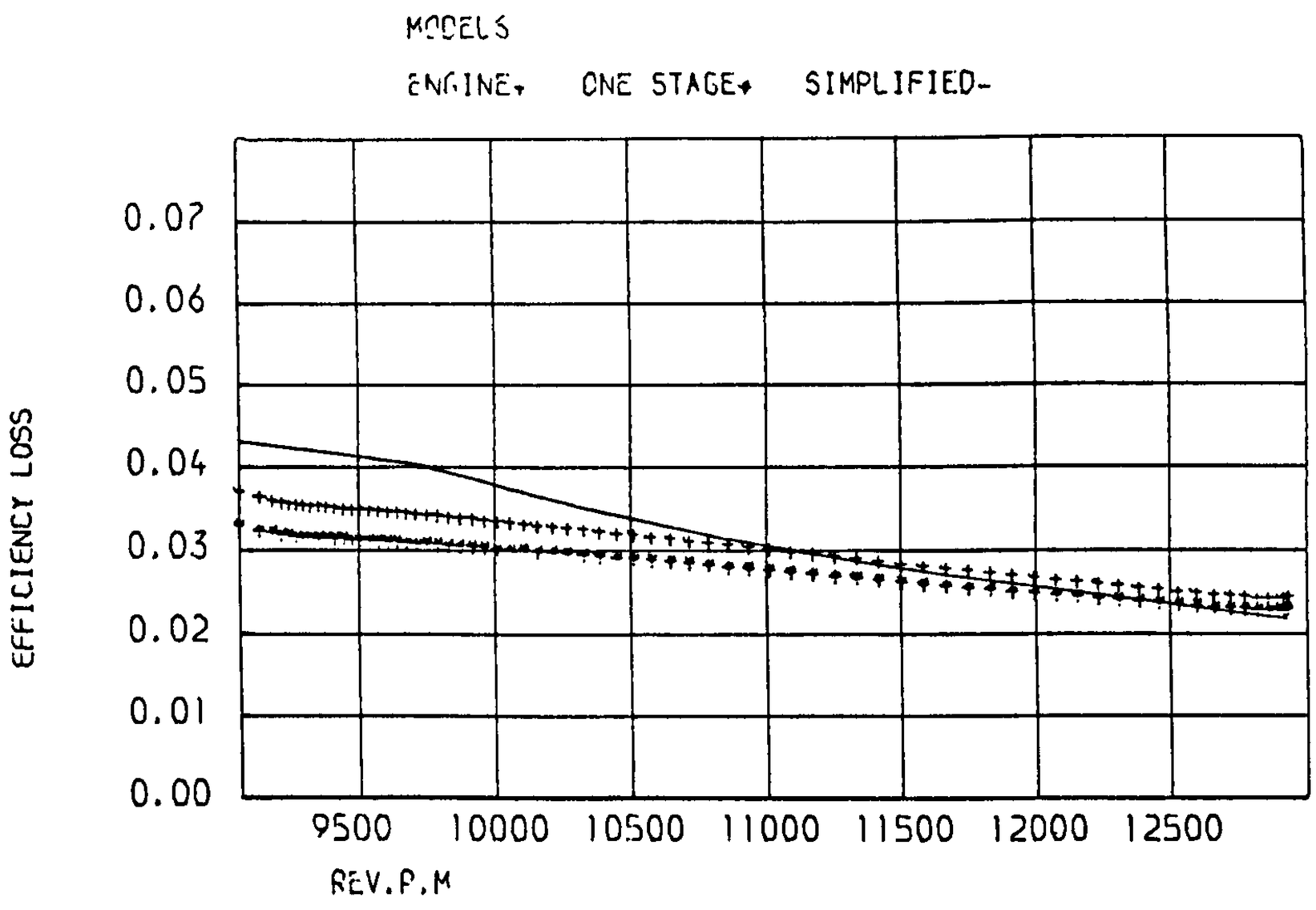

FIG. 5

EFFICIENCY LOSS COMPARED TO ZERO CLEARANCE

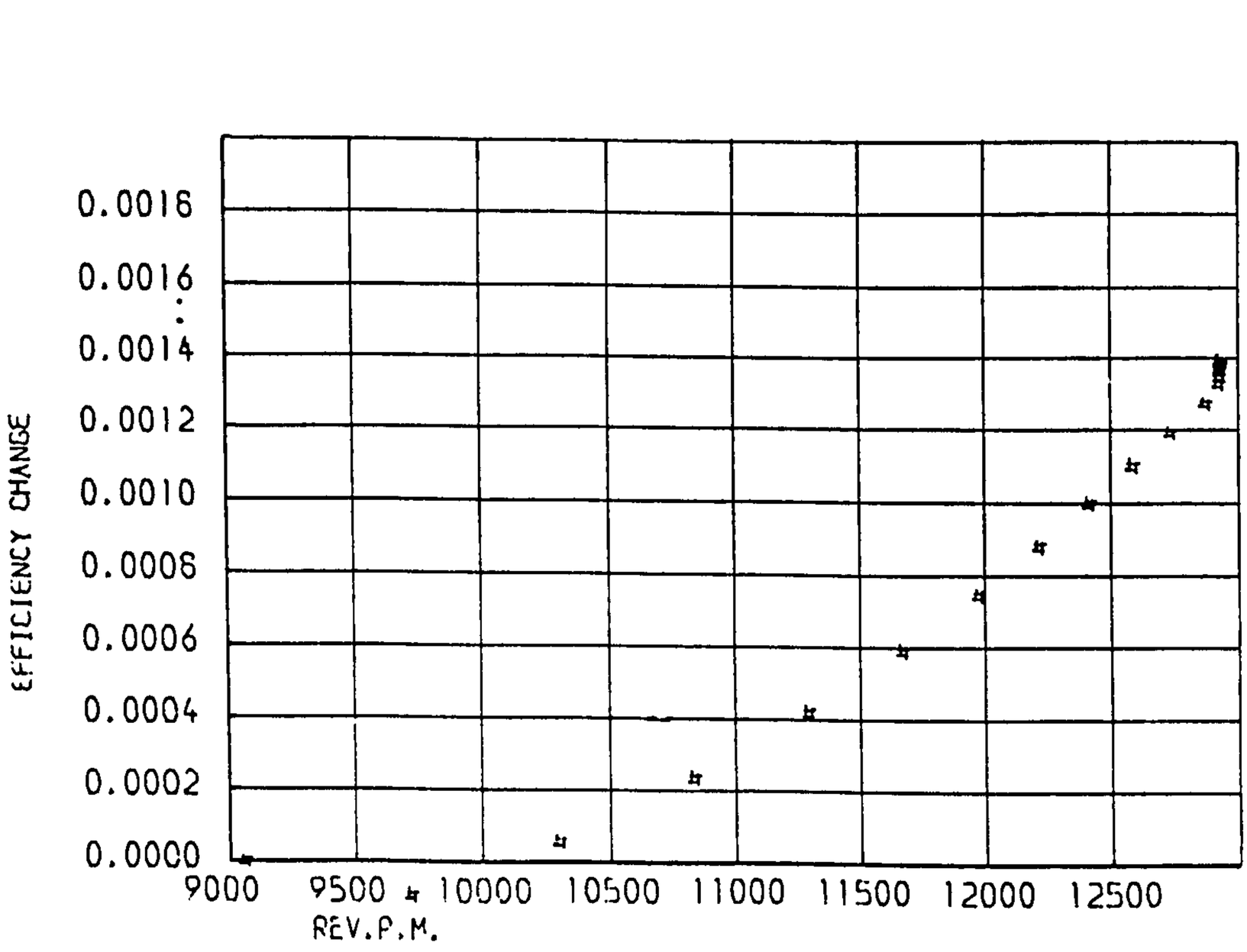

FIG. 6

EFFICIENCY CHANGE DUE TO DIFFERENCE BETWEEN TRANSIENT AND STABILISED CLEARANCE

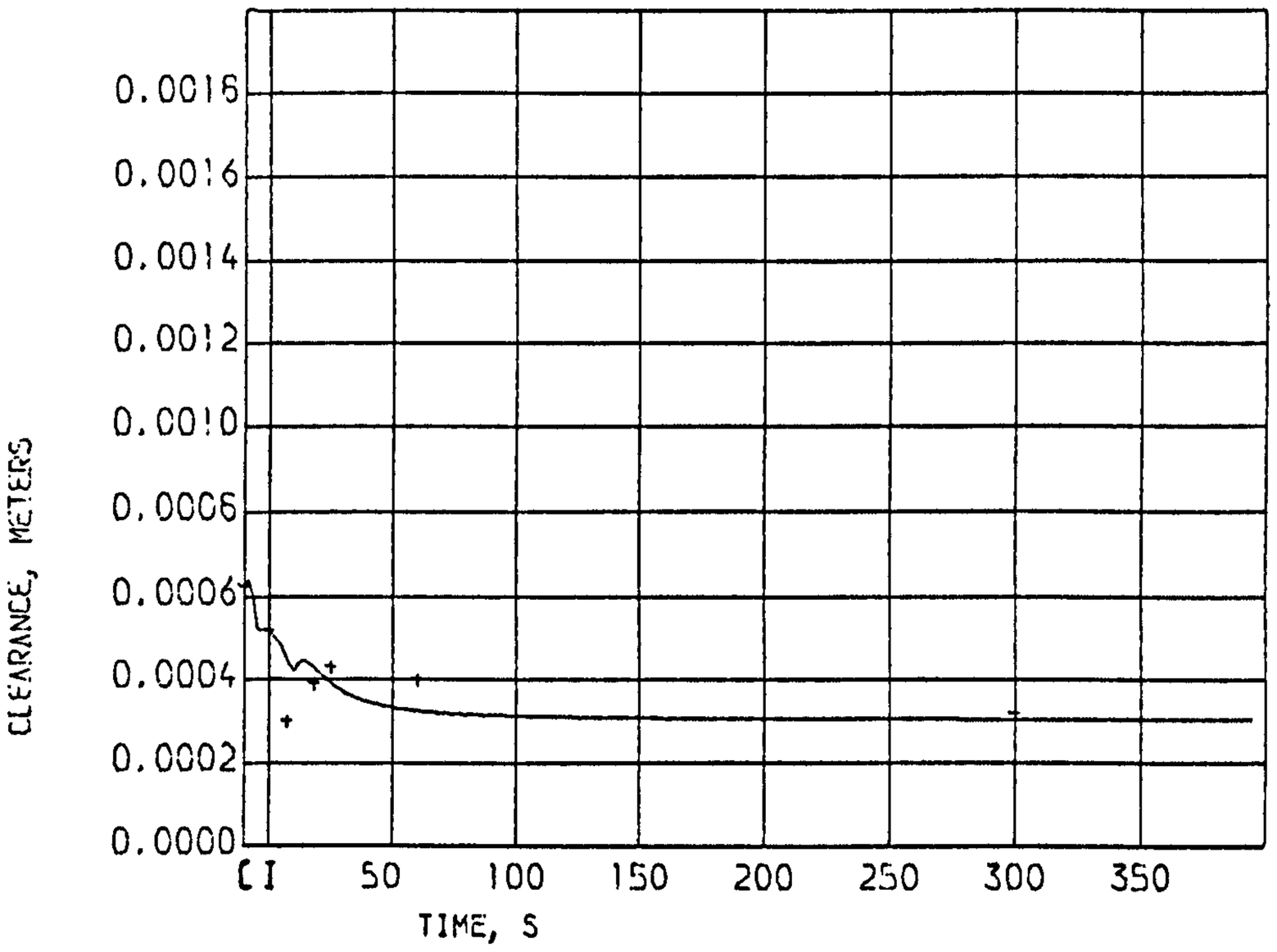

FIG. 7

PREDICTED HP COMPRESSOR OUTER REAR SEAL CLEARANCE
DURING AND FOLLOWING SEA LEVEL ACCELERATION.
PREDICTIONS FROM REF. 10 INDICATED BY +

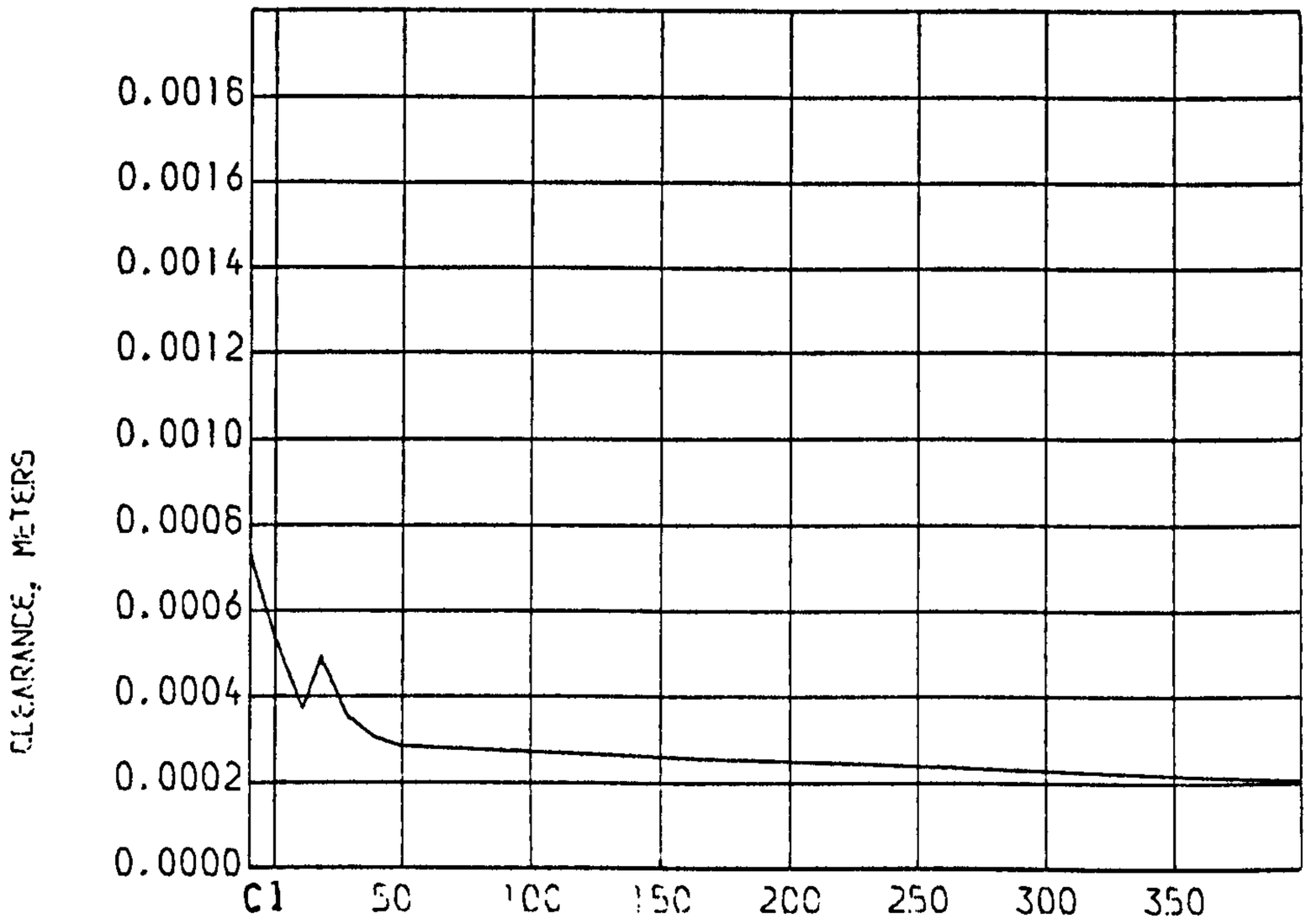

FIG. 8

PREDICTED HP TURBINE AIR SEAL CLEARANCE
DURING AND FOLLOWING SEA LEVEL ACCELERATION.
PREDICTIONS FROM REF. 5
C COLD BUILT I GROUND IDLE.

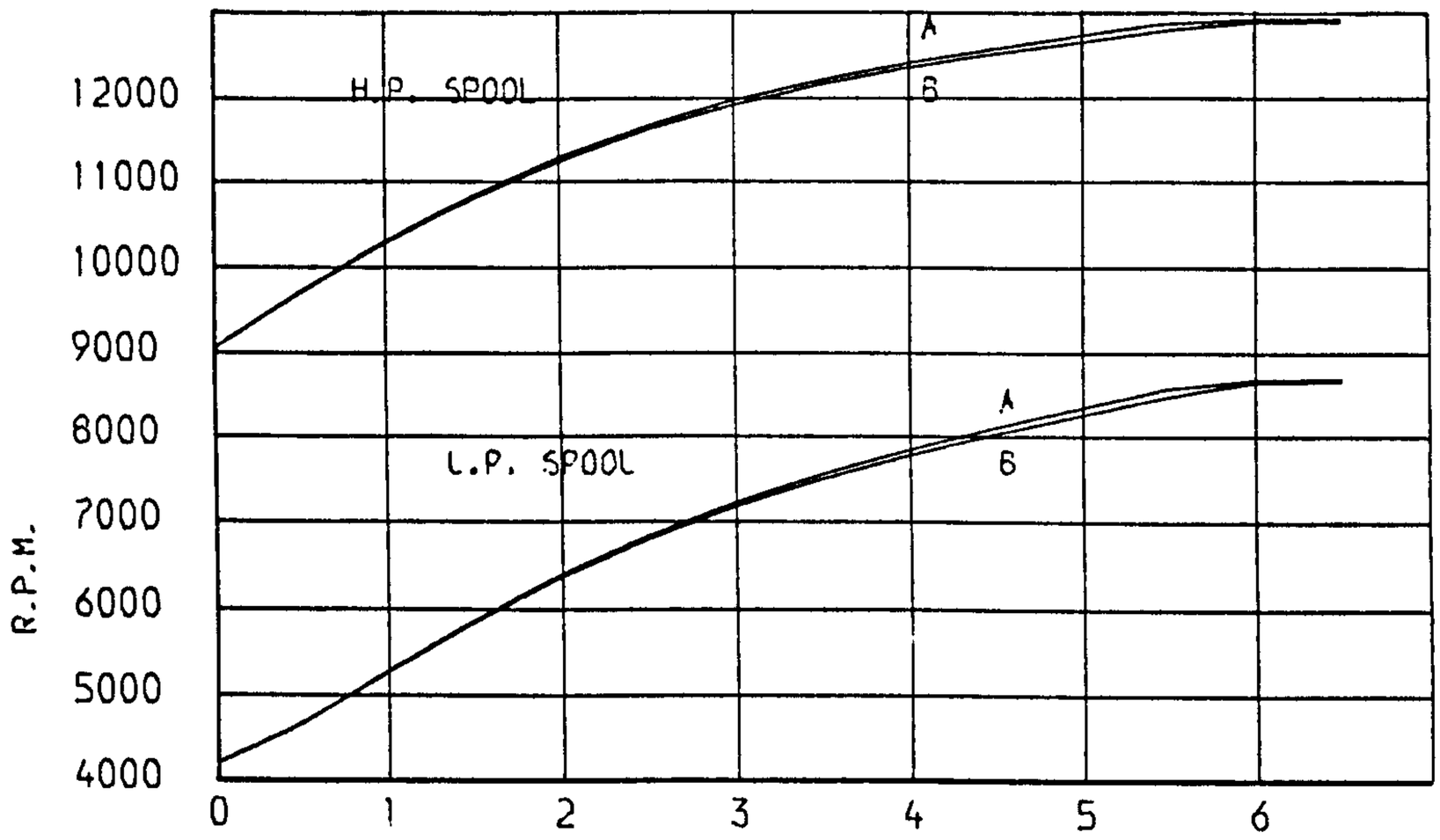

FIG. 9

EFFECT OF INCREASED SEAL OPENINGS IN THE H.P. TURBINE OF A TWO SPOOL ENGINE
A. ASSUMING CONSTANT SEAL OPENINGS
B. ALLOWING FOR SEAL OPENINGS

DISCUSSION

Ph. Ramette, Fr.

(a) In the Nusselt Number expressions in terms of Reynolds Numbers, what are the reference lengths which you have taken in your model, for a blade or for a disc?

(b) Is the equivalent stage you describe in your paper equivalent to the full high pressure compressor with 12 stages that you have studied?

Author's Reply

(a) The reference lengths used to obtain the Reynolds Number in the Nusselt Number expression are:
For the blades, blade-chords in both expressions for the disc outer section was the radial distance from the axis and for the casing the axial distance from the beginning of each stage.

(b) Yes. The idea of the equivalent stage is to represent the full compressor by one stage only. It was found that taking averages of the different dimensions and properties of the compressor gave results that were considered satisfactorily similar to the full compressor (Fig. 5).

Publication 28
84-GT-245

THE AMERICAN SOCIETY OF MECHANICAL ENGINEERS
345 E. 47 St., New York, N.Y. 10017

A STUDY OF THE PREDICTION OF TIP AND SEAL CLEARANCES AND THEIR EFFECTS IN GAS TURBINE TRANSIENTS

P. Pilidis, Research Associate
Caledonian Airmotive Ltd.
Prestwick, Scotland

N.R.L. Maccallum, Reader
University of Glasgow
Glasgow, Scotland

ABSTRACT

Clearances of compressor and turbine blade tips and seals alter during and following speed transients. These changes affect the performance of the components and hence of the engine..

This paper describes models for the prediction of bladetip clearance changes and seal clearance changes. These models have been applied to the H.P. Compressor and H.P. Turbine and to two seals controlling air flows in a Two-spool Bypass Engine. The predicted acceleration rates appear to be more influenced by the changes in the seal clearances than by the tip clearance changes.

The increases in computing time in the engine transient program which result from inclusion of the model are acceptable.

NOMENCLATURE

A = aspect ratio
C = clearance
C_p = specific heat at constant pressure
D = diameter
E = Young's Modulus
g = acceleration due to local gravity
Gr = Grashof Number

$$= \frac{l^3 \theta a g}{\nu}$$

h = local heat transfer coefficient
H = height
k = fluid thermal conductivity
l = characteristic length, blade chord
L = axial length of stage
M = mass
Nu_b = average Nusselt Number for blade (= hl/k)
Nu_r = local Nusselt Number on disc (= hR/k)
Nu_{ic} = Nusselt Number for inner surface of casing (= h(D$_o$ - D$_i$)/k)
Pr = Prandtl Number
R = radius
Re_r = local rotational Reynolds Number (= $\omega R^2/\nu$)
Re_b = Reynolds Number over blade (= ul/ν)
Re_{ic} = Reynolds Number for inner surface of casing (see Eq. 4)
T = absolute temperature
u = average gas velocity
V = volume of disc section
Va = axial velocity of fluid
Vt = blade tip tangential velocity
α = coefficient of cubical expansion
β_m = mean air angle (tan β_m = ½(tan β_i + tan β_o))
Δ = difference or change
ϵ = effectiveness
η = efficiency
θ = temperature difference
λ = non-dimensional clearance (= C/H_b)
ν = kinematic viscosity
ψ = blade loading (= $2C_p\Delta T_s/Vt^2$)
ω = angular velocity

Subscripts

av = average
b = blade
bt = blade tip
c = cooling air
d = disc
g = gas
h = hub of blade
i = inner, or inlet
j = j'th section
m = mean
mf = final metal (temperature)
o = outer, or outlet
r = at a radius
s = stage

1. INTRODUCTION

It is desirable to develop accurate methods for predicting the transient behaviour of gas turbines. The earliest programs for such predictions used equilibrium characteristics of the components and ignored alterations in these, such as due to heat absorption or tip clearance changes. Thomson (1)[1] quotes underpredictions of acceleration time of 20 to 30 per cent as compared to the real engine, when using these simplified procedures.

The influence of the non-adiabatic flow (a direct heat transfer effect) has subsequently been studied for a Single-spool Engine (2) and for a Two-spool Bypass Engine (3).

Alterations in tip clearances cause changes in component efficiencies. This can be regarded as an indirect effect of heat transfer, although tip clearances are also influenced by centrifugal and pressure effects. Another indirect effect of heat transfer lies in the response of seals which control cooling air flows.

The objects of the present paper are to develop models for representing tip clearance changes and to use these models to predict the effect of tip clearance changes during transients on the performance of the various components and hence of the engine. The models used in this work have been described briefly in a previous paper (4). More detailed descriptions are given in this paper. The transient program for the Two-spool Bypass Engine (3) has been extended to include these models so as to enable the calculation of the desired effects on engine transient response.

2. DETAILED DESCRIPTION OF THE METHOD

Gas turbines have to operate over a range of steady-running conditions. The mechanical and thermal loadings of the components vary, producing small changes in the dimensions in both the radial and axial directions. These changes can result in relative movements between rotating and stationary components, thus causing varying tip clearances and off-design seal mass flows. During accelerations and decelerations of the engine these movements can be modified by delays in the temperature responses.

In this paper, the radial changes only are considered. For much of this section the H.P. compressor of a typical two-spool bypass engine has been selected to demonstrate how the representation of a multi-stage turbo-machine can be simplified, still retaining reasonable accuracy.

2.1 Thermal Effects

2.1.1 Model for Blade Tip Movement. The movement of the blade tip depends on the responses of the disc and of the blade.

Considering first the disc (Fig. 1), some faces are rotating adjacent to stationary faces, while other faces form walls of what are effectively rotating chambers. With regard to faces adjacent to stationary walls, several investigators (for example, (5) - (7)) have examined the heat transfer coefficients and/or the drag characteristics. The variables studied included the radial inflow or outflow of coolant and the influence of a shroud. It was decided to base the heat transfer expressions to be used in the present work on experimentally derived correlations. Unfortunately in none of the experimental work did the conditions attain those in the engine, particularly with regard to the rotational

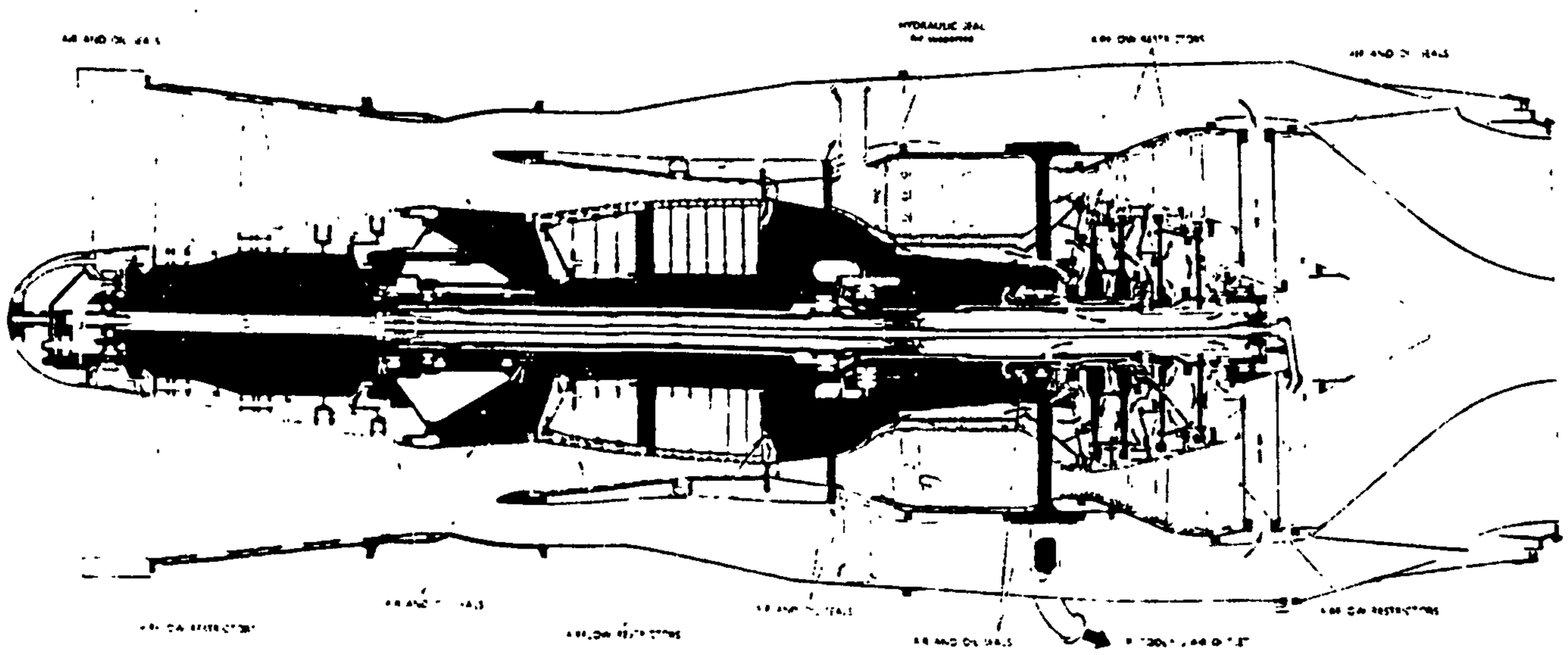

FIG. 1 GENERAL ARRANGEMENT OF TWO-SPOOL BYPASS ENGINE

1. Underlined numbers in brackets designate references at end of paper.

Reynolds Number - the highest value in experiments being 4 x 10^6 as compared with typically 12 x 10^6 in the engine. At the highest Reynolds Number of the experimental tests, with typical gap distances between the rotating and stationary discs and with typical shroud clearance and typical outflow of coolant the drag coefficient and heat transfer coefficient were found to be about 30 per cent higher than those for a free rotating disc. The free rotating disc correlation can be extended to Reynolds Numbers of 12 X 10^6. Assuming in the typical engine situation with an adjacent stationary face, a shroud and a coolant mass flow, that the coefficients are still 30 per cent higher than for a free disc, then the correlation for local Nusselt Number is (8):

$$Nu_r = 0.0253\ (Re_r)^{0.8} \qquad (1)$$

This correlation is not greatly sensitive to shroud clearance or coolant mass flow changes - doubling the coolant mass flow increases the Nusselt Number by 10 per cent, while doubling the shroud clearance lowers it by 5 per cent. It is suggested that for the present work Eq. (1) gives an adequate general correlation.

Considering now the rotating faces which form the walls of rotating chambers, the heat transfer mechanism is effectively natural convection in a high gravity field, the value of the gravitational acceleration being a function of both the rotational speed and the local radius. For this situation the following equation is suggested:

$$Nu_r = 0.12\ (Gr \cdot Pr)^{0.33} \qquad (2)$$

The above correlations have previously been used (8) to predict the temperature distributions in a turbine disc both during transients and in steady-running conditions. The steady-running temperature distributions were satisfactorily compared with results from thermal paint observations, predicted temperatures generally being within 15 deg. K of the observed values.

The present work is aimed at producing simple models to describe the movements of blade tips, casings etc. It would be preferable if the rather complicated shape of a compressor or turbine disc could be simplified. It is proposed that a deep disc rotor arrangement can be represented by three components - a thick hub, a thin diaphragm and an outer section or rim (Fig. 2). Comparisons between this grossly simplified model and the rigorous finite element transient (9) conduction analysis are given later in this paper.

With regard to the response of turbine blades. for simplicity, uncooled blades will be considered initially. A suitable correlation for heat transfer between the gas stream and turbine blade surfaces has been given by Halls (10):

$$Nu_b = 0.235\ (Re_b)^{0.64} \qquad (3)$$

For compressor blades, one approach has been to adopt a weighted average between laminar and turbulent boundary layers developing on flat plates (11). The results of this method have been found to be within five per cent of the results obtained by applying Halls' turbine correlation to the compressor blades. Therefore for convenience

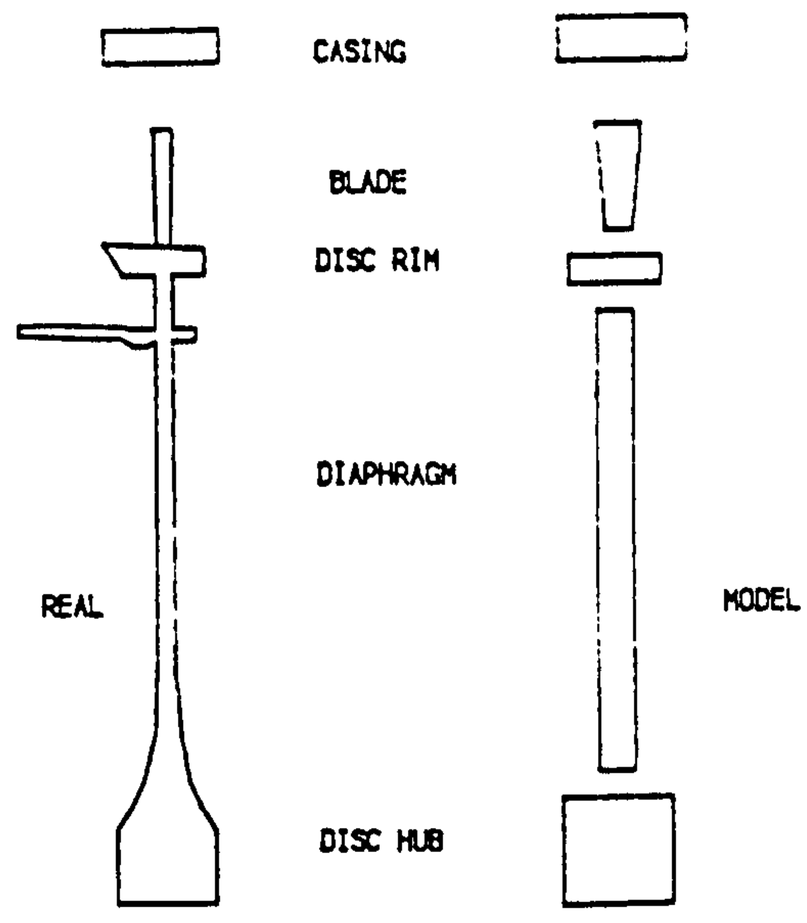

FIG. 2
REPRESENTATION OF A TYPICAL STAGE.

in the present work, which is intended to produce a model applicable to both compressor and turbine tip movements, Halls' correlation is used for all blades.

2.1.2 Model for Casing Movement. The casing structures can be complex, with inner and outer surfaces subjected to gases or air at differing temperatures and pressures, moving with differing velocities. In addition there may be spaces within the casing through which certain air or gas flows pass. At the present stage of development of the method, the effects of these cavities have been ignored, and the casings treated as solid walls.

In order to estimate the heat transfer coefficient at the internal surface of the casing, the approach used has been to regard this as a cylinder in which a smaller cylindrical shape is rotating. The heat transfer coefficient in this case is found from (12):

$$Nu_{ic} = 0.015[1 + 2.3\ (D_o - D_i)/L]\ [D_o/D_i]^{0.45} \times [Re_{ic}]^{0.8}[Pr]^{0.33} \qquad (4)$$

In this case Re_{ic} is given by:

$$Re_{ic} = (Va_m^2 + Vt^2/2)\ (D_o - D_i)/\nu$$

In applying Eq. (4) to the present work, the linear dimension, L, used was the axial length of the blade pair, it being assumed that the end-wall boundary layer is effectively restarted at each blade pair.

For the outer surface of the casing, the expression used was that for a developing turbulent boundary layer on a flat plate.

2.2 Mechanical Effects

The mechanical effects cause growth due to the change in the "pull" of the blades and of the disc sections. Pressure difference changes across a section may also cause growth, as may the effect of accelerating, or decelerating, the disc.

2.2.1 Disc. For simplicity in developing the model, it was assumed that the disc could be represented by the same three rings as in the thermal model. The predicted growths have been compared with those given by a finite element analysis. It was found that a multiplying factor of 1.3 had to be applied to the predictions of the three-ring model to bring them into agreement. (In the use of this three-ring model under the varying thermal and mechanical conditions, continuity of radial dimension at the interface was maintained.)

Disc distortion in the angular direction during a transient was calculated, but the resulting radial movement was negligible.

2.2.2 Blades. The blades are assumed to be rods of uniform cross-sectional area with or without an added shroud. The procedure was compared with calculations of elongation using the finite element method and the results were in good agreement.

2.2.3 Casing. With regard to the casing, the only relevant mechanical loading considered is the pressure change during the transient and its effect is found to be very small, about one per cent of the total movement of the rotor due to mechanical effects.

2.3 Clearance Movements

Once all these effects on the dimensions of the rotor stage or component are calculated, they are added to obtain the resulting change in the clearance.

All material, gas and air properties are calculated as functions of the temperature of the metal or fluid. In the prediction procedure it is of course possible to change the material in any section very easily.

The methods described in the preceding sections have been applied to the 12 stages of the H.P. Compressor of a Two-spool Bypass Engine. The Engine is illustrated in Fig. 1. The rotor system uses deep discs and these are surrounded by air drawn from the fifth and sixth stages. After circulating round these discs this air discharges to the bypass duct. The outer sections of the rotor discs, adjacent to the blade platforms, are effectively in contact with the air passing through the compressor. The predicted blade tip clearance movements for Stages 1, 6 and 11 during and following an acceleration from idle speed at sea level, static, are illustrated in Fig. 3. Looking at the clearance paths at the beginning of the transient, there is a sharp decrease in tip clearance due to mechanical effects, and the fast thermal growth of the blades. The thermal response of the casing is slower than that of the blades. Much of this takes place after the speed transient is completed, producing an increase in tip clearance. The disc has the slowest response and the final slow decrease in clearance is due to the slow expansion of the disc, which takes five minutes or more.

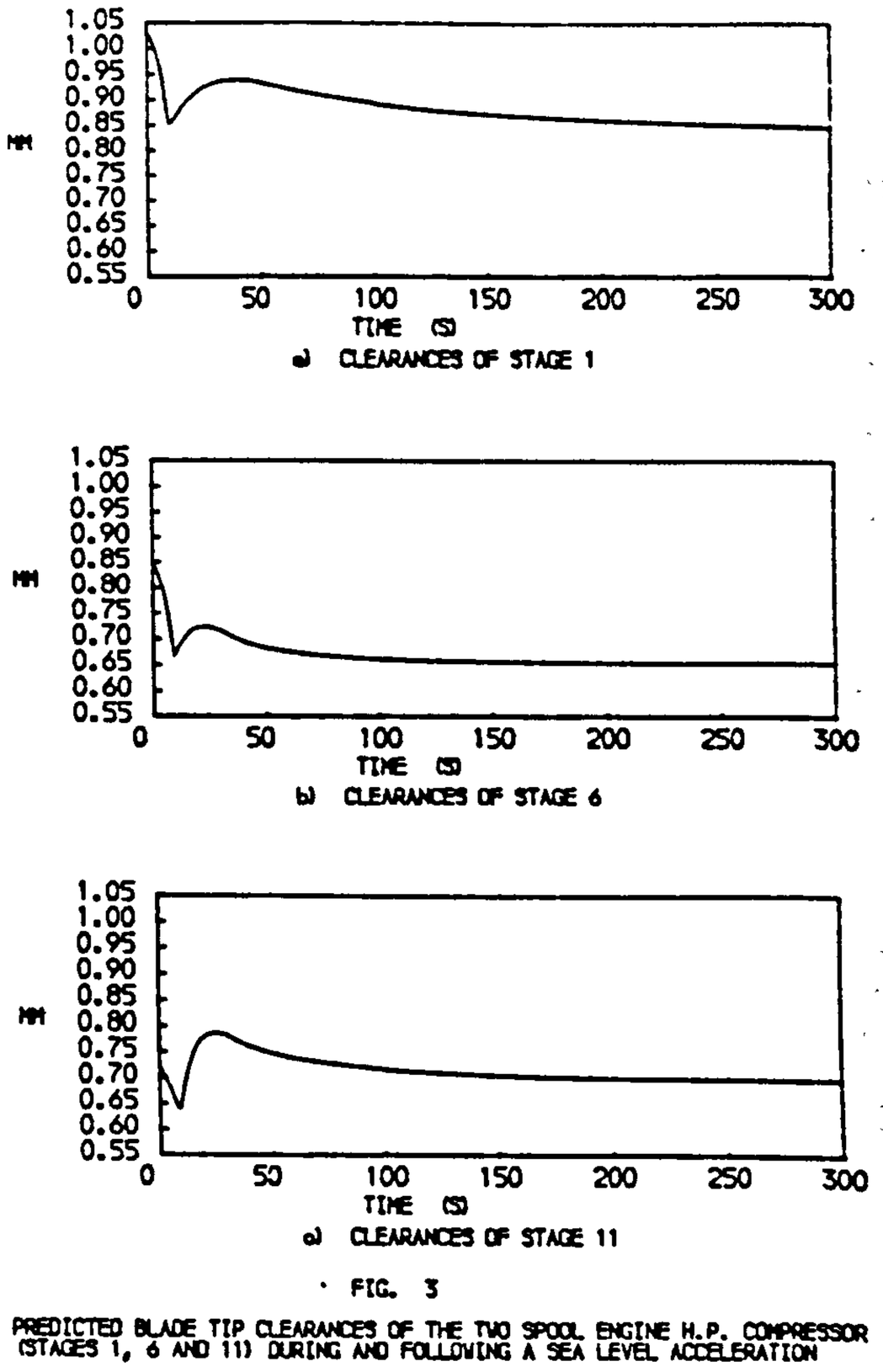

FIG. 3

PREDICTED BLADE TIP CLEARANCES OF THE TWO SPOOL ENGINE H.P. COMPRESSOR (STAGES 1, 6 AND 11) DURING AND FOLLOWING A SEA LEVEL ACCELERATION

It is interesting to notice that for Stage 1 the clearance of the end of the thermal transient is smaller than that at the end of the speed transient, for Stage 6 they are similar, while for Stage 11 the opposite to Stage 1 is the case. This is due to the effect of the air inside the shaft, this, as stated above, being drawn from between the fifth and sixth stages of the Compressor. Therefore the air inside the shaft is hotter than the core air for Stage 1, the two air streams are at similar temperatures for Stage 6 and the core air is hotter than the shaft cooling air at Stage 11. The cooling air dominates the expansion of the disc, whereas the core air dominates the expansion of the blades and the casing. This explains the different end-points of the clearance paths as compared to the clearance at the end of the speed transient.

To indicate the relative rates of thermal response of the various components, the time constants for the major components of Stage 5 are shown in Tables 1 and 2 at three instants during the acceleration and three instants during a deceleration respectively. The heat transfer coefficient is the only parameter affecting this constant, since, for a given

configuration, the geometry is fixed and the material property changes due to variations in temperature are small. It is seen that the changes in the time constants of the disc hub and the diaphragm follow a similar pattern. A small difference in the pattern of these two sections arises because in this arrangement the diaphragm consists of two surfaces perpendicular to the axis of rotation, while the hub has an additional surface parallel to the axis of rotation, the latter affecting the average magnitude of the heat transfer coefficient for this section. A different pattern can be observed in the time constants for the disc outer section and the blades. Here the two sections are subjected to the same fluid flow. Also it was found that although different correlations were used to evaluate the heat transfer coefficients, these were of similar magnitudes. This explains the similar behaviour of these two sections. The casing on the other hand is influenced by two fluid flows and so exhibits a pattern peculiar to itself.

Table 1.

Stage 5, Two-spool Bypass
Engine-H.P. Compressor.

Time constants during an acceleration
at sea level, static.

Time in transient	2s	6s	10s
Disc hub	108s	66s	37s
Disc diaphragm	38s	17.8s	9.6s
Disc outer section	12.7s	9.0s	5.5s
Blade	2.3s	1.6s	1.0s
Casing	10.4s	7.6s	4.8s

Table 2.

Stage 5, Two-spool Bypass
Engine-H.P. Compressor.

Time constants during a deceleration
at sea level, static.

Time in transient	3s	6s	10s
Disc hub	60s	55s	62s
Disc diaphragm	21s	20s	23s
Disc outer section	13.1s	15.0s	26.0s
Blade	2.0s	2.3s	3.5s
Casing	6.1s	4.9s	12.5s

3. SIMPLIFIED METHOD TO BE INCLUDED IN TRANSIENT PROGRAM

It would be excessively cumbersome to include each individual blade row of each compressor into the transient program for the engine. The use of single "equivalent" stages instead of complete components would be highly desirable. A single equivalent stage can give satisfactory heat transfer rates (3). A single equivalent stage has therefore been developed for the H.P. Compressor described in the previous section, with the aim of making simple predictions of tip clearance changes and associated efficiency changes. The single equivalent stage uses averaged dimensions of the 12 stages and averaged material properties of specific heat, thermal expansion coefficient, Young's modulus and density. A further simplification of the modelling of the disc is described below.

3.1. Thermal Growth

The subdivision of the equivalent disc as described in Section 2 is retained for the calculation of thermal effects. As in the previous more complex model. the various rotor sections are assumed individually to have infinite thermal conductivity, material properties are assumed to be constant throughout the relevant temperature range, although air and gas properties are still calculated as a function of temperature. The process ensuring continuity of the radial dimension of the disc section interfaces however is eliminated. Instead an average disc temperature is found by using Eq. (5).

$$T_{av} = \Sigma V_j T_j / \Sigma V_j \qquad (5)$$

The thermal expansion of the "characteristic" disc is thus obtained. It will be shown later that this approximation provides adequate accuracy.

With regard to the thermal growths of the blades and the casing, the method of calculation is the same as described in the previous section.

3.2 Centrifugal Growth

3.2.1 Disc. The centrifugal growth is simplified for this model by calculating the expansion of a disc of the same inner and outer radii and of a uniform thickness equal to the minimum diaphragm thickness. To check the validity of this simplification, growths were compared with those obtained from finite element analysis. It was found that the introduction of the same factor of 1.3 as in section 2.2.1 gave satisfactory agreement. The resulting expression for centrifugal growth of the disc is given in Eq. (6), where the first term in brackets represents the pull of the blades on the disc.

$$\Delta R_d = 1.3 R_o \omega^2 \left[\frac{\Sigma M_b}{l} \frac{(R_o^2+R_i^2)}{R_o^2-R_i^2} + \rho_d (R_i^2(3+\sigma)+R_o^2(1-\sigma)) \right] \qquad (6)$$

where the characteristic length, l, is the diaphragm thickness.

In Section 2.2 pressure effects were found to be very small, so they are ignored in this simplified analysis.

3.2.2 Blades. The centrifugal growth of the blades is calculated as described in Section 2.2.2. Hence Eq. (7) is obtained from integral calculus.

$$\Delta H_b = (R_{bt}^3/3 + R_h^3/6 - R_{bt}^2 R_h/2)\rho_b \omega^2 / E_b \qquad (7)$$

3.3 Efficiency Loss

The component being considered is simplified to a single-stage equivalent compressor or turbine (4). The tip clearance at that condition is estimated as indicated above, and the efficiency reduction relative to zero tip clearance is found from the relation (13):

$$\Delta\eta = \frac{0.7\lambda\psi}{\cos\beta_m}\left[1 + 10\left(\frac{\varphi\lambda\Lambda}{\cos\beta_m}\right)^{0.5}\right] \qquad (8)$$

As an illustration, the efficiency changes in the H.P. Compressor of the Two-spool Bypass Engine, relative to zero tip clearance, have been calculated during a sea level acceleration transient using the simplified procedure described above. The results, labelled "simplified" are shown in Fig. 4. For comparison, the predictions of the single equivalent stage model using the more precisely calculated disc expansion, as described in Paragraph 2.2.1, are shown alongside, marked "one stage". The efficiency changes that are predicted by treating all twelve stages individually are also given, labelled "engine". It can be seen that the results of the two simplified methods are in close agreement with the results from the stage by stage analysis, discrepancies for the "simplified" model never exceeding 0.3 per cent of efficiency. The "simplified" procedure has therefore been adopted as satisfactory for use in the engine transient program.

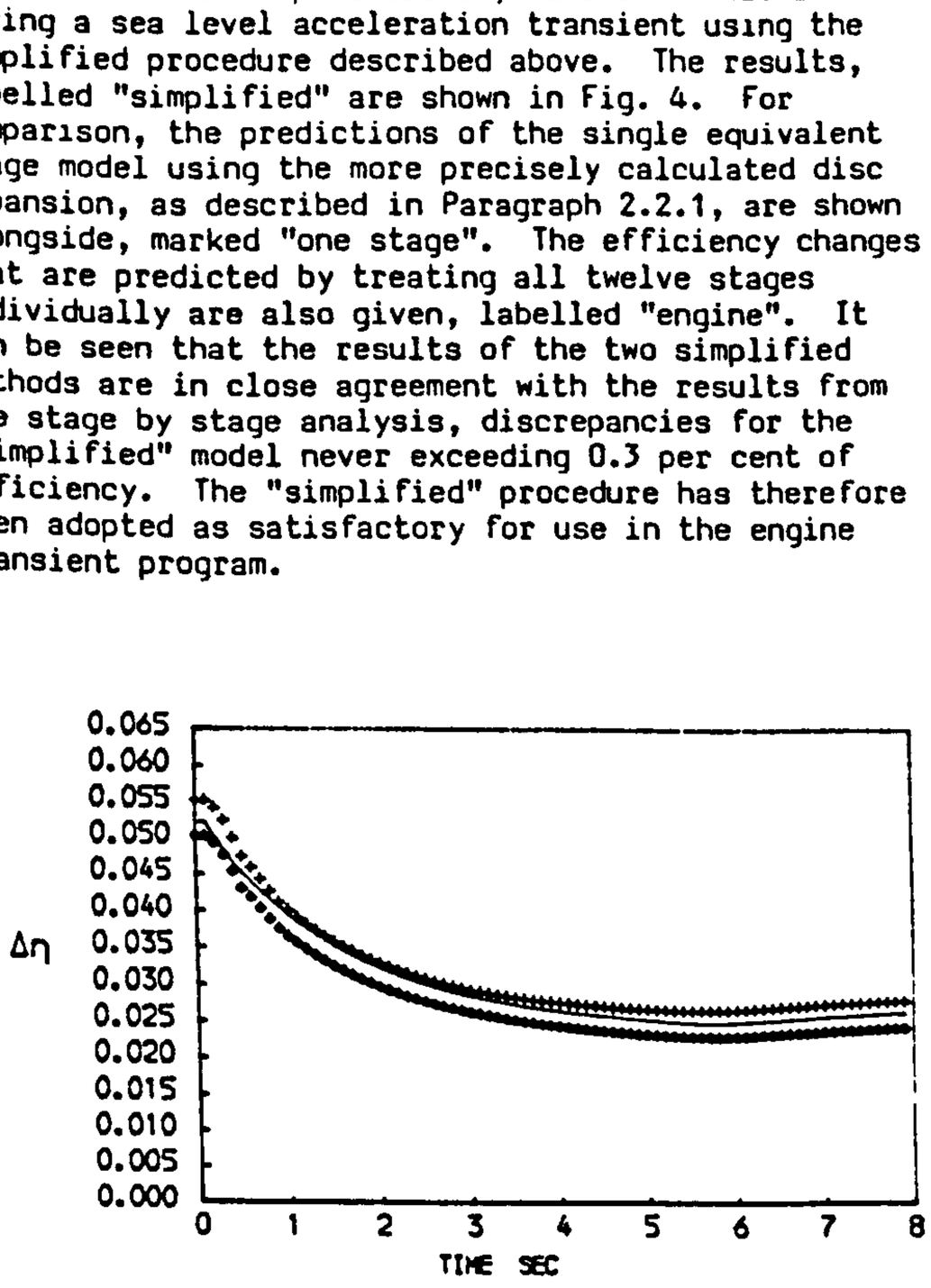

FIG. 4
EFFECTS OF CLEARANCE MOVEMENTS ON H.P. COMPRESSOR EFFICIENCY
EFFICIENCY LOSS COMPARED TO ZERO CLEARANCE
MODELS. ENGINE + ONE STAGE • SIMPLIFIED—

The next step in the analysis is the calculation of the efficiency loss compared to the stabilised value of clearance at that particular speed and inlet conditions. Stabilised clearances at the desired conditions are evaluated using the same methods and hence stabilised values of effiency loss due to clearance openings are obtained. A difference in efficiency is found by subtracting the stabilised efficiency loss from the transient efficiency loss, and the efficiency of the component obtained from the characteristics may then be modified accordingly. This difference is shown in Fig. 5. It is seen that in this compressor, the changes in efficiency are very small.

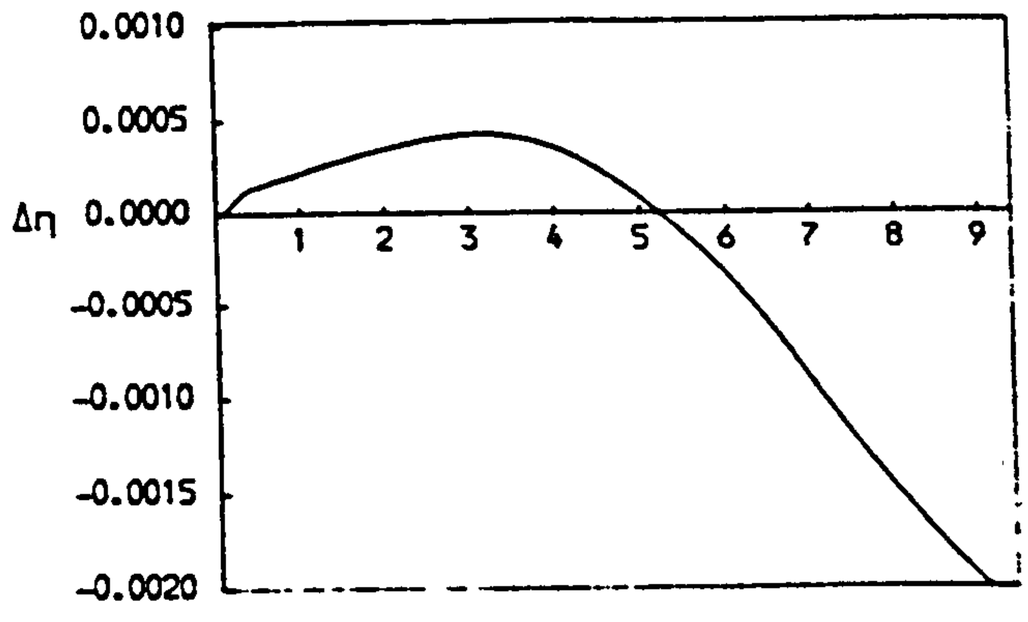

FIG. 5
EFFECTS OF CLEARANCE MOVEMENTS ON COMPRESSOR EFFICIENCY
EFFICIENCY CHANGE DUE TO DIFFERENCE BETWEEN
TRANSIENT AND STABILISED CLEARANCES

4. APPLICATION TO THE TWO-SPOOL BYPASS ENGINE

4,1 H.P. Compressor

The transient program of reference (3) has been extended to include the models described. By means of these the clearance of the "simplified" equivalent single-stage of the H.P. Compressor is calculated at each time step both in the transient and for steady running at that speed and compressor conditions. The clearances during the transient predicted by this simplified model are shown in Fig. 6. The predictions of the single-stage equivalent model using the more precise expansion (Paragraph 2.2.1) are also shown on this Figure (labelled "one stage"), confirming that the "simplified" model (which the engine transient program uses) and the "one stage" model are in good agreement.

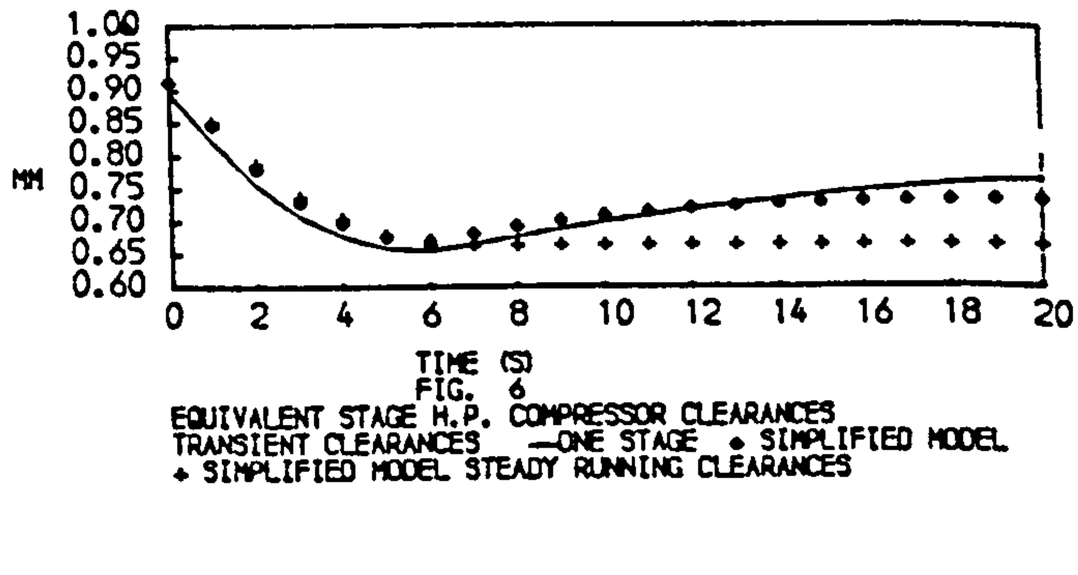

FIG. 6
EQUIVALENT STAGE H.P. COMPRESSOR CLEARANCES
TRANSIENT CLEARANCES —ONE STAGE • SIMPLIFIED MODEL
+ SIMPLIFIED MODEL STEADY RUNNING CLEARANCES

The modified efficiency is then used for calculating the next incremental acceleration in the transient. As indicated on Fig. 5, the changes in efficiency of the compressor of this engine are very small, and on average give improved efficiencies. Their effects on the acceleration are slight, reducing acceleration times by less than 1 per cent.

4.2 H.P. Turbine

The models for the blade/disc arrangement can accommodate both shrouded and unshrouded blades - in the former case the centrifugal expansions are greater due to the weight of the shroud. Also, the thermal model for the blades can incorporate the cooling arrangement, using the simple relation:

$$T_{mf} = T_g - \epsilon (T_g - T_c) \qquad (9)$$

where T_{mf} is the final metal temperature if that transient condition were maintained (this is the temperature which can be regarded as driving the heat transfer) and ϵ is the cooling "effectiveness" (a value of 0.6 being typical for a blade cooled by inner passageways).

Predicted tip clearances in the H.P. Turbine during a sea level acceleration are shown in Fig. 7. The predictions for two alternative blading arrangements are presented. In the first, the blades are unshrouded and uncooled (labelled "simple") while in the second they are both shrouded and cooled (labelled "S & C"). Both arrangements start with the same cold clearance. It can be seen that the additional expansion produced by the weight of the shroud is approximately balanced by the reduction in thermal expansion that results from cooling the blades.

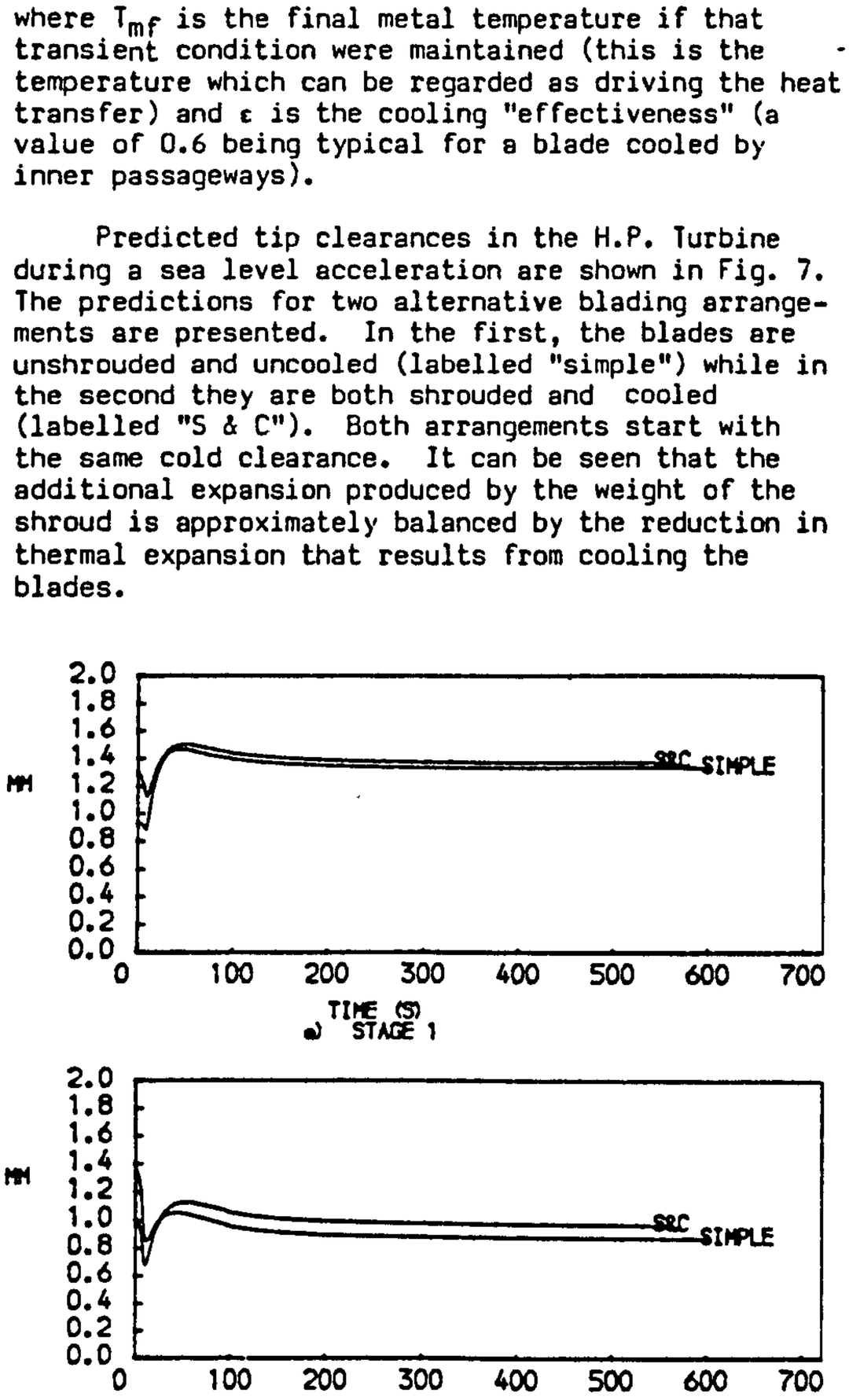

FIG. 7
CLEARANCES OF A TWO SPOOL BYPASS ENGINE H.P. TURBINE
SIMPLE. SIMPLE BLADE S&C. SHROUDED AND COOLED BLADE

In the real Engine the blades and nozzle guide vanes are shrouded and the early rows are cooled. For this scheme, the tip clearance movements have been determined for each row. These movements were transferred into efficiency changes using the correlation of Eq. (8), with the suggested modification (14) of reducing the efficiency changes by 80 per cent for shrouded nozzle guide vanes. It is estimated that a smaller reduction, say 50 per cent, should be applied to the efficiency changes for shrouded blades. The resulting efficiency values during the transient are only slightly different from the corresponding steady-running values, the difference being in the direction of improved efficiency. Inclusion in the transient program produced very small reductions in acceleration times - less than 1 per cent. None the less, in view of the assumptions that have been made in the study of the turbine, further work should be carried out to improve the analysis.

In view of the small effects resulting from inclusion of transient tip clearance changes in the H.P. Compressor and H.P. Turbine, it was considered unnecessary to make similar analyses in the L.P. Compressor and L.P. Turbine, which are subjected to less rigorous temperature changes.

4.3 Procedure for Estimation of Seal Clearance Movements

The methods and model used for tip clearance can be adapted for making estimates of seal clearance movements during transients. In the Two-spool Bypass Engine two important seals are the H.P. Compressor 12th Stage Outer Seal and the H.P. Cooling Air Seal on the H.P. 1 Turbine Disc.

4.3.1 H.P. Compressor 12th Stage Outer Seal. The movements of this Seal have been studied previously by Lim (15) using finite difference methods. The predictions of Lim and of the present methods are compared on Fig. 8(a). The agreement is sufficiently close to allow the present model to be used for seal clearance predictions during transients. It is seen that during most of the acceleration speed transient, seal clearances exceed their maximum speed stabilised values by more than 30 per cent.

4.3.2 H.P. Cooling Air Seal on H.P.1 Turbine Disc. The movements of this Seal have been studied previously by finite difference methods (8). The results of reference (8) are compared to the present methods in Fig. 8(b). It is seen that the seal clearances during the acceleration speed transient exceed the maximum speed stabilised clearance by about 100 per cent.

4.3.3 Effects of Seal Clearance Movements in Transients. In the early programs for predicting the acceleration rates of gas turbines it would probably be assumed that cooling and bleed air flows remained a constant fraction of the core air flow during the transient. However it has been illustrated that seal clearances during the speed transient can be very much higher than the maximum speed or the design clearances. Consequently these cooling and bleed flows, expressed as fractions, will exceed the design fractions.

Allowances for the clearance movements of the H.P. Compressor 12th Stage Outer Seal and of the H.P. Cooling Air Seal on the H.P. 1 Turbine Disc have been included in the engine transient program, and the results for a sea level acceleration are illustrated in Fig. 9. For the acceleration, the fuel flow, as a non-dimensional group, was scheduled as a function of the H.P. Compressor pressure ratio. It is seen that the additional loss of air through these seals during the transient causes a significant increase - about 6 per cent - in the acceleration times.

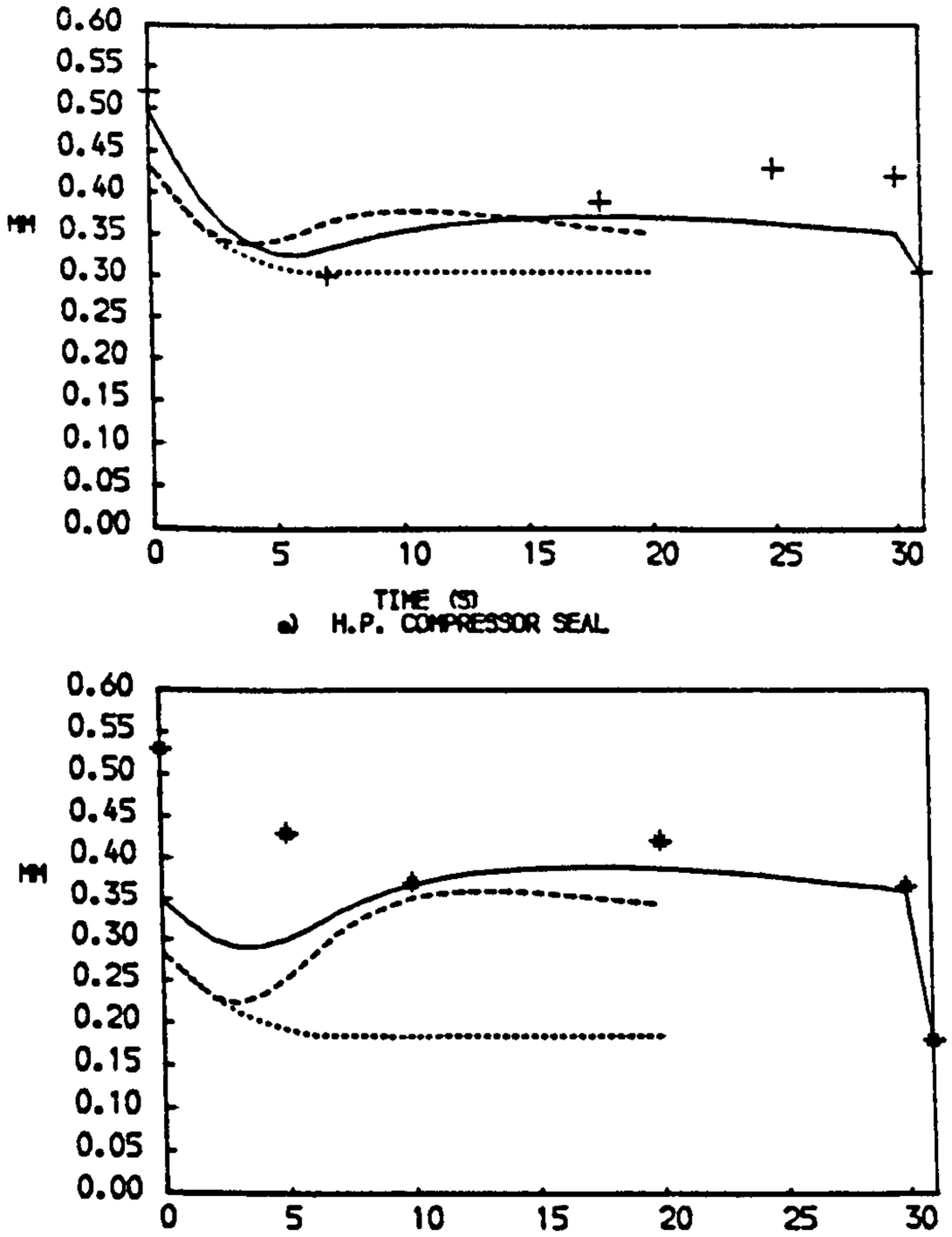

FIG. 8
CLEARANCES OF TWO SEALS OF THE TWO SPOOL BYPASS ENGINE WITH MIXED EXHAUSTS DURING AN ACCELERATION
—FULL MODEL TRANSIENT CLEARANCES
SIMPLE MODEL CLEARANCES, TRANSIENT - -, STABILISED···
ANALYSIS OF, REF. 15 +, REF. 8 ◆

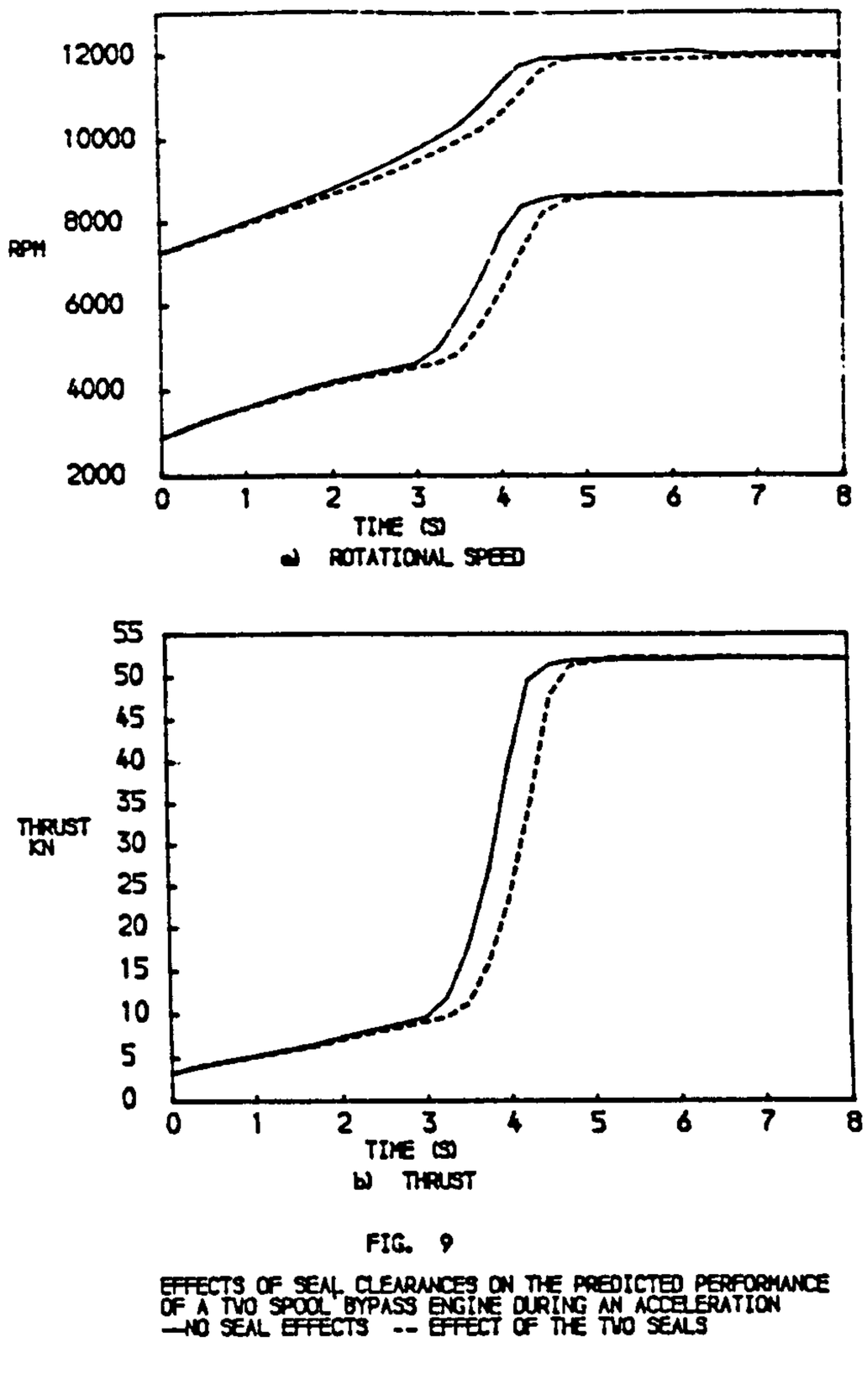

FIG. 9
EFFECTS OF SEAL CLEARANCES ON THE PREDICTED PERFORMANCE OF A TWO SPOOL BYPASS ENGINE DURING AN ACCELERATION
—NO SEAL EFFECTS -- EFFECT OF THE TWO SEALS

4.4 Decelerations

In decelerations the "heat soak" period is much longer because the reduced rotational speed at the end of the transient results in much lower values of the heat transfer coefficients. All the components were studied in both accelerations and decelerations, and no rubs were encountered.

4.5 Control of Tip Clearances during Transients

When considering, for example, the transient response of the components (disc, blade, casing) of the H.P. Compressor, it is realised that the responses of the discs would have been different, hence the transient tip clearances would have been different, if the air in which the discs rotate had been drawn from, say, a later stage of the H.P. Compressor than at present. This realisation offers the designer another method of controlling tip clearance changes.

4.6 Computing Times

The increase in computing times is not large for the inclusion of the model described in a typical engine transient program. For example, computing times were about 15 per cent longer when the model was used to calculate and apply clearance paths in three different components during an engine transient.

5. CONCLUSIONS

A simple model has been developed for calculating clearances of seals and blade tips, and for determining their effects on engine response during a transient. It also enables the study of the effects of changing materials in the engine and of altering the pattern of cooling. The procedure has been used to show that changing the cooling of compressor discs, for example, alters the tip clearance response.

Seal clearances have a larger effect than compressor blade tip clearances on the transient performance of the Two-spool Bypass Engine considered.

Further work is being carried out to assess more accurately the turbine tip clearances and their effects during a transient.

The increase in computing time is not large, amounting to about 15 per cent when the model was used to calculate and apply clearance paths in three components during the transient.

6. ACKNOWLEDGEMENT

The authors wish to thank staff of Rolls-Royce Limited and colleagues at the University of Glasgow for provision of data, for valuable comment and for encouragement.

7. REFERENCES

1. Thomson, B., "Basic Transient Effects of Aero Gas Turbines." AGARD Conference Proceedings 151, 1975.
2. Maccallum, N.R.L., "Thermal Influences in Gas Turbine Transients, Effects of Changes in Compressor Characteristics." ASME Paper 79-GT-143, 1979.
3. Maccallum, N.R.L., "Further Studies of the Influence of Thermal Effects on the Predicted Accelerations of Gas Turbines." ASME Paper 81-GT-21, 1981.
4. Pilidis, P., and Maccallum, N.R.L., "Models for Predicting Tip Clearance Changes in Gas Turbines." AGARD Conference Proceedings 324, 1982.
5. Bayley, F.J., and Owen, J.M., "The Fluid Dynamics of a Shrouded Disc System with a Radial Outflow of Coolant." Journal of Engineering for Power, Series A, Vol. 92, 1970, pp.335-341.
6. Haynes, C.M., and Owen, J.M., "Heat Transfer from a Shrouded Disc System with a Radial Outflow of Coolant." Journal of Engineering for Power, Series A, Vol. 97, 1975, pp.28-36.
7. Kapinos, V.M., "Heat Transfer from a Disc Rotating in a Housing with a Radial Flow of Coolant." Journal of Engineering Physics, Vol. 8, 1965, pp.35-38.
8. Maccallum, N.R.L., "Transient Expansion of the Components of an Air Seal on a Gas Turbine Disc." SAE Paper 770974, 1977.
9. Neilson, W., "The Finite Element Method in Transient Heat Conduction." Final Year Project, University of Glasgow, April 1973.
10. Halls, G.A., "Air Cooling of Turbine Blades and Vanes." Lecture to AGARD, Varenna, Italy, 1967.
11. Maccallum, N.R.L., "Effect of Bulk Heat Transfer in Aircraft Gas Turbines on Compressor Surge Margins." Heat and Fluid Flow in Steam and Gas Turbine Plant. Inst. Mech. Engineers, London 1974, pp.94-100.
12. Tachibana, F. and Fukui, S., "Convective Heat Transfer of the Rotational and Axial Flow between Concentric Cylinders." Bull. of Japanese Society of Mech. Engineers, Vol. 7, No. 26, 1964.
13. Lakshminarayana, B., "Methods of Predicting the Tip Clearance Effects in Axial Flow Turbomachinery." Transactions of the ASME, Journal of Basic Engineering, Vol. 92, Sept. 1970, pp.467-480.
14. Breugelmans, F.A.E., "Industrial Compressors, Aerodynamic and Mechanical Factors Affecting the Surge Line. Tip Clearance Effects in Axial Flow Compressors." Lecture Series 91, Von Karman Institute for Fluid Dynamics, 1976.
15. Lim, T.J., "An Investigation into the Seal Clearance and Temperature Response During Transient of the Stage 12 Seal of the H.P. Compressor of a Twin-Spool Bypass Jet Engine." Final Year Project, University of Glasgow, April 1980.

Publication 29

Reprinted From

SYSTEMS & CONTROL ENCYCLOPEDIA

Theory, Technology, Applications

Editor-in-Chief

Madan G Singh

University of Manchester
Institute of Science and Technology,
Manchester, UK

PERGAMON PRESS

OXFORD · NEW YORK · BEIJING · FRANKFURT
SÃO PAULO · SYDNEY · TOKYO · TORONTO

Gas Turbines in Power Generation

Gas turbines provide one method of supplying mechanical power from a thermal source. Simple open-cycle gas turbines have many advantages as a means of providing power. They are light, of low capital cost, require no water and can be brought quickly onto load. Present plants need reasonably high-quality fuels (gaseous or liquid), but future plants will be able to use coal.

1992

Gas turbines are well suited to providing heat in addition to power. They may also be effectively used with a steam-raising circuit in the exhaust to provide additional power, with very competitive overall efficiencies.

1. Principle of Cycle

All current gas turbines operate on an approximation to the constant-pressure, or Brayton, cycle (Fig. 1). The working gas is compressed from point 1 to point 2, has heat added to it at constant pressure (to point 3) and is then expanded to the initial pressure (to point 4). This expansion invariably takes place in a turbine (or turbines), hence the name gas turbine. In the ideal simple cycle the compression and expansion are reversible and adiabatic, hence isentropic. Finally the working gas is "cooled" at constant pressure to the initial temperature. If the original gas is to be reused, this cooling is carried out in a heat exchanger and the cycle is referred to as a closed cycle. However, many gas turbines use air drawn from the atmosphere as the working gas, so the final constant pressure "cooling" occurs in the atmosphere; this is the open cycle.

2. Early Development

Initially two types of gas turbine were studied. The first operated on the constant-pressure cycle, described above, while the second employed an explosive combustion process for the heat addition, in which pressure rose. Turbines of these two types had their first runs in 1905 and 1906, respectively. The efficiencies were <0.05, significantly less than those of other contemporary heat engines. Theoretically the explosion turbine offered higher efficiency than the constant-pressure cycle turbine, but practical difficulties with nonreturn valves prevented this benefit from being realized. Continuous development of the constant pressure cycle turbine soon brought its performance ahead of

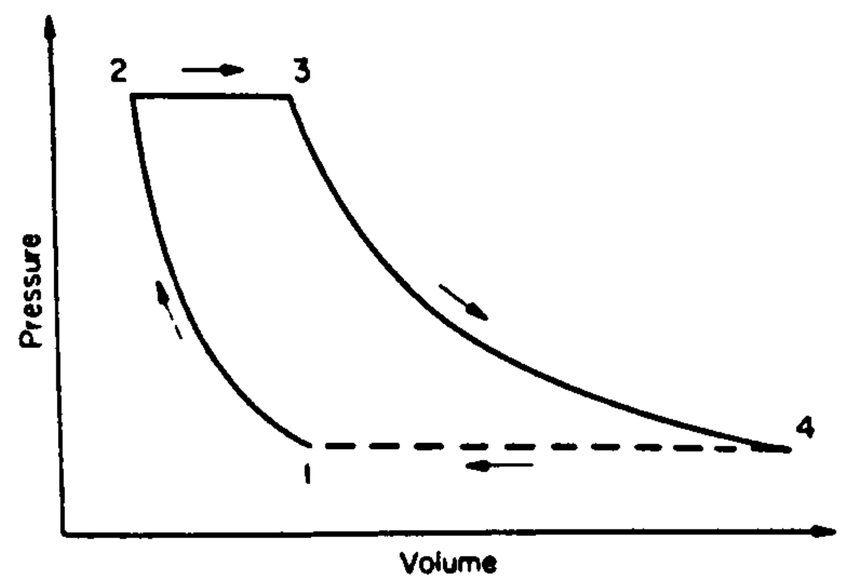

Figure 1
Constant-pressure or Brayton cycle

that of the explosion turbine. All gas turbines built since the mid-1930s have operated on the constant-pressure cycle. The first major gas turbine power plant, a closed cycle unit of 2.0 MW(e) capacity, was commissioned in Switzerland in 1939.

3. *Performance of Cycles*

The efficiency of the practical approximation to the simple cycle, without exhaust heat exchange, described in Sect. 1, is a function of the compressor and turbine efficiencies, of the compression pressure ratio and of the temperature at the inlet to the turbine. A typical relationship is shown in Fig. 2. In this example the working gas is air, the compressor and turbine have equal isentropic efficiencies of 0.8 or 0.9 (current practical range) and pressure losses cause the turbine expansion ratio to be 0.94 of the compressor pressure ratio.

Cycle efficiencies are greatly improved by increases in compressor/turbine component efficiencies, and are also improved, although less markedly, if cycle pressure ratio and turbine inlet temperature are raised in conjunction. Specific work output is considerably increased by raising the turbine inlet temperature. Current gas turbines can attain overall cycle efficiencies of 0.34–0.35.

Reduced fuel consumption, or better utilization of the energy released by the fuel, can be achieved in a variety of ways. One method, called regeneration, uses the comparatively hot gases exhausting from the turbine to heat the air after leaving the compressor and before entering the combustion chamber. This is of value only with comparatively low-pressure-ratio cycles, that is, those with a ratio of, say, less than 12 or 15 to 1 (depending on the turbine inlet temperature being used).

A second method uses the exhaust from the turbine for steam raising and subsequent power production. This is called a combined cycle. Thermal efficiencies for the combined plant in the range 0.46–0.48 are attainable.

In many applications a heat load has to be satisfied in addition to a mechanical load. The gas turbine is well suited for this, as the exhaust gases from the turbine can be used to supply the heat load. This is sometimes called combined heat and power (CHP). The name cogeneration may also be used, though it has been applied to the combined cycle as well.

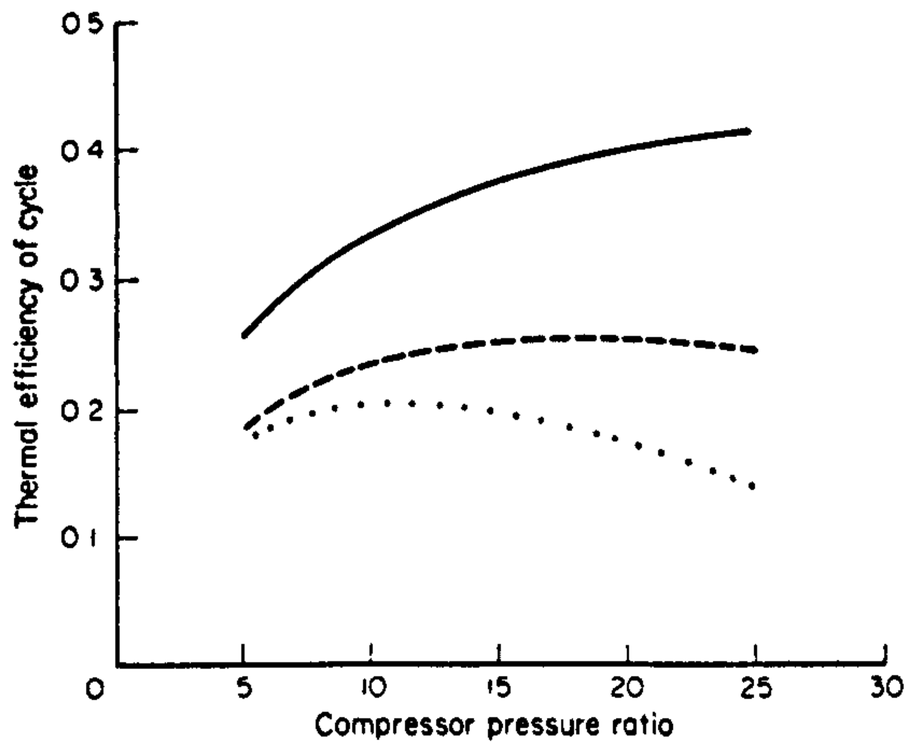

Figure 2
Cycle thermal efficiency as a function of other factors: ——, $\eta = 0.9$, $T_t = 1400$ K; – – –, $\eta = 0.8$, $T_t = 1400$ K; . . . . $\eta = 0.8$, $T_t = 1200$ K (η is compressor and turbine efficiency, T_t is turbine inlet temperature)

4. *Industrial Gas Turbines*

This name is given to all gas turbines which are not used for aircraft propulsion. Applications of industrial gas turbines include driving electrical generators, driving compressors and pumps and ship propulsion.

Current industrial gas turbines emanate from one of two different design philosophies. In the first the engine is designed solely for the above type of industrial use. Thus it must meet the requirement of long periods between major overhauls, say 100 000 h. The industrial gas turbines of the second type are derived from aircraft engine designs, which are lighter and have comparatively short times between overhauls. To adapt to the industrial application, the aircraft engine designs are modified by using heavier bearings and by "derating"—operating at lower turbine inlet temperatures. Also, the combustion system may be altered to utilize cheaper fuels.

4.1 *Shaft Arrangements*

The simplest shaft arrangement is illustrated in Fig. 3, where there is a single shaft on which are mounted the compressor and the turbine, and the load to be driven is coupled directly, or via gearing, to this shaft.

A widely used alternative has two turbines, the first to drive the compressor and the second, on a separate shaft, to drive the load (Fig. 4). This scheme is called a two-shaft gas turbine or a free power turbine. Units of this type are particularly suited to applications which require high torque outputs on startup or at low

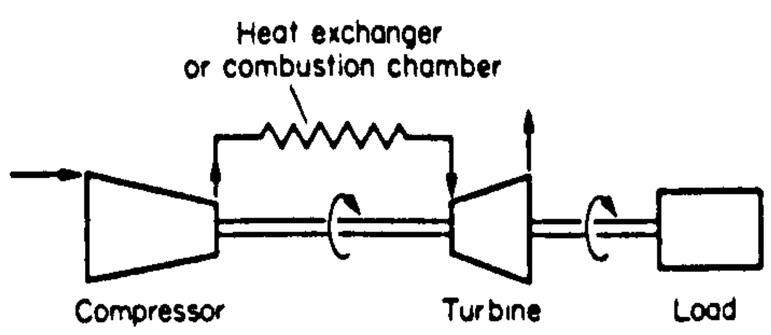

Figure 3
Single-shaft arrangement

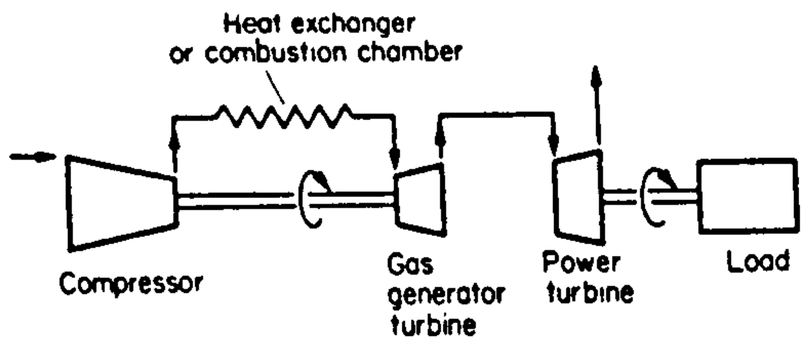

Figure 4
Two-shaft or free power turbine arrangement

rotational speeds relative to design speed. The name "gas generator" may be given to the section of the engine which comprises the compressor, the combustion chamber and the turbine which drives the compressor.

In some aero-derived gas generators, the compressions and expansions are split, the high-pressure compressor being driven by the high-pressure turbine and the low-pressure compressor by the low-pressure turbine. The shafts are coupled aerodynamically but not mechanically, and the scheme is referred to as a "two-spool" arrangement. It was adopted for high-pressure-ratio aircraft engines to achieve acceptable running and acceleration over a wide speed range without encountering surge.

4.2 Turbines

In the smallest gas turbines, for example for automotive and fire-pump applications, a radial in-flow turbine is used. The behavior is that of the centrifugal compressor in reverse.

For medium and large power units an axial flow turbine is used. The pressure ratio per stage is much higher than for an axial flow compressor—a single-stage turbine is able to drive a six- or seven-stage axial flow compressor handling the same mass flow.

4.3 Compressors

For large gas flows, axial flow compressors are used. These comprise a series of stages, each consisting of a moving and a stationary row of blades. The gas enters each row, whether moving or stationary, with a high relative velocity and is slowed down in the widening, or diffusing, passage between the blades. This deceleration gives an increase in pressure. If sufficient stages (say fifteen) are used, pressure ratios of 12 or more may be achieved.

Centrifugal compressors may be used for the smaller engines, which need lower gas flows. Angular momentum is given to the gas as it flows outwards through the passages of the impeller. Some pressure rise occurs across the impeller itself and the remainder is achieved in decelerating the high-velocity gas after it leaves the impeller tip. Pressure ratios across typical single-stage centrifugal compressors are in the range 4–8.

Axial flow compressors, which are designed for high gas flow rates, have higher efficiencies than centrifugal compressors, but this advantage disappears when designing to compress smaller flow rates.

4.4 Closed-Cycle Gas Turbines

The heat to operate these cycles is provided external to the working gas, and transferred to the gas in a heat exchanger. Any convenient gas, including air, may be used as the working gas. A gas such as helium has the advantage over air of requiring smaller turbomachinery; this saving in capital cost more than counterbalances the cost of the helium if large plants, say >50 MW(e), are considered.

Helium closed-cycle gas turbines are proposed for obtaining power from advanced gas-cooled nuclear reactors. No intermediate fluid would be needed.

5. Fuels and Combustion Chambers

A wide range of fuels may be used as heat sources, for example, natural gas, blast-furnace gas, distillate oils, residual oils, peat and also nuclear and solar energy.

If the heat results from a combustion reaction giving reasonably clean product gases, such as when using natural gas or distillate/residual oil fuels, atmospheric air may be used as the working gas and the fuel is burned in this air after its compression (i.e., the open cycle). If the products of combustion are dirty or corrosive, as in conventional burning of coal or blast-furnace gas, combustion has to be external to the working gas, which may follow either a closed or an open circuit. Schemes are now being studied in which coal is burned in the working gas (air) in a fluidized bed.

In the open-cycle gas turbine with internal combustion, the fuel is burned in the working air after it has been compressed. In present designs this is carried out in one or more combustion chambers. The combustion zone is surrounded by a flame tube or liner. Only a fraction of the total air is admitted to the primary combustion zone, this being done by an arrangement of jets, possibly with swirl, which set up recirculating flows. The fuel (gas or liquid) is injected into this zone and, once ignited from an external source, the flame is stabilized by the recirculation. The flame and combustion products are subsequently mixed with the remainder of the air to give a gas flow which is at a temperature acceptable to the turbine materials.

6. Materials of Construction

Considerable progress has been made in developing suitable materials for the various parts of the gas turbine. In axial flow compressors, steel or nickel alloys are widely used for blades, although some aero-derived engines use titanium or aluminum in early stages, these having the advantage of lightness. The material for shafts and disks is usually steel, although aero-derived engines may use titanium for the front stages and nickel alloys for the hotter rear stages.

As explained in Sect. 3, high gas temperatures at the inlet to the turbine are needed for high-specific-output, high-efficiency plants. This goal is achieved by using special alloys for the nozzle vanes and blades of the turbine and by cooling these vanes and blades, usually with high-pressure air drawn from the compressor delivery. For blades, nickel-based alloys are widely used, as they possess good creep strength. Either nickel-based or cobalt-based alloys are used for nozzle vanes. The life of blades and vanes can be greatly extended by diffusing into the surface a powder which may include aluminum, platinum or chromium. Such coatings impart excellent high-temperature corrosion resistance to the blades. Turbine disks can be made from a wide range of steels or, for the highest-temperature locations, nickel-based superalloys.

7. *Control*

Controls on industrial gas turbines are introduced so that the required output is provided, at the correct speed, without causing damage to the gas turbine. These controls operate on the fuel flow and possibly on certain variable-geometry schemes in the engine. The controls are activated by sensors on the shaft speeds and on the temperature of the gases leaving the turbine. The latter sensor is needed to prevent excessive temperatures from occurring in the turbine, and the former to maintain the correct speeds of the output shaft and of the gas generator shaft (for free power turbine arrangements). The most common variable-geometry scheme, used in free power turbine engines, operates on the throat area of the nozzle guide vanes of the power turbine. This area is controlled by the temperature sensors in the exhaust gas leaving the turbine. The fuel flow to the combustion chamber is controlled by the power demand, or for constant-output-speed applications, by the power turbine speed. At part-load, the throat area of the power turbine's nozzles is reduced to maintain the turbine gas temperature and so maintain efficiency.

See also: Fossil-Fuel Energy; Electric Generators, Rotating; Power System Operation

Bibliography

Coats R 1978 The efficient use of gas turbines for production. *Chart. Mech. Eng.* **25**(4), 51–58
Cohen H, Rogers G F C, Saravanamuttoo H I H 1972 *Gas Turbine Theory*. Longman, London
Harman R T C 1981 *Gas Turbine Engineering*. Macmillan, London
Meetham G W (ed.) 1981 *The Development of Gas Turbine Materials*. Applied Science, London
Page D M 1978 Gas turbines—the state of the art in Europe. *Chart. Mech. Eng.* **25**(4), 39–42
Starmer C 1980 Industrial gas turbines. *Chart. Mech. Eng.* **27**(4), 79–84

N. R. L. Maccallum

THE AMERICAN SOCIETY OF MECHANICAL ENGINEERS
345 E. 47 St., New York, N.Y. 10017

85-GT-209

Publication 30

A General Program for the Prediction of the Transient Performance of Gas Turbines

P. PILIDIS, Teaching Company Associate,
Caledonian Airmotive Ltd.,
Prestwick, Scotland.

N. R. L. MACCALLUM, Reader,
University of Glasgow,
Glasgow, Scotland.

ABSTRACT

The paper describes a general program which has been developed for the prediction of the transient performance of gas turbines. The program is based on the method of continuity of mass flow. It has been applied successfully to a wide range of aero gas turbines, ranging from single to three-spool and from simple jet to bypass types with or without mixed exhausts. The results for three of these engine types are illustrated. Computing times are reasonable, increasing with the complexity of the engine.

A parallel paper describes the inclusion of thermal effects in the prediction program.

NOMENCLATURE

a	exponent(variable)
A	flow area
C_1, C_2, C_3	constants
Cp	specific heat at constant pressure
f	function
f(e)	rate of convergence function (Equation 12)
$\dot{f}$	fuel flow rate
$\dot{m}$	air/gas mass flow rate
M	Mach Number
N	rotational speed
p	impulse function
P	static pressure
P_c	stagnation pressure
t	time
T	static temperature
T_c	stagnation temperature
v	velocity
X	a variable
γ	ratio of specific heats
ρ	density
ω	angular velocity

Subscripts

1	inlet
2	outlet
bp	bypass
cg	core gas
HPC	high pressure compressor
j	j'th section or shaft
t	at time t

1 INTRODUCTION

When the representation of a system is desired, a model is devised, and the behavior of this model is compared to that of the system. If the agreement is sufficiently close, the model is said to represent the system.

In the particular case of a gas turbine, the model is physical or mathematical. A physical model requires experimental work on a scaled version of the engine or its components. A mathematical model invariably involves computer programming, because of the lengthy calculations involved, particularly for the more complex engines.

The simplest modelling of the engines is by assuming a linear system to represent them. This is a good assumption for small changes from a given operating point and is the type of model used for engine control, and when studying the influence of disturbances at important points of the performance range. Thus a 'Small Change Matrix' of an engine for a given operating point or points can be obtained. However these models are not useful for large scale transients.

Another possible approach is the fundamental one, working from first principles. In this type of model, many engine parameters, in particular the pressure and temperature changes in each component, have to be

Presented at the Gas Turbine Conference and Exhibit
Houston, Texas — March 18-21, 1985

calculated from the engine's geometry. This approach suffers from the disadvantage of lengthy calculations and frequently the predictions are not of satisfactory accuracy.

A more convenient approach is to divide the above procedure into two steps. The first step is to predict the performance of the components, working from the engine's geometry. Once this has been accomplished the predicted characteristics are used for the calculation of the complete engine's steady state and transient performance. As the development proceeds and experimentally observed performance of the components becomes available, only the component performance maps need to be modified for continuing investigations. It is this type of approach that has been used in the present work, which is aimed at producing a general gas turbine prediction program.

A word of caution must be expressed at this point on the use of steady-running characteristics. However it is generally accepted (Refs.1,2)[1] that the characteristics of the components at a particular instant during a transient will differ from the characteristics observed in the steady state at the same non-dimensional speed. These changes in component performance, due to tip clearance changes, seal clearance changes and heat transfer effects have been incorporated in the program. However the inclusion of tip and seal clearance changes and thermal effects is not discussed in this paper, but is described in a parallel paper by the present authors (3).

2 THE METHOD

The method which has been developed uses the component characteristics as a basis for carrying out the performance analysis. There are two alternative procedures for carrying out the performance calculation, these being the method of 'intercomponent volumes' and the method of 'continuity of mass flow'. In the former, initial mass flows are guessed for each component and a pressure distribution through the engine is assumed. In general these mass flows will not be consistent and mass will either accumulate or diminish in the various intercomponent spaces during the subsequent short time increment. The calculation at each step is 'once-through' and requires no iterations. However very short time intervals must be used. By comparison, the method of 'continuity of mass flow' has to achieve consistency of mass flows at each section. Iterations are required, and the number of such iteration loops depends on the geometric complexity of the engine. Generally the method of 'continuity of mass flow' requires less computing time than the method of 'intercomponent volumes', but care is required in order to achieve efficient convergence of the computation. The predictions of the two procedures are in agreement, after the first few time intervals(4). The program described here uses the 'continuity of mass flow' method.

Several workers (5) - (11) have previously described procedures similar in principle to that adopted here (12). The brief outline which follows is given for completeness of this paper.

The object of the calculation procedure is to determine the acceleration that the engine will experience under various circumstances. The acceleration is a function of various parameters:

$$\frac{d\omega}{dt} = f(N_j, \dot{f}, P_{01}, T_{01}) \qquad (1)$$

The acceleration will also be a function of several other variables, such as component pressure ratios, temperature ratios, efficiencies,etc. As these parameters also depend on the rotational speed and the fuel flow, they are omitted from the above expression. The acceleration having been evaluated, the rotational speed for the next time interval is found by Euler's simple assumption that the acceleration remains constant for a particular time increment. Thus:

$$\omega_{t+dt} = \omega_t + (\frac{d\omega}{dt})_t \Delta t \qquad (2)$$

The flight speed and the altitude will define exactly the inlet conditions of the engine. Other parameters will be chosen arbitrarily to identify a point in the characteristics of the first component. The outlet parameters of the first component will define the inlet parameters of the next component. Using these procedures, the fluid variables at inlet to and outlet from each component can be calculated. Knowledge of these variables enables the calculation of a required nozzle area to discharge the flow (the program has been extended to incorporate reheat systems, if required.) In general, this required nozzle area will differ from the actual nozzle area provided. A variable, X, to be modified is then selected, and the relationship

$$\frac{dX}{X} = f(\frac{dA}{A}) \qquad (3)$$

is then used. In Eq. (3), A is the geometric area available to discharge the flow, and dA the error in the area produced by chosing the given state parameters for the current iteration. If the turbine is unchoked, the variable to be modified is the compressor pressure ratio. If the turbine is choked, the variable to be modified is the pressure ratio of the choked turbine - a previous iteration sequence will have adjusted the compressor pressure ratio to meet the capacity of the choked turbine. This variable, X, is then adjusted to bring the required nozzle area into agreement with the geometric nozzle area. Since the system is not linear, and the desired function f(dX/X) changes along the different running conditions of the engine, an iterative procedure is devised to obtain the equality between the required and the geometric nozzle areas. The desired function is assumed to be of the form:

$$f(\frac{dA}{A}) = (1 + \frac{dA}{A})^a \qquad (4)$$

where the exponent a is a variable which is continuously modified as will be outlined later.

For straight jets and for bypass engines with separate exhausts, the variable X, to be modified is chosen depending on engine configuration, the shape of the curves in the compressor characteristics and the state of the turbines. If a turbine is choked, the

1 Underlined numbers in brackets designate references at end of paper.

compressor pressure ratio is modified until the required value of the turbine capacity is obtained. Once this has been achieved, the variable to be adjusted to satisfy mass continuity at the final nozzle is the pressure ratio of the choked turbine nearest to this nozzle. The fluid velocity at this turbine is the sonic velocity, and pressure signals cannot be transmitted upstream of this point. Once the chosen parameter is modified, the process is repeated until the desired equality between required and geometric final nozzle areas is achieved. With the principle of mass continuity satisfied along the engine, the next step is to calculate the torque imbalance of the shaft(s). This torque imbalance then determines the instantaneous acceleration, which as previously stated is assumed to be constant for the given time step. The process is then repeated until a limiting time is reached.

For bypass engines with mixed exhausts there is an additional requirement. The principle of momentum conservation

$$\rho A v\, dv + A\, dP = 0 \qquad (5)$$

must be satisfied by the fraction of core gas and the fraction of bypass air to be mixed. For this purpose an infinitely thin control volume is set up in which all the mixing is assumed to occur. At entry to this control volume, the static pressures of the cold and the hot streams are equal. To obtain this equality in static pressure, an iteration loop similar to the one devised for the continuity principle has been introduced. The mixing process is assumed to occur without any momentum dissipation. If required, losses can be represented by means of a small pressure loss occurring at the final nozzle. Integrating Eq. (5) gives Eq. (6), in which momentum conservation is expressed as the impulse function being constant:

$$\sum PA\,(1 + \gamma M^2) = C_1 \qquad (6)$$

Integrating the equation of continuity of mass flow, substituting the static temperatures and pressure by stagnation temperatures and pressures, and expressing the velocity as a function of the Mach Number and the sonic velocity, Eq. (7) is obtained:

$$P_o = \frac{\dot{m}}{A}\left[\frac{R\,T_o}{\gamma}\right]^{\frac{1}{2}} \frac{\left(1 + \frac{1}{2}(\gamma - 1)M^2\right)}{M}^{\frac{\gamma+1}{2(\gamma-1)}} \qquad (7)$$

Rearranging Eq. (6), which describes momentum conservation, and substituting to obtain the stagnation pressure, gives:

$$P_{02} = \frac{\sum P_1 A_1}{A_2} \frac{\left(1 + \frac{\gamma-1}{2} M_2^{\,2}\right)^{\frac{\gamma}{\gamma-1}}}{1 + \gamma M_2^{\,2}} \qquad (8)$$

The solution to these two Equations (7 and 8) will yield the mixed flow Mach Number, and the stagnation pressure of this flow. The stagnation temperature of the mixed flow has been evaluated by means of Eq (9) which is a form of expressing energy conservation.

$$T_{02} = \frac{(\dot{m}\, C_p\, T_o)_{cg} + (\dot{m}\, C_p\, T_o)_{bp}}{(\dot{m}\, C_p)_{cg} + (\dot{m}\, C_p)_{bp}} \qquad (9)$$

The two equations obtained from mass continuity and momentum conservation are solved by an iteration process. Analytical solution is not possible.

A comment should be made on the choice of time interval used in this procedure. If the time interval is too large, the assumption of constant acceleration is not valid, and this will lead to unrealistic modelling, and could lead to instabilities in the calculations. If too small it will lead to computation times which will be longer than necessary.

2.1 Iteration Requirements of Various Configurations

The convergence process follows the nested loop approach. Before proceeding to a component, all tests on the previous components have to be satisfied. If not satisfied, the inlet parameters of the nearest upstream 'free component' are modified until a satisfactory operating point is obtained for the component in question. The term 'free component' describes a component at which the thermodynamic variables for the operation of the components downstream are generated. Three types of components can be 'free' components:- the first compressor, the first compressor of the core section in a bypass or turbofan engine with mixed exhausts, or a choked turbine.

A choice is available on the set of inlet variables for the first compressor. This is necessary because many fans and L.P. Compressors exist whose characteristics are very flat, even double valued. In this case it is desirable to start the iteration process by using the mass flow, rather than the pressure ratio as the initial input. For single-valued characteristics which are not very flat, the choice of inlet variable is irrelevant. The downstream compressors have pressure characteristics which are very steep, nearly vertical in some cases. For these compressors, the inlet parameter is the non-dimensional mass flow which is defined from the outlet parameters of the previous compressor. It is only when a 'free component' is encountered that an arbitrary pressure ratio is chosen as the input variable.

When a bypass engine with an exhaust mixer is simulated, the procedure is less sensitive to instabilities of the convergence process. To obtain the correct engine mass flow the iterations are not started from the first compressor, but from the first core compressor, thus reducing the number of components within the iteration loops. However, because of the additional iterations imposed by the requirements of static pressure balance at the mixer inlet plane, the convergence process takes longer to be achieved.

Simple jet engines, and bypass engines with separate exhausts have exactly the same convergence procedure. For the analysis of these engines, the inlet parameters of any compressor are defined by the outlet parameters of the previous compressor. The mass flow through the cold nozzle of an engine with separate exhausts is calculated from the pressure ratio across this nozzle, the fluid density and the flow area. The flow exhausted is subtracted from the total flow to obtain the flow through the core components. In a simple jet engine, the flows are basically constant, only bleeds being removed from the engine flow.

A block diagram of the above described iterative

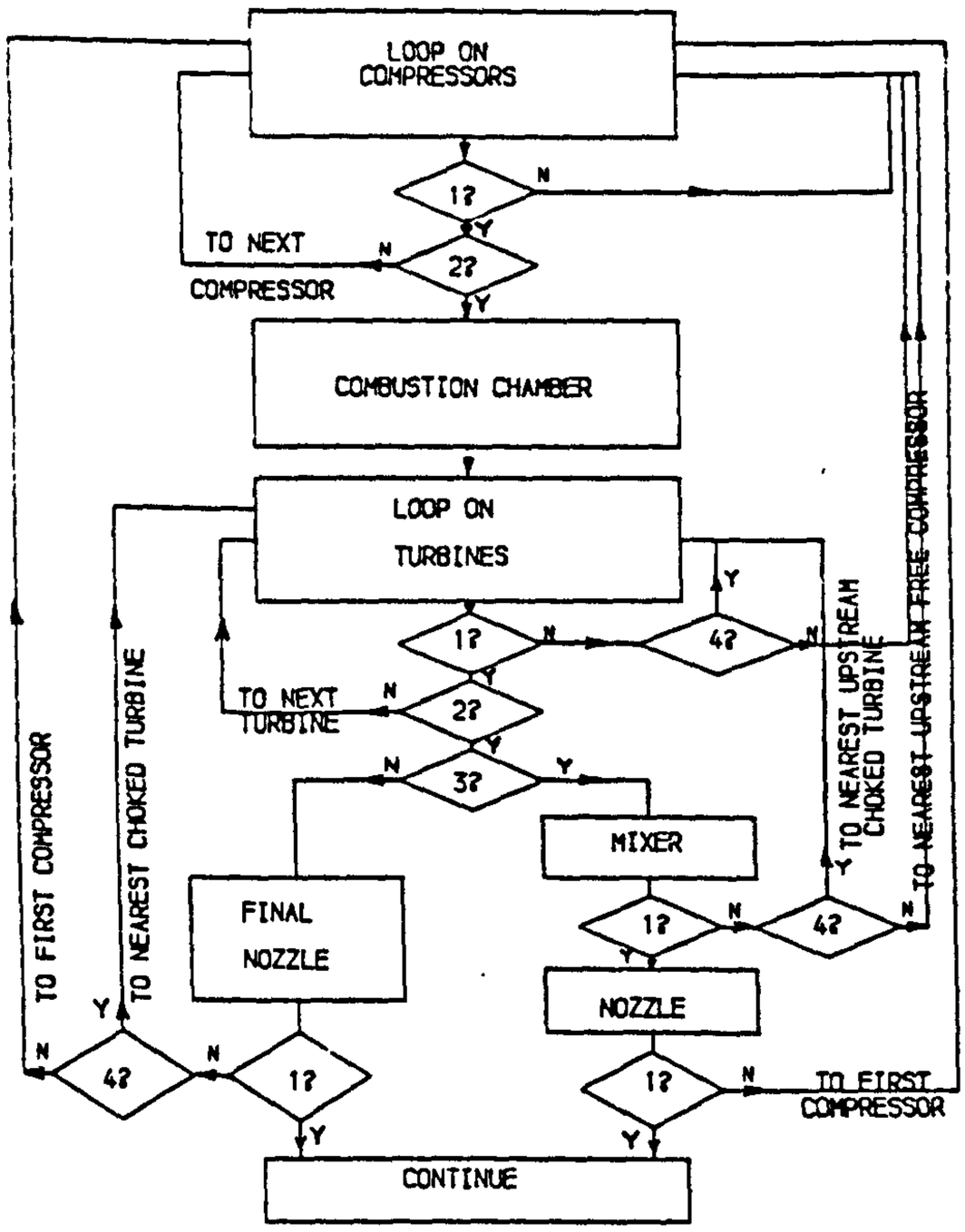

FIG. 1

BLOCK DIAGRAM OF THE MASS FLOW EVALUATION PROCEDURE
1? IS COMPONENT TEST SATISFIED?
2? IS THIS THE LAST COMPONENT OF THIS KIND?
3? DOES THE ENGINE ANALYSED HAVE A MIXER DUCT?
4? IS ANY TURBINE CHOKED?
Y = YES, N = NO

procedure is illustrated in Fig. 1. This procedure is general and can be applied to engines having any number of spools, and to simple jet engines and engines having any bypass arrangement. The engines may incorporate reheat. All bleed flow calculations, cold exhausts and individual tests have been omitted from the diagram for reasons of clarity. The remainder of the procedure, torque calculations and transient effects are not illustrated because they are straightforward.

2.2 Convergence Algorithm

The previous sections describe the procedure employed to satisfy the requirement of continuity of flow in any engine configuration. When this procedure was first applied to a single-spool turbojet engine, convergence was achieved in five or six iterations. With the adaptation of the program to more complex configurations, the total number of iterations increased greatly due to more involved algebraic loops and more nested loops. The iterating technique had to be improved to economise in computing time. One method of improving the convergence is for the index in Eq. (4) which modifies the parameter X to be a variable. This exponent should be a variable, because indirectly it is a function of the slope of the compressor characteristics for unchoked turbine conditions, and of $(dA/A)/(dP_o/P_c)$ for choked turbine conditions. It is realised that such a facility would be important in the more complex engines, where the convergence procedure is critical. In these engines a small change in the initial set of chosen parameters will produce a large change in the calculated variables at the hot end of the engine.

A procedure for continuously adjusting the index (symbol a) has been developed. Initially, 'a' is arbitrarily set to a low figure (to avoid instability) and the new parameter for the next iteration is modified as a function of the error the previous input had produced.

$$X_{t+dt} = X_t\left(1 + \frac{dA}{A}\right)^a \tag{10}$$

The error emerging at the end of the new iteration is compared with the previous error and the index 'a' is revised as follows:

$$a_{t+dt} = a_t\left(\frac{C_2}{1 - f(e)}\right)^{C_3} \tag{11}$$

where

$$f(e) = \frac{(dA/A)_t}{(dA/A)_{t-dt}} \tag{12}$$

The effect of using a range of values for C_2 and C_3 has been examined. It was found that near optimum convergence conditions were generally obtained if C_2 was given the value 0.7 and C_3 a value between 0.4 and 0.6.

2.3 Additional Features, Fuel Schedules

The program can incorporate compressor air bleed systems with the bleed value scheduled to operate on, for example, the non-dimensional speed of the compressor. The bleed flows can be returned to any part of the engine, to the bypass duct, or discharged overboard. Air flows for cooling are similarly treated.

As previously mentioned, the analysis can include the use of reheat systems. It is of course noted that normally reheat is employed when the engine is at maximum speed.

Any form of fuel scheduling can be adopted for control of accelerations and decelerations. One common method relates the non-dimensional fuel flow to the pressure ratio across the final compressor:

$$\left(\frac{\dot{f}}{N\,P_{01}}\right)_{HPC} = f\left(\frac{P_{02}}{P_{01}}\right)_{HPC} \tag{13}$$

3 APPLICATION OF THE METHOD

The prediction method has, to date, been applied successfully to eleven different configurations - most real but some hypothetical. The configurations are: - single-spool simple jet engine, single-spool turbofan with mixed exhausts, single-spool turbofan with separate exhausts, two-spool jet engine, two-spool bypass engine with separate exhausts, two-spool bypass engine with mixed exhausts, two-spool turbofan (L.P. compression system being a fan followed by an I.P. Compressor for core air, all on L.P. shaft) with separate exhausts, two-spool turbofan with mixed exhausts, three-spool jet engine, three-spool turbofan with separate exhausts, three-spool turbofan with mixed exhausts. Three of these types have been selected to demonstrate the use of the prediction method.

3.1 Two-Spool Bypass Engine with Separate Exhausts

As illustration, Figs. 2 and 3 show the results obtained when the method was used to predict the transient performance of a two-spool bypass engine with separate exhausts, when at sea level, static conditions. The fuel schedule employed is of the type specified by Eq. (13). The transient trajectories in the L.P. Compressor (Fig. 2) are seen to lie very close to the steady-running line. In the H.P. Compressor (Fig. 3), the trajectories move significantly from the steady-running line, beyond the surge line during the acceleration.. However the danger of surge may be less than indicated due to the favourable influences of heat transfer on the compressor characteristics and on the trajectory (1,2,3,12).

The steady-running lines shown in these figures were obtained by holding the fuel flow constant until the engine stabilised, then increasing the fuel by a given amount until it stabilised again. The process is repeated as required.

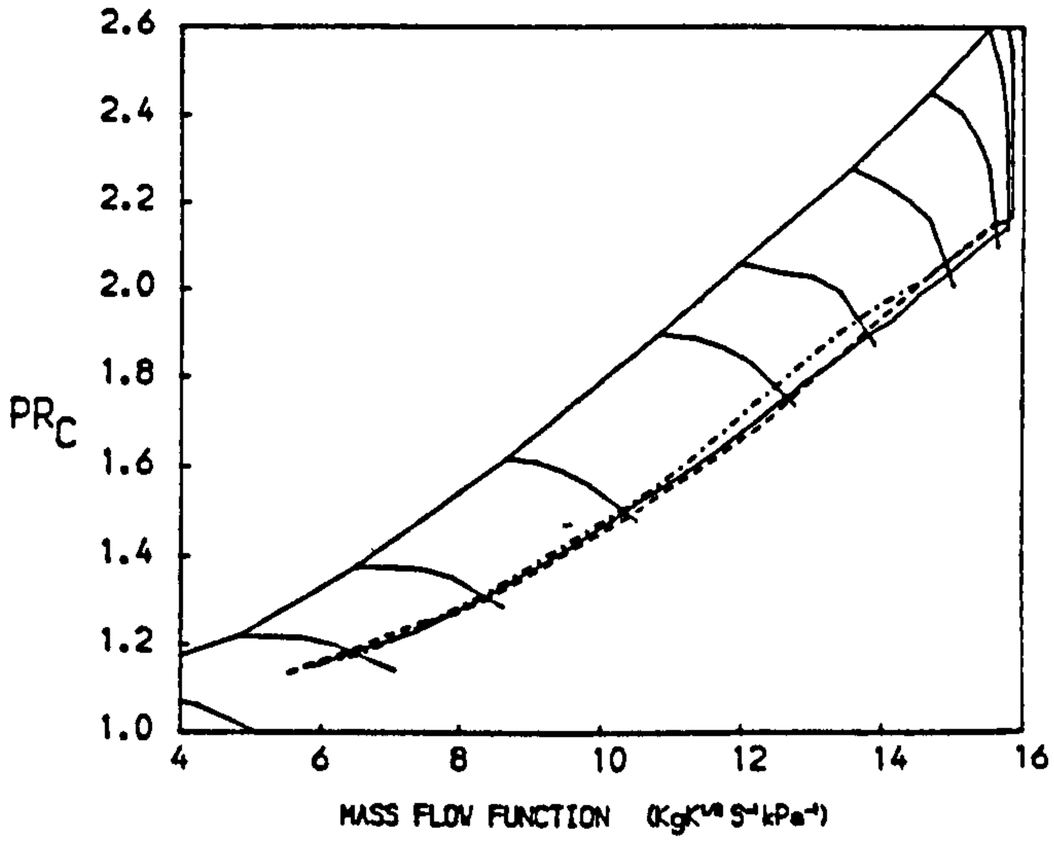

FIG. 2
PATHS ON THE CHARACTERISTC MAPS OF THE L.P. COMPRESSOR OF A TWO SPOOL BYPASS ENGINE WITH SEPARATE EXHAUSTS
-- ACCELERATION — STEADY RUNNING -·- DECELERATION

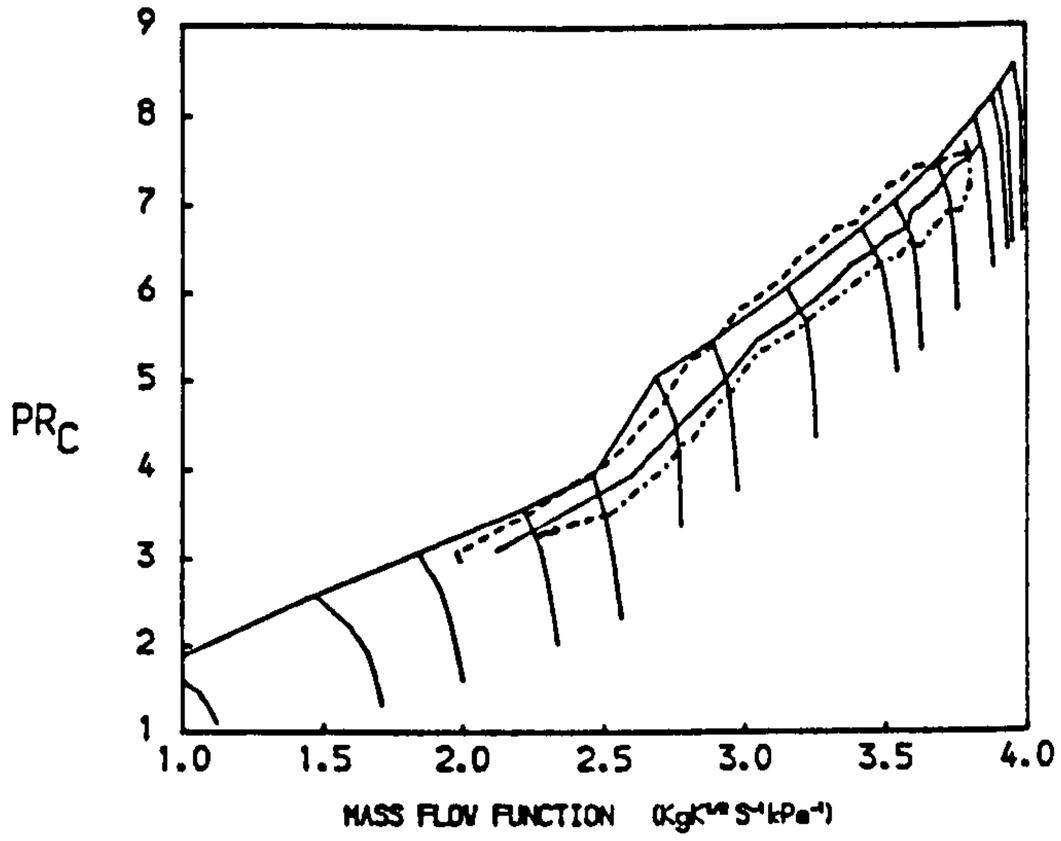

FIG. 3
PATHS ON THE CHARACTERISTC MAPS OF THE H.P. COMPRESSOR OF A TWO SPOOL BYPASS ENGINE WITH SEPARATE EXHAUSTS
-- ACCELERATION — STEADY RUNNING -·- DECELERATION

3.2 Two-Spool Bypass Engine with Mixed Exhausts

An engine with mixed exhausts using the same compressors and turbines as the bypass engine with separate exhausts, illustrated in the previous section, has been analysed. The fuel flow is controlled with a schedule which is similar to that employed in the previous engine.

In transients, again at sea level, the trajectories in the H.P. Compressor (Fig. 5) are very similar to those of the engine with separate exhausts. In the L.P. Compressor (Fig. 4) the transient trajectories move considerably further away from the steady-running line than had been the case for the engine with separate exhausts. The L.P. compressor trajectory is moved in the direction of surge in the acceleration, but there still is an adequate surge margin.

The degree of mixing in the jet pipe between the mixer and the final nozzle may not be complete. The program can be used with any specified degree of mixing. As an illustration of the adaptability of the program, it has been used to compare the steady-state performance of mixed exhaust engines with two degrees of mixing - zero and complete. The results are shown on Fig. 6. It can be seen that at the higher thrust range, the engine with complete mixing shows an advantage in better specific fuel consumption. Fig.7 shows the predicted variation of several variables during the acceleration. These are essentially similar to those of the two-spool bypass engine with separate exhausts. Therefore only the results of this engine are illustrated.

3.3 Three-Spool Turbofan with Mixed Exhausts

A hypothetical set of characteristics was used for predictions of a three-spool turbofan with mixed exhausts. The matching obtained was not good, but the characteristics have provided an adequate test for the transient predictions program. A fuel schedule of a

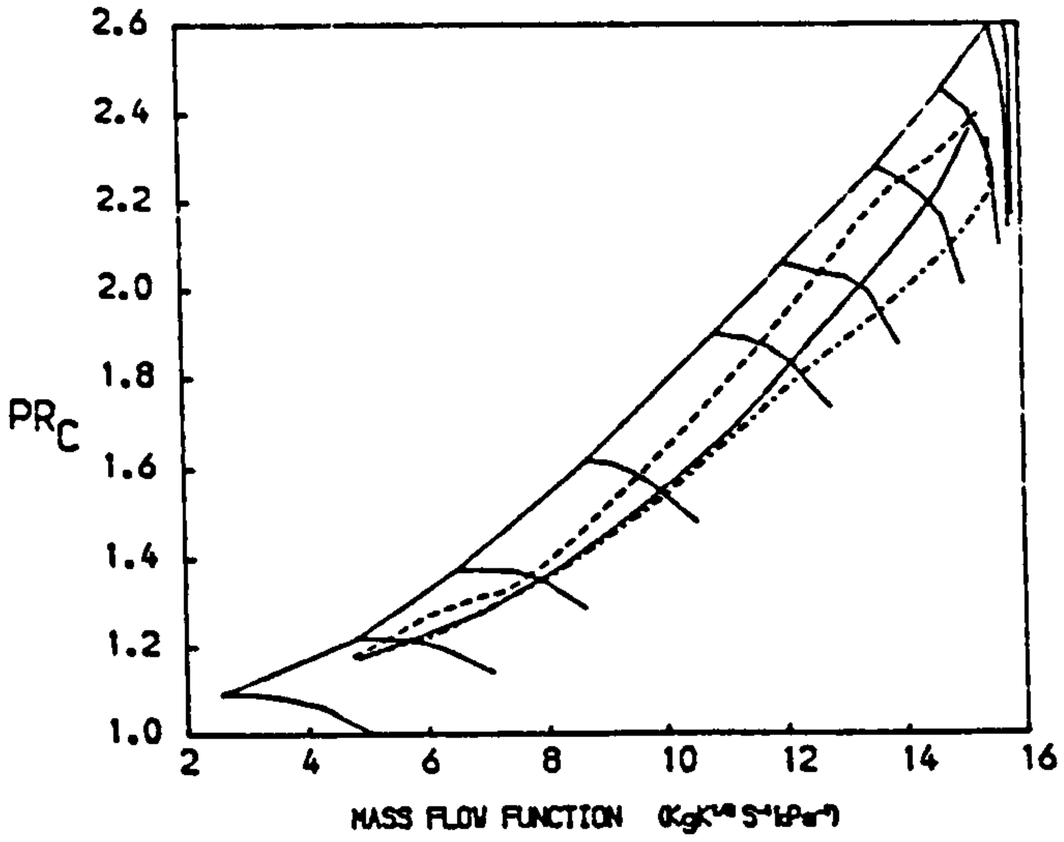

FIG. 4
PATHS ON THE CHARACTERISTC MAPS OF THE L.P. COMPRESSOR OF A TWO SPOOL BYPASS ENGINE WITH MIXED EXHAUSTS
-- ACCELERATION — STEADY RUNNING --- DECELERATION

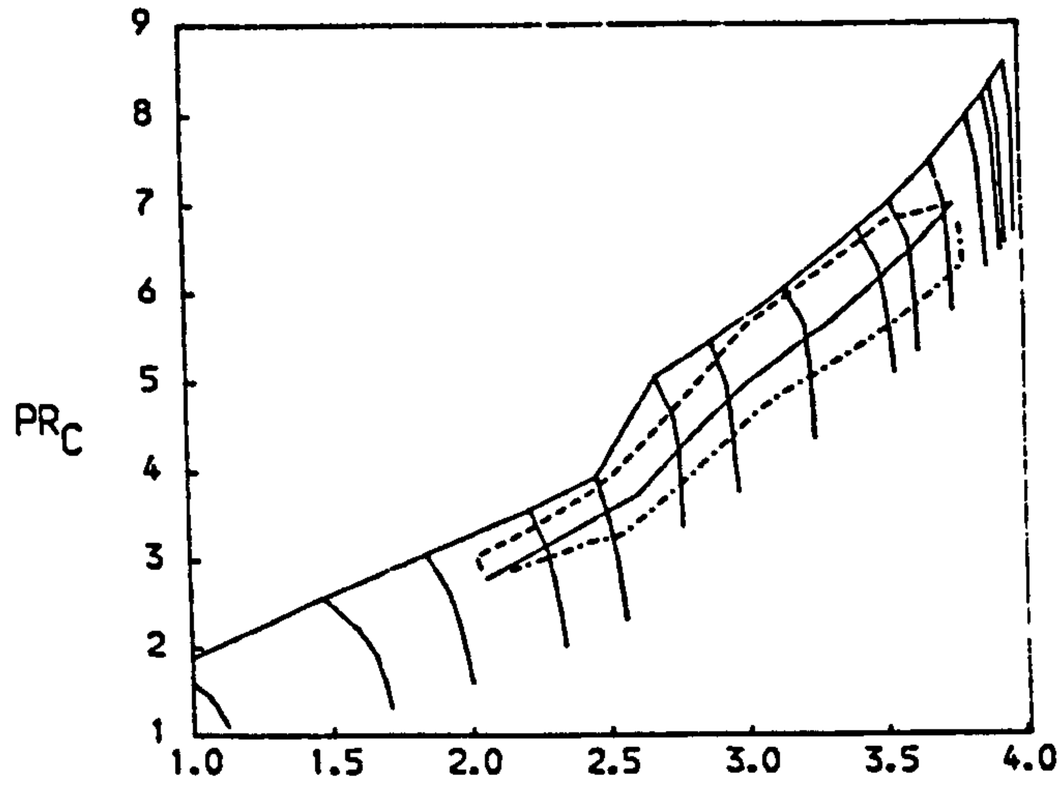

FIG. 5
PATHS ON THE CHARACTERISTC MAPS OF THE H.P. COMPRESSOR OF A TWO SPOOL BYPASS ENGINE WITH MIXED EXHAUSTS
-- ACCELERATION — STEADY RUNNING --- DECELERATION

similar type to the one employed for the two-spool engines has been used to control the fuel flow.

The predicted trajectories in the fan virtually coincide with the steady-running line, and so are not illustrated. In the I.P. Compressor (Fig. 8) the trajectories are displaced away from steady-running at the lower speed range, but over most of the remaining speed range they are close to steady-running. In the H.P. Compressor (Fig. 9) the trajectory moves towards surge in the acceleration and away from surge in the deceleration. The apparent amounts of surge margin available are not realistic, due to the poor matching of the components.

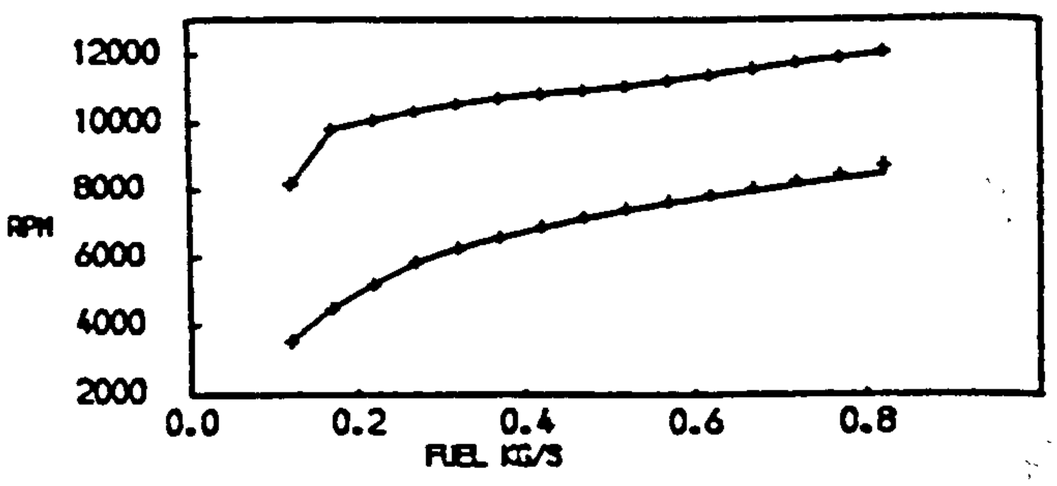

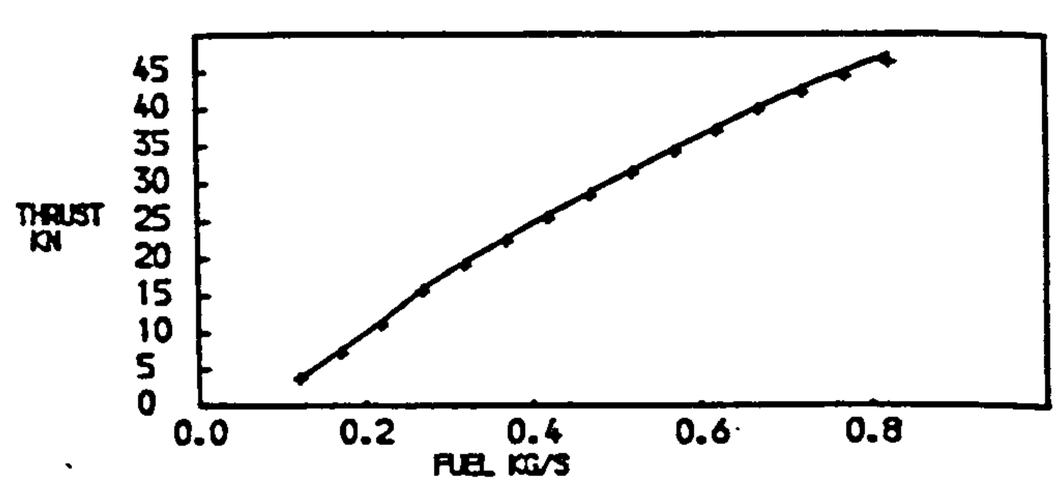

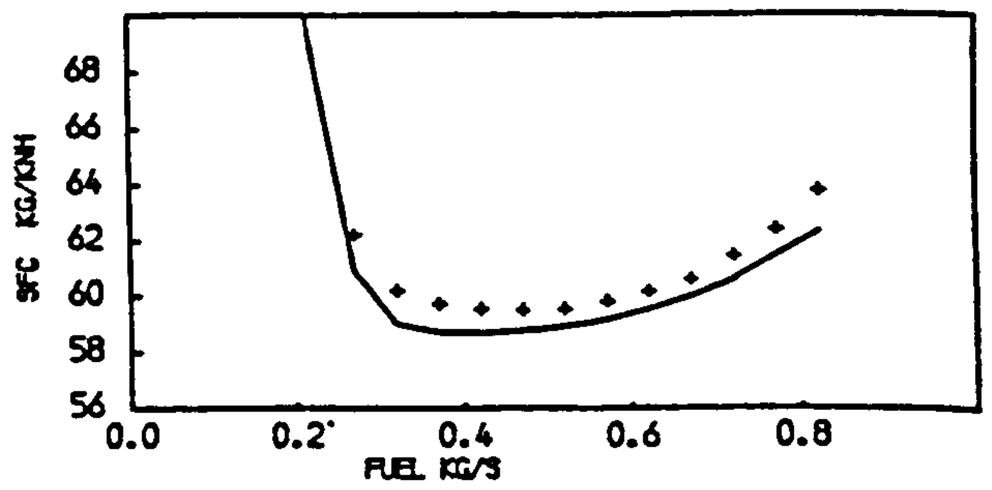

FIG. 6
EFFECT OF MIXING ON THE STEADY STATE PERFORMANCE OF A TWO SPOOL BYPASS ENGINE WITH MIXED EXHAUSTS AT SEA LEVEL STATIC CONDITIONS
+NO MIXING —COMPLETE MIXING

4 COMPUTING EFFICIENCY

It is interesting to note how the computing time is affected by the number of components (usually two per spool, except where compressions on a shaft are split) and by the introduction of mixed exhausts for a bypass engine of separate jets. Computing times, as required by an ICL 2976 Computer, are given in Fig. 10 for the range of engines considered. It can be seen that the computing time increases almost proportionately with the number of components constituting the engine. Also, engines with mixed exhausts require longer computing times than equivalent engines with separate exhausts, due to the additional convergence required in the mixing duct. In no case is the computing time requirement excessive.

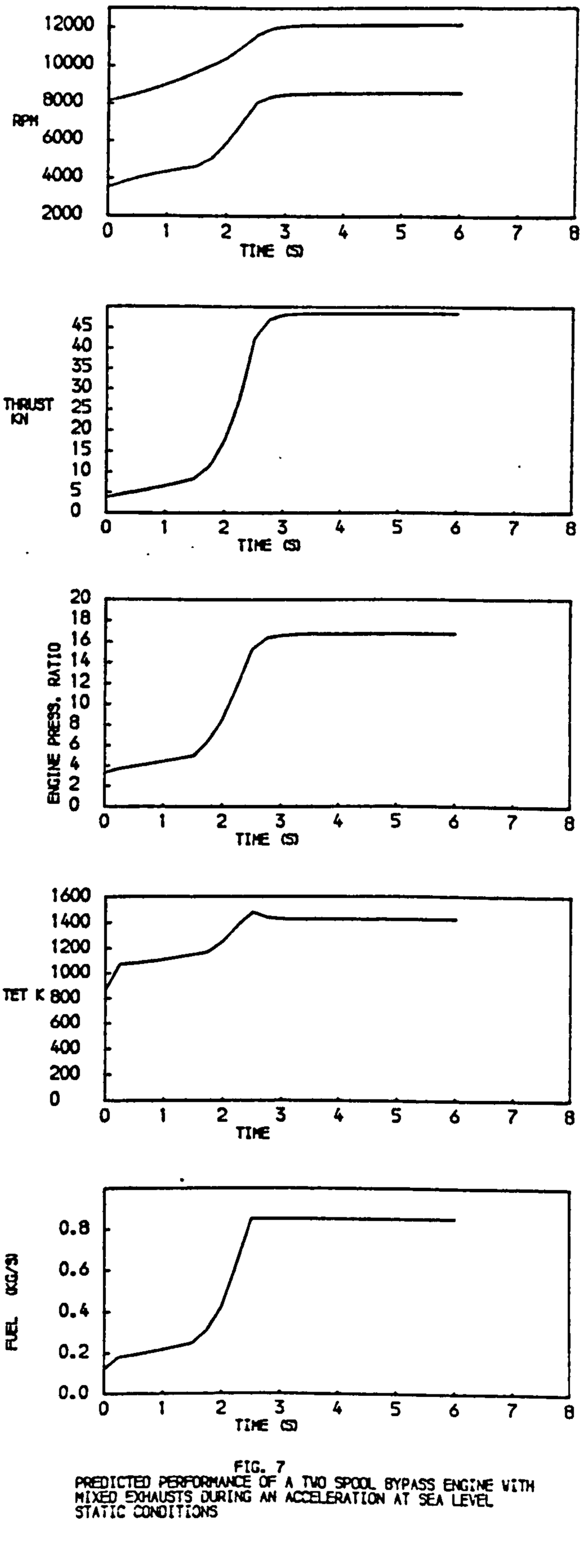

FIG. 7
PREDICTED PERFORMANCE OF A TWO SPOOL BYPASS ENGINE WITH MIXED EXHAUSTS DURING AN ACCELERATION AT SEA LEVEL STATIC CONDITIONS

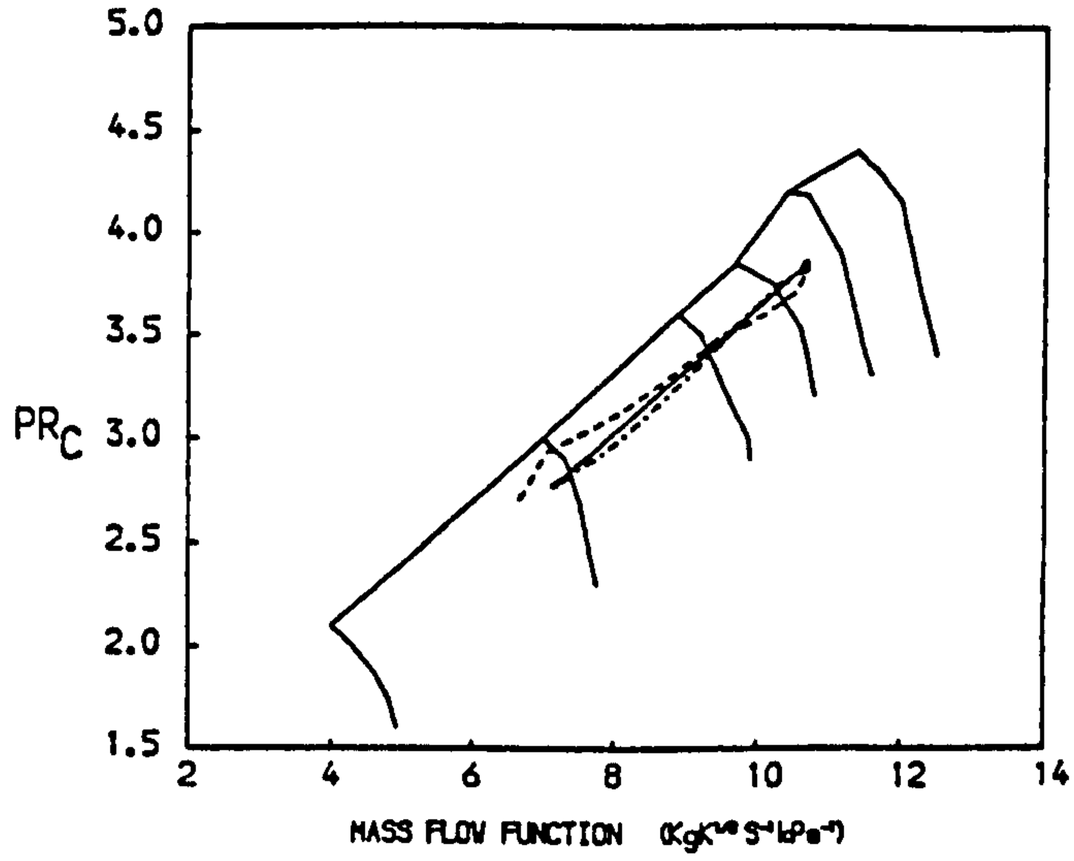

FIG. 8
PATHS ON THE CHARACTERISTC MAPS OF THE I.P. COMPRESSOR OF A THREE SPOOL TURBOFAN WITH MIXED EXHAUSTS
-- ACCELERATION — STEADY RUNNING --- DECELERATION

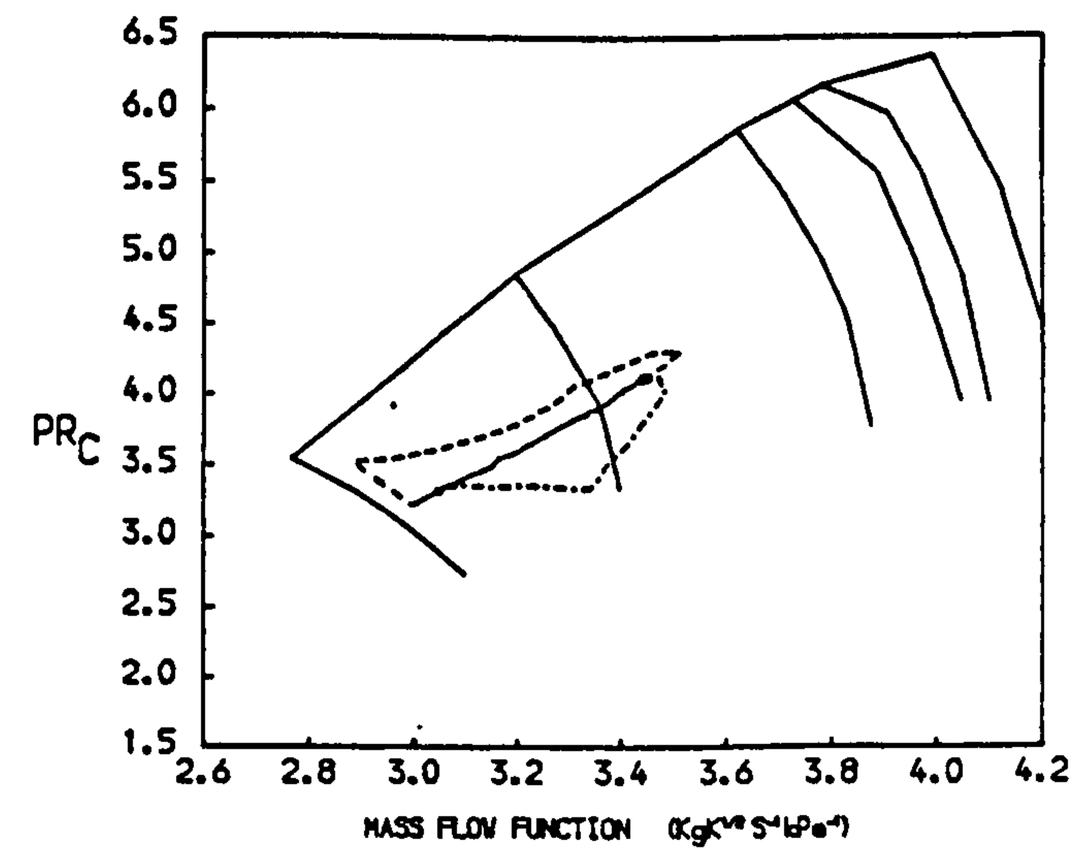

FIG. 9
PATHS ON THE CHARACTERISTC MAPS OF THE H.P. COMPRESSOR OF A THREE SPOOL TURBOFAN WITH MIXED EXHAUSTS
-- ACCELERATION — STEADY RUNNING --- DECELERATION

5 CONCLUSIONS

A general digital computer program has been developed for the prediction of the transient performance of gas turbines. The program has been applied successfully to a wide range of aero jet engines, ranging from single-spool to three-spool, and from simple jet to bypass types with or without mixed exhausts. Computing times are reasonable, increasing approximately proportionately with the complexity of the engine, as indicated by numbers of components (compressors plus turbines).

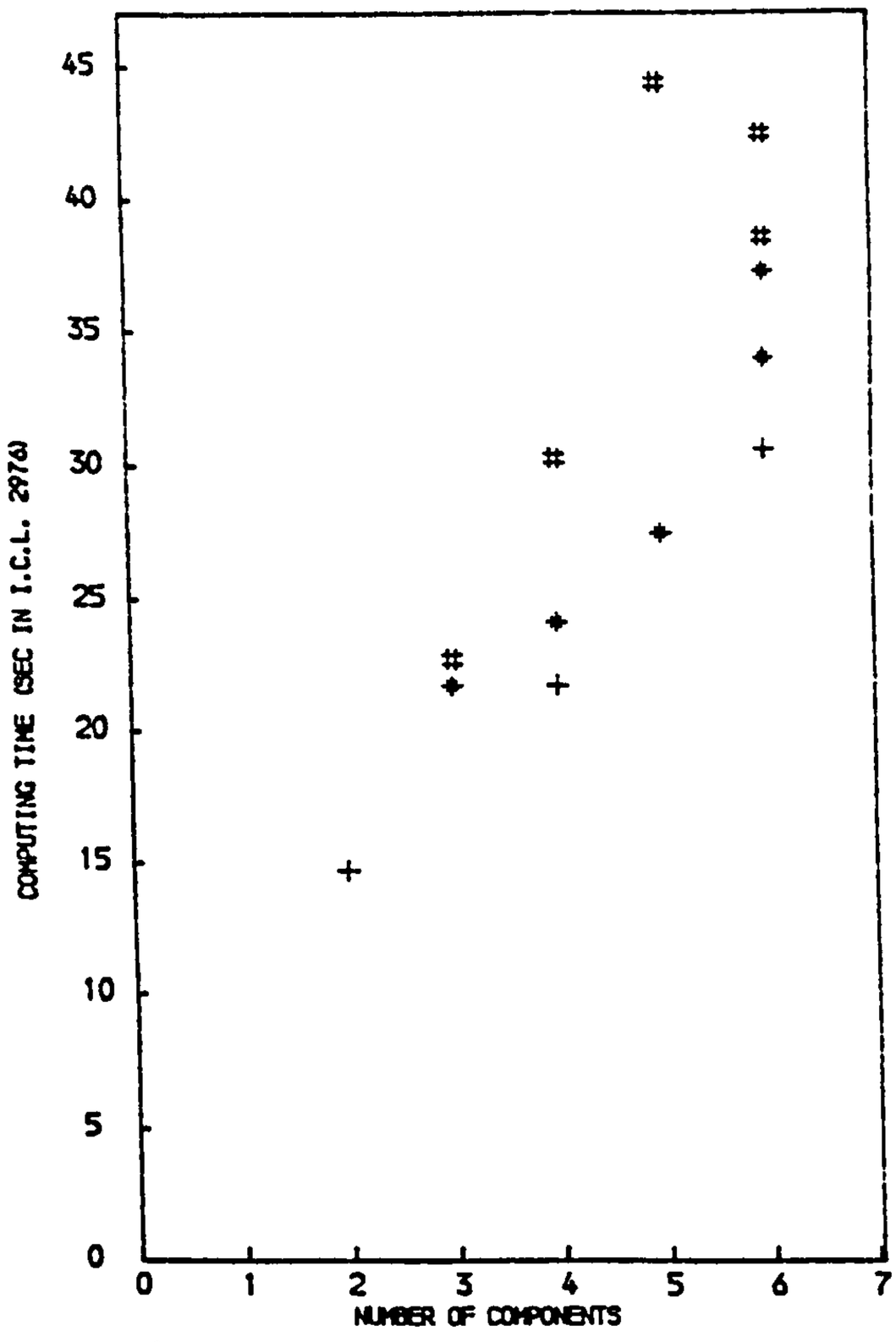

FIG. 10

COMPUTING EFFICIENCY OF THE PROGRAMME
+ TURBOJETS
# ENGINES WITH SEPARATE EXHAUSTS
• ENGINES WITH MIXED EXHAUSTS

The program does incorporate thermal effects, but that part of the program is discussed in another parallel paper. The results quoted in the present paper have not included thermal effects.

6 ACKNOWLEDGEMENT

The authors wish to thank colleagues at Rolls-Royce Limited, Caledonian Airmotive Limited and the University of Glasgow for provision of data, for valuable comment and for encouragement.

7 REFERENCES

1. Koff. B.L., 'Designing for Fighter Engine Transients',
AGARD Conference Proceedings 324, Paper 2, 1982.

2. Maccallum, N.R.L., 'Axial Compressor Characteristics During Transients',
ibid, Paper 22, 1982.

3. Maccallum, N.R.L., and Pilidis, P., 'The Prediction of Surge Margins during Gas Turbine Transients',
Paper offered to A.S.M.E. Gas Turbine Conference, March 1985.

4. Fawke, A.J., and Saravanamuttoo, H.I.H., 'Digital Computer Methods for the Prediction of Gas Turbine Dynamic Response'
S.A.E. Paper 710550, 1971.

5. Filippi, R.E. and Dugan J.F., 'Effect of Overall Compressor Pressure Ratio Division on Acceleration Characteristics of Three Hypothetical Two-Spool Turbojet Engines'
N.A.C.A. RM E56 D13, 1956.

6. Larrowe, V.L., Spencer, M.M., and Tribus, M., 'A Dynamic Performance Computer for Gas Turbine Engines',
Transactions A.S.M.E., Vol 79, Oct 1957, pp 1707-1714.

7. Durand, H.P., 'Simulation of Jet Engine Transient Performance',
A.S.M.E., Paper 65 WA/MD16, 1965.

8. Bauerfeind, K., 'Transient Performance of Jet Engines'.
M.A.N. Report 33878, 1967.

9. Saravanamuttoo, H.I.H., 'Analogue Computer Simulation of Gas Turbine Dynamic Performance',
Ph.D. Thesis, University of Bristol, 1968.

10. Szuch, J.R., 'HYDES: A generalized Hybrid Computer Program for Studying Turbojet or Turbofan Engine Dynamics',
N.A.S.A. TM X 3014, 1974.

11. Sellers, J.F., and Daniels, C.J., 'DYNGEN: A Program for Calculating Steady State and Transient Performance of Turbojet and Turbofan Engines.
N.A.S.A. TN D 7901, 1975.

12. Pilidis, P., 'Digital Simulation of Gas Turbine Performance',
Ph.D. Thesis, University of Glasgow, 1983.

Publication 31

THE AMERICAN SOCIETY OF MECHANICAL ENGINEERS
345 E. 47 St., New York, N.Y. 10017

85-GT-208

The Prediction of Surge Margins During Gas Turbine Transients

N. R. L. MACCALLUM, Reader,
University of Glasgow,
Glasgow, Scotland

P. PILIDIS, Teaching Company Associate,
Caledonian Airmotive Ltd.,
Prestwick, Scotland

ABSTRACT

This paper describes how allowance for the thermal effects of non-adiabatic flow, altered boundary layer development, changes in tip clearances and changes in seal clearances have been incorporated into a general gas turbine transient program. This program has been applied to a two-spool bypass engine. Revised predictions of surge margins in three common transients have been obtained. When the engine undergoes a 'cold' acceleration, the thermal effects on the trajectory and on the surge line give a much increased proportion of unused surge margin in the H.P.Compressor, as compared to adiabatic predictions. In a 'hot' acceleration this improvement is considerably reduced.

NOMENCLATURE

C_p	specific heat at constant pressure
$C_1,\ldots C_9$	constants
$\dot{f}$	fuel flow rate
F	ratio of heat transfer to fluid to work transfer from fluid
g	staggered gap between blades
$\dot{m}$	air flow rate
N	rotational speed
P	stagnation pressure
Q	heat flux to air
R	surge pressure ratio
T	stagnation temperature (absolute)
δ	tip clearance
ν	kinematic viscosity

Subscripts

1,2,3	inlet to, outlet from L.P. Compressor, outlet from H.P. Compressor
ad	adiabatic
b	blade aerofoil
cl	with new clearance
ht	with heat transfer
H	High Pressure
m	mean
w	wall

1. INTRODUCTION

This paper describes a study of the alterations, due to thermal effects, of compressor characteristics and of working lines in transients of gas turbines. Revised surge margins can then be examined and compared with estimates ignoring thermal effects. At this stage the study has been restricted to engines using axial-flow compressors, but an extension to the study of centrifugal compressor types is envisaged.

The 'thermal' effects which are considered to be relevant in transients are:

(a) Non adiabatic flows in compressors and turbines. In compressors this causes density changes due to heat transfer, additional to those resulting from the compression process.

(b) Changes in boundary layer development on blade aerofoils in compressors.

(c) Changes in boundary layer development on end-walls in compressors.

(d) Tip clearance changes, controlled by disc, casing and blade responses.

(e) Seal clearance changes, controlled by disc, casing and ring responses.

Presented at the Gas Turbine Conference and Exhibit
Houston, Texas — March 18-21, 1985

Effects (a) to (d) above, when applied to compressors, may alter the characteristics representing the compressor, as described in section 2 of this paper. All five effects influence the performance of the components, and hence of the engine as a whole. These changes lead to revised transient trajectories in the compressors, this being described in section 3. The procedures are then demonstrated on a two-spool bypass engine with mixed exhausts.

2. THERMAL EFFECTS ON AXIAL COMPRESSOR CHARACTERISTICS

It is known that thermal effects alter the characteristics of axial-flow compressors (1)[1], and attempts have been made (2),(3) to quantify the changes. In the present paper, the procedure adopted to quantify these changes follows the method used in reference (2), where it is described in more detail.

2.1 Pitch-line Prediction Method

The calculation is carried out stage by stage. First the limiting pressure rise is determined from Koch's correlation (4). An initial end-wall blockage factor is guessed. Assuming that Howell and Bonham's correlation (5) can be applied to the core flow through the blading in the central annulus, a pressure rise across the stage can be predicted. This is compared with the limiting, or stalling pressure rise value. From Smith's data (6), displacement thicknesses at the hub and at the casing can then be found, giving a revised end-wall blockage factor. The above calculation is then repeated until convergence on the actual end-wall blockage is obtained. This procedure is then carried out through the subsequent stages of the compressor in succession.

There are several coefficients, such as to allow for applying a low-speed correlation to a high-speed compressor, which are adjusted so that the predicted compressor characteristics, in steady-running, line up with the observed performance of the compressor. The thermal transient effects of density change due to heat transfer, modified development of boundary layers on blade aerofoils and end-walls, and tip clearance changes can then be introduced in the above method for prediction of characteristics. The means of introduction are discussed below.

2.2 Density Changes Resulting From Heat Transfer

During an acceleration of an initially 'cold' engine, there will be heat transfer from the air to the blades, platforms and casings. In a two-dimensional system, this will make the air more dense, giving it a lower axial component of velocity at a particular stage of the compressor, compared with steady-running at that speed, inlet temperature and mass flow. This alters the loading on that particular stage and thus changes the stage pressure rise. Consequently the overall pressure rise is altered.

Some study is required of which of the heat flows will affect the pitch-line density. The temperature distributions shown by Smith (6) for steady-running of a 12-stage compressor indicate that the energy dissipated into heat due to losses at the end-walls tends to remain trapped within the end-wall boundary layer. Therefore it appears that heat transfers to, or from, platforms and casings will have little influence on the temperature, hence density, of the air flow at the pitch-line (the end-wall heat transfers will alter the end-wall boundary layer thickness, as discussed later). However heat transfers to, or from the blade aerofoils will immediately influence pitch-line density. Thus the procedure adopted in the present work is to assume that only the heat transfers to, or from, the aerofoils of the blades alter the density as compared to adiabatic running.

When these effects are incorporated into the pitch-line prediction method it is found (2) that for a given inlet non-dimensional speed a new pressure ratio to non-dimensional mass flow characteristic is obtained. One method of quantifying this change is to retain the adiabatic characteristic and use a modified 'effective' speed. It is also possible for the surge pressure ratio at a particular non-dimensional mass flow to be changed. In the working region where the front stages of the compressor are the most heavily loaded, and therefore nearest to initiating surge, heat transfers to the blades, as when accelerating a 'cold' compressor, increase the effective speed and raise the surge pressure ratio (at a given mass flow). It has been suggested (7),(8) that for these small changes the binomial representation can be used and expressions are obtained such as Eq. (1) for changes in 'effective' speed:

$$\frac{\Delta N}{N} = C_1 \frac{Q}{\dot{m} C_p T_m} \qquad (1)$$

and Eq.(2) for changes in surge pressure ratio at a given mass flow:

$$\frac{R_{ht} - 1}{Rad - 1} = 1 + C_2 F \qquad (2)$$

The heat transfer coefficients used for the blades are based on established correlations, and for other areas from correlations for developing boundary layers on flat plates, as discussed in References (2),(7),(9) and (10). The blade, with its aerofoil and platform combination, can be treated as two components, comprising firstly the aerofoil and secondly a finned platform, the effectiveness of the finning depending on the instantaneous aerofoil temperature. Thus the blade aerofoil temperature, T_b, can be calculated during the transient, and using these procedures the heat flow rate to the air (or gas), $\dot{C}$ is calculated and hence the parameter F, which is the ratio of the heat flux to the air (or gas) to the power transfer from the air (or gas) in that component. The values of the coefficients C_1 and C_2 are determined for each individual compressor using the method outlined above.

These empirical expressions are used later in the engine transient program.

1. Underlined numbers in brackets indicate references at end of paper

2.3 Boundary Layer Development on Blade Aerofoils

It has been shown (9) that the separation from a convex surface in an adverse pressure gradient can occur earlier if the surface is hotter than the flowing air. This effect has been incorporated in a compressor characteristics prediction program, and the resulting movements in effective speed and in surge pressure ratio can be represented by

$$\frac{\Delta N}{N} = C_3 \frac{T_b - T_{air}}{T_{air}} \qquad (3)$$

and

$$\frac{R_{ht} - 1}{R_{ad} - 1} = 1 + C_4 F \qquad (4)$$

2.4 Boundary Layer Development on End-Walls

The effect of heat transfer on the thickness of the boundary layers on the end-walls is somewhat uncertain. The simple approximation that has been used in this program has been to assume the effect of heat transfer is similar to the effect on the thickness of turbulent boundary layers on flat plates:

$$\delta_{ht}/\delta = (\nu_w/\nu_\infty)^{0.2} \qquad (5)$$

On the basis of this assumption, small movements in effective speed and surge pressure ratio are indicated. The changes can be quantified by expressions of the type:

$$\frac{\Delta N}{N} = C_5 \frac{T_w - T_{air}}{T_{air}} \qquad (6)$$

and

$$\frac{R_{ht} - 1}{R_{ad} - 1} = 1 + C_6 F \qquad (7)$$

2.5 Summation of Effects of Heat Transfer

The effects of heat transfer on the effective speed, as indicated by Eqs. (1), (3) and (6) can be approximately summed together into:

$$\frac{\Delta N}{N} = C_7 \frac{T_b - T_{air}}{T_{air}} + C_8 \frac{\dot{Q}}{\dot{m} C_p T_m} \qquad (8)$$

The effects on surge pressure ratio, at a given mass flow, Eqs. (2), (4) and (7) can be summed into:

$$\frac{R_{ht} - 1}{R_{ad} - 1} = 1 + C_9 F \qquad (9)$$

As an illustration, the analysis has been applied to the compressors of a Two-Spool Bypass Engine, having mixed exhausts. The pitch-line prediction program (7) was used to predict the effective characteristics for a number of instants in a range of transients. There was very reasonable consistency of the values obtained for the coefficients C_7, C_8, and C_9. The mean values adopted for the I.P. Compressor were -0.07, -0.07, and 0.36. The corresponding values in the H.P. Compressor were -0.1, -0.1, and 0.36.

2.6 Tip Clearance Changes

The effect of tip clearance on the predicted characteristics can be determined, using the correlation presented by Koch (4) between the limiting pressure rise of a stage and the non-dimensional tip clearance. This method has been applied to the H.P. Compressor of the bypass engine referred to above, and it is found in the relevant range that the change in effective speed is represented by

$$\frac{\Delta N}{N} = -0.3 \frac{\Delta(\delta)}{g} \qquad (10)$$

and the change in surge pressure ratio by

$$\frac{R_{cl} - 1}{R_{ref} - 1} = 1 - 1.1 \frac{\Delta(\delta)}{g} \qquad (11)$$

The study was not extended to the L.P. Compressor as it had been found (5) that the tip clearances of that compressor in transients scarcely deviated from the corresponding steady-running values.

3. EFFECTS ON TRAJECTORIES IN TRANSIENTS

Programs have existed for many years for predicting the transient response of gas turbines to changes in fuel flow. The programs which have been published have almost invariably used equilibrium characteristics for components, and only in a few of the programs is some allowance made for heat transfer effects.

The present work is aimed at rectifying these omissions by making the allowances for changes in compressor characteristics, for tip clearance changes and for seal clearance changes in addition to the effect of heat transfer causing non-adiabatic flow. The procedure for predicting the changes in compressor characteristics has been described in the previous section. To predict tip and seal clearance changes and associated efficiency alterations use is made of the models described in Reference (10). The treatment for non-adiabatic flow has also been described previously (7).

These procedures have been incorporated in the program for the prediction of the transient performance of a two-spool bypass engine, having mixed exhausts. This program was then applied to the engine which is being used in the present work and the predicted effects on speed and thrust reponses were obtained (10).

Subsequently a general transient program,

applicable to all engine configurations has been developed (5), (11). This program as already stated incorporates all the models for tip clearances, seal clearances, and the 'direct' heat transfer effects of non-adiabatic flow and boundary layer modification.

These procedures enable the simulation of any transient situation. Three sample transients are described in the next section, intended to be an illustration of the methods developed.

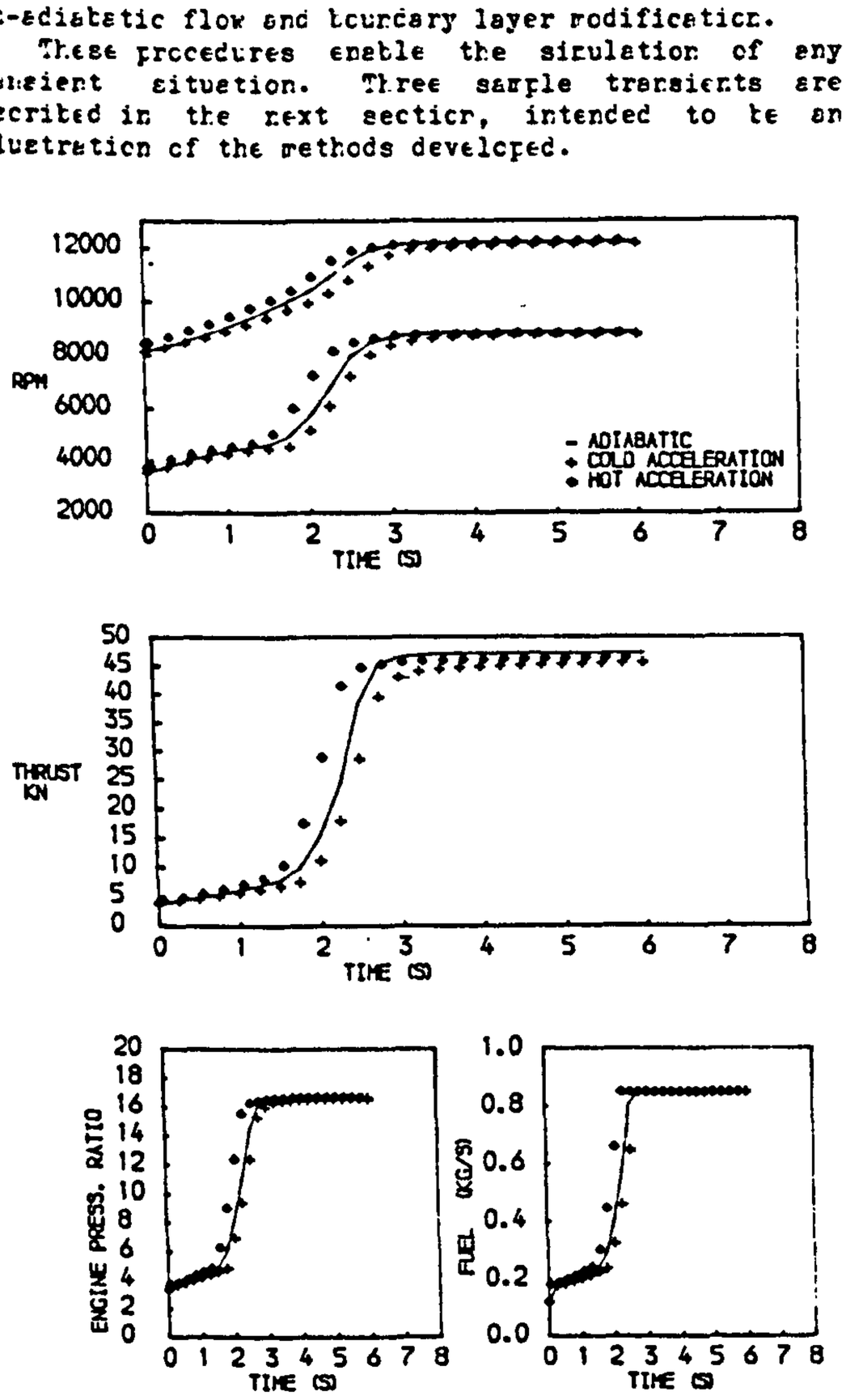

FIG. 1
PREDICTED PERFORMANCE OF A TWO SPOOL BYPASS ENGINE WITH MIXED EXHAUSTS DURING AN ACCELERATION AT SEA LEVEL STATIC CONDITIONS

4. APPLICATION: TRANSIENTS OF A TWO-SPOOL BYPASS ENGINE

The procedures described above for predicting transient trajectories and changes in compressor characteristics have been applied to the two-spool bypass engine with mixed exhausts which has already been used as an illustration in Sections 2.5 and 2.6. A range of transients has been simulated, and three of these are illustrated here. The fuel flow during the transients was controlled by a fuel schedule in which the non-dimensional fuel flow $[\dot{f}/(N_H P_2)]$ was expressed as a function of the pressure ratio across the H.P. Compressor (P_3/P_2). This type of scheduling was used for both accelerations and decelerations. The fuel flow schedules were employed between a maximum and a minimum fuel flow, determined by experimental work.

The first transient illustrated is a sea level acceleration. The predictions of speed and thrust response, and of engine pressure ratio are illustrated in Fig. 1. In the first set of calculations it is assumed that the flow in the components is adiabatic

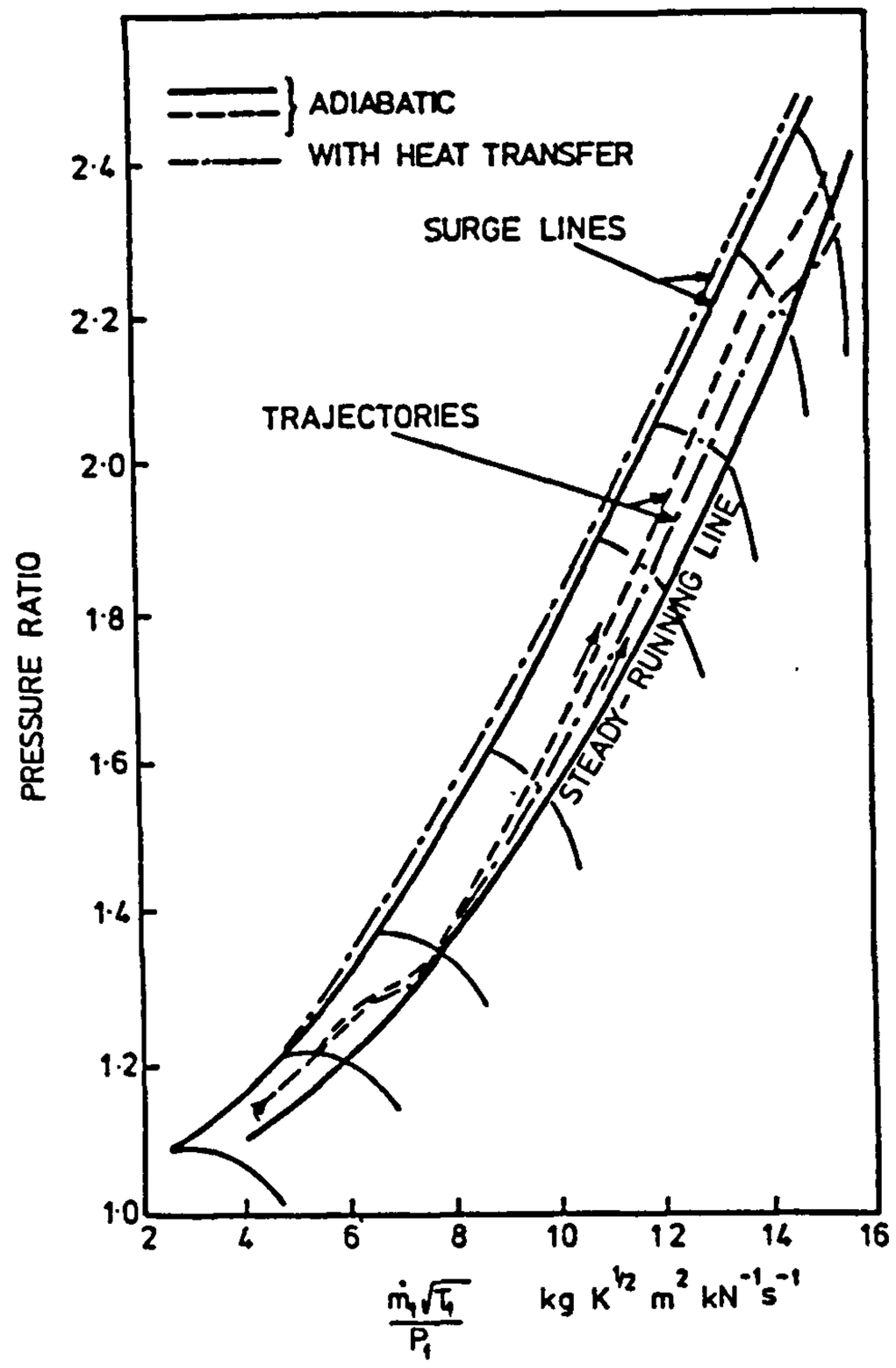

Fig. 2. PREDICTED TRAJECTORIES AND SURGE LINES IN L.P. COMPRESSOR - SEA LEVEL ACCELERATION.

and there are no thermal effects. These predictions are marked 'adiabatic'. In the second set of predictions, all the thermal effects are accounted for, including the variation of tip and seal openings, and it is assumed that prior to the acceleration the engine had stabilised at the idling speed. This set of predictions is labelled 'cold'. For the final set of calculations, the engine had first been held until stabilised at the maximum speed, then decelerated rapidly to the idling speed, and then, six seconds after starting the deceleration, the engine is reaccelerated. The predictions for this acceleration transient, which is sometimes referred to as a 'Bodie', are labelled 'hot'.

Considering first the influence of the thermal effects on the predicted acceleration of the initially 'cold' engine, it is seen that the acceleration is slower by 0.5 sec, or 15 per cent, than the adiabatic simulation. Also it is observed that when the speed transient is completed, the thrust is still about 5 per cent below the stabilised value, although the fuel flow is at its final value. The effects which appear to have the greatest influence on the dynamic response of the engine are the non-design clearances occurring in

the two air seals (10).

Turning now to the behavior of the compressors, the predicted trajectories and surge lines for the two cases of adiabatic acceleration and 'cold' acceleration are shown in Figs. 2 and 3, for the L.P. and H.P.

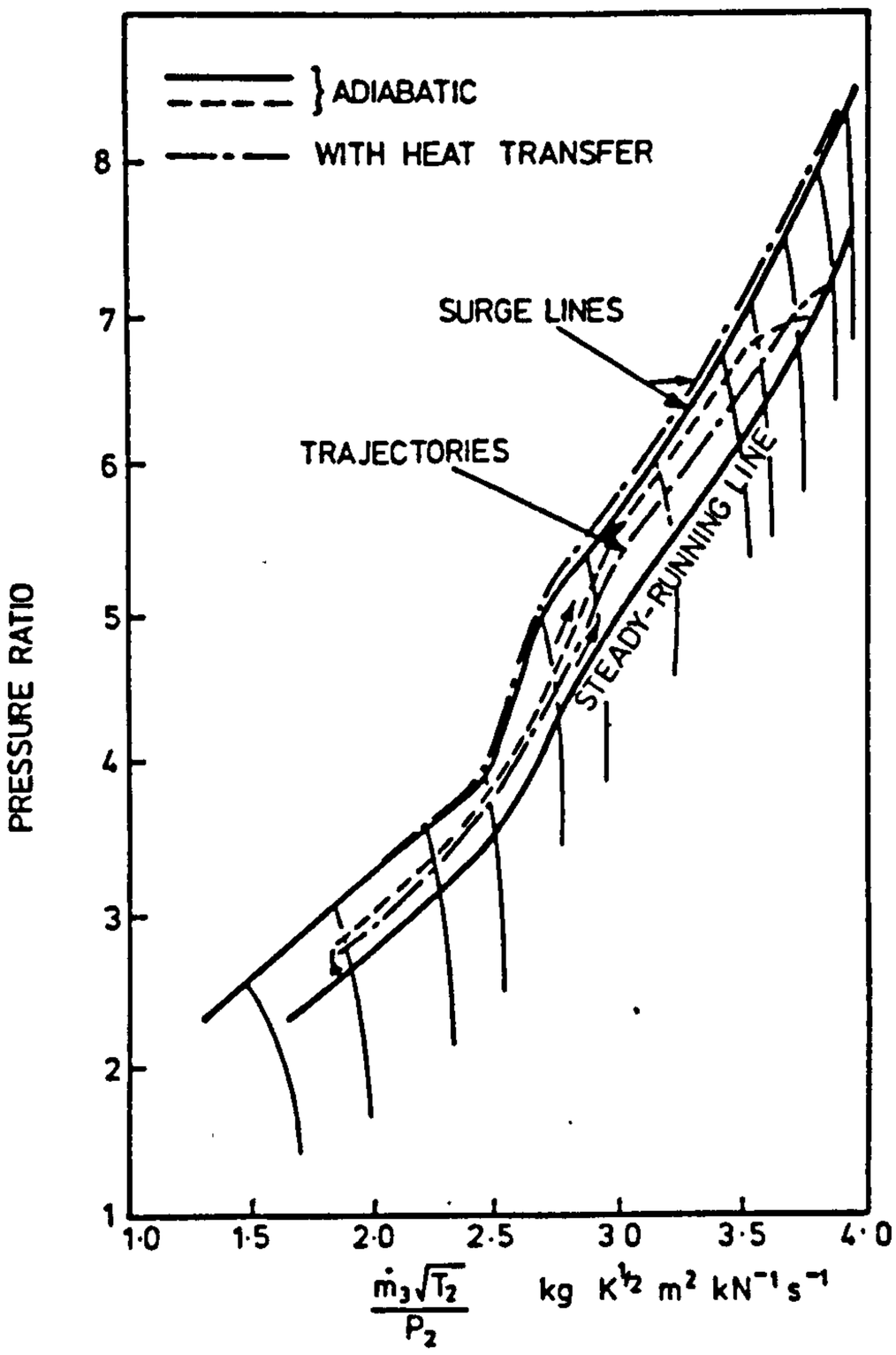

Fig. 3. PREDICTED TRAJECTORIES AND SURGE LINES IN H.P. COMPRESSOR - SEA LEVEL ACCELERATION.

Compressors respectively. In both compressors, the inclusion of heat transfer effects (ie the 'cold' case) lowers the predicted trajectories, principally due to heat absorptions altering the compressor characteristics, and to losses of H.P. cooling air through the seals. Surge lines are predicted to rise when thermal effects are included, the beneficial effects of heat absorption in the compressor outweighing the detrimental effect of the higher tip clearance in the transient (in H.P. Compressor only, the L.P. Compressor tip clearances remain close to steady-running values). Thus the inclusion of thermal effects in the prediction of surge margins in the acceleration of an initially 'cold' engine indicates that the margins are considerably greater than would have been predicted by an adiabatic procedure. Both the surge line and the transient trajectory are moved favourably. For this engine, it is only in the H.P. Compressor that trajectories come near to the surge line. With the fuel schedule used for this demonstration, adiabatic prediction indicates that about 65 percent of the surge margin in the H.P. Compressor is used - based on the distance between the

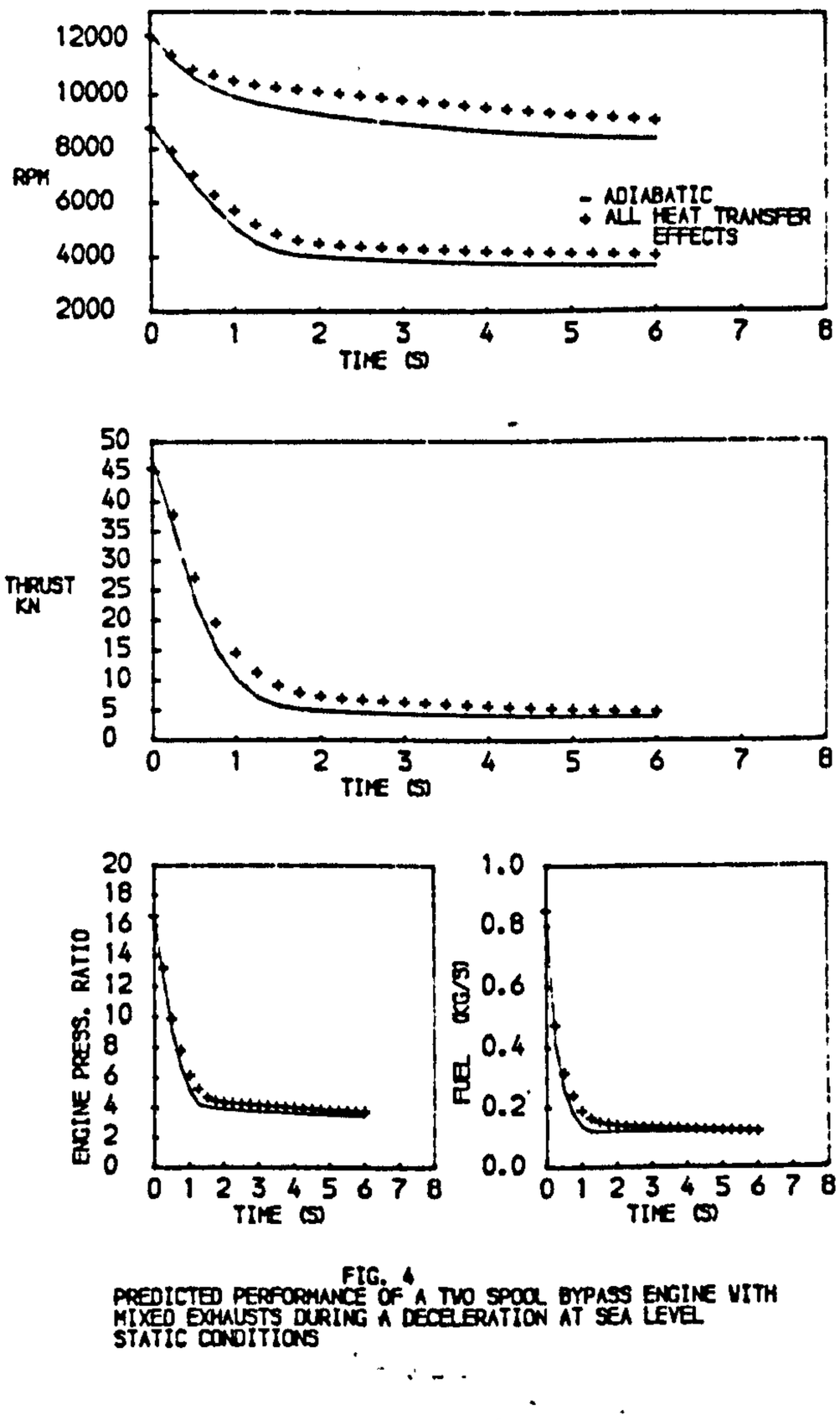

FIG. 4
PREDICTED PERFORMANCE OF A TWO SPOOL BYPASS ENGINE WITH MIXED EXHAUSTS DURING A DECELERATION AT SEA LEVEL STATIC CONDITIONS

surge line and the steady-running line. If the engine is simulated with all the thermal effects included in the model, the surge margin actually used is less than 50 percent of the steady-state surge margin.

A similar study has been made of a deceleration, again at sea level, static conditions. The predicted thrust, speed and pressure ratio responses are given in Fig. 4. It is noticed that when heat transfer effects are included, the predicted responses, particularly in the latter part of the deceleration, are significantly slower than those predicted ignoring thermal effects. This is primarily due to the relatively small air flows through the engine towards the end of the deceleration. The predicted trajectories and surge lines in the compressor are shown in Figs. 5 and 6. Inclusion of thermal effects makes only a small difference to the trajectories, raising them slightly closer to the steady-running lines. The surge lines, when thermal effects are incorporated deteriorate, particularly in the latter part of the transient. In the L.P. Compressor the trajectory at the end of the deceleration approaches, but does not touch the surge line. The deterioration of the surge lines and the raising of the transient trajectories when thermal effects are included, occur for the same reasons which caused the equivalent changes during the acceleration, discussed in the previous paragraph, though in this case the directions of all the changes are reversed.

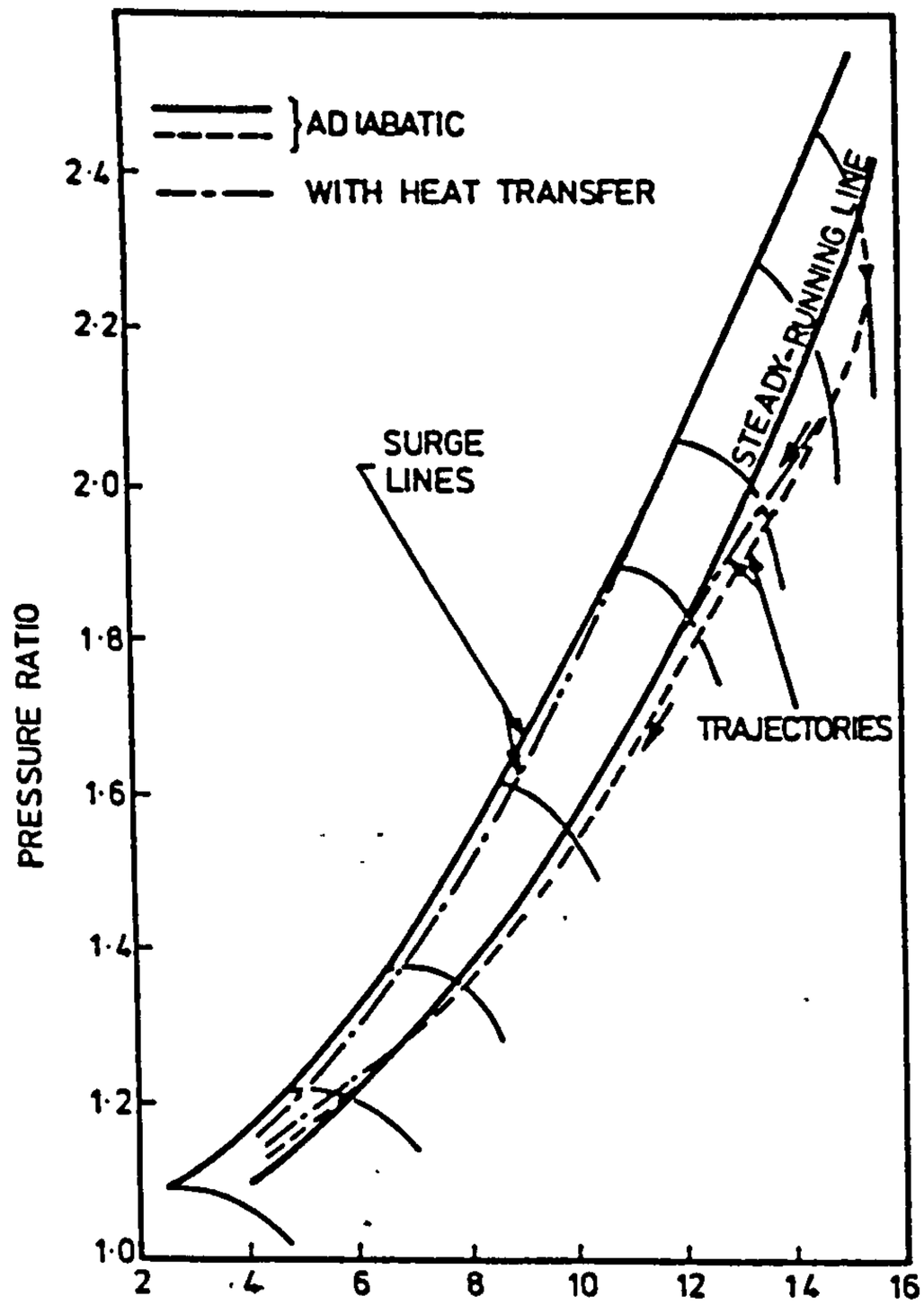

Fig. 5. PREDICTED TRAJECTORIES AND SURGE LINES IN L.P. COMPRESSOR – SEA LEVEL DECELERATION.

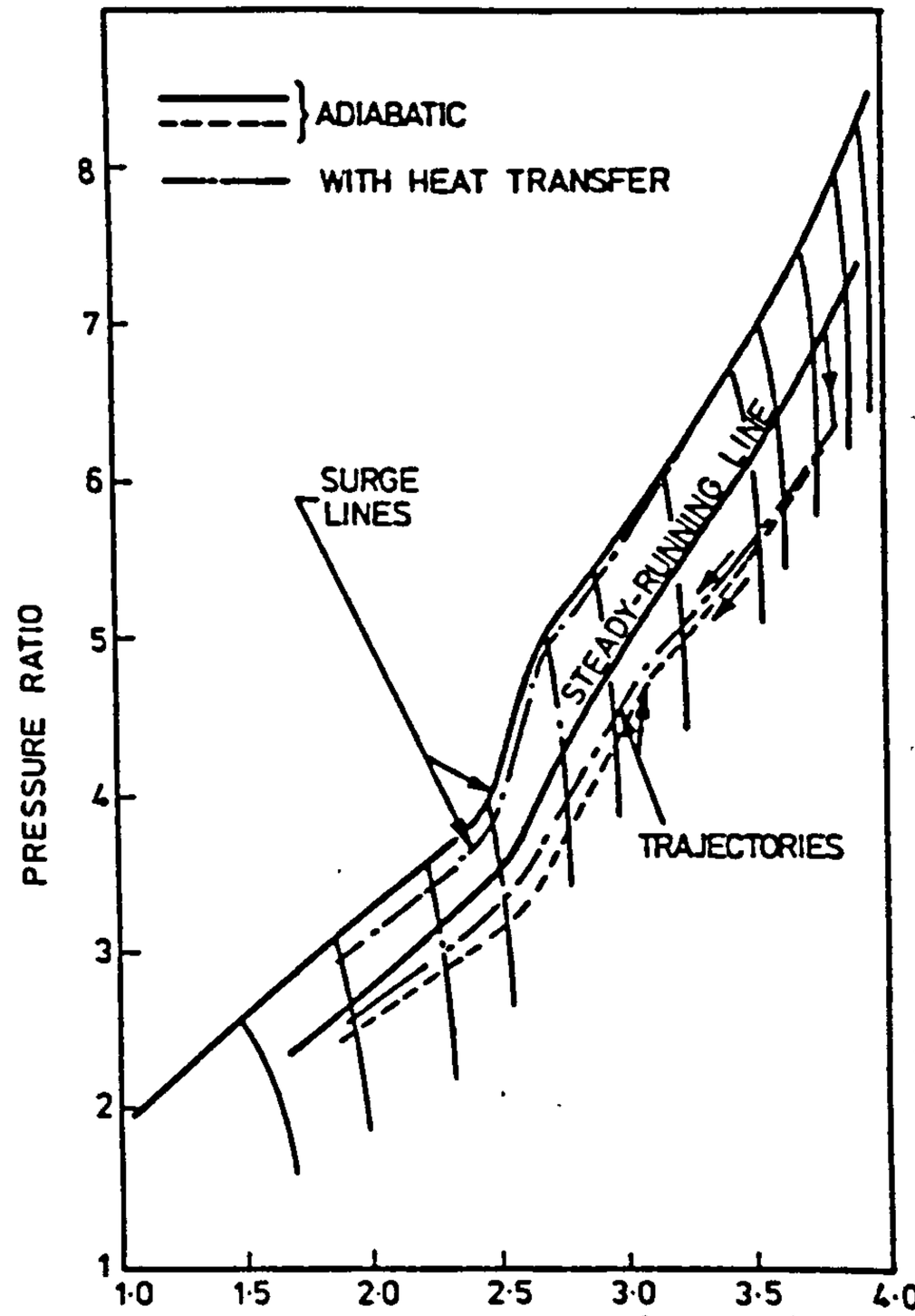

Fig. 6. PREDICTED TRAJECTORIES AND SURGE LINES IN H.P. COMPRESSOR – SEA LEVEL DECELERATION.

The observation that surge lines at the end of a deceleration are predicted to have deteriorated suggests that there is more danger of encountering surge when attempting to accelerate a 'hot' engine. This indeed has frequently been found to be the case in practice. The form of this transient test is the 'Eddie' transient, described earlier in this section. In this transient the engine is first stabilised at maximum speed, then rapidly decelerated, followed quickly by an acceleration. The thrust, speed and pressure ratio responses in such a 'hot' acceleration have already been shown in Fig. 1, where the predictions including thermal effects show significantly faster accelerations than for a 'cold' engine, and indeed than for an adiabatic engine. The corresponding trajectories and surge lines in the compressors are shown in Figs. 7 and 8 where they are compared with the equivalent predictions for the acceleration of the 'cold' engine. In the H.P. Compressor the surge margins in the 'hot' acceleration are lower than in the 'cold' acceleration. About 65 percent of the steady-running margin is used in the 'hot' case, while as previously stated, less than 50 per cent is used in the 'cold' case. The situation in the I.P. Compressor is less critical, though here again the effective surge margin is less in the 'hot' acceleration than in the 'cold' acceleration.

It might be argued that, since the 'hot' acceleration is significantly more rapid than the 'cold' one (Fig. 1) when the same fuel schedule is being used for both accelerations, then it might be worth using a less rapid schedule for 'hot' accelerations, such that the two response rates would be similar. This would ease the surge tendency in the compressors. The prediction programs used in the present work would be suitable for exhibiting such a revised accelerating fuel schedule.

5. CONCLUSION

Models for the heat transfer effects of non-adiabatic flow, altered boundary layer development, tip clearance changes and seal clearance changes have been incorporated in a general gas turbine transient program. The modelling includes the influence of these effects on the characteristics of components.

The prediction program has been applied, as an illustration, to a two-spool bypass engine with mixed exhausts. The inclusion of thermal effects in a typical 'cold' acceleration indicates considerable increases of the predicted margin between the transient trajectory and the surge line in the I.P. Compressor, which is the critical one. In a 'hot' acceleration this margin is reduced.

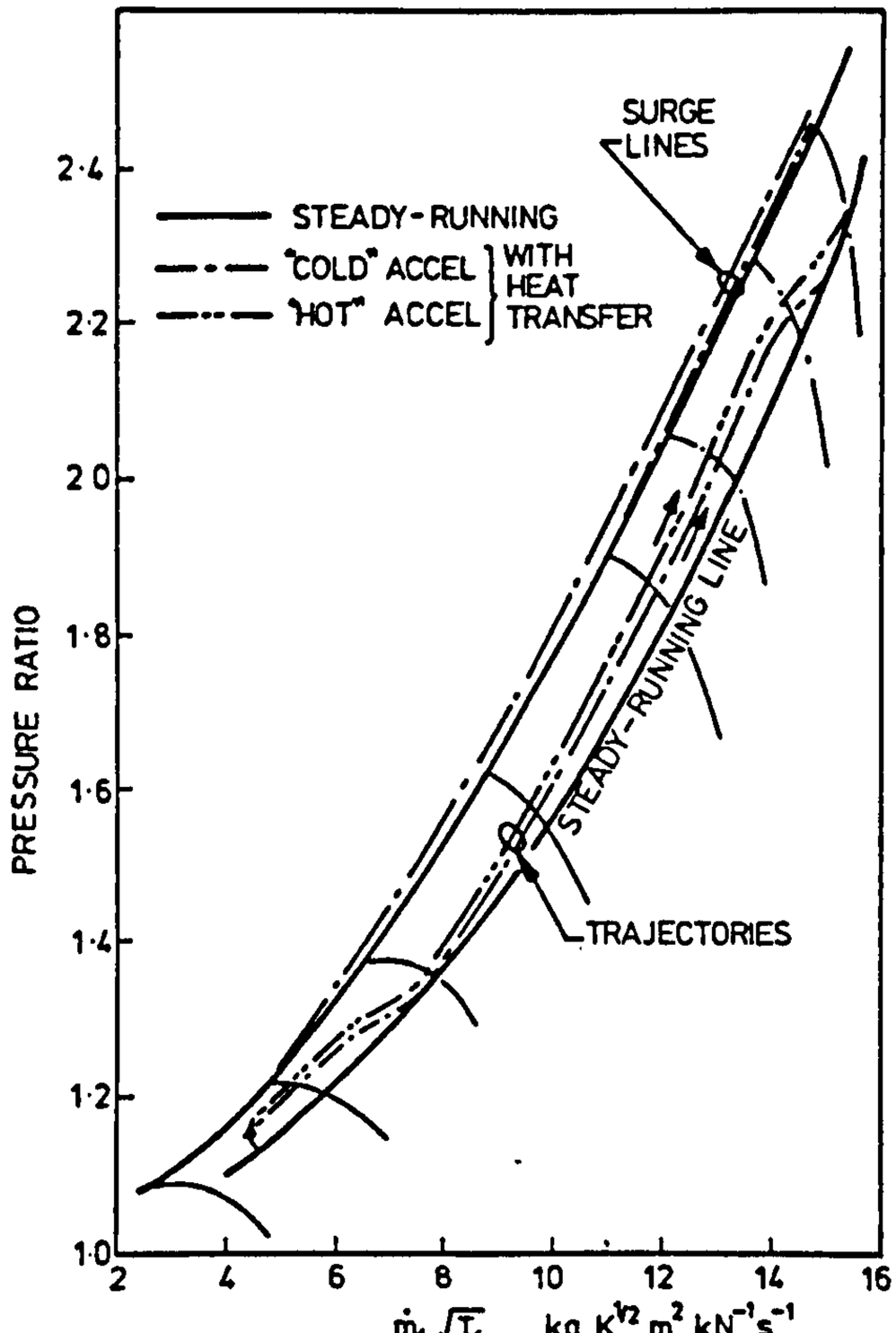

Fig. 7. PREDICTED TRAJECTORIES AND SURGE LINES IN L.P. COMPRESSOR - "COLD" AND "HOT" ACCELERATIONS AT SEA LEVEL.

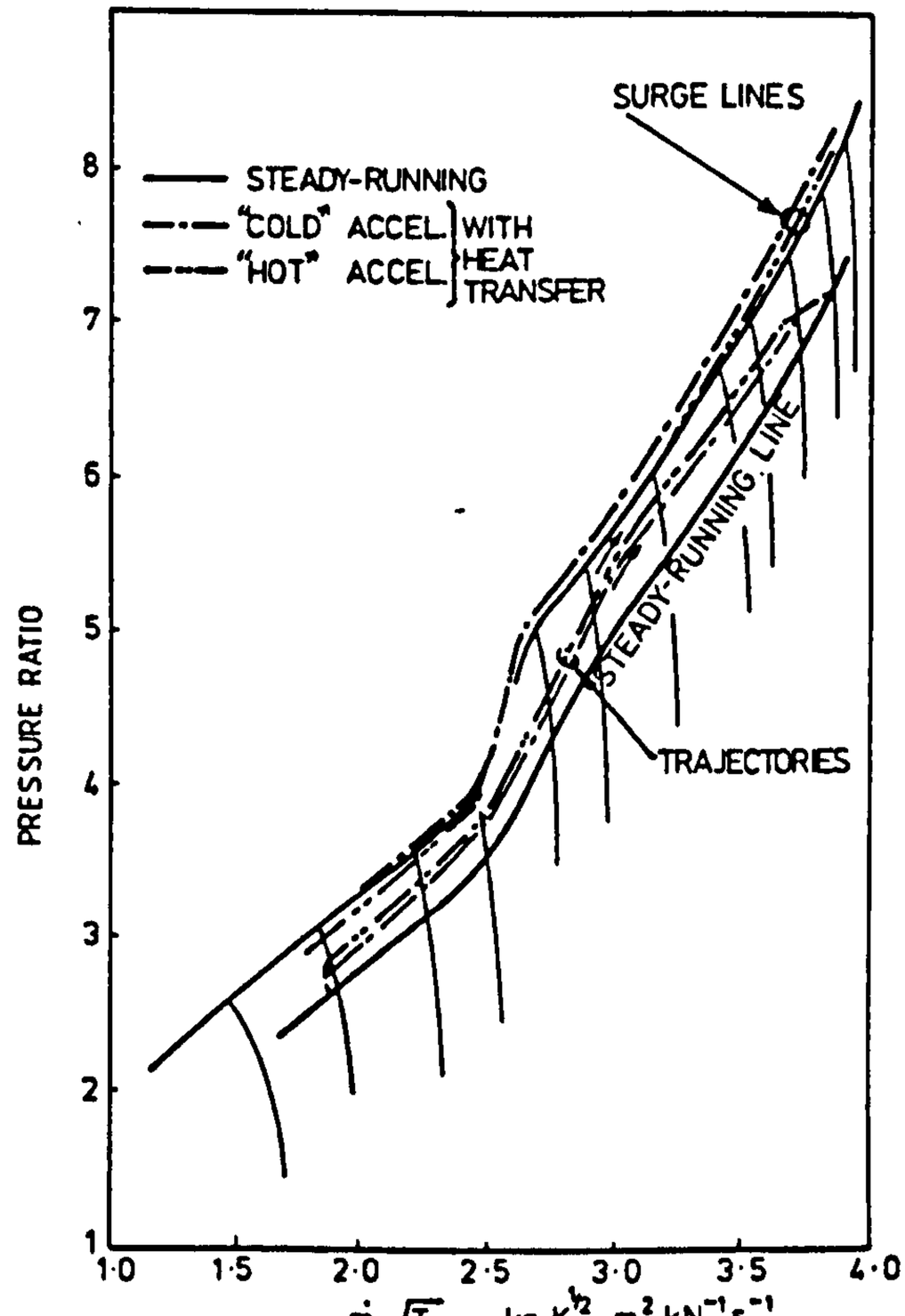

Fig. 8. PREDICTED TRAJECTORIES AND SURGE LINES IN H.P. COMPRESSOR - "COLD" AND "HOT" ACCELERATION AT SEA LEVEL.

6. ACKNOWLEDGEMENT

The authors wish to thank colleagues at Rolls-Royce Limited, Caledonian Airmotive Limited and the University of Glasgow for provision of data, for valuable comments and for encouragement.

7. REFERENCES

1. Koff. F.L., 'Designing for Fighter Engine Transients',
ACARD Conference Proceedings 324, Paper 2, 1982.

2. Maccallum, N.R.L., 'Axial Compressor Characteristics During Transients',
ibid, Paper 22, 1982.

3. Larjola, J., 'Simulation of Surge Margin Changes due to Heat Transfer Effects in Gas Turbine Transients',
A.S.M.E. Paper 84-GT-129, 1984.

4. Koch, C.C., 'Stalling Pressure Rise Capability of Axial Flow Compressor Stages',
Journal of Engineering for Power, vol 103, 1981, pp 645-656.

5. Howell, A.R. and Bonham, R.P. 'Overall and Stage Characteristics of Axial Flow Compressors',
Proceedings of the Inst. Mech. Engrs., vol 163, 1950.

6. Smith, L.H. Jr., 'Casing Boundary Layers in Multistage Axial-Flow Compressors',
Flow Research on Blading, ed L.S. Izung, Elsevier Publishing, Amsterdam, The Netherlands, 1970, pp 275-304.

7. Maccallum, N.R.L., 'Further Studies of the Influence of Thermal Effects on the Predicted Acceleration of Gas Turbines',
A.S.M.E. Paper 81-GT-21, 1981.

8. Pilidis, P., 'Digital Simulation of Gas Turbine Performance',
Ph.D. Thesis, University of Glasgow, 1983.

9. Maccallum, N.P.L. and Grant, A.D., 'The Effect of Boundary Layer Changes due to Transient Heat Transfer on the Performance of an Axial Flow Air Compressor',
S.A.E. Paper 770284, 1977.

10. Pilidis, P., and Maccallum, N.P.L., 'A Study of the Prediction of Tip and Seal Clearances and their Effects on Gas Turbine Transients',
A.S.M.E. Paper 84-GT-245, 1984.

11. Pilidis, P and Maccallum, N.P.L., 'A General Program for the Prediction of the Transient Performance of Gas Turbines',
Paper offered to the A.S.M.E. Gas Turbine Conference, 1985.

Publication 32

85-GT-158

THE AMERICAN SOCIETY OF MECHANICAL ENGINEERS
345 E. 47 St., New York, N.Y. 10017

Description of an Industry—University Liaison Rolls-Royce Scottish Factories— Glasgow University 1968-84

N. R. L. MACCALLUM, Reader
Department of Mechanical Engineering
University of Glasgow, Glasgow, Scotland

F. S. REFORD, Chief Performance and Stress Engineer,
Rolls-Royce Limited
East Kilbride, Scotland.

ABSTRACT

The paper describes the liaison that has developed between Rolls-Royce Limited (Scottish Factories) and the Department of Mechanical Engineering of the University of Glasgow and indicates the benefits that have been obtained by both sides.

Of benefit to the University have been stimulating contacts with industry, from which have come topics for meaningful investigations, both in projects by undergraduates and in research by postgraduates and staff. Students at the University have also benefited by being able to visit Rolls-Royce's Scottish Factories, and have Rolls-Royce staff give lectures to the Engineering Society.

One advantage to Rolls-Royce is that students at Glasgow University have had frequent contacts with the Company and are aware of its aims and achievements. Also, there has been technical benefit to the Company from the general research and from several specific studies carried out on a consultancy basis.

1. INTRODUCTION

This paper describes a liaison that has been built up over a period of more than 16 years between Rolls-Royce Limited (Scottish Factories) and the Mechanical Engineering Department of the University of Glasgow.

The first author, after spending several years as a lecturer at the University of Glasgow, joined the Scottish Group of Rolls-Royce Limited as a performance engineer in 1961. Some 15 months later he accepted an invitation to return to the University of Glasgow's Department of Mechanical Engineering, and he has continued in that Department to the present. There he assumed, for a period, responsibility for lectures on gas turbines in the Final Year Thermodynamics Course, and also introduced projects in that field for Final Year Students. The ground was thus prepared for the more active liaison between Rolls-Royce and Glasgow University which was shortly to begin.

In 1968 a meeting was held between representatives of Rolls-Royce and of the Mechanical Engineering Department of Glasgow University. At that meeting Alun D. Jones, at that time Chief Performance Engineer of the Scottish Group of the Company, indicated areas where performance difficulties were being experienced, and suggested that long-term fundamental research in these areas would be beneficial to the industry. The research work which followed, on what can be described as thermal effects in gas turbine transients, is described in Paragraph 2.1 below. Arising from these studies, another long-term research study - of the effects of transversely injected flows in turbines (Paragraph 2.2) - has been undertaken.

The link between the personnel at Rolls-Royce and at Glasgow University strengthened progressively as the investigations referred to above were carried out. This understanding has led Rolls-Royce to ask the University to undertake a number of specific projects. Here the emphasis was on obtaining answers to the particular problems in a short time-scale, to meet the needs of the industrial company. Three of these projects are mentioned in Paragraphs 2.3, 2.4 and 2.5.

2. CALENDAR OF PROJECTS CARRIED OUT AT UNIVERSITY

In this section five programs are described which have been, or are being carried out at the University of Glasgow. The first two are longer term research programs while the other three are short term studies carried out at the request of the Company.

In the two research type programs, for the most part deadlines have not been placed by the industrial collaborator. This arrangement is probably the more desirable when fresh approaches are being made to a problem which is not yet understood. A University environment is very suitable for this type of investigation.

Presented at the Gas Turbine Conference and Exhibit
Houston, Texas — March 18-21, 1985

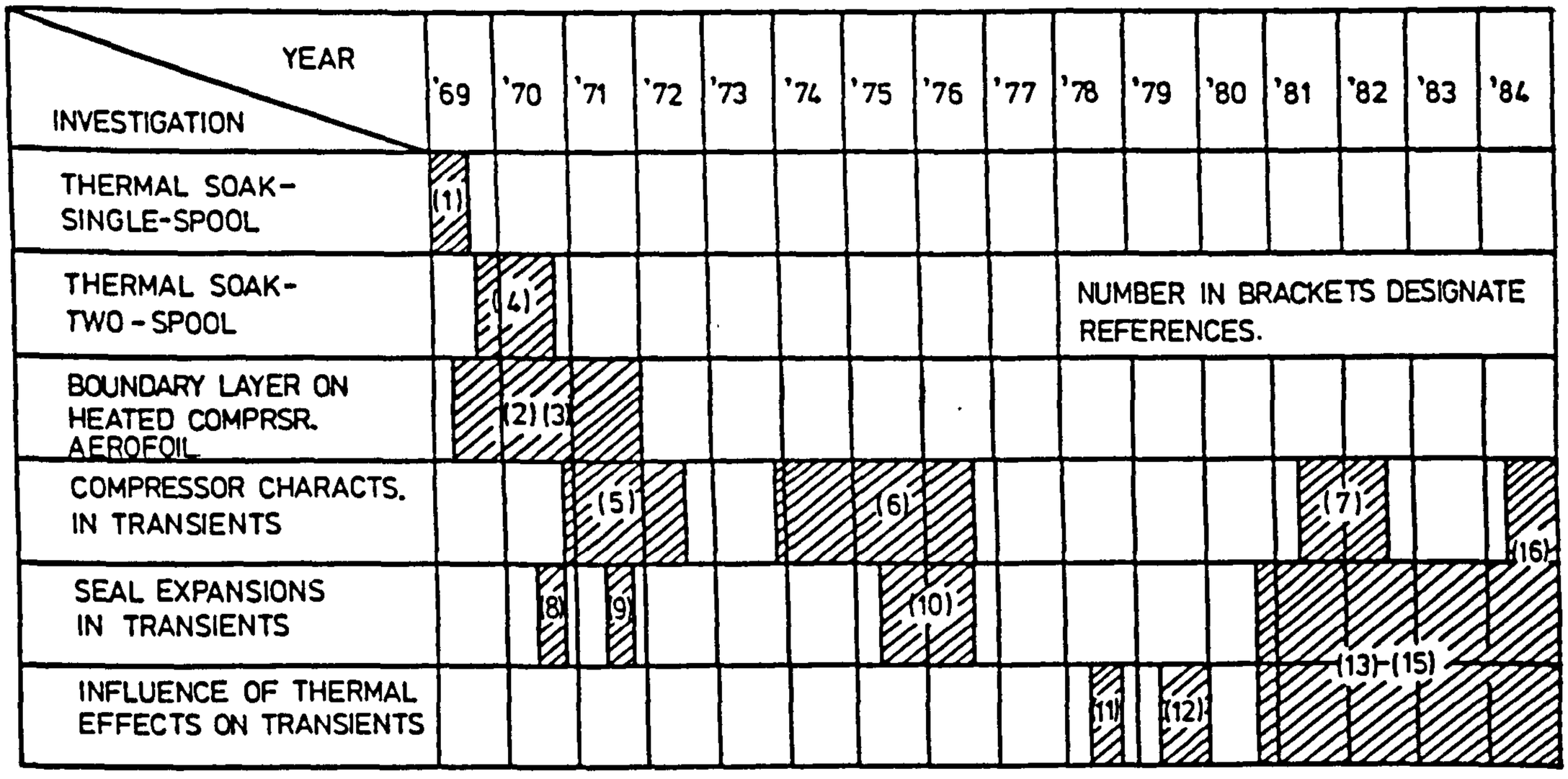

Fig.1. TIMETABLE OF STUDIES OF THERMAL EFFECTS IN GAS TURBINE TRANSIENTS.

2.1 Investigation of Thermal Effects in Gas Turbine Transients

This study initiated from the discussions between Alun D. Jones of Rolls-Royce and staff at the University of Glasgow held in 1968, when Mr. Jones indicated that one of the areas where difficulties were being experienced in aero-gas turbines was in their behaviour during and following transients. One particular difficulty was a problem sometimes encountered when attempting to re-accelerate a "hot" engine - the "Bodie" transient. Mr. Jones invited comment on these problems. In response, the first author of this paper suggested the following program:-

(a) An experimental and theoretical study of the performance of a simple single-spool engine immediately following a rapid acceleration to maximum speed.

(b) An experimental and theoretical study of the behaviour of the boundary layers on a hot compressor blade.

It was proposed that Project (a) be undertaken by the first author, possibly working with a Final Year Undergraduate Student, while Project (b) would be more suitable for a Research Student. Rolls-Royce agreed with this program and, until 1971, provided funds to support the Research Student, A.D. Grant, who worked on Project (b). The proposed studies were carried out and the results from Project (a) were reported in reference (1)[1] and from Project (b) in references (2) and (3). The time-scale under which these, and other thermal effects have been investigated is illustrated in Fig. 1.

1 Underlined numbers in brackets designate references at end of paper.

The agreement (1) found between prediction and experiment in the performance of the single-spool engine immediately following a rapid acceleration - the " thermal soak " transient - encouraged the continuation of these studies. A similar theoretical investigation was next made on a two-spool bypass engine (4).

A new line of investigation was then started by the first author:-

(c) A prediction of the alterations in the characteristics of compressors during transients due to (i) density changes resulting from heat transfers and (ii) alterations in boundary layer development as indicated by Project (b) above.

In the initial study, only the density change effect (i) was considered. This indicated significant reductions in surge margins when attempting to reaccelerate a hot engine (5). Later studies improved the technique for predicting the characteristics, and included the aerofoil boundary layer effects (6) and, most recently, the end-wall boundary layer development (7), (16). The results of these later studies added support to the initial forecasts of lowering the surge line when the engine is hot, and raising the surge line when it is cold.

It had been realised from an early stage that the engine behaviour in transients is influenced by blade tip clearances and seal clearances. Thus a further investigation was commenced:-

(d) The prediction of seal and blade tip clearances during transients.

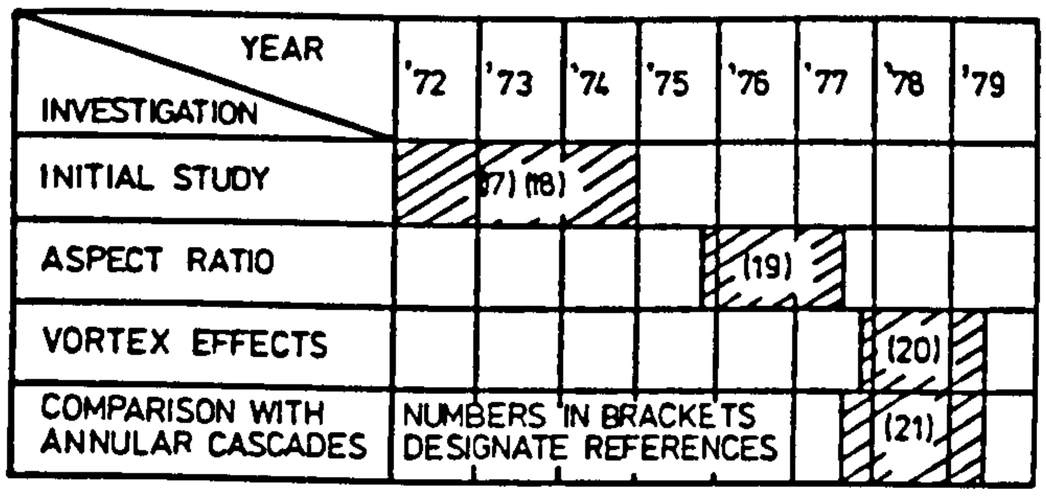

Fig.2. TIMETABLE OF STUDIES OF TRANSVERSE INJECTION.

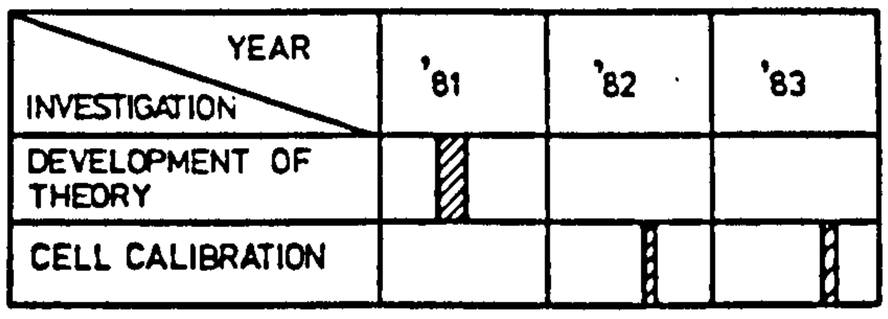

Fig.3. TIMETABLE OF STUDIES OF THRUST CORRECTION.

The first investigation, using finite difference methods, was made on a seal controlling the flow of high pressure cooling air over the front face of the first turbine disc of a two-spool engine (8). The method was then applied to a modified design (9), and a paper was subsequently published (10) describing some of this work.

About eight years after starting these investigations of thermal effects, it was decided to incorporate the results into an engine transient program, to determine the influence of these effects on the predicted acceleration and deceleration rates - Project (e). The subject of the first study (11) was the single-spool engine. Later studies have extended this to the two-spool bypass engine (12). These investigations incorporated the direct thermal effects of heat absorption and also compressor characteristics alteration. Models have since been developed by a Research Student - P. Pilidis, to describe tip clearance and seal clearance responses. These models have been included in the engine transient program (13), (14). In the most recent work (15), (16) all effects, including changes in compressor characteristics, have been incorporated in the engine transient program. This work has provided an explanation, for example, for observed acceleration rates being much lower than those predicted using steady-running component characteristics and ignoring thermal effects.

2.2 Investigation of Transversely Injected Flows in Turbines

The hotter turbine discs in aero-gas turbines are usually cooled by air drawn from the compressor delivery. The magnitude of the cooling air flow is controlled by the clearance in a seal. The investigations described above in Paragraph 2.1 have indicated that, during transients, the openings of these seals can be considerably greater than the design openings. The cooling air which passes through these seals then moves radially outwards over the turbine disc and flows transversely into the main gas stream passing through the gap between the turbine blade platforms and the inner platforms of the adjacent nozzle guide vaners. It was not known what effect this transversely injected flow might have on the main flow in the turbine. Alun D. Jones of Rolls-Royce suggested that this topic might be investigated at the University. A research program, supervised by the first author, was therefore started. Two research students have carried out the bulk of this work (references (17) to (21). Grants from the Science Research Council have provided technician support, and allowed the purchase of essential equipment. The timetable of this research programme is illustrated in Fig. 2. This program is not regarded as complete.

2.3 Thrust Corrections in Test Cells

This investigation was requested by Rolls-Royce to provide answers to specific problems relating to the conditions under which a particular engine type was being tested in a particular Test Cell. The time-scale on which answers were required was much shorter than for the research programs described earlier. This study has developed in a succession of stages, each one having to be completed reasonably swiftly. The timetable is illustrated in Fig. 3.

2.4 Model for analysis of performance of Turbine of Turbo-prop Engine

This was the shortest of the projects carried out at the University and required only a few days work. It involved a collaboration on determining the procedure for analysing the test performance of a turbo-prop engine. A first scheme was presented by Rolls-Royce. This was studied and commented on by the University, and an agreed procedure was then established.

2.5 Model for Transient Performance of a Two-Spool Turbofan Engine

As a result of the expertise which the University had built up, Rolls-Royce asked the University to carry out a research project on the transient modelling of a two-spool turbofan engine. This investigation is drawing on the results of the studies which have been described in Paragraph 2.1 above.

3. BENEFITS TO UNIVERSITY

There have been numerous benefits to the University from this link with industry.

3.1 Influence on Courses

The interaction between the University staff and the staff at Rolls-Royce has meant that the subject matter taught in the Undergraduate Courses has been more appropriate to the current and expected future needs of industry in that field. An example has been the optional course " Gas Dynamics and Thermodynamic Machines", offered to 4th Year students of Mechanical Engineering (and also available to Aeronautical Engineering students). Information deriving from the collaboration with Rolls-Royce has also been used in classes in earlier years of the Undergraduate Course.

The knowledge gained in this Industry/University link has in addition been used in a less technical course - entitled " Technology and Society" - which is offered to Arts, Social Science and Divinity Students. Lectures on the subject of " New Product Development" were illustrated with reference to the development of jet engines.

It is widely recognised that students obtain a better and more lasting understanding of a lecture if the lecturer can illustrate the subject with examples occurring in industry. Lecturers at Glasgow University have been able to provide such illustrations in various areas of gas turbine technology and manufacture thanks to the Industry/University link which has been established.

3.2 Lectures at Glasgow University by Rolls-Royce Staff

Over a long period of time, students and staff at Glasgow University have invited staff of Rolls-Royce to give lectures on the work of the Company. The link which has developed in recent years between the University and the Company has made such invitations easier. The second author has recently given one such lecture to the Engineering Society of Glasgow University.

3.3 Topics for Undergraduate Projects

For the last twenty years, Project work has formed an integral part of the Final Year Course for Honours Mechanical Engineering Students (and more recently for Ordinary Students) at Glasgow University. Performance in the Project provides 20 per cent of the assessment for the B.Sc. Degree Honours award. The Projects usually involve some research or development as this provides the student with opportunity for using initiative, and serves as an introduction to the open-ended problems which the young engineer will shortly be meeting.

It is desirable for these projects to be related to situations occurring in industry. In this context the link between the University and Rolls-Royce has been very valuable. Many topics for investigation have been offered and these have been popular with students. Topics have ranged from the performance of labyrinth seals to transient temperature distributions in air-cooled turbine blades. To date, twenty-eight projects relating to gas turbines have been undertaken. A vital requirement for the success of these projects has been the ease of obtaining information and data.

3.4 Topics for Postgraduate Research

The research programs described in Section 2 above have provided subjects for investigation by four Postgraduate Research Students. One of the Research students was sponsored for part of his period by Rolls-Royce. Two of the students were supported by Science Research Council (U.K.) Grants, while the fourth student was sponsored by a Glasgow University Scholarship. The students engaged in these projects have been stimulated and encouraged by the contacts with industry and by the relationship between their own work and the industrial application.

3.5 Visits to Rolls-Royce Scottish Factories

The ties which have been built up between the University and Rolls-Royce Limited have made it possible to arrange numerous visits by parties of students to the local Rolls-Royce Factories. The visits have been tailored to the needs of the particular groups of students. For example the students from the Technology and Society Class were more interested in seeing the modern manufacturing facility than in seeing the factory where used engines are stripped, overhauled, repaired and reassembled. By contrast, students from the Engineering Faculty preferred to see the overhaul and development work and the Test Bed Facility.

These visits have always proved well worthwhile and have been much appreciated by the students. The University staff are very conscious of the improved understanding of the subject which the students gain.

4. BENEFITS TO INDUSTRY

The liaison with Glasgow University has provided the Rolls-Royce Scottish Factories with both short and long term benefits. The term " short " embraces specific work packages subcontracted to the University within defined time-scales. The " long " term definition, on the other hand, refers firstly to the research effort, where the time-scale is less demanding, and secondly to the indirect influence on University teaching and hence on the recruitment potential of future Graduates.

Up to the present day, three short term packages have been undertaken, as described in Paragraphs 2.3 to 2.5, The technical content of the work was such that the packages could have been carried out within the Company, had the manpower resource been available. Subcontract offered a ready solution and, on the basis of the service supplied on the "long" term research, Paragraphs 2.1 and 2.2, Glasgow University was a natural choice. Two features emerged from the execution of the work. The first was that the University, as an academic institution, proved itself capable of working to defined industrial time-scales. The second was the input of a fresh approach uncluttered by past experience. All individuals and companies draw on past events or solutions in approaching a problem. In the extreme, a company can become confined by that very experience. An outsider does not suffer such confinement, particularly when, coming from a University, he has access to a wider range of disciplines through his

colleagues. Thus Rolls-Royce found that the techniques employed by the University in the "short" term packages were not necessarily "the way we would have done it". This created the stimulus to both parties of challenge and debate.

A simple example of the foregoing arose in the course of the Test Cell Correction outlined in Paragraph 2.3. All jet engines produce a lower measured thrust when tested within an enclosed structure, or test cell, than when in, say, an open field. This arises due to the airflow induced around the engine carcase by the gas jet from the engine flowing through the exhaust detuner. The difference between measured and true thrust is thus a function of the engine characteristics and the test cell geometry. All test cells must therefore be calibrated to establish the magnitude of the thrust correction. In 1981/82 one of the Company's established test cells was modified to accommodate an afterburning military engine. The engine had been in production for many years and thus had been tested in basically similar cells. The calibration test, however, revealed a thrust correction quite unlike past experience on this engine or, for that matter, any other Rolls-Royce afterburning engine. Not unnaturally the first reaction was of disbelief and the tests were repeated only to show the same effect. Due to the need to have the cell in production, the Company was faced with the requirement of entering into a fairly complex series of induced airflow measurements in order to establish the reason for the unusual correction. Lack of an immediately available resource led the Company to request the assistance of Glasgow University. The latter examined the test results, studied the plans of the test cell and then postulated a rational thermodynamic explanation based on the fluid mechanics of the nozzle gas flow and the induced, or entrained air. The theory required a relatively small amount of confirmatory measurements and so, in effect, was a very cost effective solution.

The long term research effort, started by the University in 1968, has made a significant contribution towards what is still a subject in its infancy, namely the prediction of transient engine performance. The benefits of that work are reflected in the Company's awareness of those design features which influence transient behaviour. Thus one is able to anticipate potential problems in the design of a new engine and make allowance whilst still on the drawing board. This has led to the current collaborative effort between the company and the University, Paragraph 2.5, on the predicted transient behaviour of a type of turbofan engine where little design experience exists within the Company.

Traditionally the Rolls-Royce Scottish Factories have drawn the bulk of their graduate recruitment from the local Universities of Glasgow and Strathclyde. It can be argued, therefore, that it is in the Company's long term interest to influence university teaching by promoting interaction on real problems as they arise in an industrial environment. All too often the universities are criticised for being pre-occupied with the development of academic skills rather than training young people to be able to solve the practical problems of manufacturing industry. There are many ways in which industry and the universities are approaching this problem. They range from the formal Teaching Company Scheme, sponsored in the U.K. by the Department of Industry and the Science and Engineering Research Council, to the somewhat informal liaison described in this paper. The latter blends a spectrum of fundamental research, specific problem solving and student society discussion into a productive relationship.

5. CONCLUSIONS

The liaison between the University of Glasgow and the Rolls-Royce Scottish Factories has been of benefit to both parties. The University has gained in terms of industrial participation, research funding and student exposure to a non-academic environment. The Company, in turn, has benefited by way of access to a specialist sub-contractor capable of working to industrial time-scales. A common advantage to both the University and the Company is the impact of the cross-fertilisation process on the nature and relevance of University teaching.

6. ACKNOWLEDGEMENTS

The authors wish to thank their many colleagues at Rolls-Royce and Glasgow University who have collaborated in the Industry-University Liaison described in this paper. In particular they wish to thank Alun D. Jones of Rolls-Royce who initiated the link.

7. REFERENCES

1. Maccallum, N.R.L., "Performance of turbojet engines during the 'thermal soak' transient." Proc. Instn. Mech. Engineers, 1969-70, Vol. 184, Part 3GII, 23-29.

2. Grant, A.D., "The effect of heat transfer on boundary layer stability in axial flow compressors." Heat and Fluid Flow in Steam and Gas Turbine Plant, Instn. Mech. Engineers, London, 1974, 252-258.

3. Grant, A.D., "The effect of heat transfer on boundary layer stability." Ph.D. Thesis, University of Glasgow, 1973.

4. Maccallum, N.R.L., "The performance of the Spey RB163-25 Engine during the 'thermal soak' transient." Mech. Eng. Dept. Report, University of Glasgow, 1970.

5. Maccallum, N.R.L., "The effect of 'bulk' heat transfers in aircraft gas turbines on compressor surge margins." Heat and Fluid Flow in Steam and Gas Turbine Plant, Instn. Mech. Engineers, London, 1974, 94-100.

6. Maccallum, N.R.L. and Grant, A.D., "The effect of boundary layer changes due to transient heat transfer on the performance of an axial-flow air compressor." SAE Transactions Paper No. 770284, 1977.

7. Maccallum, N.R.L., "Axial Compressor characteristics during transients." AGARD Conference Proceedings No. 324, Paper No. 22, 1982.

8. Maccallum, N.R.L., "Spey RB163-25 Engine, Transient Expansion of the components of the H.P. Air Seal on the H.P.I. Turbine Disc." Mech. Eng. Dept. Report, University of Glasgow, 1970.

9. Macccallum, N.R.L., "Spey RB163-25 Engine, Transient behaviour of modified HP Air seal on the H.P.1. Turbine disc." Mech. Eng. Dept. Reports, University of Glasgow, 1971.

10. Maccallum, N.R.L., "Transient expansion of the components of an air seal on a gas turbine disc." SAE Paper No. 770974, 1977.

11. Maccallum, N.R.L., "Thermal influences in gas turbine transients -effects of changes in compressor characteristics." ASME Paper 79-GT-143.

12. Maccallum, N.R.L., "Further studies of the influence of thermal effects on the predicted acceleration of gas turbines." ASME Paper 81-GT-21.

13. Pilidis, P. and Maccallum, N.R.L., "Models for predicting tip clearance changes in gas turbines." AGARD Conference Proceedings No. 324, Paper No. 17, 1982.

14. Pilidis, P. and Maccallum, N.R.L., "A study of the prediction of tip and seal clearances and their effects in gas turbine transients." ASME Paper 84-GT-245.

15. Pilidis, P. and Maccallum, N.R.L., "A general program for the prediction of the transient performance of gas turbines." Paper to ASME International Gas Turbine Conference, March 1985.

16. Maccallum, N.R.L., and Pilidis, P., "The prediction of surge margins during gas turbine transients." Paper to ASME International Gas Turbine Conference, March 1985.

17. Shrivastava, K.D. and Maccallum, N.R.L., "The effect of a transversely injected stream on the
18. flow through turbine cascades: Part I - Flow effects Part II - Performance changes." ASME Papers 77-GT-87 and 77-GT-88.

19. Aburwin, B.A. and Maccallum, N.R.L., "The effect of a transversely injected stream on the flow through turbine cascades: Part III - Influence of aspect ratio." ASME Paper 78-GT-24 and Journal of Engineering for Power Vol 101, 1979, 61-67.

20. Aburwin, B.A. and Maccallum, N.R.L. "Vortex effects resulting from transverse injection in turbine cascades and attempts at their reduction." ASME Paper 79-GT-18.

21. Bindon, J.P., Aburwin, B.A., and Maccallum, N.R.L., "Comparison of transverse injection effects in annular and in straight cascades." ASME Paper 79-GT-17.

An experimental investigation of the performance of equiangular annular diffusers with swirled flow

A M Elkersh, BSc, PhD
Paisley College of Technology, Scotland
A H Elgammal, BSc, PhD
Alexandria University, Egypt
N R L Maccallum, BSc, PhD, CEng, FIMechE
Department of Mechanical Engineering, Glasgow University, Scotland

An experimental study of the influence of geometrical parameters and swirl on the performance of equiangular diffusers is presented. Three diffusers were tested over a range of inlet swirls up to 45°, the swirls being of free vortex distribution.

The data presented indicate similar flow patterns for different cant angles, and show that the centrifugal forces due to swirl stabilize the flow on the outer wall, while increasing the tendency towards separation at the inner wall. Diffuser performance improves as the inlet swirl increases up to 30°, the improvement being influenced by area ratio and cant angle. A further increase of swirl causes a deterioration of performance.

NOTATION

A cross-sectional area
AR area ratio, A_2/A_1
B_1 blockage, $1 - \bar{C}_x/C_{x,\max}$
C total velocity
C_p area-averaged pressure recovery coefficient

$$C_p = \frac{(1/\mathrm{AR}) \int_{A_2} P_2 \, dA_2 - \int_{A_1} P_1 \, dA_1}{\int_{A_1} \frac{1}{2}\rho C_1^2 \, dA_1}$$

L non-dimensional axial diffuser length $= x_2/\Delta r_1$
m mass flowrate
P static pressure
r radius
Re Reynolds number

$$Re = \frac{2C_x \Delta r}{\nu}$$

T inlet hub–tip ratio $T = r_{i,1}/r_{o,1}$
x axial length
α diffuser cant angle
γ angular momentum ratio

$$\gamma = \frac{\int_{A_2} C_{\theta 2} r \, dA_2}{\mathrm{AR} \int_{A_1} C_{\theta 1} r \, dA_1}$$

Δr annulus height
λ area-averaged total pressure loss coefficient

$$\lambda = 1 - C_p - \frac{\int_{A_2} \frac{1}{2}C_2^2 \, dA_2}{(1/\mathrm{AR}) \int_{A_1} \frac{1}{2}C_1^2 \, dA_1}$$

Subscripts

1, 2 diffuser inlet and exit
i, o inner and outer walls
m meridional direction
max maximum
θ tangential direction

Superscript

– average value

The MS was received on 2 August 1984 and was accepted for publication on 20 February 1985.

1 INTRODUCTION

Annular diffusers are often used in turbo-machines to increase the static pressure and reduce the velocity of the discharge flow. Although annular diffusers have relatively simple geometry, if they are not carefully designed the flow pattern within them frequently shows large energy losses and stall. The flow pattern is further complicated if the flow entering the diffusers is swirled, which is commonly the case for flow leaving turbo-machine rotors.

In view of adverse pressure gradient and the complexity of the flow pattern in annular diffusers with swirled flow, a complete theoretical analysis and hence prediction is rarely possible. Therefore experimental methods have been of great importance in achieving some understanding of the flow behaviour, and also in assessing available theoretical predictions [for example (1)].

The influences of geometrical parameters and swirl on annular diffuser performance have attracted the interest of several research workers [for example Srinath (2), Shaalan and Shabaka (3) and Dovzhik and Kartavenko (4)]. However, the effects of these parameters in equiangular diffusers, of diverging core with equal inner and outer wall angles, have been examined by relatively fewer researchers [for example Coladipietro, Schneider and Sridhar (5) and Markowski, Lohmann and Brookman (6)]. Of these, only Coladipietro (5) has examined equiangular diffusers under flow conditions appropriate to the exit from axial fans. In his studies the average swirl angles at the diffuser inlet were limited to 20°. The aforementioned investigations indicated that equiangular diffusers are more efficient than diffusers of other geometries when the flow at diffuser inlet is swirled.

The present paper extends the studies of flow behaviour in equiangular diffusers. The data presented are obtained from an experimental investigation of the influences of geometrical parameters and swirl on annular diffuser performance (7). A comparison between the measured performance and that predicted by the authors (1) is also given.

The diffusers in question are equiangular, having cant angles of 7°, 16° and 20° and area ratios of 1.65, 2.16 and 2.16 respectively. Each of the three diffusers was tested over a range of inlet swirling flows having nominal average swirl angles of 0°, 15°, 30° and 45°, the swirls being of free vortex pattern.

2 THE EXPERIMENTAL APPARATUS AND INSTRUMENTS

The experimental rig is shown schematically in Fig. 1. The air was blown through the test diffuser by a two-stage contra-rotating axial fan, each stage being driven by a 4.92 kW motor. The annular duct upstream of the diffuser supported the swirl blade rings and allowed measurements of the flow at the diffuser inlet. A hub–tip ratio of 0.5 was chosen for the annular duct as being typical of axial flow fans.

Three swirl blade rings were designed to produce a predetermined free vortex pattern similar to that at the exit from an axial fan. Eighteen swirl blades in each ring had angles to the axial direction, at the mean height of 15°, 30° and 45° and they gave mass average swirl angles at the diffuser inlet plane of 12°, 24° and 36° respectively. The tests with zero swirl were carried out without blades. In this paper these swirl arrangements are identified by the nominal blade angles, namely 0°, 15°, 30° and 45°.

The three equiangular diverging core diffusers tested, and their geometrical parameters and inlet Reynolds numbers based on the average inlet velocity, are shown in Table 1. The outer wall of the diffusers was made of perspex or transparent styrene, thus allowing flow visualization.

Stagnation and static pressures and flow direction were measured using a three-hole cobra probe. The flow was traversed at different sections in a direction perpendicular to the diffuser walls (Fig. 2). All pressures were measured by means of a micro-manometer and the flow angles were measured using a protractor with vernier.

Table 1 Geometry of tested diffusers and inlet Reynolds numbers

Diffuser number	Geometry of the diffusers				$Re_1 \times 10^{-5}$
	T	α	L	AR	
1	0.5	7	7.88	1.65	2.85
2	0.5	16	6.10	2.16	3.60
3	0.5	20	4.80	2.16	3.60

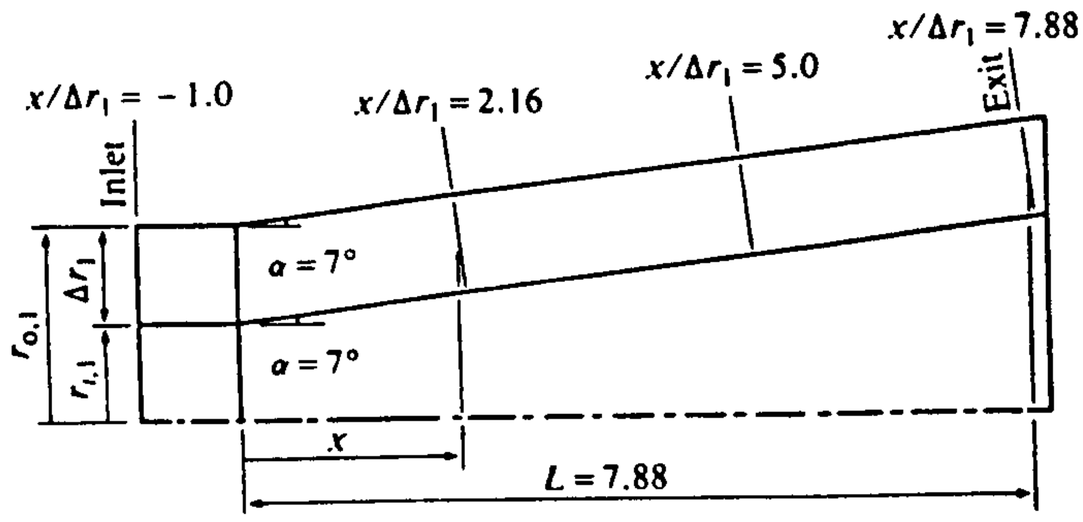

Fig. 2 Geometry of diffuser1

It was confirmed that flow was symmetric about the axis by observing the wall static pressure for each plane at four tappings equally spaced around both the inner and outer walls. The maximum variation between maximum and minimum values of the static pressure was within 4.9 per cent of the local average dynamic head. This symmetry of the flow pattern was also confirmed by means of integration of the meridional velocity profiles. The uncertainty in the diffuser performance is estimated in accordance with Kline and McClintock (8). The uncertainty of the pressure recovery coefficient was within 5 per cent. However, the uncertainty of the total pressure loss coefficient was higher, being 18 and 29 per cent with zero and high swirling flow respectively.

Turbulence measurements at the diffuser inlet were obtained using a hot wire anemometer which indicated a longitudinal turbulence intensity of 2 per cent at the mean annulus height for all swirl angles. Flow visualization was carried out by observing the movement of wool tufts.

3 RESULTS AND DISCUSSION

3.1 Flow traverses

The meridional velocity profiles at different planes along diffuser 1 are shown in Fig. 3.

The meridional velocity profile at the diffuser inlet for non-swirled flow indicates a large boundary layer thickness on the outer wall when compared with the inner wall. This may be attributed to the apparatus configuration with the longer outer wall leading to the diffuser inlet. Another feature noted in the inlet profiles is that the meridional velocities are displaced slightly towards

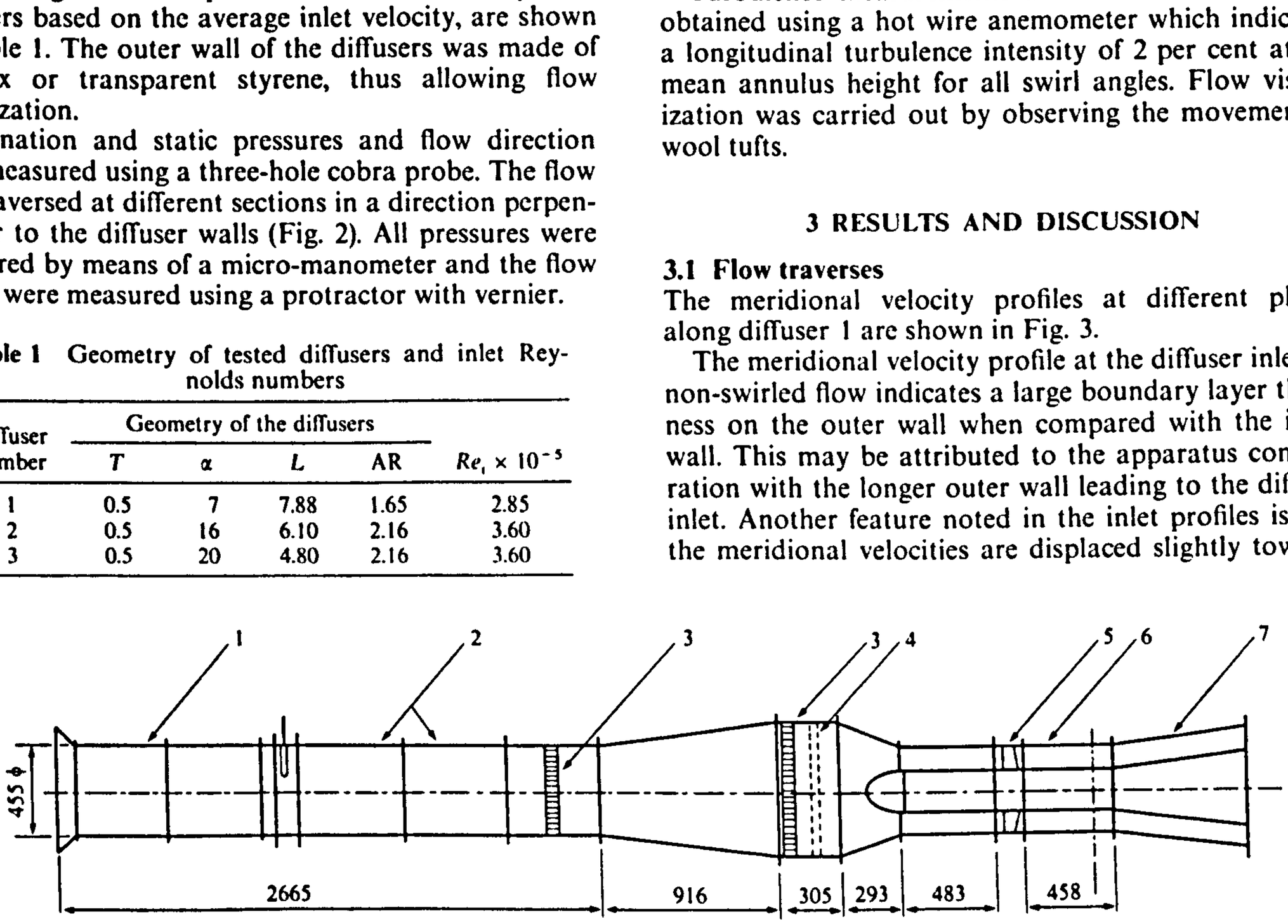

1. Inlet pipe
2. Two-stage axial fan
3. Honeycomb
4. Gauze screens
5. Swirl blade rings
6. Inlet diffuser duct
7. Annular diffuser

Fig. 1 General arrangement of the test rig (dimensions in mm)

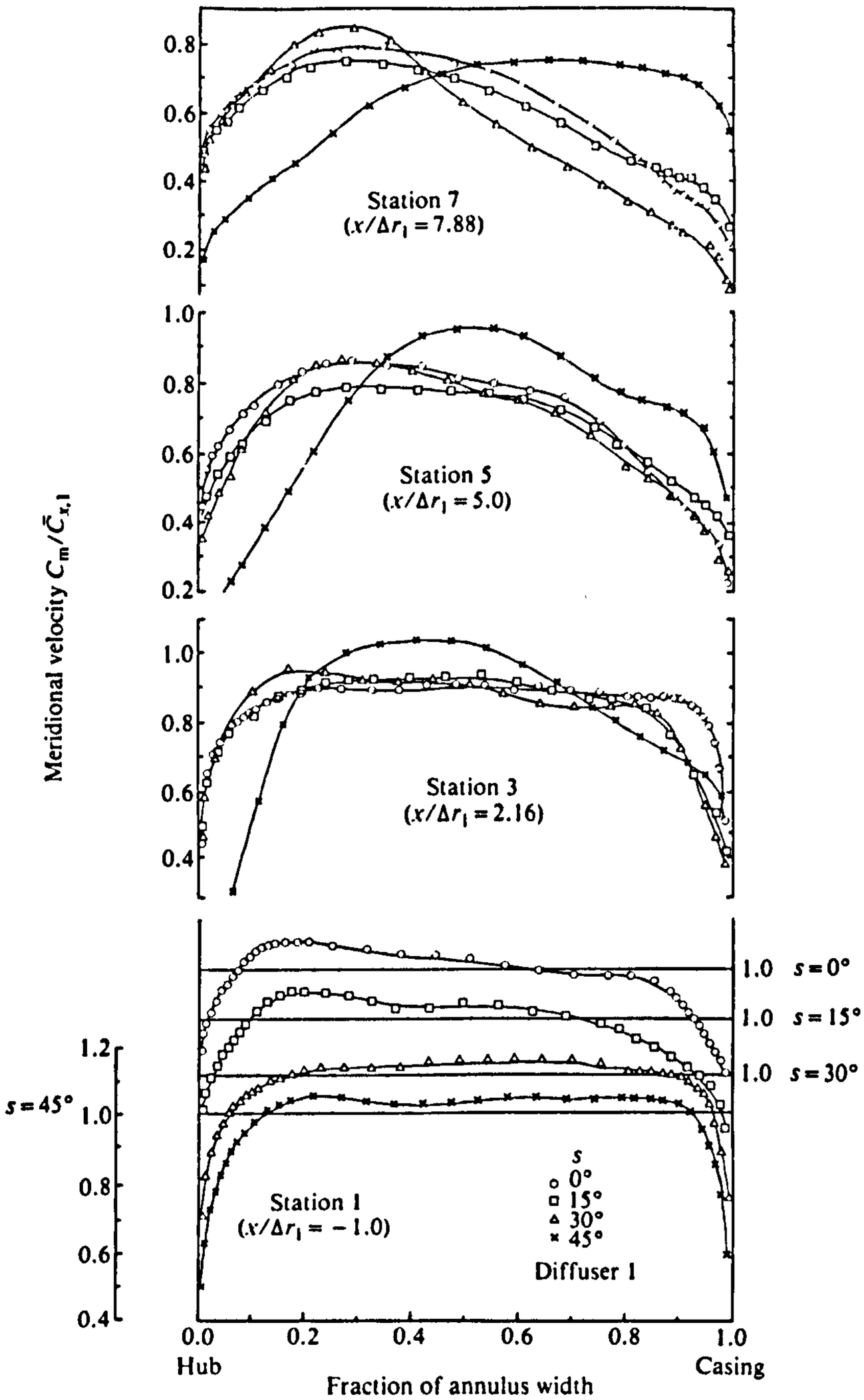

Fig. 3 Meridional velocity profiles at stations 1, 3, 5 and 7

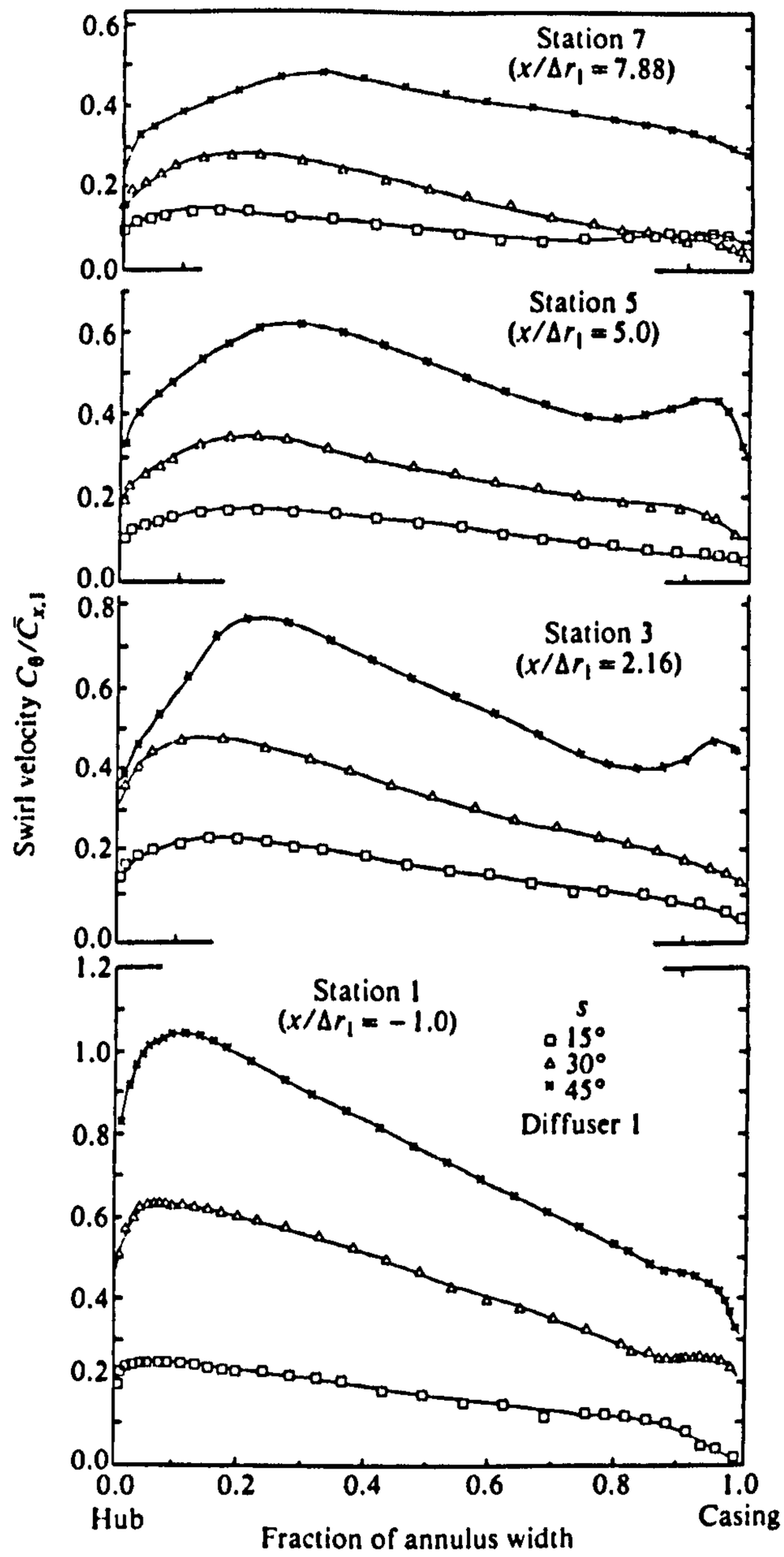

Fig. 4 Swirl velocity profiles at stations 1, 3, 5, and 7

the outer wall as the blade swirl angle is increased. This may be the result of the swirl ring configuration, in which the blade chord is longer at the hub. Associated with this displacement of the inlet profiles, there is a slight decrease in inlet blockage, from 0.04 to 0.035. This small variation in inlet blockage is considered to have little effect on the performance of the diffusers.

Considering the meridional velocity profiles within the diffuser passage and at exit, it is seen that for inlet swirl angles up to and including 30° the profiles are displaced towards the inner wall. This is partly due to the higher adverse pressure gradient along the outer wall, which causes rapid growth of the boundary layer. Another contributory factor is the different turbulence structure in the inner and outer wall layers (9). For 45° swirl, the meridional velocity profiles together with flow visualization indicate a more stable flow along the outer wall and a large-scale separation from the inner wall. This is in agreement with the findings of Dovzhik and Kartavenko (4), who attributed this behaviour to the effect of centrifugal force (dmC_θ^2/r). The effect of the centrifugal force is manifest in two ways: pressing the flow against the outer wall of the diffuser, promoting flow stabilization and delaying separation, and intensifying the tendency to flow separation from the inner wall.

The swirl velocity profiles corresponding to the meridional velocity profiles of Fig. 3 are given in Fig. 4. A free vortex pattern is predominant throughout the diffuser for swirl angles of 15° and 30°. For a swirl angle of 45°, the free vortex pattern is not maintained; this is due to the aforementioned large-scale separation. The conservation of angular momentum causes the average swirl velocity to decrease due to the increase in radius in the direction of flow.

With diffusers 2 and 3, the flow patterns were similar to those observed in diffuser 1. This indicates that the flow behaviour is practically unaffected by the limited changes in cant angle and area ratio used in the present

tests. The performance of the diffusers is, however, sensitive to these parameters as well as the swirl angle, as discussed in the following section.

3.2 Diffuser performance and comparison with predicted values

Diffuser performance, quantified in terms of area-averaged pressure recovery and total pressure loss coefficients and blockage, is presented in Figs 5 and 6. The pressure recovery coefficients for diffuser 1 are lower than those of diffusers 2 and 3 for all inlet swirl angles. This is primarily due to the smaller area ratio of diffuser 1. Diffusers 2 and 3 have the same area ratio, yet it is noted that diffuser 2 has the higher pressure recovery coefficients for all inlet swirl angles. This is attributed to the higher cant angle of diffuser 3 which results in a higher adverse pressure gradient, consequently creating a more rapid growth of the boundary layers. This also explains the lower total pressure loss coefficients of diffuser 2 compared with diffuser 1. Summarizing these effects, pressure recovery is strongly influenced by area ratio and to a lesser extent by cant angle, higher area ratios and lower cant angles giving increased pressure recovery coefficients.

The pressure recovery coefficients are increased as inlet swirl increases up to 30°. This effect is more pronounced for diffuser 1. Increasing the inlet swirl from 0 to 30°, the pressure recovery coefficients of diffusers 1, 2 and 3 are increased by 12.5, 3.5 and 8.6 per cent respectively. The higher percentage of pressure recovery increase for diffuser 1 is in agreement with the work of Coladipietro, Schneider and Sridhar (5) who showed that the effect of swirl is more pronounced for diffusers having a lower area ratio.

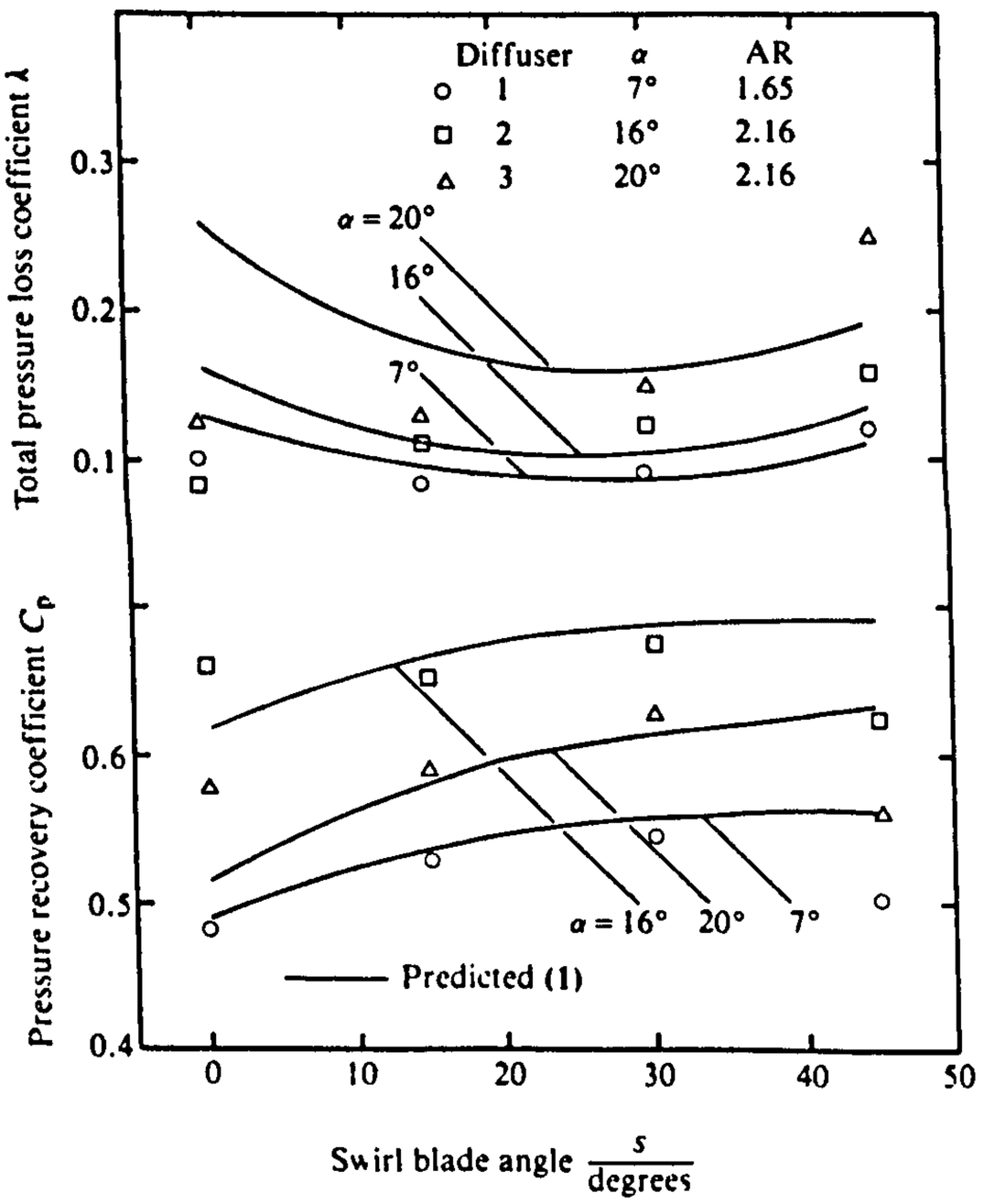

Fig. 5 Performance of equiangular diffusers

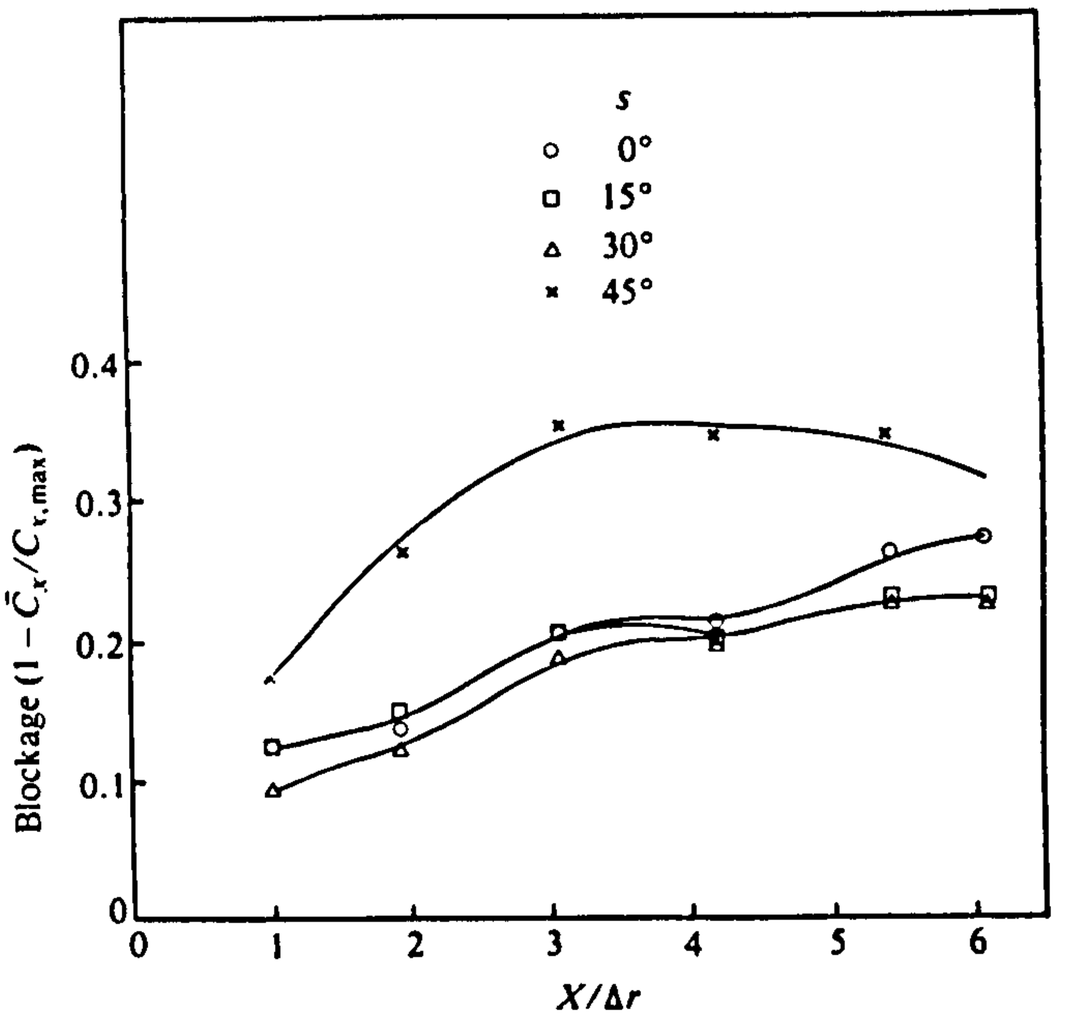

Fig. 6 Blockage distribution along diffuser 2 for different degrees of inlet swirl

The more pronounced improvement in the pressure recovery coefficient of diffuser 3 compared with diffuser 2 with increased swirl is attributed to the higher diffuser cant angle (both geometries have the same area ratio). The measurements showed that the angular momentum ratio γ is basically equal, at a value of about 0.94, for all diffusers, particularly for swirl angles up to 30°. For 45° swirl large areas of separated flow on the inner wall occur with their consequent effect on the overall performance parameters.

Figure 6 shows that the blockage increases with the increase of diffuser length for all swirl angles. At diffuser exit the blockage for 15° and 30° swirl angles is slightly lower than that of 0° swirl, which is in agreement with the increased pressure recovery coefficients for these swirl angles. The blockage for 45° swirl, however, is significantly higher when compared with lower swirl angles, which matches the flow separation and the lower pressure recovery achieved for this swirl angle.

The predicted pressure recovery coefficients (1), which are also presented in Fig. 5, are in good agreement with the measured values. Agreement is less satisfactory for the total pressure loss coefficients. This is attributed to the distorted velocity distributions at the diffuser exit, which caused higher uncertainty values already quoted in Section 2.

4 CONCLUSIONS

1. The velocity profiles in equiangular annular diffusers are practically unaffected by limited changes of cant angles (up to 20°) and area ratio (up to 3.0).
2. The effect of centrifugal force on the flow behaviour is manifest in two ways: pressing the flow against the outer wall of the diffuser, promoting flow stabilization and delaying separation, and intensifying the tendency to flow separation from the inner wall.
3. The influence of swirl on pressure recovery and the total pressure loss coefficients is very much dependent on diffuser area ratio and cant angle. For all

tested diffuser geometries, the pressure recovery coefficient improves as the inlet swirl increases up to 30° and deteriorates thereafter due to flow separation on the inner wall of the diffuser.

4. Measured diffuser performance is in good agreement with that theoretically predicted by the authors (1).

ACKNOWLEDGEMENTS

The authors would like to express their gratitude to the Department of Mechanical and Production Engineering, Paisley College of Technology, for supporting this study, and to thank colleagues at Paisley College of Technology and the University of Glasgow for their encouragement.

REFERENCES

1 **Elgammal, A. H.** and **Elkersh, A. M.** A method for predicting annular diffuser performance with swirling inlet flow. *J. Mech. Engng Sci.*, 1981, 23(3), 107–112.

2 **Srinath, T.** An investigation of the effects of swirl on the flow regimes and performance of annular diffusers with equal inner and outer cone angles. MSc thesis, 1968, Mechanical Engineering Department, University of Waterloo.

3 **Shaalan, M. R. A.** and **Shabaka, I. M. M.** Experimental investigation of the swirling-flow performance of an annular diffuser at low speed. ASME Paper 75-WA/FE-17.

4 **Dovzhik, S. A.** and **Kartavenko, V. M.** Measurement of the effect of flow swirl on the efficiency of annular ducts and exhaust nozzles of axial turbomachines. *Fluid Mech.—Sov. Res.*, 1975, 4, 156–172.

5 **Coladipietro, R., Schneider, J. H.** and **Sridhar, K.** Effects of inlet flow conditions on the performance of equiangular annular diffusers. *Trans. CSME*, 1975, 3, 75—82.

6 **Markowski, S. J., Lohmann, R. P.** and **Brookman E. T.** The performance of conical wall diffusers with swirling inlet flow. *Proc. Joint Symp. on Design and operation of fluid machinery, polyphase flow transient*, June 1978, Colorado State University.

7 **Elkersh, A. M.** Investigations into design and performance of annular diffusers. PhD thesis, 1983, Paisley College of Technology, Scotland.

8 **Kline, S. J.** and **McClintock, R. A.** Describing uncertainties in single-sample experiments. *Mech. Engng*, 1953, 75(1), 3–8.

9 **Stevens, S. J., Williams, G. J.** and **Nayak, U. S.** The influence of inlet conditions on the performance of annular diffusers. *Proc. Joint Symp. on Design and operation of fluid machinery, polyphase flow transient*, 1978, Colorado State University.

Publication 35

86-GT-208

THE AMERICAN SOCIETY OF MECHANICAL ENGINEERS
345 E. 47 St., New York, N.Y. 10017

Gas Turbine Transient Fuel Scheduling With Compensation for Thermal Effects

N. R. L. MACCALLUM, Reader,
University of Glasgow,
Glasgow, Scotland.

P. PILIDIS, Teaching Company Associate,
Caledonian Airmotive Ltd.,
Prestwick, Scotland.

ABSTRACT

Most current fuel schedules for accelerating or decelerating gas turbines use a limiting non-dimensional fuel flow expressed as a function of some engine parameter such as compressor pressure ratio. Usually the same schedule is used for, for example, accelerating 'cold' and 'hot' engines. This results in differing acceleration rates and differing usage of surge margins. The paper describes two methods of compensating the fuel schedules to account for the engine's immediately preceding temperature history. One method uses the temperature response of the aerofoil of blades in the H.P. Compressor. The second method, which appears to be an improvement, uses a 'delayed' H.P. Shaft speed signal.

1 INTRODUCTION

The procedure usually employed for accelerating (or decelerating) a gas turbine is to use a fuel flow controller which restricts the maximum (or minimum) fuel flow at that instant. These restrictions are necessary to ensure that the engine operates safely and is not endangered by surge in a compressor or excessively high gas temperatures at the turbine inlet. The relation which defines the maximum (or minimum) fuel flow is referred to as the fuel schedule, and in this schedule a non-dimensional fuel flow is expressed as a function of some engine parameters, such as pressure ratio.

Hitherto it has been the practice to use the same fuel schedule for 'handling' the engine without regard to it's immediately preceding history, for example whether the engine is 'cold' or is 'hot'. The description 'cold' used here indicates an engine which has been stabilised at the idling speed before the acceleration. The description 'hot' refers to an engine which was held at maximum speed for several minutes, thus allowing thermal stabilisation to take place before the transient, which consists of a deceleration immediately followed by an acceleration.

In a recent paper (1)* the present authors have predicted that the use of the same fuel schedule for accelerating a 'hot' and a 'cold' engine, for example, causes different rates of engine response and different usage of surge margins. In one example it was predicted that when accelerating the 'cold' engine, just under 50 percent of the surge margin was used, whereas when accelerating the 'hot' engine about 65 percent of the surge margin was used, but the acceleration time was reduced by about 20 percent, compared to the 'cold' case. The present paper describes a study that has been made of methods of compensating the fuel schedule in order to make some allowance for the previous 'thermal history' of the engine, and thereby obtain more consistent acceleration rates and more consistent usage of surge margins.

2 A NON-DIMENSIONAL FUEL SCHEDULE

The engine which has been used as an illustration in the present investigation is a two-spool bypass engine with mixed exhausts. A fuel schedule which has been used for this type of engine relates a non-dimensional fuel flow group to the pressure ratio across the H.P. Compressor.

The form of non-dimensional fuel flow group is the fuel flow rate divided by the product of the H.P. Shaft speed and the absolute pressure at inlet to the H.P. Compressor. Typical schedules for accelerating and decelerating the engine are shown in Fig. 1.

3 PREDICTED 'ADIABATIC' TRANSIENT PERFORMANCE

If thermal effects are neglected, and the processes in the engine during the transient are assumed to be 'adiabatic', the conventional transient programs can be used to predict the response of the

* Underlined numbers in brackets indicate references at the end of the paper.

Presented at the International Gas Turbine Conference and Exhibit
Dusseldorf, West Germany—June 8-12, 1986

engine in transients in which the fuel flow is limited by the fuel schedule described above and illustrated in Fig. 1. The transients that have been used as tests in the present work are an acceleration from ground idle speed and the acceleration section of a 'Bodie' transient (a deceleration of a 'hot' engine followed by a reacceleration). These two accelerations were selected because, firstly, in this engine compressor surge is approached only in an acceleration and, secondly, these two accelerations represent opposite extremes of initial conditions. For the acceleration from ground idle speed, the predicted speed and thrust responses are shown in Fig. 2(a) and the trajectories in the L.P. and H.P. Compressors are shown in Figs. 2(b) and 2(c) respectively, these predictions being

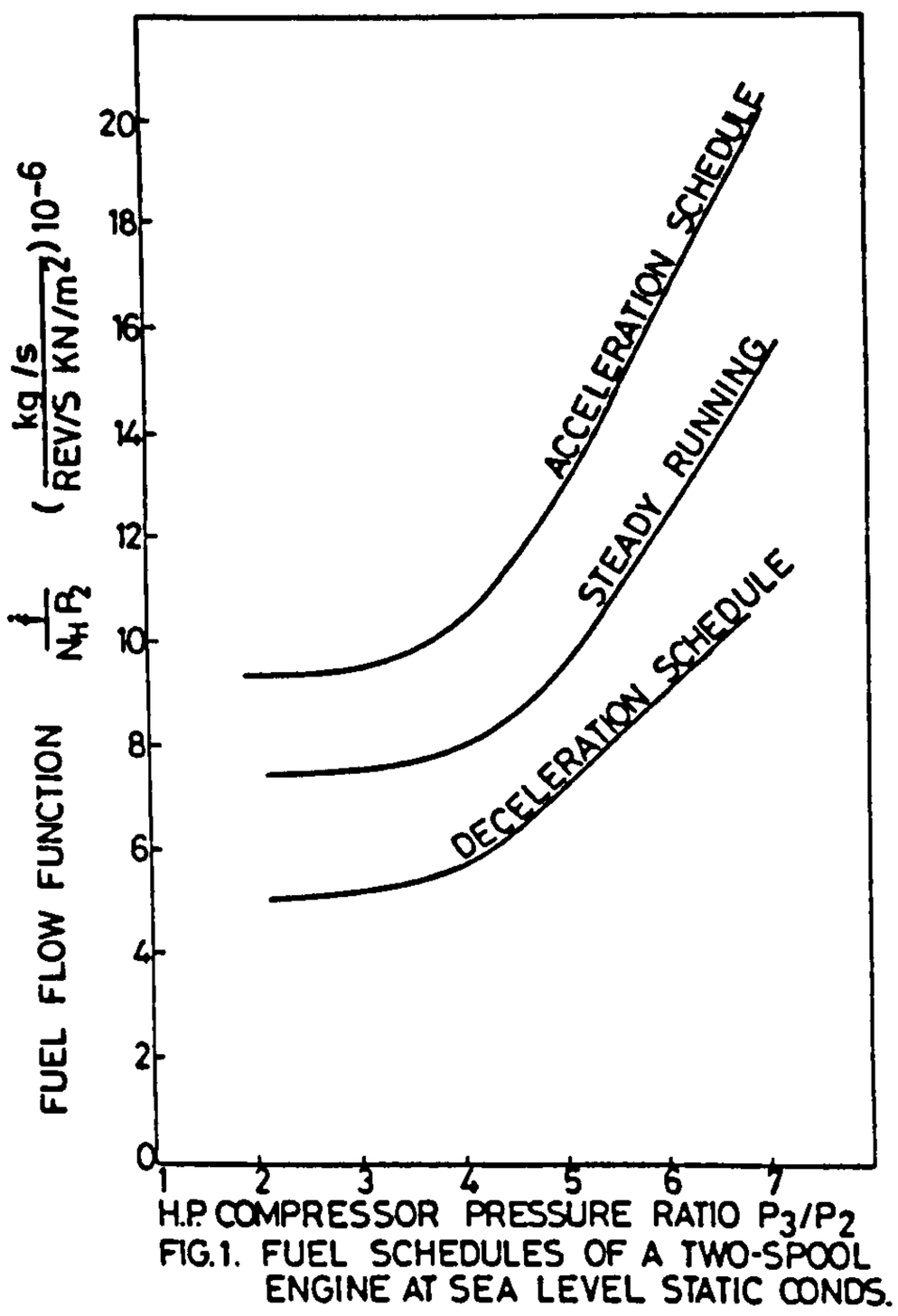

FIG.1. FUEL SCHEDULES OF A TWO-SPOOL ENGINE AT SEA LEVEL STATIC CONDS.

marked 'adiabatic'. The starting speeds for this transient were 3080 RPM for the L.P. Shaft and 7222 RPM for the H.P. Shaft. A maximum fuel flow limit of 0.71 kg/s has been used as the terminating condition for the acceleration.

The corresponding predicted results for the acceleration part of the 'Bodie' transient are shown in Figs. 3(a), 3(b) and 3(c). Again a maximum fuel flow of 0.71 kg/s has been used as the terminating condition. In this case the speeds at the start of the acceleration were 4670 and 7880 RPM for the two shafts respectively. In the case of the 'Bodie', because the

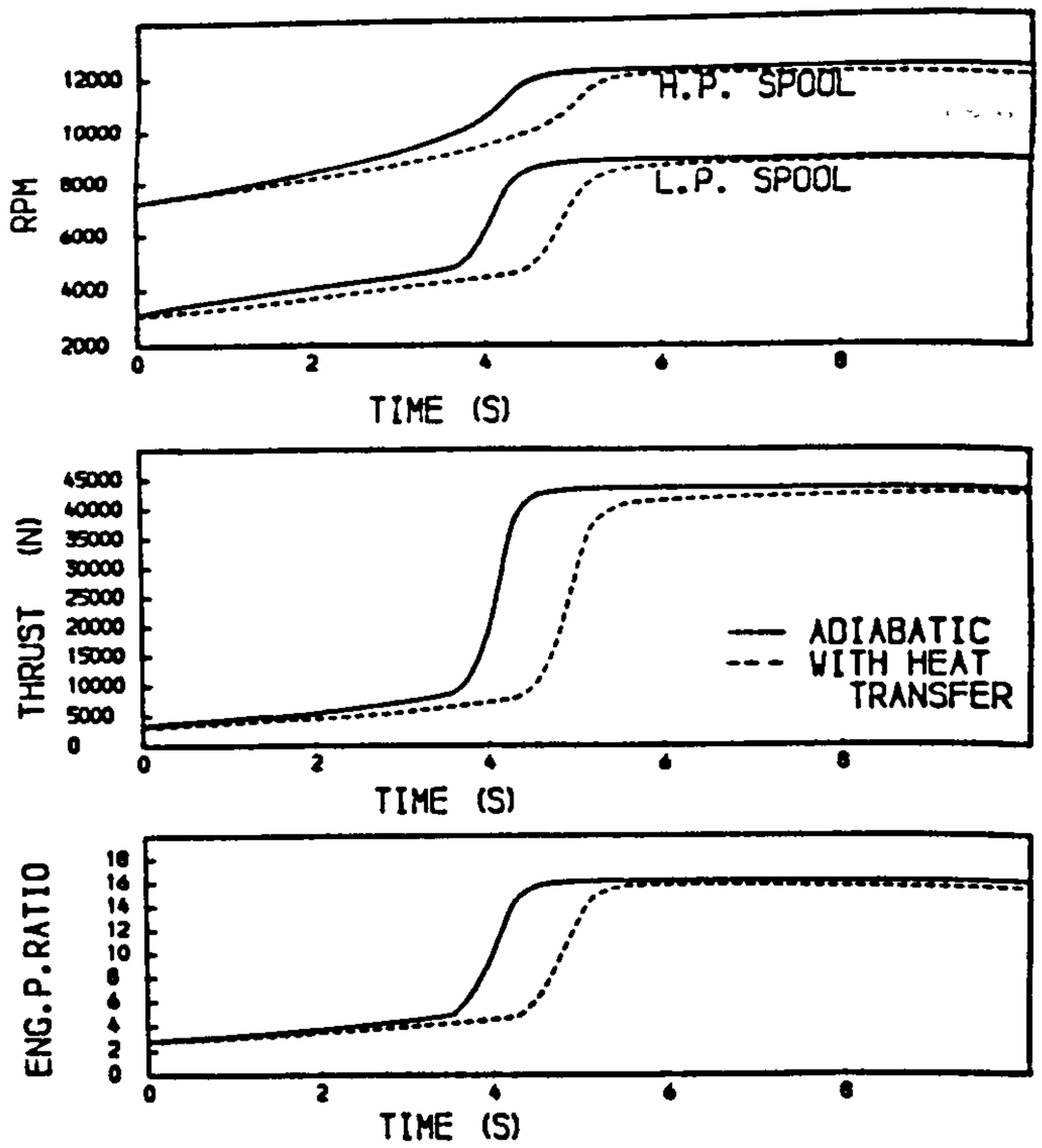

FIG 2A PREDICTED ACCELERATION OF A TWO SPOOL BYPASS ENGINE FROM GROUND IDLING AT SEA LEVEL STATIC CONDITIONS

starting speeds are higher, 90 percent of thrust is achieved in about 3 seconds as compared to the 4.2 seconds required in the acceleration from idling speeds (Fig. 2). It should also be noted that at the instant when the acceleration of the 'Bodie' is started, which is 8 seconds after starting the deceleration, the two spools have not reached mutually stabilised speeds. Consequently for the first quarter of a second of the reacceleration the speed of the L.P. Shaft drops slightly.

In both these accelerations, the trajectories in the L.P. Compressor remain very close to the steady running line, and do not approach surge. In the H.P. Compressor however the trajectories move significantly towards surge. The position of the accelerating fuel schedule line, shown in Fig. 1, dictates the proximity of the running line to the surge line. If the fuel schedule line is raised the engine will accelerate more rapidly and the trajectory in the H.P. Compressor moves closer to surge, and the opposite occurs if the fuel schedule line is lowered.

In the studies being described in this paper, attention is focused on the conditions in the H.P. Compressor during these accelerations as this is the critical location.

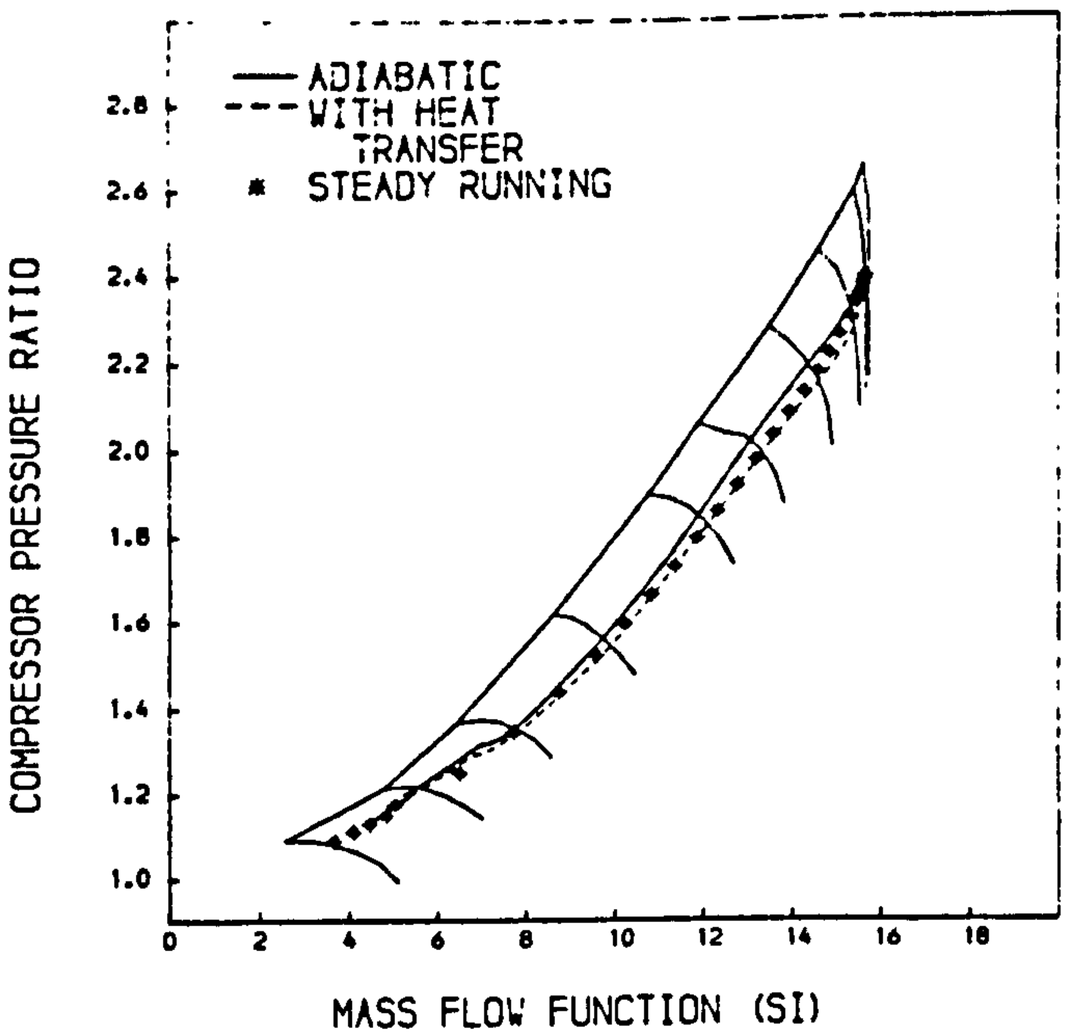

FIG 2B PREDICTED PATHS OF THE L.P. COMPRESSOR OF A TWO-SPOOL BYPASS ENGINE DURING AN ACCELERATION FROM GROUND IDLING AT SEA LEVEL STATIC CONDITIONS

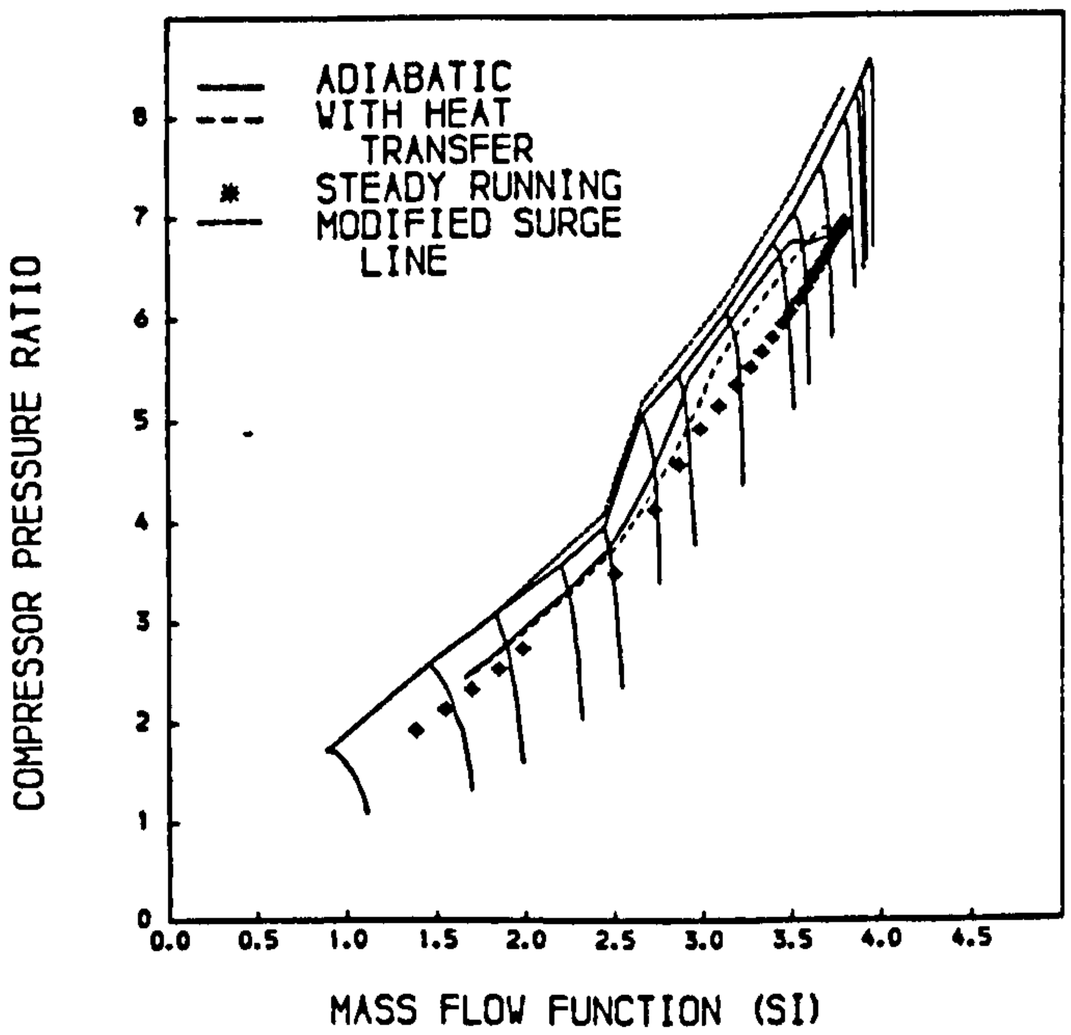

FIG 2C PREDICTED PATHS OF THE H.P. COMPRESSOR OF A TWO-SPOOL BYPASS ENGINE DURING AN ACCELERATION FROM GROUND IDLING AT SEA LEVEL STATIC CONDITIONS

4 THERMAL EFFECTS IN TRANSIENTS

In the analysis described in section 3, the following assumptions had been made:

(a) the flow in the compressors and turbines was adiabatic

(b) characteristics of compressors and turbines during the transient were the same as those recorded under steady-running conditions

(c) the small air flows, controlled by seal clearances, which are drawn from the compressor to cool various hot sections remain the same fractions of the total core air flow.

These assumptions represent a considerable simplification of what happens in practice. For example, it has been predicted that a seal clearance during an acceleration may exhibit an opening which is double that at stabilised design conditions (2). The heat transfer or thermal effects which alter the assumptions mentioned above are discussed in more detail in Reference (3) to which readers are referred. That paper describes a prediction model which is intended to take account of these effects, these being:

(a) non-adiabatic compressions and expansions

(b) changes in tip clearances

(c) changes in clearances of critical seals

(d) changes in compressor characteristics due to heat transfer, boundary layer and tip clearance effects, with particular attention being given to movements of the surge line and the constant speed lines.

The present prediction program, with the above features being incorporated, was next used to predict the responses of the two-spool bypass engine for which the 'adiabatic' predictions have already been given in Figs. 2 and 3. Inclusion of tip clearance changes in the H.P. Compressor had been found (2) to have little effect on predicted acceleration rates or compressor trajectories. The same was the case for the L.P. Compressor and Turbine. Inclusion of H.P. Turbine tip clearances produced a small improvement in response but no noticeable changes in the compressor trajectories. The two seals which are regarded as critical are at the rear of the H.P. Compressor and on the first disc of the H.P. Turbine. These seals control cooling air flows at the rear face of the H.P.

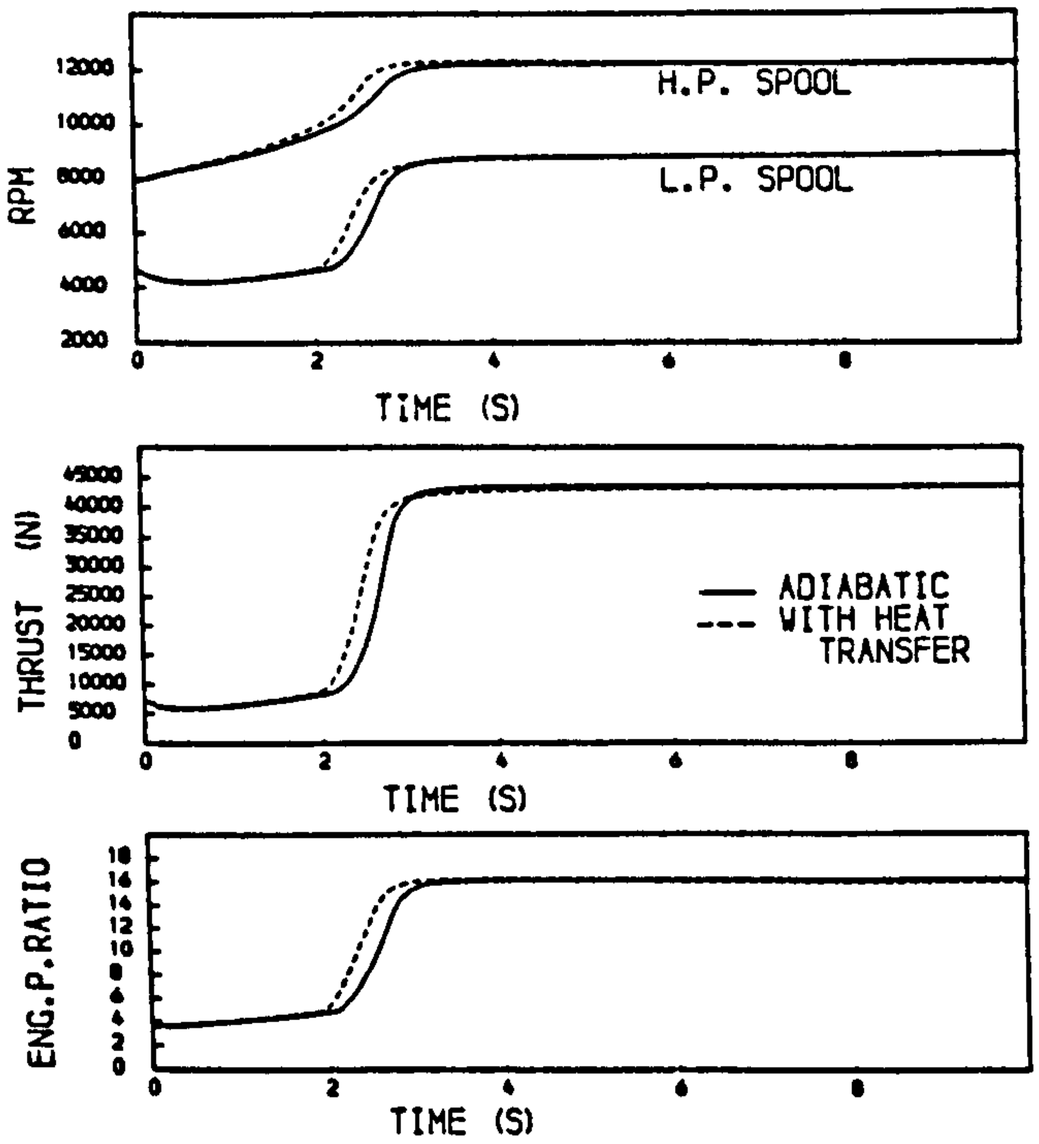

FIG 3A PREDICTED ACCELERATION OF A TWO SPOOL BYPASS ENGINE FOLLOWING AN 8 SECOND DECELERATION, AT SEA LEVEL STATIC CONDITIONS

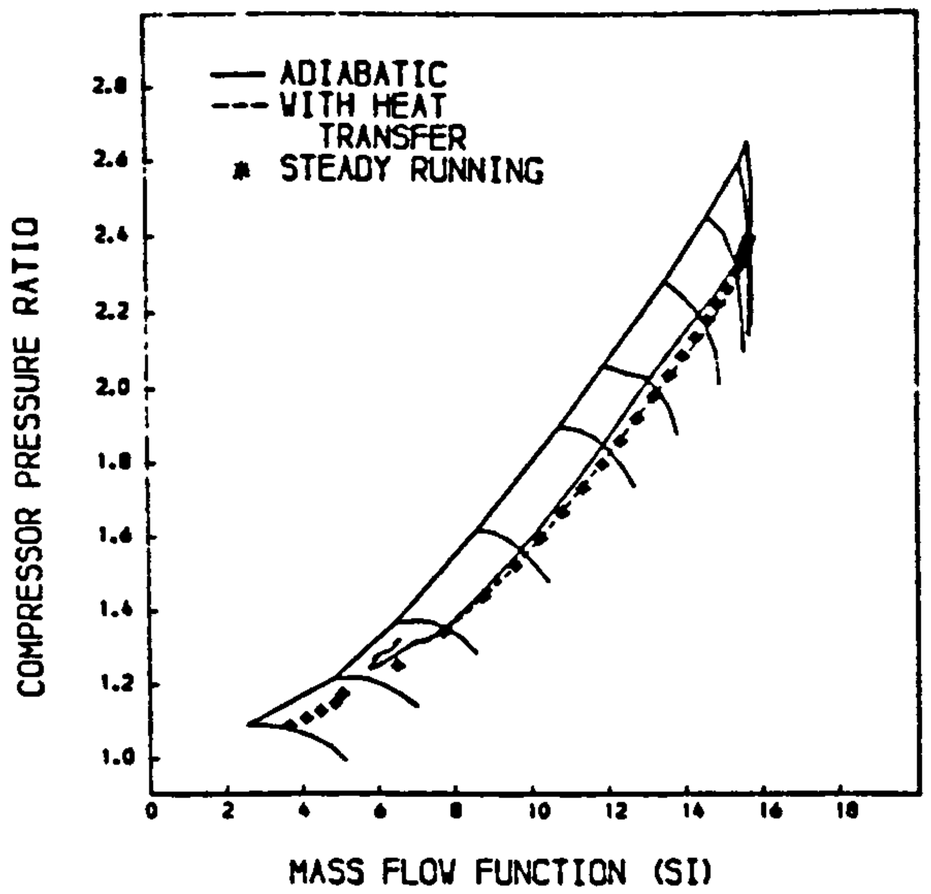

FIG 3B PREDICTED PATHS OF THE L.P. COMPRESSOR OF A TWO-SPOOL BYPASS ENGINE DURING AN ACCELERATION FOLLOWING AN 8 SECOND DECELERATION, AT SEA LEVEL STATIC CONDITIONS

Compressor and at the front disc of the H.P. Turbine.

The predicted transient performance of the engine, with allowance for the above effects is illustrated in Fig. 2 for the acceleration from ground idling speed and in Fig. 3 for the 'Bodie' transient. The altered surge lines, moved by heat transfer and tip clearance effects are also shown. The corresponding predicted adiabatic performance can be used for comparison. For the acceleration from ground idle it is observed that while the predicted surge margin usage in the H.P. Compressor based on adiabatic calculations is about 80 percent, the usage based on calculations accounting for thermal effects is about 50 percent. The predicted thrust response is about 0.8 seconds slower when account is taken of thermal effects. These results are in line with those reported elsewhere (1), (3) although in the present work a slightly different fuel schedule is being employed. In the 'Bodie' transient (Fig. 3), inclusion of the thermal effects leads to a thrust response which is about 0.2 seconds more rapid than for the adiabatic prediction, but the surge margin usage is about 70 percent as compared to 80 percent in the adiabatic prediction. The reasons for these changes have been discussed in References (1), (2) and (3).

Comparing the predictions for the more realistic cases where the thermal effects are being taken into account shows that for the 'hot' engine there is more rapid acceleration and greater surge margin usage than for the acceleration of the 'cold' engine. The same acceleration fuel schedule (Fig. 1) has been used for both situations. These results suggest that some form of adjustment might be applied to the fuel schedules to allow a greater utilisation of the surge margin, and a faster acceleration in the case of the 'cold' engine and vice versa in the case of the 'hot' engine. Two methods of achieving this are described and discussed in the next section.

It can be noted at this point that in practice in similar engines there is a greater tendency to surge the H.P. Compressor when accelerating a 'hot' engine, as compared to a 'cold' engine. A correlation has been observed by Crawford and Burwell (4) between surge in 'Bodie' transients and high rates of heat transfer from the material of the H.P. Compressor to the air flow.

5 METHODS OF FUEL SCHEDULE COMPENSATION

Since the departures from 'adiabatic' performance are, with the exception of centrifugal growth at the seals, due to the temperatures of the materials within the engine lagging behind the relevant air or gas temperatures, the first method of compensation of the fuel schedule which has been studied is based on the temperature of a characteristic component within the engine, the choice of component being discussed presently. The second method studied is based on a delayed measurement of the H.P. Shaft speed.

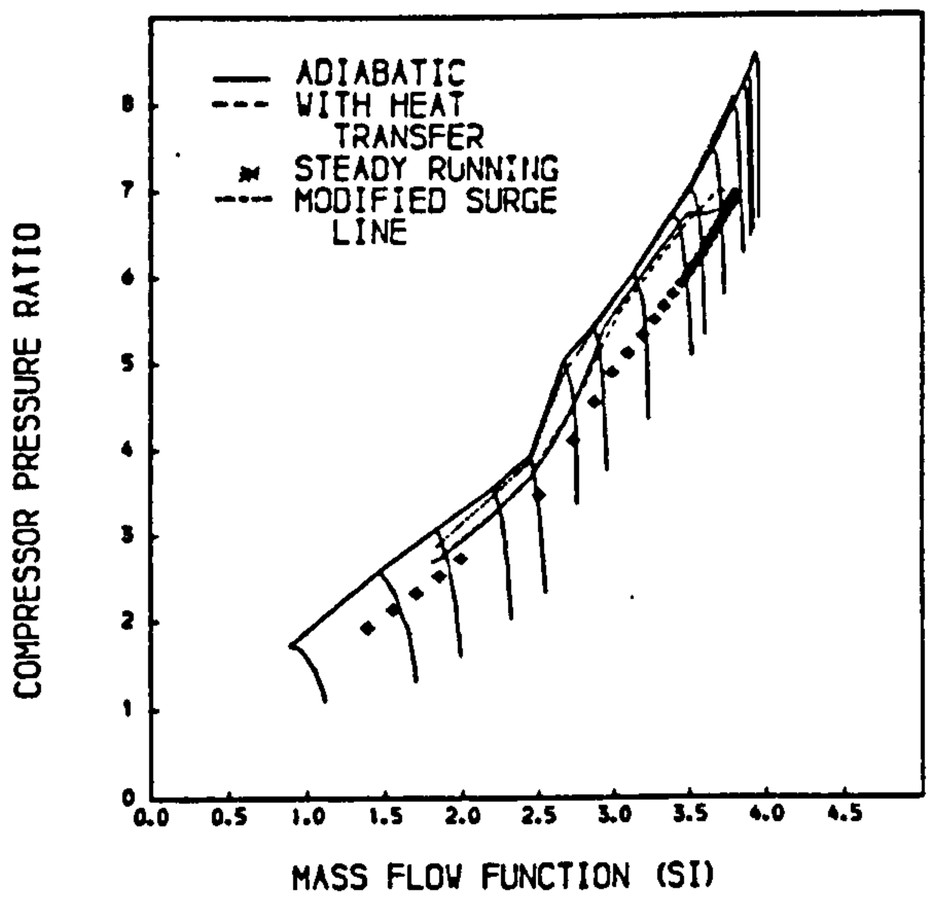

FIG 3C PREDICTED PATHS OF THE H.P. COMPRESSOR OF A TWO-SPOOL BYPASS ENGINE DURING AN ACCELERATION FOLLOWING AN 8 SECOND DECELERATION, AT SEA LEVEL STATIC CONDITIONS

5.1 Compensation by Temperature of H.P. Compressor Blades

The compressor in this engine most likely to surge in transients is seen to be the H.P. Compressor. The method of using a 'characteristic' stage to represent behaviour in a component (eg. compressor) has already been used (2). Since changes in compressor characteristics and the extent of the non-adiabatic nature of the flow in the compressor are dominantly influenced by the temperature difference between the air and the blade aerofoils, it was therefore decided to select the temperature of the aerofoil of the characteristic blade and the mean temperature of the air in the compressor to form the factor to be used in compensating the fuel schedule. This form of compensation is described by Equation 1,

$$\frac{\dot{f}}{N_H P_2} = \left(\frac{T_{m,a}}{T_{bl}}\right)^a fn\left(\frac{P_3}{P_2}\right) \qquad (1)$$

where $\dot{f}$ is the fuel flow, N_H, is the H.P. Shaft speed, P_2, and P_3, are the pressures at the inlet and outlet of the H.P. Compressor and $T_{m,a}$ and T_{bl} are the mean air temperature and the characteristic blade aerofoil temperature in the H.P. Compressor. The functional relationship shown on the right of the right hand side of Eq. (1) is the standard fuel schedule, illustrated in Fig. 1.

A range of values from 0.5 to 3.0 has been examined for the index 'a'. Typical results are given in this paper for the case in which the value of 1.0 was selected for the index. First, the fuel schedule compensating multiplier, which is the first term on the right hand side of Eq. (1), is plotted for a 'cold' acceleration on Fig. 4 and the reacceleration part of the 'Bodie' on Fig. 5. The resulting predicted engine

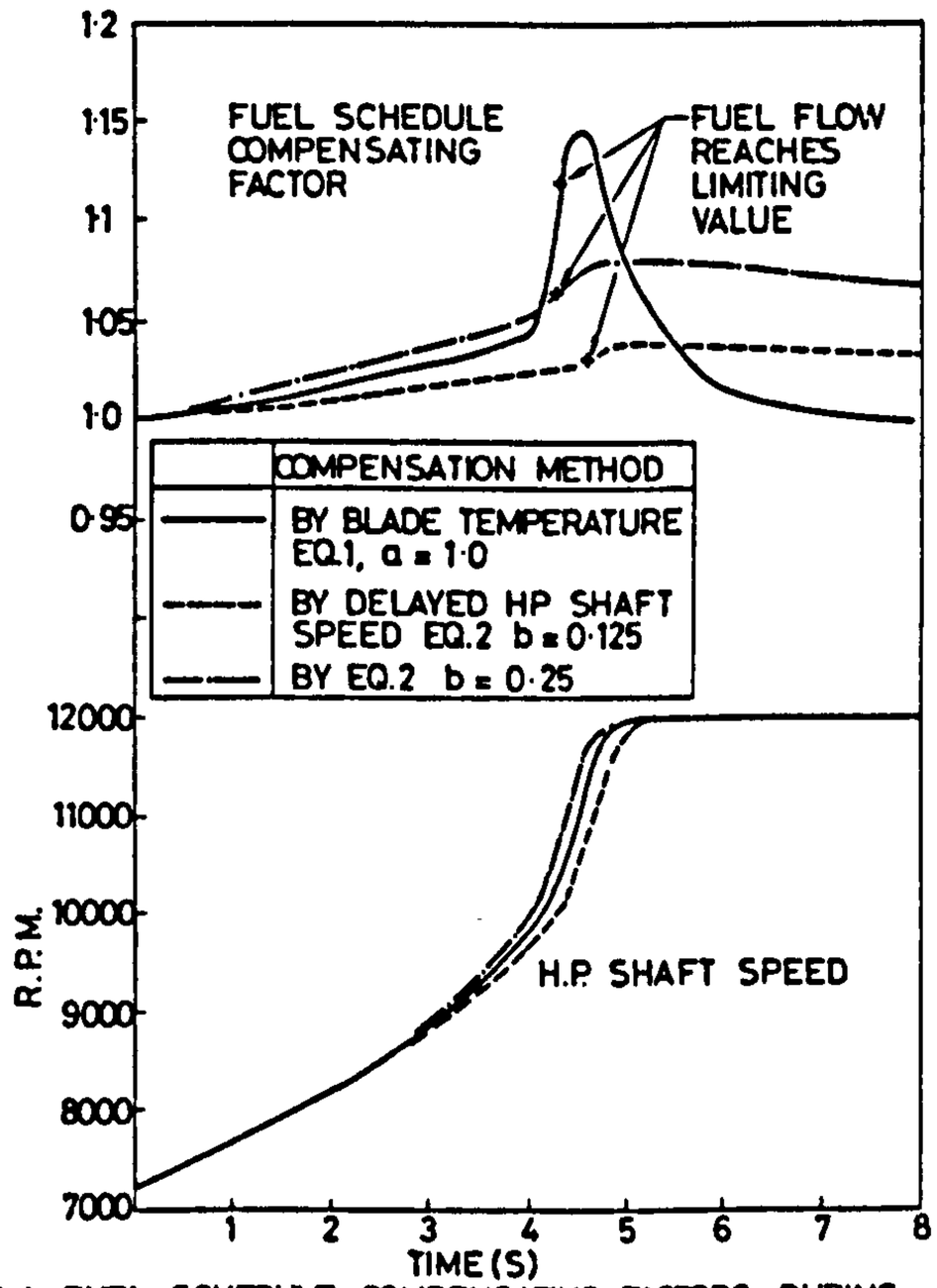

FIG.4 FUEL SCHEDULE COMPENSATING FACTORS DURING ACCELERATION FROM GROUND IDLING - AT SEA LEVEL STATIC.

responses for these transients with this compensating scheme are given in Figs. 6. and 7 respectively. The 'adiabatic' predictions are also shown alongside. The results should also be compared with the predicted responses taking account of all thermal effects (Figs.2 and 3).

In the acceleration of the 'cold' engine (Fig. 6)

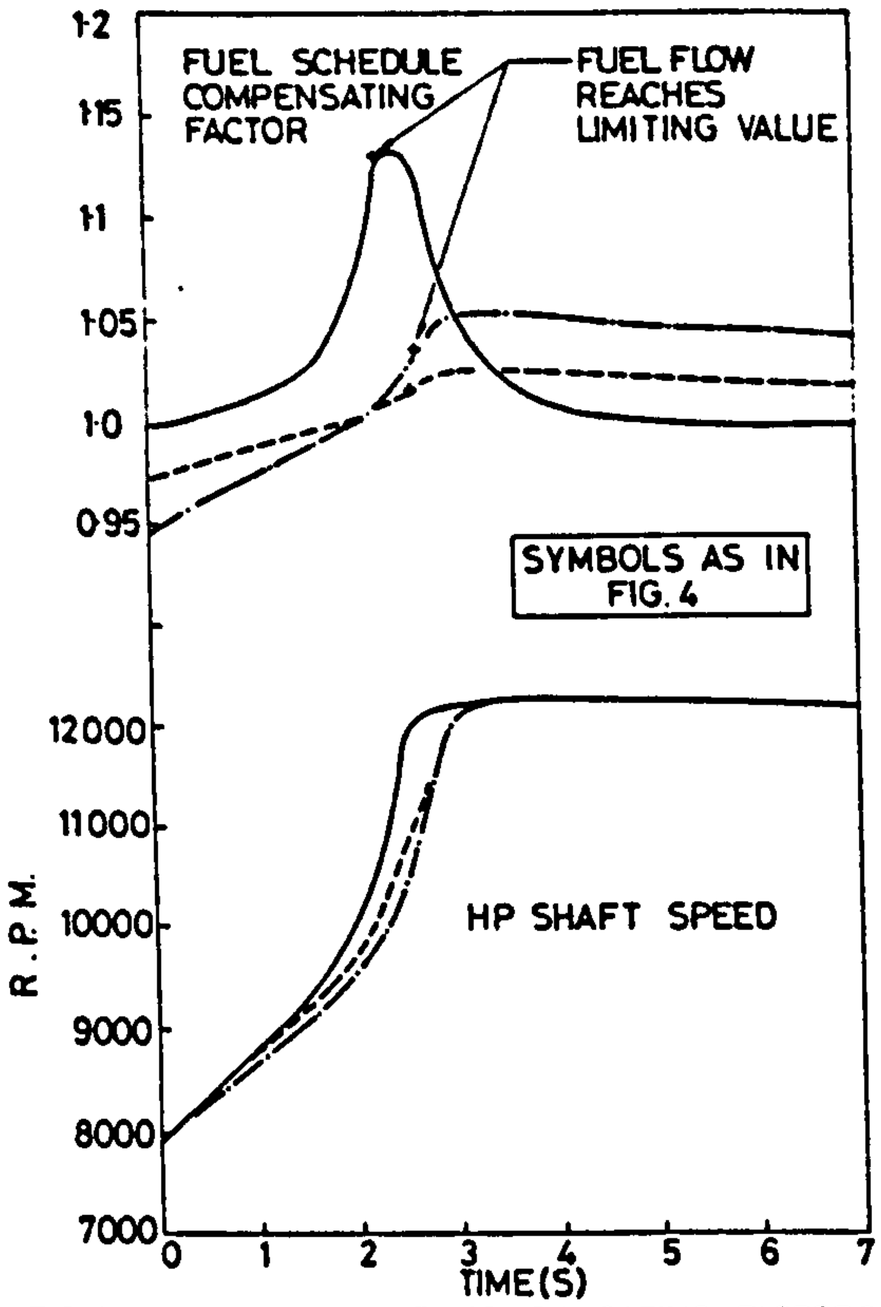

FIG 5 FUEL SCHEDULE COMPENSATING FACTORS DURING REACCELERATION FOLLOWING 6 SEC DECELERATION AT SEA LEVEL STATIC

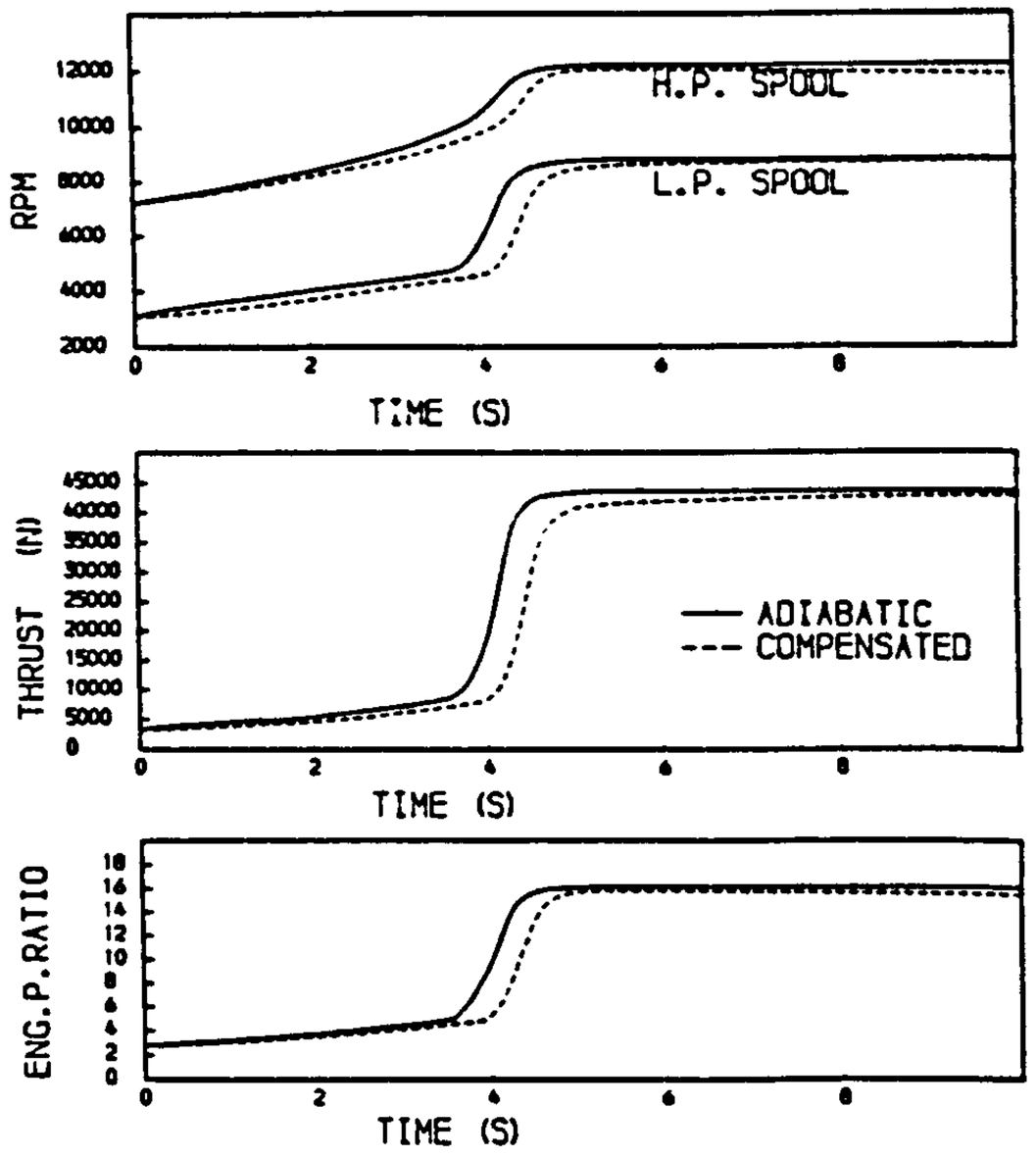

FIG 6A PREDICTED ACCELERATION OF A TWO SPOOL BYPASS ENGINE FROM GROUND IDLING AT SEA LEVEL STATIC CONDITIONS FUEL SCHEDULE COMPENSATED WITH A FUNCTION OF H.P.COMPRESSOR BLADE TEMPERATURE (EQ.1)

approximately 70 percent of the surge margin (relative to the revised surge line) is now used, as compared with about 50 percent in the case of the standard fuel schedule. The thrust response is advanced by about 0.5 seconds but still lags by about 0.4 second relative to the 'adiabatic' prediction. This represents a definite improvement in that a faster thrust response has been achieved, accompanied by an increased, but still reasonable usage of surge margin.

In the 'Bodie' transient it was decided not to introduce any compensation in the deceleration phase, since no problems are encountered during the deceleration. The effect of compensating the fuel schedule for heat transfer effects during the reacceleration is illustrated in Fig. 7. It can be observed that the thrust response is faster, by about 0.1 second and all the surge margin is used. These effects are the opposite of those intended. The explanation for this is that the temperature response of the aerofoils is too rapid, and after about one second of the reacceleration, the compensating parameter being applied to the fuel schedule is now noticeably increasing the fuel flow instead of decreasing it. This can be seen from the values of the fuel schedule compensating multiplier shown in Fig. 5. At the beginning of the reacceleration in the 'Bodie', the multiplier is effectively unity. The time constant of the temperature response of the aerofoil of the characteristic blade in the H.P. Compressor at the start of the reacceleration is about 2.5 seconds, which is clearly too short. Increasing the value of the index 'a' in Eq. 1, does not help, it merely exacerbates the problem. A more reasonable solution is to select as a correcting parameter the temperature of a more massive section of the H.P. Compressor, such as the hub of the characteristic disc.

However due to the practical difficulties of implementing such a scheme on an engine, attention has been focused on an alternative method of indicating the engine's immediately preceding 'history', a 'delayed' shaft speed signal. This method is described in the next sub-section.

5.2 Compensation by 'Delayed' H.P. Shaft Speed

In practice it will be comparatively easy to have a shaft speed signal which is delayed by a known time constant. Comparing this 'delayed' shaft speed with the actual shaft speed at that instant will give a parameter which can be an alternative way of compensating the fuel schedule. The simple method employed in the present work is described by Eq. 2:

$$\frac{\dot{f}}{N_w P_2} = \left(\frac{N_H}{N_{HD}}\right)^b fn\left(\frac{P_3}{P_2}\right) \qquad (2)$$

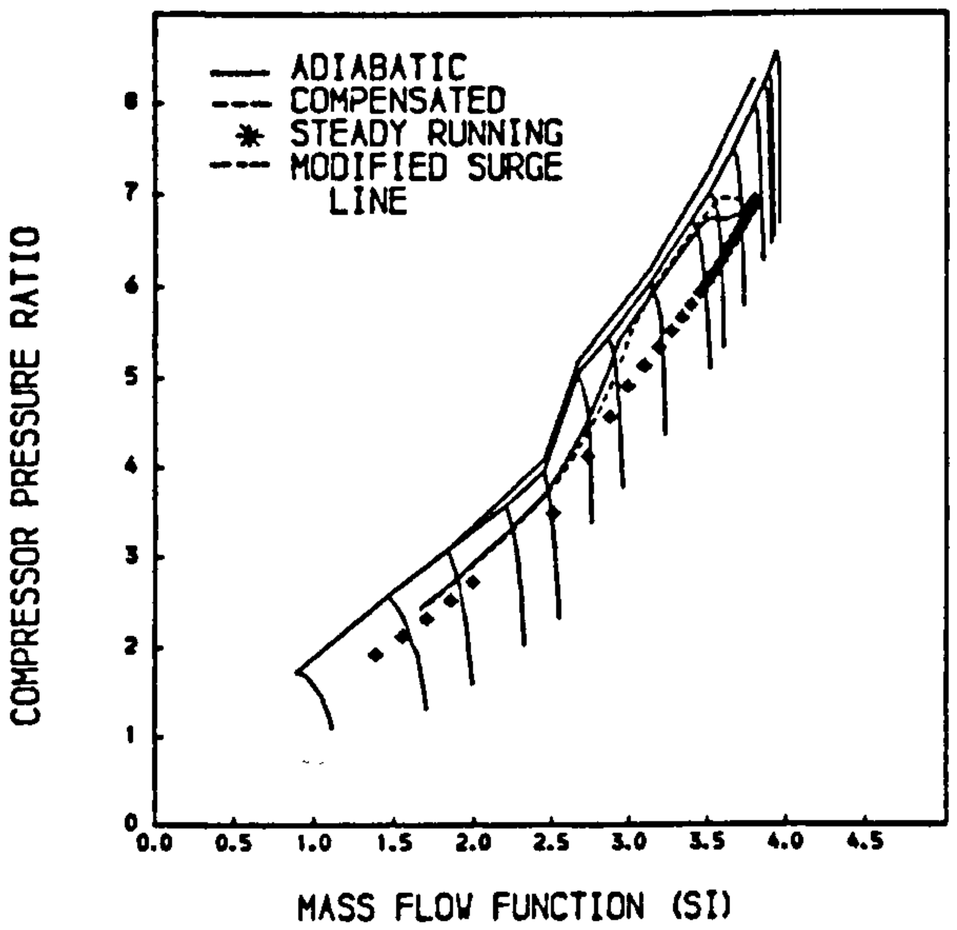

FIG 6B PREDICTED PATHS OF THE H.P. COMPRESSOR OF A TWO-SPOOL BYPASS ENGINE DURING AN ACCELERATION FROM GROUND IDLING AT SEA LEVEL STATIC CONDITIONS. FUEL SCHEDULE COMPENSATED WITH A FUNCTION OF H.P.COMPRESSOR BLADE TEMPERATURE (EQ.1)

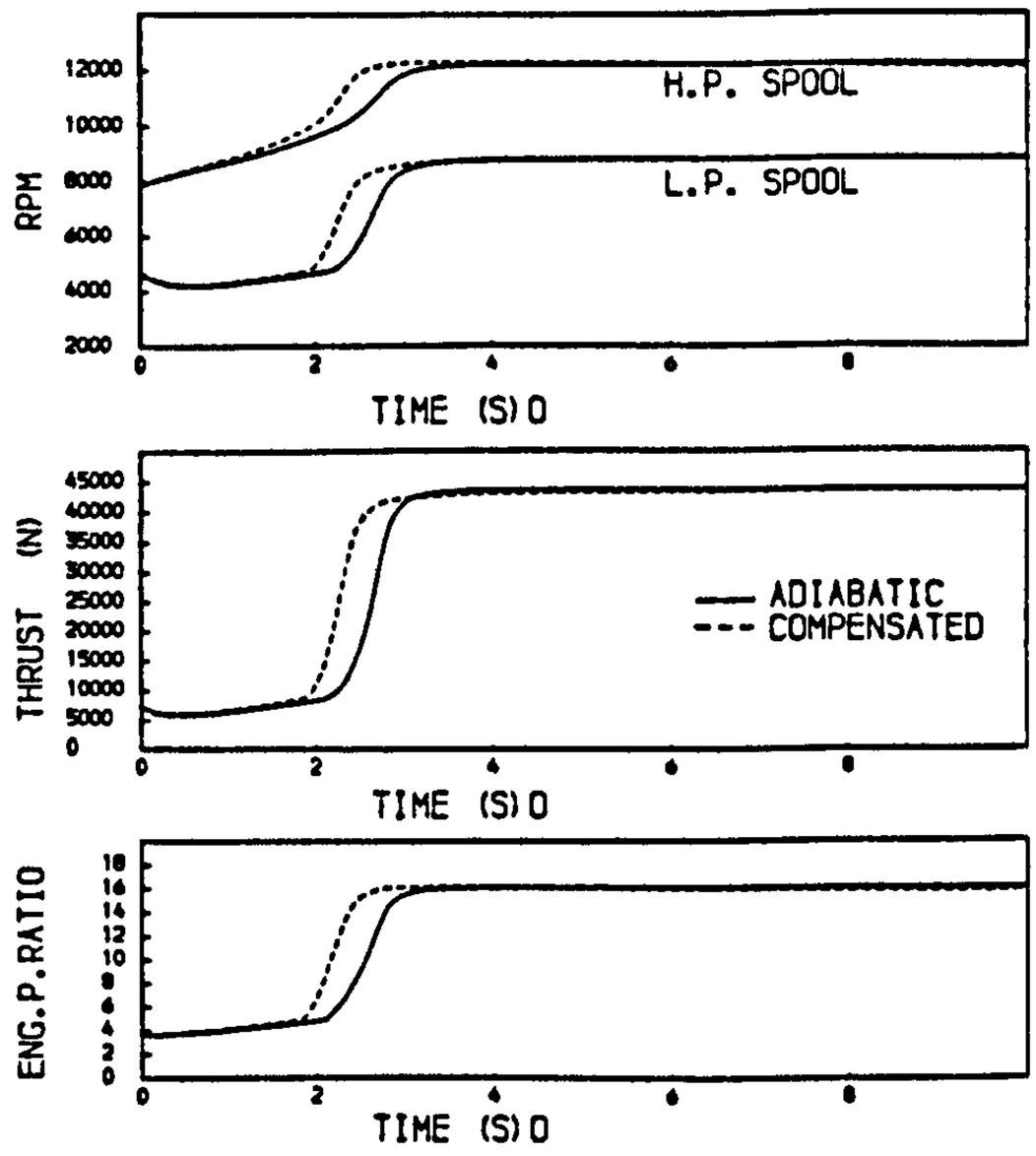

FIG 7A PREDICTED ACCELERATION OF A TWO SPOOL BYPASS ENGINE FOLLOWING AN 8 SECOND DECELERATION, AT SEA LEVEL STATIC CONDITIONS FUEL SCHEDULE COMPENSATED WITH A FUNCTION OF H.P.COMPRESSOR BLADE TEMPERATURE (EQ.1)

where N_{HP} is the signal of the H.P. Shaft speed, delayed by a time constant 'τ'. As before, a range of values for the index 'b' has been examined.

Selecting a value of 8 seconds for the time constant 'τ', coupled with a value of 1.0 for index 'b' gave a very satisfactory prediction for the acceleration of the 'cold' engine. Thrust response was 0.8 seconds faster than when employing the standard fuel schedule, which makes it virtually identical to that of the adiabatic prediction. The observed surge margin usage was of the order of 60 percent. However the response in the reacceleration of the 'hot' engine was unsatisfactory, giving a slightly faster thrust response and a greater surge margin usage than in the uncompensated case. The reason for this was, as in the case of the compensation by aerofoil temperatures, that the time constant was too short.

A time constant of 60 seconds has therefore been adopted for obtaining the 'delayed' H.P. Shaft speed. The choice of 60 seconds for the time constant was based on an average time constant for the thermal response of the components of a typical compressor disc (2). The response of the disc represents an average between the response of the heat transfer rate and the slower final response of a seal or blade tip clearance. Using the time constant of 60 seconds the predicted results with two values of index 'b', 0.125 and 0.25, are shown in Fig. 8 for the acceleration of the 'cold' engine and in Fig. 9 for the 'Bodie' transient.

As is expected, the higher value of the index 'b' produces the greater effects. The choice of 60 seconds for the time constant seems satisfactory. The combination of this time constant with a value of 0.25 for the index 'b' appears to achieve the intended aims of a reasonable improvement of the thrust response of approximately 0.8 seconds relative to the uncompensated case when accelerating the 'cold' engine, and a slowing down of the thrust response of about 0.3 seconds when reaccelerating the 'hot' engine during the 'Bodie' transient. The surge margin usage in the 'cold' acceleration rises to about 60 percent, and in the 'hot' reacceleration it is very slightly reduced, also to about 60 percent.

5.3 Implementation of Compensation Schemes

The compensation schemes described above by Eqns. 1 and 2 will be readily adaptable to digital fuel control systems, such as the FADEC seystem (5).

The second alternative -compensation by 'delayed' H.P. Shaft Speed- has been examined in the present work at sea level conditions for what can be regarded as the most testing transients -a 'cold' acceleration and a 'Bodie' acceleration- and beneficial effects have been observed. Similar benefits are being observed in predictions of behaviour at altitude.

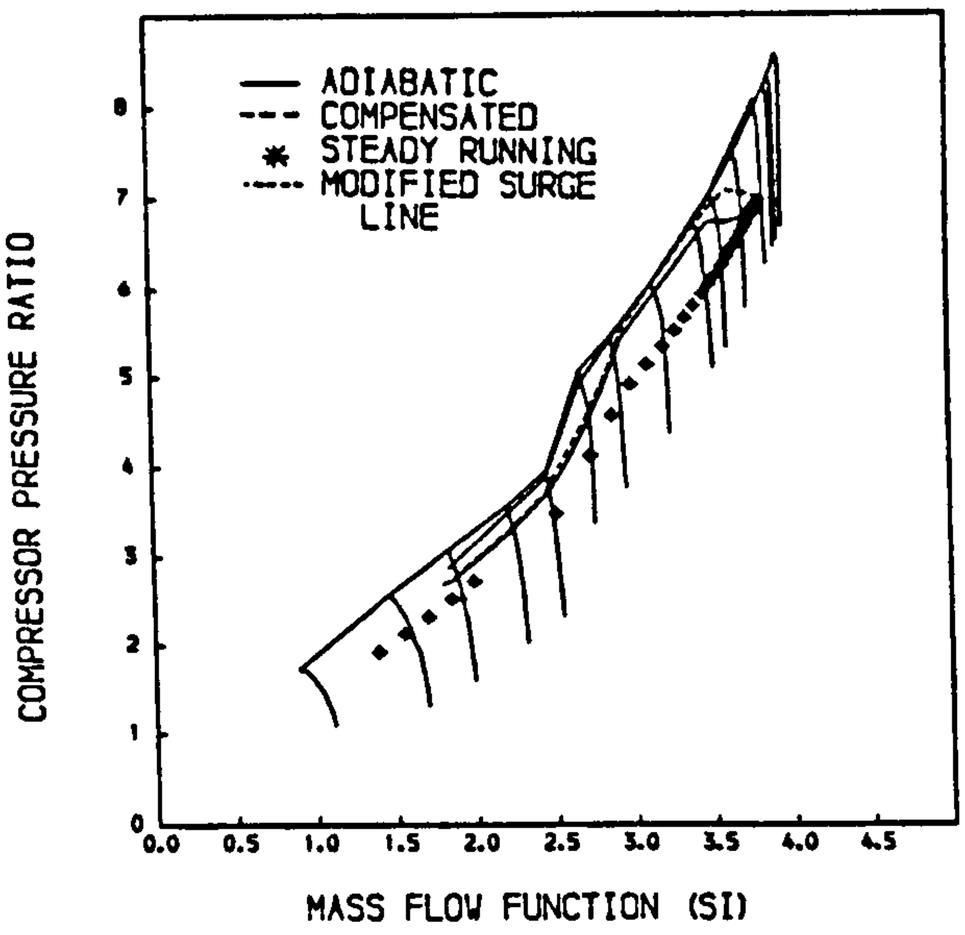

FIG 7B PREDICTED PATHS OF THE H.P. COMPRESSOR OF A TWO-SPOOL BYPASS ENGINE DURING AN ACCELERATION FOLLOWING AN 8 SECOND DECELERATION, AT SEA LEVEL STATIC CONDITIONS FUEL SCHEDULE COMPENSATED WITH A FUNCTION OF H.P.COMPRESSOR BLADE TEMPERATURE (EQ.1)

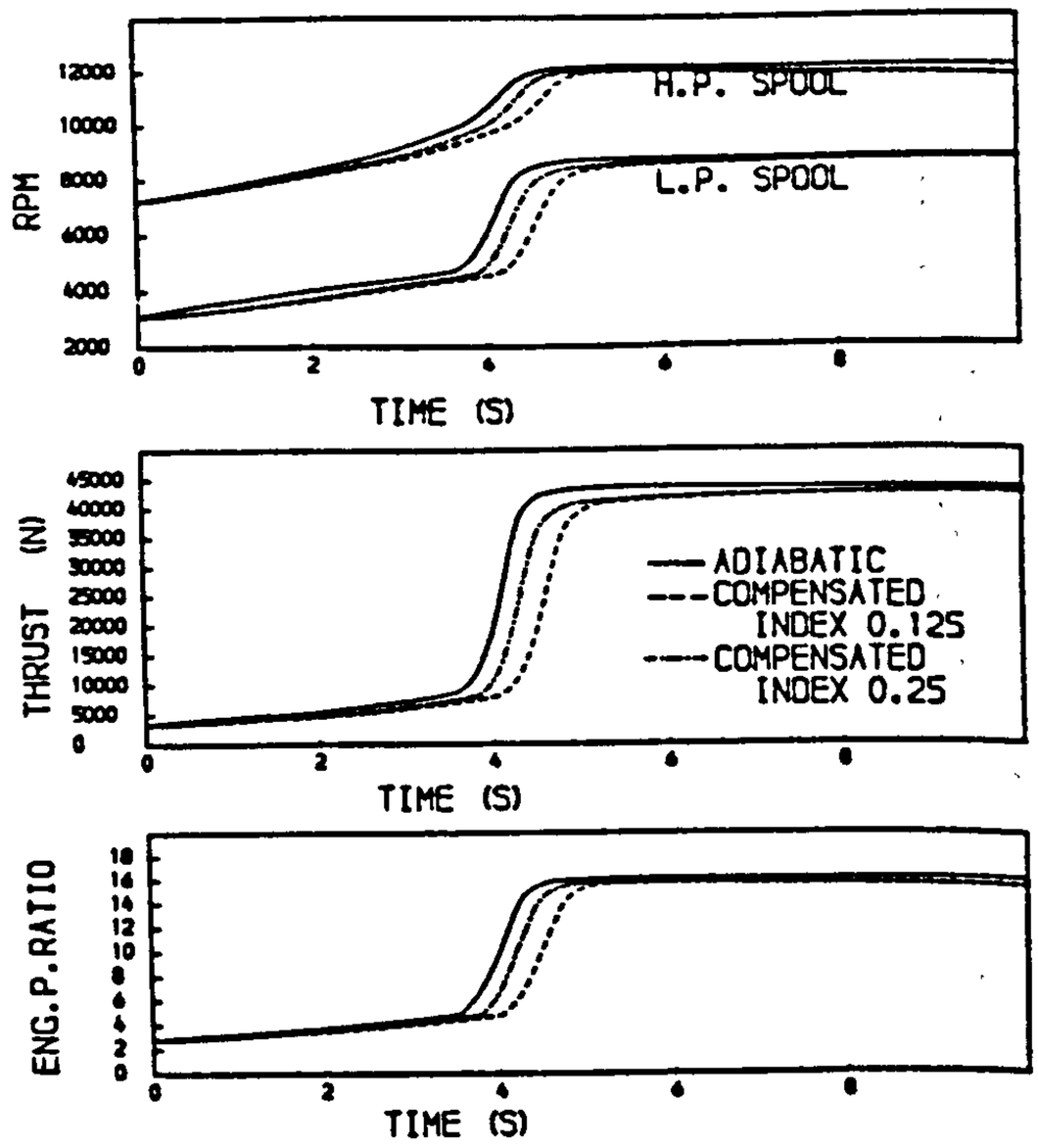

FIG 8A PREDICTED ACCELERATION OF A TWO SPOOL BYPASS ENGINE FROM GROUND IDLING AT SEA LEVEL STATIC CONDITIONS FUEL SCHEDULE COMPENSATED WITH A FUNCTION OF A DELAYED SPEED OF THE H.P. SHAFT (EQ.2)

6 CONCLUSIONS

Reasons have been presented for introducing a modifying factor which will adjust the transient fuel schedule to compensate for the immediately preceding temperature history of the engine. When accelerating a 'cold' engine this factor should enhance the acceleration rate, with greater consequent margin usage. The opposite should apply when reaccelerating a 'hot' engine, the 'Bodie' transient.

Two compensation models have been described, one based on the temperature of a characteristic component (the blades) in the H.P. Compressor, and the other on a 'delayed', H.P. Shaft speed signal. The first method induces the desired effects in a 'cold' acceleration. However the response of the blades proves too fast during a 'hot' acceleration, and the results are not satisfactory. The second model proves satisfactory during both transients if the appropriate parameters are chosen carefully (typically a time constant of 60 seconds). The latter method would also be easier to implement in practice.

7 ACKNOWLEDGEMENT

The authors wish to thank colleagues at Caledonian Airmotive Limited, Rolls Royce Limited and the University of Glasgow for provision of data, for valuable comments and for encouragement.

8 REFERENCES

1. Maccallum, N.R.L., and Pilidis, P., 'The Prediction of Surge Margins during Gas Turbine Transients',
A.S.M.E. Paper 85-GT-208, 1985

2. Pilidis, P., and Maccallum, N.R.L., 'A Study of the Prediction of Tip and Seal Clearances and their Effects on Gas Turbine Transients',
A.S.M.E. Paper 84-GT-245, 1984.

3. Pilidis, P and Maccallum, N.R.L., 'The Effect of Heat Transfer on Gas Turbine Transients',
Paper offered to the A.S.M.E. Gas Turbine Conference, 1986.

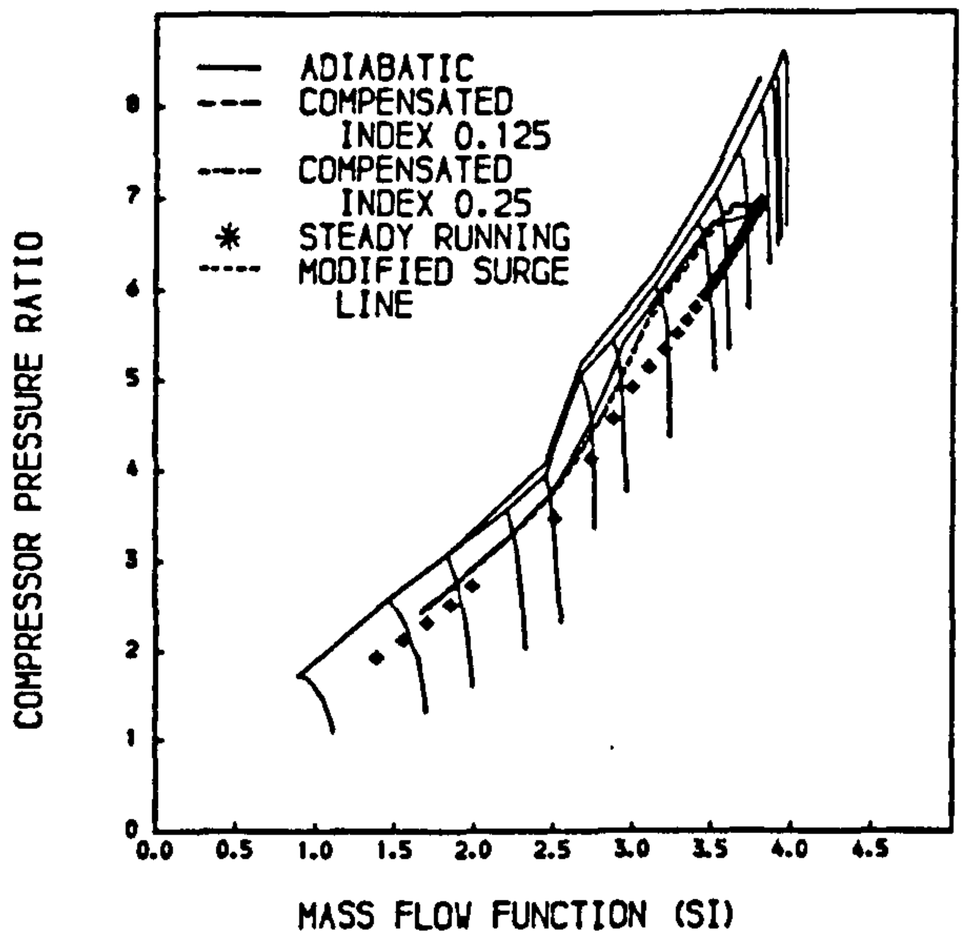

FIG 8B PREDICTED PATHS OF THE H.P. COMPRESSOR OF A TWO-SPOOL BYPASS ENGINE DURING AN ACCELERATION FROM GROUND IDLING AT SEA LEVEL STATIC CONDITIONS FUEL SCHEDULE COMPENSATED WITH A FUNCTION OF A DELAYED SPEED OF THE H.P. SHAFT (EQ.2)

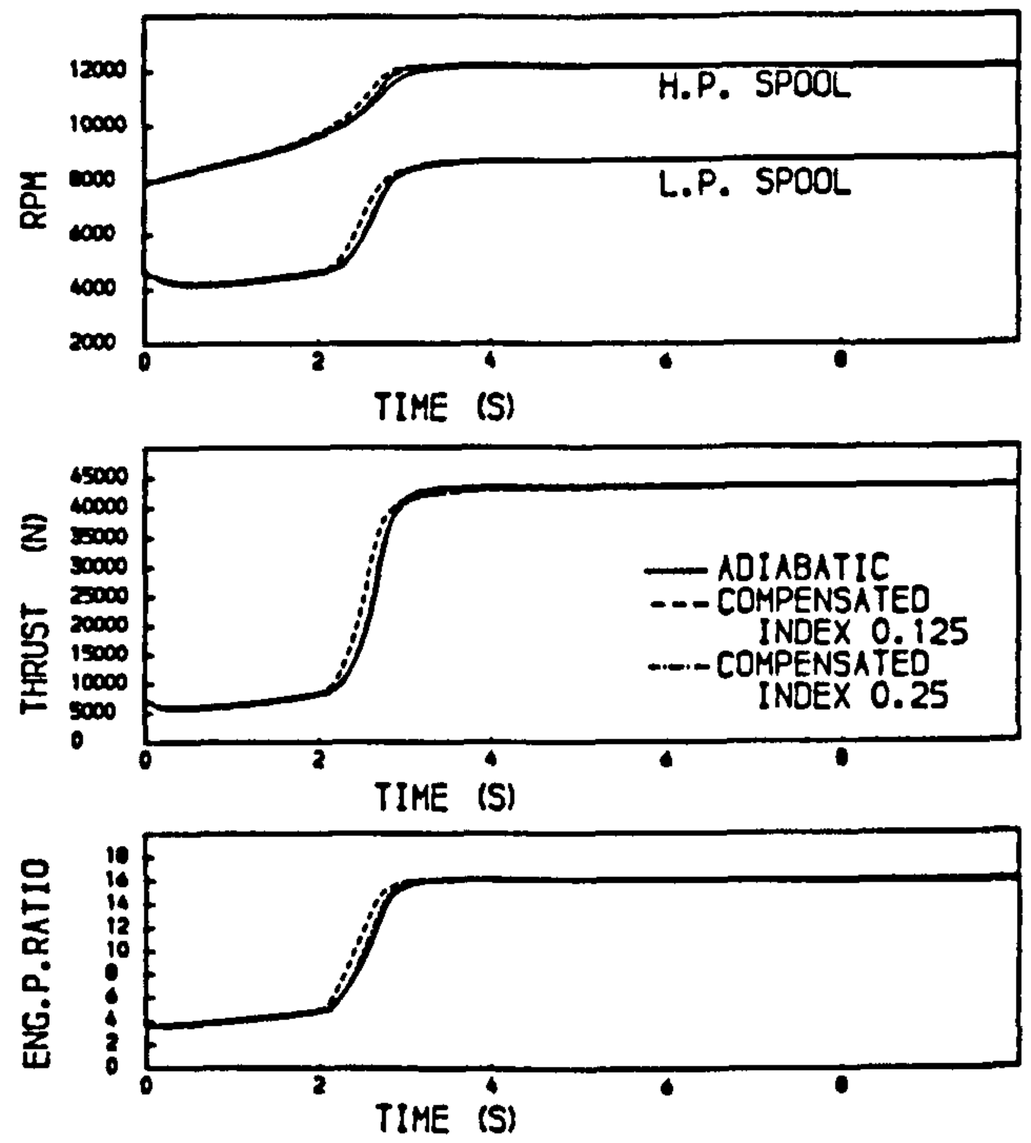

FIG 9A PREDICTED ACCELERATION OF A TWO SPOOL BYPASS ENGINE FOLLOWING AN 8 SECOND DECELERATION, AT SEA LEVEL STATIC CONDITIONS FUEL SCHEDULE COMPENSATED WITH A FUNCTION OF A DELAYED SPEED OF THE H.P. SHAFT (EQ.2)

4. Crawford, R.A. and Burwell, A.E., 'Quantitative Evaluation of Transient Heat Transfer on Axial Flow Compressor Stability', Paper AIAA-85-1352, Joint Propulsion Conference, July 1985.

5. Cantwell, H.F., 'Future Aero-Engine Control Systems, Why FADEC?', Inst. Elec. Engrs, Colloquium, London, Nov 1985.

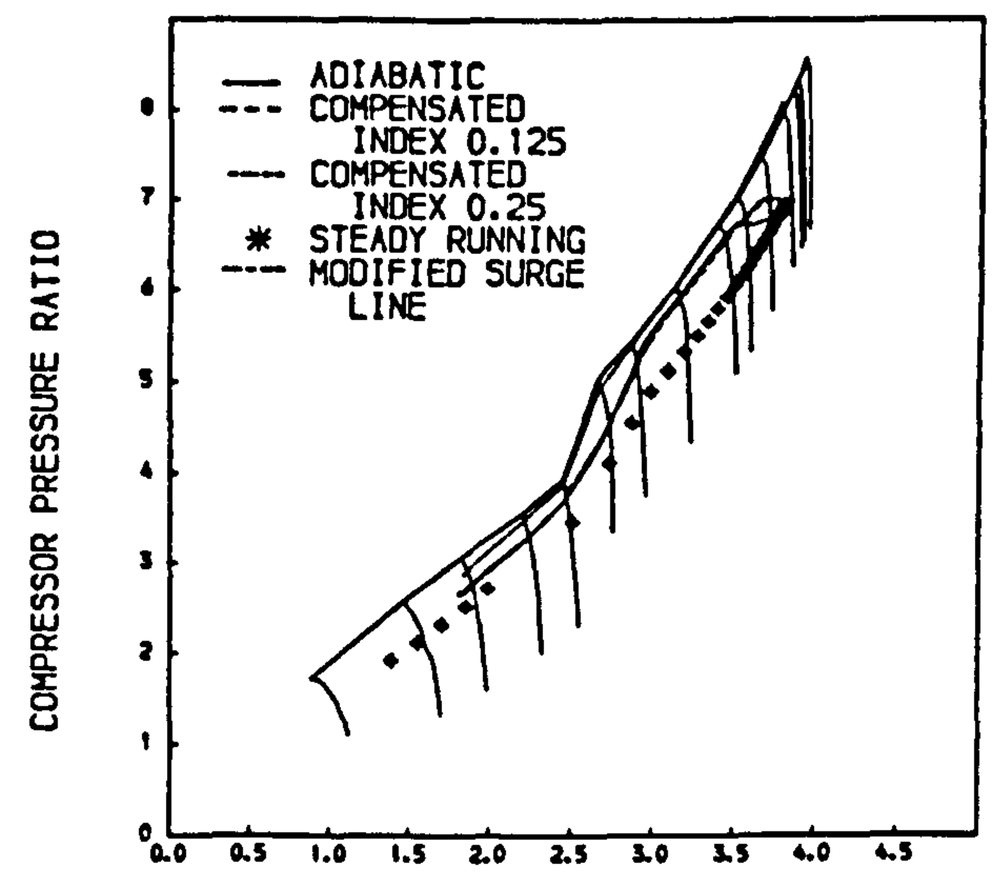

FIG 9B PREDICTED PATHS OF THE H.P. COMPRESSOR OF A TWO-SPOOL BYPASS ENGINE DURING AN ACCELERATION FOLLOWING AN 8 SECOND DECELERATION, AT SEA LEVEL STATIC CONDITIONS FUEL SCHEDULE COMPENSATED WITH A FUNCTION OF A DELAYED SPEED OF THE H.P. SHAFT (EQ.2)

Publication 36

86-GT-275

THE AMERICAN SOCIETY OF MECHANICAL ENGINEERS
345 E. 47 St., New York, N.Y. 10017

The Effect of Heat Transfer on Gas Turbine Transients

P. PILIDIS, Teaching Company Associate,
Caledonian Airmotive Ltd.,
Prestwick, Scotland

N. R. L. MACCALLUM, Reader,
University of Glasgow,
Glasgow, Scotland.

ABSTRACT

This paper describes how allowance for the thermal effects of non-adiabatic flow, altered boundary layer development, changes in tip clearances and changes in seal clearances have been incorporated into a general gas turbine transient program. These non-adiabatic effects have been investigated, modelling a two-spool bypass engine. The model has predicted events that occur in practice and also indicates which of the parameters are the most influential in the alteration of transient performance.

NOMENCLATURE

A	aspect ratio of aerofoil
c	specific heat at constant pressure
C_1 ,...C_5	constants
$\dot{f}$	fuel flow rate
f	function of
F	ratio of heat transfer to fluid to work transfer from fluid
g	staggered gap between blades
$\dot{m}$	air flow rate
n	index of expansion of gas
N	rotational speed
P	stagnation pressure
PR	pressure ratio
$\dot{Q}$	heat flux to air
R	surge pressure ratio
T	stagnation temperature (absolute)
V	blade tip velocity
β	blade angle
γ	ratio of specific heats of a gas
δ	tip clearance
η	efficiency
λ	non-dimensional clearance
φ	flow coefficient
ψ	blade loading ($2\,c\,\Delta T\,/V^2$)

Subscripts

1,2,3	inlet to, outlet from L.P. Compressor, outlet from H.P. Compressor
ad	adiabatic
b	blade aerofoil
c	compressor
ht	with heat transfer
H	High Pressure
m	mean
po	polytropic
s	stage

1 INTRODUCTION

This paper summarises a series of studies of thermal influences on the transient performance of gas turbines.

It has long been realised that heat transfer effects have an important influence on the transient performance, but until very recently, modelling was carried out either assuming adiabatic conditions, or using expedient but unrealistic models to simulate these effects.

The 'thermal' effects which are considered to be relevant in transients are:

(a) Non-adiabatic flows in compressors and turbines. In compressors this causes density changes due to heat transfer, additional to those resulting from the compression process.

(b) Changes in boundary layer development on blade aerofoils in compressors.

(c) Changes in boundary layer development on end-walls in compressors.

(d) Tip clearance changes, controlled by disc, casing and blade responses.

(e) Seal clearance changes, controlled by disc, casing and ring responses.

Presented at the International Gas Turbine Conference and Exhibit
Dusseldorf, West Germany—June 8-12, 1986

Effects (a) to (d) above, when applied to compressors, may alter the characteristics of the compressor, as described in Section 2 of this paper. All five effects influence the performance of the components, and hence of the engine as a whole. These changes lead to revised transient trajectories in the compressors and to important changes in predicted performance.

Models have been developed to represent these thermal effects. These models are described in Section 2 below. The influences of the thermal effects are then described in Section 3 and the modelling procedures are finally demonstrated in Section 4, in application to a Two-Spool Bypass Engine.

2 THERMAL EFFECTS DURING TRANSIENTS

When a gas turbine experiences a change of state, the engine materials will exchange heat with the working fluid because of the temperature changes of the latter. These heat exchanges influence the performance of the engine in an important manner (1)*. In this section the models for predicting these heat exchanges and their effects are described.

These effects have been studied by several investigators, (2), (3), (4). The description of the models given here is very brief and is intended simply to give an overall view of the investigations. Strengths and weaknesses of various models have been assessed and described fully in reference (5).

2.1 Clearances

Gas turbines are subjected to varying thermal and mechanical loading which produce small changes in both the radial and the axial dimension of the components. These changes of dimension occur during transient operation. They result in relative movements between rotating and stationary components, thus causing varying tip clearances and non-design mass flows. In the present paper only radial clearances have been investigated. Further work is required in the prediction of axial clearances, which can be important in some cases.

One of the reasons why clearance changes are experienced during transients is the thermal growth of the components. During transients the components of an engine expand at different rates because some sections absorb heat faster than others. It has been found that a convenient subdivision of the disc is possible (4). Finite element analysis indicates that thermally the disc can be treated as three sections, each of uniform temperature, a thick hub section, a thin diaphragm, and an outer rim. The blade is also treated as a discrete element, and similarly the casing.

Another factor affecting clearance openings is centrifugal expansion. The subdivision of a stage employed for the calculation of thermal growths has been utilised to obtain centrifugal growths. In the manner outlined above compressor and turbine tip clearances can be calculated.

One effect of tip clearance changes is that of modifying component efficiency. Lakhsminarayana extensively investigated clearance losses and proposed the following model (6) to evaluate the resultant efficiency loss (Eq.1).

$$\Delta\eta = \frac{0.7\,\psi\lambda}{\cos\beta_m}\left(1 + 10\sqrt{\frac{\lambda\varphi\ A}{\psi\cos\beta_m}}\right) \quad . \qquad (1)$$

Typical compressor and turbine clearance movements during an acceleration are illustrated in Fig. 1. Also shown are the resulting efficiency changes, relative to the efficiency of the component when it is

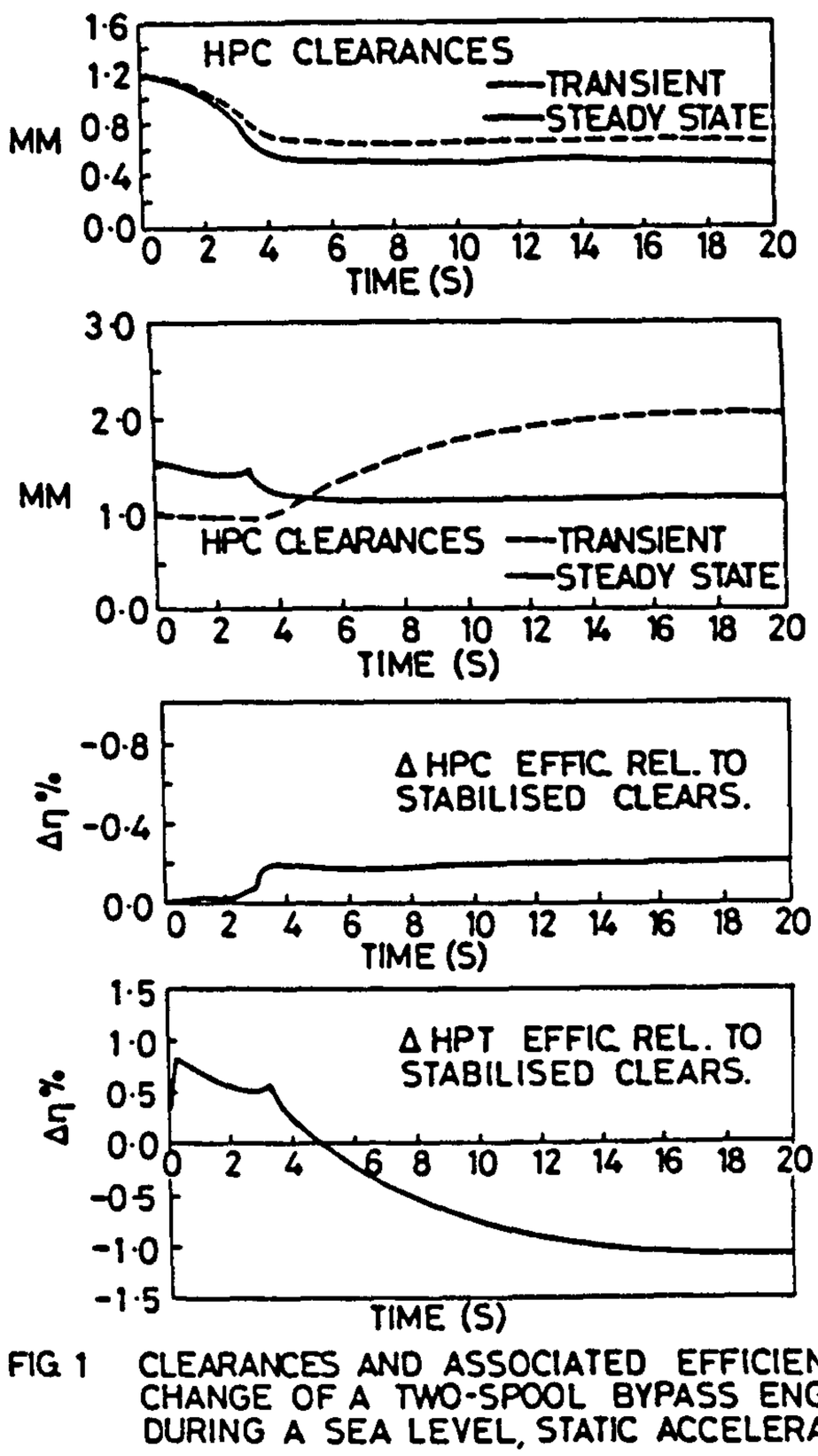

FIG. 1 CLEARANCES AND ASSOCIATED EFFICIENCY CHANGE OF A TWO-SPOOL BYPASS ENGINE DURING A SEA LEVEL, STATIC ACCELERATION.

* Underlined numbers in brackets indicate references at the end of the paper.

stabilised at that speed. The path of the efficiency changes of the H.P. Compressor is smooth, and the changes are small. Efficiency changes of the H.P. Turbine are irregular because of the changes of the turbine inlet temperature at the beginning and the end of the speed transient.

Seals restrict the amount of air bled from the engine to a predetermined quantity. The models used to

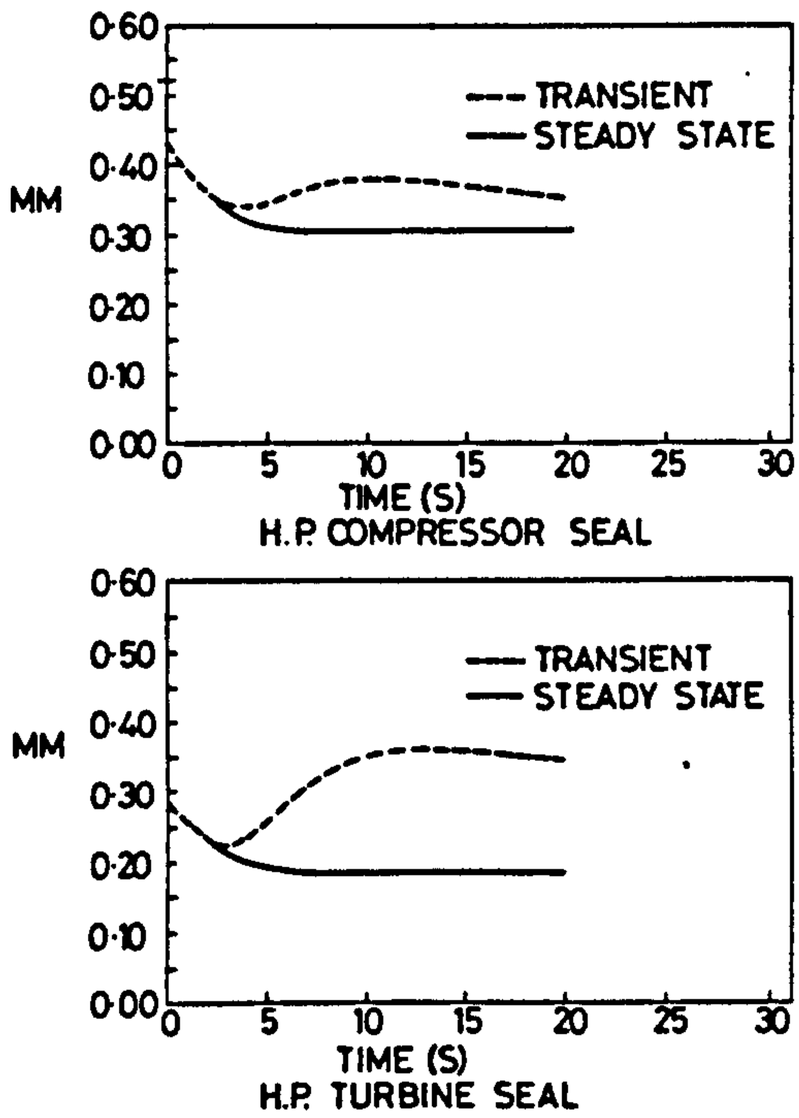

FIG.2 TRANSIENT SEAL CLEARANCES OF A TWO-SPOOL BYPASS ENGINE DURING A SEA LEVEL, STATIC ACCELERATION

predict tip clearance movements can also be used to predict seal openings during transients. Some typical predictions are shown in Fig. 2. The openings are seen to depart significantly from the design values (stabilised at the maximum speed). Wittig et al (7) have carried out experimental investigations which suggest that for a set of given engine conditions, a nearly linear relationship exists between the mass flowing through the seal and the seal opening. In view of this evidence, the present model assumes a proportional relationship between the engine mass flow and the seal opening.

2.2 Heat Capacity of the Components

During transients, engine materials and the working fluid will exchange heat. Because of this heat exchange the index of compression or expansion of the working fluid will change. Thus the performance of the various engine components will be altered. Maccallum (8) has investigated this effect. From first principles the following model has been elaborated, for compressors:

$$\frac{\eta_{ht} - 1}{\eta_{ht}} = \frac{(1-F)\,(\gamma-1)}{\eta_{po}\,\gamma} \qquad (2)$$

and for turbines:

$$\frac{\eta_{ht} - 1}{\eta_{ht}} = (1-F)\,\eta_{po}\,\frac{(\gamma-1)}{\gamma} \qquad (3)$$

2.3 Changes in Compressor Characteristics

It has been established that the characteristics of axial-flow compressors are altered by both of the above effects of tip clearance and heat capacity (1), and attempts have been made (2),(3) to quantify the changes. In the present paper, the procedure adopted to quantify these changes follows the method used in references (2) and (13), where it is described in more detail.

2.3.1 Prediction of Adiabatic Characteristics

To estimate predicted compressor characteristics a stage by stage calculation has been carried out. First the limiting pressure rise is determined from Koch's correlation (9). An initial end-wall blockage factor is guessed. Assuming that Howell and Bonham's correlation (10) can be applied to the core flow through the blading in the central annulus, a pressure rise across the stage can be predicted. This is compared with the limiting, or stalling pressure rise value. From Smith's data (11), displacement thicknesses at the hub and at the casing can then be found, giving a revised end-wall blockage factor. The above calculation is then repeated until convergence on the actual end-wall blockage is obtained. This procedure is then carried out through the subsequent stages of the compressor in succession. There are several coefficients, such as tó allow for applying a low-speed correlation to a high-speed compressor, which are adjusted so that the predicted compressor characteristics, in steady-running, line up with the observed performance of the compressor. The thermal transient effects of density change due to heat transfer, modified development of boundary layers on blade aerofoils and end-walls, and tip clearance changes can then be introduced in the above method for prediction of transient characteristics.

2.3.2 Effect of Density Changes

When a 'cold' engine is accelerated, heat will be transferred from the air to the blades and casings. In a two-dimensional system, this will make the air more dense, giving it a lower axial component of velocity at a particular stage of the compressor, compared with steady-running at that speed, inlet temperature and mass flow. This alters the loading on that particular stage and thus changes the stage pressure rise. Consequently the overall pressure rise is altered.

Thought has been given to which of the heat flows will affect the pitch-line density. The temperature distributions shown by Smith (11) for steady-running of a 12-stage compressor indicate that the energy

dissipated into heat due to losses at the end-walls tends to remain trapped within the end-wall boundary layer. Therefore it appears that heat transfers to, or from, platforms and casings will have little influence on the temperature, hence density, of the air flow at the pitch-line (the end-wall heat transfers will alter the end-wall boundary layer thickness, as discussed later). However heat transfers to, or from the blade aerofoils will immediately influence pitch-line density. The procedure adopted in the present work is to assume that only the heat transfers to, or from, the aerofoils of the blades alter the density as compared to adiabatic running.

When these effects are incorporated into the pitch-line prediction method it is found (2) that for a given inlet non-dimensional speed a new pressure ratio to non-dimensional mass flow characteristic is obtained. One method of quantifying this change is to retain the adiabatic characteristic and use a modified 'effective' speed. It is also possible for the surge pressure ratio at a particular non-dimensional mass flow to be changed.

In the working region where the front stages of the compressor are the most heavily loaded, and therefore nearest to initiating surge, heat transfers to the blades, as when accelerating a 'cold' compressor, increase the effective speed and raise the surge pressure ratio (at a given mass flow). It has been suggested (5) that for these small changes in 'effective speed' and changes in the surge pressure ratio, simple linear relationships can be used. The heat transfer coefficients used for the blades are based on established correlations, and for other areas from correlations for developing boundary layers on flat plates, as discussed in References (2),(4) and (12). The blade, with its aerofoil and platform combination, can be treated as two components, comprising firstly the aerofoil and secondly a finned platform, the effectiveness of the finning depending on the instantaneous aerofoil temperature. Thus the blade aerofoil temperature can be calculated during the transient, and using these procedures the heat flow rate to the air (or gas), Q is calculated and hence the parameter F, which is the ratio of the heat flux to the air (or gas) to the power transfer from the air (or gas) in that component.

2.3.3 Boundary Layer Development

Experiments have been carried out (12) to show that the separation from a convex surface in an adverse pressure gradient can occur earlier if the surface is hotter than the flowing air. This is directly applicable to the case of aerofoil boundary layers. A model has been incorporated in a compressor characteristics prediction program (13), and the resulting movements in effective speed and in surge pressure ratio can be represented by linear models.

The effect of heat transfer on the thickness of the boundary layers on the end-walls is somewhat uncertain. The simple approximation that has been used in this program has been to assume the effect of heat transfer is similar to the effect on the thickness of turbulent boundary layers on flat plates. On the basis of this assumption, small movements in effective speed and surge pressure ratio are indicated.

2.3.4 Tip Clearance Changes

Blade tip clearances during transients do not exhibit their equilibrium openings. Their effect on the characteristics can be determined using the correlation presented by Koch (9) between the limiting pressure rise of a stage and the non-dimensional tip clearance. This method has been applied to the H.P. Compressor of the bypass engine referred to above, and it is found in the relevant range that the change in effective speed and in surge pressure ratio can be approximated by a linear expression (13).

The study was not extended to the L.P. Compressor as it had been found (5) that the tip clearances of that compressor in transients scarcely deviated from the corresponding steady-running values.

2.3.5 Summation of Effects of Heat Transfer

The effects of heat transfer on the compressor characteristics, as indicated above can be approximated by:

$$\frac{\Delta N}{N} = C_1 \frac{T_b - T_{air}}{T_{air}} + C_2 \frac{\dot{Q}}{\dot{m}\, c\, T_m} - C_3 \frac{\Delta(\delta)}{g} \qquad (4)$$

The coefficients C_1, C_2, and C_3, represent the changes due to movements of the aerofoil boundary layer, changes in the fluid density and changes in the blade tip clearances respectively. They were obtained with the methods outlined above. A similar expression will indicate the movements of the surge pressure ratio.

$$\frac{R_{ht} - 1}{R_{ad} - 1} = 1 + C_4 F - C_5 \frac{\Delta(\delta)}{g} \qquad (5)$$

The coefficients C_4, and C_5, represent the changes due to density changes of the fluid and changes in the tip clearances repsctively.

As an illustration, the analysis has been applied to a Two-Spool Bypass Engine with mixed exhausts. The pitch-line prediction program (2) was used to predict the effective characteristics for a number of instants in a range of transients. There was very reasonable consistency of the values obtained for the coefficients C_1, C_2, C_3, C_4, and C_5. The mean values adopted for the L.P. Compressor were -0.07, -0.07, 0.3, 0.36 and 1.10. The corresponding values in the H.P. Compressor were -0.1, -0.1, 0.3, 0.36 and 1.10.

Typical heat transfer parameters in an acceleration are shown in Fig. 3 and resulting movements of compressor characteristic constant speed lines are shown in Fig. 4. The dominant effects are seen to be due to boundary layer alterations and density changes, the effects of tip clearance being small.

3 INFLUENCE OF THERMAL EFFECTS IN TRANSIENTS

In the procedures described in the previous section provision has been made for important factors that affect the performance of an engine during a transient. In this section these factors are included in the prediction of engine performance and the results compared to those of an adiabatic model. For this purpose a general transient programme was employed (5),

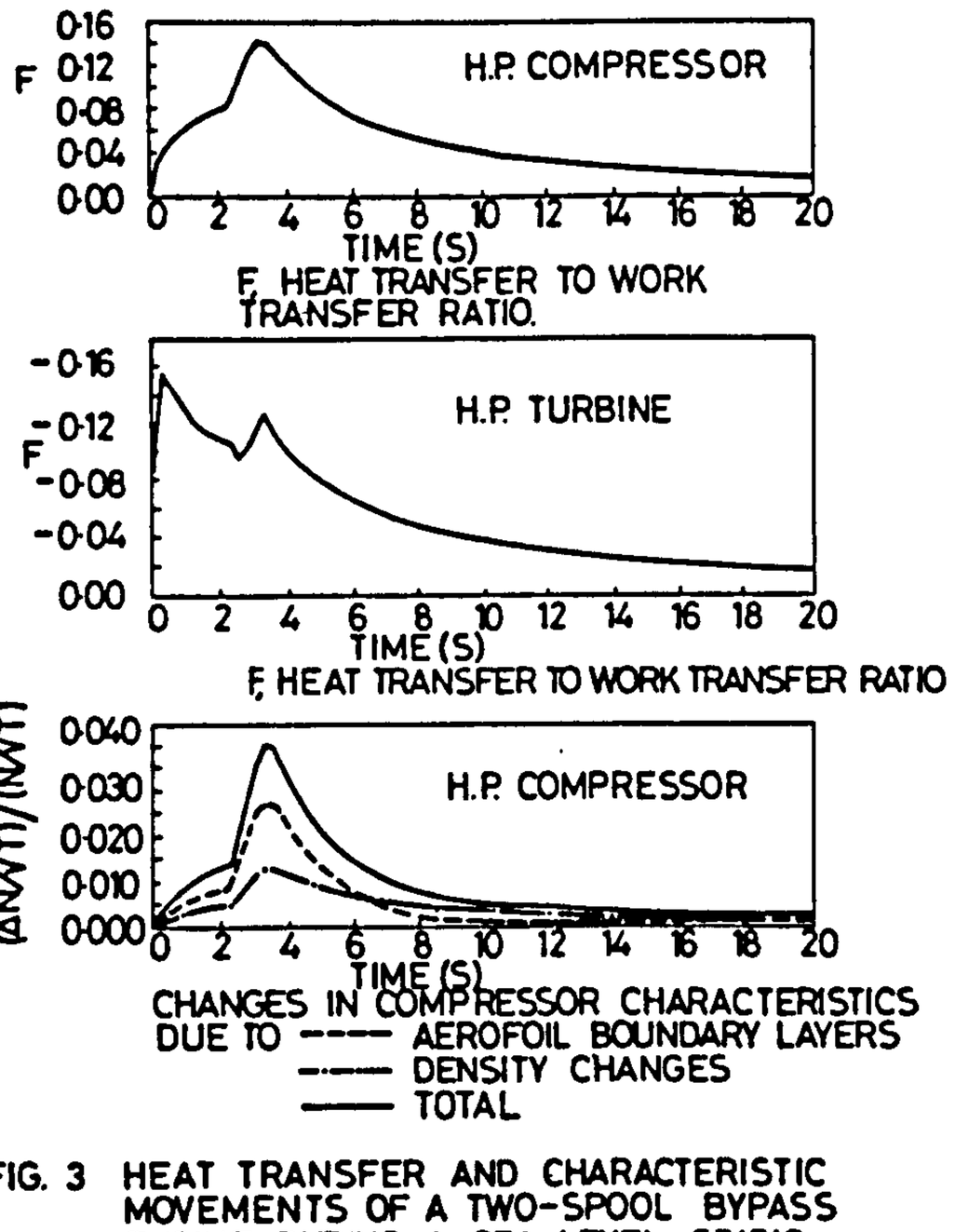

FIG. 3 HEAT TRANSFER AND CHARACTERISTIC MOVEMENTS OF A TWO-SPOOL BYPASS ENGINE DURING A SEA LEVEL, STATIC ACCELERATION.

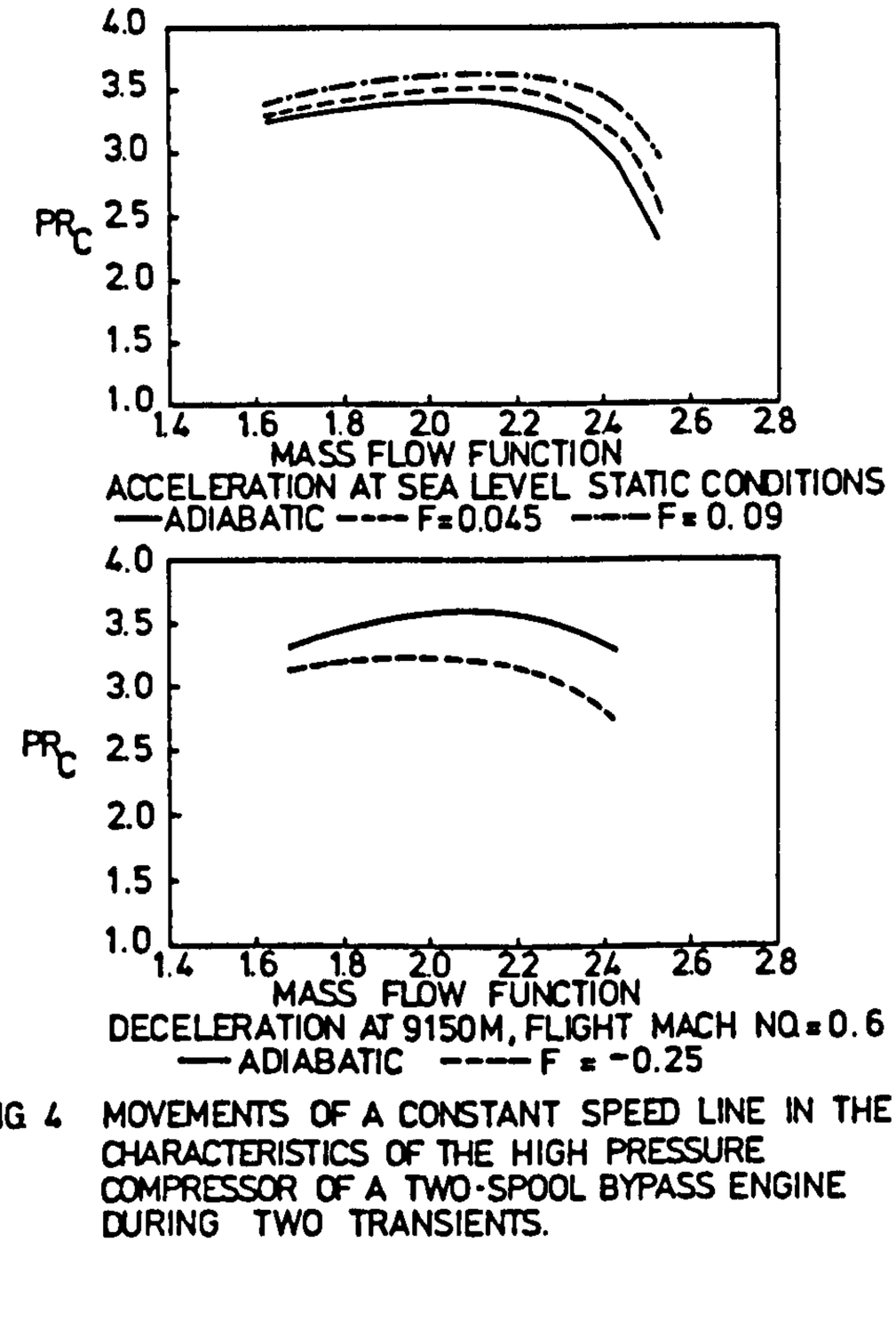

FIG 4 MOVEMENTS OF A CONSTANT SPEED LINE IN THE CHARACTERISTICS OF THE HIGH PRESSURE COMPRESSOR OF A TWO-SPOOL BYPASS ENGINE DURING TWO TRANSIENTS.

(14). For all the transients investigated the same fuel schedule was employed, a function of the H.P. Compressor pressure ratio (Eq. 6).

3.1 Clearances

As shown in Fig. 1, the tip clearances of both compressors and turbines are tighter at most points of the acceleration speed transient than they would be at the same engine conditions during the steady state. This is because the thermal growth of the blades and the centrifugal growth close the clearance very quickly, while the casing thermal expansion (which opens the clearance) becomes dominant very soon after the end of the speed transient, while the expansion of the disc is the slowest movement. The expansion of the casing is of a larger magnitude than that of the disc because the latter is cooled much more effectively.

The changes in performance due to the modified efficiencies of compressors and turbines resulting from non-design clearances are shown in Fig. 5. Only the change of the efficiency of the H.P. Turbine has a perceptible effect on the predicted performance.

Some seal clearances can have an important effect on the engine performance. Two seals have been investigated, these being a seal controlling the flow from the H.P. Compressor into the bypass duct and a seal controlling the flow of cooling air from the H.P. Compressor delivery to the first stage of the H.P. Turbine. During an acceleration transient these two seals exhibit openings which are significantly larger than their design values, these results having been shown in Fig. 2. As Fig. 6 shows, the engine is found to be very sensitive to non-design seal openings. In this case the H.P. Turbine seal has the largest effect on the transient because the ratio of maximum to stabilised seal opening is larger than that for the H.P. Compressor seal. This is so mainly because the H.P. Turbine seal has an equilibrium clearance which is half that of the H.P. Compressor seal. It is interesting to notice that the seal openings are influential in delaying the attainment of the final state of the engine. However there is no significant change to the thrust and the speed of the engine immediately after the completion of the speed transient. Their effect in the speed transient is limited to a slower dynamic response to the fuel schedule and a small increase in the turbine inlet temperature.

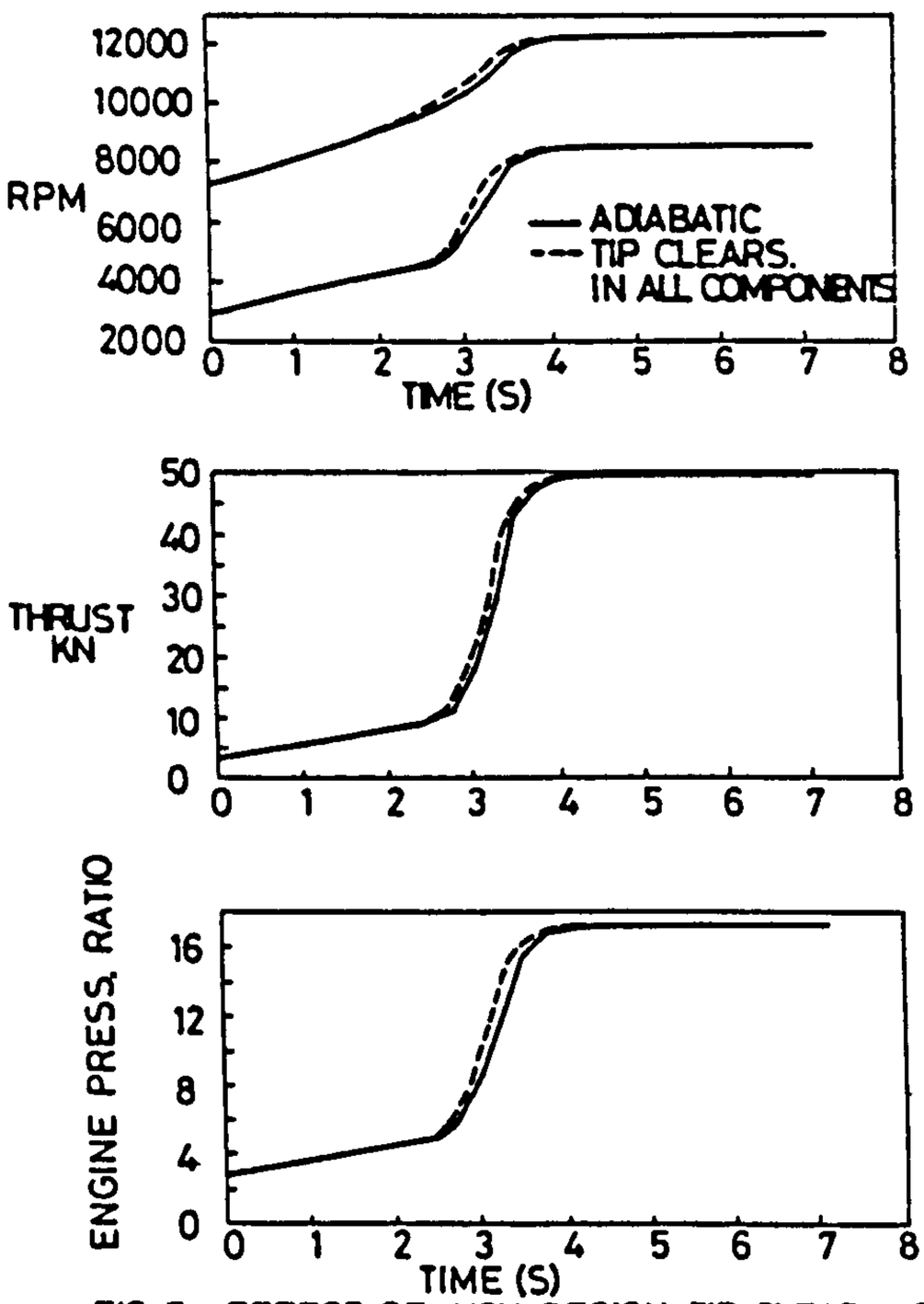

FIG. 5 EFFECT OF NON-DESIGN TIP CLEARANCES ON PREDICTED ACCEL. OF TWO-SPOOL BYPASS ENGINE – SEA LEVEL STATIC.

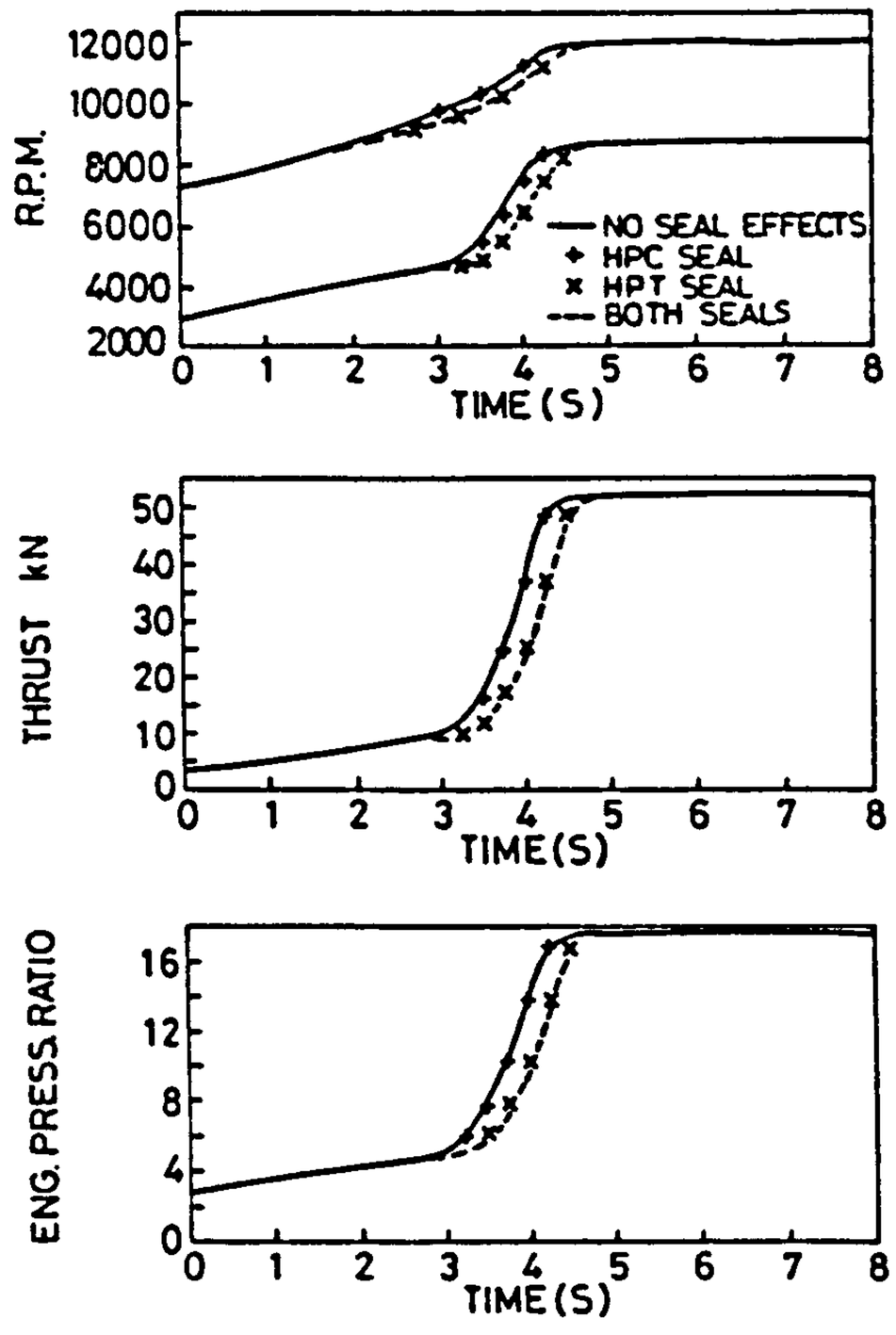

FIG.6 EFFECT OF NON-DESIGN SEAL CLEARANCES ON PREDICTED ACCEL. OF TWO-SPOOL BYPASS ENGINE - SEA LEVEL STATIC

3.2 Heat Capacities

The influence of the heat capacity of the components on the predicted transient performance is illustrated in Fig. 7. L.P. Compressor and Turbine influences are very small and their inclusion in the prediction method produces no perceptible changes to the dynamic behaviour of the engine. The inclusion of H.P. Compressor heat capacity in the prediction results in an improved response, while the opposite is true for the H.P. Turbine. When all the heat capacities are included, a small deterioration of the response is predicted. Noticeable however is the significant reduction of the thrust developed at the end of the speed transients. This effect is experienced while the components are absorbing heat. The final thrust is attained gradually as thermal equilibrium is achieved.

3.3 Changes in Characteristics

When the engine is analysed including the changes in compressor characteristics, three trends are immediately noticed (Fig. 8). The most important effect is the considerable retardation of the engine response, specially due to the changes in the H.P. Compressor characteristics. The second observation to be made is that the thrust and the pressure ratio at the end of the speed transient is the same as in the adiabatic case. Finally the rotational speed of the shafts is slightly lower than that predicted in the adiabatic case. This is because although the speed is lower than in the equilibrium conditions the 'effective speed' is that corresponding to the final steady state point. The rotational speed will gradually reach its correct value as the engine moves to thermal equilibrium.

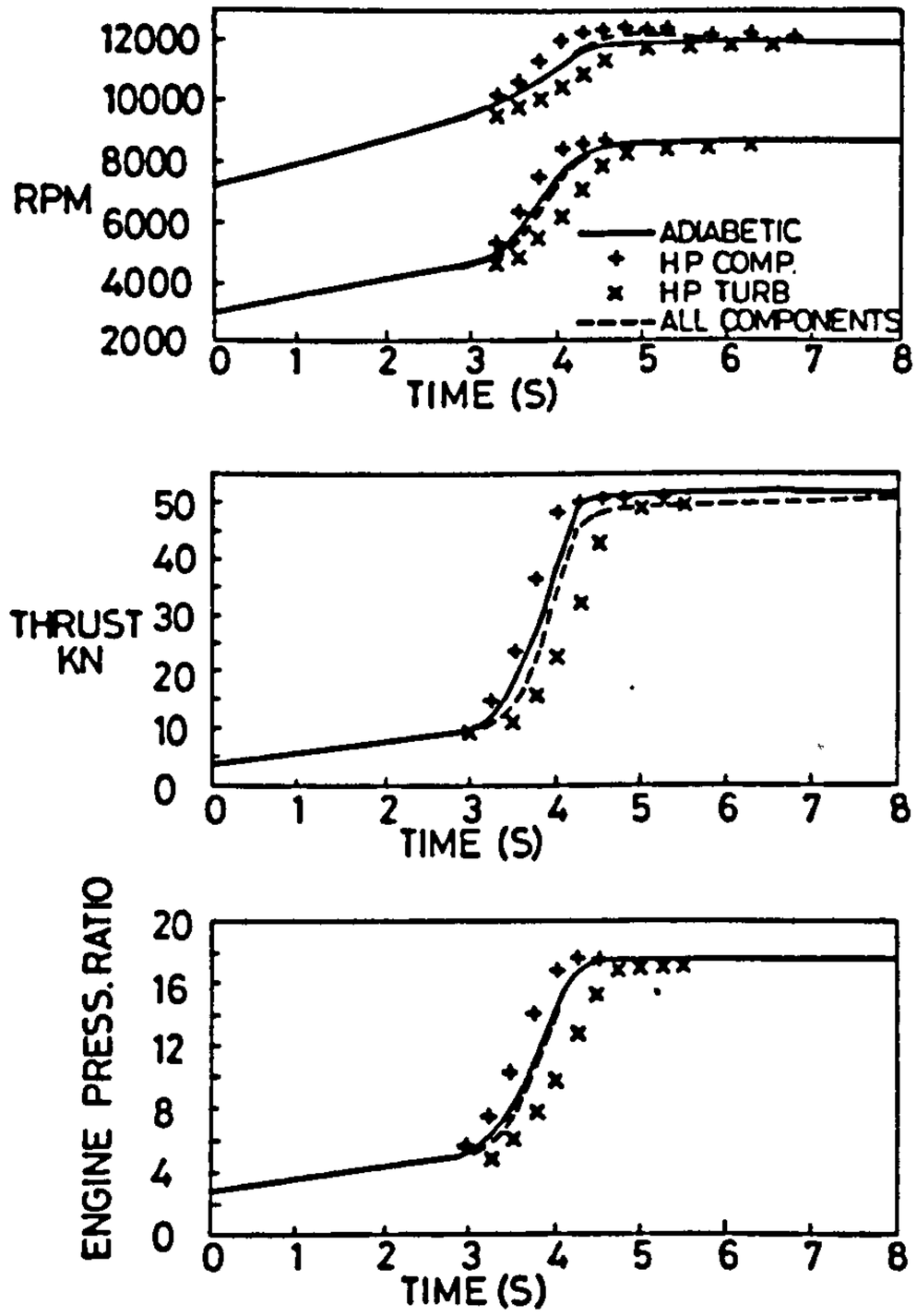

FIG.7 EFFECT OF HEAT CAPACITIES OF COMPONENTS ON PREDICTED ACCEL. OF TWO-SPOOL ENGINE - SEA LEVEL STATIC.

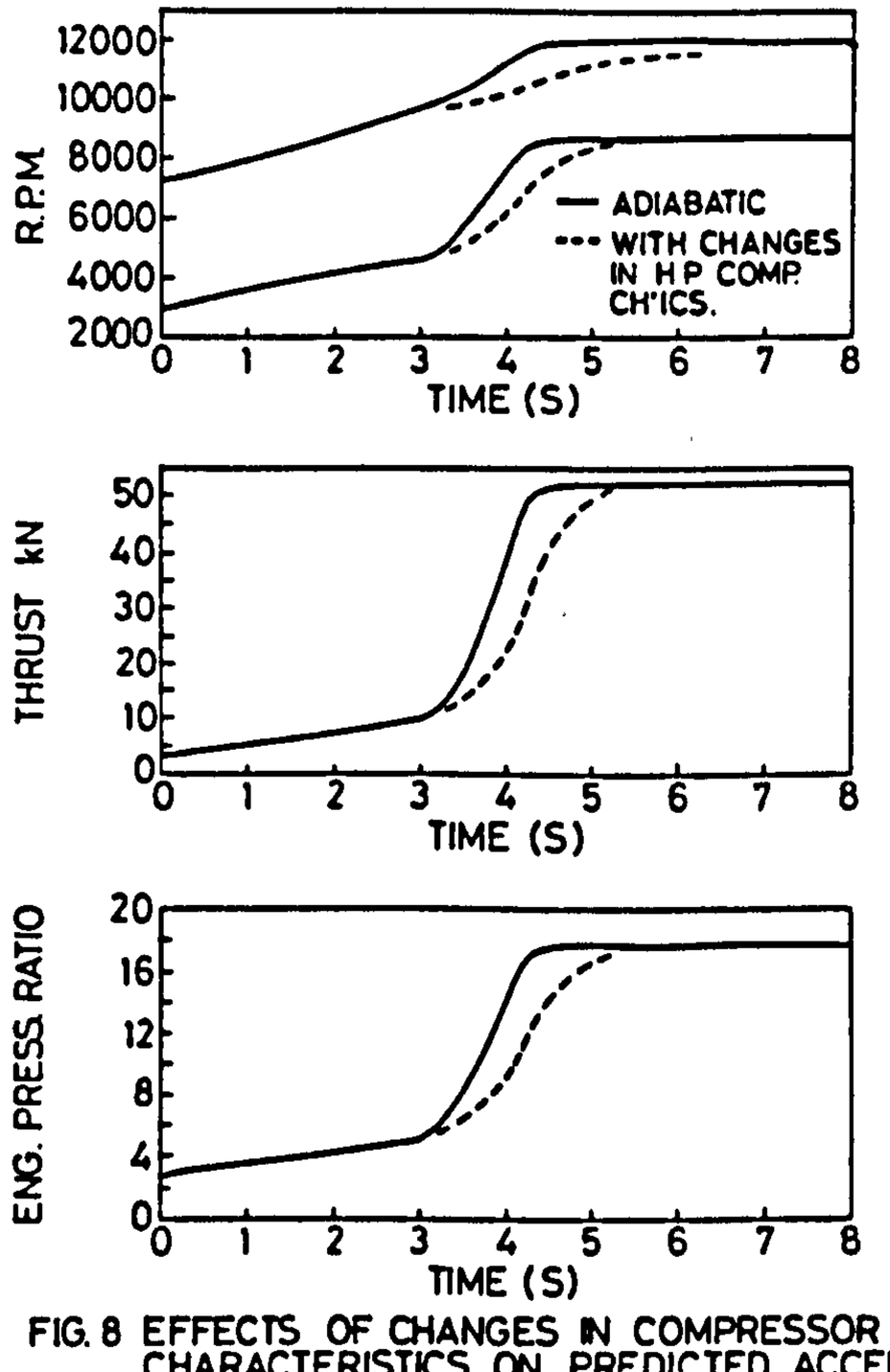

FIG. 8 EFFECTS OF CHANGES IN COMPRESSOR CHARACTERISTICS ON PREDICTED ACCEL. OF TWO SPOOL BY-PASS ENGINE - SEA LEVEL STATIC.

3.4 Inclusion of all Non-Adiabatc Effects

The inclusion of all the thermal effects result in a marked reduction in the predicted acceleration rate relative to the adiabatic simulation. In particular the last five percent of the thrust will take longer to be attained. Important movements of the surge lines can be observed. During an acceleration, the surge line moves away from the running line (Fig. 9), thus increasing the surge margin, while the opposite occurs during a deceleration.

The effects that appear to have the most important effect on the transient are the non-design seal clearances and the changes in characteristics (affecting the response rate), and the heat capacities (affecting the thrust attainable).

During decelerations the engine response is also slower when analysed as a non-adiabatic system. In this case the heat transfer effects are more noticeable because engine mass flows are much smaller at the end of the transient so the relative effects are much more important. Thermal equilibrium is attained after a longer period of time after a deceleration than during an acceleration because the heat transfer coefficients are reduced due to the lower mass flows and rotational speeds.

Thermal effects were also investigated at altitude where due to the reduced mass flows in the engine the effect of heat transfer is more important on a relatve basis than at sea level. So the changes in the performance are more noticeable.

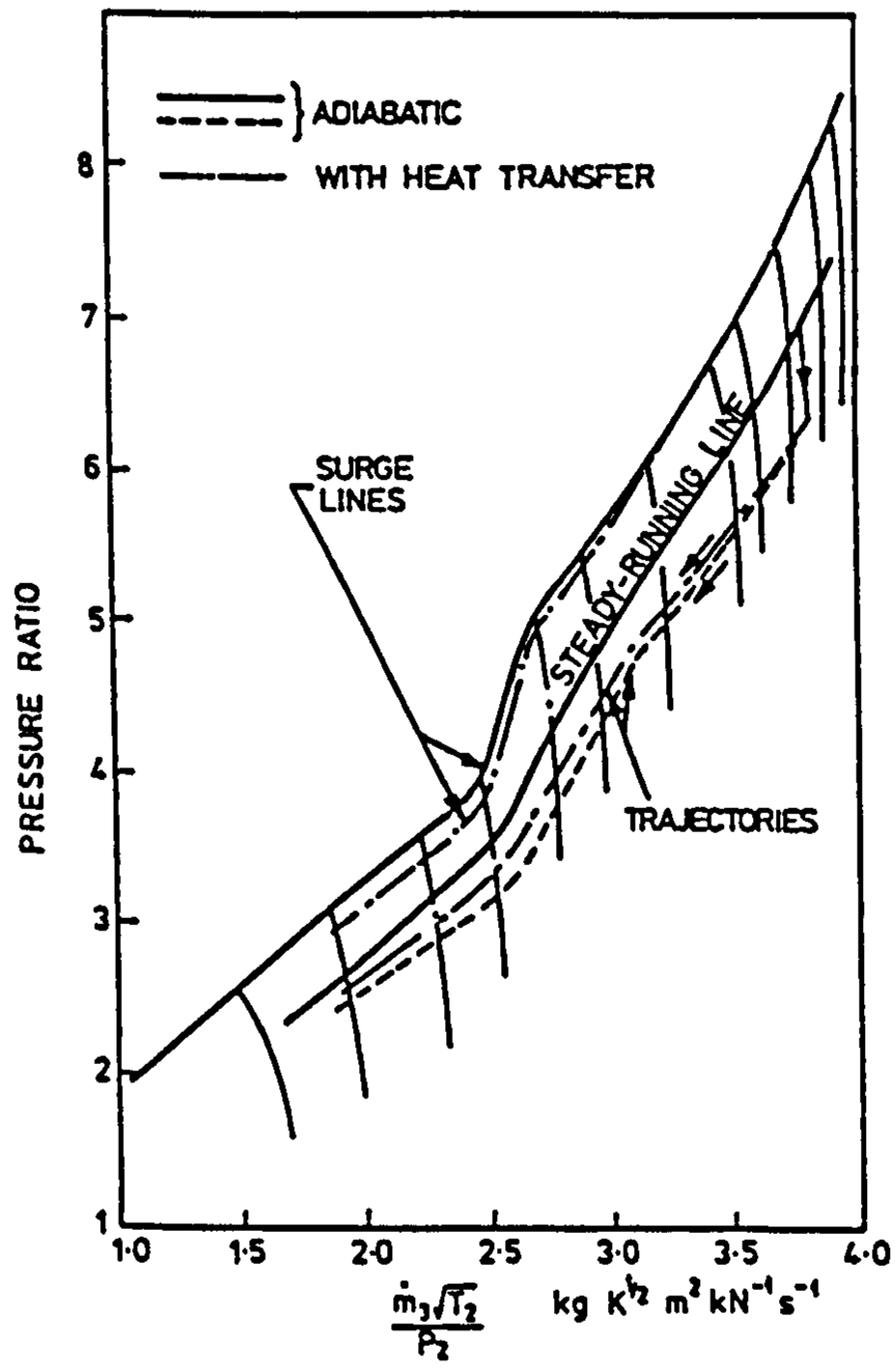

Fig.9 PREDICTED TRAJECTORIES AND SURGE LINES IN H.P. COMPRESSOR - SEA LEVEL DECELERATION.

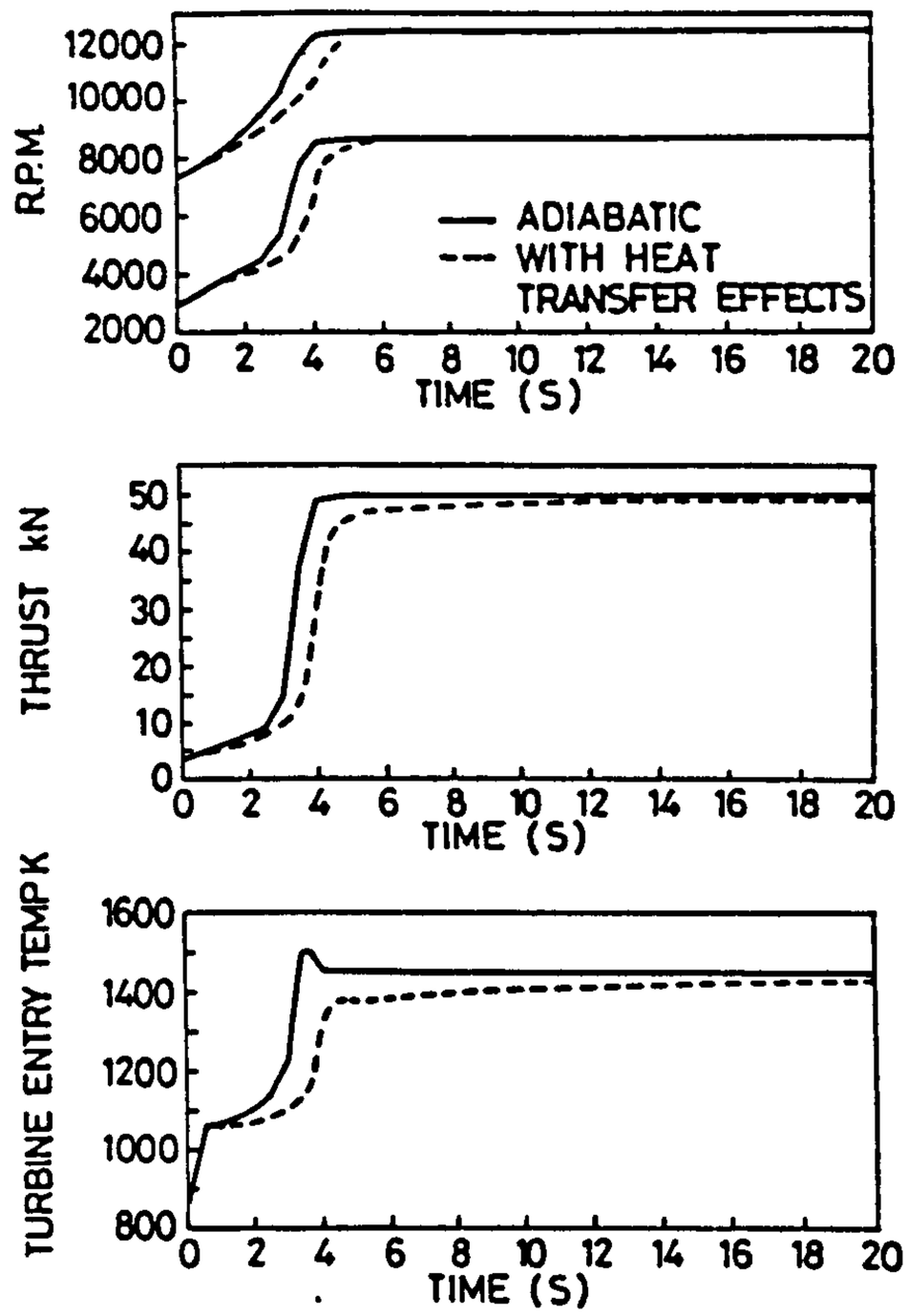

FIG.10 EFFECTS OF HEAT TRANSFER ON A MEDIUM TERM TRANSIENT OF A TWO-SPOOL BYPASS ENGINE WITH MIXED EXHAUSTS

3.5 Transients of a Two-Spool Bypass Engine

In this section a Two-Spool Bypass Engine with mixed exhausts has been used as an example to illustrate two cases in which the heat transfer effects are very noticeable: firstly the few seconds following an acceleration speed transient and secondly a 'Bodie' transient.

3.5.1 Events Following an Acceleration Speed Transient

The events occurring after an acceleration speed transient are illustrated in Fig. 10. The speed transient is completed in the first four seconds, and it is followed by a period of changes in performance due to heat transfer effects. In the analysis illustrated, once the maximum fuel flow is achieved, the fuel setting is not altered. However engine operators may change the fuel setting once the speed transient is completed. At the end of the speed transient it is evident that the rotational speed and the thrust have not reached their desired value. In addition there is some turbine temperature margin available, due to heat absorption taking place in the compressors. Thus it is a natural reaction to overfuel the engine. As the thermal stabilisation of the engine proceeds a combination of events will force the operator to reduce the fuel flow. During the period of time which immediately follows the final stages of the speed transient, the blade tip clearances start increasing. This increase in blade tip clearances coincides with the largest seal openings during the transient. The deterioration in compressor efficiency results in higher compressor delivery temperature. The larger seal opening allows a larger amount of air to bypass the combustion chamber which in turn results in a slightly smaller amount of air being supplied to the combustion chamber, thus increasing the turbine inlet temperature. This gradual temperature rise is sensed by the fuel control, which will reduce the fuel flow a few seconds after the end of the speed transient, i.e. near the point of take-off.

This phenomenon has been observed in practice. Using the present prediction procedure, such adjustments of fuel flow while the component efficiencies and seal clearances have deteriorated would cause a gradual rise in the turbine inlet temperature of some 50K.

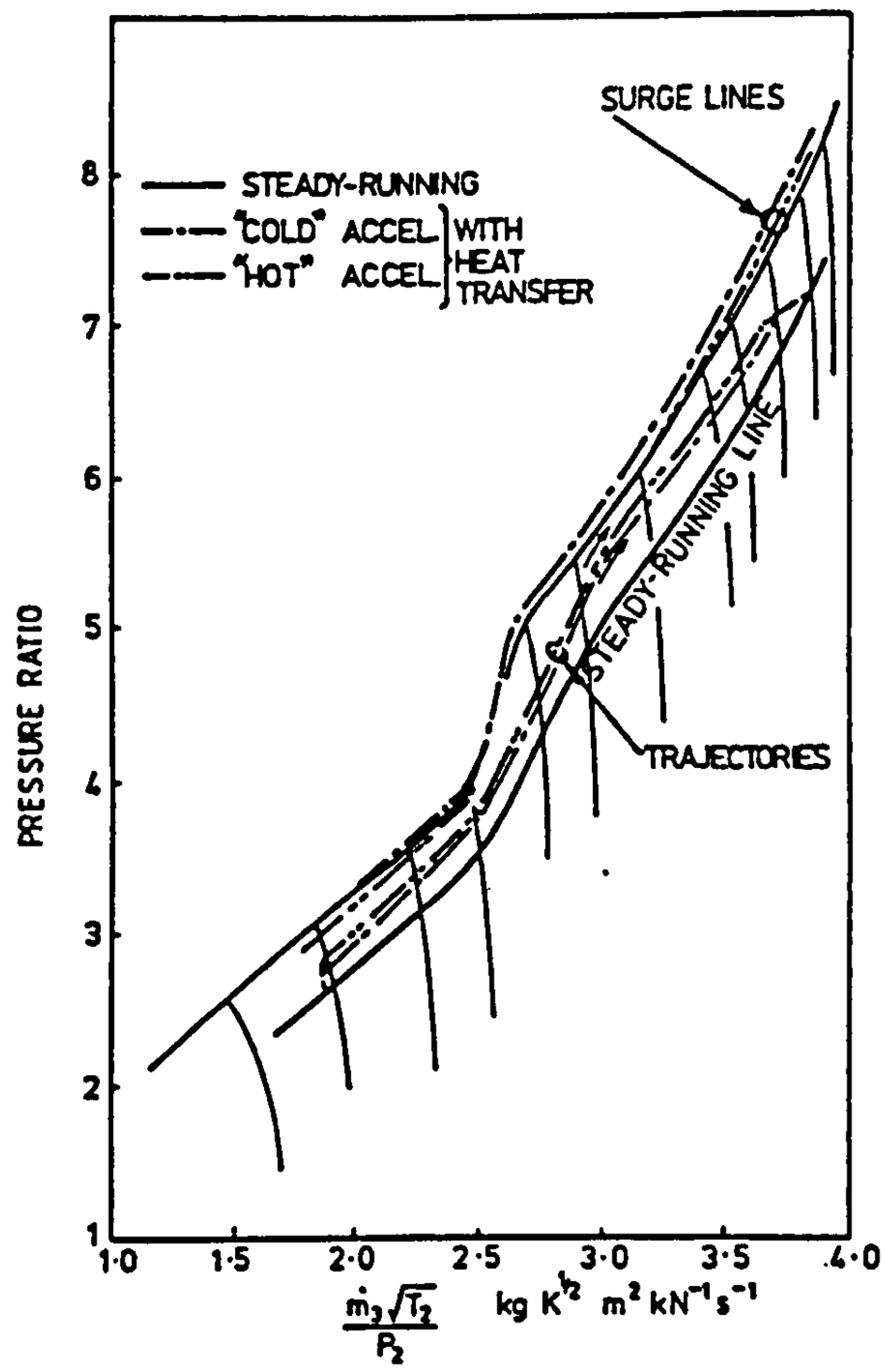

Fig.11 PREDICTED TRAJECTORIES AND SURGE LINES IN H.P. COMPRESSOR-'COLD' AND 'HOT' ACCELERATION AT SEA LEVEL.

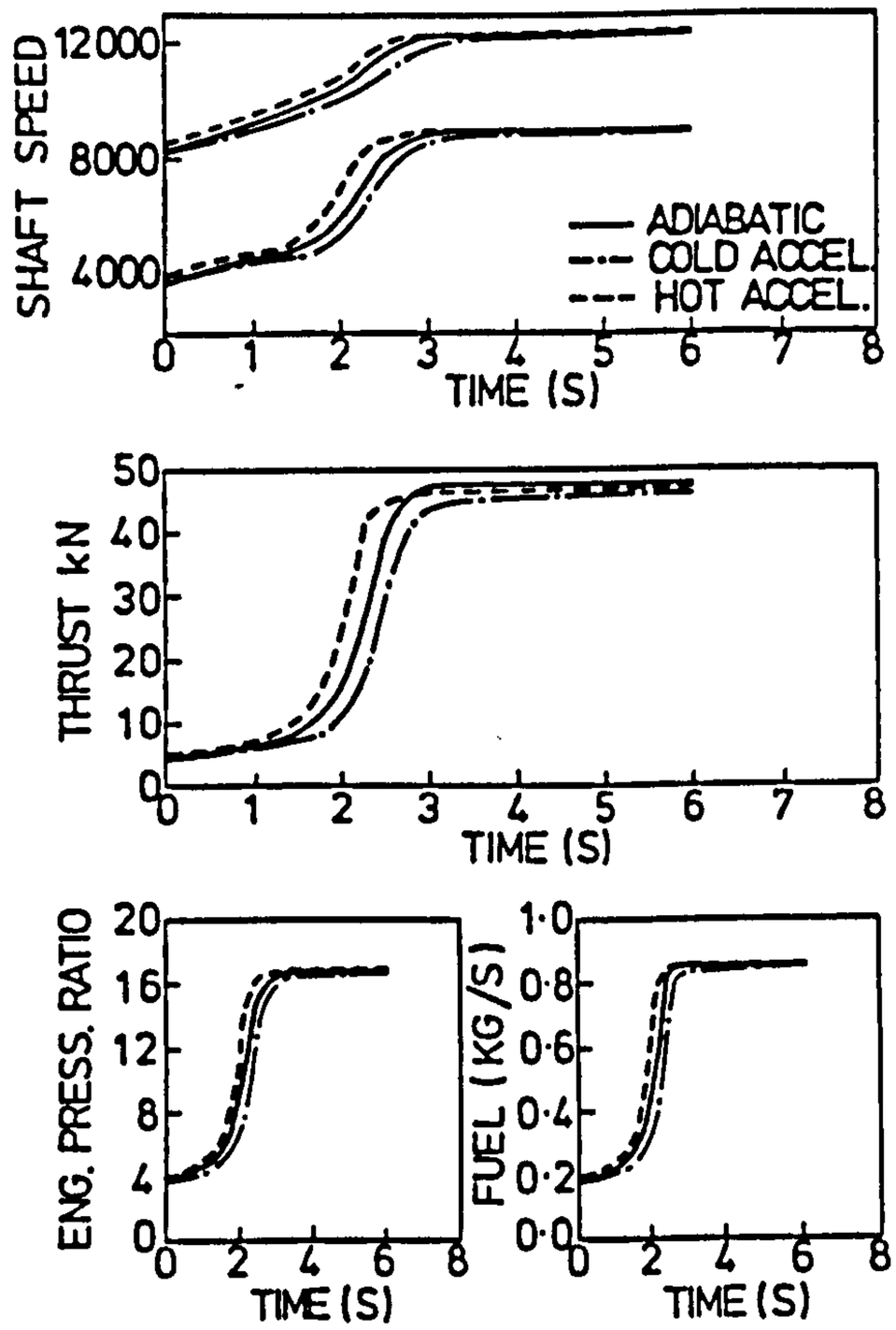

Fig.12 PREDICTED PERFORMANCE OF A TWO-SPOOL BYPASS ENGINE-SEA LEVEL ACCEL.

3.5.2 Bodie Transient

In the engine under investigation it has been shown that the surge line moves away from the running lines during an acceleration. The opposite occurs during a deceleration. Thus if there is a requirement to reaccelerate the engine immediately following a deceleration, the surge margin available is smaller than in a 'cold' acceleration. This type of transient is known as the 'Bodie' transient, in which much greater care is required when accelerating a hot engine rather than a cold one. The trajectories (13) in the performance maps are shown in Fig. 11, while the performance during this transient is shown in Fig. 12. Examination of these figures shows that the surge margin has been reduced by approximately fifteen percent. Furthermore the transient running line moves nearer to the surge line in a 'hot' acceleration than in a 'cold' one. This results in a further reduction of surge margin of a similar magnitude. Thus the net result is a reduction in the surge margin of approximately one third. Since in a cold acceleration one third of the surge margin is utilised at the beginning of the transient, the total surge margin used will be approximately two thirds.

The response to the accelerating fuel schedule is significantly faster in a 'hot' acceleration. However the thrust at the end of the speed transient is still significantly lower than that expected at the final fuel setting in the steady state.

As stated previously, the same fuel schedule was used in all the transients shown in Fig. 12, this being a non-dimensional schedule based on H.P. Compressor parameters (Eq. 6).

$$\frac{\dot{f}}{N_H P_2} = f\left(\frac{P_3}{P_2}\right) \qquad (6)$$

It can be noticed in Fig. 12 that due to the changes in the performance of the compressor, the fuel

flow increases more or less rapidly relative to the adiabatic prediction.

An investigation (15) is now being made of the inclusion of material temperature terms in the fuel schedule to allow for the history of the engine to improve control during the transients.

4 CONCLUSION

A transient performance program for gas turbines has been developed which incorporates methods to account for heat transfer effects during accelerations and decelerations. These models have been included in a very simplified form, to reduce computing times to a minimum.

The results obtained with these methods are realistic and provide an insight into the processes occurring in an engine during the transient phase. Some effects such as movement of characteristics and tip clearance movements tend to slow the speed of response of the engine. Other effects such as the heat capacity of the engine can alter the final thrust obtained at the end of the speed transient. In addition the position of the surge line during transients is not the same as in the steady state.

An understanding into these processes is necessary because many limitations in the engine design are imposed by constraints in the transient phase.

5 ACKNOWLEDGEMENT

The authors wish to thank colleagues at Caledonian Airmotive Limited, Rolls Royce Limited and the University of Glasgow for provision of data, for valuable comments and for encouragement.

6 REFERENCES

1. Koff. B.L., 'Designing for Fighter Engine Transients',
AGARD Conference Proceedings 324, Paper 2, 1982.

2. Maccallum, N.R.L., 'Axial Compressor Characteristics During Transients',
ibid, Paper 22, 1982.

3. Larjola, J., 'Simulation of Surge Margin Changes due to Heat Transfer Effects in Gas Turbine Transients',
A.S.M.E. Paper 84-GT-129, 1984.

4. Pilidis, P., and Maccallum, N.R.L., 'A Study of the Prediction of Tip and Seal Clearances and their Effects on Gas Turbine Transients',
A.S.M.E. Paper 84-GT-245, 1984.

5. Pilidis, P., 'Digital Simulation of Gas Turbine Performance',
Ph.D. Thesis, University of Glasgow, 1983.

6. Lakshminarayana, B., 'Methods of Predicting the Tip Clearance Effects in Turbomachinery.'
A.S.M.E. Journal of Basic Engineering, Sept. 1970, pp 467-482.

7. Wittig, S.L.K., Dorr, L., Kim, S., 'Scaling Effects on Clearance Losses in Labyrinth Seals'
A.S.M.E. Journal of Engineering for Power, April 1983.

8. Maccallum, N.R.L., 'Effect of Bulk Heat Transfer in Aircraft Gas Turbines on Compressor Surge Margins'.
Heat and Fluid Flow in Steam and Gas Turbine Plant.
I. Mech. Eng., London, 1974.

9. Koch,C.C., 'Stalling Pressure Rise Capability of Axial Flow Compressor Stages',
Journal of Engineering for Power, vol 103, 1981, pp 645-656.

10. Howell, A.R. and Bonham, R.P. 'Overall and Stage Characteristics of Axial Flow Compressors',
Proceedings of the Inst. Mech. Engrs., vol 163, 1950.

11. Smith, L.H. Jr., 'Casing Boundary Layers in Multistage Axial-Flow Compressors',
Flow Research on Blading, ed L.S. Dzung, Elsevier Publishing, Amsterdam, The Netherlands, 1970, pp 275-304.

12. Maccallum, N.R.L. and Grant, A.D., 'The Effect of Boundary Layer Changes due to Transient Heat Transfer on the Performance of an Axial Flow Air Compressor',
S.A.E. Paper 770284, 1977.

13. Maccallum, N.R.L., and Pilidis, P., 'The Prediction of Surge Margins during Gas Turbine Transients',
A.S.M.E. Paper 85-GT-208, 1985

14. Pilidis, P and Maccallum, N.R.L., 'A General Program for the Prediction of the Transient Performance of Gas Turbines',
A.S.M.E. Paper 85-GT-209, 1985.

15. Maccallum, N.R.L., and Pilidis, P., 'Gas Turbine Transient Fuel Scheduling with Compensation for Thermal Effects'.
Paper offered to the A.S.M.E. Gas Turbine Conference, 1986.

S A BELTAGUI BSc PhD* and N R L MACCALLUM BSc PhD†

Publication 37

Stability limits of free swirling premixed flames: Part I. Experimental correlation

The paper describes an experimental study of the stabilization of flames in unconfined premixed swirling jets. Swirl was provided by 'hubless' vane-type swirlers, the vanes being set at angles ranging from 15 to 70° to the axial direction. Two sizes of swirlers were examined, having diameters of 23.7 and 93 mm respectively. Two fuel types were used: town gas and natural gas. The studies of the mechanism of flame stabilization in jets with high degrees of swirl, and hence central recirculation, indicate that the anchoring region which controls stabilization is in the main forward flow adjacent to the central recirculation zone, within the axial distance of 0.5 to 1.0 swirler diameters from the swirler exit. The experimental observations of the weak extinction limits show that for one fuel type there is a general relationship between the absolute velocity leaving the swirler and the effective fuel/air ratio at the anchoring region

1. Introduction

It is important to understand the mechanism by which flames can be stabilized in high-velocity premixed fuel-air streams. In these systems some form of recirculation is usually employed. One convenient method of setting up such a recirculation in the centre of the flow is to introduce swirl motion. Two types of such jets have to be considered:

(*a*) free, unconfined, jets,
and (*b*) enclosed, confined, jets.

It has been shown[1] that for a furnace diameter, or main dimension, to burner diameter ratio greater than five, effects of walls on jets are minimal.

The present paper describes an investigation of the mechanism of flame stabilization in the central recirculation zone (CRZ) produced by vane type swirlers, the jets issuing directly into the atmosphere (ie free jets). A range of swirler vane angles from 15 to 70° has been examined, the observations concentrating on the weak stability, or extinction, limits. Comparisons have been made of results using two gaseous fuels: town gas and natural gas.

2. Test apparatus

The test rig consisted of air and fuel supply lines merging into a mixing chamber followed by a mixing length leading to the swirler.

Swirlers were made to the design of Mathur and Maccallum,[2] having flat vanes of inclinations to the axis of 15°, 30°, 45°, 60° and 70°. The swirlers had no central hub and the vanes met at a point on the axis of the swirler. Two sizes of swirlers were tested, having diameters for flow of 23.7 and 93 mm. Two fuel types were used: town gas and natural gas, typical compositions being given in Table 1.

In order to elucidate the mechanism of stabilization by the CRZ, temperature and gas composition surveys were made in flames stabilized by the larger swirlers (93 mm dia) at conditions approaching the extinction limit. A range of fuel-air mixtures was covered including values close to the stability limit. Temperatures were measured using a (Pt 5% Rh)–(Pt 20% Rh) thermocouple with a wire diameter of 0.25 mm and a bead diameter of 0.5 mm. The bare wire protruded 16 mm from the ceramic stem of 2.8 mm diameter, which was supported by the traversing water-cooled probe at 90 mm from the bead.[3]

Gas samples were removed using a water-cooled probe[3] and analysed for carbon dioxide using an infra-red gas analyser and for combustibles using an MSA instrument.

3. Results

Two principal flame types were observed, depending on the flow pattern produced by the swirler.

(*a*) *Weak swirl* – the case of the 15° vane swirler which produced no CRZ. The flames are stabilized in the wakes of the downstream edges of the vanes, particularly where the vanes meet on the axis. For this type of flame it was possible to obtain a complete stability loop covering both weak and rich limits, Fig. 1.

(*b*) *Strong swirl* – cases of vane angles of 30 to 60° inclusive. A stable CRZ is established downstream from the swirler, and the initial stabilizing steps take place in and around this zone. In this case the rich extinction limits occurred at extremely high equivalence ratios and apparently were not influenced by the processes within the CRZ. Attention was focused on the weak extinction limits for swirlers of vane angles 30° and above. For the smaller swirlers (23.7 mm dia), limits were observed over a tenfold range of flow velocities. With the larger swirlers (93 mm dia), air supply limitations restricted the range covered.

At the vane angle of 70° the jets issuing from the gaps between the vanes did not merge, but remained attached to the mounting which carried the swirler. The resulting 'wall-jet' flames were not examined further in the present work.

Extinction limits for the principal swirlers are shown in Fig. 1 for both fuels used, namely town gas and natural gas.

Typical sets of temperature rise contours corrected for

(*continued on p 162*)

TABLE 1 Typical percentage compositions by volume of fuels

	H_2	CO	CH_4	C_2H_6	C_3H_8	CO_2	N_2	O_2
Town gas	49	1	29	1	—	11	7	2
Natural gas	—	—	92	4	1	—	3	—

*National Engineering Laboratory, and University of Glasgow.
†Department of Mechanical Engineering, University of Glasgow.

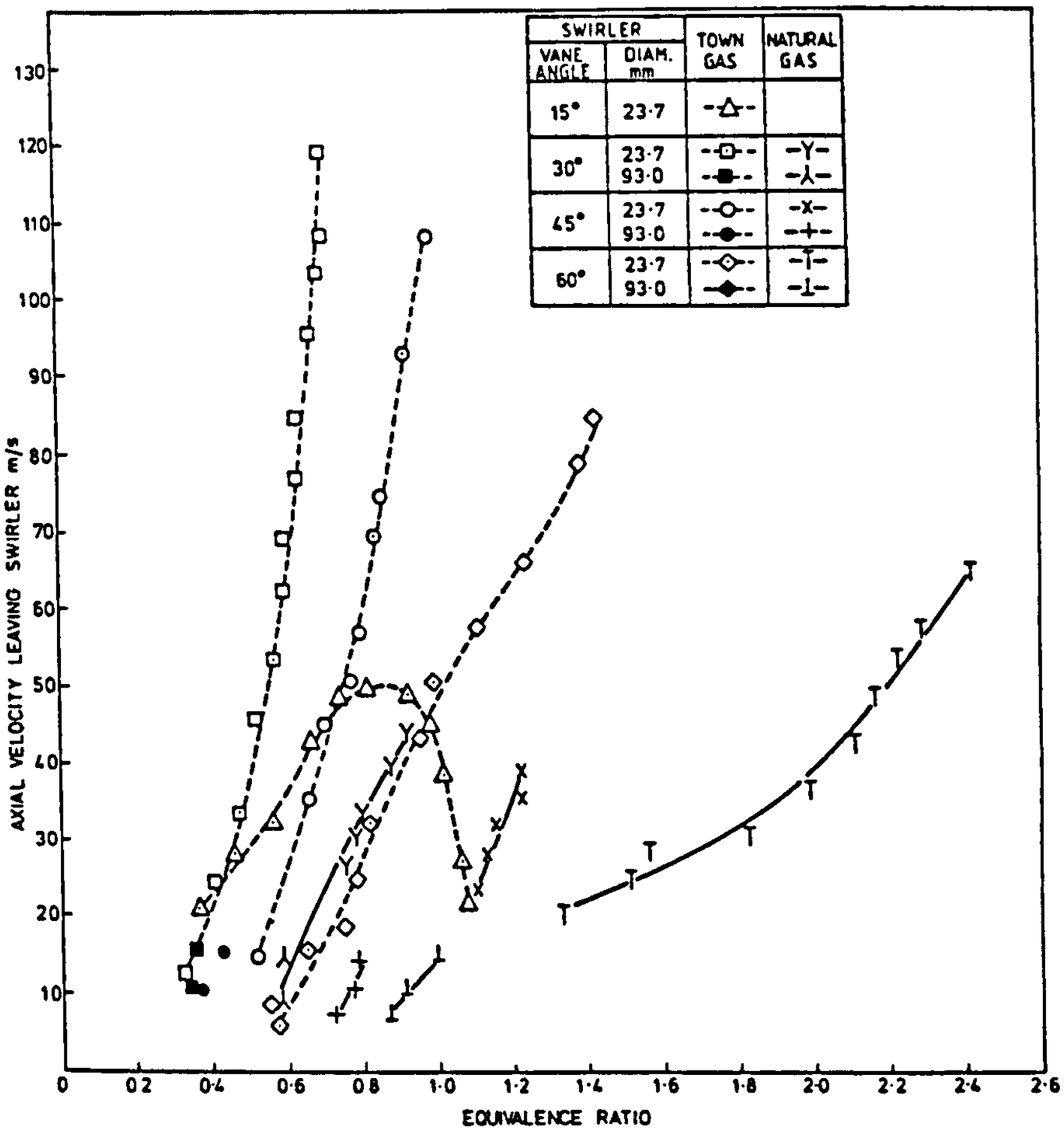

FIG 1 Weak extinction limits of flames stabilized by swirl

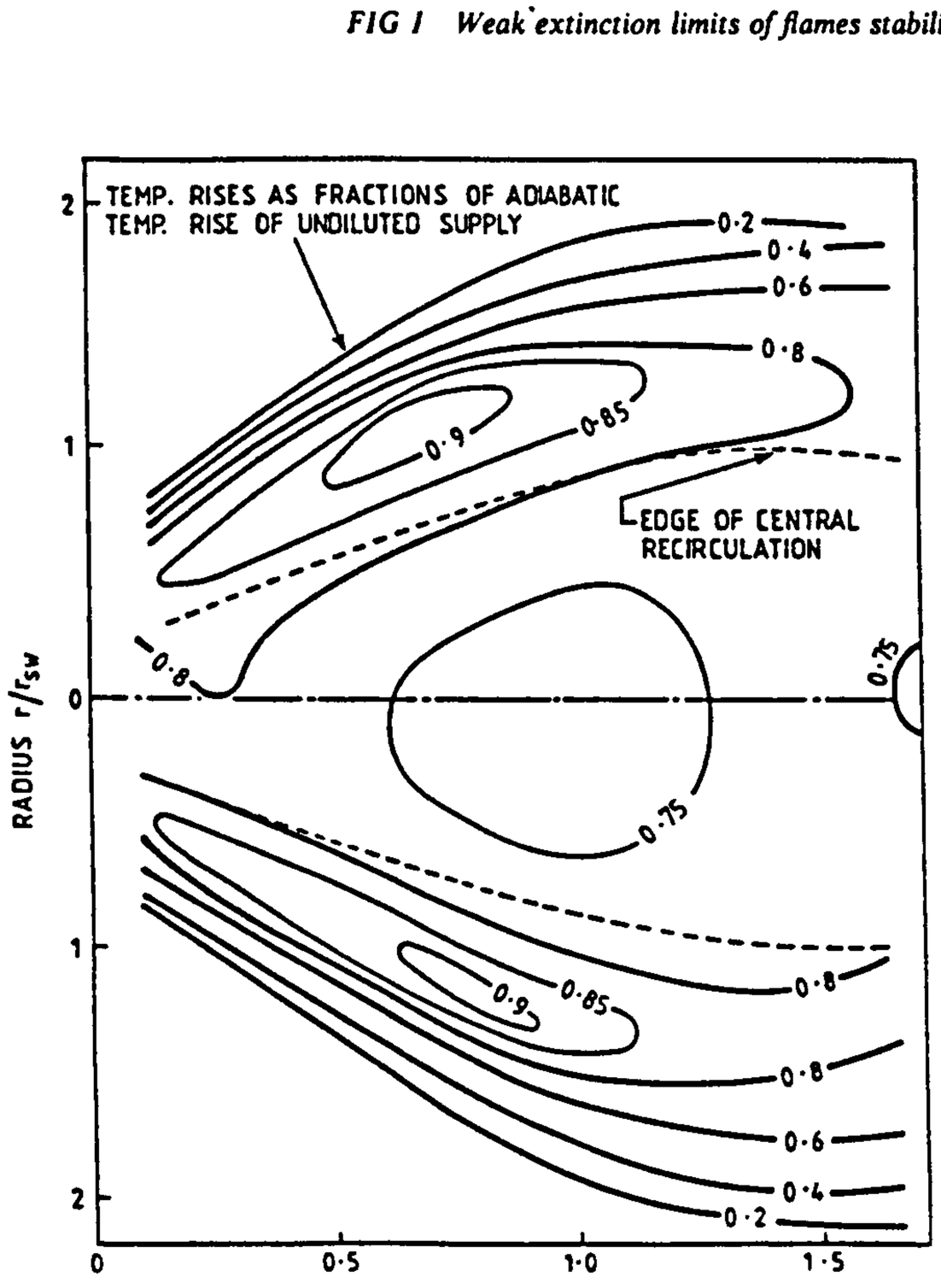

FIG. 2 Temperature rise distributions in open flame: 45° swirler, 93 mm diam, town gas, $\phi = 0.50$ (weak extinction at $\phi = 0.40$)

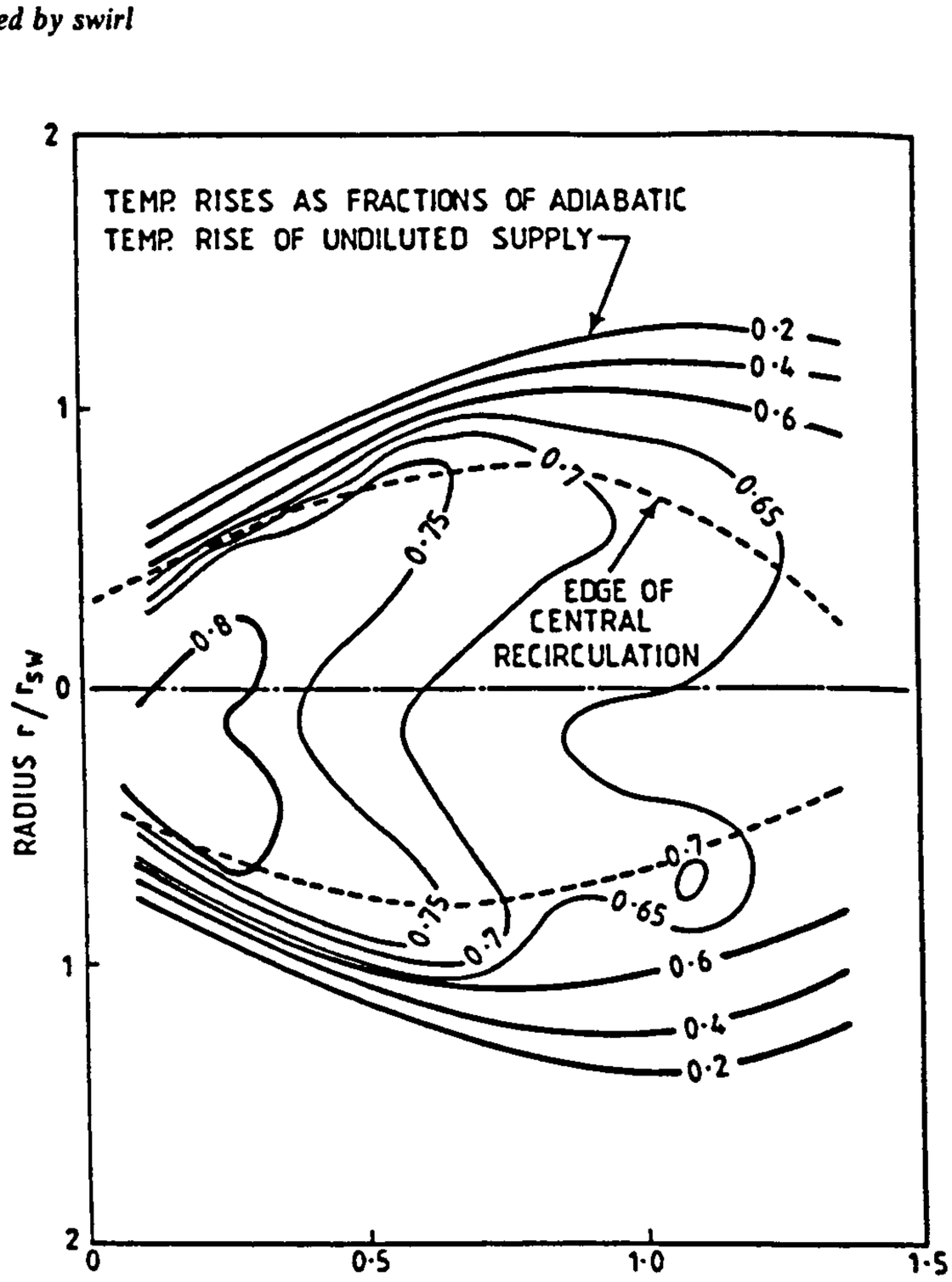

FIG. 3 Temperature rise distributions in open flame: 45° swirler, 93 mm diam, town gas, $\phi = 0.44$ (weak extinction at $\phi = 0.40$)

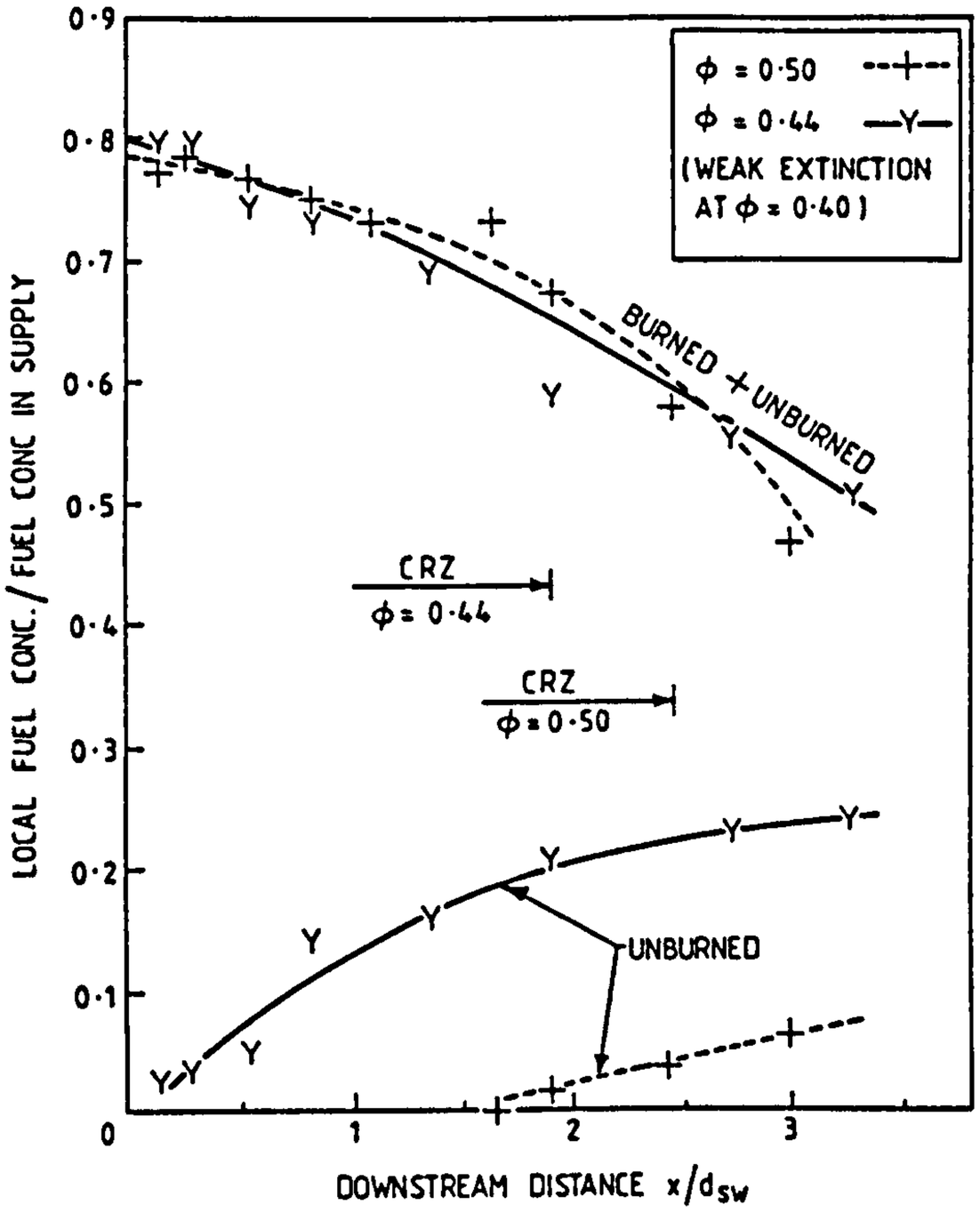

FIG. 4 Equivalent fuel concentration along axis in open flames: 45° swirler, 93 mm diam, town gas

radiation[3] are reproduced in Figs. 2 and 3 for the case of the 45° vane swirler with town gas fuel at equivalence ratios of 0.50 and 0.44. The corresponding blow-off limit occurred at an equivalence ratio of 0.40.

Results of gas sampling tests are shown in Fig. 4, where the concentrations of the burned and unburned species are expressed as fractions of the equivalent unburned fuel in the supply stream.

4. Discussion of results

Comparing the results of the weak extinction limits for the 30°, 45° and 60° swirlers, where a CRZ was set up, it is noted that although the higher vane angles produce larger and longer CRZs, they give poorer weak extinction limits reckoned on the axial flow velocity and the supply mixture strength. Similar conclusions were reached by Lutzhoft and Fetting[4] and by Albright and Alexander.[5] The explanation for this apparent deterioration of the stability limits is twofold:

(*a*) The effective flow velocity at the point of blow-off is not the axial supply velocity. A practical approximation is to take the absolute flow velocity at the swirler exit ie (axial velocity/cos (vane angle)). A similar approach has been adopted by Rawe and Kremer[6] in a study of stability of swirling diffusion flames.

(*b*) The effective fuel/air ratio (or equivalence ratio) at the critical stabilization location is not the value in the supply stream. It differs from the value in the supply stream owing to air entrainment by the boundary of the jet and then recirculation of some of this entrained air within the CRZ.

The methods of establishing the effective fuel/air ratio are described in section 6, but first there is a discussion of the mechanism of flame stabilization.

5. Mechanism of flame stabilization by swirl

The temperature surveys show that, at conditions sufficiently removed from the extinction limit, the central recirculation initiates combustion of the main forward flow and peak temperatures are observed in this forward flow within a distance of 0.5 to 1 swirler diameters downstream from the swirler exit. This is in agreement with the observations of Syred *et al*[7] and of Claypole and Syred[8] using tangential entry swirl burners. Considering the gas sampling results at these conditions removed from the weak extinction limit, there is virtually no trace of unburned gas within the CRZ, except in the vicinity of the downstream stagnation point.

At conditions closer to the weak limit, the region of maximum temperatures moves closer to the swirler and there is much less combustion in the forward stream adjacent to the CRZ. Also there is much more unburned gas present within the CRZ and the appearance of the flame becomes less steady. The amount of unburned gases inside the CRZ diminishes as one moves back towards the swirler exit. It is of significance to note that even when there is appreciable unburned gas present, the equivalent fuel concentration at any location associated with unburned plus burned gases remains essentially unaltered. This fuel concentration, as a fraction of the supply value, increases as one moves in the CRZ toward the swirler exit. For example in the case shown in Fig. 4, the equivalence ratio rises to about 0.78 of that of the supply value when adjacent to the swirler exit. The reduction in equivalent fuel concentration on the axis of the CRZ when moving in the opposite direction end is due to progressively more ambient air entrainment into the CRZ. The main forward flow becomes more diluted by ambient air as it passes the CRZ. The similar reduction in fuel concentration, when moving in the direction of the main flow, within the CRZ must mean that the CRZ is continuously being fed across its outer boundary from the forward flow, throughout the length of the CRZ. This would suggest that the location which is critical to the flame stabilization is near the upstream end of the CRZ outer boundary. It also suggests that the important recirculations which feed into this location are from immediately downstream. This point can be referred to as the anchoring point of the flame. It is also noted that, in the CRZ close to the swirler exit, the observed temperature rise, as a fraction of the adiabatic value for the undiluted supply, remains roughly constant as the weak limit is approached, although there are indications of a final slight reduction very close to the limit, which is in keeping with the observations of Zukoski and Marble[9] in flames stabilized by bluff bodies.

6. Air entrainment calculations

The amount of air entrained into the stabilization zone was determined from the temperature traverses described above. These were taken at conditions near to the extinction limits, but before appreciable unburned gases were present.

Previous work on jet entrainment[10] has indicated that it is influenced by the jet Reynolds number if it is below 2×10^4. At higher values the jet entrainment is indepen-

dent of the Reynolds number. This was taken into consideration when calculating air entrainment at extinction limits from the temperature traverses. The results of these air entrainment calculations are given in Fig. 5, indicating a linear increase of air entrainment with swirl. This is in agreement with Chigier and Chervinsky.[11] The results also indicate higher entrainment in the case of natural gas flames than with town gas flames. This increase can be explained by the fact that jet entrainment is a function of the density, as given by the relation:[10]

$$\frac{\dot{M}_e}{\dot{M}_0} = 0.32 \frac{X}{d_0} \sqrt{\frac{\rho_a}{\rho_0}} \quad \ldots \quad (1)$$

where $\dot{M}_e$ = mass entrained
$\dot{M}_0$ = nozzle flow
X = axial distance from swirler exit
d_0 = nozzle diameter
ρ_0 = nozzle flow density
ρ_a = ambient fluid density

The weak extinction results, Fig. 1, show that at a given velocity, extinction occurs at a much higher equivalence, and hence density, ratio in natural gas flames than in town gas flames. Typically, according to eqn (1), this would produce an entrainment in the natural gas flames which is 20% higher than in the town gas flames. This prediction is in line with the alterations in entrainment deduced from the temperature traverses and shown in Fig 5.

The only discrepancy which remains in the entrainments shown in Fig. 5 is the difference in the results obtained for the two swirler sizes. This difference has three possible explanations:

(*a*) The Reynolds number adjustment is not accurate.

(*b*) The chilling effect of the temperature probe is more pronounced in the flames issuing from the smaller swirlers.

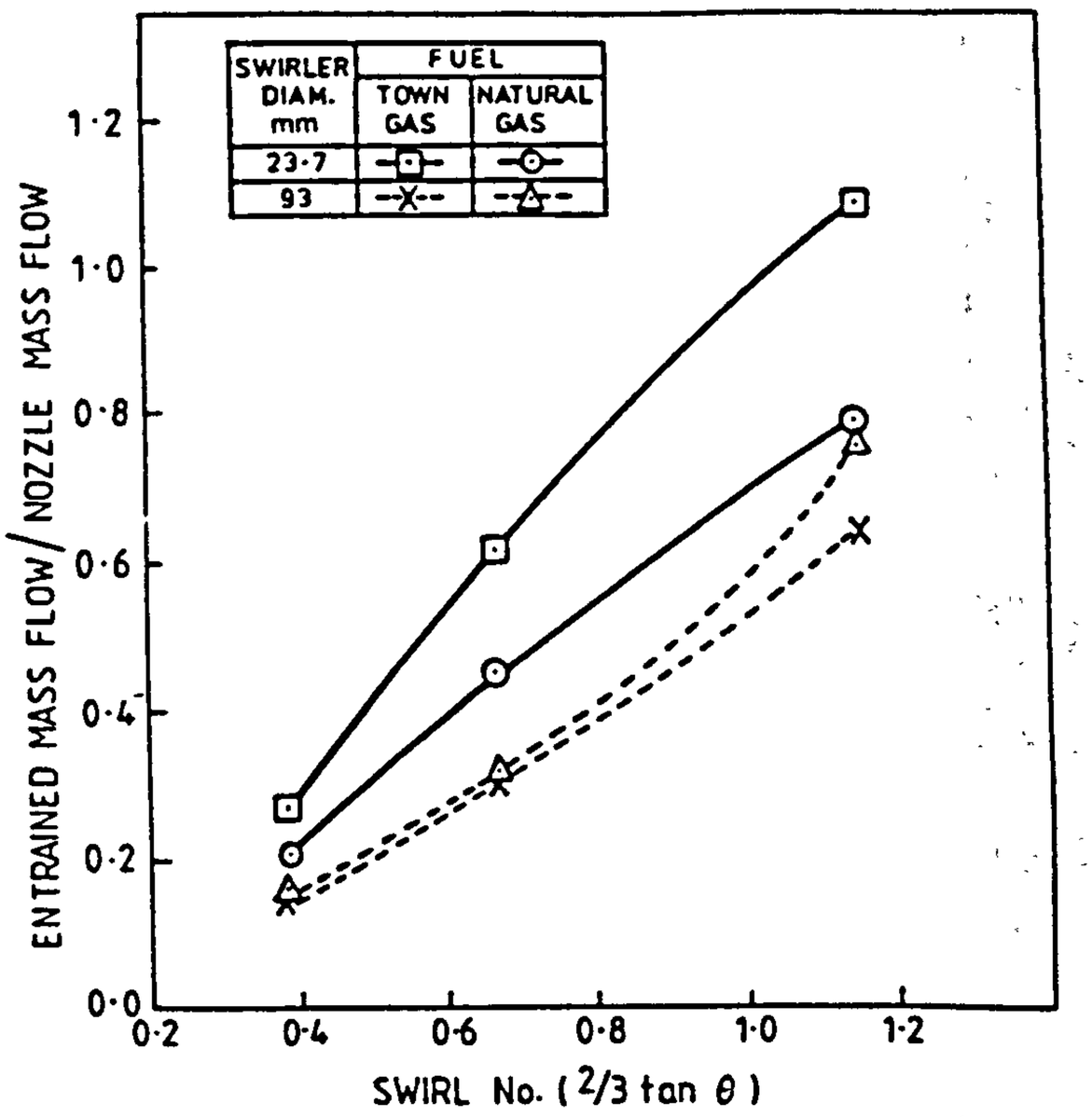

FIG. 5 Entrained mass flows at flame anchoring position for Re > 2 × 10⁴

(*c*) The radiation heat transfer is higher from the flames issuing from the larger swirlers.

7. Correlation of the weak extinction limits

The two parameters which are used here to correlate the extinction limits of these unenclosed flames are:

(*a*) The effective equivalence ratio at the point of flame anchoring, this being obtained from the supply

(*continued on p 164*)

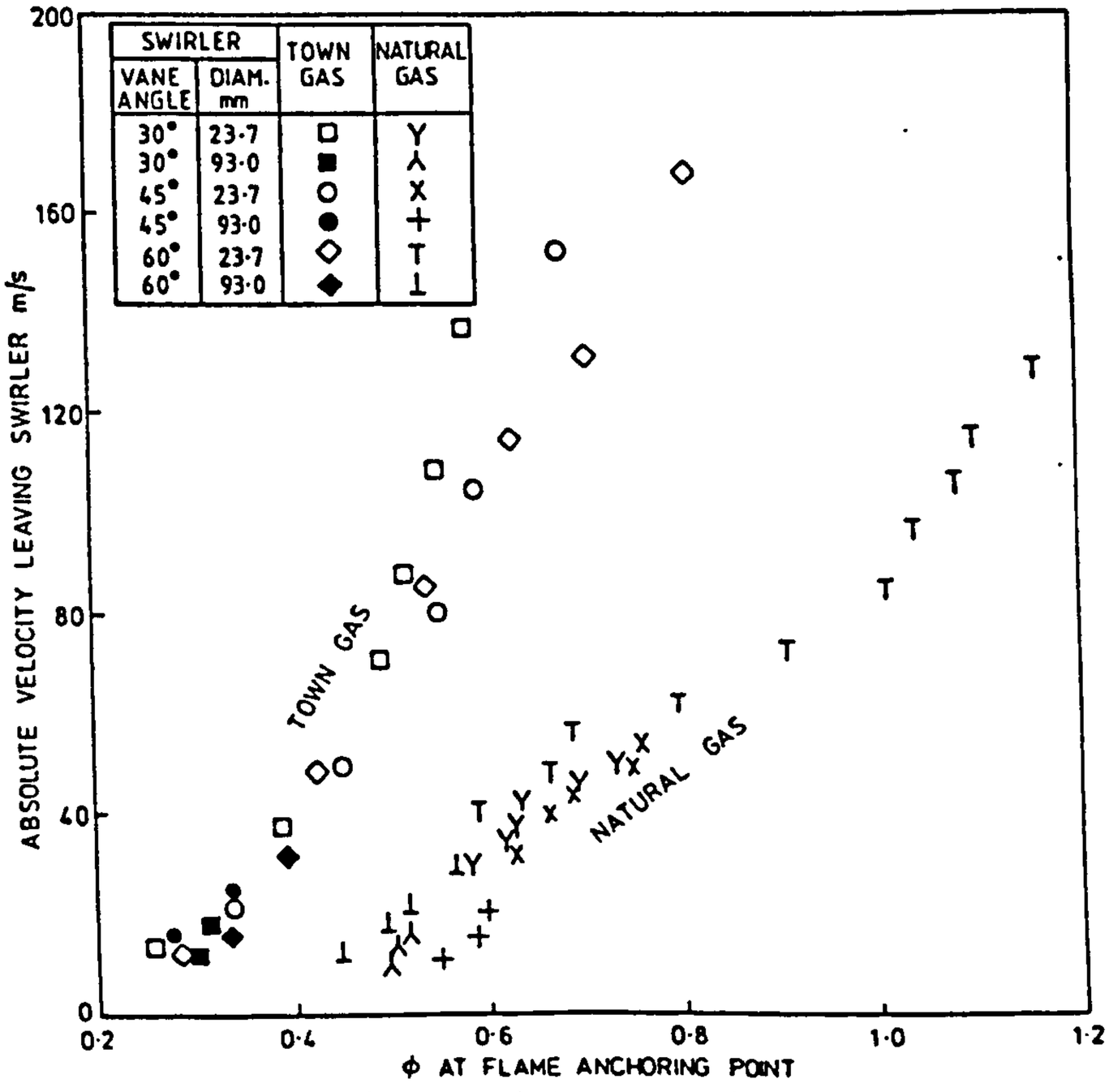

FIG. 6 Correlation of weak extinction limits – open swirled flames

value adjusted using air entrainment ratios deduced from temperature traverses.

(*b*) The absolute velocity of the jet leaving the swirler. This was taken as the average axial flow velocity leaving the swirler divided by the cosine of the swirler vane angle.

The results, for both fuels, are shown in Fig. 6. It is seen that for each fuel type a very satisfactory correlation is obtained. In the second part of this investigation,[12] a theoretical study which predicts these correlations is described.

The above statements apply to unenclosed flames where the entrained gas is ambient air. In confined flames the entrained gases will be recirculated products, either partially or completely burned. The correlation has not been tested on confined flames.

8. References

1. THRING M W and NEWBY M P. Combustion length of enclosed turbulent jet flames. 4th symp (int) on *Combustion*, 1952, pp 789–796.
2. MATHUR M L and MACCALLUM N R L. Swirling air jets issuing from vane swirlers. Part 1. Free jets. *J Inst Fuel* (now *Energy*), 1967, 40, 214–225.
3. BELTAGUI S A. Aerodynamics and modelling of vane swirled flames in furnaces. PhD thesis, Glasgow University, 1974 (May).
4. LUTZHOFT V W and FETTING F. Der Einfluss des Dralls die Stabilität von Drallflammen. *Brennst-Wärme-Kraft*, 1968, 20, 572–576.
5. ALBRIGHT L F and ALEXANDER L G. Flame stabilization in gases flowing cyclonically. Flow characteristics, temperature and gas analysis. 6th symp (int) on *Combustion*, 1956, pp 464–472.
6. RAWE R and KREMER H. Stability limits of natural gas diffusion flames with swirl. 18th symp (int) on *Combustion*, 1980, pp 667–678.
7. SYRED N, CHIGIER N A and BEÉR J M. Flame stabilization in the recirculation zone of flames with swirl. 13th symp (int) on *Combustion*, 1970, pp 617–624.
8. CLAYPOLE T C and SYRED N. The stabilization of flames in swirl combustors. *J Inst Energy*, 1982 (Mar), 55, 14–19.
9. ZUKOSKI E E and MARBLE F E. Experiments concerning the mechanism of flame blow off from bluff bodies. Proc of *Gas dynamics* symp on *Aerothermochemistry*, Northwestern University, 1956, pp 205–210.
10. RICOU F P and SPALDING D B. Measurements of entrainment by axisymmetrical turbulent jets. *J Fluid Mech*, 1961, 11, 21–32.
11. CHIGIER N A and CHERVINSKY A. Experimental investigation of swirling vortex motion in jets. *J App Mech*, 1967, 34, 443–451.
12. BELTAGUI S A and MACCALLUM N R L. Stability limits of free swirling premixed flames: Part II. Theoretical prediction. *J Inst Energy*, 1986 (Sept), 59, 165–167.

(*Paper received January 1986*)

S A BELTAGUI BSc PhD* and N R L MACCALLUM BSc PhD†

Stability limits of free swirling premixed flames: Part II. Theoretical prediction

The paper describes a general relation capable of predicting the weak extinction limits of unconfined swirling premixed jet flames. The relation is applicable to swirling jets in which the degree of swirl is sufficient to create a central recirculation. Under these conditions the region governing stabilization is in the high shear zone of the forward flow adjacent to the central recirculation. This region is regarded as a well-stirred reactor and the reaction is assumed to be quantified by a simple bimolecular kinetic equation. The activation energy, collision rate constant and reaction orders which are required can be taken from the literature for the simpler fuels. This produced satisfactory predictions for natural gas. For the more complex town gas, one constant had to be selected to give agreement with the experiment

1. List of symbols

a reaction order for oxygen
d diameter, m
E activation energy, kcal kmol^{-1}
f reaction order for fuel
k collision rate constant, m$^{3(n-1)}$ kmol^{1-n} K$^{-0.5}$ s^{-1}
L length of shear zone, m
$\dot{M}$ mass flow rate, kg s^{-1}
m ratio of inerts/oxygen by volume in mixture
MW molecular weight of air
n overall reaction order ($n = f + a$)
P pressure, atm
R universal gas constant, kcal kmol^{-1} K^{-1}
R_g gas constant (for air), m^3 atm kmol^{-1} K^{-1}
S swirl number = 0.667 tan θ
T temperature, K
t thickness of shear zone, m
U velocity, m s^{-1}
V volume of shear zone, m^3
X_f mole fraction of fuel
X_o mole fraction of oxygen
θ swirler vane angle
ε oxygen utilization efficiency
ρ density, kg m^{-3}
φ fuel equivalence ratio = (fuel/air)/(fuel/air)$_{stoichiometric}$

Suffixes

abs absolute
ax axial
e entrained
eff effective at shear zone
o swirler exit
r shear zone
t total

2. Introduction

Experimental work has been reported[1] on the mechanism of the stabilization of free swirling premixed flames in jets issuing from vane swirlers. Once significant degrees of swirl had been reached, stabilization was achieved by means of the central recirculation. It was established that the reaction takes place essentially on the forward flow adjacent to the central recirculation zone (CRZ) at an anchoring region which is close to where the fresh jet emerges from the swirler. Evidence of this is given by temperature traverses where the maximum values were obtained in this region.[1-5] It has been found that maximum velocity gradients and turbulence intensities occur there too. It is also observed that as the extinction limit is approached the flame exhibits unsteadiness, with momentary absences of flame in the centre of the CRZ, near its downstream end.

The above observations suggest the existence of a reaction zone of almost perfect mixing where the flame is stabilized. A quantitative analysis of this zone is now offered, based on the well-stirred reactor model suggested by Longwell and Weiss[6] and used successfully by various investigators.[7-10] The model offered here is a simplification of the well-stirred plus plug-flow reactors qualitatively described by Claypole and Syred[4] for stabilization by central recirculations in swirling flows.

3. Chemical kinetics model

The chemical kinetics for the reactions taking place can be reduced for the purpose of this analysis to one global bimolecular equation between fuel and oxygen. This is in effect assuming that some bimolecular step in the overall reaction chain takes place at a much slower rate than all other reaction steps. It is also assumed that the reactant concentrations are proportional to the concentrations of fuel and oxygen respectively.

Considering first the case of natural gas, as an approximation for the purpose of kinetics it may be regarded as pure methane and the stoichiometric equation may be written:

$$\varphi CH_4 + 2(O_2 + 3.76N_2) \rightarrow \varepsilon\varphi(CO_2 + 2H_2O) + 2(1 - \varepsilon\varphi)O_2 + 7.52N_2 + (1 - \varepsilon)\varphi CH_4 . \quad (1)$$

where φ is the equivalence ratio and ε is the oxygen utilization efficiency.

For town gas a simplified approximate analysis of $(0.5H_2 + 0.3CH_4 + 0.1CO_2 + 0.1N_2)$ was assumed. An equation of stoichiometry can be written assuming that all the hydrogen reacts and that all the unreacted combustibles are in the form of methane.[9,10]

The stoichiometric equations can be solved with the relevant energy equations to give the flame temperatures for a range of equivalence ratios φ at various values of the oxygen utilization efficiency ε. Also mass fractions of both fuel and oxygen, X_f and X_o, in the product gases are calculated from the stoichiometric equations as functions of φ and ε. The rate of reaction is given by the typical kinetic equation:[6,9,10]

*National Engineering Laboratory, and University of Glasgow.
†Department of Mechanical Engineering, University of Glasgow.

$$\left[\frac{\dot{M}}{VP^n}\right]_{theor} = \frac{k(m+1)(MW)X_f{}^f X_o{}^a}{\varepsilon\varphi R_g{}^n T^{n-0.5}} \exp\left[-\frac{E}{RT}\right] \quad (2)$$

The selection of the constants which appear on the right side of the above equation is now considered. For the activation energy E, a value of 40 000 kcal/kmol has been chosen for the natural gas, assuming that it will act as pure methane.[10,12] A weighted average value of 20 000 kcal/kmol has been taken for the town gas.[11,12,13] The orders of reaction, n, f and a, have been taken as being 1.8, 0.8 and 1.0 respectively[6] for both fuels. For the remaining constant, the collision rate constant k, the value of 1.29×10^{10}, as used by Kretschmer and Odgers,[10] has been chosen for the natural gas. As shown later in section 5, this gives predictions which line up closely with experimental extinction limits. There was no obvious equivalent value to be found in the literature for the collision rate constant for the fuel mixture which constitutes town gas. The procedure therefore adopted in this work has been to choose a value which, with the activation energy and orders of reaction already selected, would place the obtained predicted extinction limits in general agreement with the observed limits. The value of the collision rate constant thus chosen for the town gas is 3.1×10^8.

Inserting the above quoted values of activation energy, collision rate constant and orders of reaction in eqn (2) enabled the air loading term $[\dot{M}/VP^n]$ to be calculated for various values of equivalence ratio and oxygen utilization efficiency. For a fixed equivalence ratio, the maximum air loading was found by varying the oxygen utilization efficiency. This maximum loading, $[\dot{M}/VP^n]_{max}$, was considered to correspond to the weak extinction limit.

4. Application to stabilization zone

The above analysis is applied to what can be regarded as the 'well-stirred reaction' part of the total reaction zone. Conditions in this part determine the weak stability limits, ie flame extinction. The rest of the reaction zone is a plug-flow reactor serving to complete the burnout.[14]

The well-stirred reactor volume used is that of the maximum shear zone just outside the CRZ boundary, where the fresh forward flow is being well mixed by the heat and active species transferred from the reverse flow of combustion products.[1] As the blow-off extinction limit is approached, less combustion occurs in this volume, the remainder being completed in the reverse flow region, as illustrated in Fig. 4 of ref 1. The volume of the well-stirred reactor V is given by:

$$V = \pi L_r d_r t_r \quad . \quad . \quad . \quad . \quad . \quad . \quad . \quad (3)$$

where L_r, d_r and t_r are the length, mean diameter and thickness respectively of this maximum shear zone. Comparisons of velocity and temperature measurements indicate that the region of maximum temperature gradient coincides with the region of maximum shear.[1,15] These measurements therefore indicate that the thickness of this well-stirred reactor t_r is about 12 mm and that this dimension is almost constant for all the swirlers tested. Considering now the length L_r and mean diameter d_r of the maximum shear zone, according to the work of Bafuwa and Maccallum,[15] these vary with swirl as follows: L_r decreases from $1.0d_o$ to $0.5d_o$, while d_r increases from $1.6d_o$ to $3.2d_o$ as swirl increases. This leads to the important conclusion that the product $L_r d_r$ remains almost constant at about $1.6d_o{}^2$.

Turning to the mass flow into this zone which forms the well-stirred reactor, it is assumed that this is the sum of swirler flow plus the amount of entrainment which has occurred by that location.

$$\dot{M}_t = \dot{M}_o + \dot{M}_e$$

$$= \frac{\pi}{4} d_o{}^2 \rho_o U_{ax}(1 + \dot{M}_e/\dot{M}_o)$$

$$= \frac{\pi}{4} d_o{}^2 \rho_o U_{abs} \cos\theta(1 + \dot{M}_e/\dot{M}_o) \quad . \quad . \quad (4)$$

The entrainment ratios $(\dot{M}_e/\dot{M}_o)$ for the swirlers being examined have been evaluated from temperature measurements and are given in Fig. 5 of the earlier paper.[1] While there are minor discrepancies, attributable to Reynolds number and density difference effects, it is found that the group $((1 + \dot{M}_e/\dot{M}_o)\cos\theta)$ is almost constant at about 1.0 for all the swirlers tested. Thus eqn (4) can be simplified to:

$$\dot{M}_t = \frac{\pi}{4} d_o{}^2 \rho_o U_{abs} \quad . \quad . \quad . \quad . \quad . \quad . \quad (5)$$

Eqns (3) and (5) and the related results can now be substituted in the air loading term on the left side of eqn (2), thus:

$$\frac{\dot{M}}{VP^n} = 13 \frac{\rho_o U_{abs}}{P^n} \quad . \quad . \quad . \quad . \quad . \quad . \quad (6)$$

It is significant to note that the linear dimension of the swirler d_o has cancelled from the air loading term. For tests carried out at atmospheric pressure, the right side of eqn (6), ie the air loading term, simplifies to $(13\rho_o U_{abs})$ and for extinction limits one can write

$$U_{abs} = \frac{1}{13\rho_o}[M/VP^n]_{max} \quad . \quad . \quad . \quad . \quad . \quad (7)$$

where $[\dot{M}/VP^n]_{max}$ is obtained by the procedure described in section 3. The equivalence ratio φ_{eff} to be used in calculating this maximum loading is the effective equivalence ratio, after accounting for the diluting effect of air entrainment:

$$\varphi_{eff} = \varphi_o/(1 + \dot{M}_e/\dot{M}_o) \quad . \quad . \quad . \quad . \quad . \quad (8)$$

5. Comparison of predicted and experimental weak limits

The weak extinction limits predicted by eqn (7) above are compared with experimental limits[1] in Fig. 1. The important test is in the case of natural gas where no adjusting parameters have been involved. It is seen that for effective fuel/air ratios in the range from 0.4 to about 0.9 of the stoichiometric value there is very good agreement. Agreement would not be expected to continue into fuel-rich streams, and so this can be regarded as a very satisfactory test.

For the case of town gas, the value of the collision rate constant k had been chosen, as described in section 3 above, to give a good general agreement between the predictions of eqn (7) and the experiment. This is of course however only a multiplying factor. The shape of the predicted limit line is controlled by the activation energy and the values of the order of the reaction. These

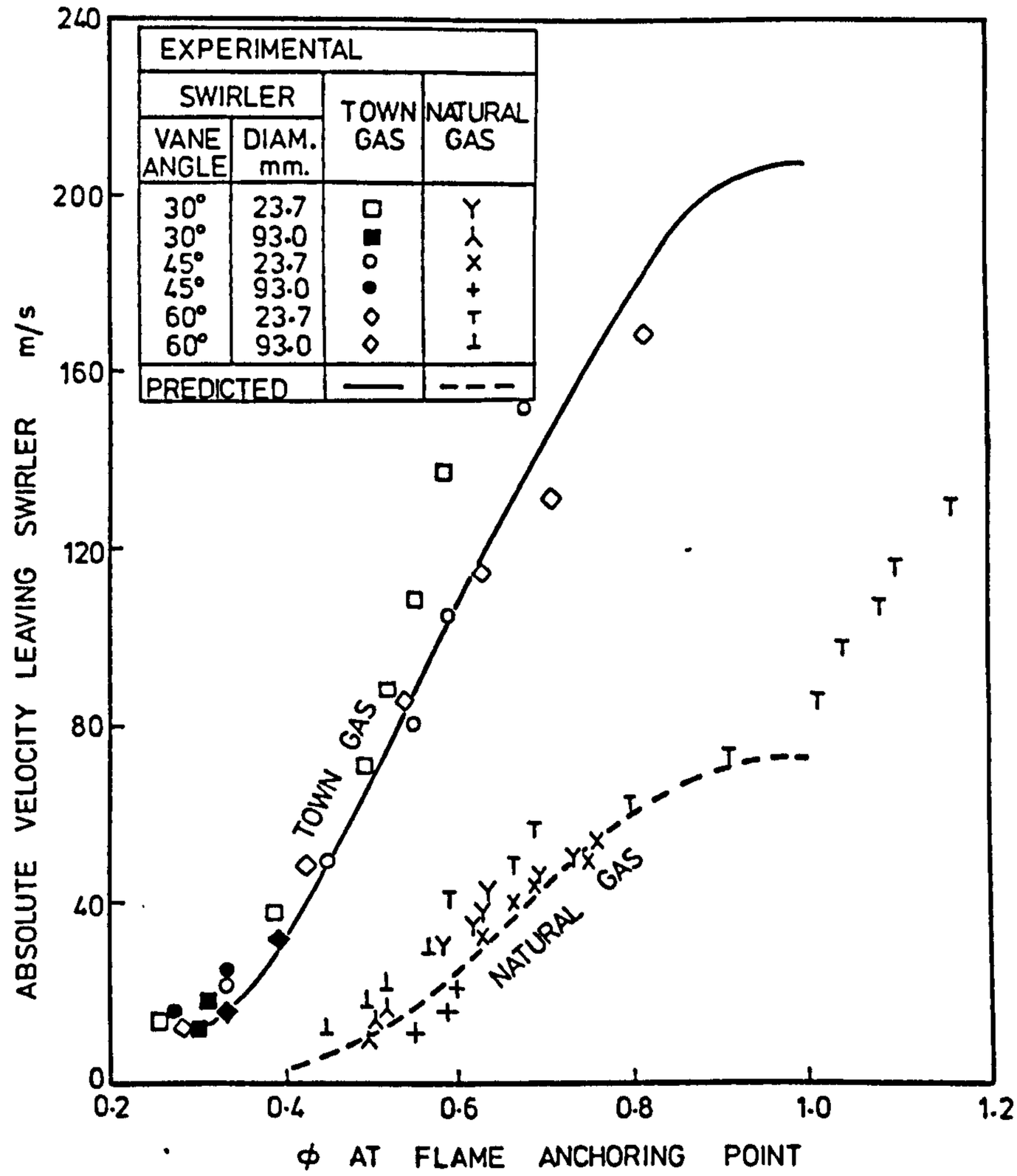

FIG. 1 Predicted and experimental weak extinction limits – open swirled flames

have been selected from the literature, using suitable weighting ratios. The resulting predicted shape agrees well with the observed extinction limit line within the expected range of effective fuel/air ratios.

This modelling of the stabilization mechanism of unconfined swirling flames, coupled with computational fluid dynamics, will aid the understanding of the processes involved.

6. Conclusion

By considering the shear flow layer adjacent to the CRZ as a well-stirred reactor and using a simple bimolecular kinetic rate equation, it has been possible to predict the air loading of swirl stabilized premixed jet flames at the weak extinction limit. The predictions are in the form of a direct relation between the absolute velocity of flow at the swirler exit section and the fuel equivalence ratio at the point of flame stabilization. When tested against experimentally obtained limiting values for two different fuels, it is seen that agreement is good.

7. References

1. BELTAGUI S A and MACCALLUM N R L. Stability limits of free swirling premixed flames: Part I. Experimental correlation. *J Inst Energy*, 1986 (Sept), 59, 160–164.
2. LUTZHOFT V W and FETTING F. Der Einfluss des Dralls die Stabilität von Drallflammen. Brennst-Wärme-Kraft, 1968, 20, 572–576.
3. SYRED N, CHIGIER N A and BEÉR J M. Flame stabilization in the recirculation zone of flames with swirl. 13th symp (int) on *Combustion*, 1970, pp 617–624.
4. CLAYPOLE T C and SYRED N. The stabilization of flames in swirl combustors. *J Inst Energy*, 1982 (Mar), 55, 14–19.
5. PEIN R, PESCHEL H and FETTING F. Recirculation zone concentrations and temperatures of bluff-body stabilized turbulent flames. *Comb Sci Technol*, 1970, 1, 327–330.
6. LONGWELL J P and WEISS M A. High temperature reaction rates in hydrocarbon combustion. *Ind Eng Chem*, 1955, 47.2, 1634–1643.
7. AVERY W H. Space heating rates and high temperature kinetics. 5th symp (int) on *Combustion*, 1954, pp 86–91.
8. STREHLOW R A. Fundamentals of combustion, International Textbook Co, Scranton, Pa, 1968.
9. BALLAL D R and LEFEBVRE A H. Weak extinction limits of turbulent flowing mixtures. *J Eng Power*, 1979, 101, 343–348.
10. KRETSCHMER D and ODGERS J. Modelling of gas turbine combustors. *J Eng Power*, 1972, 94, 173–180.
11. WEISS M A, LANG R J and LONGWELL J P. Combustion rates in spherical reactors. *Ind Eng Chem*, 1958, 50.1, 257–264.
12. HOTTEL H C, WILLIAMS G G and BAKER M L. Combustion studies in a stirred reactor. 6th symp (int) on *Combustion*, 1956, 398–411.
13. KANURY A M. Introduction to combustion phenomena. Gordon and Breach, New York, 1975.
14. BEÉR J M and CHIGIER N A. Combustion aerodynamics. Applied Science Publishers, Barking, 1972.
15. BAFUWA G G and MACCALLUM N R L. Turbulent swirling flames issuing from van swirlers. IFRF 18th Aerodynamics Panel meeting, Paris, 1970, Doc No G02/ca/3.

□

(*Paper received January 1986*)

Publication 39
HTFS RS714
NEL/HTFS 98

THE USE OF PERIPHERAL FUEL INJECTION TO IMPROVE COMBUSTION IN SWIRLING FLAMES

S A Beltagui [1] and N R L Maccallum [2]

1 National Engineering Laboratory, East Kilbride, Glasgow
2 University of Glasgow, Glasgow

ABSTRACT

An initial study has been made of the result, in a non-premixed system, of introducing the fuel - natural gas - at the outer boundary of the air jet as it enters the furnace, instead of in the conventional manner on the axis of the burner. The entering air was given a range of degrees of swirl. Velocity, pressure, temperature and species concentration profiles were measured in the resulting flows. The results confirm the potential of the system for producing high intensity flames with wide stability ranges. On comparison with central fuel injection systems, the peripheral fuel injection scheme shows the advantage of not needing such high degrees of swirl to achieve the same mixing effects - thus burner pressure drops are lower.

NOTATION

c_p	Specific heat at constant pressure	kJ kg^{-1} K^{-1}
D	Furnace diameter	m
d	Swirler diameter	m
G_d	Axial momentum flux, dynamic component = $\int 2\pi r \rho u^2 \, dr$	kg m s^{-2}
$\bar{G}_d$	Normalised axial momentum flux = $\frac{\int 2\pi r \rho u^2 \, dr}{\pi r_{sw}^2 \rho U^2}$	-
H	Sensible enthalpy flux = $\int 2\pi r \rho u h \, dr$	kJ s^{-1}
$\bar{H}$	Sensible enthalpy flux/ input energy flux	-
h	Specific sensible gas enthalpy ($c_p t$)	kJ kg^{-1}
Δp	Local pressure drop relative to ambient	N m^{-2}
r, r_{sw}	Radius, radius of swirler	m
S	Swirl number of hubless swirlers, based on swirler diameter = $\frac{1}{3}\tan\theta$	-
S*	Furnace swirl number = $T/(G_d D)$	-
T	Axial flux of tangential momentum = $\int 2\pi r^2 \rho u w \, dr$	kg m^2 s^{-2}
$\bar{T}$	Normalised tangential momentum flux = $\frac{\int 2\pi r^2 \rho u w \, dr}{\frac{2}{3}\pi r_{sw}^3 \rho U^2 \tan\theta}$	-
ΔT	Temperature rise	K
U	Average axial velocity leaving swirler	m s^{-1}
u, v, w	Local axial, radial and tangential components of velocity	m s^{-1}
$\bar{X}$	Axial distance in units of furnace diameters	-
x	Axial distance along furnace from swirler exit	m
θ	Swirler vane angle to axial direction	deg.
ρ	Density	kg m^{-3}
ϕ	Equivalence ratio	-

1. INTRODUCTION

Non-premixed combustion systems are widely used in industrial applications, in preference to premixed systems, largely for reasons of safety. In these non-premixed systems, the mixing of the fuel and oxidant plays a key role in the achievement of the important combustion aims of wide stability limits, high combustion efficiency, low emission of pollutants etc.

1.1 Shear-layer Mixing

The most obvious method of mixing in a combustion system involving jet flows is to use the turbulence generated at the shear layer of the jet boundary. For example, in the case of a central fuel jet surrounded by a concentric annular air flow there will be high shear and high property gradients in the high turbulence zone at the interface between the jets. High heat release rates can be achieved by having the regions of high fuel concentration overlap these regions of high shear stress. The mixing can be enhanced by increasing the velocity and species gradients in this region, and also by increasing the total area of the region. One method of achieving this is to place a bluff body at the centre of the fuel jet. This creates wider jets and also leads towards the establishment of a central reverse-flow zone (CRZ) where burnt gases are recirculated to mix with and ignite the fresh fuel/air flow.

Swirling the air flow can also be used to produce the effects of central recirculation and high shear stresses, it being noted that the shear stresses will occur in both the tangential and axial directions. Quarls are also frequently used, with or without swirl, to increase the jet spread rate and to help create a CRZ. The beneficial effects of swirl, however, incur the high cost of the pressure drop across the swirler, which is proportional to the square of the swirl number (Mathur and Maccallum (1967), Beer and Chigier (1972), Syred and Beer (1974)). This latter must be high to ensure the establishment of a CRZ. However, measurements of turbulence in swirling flows (Syred and Beer (1974), Oven et al (1979)) show that the high shear rates fall mainly in the outer boundary of the forward flow and that levels of turbulence in the CRZ are generally low.

The above discussion leads to the conclusion that, with or without swirl, mixing can be greatly increased through the use of a scheme where the fuel jet is the outer, annular flow and the air flow forms the central jet. The shear stresses in the mixing area are higher and the total area is increased.

1.2 Centrifugal Mixing

If swirl is to be used, it will be better utilised by fully realising the benefits of the centrifugal forces together with the density gradients occurring in a combustion system. Density gradients before ignition are caused by the difference in density of fuel and air, and after ignition by the reduction in density due to combustion.

Swirl in a variable density flow may suppress or enhance turbulence. If the radial density gradients in a rotating flow are positive, they tend to cause flow stratification and suppress turbulence.

On the other hand, negative density gradients in a rotating field will disturb the radial equilibrium and create instabilities, hence higher shear stresses and mixing rates. The lighter pockets of burnt gases will tend to move inwards and heavier pockets of reactants, unburned, will tend to travel outward, against the pressure gradient. A situation of this type can be achieved by injecting the fuel at the outer boundary of the air jet.

An advantage of this system with outer fuel injection is the reduction of the pressure loss which would otherwise have been required to establish a CRZ. Only moderate degrees of swirl should be required. The removal of the central fuel injection system also reduces the pressure loss of the air flow across the burner.

In this paper a review is given of the rather limited number of investigations that have been

made of combustion systems utilising some of the desirable effects referred to above. Then follow the results of the first part of a new experimental programme.

2. REVIEW

A multi-annular swirl burner design has been investigated by Gupta et al (1977), the fuel gas and air being injected alternately through a succession of annular openings. In this way the fuel injection was matched with the regions of high shear in the main flow. High efficiencies were reported, coupled with low emissions and low noise levels. Disadvantages of the system were its likely high cost and its high-pressure loss. Also, the design could not take advantage of the centrifugal force mixing effect.

Turning to the effects of rotation, a fundamental laboratory scale study has been made by Vranos et al (1982) of a premixed system in which combustion was initiated by a pilot flame located at the outer diameter of the chamber. The main flow in the centre of the chamber could be either unswirled or swirled. It was found that when the flow was swirled, this increased the rate of mixing and produced a much shorter flame, thus verifying the enhanced mixing effect in a swirling flow of starting the combustion at the outer radius of the chamber.

These beneficial centrifugal force effects have been used by Markowski et al (1976), Shekleton (1981) and Ahmad et al (1985) in further studies and in the design of some gas turbine combustors.

It is therefore seen that there is wide evidence to support the prediction that introducing the fuel at the outer periphery of a swirling air flow, thus starting combustion at the outer boundary, leads to enhanced mixing rates and generally shorter flames. However, it was seen that there are still wide gaps in our knowledge of such systems. Consequently, an experimental programme was planned to provide information on aspects of this type of combustion system.

3. EXPERIMENTAL PROGRAMME

3.1 Initial Tests in a Parallel-walled Combustion Chamber

In this combustion chamber (Tan and Maccallum (1983)) the inside diameter of the air supply pipe, 101 mm, equalled the inside diameter of the chamber itself. The first series of tests was carried out using a conventional arrangement with the fuel, natural gas, being introduced with, or without, swirl on the axis. The air flow passed through an annular swirler surrounding the fuel swirler, (Figure 1a).

It was found that high degrees of swirl had to be used in order to stabilise the flame - best results being obtained when using an air swirler with vane inclination of 60° to the axial direction and a gas swirler with vane inclination of 45°, the direction of flow rotation being the same in both swirlers. The average axial flow velocity at inlet to the chamber was 10 m/s.

Temperatures were measured by Pt-5%Rh/Pt-20%Rh thermocouple and time-averaged velocity and pressures by 3-hole probe (Beltagui and Maccallum (1976a)). Typical results of temperature traverses at a distance of four chamber diameters downstream from the burner are shown in Figures 2 and 3 for overall equivalence ratios of 0.6 and 0.83 respectively. Results are shown for three fuel gas swirler angles - 30, 45 and 60° - the air swirler angle being 60° in all cases. Mass flow averaged temperatures are also shown. For the 45° fuel swirler angle case these averaged temperatures have been converted to averaged completeness of combustion - Figure 4. It is seen that at the higher equivalence ratios, combustion is very incomplete even at this plane which is well downstream from the burner.

These results provided a base against which the performance of an alternative fuel introduction system was compared. In this alternative system the same annular air swirler was used. The fuel was brought along the central pipe as before, but was then carried on four radial pipes to the outer diameter of the chamber and

injected into the air flow as it left the air swirler (Figure 1b). Corresponding results with this fuel injection scheme are shown on Figures 2-4 - marked 'outer injection'. It is seen that at the higher equivalence ratios the outer injection arrangement provides a very substantial increase in completeness of combustion - from 0.37 to 0.77 at diameter of 0.83.

In view of this substantial improvement in performance, a new peripheral injection burner was designed, without a central blockage, and installed in a furnace which provided an expansion diameter ratio of 2.5. The testing of this is now described.

3.2 Peripheral Injection Burner in Furnace (D/d = 2.5)

The burner-furnace arrangement which was used for the main experimental study reported here is illustrated in Figure 5. The refractory lined furnace is of 225 mm inside diameter and 0.9 m long discharging to the atmosphere. Air is supplied on the axis at one end through an inlet tube of 93 mm inside diameter in which vane swirlers (Beltagui and Maccallum (1976a)) can be placed. The fuel - natural gas, 92%CH_4 - is introduced through an annular slit of 2 mm width around the periphery of the air swirler.

In order to define the combustion patterns, temperature and species concentrations were measured. As before, a Pt-5%Rh/Pt-20%Rh thermocouple was used to measure temperature. Concentrations of O_2 were measured by a paramagnetic analyser and of CO and CO_2 by infrared analysers.

The flow patterns were quantified by measurements of the time-averaged components of velocity, u, w and v and of the static pressure. These parameters were measured using a 3-hole pitot-type probe (tip diameter 6 mm).

The main parameters of flow velocity, swirl strength and equivalence ratio were varied as shown in Table 1.

4. RESULTS FOR PERIPHERAL INJECTION BURNER IN FURNACE (D/d = 2.5)

The flames were found to be stable for all degrees of swirl over a wide range of equivalence ratio. As swirl in the air flow was increased, the combustion became more intense and flames were shortened. However, noise levels rose significantly at the higher fuel flow rates when the swirl vane angle was increased beyond 30°.

At these higher vane angles the pressure drop across the swirler became quite marked, consequently 30° was regarded in this work as being the upper limit of vane inclination.

For each swirler, three sets of results had been obtained:

Set 1 at equivalence ratio 0.53 and inlet Reynolds number 9×10^4
Set 2 at equivalence ratio 0.38 and inlet Reynolds number 9×10^4
Set 3 at equivalence ratio 0.53 and inlet Reynolds number 6.3×10^4.

Integrations of the axial velocity profiles have been carried out at all of the traverse planes to give mass fluxes. With the exception of the first traverse plane, these integrations lay within 25 per cent of the metered flux. This agreement is considered reasonable, in view of the difficulty of measuring close to the walls. The discrepancies at the first plane are attributed to the proximity of the burner vanes and the swirler rim.

All the velocity component results have been normalised by dividing by the inlet air velocity, U. The static pressures have been normalised by the air inlet velocity head ($\frac{1}{2}\rho U^2$) and the temperature rises expressed as fractions of the theoretical temperature rise.

The results of test sets 1 and 3, when normalised as stated above, are virtually identical, confirming the similarity, already frequently reported, of flows where the Reynolds number is greater than the critical (2×10^4) and the flows are fully developed.

Comparing the results of test sets 1 and 2, it is found that changing the equivalence ratio from 0.53 to 0.38 has only minor effects on the velocity and pressure profiles. However, the combustion patterns are noticeably changed, combustion being completed in a shorter distance at the lower equivalence ratio.

For economy of space, only a selection of the results of test set 1 are illustrated in this paper. The full results are given in Beltagui and Maccallum (1985).

The sample results shown are - axial and tangential velocity components, given in Figures 6 and 7, static pressures given in Figure 8, temperature rises (corrected) in Figure 9, and concentrations of O_2 and CO in Figures 10 and 11 respectively. The concentrations of CO_2 (not illustrated) followed the inverse of the O_2 concentrations.

5. DISCUSSION OF RESULTS - PERIPHERAL INJECTION BURNER IN FURNACE

5.1 Flow Patterns

The time-averaged flow patterns, within two furnace diameters of the burner, fell into one of three classifications (Beltagui and Maccallum (1976a)):

a reduced forward velocity on the axis, and maximum forward velocities occurring at a radius displaced from the axis - the double-humped distribution, referred to as type B,

b small reverse velocities on the axis and a weak central recirculation, referred to as type C, or

c pronounced central recirculation, the reversed mass flow exceeding 10 per cent of the total flow, type D.

For the cases with combustion, taking for example the case with equivalence ratio 0.53 illustrated in Figure 6, zero swirl and 15° and 22° vane angle swirlers gave type B flows and the higher swirl angle of 30° gave a weak central recirculation - type C flow. By comparison, in corresponding isothermal tests zero swirl and 15° vane angle gave type B flows, 22° vane angle type C flow and 30° vane angle type D flow. This weakening of the central recirculation when combustion occurs is in agreement with previous work on premixed flames.

With the equivalence ratio of 0.38 (not illustrated) the axial velocity profiles were generally similar to those for equivalence ratio 0.53, except that the peak velocities occurred earlier and decayed faster, due to the shorter distance required for combustion at the lower fuel flow.

The general effects of increasing swirl are to accelerate the combustion process, so that peak axial velocities occur closer to the burner, and to increase the jet spread rate.

Considering the tangential velocity components, w, shown in Figure 7, one sees the usual Rankine-type flow with solid body central rotation surrounded by an outer free vortex. As swirl is increased the peak values of w increase and the location of the peak values is moved outwards. At these peak points the ratio of the tangential to axial components of velocity (w/u) is roughly proportional to tan θ.

It is helpful to note the static pressure distributions, typically shown in Figure 8. These show the depression in static pressure relative to ambient. The distributions are similar to those generally observed in enclosed swirling jet flows in furnaces, with greatest depressions at and around the centre of the jet and uniform pressures within the CRZ, when it exists, and in the peripheral reverse-flow zones (PRZ). Increasing the swirl increases the centre-line depression until central recirculation starts. After the reaction zone, say beyond one furnace diameter of axial distance, the pressures rise towards the ambient level. The effect of combustion is to diminish the depression in the outer region, this being where the reaction, and hence density change, is taking place. Considering centre-line pressures, tangential velocities have been increased while the density in the

central jet flow is relatively unchanged so that centrifugal effects cause a greater depression at the axis relative to the periphery. This second effect dominates so that centre-line depressions are increased when combustion is taking place. This is in contrast to the effects in the premixed case where combustion is concentrated in the centre, which diminishes the depression on the centre line and also causes less difference in pressure between centre line and PRZ.

5.2 Combustion Patterns

A good description of the combustion patterns is given by the combination of the temperature rise profiles and the gas sampling results (Figures 9-11).

It can be seen that the combustion starts at the shear layer between the air and fuel flows. Hot combustion products are the main constituents in the PRZ. The fluid flowing inside the 'cone' based on the shear layer is essentially cold air, even when there is central recirculation. This demonstrates that there is no need to create a CRZ in this peripheral injection scheme.

The maximum temperature rise occurs in the shear zone at some distance from the burner exit. In the remaining length of the flow within the furnace, these very hot gases mix with the remainder of the flow. Introducing swirl enhances the mixing by increasing the spread of the air jet, making the air meet the fuel at an angle and with a tangential velocity component. This increases the rate of mixing relative to the unswirled case where the air advances mainly with an axial component of velocity. Also, the subsequent stirring of products is more rapid and a uniform temperature is reached more readily. At the lower degrees of swirl this uniformity of temperature is not achieved within the furnace. For example, the temperature rise at the axis at the final measuring plane (x/D = 3.72) is about 75 per cent of the overall average when the 15° swirler is used and is only about 25 per cent when there is no swirl. The overall averaged normalised temperature rise at the final plane is less than unity due mainly to heat losses to the furnace walls.

It is to be noted that there is very little evidence at the furnace exit of any incomplete combustion when swirl is present. However, when there is no swirl there is up to 5%CO at the outer radii.

Considering the effect of equivalence ratio change, it is found that reducing the equivalence ratio from 0.53 to 0.38 consistently gave earlier combustion, this being seen both from the temperature rise and the species sampling tests. The sampling tests for CO confirmed virtually complete combustion by the furnace exit, even in the case without swirl.

5.3 Momentum Fluxes

It has proved valuable in modelling studies of swirling flows (Beltagui and Maccallum (1976b)) to examine the fluxes of tangential and axial momentum. The present results for axial momentum flux are given in Figure 12a and for tangential momentum flux in Figure 12b. In the former case, the value shown is the dynamic component of the axial momentum. Theoretically, the axial momentum flux should include a term representing the component due to differences in static pressure from the reference value, but in practice (Syred and Beer (1974), Beltagui and Maccallum (1976b)) it has been found more helpful to omit this term and base the flux solely on the dynamic component.

In both cases the fluxes have been normalised by input momentum, and in the case of the tangential flux the normalising group includes the term 'tan θ' as it has been shown (Kerr and Fraser (1965)) that the tangential momentum should be proportional to 'tan θ'.

In all cases the axial momentum flux shows an increase followed by a decay to a 'fully developed' value near the furnace exit. When the equivalence ratio is 0.53 the normalised fully developed flux value is about 1.2, at equivalence ratio 0.38 it is about 0.9 and in isothermal flow it is about 0.25. These

changes are in line with the relative changes expected from the density ratios.

The tangential momentum fluxes also show initial increases followed by decay to a fully developed value. According to conservation of momentum, this fully developed value should be unity in all cases. However, only with the 30° swirler is this value achieved. The lower values in the other cases are probably due to the lack of overlap of the vanes at these low inclinations to the axial direction (Beltagui and Maccallum (1976a)).

5.4 Swirl Number

Burner swirl number has been defined by Kerr and Fraser (1965) and for the case of the hubless swirlers used in the present work this definition, based on burner diameter, becomes

$$S \approx 1/3 \tan \theta.$$

Subsequently, a more representative furnace swirl number has been defined (Beltagui and Maccallum (1976b)) as

$$S^* = T/(GD)$$

where T and G are calculated from experimental velocity profiles in the fully developed region and D is the furnace diameter. Values of these swirl numbers relevant to the present tests are shown in Table 1.

The results show that combustion has the effect of reducing swirl number S* progressively as the equivalence ratio is increased. This is in line with the observations in premixed flames, largely arising from the increase in the dynamic component of the axial momentum flux due to the higher axial velocities resulting from combustion. This lowering of the swirl number S* is matched by a reduction in the conditions which create a central recirculation. For example, the CRZ observed in isothermal flow with the 22° swirler is suppressed when fuel is burned.

5.5 Degree of Combustion

The average degree of completeness of combustion at a plane can be found from integrations of the axial velocity and temperature traverses. The results are shown in Figure 13 where they have been normalised by the input energy. It is seen that as swirl is increased, this parameter increases more rapidly, indicating more intense combustion. The ideal maximum of this parameter - value unity - is reached only with the 30° swirler at the lower equivalence ratio (0.38). Because of the slower combustion in the other cases there is a larger volume of flame gases from which heat will be lost before burnout is completed.

5.6 Comparison of Peripheral with Central Fuel Injection in Furnace (D/d = 2.5)

Additional tests were carried out on similar air flow systems, but with central fuel injection (Beltagui and Maccallum (1985)). The main differences for the system with peripheral fuel injection as compared to central fuel injection can be summarised as:

a PRZ contains hot products as compared with cold flow.

b CRZ (if present) contains air as compared with hot products.

c Combustion starts at the outer surface of air jet rather than at centre.

d If there is no swirl the completeness of combustion at the furnace exit is about the same in both cases.

e With even weak swirl the peripheral injection scheme gives much more rapid mixing and combustion and more uniform temperatures at furnace exit. For example, the completeness of combustion within the furnace with peripheral injection and using the 15° swirler is similar to that obtained with the 30° swirler and central injection. The burner pressure loss is thus reduced to about one quarter, as compared to the central injection case.

The above features will aid combustion of fuels that are more difficult to burn, eg low calorific value gaseous fuels. For pulverised fuels the rapid initial mixing will assist the complete combustion of the volatiles, while the effective stirring will help burn the solids.

5.7 Future Work

The work reported here is only an early step in the development of combustion systems with outer fuel injection. Much work has to be done. Some investigations which can be foreseen at this stage are - changes of design to alleviate the high temperature being near the furnace walls, fuel injection at a group of holes around an annulus instead of through a slit, study of effect of ratio of fuel jet velocity to air jet velocity.

6. CONCLUSIONS

Flow and combustion patterns have been defined in a combustion system with peripheral injection of fuel gas. The patterns are defined by time-averaged measurements of velocity components, static pressure, temperature and species concentrations. These data sets can be used for the validation of prediction models.

Introducing a low degree of swirl in the air had the effect of reducing the flame length and the subsequent 'stirring' length. There were similar effects when the equivalence ratio was reduced.

The flow and flame processes were independent of Reynolds number, within the range examined - 6×10^4 to 9×10^4.

The axial fluxes of axial and tangential momenta showed initial rises followed by decays to the fully developed flow values. These values were functions of the input momentum and equivalence ratio and also, in the tangential momentum case, of the swirler vane angle. A furnace swirl number based on these fluxes and on the furnace diameter can be used to predict the flow type and also as a modelling criterion for isothermal tests.

Raising the swirl shortened the length for combustion and lowering the equivalence ratio had similar effects.

Comparing with central fuel injection systems, the peripheral injection systems with even weak swirl give much more rapid mixing and combustion, and uniform temperatures in shorter furnace lengths. Consequently, equivalent combustion performance can be achieved using significantly less swirl and thus much reduced fan power.

ACKNOWLEDGEMENTS

The authors wish to thank colleagues at the National Engineering Laboratory and the University of Glasgow for their advice and encouragement. Thanks are particularly due to Mr Tan H-Y of Beijing University for his work in the initial experiments at Glasgow University. The first author also wishes to thank the British Council for the award of a bursary in 1984.

REFERENCES

AHMAD, N. T., ANDREWS, G. E., KOWKABI, M. and SHARIF, S. F., (1985), "Centrifugal mixing forces in enclosed swirl flames", 20th Internat. Symp. on Combustion, The Combustion Institute, pp 259-267.

BEER, J. M. and CHIGIER, N. A., (1972), "Combustion aerodynamics", London: Applied Science Publishers.

BELTAGUI, S. A. and MACCALLUM, N. R. L., (1976a), "Aerodynamics of vane-swirled flames in furnaces", J. Inst. Fuel, Vol. 49, pp 183-193.

BELTAGUI, S. A. and MACCALLUM, N. R. L., (1976b), "The modelling of vane-swirled flames in furnaces", J. Inst. Fuel, Vol. 49 pp 193-200.

BELTAGUI, S. A. and MACCALLUM, N. R. L., (1985), "Characteristics of enclosed swirl flames with peripheral fuel injection", Report, Dept Mechanical Engineering, University of Glasgow.

GUPTA, A. K., BEER, J. M. and SWITHENBANK, J., (1977), "Concentric multi-annular swirl burner: Stability limits and emission characteristics.", 16th Internat. Symp. on Combustion, The Combustion Institute, pp 79-91.

KERR, N. M. and FRASER, D., (1965), "Swirl, Part 1: Effect on axisymmetrical turbulent jets", J. Inst. Fuel, Vol. 38, pp 519-526.

MARKOWSKI, S. J., LOHMANN, R. P. and REILLY, R. S., (1976), "The Vorbix burner - a new approach to gas turbine combustors", Trans. ASME, J. Eng Power, Vol. 98, pp 123-129.

MATHUR, M. L. and MACCALLUM, N. R. L., (1967), "Swirling air jets issuing from vane swirlers: Part 1, Free jets, Part 2, Enclosed jets", J. Inst Fuel, Vol. 40, pp 214-224 and 238-245.

OVEN, M. J., GOULDIN, F. C. and McLEAN, W. J., (1979), "Temperature and species concentration measurements in a swirl-stabilised combustor", 17th Internat. Symp. on Combustion, The Combustion Institute, pp 363-374.

SHEKLETON, J. R., (1981), "The CIVIC: A concept in vortex induced combustion for the Solar Gemini 10 kW gas turbine - Parts 1 and 2", Trans. ASME, J. Eng Power, Vol. 103, pp 34-42 and 708-717.

SYRED, N. and BEER, J. M., (1974), "Combustion in swirling flow: A review", Combustion and Flame, Vol. 22, pp 143-201.

TAN, H. Y. and MACCALLUM, N. R. L., (1983), "Combustion in rotating flows", Report, Dept Mechanical Engineering, University of Glasgow.

VRANOS, A., KNIGHT, B. A. and ZABIELSKI, M. F., (1982), "Centrifugal mixing: A comparison of temperature profiles in non-recirculating swirling and non-swirling flames", Combustion and Flame, Vol. 48, pp 109-119.

LIST OF TABLES

LIST OF FIGURES

TABLE 1

INPUT VARIABLES AND FLOW TYPES

				Flame			Isothermal	
Run No	Swirler vane angle degrees	Air velocity U m/s	Burner swirl No S	Equivalence ratio	Furnace swirl No S*	Flow type	Furnace swirl No S*	Flow type
1	0	15.0	0.0	0.53	0.0	B	0.0	B
2	0	10.65	0.0	0.38	0.0	B	-	-
3	15	15.0	0.089	0.53	0.027	B	0.094	B
4	15	15.0	0.089	0.38	0.051	B	-	-
5	15	10.65	0.089	0.53	0.031	B	-	-
6	22	15.0	0.138	0.53	0.052	B	0.238	C
7	22	15.0	0.138	0.38	0.098	B	-	-
8	22	10.65	0.138	0.53	0.056	B	-	-
9	30	15.0	0.192	0.53	0.099	C	0.386	D
10	30	15.0	0.192	0.38	0.181	C	-	-
11	30	10.65	0.192	0.53	0.082	C	-	-

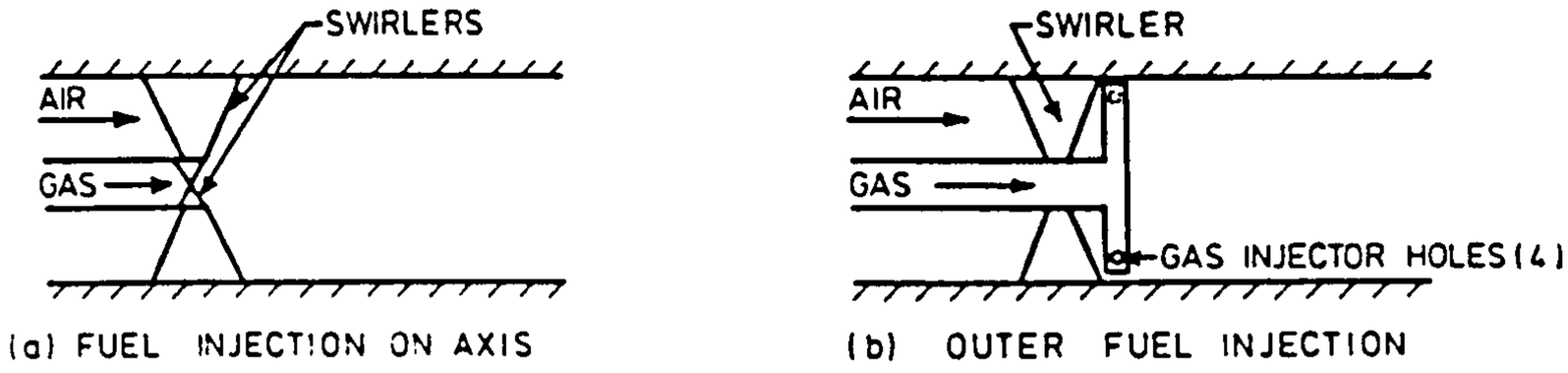

Fig.1. PARALLEL-WALLED COMBUSTER-BURNER ARRANGEMENTS

	AIR SW	GAS SW	SYM-BOL	$\bar{T}_K$
FUEL INJ ON AXIS	60°	30°	•	999
	60°	45°	x	1427
	60°	60°	△	1391
OUTER INJ.	60°	-	□	1516

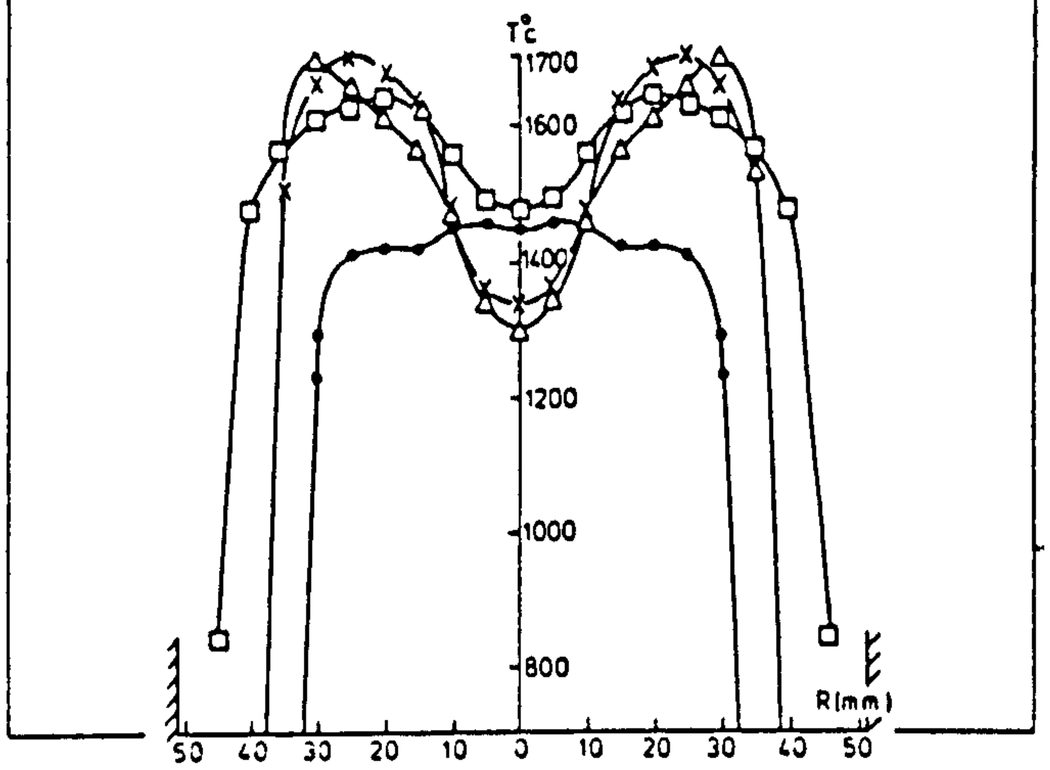

Fig 2 TEMPERATURE DISTRIBUTIONS FOR A VARIETY OF BURNER ARRANGEMENTS – x/D = 4, φ = 0 6

	AIR SW	GAS SW	SYM BOL	$\bar{T}_K$
FUEL INJ. ON AXIS	60°	30°	•	872
	60°	45°	X	976
	60°	60°	△	946
OUTER INJ.	60°	–	□	1718

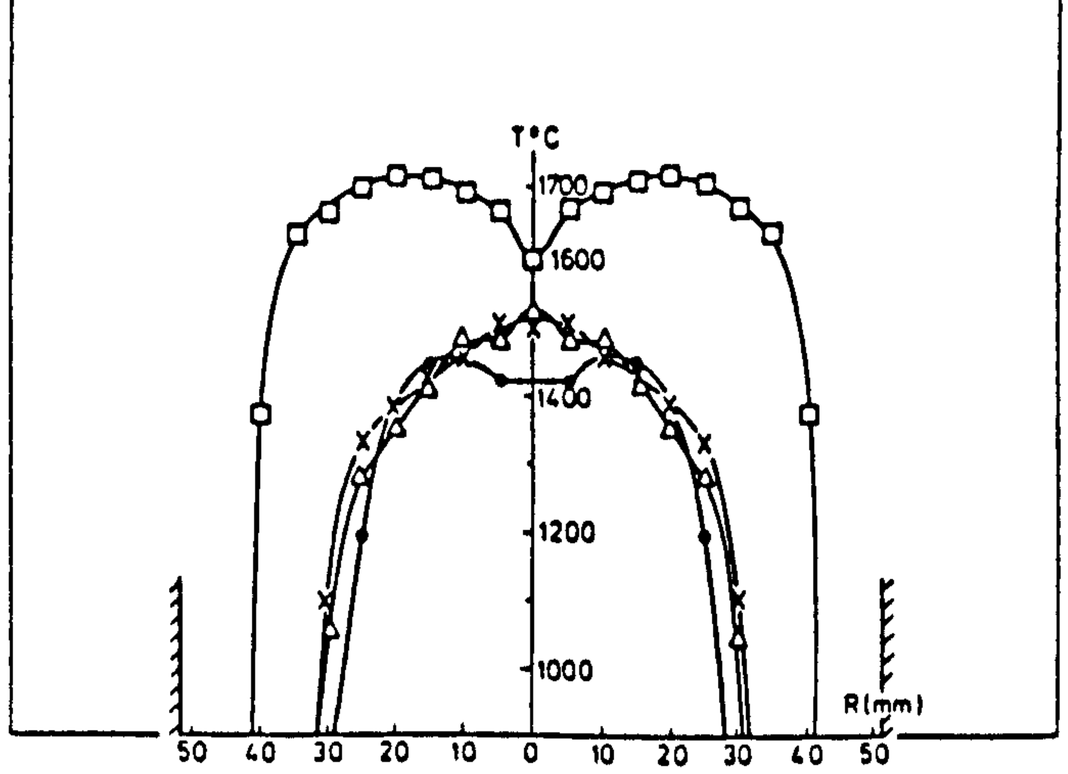

Fig.3. TEMPERATURE DISTRIBUTIONS FOR A VARIETY of BURNER ARRANGEMENTS – x/D = 4, φ = 0·83

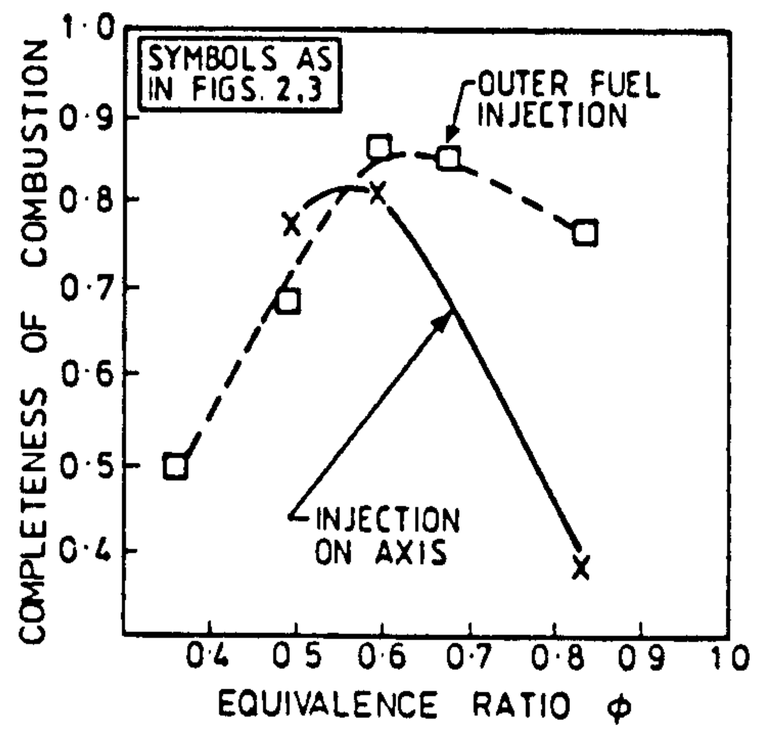

Fig.4. COMPLETENESS of COMBUSTION:– AXIS and OUTER FUEL INJECTION COMPARED

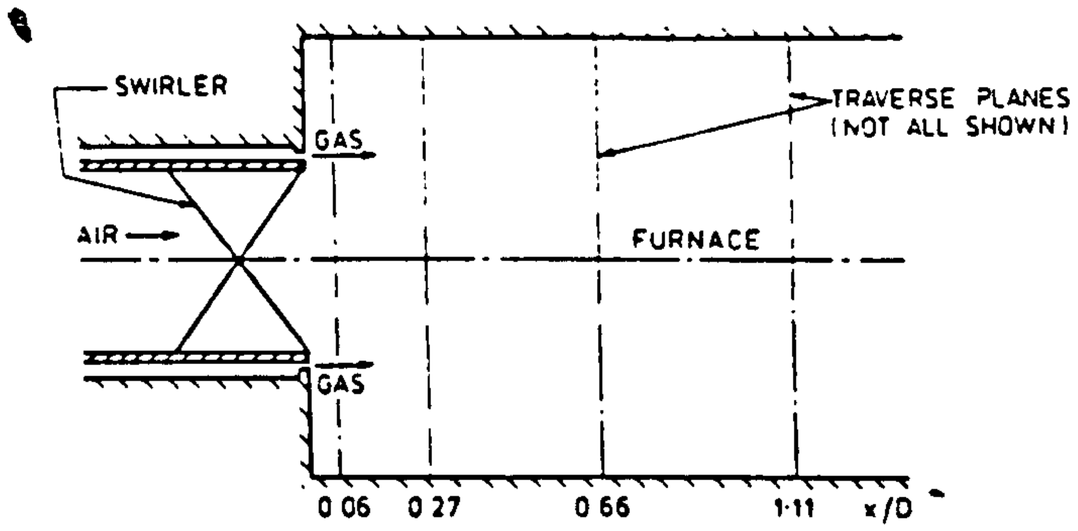

Fig 5. PERIPHERAL FUEL INJECTION BURNER IN FURNACE of D/d = 2·5

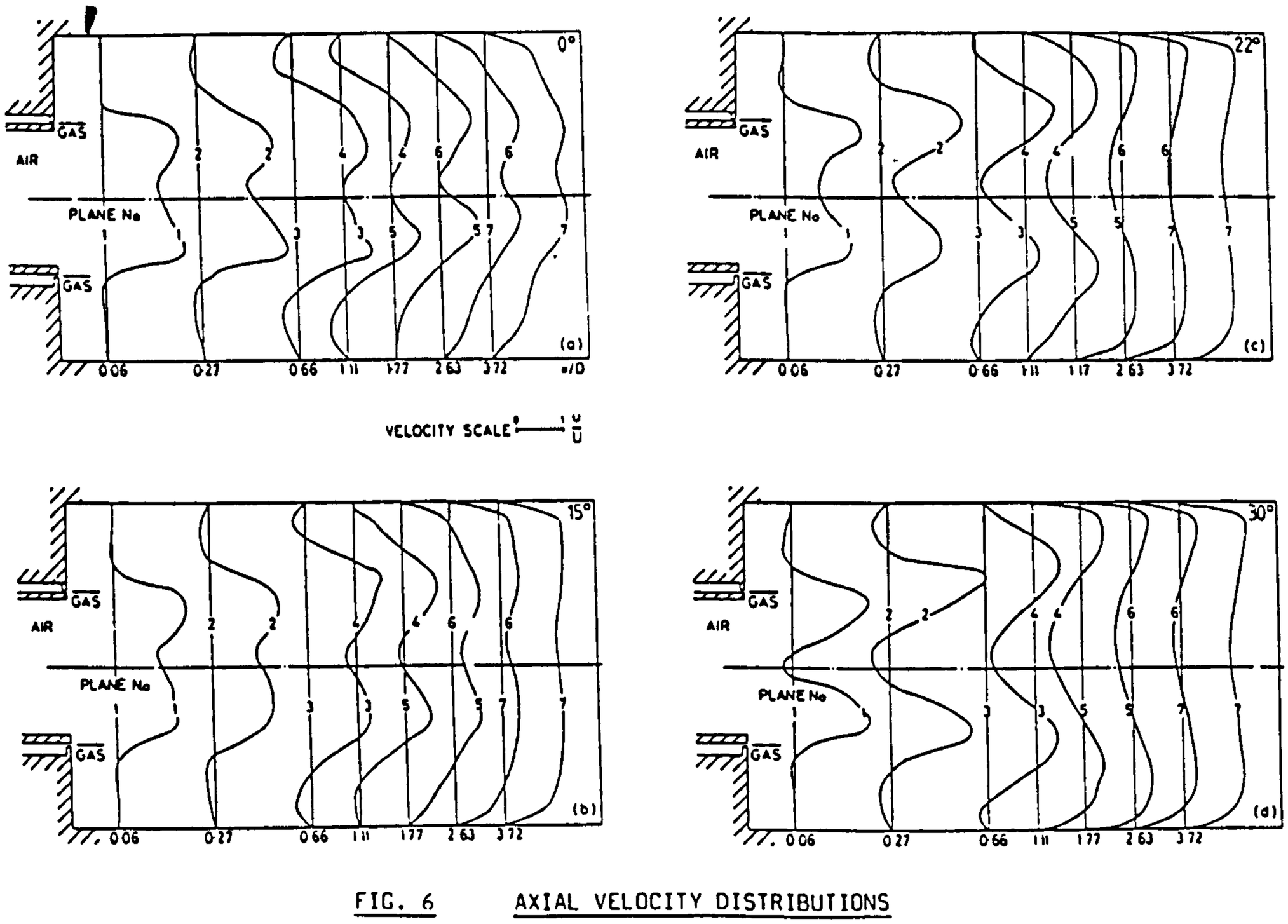

FIG. 6 AXIAL VELOCITY DISTRIBUTIONS

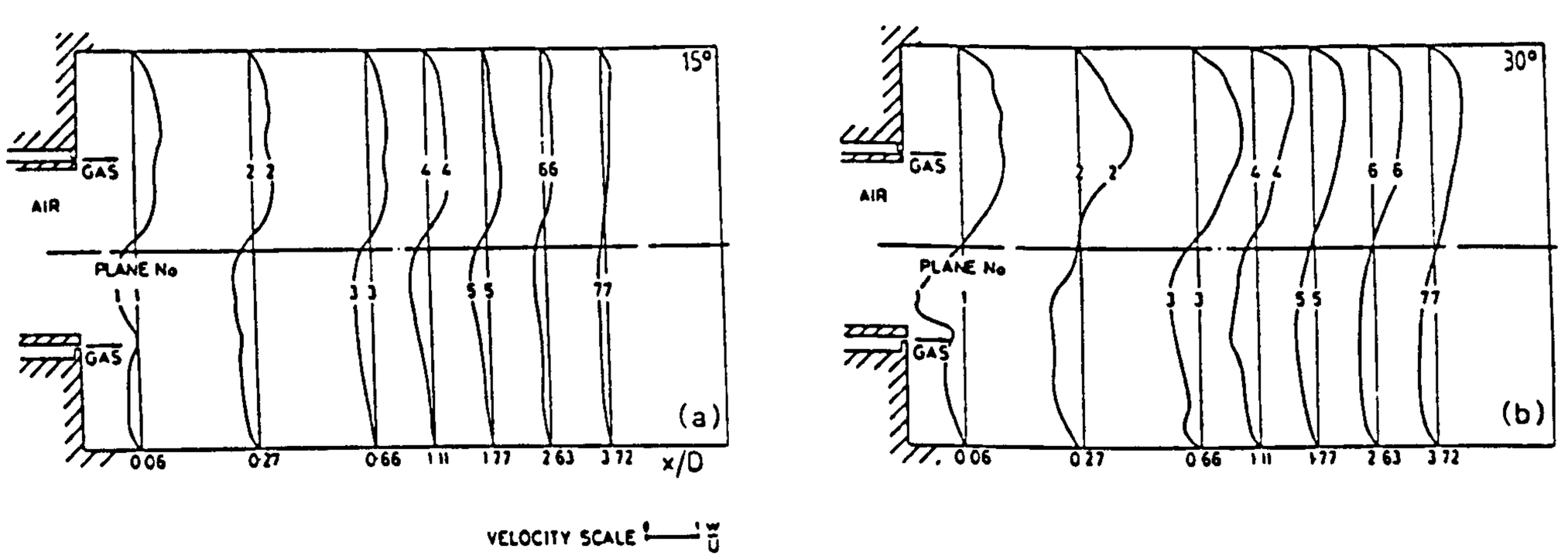

FIG. 7 TANGENTIAL VELOCITY DISTRIBUTIONS

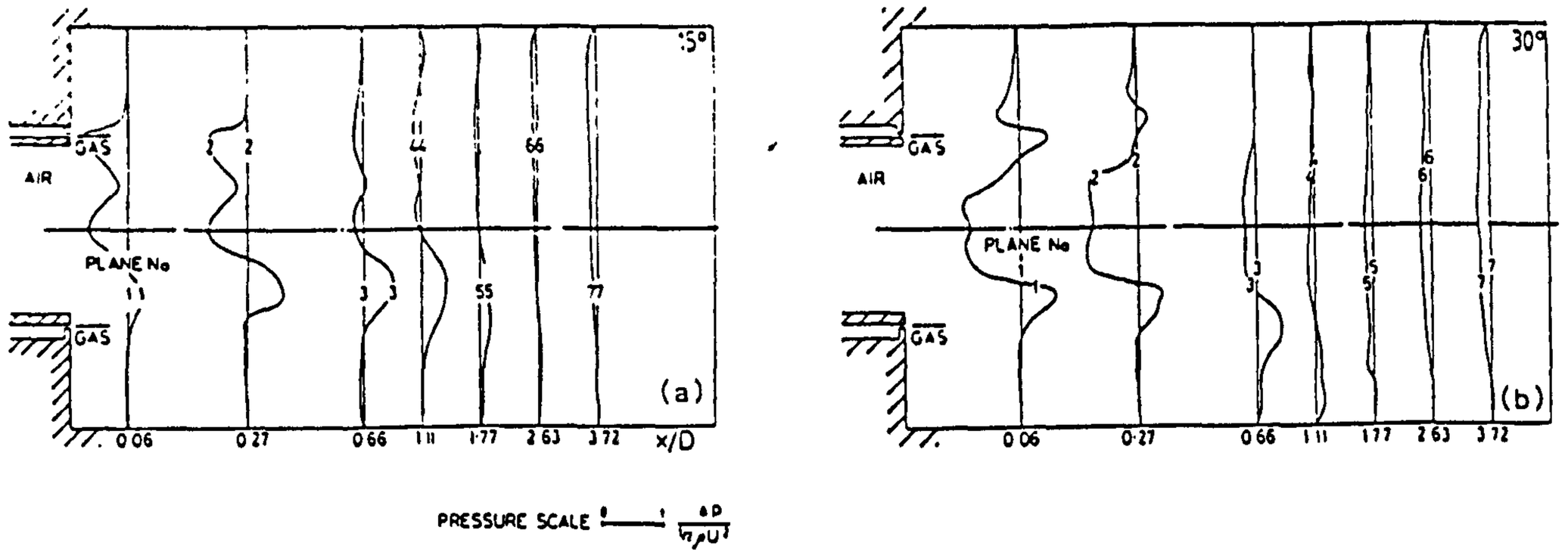

PRESSURE SCALE 0 —— 1 $\frac{\Delta P}{\eta \rho U^2}$

FIG. 8 STATIC PRESSURE DISTRIBUTIONS

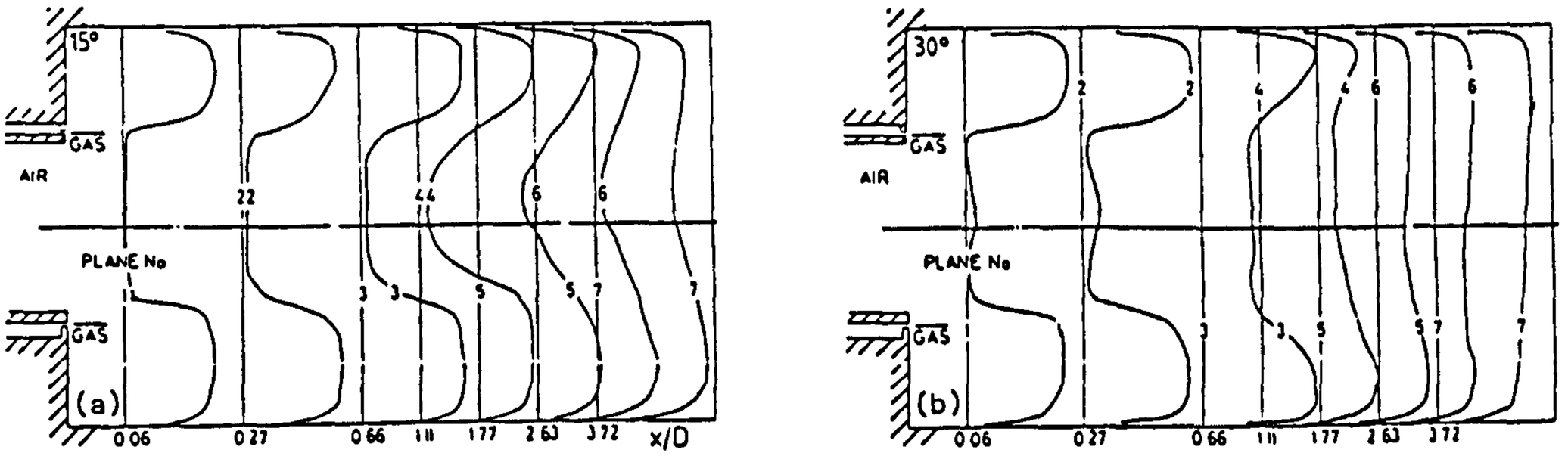

TEMPERATURE SCALE 0 —— 0·5 $\frac{\Delta T}{\Delta T_0}$

FIG. 9 TEMPERATURE RISE DISTRIBUTIONS

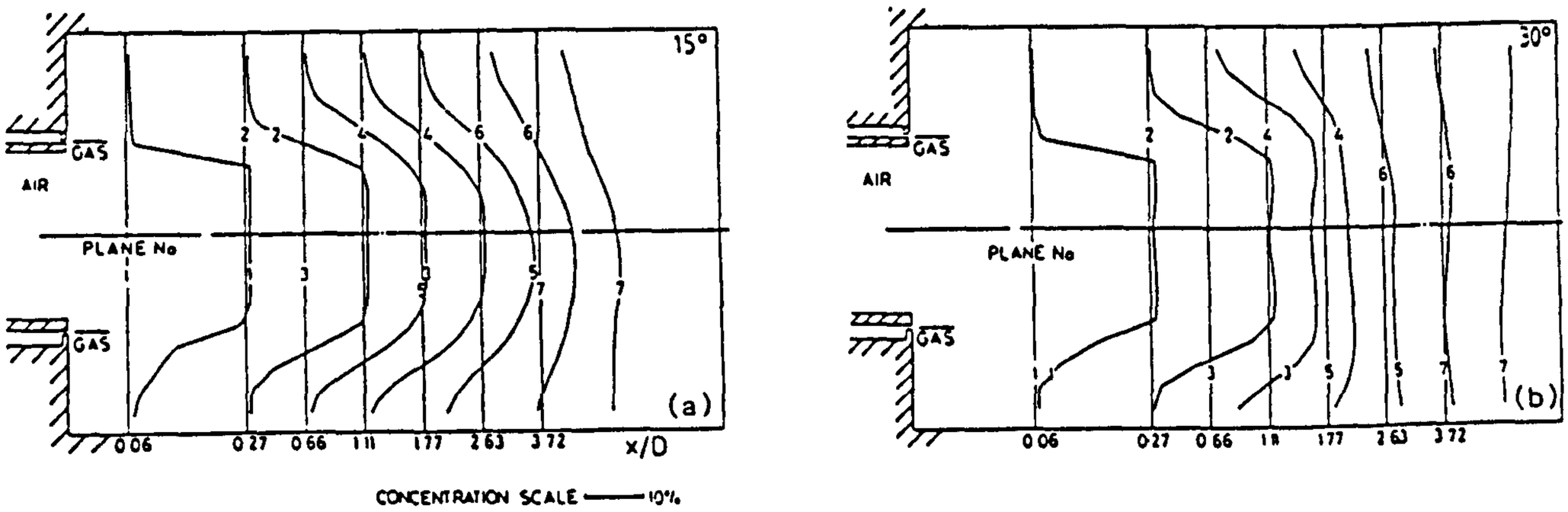

CONCENTRATION SCALE —— 10%

FIG. 10 OXYGEN CONCENTRATION DISTRIBUTIONS

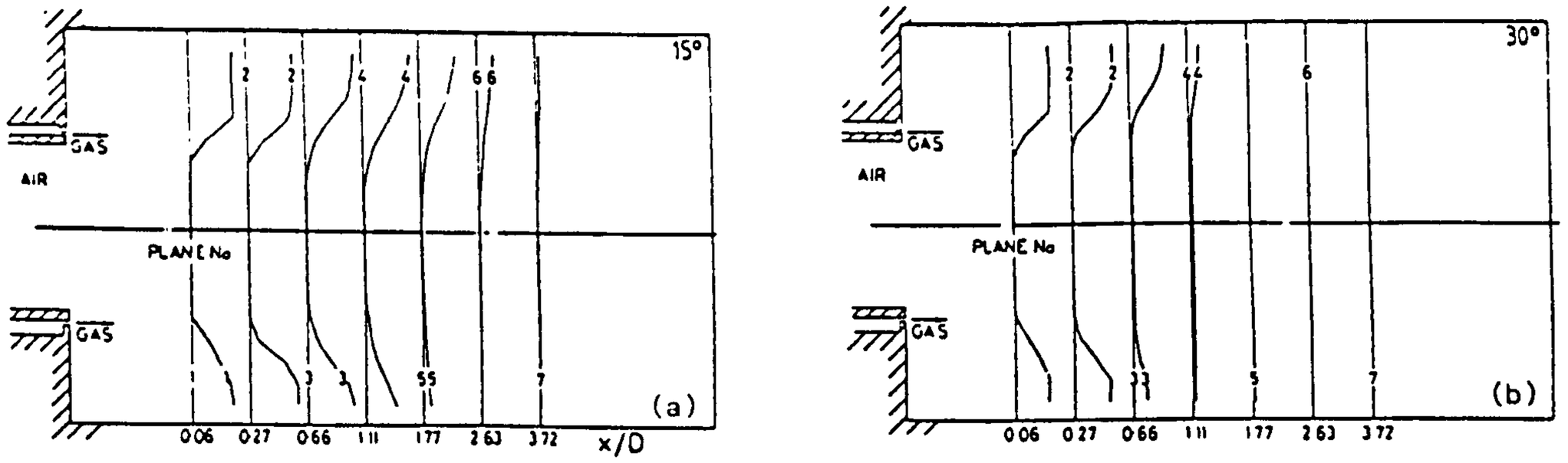

FIG. 11 CARBON MONOXIDE CONCENTRATION DISTRIBUTIONS

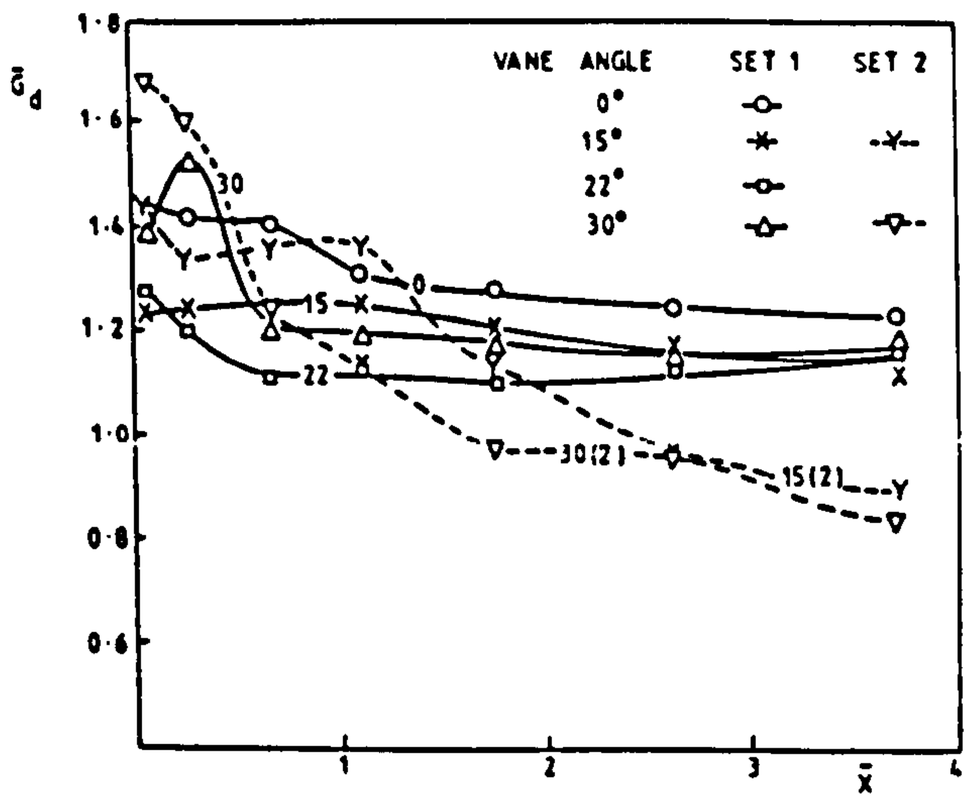

Fig.12a AXIAL MOMENTUM FLUXES

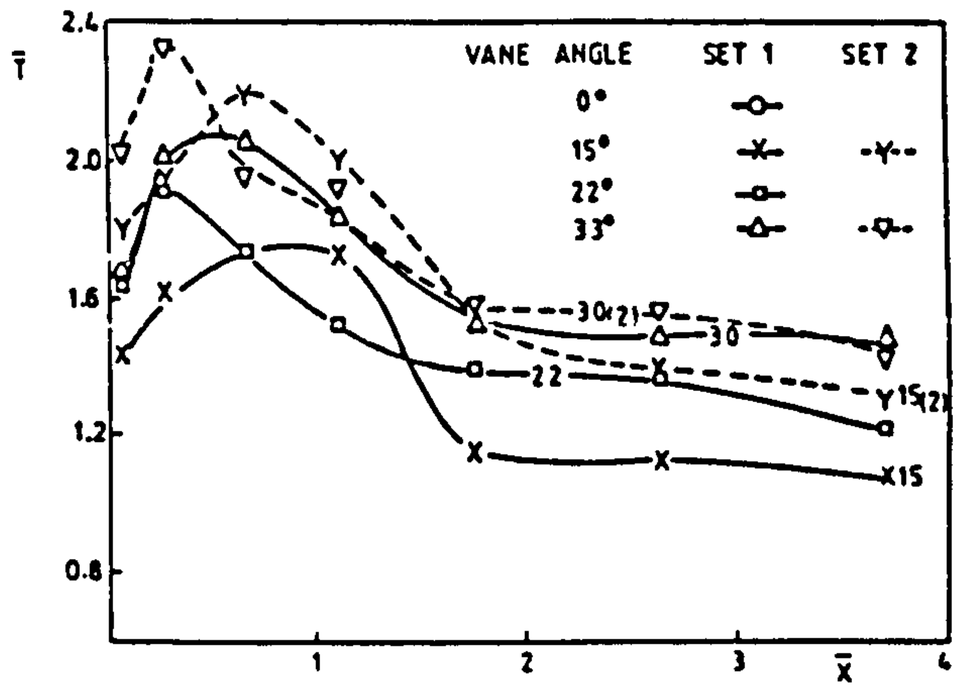

Fig.12b AXIAL FLUX of TANGENTIAL MOMENTUM

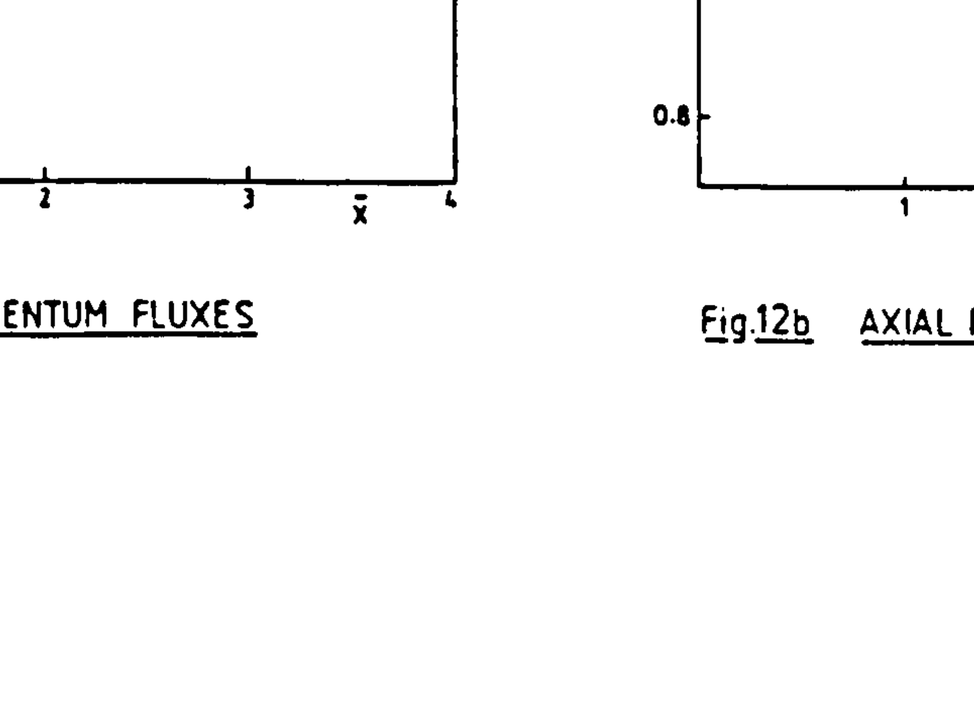

Fig.13 AXIAL FLUX of SENSIBLE ENTHALPY

S A BELTAGUI BSc PhD* and N R L MACCALLUM BSc PhDt

Publication 40

Characteristics of enclosed swirl flames with peripheral fuel injection

The conventional mechanism for combustion in a non-premixed system is by central fuel injection. To increase the mixing rate and combustion intensity, a bluff body, or a swirler which creates central recirculation, is introduced but this requires a high pressure loss. An alternative mechanism with no central recirculation makes use of the shear layer mixing at the outer jet boundary together with mixing currents created by the centrifugal forces associated with a rotating flow with negative density gradients. Such a scheme having fuel injection in the periphery of the swirling air jet has been studied experimentally under variable input conditions of flow Reynolds number, swirl strength and fuel equivalence The resulting flow and combustion patterns have been well described by detailed profiles of measured velocity components, static pressure, temperature and species concentrations. The results confirmed the potential of this system for producing high intensity flames with wide stability ranges. The effect of increasing swirl, within the low range, has been found to enhance the mixing and combustion rates and to increase the stirring of the combustion products giving uniform profiles of properties in a shorter furnace length. Reductions in fuel equivalence have produced even shorter flames. The flow and combustion patterns were confirmed to be independent of the flow Reynolds number in the fully turbulent flow range tested. Comparisons made with a similar system, but with central fuel injection, showed the superiority of the peripheral injection scheme. A furnace swirl number based on experimental momentum fluxes correlates the effects of swirl and combustion on flow patterns. The detailed profiles of the flow and combustion parameters are valuable for validation of the predictions of mathematical models as they present complete data for an unconventional combustion system

1. List of symbols

c_p	specific heat at constant pressure
d	swirler diameter
D	furnace diameter
G_d	axial momentum flux, dynamic component = $\int 2\pi r\rho u^2\,dr$
$\bar{G}_d$	normalised axial momentum flux = $\dfrac{\int 2\pi r\rho u^2\,dr}{\pi r_{sw}^2\rho U^2}$
h	specific sensible gas enthalpy ($c_p t$)
H	sensible enthalpy flux = $\int 2\pi r\rho uh\,dr$
$\bar{H}$	sensible enthalpy flux/input energy flux
Δp	local pressure drop relative to ambient
r, r_{sw}	radius, radius of swirler
S	swirl number of hubless swirlers, based on swirler diameter = $\frac{1}{3}\tan\theta$
S^*	furnace swirl number = $T/(G_d D)$
T	axial flux of tangential momentum = $\int 2\pi r^2\rho uw\,dr$
$\bar{T}$	normalised tangential momentum flux = $\dfrac{\int 2\pi r^2\rho uw\,dr}{\frac{2}{3}\pi r_{sw}^3\rho U^2\tan\theta}$
ΔT	temperature rise
u, v, w	local axial, radial and tangential components of velocity
U	average axial velocity leaving swirler
x	axial distance along furnace
$\bar{X}$	axial distance in units of furnace diameters
ρ	density
θ	swirler vane angle to axial direction

2. Introduction

There are numerous requirements which must be considered when designing a burner. These include: wide stability limits, wide turndown ratio, high combustion efficiency, high intensities of heat release, high heat transfer rates from the flame, low burner pressure drop, low emissions of pollutants and low noise. Some of these requirements are conflicting and the design has to be based on compromise. In order to achieve the best compromise, maximum use must be made of our knowledge of the key processes.

One such key process is the mixing between the fuel and the oxidant. If good mixing is achieved then the zones of highest temperature will be reduced in size and less excess air is required, giving lower oxygen concentrations in the flame zone. These results lead to reduced NO_x emissions.

As premixed combustion systems are not generally favoured in industrial applications for reasons of safety, attention must be directed towards mixing in non-premixed systems.

2.1. Shear-layer mixing

The most obvious method of mixing in a combustion system involving jet flows is to use the turbulence generated at the shear layer of the jet boundary. For example, in the case of a central fuel jet surrounded by a concentric annular air flow there will be high shear and high property gradients in the high turbulence zone at the interface between the jets. It is therefore realised that high heat release rates can be achieved by having the regions of high fuel concentration overlap these regions of high shear stress. The mixing can be enhanced by increasing the velocity and species gradients in this region, and also by increasing the total area of the region. One method of achieving this is to place a bluff body at the centre of the fuel jet. This creates wider jets and also leads towards the establishment of a central reverse-flow zone (CRZ) where burned gases are recirculated to mix with and ignite the fresh fuel/air flow.

Swirling the air flow can also be used to produce the effects of central recirculation and high shear stresses, it being noted that the shear stresses will occur in both the tangential and axial directions. Quarls are also frequently used, with or without swirl, to increase the jet spread rate and to help create a CRZ. The beneficial effects of swirl, however, incur the high cost of the pressure drop across the swirler, which is proportional to the square of the swirl number.[1,2,3] This latter must be high to ensure the establishment of a CRZ. However measurements of turbulence in swirling flows[3,4] show that the high shear

*National Engineering Laboratory and University of Glasgow, Glasgow.
†Department of Mechanical Engineering, University of Glasgow, Glasgow.

rates fall mainly in the outer boundary of the forward flow, and that levels of turbulence in the CRZ are generally low.

The above discussion leads to the conclusion that mixing can be greatly increased through the use of a scheme where the fuel jet is the outer, annular, flow and the air flow forms the central jet. Such a system will have greater potential for fuel to air mixing, with or without swirl. The shear stresses in the mixing area are higher and the total area is increased.

2.2. Centrifugal mixing

If swirl is to be used, it will be better utilised by fully realising the benefits of the centrifugal forces together with the density gradients occurring in a combustion system. Density gradients before ignition are caused by the difference in density of fuel and air, and after ignition by the reduction in density due to combustion.

Swirl in a variable density flow may suppress or enhance turbulence. If the radial gradients in a rotating flow are positive, they cause flow stratification and will suppress turbulence. In a combustion case with central fuel injection it may even cause laminarisation of the flame and an increase in the flame length.[2]

On the other hand, negative density gradients in a rotating field will disturb the radial equilibrium and create instabilities, hence higher shear stresses and mixing rates. The lighter pockets of burned gases will tend to move inwards and heavier pockets of reactants, unburned, will tend to travel outward, against the pressure gradient. A situation of this type can be achieved by injecting the fuel at the outer boundary of the air jet.

An advantage of this system with outer fuel injection is the reduction of the pressure loss which would otherwise have been required to establish a CRZ. Only moderate degrees of swirl should be required. The removal of the central fuel injection system also reduces the pressure loss of the air flow across the burner.

In this paper a review is given of the rather limited number of investigations that have been made of combustion systems that utilise some of the desirable effects referred to above. Then follow the results of the first part of a new experimental program.

3. Review

The advantages of jet shear mixing have been utilised in a combustor design by Suzuki *et al*[5,6] in which the fuel jet is directed into the main air stream. Combustion was found to be smooth, a flat flame resulted and there were low emissions of pollutants, low noise and high flame emissivity.

A multi-annular swirl burner design has been investigated by Gupta *et al*,[7] the fuel gas and air being injected alternately through a succession of annular openings. In this way the fuel injection was matched with the regions of high shear in the main flow. High efficiencies were reported, coupled with low emissions and low noise levels. The disadvantages of the system were its likely high cost and its high pressure loss. Also, the design could not take advantage of the centrifugal force mixing effect.

Turning to the effects of rotation, a fundamental laboratory-scale study has been carried out by Vranos *et al*[8] of a premixed system in which combustion was initiated by a pilot flame located at the outer diameter of the chamber. The main flow in the centre of the chamber could be either unswirled or swirled. It was found that when the flow was swirled, this increased the rate of mixing and produced a much shorter flame, thus verifying the enhanced mixing effect in a swirling flow of starting the combustion at the outer radius of the chamber.

These beneficial centrifugal force effects have been used in the designs of some gas turbine combustors: the Vorbix burner[9] and the Civic combustion chamber.[10,11]

Studies have also been made by Ahmad *et al*[12] of outer fuel injection in swirling flows. These tests too have demonstrated the superior mixing rates that can be achieved, as compared with systems with central fuel injection.

In a test of a swirling non-premixed flow through a chamber with no initial expansion, Tan and Maccallum[13] have shown that much shorter flames, and consequently much higher combustion efficiencies, could be achieved when the fuel was introduced near to the outer wall of the chamber, instead of at the axis. Also the flame was much more easily stabilised than in the central injection case where an air swirler vane inclination of higher than 45° was required.

The introduction of the fuel at locations other than the axis can also be used to reduce noise, for example Gupta *et al*[14] used a combination of radial and axial injection of natural gas fuel to obtain a significant noise reduction in a swirl-stabilised burner.

From the above it is seen that there is wide evidence to support the prediction that introducing the fuel at the outer periphery of a swirling air flow, thus starting combustion at the outer boundary, leads to enhanced mixing rates and generally shorter flames. However it was seen that there are still wide gaps in our knowledge of such systems. Consequently an experimental program was planned to provide information on aspects of this type of combustion system. The rig used for the initial tests, and the results obtained, are described in the next sections.

4. Experimental program

The aim of the experimental program was to investigate the flow and combustion patterns in a characteristic swirling flow with outer fuel injection. In addition to giving an insight into the behaviour of the system, the results would also provide a set of data to validate prediction models and also guide towards isothermal modelling of these less conventional combustion systems.

4.1. Apparatus and instrumentation

The experimental rig is based on a refractory-lined furnace, 225 mm i.d. and 0.9 m long discharging to the atmosphere. Air is supplied on the axis at one end through an inlet tube of 93 mm i.d. in which vane swirlers[15] can be placed. The fuel—natural gas, 92% CH_4—is introduced through an annular slit of 2 mm width around the periphery of the air swirler.

In order to define the combustion patterns, temperature and species concentrations were measured. A Pt-5% Rh/Pt-20% Rh thermocouple was used to measure temperature. Concentrations of O_2 were measured by a paramagnetic analyser and of CO and CO_2 by infrared analysers.

TABLE 1 Input variables and flow types

Run no	Swirler vane angle degrees	Air velocity U m s	Burner swirl no S	Flame			Isothermal	
				Equivalence ratio	Furnace swirl no S*	Flow type	Furnace swirl no S*	Flow type
1	0	15.0	0.0	0.53	0.0	B	0.0	B
2	0	10.65	0.0	0.38	0.0	B	—	—
3	15	15.0	0.089	0.53	0.027	B	0.094	B
4	15	15.0	0.089	0.38	0.051	B	—	—
5	15	10.65	0.089	0.53	0.031	B	—	—
6	22	15.0	0.138	0.53	0.052	B	0.238	C
7	22	15.0	0.138	0.38	0.098	B	—	—
8	22	10.65	0.138	0.53	0.056	B	—	—
9	30	15.0	0.192	0.53	0.099	C	0.386	D
10	30	15.0	0.192	0.38	0.181	C	—	—
11	30	10.65	0.192	0.53	0.082	C	—	—

The flow patterns were quantified by measurements of the time-averaged components of velocity—u, w, and v—and of the static pressure. These parameters were measured using a 3-hole pitot-type probe[15] of tip diameter 6 mm. Although there are some doubts regarding the use of intrusive probes for velocity measurements in swirl combustors, there is evidence that there is reasonable consistency between the results thus obtained and time-averaged readings obtained by laser anemometry.[16,17]

4.2. Test variables

The main parameters were varied as indicated below and the test conditions are given in Table 1.

(*a*) *Air swirler vane angle*—0°, 15°, 22°, 30°, giving burner swirl numbers (based on burner diameter), S, in the range zero to 0.192. Higher swirl numbers were not needed, as discussed previously.
(*b*) *Reynolds number of air flow*—9×10^4 and 6.3×10^4 corresponding to average axial air velocities at the swirler exit of 15.0 and 10.6 m/s.
(*c*) *Fuel equivalence ratio*—0.53 (limited by probe integrity) and 0.38. The corresponding heat release rates, based on total furnace volume, are 5.4 and 3.8 MW/m^3.

5. Results

The flames were found to be stable for all degrees of swirl over a wide range of equivalence ratio. As swirl in the air flow was increased, the combustion became more intense and flames were shortened. However noise levels rose significantly at the higher fuel flow rates as the swirl vane angle was increased beyond 30°. At these higher vane angles the pressure drop across the swirler became quite marked, consequently 30° was regarded in this work as being the upper limit of vane inclination.

For each swirler, three sets of results were obtained:

Set 1 at equivalence ratio 0.53 and inlet Reynolds number 9×10^4.
Set 2 at equivalence ratio 0.38 and inlet Reynolds number 9×10^4.
Set 3 at equivalence ratio 0.53 and inlet Reynolds number 6.3×10^4.

Integrations of the axial velocity profiles have been carried out at all of the traverse planes to give mass fluxes. With the exception of the first traverse plane, these integrations lay within 25% of the metered flux. This agreement is considered reasonable, in view of the difficulty of measuring close to the walls. The discrepancies at the first plane are attributed to the proximity of the burner vanes and the swirler rim.

All the velocity component results have been normalised by dividing by the inlet air velocity, U. The static pressures have been normalised by the air inlet velocity head ($\frac{1}{2}\rho U^2$) and the temperature rises expressed as fractions of the theoretical temperature rise.

The results of test sets 1 and 3, when normalised as stated above, are virtually identical, confirming the similarity, already frequently reported, of flows where the Reynolds number is greater than the critical (2×10^4) and the flows are fully developed.

Comparing the results of test sets 1 and 2, it is found that changing the equivalence ratio from 0.53 to 0.38 has only minor effects on the velocity and pressure profiles. However the combustion patterns are noticeably changed, combustion being completed in a shorter distance at the lower equivalence ratio.

For economy of space, only the results of test set 1 are illustrated in this paper. The full results are given in ref 18.

The results of test set 1 are given in Figs. 1, 2 and 3 for the three velocity components, in Fig. 4 for static pressure, in Fig. 5 for temperature rise, corrected for radiation, and in Figs. 6, 7 and 8 for the concentrations of O_2, CO_2 and CO respectively.

It is noticed that there is slight asymmetry on some occasions in the flames at the lower degrees of swirl. Possible reasons for this type of observation[3,15] can be constructional asymmetries or precessing vortices.

6. Discussion of results

6.1. Flow patterns

The time-averaged flow patterns, within two furnace diameters of the burner, fell into one of three classifications:[15]

(i) reduced forward velocity on the axis, and maximum forward velocities occurring at a radius displaced from the axis—the double-humped distribution, referred to as type B.

(ii) small reverse velocities on the axis and a weak central recirculation. referred to as type C.

or

(iii) pronounced central recirculation. the reversed mass flow exceeding 10% of the total flow—type D.

For the cases with combustion. taking for example that with equivalence ratio 0.53 illustrated in Fig. 1. zero swirl and 15 and 22 vane angle swirlers gave type B flows and the higher swirl angle of 30 gave a weak central recirculation—type C flow. By comparison. in corresponding isothermal tests (Table 1) zero swirl and 15° vane angle gave type B flows. 22° vane angle type C flow and 30° vane angle type D flow. This weakening of the central recirculation when combustion occurs is in agreement with previous work on premixed flames.

With the equivalence ratio of 0.38 (not illustrated). the axial velocity profiles were generally similar to those for equivalence ratio 0.53. except that the peak velocities occurred earlier. and decayed faster. owing to the shorter distance required for combustion at the lower fuel flow.

The general effects of increasing swirl are to accelerate the combustion process. so that peak axial velocities occur closer to the burner. and to increase the jet spread rate.

Considering the tangential velocity components. w. shown in Fig. 2(*b*). (*c*) and (*d*). one sees the usual Rankine type flow with solid body central rotation surrounded by an outer free vortex. As swirl is increased. the peak values of w increase and the location of the peak values is moved outwards. At these peak points. the ratio of the tangential to axial components of velocity (w/u) is roughly proportional to tan θ.

The radial velocity profiles. shown in Fig. 3(*a*)–(*d*). are indicators of the rate of spread of the jet. This spread obviously is more rapid as swirl is increased. For a given swirler. as the mixture burns there is a volume expansion which one would expect to increase the outward radial velocity. On the other hand. there will be a decay due to jet spread. These two factors almost balance each other for the first furnace diameter of axial distance. thereafter the radial components decay rapidly. It should be mentioned that the radial components of velocity are the most difficult to measure. and there is inevitably scatter in the results.

It is helpful to note the static pressure distributions shown in Fig. 4(*a*)–(*d*). These show the depression in static pressure relative to ambient. The distributions are similar to those generally observed in enclosed swirling jet flows in furnaces. with greatest depressions at and around the centre of the jet and uniform pressures within the CRZ. when it exists. and in the peripheral reverse-flow zones (PRZ). There are some local discontinuities near the annular fuel gas injection slit. Increasing the swirl increases the centreline depression until central recirulation starts. After the reaction zone. say beyond one furnace diameter of axial distance. the pressures rise towards the ambient level. The effect of combustion is to diminish the depression in the outer region. this being where the reaction. and hence density change. is taking place. As to centreline pressures. tangential velocities have been increased while the density in the central jet flow is relatively unchanged so that centrifugal effects cause a greater depression at the axis relative to the periphery. This second effect dominates so that centreline depressions are increased when combustion is taking place. This is in contrast to the effects in the premixed case[15] where combustion is concentrated in the centre. which diminishes the depression on the centreline and also causes less difference in pressure between the centreline and the PRZ.

6.2. Combustion patterns

A good description of the combustion patterns is given by the combination of the temperature rise profiles and the gas sampling results (Figs. 5-8).

It can be seen that combustion starts at the shear layer between the air and fuel flows. Hot combustion products are the main constituents in the PRZ. The fluid flowing inside the 'cone' based on the shear layer is essentially cold air. even when there is central recirculation. This demonstrates that there is no need to create a CRZ in this peripheral injection scheme.

The maximum temperature rise occurs in the shear zone at some distance from the burner exit. In the remaining length of the flow within the furnace. these very hot gases mix with the remainder of the flow. Introducing swirl enhances the mixing by increasing the spread of the air jet. making the air meet the fuel at an angle and with a tangential velocity component. This increases the rate of mixing relative to the unswirled case where the air advances mainly with an axial component of velocity. Also the subsequent stirring of products is more rapid and a uniform temperature is reached more readily. At the lower degrees of swirl. this uniformity of temperature is not achieved within the furnace. For example. the temperature rise at the axis at the final measuring plane (plane 7) is about 75% of the overall average when the 15 swirler is used and is only about 25% when there is no swirl. The overall averaged normalised temperature rise at the final plane is less than unity due mainly to heat losses to the furnace walls.

It is to be noted that there is very little evidence at the furnace exit of any incomplete combustion when swirl is present. However when there is no swirl. there is up to 5% CO at the outer radii.

As to the effect of equivalence ratio change. it is found that reducing the equivalence ratio from 0.53 to 0.38 consistently gave earlier combustion. this being seen both from the temperature rise and the species sampling tests. The sampling tests for CO confirmed virtually complete combustion by the furnace exit. even in the case without swirl.

6.3. Momentum fluxes

It has proved valuable in modelling studies of swirling flows[19] to examine the fluxes of tangential and axial momentum. The present results for axial momentum flux are given in Fig. 9(*a*) and for tangential momentum flux in Fig. 9(*b*). For the former. the value shown is the dynamic component of the axial momentum. Theoretically the axial momentum flux should include a term representing the component due to differences in static pressure from the reference value. but in practice[3,19] it has been found more helpful to omit this term and base the flux solely on the dynamic component.

In both examples. the fluxes have been normalised by

(*continued on p 15*)

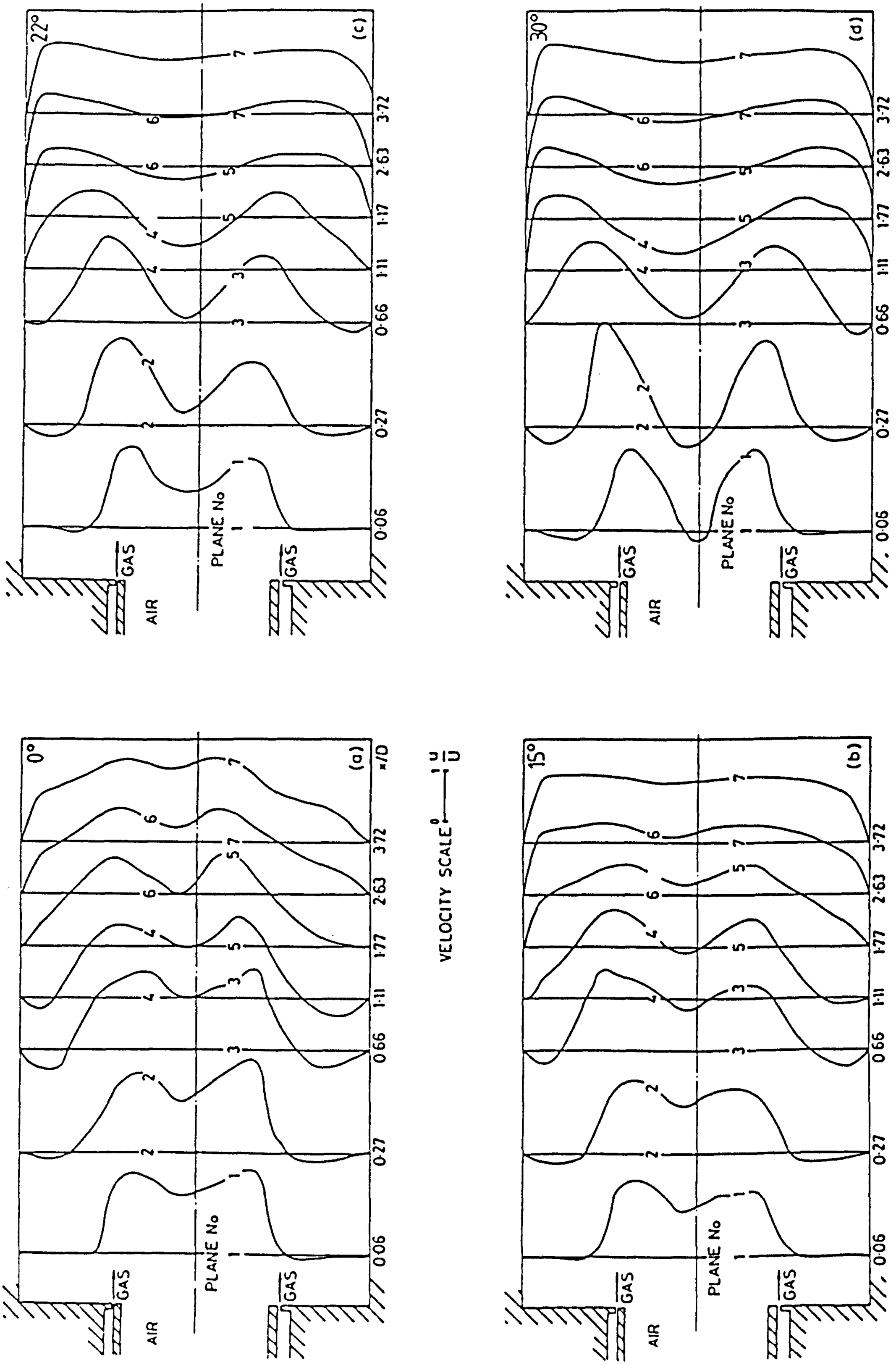

FIG. 11(a)(b)(c)(d). Axial velocity distributions

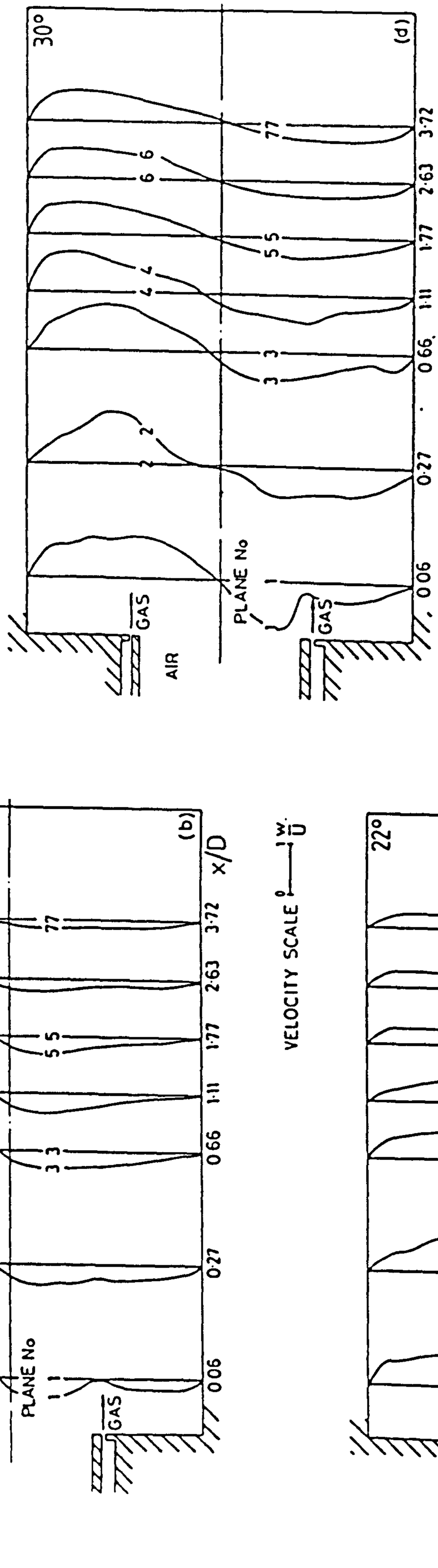

FIG. 3(b-d). Longitudinal velocity distributions

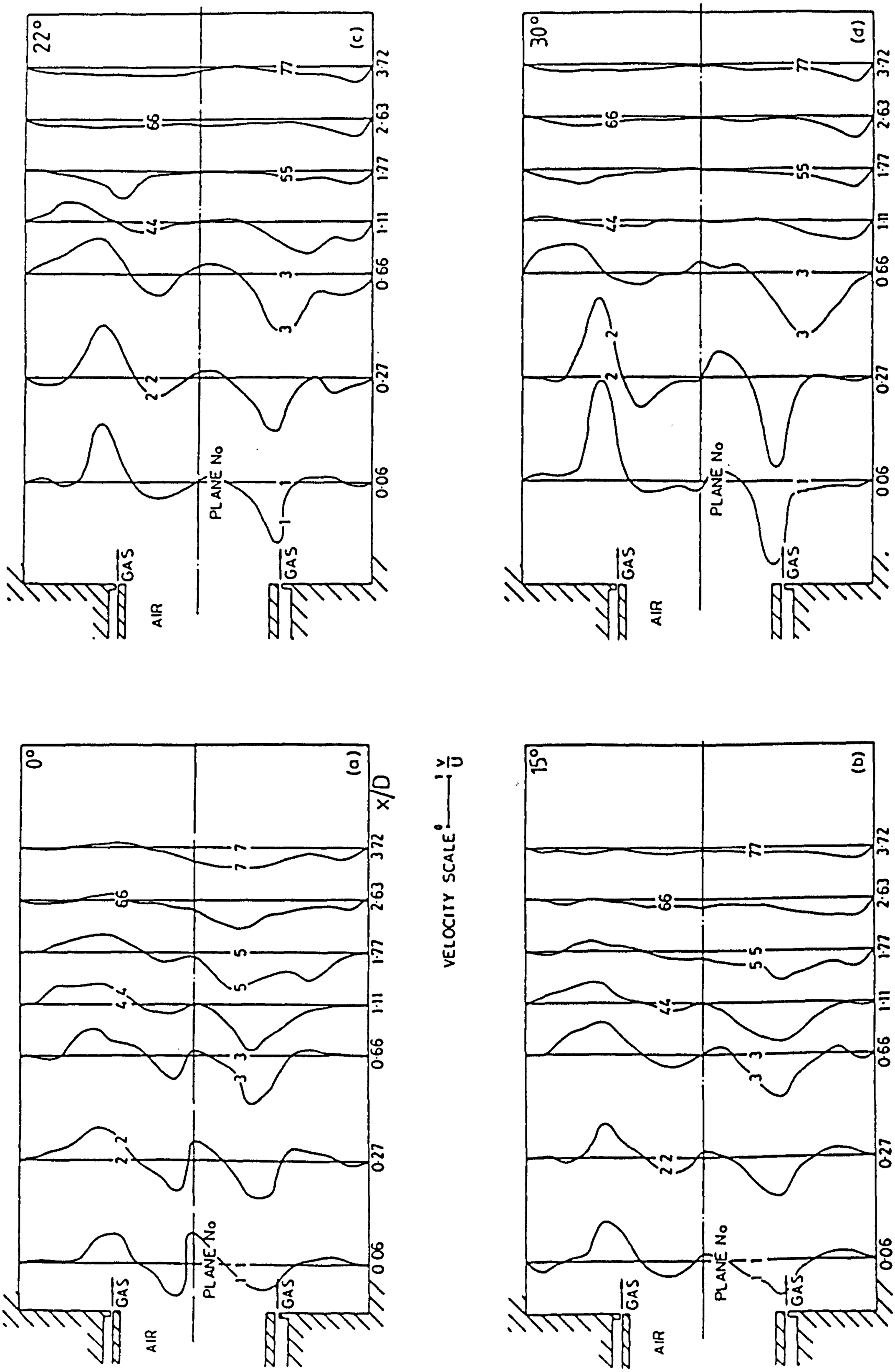

FIG. 5(a)(b)(c)(d) *Radial velocity distributions*

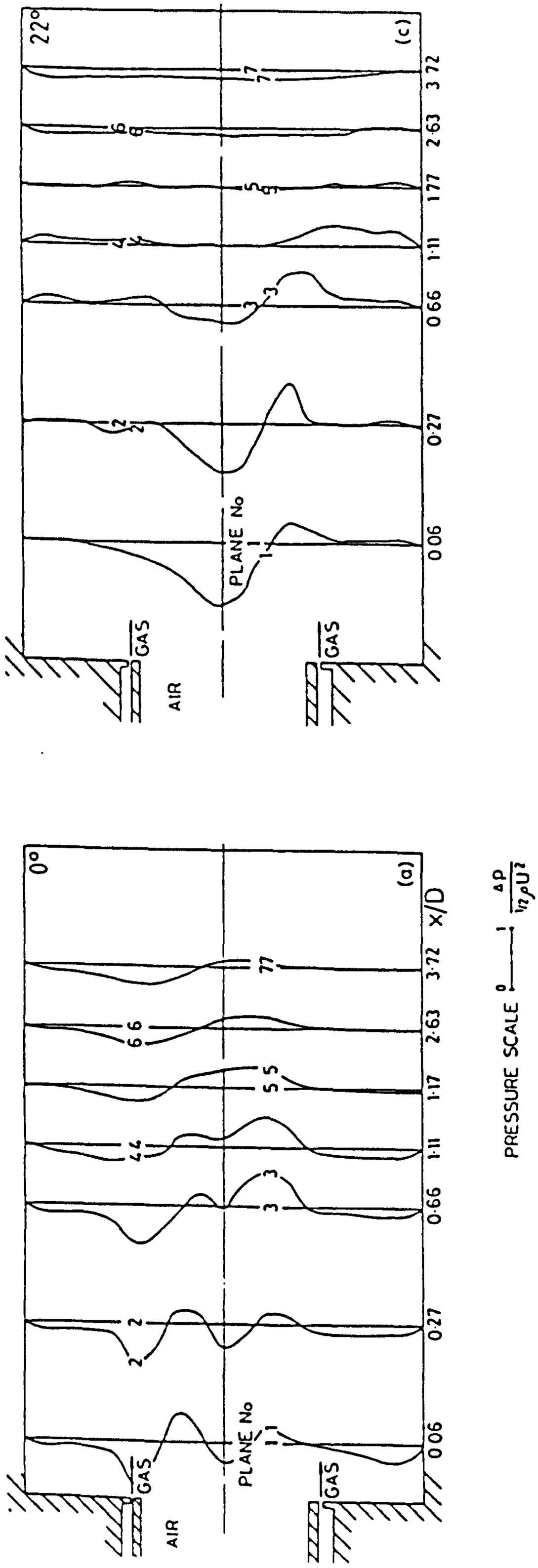

FIG. Surface and ... Static pressure distributions

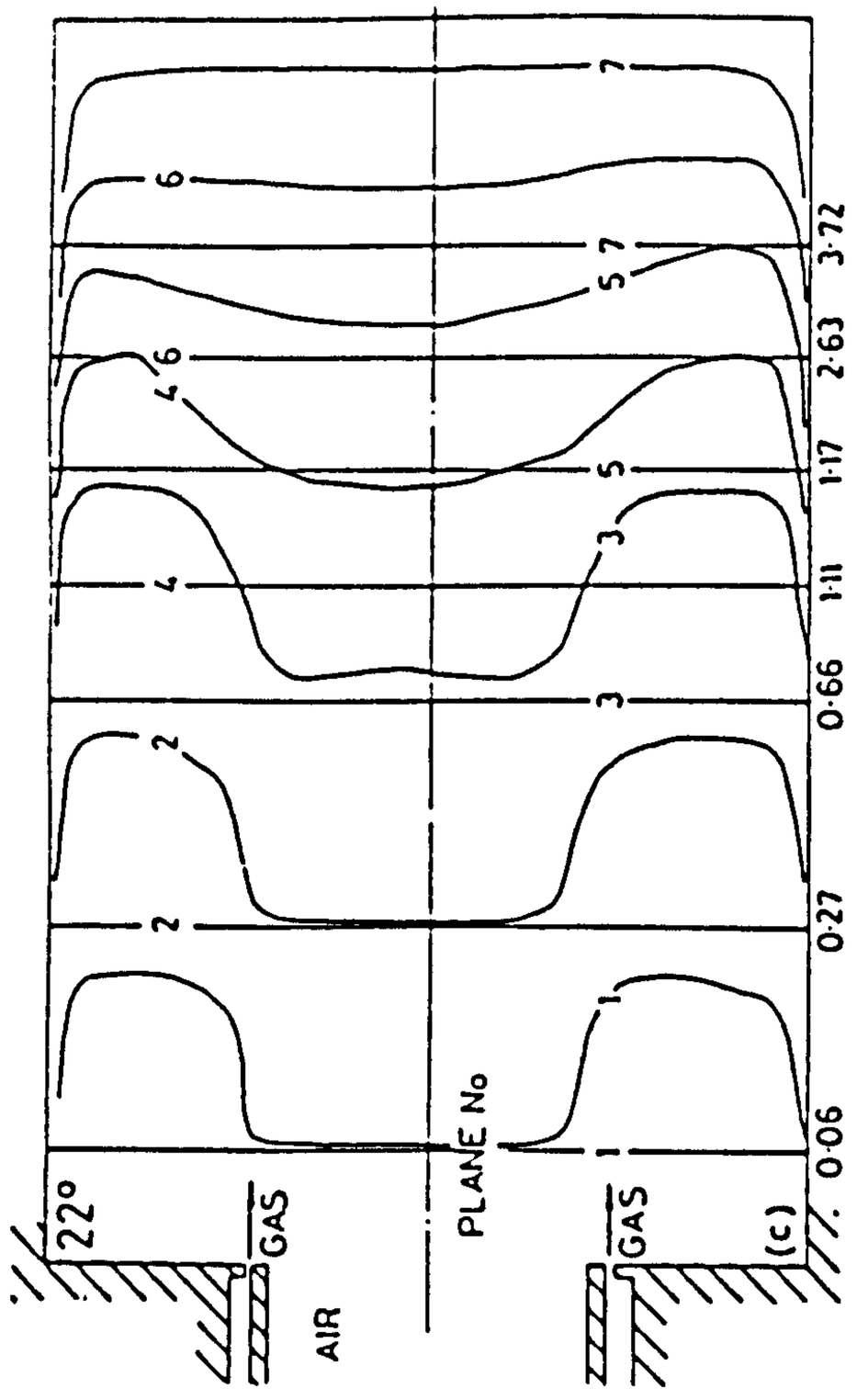

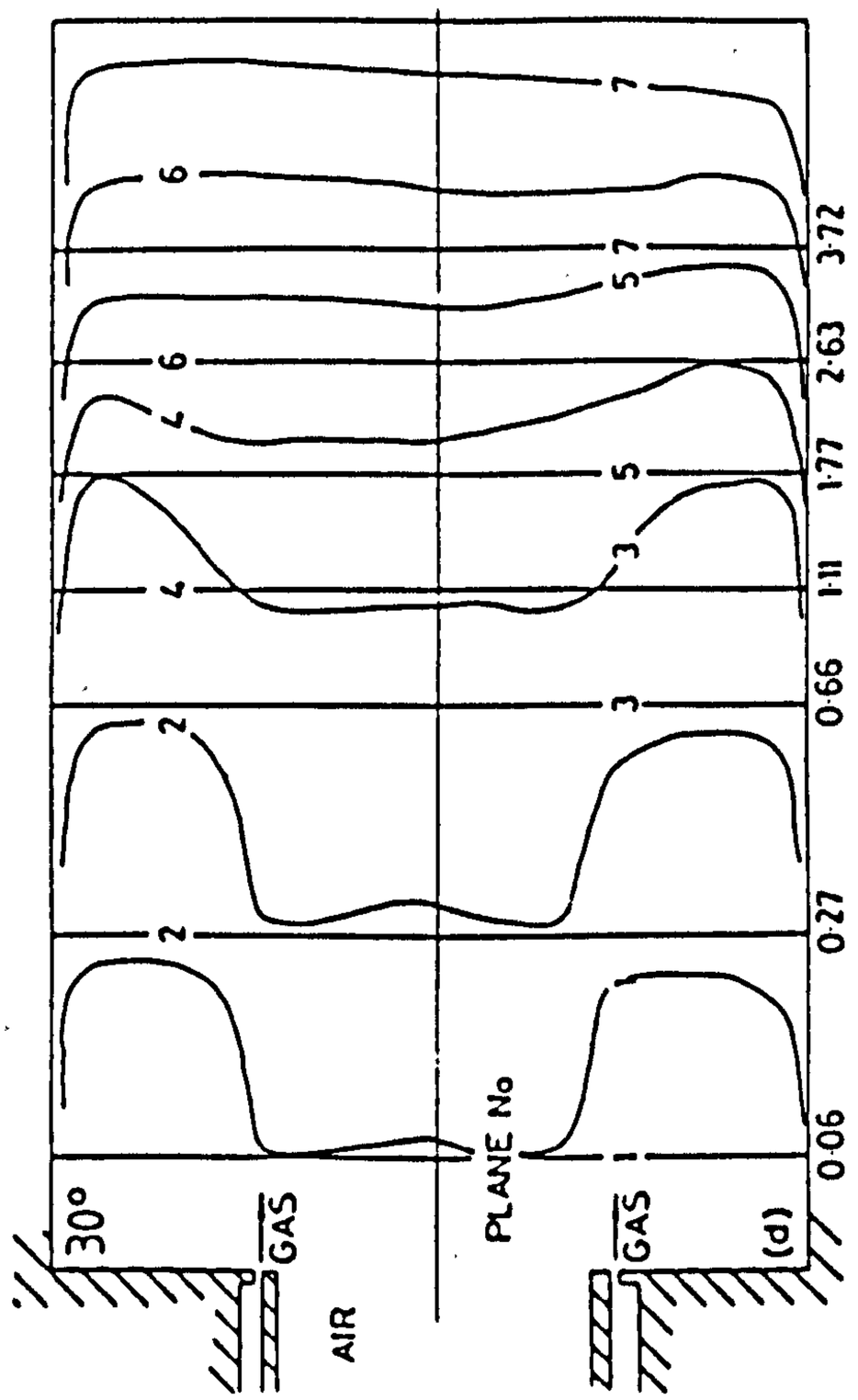

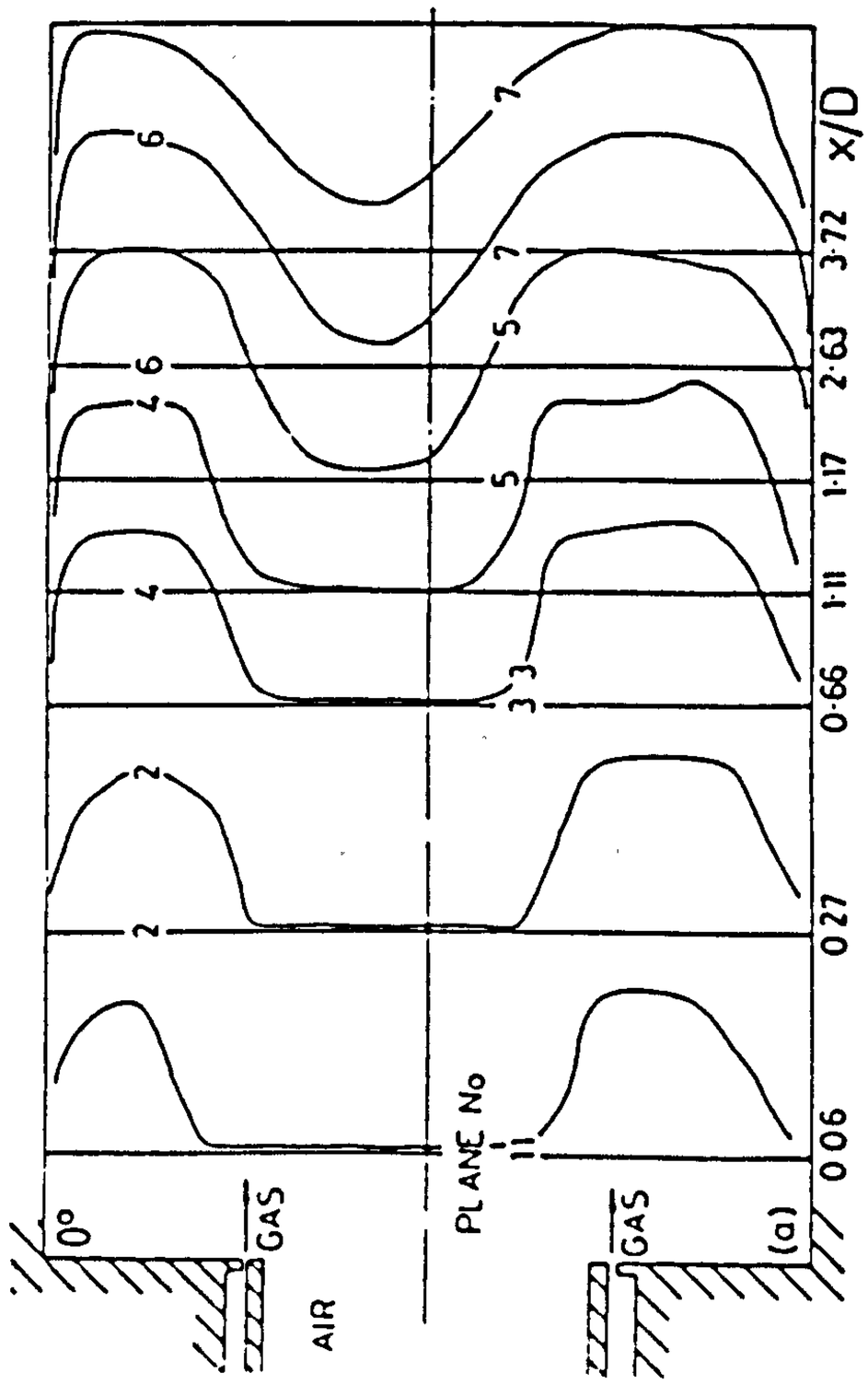

TEMPERATURE SCALE $\frac{0 \quad 0.5}{\Delta T_a}$

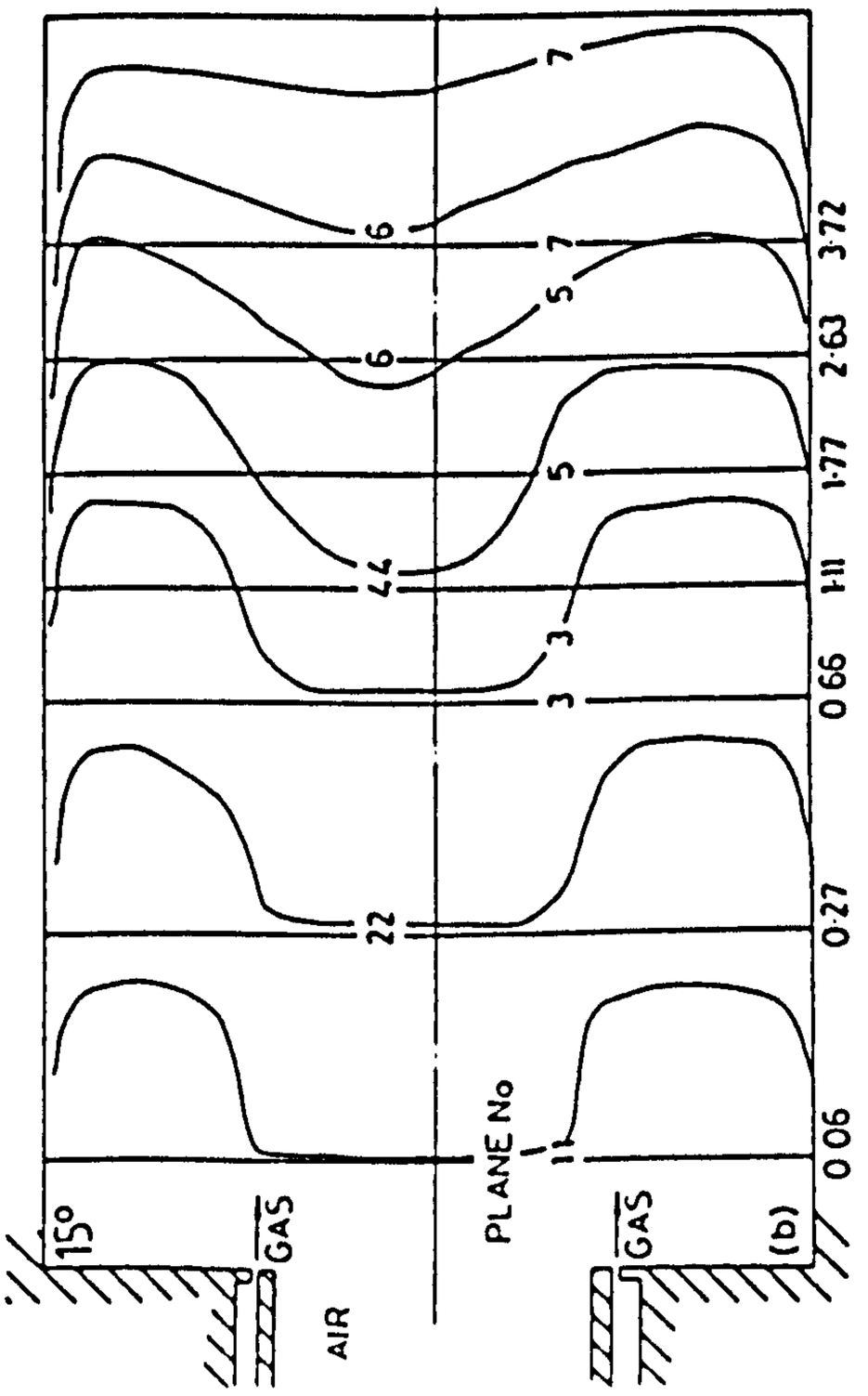

FIG. 5(a)(b)(c)(d) *Temperature rise distributions*

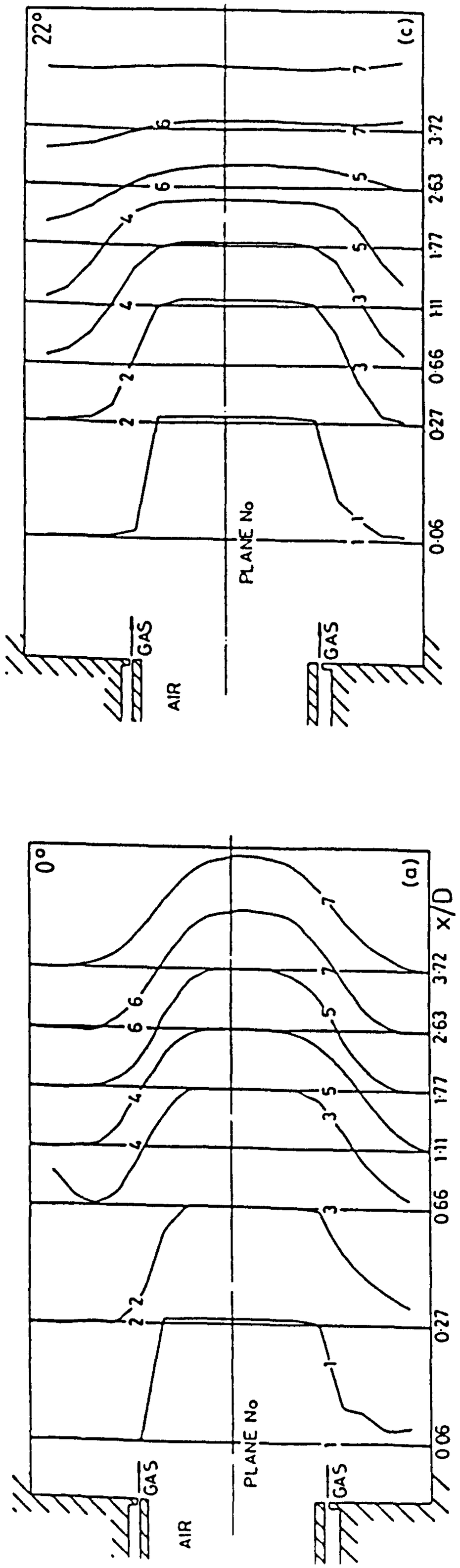

FIG. 6(a)–(d). Oxygen concentration distributions

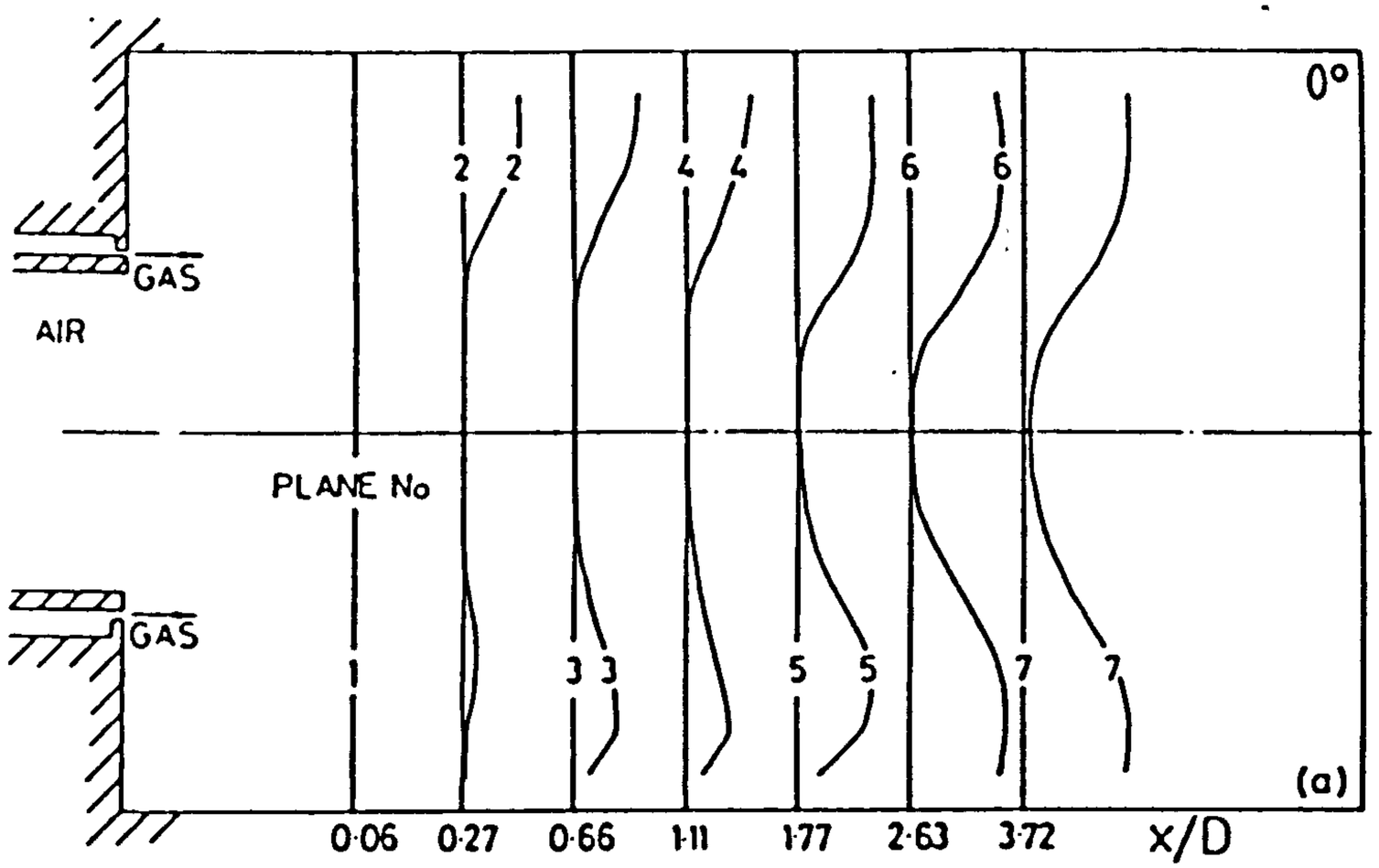

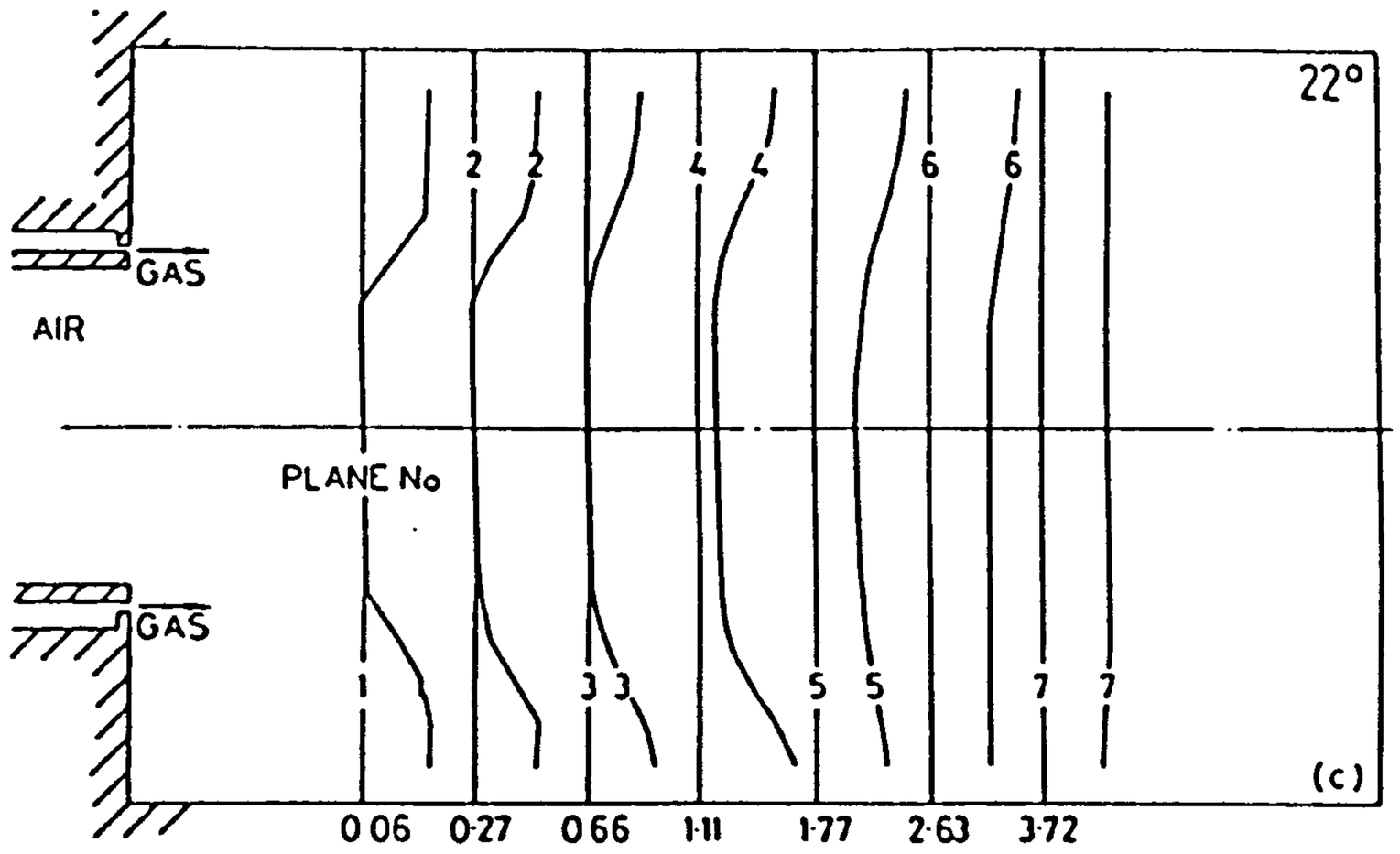

CONCENTRATION SCALE ⟵ 10%

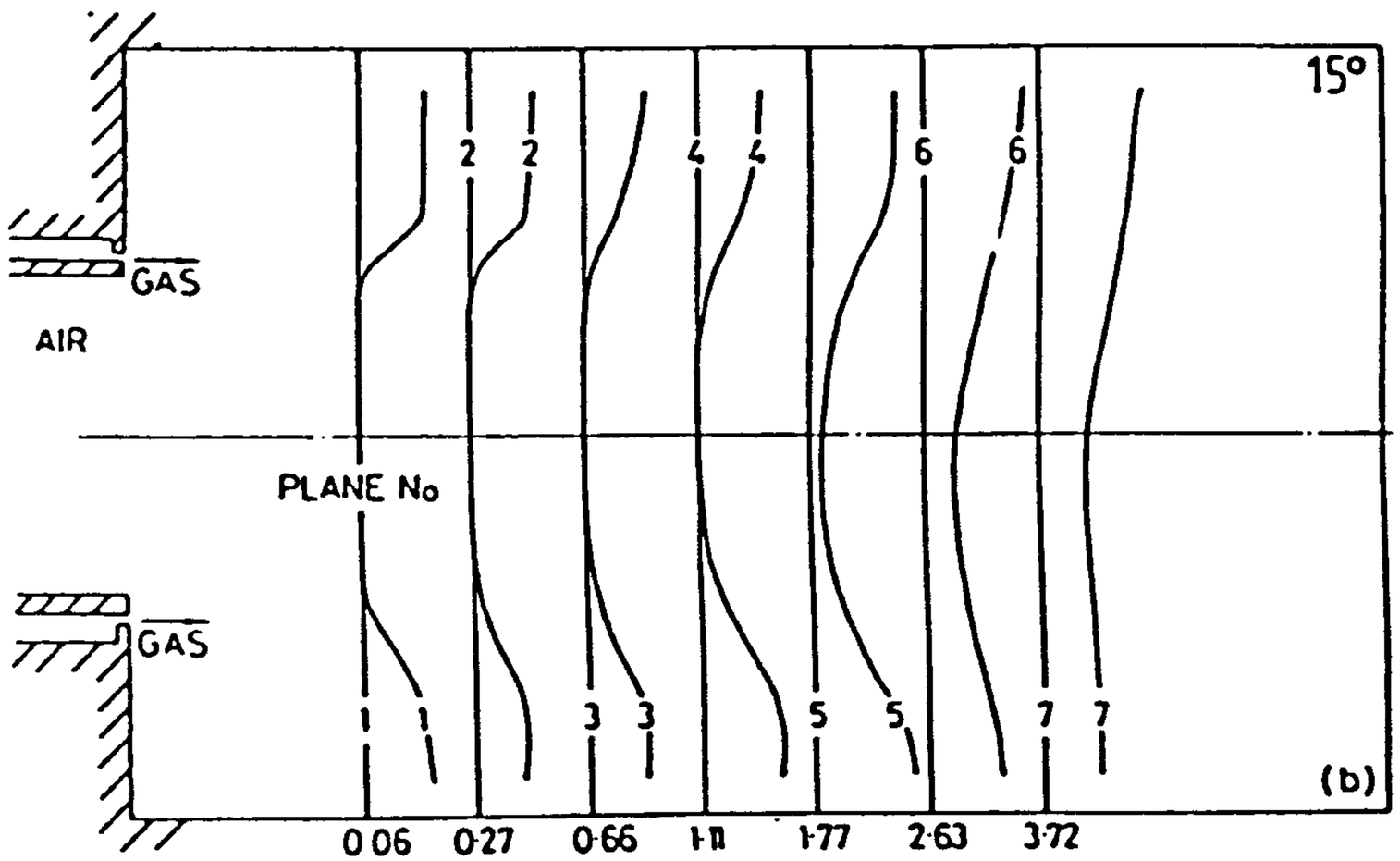

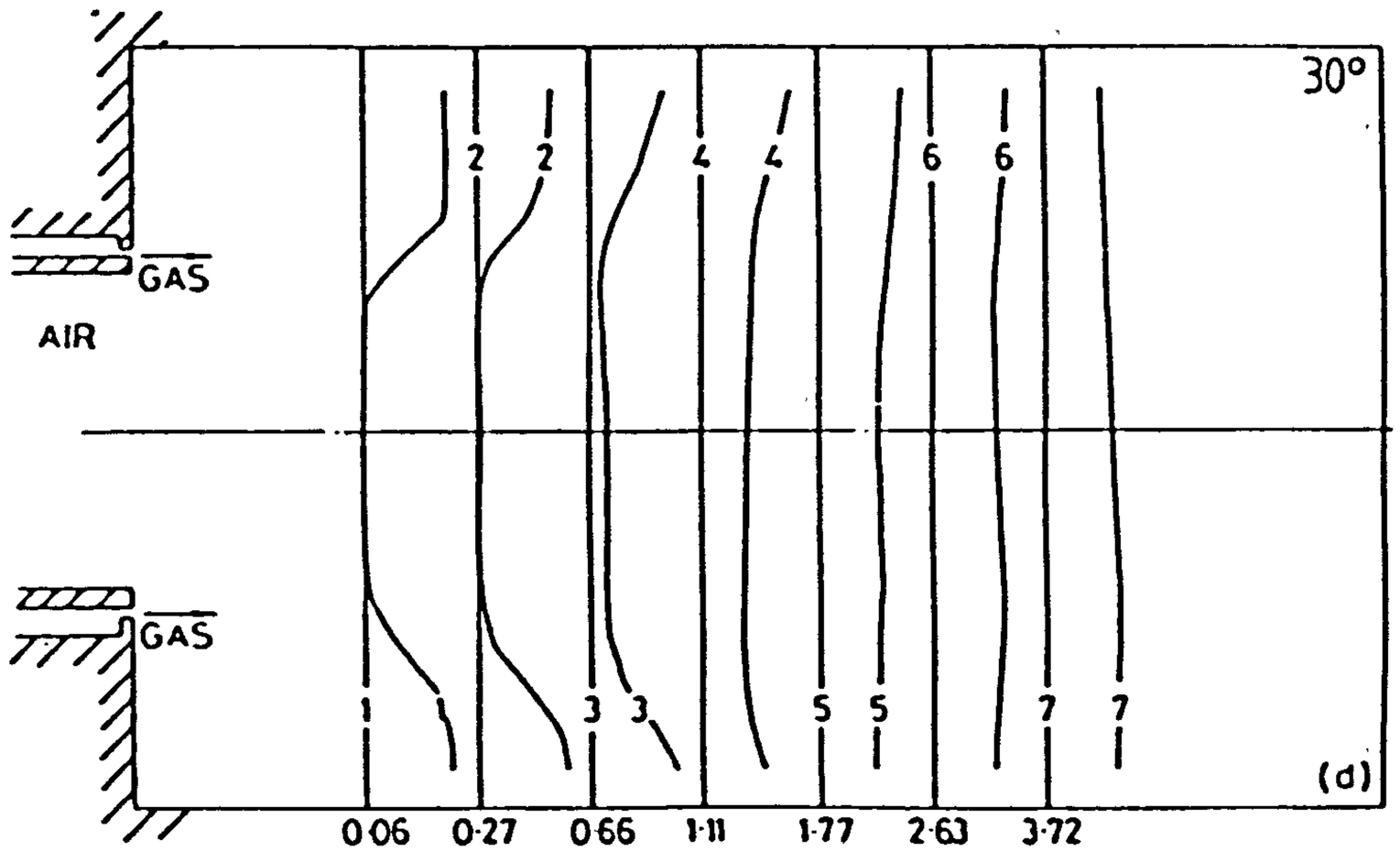

FIG. 7(a)(b)(c)(d) Carbon dioxide concentration distributions

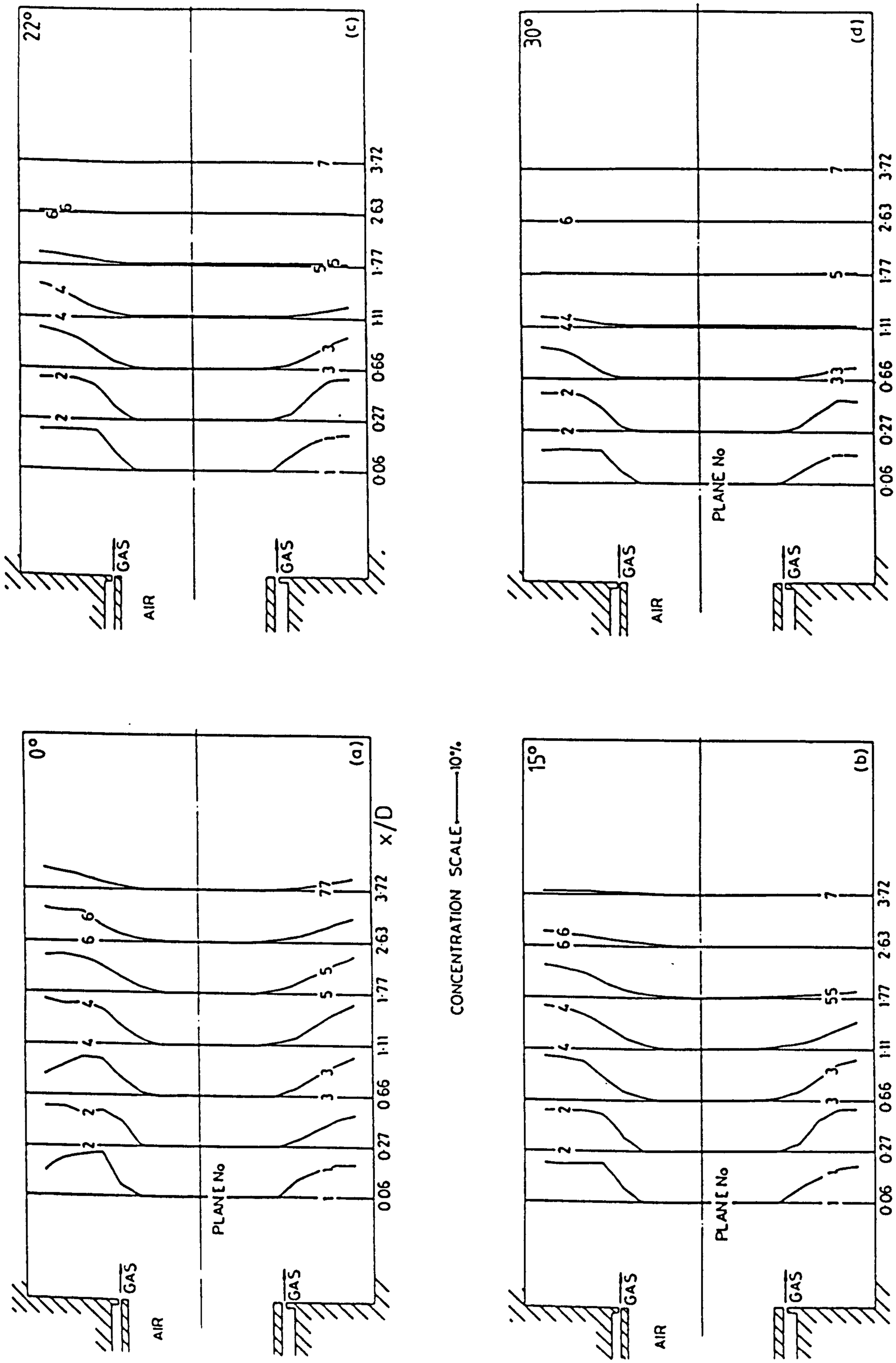

FIG. 8(a)(b)(c)(d) Carbon monoxide concentration distributions

(*continued from p 6*)

input momentum. and with the tangential flux the normalising group includes the term 'tan θ' as it has been shown[20] that the tangential momentum should be proportional to 'tan θ'.

In all cases the axial momentum flux shows an increase followed by a decay to a 'fully developed' value near the furnace exit. When the equivalence ratio is 0.53. the normalised fully developed flux value is about 1.2. at equivalence ratio 0.38 it is about 0.9 and in isothermal flow it is about 0.25. These changes are in line with the relative changes expected from the density ratios.

The tangential momentum fluxes also show initial increases followed by decay to a fully developed value. According to the law of conservation of momentum. this fully developed value should be unity in all cases. However. only with the 30° swirler is this value achieved. The lower values in the other cases are probably due to the lack of overlap of the vanes at these low inclinations to the axial direction.[15]

6.4. Swirl number

Burner swirl number has been defined by Kerr and Fraser[20] and for the hubless swirlers used in the present work this definition. based on burner diameter. becomes:

$$S = \tfrac{1}{3} \tan \theta$$

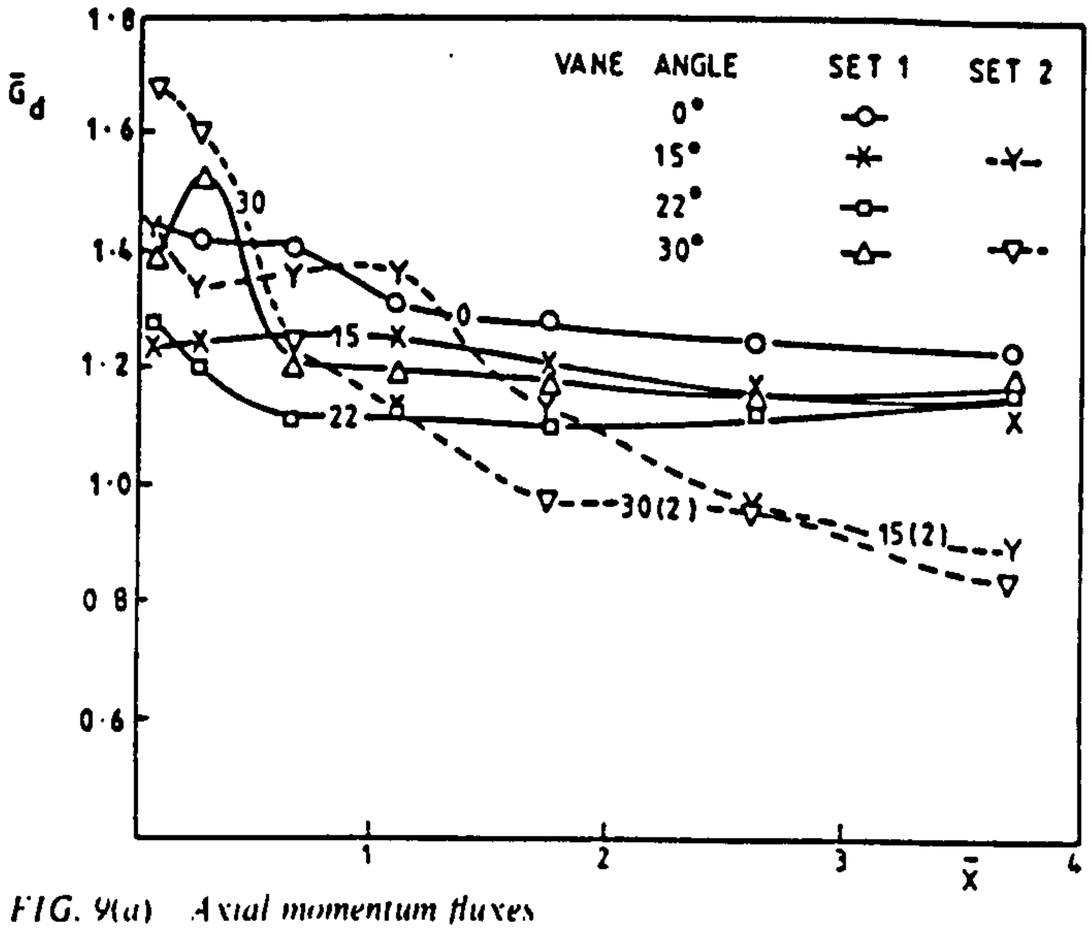

FIG. 9(a) Axial momentum fluxes

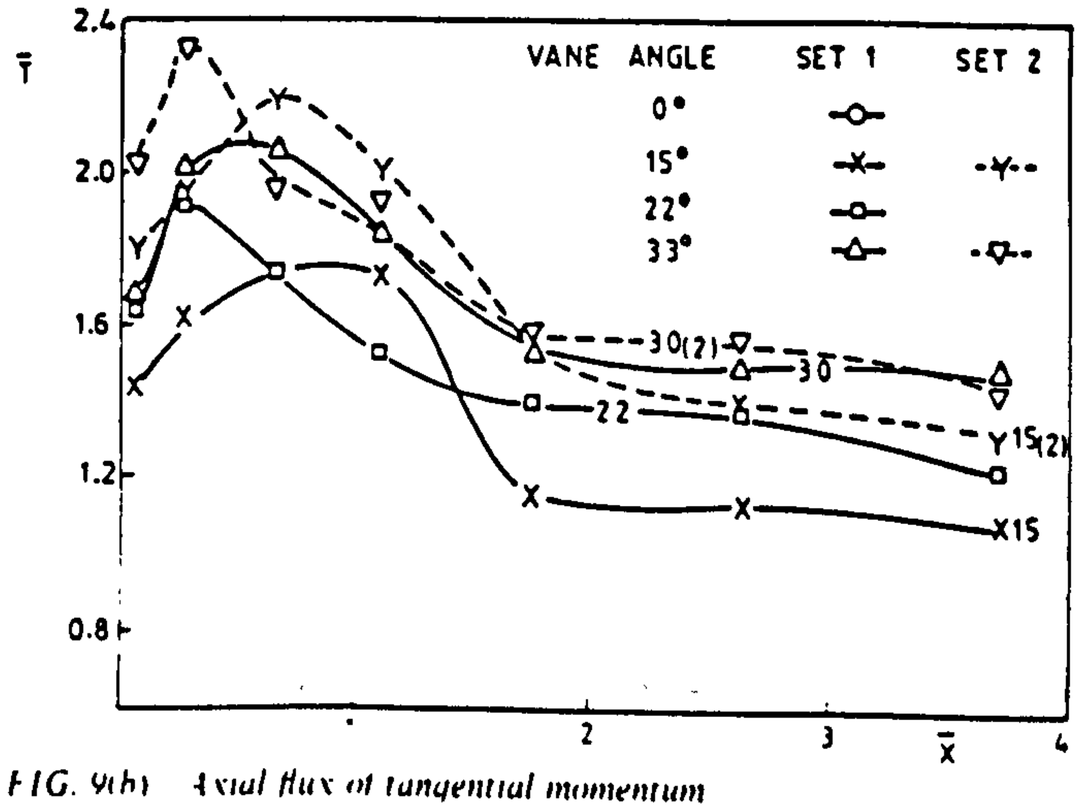

FIG. 9(b) Axial flux of tangential momentum

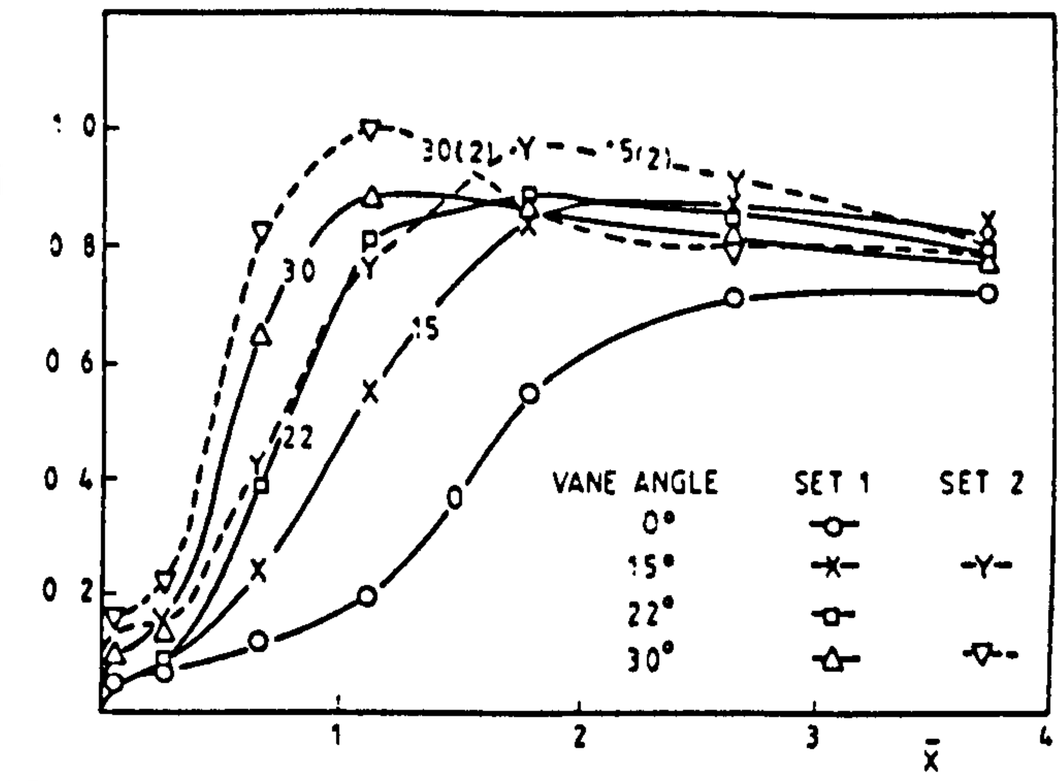

FIG. 10 Axial flux of sensible enthalpy

Subsequently a more representative furnace swirl number has been defined as[19]

$$S^* = T(GD)$$

where T and G are calculated from experimental velocity profiles in the fully developed region and D is the furnace diameter. Values of these swirl numbers relevant to the present tests are shown in Table 1.

The results show that combustion has the effect of reducing swirl number S^* progressively as the equivalence ratio is increased. This is in line with the observations in premixed flames, largely arising from the increase in the dynamic component of the axial momentum flux due to the higher axial velocities resulting from combustion. This lowering of the swirl number S^* is matched by a reduction in the conditions that create a central recirculation. For example, the CRZ observed in isothermal flow with the 22° swirler is suppressed when fuel is burned.

6.5. Degree of combustion

The average degree of completeness of combustion at a plane can be found from integrations of the axial velocity and temperature traverses. The results for the present work are shown in Fig. 10. where they have been normalised by the input energy. It is seen that as swirl is increased. this parameter increases more rapidly, indicating more intense combustion. The ideal maximum of this parameter—value unity—is reached only with the 30° swirler at the lower equivalence ratio (0.38). Because of the slower combustion in the other cases. there is a larger volume of flame gases from which heat will be lost before burnout is completed.

6.6. Comparison of peripheral with central fuel injection

Additional tests were carried out on similar air flow systems. but with central fuel injection.[18] The main differences for the system with peripheral fuel injection as compared with central fuel injection can be summarised as:

(i) The PRZ contains hot products as compared with cold flow.
(ii) The CRZ (if present) contains air as compared with hot products.

(iii) Combustion starts at the outer surface of the air jet, rather than at the centre.
(iv) If there is no swirl, the completeness of combustion at the furnace exit is about the same in both cases.
(v) With even weak swirl, the peripheral injection scheme gives much more rapid mixing and combustion, and more uniform temperatures at the furnace exit. For example, the completeness of combustion within the furnace with peripheral injection when the 15 swirler is used is similar to that obtained with the 30 swirler and central injection. The burner pressure loss is thus reduced to about one quarter, as compared with the furnace with central injection.

The features described above will aid the combustion of fuels that are more difficult to burn eg low calorific value gaseous fuels. For pulverised fuels, the rapid initial mixing will assist the complete combustion of the volatiles, while the effective stirring will help to burn the solids.

6.7. Future work

The work reported here is only an early step in the development of combustion systems with outer fuel injection. Much work has to be done. Some investigations that can be foreseen at this stage are: changes of design to alleviate the high temperature being near the furnace walls; fuel injection at a group of holes around an annulus instead of through a slit; the study of the effect of the ratio of fuel jet velocity to air jet velocity.

7. Conclusions

Flow and combustion patterns have been defined in a combustion system with peripheral injection of fuel gas. The patterns are defined by time-averaged measurements of velocity components, static pressure, temperature and species concentrations. These data sets can be used for the validation of prediction models.

Introducing a low degree of swirl in the air had the effect of reducing the flame length and the subsequent 'stirring' length. There were similar effects when the equivalence ratio was reduced.

The flow and flame processes were independent of Reynolds number, within the range examined: 6×10^4 to 9×10^4.

The axial fluxes of axial and tangential momenta showed initial rises followed by decays to the fully developed flow values. These values were functions of the input momentum and equivalence ratio and also, for the tangential momentum, of the swirler vane angle. A furnace swirl number based on these fluxes and on the furnace diameter can be used to predict the flow type and also as a modelling criterion for isothermal tests.

In comparison with central fuel injection systems, the peripheral injection systems with even weak swirl give much more rapid mixing and combustion, and uniform temperatures in shorter furnace lengths. Consequently, equivalent combustion performance can be achieved using significantly less swirl and thus much reduced fan power.

8. Acknowledgments

The authors wish to thank colleagues at the National Engineering Laboratory at the University of Glasgow for their advice and encouragement. Dr Beltagui also wishes to thank the British Council for the award of a Bursary in 1984.

9. References

1 MATHUR M L and MACCALLUM N R L. Swirling air jets issuing from vane swirlers. Part 1: free jets. Part 2: enclosed jets. *J Inst Fuel* (now *Energy*), 1967 (May), 40, 214–225; ibid 1967 (June), 40, 238–245.
2. BEÉR J M and CHIGIER N A. Combustion aerodynamics. Applied Science Publishers, London, 1972.
3. SYRED N and BEER J M. Combustion in swirling flow: A review. *Combust Flame*, 1974, 22, 143–201.
4. OWEN M J, GOLLDIN F C and MCLEAN W J. Temperature and species concentration measurements in a swirl-stabilised combustor. 17th symp (int) on *Combustion*, 1979, pp 363–374
5 SUZUKI T, MORIMOTO K, OTANI K, YAMAGATA T, ODAWARA R and FUKUDA T. Development of high efficiency burners with low NO_x emission. *J Inst Energy*, 1982 (Dec), 55, 212–215.
6 SUZUKI T, MORIMOTO K, OTANI K, YAMAGATA T, ODAWARA R and FUKUDA T. Heat transfer characteristics and practical applications of high efficiency, low NO_x emission burners. *J Inst Energy*, 1982 (Dec.), 55, 216–220.
7. GUPTA A K, BEÉR J M and SWITHENBANK J. Concentric multi-annular swirl burner: Stability limits and emission characteristics. 16th symp (int) on *Combustion*, 1977, pp 79–91.
8. VRANOS A, KNIGHT B A and ZABIELSKI M F. Centrifugal mixing: A comparison of temperature profiles in non-recirculating swirling and non-swirling flames. *Combust Flame*, 1982, 48, 109–119.
9. MARKOWSKI S J, LOHMANN R P and REILLY R S. The Vorbix burner—A new approach to gas turbine combustors. *Trans ASME, J Eng Power*, 1976, 98, 123–129
10. SHEKLETON J R. The CIVIC: A concept in vortex induced combustion for the Solar Gemini 10 kW gas turbine. *Trans ASME, J Eng Power*, 1981, 103, 34–42
11. SHEKLETON J R. The CIVIC: A concept in vortex induced combustion. Part 2. *Trans ASME, J Eng Power*, 1981, 103, 708–717.
12 AHMAD N T, ANDREWS G E, KOWKABI M and SHARIF S F. Centrifugal mixing forces in enclosed swirl flames. 20th symp (int) on *Combustion*, 1985, pp 259–267.
13. TAN H Y and MACCALLUM N R L. Combustion in rotating flows. Report, Dept Mechanical Engineering, University of Glasgow, 1983 (Feb).
14. GUPTA A K, SYRED N and BEÉR J M. A low-noise burner for swirl-stabilised natural gas flames. *J Inst Fuel* (now *Energy*), 1973 (Mar), 46, 119–123.
15. BELTAGUI S A and MACCALLUM N R L. Aerodynamics of vane-swirled flames in furnaces. *J Inst Fuel* (now *Energy*), 1976 (Dec), 49, 183–193.
16. GOULDIN F C, DEPSKY J S and LEE S-L. Velocity field characteristics of a swirling flow combustor. *AIAA J*, 1985, 23, 95–102.
17. RALSTON T and SYKES J. Velocity measurements of cold flows through a variable swirl burner at the National Engineering Laboratory. Communication to IFRF Members meeting, 1985.
18. BELTAGUI S A and MACCALLUM N R L. Characteristics of enclosed swirl flames with peripheral fuel injection. Report, Dept Mechanical Engineering, University of Glasgow, 1985 (Dec)
19 BELTAGUI S A and MACCALLUM N R L. The modelling of vane-swirled flames in furnaces. *J Inst Fuel* (now *Energy*), 1976 (Dec), 49, 193–200.
20. KERR N M and FRASER D. Swirl. Part I. Effect on axisymmetrical turbulent jets. *J Inst Fuel* (now *Energy*), 1965 (Dec), 38, 519–526.

(*Paper received January 1987*)

BRITISH FLAME DAYS CONFERENCE Publication 41

SEPT. 1988

THE EFFECT OF FUEL INJECTION MODES ON COMBUSTION OF SWIRLING FLOWS

S A Beltagui, N R L Maccallum and T Ralston

Glasgow University and The National Engineering Laboratory

SUMMARY

Two fuel injection modes are examined as alternatives to conventional central fuel injection in the axial direction. These alternatives are (a) introduction of the fuel around the periphery of the air jet, and (b) injection radially outwards from the central axis, across the entering air flow. The fuel used was natural gas.

It is seen that peripheral injection exploits the benefits of both shear-layer mixing and peripheral mixing. Thus it requires less swirl and less fan power than central fuel injection.

Radial fuel injection, when suitably designed, also shows good combustion performance without requiring high swirl.

1. LIST OF SYMBOLS

d	burner throat diameter
d_q	quarl exit diameter
D	furnace diameter
G	axial momentum flux, velocity component only
r	radius
S	swirl number, based on burner exit radius $= \frac{2T}{Gd}$ $= \frac{2}{3} \tan \Theta$ for hubless swirlers
T	axial flux of tangential momentum
x	axial distance
Θ	vane angle to axial direction

2. INTRODUCTION

One of the most important factors in the control of flame performance is the mixing of fuel and oxidant (air). The effectiveness of this mixing controls combustion intensity, stability, heat release and formation of pollutants[1].

The fuel can be thoroughly mixed with the air prior to entering the combustion chamber – the "pre–mix" configuration, or the mixing can occur within the combustion chamber itself – the "non–premix" configuration. Also, some combination of these two may be adopted.

In systems which are of the "non–premix" type, there are two physical processes that can be adopted to achieve mixing within the combustion chamber. These are respectively shear layer mixing and centrifugal mixing. Shear layer mixing is effectively utilised if the fuel is injected into the regions of maximum shear in the air stream. Centrifugal mixing effects can be utilised by swirling the flow and creating favourable density gradients within the flows of air, fuel and products.

In the present work, investigations have been made of "non–premix" combustion in furnaces using two types of swirl generator – axial vane and moving block – and also, in the former case, using two locations for fuel injection – on the axis and at the periphery of the air jet. Where fuel injection on the central axis was used, studies covered injection both in the axial and radial directions.

3. NON–PREMIX BURNERS – FUEL INJECTION MODES

The most common method of fuel injection is axially through the centre of the burner (Fig. 1(a)). Some dual fuel burners use spuds (Fig. 1(b)) located away from the centre to inject the gas fuel while the centre pipe carries the other fuel.

Fuel injection at the periphery of the entering air jet (Fig. 1(c)), as an alternative to central fuel injection, has been studied in the present work and it will be seen that this offers certain advantages of enhanced mixing.

Another variation from conventional central axial fuel injection is to inject the fuel radially from the central axis across the entering air jet (Fig. 1(d)). Burners of this type have been included also in the present study and they too have some attractive characteristics.

There are many possible practical configurations, which may be some form or combination of these alternatives. While it is obviously not possible to test all these configurations, it is considered that the results obtained on simple basic systems such as those reported here will provide a basis for predicting the performance of more complex configurations.

The present work has used gas as the fuel. Aerodynamics has a predominant influence on the combustion of all types of fuel. The present results, in which the aerodynamic parameters are defined, will also be of use to the designer of burner–furnace systems which are to use liquid or solid fuels.

4. PERIPHERAL FUEL INJECTION

Injection of the fuel around the outer periphery of the air jet makes use of the high shear zones around the air jet[2]. Further, if the air jet has been swirled, centrifugal buoyancy forces are set up which differ between the air, the fuel and the hot flame products. These will tend to move the cold air outwards and the hot flame products inwards. If the fuel is less dense than air, e.g. natural gas, then it too will tend to move inwards. Thus for the case of natural gas, injection of the fuel at the outer periphery of the swirled air jet leads to effective mixing. For the case of heavier than air fuels, such as propane/butane gas or liquids or solids, fuel injection in the outer regions of the air jet will still offer the advantages of rapid mixing in the high shear zones and the centrifugally enhanced mixing of outer flame gases and incoming cold charge.

Two burner–furnace arrangements employing peripheral, or outer fuel injection have been examined at Glasgow University as part of the present investigation. The fuel was natural gas. The first arrangement is illustrated in Fig. 2(b), the combustor in this case being parallel–walled i.e. there was no expansion of the main flow area at exit from the burner, the constant combustor inside diameter being 0.1m. Comparative tests were carried out in the same combustor but with a central fuel injection burner (Fig. 2(a)). The second burner–furnace configuration used a peripheral injection burner as shown in Fig. 1(c), firing into a refractory–lined furnace of inside diameter 0.23m. The burner air jet outer diameter is 0.093m so the furnace to burner diameter ratio was 2.5. The annular slit through which the fuel was introduced was 2mm wide, around the periphery of the air jet. Again, comparative tests were made with a burner using central fuel injection. In all cases, vane swirlers[3] were used to give a range of degrees of swirl to the entering air jet.

The tests included time–averaged velocity (3–dimensional), pressure and temperature traverses carried out at a range of planes in the furnace. Illustrations of the results are given in Figs. 3, 4 and 5.

The degrees of completeness of combustion achieved within the parallel–walled combustor are given in Fig. 3. In this case, at low equivalence ratios – less than 0.5 of stoichiometric – outer fuel injection offers no advantage over central fuel injection in so far as completeness of combustion is concerned. However at equivalence ratios greater than 0.6 the outer fuel injection arrangement gives very significant enhancements to the completeness of combustion.

Typical relative temperature contour results from the tests in the furnace, with diameter expansion ratio (D/d) of 2.5, are shown in Fig. 4 (central fuel injection) and Fig. 5 (peripheral fuel injection). Results are given for two of the degrees of air inlet swirl used – vane inclinations of 15^{o} and 30^{o} to the axial direction (Swirl Nos., S, of 0.18 and 0.385 respectively). The detailed tests were carried out only at one overall equivalence ratio – 0.53 – however observation of operation at the lower equivalence ratio of 0.38[2] did not indicate the deterioration in completeness of combustion seen in the parallel–walled combustor at low equivalence ratios (Fig. 3). In this expansion case, comparison of the fuel injection methods with the same degrees of air inlet swirl shows that peripheral injection leads to the general combustion of the fuel taking place much earlier. In the former cases there are much steeper temperature gradients close to the fuel injection location. Also, the more general combustion starts earlier in the former cases – for example, with the 15^{o} vane swirler and central injection it gets under way only after about 1.5 furnace diameters, whereas with peripheral injection it is

already well advanced at an axial distance of 1.0 x furnace diameter. Another benefit of peripheral fuel injection is that the temperature profiles following the completion of combustion are much more uniform. Increasing the degree of swirl given to the inlet air also helps to make these temperature profiles more uniform. It is seen that the change achieved in this direction by using the 30^{o} vane swirler as compared with the 15^{o} vane swirler is more marked in the peripheral injection system than in the system using central fuel injection.

It is important to note that when using gaseous fuel, successful combustion can be achieved without the necessity of establishing a central reverse-flow zone (CRZ) - the 30^{o} vane angle swirler in the inlet air does create a CRZ, whereas the 15^{o} vane swirler does not, yet combustion is stable in the latter case, and comparatively rapid when using peripheral injection.

5. RADIAL FUEL INJECTION

In applications where peripheral fuel injection is not practical or suitable, equivalent benefits may be achieved by injecting fuel radially outwards from the central axis of the burner and across the entering air flow. Comparisons between axial fuel injection and injection at a range of inclinations to the axis, leading to the radial, have been given by Leuckel and Fricker[4,5]. When properly designed, the radial fuel jets will interact with the main air flow producing or at least promoting the creation of a CRZ through aerodynamic blockage. This means that stability can be achieved with low, or even no swirl.

To study this system, tests have been carried out on a furnace, and its isothermal model, these facilities being situated at the National Engineering Laboratory (NEL). The aerodynamic effects of the fuel jets, particularly within the quarl and the near-chamber zone, were carefully examined in the isothermal model, emphasis being placed on the establishment of the CRZ. Measurements within the flame in the furnace confirmed these isothermal model results, and gave data on combustion parameters such as temperature and species concentration. Further details of these tests are now given.

5.1 The NEL Furnace

The NEL furnace is a watercooled upfired cylindrical furnace, Fig. 6, of 1m internal diameter and 3m high. The furnace is fired by natural gas through a moving block burner (IFRF), with 25^{o} half angle quarl of (d_q/d) ratio 1.8 Fig. 1(a). The fuel injector used is a central pipe with radial holes. Two injectors were investigated, both of 35 mm diameter and having 5 mm bore fuel nozzles. The number of these fuel jets was either 16, Injector I, or 8, Injector II. The injection plane coincides with the quarl throat. The isothermal model of the furnace system where the aerodynamic measurements were carried out constituted the full scale burner and quarl discharging into a chamber scaled according to the Thring-Newby criterion.

The velocity profiles within the quarl and chamber were measured using a 5-hole probe of 3mm tip diameter. Cases considered included main flow with no injector flow and main flow with either Injector I or Injector II operative. In each case five swirl settings were tested, Swirl Number, defined in List of Symbols, ranging from 0.0 to 4.0.

5.2 Isothermal Model – Experimental Results

In this work air was used in place of natural gas as the fluid which was injected. The flow rate of the injected air was matched to the main air flow to maintain the same ratio of "injected" fluid momentum to main air flow momentum as if firing on natural gas in the furnace.

A main aim was to measure axial components of velocity within the quarl and in the near–burner area. This would give definition of the existence, or otherwise, of a possible CRZ in this location. It was found that both degree of swirl and manner of fuel gas injection affected the creation of the CRZ. For example, the use of Injector I – with 16 jets – led to the establishment of a CRZ starting in the quarl, even with no swirl in the inlet air flow. However in the corresponding non–swirl case with Injector II there was no CRZ. As typical of the results, profiles of the axial component of velocity within the quarl are given in Fig. 7 for this case of Injector I with zero inlet swirl. This shows a distinct CRZ within the quarl, the diameter of the CRZ extending near the exit to about 0.6 of the local quarl diameter. The reason for the ability of Injector I to create a CRZ, whereas Injector II does not is thought to be that Injector I has 16 jets and therefore closer inter–jet spacing whereas Injector II has only 8 jets. It should be noted that in these tests Injector II will give the jets double the outward radial velocity, and momentum, than in the case of Injector I, the ratios of radial velocity of the "fuel" to the axial component of velocity of the air flow being about 4 with Injector II and 1 with Injector I. It is possible that the velocity ratio of 4 is excessive and causes the "fuel" to penetrate to the outer wall of the annulus with insufficient interaction and mixing with the air flow. It is concluded that the geometry of the fuel jet system is more important in controlling mixing than fuel jet momentum.

A representation of the CRZ boundary observations is given in Fig. 8(a) for Injector I and Fig. 8(b) for Injector II, the boundaries being illustrated for a range of inlet swirls. It is seen that when swirl is introduced at the Swirl Number, S, level of 0.45, use of Injector I still gives a slightly more pronounced CRZ. However at the highest swirl levels (S = 2.25) the CRZ's within the quarl look to be very similar but in the furnace itself the use of Injector II gives the stronger CRZ. It is to be noted that in both cases at this high swirl the CRZ in the furnace extends downstream to beyond the furnace exit.

To summarise, the results of the aerodynamic measurements indicate that at low swirl, the aerodynamic effect of the fuel jets is predominant, whereas at high swirl, centrifugal effects take over. The main feature observed is that the creation of a CRZ depends on the interaction of the fuel jets with the main air flow. This interaction is a function of the velocity ratio, fuel jet spacing and jet direction relative to the air jet.

More detailed presentation of the results from these tests, including velocity and pressure profiles, is given by Beltagui et al [6,7].

5.3 Furnace Results

The observations include temperature, concentration and velocity profiles for conditions using Injector I. Four swirl settings were selected, Swirl Number, S, ranging from 0.0 to 2.25. A fixed firing rate of 400 kW was used, with 5% excess air (equivalence ratio 0.95).

The aerodynamic measurements within the flame indicate the existance of the CRZ at all the swirl settings tested. The CRZ boundaries are illustrated in Fig. 9.

While the maximum diameter of this zone is almost the same for all cases, the length increases from 0.15 m to 0.26 m as Swirl Number, S, is raised from zero to 2.25. It is to be noted that at the highest swirl setting (S = 2.25) the CRZ has a finite length of approximately 0.26 furnace diameters in this flame case, whereas in the isothermal condition the CRZ extended to beyond the furnace exit (Fig. 8(a)). This closing of the CRZ is a commonly observed effect of the introduction of combustion. It is interesting, in comparing the results obtained in the furnace (Fig. 9) and those obtained in its isothermal model (Fig. 8(a) and (b)) to consider if the dimensions of the CRZ are functions of the furnace diameter, D, or alternatively of the burner diameter, taken in this case as the quarl exit diameter. It had been found in cases of strong swirl – vane angles of 45^{o} and 60^{o} – with pre–mixed flows, that the CRZ dimensions of maximum diameter and length were proportional to the furnace diameter[8]. In these cases the CRZ cross–section represented a large fraction of the furnace cross–section, its maximum diameter being about 65% of the furnace diameter. However in the present work swirl levels are lower and the maximum diameter of the CRZ is small compared to the furnace diameter – 14% in the combustion case and 28% in the isothermal model. It would appear in this case of lower swirl and less confined flow that the CRZ dimensions are controlled by the burner size and flow conditions.

A typical relative temperature distribution is shown in Fig. 10, this representing the results with zero swirl and using Injector I.

When swirl is then introduced, combustion is completed earlier in the furnace and the temperature gradients in the near burner zone become much steeper. More complete results describing these effects will be published shortly.

6. CONCLUSIONS

For non–premix furnace combustion systems it can be advantageous to introduce the fuel in a way other than the conventional one of axially at the centre of the air inlet jet. Two alternatives have been examined – injection around the periphery of the air jet and injection radially outwards from the central axis across the entering air jet.

Peripheral fuel injection, particularly when coupled with swirl, exploits the benefits of both shear–layer and centrifugal mixing. Thus less swirl is required, and less fan power, to produce the same degree of mixing and combustion rate as in a central injection system.

When radial fuel injection is used, the fuel jets interact better with the air flow than axial fuel jets. The geometry of the Injector is significant. For example an Injector having sixteen fuel jets, with velocity ratio of 2 relative to the air velocity is preferable to one having eight jets at velocity ratio of 4. The former arrangement, by producing aerodynamic blockage, causes a central recirculation zone to be established, even without giving swirl to the air flow. Again, this will lead to a reduction in the fan power required.

7. ACKNOWLEDGEMENT

Part of this work was carried out under the research programme of the Heat Transfer and Fluid Flow Service (HTFS) and was supported by the Department of Trade and Industry. This Paper is Crown Copyright.

8. REFERENCES

1. Gupta, A.K., Lilley, D.G. and Syred, N. Swirl Flows. Abbacus Press, 1984.

2. Beltagui, S.A. and Maccallum, N.R.L. Characteristics of enclosed swirl flames with peripheral fuel injection. J. Inst Energy, 1988 (March), 61, 3–16.

3. Mathur, M.L. and Maccallum, N.R.L. Swirling air jets issuing from vane swirlers: Part 1 Free Jets. J. Inst Fuel (now Energy), 1967 (June), 40, 214–224.

4. Leuckel, W. and Fricker, N. The characteristics of swirl–stabilized natural gas flames, Part 1: Different flame types and their relation to flow and mixing patterns. J. Inst Fuel (now Energy), 1976 (June), 49, 103–112.

5. Fricker, N. and Leuckel, W. The characteristics of swirl–stabilized natural gas flames, Part 3: . The effect of swirl and burner mouth geometry on flame stability. J. Inst Fuel (now Energy), 1976 (June), 49, 152–158.

6. Beltagui, S.A., Fuggle, R.N. and Ralston, T. Aerodynamics and mixing within the quarl of a variable–swirl burner. 1st European Conference on Industrial Furnaces and Boilers, 1988 (March), Lisbon, Portugal.

7. Beltagui, S.A., Fuggle, R.N. and Ralston, T. An isothermal study of the aerodynamics of the flow issuing from a variable–swirl burner. 1st World Conference on Experimental Heat Transfer, Fluid Mechanics and Thermodynamics, 1988 (Sept.), Dubrovnik, Yugoslavia.

8. Beltagui, S.A., and Maccallum, N.R.L. Aerodynamics of vane–swirled flames in furnaces. J. Inst Fuel (now Energy), 1976 (Dec), 49, 183–193.

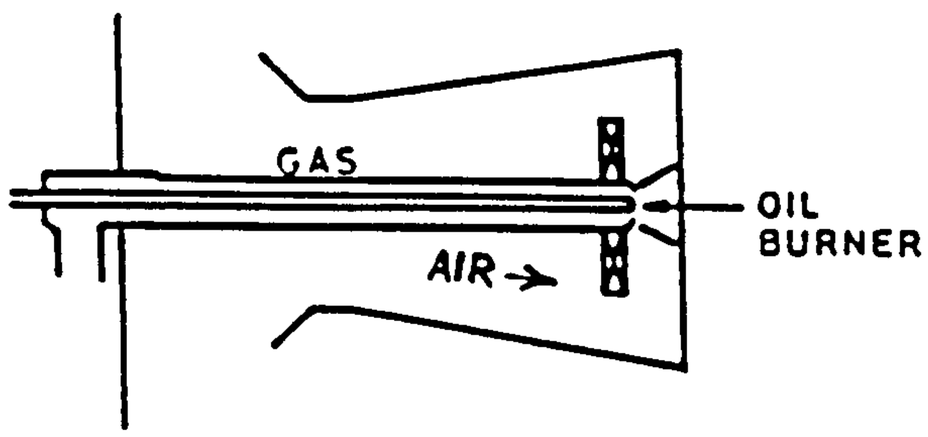

(a) Central fuel injection

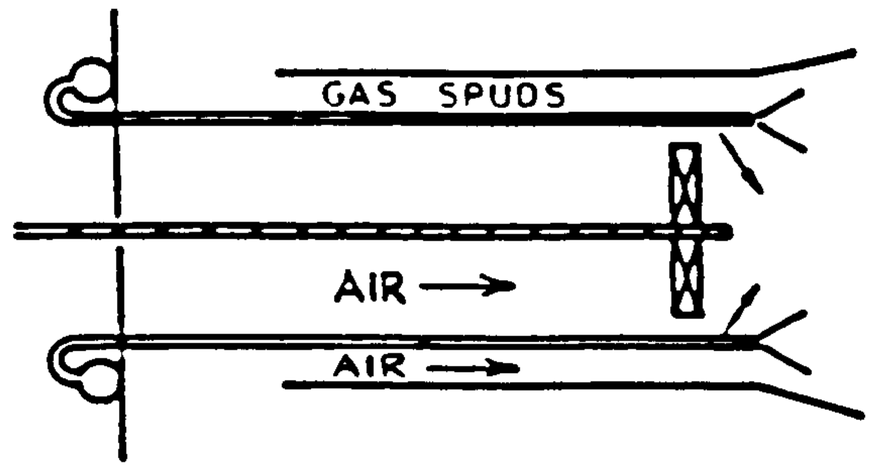

(b) Annular fuel injection

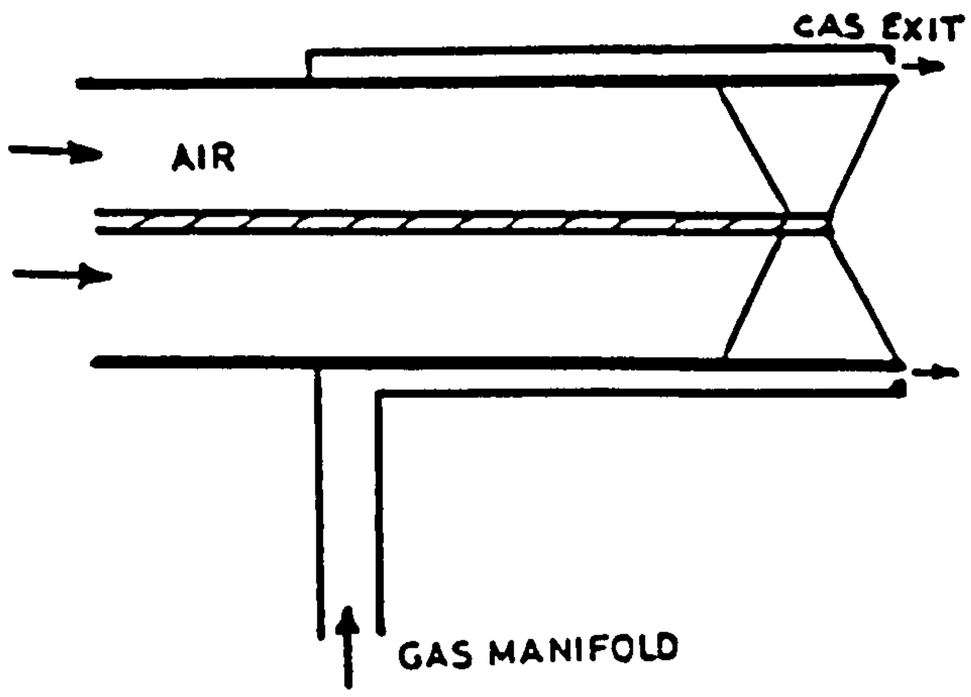

(c) Peripheral fuel injection

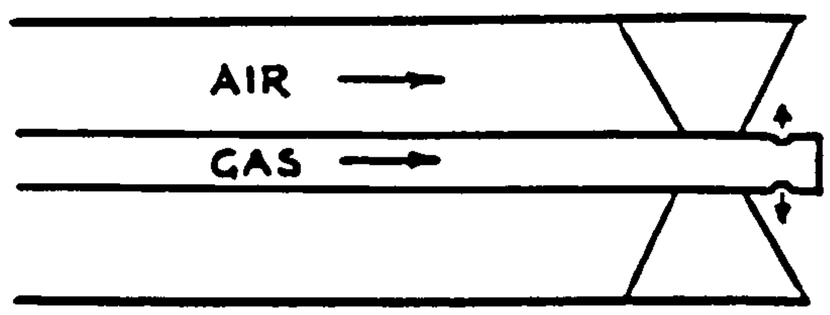

(d) Radial Fuel Injection

Fig. 1 BURNER ARRANGEMENTS (FURNACES NOT SHOWN)

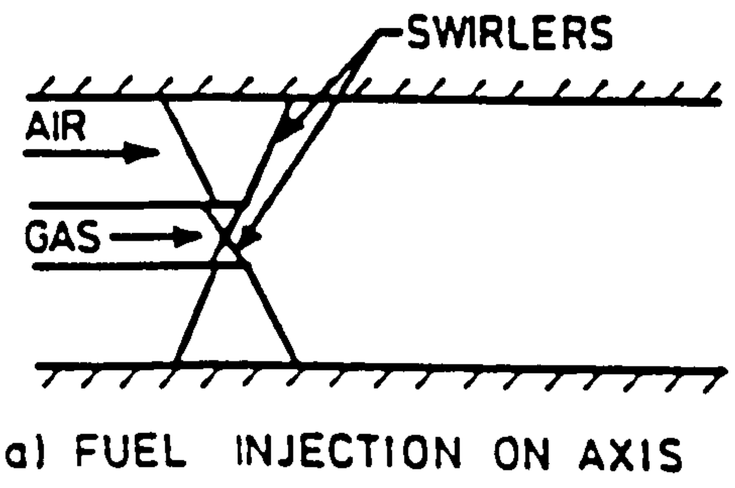

(a) FUEL INJECTION ON AXIS

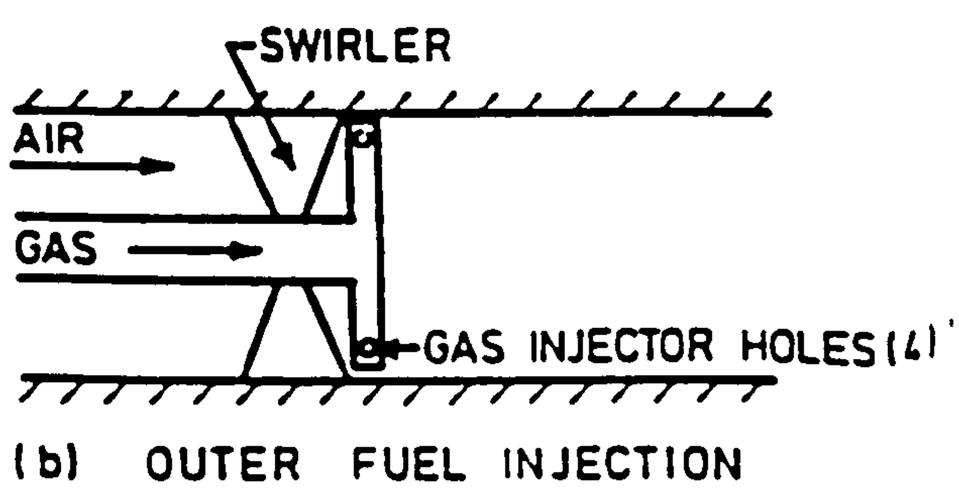

(b) OUTER FUEL INJECTION

Fig. 2 PARALLEL-WALLED COMBUSTOR-BURNER ARRANGEMENTS

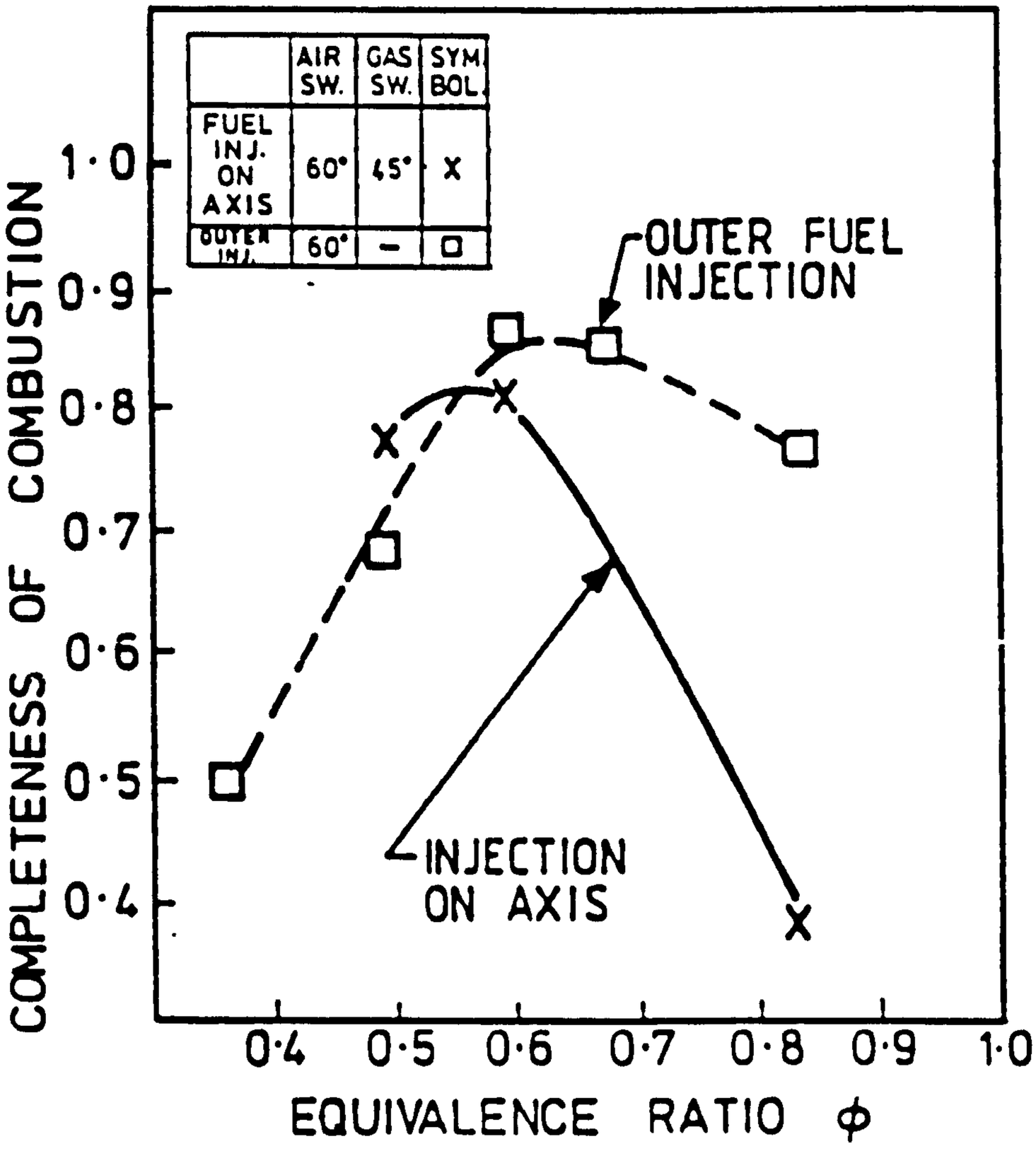

Fig. 3 COMPLETENESS of COMBUSTION:- AXIS and OUTER FUEL INJECTION COMPARED

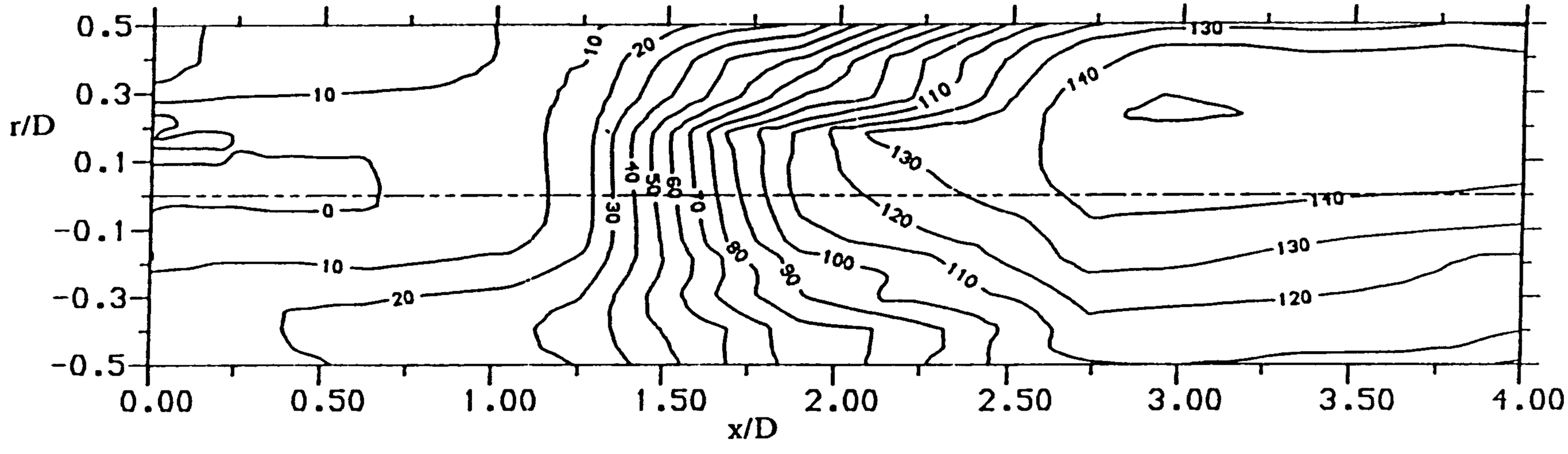

Fig. 4(a) TEMPERATURE CONTOURS FOR GLASGOW FURNACE D/d = 2.5 CENT. INJEC. 15 deg SW

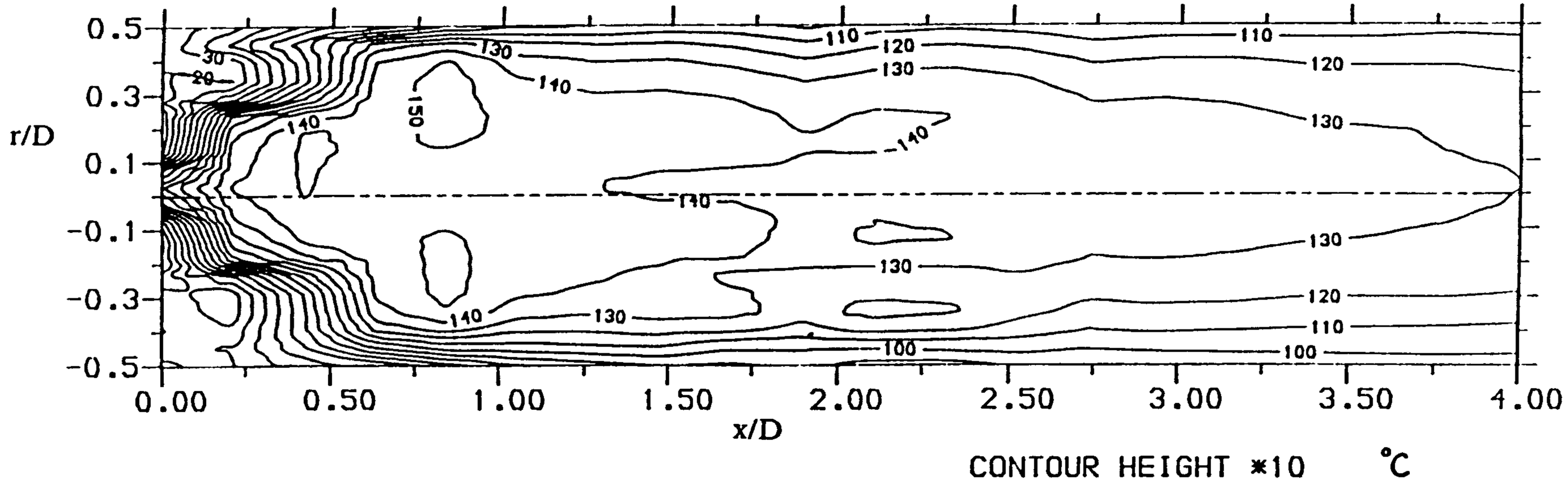

Fig. 4(b) TEMPERATURE CONTOURS FOR GLASGOW FURNACE D/d = 2.5 CENT. INJEC. 30 deg SW

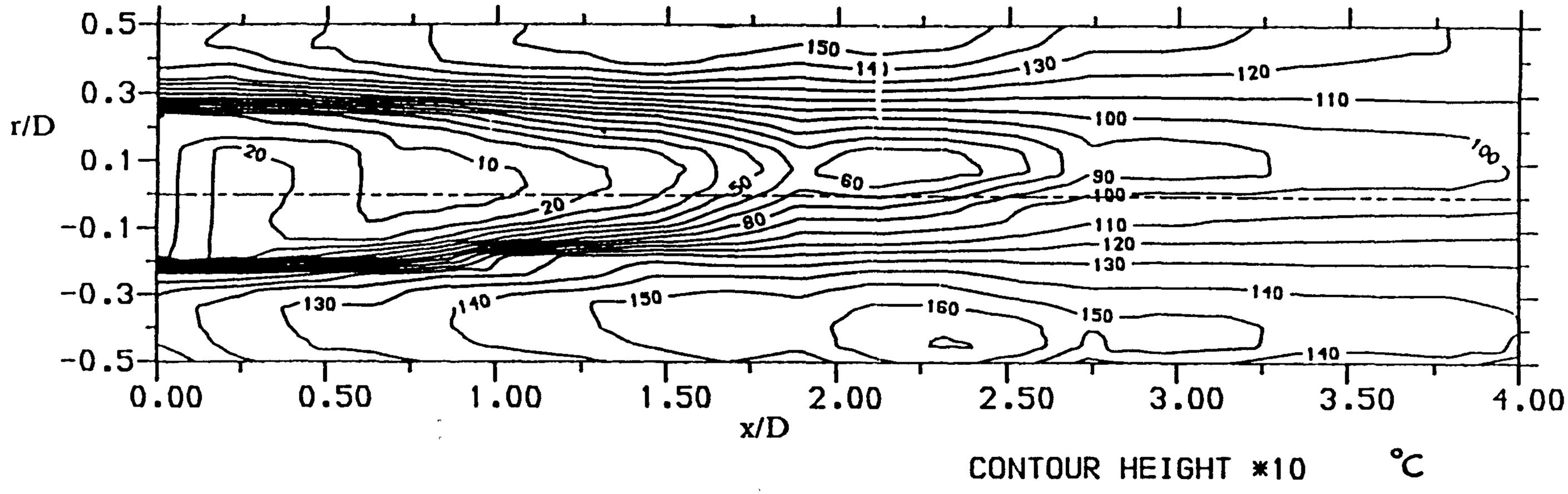

Fig. 5(a) TEMPERATURE CONTOURS FOR GLASGOW FURNACE D/d = 2.5 PERIPH INJECTION 15 deg SW

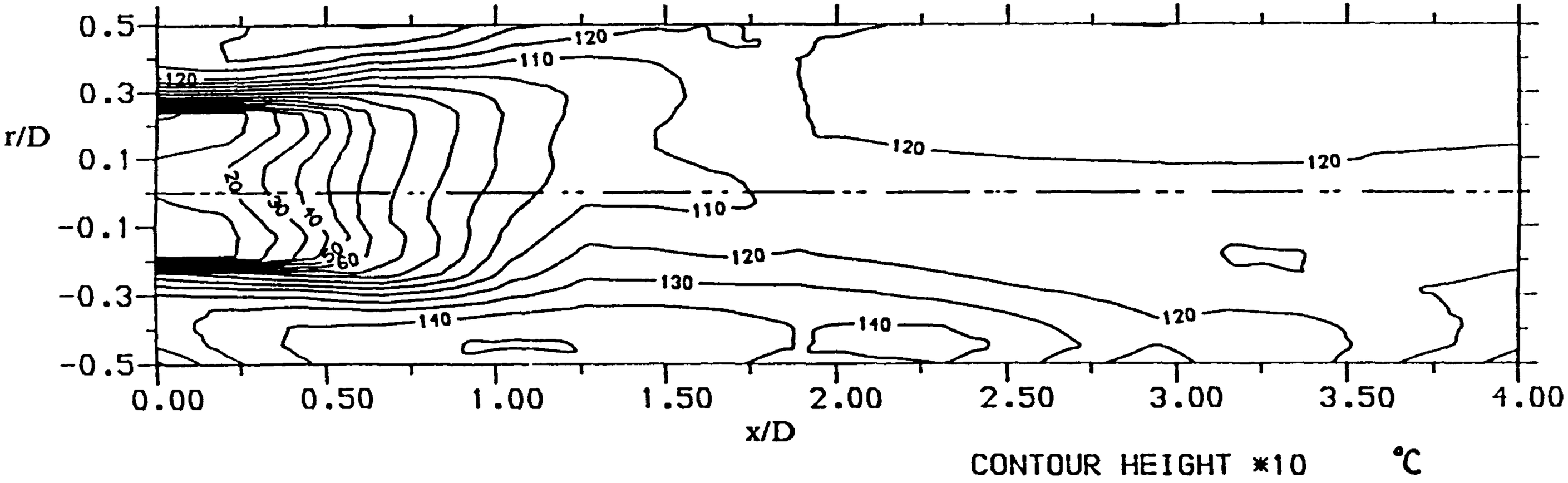

Fig. 5(b) TEMPERATURE CONTOURS FOR GLASGOW FURNACE D/d = 2.5 PERIPH INJECTION 30 deg SW

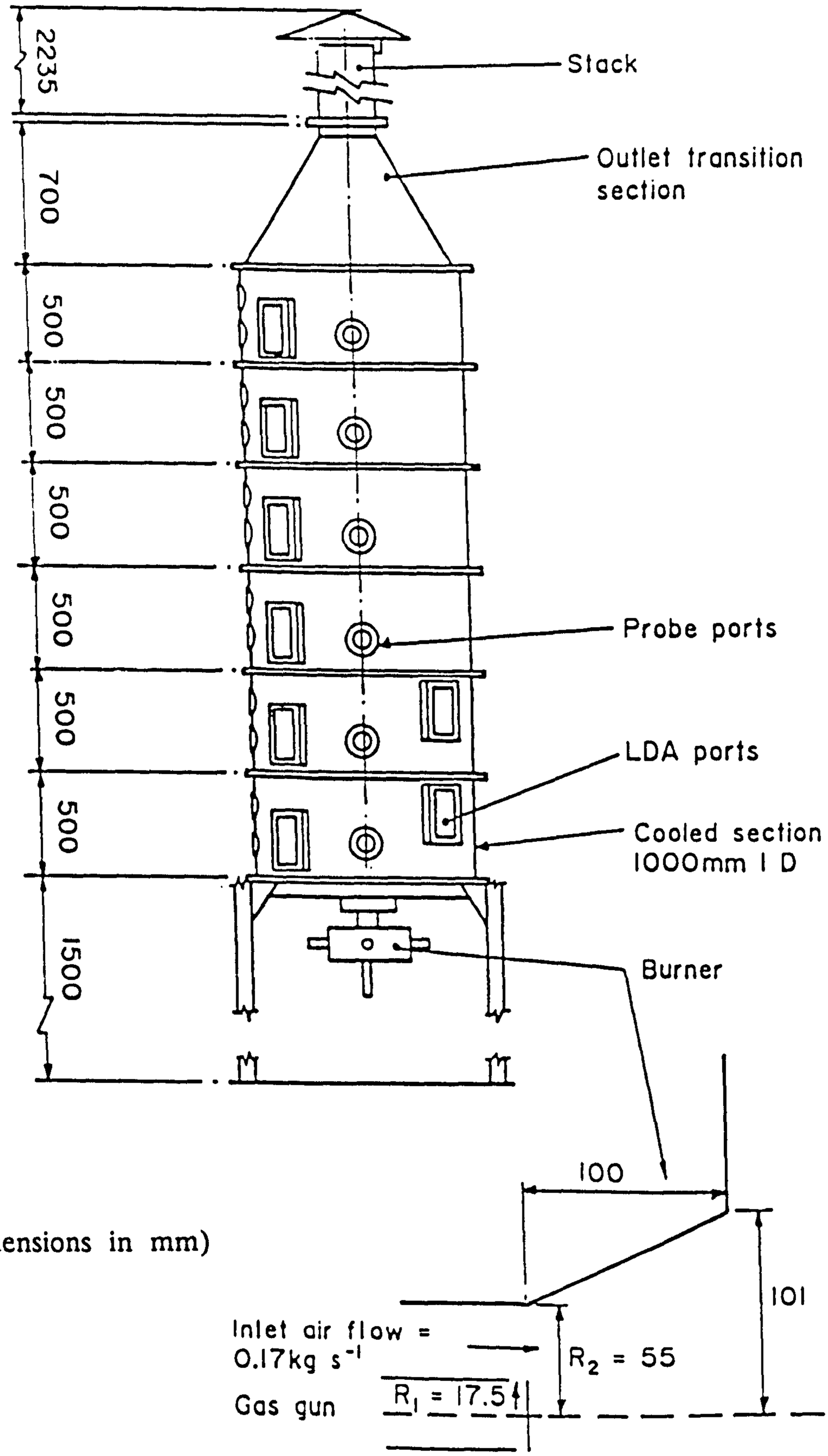

(Dimensions in mm)

Fig. 6 THE GEOMETRY OF THE QUARL AND CHAMBER – N.E.L. FURNACE

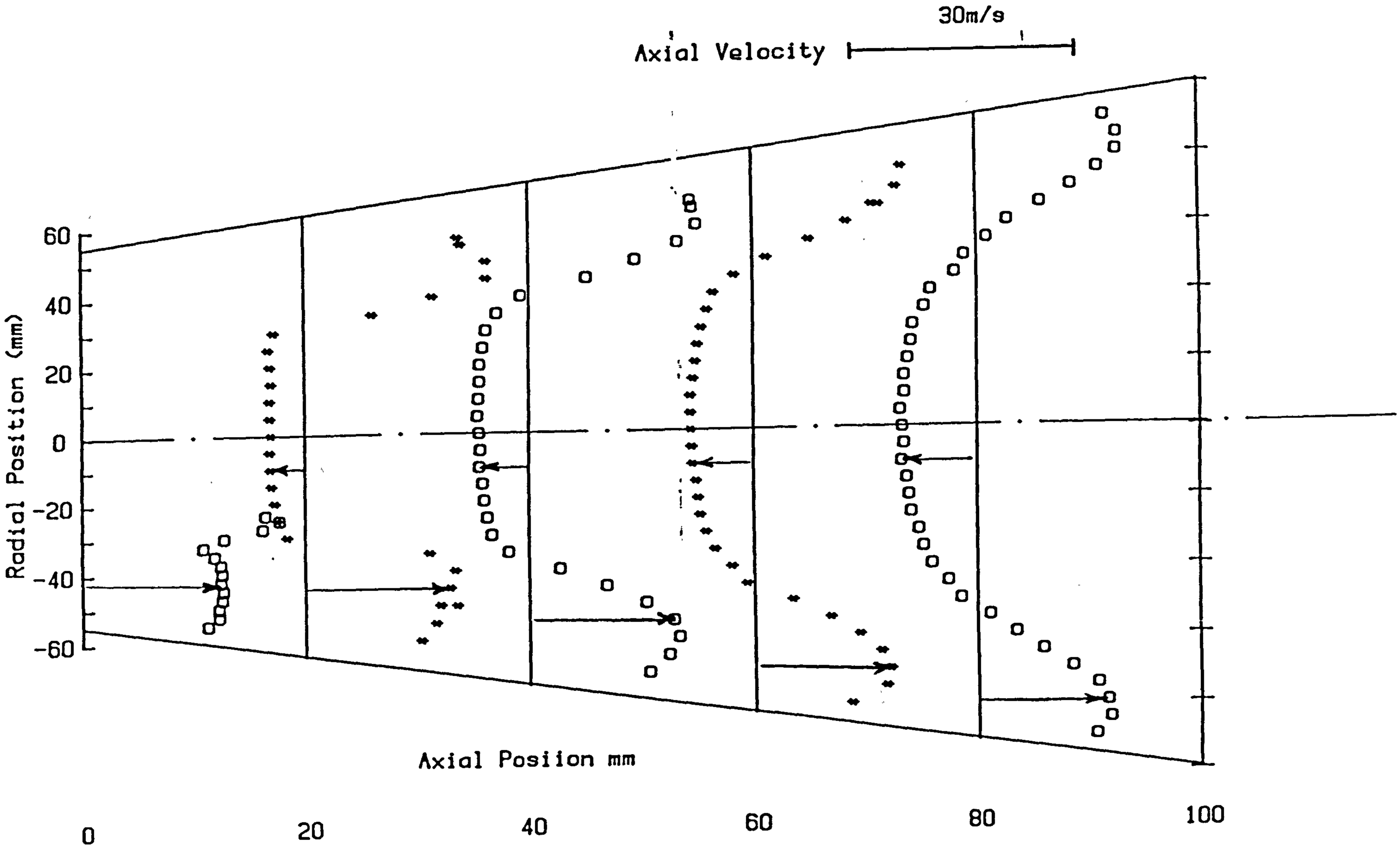

Fig. 7 AXIAL COMPONENT OF VELOCITY IN QUARL - RADIAL INJECTOR I - SWIRL No. 0.0

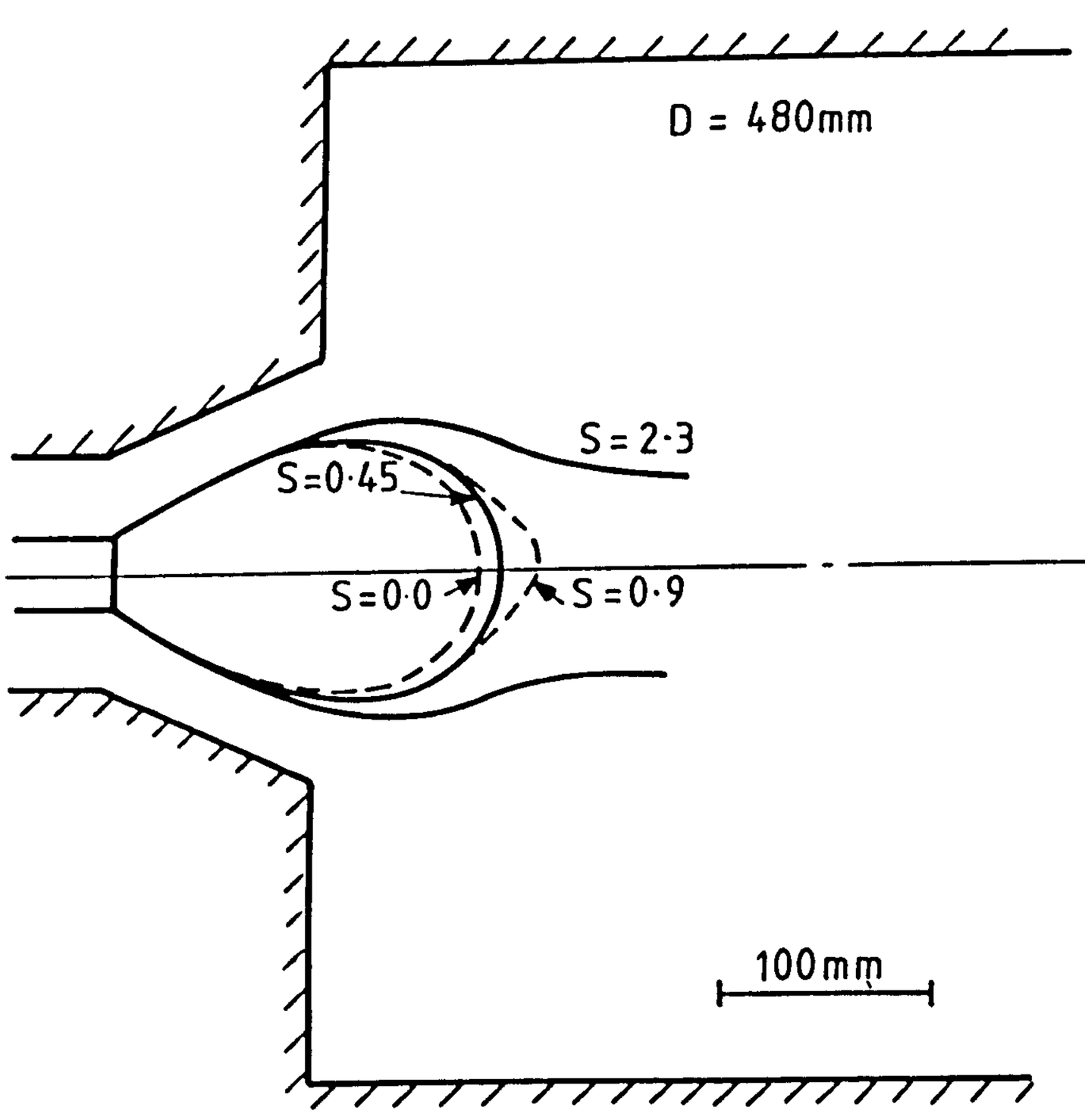

(a) WITH RADIAL INJECTOR I

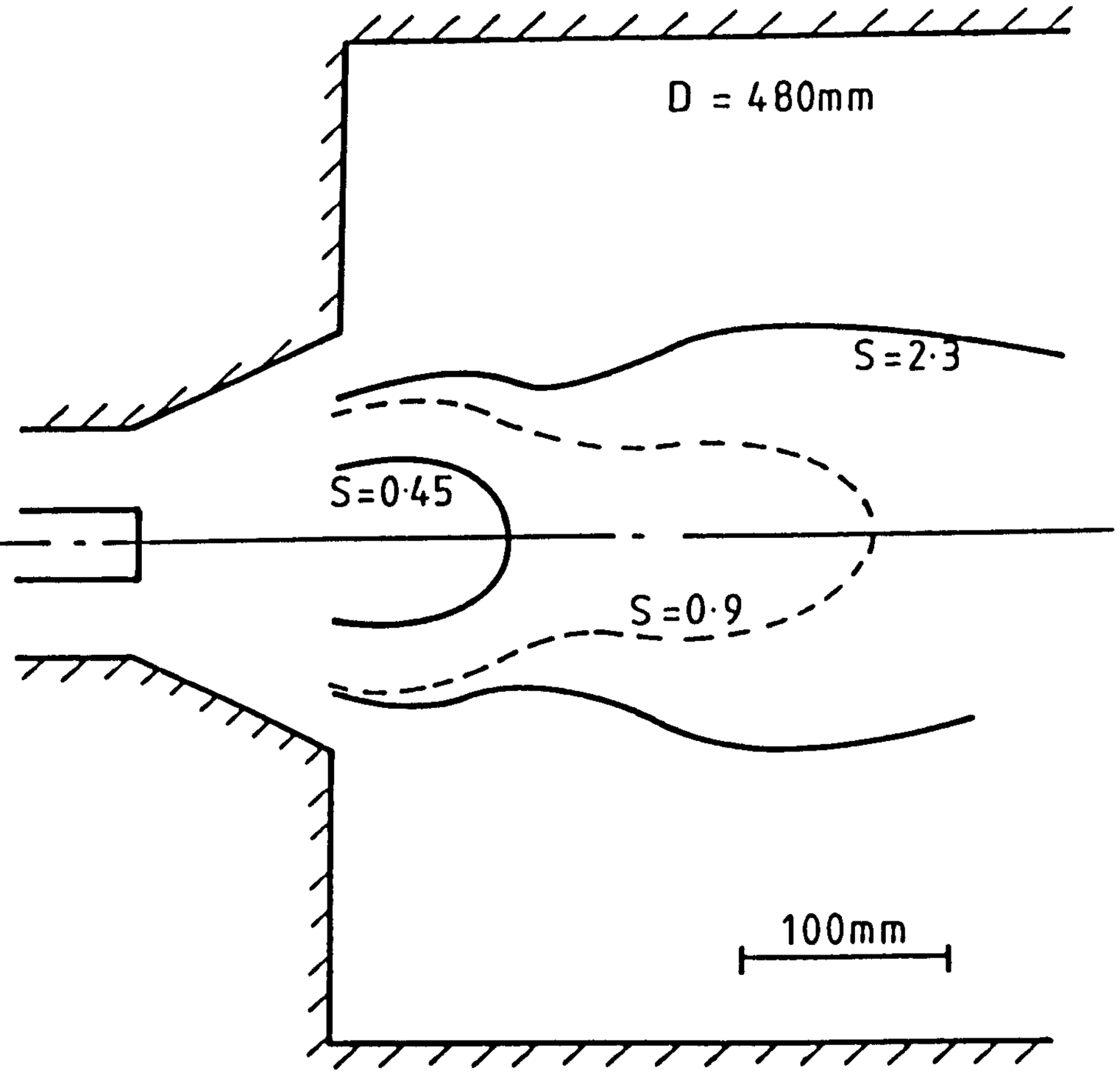

(b) WITH RADIAL INJECTOR II

Fig. 8(a,b) BOUNDARIES OF THE CENTRAL REVERSE - FLOW ZONE IN ISOTHERMAL MODEL OF N.E.L. FURNACE

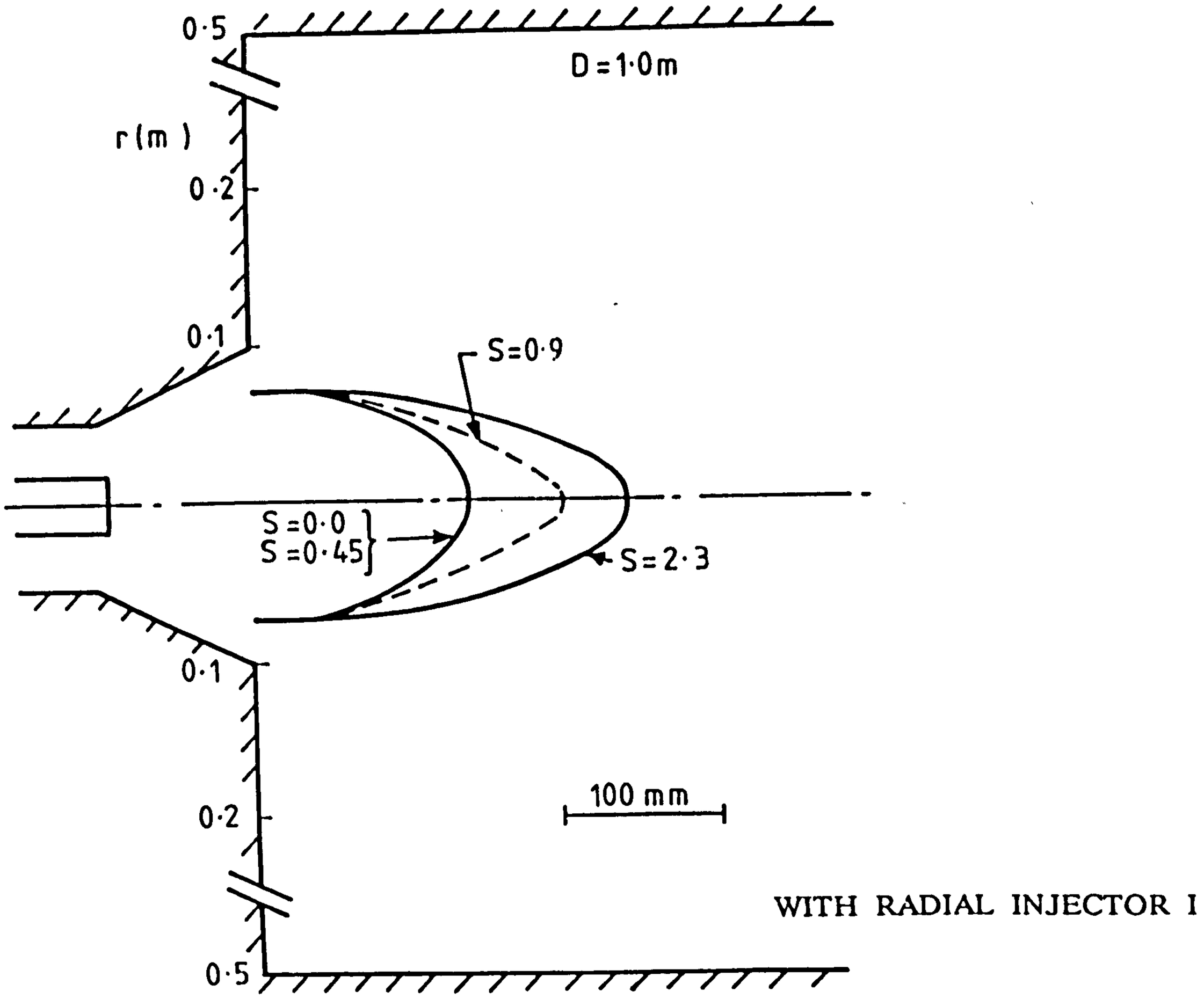

Fig. 9 BOUNDARIES OF THE CENTRAL REVERSE - FLOW ZONE FOR FLAME IN N.E.L. FURNACE

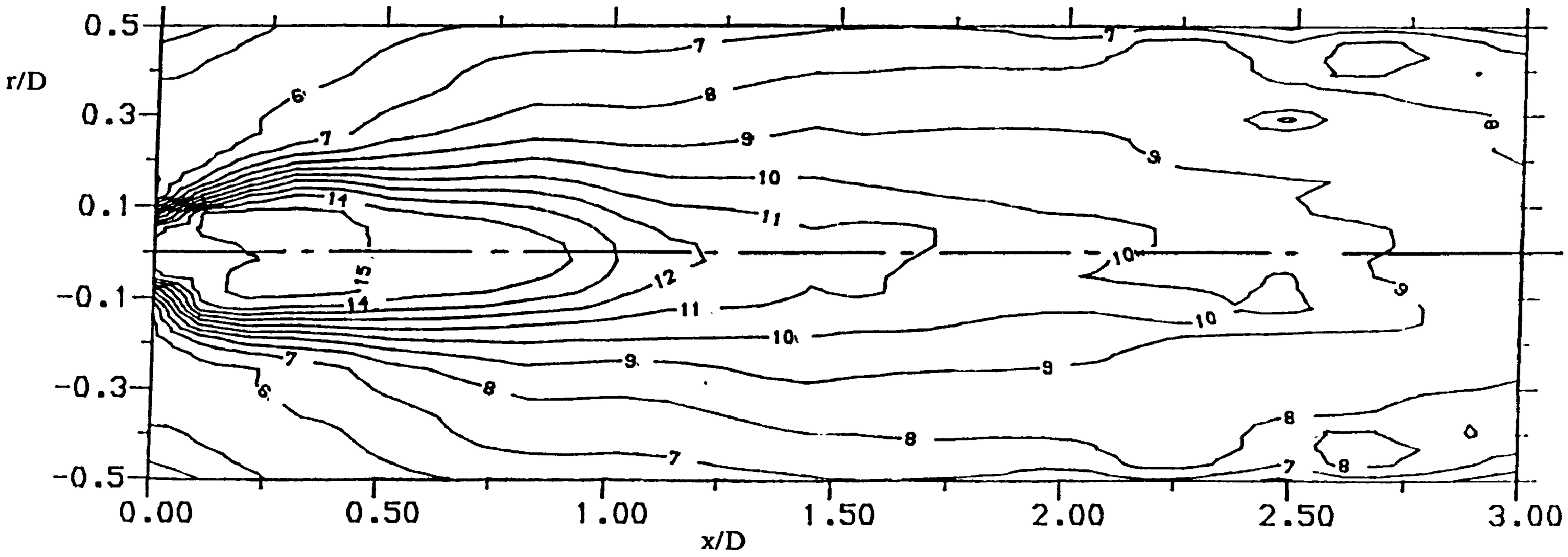

(RELATIVE TEMPERATURE VALUES)

Fig. 10 TEMPERATURE CONTOURS FOR N.E.L. FURNACE RADIAL INJECTOR I - SWIRL No. 0.0 $D/d_q = 5$

Publication 42

NOx GENERATION AND CONTROL IN CONFINED SWIRLING FLAMES - REVIEW AND PARAMETRIC STUDY

S A Beltagui[1,2], A M A Kenbar[1] and N R L Maccallum[1]

1. University of Glasgow
2. National Engineering Laboratory, East Kilbride, Glasgow

ABSTRACT

A programme of work on the control of combustion-generated NOx has started at the National Engineering Laboratory (NEL) in collaboration with Glasgow University. The main emphasis is to control the NOx generation through the aerodynamic design of the burner and its fuel injection mode. The work will involve both experimental measurements in the NEL furnace and theoretical modelling, in conjunction with the HTFS flow and combustion programs.

This paper reports on the literature survey, on NOx generation and control, carried out at the start of the work. The survey focuses on studies of the effect of burner parameters on the NOx generation in furnaces and gas turbine systems. Alternative prediction models are reviewed and the recommended model is presented.

The proposed model is applied to a well-stirred reactor to illustrate the relative importance of the main contributors to the NOx generation, namely, flame temperature, oxygen concentration and residence time.

NOTATION

k	Kinetic rate constant	cm^3/mole s
t	Residence time	s
T	Flame temperature	K
x	Number of carbon atoms in hydrocarbon	-
y	Number of hydrogen atoms in hydrocarbon	-
[ ]	Concentration	mole/cm^3 s
ϕ	Fuel/air equivalence ratio, dimensionless	-
ζ	Completeness of combustion, dimensionless	-

1. INTRODUCTION

1.1 NOx and the Environment

Combustion generated pollution is now

recognised as a threat to the environment. The most obvious air pollutant is smoke, being visible to the naked eye. Other pollutants of importance are carbon monoxide, sulphur oxides (SOx) and nitrogen oxides (NOx). Recently, attention has been focused on NOx.

NOx is a collective name for nitrogen oxides; N_2O, NO and NO_2.

Combustion produces NO and to a lesser extent NO_2. At atmospheric temperature NO is converted to NO_2 and some N_2O. Stationary sources are responsible for about half the total man-produced NOx.

Locally, NOx is toxic and is known to act through photochemical reactions as a precursor to the formation of smog and other pollutants. On a wider scale it causes damage to plant life and soil through its contribution to acid rain. It has a global effect, as N_2O is involved in depletion of the earth's ozone layer (OECD Reports (1979, 1984)).

Emission standards progressively call for tighter control on emission levels. Early regulations specify percentage reductions of the current emission levels, these reductions being achievable by the application of the most up-to-date technology. However, recent regulations for new sources prescribe specified levels of emissions in order to maintain a reasonable, healthy atmosphere (OECD Reports (1979, 1983)).

1.2 Sources and Control of Combustion Generated NOx

The main origin of combustion-generated NOx is nitrogen contained in the two combustion elements, ie air and fuel. The removal of nitrogen from air before combustion is impossible and from fuel is impractical. The nitrogen fixation is a result of the combustion environment, thus, NOx formation can be limited through careful combustion control.

It has been recognized that there are three important formation mechanisms - thermal, prompt and fuel NOx - and each has its own characteristics. The understanding of the NOx source and formation mechanism will determine the appropriate technique to be selected for NOx reduction.

Various general reviews of combustion-generated pollution have been published recently eg Sawyer (1981), Levy (1982), Clarke and Williams (1985), Lawn (1987) and Williams (1989).

The present paper begins with a very brief review of NOx formation mechanisms. Methods of reduction are described, followed by a more detailed review of those methods which relate to the present work, where control is examined in the context of gaseous combustion systems.

The last part of the paper presents a parametric study of the thermal NO formation through the application of the kinetic model to a well-stirred reactor system.

2. FORMATION OF NOx

The fundamental understanding of the chemical and physical processes leading to the formation of NOx is critical to the techniques for the minimisation of its emissions.

Three categories of NOx formed in the

combustion process have been identified according to the source of the nitrogen and the chemical kinetics of the NOx formation, as shown in Figure 1.

2.1 Thermal NOx

The 'thermal NOx' refers to that formed from the free N_2 in the air as it passes through the high temperature post-flame zone. The formation mechanism being that proposed by Zeldovich, (reactions 1,2) and further extended to include reaction 3 (Bowman (1975)).

$$O + N_2 \rightleftharpoons NO + N \qquad (1)$$

$$N + O_2 \rightleftharpoons NO + O \qquad (2)$$

$$N + OH \rightleftharpoons NO + H. \qquad (3)$$

The last reaction contribution is mainly at rich and near stoichiometric mixtures. In most cases the O atom concentration is assumed to be that in equilibrium with O_2. The main feature of the above reactions is their relatively high activation energy, thus, they are much slower than the main combustion reactions and can be decoupled from these, as will be detailed in Section 6.

An approximate formula for the overall prediction of thermal NO takes the form

$$\frac{d[NO]}{dt} = k_1(T)^{-1/2}_{eq} \exp(-E/RT) \; [O_2]^{1/2}_{eq} \; [N_2]_{eq} \text{ mole/cm}^3 \text{ s.} \qquad (4)$$

Measurements by Newhall and Shahed (1971) on H_2 flames and by Engleman et al (1973) on H_2, CO and propane flames have shown that the rates of formation in the post-flame high temperature zone follow this reaction rate law. Later measurements as reviewed by Sawyer (1981) and shown in Figure 2 confirm these results.

Thermal NOx is the main mechanism for NOx generation when burning N-free fuels such as natural gas. However, its contribution is not significant when combustion zone temperatures are less than 1500 K.

The rate of thermal NOx formation depends upon the following three parameters:

a Flame temperature - which is the main factor since NO temperature relation is exponential,

b Oxygen concentration in the post-flame zone, and

c Residence time of gas in high temperature region.

The relative importance of these parameters in contributing to thermal NOx formation is illustrated in Section 6.

The control of these three parameters is the basis of the techniques for thermal NOx reduction.

However, it must be emphasised that the local spacial and temporal variations in these parameters are as important as the mean values, eg locally fuel-rich or fuel-lean pockets could lead to different NOx production rates from those derived by mean values as discussed by Appleton and Heywood (1973).

2.2 Prompt NOx

Early workers realised that the thermal mechanism failed to predict the observed

high formation rate of NOx in the early part of some flames especially hydrocarbon rich flames (Fenimore (1971), Engleman et al (1973)). This led Fenimore (1971) to consider other reactions where the hydrocarbon fragments attack bimolecular nitrogen, producing atomic nitrogen, cyanides and amines, which subsequently oxidize to nitric oxide.

$$CH + N_2 \rightleftharpoons HCN + N \qquad (5)$$

$$C + N_2 \rightleftharpoons CN + N. \qquad (6)$$

The term 'Prompt NO" was used to describe NO formed early in combustion, through such mechanism. It was found to be of minor importance relative to thermal NO for cases of lean mixtures and of H_2 or CO flames.

The rate of prompt NO formation is not temperature sensitive and cannot be separated from the HC kinetics. Sarofim and Pohl (1973) confirmed this and tried to relate the prompt NOx formation to a partial equilibrium mechanism with overshoot of O atoms in the flame. Takagi et al (1976) measured HC and HCN in flames and related these to prompt NOx.

Measurements of prompt NOx were also made by Semerjian and Vranos (1976) in rich flames. They found that prompt NOx formation was unaffected by the temperature fluctuations in the flame. In another study it was found that increasing the pressure increased the formation of prompt NOx (Heberling (1976)). A detailed review of prompt NOx formation is given by Hayhurst and Vince (1980).

The contribution from prompt NOx is about 5 per cent of the total NOx in the case of gaseous fuels but is higher in cases of liquid and solid fuels, eg Williams (1989).

Reduction of prompt NOx formation could be achieved through the reduction of residence time in the flame reaction zone and by use of lean mixtures.

2.3 Fuel NOx

The name 'fuel NOx' refers to NOx from the nitrogen-containing compounds in the fuel. The chemical reaction mechanisms are more complex than thermal NOx and their temperature dependence is very weak.

Several prediction mechanisms for fuel NOx are proposed, eg Fenimore (1972), De Soete (1975), Takagi (1976), Roslyakov (1986) and Eberius et al (1989).

The general hypothesis is that the fuel nitrogen molecules pyrolise or react to form an intermediate nitrogen containing species, designated I (HCN or NHi i = 0, 1, 2, 3). This intermediate can then react with an oxygen containing molecule, R, to form NO, or with NO or possibly another I to form N_2.

$$\text{Fuel nitrogen} \rightarrow I \qquad (7)$$

$$I + R \rightarrow NO \qquad (8)$$

$$I + (NO \text{ or } I) \rightarrow N_2 \qquad (9)$$

The rate of conversion of fuel nitrogen to NO decreases with increased fuel nitrogen content and is independent of the type of fuel, Sawyer (1981).

This rate is also dependent on the fuel equivalence ratio. Tang et al (1981) report that maximum conversion rates occur for lean mixtures, with equivalence ratios

0.6 to 1.0. The measured conversion rates diminished for rich mixtures. Hence, control of fuel NOx is sometimes based on the reduction of oxygen in the primary combustion zone - called 'air staging'.

Fuel NOx is the major contributor in the case of solid fuels, which usually contain N-compounds. At the other extreme, natural gas is relatively free of nitrogen compounds thus thermal and prompt NOx are the main mechanisms of formation. Liquid fuels usually fall between these bounds according to their nitrogen content and combustion conditions.

3. ABATEMENT

In principle, there are three general approaches to reducing NOx emissions:

a Through the prevention of formation by combustion control. NOx is the most amenable of pollutants to prevention through modification of the combustion process, especially thermal and prompt NOx.

b Through the promotion of destruction after formation by reducing reactions in a reburning zone.

c If more reduction is needed, then treatment of the combustion products has to be implemented as a last resort. In this case, chemicals are injected in the combustion gases and reactions may occur under catalytic conditions.

The first two methods have proved sufficient in most applications.

The energy and running costs of implementing the above three techniques increase in the order they are listed above.

Some of these techniques may reduce efficiency, eg lower preheat, water injection. In power applications this is important but it could be of no effect in process applications if the process temperature is already low and thus not compromised (Pfeiffer and Altmark (1987)).

The cost of the implementation of these measures is due to

a The reduction in efficiency or loading of the plant, (Thomson and Crow (1976)),

b The initial cost of the extra equipment, and

c The cost of the materials, eg chemicals and energy used in the process by fans, injectors etc.

Some cost analysis is given in the Proceedings of the EPRI Joint Symposium on Stationary Combustion NOx Control (1982), and in OECD Report (1983).

Other factors should be considered when selecting the technique for NOx control such as the effect upon the process and on the formation and control of other pollutants, eg CO, SOx, HC etc.

The possibility of controlling both SOx and NOx simultaneously is under investigation, for example, the reduction of both by use of ozone (Lozovskii et al (1988) and Anon (1989)).

3.1 Control of Combustion

The control of combustion to prevent the formation of NOx represents the most promising and cost effective of all methods of NOx control. The extensive world-wide research on NOx formation covering different areas of applications has resulted in many practical means for NOx control. Table 1 lists the NOx control investigations reviewed. These are classified, according to the technique used and the proposed application. The principles of operation of these techniques are as follows.

a Lowering the peak combustion temperature:

A reduction of combustion peak temperature is very effective when dealing with thermal NOx but not effective for fuel NOx. Techniques leading to this aim include

i Off-stoichiometric combustion, through staged combustion,

ii Very lean combustion, flame tube premixed burner, fibre burner, cyclone combustors,

iii Reduced preheat,

iv Increased heat transfer in the burner zone,

v Flue gas recirculation, especially if the gases are cooled before recirculation, and

vi Water injection into the primary combustion zone of a burner, as used in industrial turbines and boilers, utilizes the latent heat of evaporation of water droplets to reduce temperature. This method is most effective if water is injected exactly where needed, ie in the peak temperature zone.

b Improved burner mixing thus eliminating temperature variations between lean and rich local mixtures. Uniform mixing is possible in premixed burners but stability and control may suffer. Injection of fuel in the shear layer of the air jet produces very low NOx with better stability and efficiency, eg Andrews et al (1988).

c Reduction of excess oxygen: Low excess air combustion since O_2 concentration is reduced and efficiency is increased, as in the case of staged combustion, both air staging and fuel staging are applied. Flue gas recirculation also dilutes the mixture and thus reduces O_2 concentration.

d Reduction of residence time in the flame zone and the peak temperature zone.

3.2 Destruction of NOx

By reburning in a second combustion stage, preferably using a low or N-free fuel, oil or gas. Fuels such as CO, H_2 and hydrocarbons will react with O_2 rather than NO if both exist but when O_2 is completely used up they will reduce NO to N_2.

3.3 Flue Gas Treatment

The processing of combustion products to remove NOx is used as a final measure with or without the above described methods.

In the thermal 'de-NOx' process reducing compounds, eg ammonia, urea, ozone etc are injected into the flue gases under

catalytic or noncatalytic conditions. Ammonia and other amines reduce NO in the primary combustion products in the presence of oxygen within a specified temperature range, (980-1370 K) and with certain NH3/NO equivalence, eg Muzio et al (1976) claim 78 per cent reduction at an optimum temperature of 1240 K with NH3/NO = 1/1.

Table 1 summarises a number of publications dealing with various control methods and their applications.

4. NOx IN CONFINED SWIRLING FLAMES

The review presented in the above sections dealt with general aspects of NOx formation and control. This section deals with those aspects relevant to burner flow and mixing, particular emphasis being placed on swirl stabilized gaseous flames.

4.1 Effect of Flow Pattern

Aerodynamics plays a major role in the reactions in the flame since it dictates the role and conditions under which active species are brought together before the kinetics starts to operate. The effects of flow will influence

a NOx concentration. This was found to depend on the local conditions early in the combustion process, in the developing jet in the near burner zone.

b Mixing effectiveness. This can lead to the suppression of NOx production due to the uniformity of the mixture, otherwise fuel-rich and fuel-lean pockets will exist causing higher local NOx production.

c Length scale. NOx formation was found to have a length scale dependence (Peters and Donnerhack (1981)). Those workers, studying diffusion flames, correlated this effect with Reynolds number and Froude number. NOx formation has also been related to flame stretch in a flat laminar flame (Hahn and Wendt (1981)).

d Residence time. The residence time of the combustion products in the various zones can only be controlled through the flow parameters.

e The total NOx production. This is related to the integrated producton by the flow and not by the local concentrations in the various zones. Thus, in order to establish the total mass of pollutants in the combustor, it is essential to consider the pollutant mass flow profiles as illustrated by Sadakata and Beer (1976) and Claypole and Syred (1981)).

4.2 Effect of Swirl

The application of swirl to the combustion air can have a major influence on NOx production which is dependent upon the local temperature and mixing rates in the near burner zone. In general, increased swirl will produce the following effects.

a Increased entrainment of cooled combustion products and thereby less thermal NOx, due to lower temperature and O_2 concentration.

b Increased local oxygen availability and thereby more thermal and fuel NOx.

c Increased combustion intensity and thus higher temperature and more thermal NOx.

These effects have been reported by various

investigators. Some of these studies are briefly summarised below.

i Owen et al (1976) studied the effect of swirl, fuel/air velocity ratio and pressure on the formation of pollutions from a combustor. They indicated the effect of these parameters on NOx formation and they also illustrated how small fluctuations in these flow parameters can cause large-scale fluctuations in the resulting NOx.

ii Oven et al (1978) discussed the influence of swirl on combustion and NOx formation in the light of flame quenching due to the rapid dilution and cooling of the reacting inner jet flow by mixing with the outer flow.

iii The influence of the level of swirl on the aerodynamics and NOx emissions was also studied by Claypole and Syred (1981). The effect of higher central flow recirculation is to reduce NOx emission. This reduction is a result of better mixing prior to combustion and the reduced flame peak temperature. The better mixing also tends to eliminate local imbalances of reactants. These imbalances produce local fuel-rich regions leading to more prompt NOx. The recirculation zone, despite elevated temperature did not appear to play a major role in the formation of NOx.

The last two investigations reported some NO reacting to produce NO_2 in the combustor although the measured levels may have been enhanced by probe reactions.

iv Similar effects of the flow pattern were also reported by Sadakata and Beer (1976) where NOx formation in a swirling flame was measured. They reported some NOx destruction in the central recirculating flow.

4.3 Effects of Fuel Injection Modes

a The effect of the mode of fuel injection on NOx formation has been studied by Ahmad N T et al (1985), Andrews et al (1988) and Al-Shaikhly and Andrews (1989) in gas turbine combustor configurations. The main findings support the theory of improved mixing when fuel is injected in the shear layer of the air flow - wall injection and radial injection being superior to central injection. These systems, when used with swirl flow, also utilise the centrifugal force in improving the mixing. The high mixing rates led to near premixed conditions producing minimum NOx, together with improved efficiency and turn down.

b Gupta et al (1975) studied the effect of fuel injection mode and burner geometry on NOx formation from natural gas swirling flames. Their results indicate that higher recirculation of burnt gases led to less NOx due to the lower temperature of the combustion zone. It was also shown that tangential fuel entry produced less NOx than axial/radial injection.

c Markowski et al (1976) have reported 50 per cent reduction of NOx by using a 'premix-prevap' swirl burner in a gas turbine system. The inherent instability of swirling flows was exploited to enhance the premixing process and to stir the reacting species thus approaching a lean premixed process.

d On the other hand, by effectively producing slow mixing low NOx could be

achieved, as this acts as a system staged. This was implemented in the burner of Suzuki et al (1982) where fuel was injected at an angle to the axis of the air stream. A soft flame was formed and the temperature of the flame became more uniform with lower maximum temperature and oxygen concentration.

Abassi and Fleming (1988) used the same principle in tests in a glass furnace.

e Stratified combustion produces lower NOx where two combustion regions are distinguishable, one in the primary air, the other associated with the secondary air. Meyer and Mauss (1973) illustrated this effect on a spray combustion system where the fuel was injected into a primary swirling air stream, surrounded by a non-swirling secondary stream. Low levels of NOx (50 p.p.m.) were obtained at an optimum swirl number of 0.93 even when using a fuel with 0.01 per cent nitrogen. It was also shown that flue gas recirculation could be used to reduce NOx even further.

5. THE PROPOSED PROGRAMME

The literature reviewed above reveals that use of a system employing both centrifugal and shear-layer mixing significantly inhibits NOx formation. Earlier work at Glasgow University by Beltagui and Maccallum (1988) has shown that such an aerodynamic configuration can be achieved through the peripheral injection of fuel in a swirl burner. Radial fuel injection, as currently employed in the NEL furnace programme of aerodynamic and heat-transfer measurements, can also produce good shear-layer mixing. This latter method has the merit of stabilising the flame through promotion of a central recirculation zone even without swirl (Beltagui et al (1988)).

It is thus proposed to carry out a series of measurements of the local NOx formation in flames of the above types. The programme will cover three different modes of natural gas injection:

a Central/axial fuel injection,

b Central/radial fuel injection, and

c Peripheral/axial fuel injection.

For each mode, the effect of the swirl-burner aerodynamics on NOx formation will be studied. Comparisons should provide the information needed to optimise both the fuel injection mode and swirl to achieve the best suppression of NOx formation.

HTFS also requires data from the proposed measurements to develop and validate computer models for prediction of NOx formation. This will be carried out by incorporating the thermal NOx model in a tested flow and combustion program.

6. THERMAL NOx MODELLING

In the application being presently considered, the NOx formation is mainly attributed to the thermal mechanism. Therefore, in this section the appropriate reaction rate equations are presented. Calculations are made for NOx production for a well-stirred reactor system. The results illustrate the relative effects of the main parameters, namely, flame temperature, oxygen concentration and residence time.

6.1 Model Inputs

The thermal NOx modelling equations (1), (2), and (3), as mentioned in Section 2, are well established and understood. However, their application even using a simplified overall equation (4), requires two sets of information.

The first set includes the rate constants of the reaction equations. Predictions are particularly sensitive to the value of the rate constant for the reaction (1). The uncertainty in determining these rate constants is large and recent measurements have demonstrated the need for more accurate determination of these constants. The most recently accepted value for k1 as measured by Monat et al (1978) is about 2.2 times the values used for the previous decade (Bowman (1975)).

The second set covers the local values of the flow conditions, the most critical being temperature and concentration of the main species. The determination of these values requires the solution of the momentum, heat- and mass-transfer equations, together with the chemical reaction equations for the main species (Caretto (1976)).

The flow pattern also has to be determined. The early modellers, see Table 2, applied simplifying assumptions for the flow, eg well-stirred reactor. Recently, however, more advanced programs for solving the flow equations have become available, such as TUFC (Sykes and Wilkes (1983)), PCOC (Stopford (1989)), PHOENICS (Rosten and Spalding (1987)), FLUENT (Visser et al (1987)) and FLOW3D (Burns et al (1988)).

Because of the high sensitivity of thermal NOx to temperature, it is essential that the predictions of temperature from the flow model are carefully validated.

On the other hand, chemical species concentration calculations can be performed at different levels of complexity, starting with a very fast kinetics model (mixed-is-burned) then one or two equation models and, most recently, a full set of detailed kinetics, as described by Maas and Warnatz (1989).

While the closure of these two sets of equations, ie flow and chemistry, is possible, it may prove prohibitively expensive for cases of industrial interest, so some compromises may have to be made.

A two-step approach has been adopted by Pericleous et al (1988) to model the formation of NOx in a combustion system with swirling flow and fuel injected either tangentially or axially. The first step involves the main exothermal reaction of methane in air which is considered to be mixing controlled and the second involves the solution of the Zeldovich reaction scheme for the generation of NOx. The results demonstrate the potential of these models to predict quantitatively the effects of burner geometry on the flame structure and, consequently, on NOx emission. The same approach has been adopted by Kudryavtsev (1988) for jet flow in order to model the combustion of gaseous fuel in a steam boiler furnace. Modelling studies of the effect of peripheral fuel injection on NOx formation were also reported by Sabo et al (1988), indicating NOx levels of about 50 per cent of those from equivalent central injection systems.

6.2 The Proposed Model

6.2.1 Combustion calculations

As indicated above, gas conditions required for the calculation of thermal NOx include temperature and species concentrations. The values of these quantities were calculated for methane combustion in a well-stirred reactor assuming a global one-step reaction given by the stoichiometry equation

$$\phi C_x H_y + \left(x + \frac{y}{4}\right)(O_2 + 3.76N_2) \rightarrow$$

$$\zeta\phi x CO_2 + \zeta\phi \frac{y}{2} H_2O + (1 - \zeta)\phi C_x H_y +$$

$$+ (1 - \zeta\phi)\left(x + \frac{y}{4}\right)O_2 + 3.76\left(x + \frac{y}{4}\right)N_2 \quad (10)$$

where ϕ is the equivalence ratio and ζ is the degree of combustion.

Equilibrium conditions were assumed using a dissociation factor as given by Fairweather (1985) to calculate the adiabatic flame temperature.

The actual flame temperature was then calculated after making allowance for radiative heat transfer, with radiation parameters approximating to the NEL furnace conditions. Results are compared with adiabatic temperatures in Figure 3a. This was carried out to compare NOx formation under adiabatic and heat-transfer conditions.

6.2.2 NOx model

The formulation of the model described here was based on the following assumptions:

a NO formation when firing lean and near-stoichiometric gaseous fuels is mainly thermal and strongly dependent on temperature.

b NO formation rate is much slower than the hydrocarbon reaction rate and that most of NO is formed after the hydrocarbon reactions reach equilibrium.

c The calculation of NO (nitric oxide) is sufficient for determining NOx. NO_2 (nitrogen dioxide) may also form in the furnace. However, the total NOx ($NO + NO_2$) is not affected by the amount of NO_2 formed (Toof (1986)).

Thermal NO was calculated via the extended Zeldovich mechanism reactions 1, 2 and 3. Additional reactions involving NO formation from N_2O are sometimes considered but usually account for less than 1 per cent of the NOx formed thus they are not included here.

The general NO formation production equation will have the form

$$\frac{d[NO]}{dt} = 2k_1[O][N_2]\left\{\frac{1 - [NO]^2/K[O_2][N_2]}{1 + k_{-1}[NO]/(k_2[O_2] + k_3[OH])}\right\} \quad (11)$$

where $K = (k_1/k_{-1})(k_2/k_{-2})$.

At this stage for lean mixtures the contribution of reaction 3 can be neglected. Assuming steady-state concentrations of N and H atoms, the rate of NO formation could be approximated by

$$\frac{d[NO]}{dt} = 2k_1[O]_{eq}[N_2]_{eq} \quad (12)$$

where

$$k_1 = 1.82 \times 10^{14}$$

$$\exp [-38\ 370/T] \text{ cm}^3/\text{mole.s}$$

(Monat et al (1978).

Assuming 0/02 equilibrium, then (0) concen-- tration is given by

$$[O]_{eq} = \{K_0/(RT)^{1/2}\}[O_2]_{eq}^{1/2} \qquad (13)$$

where

$$K_0 = 3.6 \times 10^3 \exp(-31\ 090/T)^{1/2} (\text{atm})^{1/2}.$$

Substituting these rate constants in equation (12), the final NO production-rate equation becomes

$$\frac{d[NO]}{dt} = 1.44 \times 10^{17} T^{-1/2} \exp(-69\ 460/T)$$

$$[O_2]^{1/2}[N_2] \text{ (mole/cm}^3\text{s)}. \qquad (14)$$

6.2.3 Model results

Using the above simplified analysis, values of NO formed under various input conditions of equivalence ratio and degree of combustion are calculated. These simple model predictions are used to illustrate the relative contribution of input conditions to thermal NO production. In all cases the fuel is methane and the inlet air and fuel temperatures are 300 K.

Figure 3b shows the effect of heat transfer on NO formation at constant degree of combustion ζ of 0.95. Flame temperature values in all the subsequent figures are those in which heat transfer is considered.

Both Figures 3b and 4 illustrate the strong dependence of thermal NO on flame temperature.

To examine the effect of the degree of combustion on NO formation, the results are shown in Figure 5 for ζ values of 0.80, 0.85 and 0.95. It is obvious that at a given value of the equivalence ratio, the increase in the degree of combustion results in a higher flame temperature and hence higher NO formation.

Figure 6 shows that NO formation is not as sensitive to O_2 concentration as it is to flame temperature. Despite the decay of O_2 concentration with the increase of equivalence ratio, NO continues to increase exponentially with the flame temperature.

Finally, the effect of residence time on NO formation is illustrated in Figure 7. It is clear that reduction in residence time of gas in the high temperature region reduces NO formation.

7. SUMMARY AND CONCLUSIONS

Nitrogen oxides are generated in combustion systems either by fixation of atmospheric nitrogen, through thermal and prompt mechanisms or by conversion from N-containing compounds in fuel. Nitrogen oxides are products of the combustion environment and their control should start with the modification of the combustion to prevent their formation. The next level of control involves the destruction of formed NOx in a reburning or second stage zone. If neither method achieves adequate reduction, treatment of combustion products through catalytic reduction or other methods has to be undertaken. Alternative techniques based on the above principles are reviewed with

particular emphasis on those based on combustion control for prevention of NOx formation.

In most gaseous combustion systems the major contributor to the overall NOx emission is thermal NOx. Methods of thermal NOx control are principally based on the reduction of one or more of the following flame parameters; temperature, excess oxygen concentration and residence time in the post-flame zone. The present review illustrates that the aim of NOx reduction can be achieved through the careful control of the aerodynamics and mixing in the near-burner zone.

An experimental program has been proposed which will focus on the effects of swirl and fuel injection modes on NOx formation in natural gas flames in a cylindrical furnace.

The mathematical modelling of NOx formation in this case is also under investigation. A first step is presented here offering a simple parametric study of the relative importance of the combustion parameters on the NOx formation. The calculations are based on the thermal NO mechanism applied to a well-stirred reactor.

ACKNOWLEDGEMENTS

The authors wish to thank colleagues at the National Engineering Laboratory and the University of Glasgow for their advice and encouragement. This work was supported in part by the Management Board of the National Engineering Laboratory.
A M A Kenbar wishes to acknowledge the support of the Government of Iraq.

REFERENCES

ABASSI, H. A. and FLEMING, D. K., (1988), Ceram. Eng. Sci. Proc., Vol. 9, No 3-4, pp 168-177.

ABDALLA, A. Y., BRADLEY, D. and CHIN, S. B., (1989), Joint Meeting of the British and French Sections of the Combustion Institute, Rouen, pp 29-32.

AHMAD, N. T., ANDREWS, G. E., KOWKABI, M. and SHARIF, S. F., (1985), 20th Internat. Symp. on Combustion, pp 259-267.

AHMAD, T., PLEE, S. L. and MYERS, J. P., (1985), J. Eng. Gas Turbine Power, Vol. 107, No 1, pp 48-53.

AL-SHAIKHLY, A. F. A., ANDREWS, G. . and ANIAGOLU, C. O., (1989), Joint Meeting of the British and French Sections of the Combustion Institute, Rouen, pp 5-8.

ANDREWS, G. E. et al, (1988), British flame days, Imperial College, London.

ANON, (1989), "Control of NOx emission from large combustion plant", The Chem. Eng., March, pp 33-40.

APPLETON, J. P. and HEYWOOD, J. B., (1973), 14th Internat. Symp. on Combustion, pp 777-786.

BARNES, F. H., BROMLY, J. H., EDWARDS, J. J. and MANDYCZEWSKY, R., (1988), J. Inst. Energy, Vol. 61, pp 184-188.

BELTAGUI, S. A., FUGGLE, R. N. and RALSTON, T., (1988), HTFS RS 756, NEL/HTFS 113.

BELTAGUI, S. A. and MACCALLUM, N. R. L., (1988), J. Inst. of Energy, pp 3-16.

BOWMAN, C. T., (1975), Prog. Energy Comb. Sci., Vol. 1, pp 33-45.

BREEN, B. P., BELL, A. W., De VOLO, N. B., BAGWEKK, F. A. and ROSENTHAL, K., (1971), 13th Internat. Symp. on Combustion, pp 391-401.

BROWN, T. D., MITCHELL, E. R. and LEE, G. K., (1973), First European Symp. on Combustion, Sheffield, pp 487-492.

BURNS, A. D. et al, (1988), Harwell Report AERE-R 13148.

CARETTO, L. S., (1976), Prog. Energy and Comb. Sci., Vol. 1, pp 47-75.

CLARKE, A. G. and WILLIAMS, A., (1985), HTFS Design Report DR32, Part 10.

CLAYPOLE, T. C. and SYRED, N., (1981), 18th Internat. Symp. on Combustion, pp 81-89.

DE SOETE, G. G., (1975), 15th Internat. Symp. on Combustion, pp 1093-1099.

DESTEFANO, J. T., (1985), Ceram. Eng. Sci. Proc., Vol. 6, No 3-4, pp 241-248.

EBERIUS, H., JUST, Th., KELM, S. and WARNATZ, J., (1989), Joint Meeting of the British and French Sections of the Combustion Institute, Rouen, pp 17-20.

ENGLEMAN, V. S. et al, (1973), 14th Internat. Symp. on Combustion, pp 755-765.

EPRI, (1982), Proc. of the Joint Symp. on Stationary Combustion NOx Control, Vols 1 and 2. Elect. Power Research Institute, Palo Alto, California.

FAIRWEATHER, M., (1985), HTFS Design Report DR32, Part 2.

FENIMORE, C. P., (1971), 13th Internat. Symp. on Combustion, pp 373-380.

FENIMORE, C. P., (1972), Combustion and Flame, Vol. 19, pp 289-296.

FLAMENT, P. and BURY, F., (1989), Joint Meeting of the British and French Sections of the Combustion Institute, Rouen, pp 239-242.

FLETCHER, R. S., (1973), 1st European Symp. on Combustion, Sheffield, pp 445-450.

FLETCHER, R. S. and HEYWOOD, J. B., (1971), AIAA Paper No 71-123, New York, N. Y.: American Institute of Aeronautics and Astronautics.

FOSTER, P. J., (1974), HTFS Design Report DR32, Part 5.

GODRIDGE, A. M., (1986), Int. Flame Research Foundation, 8th Members Conference, Netherlands.

GUPTA, A. K., SYRED, N. and BEER, J. M., (1975), 15th Internat. Symp. on Combustion, pp 1367-1378.

HADVIG, S., MADSEN O, H. and JENSEN, J., (1988), British Flame Days, Imperial College, London.

HAHN, W. A. and WENDT, J. D. L., (1981), 18th Internat. Symp. on Combustion, pp. 121-131.

HAYHURST, A. N. and VINCE, I. M., (1980), Prog. Energy Comb. Sci., Vol. 6, pp 35-51.

HEBERLING, P. V., (1976), 16th Internat. Symp. on Combustion, pp 159-168.

HIRAI, T., NAGAI, N. and TAKADO, J., (1987), Int. J. JSME, Vol. 30, No 260, pp 303-309.

HUNTER, S. C., HALL, R. E. and CARTER, W. A., (1978), ASME Paper No 78-WA/APC-8.

KNILL, K. J., (1987), Int. Flame Research Foundation Doc. No G13/a/3.

KOTLER, V. R. and IMANKULOV, E. R., (1986), Thermal Eng., Vol. 33, No 1, pp 12-14.

KRETSCHMER, D. and ODGERS, J., (1973), ASME Paper No 73-WA/GT-6.

KUDRYAVTSEV, N. Yu. and VOLKOV, E. P., (1988), Thermal Eng., Vol. 35, No 4, pp 219-222.

LAWN, C. J., (Ed.), (1987), "Principles of combustion engineering for boilers", Academic Press.

LEFEBVRE, A. H., (1975), 15th Internat. Symp. on Combustion, pp 1169-1180.

LEVY, A., (1982), 19th Internat. Symp. on Combustion, pp 1223-1242.

LEWIS, G. D., (1981), ASME Paper No 81-GT-119.

LOZOVSKII, V. A. et al, (1988), Thermal Eng., Vol. 35, No 8, pp 20-22.

LUKOSHYAVICHYVS, V. P., TSIRUL'NIKOV, L. M. and SHVENCHYANAS, P. P., (1986), Thermal Eng., Vol. 33, No 7, pp 9-12.

MAAS, V. and WARNATZ, J., (1989), Joint Meeting of the British and French Sections of the Combustion Institute, Rouen, pp 133-137.

MARKOWSKI, S. J., LOHMANN, R. P. and REILLY, R. S., (1976), ASME J. of Eng. Power, pp 123-129.

MEIER, J. G. and VOLLERIN, B. L., (1976), 16th Internat. Symp. on Combustion, pp 63-76.

MELLOR, A. M., (1980), Prog. in Energy and Comb. Sci., Vol. 6, pp 347-358.

MELLOR, A. M. and WASHAM, R. A., (1979), ASME Paper No 79-GT-194.

MEYER, G., and MAUSS, F., (1973), First European Symp. on Combustion, Sheffield, pp 475-480.

MIRZAIE, H. and SYRED, N., (1989), Joint Meeting of the British and French Sections of the Combustion Institute, Rouen, pp 61-64.

MIZUTANI, Y. and KATSUKI, M., (1976), Bulletin of JSME, Vol. 19, pp 1360-1366.

MONAT, J. P., HANSON, R. K. and KRUGER, C. H., (1978), 17th Symp. (Int.) on Combustion, pp 543-552.

MONAT, J. P., HANSON, R. K. and KRUGER, C. H., (1978), 17th Internat. Symp. on Combustion, pp 543-552.

MULHOLLAND, J. A. and HALL, R. E., (1987), J. Eng. Gas Turbine Power, Vol. 109, pp 207-214.

MUZIO, L. J. ANAND, J. K. and TEIXEIRA, D. P., (1976), 16th Internat. Symp. on Combustion, pp 199-208.

NEWHALL, H. K. and SHAHED, S. M., (1971), 13th Internat. Symp. on Combustion, pp 381-389.

NOVOSELOV, S. S. et al, (1986), Thermal Eng., Vol. 33, No 9, pp 30-33.

NUTCHER, P. B., (1984), Plant/Operations Progress, Vol. 3, No 3, pp 168-173.

OECD, (1979), "Photochemical oxidants and their precursors in the atmosphere", OECD Report

OECD, (1983), "Control technology for nitrogen oxide emissions from stationary sources", OECD Report.

OECD, (1984), "Emission standards for major air pollutants", OECD Report.

OVEN, M. J., GOULDIN, F. C. and McLEAN, W. J., (1978), 17th Internat. Symp. on Combustion, pp 363-374.

OWEN, F. K., SPADACCINI, L. J. and BOWMAN, C. T., (1976), 16th Internat. Symp. on Combustion, pp 105-118.

PERICLEOUS, K. A., CLARK, I. W. and BRAIS, N., (1988), British Flame Days, Imperial College, London

PETERS, N. and DONNERHACK, S., (1981), 18th Internat. Symp. on Combustion, pp 33-42.

PFEIFFER, R. and ALTMARK, D., (1987), Research and Development Forum, June, Osaka, Japan.

RITZ, J., KOLB, T., JANSOHN, P. and LEUCKEL, W., (1989), Joint Meeting of the British and French Sections of the Combustion Institute, Rouen, pp 37-40.

ROSLYAKOV, P. V., (1986), Thermal Eng., Vol. 33, No 1, pp 23-26 and Vol. 33, No 9, pp 499-502.

ROSTEN, H. I. and SPALDING, D. B., (1987), Phoenics Reference Manual, Cham.

RUBINS, P. M. and MARCHIONNA, N. R., (1976), AIAA Paper No 76-612, New York, N.Y.: American Institute of Aeronautics and Astronautics.

SABO, Sh., DVOINISHNIKOV, V. A. and VILENSKII, T. V., (1988), Thermal Eng., Vol 35, No 9, pp 534-537.

SADAKATA, M. and BEER, J. M., (1976), 16th Internat. Symp. on Combustion, pp 93-103.

SADAKATA, M., FUJIOKA, Y. and KUNII, D., (1981), 18th Internat. Symp. on Combustion, pp 65-72.

SAROFIM, A. F. and POHL, J. H., (1973), 14th Internat. Symp. on Combustion, pp 739-754.

SAWYER, R. F., (1981), 18th Internat. Symp. on Combustion, pp 1-22.

SCHEFER, R. W. and SAWYER, R. F., (1976), 16th Internat. Symp. on Combustion, pp 119-133.

SEMERJIAN, H. and VRANOS, A., (1976), 16th Internat. Symp. on Combustion, pp 169-179.

SHAW, H., (1973), ASME Paper No 73-WA/GT-1.

SIDDIQUI, A. A., TENINI, J. W. and KILLION, L. D., (1976), Hydrocarbon Processing, Oct., pp 94-97.

SIGAL, I. Ya., KOSINOV, O. I., DUBOSHII, A. N. and NIZHNIK, S. S., (1986), Thermal Eng., Vol. 33, No 7, pp 6-9.

SIMACHEV, V. Y. et al, (1988), Thermal Eng., Vol. 35, No 3, pp 171-175.

SKORIK, L. D. et al, (1986), Thermal Eng., Vol. 33, No 7, pp 58-59.

SMART, J. and WEBER, R., (1987), Int. Flame Research Foundation, Doc. No F 037/a/18.

STOPFORD, P. J., (1989), PCOC Users Manual, AERE-R12626.

SUZUKI, T. et al, (1982), J. Inst. Energy, Vol. 55, Part 1, pp 212-215, Part 2, pp 216-220.

SYKES, J. and WILKES, N. S., (1983), TUFC2 Program Users Manual, Harwell Report AERE-R11027.

TAKAGI, T. OGASAWARA, M., DIAZO, M. and TATSUMI, T., (1976), 16th Internat. Symp. on Combustion, pp 181-189.

TANG, S., CHURCHIL, S. W. and LIOR, N., (1981), 18th Internat. Symp. on Combustion, pp 73-80.

THOMSON, S. T. and CROW, R. H., (1976), Proc. API Refin. Dep. Midyear 41st Meeting, Vol. 55, pp 567-574.

TOOF, J. L., (1986), ASME J. Eng. Gas Turbine Power, Vol. 108, pp 340-347.

TOUCHTON, G. L., (1984), ASME Paper No 84-GT-152.

TSIRUL'NIKOV, L. M. et al, (1986), Thermal Eng., Vol. 33, No 9, pp 503-506.

TUTTLE, J. H., COLKET, M. B., BILGER, R. W. and MELLOR, A. M., (1976), 16th Internat. Symp. on Combustion, pp 209-219.

VISSER, M., BOYSAN, F. and WEBER, R., (1987), Int. Flame Research Foundation, Doc. No F 336/a/9.

WAIBEL, R. and NICKESON, D., (1986), Int. Flame Research Foundation, 8th Members Conference, The Netherlands.

WILLIAMS, A., (1989), Joint Meeting of the British and French Sections of the Combustion Institute, Rouen, pp A1-A11.

YAMAGISHI, K. et al, (1975), 15th Internat. Symp. on Combustion, pp 1157-1166.

LIST OF TABLES

LIST OF FIGURES

4 Variation of NO formation with flame temperature

5 Effect of degree of combustion on NO formation

6 Variation of flame temperature, O_2 and NO with equivalence ratio

7 Variation of NO formation with residence time.

TABLE 1

REVIEW OF NOx EMISSION CONTROL METHODS

Investigators	Techniques	Applications
EPRI 1982 NOx Symp.	Review of all techniques and applications	Utility, process.
OECD NOx Control for Stationary Sources, 1983	Review of techniques	Utility, process.
Breen et al, 1971	General review	Utility
Sawyer, 1981	General review	Utility
Lefebvre, 1975	General review	Gas turbine
Foster, 1974	General review	Furnaces
Ahmad, N. T. et al, 1985 Andrews et al, 1988 Al-Shaikly et al, 1989	Burner controlled mixing, shear layer fuel injection, both axial and radial	Gas turbine Process
Markoski et al, 1976	Premix-prevap swirl burner	Gas turbine
Gupta et al, 1975	Fuel injection control burner geometry and swirl	Process
Suzuki et al, 1982	Controlled slow mixing, low temperature, internal FGR	Steel processing
Pfeiffer and Altmark, 1987	Low temperature premixed radiant tube burner	Process, gas turbine, small boiler
Mirzaie and Syred, 1989	Cyclone low temp. very lean combustion	Process, low CV fuels
Schefer and Sawyer, 1976	Lean combustion opposed jet system	Gas turbine
Meier and Volleron, 1976	High swirl with FGR	Domestic boilers
Barnes et al, 1988	Radiant burner	Domestic heating
Hadvig et al, 1988	Fibre burner	Boiler
Ritz et al, 1989	Reburn with NH_3 mixed with fuel	Boilers
Mulholland and Hall, 1987	Reburn with gas or oil fuel	Packaged boiler
Hunter et al, 1978	Combustion modification, review	Various processes

T A B L E 1 (contd)

Investigators	Techniques	Applications
Siddiqui et al, 1976	Review of techniques	Fired heaters
Nutcher, 1984	Review of air and fuel staging and FGR	Fired heaters
Destefano, 1985	NH_3 injection	Glass furnace
Abassi et al, 1988	Low excess air and slow mixing	Glass furnace
Tsirul'nikov et al, 1986	Low excess air, FGR and steam injection	Utility
Meyer and Mauss, 1973	Stratified combustion, swirl and FGR	Fundamental
Abdalla et al, 1989	Stratified, well-stirred reactor	Fundamental
Oven et al, 1979	Stratified swirl burner	Fundamental
Waibel and Nickeson, 1986	Fuel and air staging with FGR	Process refinery
Yamagushi et al, 1975	Air staging	Boiler
Kotler and Imankulav, 1986	Air staging, swirl	Utility
Hirai et al, 1987	Air staging, swirl	Boiler, process
Sadakata et al, 1981	Air staging, preheat	Model
Knill, 1987	Review of fuel staging, pf.	Utility
Smart and Weber, 1988	Internal air staging and precombustor	Utility
Flament and Bury, 1989	Fuel staging, central and peripheral injection	Boilers
Brown et al, 1973	FGR	Boiler
Sigal et al, 1986	FGR	Utility
Godridge, 1986	FGR	Utility
Lukoshyavichyvs et al 1986	Water spraying	Utility
Novoselov et al, 1986, Lozovskii, 1988 and Simachev et al, 1988	Reduction of NOx and SOx by ozone	Utility
Skorik et al, 1986	Ammonia injection	Utility

TABLE 2

REVIEW OF NOx MODELLING WORK

INVESTIGATORS	NOx Mechanism	Hydrocarbon Kinetics	Flow Modeling	Remarks
a)Fletcher and Heywood,1971. b)Fletcher,1973	a) Thermal b) Thermal	a) Equilibrium b) 2-step reaction	a) 1.D.M b) 2.D.M	a) Fluctuations b) Premixed
Appleton and Heywood,1973.	Thermal & Fuel		1.D.M	Fluctuations
Fletcher, 1973	Thermal	Equilibrium	W.S.R	Fluctuations
Engleman et al,1973	Thermal	Semi-detailed	W.S.R	premixed
Shaw, 1973	Thermal & Prompt	Equilibrium	W.S.R	
Kretschmer and Odgers,1973	Thermal	1-step reaction	W.S.R	
Tuttle et al,1976	Thermal	Emperical	W.S.R	
Rubins and Marchionna,1976.	Thermal	Equilibrium	Multiple W.S.R	
Mizutani and Katsuki,1976	Thermal	1-step reaction	2.D.M	
Mellor and Washam, 1979, Mellor, 1980.	Thermal		W.S.R	
Lewis ,1981	Thermal	Equilibrium	W.S.R	
Sadakata et al, 1981	Thermal	Equilibrium	1.D.M	Air staging
Peters and Donnerhack,1981	Thermal	Equilibrium	2.D.M	Boundary layer
Touchton, 1984.	Thermal	Equilibrium	Multiple W.S.R	steam injection
Ahmed T et al, 1985	Thermal	1-step reaction	2.D.M	
Toof, 1986	Thermal,prompt and fuel	Equilibrium		
Sabo et al ,1988	Thermal & Fuel	Equilibrium/1-step	3.D.M	Cenral/peripheral injection
Pericleous et al,1988	Thermal	1-step + turbulence	3.D.M	Central/peripheral injection
Kudryavtsev & Volkov, 1988	Thermal	1-step + turbulence	2.D.M	Boundary layer

1 D.M = One Dimensional Model.
2.D.M = Two = =
3.D.M= Three = =
W.S.R = Well stirred Reactor.

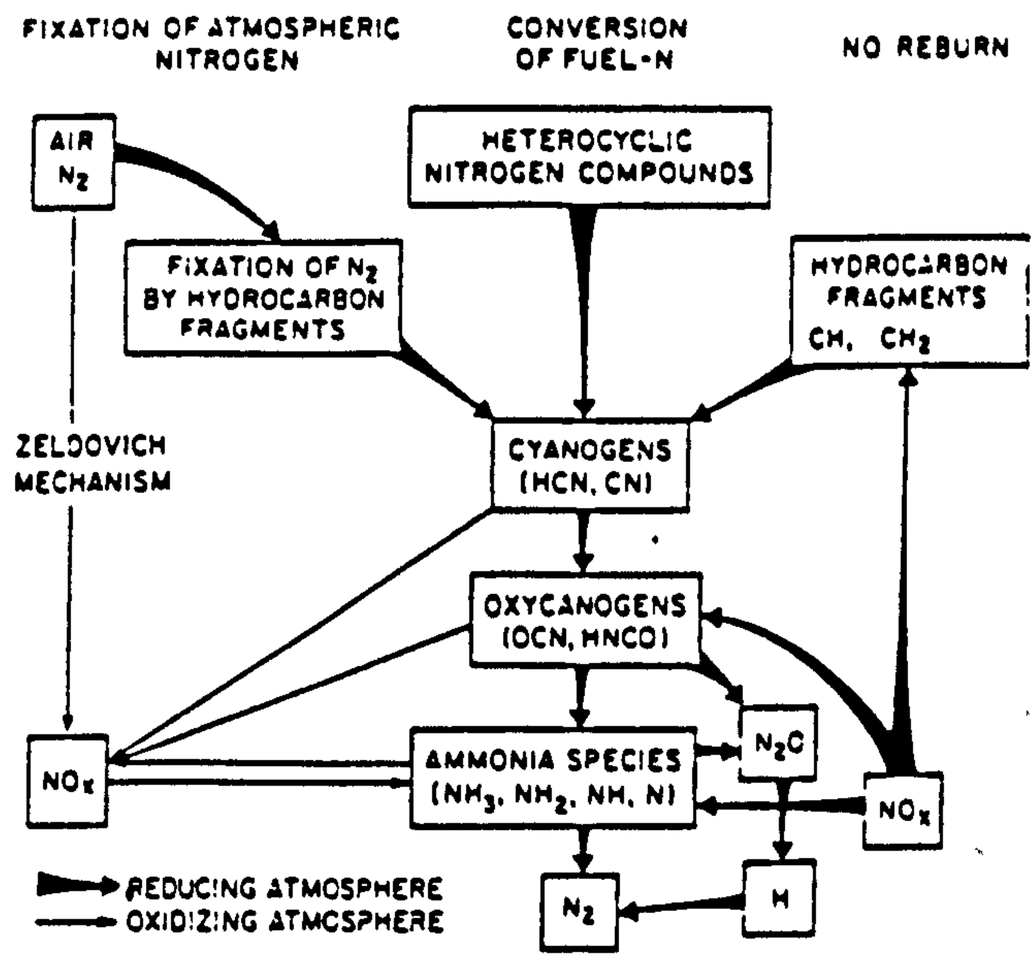

FIG.1: POTENTIAL NOx FORMATION ROUTES

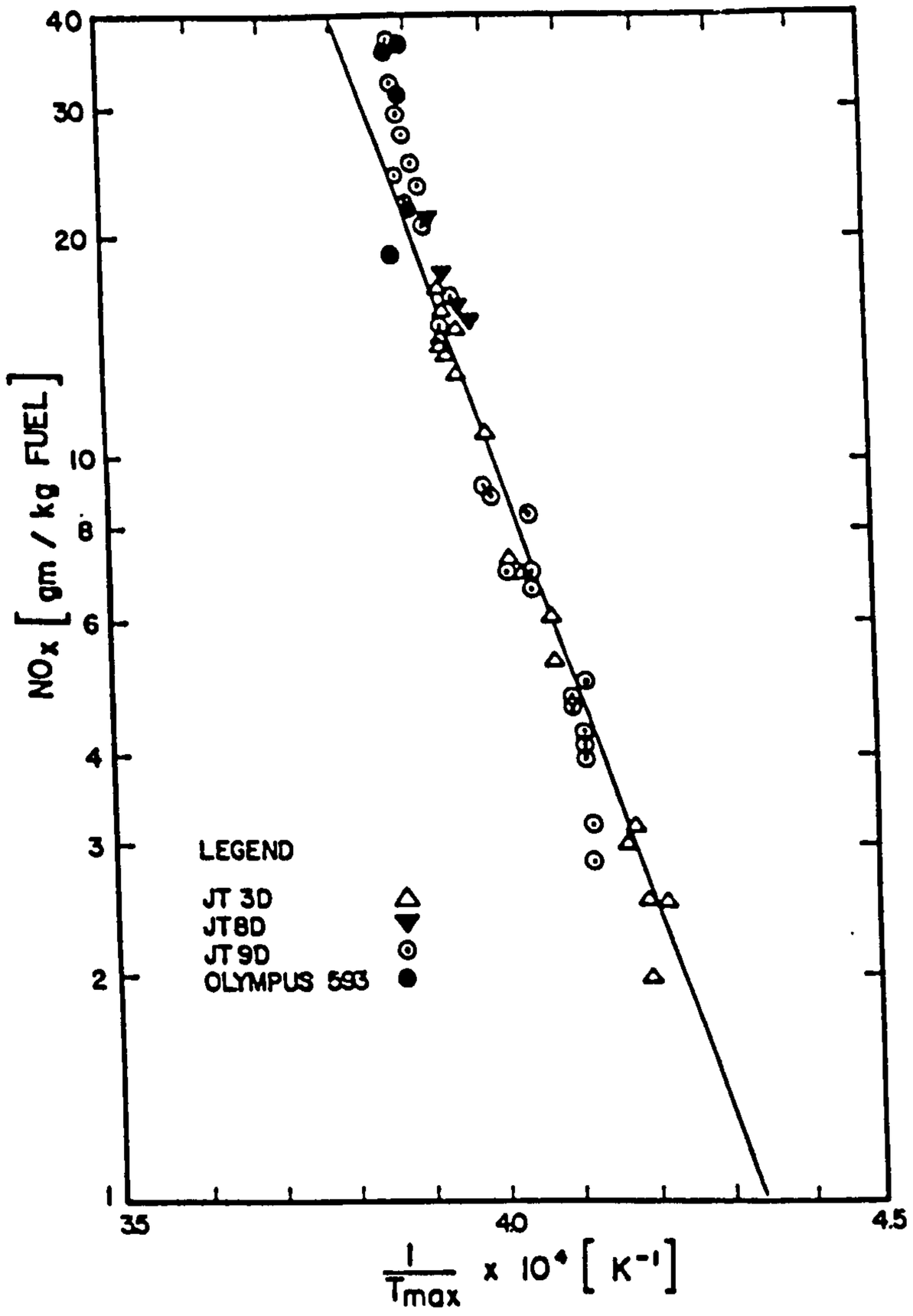

FIG.2: THERMAL NO-EXPERIMENTAL VS PREDICTIONS

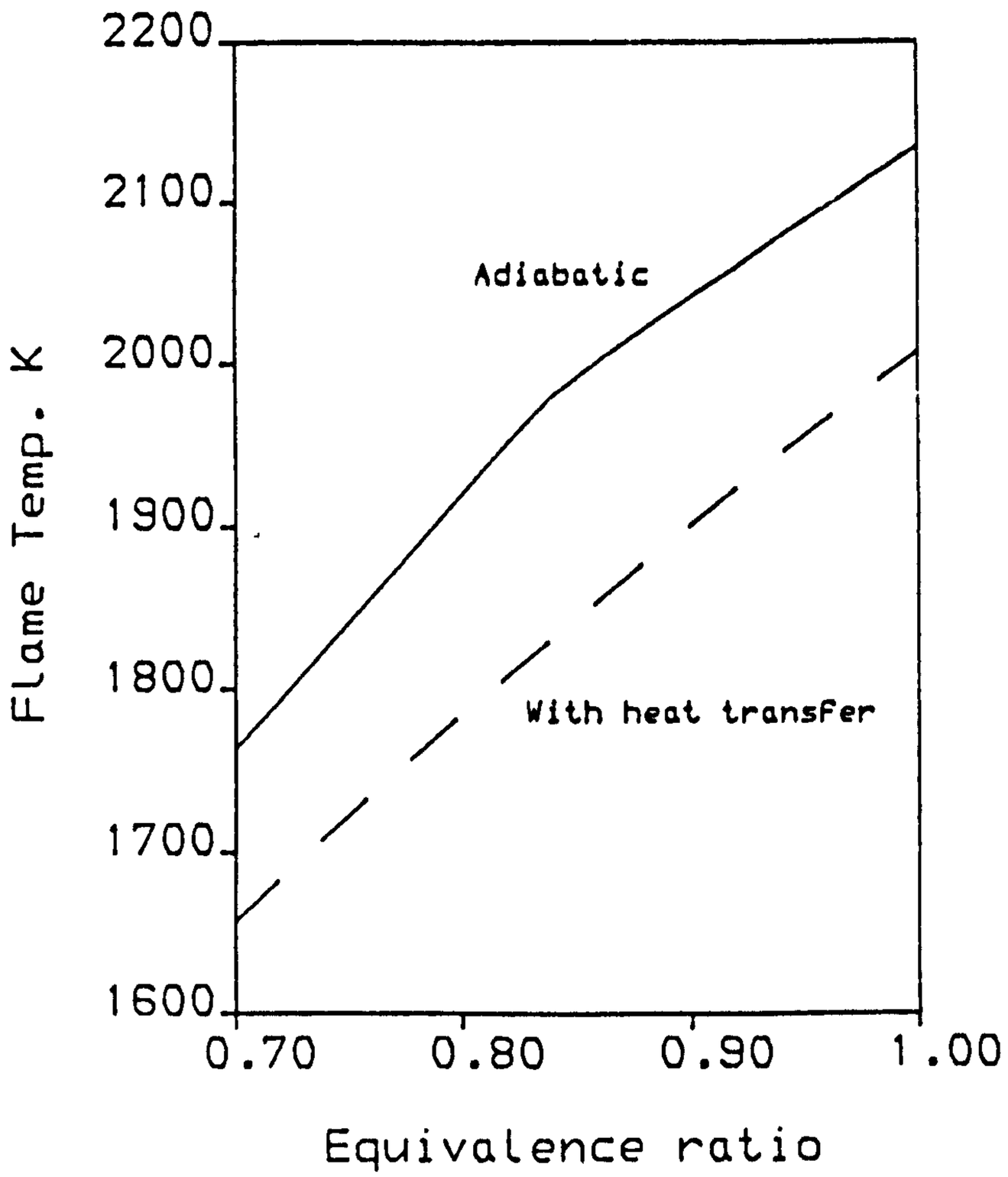

FIG.3a:EFFECT OF HEAT TRANSFER ON FLAME TEMPERATURE

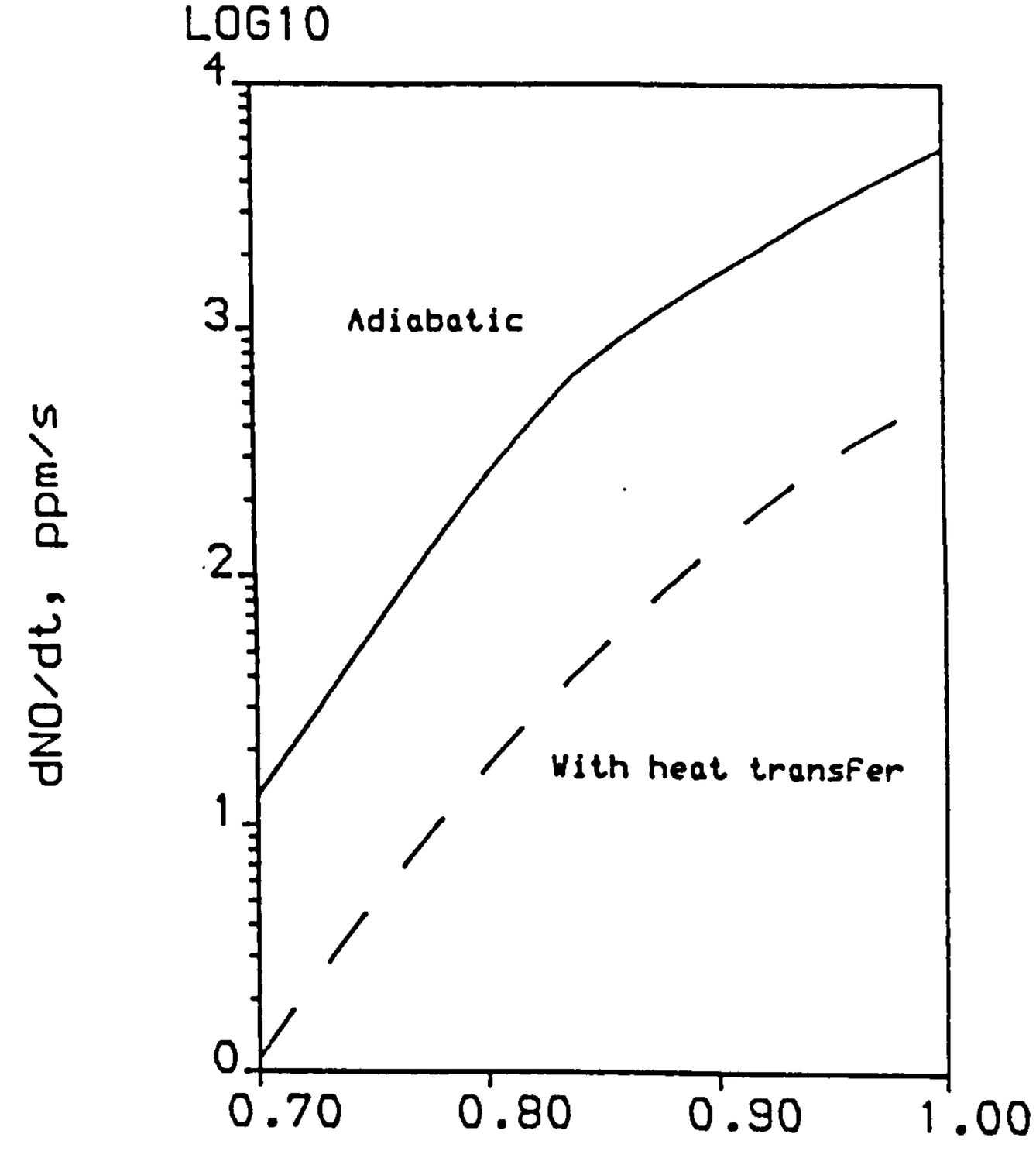

FIG.3b: EFFECT OF HEAT TRANSFER ON NO FORMATION

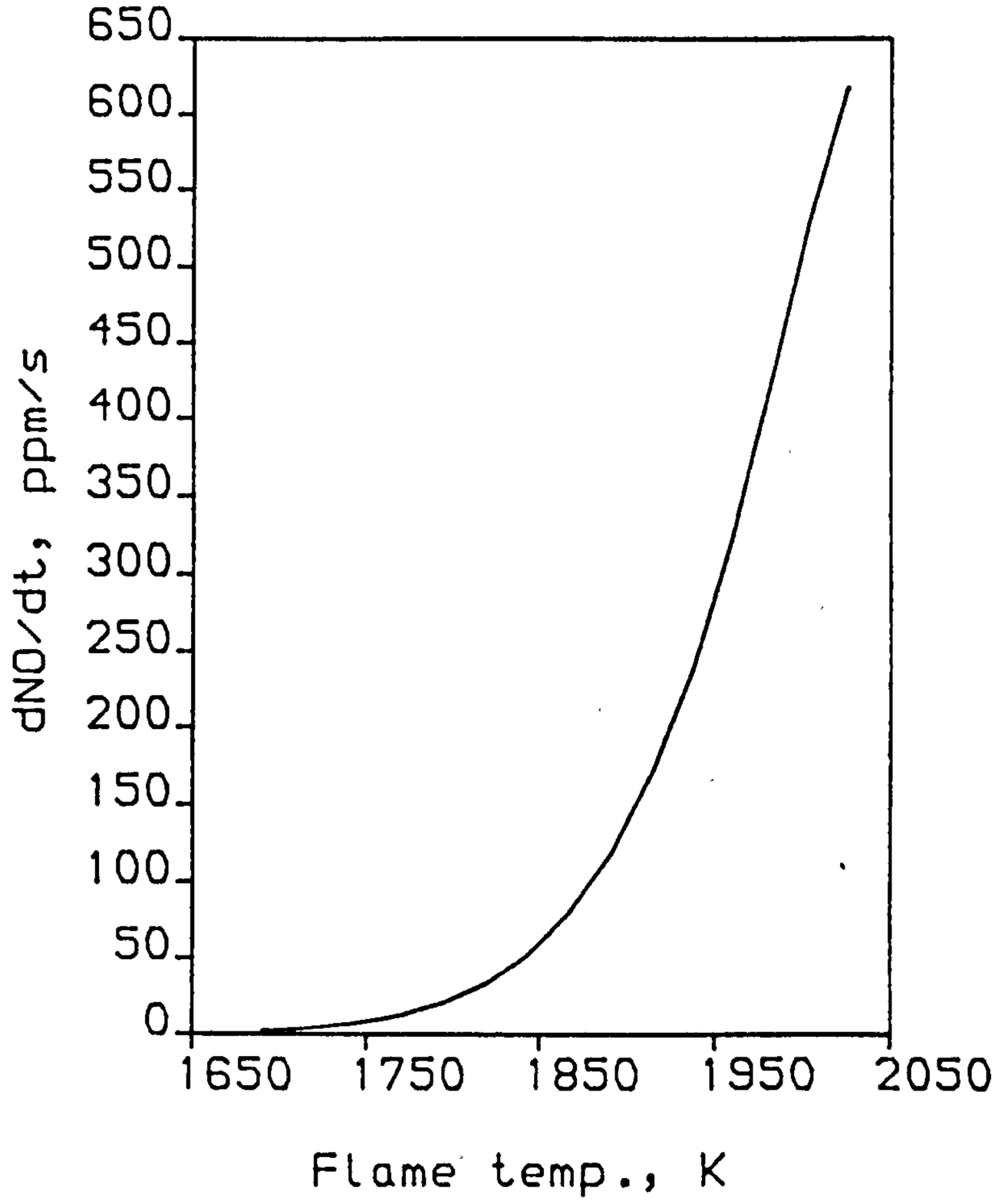

FIG.4:VARIATION OF NO FORMATION WITH FLAME TEMPERATURE

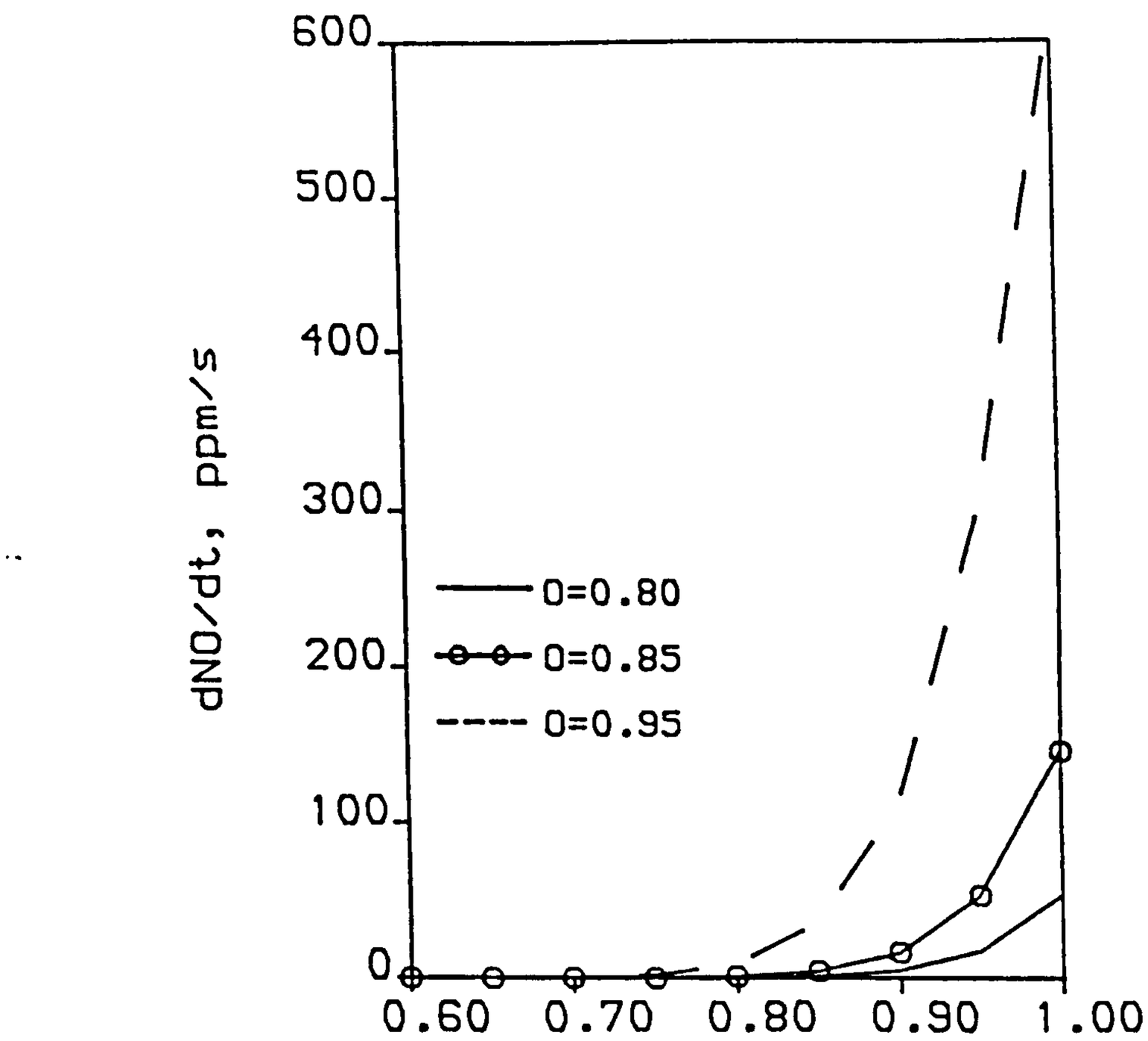

FIG.5: EFFECT OF DEGREE OF COMBUSTION ON NO FORMATION.

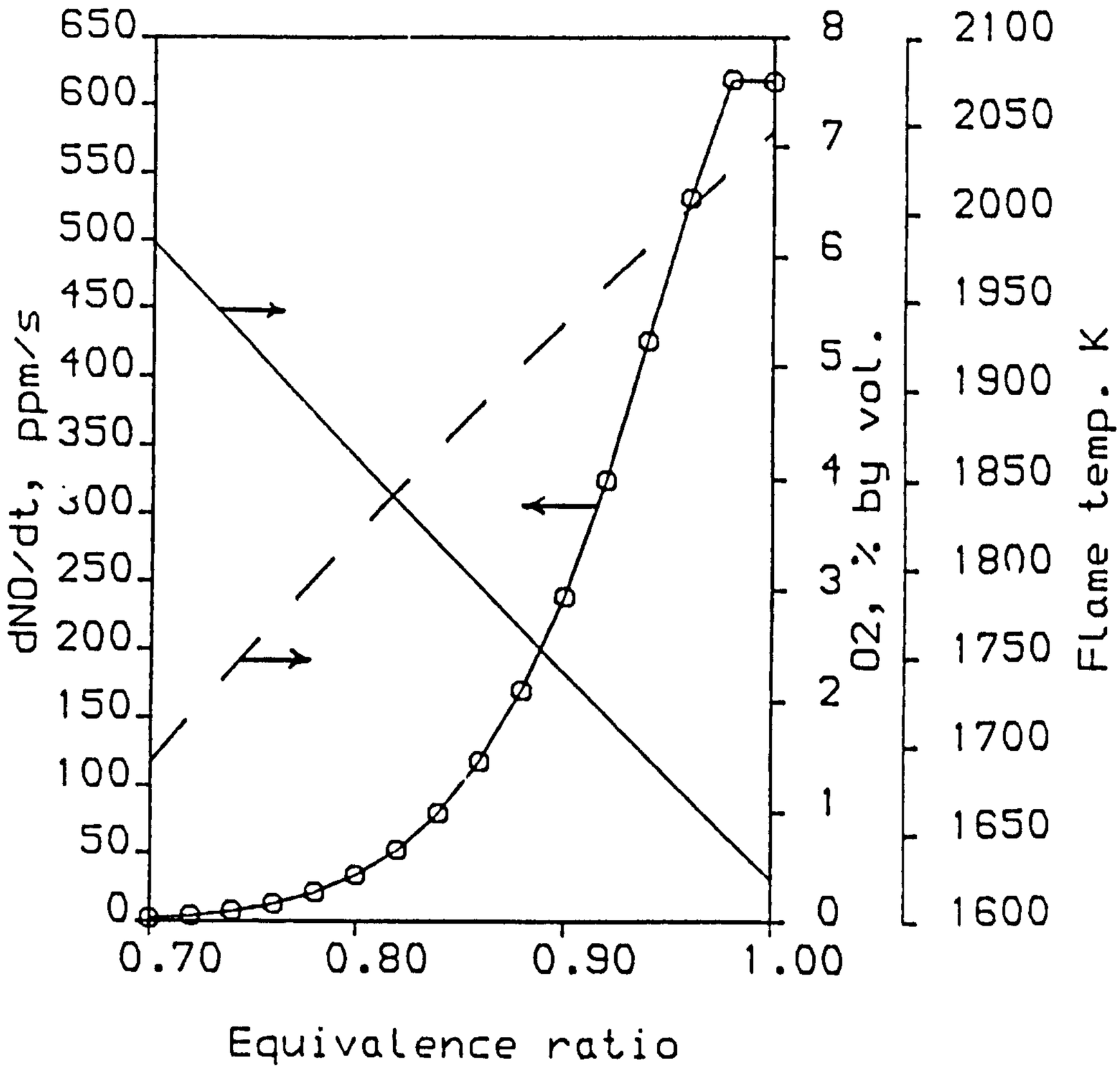

FIG.6: VARIATION OF FLAME TEMPERATURE, O2 AND NO WITH EQUIVALENCE RATIO.

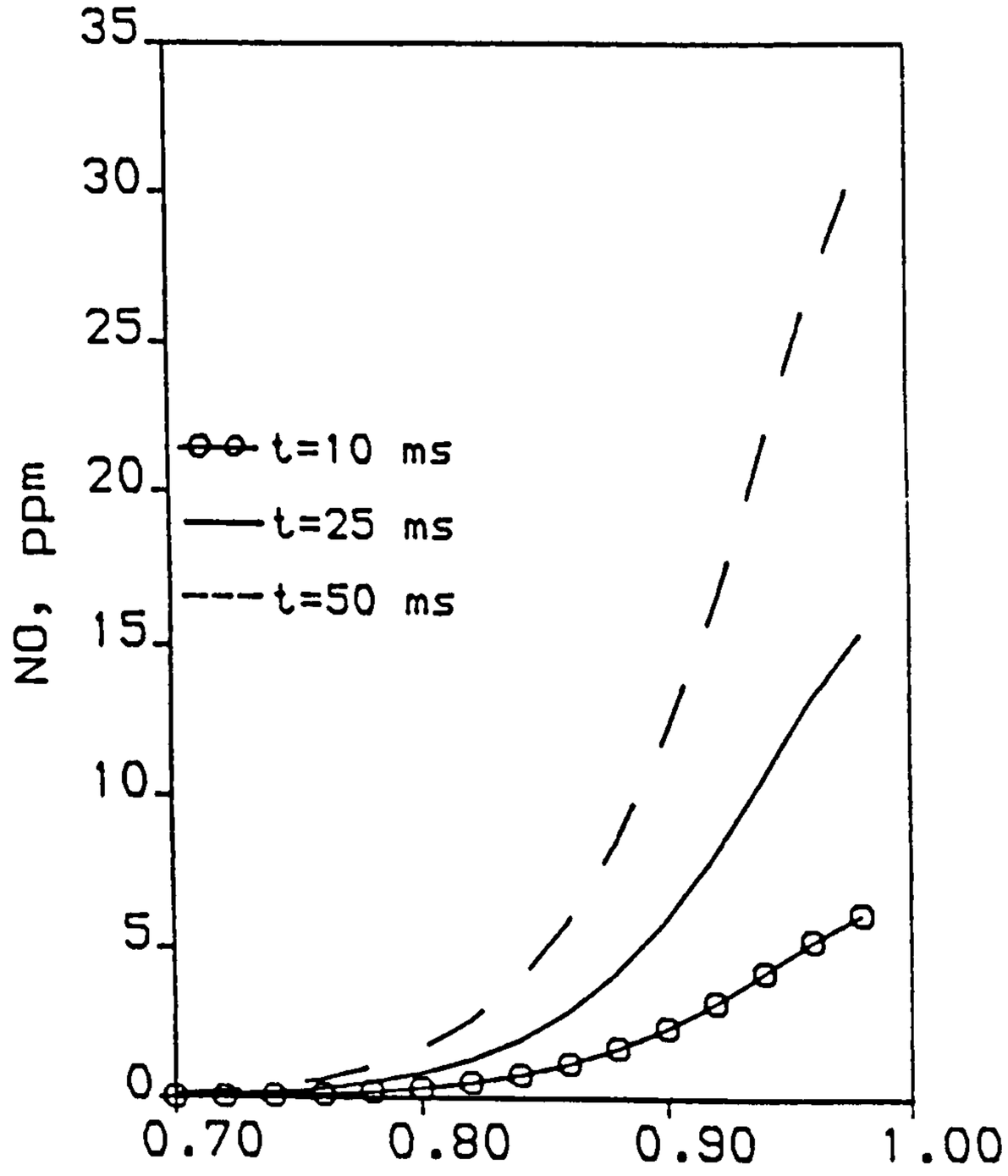

FIG.7:VARIATION OF NO FORMATION WITH RESIDENCE TIME

Presented at I. Mech. E. Seminar Publication 43
"Gas Turbines - Technology and Development"
2nd Nov 1989
London.

THE TRANSIENT BEHAVIOUR OF AIRCRAFT GAS TURBINES

N.R.L. Maccallum and O.F. Qi

University of Glasgow, 15 September 1989

SYNOPSIS Given the need for aircraft gas turbines to be able to accelerate and decelerate rapidly, the Paper explains the importance of computational procedures which can predict the transient behaviour. The early procedures were inadequate in predicting 'real engine' behaviour. The paper describes 'thermal effects' which are now incorporated in the prediction method. These developments are demonstrated on a typical two-spool turbofan, and the earlier 'real engine' anomalies can now be predicted with good accuracy. Developments of fuel control systems are discussed briefly.

NOTATION

C_1, C_2, C_3, C_4	coefficients defined in Eqns. 7, 8
C_p	specific heat of air/gas at constant pressure
f	ratio of heat transfer to air/gas to work transfer from air/gas in element of compressor or turbine
$\dot{f}$	fuel flow rate
g	blade staggered spacing
h	blade length
m	polytropic index of non-adiabatic path
$\dot{m}$	air/gas mass flow rate
n	polytropic index of adiabatic path
N	shaft rotational speed
$\dot{N}$	'N dot' - rate of change of shaft rotational speed
P	pressure
R	compressor pressure ratio at surge
T	temperature
U	blade tip speed
V	air/gas velocity
β	air/gas angle
γ	isentropic index
δ	tip clearance
λ	non-dimensional clearance (δ/h)
η	small-stage efficiency
ρ	air/gas density
φ	flow coefficient (V_{ax}/U)
ψ	blade loading coefficient $= \frac{2\ C_p\ \Delta t}{\rho\ U^2}$

Subscripts

ad	adiabatic
ax	axial
b	blade
ht	with heat transfer
H	H.P.
m	mean, mean temperature of air
pc	polytropic in compressor
pt	polytropic in turbine
24	inlet to I.P. compressor
26	inlet to H.P. compressor
3	exit from H.P. compressor

1. INTRODUCTION

Gas turbines are extensively used for the propulsion of aircraft. It is essential that these engines can be accelerated from idling speed to maximum speed, and vice versa, in as short times as possible. The two situations which must be avoided during these transient movements are (i) encountering surge in a compressor and (ii) allowing gases at excessive temperature to enter the turbine. It is the first of these situations that is the more difficult to avoid. Surge occurs when a compressor is forced to operate at too high a pressure ratio for that value of non-dimensional rotational speed. Thus the possibility of encountering surge can be eased by matching of the components of the engine (compressor, turbine and final nozzle for a single-spool engine) so that the steady-running line lies well below the surge line. On the other hand, the engine, when at its design condition, must operate at a high pressure ratio in order to achieve good cycle efficiency and hence good fuel economy. It is thus essential, when designing an engine, that the transient behaviour, such as compressor pressure ratio excursions, is well understood. Ideally, an accurate transient prediction procedure should be used.

The purpose of this Paper is to summarise the development of transient prediction procedures, indicating the shortcomings of early procedures and explaining how these shortcomings have been overcome. Finally, this Paper indicates how the use of these improved transient prediction methods can suggest new engine control strategies.

2. PREDICTION OF TRANSIENT PERFORMANCE - ADIABATIC PROCEDURE

The two methods most commonly used to predict the transient behaviour of gas turbines are the 'Continuity of Mass Flow' method and the 'Inter-Component Volume' method.

2.1 'Continuity of Mass Flow' (CMF) Method

In this method it is assumed that at any given instant the mass flow out of the engine matches with the mass flow into it, allowances having been made for bleeds and fuel flow. The calculation starts with a guessed pressure ratio, or mass flow, at the first compressor or fan. This then leads to a set of conditions at entry to the next component. The calculation, with further guesses where necessary, proceeds through the engine. The mass flow at the turbine(s) and nozzle must be consistent with the

non-dimensional characteristics of these components. Tests at these locations will cause iterations in which the initial guesses of pressure ratio(s) or mass flow(s) are revised until continuity of mass flow is achieved. Energy balances are now carried out on the shaft(s) of the engine and instantaneous acceleration rate(s) determined. The procedure of Newton is then adopted in which it is assumed that this acceleration will continue throughout the next time interval. This gives new shaft speed(s) which form the starting point for the calculation procedure at the next instant.

The number of iterative loops (frequently nested) which are required depends on the complexity of the engine. For example, for a single-spool engine operating in a range where the turbine is not choked, only one iterative loop is required. By contrast, five iterative loops may be required for a two-spool turbofan with mixed exhausts. Further description of the CMF method is given in Ref. (1), where it is referred to as the 'Iterative' method.

Difficulties have been experienced (2) in achieving convergence of this procedure when simulating the more complex configurations. However the method has the advantage of requiring significantly less computing time that the alternative, the 'Inter-Component Volume' method. Also, the initial guesses need not be accurate because no results emerge until the iterations have converged on the true pressure ratios etc. The weakness of the procedure obviously is that no allowance is made for the accumulation of air, or gas, mass during the transient within the components and ducts of the engine.

2.2 Inter-Component Volume' (ICV) Method

In this method, allowance is made for the accumulation of mass within the components and ducts. The procedure requires an initial estimate of the pressure distribution along the engine at the conditions corresponding to the start of the transient. Inter-component volumes are identified which include an appropriate proportion of the preceding component and an appropriate proportion of the next component. The initially provided pressure distribution will give mass flows into, and out of, these inter-component volumes. In general, these mass flows will not match, thus air/gas mass will accumulate, or diminish, and the pressure in that volume will rise or fall during the subsequent time interval. This new pressure distribution forms the starting point for the calculation at the next time instant. Further description of this procedure is given in Ref. (1). The calculation is essentially a straight-through procedure with no iterations. In practice some iteration may be required in order to achieve the correct working point on the characteristics of the first turbine. Because of the small values of the inter-component volumes compared to the large magnitudes of the air/gas mass flow rates, very short time intervals have to be used otherwise instabilities occur. Thus computing times are significantly longer than for the CMF method described previously. Also, poor initial values for the pressure distribution in the engine will lead to erroneous results for the first number of time intervals. This can be overcome by having a 'stabilisation' period prior to the transient.

2.3 Fuel Control

In the Introduction it was indicated that, during transients, excursions of a compressor pressure ratio into surge must be avoided. This limitation is achieved by a fuel control system.

For many engines, the engine behaves as though it were 'non-dimensional' over much of its working range. Therefore some fuel control systems have been developed in which the fuel flow, in non-dimensional form, is made a function of some engine non-dimensional parameter. One system that has been applied, for example, to some two-spool turbofan engines is of the form:-

$$\frac{\dot{f}}{N_H \, P_{26}} = fn\left(\frac{P_3}{P_{26}}\right) \qquad \ldots\ldots\ldots(1)$$

Typical acceleration and deceleration schedules of this type are illustrated in Figure 1.

In practice, when the power lever angle is moved rapidly to accelerate, or decelerate, an engine, the fuel flow does not change instantaneously from the steady-running value to the value defined by the acceleration, or deceleration schedule. Instead there is a gradual change which may extend over a period of about 0.5 second. This has been simulated, in the prediction work described in the Paper, by 'ramping' the fuel flow from the steady-running to the transient schedule value over a finite time span. A time span of 0.5 second has been used in the present work.

2.4 Comparison of Predictions of CMF and ICV Methods

The first published comparison of the predictions of these two methods was by Fawke and Saravanamuttoo (1). They found little difference in the predictions, when applied to a single-spool engine, except in the first fractions of a second, in reponse to a step change in fuel flow, the ICV method predicting a more gradual movement of the compressor pressure ratio.

In a recent study (3), in this case of a two-spool turbofan engine with mixed exhausts, the first of the present authors found that the predictions by the two methods of speed change and thrust response were in fair agreement, the responses predicted by the ICV method being about 4 per cent slower. For the transient trajectories in the compressors, the two predictions in the fan and Intermediate Pressure (I.P.) Compressor were very similar. However in the High Pressure (H.P.) Compressor, the trajectory predicted by the ICV method during the first one or so seconds of a rapid transient moves less from the steady-running line than does that predicted by the CMF method.

The predictions given by the ICV method are of course the more accurate because this procedure includes an effect – mass accumulation - ignored in the CMF method. However, as mentioned earlier, the latter method requires significantly less computing time, which may be important when real-time simulation is required.

2.5 General Comments on Predictions

The comments given below are based on the predictions of the ICV method, which is taken as the reference prediction method. As discussed above, the predictions from the CMF method are in general agreement with those from the ICV method, with the exception of magnitude of trajectory displacement in the H.P. compressor only, as described.

Considering first a single-spool engine, it is predicted for an acceleration that the transient 'trajectory' in the compressor will run at pressure ratios higher than the steady-running values. Simple study of the sequence of events will confirm that this movement of the trajectory is to be expected - the higher fuel flow will raise the temperature of the gases at inlet to the turbine, but the non-dimensional flow capacity of the turbine will still be roughly the same so the pressure at inlet to the turbine has to rise, hence the compressor pressure ratio has to rise. In a deceleration the transient trajectory in the compressor drops below the steady-running line.

For multi-spool engines, the trajectory in the H.P. compressor follows the same behaviour as that in the compressor of the single-spool engine described above. The directions of the trajectory movements in the Low Pressure (L.P.) and I.P. compressors of multi-spool engines depend on a number of factors such as the relative inertias of the

shafts, whether any of the compressors have variable geometry such as Inlet Guide Vanes, and finally the engine configuration- turbojet, bypass with mixed exhaust, or bypass with separate exhaust nozzles.The predicted acceleration thrust response of a typical two-spool turbofan with mixed exhaust is shown in Figure 2, the prediction in this case being marked 'Adiabatic'. The engine was using the control system having the acceleration schedule illustrated in Figure 1 with the ramped fuel increase over 0.5 second at the start of the transient. The predicted trajectories in the I.P. and H.P. compressors are shown in Figures 3 and 4 respectively, again marked 'Adiabatic'.

2.6 Some Comparisons with Actual Engine Behaviour

In practice there are some significant discrepancies between the predictions given by the above methods and the performance of actual engines. Three of these cases are cited here.

Firstly, it has been observed (4, 5) that the time taken for an engine to complete a speed transient can be 20 to 30 per cent longer than that predicted by the methods described in Paragraphs 2.1 and 2.2.

Secondly, when the speed transient has been completed in an acceleration, the thrust developed may still be significantly below that which is developed when the conditions in the engine are fully stabilised. For example, it has been observed for a typical single-spool engine (6) that the thrust at the conclusion of the speed transient was 1.5 to 2 per cent below the stabilised value.

Thirdly, it has frequently been observed that, when engines are re-accelerated immediately following a rapid deceleration - the 'Bodie' transient, surge in a compressor is more likely to occur than when accelerating a 'cold' engine at equivalent conditions. Some quantitative data on this occurrence has recently been obtained by Crawford and Burwell (7).

It is obvious that the simple prediction procedures described in Paragraphs 2.1 and 2.2 are not capable of explaining these real engine results.

Studies of 'thermal effects' (4 to 6 and 8 to 19) have been made, resulting in quantitative relationships which can be included in the above general engine transient programs. The introduction of these allowances for 'thermal effects' goes much of the way towards explaining the above mentioned real engine results. These 'thermal effects', and their modelling, are described in the next Section.

3. THERMAL EFFECTS

The 'thermal effects' which are considered to be relevant are:

(i) Heat absorption in fans, compressors and turbines.
(ii) Heat absorption in combustion chambers.
(iii) Changes in characteristics of compressors due to heat transfer (excluding tip clearance effects).
(iv Changes in efficiencies of compressors and turbines due to tip clearances not being stabilised values.
(v) Air flows through seals differing from design proportions due to seal clearances during the transient differing from design stabilised values.
(vi) Delay in the response of the combustion process.

3.1 Heat Absorption in Fans, Compressors and Turbines

In adiabatic flow in a fan or compressor, elemental changes in temperature and pressure are related by the small-stage or polytropic efficiency, η_{pc}:

$$C_p\, dT = \frac{1}{\eta_{pc}}\, v dP \qquad \ldots\ldots\ldots(2)$$

This leads to the relation between the index of compression, n, and the isentropic index, γ:

$$\frac{n-1}{n} = \frac{1}{\eta_{pc}}\,\frac{\gamma-1}{\gamma} \qquad \ldots\ldots\ldots(3)$$

If the flow is not adiabatic, due to heat transfer between the air and the compressor materials during the transient, the above equations are modified to:

$$C_p\, dT = (1-f)\frac{1}{\eta_{pc}}\, v dT \qquad \ldots\ldots\ldots(4)$$

and

$$\frac{m-1}{m} = \frac{1-f}{\eta_{pc}}\,\frac{\gamma-1}{\gamma} \qquad \ldots\ldots\ldots(5)$$

where f is the ratio of the heat transfer to the air in an element to the work transfer from the air in that element. Symbol m represents the index of this non-adiabatic, polytropic compression. It is assumed that the ratio, f, is constant along the compressor.

The equivalent final relation for non-adiabatic polytropic expansion in a turbine is:

$$\frac{m-1}{m} = (1-f)\eta_{pt}\,\frac{\gamma-1}{\gamma} \qquad \ldots\ldots\ldots(6)$$

The ratio, f, can be quite significant and can rise, numerically, to 0.2 in a compressor and 0.35 in a turbine in the sea level transients of a two-spool engine described later in this paper.

3.2 Heat Absorption in Combustion Chamber

In a transient there will be heat tranfers between the materials which form the combustion chamber flame tube and casing and the air/gas which is passing through the chamber. In the early stages of a transient these can represent significant fractions of the changes in fuel flow. A procedure for quantifying this effect is given in Ref. (19).

3.3 Changes in Characteristics of Compressors

During a transient there are several effects taking place in a compressor which will alter the overall characteristics.

Firstly, the heat transfer will change the density at subsequent stages, thus altering the ratio of axial velocity to blade speed in these later stages. This therefore changes the matching between stages and changes the overall pressure rise that will be achieved at the particular non-dimensional inlet mass flow (9, 11, 14).

A second effect is that the boundary layers of the flows over the aerofoils may be altered. For example, heat transfer from the suction surface of a blade to the air, as occurs during a deceleration, will cause a more rapid thickening of the boundary layer, and may lead to earlier separation (10).

A third effect is that heat transfer at the end-walls i.e. at the casings and hubs, will alter the development of the end-wall boundary layers, and thus the pressure rise capability of the stages.

The impact of the above effects on the overall characteristics of a compressor have been investigated (14). A typical change in an H.P. compressor characteristic at an instant in an acceleration of an initially 'cold' engine is shown in Figure 5. It is seen that the constant speed characteristic is moved to what is effectively a higher value, and also the surge pressure ratio - at a mass flow - is raised. These effects can be quantified (12, 17) by the following relationship for change in effective speed:

$$\frac{\Delta N}{N} = C_1\,\frac{T_b - T_{air}}{T_{air}} + C_2\,\frac{\dot{Q}}{\dot{m}\, C_p\, T_m} \qquad \ldots\ldots\ldots(7)$$

and for the revised surge pressure ratio, the relationship:

$$\frac{R_{ht} - 1}{R_{ad} - 1} = 1 + C_3 f - C_4 \frac{\Delta(\delta)}{g} \qquad \ldots\ldots\ldots(8)$$

For the H.P. compressor of the typical two-spool turbofan the coefficients C_1, C_2, C_3 and C_4 have been predicted (17) to have the values – 0.1, – 0.1, 0.36 amd 1.1 respectively.

3.4 Tip Clearance Changes and Effect on Efficiency

Tip clearance changes in general depend on both radial and axial growths (or contractions) during the transient. At this stage only radial growths have been modelled (16). A brief summary is now given of how that model was developed. More complete details are given in the original Paper and Ref. (15).

Tip clearance movements depend on the growths of discs, blades and casing. Considering first the disc, this was considered to be represented by the following - a massive hub, a comparatively thin diaphragm and then an outer rim to which the blade is attached. The hub and diaphragm temperatures are controlled primarily by air drawn from an appropriate stage in a compressor. The 'rim' temperature follows the influences of both the internal air and the external gas flow. Appropriate heat transfer correlations are used for all surfaces. Disc tip expansions were then calculated, assuming that the interfaces were not allowed to move apart. This disc tip expansion was then compared with the predictions of a finite element analysis of the complete disc, considered as a unity. It was found that the movements predicted by the simplified model had to be scaled up by a factor of 1.3 to align them with the predictions of the finite element analysis. Centrifugal growth has also been allowed for. The expansions of the blades are more easily calculated, the procedure being able to cater for cooled blades. Lastly casing expansions were found, the casing temperature responding to the temperature of the internal gas flow and to the temperature of external flows such as air in the by-pass duct.

To illustrate results that are obtained from this procedure, as incorporated in an engine transient program, predicted movements for the components of a characteristic stage in the H.P. compressor of a two-spool turbofan are given in Figure 6, the transient in this case being a rapid acceleration at sea level of an initially 'cold' engine. It is seen that during the speed transient, which lasts about 10 seconds, there is only slight thermal growth of the disc itself - about 10 per cent of the total thermal growth between the starting speeds and the stabilised conditions at the final fuel flow. The averaged time constant of the disc response is about 15 seconds at the end of the speed transient. The characteristic blade on the other hand shows comparatively rapid thermal response, with a final time constant of about 1.0 second. The casing shows a response intermediate between these extremes, with a final time constant of about 5 seconds. The combination of these thermal growths, plus disc centrifugal growth, gives the tip clearance movement, which reduces in the speed transient primarily due to centrifugal growth. During the speed transient the tip clearances are tighter than stabilised values by up to 0.1 mm.

The prediction shows that tip clearances during the transient will, in general, differ from the stabilised values that applied when the set of efficiency values for the component in question was determined. Consequently adjustments to efficiencies are required. The relationship of Lakshminarayana (20) is used to establish the efficiency losses due to the clearances in both the datum and transient cases. The change in efficiency which arises during the transient is then obtained by difference. For reference, Lakshminarayana's relationship is:-

$$\Delta\eta = \frac{0.7\lambda\psi}{\cos\beta_m}\left[1 + 10\left(\frac{\varphi\lambda A}{\psi\cos\beta_m}\right)^{0.5}\right] \qquad \ldots\ldots\ldots(9)$$

For the case illustrated in Figure 6, the tightening of the tip clearance of 0.1 mm is estimated to be worth an improvement in compressor efficiency of about 0.6 per cent.

3.5 Seal Clearance Changes

The methods and model used for tip clearance radial movements can be adapted to predict radial movements at seals. In the present Paper a two-spool turbofan engine is used as the basis for illustrations. For this engine, the seals which are regarded as being most important are an outer seal at the final stage of the H.P. compressor and a seal on the H.P.1 Turbine Disc. The models for these seals have been included in the final program which is used to predict the transient performance of the engine.

3.6 Combustion Delay

It has been suggested that there may be delay between an alteration in fuel flow and the subsequent change in the effective rate at which heat is released in the combustion chambers. However it has been found by Saravanamuttoo (21) that the delay is significant only in engines using vapourising burners. The two-spool turbofan used as illustration in the present work has pressure jet burners, so in this case no delays of this type are expected.

4. PREDICTIONS OF TRANSIENT PERFORMANCE WHEN ACCOUNTING FOR THERMAL EFFECTS

The transient programs (CMF and ICV) described in Section 2 have been extended to include the models of the various thermal effects indicated in Section 3. The resulting predictions for two transients are illustrated here, these transients being firstly, an acceleration of a 'cold' engine and secondly, a deceleration from maximum speed immediately followed by a re-acceleration (the 'Bodie' transient), both transients being at sea level, with flight Mach Number 0.2. The engine used for the illustration is the two-spool turbofan with mixed exhausts, already referred to. Only the predictions from the ICV method are shown.

4.1 Predictions for Acceleration of 'Cold' Engine

The predicted thrust response is given in Figure 2, marked 'With Thermal Effects'. It is seen that the predicted time for the completion of the major portion of the thrust increase is now some 2 to 2.5 seconds longer than has been predicted using the simple 'adiabatic' procedures (Section 2). The major contributions to this delay, indicated by the procedure adopted, are – heat absorption in the combustion chamber metal, higher tip clearances in the H.P. turbine and increased clearance in the seal on the cooling air at the H.P.1 Turbine Disc. Heat absorptions in the H.P. compressor and in the H.P. and L.P. turbines also contribute, although to lesser extents.

It is also to be noted that at the completion of the speed transient and when the fuel flow is at its final value - say at 14 seconds after the start of the transient - the thrust developed is some 2.3 per cent below its final value. This is primarily due to heat absorptions in the compressors and turbines.

Considering now the trajectories predicted in the fan and compressors, the predicted transient operating points in the fan lie very close to the steady-running states and so little further comment is required for that component.

In the I.P. compressor the predicted trajectory during the acceleration (Figure 3) lies below the steady-running line. This is primarily due to the relatively low inertia of the H.P. shaft, compared to the L.P. shaft and to the variable inlet guide vanes on the H.P. compressor which, in their turning range, allow a considerable increase in non-dimensional mass flow for a relatively small increase in non-dimensional speed. The predicted trajectory in the I.P. compressor is hardly affected by the inclusion of the thermal effects.

In the H.P. compressor the predicted trajectory in the acceleration (Figure 4) rises above the steady-running line – as discussed in Paragraph 2.4 However the inclusion of the 'thermal effects' in the prediction procedure gives a much reduced departure from steady-running, now about 60 per cent in the critical region, of that predicted by the adiabatic procedure. The most significant factors causing this reduction in excursion are the heat absorption in the H.P. compressor, and resulting change in characteristics, plus heat absorption in the combustion chambers. The revised surge line, as altered by the heat transfer effects (Equation 8), is also indicated.

4.2 Predictions for Deceleration and Re-acceleration of 'Hot' Engine (Bodie Transient)

The procedures have also been used to predict the performance during a typical transient of this type, again using the two-spool turbofan, with fuel schedule as in Figure 1, as illustration. After the thrust drop in the deceleration, the thrust increase in the re-acceleration was found to be more rapid than that for a 'cold' engine accelerating from the same speeds, and indeed more rapid than predicted by the adiabatic procedure. The more rapid response is due to the summation of virtually all the effects - the heat already stored in the components, and clearances being closer to design condition values.

With regard to the trajectories in the compressors, that in the I.P. compressor (Figure 7) moves upwards from the steady-running line, and towards surge during the deceleration - this being the inverse of the situation in the acceleration, discussed previously. When the re-acceleration takes place the trajectory moves downwards to follow very closely the trajectory that had been predicted for the acceleration of the 'cold' engine. In both the deceleration and re-acceleration, allowing for heat transfer has little effect on the trajectory, as compared with the 'adiabiatic' trajectory. The only noticeable effect, apart from the lowering of the LP shaft speed at the turning point, is a slight easing of the trajectory at the start of the deceleration, mainly due to heat being released from the combustion chamber material.

In the H.P. compressor (Figure 8), during the deceleration the trajectory drops below the steady-running line. However heat transfer effects, particularly the heat transfer and change of characteristics in the H.P. compressor, tend to move the path back towards, and over the steady-running line. When the re-acceleration then takes place the trajectory moves significantly above the predicted accelerating trajectory for the 'cold' engine. Also the surge line is lowered for the first part of the re-acceleration. Surge in this re-acceleration of the 'hot' engine is forecast for this particular example, whereas the acceleration of the 'cold' engine is predicted to be well clear of surge (Figure 4).

5 DEVELOPMENTS TO FUEL CONTROL SYSTEM

It is seen from the above that the control system described in Paragraph 2.3 does not allow consistent utilisation of surge margin. One means that has been proposed of rectifying this is to compensate the controller, introducing a multiplying factor to the fuel fow - this factor being determined by the engine's preceding history. For example, the factor could be a function of a component's temperature e.g. a disc's temperature, or a function of a 'delayed' shaft speed (22).

Another method of achieving consistent surge margin utilisation, is to use a controller whIch ensures that the engine accelerates, or decelerates, at predetermined rates - the N dot (or $\dot{N}$) controller - the acceleration being some function of shaft speed. Achieving a consistent acceleration rate ensures a more consistent trajectory in the compressor(s), provided of course that the compressor(s) and turbine(s) are not deteriorating.

6. CONCLUSIONS

The predictions from the common transient computational procedures - Continuity of Mass Flow (CMF) and Intercomponent Volume (ICV) - have been compared for a two-spool turbofan engine. There is a general similarity in the predictions, but some differences did appear - the CMF method predicts a thrust response which is about 4 per cent more rapid and also a more severe trajectory excursion in the H.P. compressor during those portions of transients where rapid changes are occurring. The predictions of the ICV method are the more valid, as air/gas packing is now accounted for.

The use of these procedures, and assuming adiabatic flow, however fails to predict some important features of 'real engine' performance – slower than predicted speed and thrust response (discrepancy typically 25 per cent), low thrust when speed transient has been completed and tendency to surge when re-accelerating a 'hot' engine. When models for thermal effects are included in the prediction procedure, it is demonstrated that these apparent anomalies in 'real engine' behaviour can now be accurately predicted. The thermal models which have been introduced are described.

REFERENCES

(1) FAWKE, A.J. and SARAVANAMUTTOO, H.I.H. Digital computer methods for prediction of gas turbine dynamic response. SAE Paper 710550, 1971.

(2) FAWKE, A.J. Digital computer simulation of gas turbine dynamic behaviour. PhD Thesis, 1970, University of Bristol.

(3) MACCALLUM, N.R.L. Comparison of CMF and ICV methods for predicting gas turbine transient response. Department of Mechanical Engineering Report, University of Glasgow, August 1989.

(4) BAUERFEIND, K. A new method for the determination of transient jet engine performance based on the non-stationary characteristics of the components. AGARD Conf. Proc. No 34, Part 2, 1968.

(5) THOMSON, B. Basic transient effects of aero gas turbines. AGARD Conf. Proc. No 151, 1975.

(6) MACCALLUM, N.R.L. The performance of turbojet engines during the 'thermal soak' transient. *Proc. Instn mech Engrs.* 1969-70, 184, (Pt 3G(II)), 23-29.

(7) CRAWFORD, R.A. and BURWELL, A.E. Quantitative evaluation of transient heat transfer on axial flow compressor stability. AIAA/SAE/ASME/ASEE 21st Joint Propulsion Conference. Paper AIAA-85-1352, 1985.

(8) FAWKE, A.J. and SARAVANAMUTTOO, H.I.H. Digital computer simulation of the dynamic response of a twin-spool turbofan with mixed exhausts. *Aeronautical Journal* 1973, 24, 471-478.

(9) MACCALLUM, N.R.L. Effect of 'bulk' heat transfers in aircraft gas turbines on compressor surge margins. Instn. mech. Engrs. Conference Publication 3, 1973.

(10) GRANT, A.D. The effect of heat transfer on boundary layer stability in axial flow compressors. ibid.

(11) MACCALLUM, N.R.L. and GRANT, A.D. The effect of boundary layer changes due to transient heat transfer on the performance of an axial-flow air compressor. S.A.E. Trans, 1977, 86, 770284.

(12) MACCALLUM, N.R.L. Thermal influences in gas turbine transients - effects of changes in compressor characteristics. ASME Paper 79-GT-143, 1979.

(13) MACCALLUM, N.R.L. Further studies of the influence of thermal effects on the predicted accelerations of gas turbines. ASME Paper 81-GT-21, 1981.

(14) MACCALLUM, N.R.L. Axial compressor characteristics during transients. AGARD Conf. Proc. No 324, 1982.

(15) PILIDIS, P. Digital simulation of gas turbine performance. PhD Thesis, 1983, University of Glasgow.

(16) PILIDIS, P. and MACCALLUM, N.R.L. A study of the prediction of tip and seal clearances and their effects in gas turbine transients. ASME Paper 84-GT-245, 1984.

(17) MACCALLUM, N.R.L. and PILIDIS, P. The prediction of surge margins during gas turbine transients. ASME Paper 85-GT-208, 1985.

(18) PILIDIS, P. and MACCALLUM, N.R.L. The effect of heat transfer on gas turbine transients. ASME Paper 86-GT-275, 1986.

(19) MACCALLUM, N.R.L. and CHIA, B.H. Thermal modelling of an aero gas turbine combustor. Department of Mechanical Engineering Report, University of Glasgow, August 1989.

(20) LAKSHMINARAYANA, B. Methods of predicting the tip clearance effects in axial flow turbomachines. *J. basic Engng.*, 1970, 92, 467-480.

(21) SARAVANAMUTTOO, H.I.H. Private Communication, 1973.

(22) MACCALLUM, N.R.L. and PILIDIS, P. Gas turbine transient fuel scheduling with compensation for thermal effects. ASME Paper 86-GT-208.

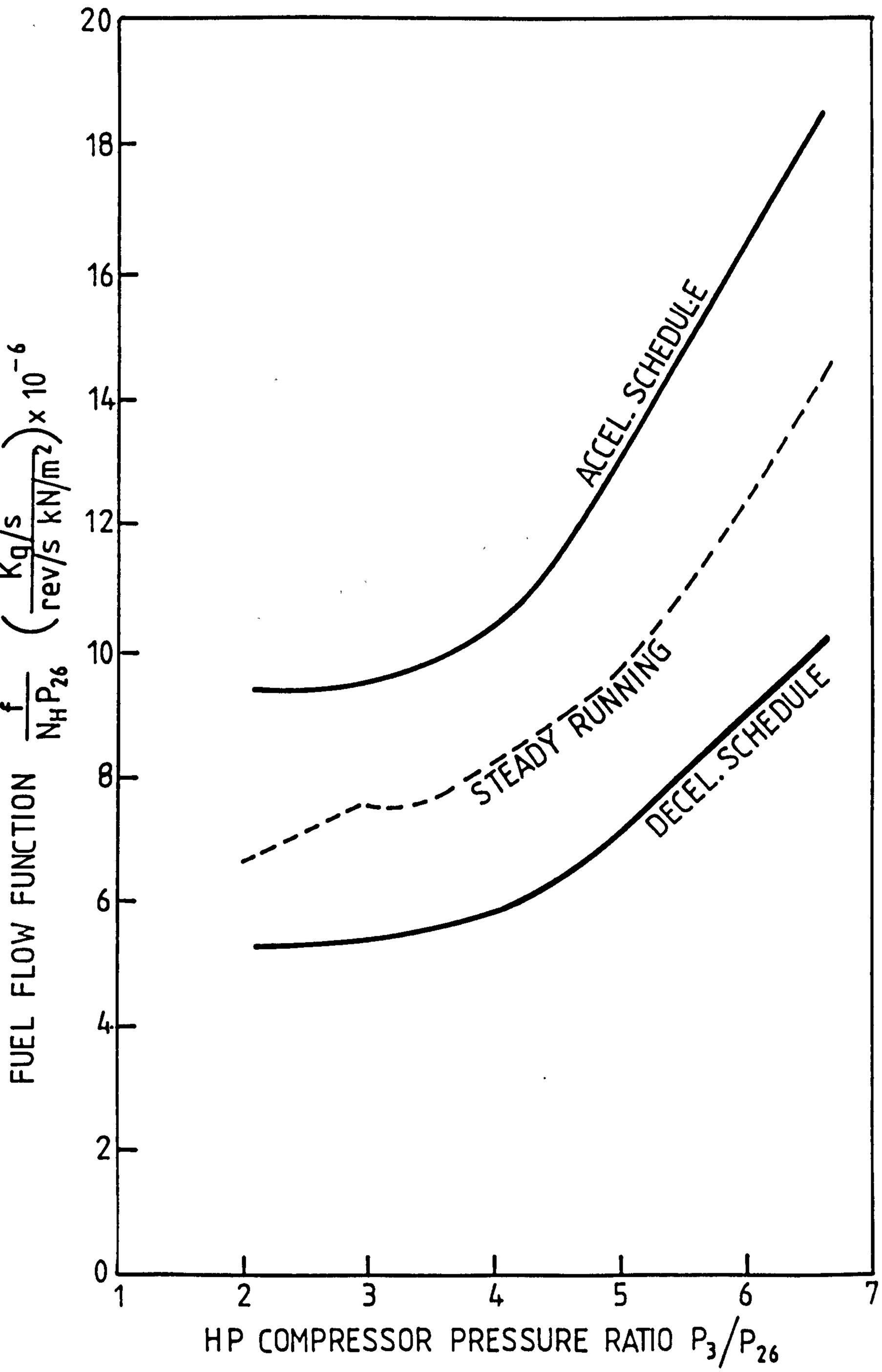

Figure 1 A SIMPLE FUEL CONTROL PAIR OF SCHEDULES

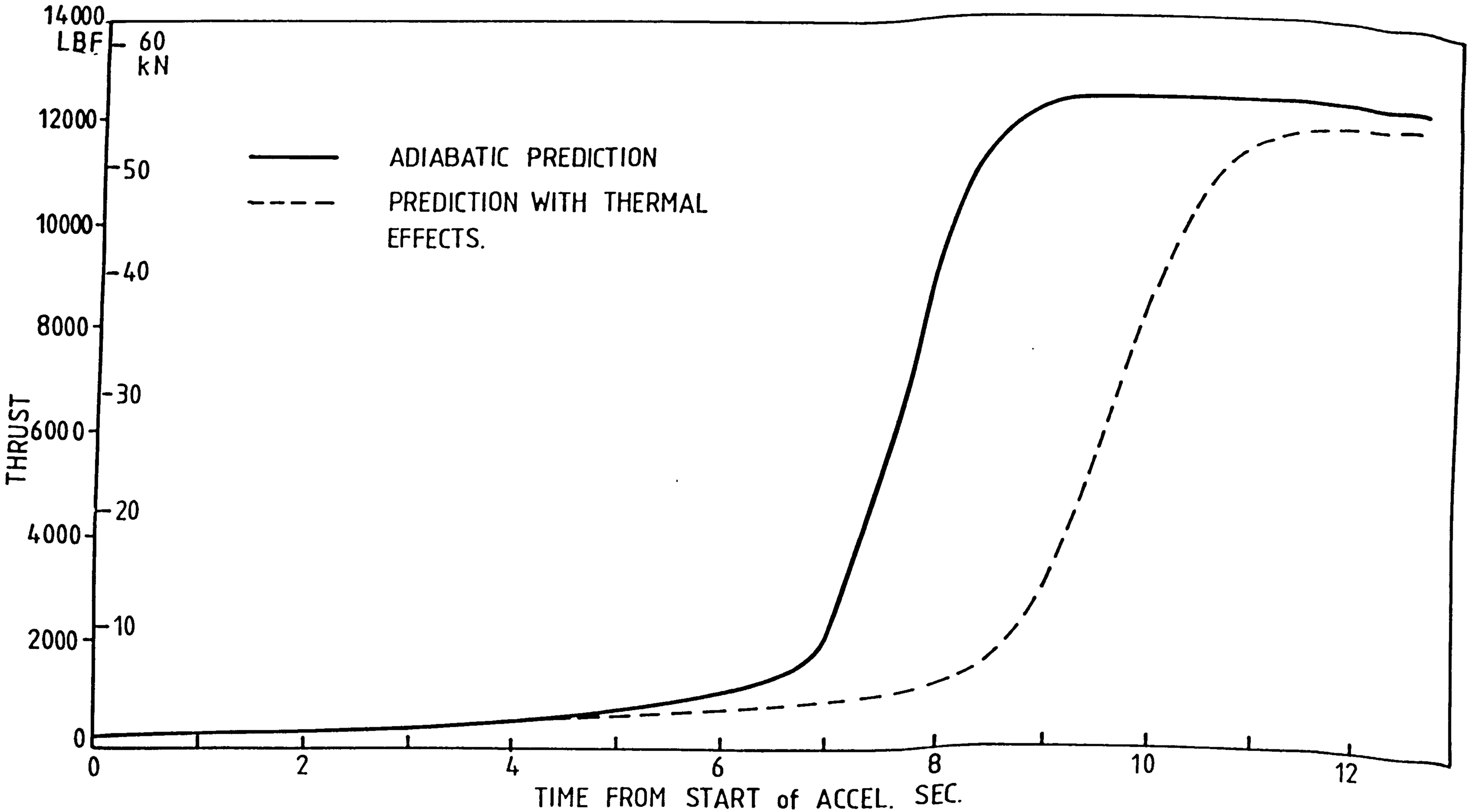

Figure 2 PREDICTED THRUST RESPONSE IN ACCELERATION - SEA LEVEL, MACH 0.2

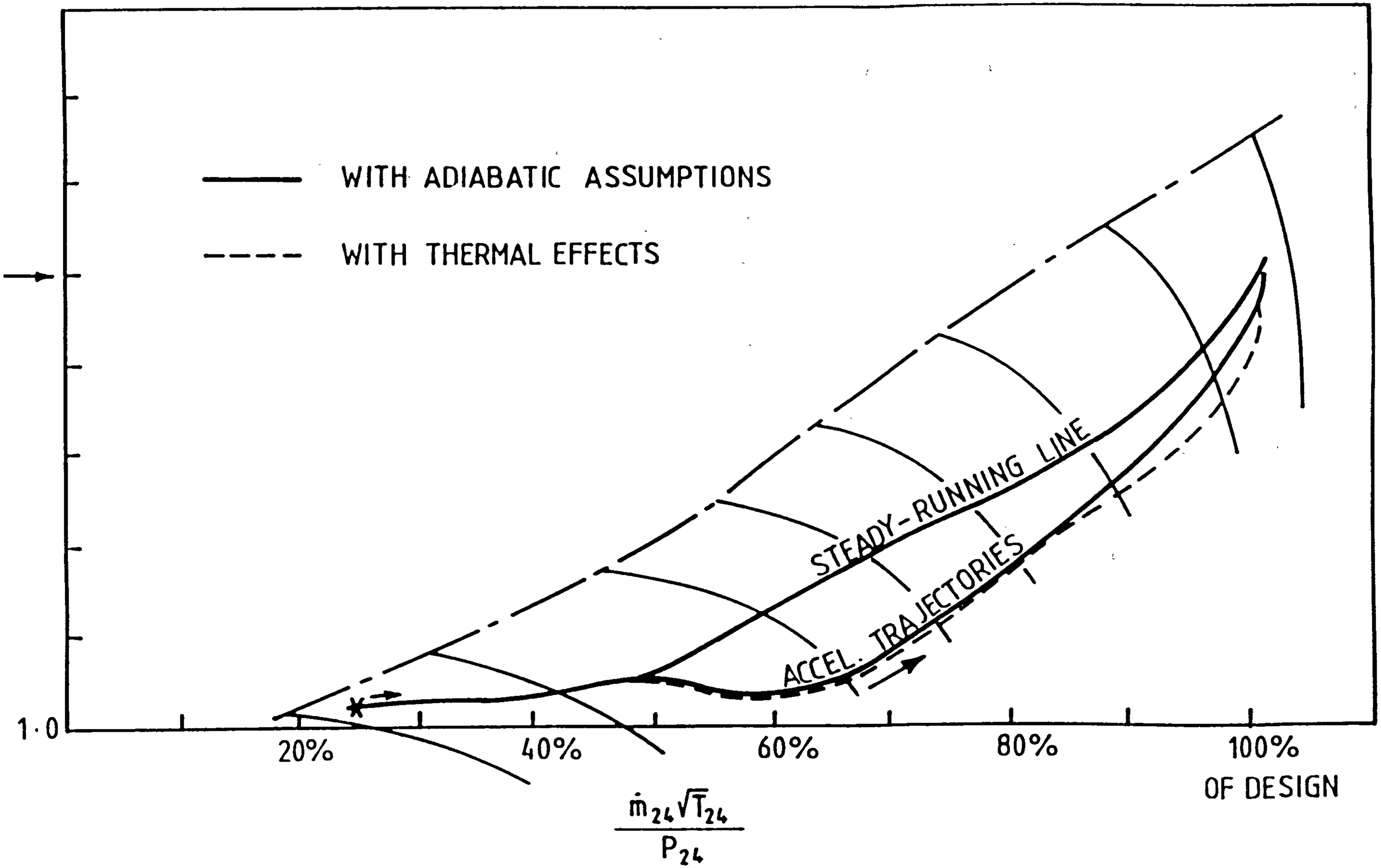

Figure 3 TWO-SPOOL TURBOFAN - PREDICTED TRAJECTORY IN I.P. COMPRESSOR - ACCELERATION AT SEA LEVEL, MACH 0.2

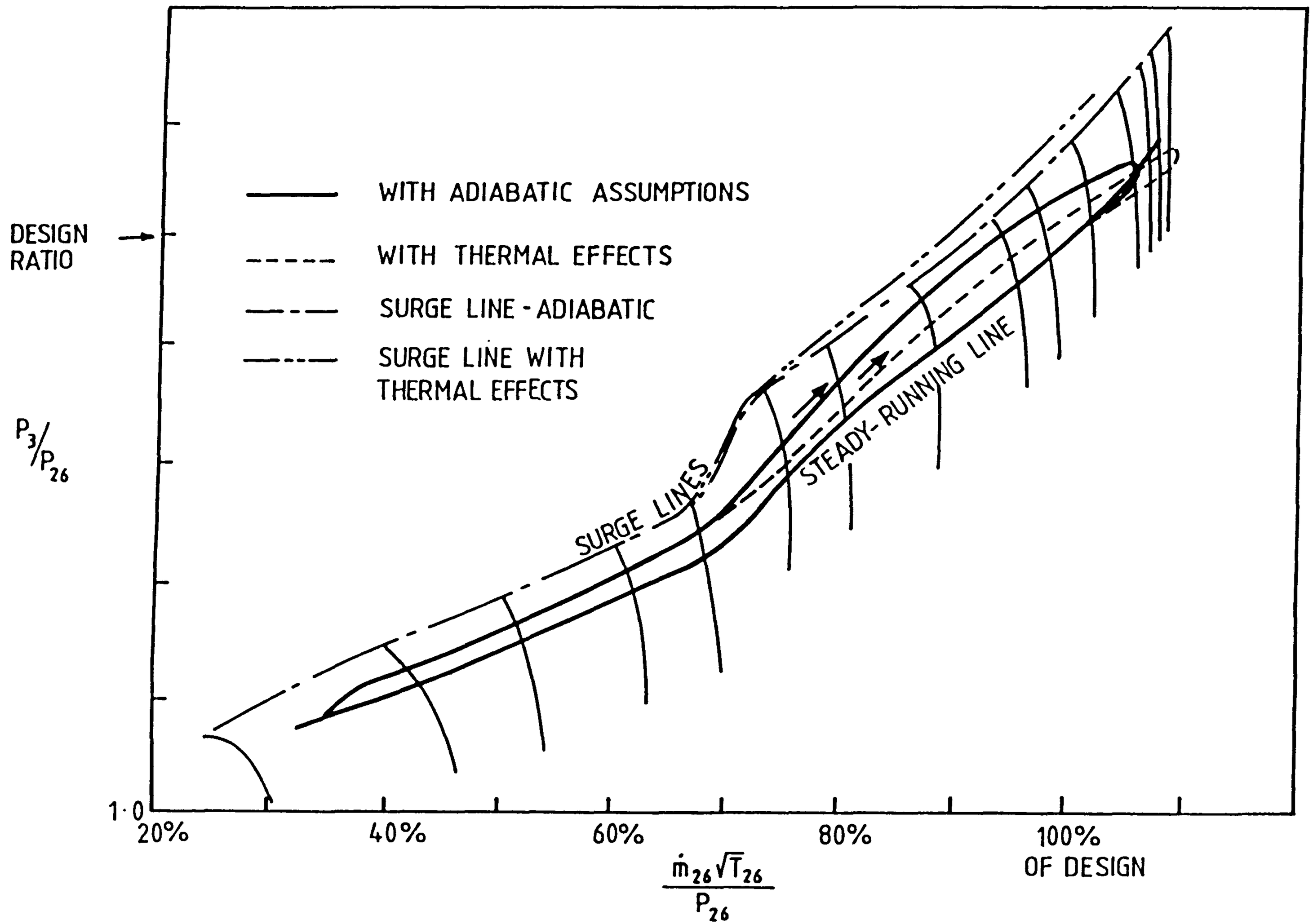

Figure 4 TWO-SPOOL TURBOFAN - PREDICTED TRAJECTORY IN H.P. COMPRESSOR - ACCELERATION AT SEA LEVEL, MACH 0.2

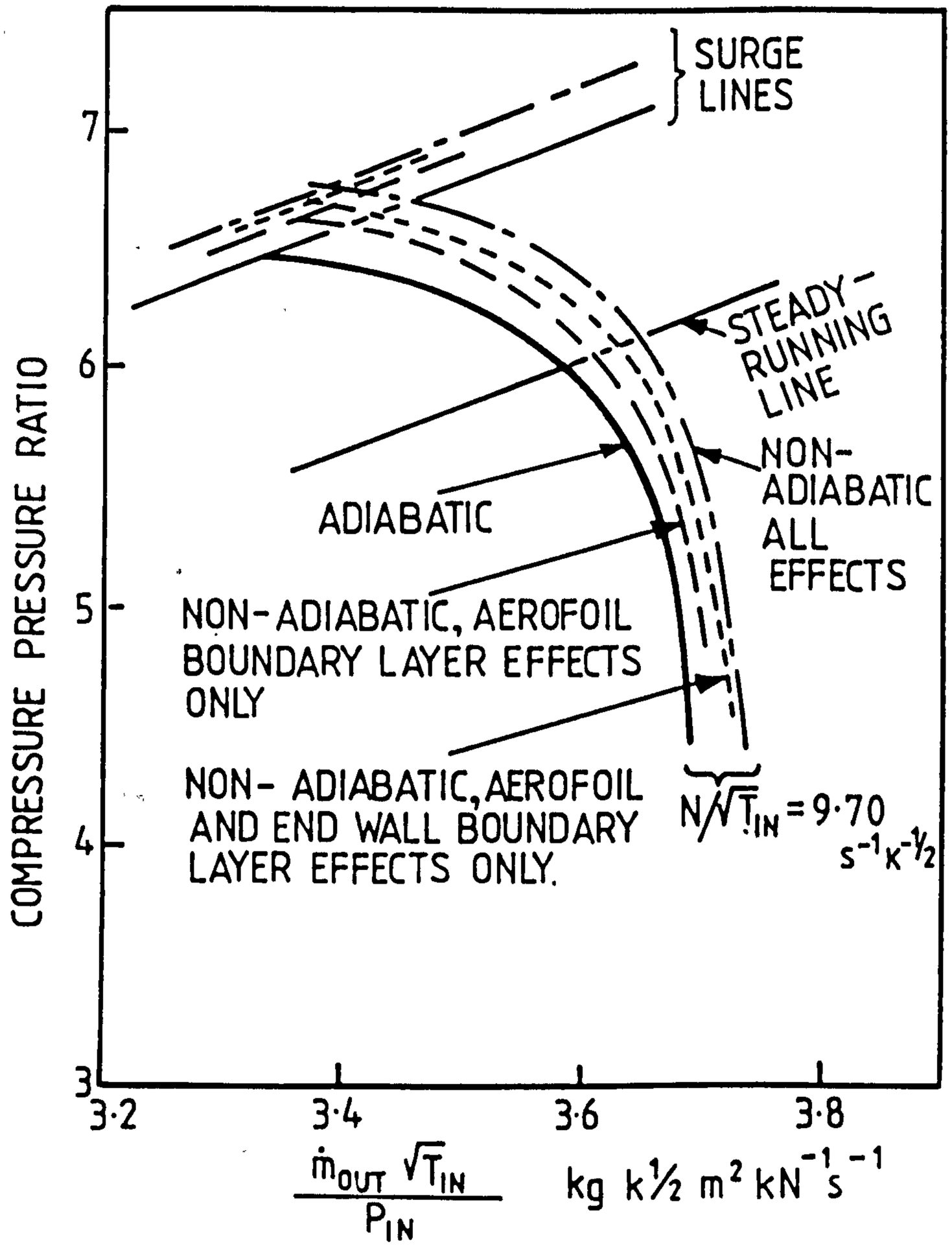

Figure 5 EFFECTS PREDICTED ON TYPICAL H.P. COMPRESSOR CHARACTERISTICS AT 6 SEC. IN SEA LEVEL ACCELERATION

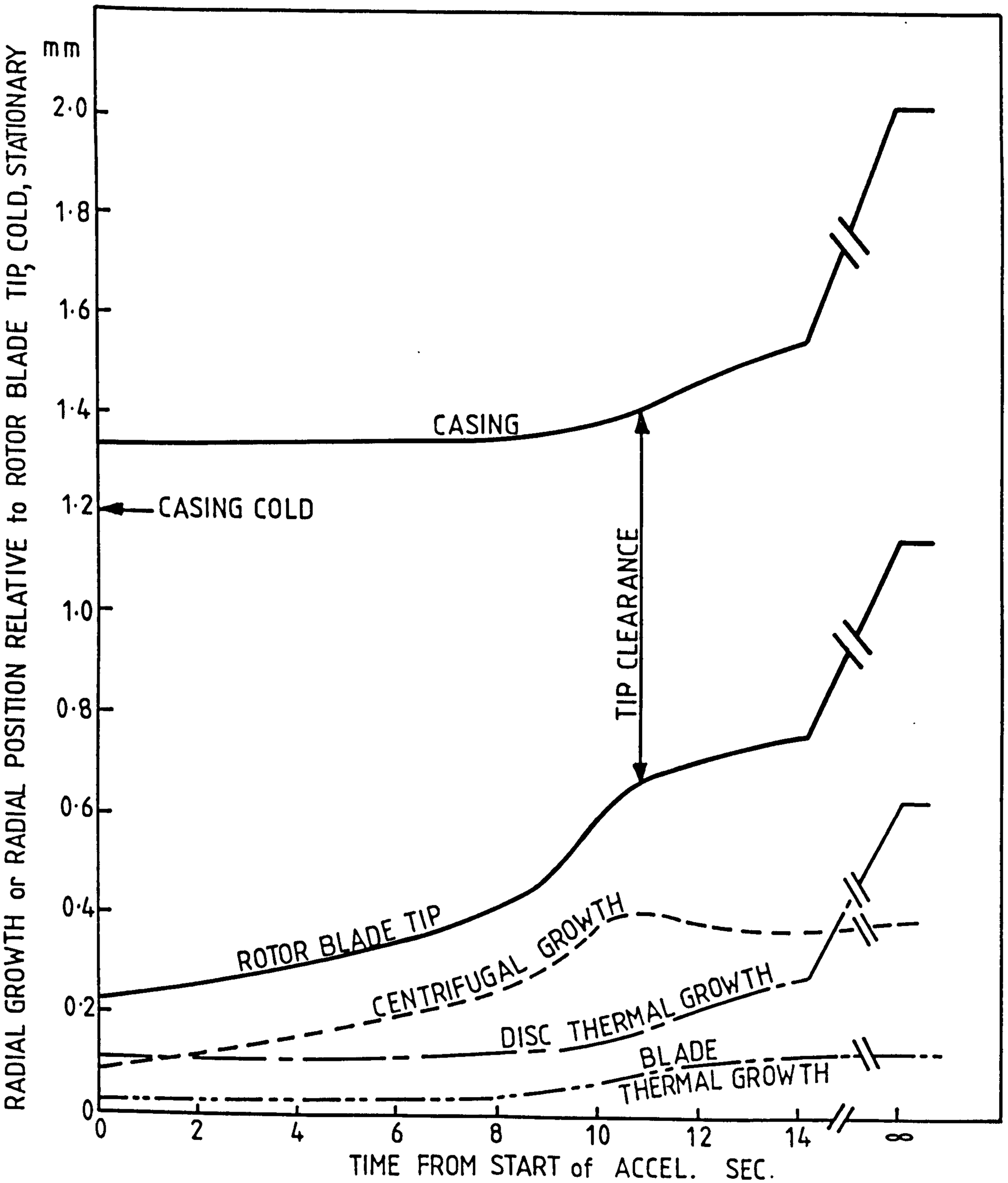

Figure 6 TWO-SPOOL TURBOFAN H.P. COMPRESSOR - CHARACTERISTIC STAGE - MOVEMENTS OF DISC, BLADE AND CASING DURING ACCELERATION - SEA LEVEL, MACH 0.2

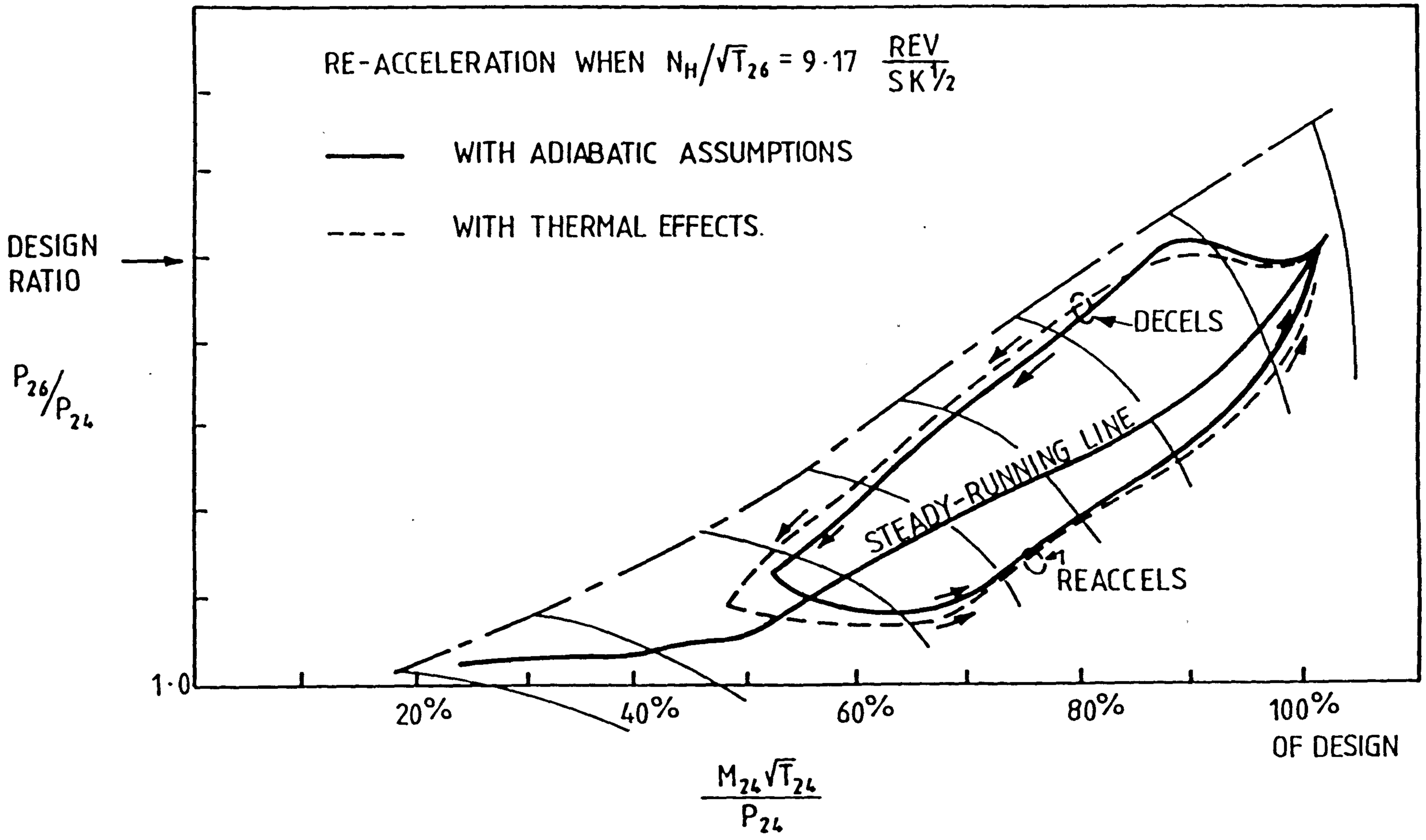

Figure 7 TWO-SPOOL TURBOFAN - PREDICTED TRAJECTORY IN I.P. COMPRESSOR - BODIE TRANSIENT AT SEA LEVEL, MACH 0.2

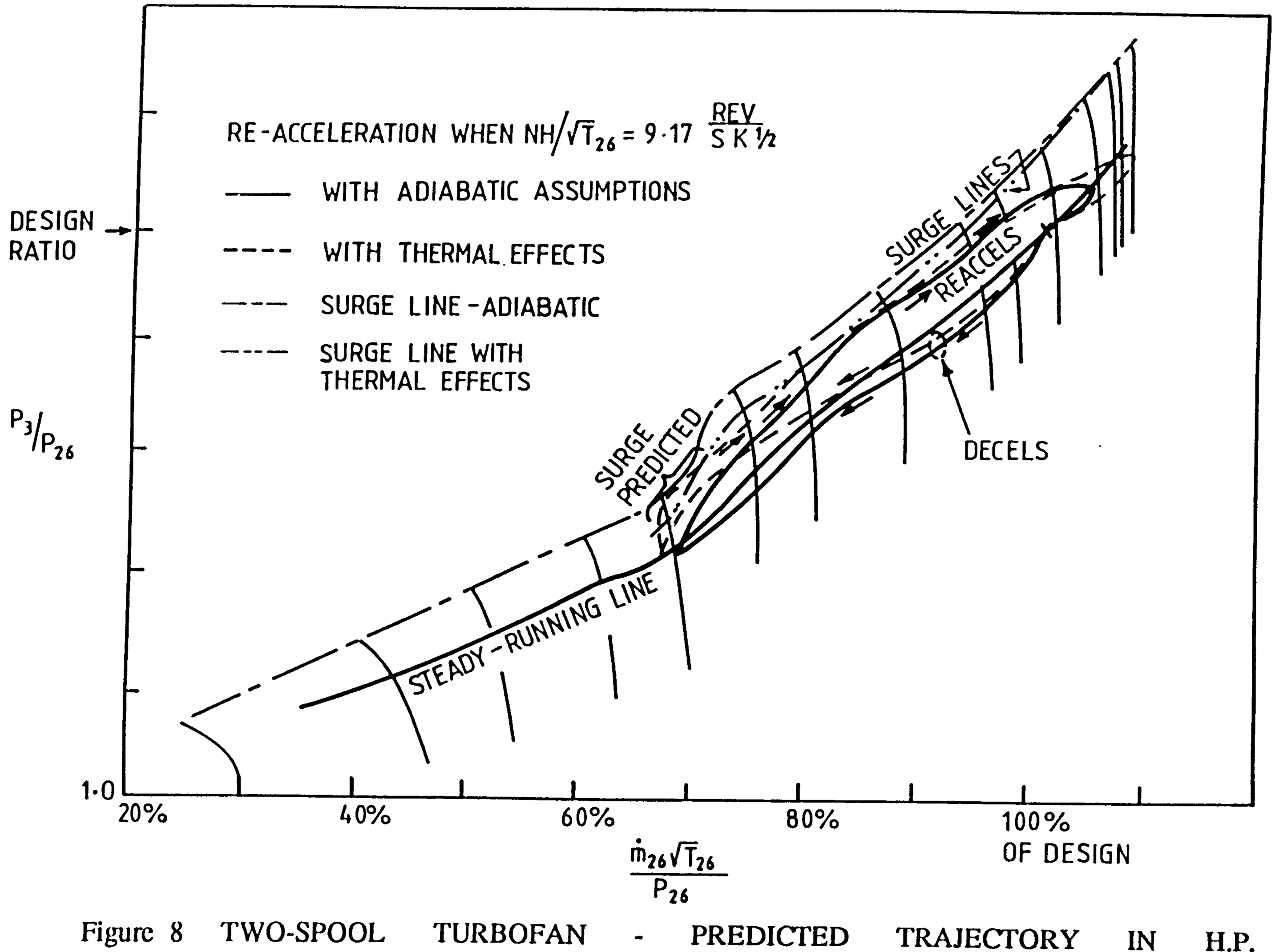

Figure 8 TWO-SPOOL TURBOFAN - PREDICTED TRAJECTORY IN H.P. COMPRESSOR - BODIE TRANSIENT AT SEA LEVEL, MACH 0.2

THE AMERICAN SOCIETY OF MECHANICAL ENGINEERS
345 E. 47 St., New York, N.Y. 10017

92-GT-392

The Society shall not be responsible for statements or opinions advanced in papers or in discussion at meetings of the Society or of its Divisions or Sections, or printed in its publications. Discussion is printed only if the paper is published in an ASME Journal. Papers are available from ASME for fifteen months after the meeting.

Publication 50

Improving Dynamic Response of a Single-Spool Gas Turbine Engine Using a Nonlinear Contoller

O. F. QI, N. R. L. MACCALLUM and P. J. GAWTHROP

Department of Mechanical Engineering
University of Glasgow
Glasgow G12 8QQ
U.K.

Abstract: This paper describes the design of a closed-loop nonlinear controller to improve the dynamic response of a single-spool gas turbine engine. The nonlinear controller is obtained by scheduling the gains of multivariable compensators as a function of engine non-dimensional shaft speed. The compensators, whose outputs are fuel flow and nozzle area, are designed using optimal control theory based on a set of linear models generated from a nonlinear engine simulation. Investigations are also made into developing simple algorithms to obtain an analytical expression for the compressor given its characteristic. The detailed process of developing a nonlinear simulation model for the engine is also described. The open-loop fuel controller is studied using the digital simulation.

NOMENCLATURE

a_i, b_i, c_i	=	parameters for the polynomials.
A_b	=	compressor bleed valve area.
A_e	=	final nozzle area.
c_p	=	specific heat.
F	=	engine thrust.
J	=	shaft inertia.
$\dot{m}_f$	=	fuel flow.
Ma	=	engine flight Mach number.
N	=	engine shaft speed.
P	=	pressure.
s	=	Laplace transform.
T	=	temperature.
u_0	=	flight speed.
u_5	=	exit speed.
V	=	intercomponent volume size.
W	=	power.
γ	=	isentropic index.
η	=	isentropic efficiency.

SUBSCRIPT

0	=	total flow property.
1,2,3,4,5	=	engine station number.
amb	=	ambient conditions.
crit.	=	nozzle critical condition.
c	=	compressor.
n	=	nozzle.
t	=	turbine.
is	=	isentropic.
ss	=	steady-state value.

1 INTRODUCTION

The control designers of modern aircraft gas turbine engines use a variety of sensors and actuators in transient and steady-state operations. Classical designs have relied on hydromechanical fuel controls, i.e., a speed governor for gross transient response with more sophisticated control action used in steady-state regulation and trim. The use of a multivariable control system in gas turbine engines allows an integrated control action to meet steady-state and transient performance requirements. It thus is possible to apply optimal control theory to the design of a closed-loop nonlinear control system intended for operation over the entire power range. The advantages of this control system are DeHoff and Hall (1976);

- Enhanced performance from cross-coupled controls
- Maximum use of engine variable geometry
- A systematic design procedure that can be applied efficiently.

2 MODELING APPROACH

The method of modeling that allows greater insight into the dynamic behavior of a gas turbine engine is based upon the characteristics for each of the engine components. A gas turbine engine comprises a number of components such as compressors and turbines, and the behavior of each of these is well understood. The interactions between the components are fixed by the physical layout of the engine. Thus, for a given engine, if all component characteristics and the engine layout are known, then the gas turbine engine is precisely defined and its dynamic behavior can be expressed mathematically Fawke and Saravanamuttoo (1971).

2.1 MODELING THE COMPRESSOR

The performance of the compressor in a gas turbine engine is very important, especially during transients. In the past, the steady-state characteristics have been used to model this component and computer simulation therefore involves calculating the mass flow or pressure ratio by various interpolation techniques. It is desirable to develop algorithms to enable an analytical expression to be obtained given the compressor characteristics. Unfortunately, relatively little work has been done in this regard. In this section, two simple algorithms are proposed. The first is specific to the present application, and the other is useful for theoretical modeling.

Presented at the International Gas Turbine and Aeroengine Congress and Exposition
Cologne, Germany June 1-4, 1992

2.1.1 USING THE POLYNOMIAL CURVE FITTING

The direct approach is to fit a polynomial to the given characteristic. Examining the shape of a typical compressor characteristic, it is clear that a second order polynomial will be adequate to describe this set of curves. Suppose the pressure ratio can be related to the non-dimensional mass flow as:

$$z = a_1 x^2 + a_2 x + a_3 \tag{1}$$

and the coefficients $a_i, i = 1, 2, 3$ are further assumed to be a second order polynomial of non-dimensional speed:

$$a_i = b_{1i} y^2 + b_{2i} y + b_{3i} \tag{2}$$

Substituting eqn. 2 into eqn. 1, a general nonlinear polynomial, relating pressure ratio to non-dimensional mass flow and shaft speed, can expressed as:

$$z = c_1 x^2 y^2 + c_2 x^2 y + c_3 x y^2 + c_4 x^2 + c_5 y^2 + c_6 x y + c_7 x + c_8 y + c_9 \tag{3}$$

where x stands for non-dimensional mass flow, y for non-dimensional shaft speed, and z for pressure ratio. The coefficients c_i in the equation 3 are obtained from a_i and b_i. By using the nonlinear least-squares fitting method, the coefficients c_i can be determined. The fitting result is shown in Fig.1.

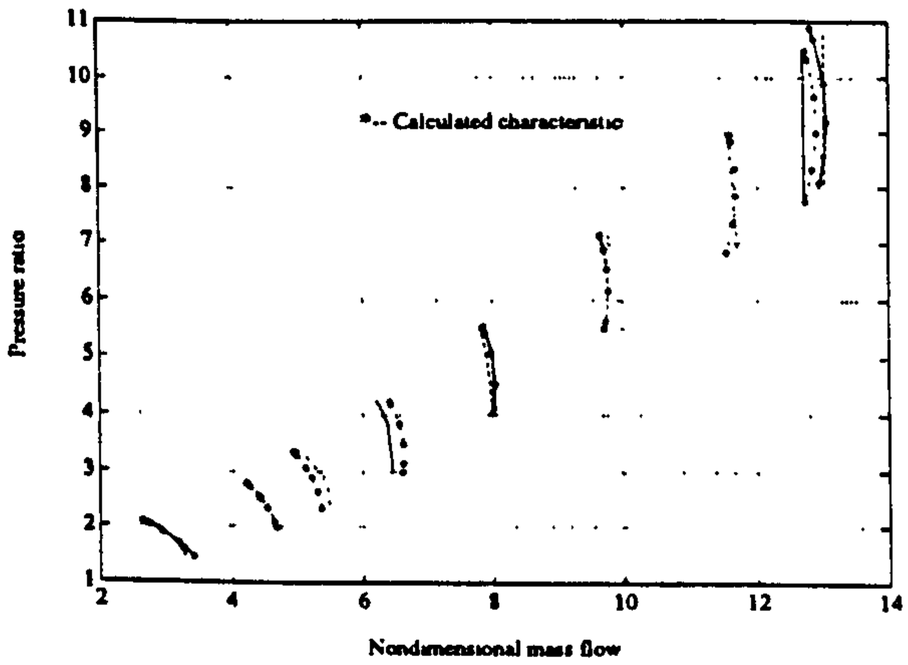

Figure 1: CHARACTERISTIC FITTING USING THE POLYNOMINAL

2.1.2 USING AN ODD GENERIC POLYNOMIAL

An odd-polynomial compressor characteristic is defined by the function Harris and Spang (1991):

$$\phi(x) = \frac{2n^3 + 1}{2n^3} x - \frac{1}{2n^3} x^{2n^3+1} \tag{4}$$

where x and n are the scaled non-dimensional mass flow and speed respectively. All such functions have the same value at $x = 1$, as shown in Fig.2

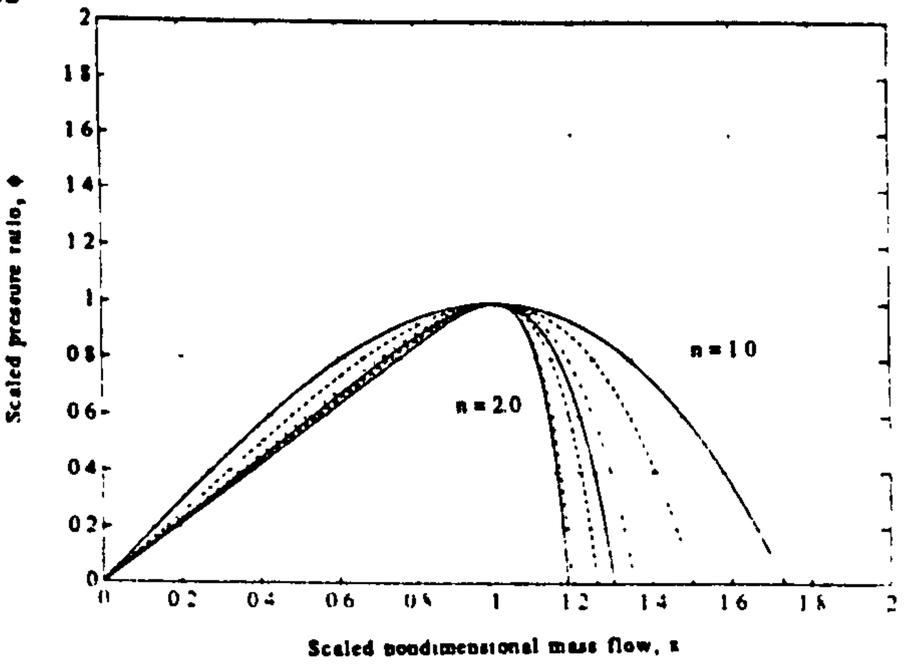

Figure 2: AN ODD POLYNOMIAL CURVE

This unique feature of the equation 4 aids in obtaining the compressor characteristic by dynamic scaling. At each non-dimensional speed, the values of pressure ratio and non-dimensional mass flow are scaled from the reference surge values. The reference scaling value (the surge point) changes as the compressor speed is varied.

The resultant map is shown in Fig 3. There is no significant physical meaning for the region, where at a speed, the non-dimensional mass flow is less than the surge line value.

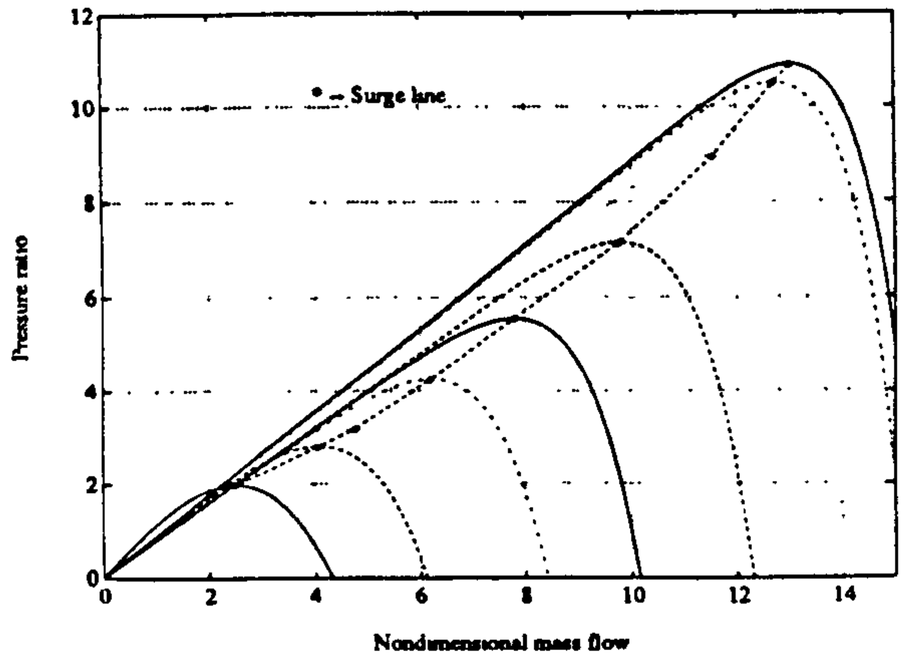

Figure 3: THE CHARACTERISTIC GENERATED USING ODD-POLYNOMIAL

2.2 THERMODYNAMIC MODEL OF THE ENGINE

Using the above approach to modeling the compressor (Fig.1), a nonlinear simulation model could be developed for the engine (Fig.4).

The modeling procedure using the intercomponent volume method Eveker and Nett (1991) is described in this section.

Component A is the inlet. In this component, it is assumed that flow is adiabatic. Using an isentropic efficiency to account for the pressure loss, the conditions at the inlet to the compressor can be calculated using the following equations:

$$T_{01} = T_{amb}(1 + \frac{\gamma + 1}{2} Ma^2) \tag{5}$$

$$T_{01,s} = T_{amb} + \eta_{is}(T_{01} - T_{amb}) \tag{6}$$

$$P_{01} = P_{amb}(\frac{T_{01,s}}{T_{amb}})^{\gamma - 1/\gamma} \tag{7}$$

Component B is the compressor. It is modeled empirically using the fitted polynomial, which gives the non-dimensional mass flow across the compressor:

$$\frac{\dot{m}_c \sqrt{T_{01}}}{P_{01}} = F_c(N, P_{02}, P_{01}, T_{01}) \tag{8}$$

The total temperature rise is found by using the isentropic efficiency factor η_c in the following manner:

$$T_{02} = T_{01}(1 + \frac{1}{\eta_c}((\frac{P_{02}}{P_{01}})^{\gamma - 1/\gamma} - 1)) \tag{9}$$

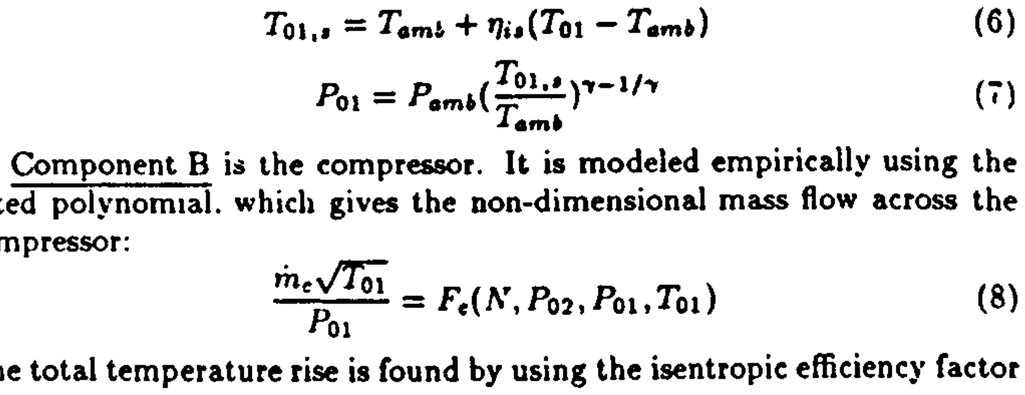

Figure 4: SINGLE-SPOOL ENGINE

Component C is a volume representing the volume of the compressor plus combustor. Here it is assumed that the flow is adiabatic and the flow properties are spatially uniform. The discretized continuity equation combined with the isentropic relation results in:

$$\frac{d}{dt}P_{02} = \frac{\gamma R T_{02}}{V_2}(\dot{m}_c - \dot{m}_b - \dot{m}_t + \dot{m}_f) \tag{10}$$

Component D is the compressor bleed valve. In this engine, a bleed valve at compressor exit has been introduced. It is modeled with an empirical orifice relation which gives:

$$\dot{m}_b = A_b\sqrt{\frac{2P_{amb}}{RT_{amb}}(P_{02} - P_{amb})} \tag{11}$$

Component E is the combustor. In the combustor, the total pressure loss is assumed to be a fixed percentage of its inlet pressure P_{02}, which gives

$$P_{03} = k_{loss}P_{02} \tag{12}$$

The total temperature rise is given by the steady-state energy equation in the combustor:

$$T_{03} = T_{02} + \frac{\eta_f \dot{m}_f Q_f}{(\dot{m}_c + \dot{m}_f - \dot{m}_b)c_p} \tag{13}$$

Component F is the turbine. It is modeled empirically with the steady-state turbine performance map, which gives the nondimensional mass flow across the turbine, thus:

$$\dot{m}_t = \frac{P_{03}}{\sqrt{T_{03}}}T(\frac{P_{03}}{P_{04}}) \tag{14}$$

The total temperature drop is found by using the isentropic efficiency factor η_T in the following manner:

$$T_{04} = T_{03}(1 - \eta_t((\frac{P_{04}}{P_{03}})^{\gamma-1/\gamma} - 1)) \tag{15}$$

Component G is the volume of the turbine plus nozzle. As in the case of the volume C, the exit total pressure P_{04} is modeled using the dynamic equation as;

$$\frac{d}{dt}P_{04} = \frac{\gamma R T_{04}}{V_4}(\dot{m}_t - \dot{m}_n) \tag{16}$$

Component H is the propulsion nozzle. Here it is assumed that the flow is adiabatic. By using an isentropic efficiency factor to account for flow loss, the algebraic continuity equation can be put into the form:

$$\frac{\dot{m}_n\sqrt{T_4}}{P_4} = \frac{u_5}{\sqrt{T_{04}}}\frac{A_p}{R}\frac{P_5}{P_{04}}\frac{T_{04}}{T_5} \tag{17}$$

where

$$\frac{u_5}{\sqrt{T_{04}}} = \sqrt{2c_p\eta_n(1 - (\frac{P_5}{P_{04}})^{\gamma-1/\gamma})} \tag{18}$$

and

$$\frac{T_5}{T_{04}} = 1 - \eta_n(1 - (\frac{P_5}{P_{04}})^{\gamma-1/\gamma}) \tag{19}$$

The preceding equations hold only if the nozzle is not choked. If the nozzle is choked, i.e. $P_{05}/P_{04} \leq P_{crit}/P_{04}$, then:

$$\frac{\dot{m}_n\sqrt{T_{04}}}{P_{04}} = \frac{u_5}{\sqrt{T_{04}}}\frac{A_p}{R}\frac{P_{crit}}{P_{04}}\frac{T_{04}}{T_{crit}} \tag{20}$$

where

$$\frac{P_{crit}}{P_{04}} = (1 - \frac{1}{\eta_n}(\frac{\gamma-1}{\gamma+1}))^{\gamma/\gamma-1} \tag{21}$$

and

$$\frac{T_{crit}}{T_{04}} = \frac{2}{\gamma+1} \tag{22}$$

and

$$\frac{u_5}{\sqrt{T_{04}}} = \sqrt{\frac{2\gamma R}{\gamma+1}} \tag{23}$$

Using the momentum equation applied to the entire engine and ignoring the unsteady terms which are negligible compared to the momentum flux term, an estimate of thrust of the engine is calculated:

$$F = \dot{m}_n u_5 - \dot{m}_c u_0 + A_p(P_5 - P_{amb}) \tag{24}$$

Component I is the compressor/turbine spool. This dynamic equation comes from a power balance on the spool which gives:

$$JN\frac{d}{dt}N = W_t - W_c \tag{25}$$

where $W_c = \dot{m}_c c_p(T_{02} - T_{01})$ and $W_t = \dot{m}_t c_p(T_{03} - T_{04})$. The governing equation is therefore

$$JN\frac{d}{dt}N = \dot{m}_t c_p(T_{03} - T_{04}) - \dot{m}_c c_p(T_{02} - T_{01}) \tag{26}$$

An information flow diagram for the model described above is given in Fig.5, which shows where the parameters and inputs enter into the model structure.

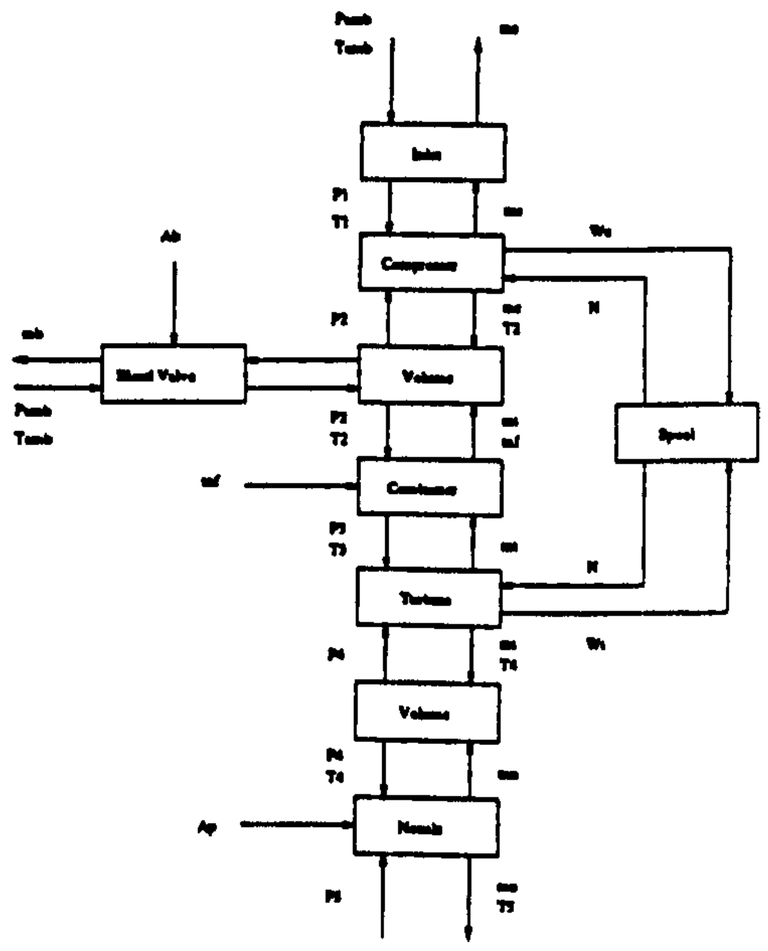

Figure 5: INFORMATION FLOW DIAGRAM FOR SINGLE-SPOOL ENGINE

3 OPEN-LOOP FUEL CONTROLLER

When using the open-loop fuel controller, it has been a common practice to meter fuel flow to the engine as a function of compressor pressure ratio. In this method, the fuel at a fixed compressor pressure ratio will change with the engine inlet condition. As a result, acceleration rate will vary as a function of the inlet condition.

This could be avoided by scheduling fuel non-dimensionally during transients. Therefore, the open-loop fuel group usually incorporates inlet pressure and temperature, the nondimensional fuel flow group becomes $\dot{m}_f/(P_1\sqrt{T_1})$.

Using such a group will involve the measurement of inlet temperature which is generally slow in response compared with the measurements of speed and pressure. A alternative non-dimensional parameter could be obtained by dividing the group above by non-dimensional speed $N/\sqrt{T_1}$, which gives

$$\frac{\dot{m}_f}{P_1\sqrt{T_1}}/\frac{N}{\sqrt{T_1}} = \frac{\dot{m}_f}{P_1 N} \tag{27}$$

In the common open-loop controller, using the fuel group of this form, only shaft speed and inlet pressure need to be measured, and is made a function of the compressor pressure ratio.

4 GENERATING LINEAR MODELS

Before linearising the nonlinear model, it is necessary to normalize the nonlinear engine model. The nonlinear model includes the physical units of the performance variables and scaling of their physical units is necessary to make their interactions easier to compare and understand. For this single-spool engine, the physical maximum limits of the variables, shown in table 1, were used as scaling values.

Variable	Scaling value	Physical unit
N	8193.80	rpm
P_2	1005.70	KN/m^2
T_3	1250.80	K
P_4	315.780	KN/m^2
F	59243.0	N
$\dot{m}_f$	1.40000	kg/s
A_p	0.32000	m^2

Table 1: Scaling values for the single-spool turbojet engine

4.1 LINEARISING THE NONLINEAR MODEL

Suppose a gas turbine engine can be represented by the following nonlinear differential and algebraic equations.

$$\begin{aligned} \dot{x} &= F(x,u) \\ y &= G(x,u) \end{aligned} \tag{28}$$

In deriving linear models, we assume that functions F and G are continuous and differentiable. If the system described by equation 29 is in a steady state condition, i.e., constant input u_{ss} producing constant state x_{ss} and constant output y_{ss}, then the combination (u_{ss}, x_{ss}, y_{ss}) satisfies:

$$\begin{aligned} 0 &= F(x_{ss},u_{ss}) \\ y_{ss} &= G(x_{ss},u_{ss}) \end{aligned} \tag{29}$$

The point (u_{ss}, x_{ss}, y_{ss}) is termed an equilibrium operating point of the gas turbine engine. Perturbating the control input with δu results in state and output perturbation δx and δy, respectively and control input, state and output become $u = u_{ss} + \delta u$, $x = x_{ss} + \delta x$ and $y = y_{ss} + \delta y$, and the equation 29 follows:

$$\begin{aligned} \dot{x}_{ss} + \delta\dot{x} &= F(x_{ss} + \delta x, u_{ss} + \delta u) \\ y_{ss} + \delta y &= G(x_{ss} + \delta x, u_{ss} + \delta u) \end{aligned} \tag{30}$$

Because of the continuity requirements imposed on the functions of F and G, equation 31 can be expanded in a Taylor series about the point (u_{ss}, x_{ss}). Ignoring the higher order items and noting $\dot{x}_{ss} = 0$ $y_{ss} = G(x_{ss}, u_{ss})$, we obtain;

$$\begin{aligned} \delta\dot{x} &= A\delta x + B\delta u \\ \delta y &= C\delta x + D\delta u \end{aligned} \tag{31}$$

The constant matrices A, B, C, D have the dimensions of n×n, n×m, r×n, r×m respectively and are given by;

$$A = \frac{\partial F_i}{x_j} \quad B = \frac{\partial F_i}{u_j} \quad C = \frac{\partial G_i}{x_j} \quad D = \frac{\partial G_i}{u_j} \quad i = 1,2,...,n. \quad j = 1,2,...,r. \tag{32}$$

This equation approximates the dynamic behavior of the nonlinear gas turbine engine in a small region about the operating point ($u = u_{ss}$, $x = x_{ss}$).

Remark 1 : Linear models of a gas turbine engine can be generated in many ways, e.g. numerically from the nonlinear simulation, or directly from engine test data. A common method is to utilize a nonlinear hybrid or digital engine simulation. This procedure is computationally efficient; but often, linearised behavior is dependent on the perturbation size.

Remark 2 : Linear models generated numerically do not contain the most convenient parameterization of dynamics and sometime contain far too complex a description to be practically utilized for control design. It is likely that a design model including engine, actuator and sensor dynamics could be a high order system. In this case, model reduction will be the first important step to establish an effectively simple model which includes only elements important to the desired control function.

4.2 COMPARING LINEAR, NONLINEAR MODEL

After nine linear models have been obtained, it is necessary to compare their performance with those of the nonlinear model. Time-domain simulation has been conducted in which linear and nonlinear model are subject to a series of the equal step change in fuel flow. The results for operating point 1 are shown in Fig.18. It is shown that linear models have approximately the same dynamics as the nonlinear model at most of the operating points.

5 NONLINEAR CONTROLLER DESIGN

The nonlinear control synthesis procedure derived here is based on linearising the engine nonlinear model at a set of closely-spaced steady-state operating points and applying the linear optimization method to the linear models. The nonlinear control problem is thereby reduced to a series of linear control problems. This permits the use of established analytical and numerical methods associated with linear optimal control theory. At each operating point, an optimal linear feedback controller is generated by minimizing a quadratic performance criterion. Weighting factors within each performance criterion enable the control designer to satisfy performance specifications by trading off system response against control actuation rate. Nonlinear feedback control is then constructed by combining the series of linear controllers into a single nonlinear controller whose feedback gains vary with states.

5.1 CHOICE OF CONTROLS AND OUTPUTS

The nonlinear model for this engine has four states. In order to improve the dynamic response, the final nozzle area is used as control input as well as fuel flow.

5.2 LINEAR QUADRATIC REGULATOR(LQG)

Given a linearised model corresponding to a engine operating point, the standard linear optimal design technique can be used to determine full state feedback gains by minimizing a quadratic performance index Bryson and Ho (1969);

$$J = \frac{1}{2}\int_0^\infty (\delta x^T Q \delta x + \delta u^T R \delta u) dt \tag{33}$$

and solving the corresponding Riccati equation;

$$A^T P + PA + PBR^{-1}B^T P - Q = 0 \tag{34}$$

The state feedback gains are;

$$\delta u = -R^{-1}B^T P \delta x \tag{35}$$

To satisfy the steady state performance, the control actuation rates are introduced by augmenting the linearised model with m integrators . Fig.6 depicts the resultant structure. It should be noted that δ has been omitted in the Figures.

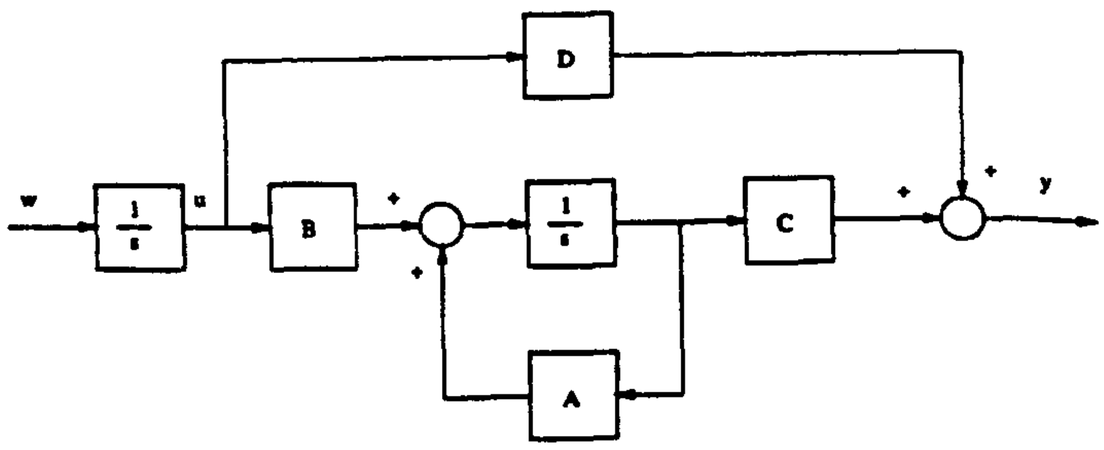

Figure 6: LINEARISED MODEL AUGMENTED BY M INTEGRATORS

The augmented system equation becomes;

$$\begin{aligned} \delta\dot{x} &= A\delta x + B\delta u \\ \delta\dot{u} &= \delta w \\ \delta y &= C\delta x + D\delta u \end{aligned} \tag{36}$$

Note that the order of the overall system i.e. the system whose input is δw and output is δy. is n+m. The original control variable δu, which is now the output of integrators, becomes a state vector. The vector δw is the new m × 1 control vector, and $\delta\hat{x} = [\delta x \delta u]^T$ is the new (n+m)×1 state variables. The overall perturbational system is then given by;

$$\begin{aligned} \delta\dot{\hat{x}} &= \hat{A}\delta\hat{x} + \hat{B}\delta w \\ \delta y &= \hat{C}\delta\hat{x} \end{aligned} \tag{37}$$

The matrices $\hat{A}$, $\hat{B}$ and $\hat{C}$ are (n+m)×(n+m), (n+m)×m, and p×(n+m) and can be partitioned into;

$$\hat{A} = \begin{bmatrix} 0 & 0 \\ A & B \end{bmatrix} \quad \hat{B} = \begin{bmatrix} I \\ 0 \end{bmatrix} \quad \hat{C} = \begin{bmatrix} C & D \end{bmatrix} \tag{38}$$

Applying LQG to the augmented model and minimizing the quadratic performance index leads to the state feedback gains;

$$\delta w = -K\delta\hat{x} = \begin{bmatrix} K_{11} & K_{12} \end{bmatrix} \begin{bmatrix} \delta u \\ \delta x \end{bmatrix} \tag{39}$$

The resultant control structure is shown in Fig.7. The gain matrix M has been added to the closed-loop system to permit the consideration of command inputs δr and an equation defining M will be derived later. This standard linear optimal control structure may not guarantee the output δy tracking the commanded input δr despite the addition of m integrators to the linearised system equation. This is because the control commands there are not generated by the integral of the error between the desired and the actual output Athans, et al (1986).

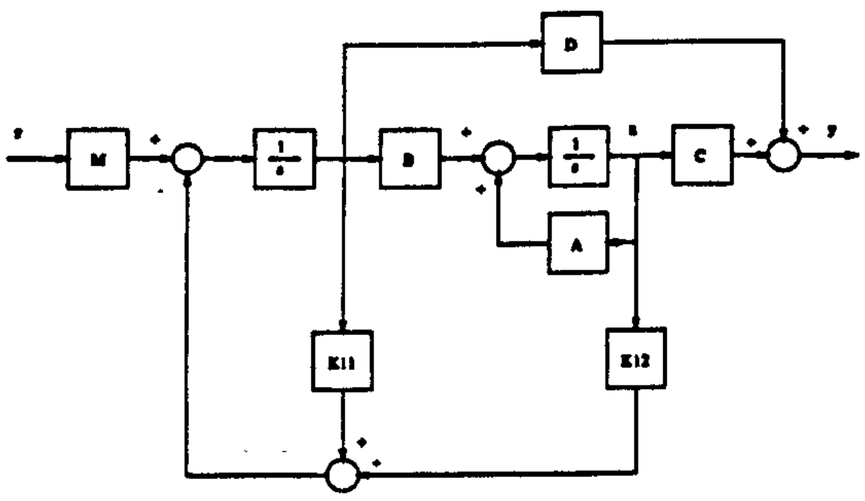

Figure 7: LQG DESIGN FOR THE AUGMENTED LINEARISED MODEL

5.3 OPTIMAL INTEGRAL CONTROL

An integral control structure drives a dynamic system to its proper state using control commands derived by integrating the errors between the desired and actual output Szuch et al (1977), Rosenblad (1990). Consequently, an optimal integral controller is an improvement over standard linear optimal control because it ensures zero steady-state errors even in the presence of plant parameter variations. Given an optimal feedback gain K, it is possible to derive an equivalent optimal integral control structure to eliminate steady-state error. The desired structure is shown in Fig.8.

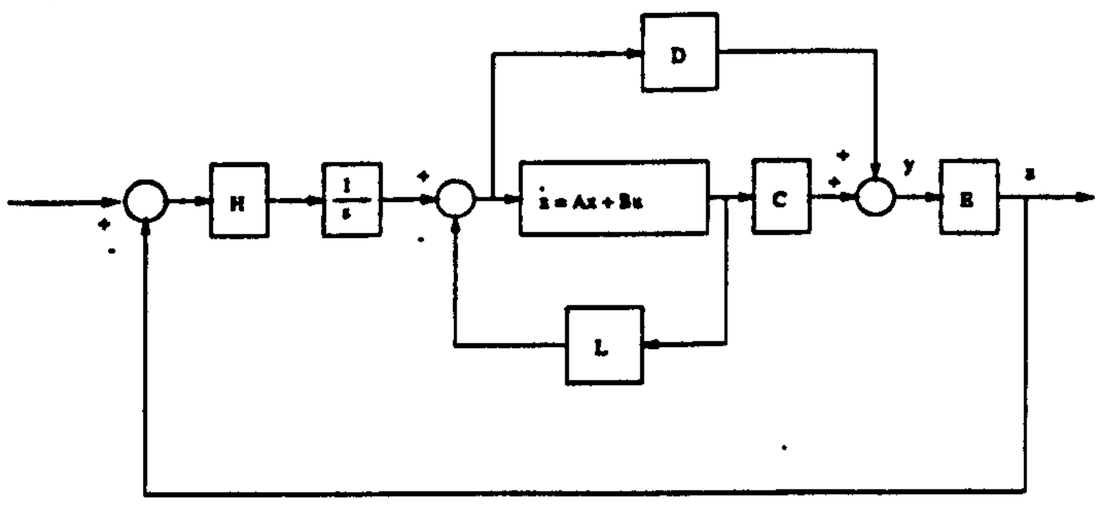

Figure 8: OPTIMAL INTEGRAL CONTROL STRUCTURE

Because there are m independent control variables, the steady-state values of m outputs can be specified independently if p $\geq$ m. Hence δr is an m vector. With no loss of generality, the p components of the output vector δy can be ordered such that the steady-state values of first m components are is desired to be specified. If a partitioned matrix E is defined as $E = [I \;\; 0]$ and $\delta z = E\delta y$, then δz is m×1 measured output vector, and thus required to track the command δr. The desired integral matrix H and L are yet to be determined. Note that the original feedback gain matrix K has m×(n+m) known elements. while the integral control gain matrices H, L have a combined total $m^2 + mn$ unknown elements, the integral control gains will be established by deriving an explicit relationship between the m×(n+m) H, L unknowns and m×(n+m) K knowns. It is clear from Fig.8 that the following equations hold:

$$\delta u(s) = \frac{1}{s}H(\delta r(s) - \delta z(s)) - L\delta x(s) \tag{40}$$

$$s\delta u(s) = H(\delta r(s) - \delta z(s)) - sL\delta x(s) \tag{41}$$

$$s\delta x(s) = A\delta x(s) + B\delta u(s) \tag{42}$$

$$\delta z(s) = E\delta y(s) = EC\delta x(s) + ED\delta u(s) \tag{43}$$

$$s\delta u(s) = H\delta r(s) - (HEC + LA)\delta x(s) - (HED + LB)\delta u(s) \tag{44}$$

From the Fig.8;

$$s\delta U = M\delta r(s) - K_{11}\delta u(s) - K_{12}\delta x(s) \tag{45}$$

For any command δr, it is desired that the control modes in Fig.7 and 8 yield identical state and control variable time responses. This equivalence is accomplished by equating the δx, δu and δr coefficients on the right hand sides of the above two equations, leading to;

$$K_{11} = HED + LB \quad , K_{12} = HEC + LA, \quad M = H \tag{46}$$

Given the system matrices A, B, C, D and the optimal feedback gain matrix K, the above equation provides an explicit means for uniquely determining the integral control gain matrix H, L. If the system matrices A, B, C, D are perfectly known and H, L and M are determined from the above equations, then the responses of these systems in Fig.7 and 8 to arbitrary command input will be identical. Unlike the standard control mode in Fig.7, however, the integral controller assures zeros steady-state output errors even when unknown parameter variations occur in the system equations.

6 NONLINEAR CONTROL SYNTHESIS

The optimal linear control synthesis method described in the preceding section is carried out at all the steady-state operating points, and as the result, a series of optimal incremental feedback controls δu can be obtained. The gain matrix H and L are computed using the resultant state feedback gain K (Hackney, Miller and Small (1978)).

The weighting matrices Q and R in the present study are selected as:

$$Q = \begin{bmatrix} 10 & 0 & 0 & 0 & 0 \\ 0 & 10 & 0 & 0 & 0 \\ 0 & 0 & 1 & 0 & 0 \\ 0 & 0 & 0 & 1 & 0 \\ 0 & 0 & 0 & 0 & 1 \end{bmatrix} \quad R = \begin{bmatrix} 1 & 0 \\ 0 & 1 \end{bmatrix} \tag{47}$$

for all the linear optimal compensator designs. Selection of weighting matrices Q and R in this way, along with the continuity requirement imposed upon F and G assure that the optimal feedback gains H and L vary smoothly from one operating point to another.

Since a operating point is defined by the state x, H and L become functions of x ,i.e., $H = H(x)$ and $L = L(x)$. These matrices may be converted to continuous functions of x using any of several interpolation schemes. With H and L continuous functions of state, it is possible to develop a relationship defining a nonlinear optimal control $u(t)$.

From the Fig.8, the optimal incremental control is defined by:

$$dU(s) = L(x)dx(s) + \frac{1}{s}H(x)(r(s) - z(s)) \tag{48}$$

The optimal control $u(t)$ can now be obtained from the path integral:

$$\begin{aligned} u(t) &= u(0) + \int_{u(0)}^{u(t)} du \\ &= u(0) + \int_{x(0)}^{x(t)} L(x)dx + \int_0^t \int_{r(0)-z(0)}^{r(t)-z(t)} H(x)(dr(\tau) - dz(\tau))d\tau \end{aligned} \tag{49}$$

By definition, the gain matrix H(x) is a function of x alone, i.e, it is independent of r and z, hence H(x) can be removed from the first integration, resulting in:

$$u(t) = u(0) + \int_{x(0)}^{x(t)} L(x)dx + \int_0^t H(x) \int_{r(0)-z(0)}^{r(t)-z(t)} (dr(\tau) - dz(\tau))d\tau \tag{50}$$

$$u(t) = u(0) + \int_{x(0)}^{x(t)} L(x)dx + \int_0^t H(x)(r(\tau) - z(\tau))d\tau \tag{51}$$

The above equations make use of the fact that $r(0) = z(0)$ for a system controlled by the integral mode and initially in a steady state condition. In the computer implementation, each entry in the H and L is scheduled as a function of speed; for example, $H(1,1)$ is;

$$H(1,1) = f_1 exp(-\lambda_1 * N) + f_2 exp(-\lambda_2 * N) \qquad (52)$$

and the scheduling result is shown in Fig.9

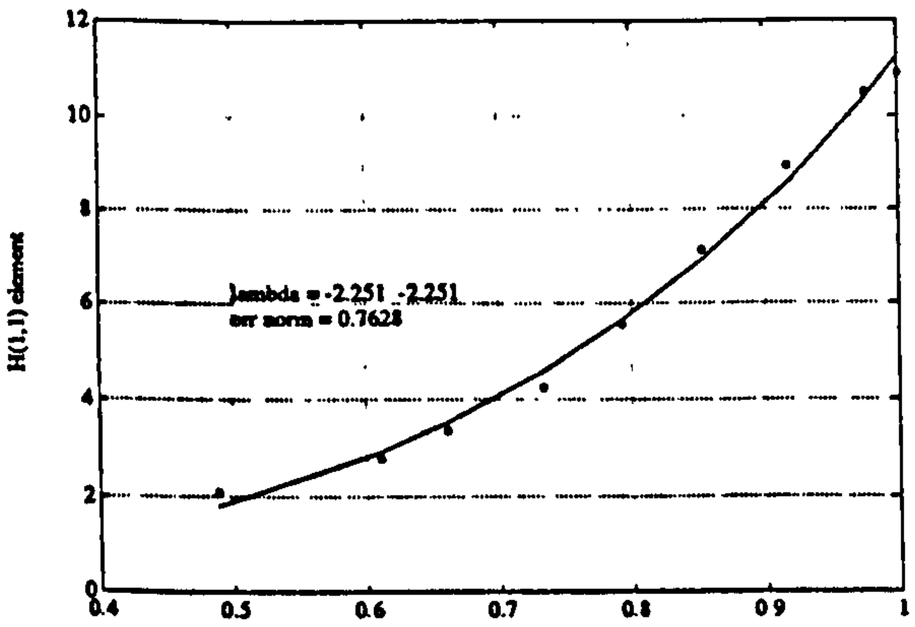

Figure 9: VARIATION OF H(1,1) WITH NON-DIMENSIONAL SPEED

7 SIMULATION RESULTS

In this section, we present the simulation results based on the open-loop fuel controller and the multivariable nonlinear controller.

Simulations shown in Fig.10 through 12 show that the pressures and shaft speed responses are much faster than that of the open-loop fuel controller. This is due to the fact that nozzle area has been opened at the start of the transient, while allowing more fuel flow to be injected to achieve fast response. The variations of fuel flow and final nozzle area are shown in Fig.13 and 14. It can be seen that for the open-loop fuel controller, the final nozzle area is fixed while in the nonlinear controller, this area is modulated with fuel flow. The gain of thrust response is shown in Fig.15 where 95% of rated thrust response is achieved in about 5 second while for the open-loop fuel controller, this time is about 7 second. In the Fig.16, the turbine inlet temperature response is shown to be improved significantly. There is no overshoot of the nominal design value and the initial jump in this temperature contributes greatly to the fast response in the shaft speed and engine thrust. Fig.17 indicates that the transient trajectory with nonlinear controller make more use of low speed surge margin than the open-loop fuel controller, increasing the overfueling capacity of the engine. In the high speed range, this trajectory lay well below that of the open-loop fuel controller, therefore avoiding the turbine temperature overshoot.

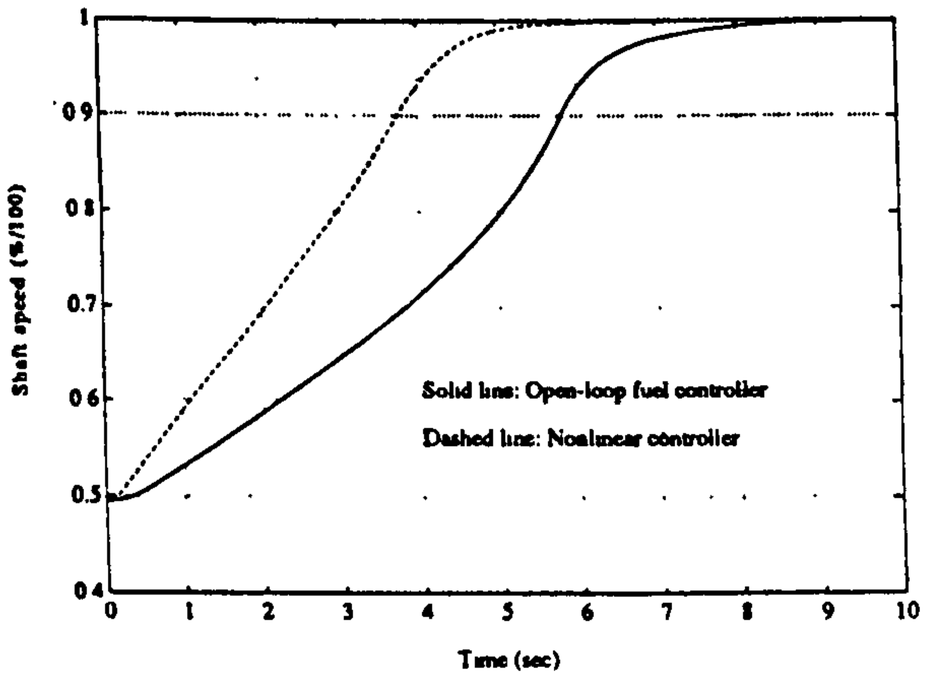

Figure 10: COMPARISON OF SHAFT SPEED RESPONSE

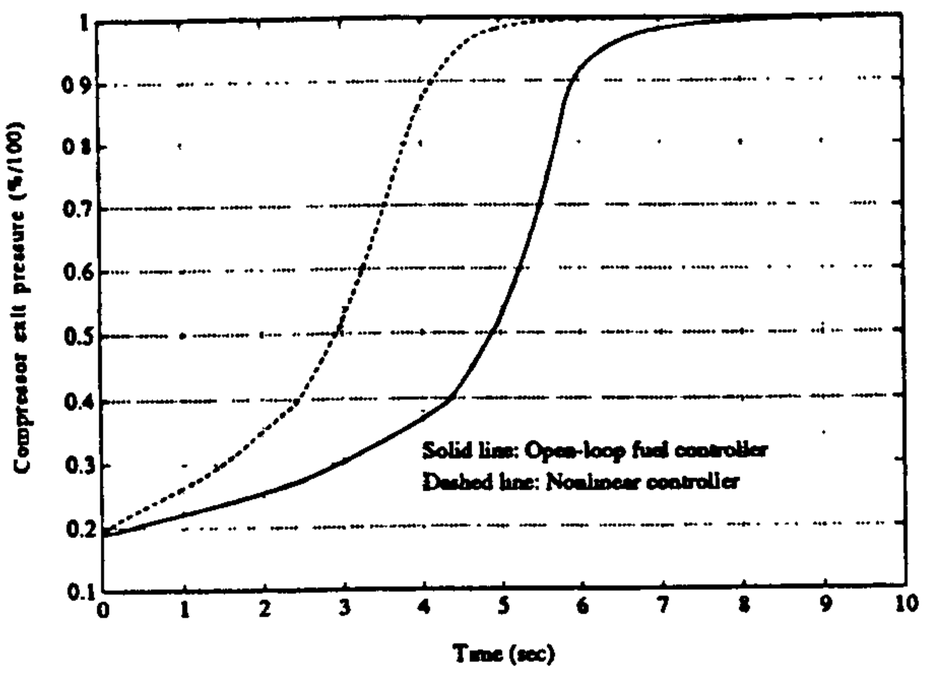

Figure 11: COMPARISON OF COMPRESSOR EXIT PRESSURE RESPONSE

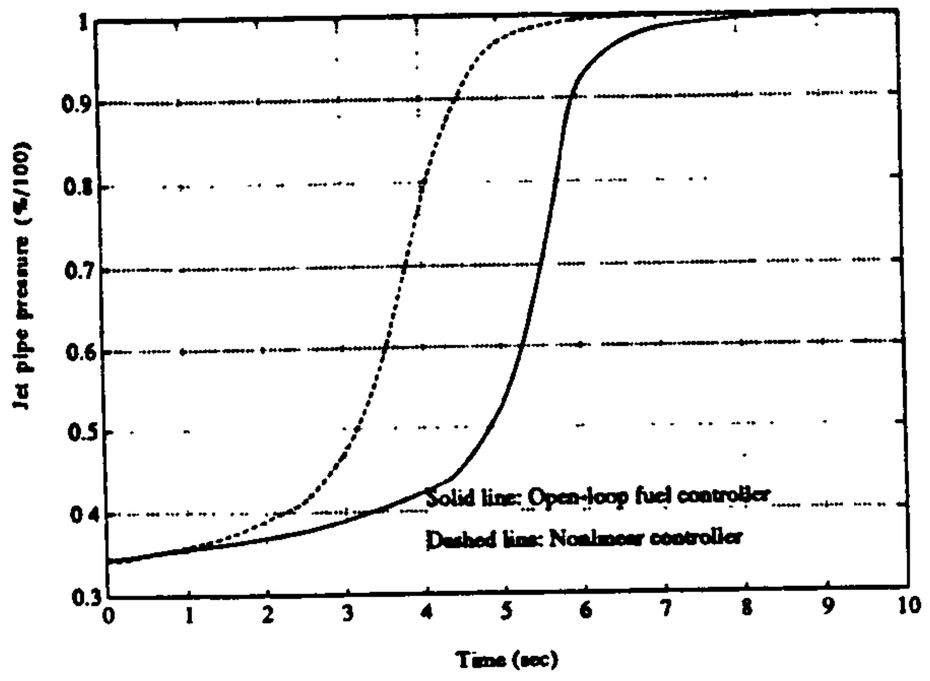

Figure 12: COMPARISON OF JET PIPE PRESSURE RESPONSE

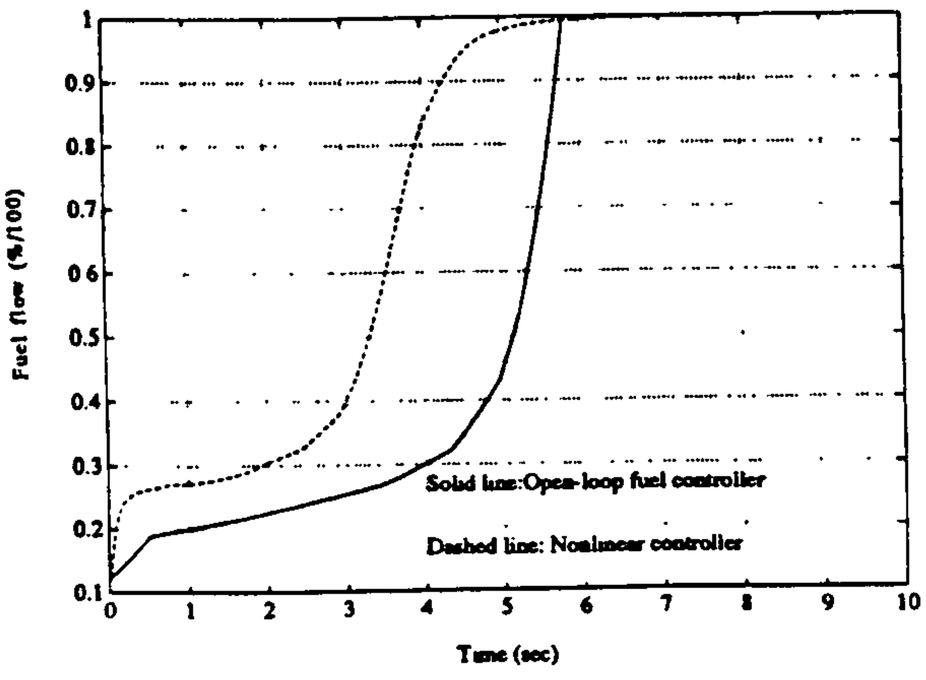

Figure 13: COMPARISON OF FUEL FLOW OF THE CONTROLLERS

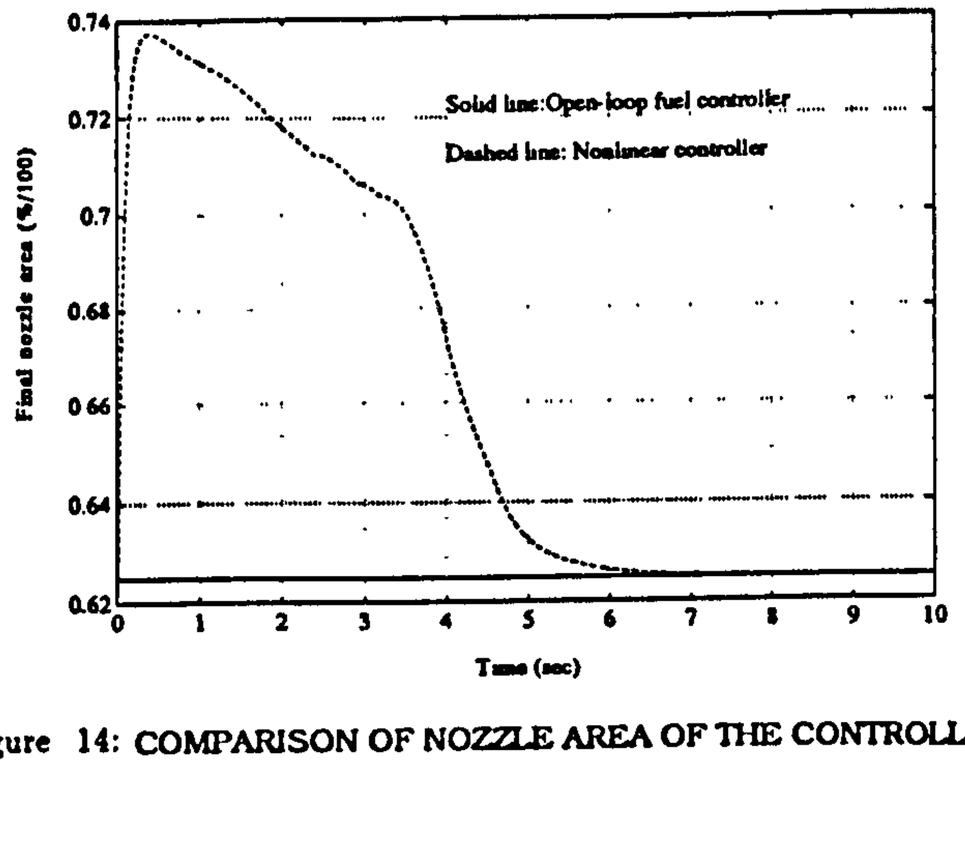

Figure 14: COMPARISON OF NOZZLE AREA OF THE CONTROLLERS

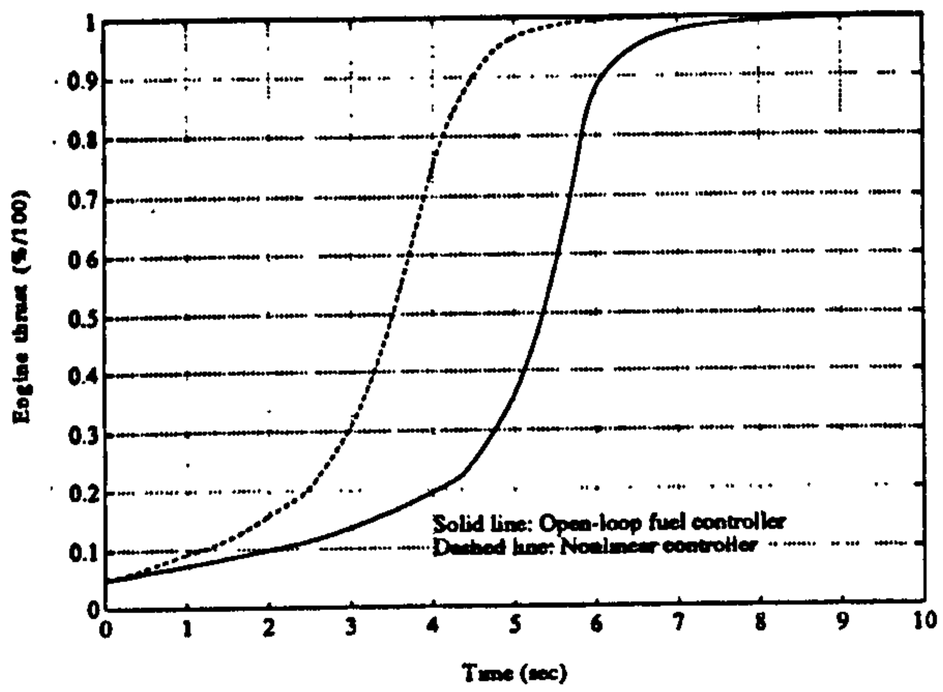

Figure 15: COMPARISON OF ENGINE THRUST RESPONSE

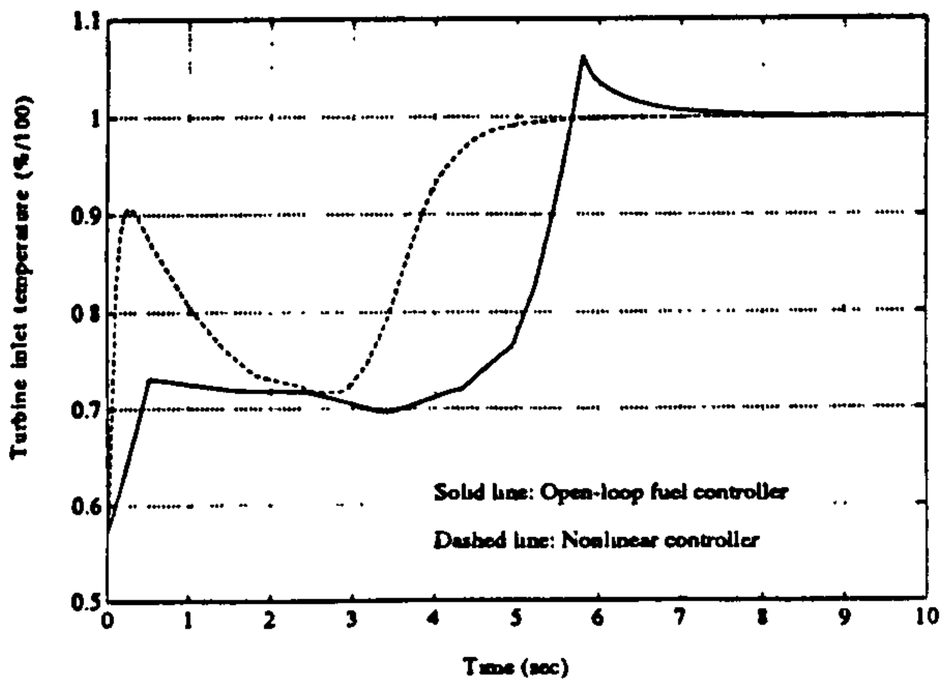

Figure 16: COMPARISON OF TURBINE INLET TEMPERATURE RESPONSE

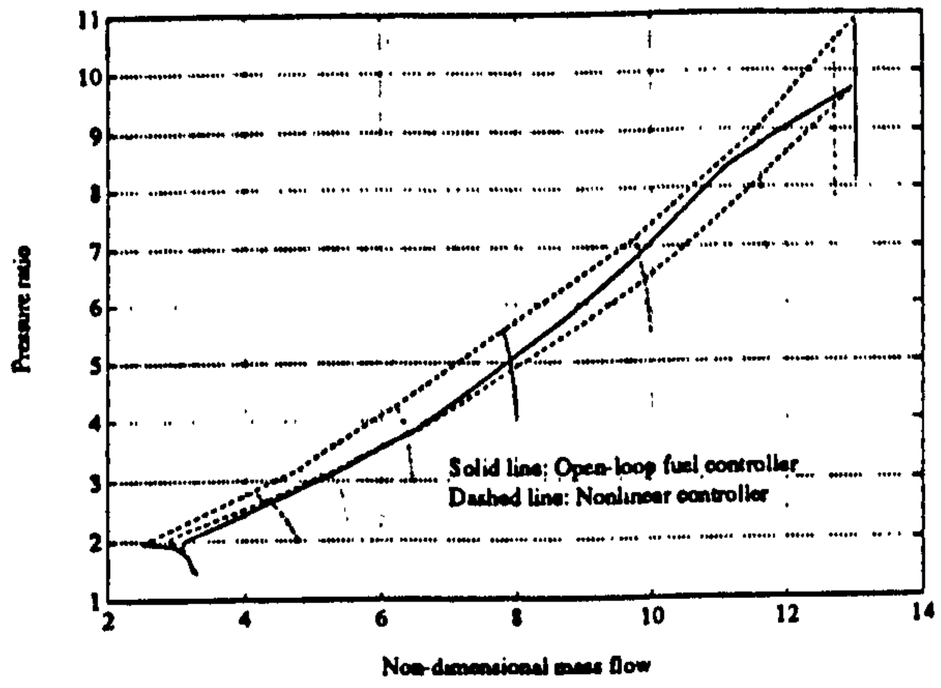

Figure 17: COMPARISON OF TRANSIENT TRAJECTORY ON COMPRESSOR CHARACTERISTIC

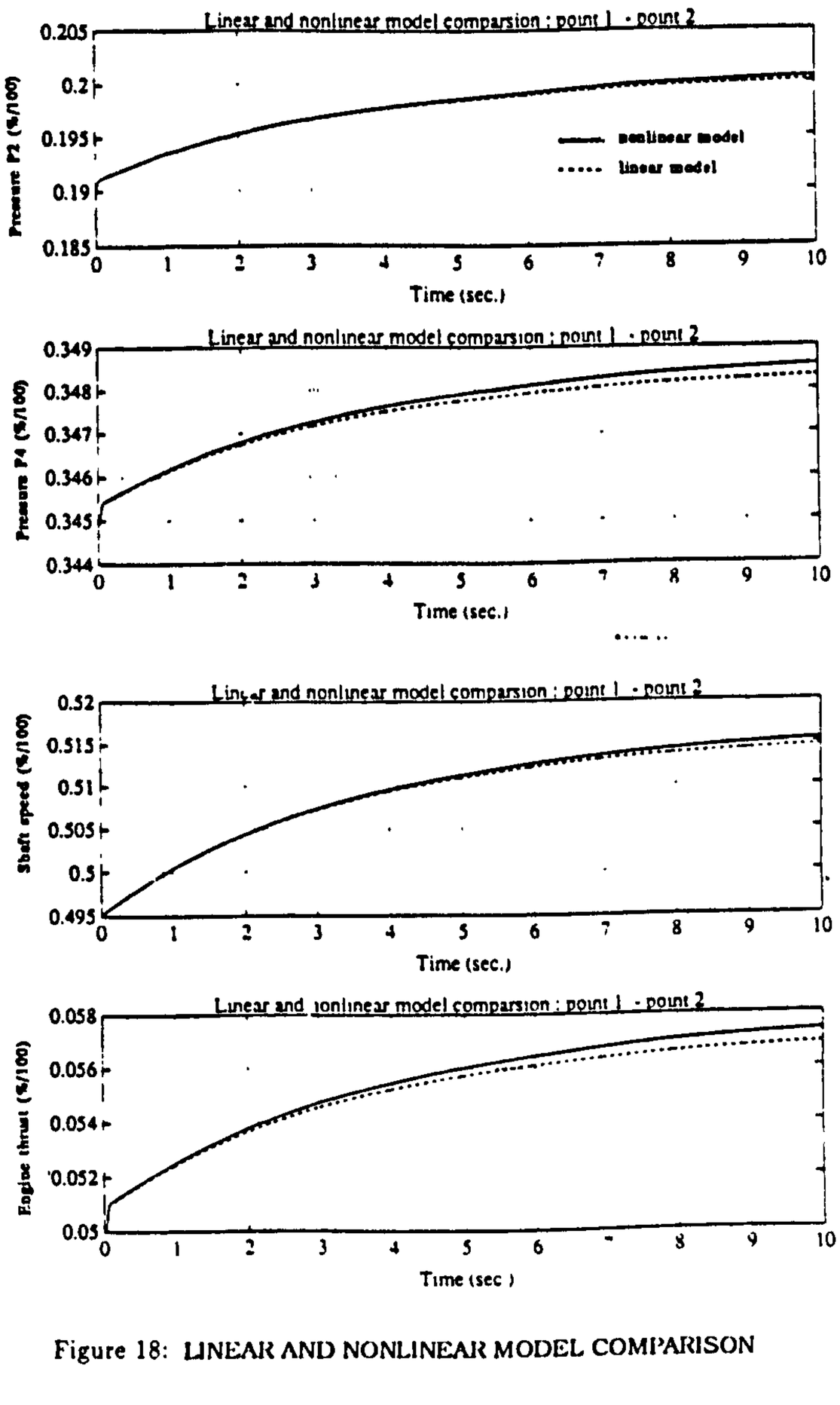

Figure 18: LINEAR AND NONLINEAR MODEL COMPARISON

8 CONCLUSIONS

In this paper, the work into modeling and control of a single-spool gas turbine engine has been described. The algorithms proposed for approximating a compressor enable an analytical expression to be obtained, therefore the simulation time step can be increased. Simulations have shown that a multivariable nonlinear controller could greatly improve the engine dynamic response. The results of this application demonstrate that the design tool is valid and the design method provides a systematic way for synthesizing a multivariable nonlinear controller. The selection of the weighting matrices is specific to the present study. Using non-dimensional speed as a scheduling variable is based on our understanding that this slow-changing variable will guarantee the stability of the nonlinear controller. These will need further study. Since the nonlinear controller is obtained based on the linear design method, it can not directly provide optimal performance for large perturbation transients of a nonlinear system.

9 ACKNOWLEDGMENT

The first author wishes to thank British Council and Chinese Government for the financial support during this research.

10 REFERENCES

M. Athans, et al 1986, " *Linear-Quadratic Gaussian with Loop Transfer Recovery Methodology for the F-100 Engine.* " IEEE Journal of Guidance and Control, Vol.9, No.1, pp.45-52

A.E. Bryson and Y.C. Ho 1969, " *Applied Optimal Control.* " Ginn Blaisdell, Walthham, Mass.

R.L. DeHoff and W.E.Jr. Hall 1976, " *Design of a Multivariable Controller for an Advanced Turbofan Engine.* " Presented at the 1976 IEEE conference on Decision and Control, Clearwater Beach, Florida

K.M. Eveker and C.N. Nett 1991, " *Model Development for Active Surge Control/Rotating Stall Avoidance.* " Proceedings of American Control Conference, pp.3166-3172, Boston, Mass.

A.J. Fawke and H.I.H. Saravanamuttoo 1971, " *Digital Computer Methods for Prediction of Gas Turbine Dynamic Response.* " Paper 710550 presented at SAE Mid-Year Meeting, Montreal, Que., Canada.

R.D. Hackney, R.J. Miller and L.L. Small 1978, " *Engine Criteria and Models for Multivariable Control System Design.* " Alternative for Linear Multivariable Control, ed. by M.K. Sain, J.L. Peczkowski and J.L. Melsa NEC Chicago

L.P. Harris and H.A. Spang III 1991, " *Compressor Modeling and Active Control of Stall/Surge Operation.* " Proceedings of American Control Conference, pp.2392-2397, Boston, Mass.

L.E. Rosenblad 1990, " *Evaluation of Control Techniques for Aircraft Propulsion Systems.* " J. of Engineering for Gas Turbines and Power. Vol.112, pp.229-232.

Szuch et al 1977, " *F-100 multivariable Control Synthesis: Program-Evaluation of a Multivariable Control Using a Real-time Engine Simulation.*" NASA TP 1056.

For International Journal of Experimental Thermal Science
1993, 6, 147-155.

COMPARISON OF MEASURED ISOTHERMAL AND COMBUSTING CONFINED SWIRLING FLOWS - PERIPHERAL FUEL INJECTION

Beltagui S.A., Kenbar A.M.A. and Maccallum N.R.L.

Glasgow University and National Engineering Laboratory

ABSTRACT

The study focused on a burner system where the fuel was injected around the outer periphery of the swirled air jet. This type of burner has advantages in achieving better mixing and rapid combustion.

Measurements of the velocity components and static pressure were made in the furnace, of confinement ratio D/d = 2.5, under both combusting and isothermal conditions. In the combusting case, temperatures and species concentrations were also measured.

The effect of axial flow acceleration, caused by combustion on the observed flow patterns, was a weakening or even cancellation of the central reverse-flow zone. For a given swirler, combustion led to a significant increase in the measured axial momentum flux (dynamic component), a small increase in the tangential momentum flux and thus a reduction in the furnace swirl number, S^*, based on these momentum fluxes. This furnace swirl number, S^*, was successful in correlating these changes in flow pattern.

1. INTRODUCTION

In swirling flames the aerodynamics of the near burner region play a major role in controlling the mixing and combustion patterns. The study of this flow in furnaces is very complex and expensive.

The flow patterns can be determined either from physical model tests or analytical models e.g. based on computational fluid dynamics (CFD). The CFD model predictions of furnace flow and heat transfer still need validation. The validation process is speeded if done in steps starting with isothermal non-reacting flow. Physical models, designed to specific scaling criteria, are often used to obtain data which can be correlated to the actual system. The formulation of the scaling criteria is based on experimental data from model and prototype systems.

Measurements taken from these physical models can also be used to assess the validity of the CFD solutions. Presently a combination of scaled physical models and CFD models is believed to be the optimum design procedure [1,2]. The success of such modelling accelerates the process of furnace system design to meet different operating and environmental requirements.

Considering the physical models, comparisons of isothermal and combusting swirling flows have been reported for free expanding flows [e.g. 3-5]. However, few published studies cover confined flows. One of these studies describes the case of premixed flames in furnaces having D/d values of 5 and 2.5 [6,7]. The case of a highly confined flow, D/d = 1.13, non-premixed and with a central-fuel gun is reported in reference [8]. Previous investigations of non-premixed flames have covered the conventional systems where the fuel is injected through a central fuel-gun. The subject of the present paper is the extension of these comparisons to a system having a peripheral fuel-injection burner.

Combustion systems frequently use swirl to aid mixing and, possibly, recirculation to ensure flame stability. Several forms of non-dimensional Swirl Numbers have been used to establish appropriate physical models. The paper includes an assessment of the alternative definitions of swirl number [7-11], and a method of relating the combusting flow swirl number to the isothermal flow value.

2. PERIPHERAL FUEL-INJECTION BURNER STUDIES

In most practical combustion systems the mixing of the fuel and air is achieved in the early part of the combustion system. Non-premix burners vary in the method of injecting the fuel into the air stream to achieve efficient and stable combustion. Many conventional burner flows consist of two concentric jets, the inner for fuel and the outer for air. Mixing and consequently combustion take place at the shear layer between the two jets. Swirling the air is often applied to enhance the mixing and help stabilise the flame by recirculating some hot combustion products at the centre of the flow. To create this central reverse flow, however, requires high degrees of swirl. The supply air pressure needed to promote high swirl represents expensive fan power requirement.

At Glasgow University a burner with a peripheral fuel-injection scheme is under study, Fig. 1.

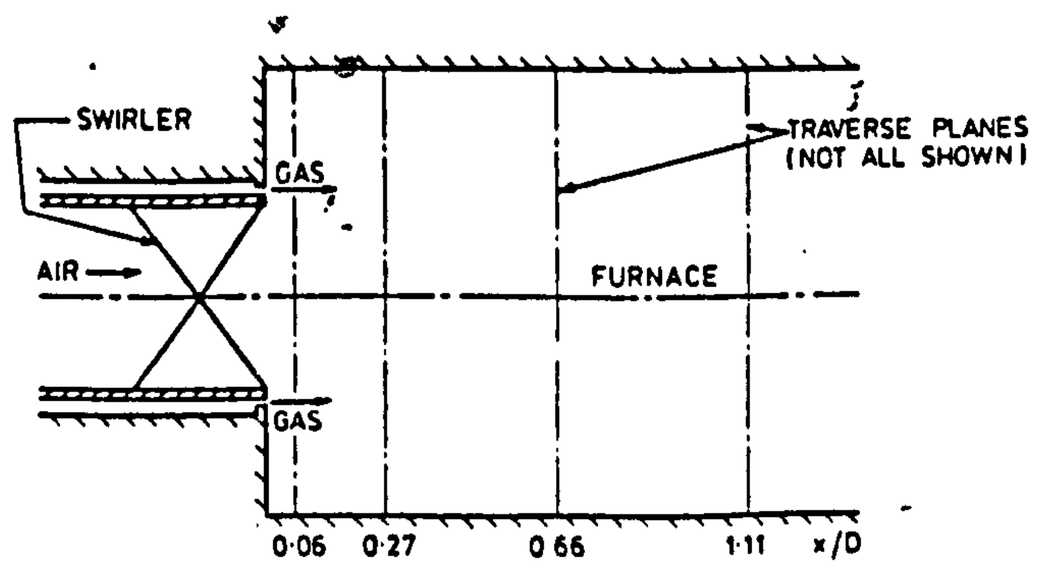

Fig. 1- Furnace With Peripheral Fuel Injection Burner

The fuel is injected axially through an annular slot running around the periphery of the air swirler. With this burner, combustion takes place at the outer boundary of the air jet, thus creating favourable radial density gradients which, with swirl, enhance mixing, as compared with the central fuel injection case where combustion starts around the central axis. This system also utilises the larger shear-layer area at the boundary of the air jet. In this system flame stability can be achieved without the need for a central recirculating flow. Thus only low to moderate swirl is required. An experimental study has been carried out of the aerodynamics of this system under both isothermal and reacting conditions. Details of the combustion case were discussed in a previous paper [12]. The data measured on this system are being used to assess physical modelling principles and also to validate CFD procedures [13].

The aim of the present contribution is to quantify the effect of combustion in modifying the isothermal flow field. The effects of swirl and fuel/air ratio on the flow patterns are studied with the aim of formulating similarity criteria for modelling this system. The experimental results are presented in the form of radial profiles of the time-averaged velocity components and static pressure. Integrated momentum fluxes, and resulting similarity criteria, are then given.

3. EXPERIMENTAL PROGRAMME

3.1 Apparatus

The experimental rig is based on a refractory lined furnace of 225 mm inside diameter and 0.9 m long. The air is introduced through a vane swirl burner of 93 mm inside diameter, Fig. 1. The fuel, natural gas, is injected through an annular slit of 2 mm width around the periphery of the air swirler.

3.2 Instrumentation

The flow patterns were quantified through the measured fields of the three time-averaged velocity components and the static pressure.

For the isothermal flow these were measured using a 5-hole pitot type probe of tip diameter 3 mm, in conjunction with a specialised data acquisition system [11]. The mixing pattern was determined through the measurement of the concentration of CO_2 used as tracer in the air simulating the fuel flow.

For the combusting flow a water cooled 3-hole probe of tip diameter 6 mm was used for the velocity measurements. The combustion pattern was defined by the measured fields of temperature and concentrations (CO_2, CO, O_2). Local temperatures were measured by *Pt/5%Rh-Pt/20%Rh* bare-wire thermocouples. Radiation corrections were neglected as they were always less than 50 deg C. Gas samples were drawn through a special water cooled probe and analysed for CO and CO_2 using infra-red analysers and for O_2 using a paramagnetic analyser.

The above parameters were measured at 12 mm radial increments across each of seven traverse planes, these being located at distances of: 0.06; 0.27; 0.66; 1.11; 1.77; 2.63 and 3.72 furnace diameters from the burner exit.

Although the probes used for the measurements are intrusive, considerable evidence exists from work on similar systems [3, 14] that probe results for velocity are in agreement with those measured by LDA. Where discrepancies occur, these are in regions of low axial velocity and relatively high radial velocity.

Reported velocity values were found repeatable within ±0.5 m/s. Mass integration of the measured axial velocity distribution at any section compared well with the metered flow values, within 25%. This is considered reasonable in view of the difficulty in measuring near the walls. The error maximum in mass corresponds, for example, to an error of less than 0.7 m/s in the axial velocity at the section nearest to the wall.

There is therefore reasonable confidence in the axial and tangential velocity components measurements, but less confidence in the radial component values.

3.3 Input Variables

The main input parameters varied were:

1. Air swirler vane angle, θ :- 0°, 15°, 22°, 30° corresponding to Burner swirl numbers S (= $1/3\tan\theta$):- 0.0, 0.089, 0.138, 0.192.
2. Inlet air velocity :-10.6 and 15.0 m/s corresponding to Reynolds Numbers 6.3 x 10^4 and 9.0 x 10^4 based on swirler conditions.
3. Fuel equivalence ratio, φ :- 0.53 and 0.38 at the higher air flow rate (corresponding to heat release rates 3.8 and 5.3 MW/m³ of furnace volume) and 0.53 at the lower air flow rates.

Thus for each swirler a total of three sets of measurements were performed in the combustion case and two sets for the isothermal case, as summarised in Table 1.

Table 1 : Input variables, Swirl numbers and CRZ sizes

			Combustion			Isothermal	
Swirler vane angle °	Air velocity U_o m/s	Burner Swirl No.	ø	Furnace Swirl No.	CRZ Size	Furnace Swirl No.	CRZ Size
0	15.0	0.0	0.53	0.0	-	0.0	-
0	10.6	0.0	0.38	0.0	-	-	-
15	15.0	0.089	0.53	0.027	-	0.094	-
15	15.0	0.089	0.38	0.051	-	-	-
15	10.6	0.089	0.53	0.031	-	-	-
22	15.0	0.138	0.53	0.052	-	0.238	small
22	15.0	0.138	0.38	0.098	-	-	-
22	10.6	0.138	0.53	0.056	-	-	-
30	15.0	0.192	0.53	0.099	small	0.386	large
30	15.0	0.192	0.38	0.181	small	-	-
30	10.6	0.192	0.53	0.082	small	-	-

4. FLOW PATTERNS

Comparisons of the flow pattern results at the two inlet air velocities (10.6 and 15.0 m/s), show almost complete similarity between the two cases, thus confirming the independence of the flow from Reynolds Number, within the range of these tests. Consequently, only the results at the higher velocity are illustrated in the figures. Also, for brevity, the tangential and radial components of time-averaged velocity and static pressure are shown for only one swirler, 30°, and, further, in the combusting case only the data from the higher equivalence ratio (0.53) are presented.

4.1 Axial Velocity Profiles

Axial velocity profiles are of principal importance since they illustrate the jet boundary, degree of expansion and regions of high velocity gradient. They also define the boundaries of the forward and reversed flow zones.

The velocity profile observed at the first traverse plane (X/D = 0.06 which is equivalent to X/d = 0.15) indicates effectively the axial velocity distribution leaving the swirler. It is seen that the profiles at this plane indicate a velocity redistribution towards the outer radii, Figs. 2-4. This effect increases with swirl. These data are of value for specifying input conditions for CFD prediction procedures [13].

The measured axial velocity profiles for isothermal flow and combusting flow are shown in Figs. 2-4 for swirlers having vane angles 0°, 22° and 30°. The axial velocity profiles show the forward flow to be mainly in the outer part of the jet with peak velocities increasing with swirl. The boundaries of forward and reverse flow in the isothermal and combusting cases are compared in Fig. 5. The sizes of the central reverse-flow zone (CRZ) and the locations of the jet outer boundary are indicated.

The following are the main observations made on comparing the combusting with the isothermal flows:

1. The forward flow velocities increase due to the expansion caused by combustion. The increase is a function of the location of the flame front and heat release, being nearer to the burner for the lower equivalence ratio.

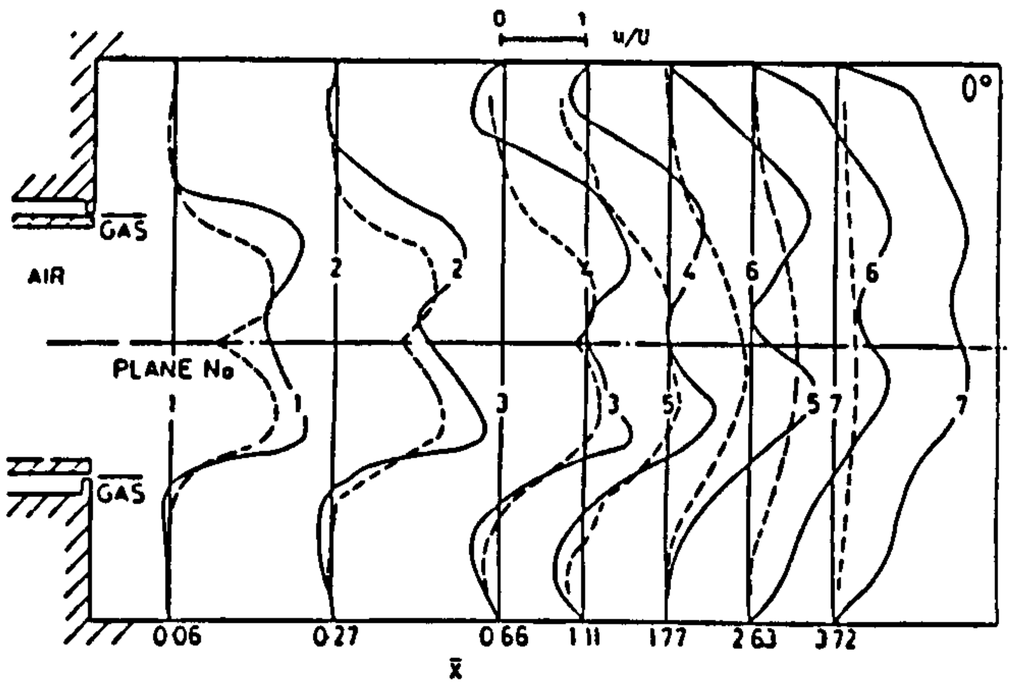

Fig. 2- Axial velocity distributions, 0° vane swirler.

. . . . isothermal
——— combustion

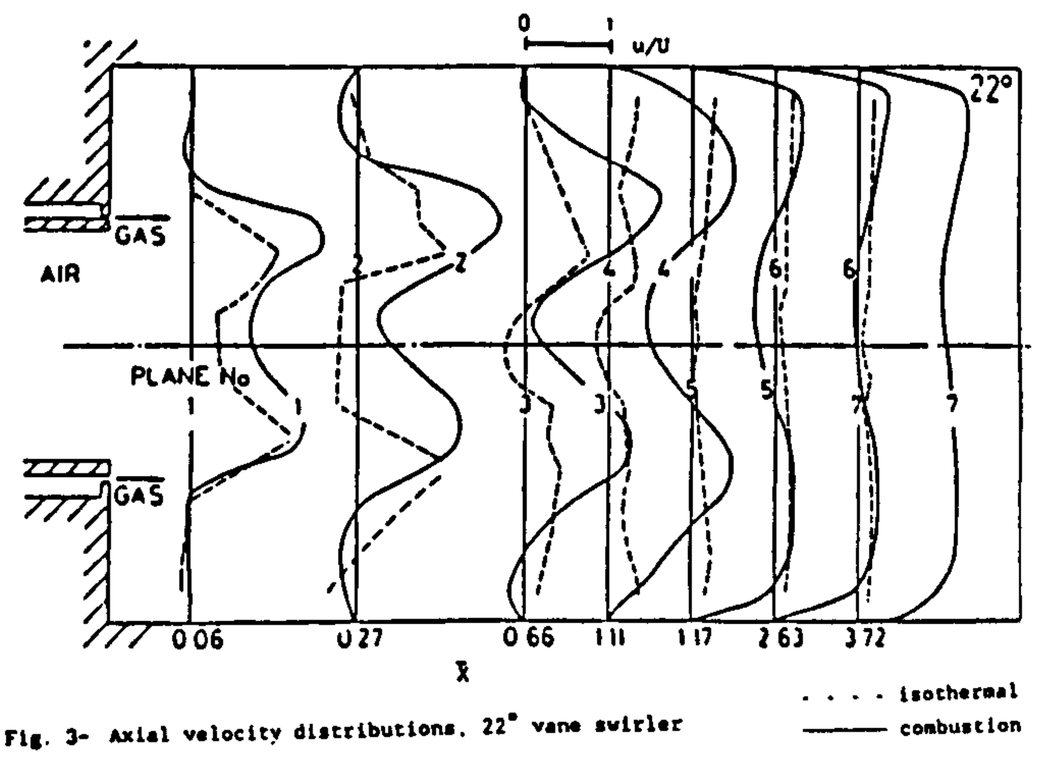

Fig. 3- Axial velocity distributions, 22° vane swirler

. . . . isothermal
——— combustion

2. The CRZ is very much reduced by combustion. Isothermal flow shows a CRZ for swirler vane angles 22° and 30°. For combusting flow there is no CRZ for the 22° vane angle and a small zone for the 30° swirler. This is a consequence of the expansion mentioned above. These observations agree with previously reported work [3-8], for central injection and premixed cases.

3. For the unswirled and low swirl cases (0°, 15°), combustion has little effect on the position of jet wall impingement. In the higher swirl cases (22°, 30°) the outer jet spread with combustion is less rapid than in the isothermal conditions. This is probably due to the combination of the reduction of the CRZ and the creation of the highest temperatures, and hence lowest densities, in the outer recirculation zones.

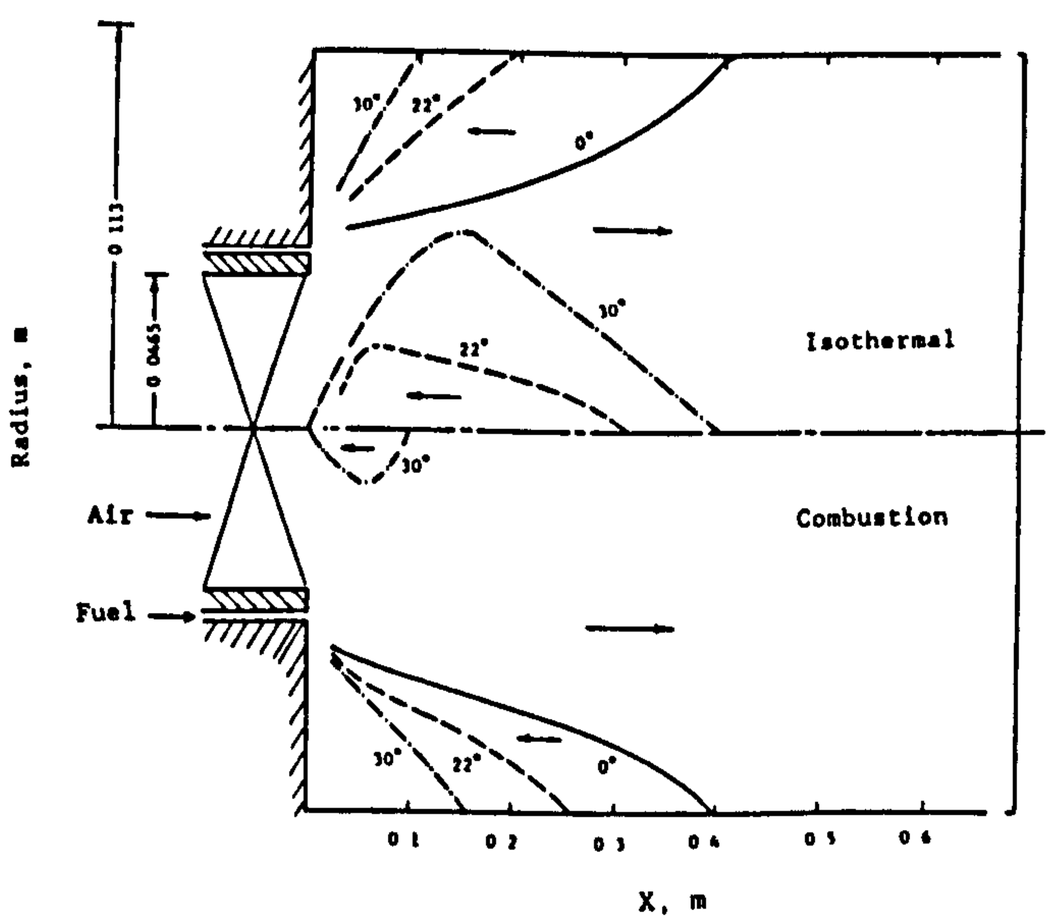

Fig. 5- Flow Boundaries

4.2 Tangential Velocity Profiles

As illustration, the results are shown for the 30° swirler, Fig. 6, both isothermal and combustion cases being presented. The profiles, approximate to Rankine-vortex flow. The peak values of the tangential velocity appear in the vicinity of the axial velocity maxima. Within the CRZ, the tangential velocity profiles approximate to solid body rotation. Both isothermal and combusting flows leave the swirler with the same tangential velocity. In the isothermal case the tangential velocities diminish as the flow expands along the wall. In the combusting case, the high initial tangential velocities extend across the outer recirculation zone. These velocities remain high along the combustion region of the furnace.

4.3 Radial Velocity Profiles

Sample profiles of both isothermal and combusting flows are shown in Fig. 7 for the 30° swirler only. The sign convention is that in the upper half of the diagram, positive values correspond to inward radial velocity components. In the lower half of the diagram, the convention is reversed. Thus for a perfectly symmetric jet, the distribution should be diagonally symmetric. The trends of the radial velocity profiles are consistent with the jet expansion behaviour suggested by the axial velocity distributions. The distributions in both isothermal and combusting cases show that, close to the swirler, the radial components are of the same order as the axial velocity components. Combustion tends to increase the magnitude of radial velocities, mainly due to the increased buoyancy forces caused by radial density gradients [12].

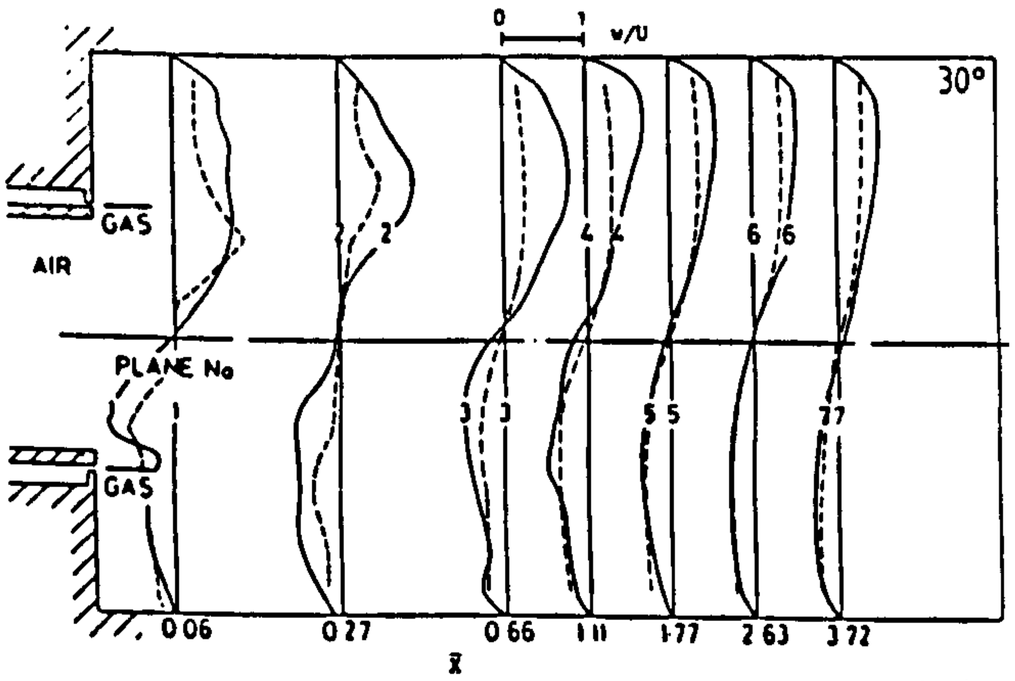

Fig. 6- Tangential velocity distributions, 30° vane swirler. — — — isothermal ——— combustion

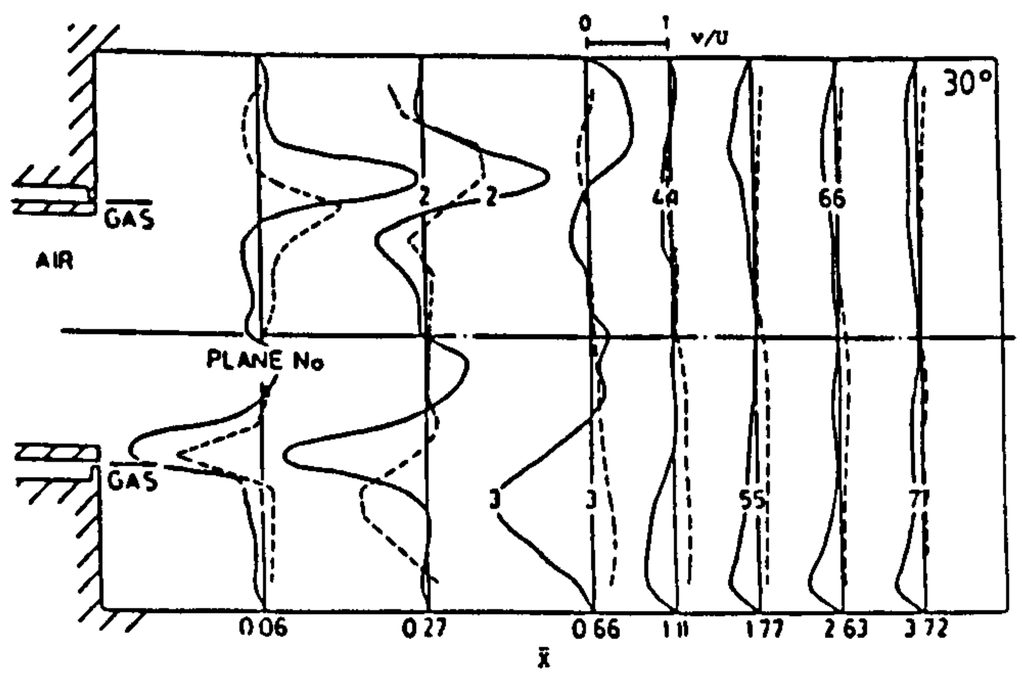

Fig. 7- Radial velocity distributions, 30° vane swirler — — — isothermal ——— combustion

4.4 Static Pressure Profiles

The static pressure profiles are mostly sub-atmospheric with a minimum at the centreline and rising to near, or above, atmospheric close to the walls. Within the CRZ, the static pressures are almost uniform. These features are illustrated in Fig. 8, for isothermal and combusting flows with the 30° swirler. These pressures recover towards the ambient value as the flow proceeds to the furnace exit. The radial pressure gradients are much higher in the combustion case for all swirlers due to the density gradients caused by combustion.

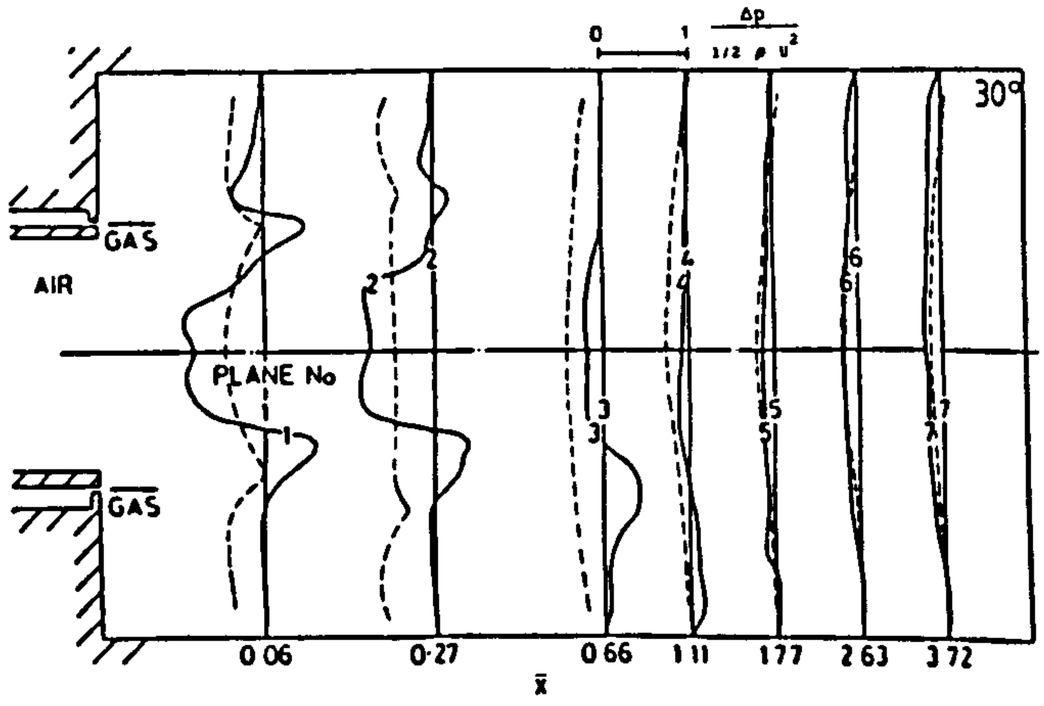

Fig 8- Static pressure distributions, 30° vane swirler. — — — isothermal ——— combustion

5 MOMENTUM FLUXES

The experimental profiles of axial and tangential velocity have been integrated to give axial fluxes of axial and tangential momentum respectively.

5.1 Axial Momentum Flux

It is accepted practice [1,2,7-12] that it is the dynamic component, G_d, of the axial momentum flux which has greatest bearing on flow development in a confined furnace. Therefore, the present work has been focused on this dynamic component, G_d, of the axial momentum flux. Examples of the resulting flux values $\bar{G}_d$, normalised by the theoretical axial momentum flux at the swirler exit, are shown in Fig. 9.

In the isothermal case they decay along the furnace from the initial value at exit from burner to about 0.22 of the initial value, at the downstream end of the furnace. This compares with the value of 0.19 predicted by a simple one-dimensional analysis (Appendix I). For the combusting flow, at equivalence ratio 0.53, near the burner there is a rise to a normalised value of about 1.8, at a position related to the flame front, followed by decay to about 1.2 at the furnace exit. At the lower equivalence ratio (φ = 0.38) the normalised flux value at furnace exit is about 0.9.

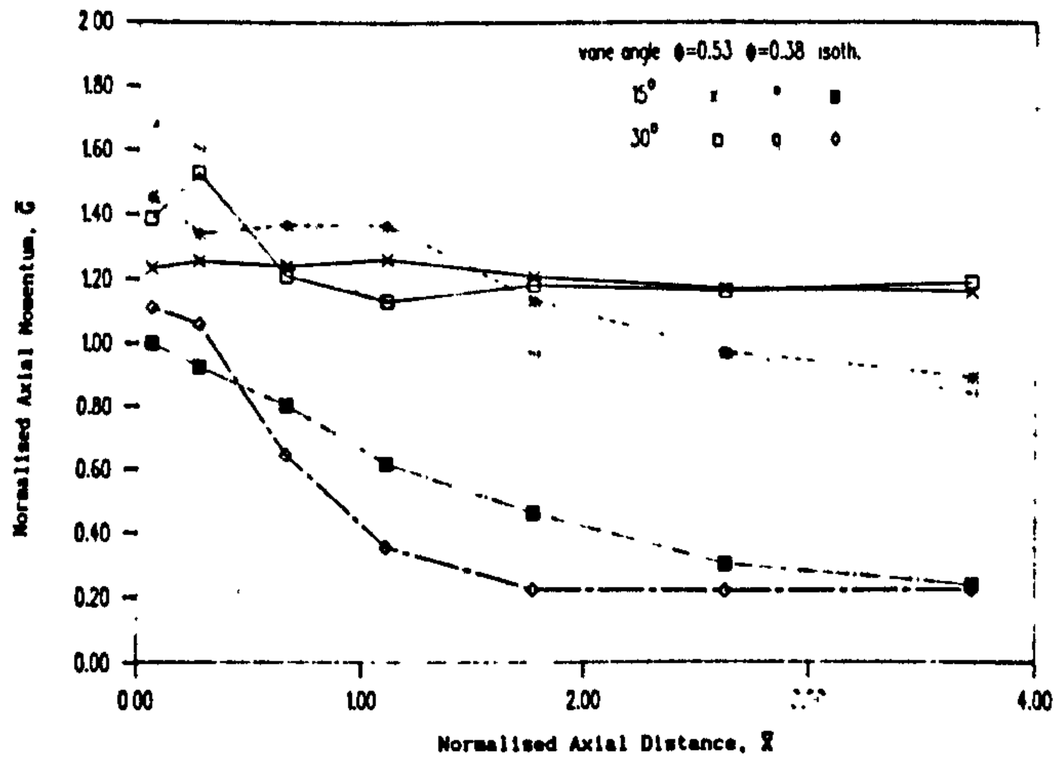

Fig. 9- Axial Momentum Flux

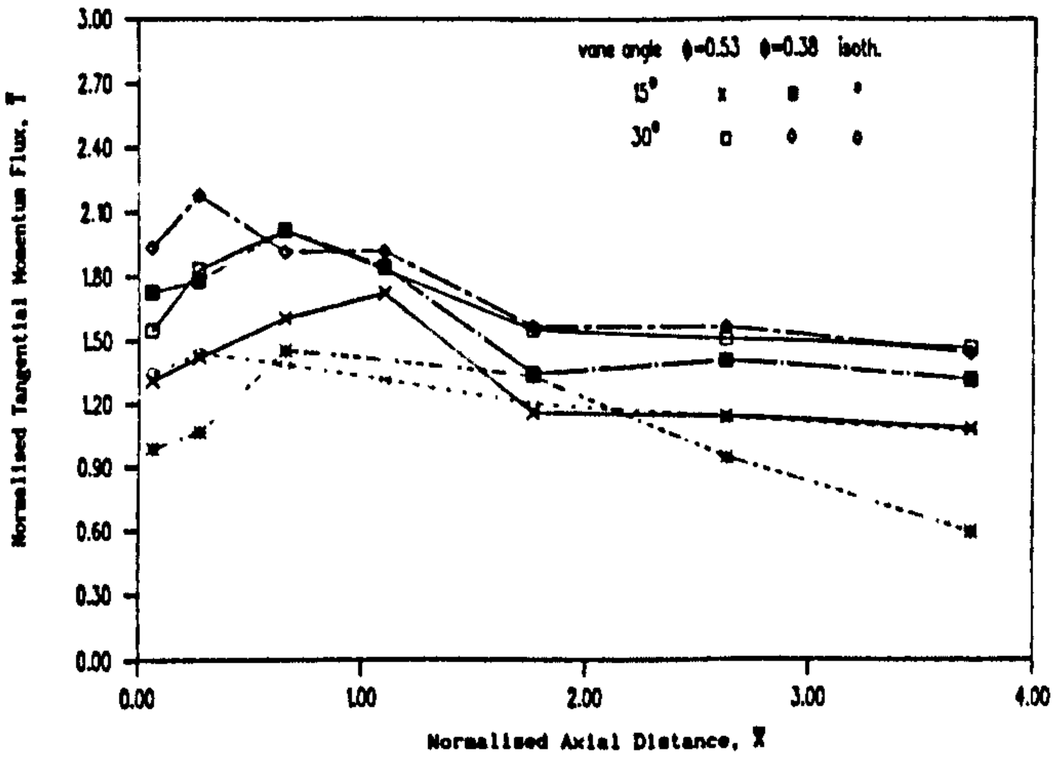

Fig. 10- Axial Flux of Tangential Momentum

The simple one-dimensional analysis predicts that the values at exit should be about 0.9 and 0.7 respectively for these equivalence ratios. The reason for the experimental flux values exceeding the one-dimensional theory values is that the actual velocity profiles in the furnace are non-uniform. This being more marked close to the burner, particularly in the higher swirl cases.

It is worth noting that the observed ratios of axial momentum flux at furnace exit in the burning, as compared to the isothermal cases, are about 5.5 (φ = 0.53) and 4.1 (φ = 0.38). These values agree closely with the one-dimensional analysis predictions of 4.7 and 3.8.

5.2 Tangential Momentum Flux

Examples of the tangential momentum fluxes, as obtained by integration of the measured velocity profiles, are shown in Fig. 10. The fluxes have been normalised ($\bar{T}$) by the theoretical tangential momentum of the flow leaving the burner, assuming that the axial velocity at that plane is uniform and that all the air flow leaves at the angle the burner swirler vanes make to the axial direction. It is noted that the measured values of $\bar{T}$ at the first traverse plane ($^X/_d$ = 0.15) are in all cases greater than unity. This is principally due to the non-uniformity in the air flow distribution leaving the swirler, previously commented on in Section 4.1. The axial velocity distributions taken at the first traverse plane, Figs. 2-4, show that the axial velocities are higher at the outer radii of the swirler. The tangential components of velocity, Fig. 6, when compared with the axial velocity components, confirm that the flow is deflected to the swirler vane angle. Thus, due to the redistribution of the flow, the tangential momentum flux will be higher than that predicted by the uniform velocity model. This flow redistribution becomes more pronounced as swirl is increased.

For the isothermal cases the normalised fluxes have early values of about 1.3 and then decay to about 0.9 as the flow approaches the furnace exit. In the burning cases the normalised fluxes start with values of about 1.7 and then decay to about 1.3, this value not being significantly altered by equivalence ratio. The observed ratio of axial flux of tangential momentum at furnace exit in the burning case as compared to isothermal (coefficient F_3) is about 1.4. This ratio is discussed, and used, in Section 6.1.

Comment should be made on the apparent increases in tangential momentum fluxes observed between the first and second or third traverse planes. It is suggested that these apparent increases are due in part to the integrations having ignored turbulent shear stresses. Also there is the possibility of experimental inaccuracy in the data, giving rise to magnified errors in the integrated flux values. The correlations which are given in the subsequent Section are however based on the fluxes approaching the furnace exit where the above difficulties are not significant.

6. SWIRL NUMBER

For modelling swirl flames a scaling parameter is needed as a measure of the swirl intensity given to the flow. There have been a number of definitions for this parameter. The two most commonly recognised are:-

a) Burner swirl number, defined as -

$$S = {}^{T}/(G_d . d) \qquad \ldots\ldots (1)$$

where T is the axial flux of tangential momentum at the swirler exit,
G_d is the flux of axial momentum, dynamic component, at the swirler exit, and
d is the swirler diameter.

This parameter gives a good indication of the degree of swirl imparted to the flow within the swirler. it is successful in correlating the flow close to the swirler in isothermal free flows. However, it does not account for the effects created by expansion into a furnace confinement, suddenly or via a quarl. Nor are the effects of the flow expansion caused by combustion accounted for.

The effect of area expansion, for isothermal flows, was introduced by using a swirl number based on the quarl exit diameter [9], or the furnace diameter [7, 10, 11].

b) Furnace swirl number, defined as -

$$S^* = {}^{T}/(G_d . D) \qquad \ldots\ldots (2)$$

where T and G_d are the integrated fluxes of tangential and axial momenta measured at the furnace exit respectively

and D is the furnace diameter. This definition was proposed by Beltagui and Maccallum [7] where it was applied successfully to characterise the general flow patterns in two furnaces for isothermal and premixed combustion conditions.

This number proved to be a better index of the flow pattern in furnaces [e.g. 10]. It takes account of the furnace to burner ratio as well as the effect of combustion. However its evaluation requires more experimental measurement. The value of the integrated S^* for the combustion flow is lower than for the isothermal flow. It is also a function of the equivalence ratio, or temperature rise due to combustion, being lower for the higher equivalence ratio. A value of $S^* = 0.1$ was found to define the onset of a CRZ in the flow, for both isothermal and combusting flows, in two furnace confinements ratios ($^D/_d$).

The values of S^* calculated from the experimental data for the present work are given in Table 1 and Fig. 11. The values and flow patterns confirm the validity of the swirl number S^* in characterising the flow patterns of swirling flows, both isothermal and combusting, the initial value for the establishment of a CRZ again being 0.1.

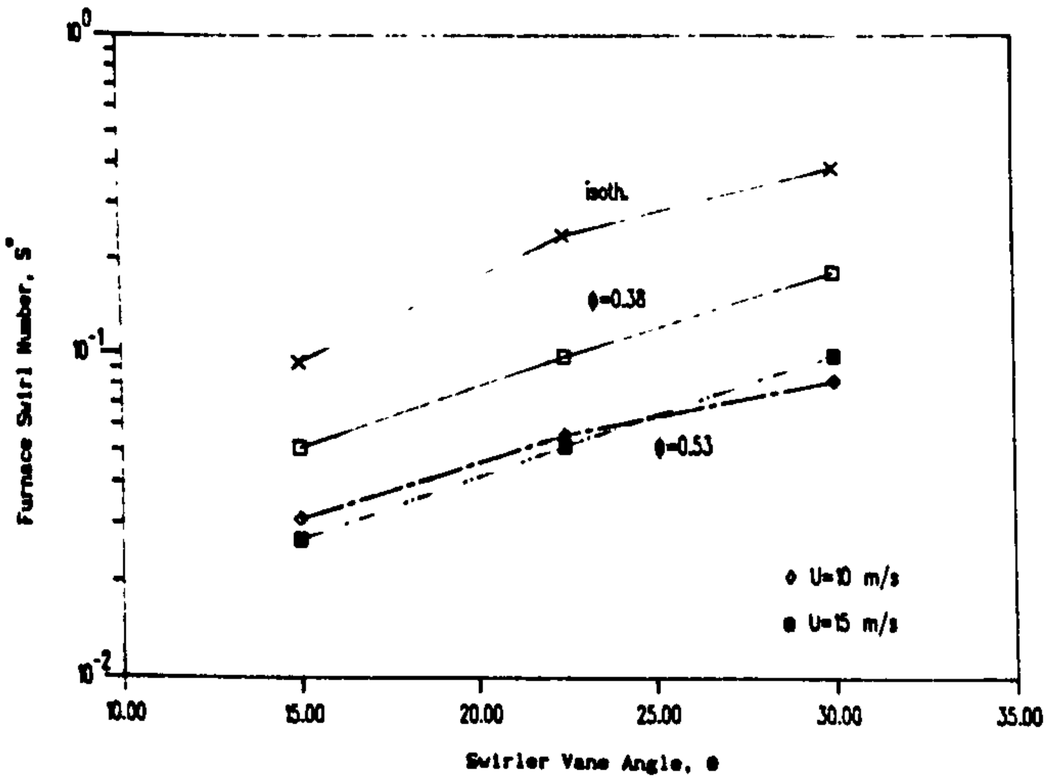

Fig. 11- Furnace Swirl Number

6.1 Swirl Number Prediction

It would be useful to predict the value of S^* for the combusting flow from data measurements in isothermal models. A simple correlation to relate the combusting flow furnace swirl number to the isothermal flow value has been proposed [7], see Appendix II, as follows:

$$S^*_{comb}/S^*_{isoth} = \{F_2 . F_3\}/\{F_2+F_1(d/D)^2((\rho_u/\rho_b)-1.0)\} \quad .....(3)$$

where;

F_1 is the ratio of the actual pressure drop across the flame front to the predicted value, based on simple one-dimensional analysis,

F_2 is the ratio of the isothermal dynamic axial momentum at furnace exit to the furnace inlet value,

F_3 is the ratio of the combustion tangential momentum flux at furnace exit to the corresponding isothermal value.

Applying the simple one-dimensional analysis (Appendix I) to the present configuration it was predicted that the coefficient F_2 should have the value of 0.19. The value obtained from the experimental results, Fig. 9, is 0.22. It is to be expected that the experimental value will be somewhat higher than that predicted by the one-dimensional analysis, due to the non-uniformity of the flow distribution at the swirler exit.

The value of coefficient F_3 has to be deduced from experimental data. For the present system it was found to have the value 1.4 (Section 5.2). It is noteworthy that the value of this coefficient in this novel non-premixed system is the same as that previously obtained for premixed combustion [7].

The value of coefficient F_1 has to be obtained also from the experimental data. It is found that the values of 1.6 and 1.0 provide the best fits with the results observed at the equivalence ratios of 0.53 and 0.38 respectively. These values for F_1 are significantly lower than the value of 2.1 obtained for the premixed town gas case [7]. This had been anticipated in that paper.

The above work has illustrated how the coefficients F_1, F_2, F_3 were obtained and Eq. 3 applied in the present case. To apply Eq.3 to a different configuration, the value of F_2 can be obtained from isothermal model tests. The values of F_1 and F_3 can be evaluated from a limited number of scaled model tests. Additionally, an estimate of F_2 is given by the analysis in Appendix I. This can be made more general if the velocity distribution leaving the swirler is known.

7. CONCLUSIONS

Study of the results obtained in the isothermal and combusting tests (on a peripheral fuel injection system), for the range of inlet air velocities (10.6 and 15.0 m/s) and swirler vane angles (0° to 30°), leads to these conclusions:

1. The flow patterns are independent of Reynolds Number within the range tested.
2. The modification of the flow pattern resulting from combustion has been quantified. The modification is due to the flow acceleration associated with the combustion heat release. In the present system the heat release takes place at the shear-layer on the boundary of the air jet, as compared to the centre in the case of central fuel-injection systems.
3. The radial gradients of both radial velocity and static pressure increase with combustion.
4. The integrated axial momentum flux (dynamic component) in the isothermal case shows the lowering predicted by the simple one-dimensional analysis. In the combusting case there is a sharp rise in the vicinity of the flame front, followed by gradual decay to a value similar to that predicted by the simple analysis.
5. The integrated tangential momentum flux in the isothermal case shows a decay along the furnace. With combustion this flux rises near the flame front and then decays, but remains above the isothermal value.
6. The furnace swirl number, S^*, calculated from the developed momentum fluxes at the furnace exit, is reduced by combustion. This swirl number is successful in correlating the change in flow patterns, a value of 0.1 for S^* being the critical value for onset of a CRZ.
7. A means is presented of predicting the combusting furnace swirl number, and hence flow pattern, from isothermal and limited small-scale model tests.
8. The data, covering both isothermal and reacting flows, is valuable in assessing the capability and reliability of mathematical models (CFD) in simulating swirling flows.

NOMENCLATURE

d	swirler diameter
D	furnace diameter
F_1, F_2, F_3	factors defined in Sec.6.1 and Appendix II
M	mass flow rate
G_d	axial momentum flux, dynamic component $= \int 2\pi r \rho u^2 dr$
$\bar{G}_d$	normalised axial momentum flux, $\int 2\pi r \rho u^2 dr \,/\, \rho \pi r_{sw}^2 U_o^2$
S	burner swirl number, based on swirler diameter $= {}^1/_3 \tan\theta$
S^*	furnace swirl number $= T/(G_d.D)$, Eq.2
T	axial flux of tangential momentum $= \int 2\pi r^2 \rho u w dr$
$\bar{T}$	normalised axial flux of tangential momentum $= \int 2\pi r^2 \rho u w dr \,/\, {}^2/_3 \pi r_{sw}^3 U_o^2 \tan\theta$
u, v, w	local axial, radial and tangential components of velocity
U_o, W_o	average axial and tangential velocity components at swirler exit
U_x, W_x	average axial and tangential velocity components at furnace exit
X	axial distance along furnace
$\bar{X}$	axial distance in units of furnace diameters
θ	swirler vane angle to axial direction
ρ	density
φ	fuel equivalence ratio

REFERENCES

1. Gupta, A.K., Lilley, D.G. and Syred, N., *Swirl flows.* Abacus Press, 1984.
2. Gupta, A.K. and Lilley, D.G., *Flow field modelling and diagnostics.* Abacus Press, 1985.
3. Hillemanns, R., Lenze, B. and Leuckel, W., *Flame stabilization and turbulent exchange in strongly swirling natural gas flames.* 21st Symposium (Int.) on Combustion, The Combustion Institute, pp1445-1453, 1987.
4. Fujii, S., Eguchi, K. and Gomi, M., *Swirling jets with and without combustion.* AIAA, 19(11), pp1438-1442, 1981.
5. Yoon, J.K. and Shin, H.D., *Time-mean structures of the swirling flow with and without flame.* J. Inst. Energy, 60, pp138-142, 1987.
6. Beltagui, S.A. and Maccallum, N.R.L., *Aerodymanics of vane-swirled flames in furnaces.* J. Inst. Fuel, 49, pp183-193, 1976.
7. Beltagui, S.A. and Maccallum, N.R.L., *The modelling of vane-swirled flames in furnaces.* J. Inst. Fuel, 49, pp194-200, 1976.
8. Dugue, J. and Weber, R., *The effect of combustion on confined swirling flows.* International Flame Research Foundation (IFRF), Doc. No. K70/a/8. 1989.
9. Criesta, E-D. B., *Prediction of central recirculation zone size for a complete burner-quarl-furnace system.* AIAA. 25(3), pp457-463, 1987.
10. Hagiwara, A. and Bortz, S., *Studies on the near field aerodynamics of swirl burners, flow visualization and hot wire measurements in isothermal swirling flows.* IFRF Doc. No. F259/a/1, 1986.
11. Beltagui, S.A. and Ralston, T., *An isothermal model study of aerodynamics and mixing in the flow issuing from a variable-swirl burner.* NEL Report DC/370, 1984.
12. Beltagui, S.A. and Maccallum, N.R.L., *Characteristics of enclosed swirl flames with peripheral fuel injection.* J. Inst. Energy, 61, pp3-16, 1988.
13. Kenbar, A.M.A., Beltagui, S.A. and Maccallum, N.R.L., *Modelling the combustion aerodynamics for a peripheral system.* Report, Dept. of Mechanical Engineering, University of Glasgow, August 1990.
14. Aoki, K., Shibata, W. and Nakayama, Y., *Study on the flow with a swirl flow in a cylindrical combustor.* 2nd report, Characteristics of turbulence for the swirl number. Bulletin of JSME, 29, pp4113-4121, 1986.

APPENDIX I

One-dimensional Momentum Analysis

The analysis presented here is meant to clarify and give simple predictions for the changes in the axial and tangential momenta between the inlet and exit of the furnace.
It is assumed that the axial flow velocity is uniform across the flow area.

Mass flow rate into furnace M;

$$M = {}^\pi/_4 \; d^2 \; \rho_u U_o$$

The same mass flow rate at furnace exit;

$$M = {}^\pi/_4 \; D^2 \; \rho_b U_x$$

Axial momentum flux, dynamic component, at swirler exit, furnace inlet;

$$G_{do} = {}^\pi/_4 \; d^2 \; \rho_u U_o^2$$

Axial momentum flux, dynamic component, at furnace exit;

$$G_{dx} = {}^\pi/_4 \; D^2 \; \rho_b U_x^2$$

Thus, the normalised axial momentum flux, furnace exit;

$$\bar{G}_{dx} = ({}^d/_D)^2 \; (\rho_u/\rho_b)$$

For the isothermal flow;

$$\bar{G}_{dx,isoth} = ({}^d/_D)^2 = F_3$$

For the present system, the burner equivalent diameter is $d = 0.097$ m and the furnace diameter, $D = 0.225$ m, thus;

$$\bar{G}_{dx,isoth} = 0.19$$

For the combusting flows, furnace assumed to be adiabatic;

$$\varphi = 0.53 \;,\; \rho_u/\rho_b = 4.7 \;,\; \text{then} \;\; \bar{G}_{dx,comb} = 0.87$$
$$\varphi = 0.38 \;,\; \rho_u/\rho_b = 3.8 \;,\; \text{then} \;\; \bar{G}_{dx,comb} = 0.71$$

The ratio of combusting to isothermal axial momenta is given by;

$$\bar{G}_{dx,comb} \;/\; \bar{G}_{dx,isoth} = \rho_u/\rho_b$$

and therefore has the values 4.7 and 3.8 for $\varphi = 0.53$ and 0.38 respectively.

Considering the tangential momenta, axial flux at swirler exit;

$$T_e = \pi/_{12}\ d^3 \rho_u U_e W_e$$

Axial flux of the tangential momentum at furnace exit;

$$T_x = \pi/_{12}\ D^3 \rho_b U_x W_x$$

Thus the normalised tangential momentum flux at furnace exit;

$$\bar{T} = \bar{G}_{dx}\ (D/_d)\ ((W_x/U_x)\ /\ (W_e/U_e))$$

The tangential momentum flux is conserved, in the ideal frictionless case. Consequently there is a reduction of the tangential velocity component;

$$W_x/W_e = d/_D$$

The simplified model used in the above analysis is however limited. In the situations observed experimentally in this work, there was a redistribution of the flow leaving the swirler from the simple uniform axial velocity assumed in the model (Section 4.1). The redistribution gave higher axial velocities at the outer radii of the swirler. Thus the fluxes of tangential momentum were higher than those predicted by the simple model.

APPENDIX II

Furnace Swirl Number Prediction

The furnace swirl number is defined as; $S^* = T/(G_d . D)$.
The axial momentum flux is increased due to combustion by an amount equal to the pressure drop across the flame front. For one-dimensional flow, this pressure drop is given by;

$$\Delta p = \rho_u U^2\ (d/_D)^4\ ((\rho u/\rho_b) - 1.0)$$

For the actual flame the pressure drop will be F_1 times the above Δp.
The ratio of the isothermal axial momentum flux at furnace exit to its value at inlet is taken as F_2, Appendix I.
Thus the ratio of the normalised axial momentum flux in the combusting flow to that in the isothermal flow is given by;

$$\bar{G}_{dx,comb}\ /\ \bar{G}_{dx,isoth} = F_2 + F_1\ (d/_D)^2\ ((\rho u/\rho_b) - 1.0)$$

For the normalised axial fluxes of tangential momentum at furnace exit, the ratio for the combusting flow to that for the isothermal flow is taken as F_3.
Thus, for the furnace swirl number, the ratio of the combusting flow value to the isothermal flow value is given by;

$$S^*_{comb}/S^*_{isoth} = \{F_2 . F_3\}/\{F_2 + F_1 (d/D)^2\ ((\rho_u/\rho_b) - 1.0)\} \quad .....(3)$$

FIRST INT. CONF. ON COMBUSTION AND EMISSIONS CONTROL, INSTITUTE OF ENERGY, CARDIFF, 1993

HEAT TRANSFER AND EMISSION STUDIES IN A GAS FIRED FURNACE

Beltagui[1,2] S A, Kenbar[1,2] A M A and Maccallum[1] N R L

1-Glasgow University
2-National Engineering Laboratory (NEL).

ABSTRACT

This paper presents results from an extensive programme of studies aimed at improved combustion performance with reduced pollutant emissions. In these studies characteristics of swirling flames in a natural-gas fired furnace are investigated through detailed measurements of the aerodynamics, combustion, heat transfer and pollutants emissions.
This paper presents comparisons of combustion performance, heat transfer and pollutant formation when using three different fuel injection schemes with a variable swirl burner in a semi -industrial scale furnace system. The data gained provide the information needed to optimise the fuel injection mode, swirl and mixture ratio to achieve the best combustion performance with minimum pollutant formation.
In addition to providing more insight into the processes involved results of these studies are also being used for the validation of furnace prediction models. These models can then be used for the appropriate optimisation of the design.

1. INTRODUCTION

Furnace system design and operation requires careful characterisation and optimisation of complex flow and combustion parameters in order to satisfy various requirements, some of which may be conflicting. Although Computational Fluid Dynamic (CFD) techniques are being progressively used in furnace design, there is still a great need for experimental testing. A combined approach using validated models to predict detailed information to supplement experimental testing of new designs is recommended. This is being implemented in the NEL furnace facility where measurements are performed to test new designs and validate CFD predictions.

In a collaborative research programme between Glasgow University and NEL, extensive studies aimed at improved combustion performance with reduced pollutant emissions are being carried out. In this programme characteristics of swirling flames in a semi-industrial size gas fired furnace are investigated through detailed measurements of flow, combustion, heat transfer and pollutants.

The extensive data sets gained are being used in developing and testing theoretical models of furnace flow, combustion and heat transfer produced by Heat Transfer and Fluid Flow Service, HTFS such as PCOC [1] and ZONE [2]. The data is also used for assessing general CFD codes such as PHOENICS [3] and FLOW3D [4]. These models can then be used for the appropriate optimisation of the design.

This paper presents comparisons of combustion performance and pollutant formation when using three different fuel injection schemes with a variable swirl burner. The data gained provide the information needed to optimise both the fuel injection mode and swirl to

achieve the best combustion performance with minimum pollutant formation.

2. FUEL INJECTION MODES

In industrial burners, mixing between air and fuel occurs within the combustion chamber by shear layer mixing. Swirling the air flow can increase shear mixing and enhance it with centrifugal mixing. The utilisation of the full benefits of these two mixing mechanisms depends mainly on the fuel injection mode and swirl. The effects of fuel injection mode on swirling flames were investigated by many workers as reviewed in [5-8].

Shear layer mixing is effectively utilised if the fuel is injected into the regions of maximum shear in the air stream. Centrifugal mixing effects can be utilised by creating favourable density gradients within the flow. The most common method of fuel injection is axially at the centre of the air flow. This method does not utilise the full potential of the shear layer mixing.

Shear layer mixing is enhanced if the fuel is injected radially from the centre axis across the entering air jet. With proper design the fuel jets can be used to produce the central reverse-flow zone (CRZ) required for flame stability instead of using high swirl as illustrated by tests on the NEL furnace [1].

An alternative to the central axial fuel injection, is to inject the fuel at the periphery of the entering air jet [5]. This system utilises both shear layer and centrifugal mixing resulting in efficient mixing and hence high combustion intensity.

The peripheral fuel injection system was investigated in an adiabatic furnace [5]. Stable flames were obtained even without a CRZ. The peripheral injection produced higher intensity flames with wider stability ranges relative to the central axial fuel injection.

In order to provide reliable comparisons, the present work was carried out on the NEL test facility which represents a semi-industrial scale furnace system. Detailed data were gained for the three fuel injection methods with variable swirl and fuel/air ratios [1,2,6,7,8].

3. EXPERIMENTAL FACILITY AND TEST CONDITIONS

The NEL furnace is a model of a cylindrical upshot fired heater. The apparatus consists of a water cooled chamber of 1 m diameter, by 3 m high, which is segregated into six cooling sections. The rig is extensively instrumented for detailed traverses of the flow field. The burner uses a moving block swirl-generator [9], followed by a quarl as shown in Fig. 1.

3.1 Fuel Injection Systems

Figure 1 illustrates the burner and the three fuel injection systems.

a- Central axial fuel injection.

b- Central radial fuel injection. Fuel is injected by a 35 mm diameter concentric gas gun, radially through 16 nozzles of 5 mm bore.

c- Peripheral axial fuel injection. Two alternative arrangements for fuel entry were used, either an annular continuous slit around the periphery of the air inlet, or a set of 60 holes, having the same total flow area as the continuous slit. Both arrangements produced flames of virtually identical geometry and appearance. Thus the detailed measurements were taken for the continuous slot arrangement only. For brevity, the above three injection modes

will be referred to as axial, radial and peripheral.

3.2 Air Entry Schemes

It was found that a stable flame could only be achieved if enough swirl (S > 0.8) was applied to the air flow to produce a CRZ near the burner. Otherwise, a CRZ was aerodynamically created by introducing a fraction of the combustion air radially outward through a central gun. Thus when 10 % of the combustion air was supplied through the central gun, a stable flame was achieved even without swirl

3.3 Swirl Range

Measurements of the flow and combustion patterns were carried out for four swirl settings, swirl numbers S values: 0.0, 0.45, 0.9 and 2.25.

3.4 Firing Rate and Mixture Ratio

All detailed in-furnace measurements were carried out at 400 kW and 5% excess air. Stack measurements, covered a wide range of input fuel-equivalence ratio, namely 0.70 to 1.35. Some additional heat transfer tests were performed at 300 kW and at 20 % excess air ratio.

4. MEASUREMENTS

Detailed results of the measurements to be used here for the radial fuel injection were reported in [1,2,11]. The peripheral fuel injection results were reported in [7,8]. The axial fuel injection measurements in [6,8].

4.1 In-furnace Measurements

Detailed mapping of the flow field was made through radial traverses at 13 axial planes along the furnace. A calibrated spherical head five-hole pitot probe of 8 mm tip diameter [8,10] was used for velocity measurements. The gas temperature was measured using a suction pyrometer [10]. For concentration measurements, a special water cooled stainless steel sampling probe [12] was used. For NOx and HC analysis, the gas sample passes through a heated sample line to the NOx chemiluminescent and hydrocarbon flame ionization detector analysers respectively. For CO, CO_2 and O_2 analysis, the sample was cooled and dried before passing to Infra-red absorption analysers for CO and CO_2, and a paramagnetic analyser for O_2.

Heat flux distributions along the furnace were measured. Total heat flux was measured using both calorimetry and heat-flux probe [2,10]. A radiometer probe was used to measure the radiant heat flux. Measurements also include the furnace inside wall temperature..

4.2 Stack Measurements

These include concentrations of CO, CO_2, O_2 , HC and NOx and flue gas temperature.

5. FLAME BEHAVIOUR

The flames studied were all stabilised through recirculation of some combustion products.

The axial fuel injection resulted in a stable flame only for swirl above S=0.9. This flame was characterised with non-uniformity and yellow colour. Compared with other fuel

injection modes, this flame was the longest.

The radial fuel injection achieved a stable flame without and with swirl. The flame intensity increased with swirl over the range tested, S=0.0 to 2.25.

The peripheral fuel injection basic scheme achieved stable flames only with swirl above S=0.80. The flame with S=0.90 show some non-uniformity in shape. The alternative scheme, where 10% of the combustion air was introduced radially through the central gun to create a CRZ, achieved a stable flame even without swirl.

6. FLOW PATTERNS

The flow patterns are defined by the radial distributions of the measured three time-averaged velocity components and static pressure.

6.1 Axial Velocity Profiles

A sample of the velocity profiles is given in Fig. 2. The measured flow patterns have essentially the same shape, type D, as classified by Beltagui and Maccallum [12]. In this flow pattern, the flow near the burner consists of a CRZ surrounded by an annular jet containing the main forward flow. Outside the forward flow a weak external reverse-flow zone (ERZ) extended to the walls. Velocities in the ERZ are very low due to the low confinement.

For the forward flow, the value of peak velocity increases with swirl. The high velocity gradients at the boundaries increase even further with swirl. These gradients enhance the shear forces at the jet boundaries, leading to higher mixing rates. These features result in short intense flames.

Along the furnace, both the rate of decay of maximum velocity and the recovery of the centreline axial velocity increase with swirl.

6.2 Flow Boundaries

Figure 3 defines the boundaries of the flow extracted from the velocity profiles, and defines the flow zones. Both the jet radial expansion and the size of the CRZ increase with swirl. The flow structure inside the furnace can be divided into four distinct zones: Near burner forward-flow zone (main reaction zone), CRZ, fully developed-flow zone and ERZ.

6.3 Tangential Velocity Profiles

The tangential velocity values indicate the local swirl strength which contributes to mixing and combustion. The high swirl jets show a Rankine-vortex flow with solid body central rotation surrounded by an outer free vortex. The rate of decay of the tangential velocity increases with swirl.

6.4 Radial Velocity Profiles

The radial velocity values indicate the direction and magnitude of the jet spread. Both the magnitude of the radial velocity and its rate of decay along the furnace increase with swirl. The measured features are consistent with the jet expansion behaviour suggested by the axial velocity distributions.

7. COMBUSTION PATTERNS

The relative combustion patterns over the range of fuel injection and swirl studied, are demonstrated by the in-furnace measurements of temperature and species concentrations (CO, CO_2, O_2 and NOx). These measurements give useful data to quantify the main features of the flame performance which include; mixing, combustion intensity, flame symmetry, heat release and pollutant formation.

Samples of the results are given in Figs 4,5 showing CO and temperature contours, for radial injection for the swirl settings of S = 0.0 and 2.25. The results illustrate the strong influence of fuel injection mode and swirl on combustion. Since the most important information is required near the burner, Figs. 6,7 show radial profiles for two planes at distance, X , from the burner exit of 45 and 200 mm.

Generally, the flames are of the short intense type associated with high mixing rates and central reverse flow. All profiles illustrate good flame symmetry except for the case of axial fuel injection, where a degree of asymmetry is noted nearer the burner and at the lower swirls. This asymmetry is due to slow combustion and thus low jet expansion.

The following notes discuss the mixing and combustion for each of the three fuel injection modes dealing with the four zones of the flow field.

7.1 Main Reaction Zone:

The measurements show that the main reaction zone length decreases with swirl. Combustion starts within the quarl, as shown by CO, CO_2 and O_2 values at X =45 mm where the minimum value of CO_2 is between 2.5% and 4.0%. The steepest axial and radial gradients, of both concentrations and temperature, occur at the plane nearest to the burner. These gradients increase as swirl is increased.

Further downstream, these gradients decay more rapidly at the higher swirl, resulting in near-uniform temperature profiles for S=2.25 at a plane 1.0 m downstream of the burner. By comparison, with low swirl, radial temperature gradients are evident even at furnace exit. Thus, increased swirl not only increased combustion intensity, but also enhanced the stirring of the post-flame gases.

Of the three fuel injection modes, the axial injection system produces the longest reaction zone with the lowest peak temperature value.

For the peripheral fuel injection, combustion starts earlier, the temperature of the combustion products then decreases due to both heat transfer and entrainment and subsequent rapid mixing with the cooler externally recirculated gases just downstream of the burner exit. Thus although combustion is more intense the peak reaction zone temperature for the peripheral fuel injection is lower than for the radial injection.

The flame length, defined by the distance from the quarl exit up to the point where the CO concentration is less than 0.5 %, is reduced by swirl. For example with the radial fuel injection it is reduced from about 1.5 m for S=0.0 to 0.5 m for S=2.25.

At the high swirl, S=2.25, all fuel injection modes exhibit nearly the same flame diameter.

However, in the peripheral fuel injection the lower swirl, S=0.9, exhibits a flame envelope which is wider than with the radial fuel injection mode.

7.2. Central Reverse-flow Zone, CRZ

Small concentrations of HC and CO exist along the CRZ, for the lower swirl flames where the CRZ receives mixtures with reactions still in progress. As swirl is increased these concentrations diminish to zero.

Within the CRZ, temperature profiles become more uniform as swirl is increased, due to enhanced radial stirring of the gases. The centreline temperature is close to the maximum temperature measured at the particular traverse plane.

7.3. Fully Developed Flow Zone

Downstream of the reaction zone, CO and HC decay to zero, and CO_2 and O_2 attain their uniform values of complete combustion.

7.4 External Reverse-flow Zone, ERZ

This zone contains mainly products of complete combustion from the above region. However very low concentrations of CO and HC are entrained from the outer boundary of the forward flow where reactions are still in progress.

The highest ERZ temperature is observed with the axial fuel injection where the flame is longest. Heat transfer to the furnace walls reduces the temperature of the gases in this zone as they travel towards the burner end.

8. HEAT TRANSFER

8.1. Heat Flux Distributions

Axial distributions of heat fluxes for representative tests are given in Fig 8, which shows both calorimetry and probe measured total heat flux in addition to the radiant probe measured heat flux component. High swirl is associated with short intense flames with high heat transfer near the burner. Low swirl results in longer flames with more uniform heat transfer along the furnace. The peak total heat flux increases in value and moves towards the burner as swirl is increased.

Although both convection and radiation contributions are affected by swirl, the measurements show that the convection is affected in a more pronounced manner, both in magnitude and position. The jet spread increases with swirl, reducing the length of the ERZ bringing the jet impinging point nearer to the burner thus enhancing the convective heat transfer contribution.

8.2. Overall Heat Transfer

This is measured by the furnace heat-transfer efficiency, defined as the ratio of the heat absorbed by the cooling water to the total energy input at the burner. Values of this efficiency for the three fuel injection modes at 400 kW and 5% excess air are plotted in Fig 9. Furnace efficiency was also measured for higher excess air, up to 35% and for lower firing rate of 300 kW. The results lead to the following conclusions:

1- The highest heat-transfer efficiency is produced by the peripheral fuel injection followed by the radial injection
2- For the same input energy and excess air the efficiency increases with swirl.
3- For the same excess air lower input energy produces a higher efficiency.
4- For the same input energy and swirl higher excess air reduces efficiency.

The conclusions indicate that the radiant component of the heat transfer is the dominate part. Higher efficiency at reduced loading, results from the effective maintenance of the radiant contribution mitigating the reduction in convection associated with reduced loading.

9. FORMATION OF POLLUTANTS

The pollutant formation was determined by the stack emissions of CO, HC and NOx measured over the range of equivalence ratio, ϕ, 0.70 to 1.35 for the three fuel injection modes.

The measured CO and HC concentrations show that for both the peripheral and radial fuel injection modes an excess air of 5% is sufficient to guarantee complete combustion. The corresponding value of excess air for the axial fuel injection is 10 %.

Before dealing with the NOx emissions from the stack, the in-furnace detailed NOx surveys are discussed.

9.1 NOx Concentrations

NOx concentration measurements are represented in Fig. 10 by full contours for radial fuel injection system with S=0.0 and 2.25. Comparative profiles of NOx concentration profiles at two near burner levels are given in Fig 11. The results are discussed in relation with the temperature and species concentration fields dealing with the four flow field zones defined in Section 7.

9.1.1. Main Reaction Zone:

All fuel injection modes show steep gradients of NOx concentrations in both radial and axial directions. The rate of NOx reactions follows closely that of the main combustion reaction. Comparison of the NOx profiles at X= 45 mm, Fig. 11, with the corresponding temperature profiles, Fig. 7, shows a high degree of similarity. The maximum NOx concentrations increase towards the boundary of the CRZ where the maximum mixing and combustion intensity occur.
In general, the peak NOx concentrations occur with the highest swirl. However, for both axial and peripheral fuel injection systems, increasing swirl from 0.90 to 2.25, resulted in a decrease in NOx formation even though the temperature level has increased. It is suggested that this decrease in NOx at the higher swirl is due to the increased mixing rate leading to reduced concentration fluctuations and to shorter residence time.

9.1.2 Central Reverse-flow Zone, CRZ

The concentrations of NOx here depend on the length of the CRZ relative to that of the reaction zone. This will also decide whether any further reactions will take place within the CRZ.

Figure 11 shows that at both planes, for the lower swirl, the radial fuel injection mode

produces the minimum value of NOx compared with other injection modes. These low concentrations indicate that this zone receives mixtures which are still reacting, as confirmed by the high CO concentrations shown in Fig 6. At the higher swirl with the radial fuel injection, increased NOx concentrations within the CRZ were observed. This increase indicates that gases with higher temperature and thus higher NOx concentrations enter the CRZ, where further NOx reactions take place, resulting in the highest NOx concentrations compared with the other fuel injection modes.

The profiles of NOx within the CRZ, Fig. 11, and the corresponding temperature profiles, Fig. 7, show that the increase in NOx concentration within this region is mainly due to the entrainment from the forward flow and not due to reactions within this zone. For example at the 45 mm plane, higher NOx concentrations are measured for the lower swirl, although the temperature is lower. Further downstream at the 160 mm plane the temperature levels at both swirl settings are about the same, yet higher levels of NOx are observed at the lower swirl.

9.1.3. Fully Developed Flow Zone

Constant NOx concentrations were measured throughout this region and these equal the value measured at the stack, Fig.12.

9.1.4. External Reverse-flow Zone, ERZ

This zone contains mainly combustion products from the fully developed zone with some flow entrained from the outer boundary of the reaction zone. Figure 11 shows that NOx concentration within this zone increases with axial distance from the burner until it reaches the fully developed value.

The above discussion of NOx measurements show that the NOx formation rates are affected by the flame temperature, residence time of hot gases in the reaction zone and the concentration fluctuations. These conclusions are confirms that in these flames NOx is formed by the Zeldovich mechanism, although there may be some prompt NOx.

9.2. Overall NOx Emissions

Stack measured NOx concentrations, given in mg/m^3 corrected to 3% excess O_2, are presented in Fig. 12. For the range of ϕ covered by the data, the lowest NOx concentrations are observed with the axial fuel injection. This is due to the lower combustion intensity and thus the lower flame temperature in the reaction zone.

For the lean mixtures tested ($\phi < 1$), , the peripheral fuel injection mode produced significant decrease in NOx formation with increased excess air, while the radial and axial fuel injection modes gave an increase in NOx formation. The differences observed here are mainly dependent on the peak flame temperature. The peripheral fuel injection mode, is the only mode where increased excess air leads to a decrease in the peak temperature. This is due to the higher rates of mixing before and after combustion in this mode. In the other injection modes the increase in local O_2 concentration becomes the controlling factor.

At fuel-rich conditions ($\phi > 1$), all fuel injection modes exhibit a sharp decrease in NOx formation with increased ϕ. This decrease is the result of both lower peak temperature and lower O_2 concentrations.

The above analysis confirms that the peripheral fuel injection is the only method which offers both air and fuel-staging as means of suppressing NOx formation. In applications where lean combustion can be used, only peripheral fuel injection offers the possibility of reducing NOx formation compared with the other fuel injection modes.

CONCLUSIONS

1- Flame stability: All flames were stabilised by the central reverse flow. A minimum swirl of S=0.8 is required to create this CRZ. For peripheral fuel injection mode, a stable flame was achieved by feeding a fraction of the air flow radially through the centre to create a CRZ. For the radial fuel injection, the fuel jets created a CRZ, thus it was possible to achieve stable flame even without swirl.

2- Flame behaviour: The central axial fuel injection produced a long flame with a yellow appearance and non-uniformities. The radial and peripheral fuel injection modes resulted in intense, shorter blue flames.

3- Flow patterns: These patterns show the flow boundaries defining the jet expansion in the radial and axial directions. It also define the central and outer reverse-flow zones.

4- Combustion patterns: These display the following features:

a- Good flame symmetry except for the central axial fuel injection.
b- The peripheral fuel injection achieves the highest rates of mixing and combustion followed by the radial fuel injection.
c- With the peripheral fuel injection combustion occurs at the outer boundary of the swirled air flow, while in the other modes it is mainly on the boundary of the CRZ.
d- Swirl increases the mixing and thus combustion intensity.

5- The peripheral fuel injection has the maximum heat transfer efficiency followed by the radial fuel injection. Swirl enhances the total heat transfer and produces higher peak flux at locations nearer the burner. Increased excess air reduces heat-transfer efficiency whereas lower firing rate leads to higher efficiency.

6- Measurements of NOx confirmed its formation by the thermal mechanism with dependence on flame temperature, concentration fluctuations and residence time,

7- Complete combustion can be guaranteed with excess air of 5% for both the peripheral and radial fuel injection modes. The higher value of 10% was needed for the axial fuel injection.

8- For the 5% excess air firing, the lowest overall NOx formation was observed with the central axial fuel injection.This was the result of the lower temperature levels caused by the slower combustion in this system.

9- At fuel-rich conditions, increasing the fuel-air ratio resulted in sharp decrease in NOx formation for all fuel injection modes.

10- At fuel-lean conditions, the peripheral fuel injection gave a reduction in NOx formation,

with increased excess air, while the other two fuel injection modes produced some increase in NOx formation.

REFERENCES

1. BELTAGUI S A, FUGGLE R N, KENBAR A M A, RALSTON T, MARRIOTT N and STOPFORD P J. Modelling a gas-fired furnace flow and combustion using the PCOC Code, Proc.of the Euroteck Direct 91 Conference, I. Mech. E., pp.51-58, Birmingham, July, 1991.

2. BELTAGUI S A, FUGGLE R N and RALSTON T. Measurements and prediction of heat transfer in the NEL furnace. Second UK National Heat Transfer Conf., Glasgow, 1988.

3. KENBAR A M A, BELTAGUI S A and MACCALLUM N R L. Flow and combustion modelling of gas fired furnace with peripheral fuel injection burner. Presented at the 5th Int. PHOENICS Users Conf. Nice, 1992.

4- BRØNNUM A Sc, RASMUSSEN I R and BELTAGUI S A. FLOW3D modelling of the flow, combustion and heat transfer in a furnace with swirl burner. Presented at the first FLOW3D users Conf., Oxford, May 1993

5. BELTAGUI S A and MACCALLUM N R L. Characteristics of enclosed swirl flames with peripheral fuel injection, J. Inst. Energy, **61**, 3-16, 1988.

6. KENBAR A M A, BELTAGUI S A and MACCALLUM N R L. Effect of fuel injection modes on the combustion pattern and pollution formation in a gas fired furnace, Second Int. Conf. on Combustion Technologies for a Clean Environment, Portugal, July 1993.

7. KENBAR A M A, BELTAGUI S A, and MACCALLUM N R L. Combustion aerodynamics of a gas fired furnace with peripheral fuel injection. Third World Conf. on Experimental, Heat Transfer, Fluid mechanics and Thermodynamics, To be held in Honolulu, Oct. 1993.

8. KENBAR A M A, Combustion aerodynamics and pollutant formation in gas-fired furnaces. Ph.D. Thesis, Dept. of Mech. Eng., University of Glasgow, 1991.

9. LEUCKEL W and FRICKER N. The characteristics of swirl-stabilised natural gas flames, Part 1: Different flame types and their relation to flow and mixing patterns, J. Inst. Fuel, **49**, pp 103-112, 1976.

10. CHEDAILLE J and BRAUD Y. Measurements in flames. Edward Arnold, London, 1972.

12. KENBAR A M A, BELTAGUI S A, RALSTON T and MACCALLUM N R L. Measurement and modelling of NOx formation in a gas fired furnace. Proc. of the First Int. Conf. on Combustion Technologies for a Clean Environment, Portugal, Sept. 1991.

13. BELTAGUI S A and MACCALLUM N R L. Aerodynamics of vane-swirled flames in furnaces, J. Inst. Fuel, **49**, 183-193, 1976.

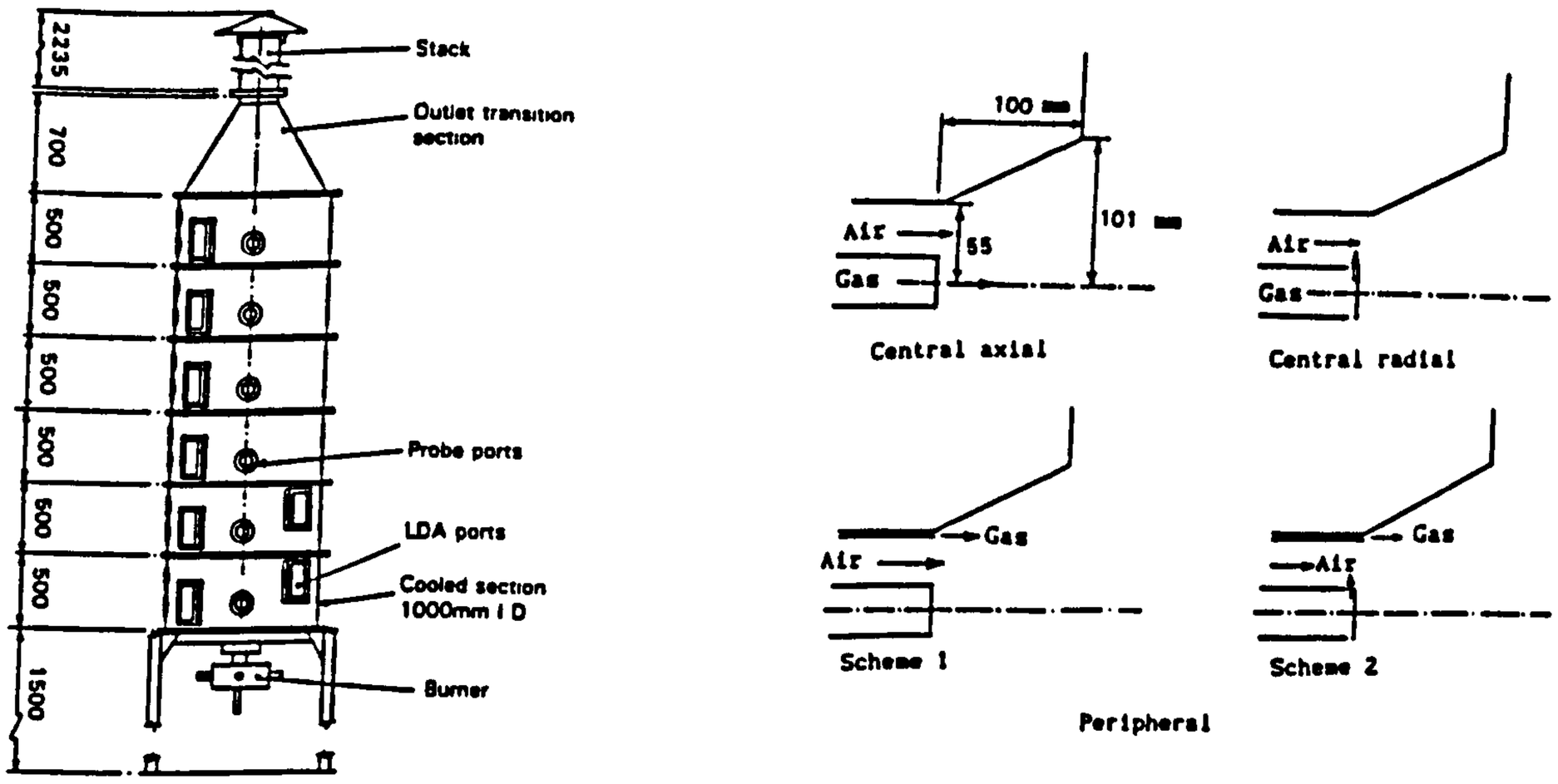

Figure 1- Furnace and burner system.

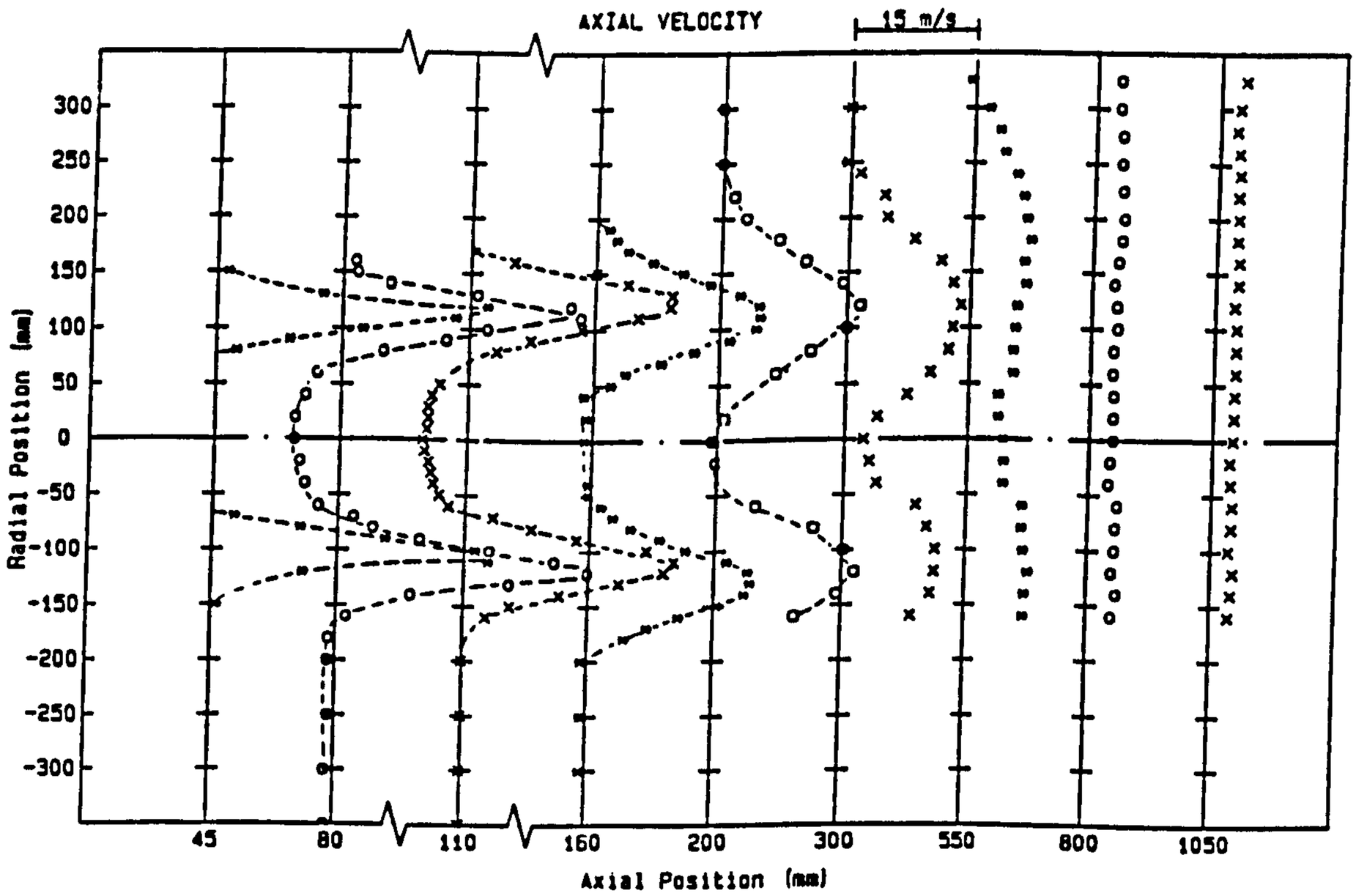

Figure 2- Axial velocity distributions, radial fuel injection, S=2.25 .

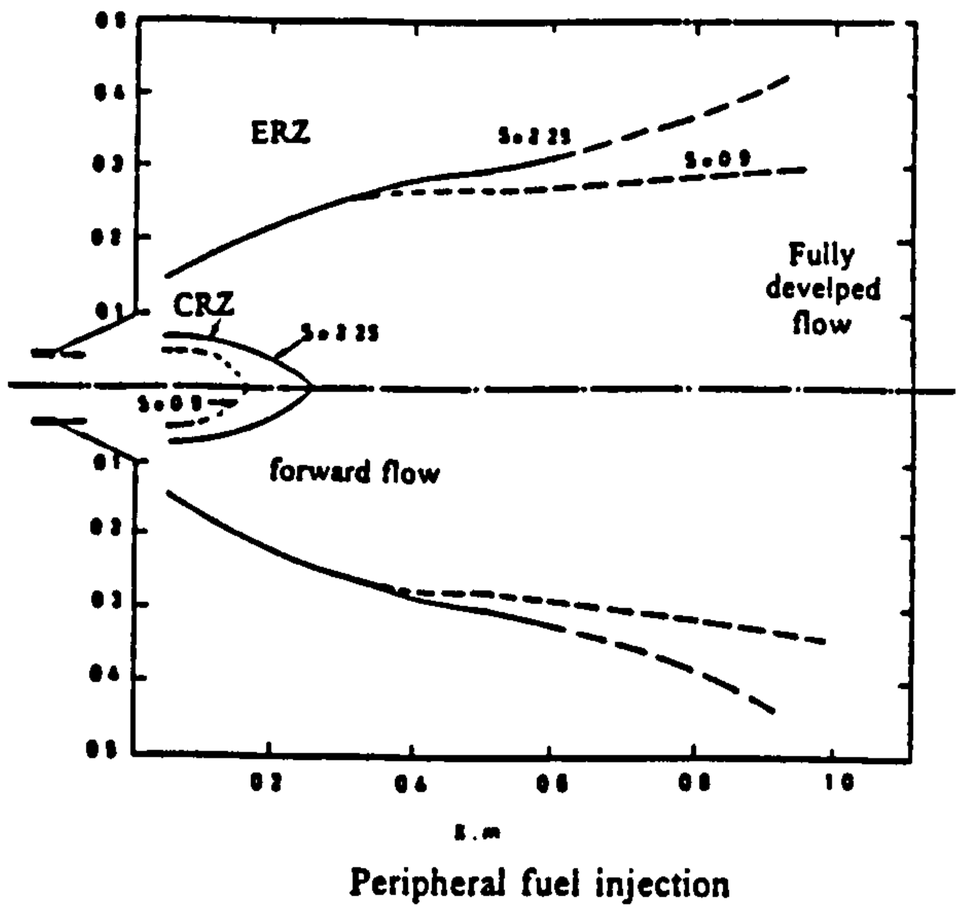

Figure 3- Flow Boundaries, radial and peripheral.

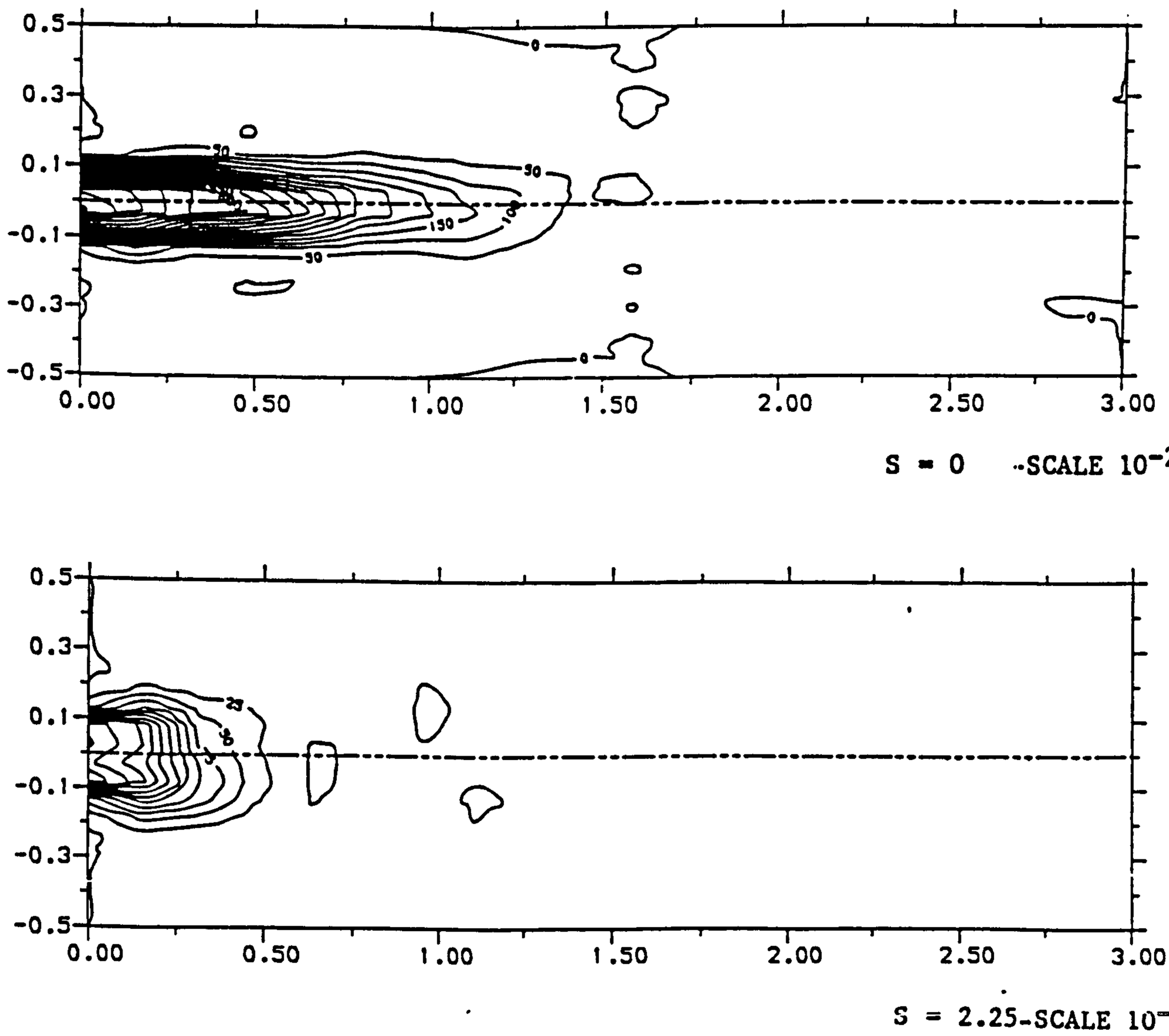

Figure 4- CO contours, radial fuel injection.

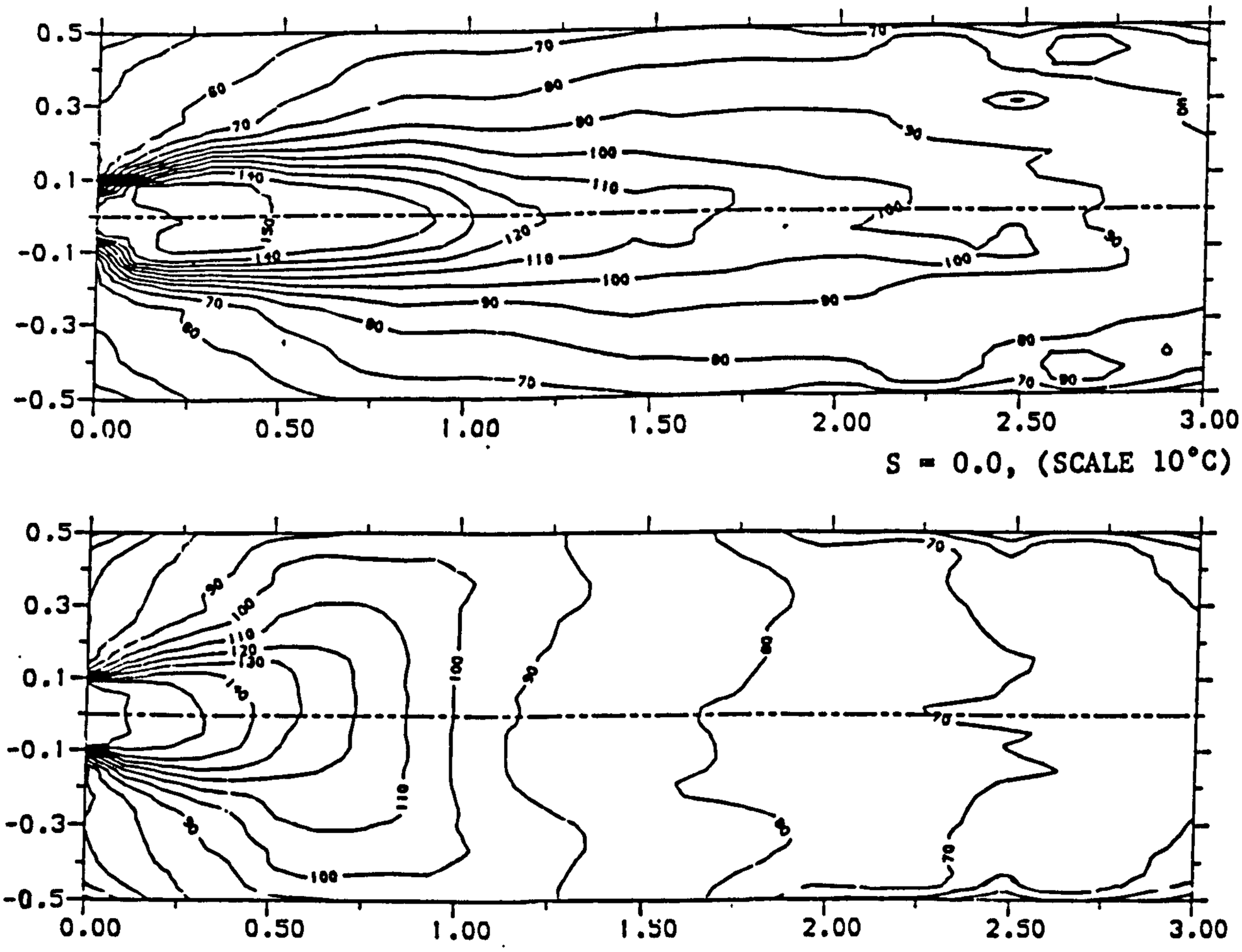

Figure 5- Temperature contours, radial.fuel injection.

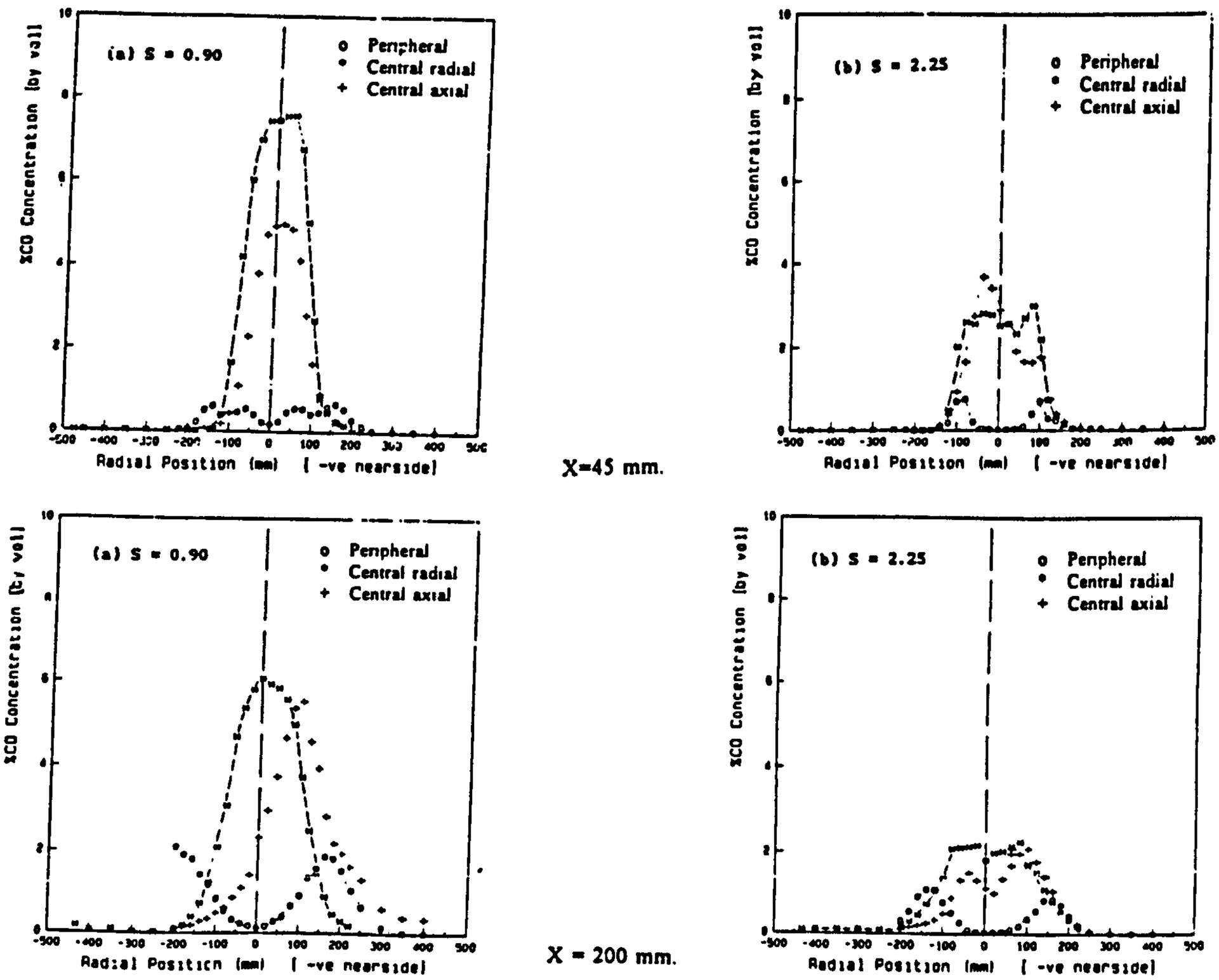

Figure 6- CO Profiles, X = 45 mm, X = 200 mm.

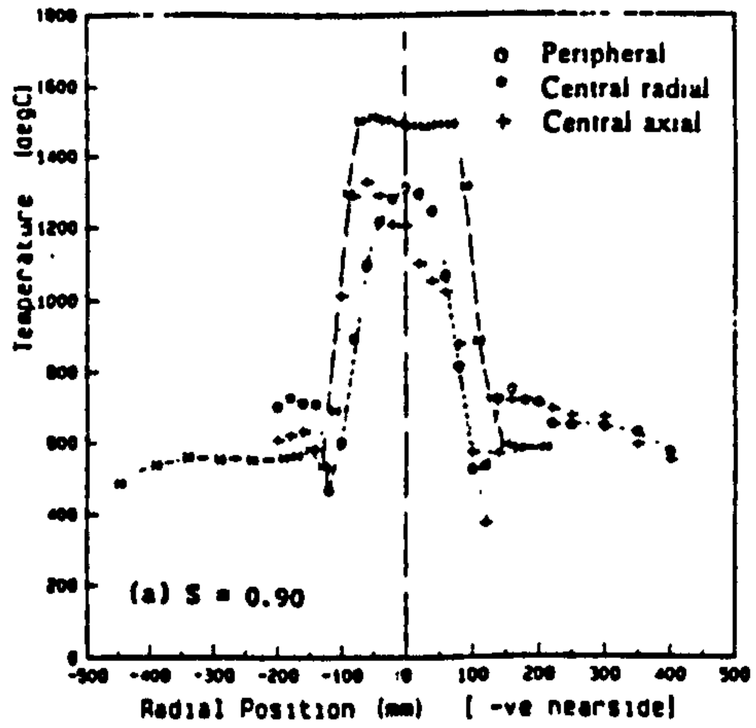

X = 45 mm.

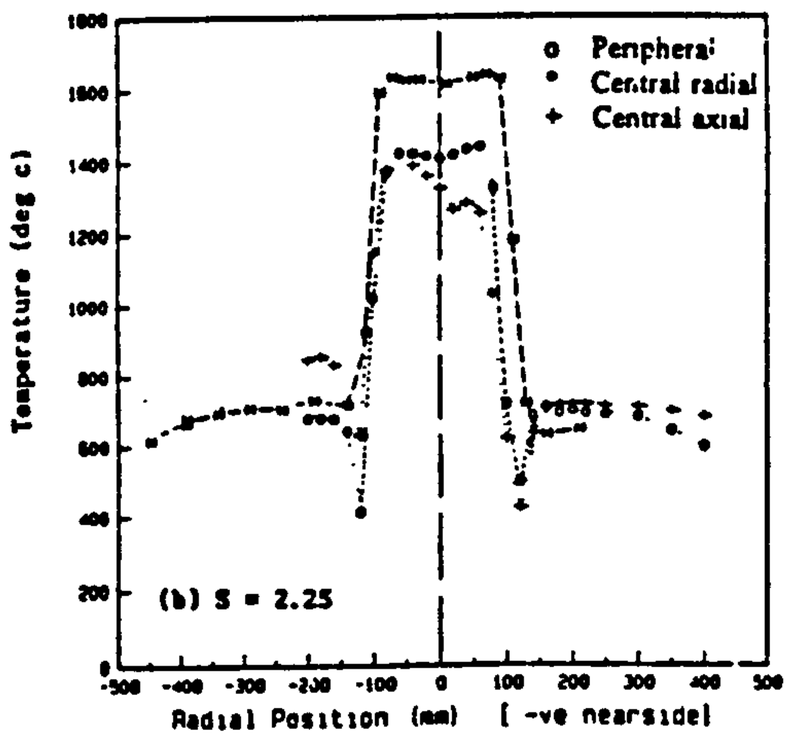

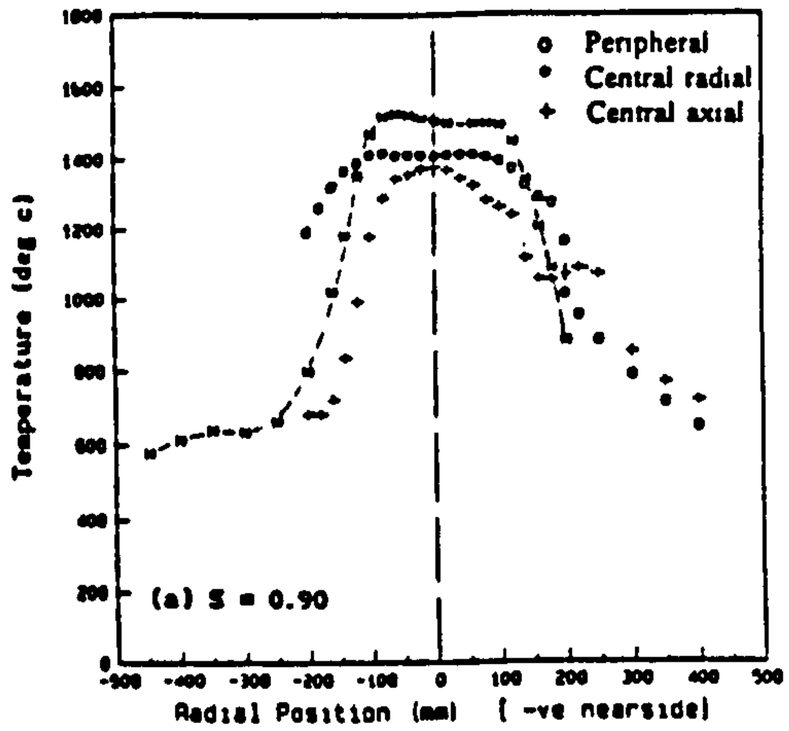

X = 200 mm.

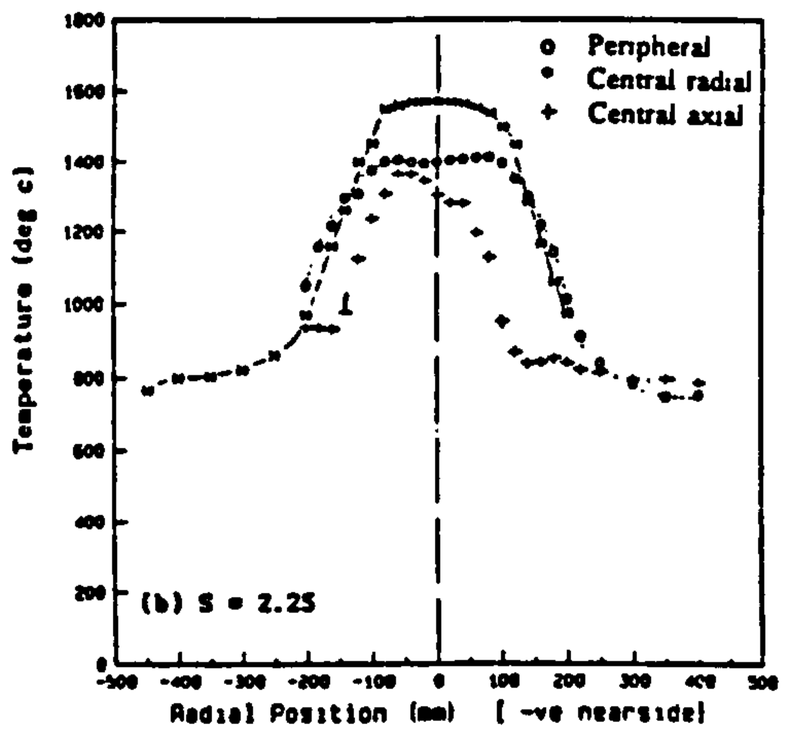

Figure 7- Temperature Profiles X = 45 mm and X = 200 mm

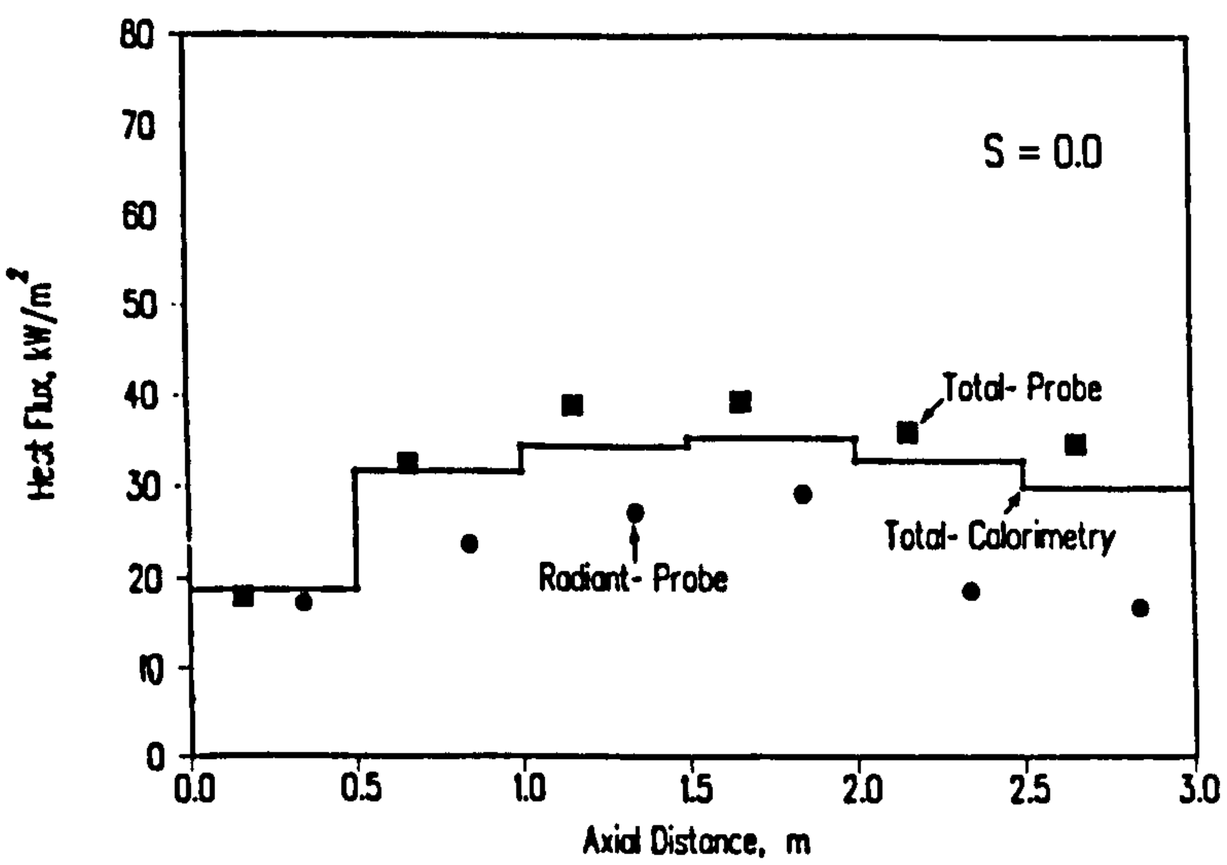

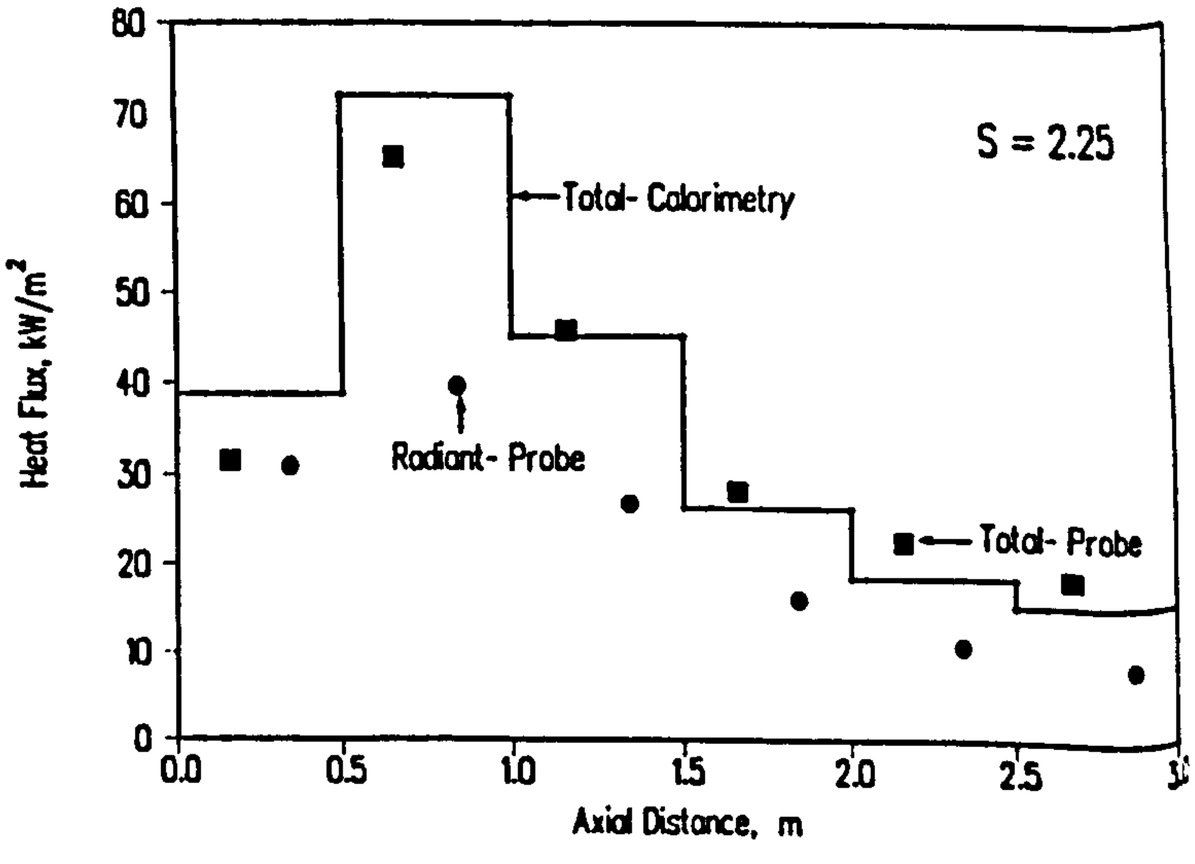

Figure 8- Heat Flux Distributions, radial fuel injection.

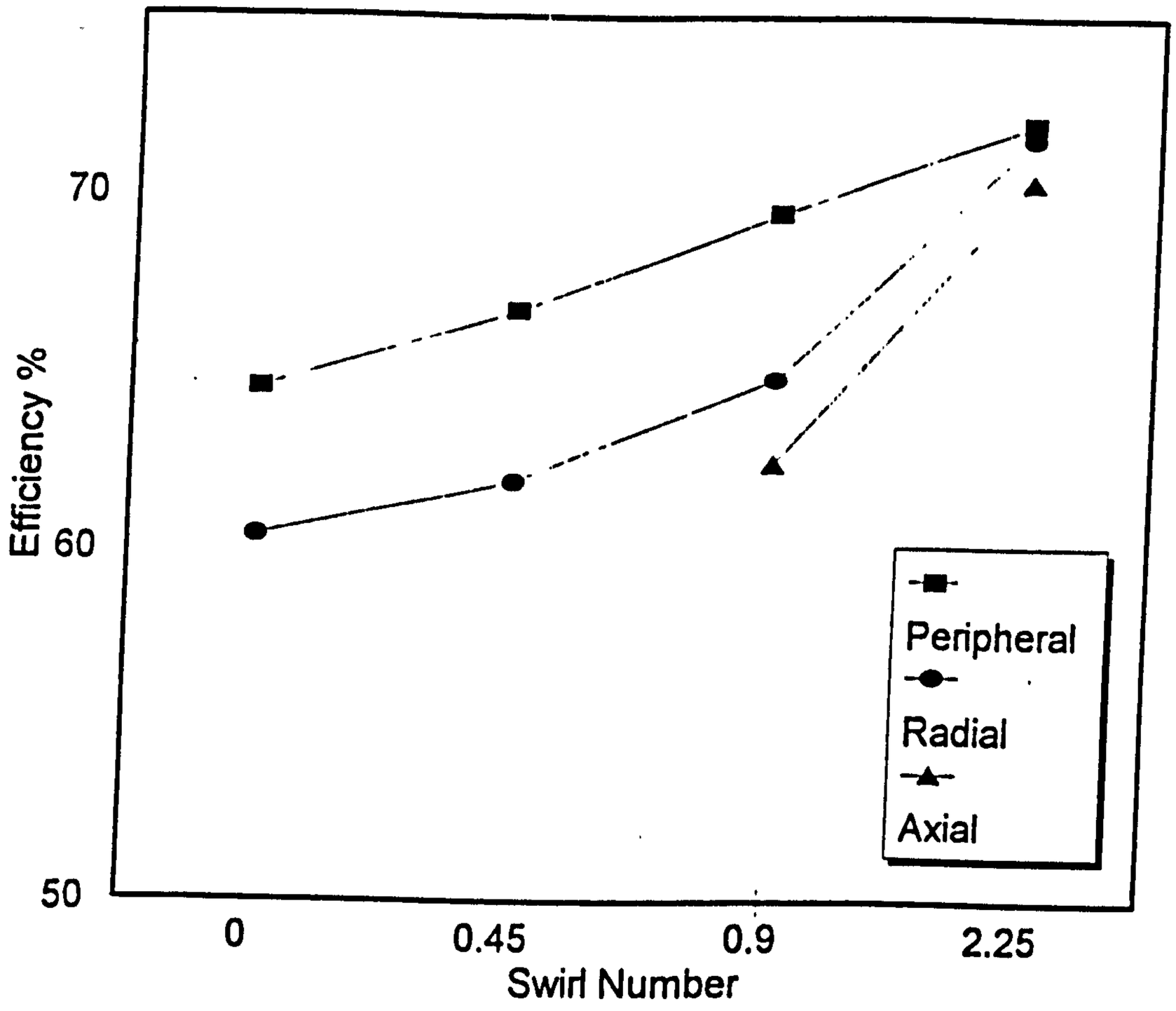

Figure 9- Heat transfer efficiency.

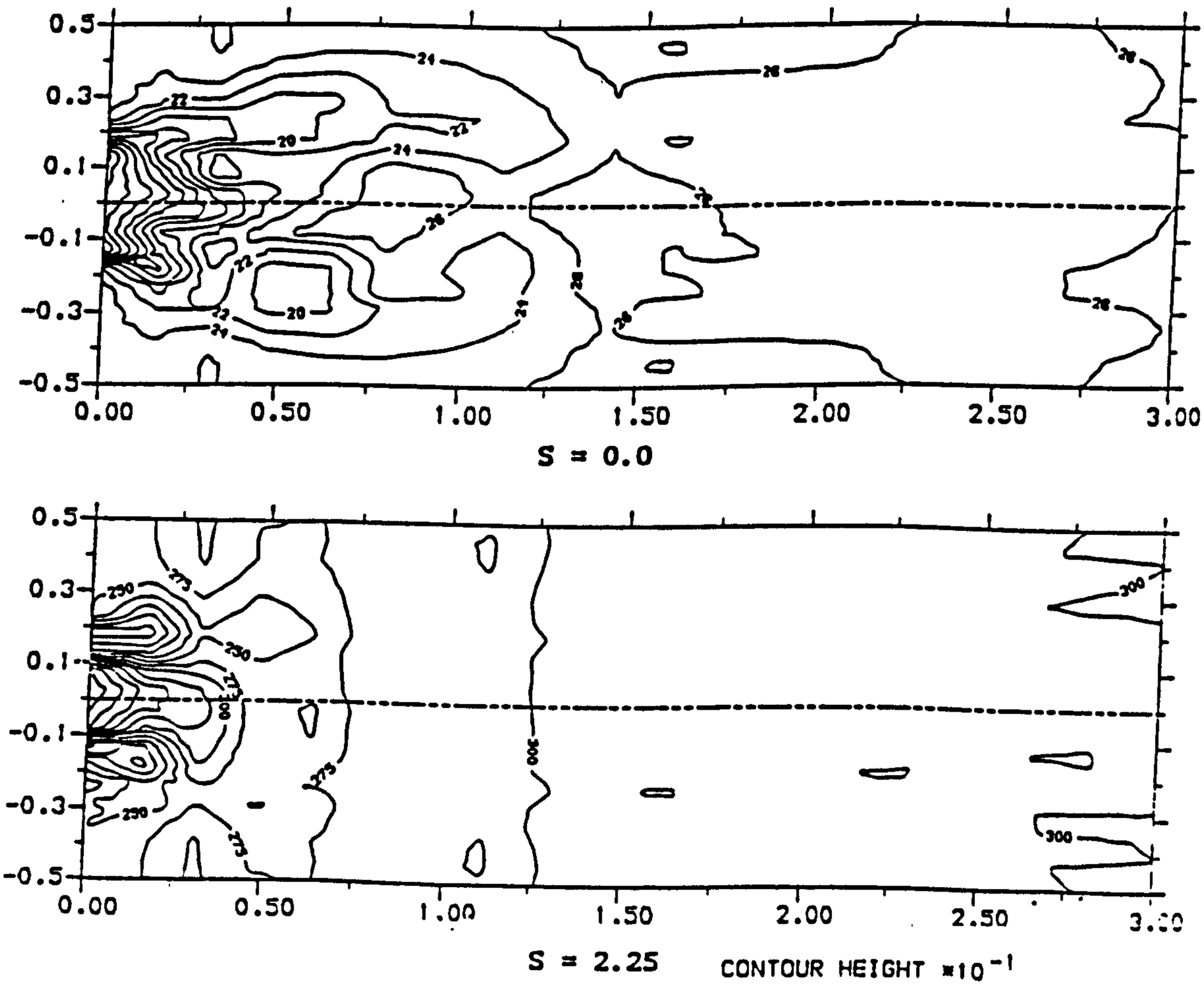

Figure 10- NOx Contours, radial fuel injection.

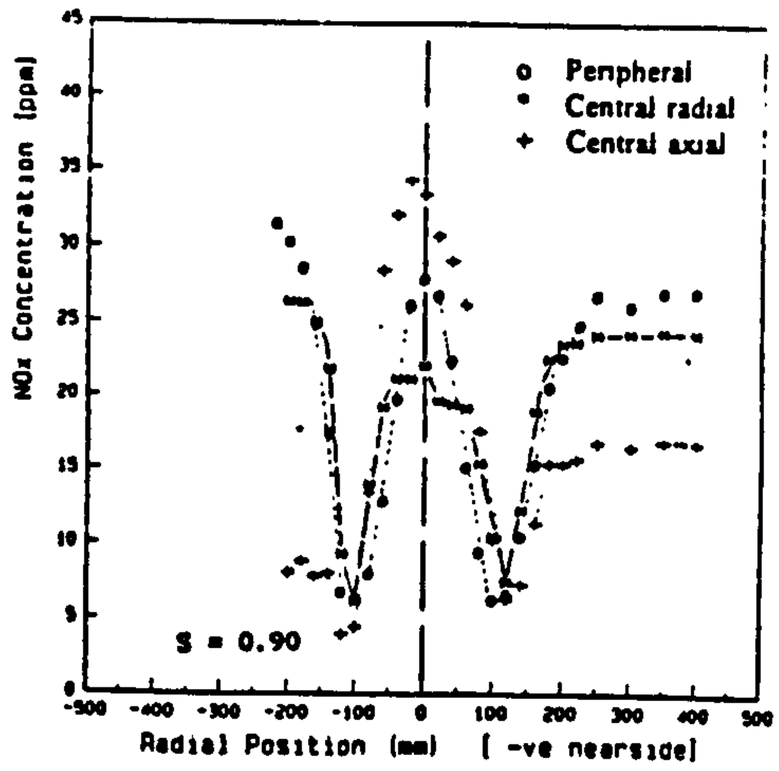

X = 45 mm.

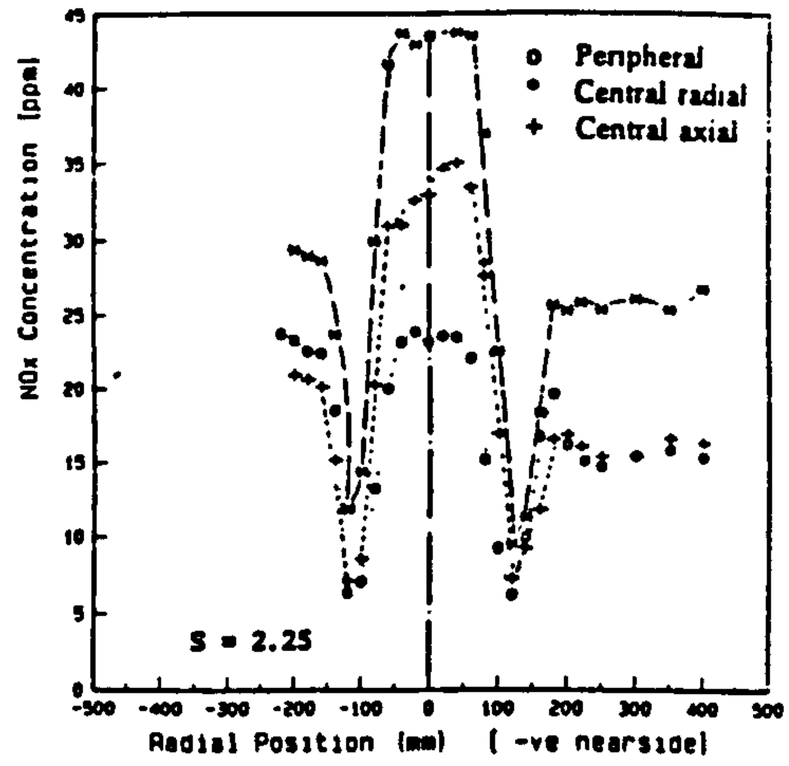

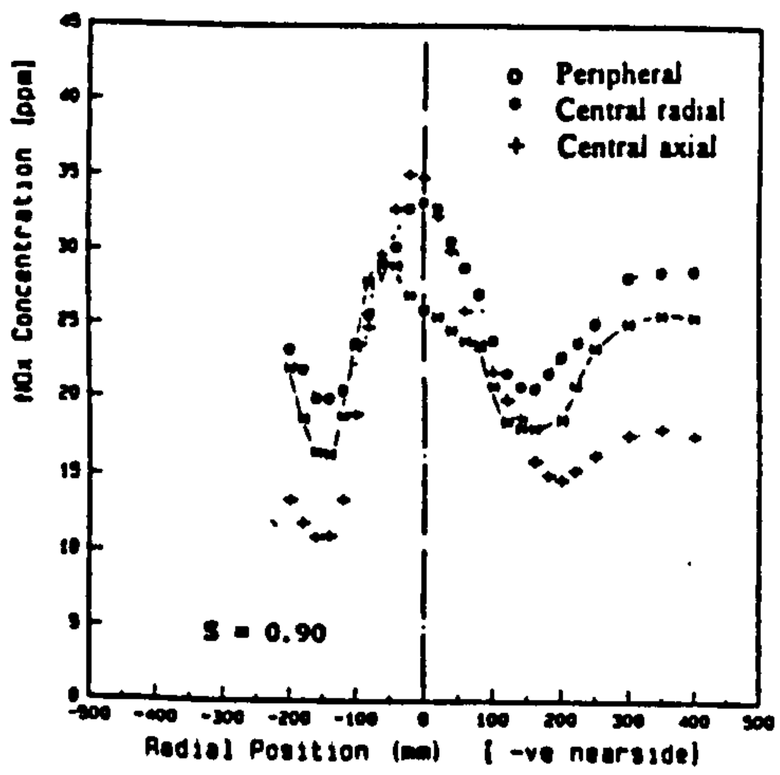

X = 200 mm.

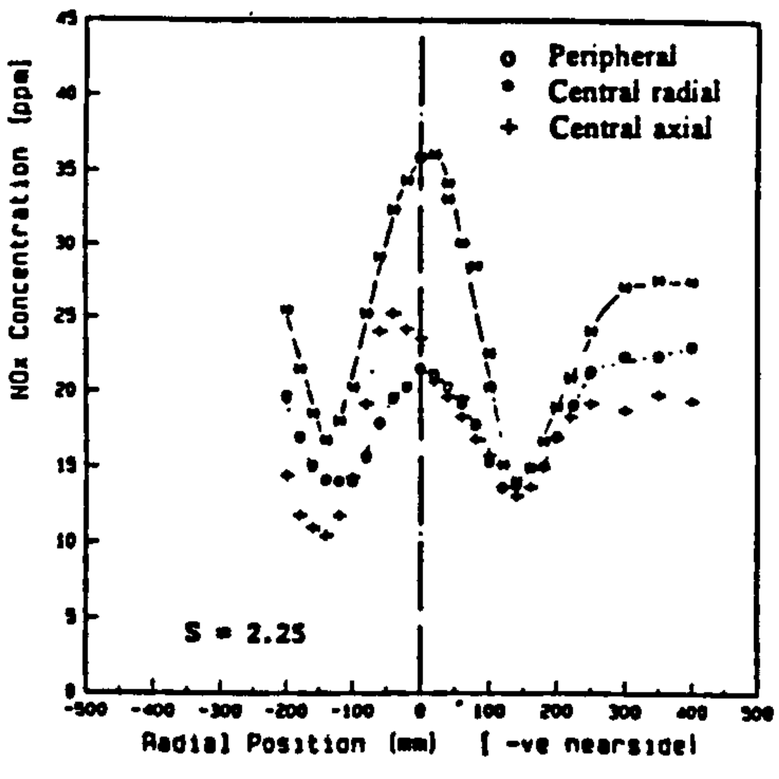

Figure 11- NOx Profiles, X= 45 mm and X = 200 mm.

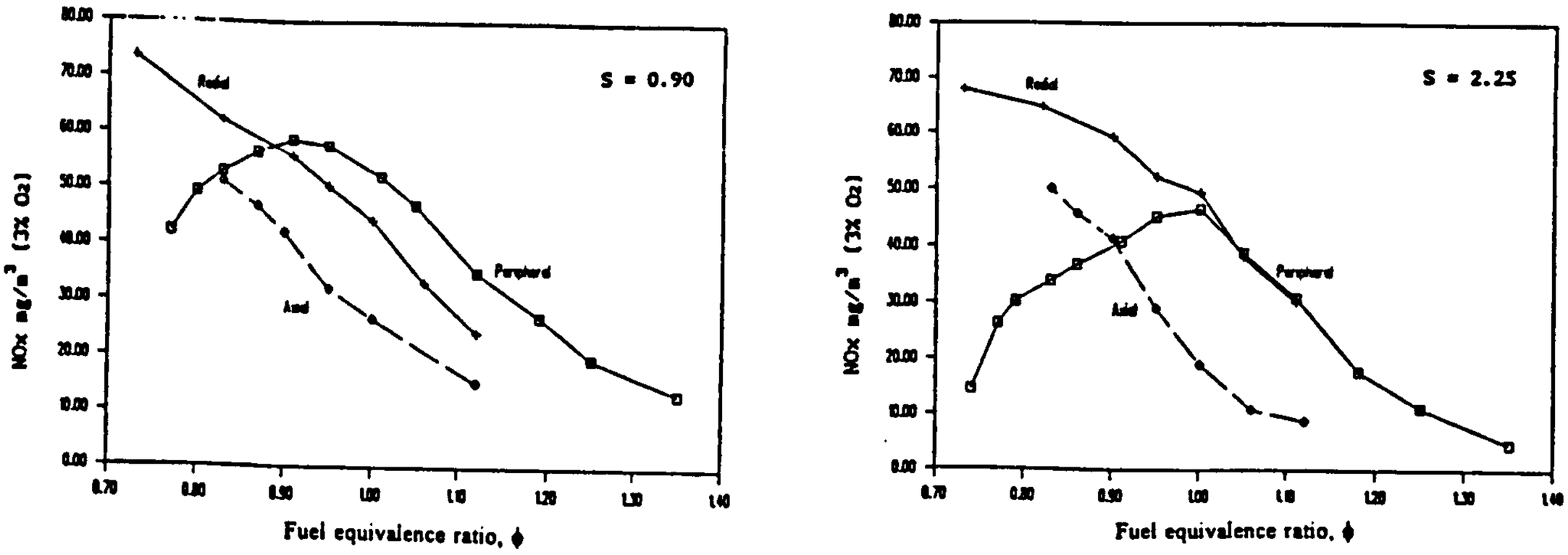

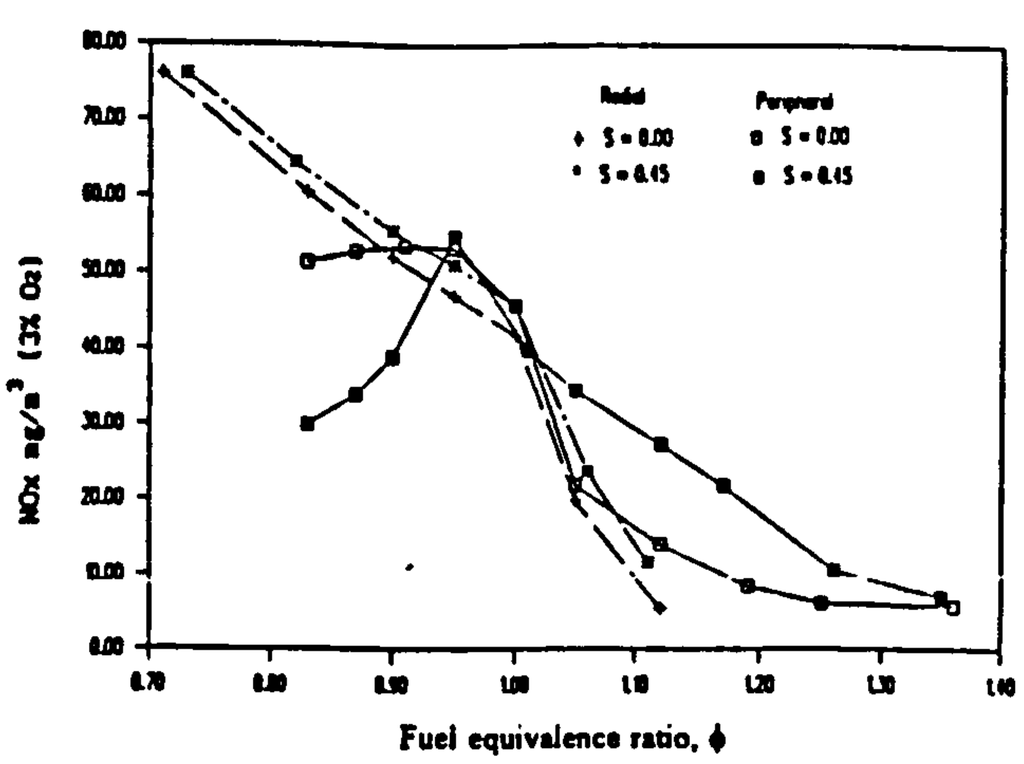

Figure 12- Stack Measured NOx Emissions.

COMMERCIAL - IN CONFIDENCE

HTFS RS 93-929
NEL/HTFS

PREDICTION OF FLOW AND COMBUSTION PATTERNS OF PERIPHERAL FUEL INJECTION BURNER IN THE NEL FURNACE

S A Beltagui[1,2] , A M A Kenbar[1,2] and N R L Maccallum[2]

1- HTFS, NEL
2- Glasgow University

ABSTRACT

An assessment is made of the ability of a CFD code to model the flow, combustion and heat transfer of swirling flames in furnaces. Predictions were made for the HTFS furnace facility at NEL using a swirl burner with peripheral fuel injection scheme. This configuration is a novel test case of the generality of the codes. The predictions were made using the PHOENICS code, with turbulence and combustion represented by k-ε and 'eddy break-up' models respectively. Radiation heat transfer was modelled by the flux method. Reasonable agreement between prediction and measurement was achieved for S=0.90, but less agreement for S=2.25 swirl.

NOTATION

a,b	Eddy break-up constants	-
C	Constant in kinetic energy of turbulence	-
h	Convective heat transfer coefficient	W/m^2K
k	Kinetic energy of turbulence	m^2/s^2
l	Characteristic dimension	m
M	Mass fraction	kg/kg
q	Wall heat flux	W/m^2
R	Rate of chemical reaction	kg/m^3s
S	Burner Swirl number	-
s	Stoichiometric air-fuel ratio	kg_f/kg_o
T	Temperature	K
t	time	s
U	Time-mean axial velocity	m/s
V	Time-mean radial velocity	m/s
W	Time-mean swirl velocity	m/s

Greek

α	Absorptivity	-
ε	Rate of dissipation of kinetic energy of turbulence	m^2/s^3
ε	Emissivity	-
ρ	Density	kg/m^3
σ	Stefan-Boltzman constant	W/m^2K^4

Subscript

f	Fuel
g	gas
o	Oxidant
p	product
w	wall

1. INTRODUCTION

Computational fluid dynamic (CFD) codes are being progressively used to help furnace designers. Furnace system design requires careful characterisation and optimisation of complex flow and combustion phenomena. The use of CFD is reducing the exclusive reliance on empirical methods

and measurements on scaled test units, by supplying detailed information of a proposed new design or modification. The mixed approach of physical model testing and CFD simulation reduces the time and cost of development.

Recently, numerical models capable of predicting the flow patterns and heat transfer characteristics have been developed and widely used for such furnaces. In addition to being required to handle turbulence, heat transfer and chemical reaction, these models must also be able to deal with complex geometries. Many detailed reviews of research in this field are given in literature, as reviewed by Kenbar et al (1991-a).

An assessment is made of the ability of a CFD code to model the aerodynamics, combustion and heat transfer of swirling flames in furnaces in a collaborative project between Glasgow University and HTFS (NEL).

These prediction procedures have been applied progressively to the case of swirling flows in furnaces. The simplest case- isothermal flow expanding into a furnace- were predicted by Beltagui et al (1991). Combusting flows where the fuel was injected in the centre of the swirled air jet have also been predicted by Beltagui et al (1991).

Recent advances in burner design to meet operational and environmental requirements have resulted in burners with other modes of fuel injection. An example is a burner with fuel injected at the periphery of the swirled air flow, studied in an experimental furnace system by Beltagui and Maccallum (1988). In that burner the mixing and combustion patterns are significantly different from those of the central fuel injection case due to the utilisation of the combined effects of shear-layer and centrifugal mixing. Therefore predicting the aerodynamic and combustion patterns of such a combustion system represents a new test for the generality of the modelling procedures. These predictions were carried out by Kenbar et al (1991-a) for the flow in a cylindrical adiabatic furnace using the PHOENICS Code. The flow dealt with has low to medium swirl and the results were encouraging for the low swirl flows, but less good for the medium swirl.

The peripheral fuel injection has recently been implemented in the NEL furnace system, and the measured flow and combustion patterns were reported by Kenbar et al (1991-b). The purpose of the present study is therefore to investigate the ability of the CFD procedure to deal with this peripheral fuel injection in the NEL furnace system. The present application geometry includes a high swirl burner with a quarl, discharging in a water cooled furnace chamber.

The governing equations are solved by the finite difference procedure embodied in the PHOENICS Code (Ludwig et al (1989)). Turbulence is modeled by the standard k-ε model (Bradshaw et al (1981), Gupta and Lilley (1985)) and combustion by the 'eddy break-up' model (Spalding (1970) and Magnussen and Hjertager (1976)). Radiation heat transfer is modelled by the flux method (Gupta and Lilley (1985)).

The predicted aerodynamic and combustion patterns are compared with the measured patterns. An assessment is made of the degree of agreement with the measurements and suggestions are made for further improvements to the models of flow, combustion and heat transfer.

2. EXPERIMENTAL DATA

This data is part of an HTFS extended research effort to study the combustion characteristics of swirling flames using the NEL furnace system. In addition to providing more insight into the processes involved, the results of these studies were also used for the validation of the HTFS mathematical modelling programs, such as PCOC, Beltagui et al (1991).

2.1 NEL Furnace System

The furnace is a model of an upshot fired heater. The apparatus is a cylindrical combustion chamber of 1 m diameter and 3 m height. The water-cooled chamber wall has six separate sections. The furnace is fired by natural gas through a variable swirl burner with a quarl. More details of the furnace and

measuring equipment were given by Beltagui et al (1988-a and 1989) and Kenbar et al (1991-b).

The fuel was injected axially at the outer periphery of the air stream as shown in Fig. 1, through an annular slit of 2.5 mm width around the air inlet. It was found that a stable flame can only be achieved if a central recirculating-flow zone (CRZ) exists near the burner. This can be created either by swirling the air flow or by injecting a fraction of the air flow radially from a central gun across the air flow. The results presented here are for the case of swirling flow.

2.2 Measurements Conditions

The detailed in-furnace experimental measurements were taken under fixed firing conditions of 400 KW and 5% excess air. Two settings of air swirl were surveyed, with swirl number, S values 0.9 and 2.25.

The results present complete mapping of the flow and combustion patterns within the furnace. The experimental measurements for the aerodynamic patterns include the three time-averaged velocity components and static pressure. Those for the combustion patterns covered temperature and species concentrations- HC, CO_2, CO, O_2 and NOx.

2.3 Measurements

Radial traverses were carried out at 13 planes along the furnace, at axial positions from the quarl exit that were closely spaced near the burner. At each plane 13 to 26 measurement points were covered according to the gradients of the variable being measured. The gas temperature was measured using suction pyrometer with shielded S-type thermocouple. A calibrated spherical head five-hole pitot probe of 8 mm tip diameter, was used for the measurements of the three time-averaged velocity components and static pressure, Chedaille and Braud (1972).

A special water cooled stainless steel sampling probe (Kenbar and et al (1991-c)) was used to draw samples for concentration measurements. Chemiluminescent and flame ionisation analyzers were used for NOx and HC analysis respectively. Infra-red analyzers were used for CO, CO_2 and a paramagnetic analyzer for O_2.

3. PREDICTION PROCEDURE

The predictions have been made by solving the finite-difference formulations of the governing equations for the conservation of mass and three components of momentum. Turbulence is modelled by solving two differential equations for the turbulence kinetic energy and its dissipation rate (standard k-ε model). The combustion modelling was performed by solving differential equations for fuel mass fraction and mixture fraction, together with the energy equation. The radiation heat transfer from the flame gases was modelled by the flux method.

3.1 Combustion Model

In turbulent reacting flows, the modelling of the rate of reaction, and consequently the heat release rate, is essential to the evaluation of the local gas temperature and density, the latter being a major factor in the momentum and mass conservation equations.

In the present non-premixed system, the flame is considered as diffusion controlled. As was discussed before, Beltagui et al (1991), the combustion rate in this forced draught system is modelled using the 'eddy break-up' model of Spalding (1970) and Magnussen and Hjertager (1976). This model assumes that the reactants are homogeneously mixed in the fine-scale dissipative eddies of the turbulence. The chemical reaction is represented by a one-step reaction between the fuel and oxidant. The present formulation includes the effect of the hot product concentration, which has proved significant. The rate of the reaction is dependant on the concentration of the limiting reactant as given by:

$$R = a\,\rho\,\mathrm{Min}\,[\,M_f\,,\,M_o/s\,,\,b^*M_p/(1+s)] \qquad (1)$$

where M_f, M_o and M_p are the mean mass fractions of fuel, oxidant and product respectively, s is the stoichiometric ratio and a and b are 'eddy break-up' constants. The values of a and b were taken to be 2.0 and 0.5 respectively, Beltagui et al (1991).

The local gas temperature was calculated from the

enthalpy using temperature dependant specific heat values for each of the three species. The perfect gas law was used for the density calculation.

3.2 Heat Transfer Model

The radiation heat transfer from the flame gases was modelled by the Flux method. The mean absorption coefficient for the furnace gases was taken to be 0.355 m. Convective heat transfer contribution was considered through the wall boundary condition.

3.3 Boundary Conditions

The calculation domain comprised the burner quarl and furnace. The burner geometry was represented by a cylindrical inlet followed by the conical quarl discharging into the furnace space.

The inlet mean velocity components and static pressure values at the burner throat were based on experimental measurements carried out on a full scale isothermal model of the burner, Beltagui et al (1988-b).

The corresponding k and ε values have been calculated as follows:

$$k = C * 0.0325 (U^2 + V^2 + W^2) \quad (2)$$

$$\varepsilon = k / 0.548\ l \quad (3)$$

where l is a characteristic dimension for the flow stream taken as swirler radius for air and annular slot width for fuel. The values of the constants in Eqns. 2 and 3 have been deduced from experimental measurements in similar flow systems as reported by Nejad et al (1989).

The flow boundary conditions at the solid walls have been described by the log-law. The heat transfer at the walls was modelled by a special formulation to take account of both radiation and convection components, according to the heat flux equation;

$$q_w = h (T_g - T_w) + \sigma (\varepsilon_g T_g^4 - \varepsilon_w T_w^4) \quad (4)$$

At this stage a constant value of the convective heat-transfer coefficient h, was applied for each swirl setting, namely 23 and 30 W/m^{2}K for 0.9 and 2.25 swirl numbers respectively, as suggested by Beltagui and Ralston (1991).

3.4 Computational Details

The furnace geometry was represented by an axisymmetric non-uniform grid of 45 axial by 47 radial nodes. Within the burner, particularly the fuel exit, the grid spacing in the radial direction was reduced to 0.44 mm. The quarl wall was represented by a series of 10 steps.

The upwind numerical differencing scheme was used, with under-relaxation parameters for all the variables. At least 1000 sweeps were required to obtain a satisfactorily converged solution with normalised mass residuals of less than 0.5×10^{-4}. A typical calculation of 1000 sweeps required about 40 minutes of CPU time on a Silicon Graphics IRIS Workstation.

The predictions are influenced by the specified inlet conditions. In the present case, the inlet conditions for enthalpy and concentrations were known. The values of the time-averaged three velocity components were also known from experimental measurements. The turbulence kinetic energy and rate of dissipation were, however, not measured. Estimates of the turbulence kinetic energy were made based on some experimental data on similar systems, Nejad et al (1989). The final predictions were found to be influenced by the value of the constants in Eqns. 2 and 3. The results presented here are based on the value of C=1.0.

4. RESULTS

A representative selection of the predictions for the 0.90 swirl case is presented in Figs 2-4, together with the corresponding experimental measurements. The selected variables are the axial and tangential components of the time-mean velocity.

4.1 Flow Patterns

The measured flow boundaries, as defined by the

forward flow and both the central and external reverse-flow zones, for the two swirls tested, were essentially the same, type D, according to the classification of Beltagui and Maccallum (1976). In this pattern, the flow near the burner consists of a CRZ surrounded by an annular jet containing the main forward flow. Outside the forward flow a weak external reverse-flow zone (ERZ) extends to the walls. The very low velocities in the ERZ observed here are due to the low confinement, manifested by the furnace to quarl diameter ratio of 5.

Downstream from the quarl exit, the jet radial expansion increases with swirl, thus bringing the jet impingement point with the furnace wall nearer to the burner. It is noted that both the length and maximum diameter of the CRZ increase with swirl.

4.1.1 Axial velocity profiles

Predicted and measured axial velocity profiles for S=0.9 case are shown in Fig 2. Peak forward velocities- predicted and measured- increase with increased swirl. The high velocity gradients at the boundaries of the forward flow enhance the shear forces at the jet boundaries. This leads to higher mixing and combustion rates, resulting in short intense flames. Predictions generally match the measurements but there are some differences as follows:

i Swirl increases jet expansion, but the predicted increase is less than that measured.

ii The predicted decay of the peak velocities, all three components, and their radial gradients is more rapid than that measured.

iii Although the flow reversal at the centre of the jet was predicted, the predicted size of the CRZ is less than that measured.

4.1.2 Tangential velocity profiles

Figure 3 illustrates the radial profiles of the tangential velocity component in the furnace chamber. Prediction and measurements both show Rankine-Vortex type flow with solid body rotation in the central region. The peak tangential velocities coincide with the zones of peak axial velocity.

4.1.3 Radial velocity profiles

In general the radial velocity component gives a measure of the jet spread. Both the magnitude of the radial velocity and its rate of decay along the furnace increase with swirl.
The predicted radial velocity profiles in the near-burner zone follow the shape of the experimentally measured profiles but the predicted values are much lower than those measured. Further downstream, the predicted radial velocities decay much faster than the measured. These features are consistent with the corresponding predicted decay of the axial velocities in this region.

4.1.4 Static pressure distributions

There is generally good agreement between prediction and measurement, with sub-atmospheric pressure near the centreline, rising to near, or slightly above, atmospheric close to the walls. This pattern is typical of static pressure distributions associated with confined swirling flows, with greatest depressions at and around the centre of the jet and uniform pressure distributions within the reverse-flow zones. The radial gradients of the static pressure increase with increased swirl.

4.2 Combustion Patterns

These are defined by the distributions of temperature and species concentrations within the furnace.
The flow field can be divided into four zones:

A Main reaction zone (near burner forward flow).
B Central reverse-flow zone (CRZ).
C Fully developed flow zone.
D External reverse-flow zone (ERZ).

The measurements show that most of combustion reactions take place in the reaction zone, A, leading to uniform concentration distributions in the fully developed flow zone, C. Measurements show reverse flows to be mainly products of combustion.

There is general agreement between predictions and

measurements for all these zones except for the CRZ. While the measured concentrations within the CRZ indicate products of combustion, the predictions indicate almost fresh air.

Both prediction and measurements of temperature and species concentration show that combustion commences within the quarl.

4.2.1 Temperature distributions

Predicted and measured profiles for S= 0.9 swirl case are shown in Fig 4. The developing profiles are generally well predicted except in the very near burner zone and near the centreline, where prediction shows the CRZ to be mainly cold air, whereas the measured flow in this area is mostly of combustion products.

Predicted and measured temperature profiles near the burner show high temperatures within the ERZ. The lowest temperatures are those of the unburned central inlet air flow. The maximum temperature at any level lies on the boundary of the fresh charge where combustion is initiated at the shear layer between the air and fuel jets. Further downstream, the agreement between the predicted and measured profiles improves.

The predicted effect of swirl on the temperature profiles is less than that measured. This indicates that the effect of radial mixing between the flow streams is not adequately predicted.

4.2.2 Species concentration distributions

The predicted oxidant and product concentrations are consistent with each other, and with the predicted temperature profiles. Thus the degree of agreement between the predicted and observed species concentration is similar to the agreement for the temperature profile. The comments made in Section 4.2.1 about the temperature profiles therefore apply also to the concentration profiles.

5. DISCUSSION OF RESULTS

While the main features of the flow and combustion patterns have been reasonably predicted, as demonstrated by the comparison with the measured patterns, there are some discrepancies, particularly in the higher swirl case (S=2.25).

Considering the flow pattern, the radial gradients of velocity components especially near the centreline are underpredicted. This is a feature of the standard k-ε turbulence model and has been reported by other investigators, for example see Mahmud et al (1987), Nejad et al (1989), Jones and Pascau (1989) and Kobayashi and Yoda (1987). The is attributed to the body forces which arise from the effects of curvature, recirculation, swirl and buoyancy. These forces interact selectively with different normal and shear stresses making the use of the isotropic turbulence assumption inappropriate, Sloane et al (1986) and Leschziner (1989).

The present investigation is of a special flow configuration where the body forces play an important role. In this furnace, using the peripheral fuel-injection scheme, combustion starts at the outer shear layer of the air jet. The centrifugal forces created in this system due to the density gradients are expected to increase further the effect of body forces on the turbulent flow (Leschziner (1989) and Beltagui and Maccallum (1988)). Trials to overcome the model deficiency through the use of a modified anisotropic form of the turbulent eddy viscosity based on the k-ε model for some simpler flow situations have been presented by Kobayashi and Yoda (1987) and others. However, these models are not yet of a general form.

Rigorous models solving the complete Reynolds stress equations should have the degree of generality required. However, these models were not available in general CFD codes. Another reason for not using these is the expensive computational time penalty involved. Recently, this situation has improved and predictions are being made using the Reynolds stress equations.

Considering the combustion patterns, as represented by the temperature and species concentration fields, while previous predictions were in good agreement for the low and non-swirled flow case, less satisfactory agreement is obtained for the highly

swirling flows presented here. There are three reasons for these deficiencies:

i The weakness in the turbulence modelling, as explained above, led to lower mixing rates in the radial direction as indicated by the lower degree of uniformity in the temperature and species concentration profiles, compared to the measured profiles. The underprediction of mixing is more apparent in the higher swirl flow.

ii The simplified combustion model, which is also governed by the turbulence properties through the "eddy break-up" model, is not sufficient.

iii The flux model for radiation heat transfer is too simple to model the heat transfer accurately.

6. CONCLUSIONS

The general agreement between predicted and measured flow and combustion patterns is encouraging considering that the procedure used the standard k-ε turbulence model, with simple combustion and radiation models.

The main flow and combustion patterns of a high swirling flame using a peripheral fuel injection burner were reasonably predicted. However, the enhancement of mixing caused by the combined effects of swirl and density gradients, was not adequately predicted. This weakness highlights the importance of modelling the contribution of the body forces to the turbulence exchange coefficients.

Further work is being carried out using the FLOW3D code to model the same flow configuration.

ACKNOWLEDGEMENTS

This work is part of an HTFS project which receives support from the U.K. Department of Trade and Industry.

REFERENCES

BELTAGUI, S. A. and MACCALLUM, N. R. L., (1976), "Aerodynamics of vane-swirled flames in furnaces", J. Inst. of Fuel, vol. 49, pp. 183-193.

BELTAGUI, S. A. and MACCALLUM, N. R. L., (1988), "Characteristics of enclosed swirl flames with peripheral fuel injection", J. Inst. of Energy, March, pp. 3-16.

BELTAGUI, S. A., FUGGLE, R. N. and RALSTON, T., (1988-a), "Combustion pattern measurements for swirling flames in the NEL furnace", HTFS Research Symp., RS 756, NEL/HTFS 113.

BELTAGUI, S. A., FUGGLE, R. N. and RALSTON, T., (1988-b), "Aerodynamic and mixing within the quarl of a variable swirl burner (experimental and theoretical study)", First European Conference on Industrial Furnaces and Boilers (INFUB), Lisbon, Portugal.

BELTAGUI, S. A., FUGGLE, R. N., KENBAR, A. M. A. and RALSTON, T., (1989), "Measurements of swirling flames aerodynamics in the NEL furnace", HTFS Research Symp., RS 826, NEL/HTFS 125.

BELTAGUI, S. A. and RALSTON, T., (1991), "The prediction of convective heat-transfer from swirling flames", Second European Conference on Industrial Furnaces and Boilers (INFUB), Algarve, Portugal. Also HTFS RS845.

BELTAGUI, S. A., FUGGLE, R. N., KENBAR, A. M. A., RALSTON, T., MARRIOTT, N. and STOPFORD, P. J., (1991), "Modelling a gas-fired furnace flow and combustion using the PCOC code", Eurotech Direct, I Mech E, Birmingham, Paper No. C413/054.

BRADSHAW, P., CEBECI, T. and WHITELAW, J. H., (1981), "Engineering calculation methods for turbulent flow", Academic Press, London.

CHEDAILLE, J and BRAUD, Y, (1972),

"Measurements in flames", Edward Arnold publishers, London.

GUPTA, A. K. and LILLEY, D. G., (1985), "Flow field modelling and diagnostics" ABACUS Press, Tunbridge Wells, Kent, England.

JONES, W. P. and PASCAU, A., (1989), "Calculation of confined swirling flows with a second moment closure", ASME, J. of Fluids Eng., Vol. 111, 248,255.

KENBAR, A. M. A., BELTAGUI, S. A. and MACCALLUM, N. R. L.(1991-a), "Modelling the combustion aerodynamics for a peripheral injection system", HTFS Research Symposium paper, RS878, NEL/HTFS 144.

KENBAR, A. M. A., BELTAGUI, S. A. and MACCALLUM, N. R. L.(1991-b), "Peripheral fuel injection burner in the NEL furnace- Flow and combustion patterns", HTFS Research Symp., RS 878, NEL/HTFS 144.

KENBAR, A. M. A., BELTAGUI, S. A., RALSTON, T. and MACCALLUM, N. R. L. (1991-c), "Measurement and modelling of NOx formation in a gas fired furnace" First Int. Conference on Combustion Technologies for clean environment, Portugal.

KOBAYASHI, T. and YODA, M., (1987), "Modified k-ε model for turbulent swirling flow in a straight pipe", JSME, Internat. Journal, Vol. 30, No. 259, 66-71.

LESCHZINER, M. A., (1989), "Modelling turbulent recirculating flows by finite-volume methods - current status and future directions", Int. J. Heat and Fluid Flow, Vol. 10, No. 3, 186-202.

LUDWIG, J. C., QIN, H. Q. and SPALDING, D. B., (1989), "The PHOENICS Reference Manual", CHAM TR/200, CHAM LTD.

MAGNUSSEN, B. F. and HJERTAGER, B. H., (1976), "On mathematical modelling of turbulent combustion with special emphasis on soot formation and combustion", 16th Symp. (Int). on Combustion, 719-730.The Combustion Institute, Pittsburgh, PA.

MAHMUD, T., TRUELOVE, J. S., WALL, T. F., (1987), "Flow characteristics of swirling coaxial jets from divergent nozzles", ASME, J. of Fluids Eng., vol. 109, 275-282.

NEJAD, A. S., VANKA, S. P., FAVALORO, S. C., SAMIMY, M. and LANGENFELD, C., (1989), "Application of laser velocimetry for characterization of confined swirling flow", ASME J. Eng. for Gas Turbines and Power, vol. 111, 36-45

SLOANE, D. G., SMITH, P. J. and SMOOT, L. D., (1986), "Modelling of swirl in turbulent flow systems", Prog. Energy Combust. Sci., Vol. 12, 163-250.

SPALDING, D. B., (1970), "Mixing and chemical reaction in steady confined turbulent flames", 13th Symp. (Int.) on Combustion, 649-658.The Combustion Institute, Pittsburgh, PA.

LIST OF FIGURES

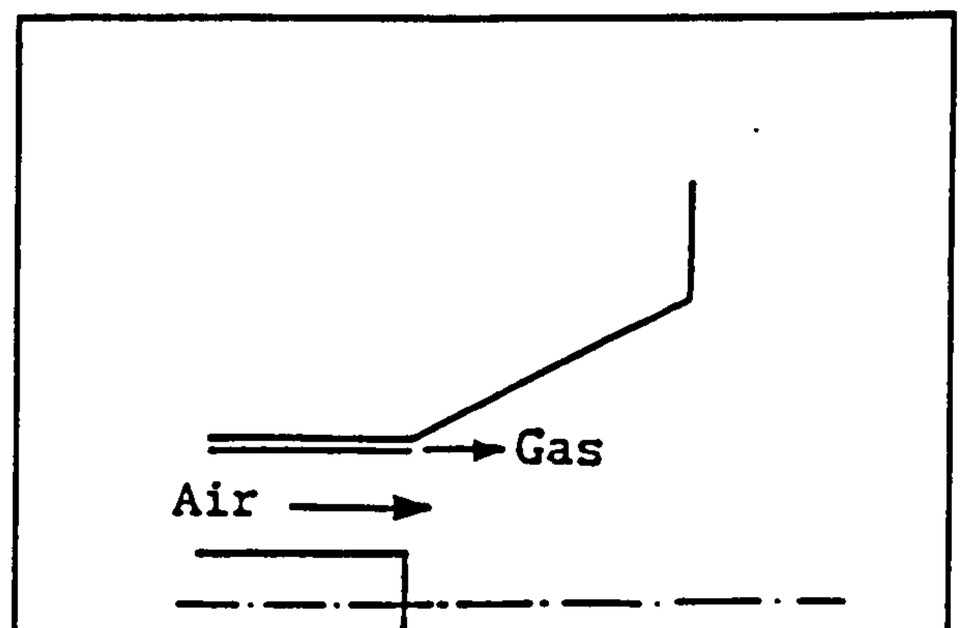

FIG 1: Peripheral fuel-injection burner system

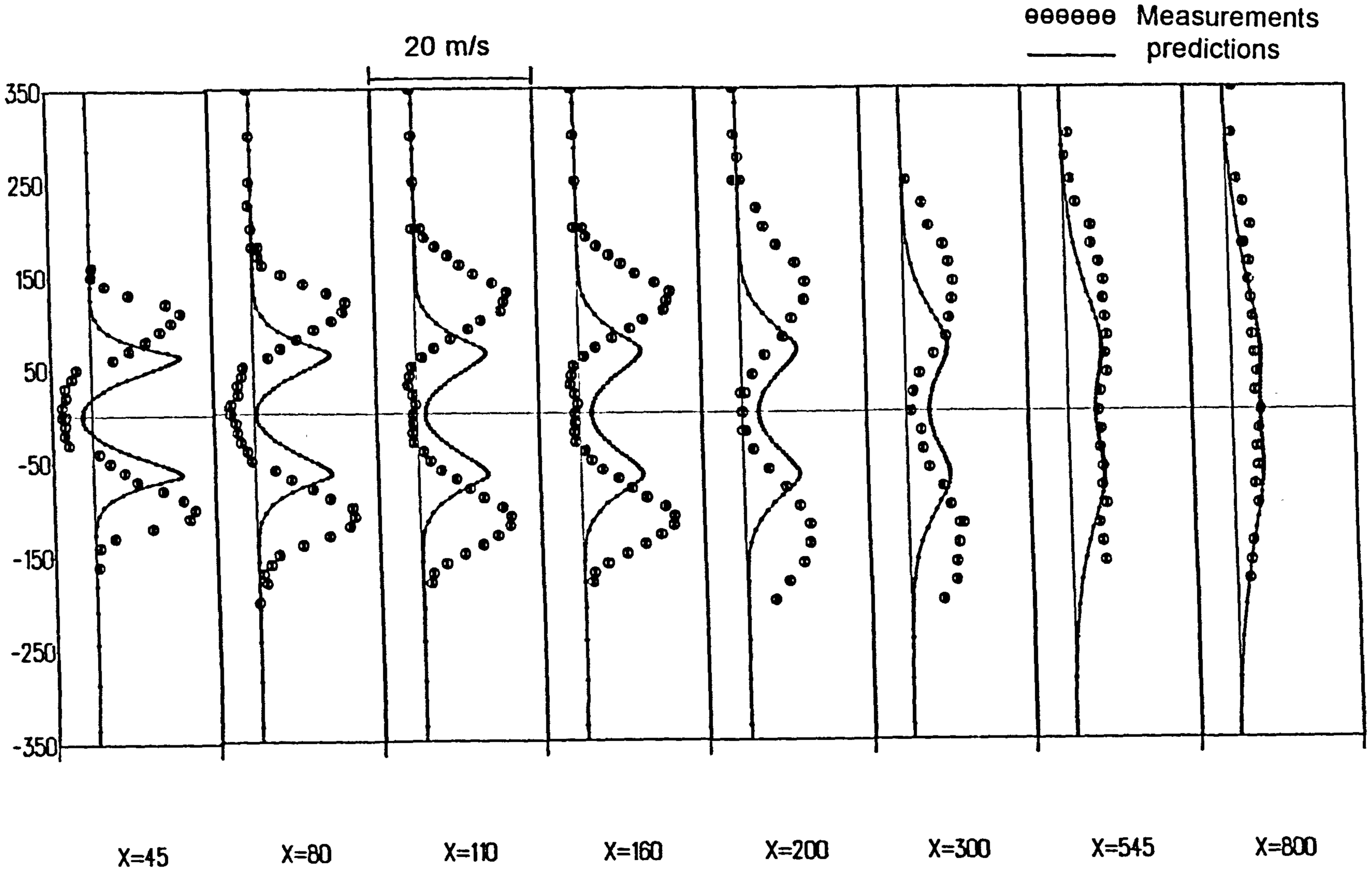

Figure 2: Axial Velocity Profiles, S=0.9

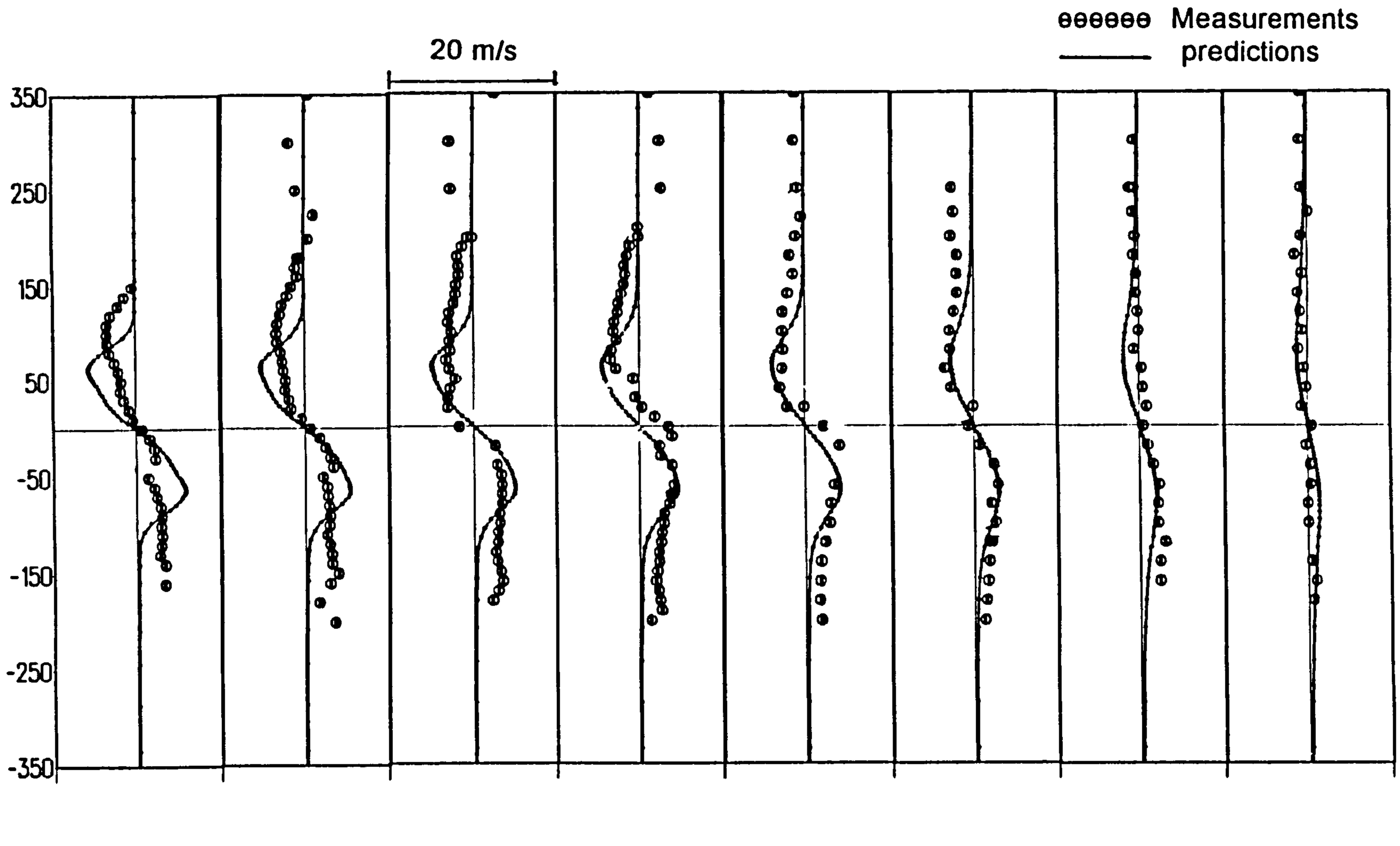

Figure 3: Tangential Velocity Profiles, S=0.9

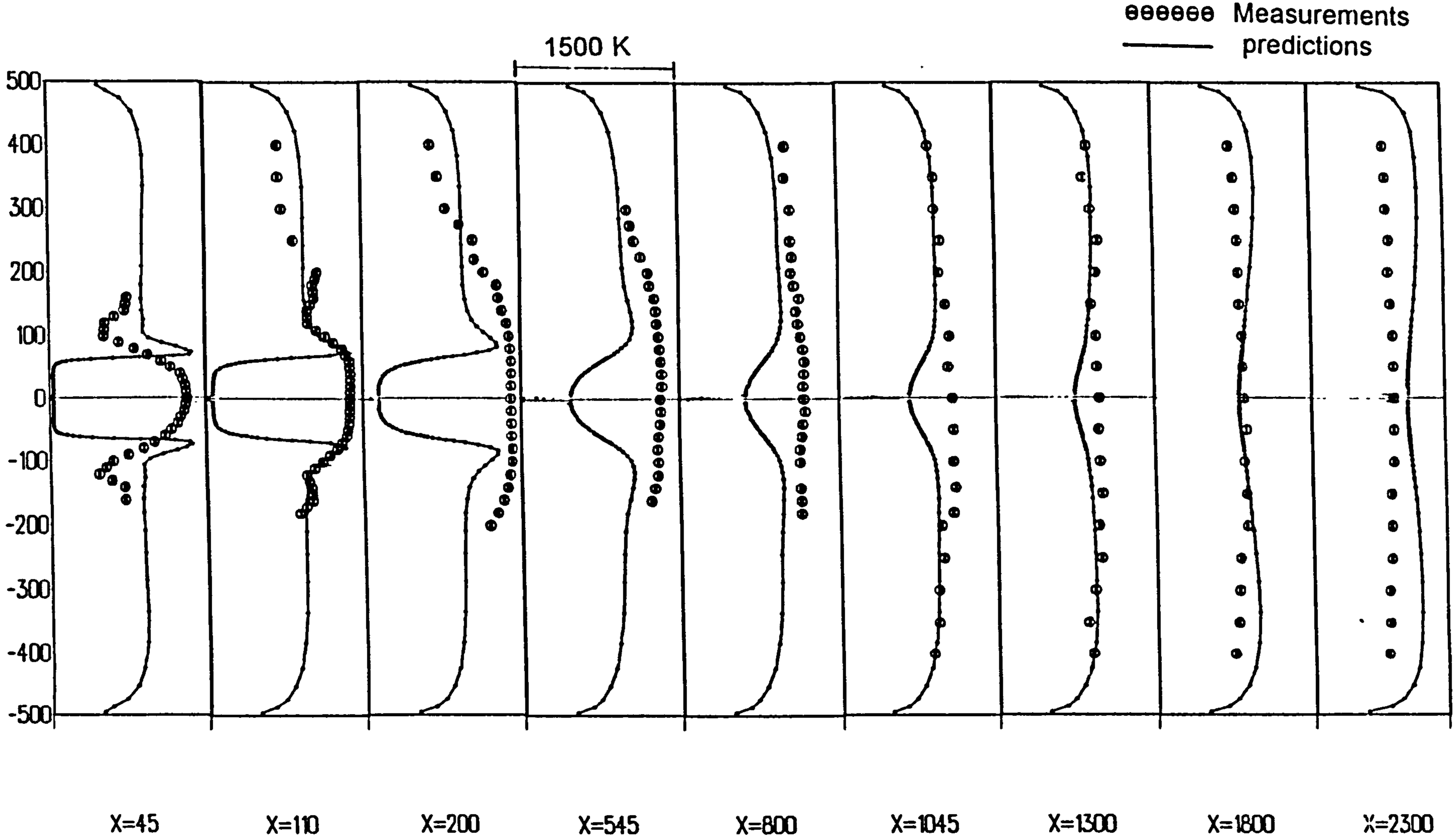

Figure 4: Temperature Profiles, S=0.9

THIRD WORLD CONFERENCE ON EXPERIMENTAL HEAT TRANSFER, FLUID MECHANICS AND THERMODYNAMICS - HONOLULU 1993

COMBUSTION AERODYNAMICS OF A GAS FIRED FURNACE WITH PERIPHERAL FUEL INJECTION

A.M.A. Kenbar [1,2], S.A. Beltagui [1,2] and N.R.L. Maccallum [1]

1- The University of Glasgow, Glasgow, UK.
2- National Engineering Laboratory (NEL), East Kilbride, Glasgow, UK.

ABSTRACT

The work presented in this paper is part of a research programme to study the combustion characteristics of swirling flames in furnace systems. These studies are aimed at improving combustion performance with reduced pollutant emissions. In addition to providing more insight into the processes involved ie, aerodynamics, combustion, heat transfer and formation of pollutants, results of these studies are also needed for the validation of furnace prediction models.

This paper presents measured flow and combustion patterns carried out on a semi-industrial scale natural-gas fired furnace. The burner utilises a non-conventional fuel-injection scheme where the fuel is injected around the periphery of the swirling air jet. The furnace is a water cooled cylindrical combustion chamber of 1 m diameter and 3 m height, fired by natural-gas through a variable swirl burner with a quarl.

The measurements of the flow and combustion patterns were carried out for two air swirl intensities, Swirl Numbers 0.9 and 2.25, through radial traverses at 13 axial planes along the furnace. The flow patterns are defined by the radial distributions of the measured three time-averaged velocity components and static pressure. Also presented are the combustion patterns in the form of measured contours of temperature and species concentrations of O_2, CO_2, CO, HC and NOx.

The results demonstrate that peripheral fuel injection produces high rates of mixing leading to better combustion efficiency and heat transfer. The axial velocity profiles define the main shear areas and the forward and reverse flow zones. The temperature and concentration fields illustrate the progress of combustion reactions to completion and the formation of pollutants.

The data obtained by the detailed measurements is being used for the validation and development of the mathematical models for prediction of furnace flows.

INTRODUCTION

Furnace system design requires careful characterisation and optimisation of complex flow and combustion phenomena. Although Computational Fluid Dynamic (CFD) techniques are being progressively used in furnace design, there is still a great need for experimental measurements to test new designs and validate CFD predictions. Thus a mixed approach of physical model testing and CFD simulation reduces the time and cost of development.

This approach is being followed in this research programme to study the combustion characteristics of swirling flames in furnaces. This programme is aimed at improving combustion performance with reduced pollutant emissions.

In non-premixed industrial burners, mixing occurs within the combustion chamber by shear layer mixing between the air and fuel streams. Swirling the air flow can be used to increase shear mixing and enhance it with centrifugal mixing. The utilisation of the full benefits of these two physical processes in a practical combustion system depends mainly on the method of fuel injection.

Shear layer mixing is effectively utilised if the fuel is injected into the regions of maximum shear in the air stream. Centrifugal mixing effects can be utilised by creating favourable density gradients within the flow of air, fuel and products. The most common method of fuel injection is axially at the centre of the burner air flow. This method does not utilise the full potential of either shear layer or centrifugal mixing.

As an alternative to the central fuel injection, the fuel can be injected at the periphery of the entering air jet [1,2]. This system offers better shear layer and centrifugal mixing, thus resulting in efficient mixing and hence high combustion intensity. The flame stability was achieved through either the central or outer reverse flow of hot products. This system and similar systems have been examined by a number of investigators, reviewed in [1].

The peripheral fuel injection system was studied [1]

in an adiabatic furnace of 0.225 m inside diameter and 0.9 m long. This system resulted in a stable flame even without a central reverse-flow zone (CRZ), thus only low swirl settings, up to that which is formed a CRZ, were used. Compared to the central axial fuel injection, the peripheral injection produced higher intensity flames with wider stability ranges. This work gave strong evidence in support of fuel injection at the outer periphery of the swirled air flow. However, these findings are related to a small scale adiabatic furnace where the flame stability is easier to achieve when compared with large non-adiabatic furnace systems which exist in industry. It is necessary to test this scheme in a non-adiabatic industrial size furnace systems. Thus the present work was carried out on the NEL test facility which represents a semi-industrial scale furnace system. The main objectives of the NEL programme were:

First, to acquire data to study different fuel injection methods in a semi-industrial scale application. This should provide more insight into the processes involved, that is, aerodynamics, combustion, heat transfer and formation of pollutants. This information is needed to optimise both the fuel injection mode and swirl to achieve the best combustion performance with minimum pollutant formation. In this paper detailed measurements of the flow and combustion patterns using the peripheral fuel injection scheme are presented. Comparisons with other fuel injection systems are given in reference [3].

Second, to provide an extensive data bank which is used in developing and testing the theoretical programs for furnace flow and combustion. These include both furnace specific codes eg PCOC [4] and more general CFD codes, eg PHOENICS [5].

EXPERIMENTAL PROGRAMME

NEL Furnace System

The NEL furnace models an upshot fired heater. The furnace is a water cooled cylindrical combustion chamber of 1 m diameter and 3 m height.

The furnace is fired by natural gas through a variable swirl burner with a quarl. The burner uses a moving-block swirl generator. Two air swirl settings were tested with Swirl Numbers S = 0.9 and 2.25.

The Swirl Number is defined as the ratio of tangential to axial momentum fluxes divided by the burner throat radius. More details of the furnace and measuring equipment were given in references [6,7].

Entry Flow Arrangements

Fuel entry arrangements. The fuel was injected axially at the outer periphery of the swirled air stream, Fig. 1. Two alternative arrangements have been used. In arrangement A, the fuel entered through an annular slit of 2.5 mm width around the periphery of the swirled air. The velocity of the gas leaving the slit was 12 m/s. In arrangement B, the fuel was injected through 60 holes, each 4 mm diameter. These holes were designed to maintain the same flow area as the continuous slit of arrangement A.

Both arrangements, A and B, produced flames of virtually identical geometry and appearance. Thus the detailed measurements were taken for arrangement A only.

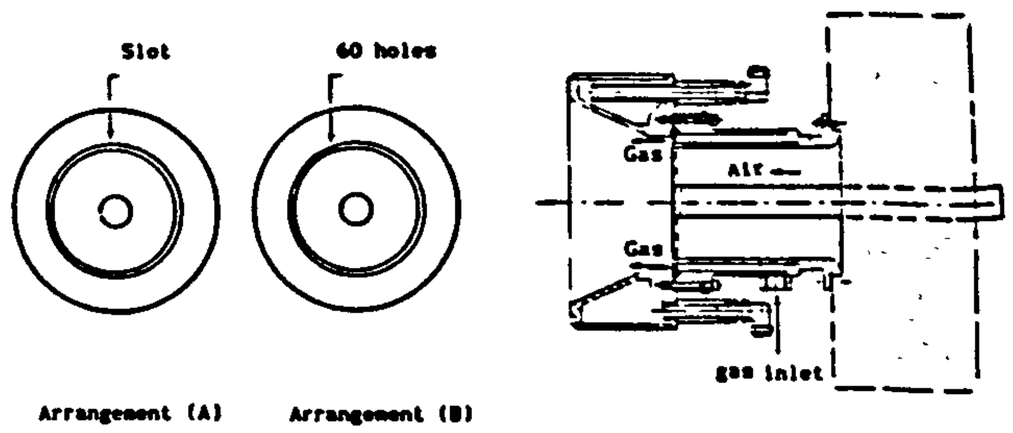

Fig. 1 Air and fuel entry arrangements.

Air entry schemes. In Scheme 1 all the air entered through the burner throat, Fig. 1. It was found that a stable flame could only be achieved if enough swirl (S > 0.8) was applied to the air flow to produce a CRZ near the burner. However, of the two swirl settings investigated above this value, the one close to the stability limit (S=0.9) produced a flame characterised by some non-uniformity in shape when compared with the higher swirl flame (S= 2.25).

An alternative way of achieving the CRZ is to create an aerodynamic blockage by introducing part of the combustion air radially outward through a central gun. The gun used, Fig. 1, has 16 holes each 5 mm diameter, spaced on its outer periphery. Thus in Scheme 2 about 10 % of the combustion air was supplied through the central gun. In this case a stable flame was achieved even without swirl.

Measurements Conditions

Experimental measurements were performed to

produce complete mapping of the flow and combustion patterns within the furnace. These measurements were carried out for the air entry Scheme 1.

The experimental measurements for the aerodynamic patterns include the three time-average velocity components and static pressure. Those for the combustion patterns covered temperature and species concentrations, that is HC, CO, CO_2, O_2 and NOx. These measurements were taken under fixed firing conditions of 400 KW and 5% excess air.

MEASUREMENTS

Radial traverses were carried out at 13 planes along the furnace, being closely spaced near the burner. Some extended traverses were made to check for flow symmetry and intrusive effects of probes. The probe effects were found to be minor and the flow symmetry very reasonable. Repeatability tests gave velocity values repeatable within ±0.5 m/s. Between 13 and 26 measurement points were used in each plane depending on the gradient of the variable being measured. The absolute positioning of the probe relative to the furnace wall and base plate was achieved to within ± 2 mm.

The gas temperature was measured using a suction pyrometer [8], which has an overall shield diameter of 15 mm and uses an 'S' type thermocouple. The suction rate corresponds to a gas velocity of 150 m/s at the hot junction. The measured probe efficiency [8] was found to be 99%, thus temperature measurements needed no correction. Temperature measurements were repeatable to within ± 10 K.

A spherical head five-hole pitot probe of 8 mm tip diameter [7,8] was used for the measurements of the three time-averaged velocity components and static pressure. The probe was recalibrated in a special rig before the start of the measurements [7].

Although the probe is intrusive, it has been confirmed in the present furnace that the velocity values obtained are generally within ±1 m/s of those measured by LDA. Similar comparisons elsewhere reached the same conclusion, eg [9]. It is only in regions of low axial velocity and relatively high radial velocity that discrepancies occur between measurements by the two methods. There is therefore reasonable confidence in the axial and tangential velocity components measurements, but less confidence in the radial component values.

Mass integration of the measured axial velocity distribution at any section compared well with the metered flow values, within 25%.

For concentration measurements, a special water cooled stainless steel sampling probe [6] was used. For NOx and HC analysis, the gas sample passes through a heated sample line to the NOx chemiluminescent and hydrocarbon flame ionization detector analysers respectively. For CO, CO_2 and O_2 analysis, the sample was passed through a water trap, condenser and chemical dryers before being introduced to the analysers. Infra-red absorption analysers were used for CO and CO_2. A paramagnetic analyser measured the concentration of O_2. Each analyser was calibrated against known concentrations of the gas to be measured. The time-mean values of all measured variables are those averaged over a period of 1 minute, after sufficient time was allowed for purging the sampling lines and analysers. The concentration measurements were checked for repeatability and the maximum deviation was within ± 1% of the full scale for each analyser.

FLOW PATTERN RESULTS

These are defined by the measured profiles of the three time-averaged velocity components and static pressure.

Axial Velocity Profiles

These profiles are given in Fig. 2. The forward and

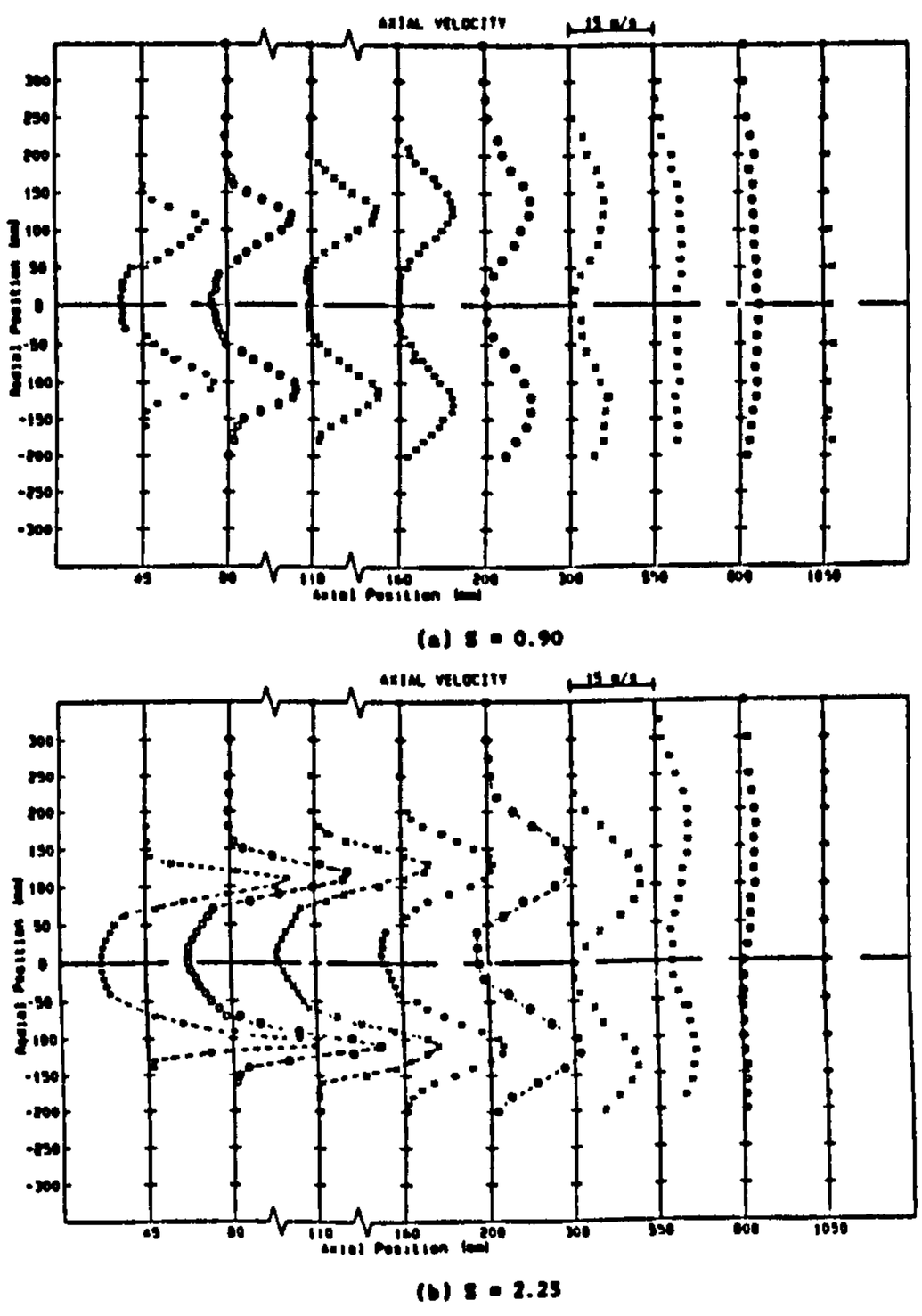

(a) S = 0.90

(b) S = 2.25

Fig. 2 Axial velocity profiles.

reverse flow boundaries in each plane are defined by these profiles. For the two swirls tested, the flow patterns are essentially the same, type D, according to the classification of Beltagui and Maccallum [10]. In this flow pattern, near the burner, the flow consists of CRZ surrounded by an annular jet containing the main forward flow. Outside the forward flow a weak external reverse-flow zone (ERZ) extended to the walls. The very low velocities in the ERZ observed here are due to the low confinement, the furnace to quarl diameter ratio being 5.0.

For the forward flow, the value of peak velocity increases with increased swirl. The high velocity gradients at the boundaries of the forward flow increase even further with increased swirl. These gradients enhance the shear forces at the jet boundaries, leading to higher mixing and combustion rates. These features result in the short intense flames associated with the high swirl flows.

The rate of decay of maximum velocity along the furnace is accelerated at high swirl, this being associated with the jet area expansion- see next paragraph. The recovery of the centreline axial velocity is enhanced with swirl.

Flow Boundaries

Figure 3 defines the boundaries of the forward flow and both the central and outer reverse-flow zones for the two swirls. For the first 250 mm distance from

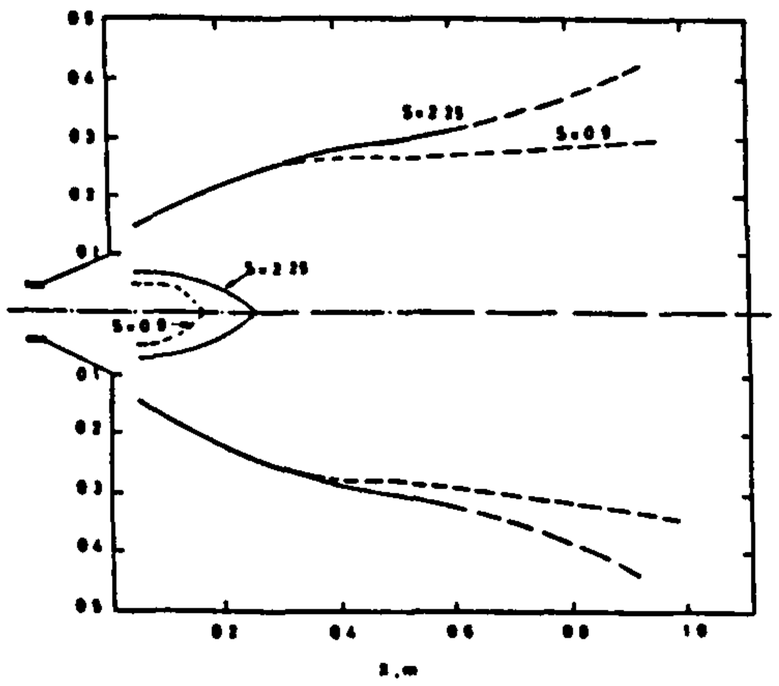

Fig. 3 Flow boundaries.

the quarl exit, the jet radial expansion is nearly the same for both swirls. Further downstream, the jet radial expansion increases with swirl, thus bringing the jet impingement point with the furnace wall nearer to the burner. It is noted that both the length and maximum diameter of the CRZ increase with swirl.

Tangential Velocity Profiles

These profiles are presented in Fig. 4. The tangential

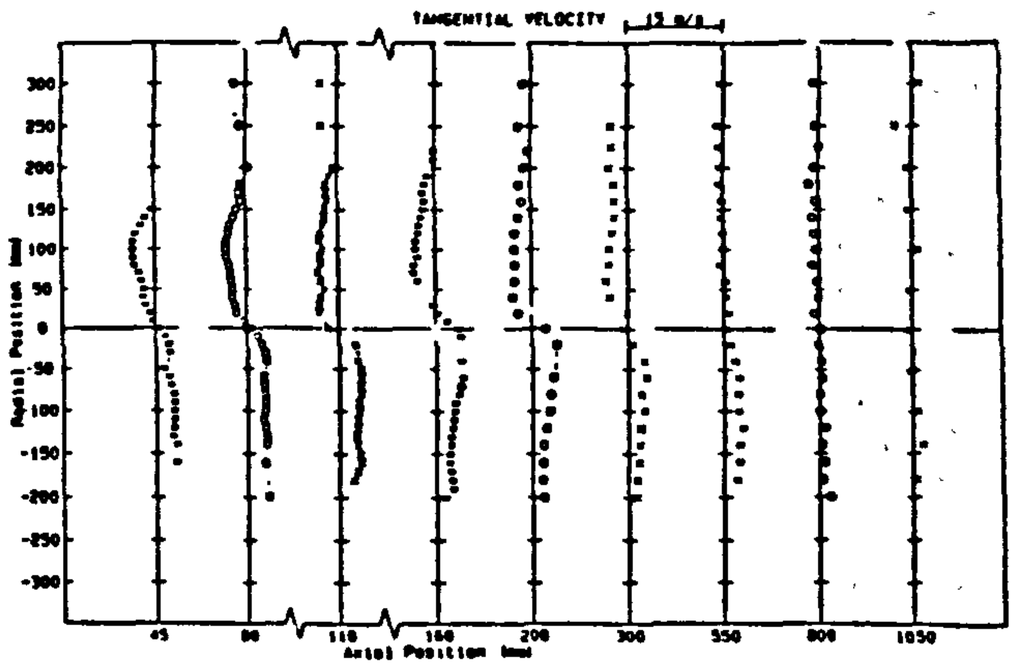

Fig. 4 Tangential velocity profiles.

velocity values are an indication of the local swirl strength which contributes to mixing and combustion. The high swirl jet approximates to the usual Rankine-vortex flow with solid body central rotation surrounded by an outer free vortex. At planes from the furnace inlet to about 300 mm downstream, the tangential velocity values in the high swirl, are about twice the corresponding values of the lower swirl. However, the rate of decay of the tangential velocity increases with swirl so that the tangential velocities in both swirls decay to very low values by about 800 mm downstream.

Radial Velocity Profiles

These profiles are similar for both swirl settings although the magnitudes of radial velocities are higher at the higher swirl. The profiles for the higher swirl (S=2.25) only are shown in Fig. 5. In the upper half of the diagram, positive values correspond to outward radial velocity components, with the reverse convention in lower half.

As mentioned in "Measurements" Section, it is believed that the probe measurements exaggerate the radial velocity values, in the regions of low

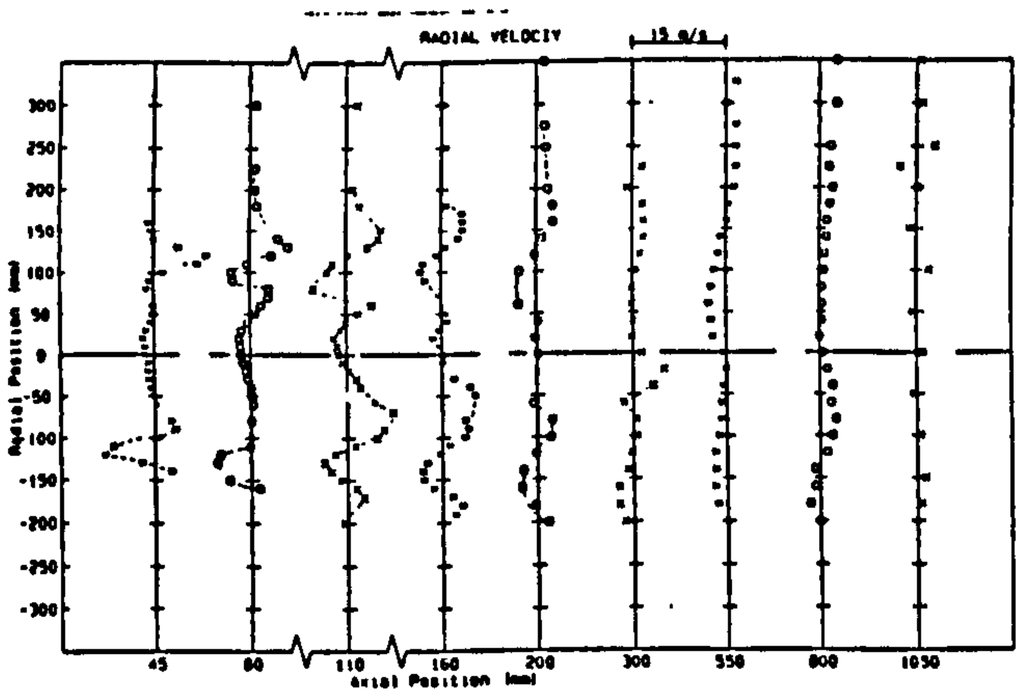

(b) S = 2.25

Fig. 5 Radial velocity profiles.

axial velocity and peak radial velocity. Consequently, excessive reliance should not be placed on the measured radial velocities. However the radial velocity values are an indicator of the direction and magnitude of the jet spread. Both the magnitude of the radial velocity and its rate of decay along the furnace increase with swirl. The features shown in Fig. 5 are consistent with the jet expansion behaviour suggested by the axial velocity distributions.

Static Pressure Profiles

Static pressure distributions indicate that all pressure values are below ambient pressure with maximum depressions near the burner. These distributions are similar to those generally observed in enclosed swirling jet flows in furnaces, with greatest depressions at and around the centre of the jet and flat pressure distributions within the reverse-flow zones. Increased swirl, above the value corresponding to the onset of the CRZ, increases the centreline depression resulting in a larger CRZ. The radial gradients of the static pressure are higher in the higher swirl case and it takes a longer axial distance to reach a uniform pressure distribution in this case.

COMBUSTION PATTERNS RESULTS

The flames observed were of the short intense type associated with high mixing rates and central reverse flow. Combustion patterns are represented by the distributions of time-averaged temperature and species concentrations within the furnace.

Temperature Distributions

These are presented as contours in Fig. 6. Temperature profiles are also shown in Fig. 7, for three of the axial positions along the furnace. These figures give an indication of the effect of swirl on the rate of combustion as well as the symmetry of the flame.

Generally, the profiles shown in Fig. 7, illustrate a good degree of symmetry, particularly for the higher swirl case. The slight asymmetry in the lower swirl case near the burner may be caused by slight variation in the width of the slit used for the fuel gas injection, see also [1].

The temperature contours indicate that combustion starts within the quarl, a fact confirmed by the measured species concentrations.

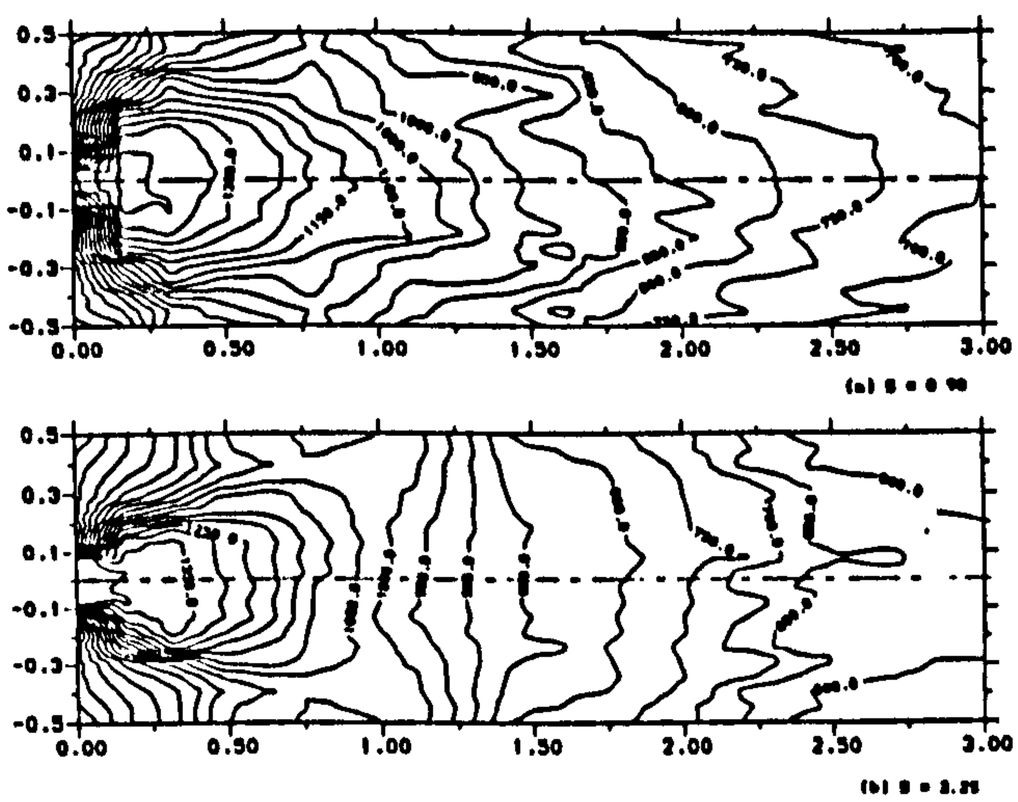

Fig. 6 Temperature contours.

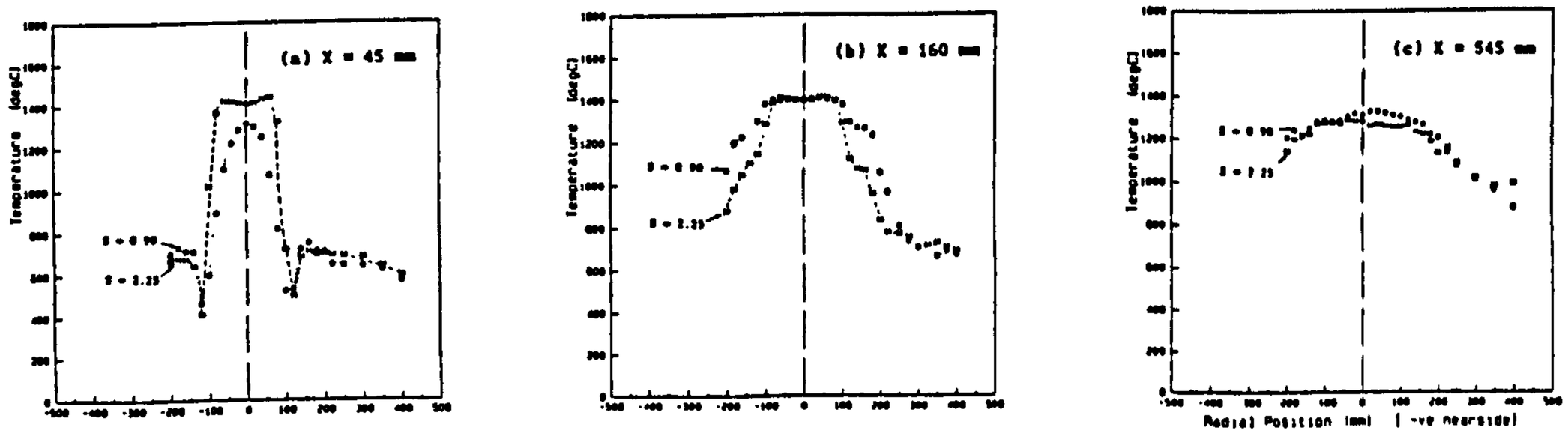

Fig. 7 Radial temperature profiles.

The temperature contours also show that the maximum temperature and steepest radial temperature gradients occur nearer to the burner as swirl is increased from 0.9 to 2.25. Further downstream, these gradients decay much more rapidly at the higher swirl. Away from the furnace walls, for the higher swirl case, near-uniform temperature profiles are reached at a plane of 1 m downstream of the burner. However, for the lower swirl, radial temperature gradients are evident even at furnace exit. Thus, increased swirl not only increased combustion intensity, but also enhanced the stirring of the post-flame gases.

Within the CRZ, temperature profiles are mostly uniform for both swirl cases. The temperature at the centreline is always close to the maximum temperature measured at this traverse plane. Within the ERZ, Fig. 7 shows that for both swirl settings the gas temperature decreases from about 1000 C at 545 mm to about 600 C at 45 mm, this being due to heat transfer to the furnace walls.

Main Species Concentrations

Complete surveys of concentrations of HC, CO, CO_2, O_2 and NOx were performed along the furnace. For brevity, only some radial profiles are presented at two planes close to the burner (Fig. 8-11) where local combustion information is required. This information includes the effect of swirl and the degree of mixing on combustion intensity and flame size.

The concentration profiles shown in Figs. 8-11 exhibit the same degree of symmetry as described for the temperature profiles.

On inspection of the complete profiles, the flow field can be divided into four zones:

A- The main reaction zone (near burner forward flow).
B- The central reverse-flow zone (CRZ).
C- The fully developed flow zone.
D- The external reverse-flow zone (ERZ).

Most of combustion occurs in the reaction zone (A) leading to uniform concentration distributions in the fully developed flow zone (C), as detailed below:-

A- In the reaction zone, the concentrations of HC and CO are higher in the case of S= 0.9. This shows that the degree of mixing and consequently completeness of combustion are lower. This is also confirmed by the lower measured CO_2 and the higher O_2 in this region. As swirl is increased, high CO_2 peaks are observed in the annular forward jet, and correspondingly lower O_2, CO and HC, consistent with increased combustion intensity. The flame envelope is therefore smaller in the case of S=2.25. From the CO contours it can be estimated that the flame diameter for the higher swirl is about 0.8 that for the lower swirl, in contrast with the wider jet spread.

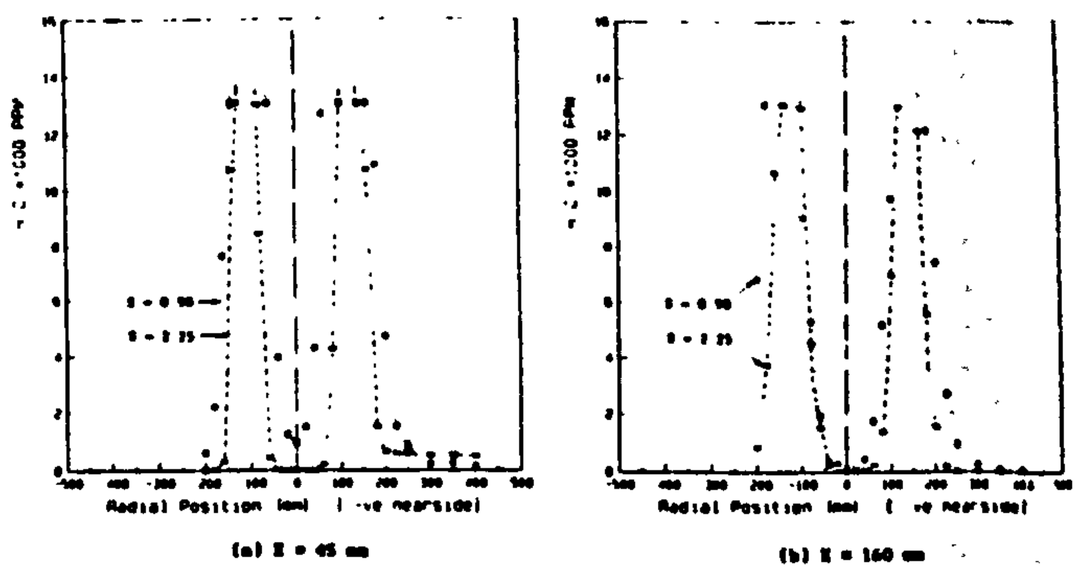

Fig. 8 Radial HC profiles.

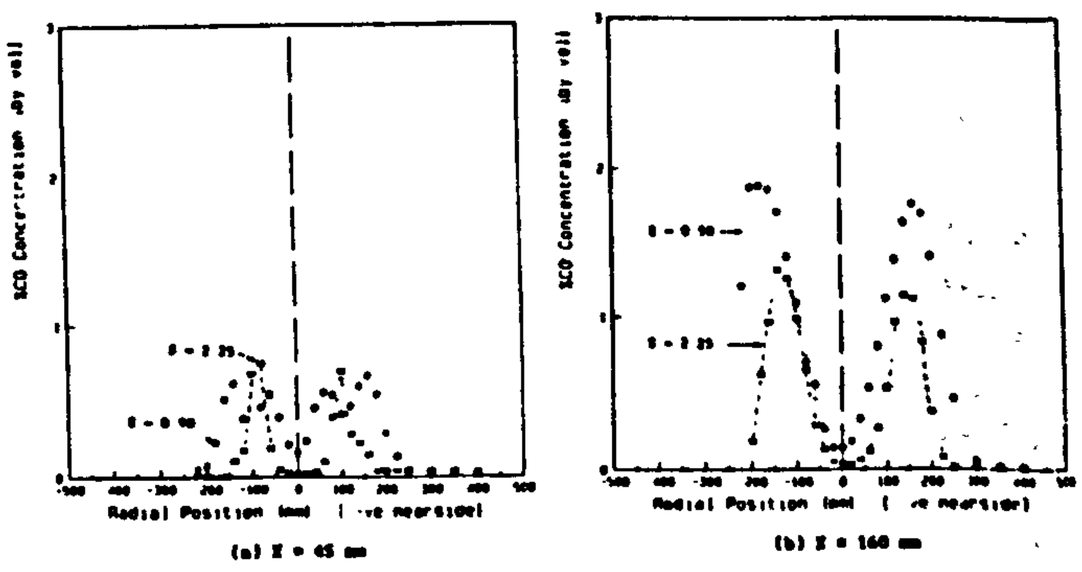

Fig. 9 Radial CO profiles.

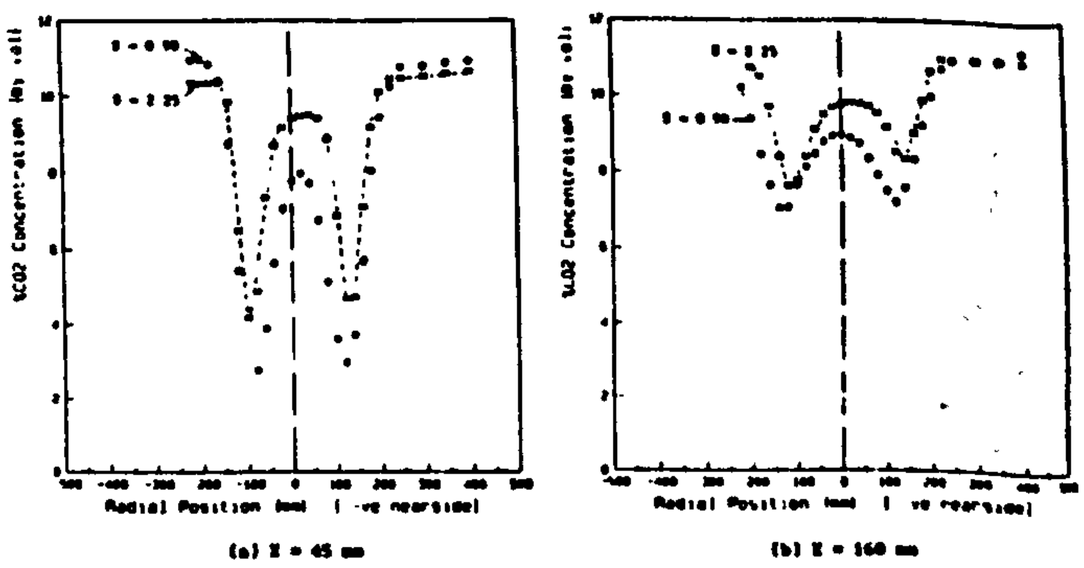

Fig. 10 Radial CO_2 profiles.

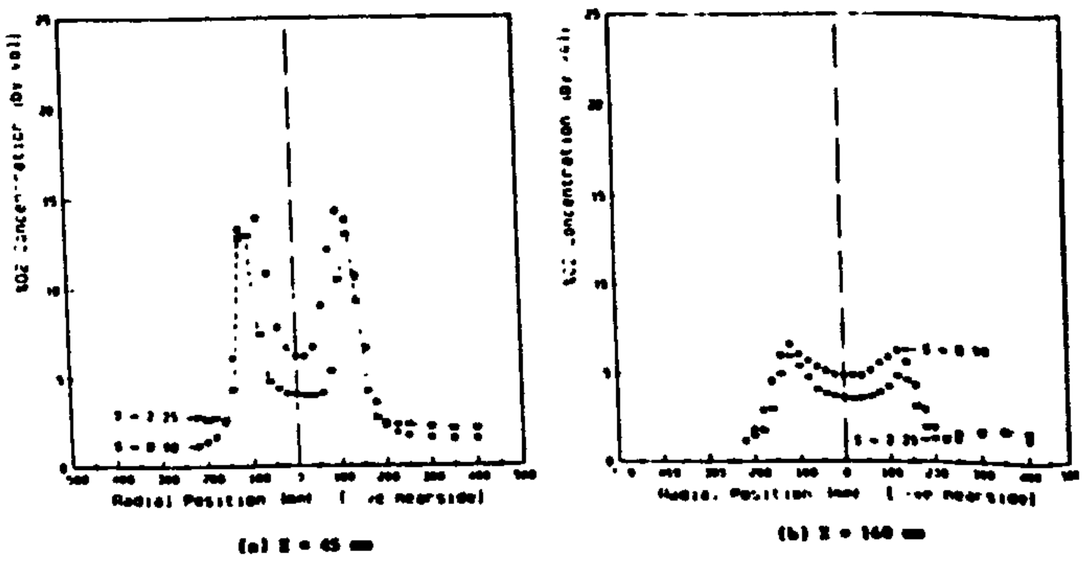

Fig. 11 Radial O_2 profiles.

The minimum value of CO_2 at the first measuring section, 45 mm from quarl exit, Fig. 10(a), varies between 2.5% and 4.0%, confirming that combustion commences within the quarl. This is also confirmed by the maximum value of O_2 concentration at this section.

The measurements show that the main reaction zone ends at about 500 mm. Beyond this distance, concentrations of CO and HC decay to zero, and concentrations of CO_2 and O_2 attain their uniform values of 11.5 % and 1 % respectively, representing complete combustion.

B- Within the CRZ, concentrations of HC and CO are nearly zero in the case of S= 2.25. However for S= 0.90, small concentrations exist along the CRZ. This indicates that the CRZ of the lower swirl flame receives mixtures with reactions still in progress.

C- As mentioned in (A) above, the fully developed flow zone extends from about 500 mm downstream from the quarl to the furnace exit.

D- In the ERZ, although gases circulating in this region are mainly products of complete combustion, very low concentrations of CO and HC are observed for both swirls. These concentrations are entrained from the outer boundary of the forward flow where reactions are still in progress.

axial directions. The rate of NOx formation follows closely the rate of the main combustion reactions as indicated by the temperature and main species concentrations. Comparison of the NOx profiles at 45 mm from quarl exit Fig. 12 with those of the temperature Fig. 7 shows that NOx profiles are similar to the temperature profiles for each swirl case. At the 545 mm plane from the quarl exit, NOx profiles become almost uniform across the furnace. These features indicate that NOx in this case is formed by the thermal mechanism.

However it is noted that the NOx concentration levels are significantly higher for the lower swirl case. This cannot be completely explained by the temperature variation alone. Two other factors must also be considered:

a- Longer residence time, due to the slower reaction.

b- Higher fluctuations in the concentrations as observed from the flame shape.

B- The profiles of NOx within the CRZ, Fig. 12, and the corresponding temperature profiles, Fig. 7, show that NOx concentrations within this region are mainly due to the entrainment from the forward flow and not due to reactions within this zone. For example at the 45 mm plane, higher NOx concentrations are measured for the lower swirl, although the

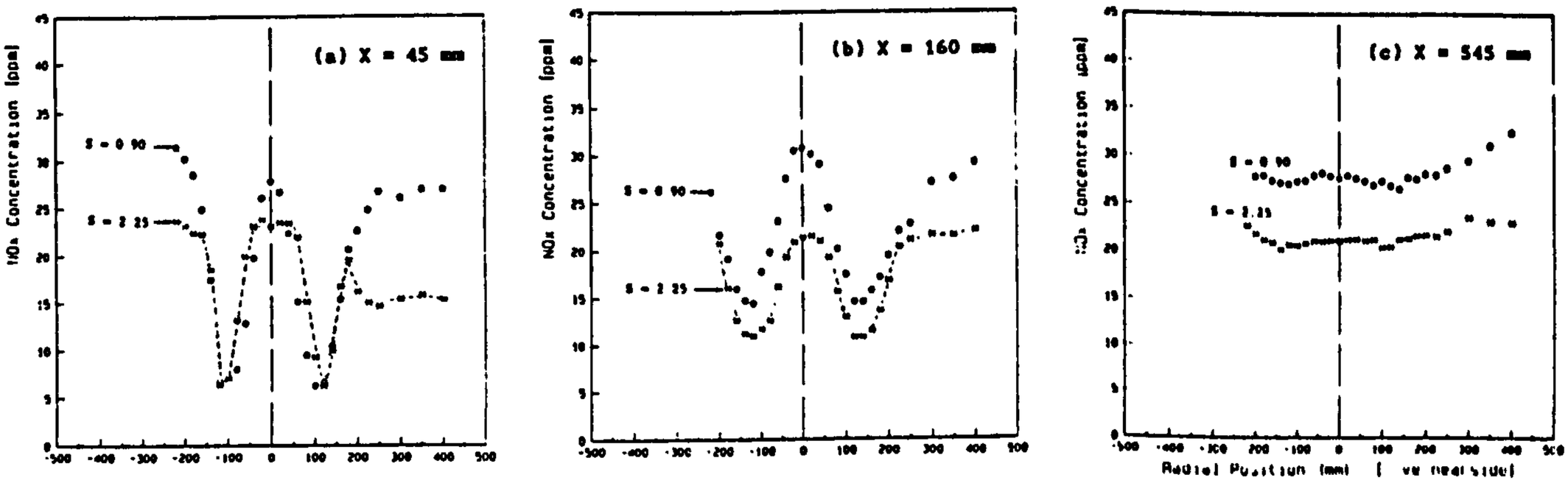

Fig. 12 Radial NOx profiles.

NOx Concentrations

The results of NOx measurements for the two swirl settings surveyed are represented in Fig. 12 by some illustrative NOx profiles at near burner planes. These results are discussed in relation with the temperature and species concentration fields described above, using the same four flow field zones defined above.

A- The reaction zone is characterised by steep gradients of NOx concentration in both the radial and

temperature is lower. Further downstream at the 160 mm plane the temperature levels at both swirl settings are about the same, yet higher levels of NOx are observed at the lower swirl.

C- In both swirl settings, constant NOx concentrations were measured throughout this region and these equal the value measured at the stack. The lower swirl, S= 0.9, produced the higher NOx value of 32 ppm compared to only 26 ppm at S= 2.25.

D- The flow in the ERZ comes mainly from the fully developed flow with some flow entrained from the outer boundary of the reaction zone. Figure 12

shows that NOx concentration within this zone increases with axial distance from the burner until it reaches the fully developed value.

The discussion of NOx results described above confirms that its formation in these flames is mainly by the Zeldovich mechanism, although there may be some prompt NOx. The formation rates are affected by the flame temperature, residence time of hot gases in reaction region and the concentration fluctuations. The last two of these factors lead to higher NOx values in the lower swirl case.

CONCLUSIONS

1- With the use of the air entry Scheme 1 with the peripheral injection system, a minimum swirl (S=0.8) was required to achieve a CRZ stabilised flame. In Scheme 2, a CRZ was created by introducing some of the combustion air radially outward through a central gun, thus a stable flame was established even without swirl.

2- The flow patterns presented for Scheme 1 with peripheral injection were represented by distributions of the three time-averaged velocity components and the static pressure. These measurements have given clear pictures of flow expansion in the radial and axial directions, also of the flow boundaries and thus the central and external reverse-flow zones (CRZ and ERZ). The effect of swirl on the size of the CRZ was found to be significant with this injection system due to the increased influence of centrifugal forces.

3- An assessment of the combustion patterns has been obtained from the measurements of temperature and species concentrations. Good flame symmetry was obtained. Increasing swirl enhanced the mixing and thus combustion intensity.

5- Measurements of the local NOx concentrations have shown that its formation is through the thermal mechanism, with strong dependence on local flame temperature and O_2 availability. The NOx formation rate is thus dependent on the degree of mixing and local concentration fluctuations. In addition it depends on the residence time within the reaction zone. Consequently, at the higher swirl, higher mixing led to reduced NOx formation.

ACKNOWLEDGEMENTS

Part of this work was carried out under the research programme of Heat Transfer and Fluid Flow Service (HTFS) which receives support from the UK Department of Trade and Industry.

REFERENCES

1. Beltagui, S.A., and Maccallum, N.R.L., Characteristics of Enclosed Swirl Flames with Peripheral Fuel Injection, J. Inst. of Energy, 61, 3-16, 1988.
2 Beltagui, S.A., Kenbar, A.M.A and Maccallum, N.R.L, Comparison of Measured Isothermal and Combusting Confined Swirling Flows- Peripheral Fuel Injection, Proc. 2nd World Conference on Experimental Heat transfer, Fluid Mechanics and Thermodynamics, pp. 118-125, Elsevier Pub., 1991.
3. Kenbar, A.M.A, Beltagui, S.A. and Maccallum, N.R.L, Effect of Fuel Injection Modes on the Combustion Pattern and Pollution Formation in a Gas Fired Furnace, Submitted to the 2nd Int. Conf. on Combustion Technologies for a Clean Environment, to be held in Portugal , July 1993.
4. Beltagui, S.A., Fuggle, R.N., Kenbar, A.M.A., Ralston, T., Marriott, N. and Stopford, P.J., Modelling a Gas-fired Furnace Flow and Combustion Using the PCOC Code, Proc. of the Euroteck Direct 91 Conference, I. Mech. E., pp.51-58, Birmingham, July, 1991.
5. Kenbar, A.M.A, Beltagui, S.A. and Maccallum, N.R.L, Modelling the Combustion Aerodynamics for a Peripheral Injection Flow, 5th Int. PHOENICS Users Conference, Nice, France, Sept.1992.
6. Kenbar, A.M.A, Beltagui, S.A., Ralston, T and Maccallum, N.R.L, Measurement and Modelling of NOx Formation in a Gas Fired Furnace, Proc. of 1st Int. Conf. on Combustion Technologies for a Clean Environment, Vilamoura, Portugal, Sept., 1991.
7. Kenbar, A.M.A., Combustion Aerodynamics and Pollutant Formation in Gas-fired Furnaces. Ph.D. Thesis, Mech. Eng. Dept., University of Glasgow, 1991.
8. Chedaille, J. and Braud, Y., Measurements in Flames, Edward Arnold , London, 1972.
9. Hillemanns, R., Lenze, B. and Leuckel, W., Flame Stabilization and Turbulent Exchange in Strongly Swirling Natural Gas Flames, 21st Symposium (int.) on Combustion, The Combustion Institute, Pittsburg, pp. 1445-1453, 1987.
10. Beltagui, S.A. and Maccallum, N.R.L., Aerodynamics of Vane-swirled Flames in Furnaces, J. Inst. Fuel, 49,183-193, 1976.

SECOND INT. CONF. ON COMBUSTION TECHNOLOGIES FOR A CLEAN ENVIRONMENT, LISBON, PORTUGAL, 1993

EFFECT OF FUEL INJECTION MODES ON THE COMBUSTION PATTERN AND POLLUTANT FORMATION IN A GAS FIRED FURNACE

A M A Kenbar[1,2], S A Beltagui[1,2], T Ralston[2] and N R L Maccallum[1]

1- Glasgow University

2- Heat transfer and Fluid Flow Services (HTFS), NEL, East Kilbride, Glasgow

ABSTRACT

This paper presents comparisons of combustion patterns and pollutant formation when using three different fuel injection schemes. In a semi-industrial size gas fired furnace, two fuel injection modes- radial outwards and peripheral axial, were examined as alternatives to the central axial mode. The radial fuel injection mode produced widest flame stability range. However the peripheral injection resulted in better mixing and combustion intensity. The results of pollutant measurements (NOx, CO and HC) indicate that the peripheral mode offer a wider scope for NOx reduction through the use of lean combustion and both air and fuel staging.

The data gained provide the information needed to optimise both the fuel injection mode and swirl to achieve the best combustion performance with minimum pollutant formation.

Theoretical predictions of the overall NOx formation under the above conditions are compared with stack measured values for the three fuel injection schemes above. The results of predictions are encouraging.

key words: Fuel injection modes, Combustion generated NOx, NOx-modelling, Furnace, Swirl, Combustion patterns.

INTRODUCTION

The work presented in this paper is part of collaborative research programme between Glasgow University and NEL aimed at:

First, to acquire a complete and reliable data set to compare three fuel injection modes, radial outward, peripheral axial and central axial in a semi-industrial scale application. These comparisons should provide the information needed to optimise both the fuel injection mode and swirl to achieve the best combustion performance with minimum pollutant formation.

Second, to provide an extensive data bank which is valuable in developing and testing the Heat Transfer and Fluid Flow Services (HTFS) mathematical models of furnace flow and combustion ,eg, PCOC (Beltagui et al (1991)) and heat transfer, eg, ZONE (Beltagui et al (1988)) and FIHR. The data is also needed to develop and validate NOx models such as the model suggested by Kenbar et al (1991).

In industrial burners, mixing between air and fuel occurs within the combustion chamber by shear layer mixing. Swirling the air flow can be used to increase shear mixing and enhance it with centrifugal mixing. The utilisation of the full benefits of these two physical processes in a practical combustion system depends mainly on the method of fuel injection.

Shear layer mixing is effectively utilised if the fuel is injected into the regions of maximum shear in the air stream. Centrifugal mixing effects can be utilised by creating favourable density gradients within the flow of air, fuel and products.

The most common method of fuel injection is axially at the centre of the air flow. This method does not utilise the full potential of the shear layer mixing.

Another variation from the above is to inject the fuel radially from the centre axis across the entering air jet. In this method the fuel flow can be used to produce the central reverse flow required for flame stability instead of using high swirl, as demonstrated by tests on the NEL furnace reported by Beltagui et al (1991).

The effect of swirl and fuel injection method on stability and intensity of gas flames in furnaces has also been studied by Leuckel and Fricker (1976) and Fricker and Leuckel (1976). The fuel was injected at the axis of the burner in four arrangements- axial jet, annular axial jet, diverging jets and axial through multi-throttle jets. Two distinct flame forms were observed in these tests. First, long asymmetric flame was observed with central axial fuel injection where the fuel jet penetrates completely the central reverse-flow zone (CRZ). Second, a short intense blue flame with a high degree of symmetry observed with the other fuel injection methods. Similar conclusions were reached by Hallet and

Günther (1978), Gupta et al (1973) and Milosavljevic et al (1990)

As an alternative to the central fuel injection, the fuel can be injected at the periphery of the entering air jet as reviewed by Beltagui and Maccallum (1988) This system offers the possibility of employing both shear layer and centrifugal mixing, thus resulting in efficient mixing and hence high combustion intensity.

Thus there is strong evidence in support of fuel injection either radially outwards or at the outer periphery of the swirled air flow. These two fuel injection modes lead to enhanced mixing rates and generally shorter flames that can be stabilised at no swirl or a low degree of swirl

Although the above investigations covered the three methods of fuel injection, complete and detailed information is not available for the same furnace system in order to provide reliable comparisons between their performances, particularly as to pollution formation.

This information has been gained in the NEL furnace programme covering the three fuel injection systems tested under the conditions described in the next section.

EXPERIMENTAL PROGRAMME

The NEL furnace is a model of a cylindrical upshot process heater, 3 m high by 1 m diameter, fired by natural gas through a variable swirl burner with a quarl. The apparatus is described in detail by Beltagui et al (1988). The three fuel injection modes investigated were:

a- Central axial fuel injection

b- Central radial fuel injection

c- Peripheral axial fuel injection

Figure 1 illustrates the furnace and fuel injection systems. The experimental data falls into two main groups:

In-Furnace Measurements

These data constitute complete mapping of the aerodynamic patterns (three time-average velocity components and static pressure) and the combustion patterns (temperature and species concentrations- CO, CO_2, O_2 and NOx) within the furnace. Mapping of HC concentrations was also performed for the peripheral fuel injection system only. The data was obtained for a fixed firing rate of 400 KW and 5% excess air (ϕ=0.95). Tests were generally carried out at four swirl numbers, S= 0.0, 0.45, 0.9 and 2.25. However only self-sustained flames were studied in detail.

Stack Measurements

Concentrations of CO, CO_2, O_2 and NOx were measured in the stack for 400 KW and 360 KW firing rates under a range of input fuel equivalence ratio 0.70 to 1.35. Concentrations of HC were also measure under the same conditions for the peripheral fuel injection system only.

The results of these investigations (In-furnace and stack) for the radial fuel injection were reported by Beltagui et al (1991) and Kenbar et al (1991). The peripheral fuel injection results were reported by Kenbar et al (1993). The central axial fuel injection measurements were reported by Kenbar (1991).

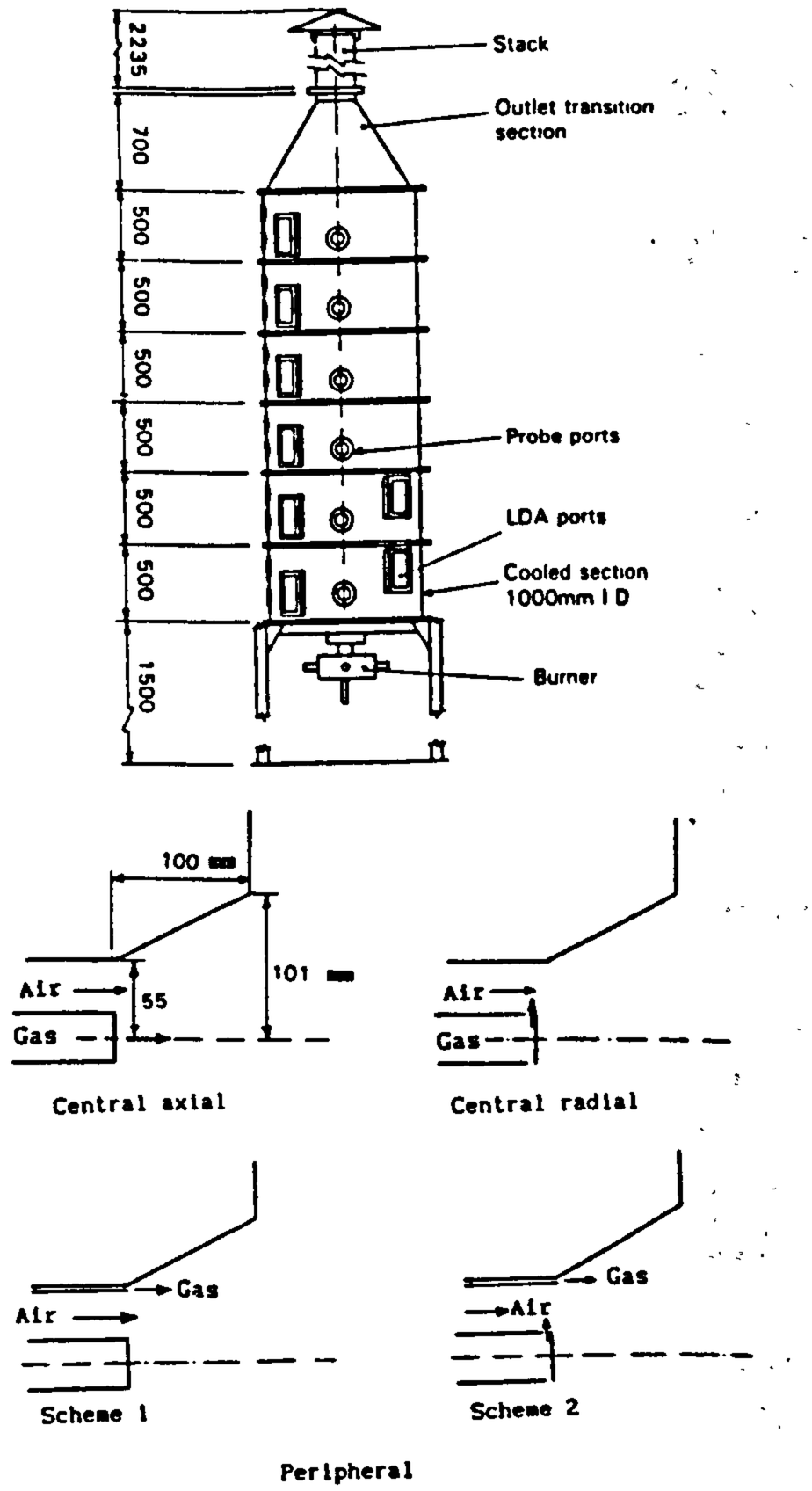

FIG 1: Schematic of furnace and fuel iniection systems

FLAME BEHAVIOUR

The flames studied were all stabilised through recirculation of some combustion products. Flame behaviour for the three methods of fuel injection can be summarised as follows:

a- For the central axial fuel injection the flame was established only for the cases with swirl numbers, S=0.9 and 2.25. The flames were stable but characterised with non-uniformity and yellow colour. Compared with other fuel injection modes, this flame was the longest.

b- For the central radial fuel injection a stable flame was achieved without and with swirl. The flame intensity increased with swirl over the range tested, S=0.0 to 2.25.

c- For the peripheral fuel injection, two schemes were tested, Fig 1. In the basic scheme (Scheme 1) stable flames were achieved only with swirl above S=0.80. For the case with S=0.90, the flame was characterised with some non-uniformity in shape as compared with the higher swirl flame S=2.25.

In Scheme 2 a fraction of the combustion air, about 10 %, was introduced through the central gun to create a CRZ. This scheme produced stable flames even without swirl.

FLOW PATTERNS

The complete mapping of the flow structure inside the furnace has been performed for the radial and peripheral fuel injection systems only. This has resulted in identifying four distinct flow zones within the furnace: near burner forward flow (main reaction zone), central reverse flow (CRZ), fully developed flow and external reverse-flow zones (ERZ) as shown in Fig 2. This division helps in the analysis of the combustion patterns. The main features of the flow patterns for the two fuel injection systems are generally similar. The main forward flow occurs in an annular jet with a CRZ in the centre and a large weak ERZ surrounding it. The CRZ size has increased with swirl. The jet width is indicated by the flow boundaries of the forward flow. For space limitation, flow patterns measurements are not presented in this paper.

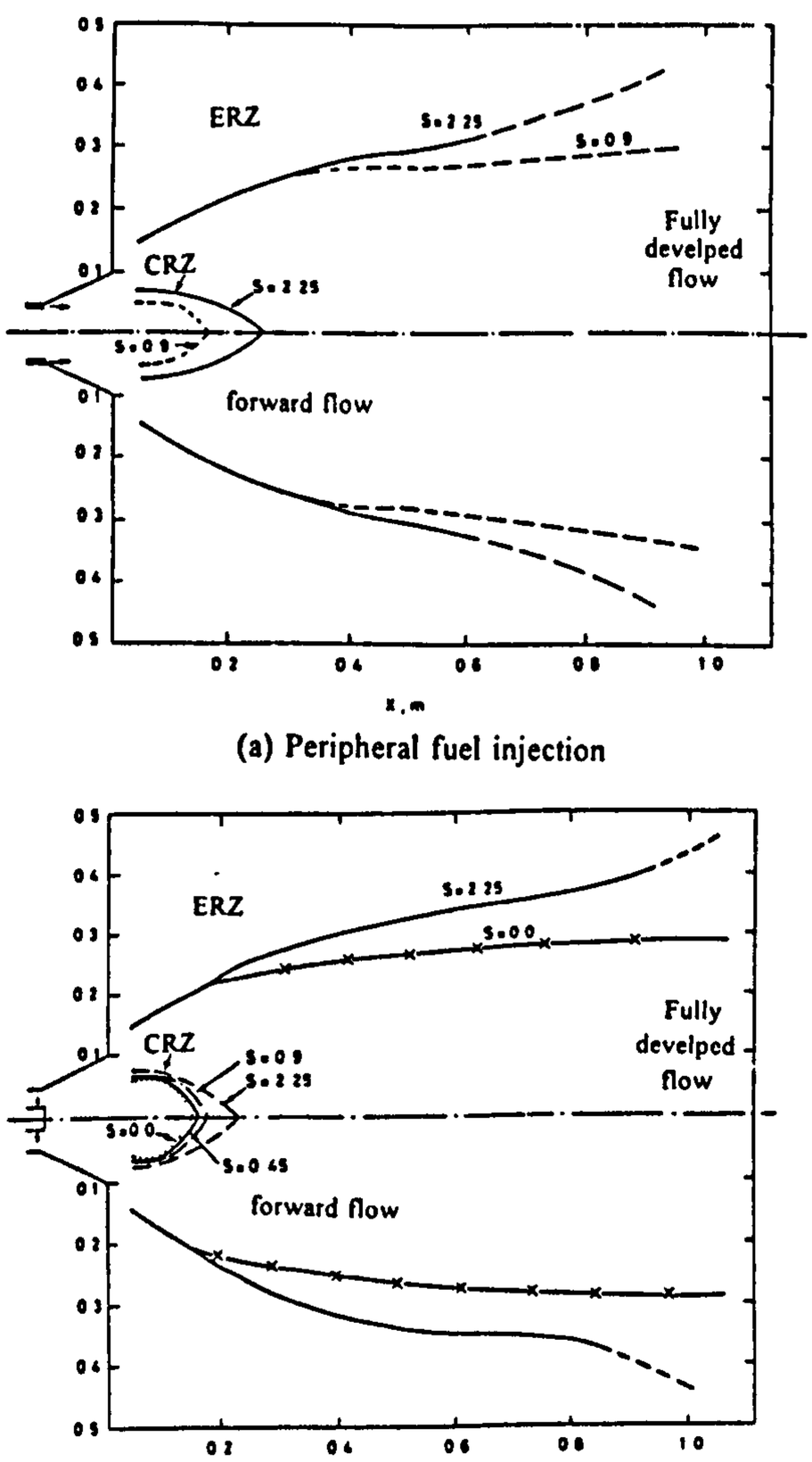

(a) Peripheral fuel injection

(b) Radial fuel injection

FIG 2: Flow boundaries

COMBUSTION PATTERNS

The important information required to assess the combustion performance of the three fuel injection modes is obtained from the results of measurements near the burner zone. The information inferred from these results include mixing, combustion intensity, flame symmetry, heat release and pollutant formation. Comparisons are therefore presented for two selected planes near the burner- at X=45 mm and X=200 mm from quarl exit.

Temperature Distributions

Comparison of the temperature distributions are given in Figs 3 and 4. All profiles illustrate good flame symmetry except for the central axial fuel injection. The highest degree of asymmetry is noted at the plane nearest to the burner and at the lower swirl, where the gas jet is deflected to one side. This observation is attributed to the slow combustion rate and thus low jet expansion. Similar observations were reported by other workers, eg Leuckel and Fricker (1976).

The mixing and combustion intensity in each of the three fuel injection modes, will be discussed for the four zones of the flow field.

The main reaction zone. This zone covers the forward flow near the burner. In all three fuel injection modes, the steepest temperature gradients occur at the plane nearest to the burner, X=45 mm, and the temperature gradients increase as swirl is increased. The longest reaction zone with the lowest peak temperature value is associated with the central axial injection system.

Although the radial fuel injection gives reaction zone temperature higher than the peripheral injection, this does not necessarily reflect higher combustion intensity. For the peripheral fuel injection with higher mixing rates, combustion starts earlier and at locations closer to the furnace walls. The temperature of the combustion products then decreases due to the high rate of entrainment and subsequent rapid mixing with the relatively cool externally recirculated gases just downstream of the burner exit. The heat transfer effect on the peak temperature is more pronounced because of the earlier combustion. This earlier combustion is confirmed by the measured species concentrations.

Central reverse-flow zone (CRZ). The gases entrained into the CRZ are those with the peak temperatures described above. All injection modes show an increase in this temperature as swirl increased from S=0.9 to 2.25. The temperature distribution within this zone becomes more uniform with increased swirl which enhances the radial stirring of the gases.

The fully developed zone and ERZ. In all cases, the gases circulated in the ERZ come mainly from the fully developed flow region further downstream. The highest ERZ temperature is observed with the central axial fuel injection where the flame is longest. The temperature in all cases decreases during the upstream travel of the gases, due to heat transfer to the furnace walls.

Concentrations of CO, CO_2 And O_2

Comparative profiles for these species concentrations are given at X=45 mm and X=200 mm, in Figs 5 to 10. From these figures, the following comments are made:

1- In all fuel injection modes combustion commences within the quarl,

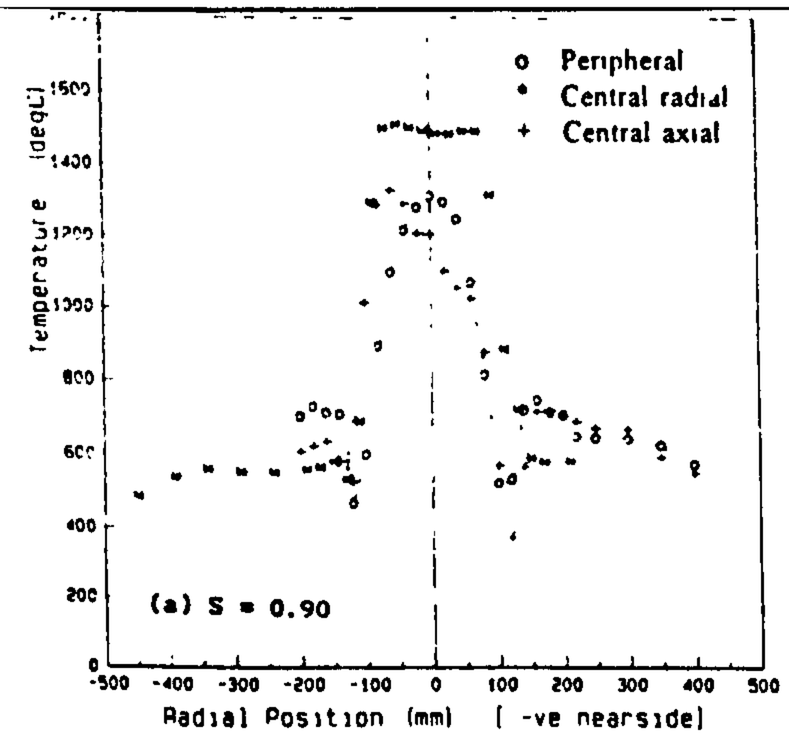

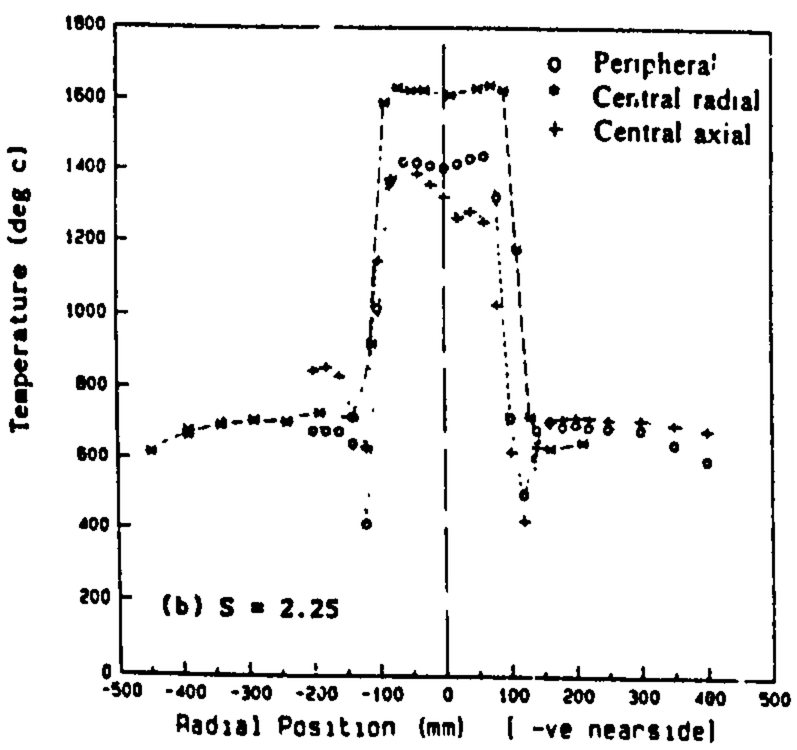

FIG 3: Radial temperature profiles, X = 45 mm.

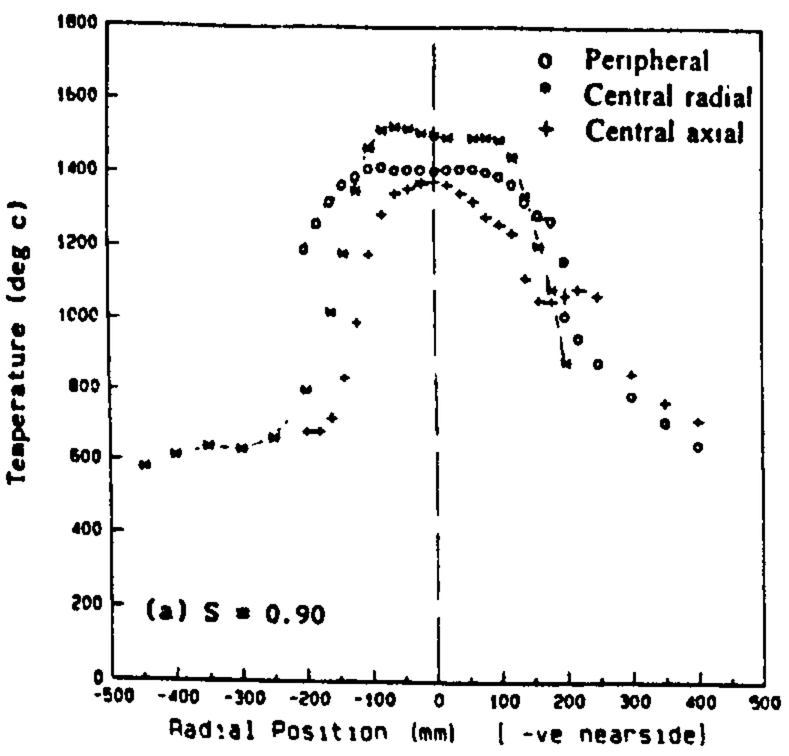

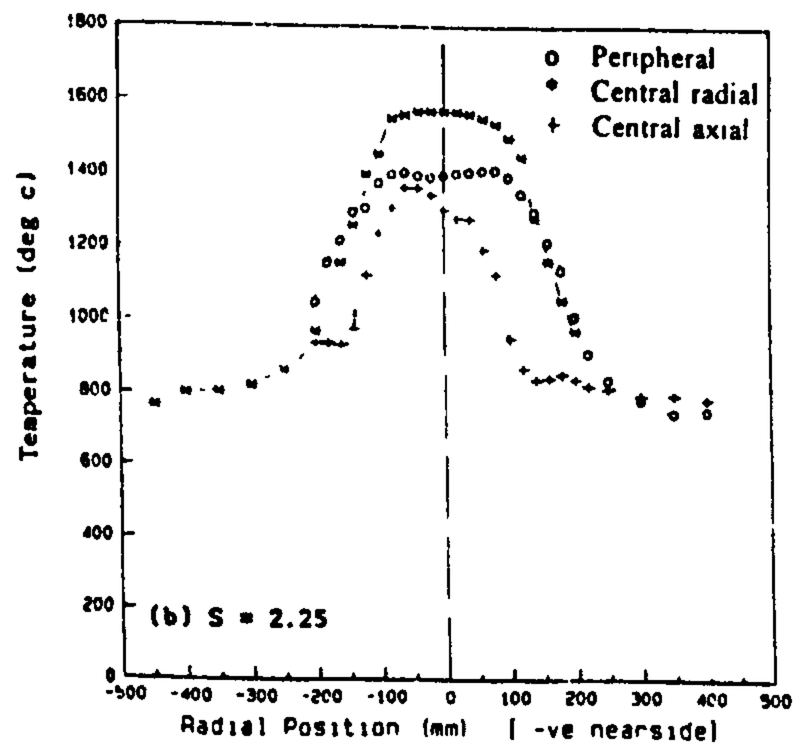

FIG 4: Radial temperature profiles, X = 200 mm.

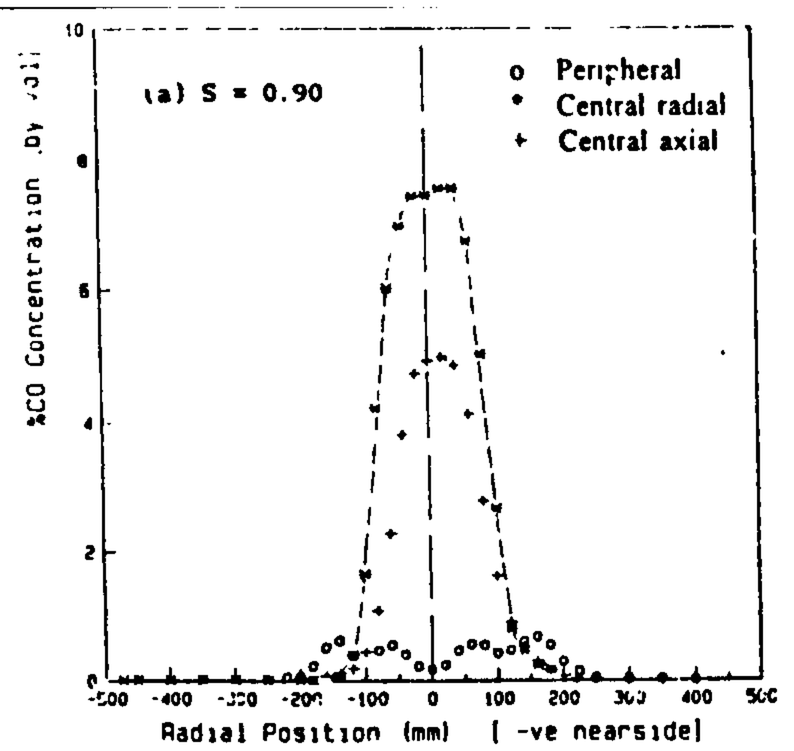

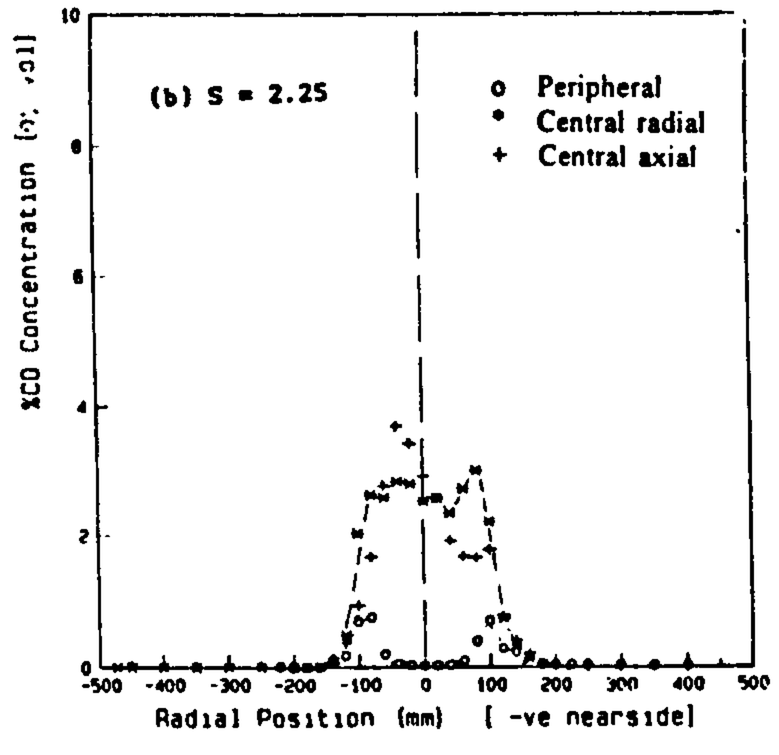

FIG 5: Radial CO profiles, X = 45 mm.

see concentrations of CO_2 and O_2 at X=45 mm.

2- The effect of increased swirl is to increase mixing and combustion intensity as seen through the reduction in both O_2 and CO and the increase in CO_2 in both planes.

3- At both planes, the lower swirl in the peripheral fuel injection exhibits a flame envelope which is wider than with other fuel injection modes, Figs 5 and 6. At the higher swirl of S=2.25, all fuel injection modes exhibit nearly the same flame diameter.

4- The lowest concentrations for O_2 and CO (and the highest for CO_2) within the flame are observed with the peripheral fuel injection mode, Figs 7 and 8, thus indicating the highest rates of mixing and combustion intensities of all three methods.

5- Within the ERZ, the low CO and O_2 values and the high CO_2 indicate that the gases circulated in these regions are mostly the products of complete combustion. The highest values of CO_2 and the minimum values of CO are observed with the peripheral fuel injection.

NOX CONCENTRATIONS

Comparative profiles of NOx concentrations are given in Figs 11 and 12. Complete contours of NOx concentrations for the radial fuel injection are given by Kenbar et al (1991) and for the peripheral fuel injection by Kenbar (1991). The NOx formation will be discussed in relation with the temperature and main species concentrations.

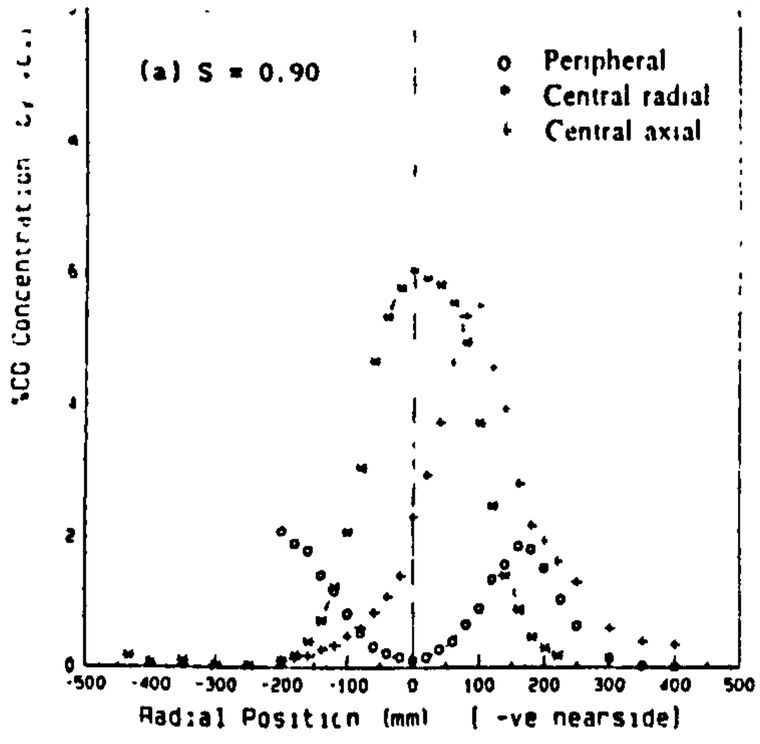

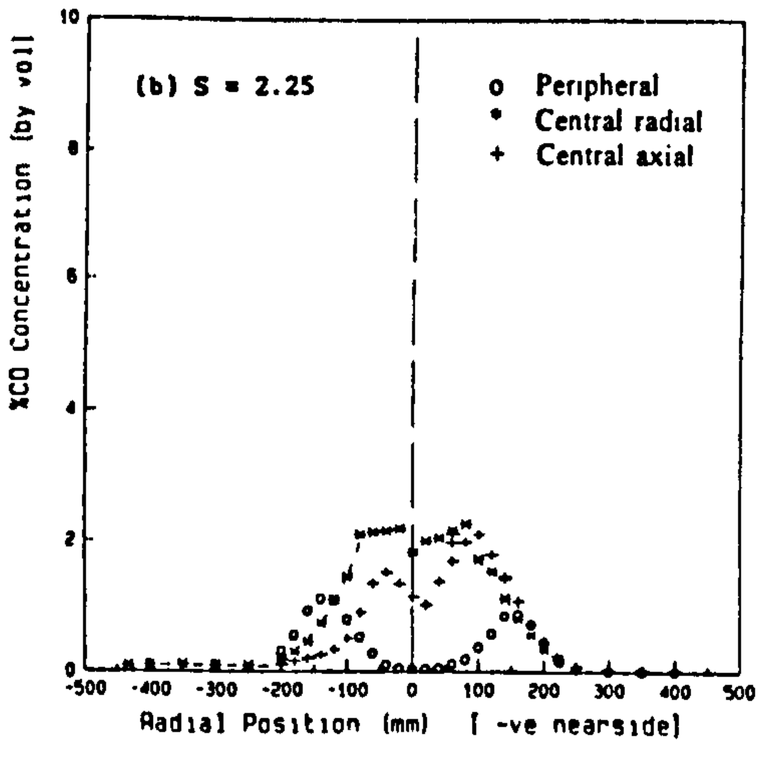

FIG 6: Radial CO profiles, X = 200 mm.

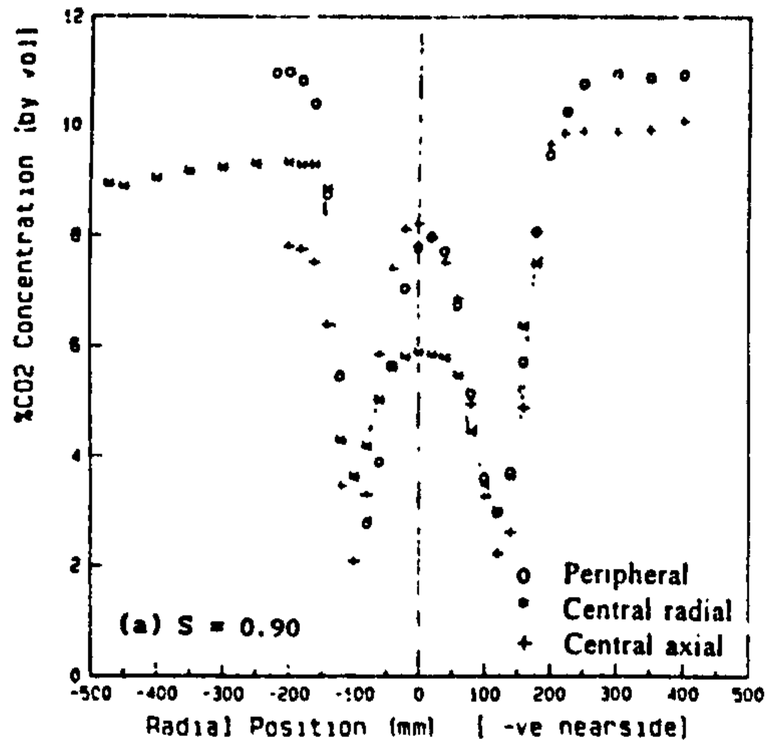

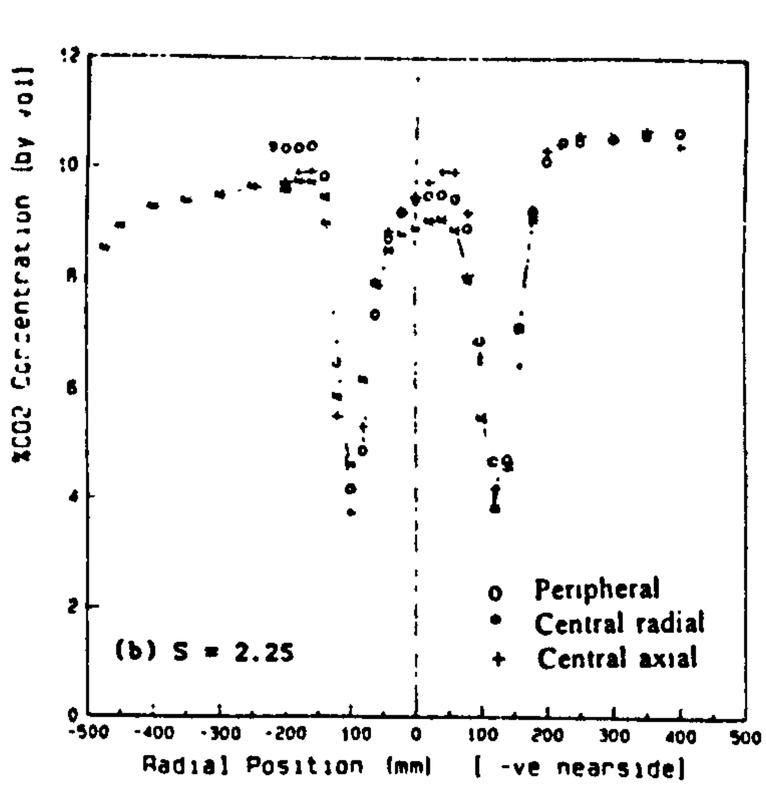

FIG 7: Radial CO_2 profiles, X = 45 mm.

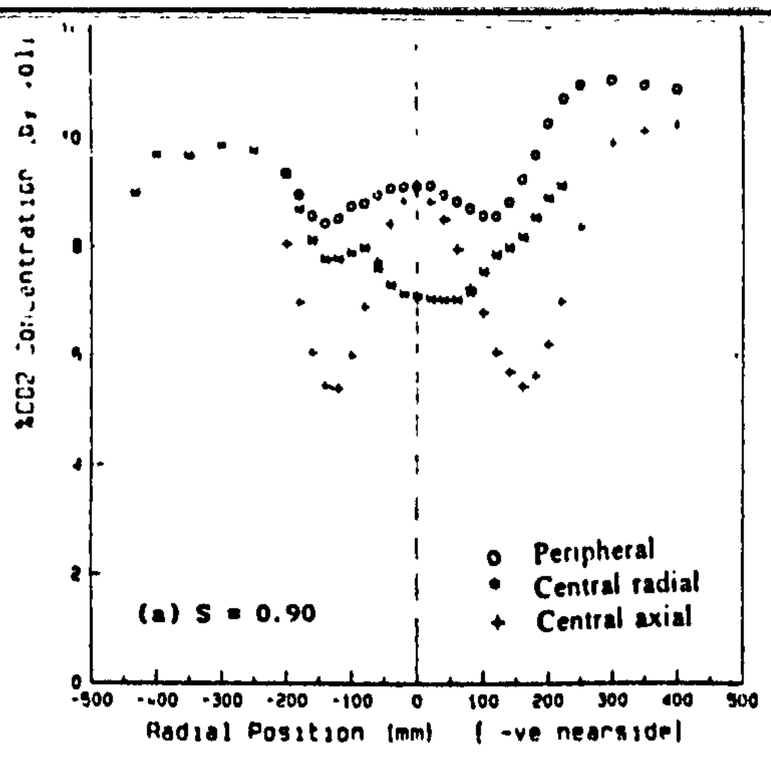

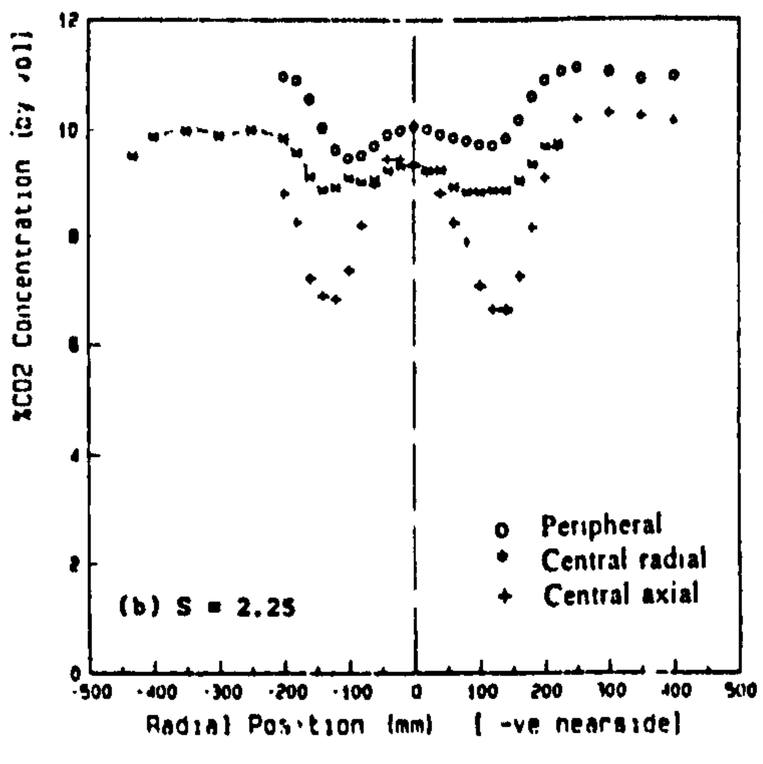

FIG 8: Radial CO_2 profiles, X = 200 mm.

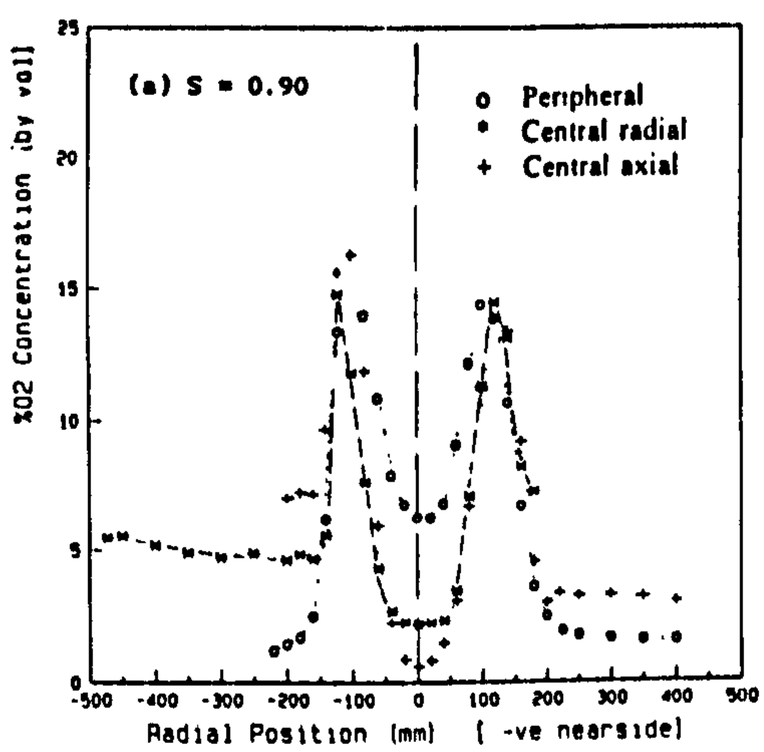

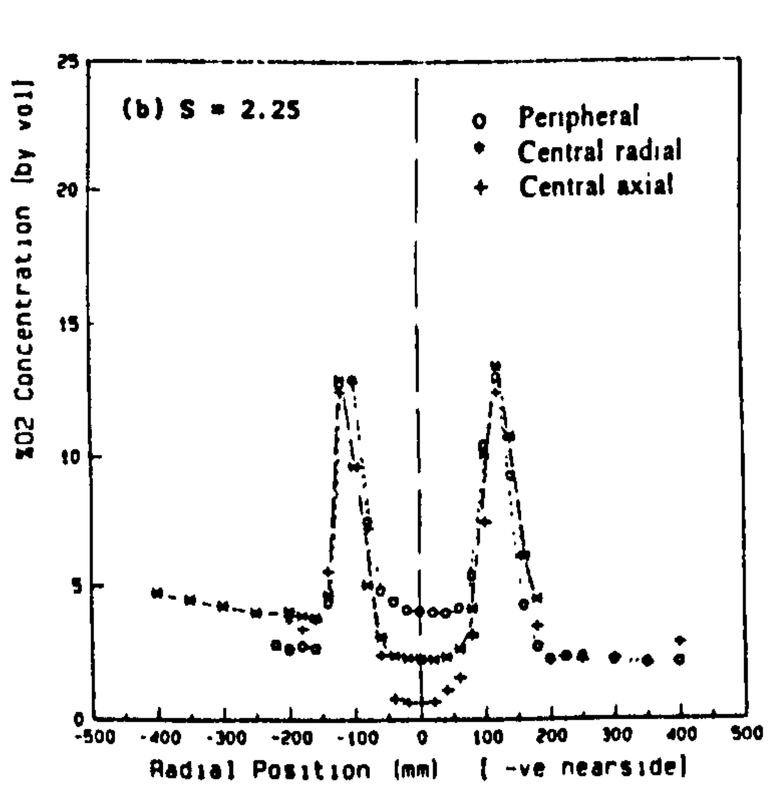

FIG 9: Radial O_2 profiles, X = 45 mm.

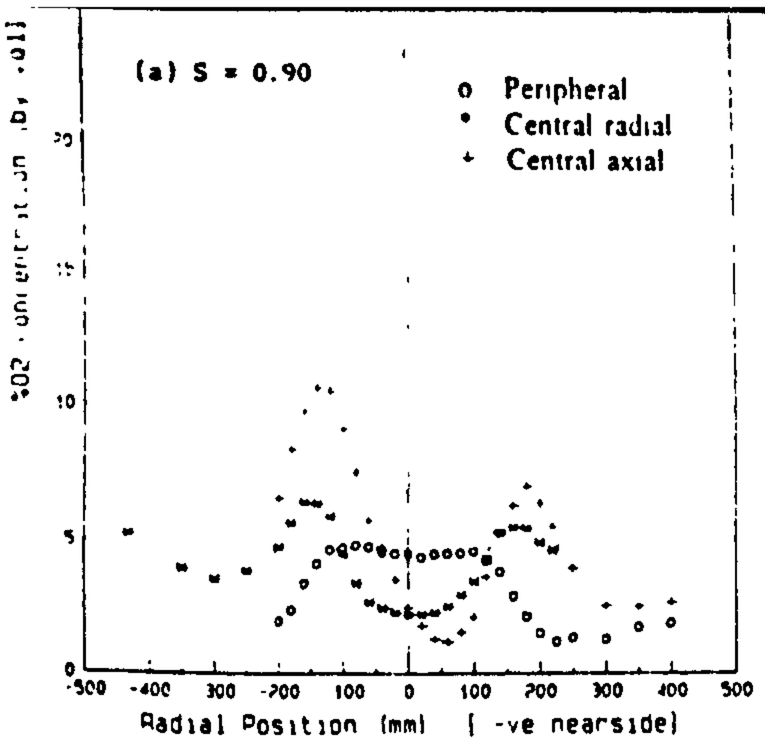

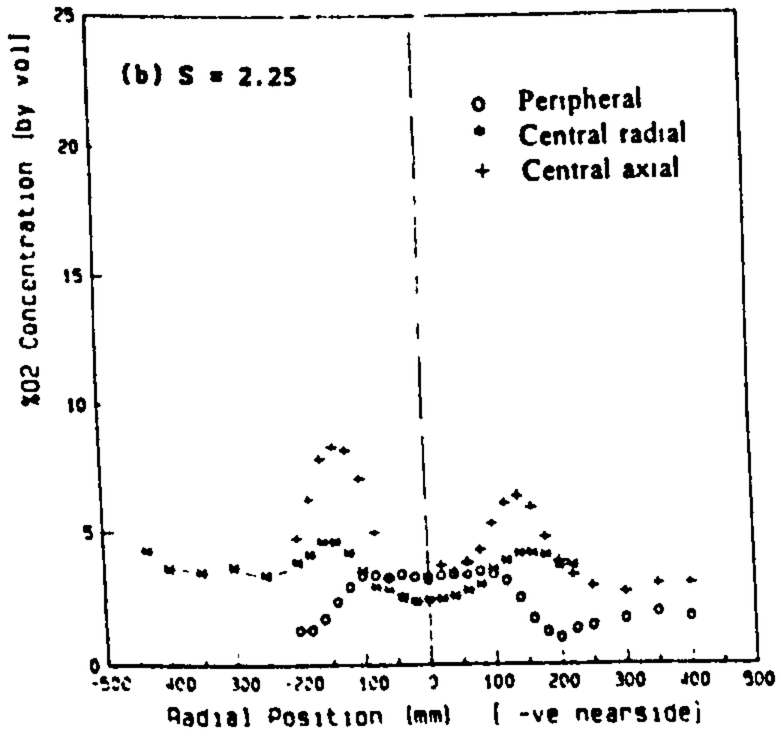

FIG 10: Radial O_2 profiles, X = 200 mm.

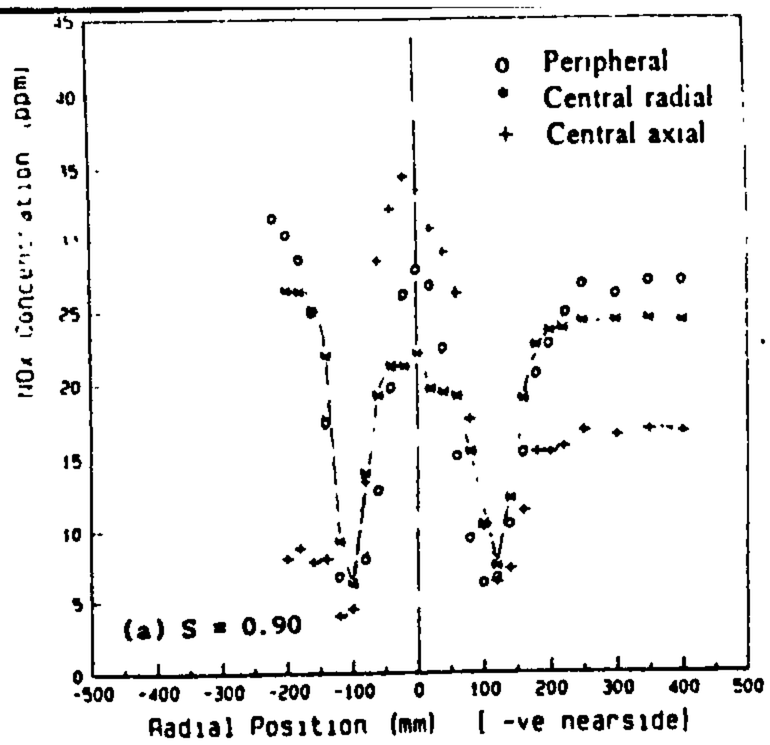

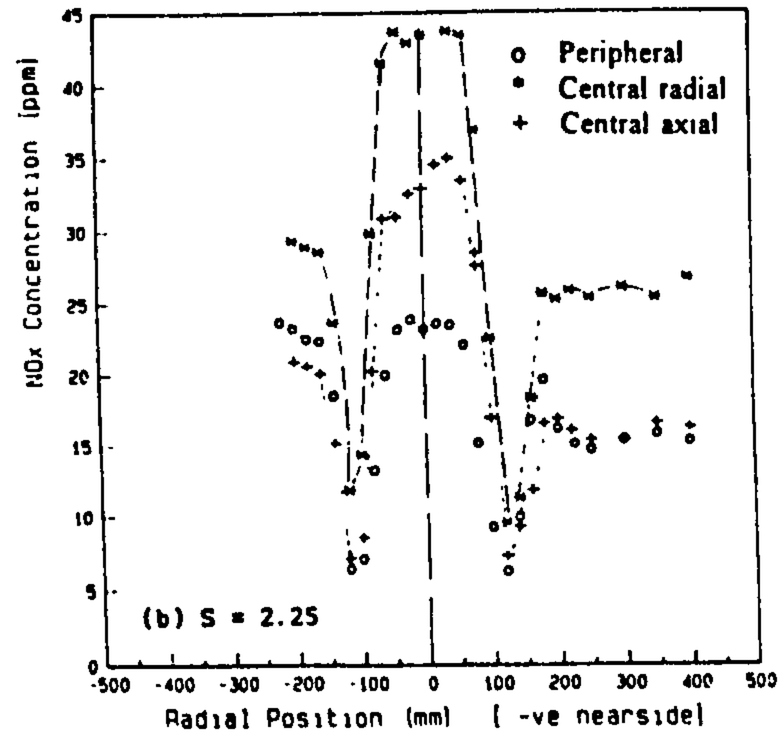

FIG 11: Radial NOx profiles, X = 45 mm.

The main reaction zone. All fuel injection modes show steep gradients of NOx concentrations in both radial and axial directions. The rate of NOx reactions follows closely that of the main combustion reaction. The increase in the minimum NOx value within this zone when moving from X=45 mm to X=200 mm indicates the newly formed NOx. The maximum NOx concentrations increase towards the boundary of the CRZ where the maximum mixing and combustion intensity occur.

Central reverse-flow zone (CRZ). The concentrations of NOx here depend on the length of the CRZ relative to that of the reaction zone. This will also decide whether any further reactions will take place within the CRZ.

At both planes X=45 mm and X=200 mm, for the lower swirl, the radial fuel injection mode, shows the minimum values of NOx compared with other injection modes These low concentrations indicate that this zone receives mixtures which are still reacting, as confirmed by the high CO concentrations shown in Figs 5 and 6. At the higher swirl with the radial fuel injection, NOx concentrations increase within the CRZ. This increase indicates that gases with higher temperature and thus higher NOx concentrations enter the CRZ, where further NOx reactions take place, resulting in the highest NOx concentrations compared with the other fuel injection modes.

The rate of NOx formation depends on flame temperature, residence time and O_2 concentration. The local values of these parameters are highly dependant upon the concentration fluctuations within the flow

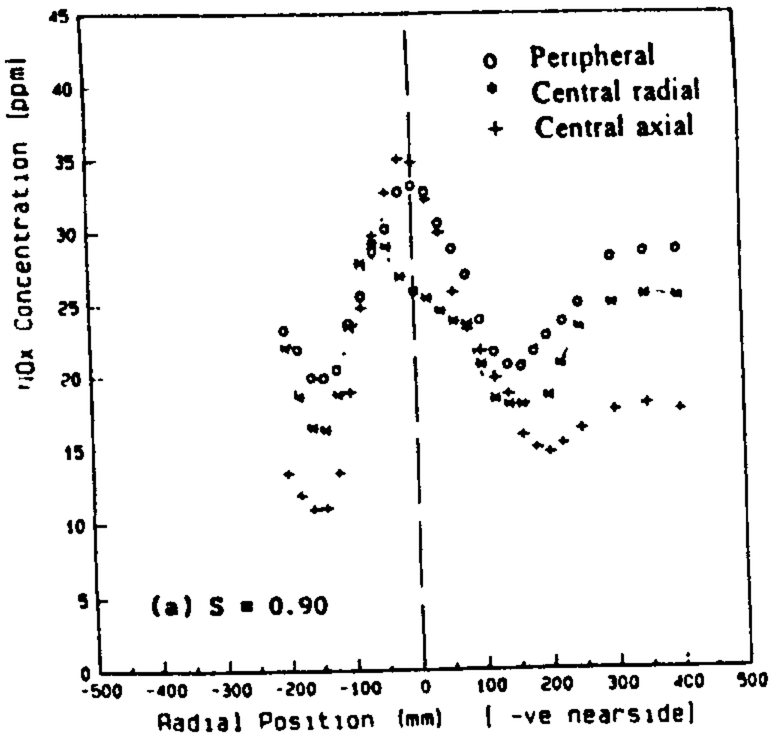

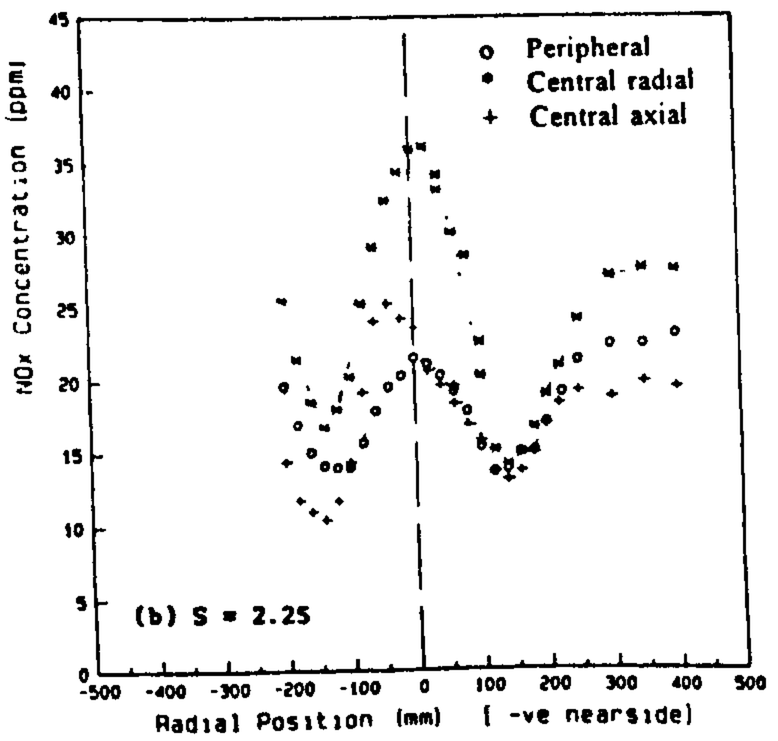

FIG 12: Radial NOx profiles, X = 200 mm.

The latter is mainly dictated by the method of fuel injection and swirl. For both central axial and peripheral fuel injection systems, increasing swirl has resulted in a decrease in NOx formation even though the temperature level has increased. It is suggested that this decrease in NOx formation at the higher swirl is due to the increased mixing rate leading to reduced concentration fluctuations and to the shorter residence time.

The fully developed zone and ERZ. The minimum measured NOx concentrations in the fully developed flow were observed with axial fuel injection, leading to minimum values of NOx concentrations in the ERZ. For the peripheral fuel injection, the low swirl produced the highest NOx values in the fully developed region, while the high swirl with this injection demonstrated NOx values less than those of the radial fuel injection. All NOx values in the fully developed flow zone are the same as the values measured in the stack as discussed below.

OVERALL FORMATION OF POLLUTANTS

The pollutant formation as measured by the stack emissions of CO and NOx concentrations will be compared over the range of equivalence ratio, ϕ, 0.70 to 1.35 for the three fuel injection modes and for the swirl range, S=0 to 2.25.

CO Concentrations

The measured CO concentrations show that for both the peripheral and radial fuel injection modes an excess air of 5% is sufficient to guarantee complete combustion. This is confirmed by the very low concentrations of HC (55 ppm) measured for the peripheral injection system in the stack. The value of excess air required to complete combustion for the central axial fuel injection system is 10 %.

NOx Concentrations

NOx concentrations, given in mg/m^3 corrected to 3% excess O_2, are shown in Fig 13. For the range of ϕ covered by the data, the lowest NOx concentrations are observed with the central axial fuel injection. This is due to the lower combustion intensity and thus the lower flame temperature in the reaction zone.

For the lean mixtures tested, the peripheral fuel injection mode produced significant decrease in NOx formation with increased excess air, while the radial and axial fuel injection modes gave an increase in NOx formation. The differences observed here are mainly dependent on the peak flame temperature. The peripheral fuel injection mode, is the only mode where increased excess air leads to a decrease in the peak temperature. This is due to the higher rates of mixing before and after combustion in this mode. In the other injection modes the increase in local O_2 concentration becomes the controlling factor.

At fuel-rich conditions (ϕ >1), all fuel injection modes exhibit a sharp decrease in NOx formation with increased ϕ. This decrease is the result of both lower peak temperature and lower O_2 concentrations.

Figure 13 also show that increased swirl reduces NOx with the peripheral fuel injection mode. This is due to the reduction in

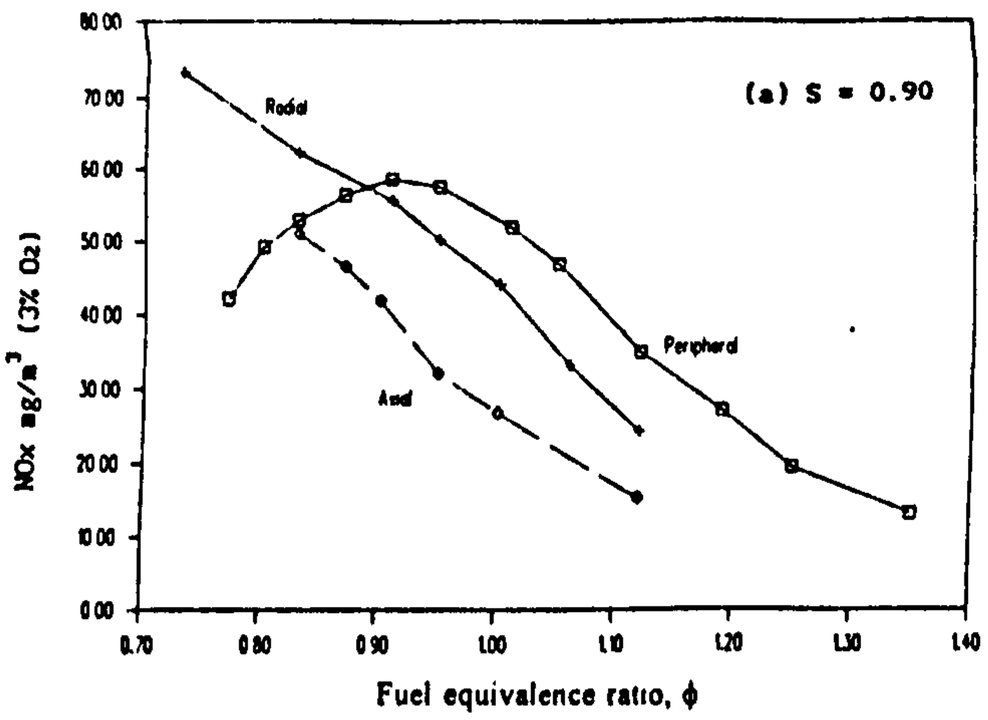

FIG 13: Overall NOx concentrations, S=0.90 and 2.25.

concentration fluctuations as described earlier.

For the non-swirled and low swirl cases, Fig 14 compares the radial and peripheral fuel injection modes. The results show the same trends as for the higher swirls mentioned above.

The above results show that the peripheral fuel injection is the only method which offers both air and fuel-staging as means of suppressing NOx formation. In applications where lean combustion can be used, only peripheral fuel injection offers the possibility of reducing NOx formation compared with the other two fuel injection modes.

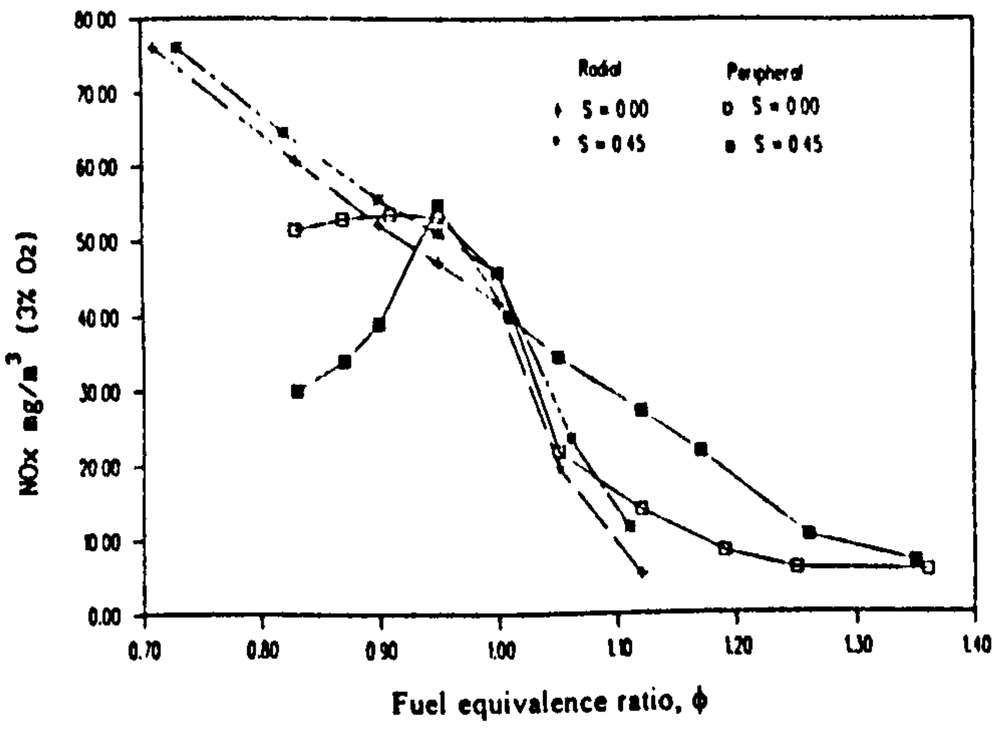

FIG 14: Overall NOx concentrations, S=0 0 and 0.45.

MODELLING OF NOx FORMATION

Theoretical predictions of the overall NOx formation are made using a well-stirred reactor model based on the Zeldovich mechanism with account for the species concentration fluctuations. This model has been fully described by Kenbar et al (1991). The model was used to predict the variation of stack emitted NOx with fuel/air ratio (equivalence ratio) for the three fuel injection modes.

Model Results

The model requires as input the values of mixedness of fuel/air jets (S_o) and the mean residence time (t) within the reaction zone.

The experimental study of NOx formation described earlier has shown that these two parameters are affected more by fuel injection mode than by swirl. Changes in swirl intensity have resulted in a very small change in stack measured NOx, therefore, the model has been tested for a single swirl value S=0.9.

An estimate of the average value of standard deviation (σ) of temperature for each fuel injection mode was obtained from the experimental measurements. The rate of collection of temperature measurements was 30 Hz. The standard deviation was calculated for 200 readings taken at each traverse position. The corresponding average values of S_o, were 0 65, 0.7 and 0.8 for central axial, central radial and peripheral fuel injection modes respectively.

A mean value of residence time (t) in the reaction zone was calculated from the zone length and the average flow velocity in this zone, both deduced from experimental measurements. The reaction zone has been assumed to end when CO concentrations decay to less than 0.5%.

However in the case of axial fuel injection, complete mapping of the flow and combustion patterns was not performed, therefore it was not possible to estimate the residence time accurately. An indication of the value of residence time has been based on the similarity of CO concentrations with the radial fuel injection at the measured axial level of X=200 mm and from the visual observation of flame length.

Comparison of model predictions and experimental measurements, are given in Figs 15 to 17 for central axial, central radial and peripheral fuel injection modes respectively. For all cases, the agreement between the model results and measurements is considered good. However, for the peripheral fuel injection mode, the predicted profile is slightly shifted to one side. This shift could be explained by two reasons.

Firstly, the value of ϕ was taken for simplicity to be the input value rather than the actual mean value in the reaction zone. It is expected that during the air/fuel jets progress to the reaction zone, the value of the effective equivalence ratio will differ from the burner input value due to the dilution with flows circulating from the CRZ and the ERZ. This effect seems to be significant in the case of peripheral fuel injection due to the fact that the mixing in this system is higher than in the other fuel injection modes as discussed earlier.

Secondly, the estimate of S_o was based on experimental measurements taken at fixed equivalence ratio (ϕ=0.95), and used for all values of equivalence ratio in the prediction. It is expected however that S_o will vary with ϕ and thus the predicted NOx profile.

Considering the simplicity of the model presented in this stage, it could be said that the present model is capable of giving a good prediction of the maximum value of NOx for different types of fuel injection modes. It also give the correct trend of NOx at the fuel lean and fuel rich conditions observed in the measurements. These results are

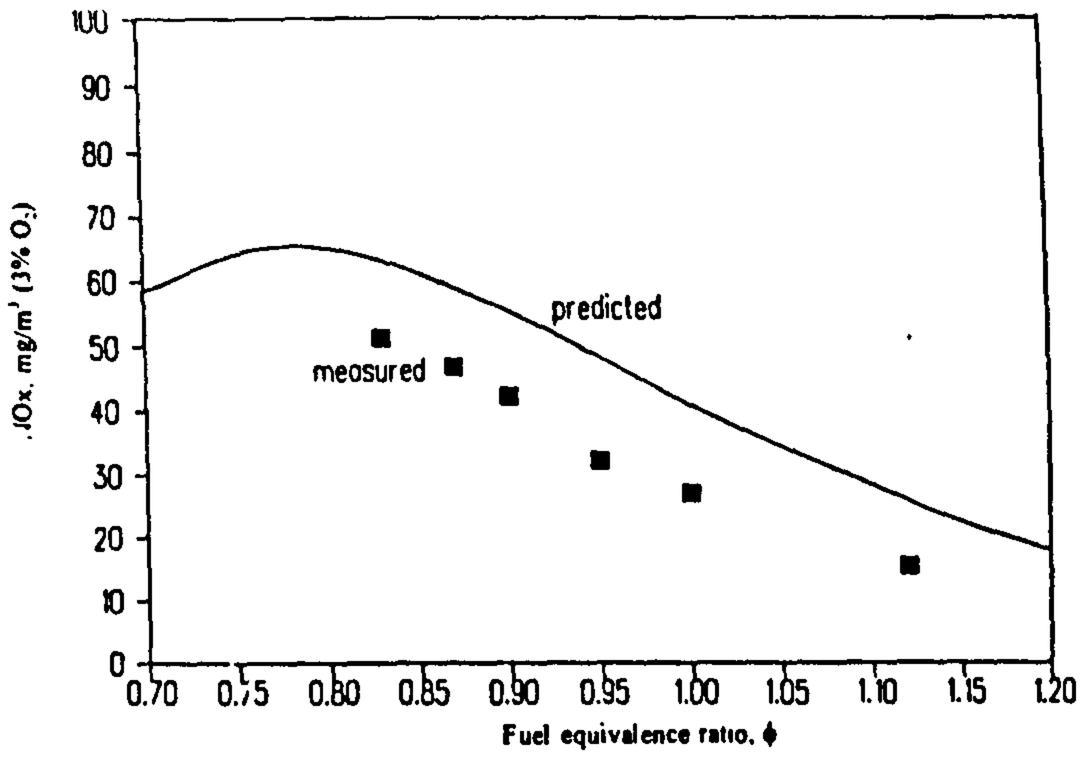

FIG 15: Predicted and measured NOx concentrations, central axial fuel injection, S=0.90

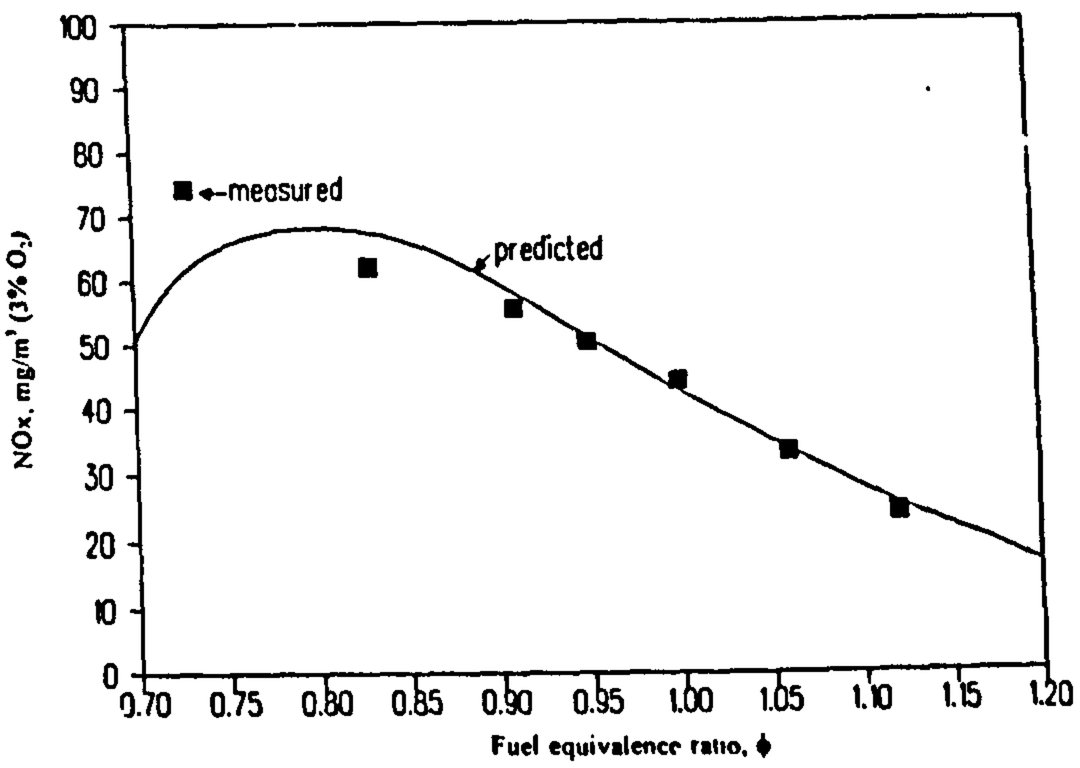

FIG 16: Predicted and measured NOx concentrations, central radial fuel injection, S=0.90

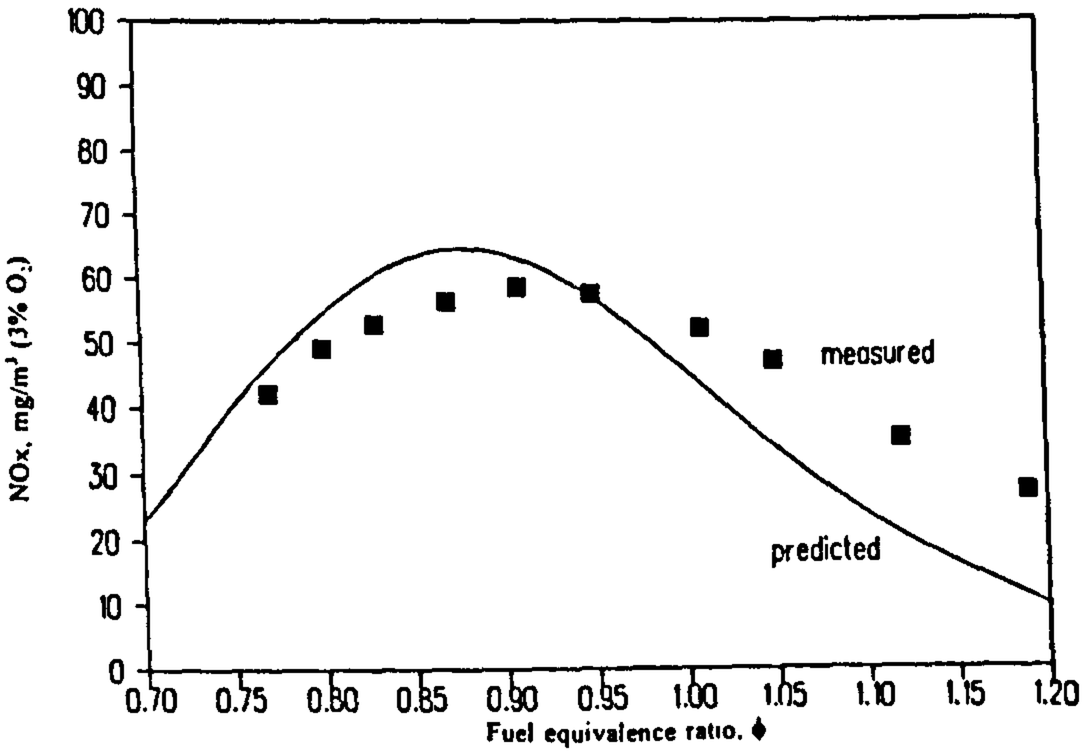

FIG 17: Predicted and measured NOx concentrations, peripheral fuel injection, S=0.90

valuable for practical engineering purposes.

This study has also highlighted the importance of accounting for the concentration fluctuation of species in the NOx prediction models.

CONCLUSIONS

1- Flame stability: All flames were stabilised by the central reverse flow. For the central radial fuel injection, the fuel jets created a central reverse-flow zone (CRZ), thus it was possible to achieve stable flame without swirl. For both central axial and peripheral fuel injection modes, a minimum swirl (S=0.8) was required to achieve a CRZ stabilised flame. In Scheme 2 of the peripheral fuel injection, feeding a fraction of the air flow radially through the centre produced stable flame without swirl.

2- Flame behaviour: The central axial fuel injection produced a long flame with a yellow appearance and non-uniformities. The central radial and peripheral fuel injection modes resulted in intense, shorter blue flames.

3- Combustion patterns: While good flame symmetry was obtained with the central radial and peripheral fuel injection modes, a high degree of flame asymmetry was observed with the central axial fuel injection. The effect of swirl in all fuel injection modes is to increase the mixing and thus combustion intensity. With the peripheral fuel injection, combustion occurs at the outer boundary of the swirled air flow, while in the other modes it is mainly on the boundary of the CRZ. The highest rates of mixing and combustion were achieved with peripheral fuel injection, due to the utilisation of the full benefits of shear layer and centrifugal mixing.

4- NOx formation has a strong dependence on flame temperature, concentration fluctuations and residence time, thus confirming its formation by the thermal mechanism. The effect of swirl on the local NOx values was more significant than on the overall NOx formation.

5- The stack-measured CO data show that complete combustion can be guaranteed for peripheral and central radial fuel injection modes with only 5% excess air. The corresponding value for the central axial fuel injection is 10% .

6- For the 5% excess air firing conditions, the lowest overall NOx formation was observed with the central axial fuel injection.

At fuel-lean conditions, the peripheral fuel injection gave a reduction in NOx formation, with increased excess air, while the other two fuel injection modes produced some increase in NOx formation.

At fuel-rich conditions, reducing air-fuel ratio gave sharp decrease in NOx formation.

The peripheral fuel injection was therefore the only system to offer NOx reduction by lean combustion, fuel-staging and air-staging. With the central radial and central axial injection modes, only air-staging is useful in reducing NOx formation.

7- Predictions of the variation of stack NOx with fuel equivalence ratio for the three types of fuel injection systems tested are good.

ACKNOWLEDGEMENTS

The authors wish to thank colleagues from the National Engineering Laboratory (NEL) and the University of Glasgow for their advice and encouragement. This work was supported in part by the management of the NEL.

REFERENCES

Beltagui, S.A., Fuggle, R.N. and Ralston, T. (1988). Measurements and prediction of heat transfer in the NEL furnace, *Second UK National Heat Transfer Conf.*, Glasgow.

Beltagui, S.A. and Maccallum, N.R.L. (1988). Characteristics of enclosed swirl flames with peripheral fuel injection,. *J. Inst. of Energy*, Vol. 61, pp. 3-16.

Beltagui, S.A., Fuggle, R.N., Kenbar, A.M.A., Ralston, T., Marriott, N. and Stopford, P.J. (1991). Modelling a gas-fired furnace using the PCOC code, *Eurotech Direct*, IMechE, Birmingham. Paper C413/054.

Fricker, N. and Leuckel, W. (1976). The characteristics of swirl-stabilised natural gas flames, Part 3: The effect of swirl and burner mouth geometry on flame stability, *J. Inst. of Fuel*, Vol. 49, pp. 152-158.

Gupta, A.K., Syred, N. and Beer, J.M. (1973). A low-noise burner for swirl-stabilised natural gas flames, *J. Inst. of Fuel*, Vol. 46, pp. 119-123.

Hallet, J. and Gunther, R. (1978). The influence of burner-data on shape and properties of swirling flames, *Ger. Chem. Eng.* Vol. 1, pp. 340-346.

Kenbar, A.M.A. (1991). Combustion aerodynamics and pollutant formation in gas-fired furnaces, *Ph.D. Thesis*, Dept. of Mech. Eng., University of Glasgow.

Kenbar, A.M.A., Beltagui, S.A., Ralston, T. and Maccallum, N R L. (1991). Measurement and modelling of NOx formation in a gas fired furnace, *1st (Int.) Conference on Combustion Technologies for Clean Environment*, Vol. 1, Algarve, Portugal.

Kenbar, A.M.A., Beltagui, S.A., and Maccallum, N.R.L. (1993) Combustion aerodynamics of a gas fired furnace with peripheral fuel injection, *Third World Conf. on Experimental, Heat Transfer, Fluid Mechanics and Thermodynamics*. To be held in Honolulu, Oct.

Leuckel, W. and Fricker, N. (1976). The characteristics of

swirl-stabilised natural gas flames, Part 1: Different flame types and their relation to flow and mixing patterns, *J. Inst. of Fuel*, Vol. 49, pp.103-12.

Milosavljevic, V.D., Taylor, A.M.K.P. and Whitelaw, J.H. (1990). The influence of burner geometry and flow rates on the stability and symmetry of swirl-stabilised non-premixed flames, *Combustion and Flame*, Vol. 80, pp. 196-208.

NOTATION

S	Burner swirl number, (ratio of axial flux of tangential momentum to the product of axial momentum flux and burner radius)	-
S_o	Mixedness factor, unity for perfect mixing	-
t	Residence time	s
X	Axial distance along furnace from burner exit	mm
ϕ	Fuel/air equivalence ratio	-
σ	Standard deviation	-

Combust. Sci. and Tech., 1993. Vol. 93. pp. 173-192
Photocopying permitted by license only

Measurement and Modelling of NO_x Formation in a Gas Fired Furnace

A. M. A., KENBAR[1,2], S. A. BELTAGUI[1,2], T. RALSTON[2] and N. R. L. MACCALLUM[1]
1–University of Glasgow
2–Heat Transfer and Fluid Flow Service (HTFS), NEL, East Kilbride, Glasgow

Abstract—This paper reports results of NO_x measurements carried out on a gas fired furnace using radial fuel injection. The data consists of a complete mapping of NO_x concentration in the furnace under variable swirl conditions. Swirl produced locally higher NO_x concentrations but little overall increase. Measured stack NO_x variations with burner input conditions indicate that, for this system, operating with a fuel-rich mixture is more effective in suppressing NO_x formation than with excess air operation. The data is needed for testing and developing theoretical models. Theoretical predictions of the overall NO_x formation are made using a well-stirred reactor model based on the Zeldovich mechanism with account for the species concentration fluctuations. The model predictions compare satisfactorily with the measurements.

Key Words: Combustion-generated NO_x, NO_x-Measurement, NO_x-modelling, Furnace, Swirl, Natural-gas, Fuel/air ratio.

NOTATION

$[N_2]$	Nitrogen concentration	mol/cm^3 s
$[O_2]$	Oxygen concentration	mol/cm^3 s
S	Burner swirl number, (ratio of axial flux of tangential momentum to the product of axial momentum flux and burner radius)	—
s	Mixedness factor, unity for perfect mixing	—
T	Flame temperature	K
t	Residence time	s
X	Axial distance along furnace from burner exit	mm
Z	Fluctuation parameter, see Equation 3	—
ϕ	Fuel/air equivalence ratio	—
$\bar{\phi}$	Mean value of ϕ	—
σ	Standard deviation	—

INTRODUCTION

The need to protect the environment from combustion generated NO_x has led to considerable demand to improve burner design. The present paper is part of a study on the effect of burner parameters on the formation of NO_x in gas fired furnaces. These parameters include fuel injection, firing rate, swirl and the mixture fuel/air ratio. These parameters are interrelated and vary from one combustion system to another. Thus it is important to investigate their effects on the level of NO_x emissions. This study makes a significant contribution to the understanding of the main factors involved in the formation of NO_x in these flames. The work also provides a valuable data-base for the assessment and validation of the theoretical models for NO_x prediction.

The present paper concentrates on the effect of swirl and mixture fuel/air ratio on NO_x formation when using a radial-outwards gaseous fuel injector. Swirl is an important feature of burner design since it provides satisfactory flame stability by creating a central reverse-flow zone. The mixture fuel/air ratio is an important parameter in burner operation. Other work to study the effect of the fuel injection modes is reported by Kenbar *et al.* (1991).

In a previous paper (Beltagui *et al.* 1989) an extensive review was made of the NO_x formation mechanisms and methods of abatement. The effect of swirl as observed by previous workers was included and it was realised that it is linked to other parameters, such as fuel injection mode and fuel/air ratio.

The aerodynamics and combustion patterns of the swirling flames in the National Engineering Laboratory (NEL) furnace have already been extensively studied through detailed measurements of the velocity components, gas temperature and species concentrations of CO_2, CO and O_2.

These measurements were carried out in the NEL furnace fired by natural gas through a variable-swirl burner with a quarl. The fuel gas was injected from a central gun radially outward. Four swirl settings were considered, burner swirl numbers ranging from 0.0 to 2.25. The availability of this complete set of data is useful in testing and developing the furnace flow and heat transfer codes, such as the HTFS program PCOC (Stopford, 1989). Part of these measurements and comparisons with modelling using PCOC were reported by Beltagui *et al.* (1991).

The present paper offers two data sets:

The first illustrates complete mapping of NO_x concentrations produced under different swirl levels, but with the same firing conditions, in order to study the effect of swirl on NO_x formation.

The second illustrates the effects of the mixture fuel/air ratio on the overall NO_x emissions as measured in the stack.

The results show that while the effect of swirl on the local NO_x concentration in the near burner zone is significant, it was of secondary importance downstream. The results also demonstrate that increasing excess air above the level required for complete combustion led to an increase in the overall NO_x emission level. However by operating with a fuel-rich mixture, NO_x formation was suppressed significantly.

The paper also presents a simple engineering model which can be used to predict the overall thermal-NO_x formation for furnaces and its variation with input conditions, eg fuel injection mode and equivalence ratio. The model is based on the well-stirred reactor concept with account being taken for local concentration fluctuations. The inputs to the model are limited to the residence time in the reaction zone and the fuel/air mixing parameter. The agreement between model-predicted and measured concentrations was satisfactory.

EXPERIMENTAL PROGRAMME

The aims of the experimental programme were:

a—To produce complete mapping of the local NO_x concentrations within the furnace under a range of swirl intensities. This set of data illustrates the NO_x formation processes in this system. It is also required for the assessment and development of the modelling procedures.

b—To investigate the effect of two burner parameters, namely, swirl and fuel-air ratio on the overall NO_x formation as measured in the stack.

Both sets of results have been analysed and discussed in the light of the temperature, concentrations and velocity measurements reported earlier by Beltagui *et al.* (1991).

The NEL furnace is a model of a cylindrical upshot fired heater. The apparatus is described in detail by Beltagui *et al.* (1988-a). The furnace is fired by natural gas through a variable swirl burner with a quarl. The burner used in this study utilises the moving-block swirl generator of the International Flame Research Foundation (IFRF).

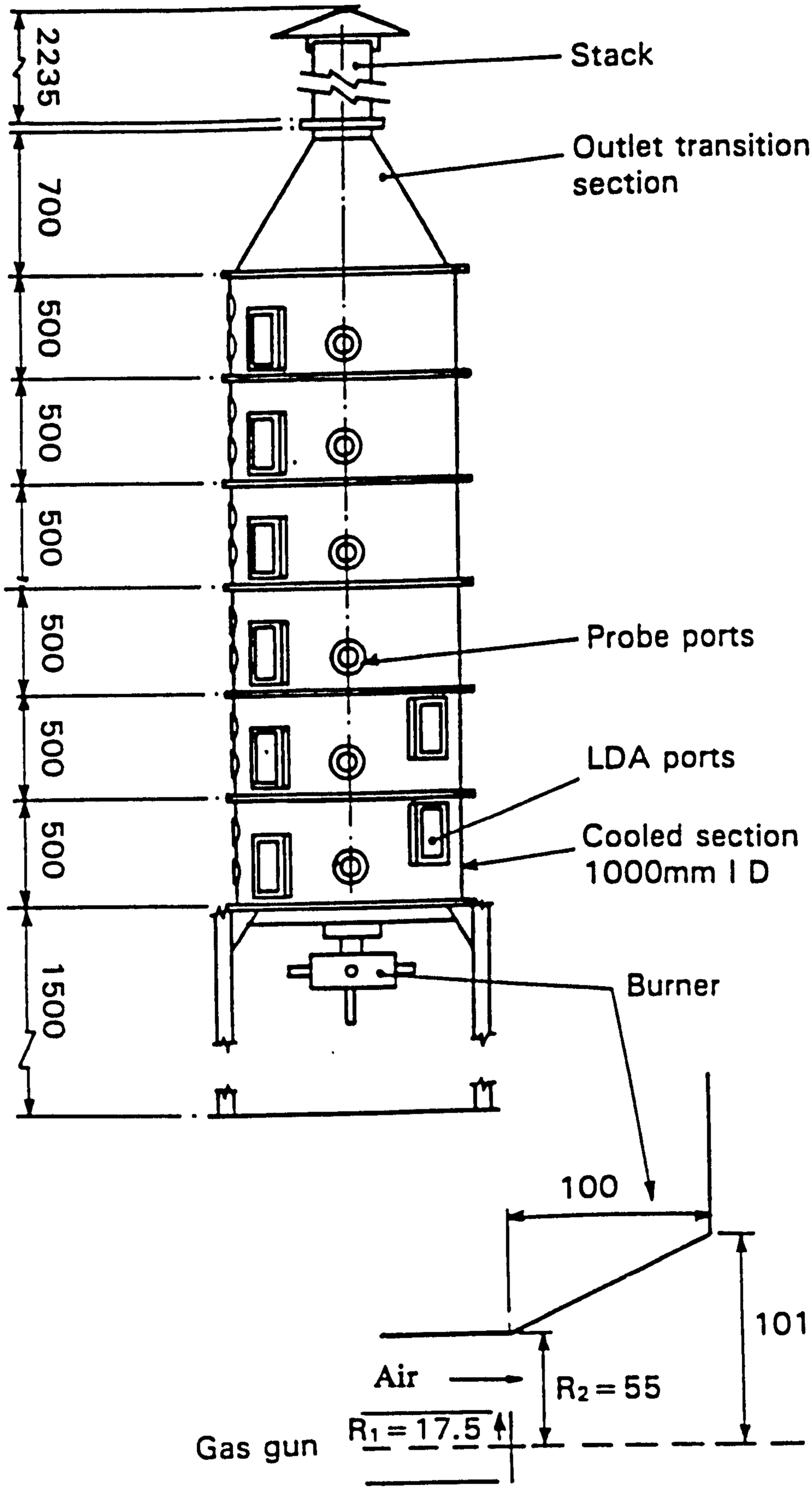

FIGURE 1 Schematic of furnace and burner

The fuel is injected radially outward from the centre of the air jet through 16 holes on the periphery of the fuel gun. Figure 1 illustrates the furnace and burner system. More details of the burner are given by Beltagui and Ralston (1985).

Four swirl settings were considered, with burner swirl number values, S = 0.0, 0.45, 0.9 and 2.25. Air and fuel flow rates were metered by orifice plates. The flow rates of air and fuel during each run were controlled to within ± 1%. Detailed natural gas analysis, obtained from British Gas, indicated that, over the period of the tests the main fuel properties were constant to within ± 2% for the calorific value and ± 1.2% for density and stoichiometric ratio.

In the first set of measurements the furnace firing rate was constant at 400 KW with 5% excess air. In the second set, firing rates of 400 KW and 360 KW were used with a wide range of fuel/air ratios, corresponding to a range of the equivalence ratio, ϕ of 0.71 to 1.1, (excess air 40% to -10%).

MEASUREMENTS AND INSTRUMENTATION

Radial traverses were carried out at 13 planes along the furnace, located at axial distances from the quarl exit of 45, 80, 110, 160, 200, 300, 545, 800, 1045, 1300, 1800, 2300 and 2800 mm.

Additional traverses were made at some of these planes along other radii to check the flow symmetry and probe intrusive effect. Repeatability tests were also performed. In each level the NO_x sampling probe was traversed for at least 1.5 radii to confirm the flow symmetry. The measurement points were spaced 20 to 50 mm according to the gradients of the NO_x concentration being measured. Between 13 and 26 measurement points were made in each plane.

The probe used in the measurements is a water cooled stainless steel probe. After leaving the probe, the gas sample passes through a heated sample line to the NO_x chemiluminescent analyser. The analyser calibration was checked before and after each traverse. The maximum drift in the calibration was within ± 2% of the full scale. The time-mean NO_x concentration values reported are those averaged over a period of 1 minute.

Although all the results are presented in terms of NO_x concentration, it should be appreciated that NO is the main constituent of the measured NO_x value.

The probe radial traverse and the data collection rate were all controlled by a microcomputer in conjunction with a specialised data acquisition system described by Beltagui and Ralston (1985).

Sampling Conditions

In order to obtain a representative sample, the chemical constitution of the sampled mixture should be maintained, by freezing all undergoing reactions within the sample. Cooling the sample down to a temperature of 300°C is sufficient to freeze these reactions (Chedaille and Braud, 1972).

Excessive, uncontrolled cooling of the gas sample could lead to water vapour condensation along the sampling system. The problem of surface absorption of NO_x on the probe and sample line is aggravated by the presence of absorbed films of moisture and hence is most serious when sampling wet gases from flames (Allen, 1973 and De Soete, 1989).

Furthermore, almost all gas analysers are subject to serious interference from water. The use of desiccants has been found to absorb nitrogen dioxide NO_2 to varying degrees. Cold traps also remove NO_2 and water vapour simultaneously (Allen, 1973).

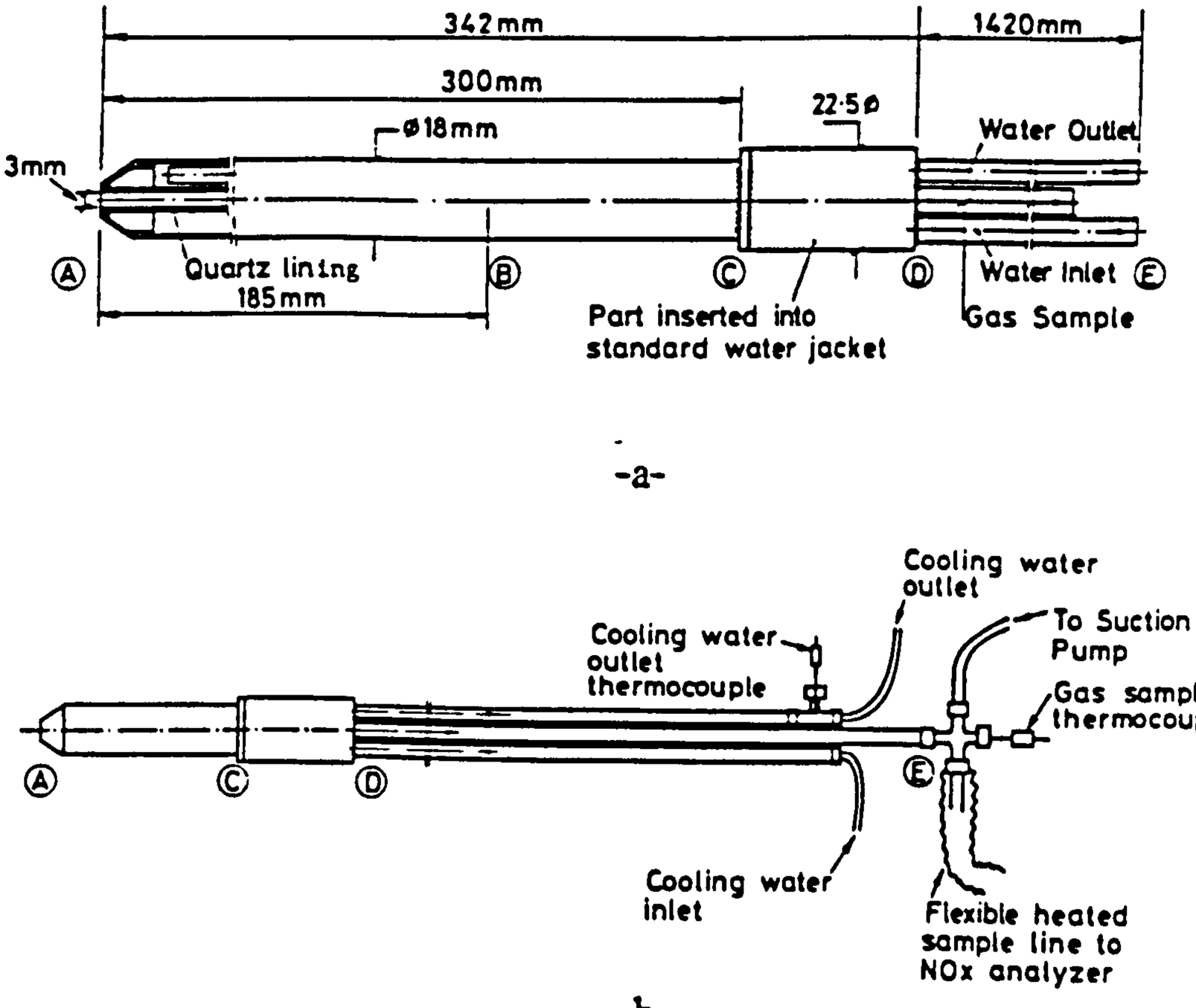

FIGURE 2 NO_x sampling system

The choice of probe material is also important for NO_x sampling to ensure no probe reactions or surface ageing with the sampled gas. A system of water cooled stainless steel probe and a teflon heated sample line was found satisfactory for NO_x measurements by Allen (1973) and Tuttle (1974). Stainless steel probes were also used satisfactorily by Oven *et al.* (1978), Sadakata *et al.* (1980), Ahmad *et al.* (1984) and Mulholland *et al.* (1987).

A water cooled stainless steel probe and a teflon sampling line were therefore used in the current measurements. The receiving part of the probe was lined with quartz to avoid the possibility of ageing especially at the high temperature region.

In order to withdraw a local representative sample, isokinetic sampling is generally recommended. However, in turbulent recirculating flows isokinetic sampling is difficult to achieve due to the large velocity fluctuations especially in the recirculating zones. In the present work, the suction velocity was adjusted to be of similar magnitude to the average flow velocity in the furnace.

Sampling Probe

Figure 2 shows the NO_x sampling system. The tip length A-C is exposed to the flame. The sample tube length D-E passes through a water-cooled probe carrier to convey the sample to the heated sample line. The probe cooling system was designed to control the sample gas temperature at D to 300°C and at E to close to 150°C.

Complete control on the sample temperature under all the operating conditions, without subjecting the probe to excessive heating, has been achieved through the following steps:

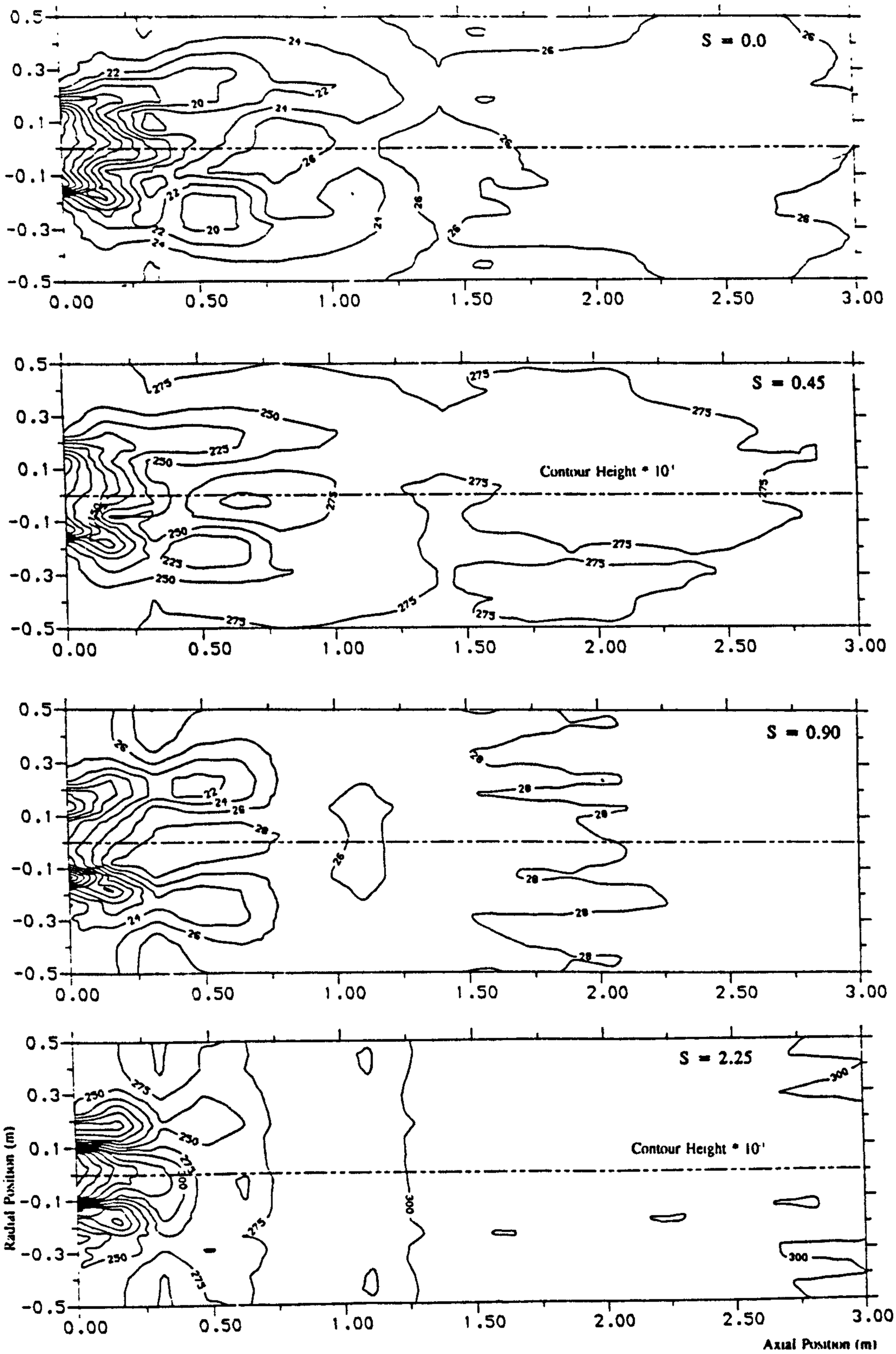

FIGURE 3 NO_x contours

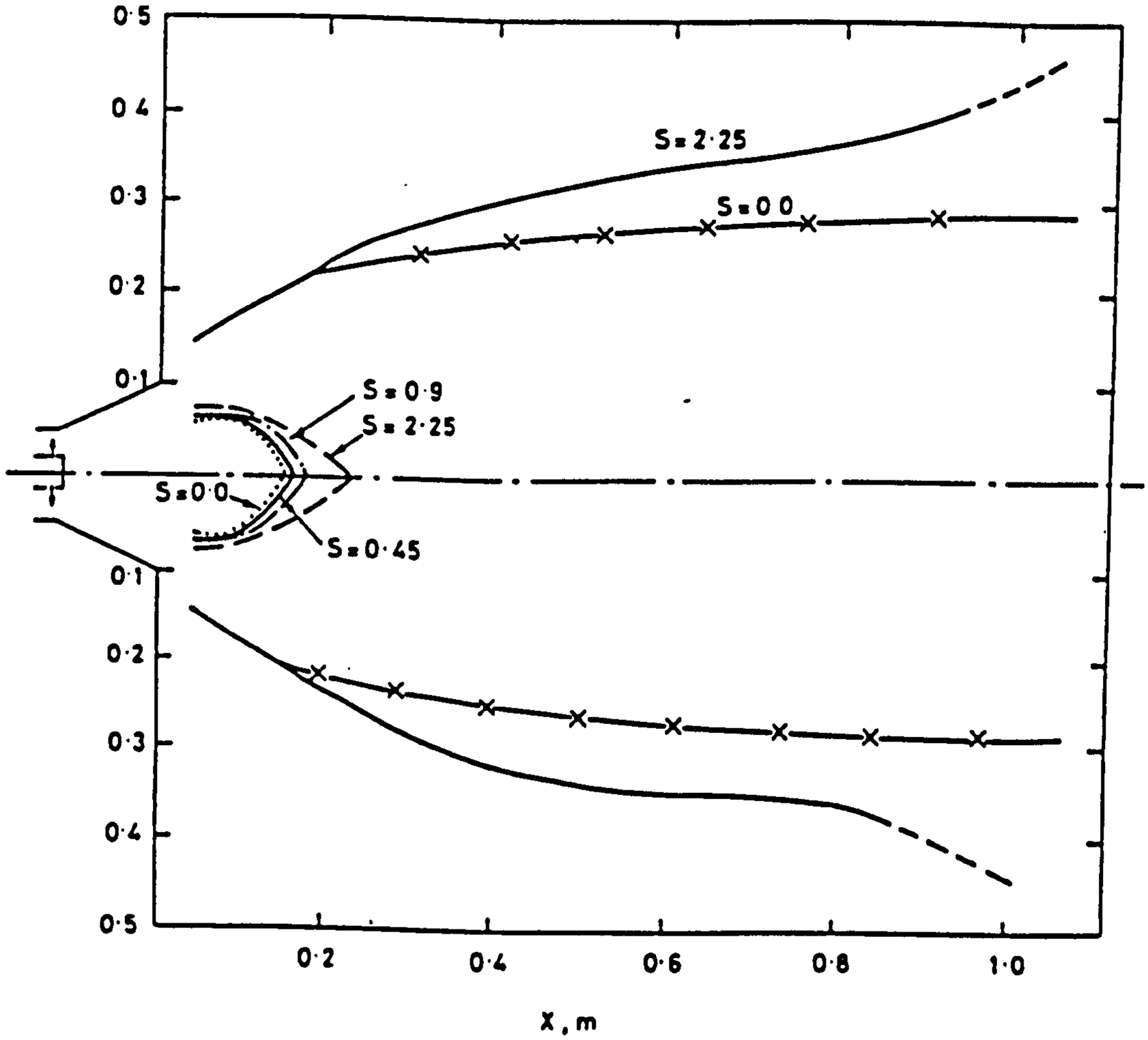

FIGURE 4 Flow boundaries

a—Controlling the cooling water temperature supplied to the probe.

b—Insulating the probe cooling water tubes in contact with the sample tube, length D-E.

c—To compensate for any further heat losses the sample tube D-E was electrically heated

Before the measurements were started, the probe performance was tested in the furnace under a range of operating conditions. Two thermocouples fitted to monitor the sample temperature at points D and E, gave readings within the probe design range.

EXPERIMENTAL RESULTS AND DISCUSSION

Before starting the detailed NO_x measurements and also at the conclusion of the series of measurements, tests were carried out to ensure repeatability of themeasurements. These tests were carried out at axial positions of 200 and 300 mm for all swirl settings. Repeatability of the measurements to within ± 2 ppm was obtained at all swirl settings.

The effect of probe presence in the flame on the local NO_x concentration was also investigated by traversing the probe through two ports, radially opposite, at the X = 200 mm plane. For all swirl numbers no flame disturbance by the probe was observed. Similar observations were reported by Oven *et al.* (1978) and Amad *et al.* (1984).

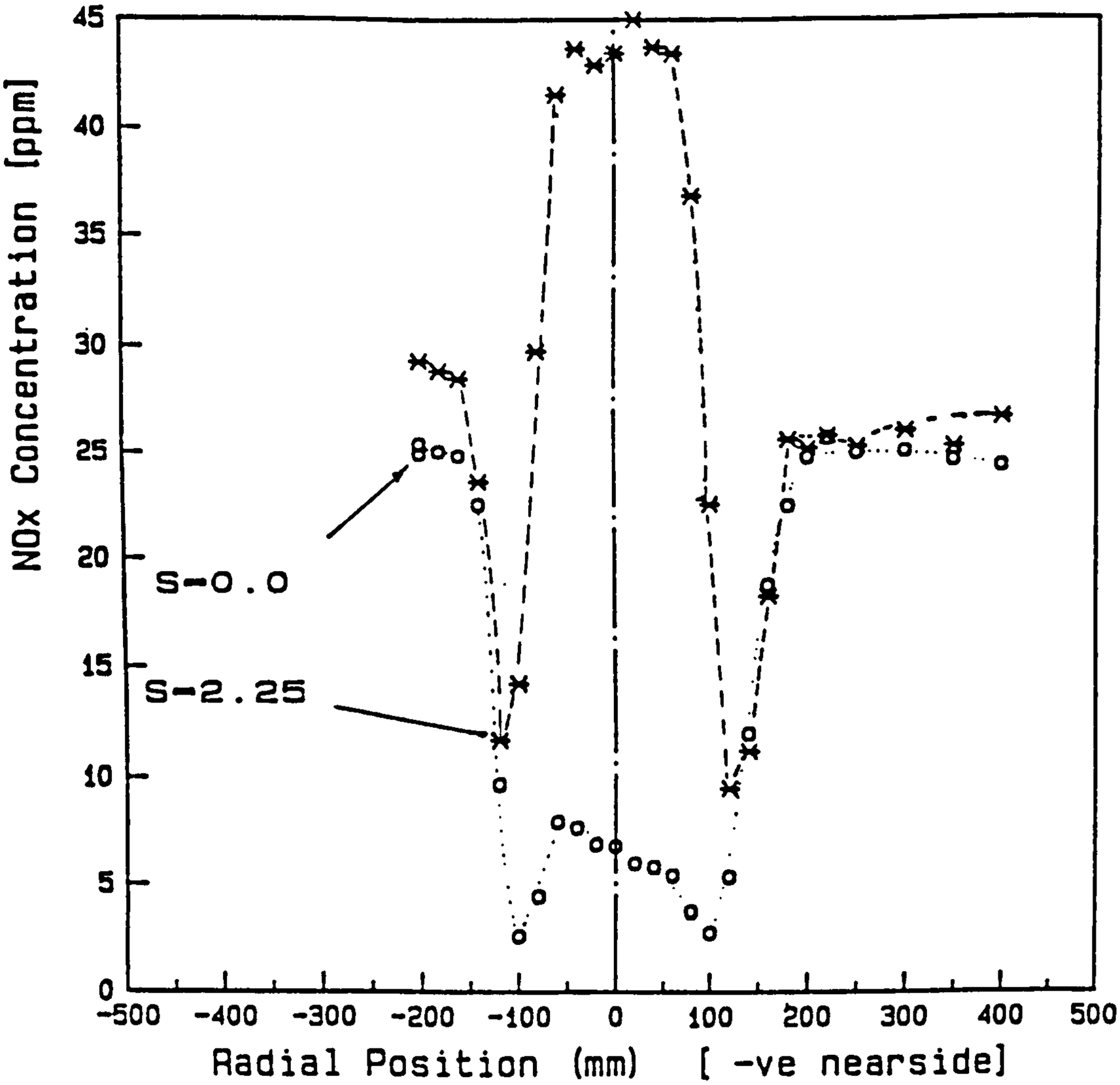

FIGURE 5-a Radial NO_x profile, axial position 45 mm

In-Furnace Measurements

The results of these measurements are presented in Figure 3 as contours of the NO_x concentration field for the four swirl settings surveyed. The above NO_x contours are discussed in relation with the experimental data for the flow and combustion fields reported earlier by Beltagui *et al.* (1991). Figure 4 illustrates the flow boundaries as determined from the flow field measurements, indicating the forward and reverse flow zones.

Some illustrative radial NO_x profiles at three planes near the burner are presented in Figures 5-7, together with the corresponding temperature profiles.

For the present discussion, the flow field can be divided into three zones:

1. The main reaction zone (forward flow zone)
2. The central reverse-flow zone (CRZ).
3. The fully developed flow zone

In general it is seen that most of the NO_x formation takes place in the first zone. Some further reactions occur in the second, leading to uniform concentration distributions in the third zone. The processes occurring in these zones are now discussed.

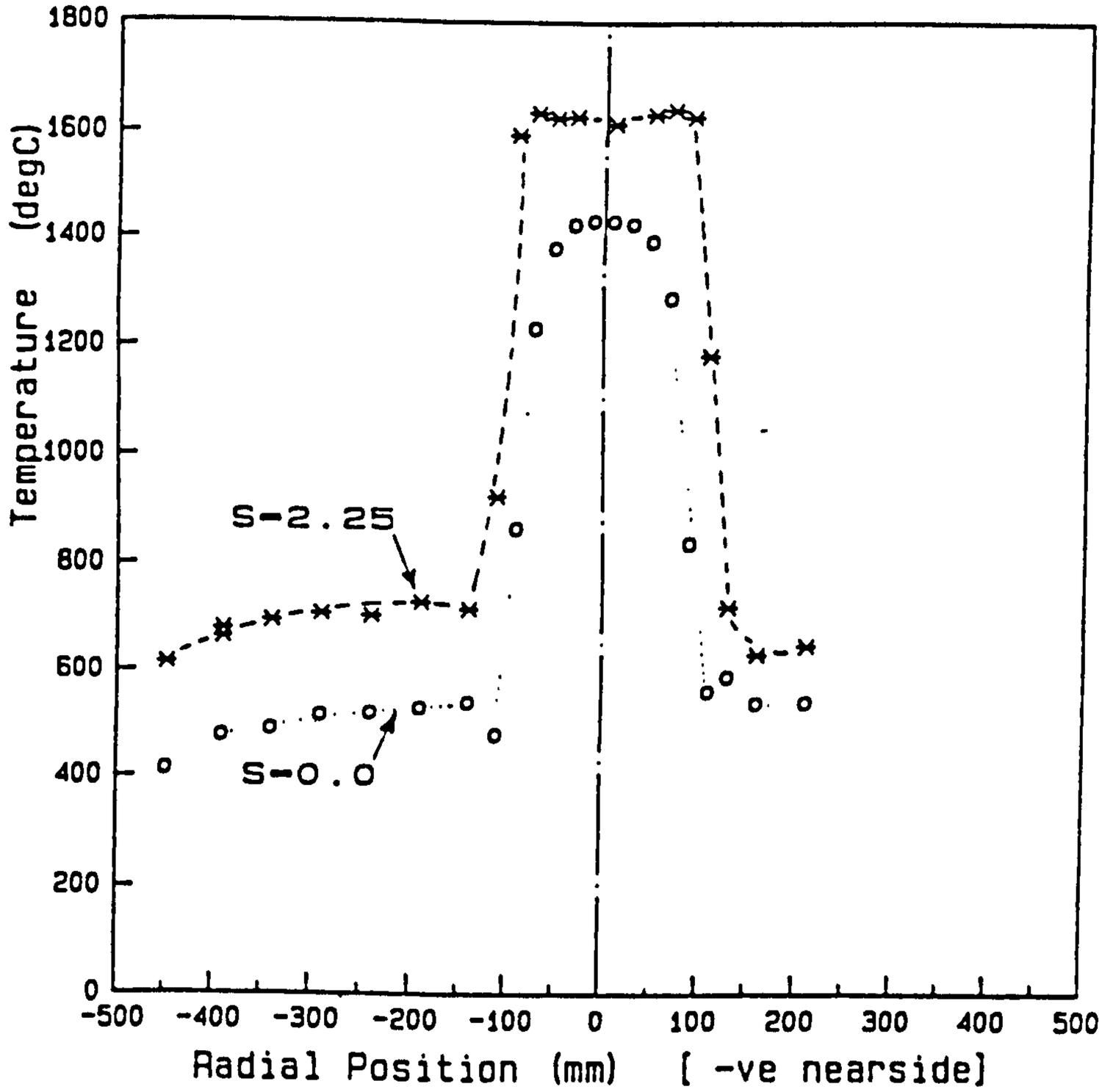

FIGURE 5-b Radial temperature profile, axial position 45 mm

The main reaction zone

This region covers the area containing the forward flow of the fresh mixture discharged from the burner. It is regarded as extending to the point where NO_x concentration becomes uniform across the whole radial profile. The length of the reaction zone decreases from 1.15 m to 0.42 m over the swirl range 0.0 to 2.25. This is in agreement with flame length values estimated from the measured CO concentration. Figures 5-7, show sample profiles of NO_x with those of temperature for three levels near the burner. The figures demonstrate the relation between NO_x concentration and temperature for the cases of swirl numbers 0.0 and 2.25. The main reaction zone is characterised by steep gradients of NO_x concentration in both the radial and axial directions. The rate of NO_x formation follows closely the rate of the main combustion reactions as indicated by the temperature and main species concentrations. The axial distance from the burner to the position of maximum NO_x concentration decreases as swirl is increased. Figure 8 illustrates this further where the minimum NO_x value at any plane is plotted versus the furnace length. The increase in the plane-minimum value of NO_x from one plane to the next indicates the newly formed NO_x. Radial profiles show higher NO_x concentrations on both sides of the minimum value due to mixing with the reverse flow on the boundaries of this region.

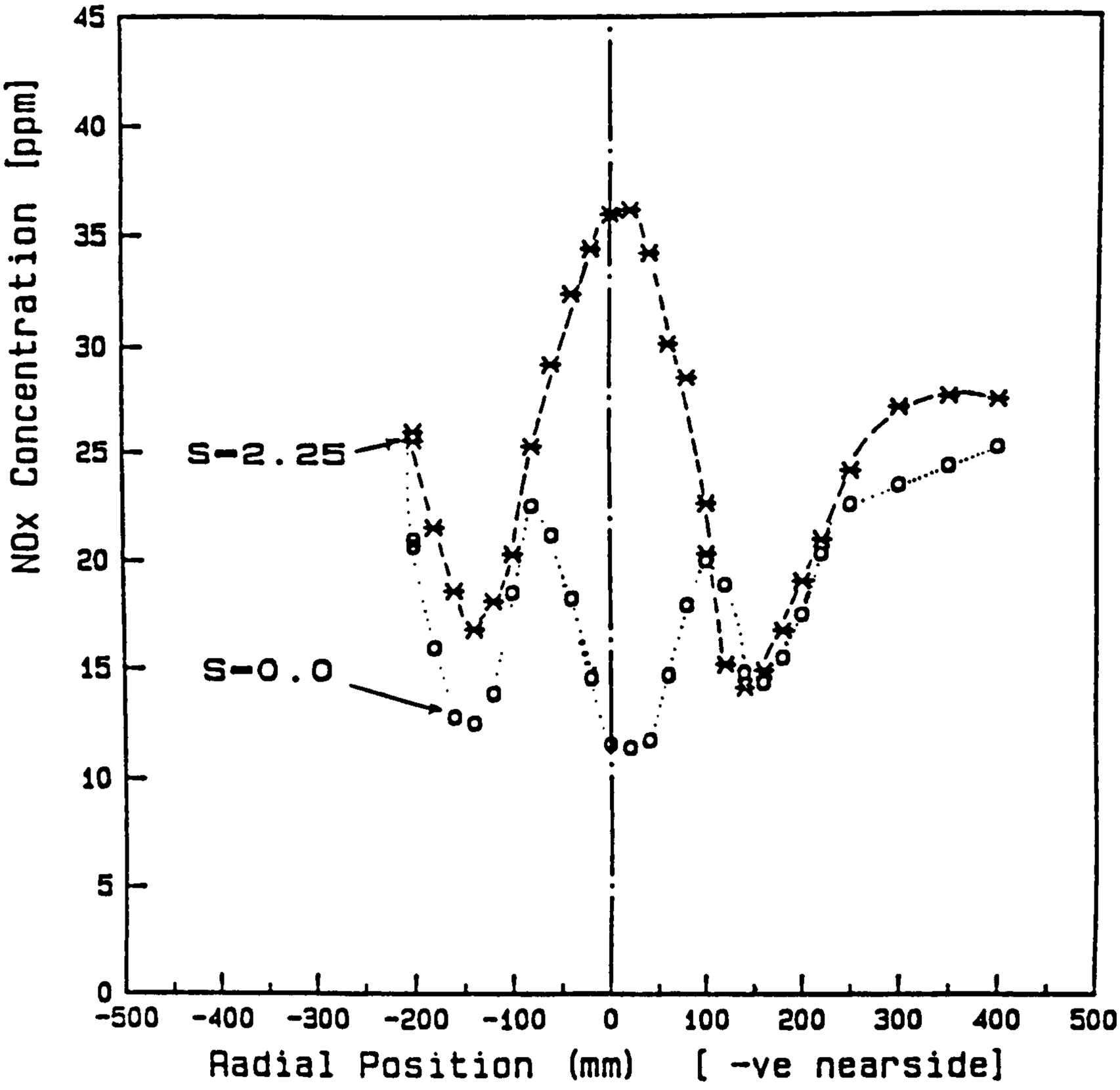

FIGURE 6-a Radial NO_x profile, axial position 200mm

Central reverse-flow zone

The flow entrained into this zone has come from the forward flow described above. Thus reactions here depend on the length of the CRZ relative to that of the reacting zone.

Figure 9 shows the variation of the NO_x concentration at the centreline with axial distance along the furnace.

For low swirl the CRZ is much shorter than the reaction zone, thus the CRZ receives a mixture with reactions still in progress and with low NO_x concentration and low temperature values. In this case it was found that no more NO_x reactions take place within this zone. A decrease of NO_x concentration occurs due to dilution with fresh mixture entrained nearer the burner end, Figure 9.

As swirl is increased the CRZ lengthens and the reaction zone shortens but is still longer than the CRZ. Thus gases with higher NO_x concentrations and at higher temperatures enter the CRZ where further NO_x reactions take place producing peak concentrations near the burner, as shown in Figure 9, with S=2.25.

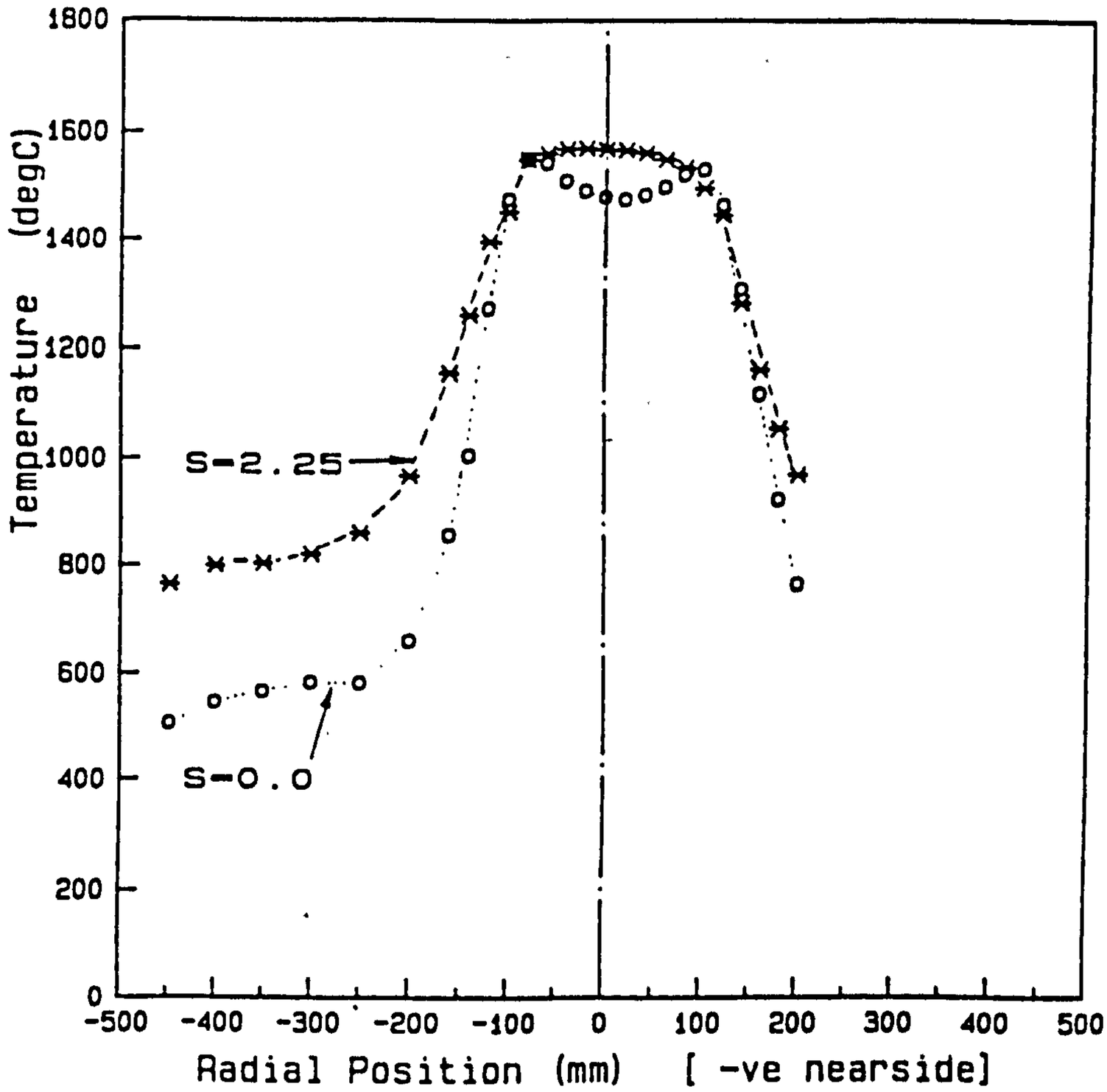

FIGURE 6-b Radial temperature profile, axial position 200 mm

Fully developed-flow zone

This region covers the fully developed forward flow downstream from the reaction zone and the reverse flow in the outer recirculating flow. At each swirl setting constant NO_x concentrations were measured throughout this region and these equal the value measured at the stack. This value varied from about 25 ppm to 30 ppm over the range of swirl studied (Figures 5-7). Within the outer reverse-flow zone some dilution of the flow occurs through entrainment from the forward flow giving lower NO_x concentrations at the planes nearer to the burner.

Discussion of the results

In the present system burning natural gas. NO_x is formed by the thermal mechanism. Some additional NO_x may be formed within the flame, as prompt NO_x. The present data was obtained in a lean flame with 5% excess air, thus little or no prompt NO_x is expected (eg Sarofim and Pohl, 1972, Semerjian and Vranos, 1976 and Williams, 1989).

The rate of thermal NO_x reaction is dependent on three parameters, namely temperature, O_2 concentration and residence time. The close relation between the temperature and NO_x profiles presented at Figures 5-7 confirms that NO_x has been formed by the thermal mechanism.

Turning now to the effect of swirl, the experimental results indicate that the overall effect of swirl on the final NO_x emission from the furnace is small. Over the range of

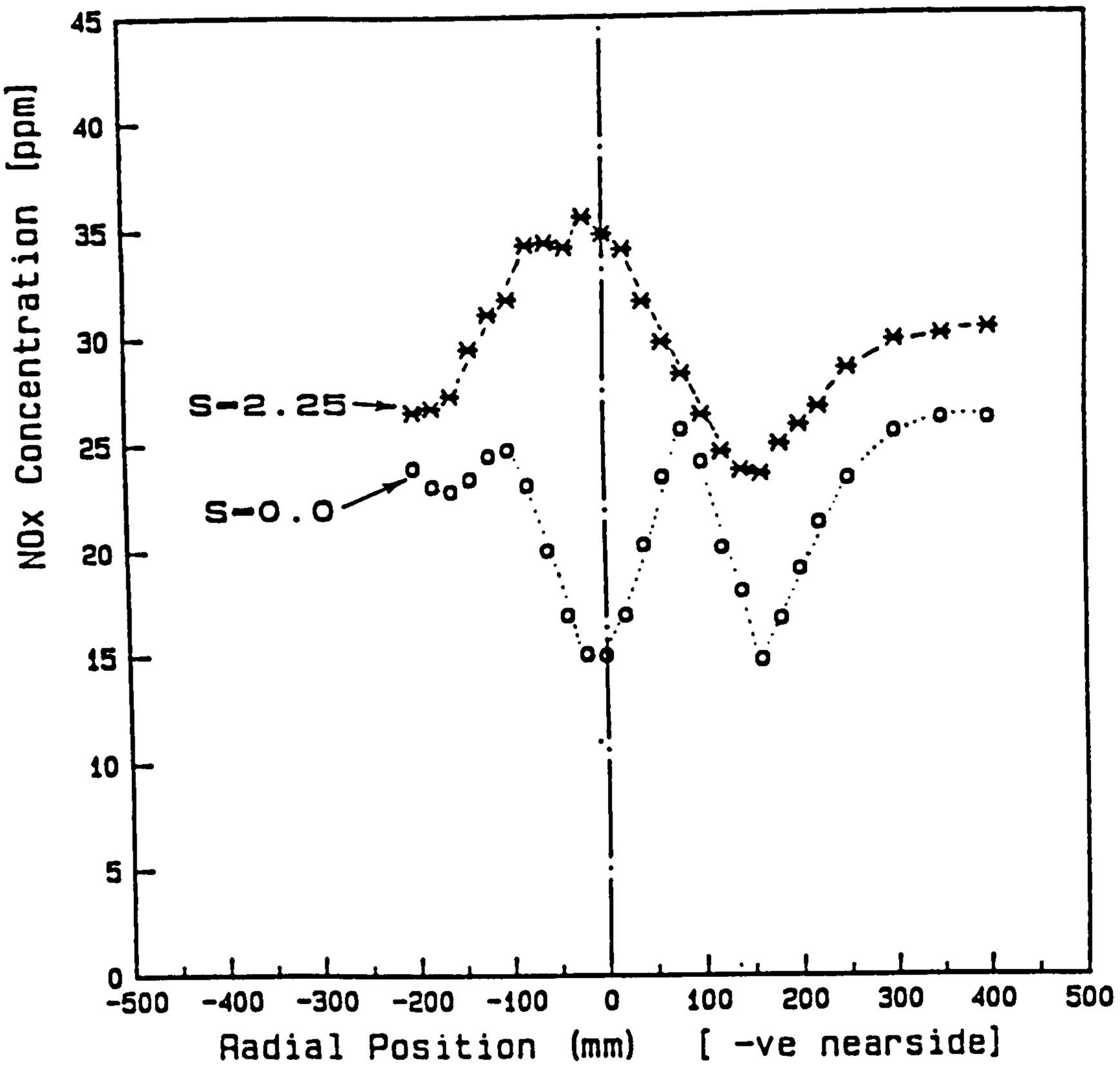

FIGURE 7-a Radial NO_x profile, axial position 300mm

swirl studied, swirl numbers 0 to 2.25, the stack NO_x concentration only varied from 25 to 30 ppm.

The NO_x formation in the forward flow reaction zone, as shown by Figure 8, is nearly the same for all swirls, as measured by the increase of NO_x over the length X = 0.045 to X = 1.15 m. The value of NO_x concentration near the burner is the result of flow from the CRZ mixing with the fresh flow.

Thus it can be assumed that all the increase in NO_x due to swirl is caused by the reactions taking place within the CRZ. These reactions seem to be most active in the highest swirl case (2.25) as illustrated by Figure 9.

Thus although swirl increases the rate of the main combustion reaction resulting in a shorter flame, it does not contribute to higher NO_x generation within the forward flow. This is due to the higher swirl giving reduced residence time in the shorter high temperature forward flow zone.

It is also realised that the mixing is affected more by the fuel injection system, than by swirl. The mixing pattern in the present system is governed by the radial fuel injection mode. This can be confirmed by the general similarity of the flow patterns obtained for all swirl cases tested, eg even for zero swirl a CRZ is created (Beltagui *et al.* 1989-a).

The use of different fuel injection modes produces different stability ranges and flow patterns, (Beltagui *et al.* 1988-b). The use of central axial fuel injection in this same

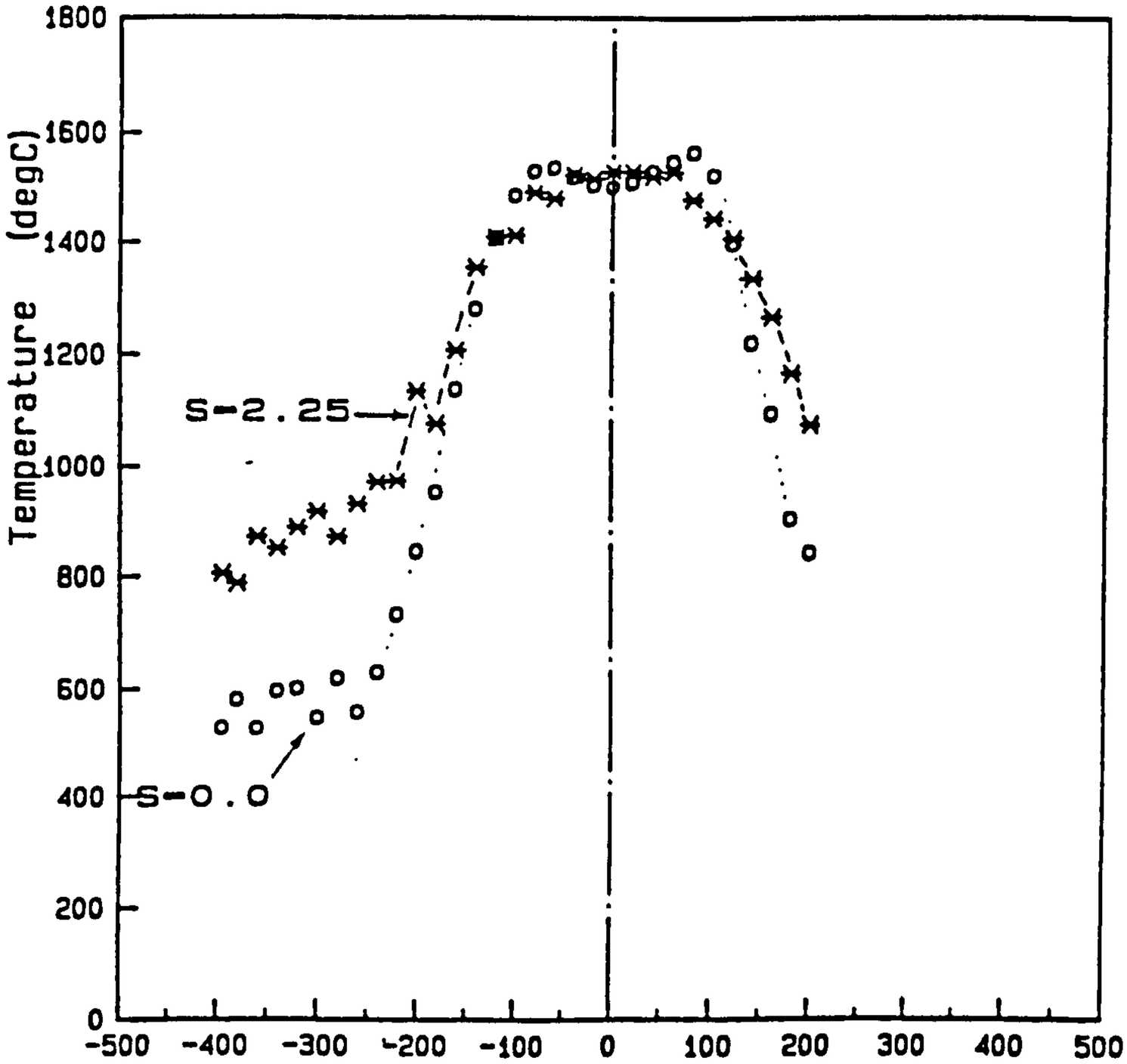

FIGURE 7-b Radial temperature profile, axial position 300 mm

burner system produced significantly lower NO_x emissions for the same swirl although the stability range was seriously reduced (Kenbar *et al.* 1991). Work by Andrews *et al.* (1988) and Al-Shaikhly *et al.* (1989) has also demonstrated the significant effect of fuel injection mode on NO_x formation.

NO_x Variation With Mixture Fuel/Air Ratio

The second set of measurements was aimed at finding the effect of fuel/air ratio upon NO_x formation as measured in the stack. The tests used initially the same input firing rate of 400 KW and covered the same swirl range as for the first set. The fuel equivalence ratio (ϕ) range was 0.71 to 1.10 (40% excess air to 10% deficient air respectively). These tests were also performed at the lower rate of 360 KW. The observed effect of this reduction upon NO_x formation is negligible.

The stack measured NO_x concentrations are given (in mg/Nm^3 corrected to 3% O_2) in Figure 10, for the four swirl settings tested. As discussed above the effect of swirl on the overall NO_x emissions is not significant, especially with the lean mixtures.

Lean mixtures

As the excess air was increased from 5% up to 40% ($\phi = 0.95 - 0.71$), the stack measured NO_x concentration increased in proportion to the excess air for all swirl settings (Figure

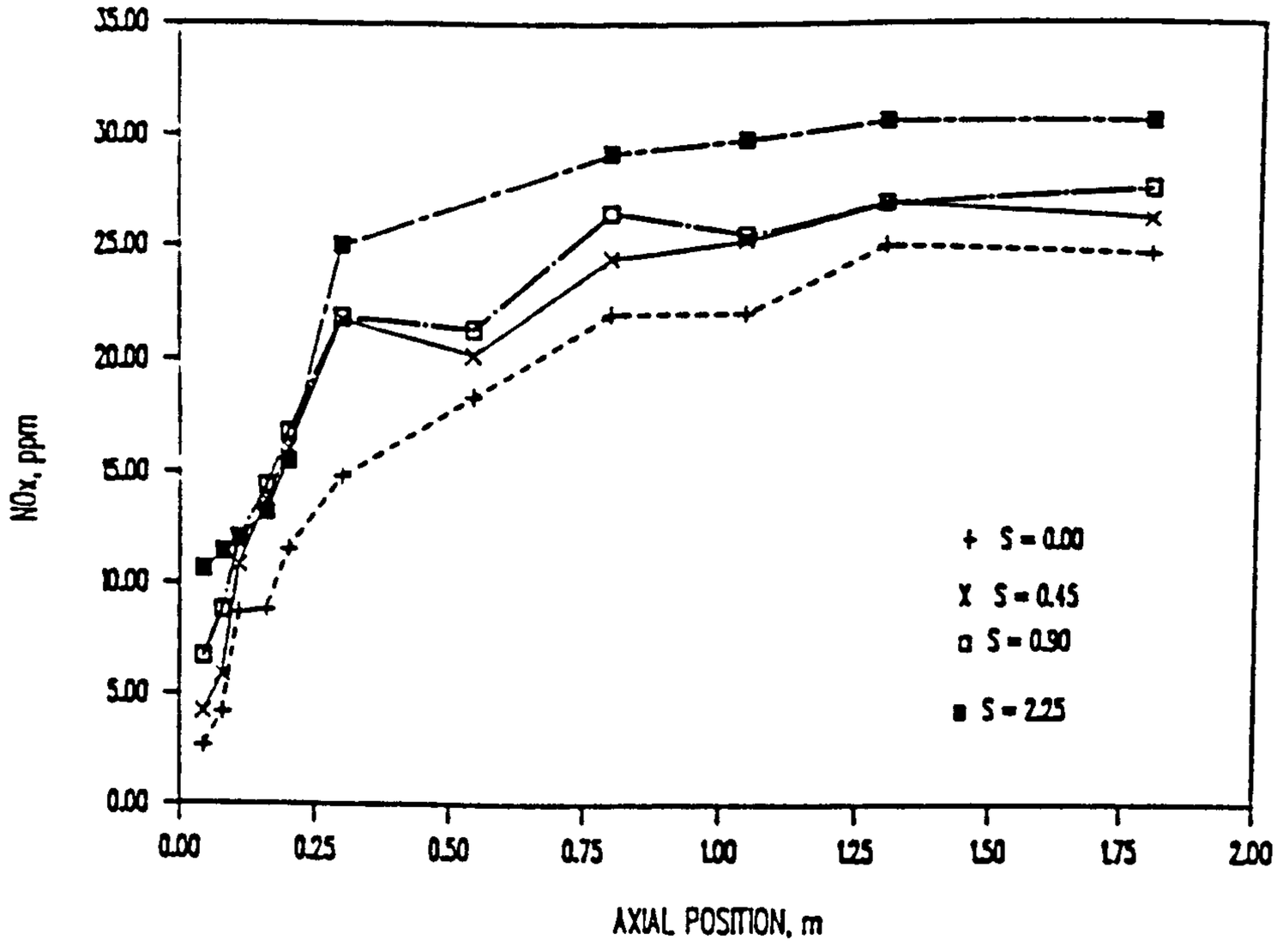

FIGURE 8 Variation of minimum NO_x concentrations along the furnace

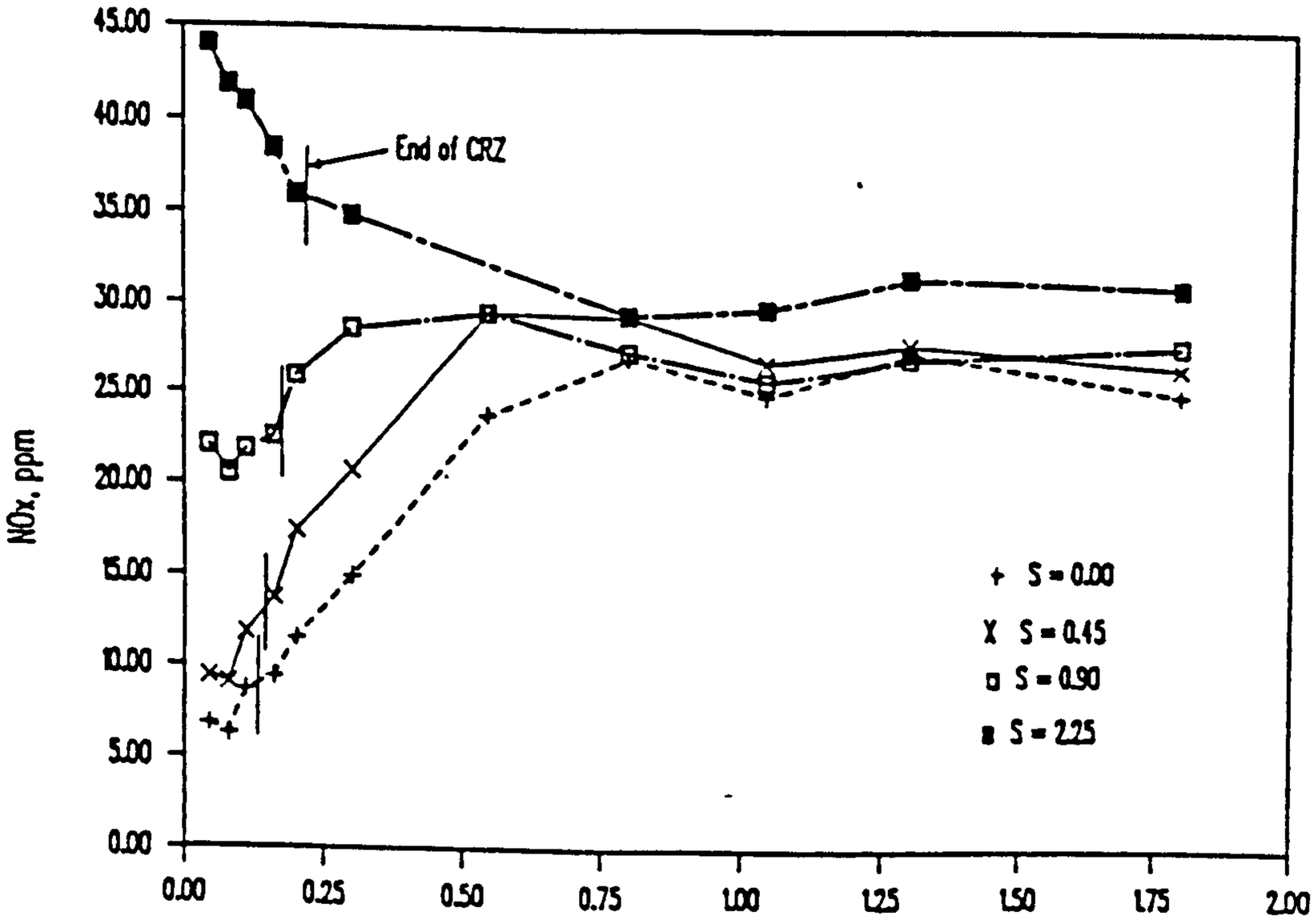

FIGURE 9 Variation of centreline NO_x concentrations along the furnace

10). This indicates that the effect of the increased air upon the local temperature of the NO_x reaction zone is minor, but there is an increase in NO_x due to the increased O_2 concentration.

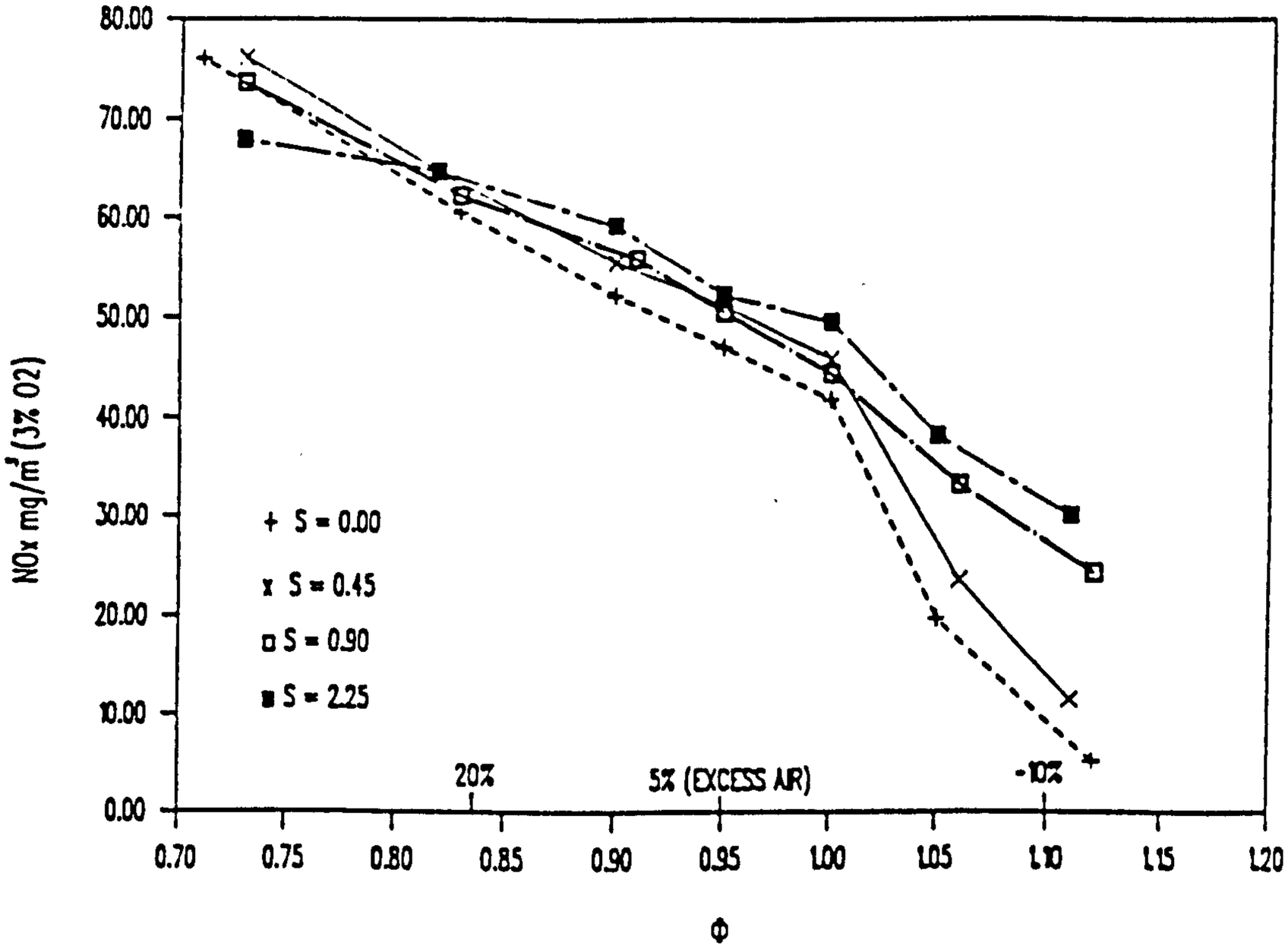

FIGURE 10 Variation of overall NO_x concentration (corrected to 3% O_2) with fuel equivalence ratio.

Rich mixtures

The measured NO_x emissions when burning fuel-rich mixtures with ϕ up to 1.11, are given by Figure 10. These results exhibit a very sharp decrease of NO_x as ϕ was increased, this decrease is more pronounced for the lower swirl settings.

The formation of NO_x occurs in localised regions where combustion products at adiabatic flame temperature and unused oxygen coexist. For rich mixtures the effects of lower temperature and lack of oxygen both work together towards reducing NO_x formation.

Some of the measured NO_x could be formed within the flame zone by the prompt mechanism although this is unlikely within the relatively modest maximum value of ϕ tested (1.1). The above results indicate that, for the present burner system, air staging is the only effective technique in reducing NO_x formation through combustion control.

MODELLING OF NO_x FORMATION

The aim of this modelling work is to produce a simple engineering model which can be used to predict the overall NO_x formation for furnaces. The model should be able to predict the variation of NO_x formation with input conditions, mainly fuel injection mode and equivalence ratio. The model is based on the well-stirred reactor concept with account being taken for local concentration fluctuations. The inputs to the model are limited to the residence time in the reaction zone and the fuel-air mixing parameter.

In a natural-gas fired furnace system NO_x is formed by fixation of atmospheric nitrogen. The main mechanism for this process is known to be the thermal one. This reaction mechanism, assumes post flame NO_x formation and is usually modelled by the Zeldovich equations. The rate of thermal NO_x reaction is dependent on three parameters, namely, temperature, O_2 concentration and residence time within the reaction zone.

It is widely acknowledged that the fluctuations in temperature and O_2 concentration have to be taken into account when calculating thermal NO_x, especially in continuous combustion systems such as gas turbines and furnaces.

Thermal NO Model

The thermal NO formation rate, based on the extended Zeldovich mechanism, is well established. The rate equation was reduced by Beltagui *et al.* (1989-b) to the form:

$$\frac{d\,\mathrm{NO}}{d\,t} = 1.44 \times 10^{17}[\mathrm{N2}][\mathrm{O2}]^{1/2}(T)^{-1/2}\ \exp\left(-69460/T\right)\ mole/cm^3 \qquad (1)$$

The application of this equation requires values of all the variables in the RHS as they exist within the NO reaction zone. Since the rate of this reaction is slower than the main combustion reactions, it is possible to assume that reactions of the main species progress to completion before NO reactions start. Thus the values of temperature and concentrations of O_2 and N_2 can be calculated.

However when using measured time-averaged temperatures it was found that NO was underpredicted, sometimes by two orders of magnitude (Sadakata and Beer, 1976). In the present work the predicted NO values were one order of magnitude lower than those measured. The explanation for these underpredictions lies in the existence of concentrations and temperature fluctuations within the NO reaction zone.

The earlier attempts to measure these fluctuations were limited by the speed of response of thermocouples. Generally this is too slow to follow the temperature fluctuations beyond 1 kHz (Sadakata and Beer, 1976).

Recent measurements using CARS technique give a much better indication of the range of the temperature fluctuations, for example LaRue *et al.* (1984) measured a 500 K peak to peak range.

These temperature fluctuations are caused by concentration fluctuations. Since the NO reactions take place "immediately" after the main reactions, both temperature and concentration fluctuations have a considerable influence on the NO formation rate.

On the other hand, it is suggested by some investigators that the temperature in the NO reaction zone is the stoichiometric adiabatic flame temperature (Toof, 1986 and Takagi *et al.* 1976). Vranos (1974) assumed that the thermal NO reactions are not faster than the mixing rates so most thermal NO is formed at or near $\phi = 1.0$. This assumption follows from the fact that stoichiometric mixtures have the highest probability of reaction.

When using finite difference solutions of the flow and combustion equations, eg. PCOC (Stopford, 1989), the effect of concentration fluctuations can be taken into consideration through the solution of an extra differential equation (Elghobashi and Pun, 1974). For the present work considering a well-stirred reactor model, a stochastic approach was adopted to estimate the fluctuating components of concentration about the mean value.

Model Assumptions

Assuming the reaction zone to be one well-stirred reactor and using Equation 1, the following analysis is carried out to account for the effect of concentration fluctuations.

On the microscale of mixing, it is assumed that at any location within the well-stirred reactor, the fuel air mixture will have a random distribution of parcels with values of ϕ which have a Gaussian distribution about the mean value $\bar{\phi}$. This assumption agrees with experimental measurements in jet flows as reviewed by Chatwin and Sullivan (1990). The spread of this distribution is dependant upon the value of the standard deviation σ. The value of σ is linked to the mixedness, s, of the mixture by the relation (Appleton and Heywood, 1972 and Fletcher, 1973):

$$\sigma = (1 - s)\bar{\phi} \tag{2}$$

Introducing Z as a non-dimensional parameter of fluctuation gives:

$$Z = (\phi - \bar{\phi}) / \sigma \tag{3}$$

The probability density function (p.d.f.) of the distribution function of ϕ is written as:

$$f(\phi) = (2\pi)^{-1/2} \exp\left(-Z^2/2\right) \tag{4}$$

Integrating the area under the above distribution function, leads to the cumulative density function (c.d.f.) of ϕ:

$$F(\phi) = \int_{-\infty}^{\phi} (2\pi)^{-1/2} \exp\left(-Z^2/2\right) dZ \quad -[\infty < \phi < \infty \tag{5}$$

For standard Gaussian distribution, the value of $F(\phi)$ is usually between 0 and 1. A stochastic process (Kenbar, 1988) has been implemented to produce the variable Z from Equation 5 using randomly generated values of $F(\phi)$ using an appropriate random number generator. From Equation 3 above and at known values of $\bar{\phi}$ and σ the stochastic value of ϕ has been predicted. This process gives the Gaussian distribution of ϕ about $\bar{\phi}$.

Of the different parcels, those with ϕ close to unity (ie stoichiometric) have the maximum probability of combustion and thus react first. The products of this reaction will be at the adiabatic stoichiometric flame temperature. The NO reaction will take place effectively at this flame temperature. The required oxygen is assumed to come from the excess air of the unburnt lean parcels with $\phi < 1$. These values are substituted in Equation 1.

Finally a mean value of residence time in the reaction zone was calculated for each swirl case from the length and the average flow velocity in the reaction zone.

Prompt NO_x

Although prompt NO_x was initially defined as NO_x formed in the flame front, it sometimes refers to NO_x resulting from N_2 via reactions other than the Zeldovich mechanism. Detailed models of prompt NO_x are not available yet, because the amounts of prompt NO_x are small compared to other sources of NO_x, and because it seems to occur mainly in very rich flames. It can be important in fuel-rich pockets of diffusion flames. Rate equations were suggested by Fenimore (1970) and De Soete (1974).

In the present analysis both equations were used to estimate prompt NO_x. The results indicate the contribution by this mechanism to be very small, less than 1 ppm.

Model Results

The above model was tested by application to the conditions of the stack measurements to predict the effect of fuel/air ratio (equivalence ratio) on the overall NO_x emission from the furnace. The value for the standard deviation σ can be estimated from the measurements of the fluctuations of concentrations and temperatures in jet flows, as

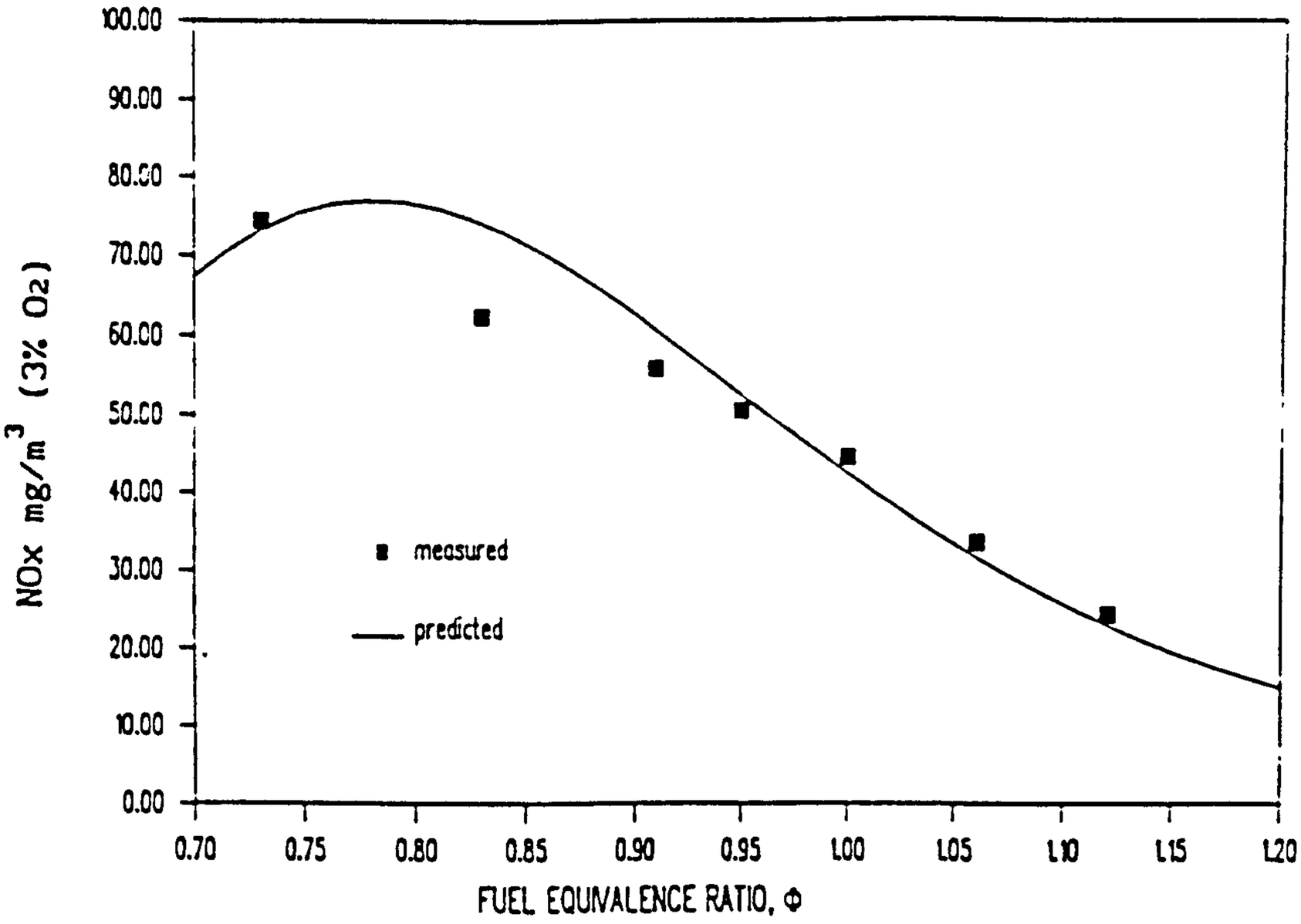

FIGURE 11 Comparison of predicted and measured NO_x concentration, S = 0.90

reported by Becker (1974). His results give an estimated value of 0.70 for the mixing parameter s in Equation 2.

The results for the medium swirl case with S = 0.90 are presented in Figure 11. The agreement between the model predictions and measurements is considered satisfactory and very encouraging considering the simplicity of treating the reaction zone as one well-stirred reactor. As earlier stated, the observed effect of swirl on NO_x formation in the present system is small and therefore could not be used as a reliable test of this model. The model is also being used to model other fuel injection modes. The input data required are only the mixedness of the fuel-air jets and the mean residence time within the reaction zone.

CONCLUSIONS

Two sets of experimental measurements have been carried out in the NEL furnace, when using a variable swirl burner with central radial fuel injection. The first set covers a complete mapping of NO_x concentrations carried out at different swirl settings. In the second set, the effect of fuel/air ratio on the overall NO_x emissions in the stack has been measured.

The reliability of these measurements has been checked by carrying out tests of repeatability and of the probe intrusion effect. NO_x concentration profiles have shown reasonable degree of symmetry. This is important for the meaningful comparison with the axisymmetric numerical predictions.

From the experimental measurements the following conclusions can be drawn:

1— NO_x formation occurred mainly at the high temperature regions downstream of the combustion zone (flame front), hence confirming that NO_x has been formed by thermal reactions which follow the main combustion.

2— For the present burner system, increased swirl did not contribute significantly to increased stack NO_x emissions. At zero swirl, NO_x concentration measured at the stack was about 25 ppm while at the high swirl (S=2.25). NO_x concentration was about 30 ppm.

3— Increased swirl has contributed only to increased local NO_x concentrations in the central recirculation zone.

4— Increasing excess air, from zero up to 40%, led to a slightly more than proportionate increase in the NO_x emissions.

5— At rich flame conditions, increased fuel equivalence ratio resulted in marked reduction of NO_x emission. This finding supports the use of air-staged combustion for NO_x reduction.

Theoretical predictions of the overall NO_x formation under the above test conditions have been made using a well-stirred reactor model based on the extended Zeldovich mechanism. The model takes account of the fluctuations of the concentrations of fuel and oxidant in the NO_x reaction zone. A stochastic analysis has been adopted to calculate the effect of these fluctuations on the NO_x formation rate. The results of these predictions compare satisfactorily with the measurements and confirm the relationship between NO_x formation and equivalence ratio.

ACKNOWLEDGEMENTS

The authors wish to thank colleagues at the National Engineering Laboratory (NEL) and the University of Glasgow for their advice and encouragement. This work was supported in part by the Management Board of NEL.

REFERENCES

Ahmad, N. T., Andrews, G. E., Kowkabi, M. and Sharif, S. F. (1984). Centrifugal mixing forces in enclosed swirl flames. *20th Symp. (Int.) on Combustion*, pp 259-267.

Allen, J. D. (1973). A review of methods of analysis for oxides of Nitrogen. *J. Inst. of Fuel*, **46**, pp. 123-133.

Al-Shaikhly, A. F. A., Andrews, G. E. and Aniagolu, C. O. (1989). Jet shear layer turbulent diffusion flames for ultra-low NO_x emission. Joint meeting of the British and French Sections of The Combustion Institute, Rouen, pp. 5-8.

Andrews, G. E., Abdul Aziz, M. M., Abdul Hussain U. S. *et al.* (1988). High intensity burner with low NO_x emissions. British Flame Days, Furnace Combustion Research and Its Applications, The Institute of Energy, London.

Appelton, J. P. and Heywood, J. B. (1972). The effects of imperfect fuel-air mixing in a burner on NO formation from nitrogen in the air. *14th Symp. (Int.) on Combustion*, pp. 777-786.

Becker, H. A. (1974). Effects of concentration fluctuations in turbulent diffusion flames. *15th Symp. (Int.) on Combustion*, pp 601-615.

Beltagui, S. A. and Ralston, T. (1985). An isothermal model study of aerodynamics and mixing in the flow issuing from a variable-swirl burner. *HTFS Research Symp.*, RS 602, NEL/HTFS 63, also NEL Report DC/355.

Beltagui, S. A., Fuggle, R. N. and Ralston, T. (1988-a). Measurement and prediction of heat transfer in the NEL furnace. I.Mech.E./I.Chem.E./Heat Transfer Society, *2nd UK National Heat Transfer Conference, Glasgow*, pp. 1219-1232, Mechanical Engineering Publications.

Beltagui, S. A., Maccallum, N. R. L. and Ralston, T. (1988-b). The effect of fuel injection modes on combustion. British Flame Days, Imperial College, London.

Beltagui, S. A., Kenbar, A. M. A. and Maccallum, N. R. L. (1989-b). NO_x generation and control in confined swirling flames—review and parametric study. *HTFS Research Symp.*, RS 827, NEL/HTFS 123.

Beltagui, S. A., Fuggle, R. N., Kenbar, A. M. A., Ralston, T., Marriott, N. and Stopford, P. J. (1991). Modelling a gas-fired furnace using the PCOC code. Paper accepted for presentation at the Euroteck Direct 91, Birmingham, 2-4 July.

Chatwin, P. C. and Sullivan, A. N. (1990). A simple and unifying physical interpretation of scalar fluctuation measurements from many turbulent shear flows. *J. Fluid Mech.*, **212**, pp. 533-556.

Cheadaille, J. and Braud, Y. (1972). Industrial Flames. Vol. 1, Measurements in flames. Edward Arnold Publishers, London.

De Soete, G. G. (1974). Overall reaction rates of NO and N_2 formation from fuel nitrogen. *15th Symp. (Int.) on Combustion*, pp 1093-1102.

De Soete, G. G. (1989). N_2O analysis techniques: Gas chromatography with EC detection: sampling techniques. 1st topic Oriental meeting TOTeM1, IFRF, Amsterdam.

Elghobashi, S. E. and Pun, W. M. (1974). A theoretical and experimental study of turbulent diffusion flames in cylindrical furnaces. *15th Symp. (Int.) on Combustion*, pp. 1353-1365.

Fenimore, C. P. (1970). Formation of nitric oxide in premixed hydrocarbon flames. *13th Symp. (Int.) on Combustion*, pp. 373-380.

Fletcher, R. S. (1973). The prediction of nitric oxide formation in combustion systems. *1st European Symp. on Combustion*, Sheffield, pp. 445-450.

Kenbar, A. M. A., Beltagui, S. A. and Maccallum, N. R. L. (1991). Effect of fuel injection modes on the combustion patterns and pollution formation in the NEL furnace. *HTFS Research Symp.*, RS 877, NEL/HTFS 146, pp.183-206.

Kenbar, A. M. A. (1988). MSc thesis, Dept. of Mech. Eng., University of Glasgow.

LaRue, J. C., Samuelsen, G. S. and Seiler, E. T. (1984). Momentum and heat flux in a swirl-stabilized combustor. *20th Symp. (Int.) on Combustion*, pp. 277-285.

Mulholland, J. A. and Hall, R. E. (1987). Fuel oil reburning application for NO_x control to fire tube package boilers. *J. Eng. Gas Turbine Power*, **109**, pp. 207-214.

Oven, M. J., Gouldin, F. C. and McLean, W. J. (1978). Temperature and species concentration measurements in a swirl-stabilized combustor. *17th Symp. (Int.) on Combustion*, pp. 363-374.

Sadakata, M. and Beer, J. M. (1976). Spatial distribution of Nitric Oxide formation rates in a swirling turbulent methane-air flame. *16th Symp. (Int.) on Combustion*, pp. 93-103.

Sadakata, M., Fujioka, Y. and Kunii, D. (1980). Effects of air preheating on emissions of NO, HCN and NH_3 from a tow-staged combustor. *18th Symp. (Int.) on Combustion*, pp. 65-72.

Sarofim, A. F. and Pohl, J. H. (1972). Kinetics of Nitric Oxide formation in premixed laminar flames. *14th Symp. (Int.) on Combustion*, pp. 739-754.

Semerjian, H. and Vranos, A. (1976). NO_x formation in premixed turbulent flames. *16th Symp. (Int.) on Combustion*, pp. 169-179.

Stopford, P. J. (1989). PCOC Users Manual, AERE-R12626.

Takagi, T., Ogasawara, M. and Daizo, M. (1976). NO_x formation from nitrogen in fuel and air during turbulent diffusion combustion. *16th Symp. (Int.) on Combustion*, pp 181-189.

Toof, J. L. (1986). A model for the prediction of thermal, prompt and fuel NO_x emission from combustion turbine. *ASME J. Eng. Gas Turbine and Power*, **108**, pp. 340-347.

Tuttle, J. H., Shisler, R. A. and Mellor, A. M. (1974). Nitrogen Dioxide formation in gas turbine engine: Measurements and measurement methods. *Comb. Sci. and Tech.*, **9**, pp. 261-271.

Vranos, A. (1974). Turbulent mixing and NO_x formation in gas combustors. *Combustion and Flame*, **22**, pp. 253-258.

Williams, A. (1989). Combustion-Generated NO_x. Joint meeting of the British and French Sections of The Combustion Institute, Rouen, pp. A1-A11.

MEASUREMENT OF CO AND NO_x POLLUTANTS IN A GAS-FIRED FURNACE

N.R.L. Maccallum [1], S.A. Beltagui [1,2] and A.M.A. Kenbar [1,2]

1. University of Glasgow, UK
2. National Engineering Laboratory, East Kilbride, UK

Paper presented to:

"Measurement and Control Techniques on Environmental Protection" Symposium, Technical University of Budapest, 7 - 9 June 1993.

1. INTRODUCTION

This paper describes the instrumentation and sampling probes used for measuring levels of pollutants in a gas-fired furnace.

The Furnace and the range of Burners used have been described in another Paper to this Symposium (Ref. 1). The pollutants of importance are CO, NO_x and HC. In order to assist the understanding of how these pollutants are formed, measurements were also made of CO_2, O_2 and of the velocity components and temperature.

2. GAS SAMPLER

2.1 Design of Sampler

For sampling for NO_x there are a number of conditions that must be satisfied:

(i) The chemical constitution of the sampled mixture must be retained at the composition which it had when it was withdrawn from the gas stream in the furnace. So the evolution process must be stopped quickly - hence the design is aimed to cool the sample quickly to below 300^0C.

(ii) Excessive cooling leads to condensation of water vapour and this water will absorb NO_x. So condensation must be avoided. Dessicants which absorb H_2O also absorb NO_2. Cold traps take out water but also absorb NO_2. The solution adopted in the present work is to ensure that the sample temperature does not drop below 150^0C.

(iii) Probe material must not react with sample.

(iv) Probe material should not age.

The probe used was designed to meet the above conditions. It is shown in Fig. 1. The probe itself is in stainless steel and the receiving portion, where the gases are hottest, is lined with a quartz tube to minimise ageing. The water cooling system is controlled so that the sample gas temperature is not above 300^0C at D (Fig. 1) and also not below 150^0C at E, the temperatures at these locations being continuously monitored by thermocouples. The control was achieved thus - the temperature of the cooling water supply was increased by mixing in some of the hot-water return if the temperature of the sample at E was dropping below 150^0C. The cooling water inlet flow rate was controlled to keep the temperature at D below 300^0C.

2.2 Sampling Flow Rate

Ideally the entry opening into the sampler should face the flow direction and the velocity with which the sample enters the probe should equal the magnitude of the flow velocity - iso-kinetic sampling. However in the highly turbulent reaction zones being examined in furnaces or combustors, there are very substantial fluctuations in flow velocity and direction. For simplicity, in the present work which is studying the combustion of a gaseous fuel, a constant sampling velocity of 15 m/s has been used. As a check, in some cases this sampling velocity was changed by more than a factor of 2:1. This change had no influence on the composition of the sample extracted from a particular location. Thus it appears that, when burning gaseous fuels, a wide range of sampling velocity can be used. The velocity of 15 m/s allowed reasonably rapid purging of the analysers between readings being taken.

3. ANALYSERS

3.1 NO_x

This was measured by a Chemiluminescent Analyser (Analysis Automation Limited, Type AAL 443). As this measures NO, the sample was first passed through a catalytic converter which converted NO_2 to NO. Thus the Analyser gave the value of total NO_x.

3.2 CO, CO_2 and HC

CO and CO_2 were measured by infra-red gas analysers - Analytic Development Company 3M/24-4052 and 4L/24-4051 respectively.

Flame Ionisation

Unburned HC was measured by a Hydrocarbon Analyser (Signal, Series 3000).

3.3 Calibrations

Calibrations of all analysers were checked, at least daily, against standard gases of known composition.

4. USE OF SAMPLING AND ANALYSING EQUIPMENT

The equipment was used extensively in the testing of the Gas-Fired Furnace reported in Ref. 1. The performance of the equipment was very satisfactory and results were repeatable.

The results obtained have been very valuable in giving an insight into the mechanisms by which the pollutants NO_x and CO are formed. They have also helped guide the formulation of a model to represent the formation of NO_x. This work is fully reported in Ref. 1.

References

1. N.R.L. Maccallum, S.A. Beltagui and A.M.A. Kenbar, "Combustion Patterns and Pollutant Formation in a Gas-Fired Furnace", Symposium - "Measurement and Control Techniques on Environmental Protection", Technical University of Budapest, 7 - 9 June 1993.

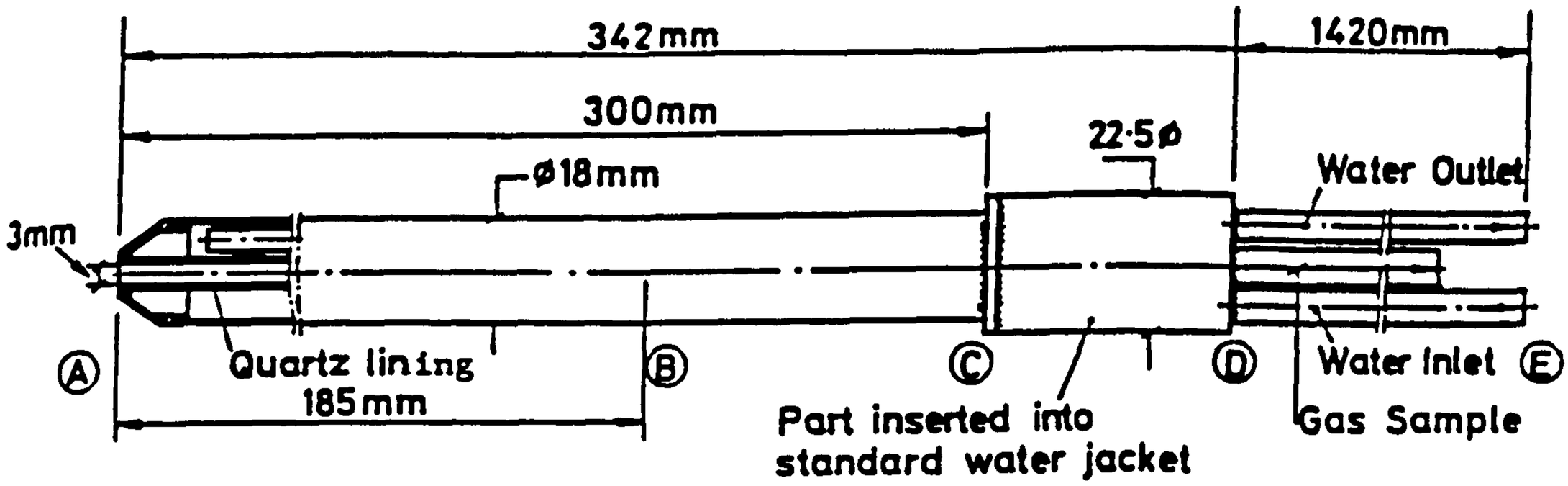

-a-

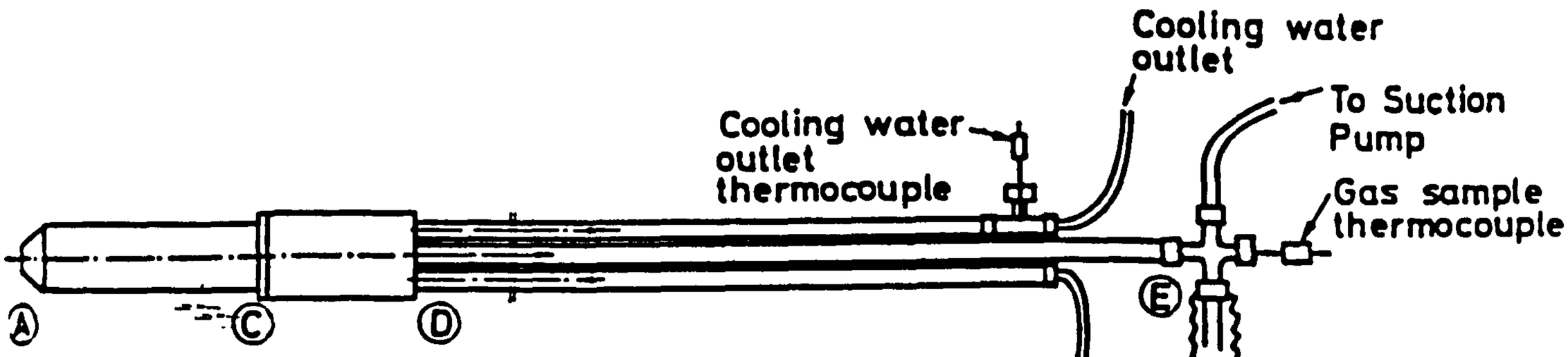

-b-

FIG. 1 NO_x sampling system

COMBUSTION PATTERNS AND POLLUTANT FORMATION IN A GAS-FIRED FURNACE

N.R.L. Maccallum[1], S.A. Beltagui[1,2] and A.M.A. Kenbar[1,2]

1. University of Glasgow, UK
2. National Engineering Laboratory, East Kilbride, UK

Paper presented to:

"Measurement and Control Techniques on Environmental Protection" Symposium, Technical University of Budapest, 7 - 9 June 1993.

1. INTRODUCTION

Combustion patterns and pollutants have been observed in a water-cooled furnace, fired by natural gas. The furnace, in a vertical, upwards-firing position, is of 1m inside diameter and 3m high. The typical heat release rate is 400 kW (Fig.1). The burner - of International Flame Research Foundation (IFRF) design - has adjustable blocks in the air entry which give varying degrees of swirl to the air (Fig.2), Swirl Numbers for the emerging flow ranging in the present work from 0.0 to 2.25. (Swirl Number, S, is defined by (axial flux of tangential momentum/axial flux of axial velocity momentum x burner throat radius)).

Three methods of injecting the fuel have been examined (Fig.3) - (i) central axial injection, (ii) outwards radial injection from a gun on the burner axis and (iii) injection from a narrow slot, or alternatively a series of axial holes, around the periphery of the air jet leaving the burner (Scheme 1). In a variation of the peripheral method, some 10% of the total air was injected radially outwards from the central gun (Scheme 2). This provided very helpful aerodynamic blockage which assisted flame stability at lower swirl settings. The Peripheral Fuel Injection technique takes advantage of the advantageous buoyancy effects in swirl and also the longer perimeter of the shear layer mixing zone.

The furnace walls were water-cooled. About 45% of the thermal energy released in the furnace was transferred to the walls by radiation, this fraction being almost independent of swirl. The fraction transferred by convection varied from about 20% at zero/low swirl to about 30% with high swirl (S = 2.25).

The work reported in this Paper summarises an investigation, parts of which have already been published. (Refs 1, 2 and 3).

2. AERODYNAMIC AND COMBUSTION PATTERNS

Time-averaged velocity components (in the 3 directions) were measured throughout the furnace, using a 5-hole velocity probe. This also gave static pressure distributions. Results were taken with the two higher degrees of swirl - S = 0.9 and S = 2.25, as the flame was stable with these swirl settings for all three modes of fuel injection. An excess air level of 5% was used for all these tests. It was found in the case of central axial fuel injection that, while the flame was stable at these higher swirl levels, the flame was long and combustion was not complete at the furnace exit - typical CO level 0.1%. Heat transfer from this flame was also low. On the other hand, with the radial outward and with the peripheral fuel injection modes, combustion was rapid and CO levels at furnace exit were always less than 0.01%. Heat transferences from these flames were high - in the range of 65 to 75% (total of radiation plus convection).

Consequently, due to this superior performance of radial outwards and peripheral injection modes over the more straightforward central axial injection mode, this paper concentrates on results for the radial outwards and peripheral injection modes.

2.1 Velocity Distributions

Typical axial velocity distributions across the furnace are shown in Fig.4 for the Peripheral Fuel Injection Mode (Scheme 1) and in Fig.5 for the Radial Outwards Injection Mode, results for the two degrees of swirl (S = 0.9 and S = 2.25) being given. It will be noticed that, with both Modes, the size of the Central Reverse-Flow Zone (CRZ) increases with Swirl. The jet expansion when using Peripheral Injection is slightly more rapid in the early stages than in the Radial Injection case.

The boundaries of the main forward flow with the central reverse and external reverse flow zones (ERZ) are shown, for the two Injection Modes, in Figs. 6 and 7.

Profiles of the corresponding tangential components of velocity are shown in Figs. 8 and 9. It is seen that, for both Injection Modes, the profiles are essentially similar, having the typical Rankine Vortex form of a core having solid body rotation surrounded by a free vortex. The tangential velocities are highest close to the burner quarl exit, and spread and diminish on moving downstream along the furnace.

2.2 Temperature Distributions

Temperatures were measured by suction pyrometer. Typical time-averaged results are shown in Figs. 10 and 11, giving profiles at distances of 45mm and 200mm respectively from the burner quarl exit. Temperatures are shown in this case for all three Injection Modes. The experimental conditions of air and gas flows were as previously described, I.e. there was 5% excess air.

For the Central Axial Injection Mode, flame asymmetry and inefficient mixing - leading to lower temperatures - are seen. With Peripheral Injection, the temperatures are reduced at the axis and are, relatively, highest at the outer shear layer of the main forward jet. The temperatures are also somewhat higher in the external reverse flow zones.

It is to be noted that increasing the swirl accelerates the mixing and advances the combustion process.

2.3 Species Concentration Distributions

Gas samples were taken and analysed (for CO_2, O_2, HC, CO and NO_x) at the same flow conditions as for the velocity and temperature measurements. The sampling and analysis methods are described in Ref.4.

Firstly, considering the concentrations of CO_2, these generally reflect how far the combustion process has advanced. Typical results are given in Fig.12 where concentration contours along the furnace are shown for the Peripheral Fuel Injection Mode (Scheme 1). It is seen that increasing swirl leads to shorter, more intense flames. This conclusion duplicates that drawn from the temperature distributions.

Carbon monoxide (CO) was also measured and results are shown in Figs. 13 and 14, profiles being given at distances of 45mm and 200mm respectively from the burner quarl exit. Concentrations are given for all these Injection Modes. The lowest ultimate values of CO concentration are obtained with the Peripheral Fuel Injection Mode.

Concentrations of total oxides of nitrogen (NO_x) were also measured. As an illustration of the processes within the complete furnace, contours (ppm) for the case with Peripheral Fuel Injection (Scheme 1) at swirl levels of S = 0.9 and S = 2.25 are shown in Fig. 15. It can be seen that the rate of NO_x formation follows the rate of the main combustion reaction, as indicated by the temperature and the concentrations of the reacting species. At the higher swirl setting, the concentrations of NO_x leaving the furnace are rather lower (24 to 26 ppm) than those observed at the lower swirl setting (30 to 33 ppm) - see also Fig. 18. This is attributed to the better mixedness achieved with the higher swirl, as will be discussed in Section 3.

Local concentrations of NO_x are also illustrated in Figs. 16 and 17 at two traverse planes close to the burner quarl exit. The lowest local NO_x values occur where there are high forward components of velocity, thus with shorter residence times up to that instant in the reaction zone.

2.4 Furnace Exit Measurements

In addition to the above measurements shown in Figs. 4 to 17 inclusive which were taken at one fuel/air ratio only - 5% excess air (i.e. equivalence ratio of 0.95), further experiments were carried out in which the equivalence ratio was varied between 0.7 and 1.35 and the concentrations of the species in the furnace exit gases measured. The three methods of fuel injection were investigated, over the swirl range giving stable flames. Results for NO_x concentrations, converted to correspond to 3% O_2, are shown in Figs. 18 to 20. In Fig. 18 the two alternative Schemes for peripheral injection (see Fig. 3) are compared. Stable flames could be obtained with Scheme 1 - only at the higher swirl settings i.e. $S > 0.8$, whereas Scheme 2 provided stable flames even at zero swirl. Due to the stability limitation of Scheme 1 the comparison is restricted to the cases at $S = 0.9$ and $S = 2.25$. For the case of $S = 0.9$, Scheme 2 gives significantly lower NO_x emissions than Scheme 1. This is attributed to the better mixedness achieved in Scheme 2, whereas with Scheme 1, which is closer to its stability limit, there are greater fluctuations in the concentrations of the reactants. The influence this has on the formation of NO_x is discussed in Section 3. At the higher swirl setting of $S = 2.25$ the mixedness achieved with Scheme 1 is much improved and the NO_x levels are reduced and are much closer to those achieved with Peripheral Injection Burner Scheme 2. The effect of equivalence ratio in these peripheral injection methods should also be noted. It is seen that the NO_x emissions have a maximum at an equivalence ratio of fairly close to, or slightly on the fuel-weak side of, stoichiometric. The NO_x emissions drop markedly on moving to both the fuel-weak and fuel-rich sides of stoichiometric. This indicates the potential for both air and fuel staging as means of reducing NO_x formation.

The effect of swirl in the case of Peripheral Injection (Scheme 2) can be investigated by comparing Figs. 18 and 19. It would appear that, once swirl is introduced, there is little further effect (comparing tests taken at $S = 0.45$, 0.9 and 2.25). When there is zero swirl ($S = 0.0$), furnace exit NO_x is somewhat higher on the fuel-weak side and lower on the fuel-rich side.

Comparisons of the effects of modes of fuel injection are given in Fig. 19 (for $S = 0.0$, 0.45) and Fig. 20 (for $S = 0.9$, 2.25). It is seen that the simple central axial fuel injection appears to give generally the lowest values of NO_x emissions. However these low quantities of NO_x are attributed to the slower reaction rates when central axial fuel injection is being used. A greater distance downstream has to be travelled before the main reactions are complete. By that distance there has been significant heat transfer from the burning gases. Hence the peak temperatures achieved are lower (Figs. 11 and 10). Hence the NO_x formation, which is heavily temperature dependent, is less.

Considering the performances with the central radial outwards and the peripheral injection modes, it has been noted already that the latter method leads to reduced NO_x emission if the fuel/air ratio is changed from stoichiometric in either the fuel-weak or fuel-rich directions. However with the central radial mode it appears that the reduction in NO_x occurs only in the fuel-rich direction. On this fuel-rich side at the swirl values of S = 0.45 and 0.9 the central radial method appears to be a little better than the peripheral method. At the highest swirl (S = 2.25) there is nothing to choose between the two. The superiority in performance of the peripheral injection mode on the fuel-weak side is noteworthy and is evident at all swirl settings.

The question that now has to be answered is "Is it possible to derive a model for the formation of NO_x which will satisfactorily predict the above results when working from the relevant initial data?"

3. MODEL FOR FORMATION OF NO_x

In general, there are three mechanisms by which NO_x may appear in the products of combustion - by the "thermal" mechanism, by the "prompt" process and lastly, from the nitrogen compounds in the fuel itself.

3.1 Thermal NO_x

In the "thermal" process nitrogen from the air is oxidised as it passes through the high temperature post-flame region. The major reactions are considered to be:

$$O + N_2 \rightleftharpoons NO + N \qquad \text{(Zeldovich) ..... 1}$$

$$N + O_2 \rightleftharpoons NO + O \qquad \text{(Zeldovich) ..... 2}$$

Also, in fuel-rich mixtures:

$$N + OH \rightleftharpoons NO + H \qquad \text{(Bowman) ..... 3}$$

The concentration of O to be used is that which is in equilibrium with molecular oxygen, O_2.

The above reactions have high activation energies and these are much slower than the main combustion reactions. Thus the NO reactions can be decoupled from the main combustion reaction.

The local rate of NO_x formation by the thermal mechanisms depends on (i) the flame temperature, (ii) the oxygen concentration in the post-flame zone and (iii) the residence time in the high temperature zone. Local variations of these parameters with space and time are important (Ref 5).

3.2 Prompt NO_x

High NO_x formation rates have been observed in the early parts of some flames (e.g. fuel-rich hydrocarbon flames). These rates were much more rapid than the Zeldovich mechanism.

Reactions, involving cyanides and amines have been suggested. The NO_x formed in these fast reactions in the early parts of flames is called "prompt" NO_x.

When gaseous fuels are burned lean or near stoichiometric, the "prompt" NO_x is usually less than 5 per cent of total NO_x. This is ignored in the prediction model which is proposed in Section 3.5.

3.3 Fuel NO_x

Nitrogen bound in the initial fuel can lead to NO_x in the product gases. For natural gas, the fuel in the present study, there are no nitrogen compounds and so this mechanism is not considered.

3.4 Modelling of Thermal NO_x formation

The following assumptions were first made:

(i) When firing lean or near-stoichiometric rich mixtures of gaseous fuels the dominant mechanism for the formation of NO is the thermal process.

(ii) The NO formation rate is slower than the hydrocarbon combustion rate, so most of the NO is formed after the hydrocarbon reactions reach equilibrium.

(iii) The calculation of NO formation is sufficient for predicting the NO_x formation.

With these assumptions and using the time-averaged concentrations, temperatures, etc, however, the NO_x is usually seriously underpredicted, in typical cases by a factor of 1:10.

The explanation that is put forward for this underprediction is that there are fluctuations of concentrations of reactants, and hence of temperatures in the reaction zone. To model this, the concept of collections of parcels of gases about to react, or reacting, is introduced. These parcels have individual equivalence ratios, ϕ, in a Gaussian distribution about the mean, $\overline{\phi}$. A mixedness parameter, S_o, is now introduced relating the standard deviation, σ, to $\overline{\phi}$:

$$\sigma = (1 - S_0)\overline{\phi} \qquad \text{..... 4}$$

For the case of complete mixedness, S_o is unity.

3.5 Proposed Model for Thermal NO formation

The proposed model has the following features:

(i) Those parcels with ϕ close to unity have maximum probability of combustion and thus react first.

(ii) Products of this reaction will be at the adiabatic stoichiometric flame temperature. The NO formation reaction takes place at this temperature.

(iii) The required oxygen comes from unburnt lean parcels with ϕ less than 1.0.

(iv) A mean value of residence time is estimated from the observations of the length of the reaction zone - taken as the distance until CO content is less than 0.5% - and the flow velocity in the reaction zone - taken as being the peak velocity.

The input data required for the model then are the average equivalence ratio, $\overline{\phi}$, and the experimentally derived parameters of mixedness, adiabatic stoichiometric flame temperature, reaction rate constants and residence time.

In the present work the mixedness, S_o, for each of the fuel injection methods, was estimated from a set of 200 instantaneous temperature measurements, taken at $\overline{\phi}$ = 0.95 and with Swirl Number, S = 0.90.

The results were:

$S_o = 0.65$ for central axial injection

$S_o = 0.7$ for radial outwards injection

$S_o = 0.8$ for peripheral injection (Scheme 1).

The adiabatic stoichiometric flame temperature for the natural gas fuel has been taken as 2222 K (Ref. 6).

The reaction rate equation used, with constants (Refs. 7,1) is:

$$\frac{dNO}{dt} = 1.44 \times 10^{17} [N_2][O_2]^{\frac{1}{2}} \; T^{-\frac{1}{2}} \exp(-69460/T) \quad \text{mole/cm}^3\text{sec} \quad .... \; 5$$

3.6 Comparison of Predictions of Model with Observations

The model for the formation of NO by the thermal mechanism has been applied to the test conditions given in the latter part of Section 2.4 and which gave the experimental results shown in Figs. 18 to 20. It has been assumed that the quantities of NO_x formed by the prompt mechanism are small and these have been omitted from the predictions.

The comparisons are given in Figs. 21 to 23 for the three fuel injection methods respectively - central axial, radial outwards and peripheral (Scheme 1). For the central axial case (Fig. 21) the NO_x level is over-predicted by about 40% at the 0.95 equivalence ratio condition and by higher fractional margins at higher equivalences and lower margins at lower equivalences. This over-prediction is attributed to the somewhat slower combustion in this case with there now being more heat transfer from the zone in which the reactions take place, hence lower temperatures. However the theoretical model ignores this heat transfer. Due to the poor mixedness ($S_o = 0.65$) of this central axial injection method, the predicted peak in the NO_x formation, as a function of ϕ, occurs at ϕ of about 0.78, which was below the experimental range covered. So the model could not be tested for this predicted feature. The omission of prompt NO_x from the predictions could lead to under-prediction in the very fuel-rich region (Section 3.2), but this was not very evident when using central axial injection.

The corresponding comparison for the radial outwards fuel injection method is shown in Fig. 22. Here there is a very satisfactory agreement between prediction and observation, except at the weakest equivalence ratios - less than 0.80. The predicted reduction in NO_x formation in this range is not apparently observed.

Finally the observations and predictions for the peripheral fuel injection method (Scheme 1) are compared in Fig. 23. In this case the reduction in NO_x emissions at the lower equivalence ratios is both predicted and observed. For equivalence ratios of less than unity there is generally satisfactory agreement between prediction and observation. However the observed reduction in NO_x formation as equivalence ratio increased into the fuel-rich region is significantly less marked than that predicted. This may be partly explained if the prompt NO_x is included in the prediction.

Comparing the radial (Fig. 22) and peripheral (Fig. 23) methods of fuel injection, it has already been noted that with the latter a significant reduction in NO_x formation is observed as equivalence ratio (ϕ) is reduced below 0.90. With the former no reduction is observed. The model described in the present work does predict a reduction in both cases, this reduction beginning at $\phi = 0.86$ in the peripheral injection case, and at $\phi = 0.79$ in the radial injection case. This movement of the maximum of the predictions is due to the differences in mixedness parameter, S_0 - the temperature measurements giving it the value 0.7 for the radial injection and 0.8 for the peripheral injection cases. Thus the model does indeed offer differences in predictions, in the correct direction, on the fuel-weak side between these two injection methods, but the difference is not as substantial as that observed.

4. CONCLUSIONS

Three methods of injecting the gaseous fuel into a 400 kW furnace have been examined. The resulting combustion patterns have been observed, and the emissions of pollutants noted.

The fuel injection methods have influence both on the flame aerodynamics and on the formation of pollutants. The lowest total pollutant formations (considering NO_x, CO and HC) were obtained using either radial fuel injection or peripheral fuel injection. In both cases the total emissions of NO_x are reduced by operating in the fuel-rich region - this demonstrates the possibility of air-staging for "clean" combustion. The peripheral injection method also showed reductions in NO_x when moving into the fuel-weak region - hence the possibility in this case of fuel-staging.

A model has been proposed for the formation of NO, based on the thermal reactions and on measurements of the mixedness of the fuel and air in the reaction zone. This model gives predictions which are in encouraging agreement with the observations.

References

1. A.M.A. Kenbar, "Combustion Aerodynamics and Pollution Formation in Gas-Fired Furnaces", Ph.D. Thesis, University of Glasgow, 1991.

2. A.M.A. Kenbar, S.A. Beltagui, T. Ralston and N.R.L. Maccallum, "Measurement and Modelling of NO_x Formation in a Gas-Fired Furnace", 1st (Int) Conference on Combustion Technologies for a Clean Environment, Algarve, Portugal, 1991.

3. A.M.A. Kenbar, S.A. Beltagui and N.R.L. Maccallum, "Effect of Fuel Injection Modes on the Combustion Pattern and Pollutant Formation in a Gas-Fired Furnace", 2nd (Int) Conference on Combustion Technologies for a Clean Environment, Lisbon, Portugal, 1993.

4. N.R.L. Maccallum, S.A. Beltagui and A.M.A. Kenbar, "Measurement of CO and NO_x Pollutants in a Gas-Fired Furnace", Symposium - Measurement and Control Techniques on Environmental Protection, Technical University of Budapest, 7 - 9 June 1993.

5. J.P. Appleton and J.B. Heywood, "The Effects of Imperfect Fuel-Air Mixing in a Burner on NO Formation from Nitrogen in the Air", 14th Symposium (Int) on Combustion, 1972, pp777-786.

6. G.A. Karim and R. Singh, "A Thermodynamic Investigation of the Combustion of Methane", Jour. Institute of Fuel, Vol.40, Oct.1967, pp447-455.

7. S.A. Beltagui, A.M.A. Kenbar and N.R.L. Maccallum, "NO_x Generation and Control in Confined Swirling Flames - Review and Parametric Study", HTFS Research Symposium, 1989, Paper RS 827, NEL/HTFS 123.

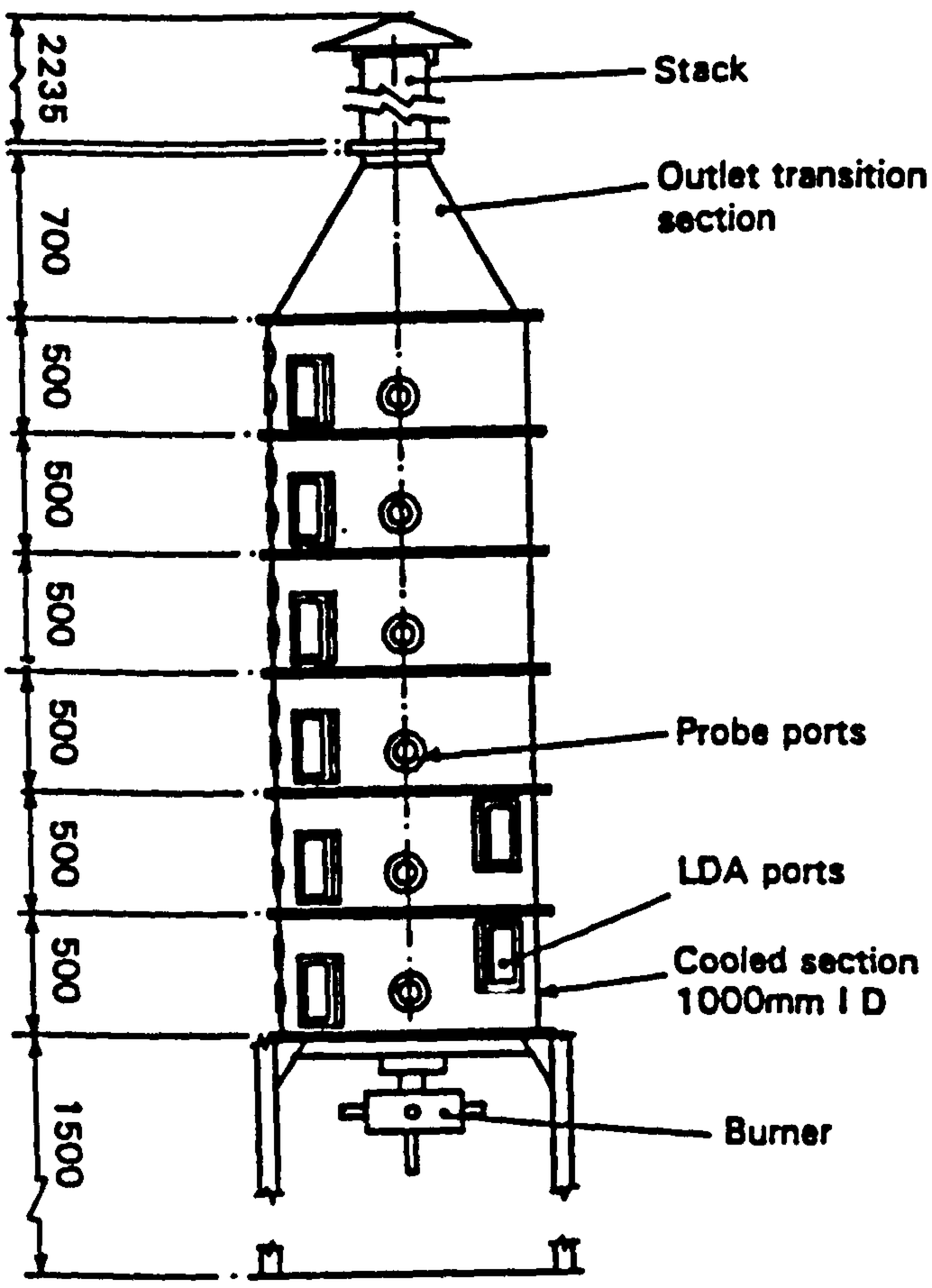

Fig. 1 Schematic of the NEL furnace

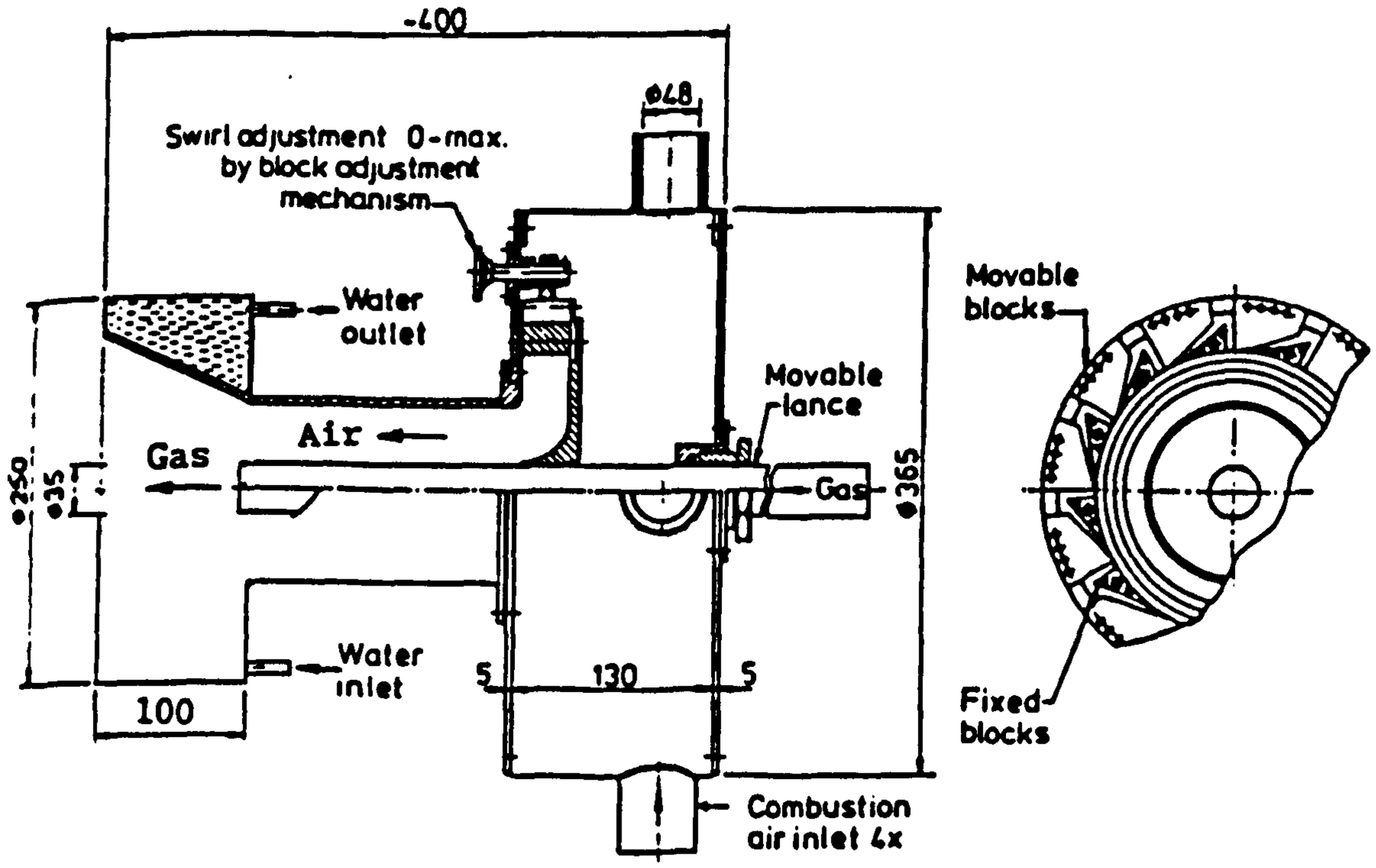

Fig. 2 Central axial fuel injection

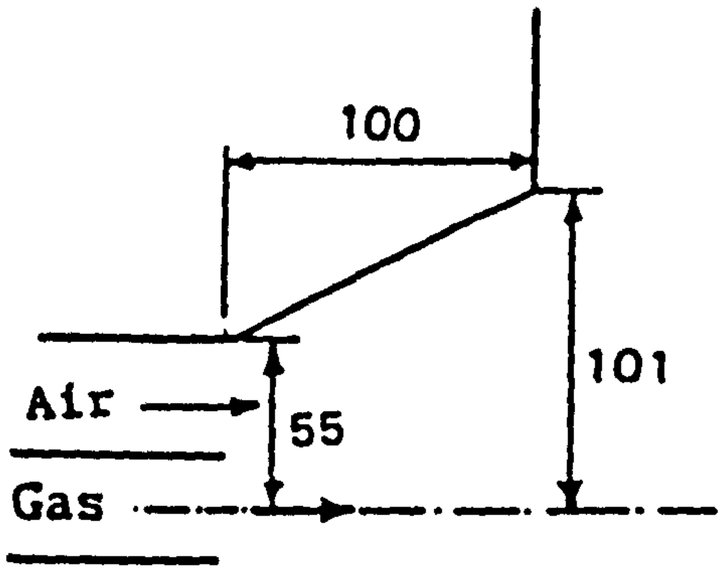

(i) Central axial

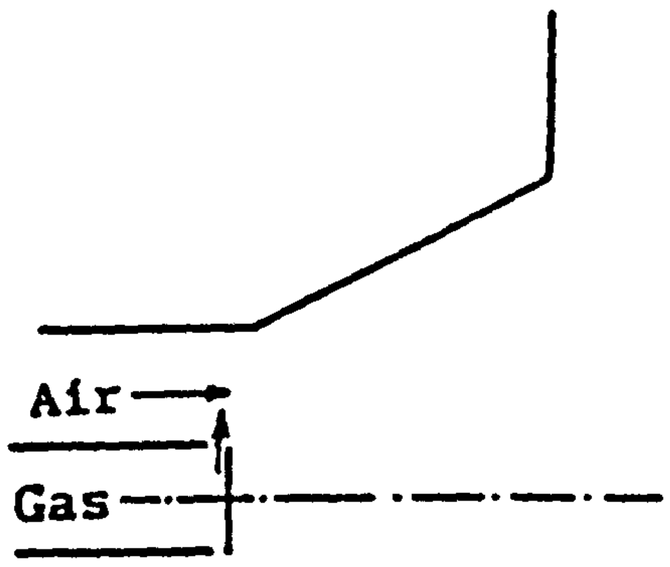

(ii) Central radial

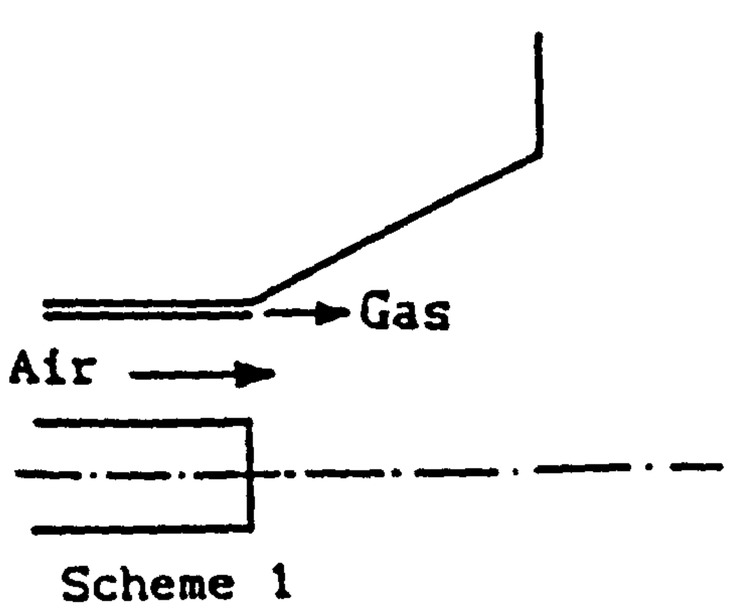

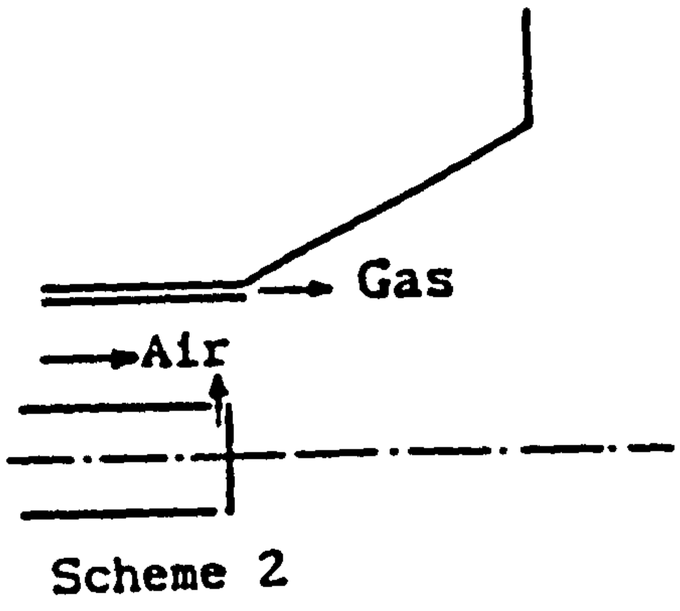

(iii) Peripheral

Fig. 3 Schematic of fuel injection systems

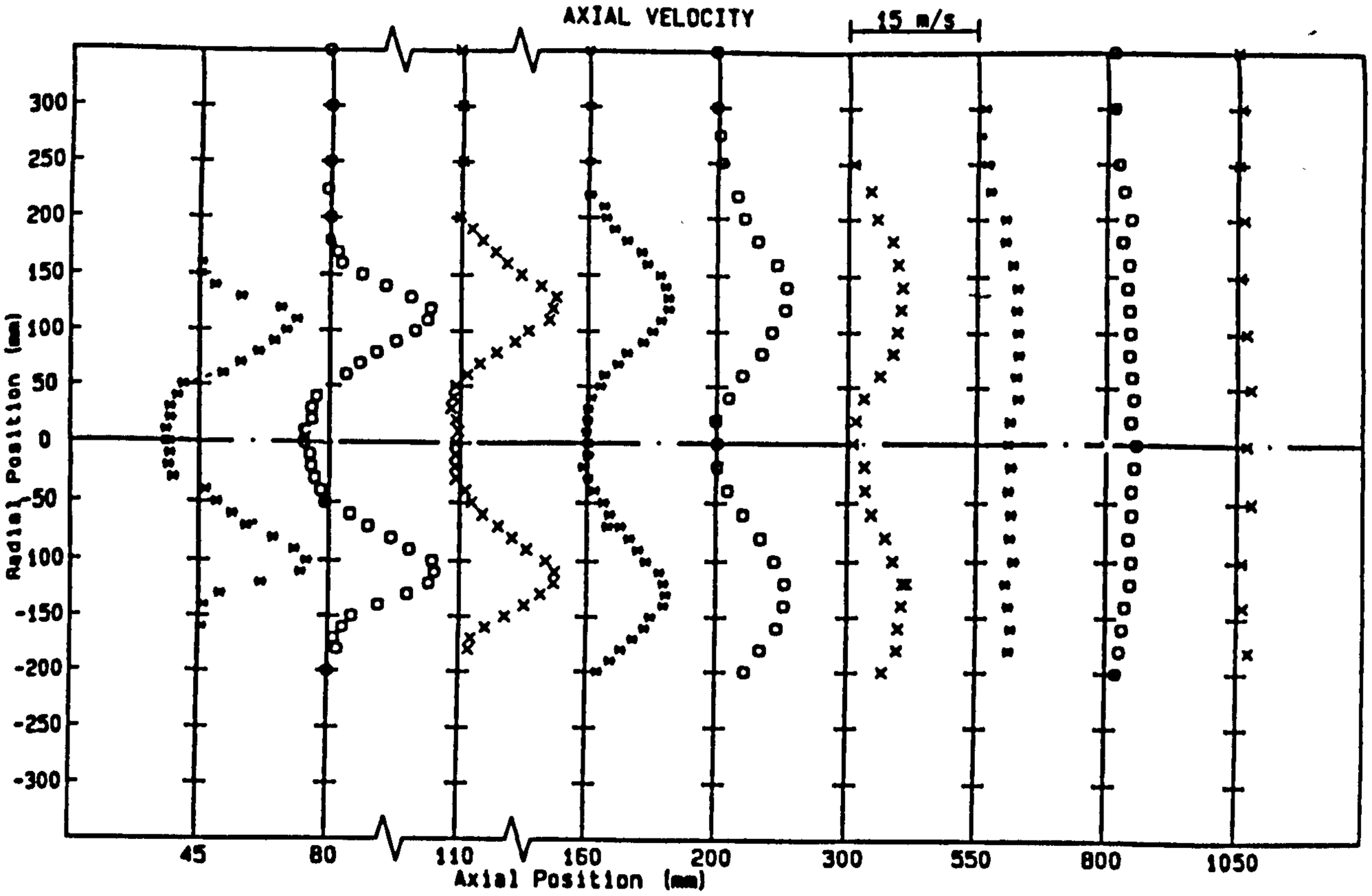

(a) S = 0.90

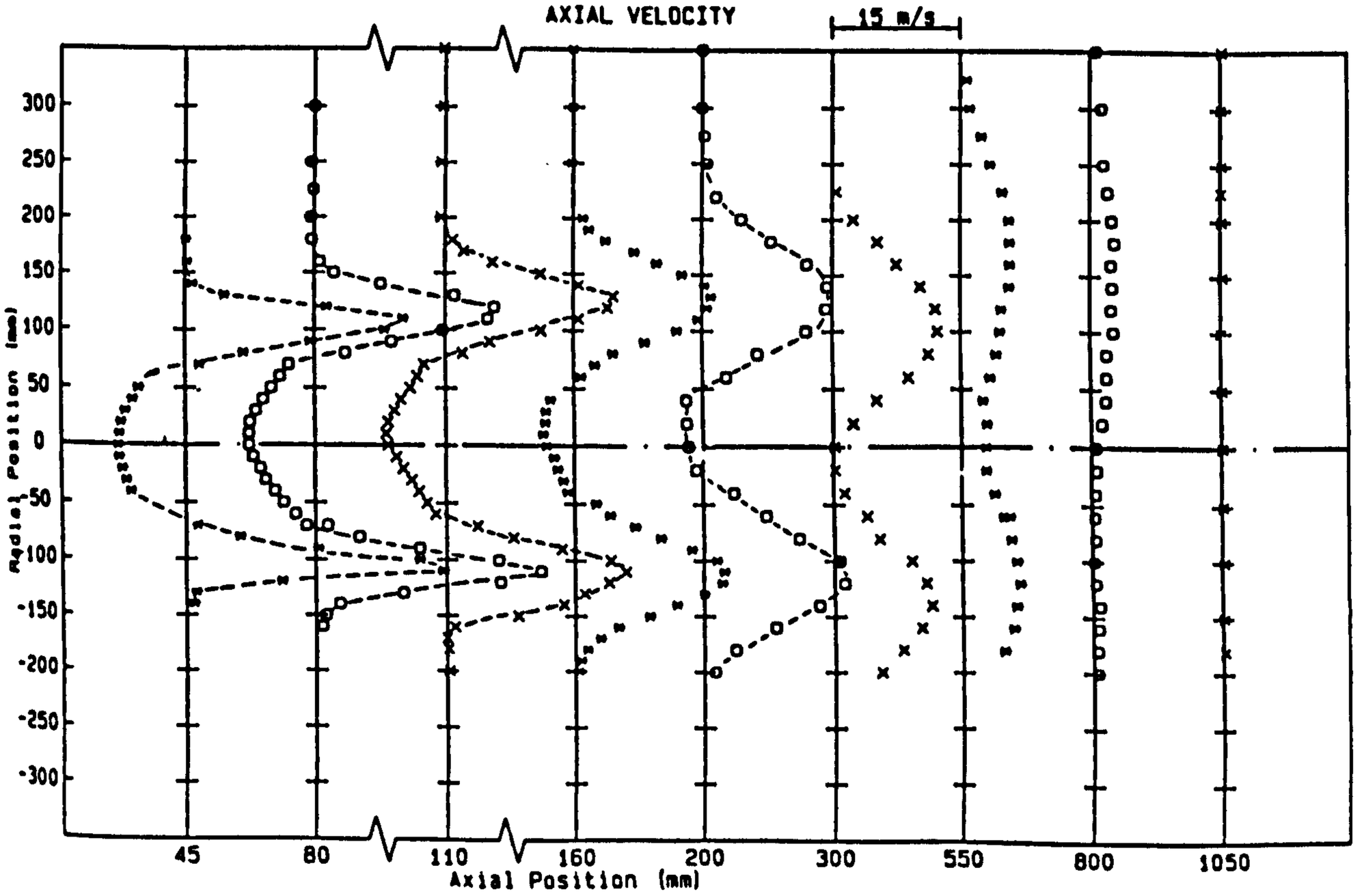

(b) S = 2.25

Fig. 4 Axial velocity profiles, peripheral fuel injection, Scheme 1

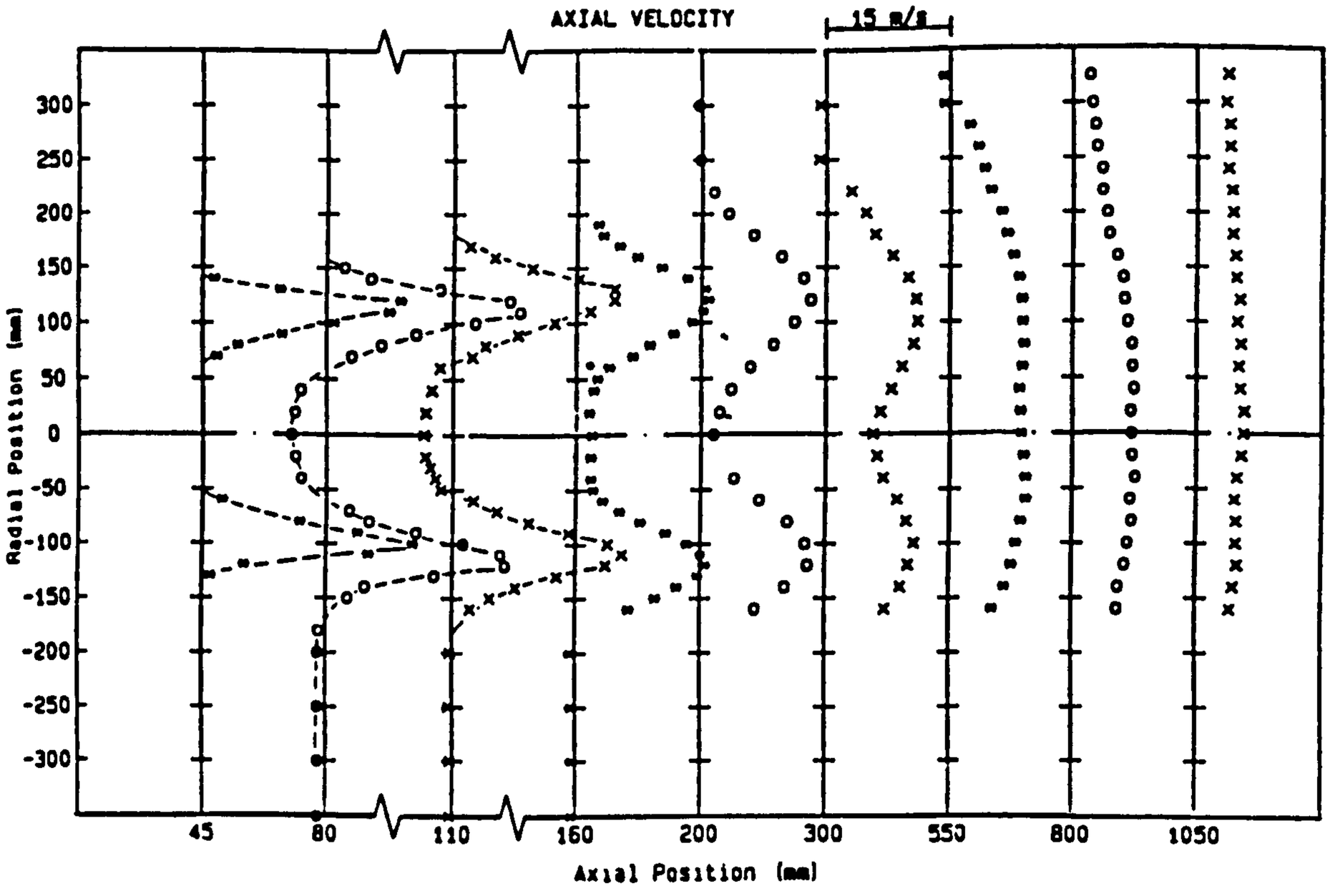

(a) S = 0.90

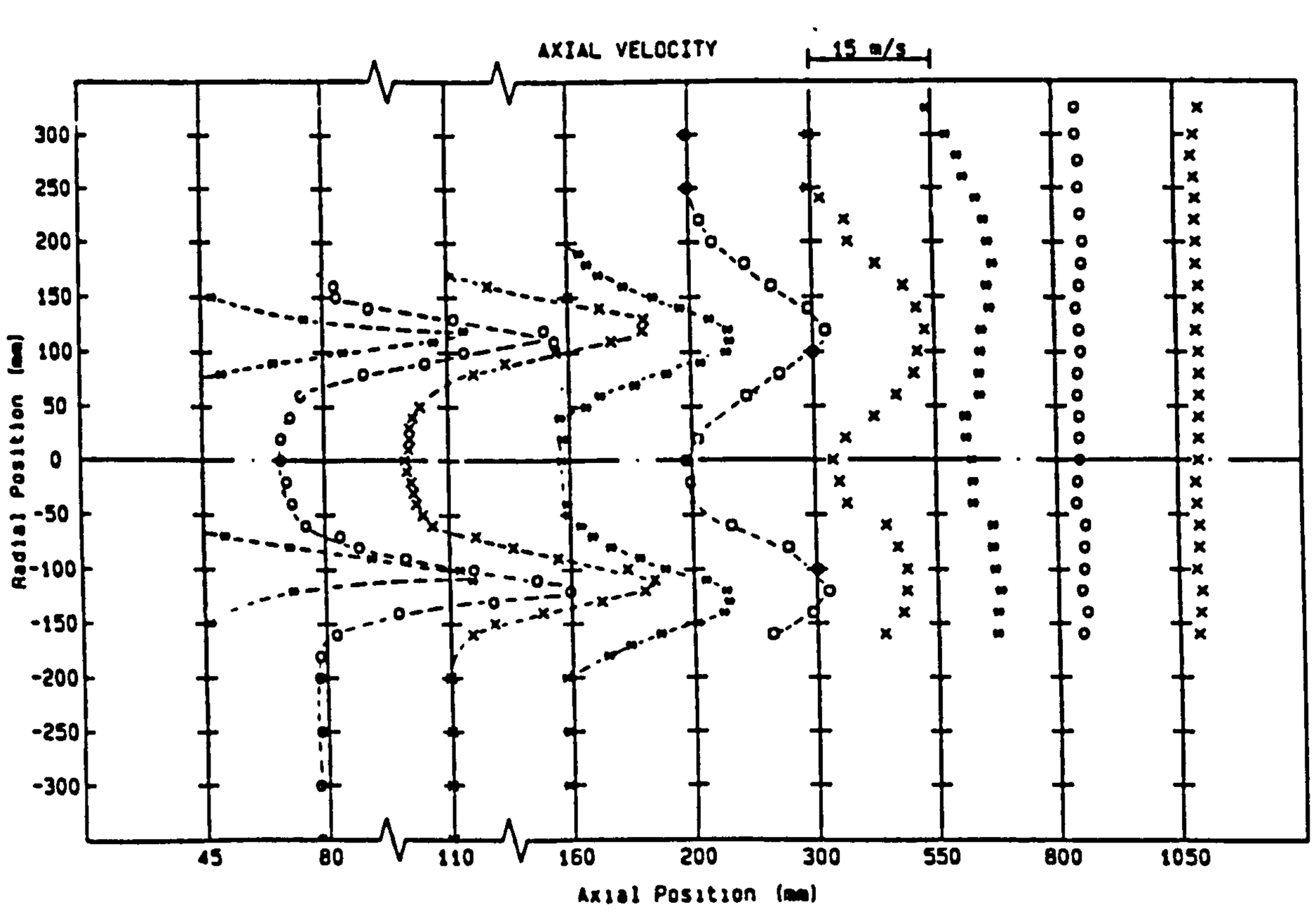

(b) S = 2.25

Fig. 5 Axial velocity profiles, radial fuel injection

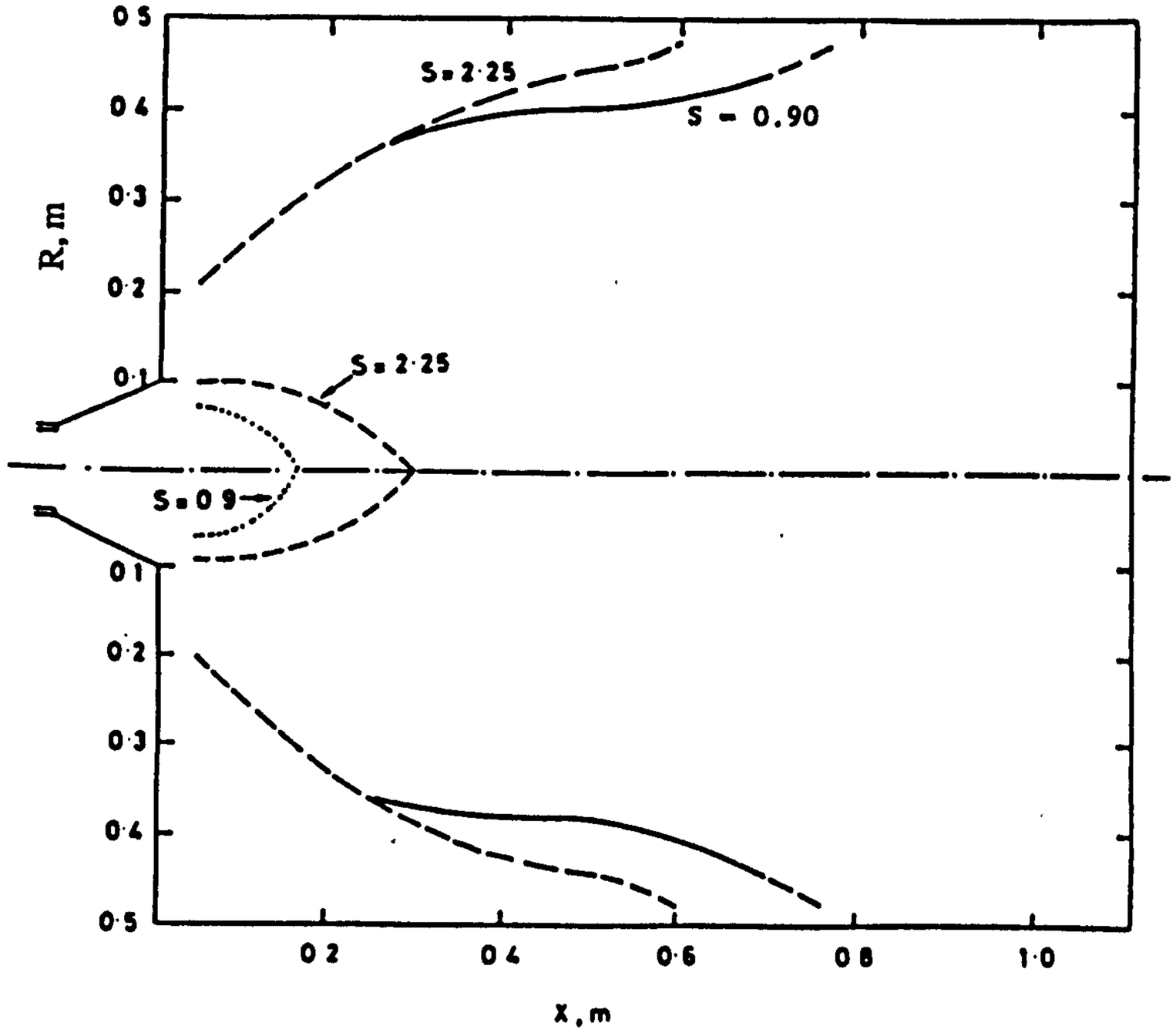

Fig. 6 Flow boundaries, peripheral fuel injection, Scheme 1

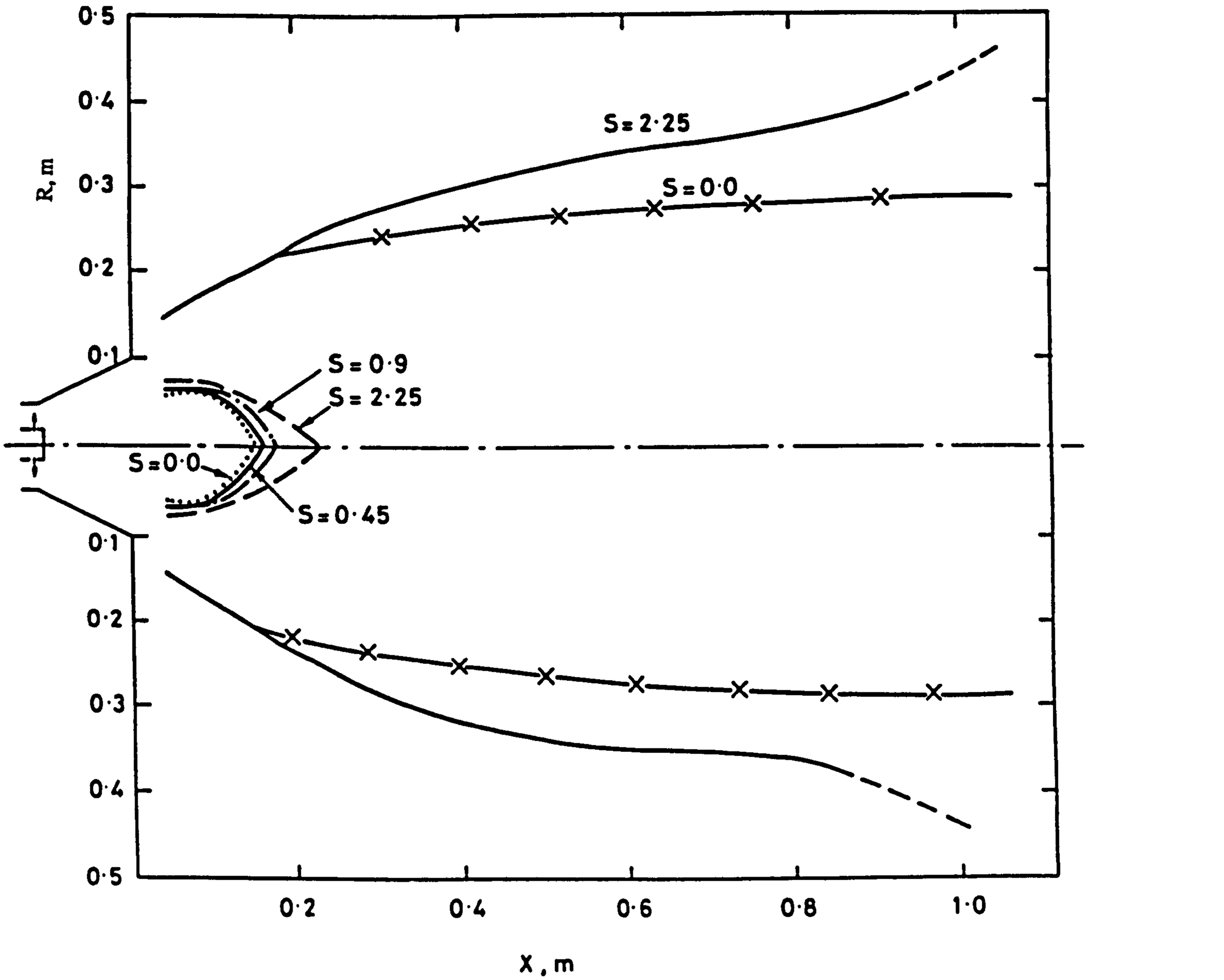

Fig. 7 Flow boundaries, radial fuel injection

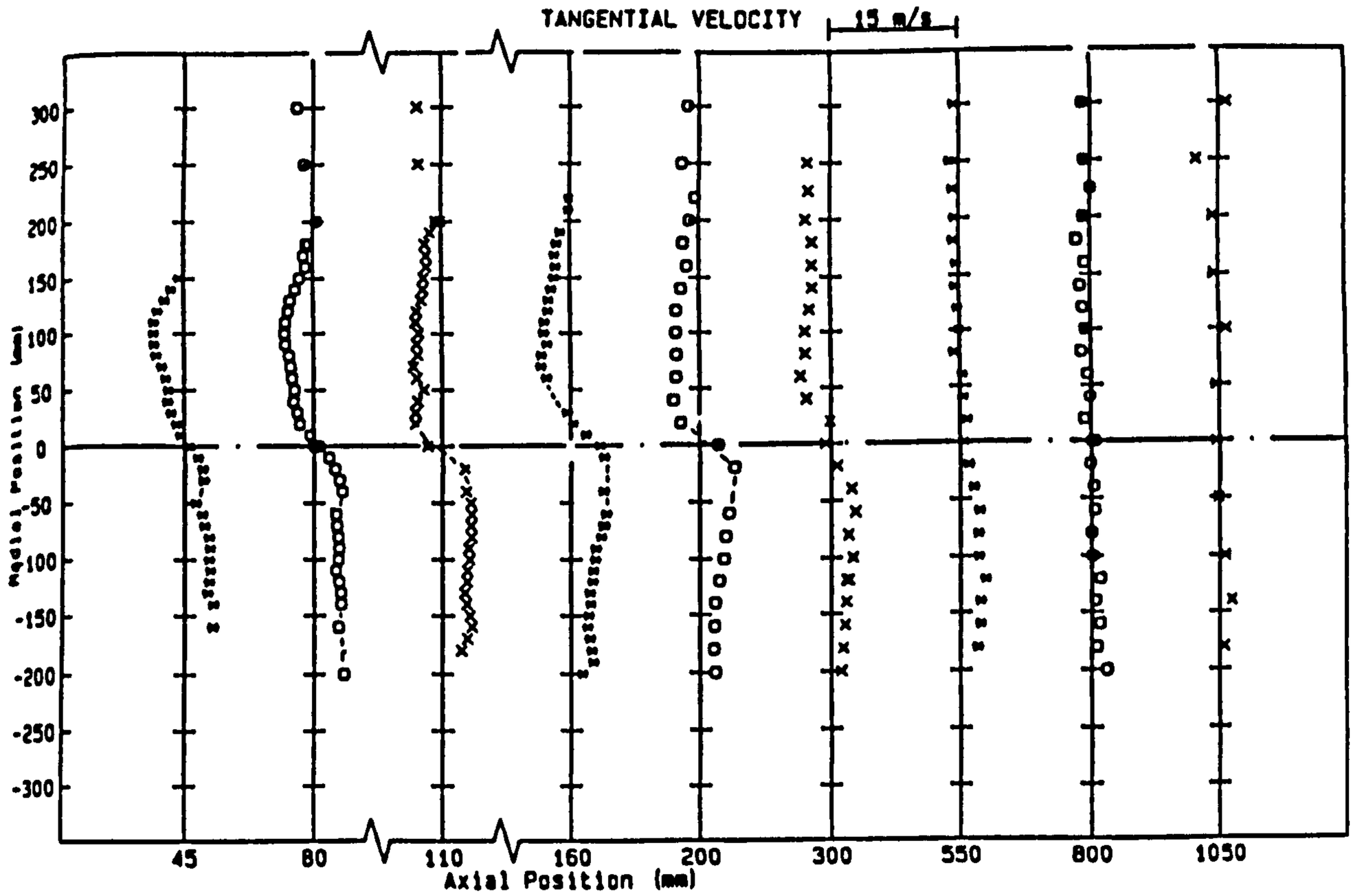

(a) S = 0.90

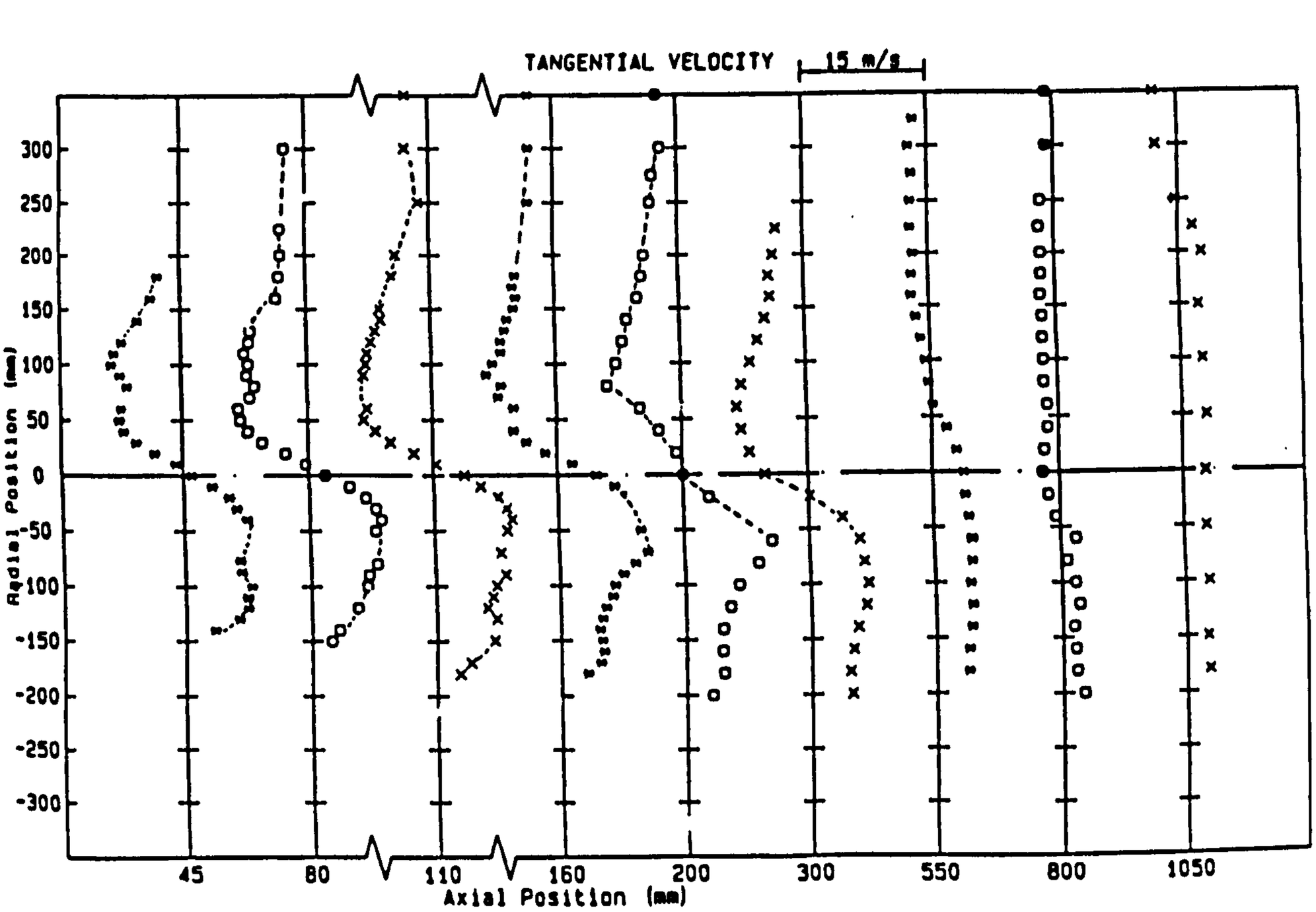

(b) S = 2.25

Fig. 8 Tangential velocity profiles, peripheral fuel injection, Scheme 1

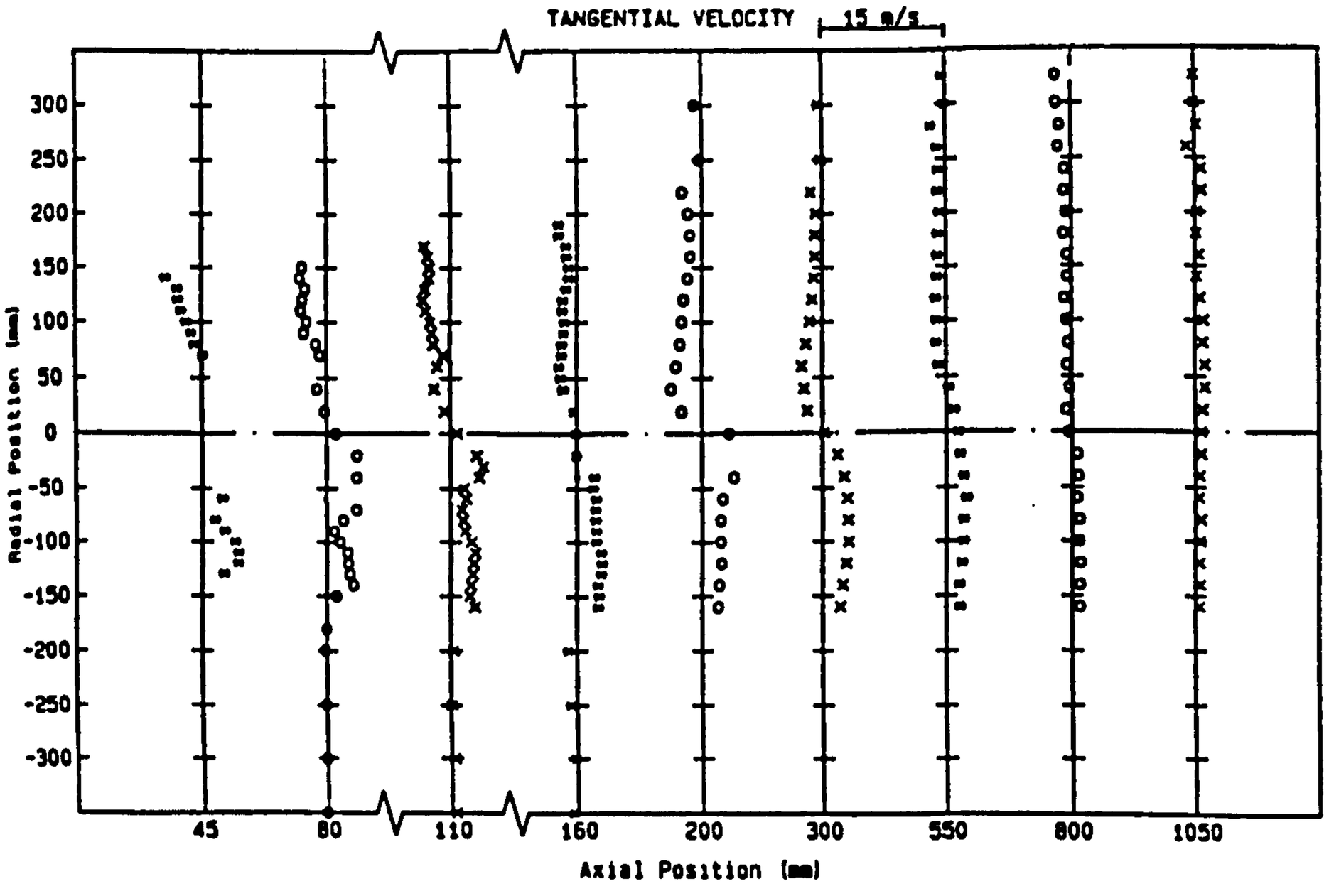

(a) S = 0.90

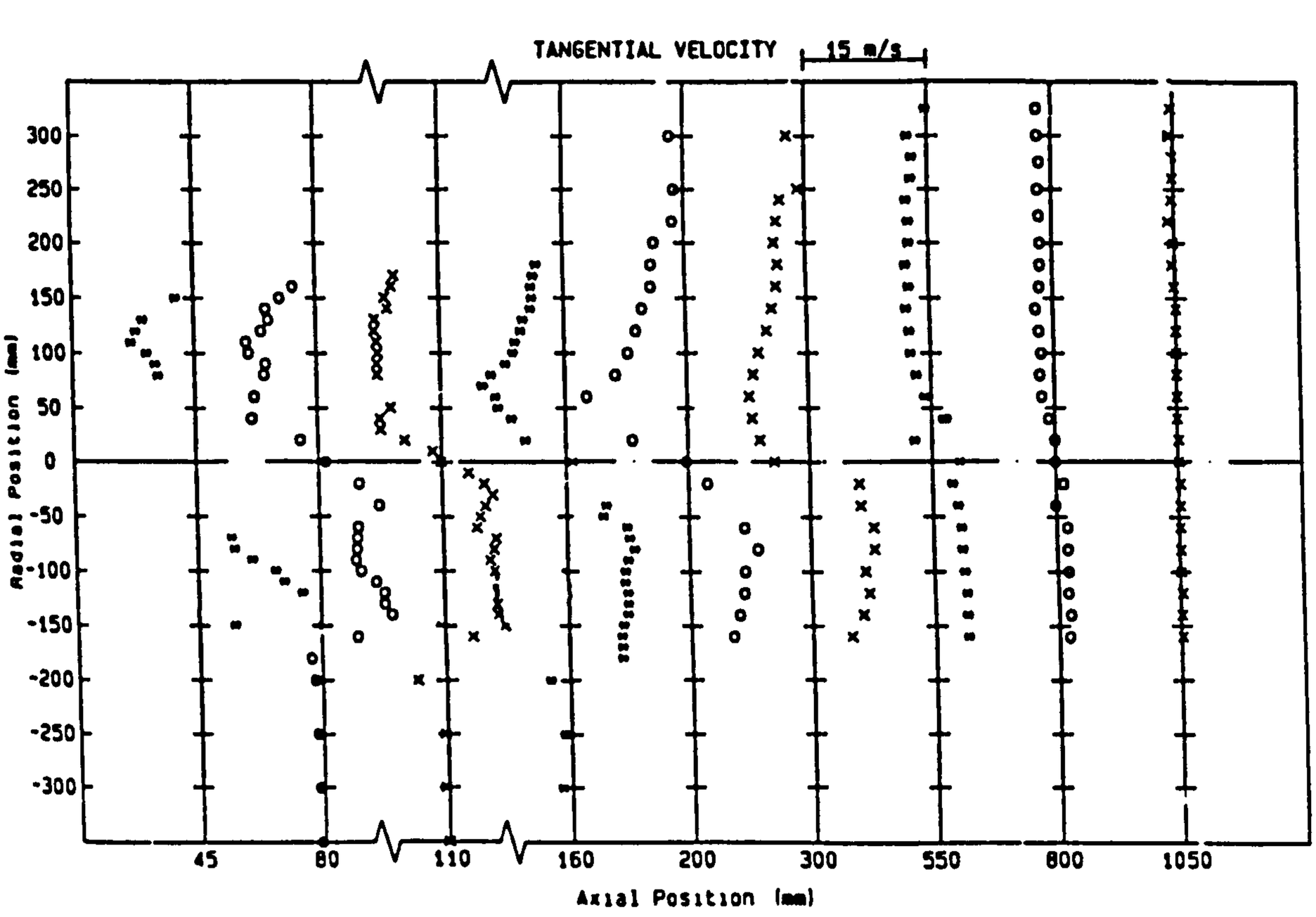

(b) S = 2.25

Fig. 9 Tangential velocity profiles, radial fuel injection

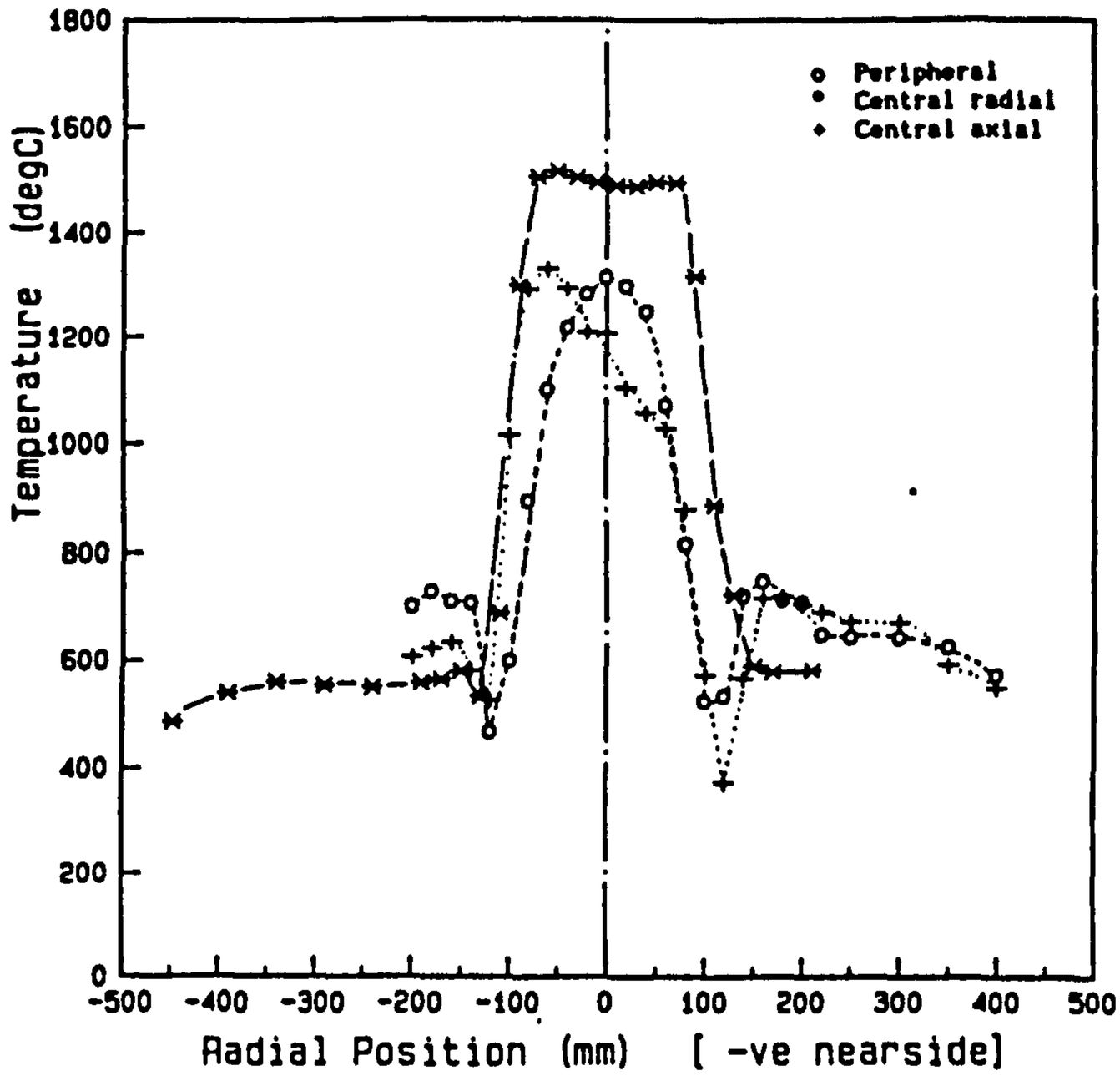

(a) S = 0.90

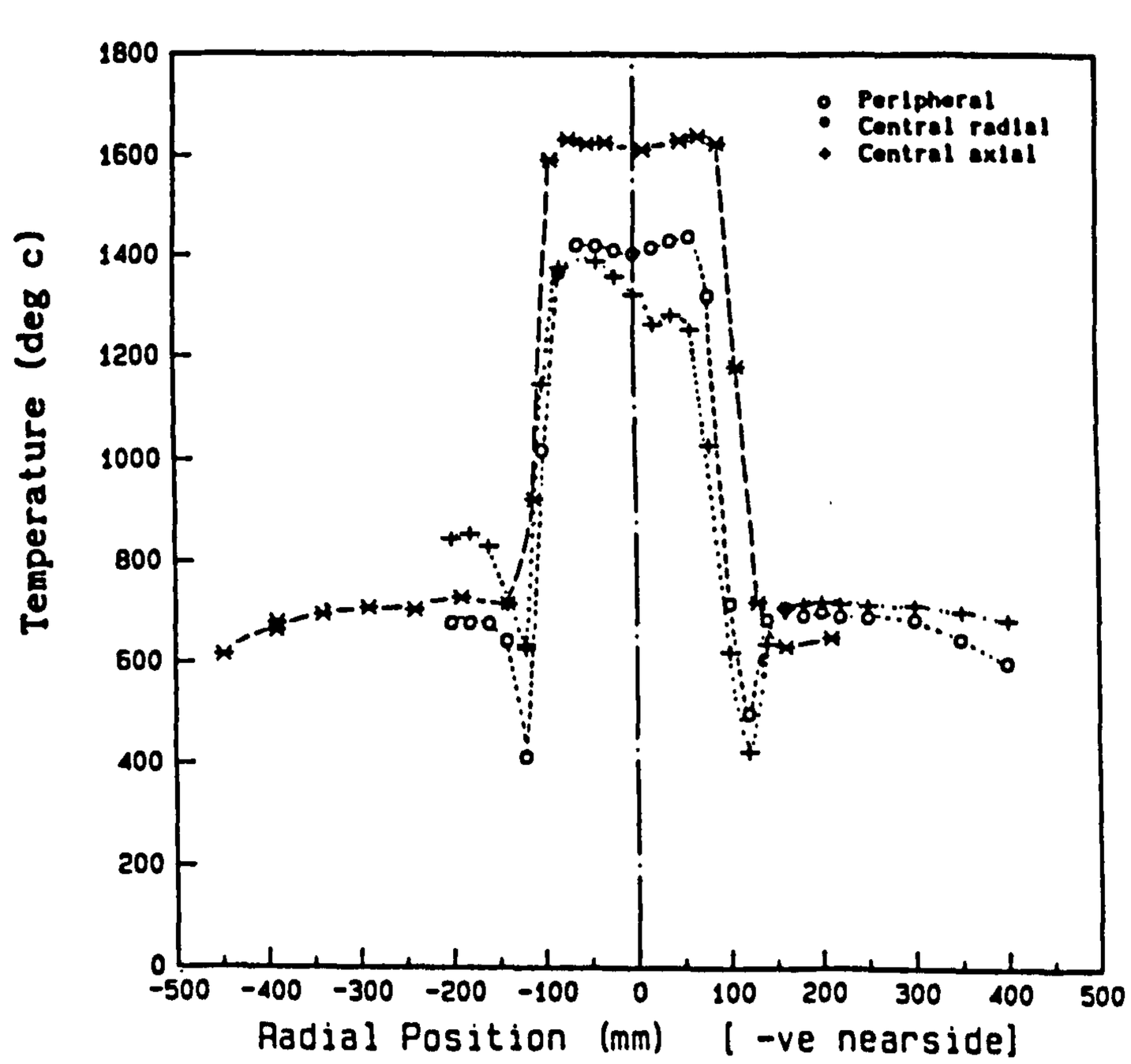

(b) S = 2.25

Fig. 10 Radial temperature profiles, X = 45 mm, peripheral, radial and axial fuel injection modes

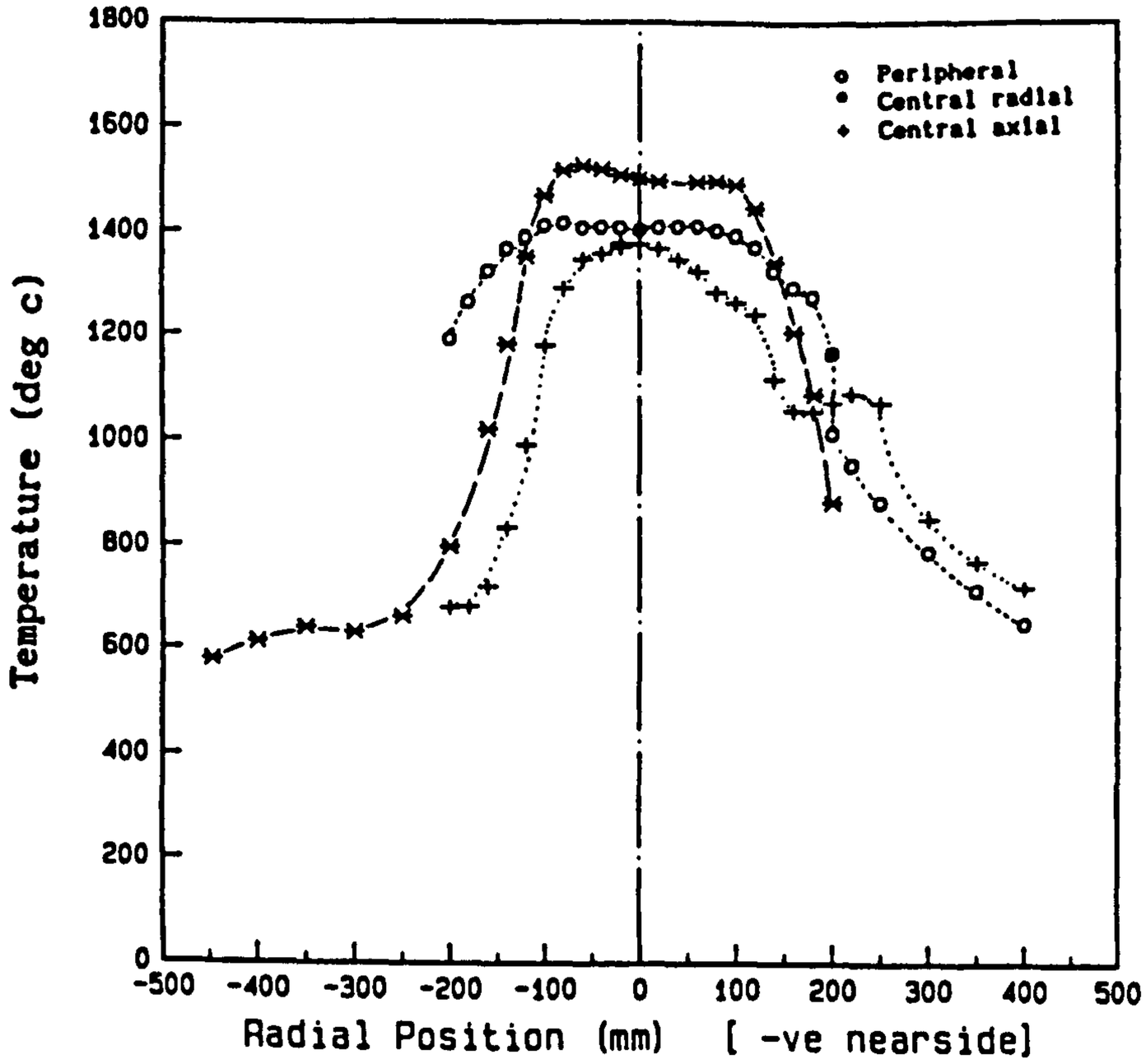

(a) S = 0.90

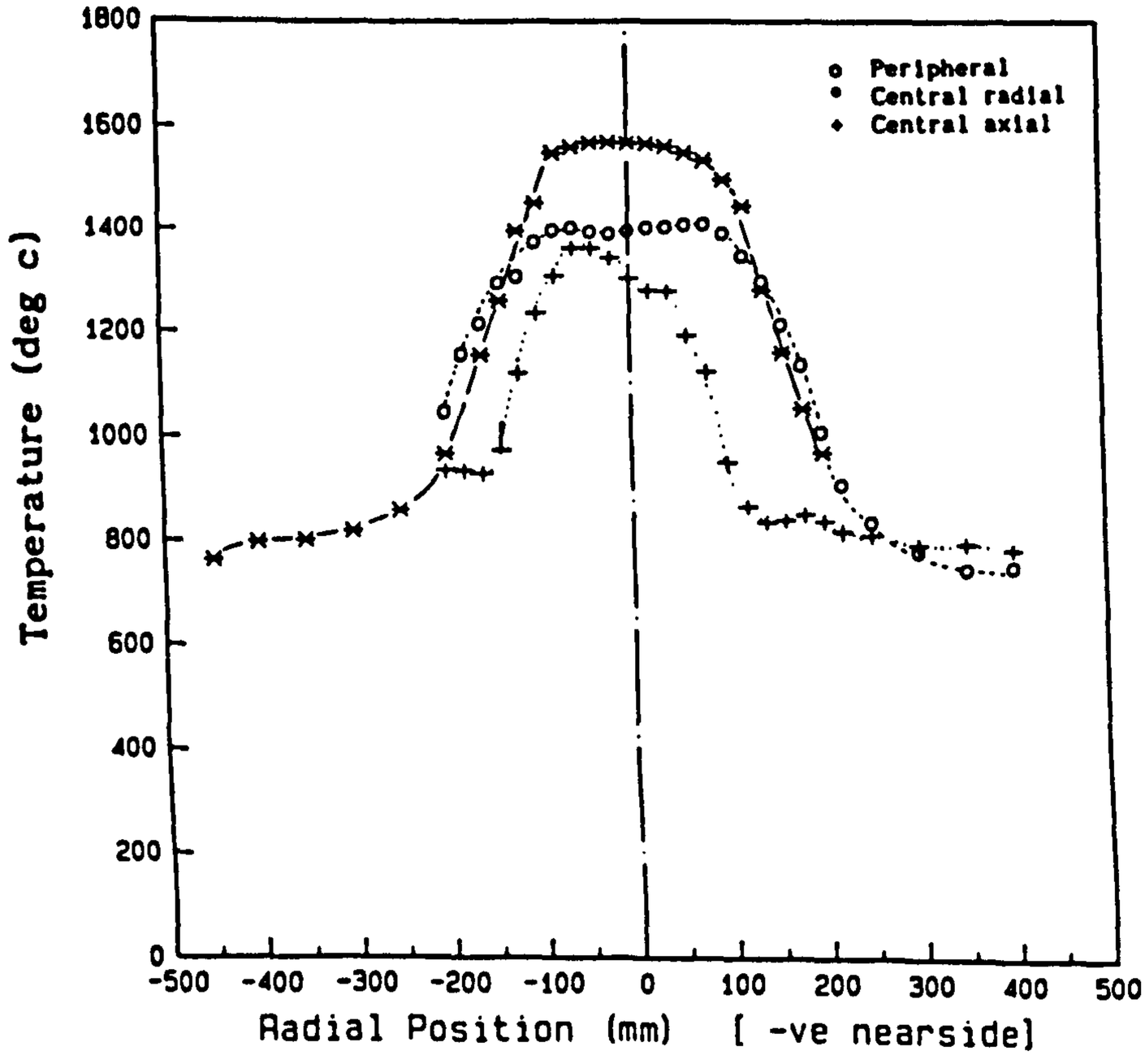

(b) S = 2.25

Fig. 11 Radial temperature profilesl, X = 200 mm, peripheral, radial and axial fuel injection modes

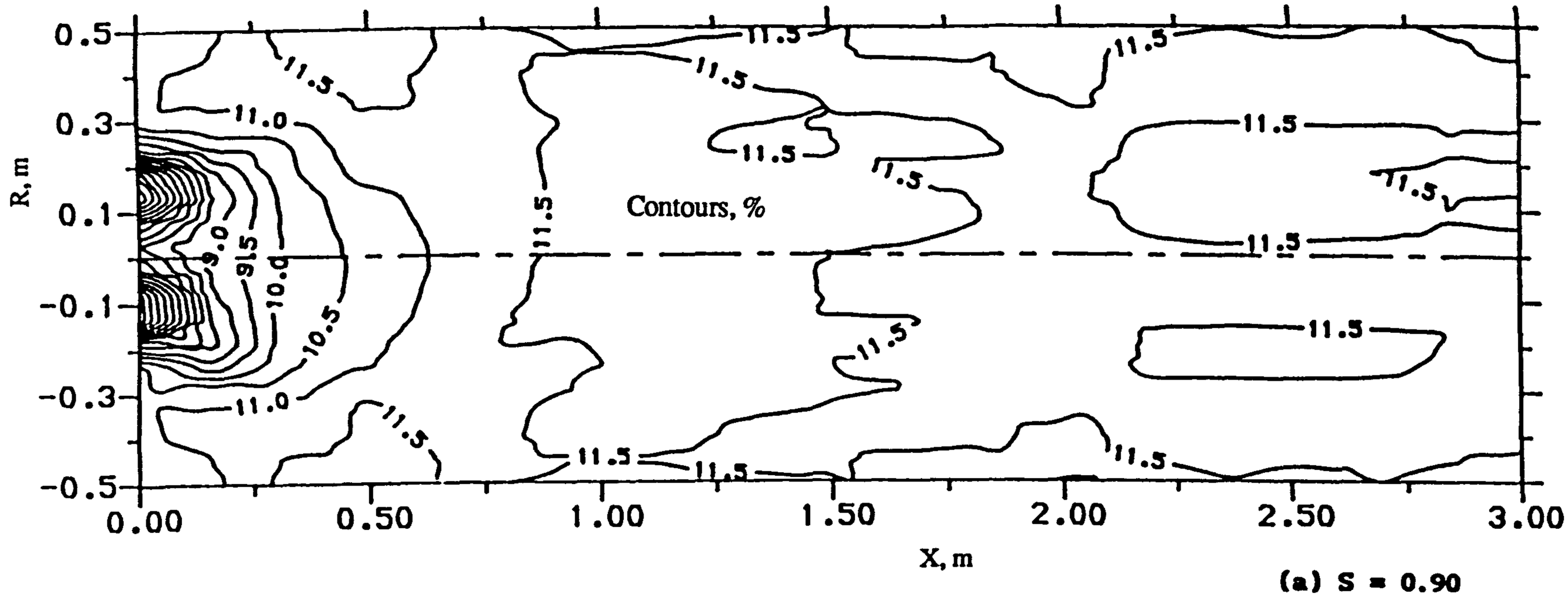

Fig. 12 CO_2 contours, peripheral fuel injection, Scheme 1

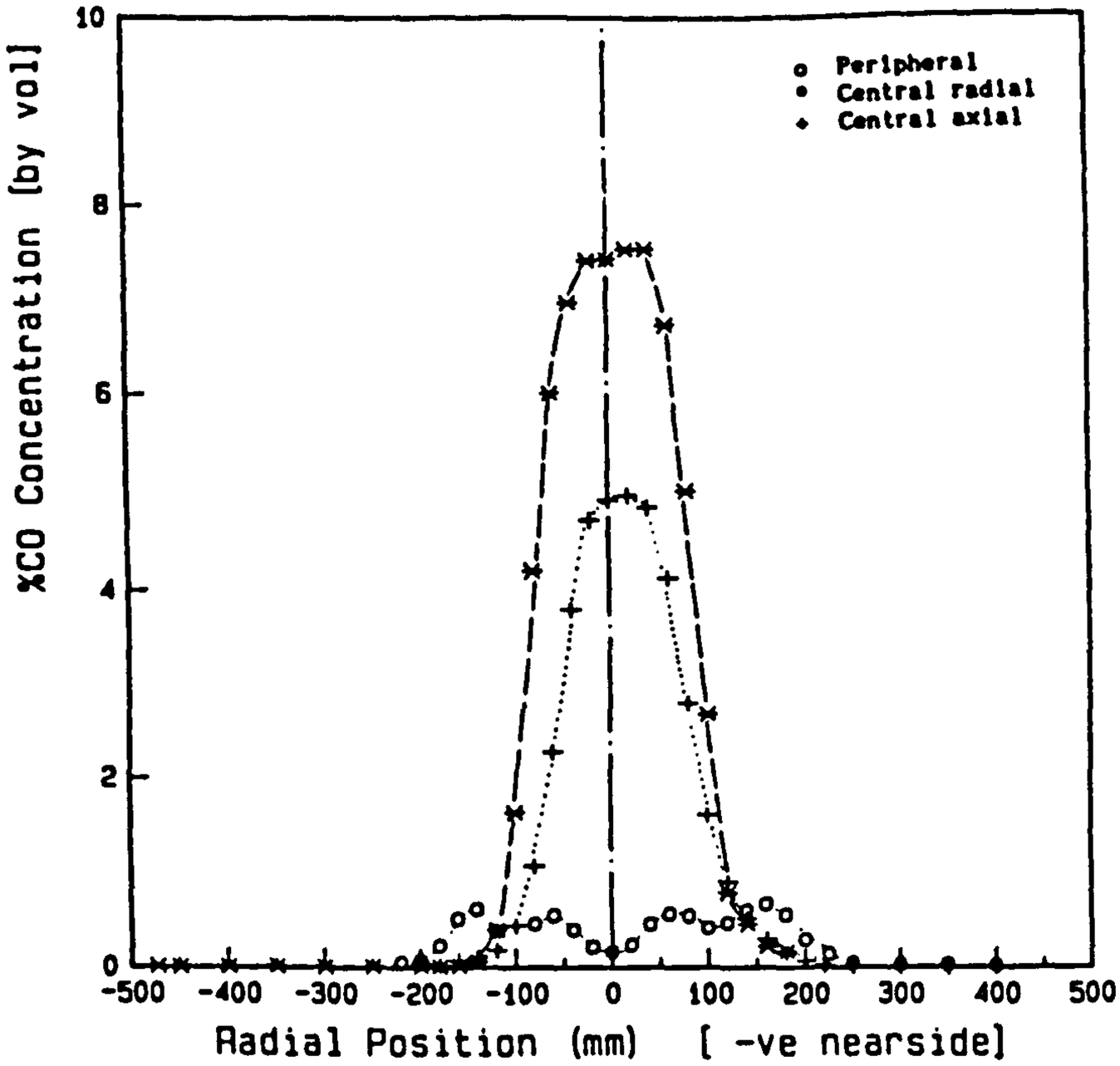

(a) S = 0.90

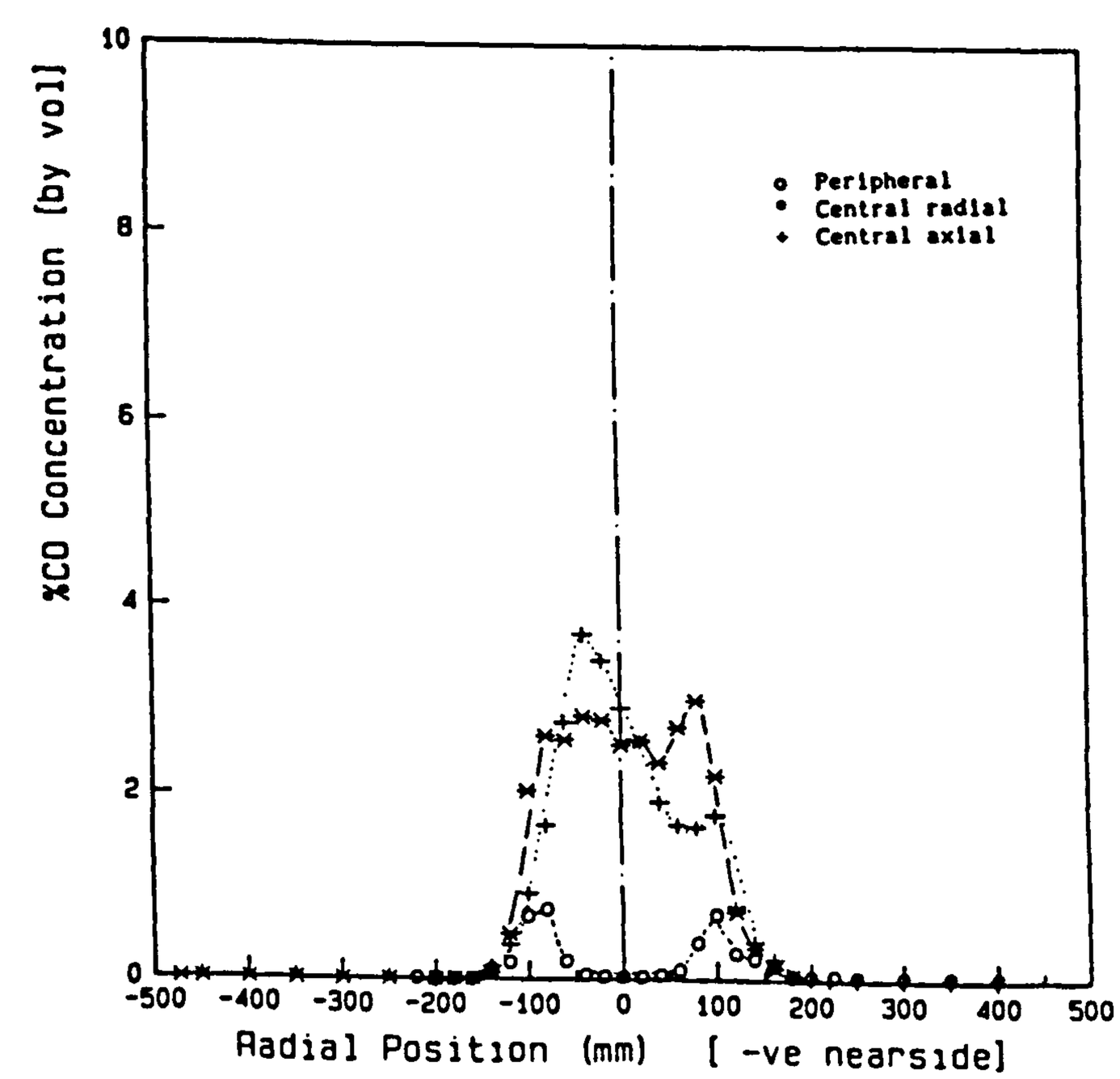

(b) S = 2.25

Fig. 13 Radial CO profiles, X = 45 mm, peripheral, radial and axial fuel injection modes

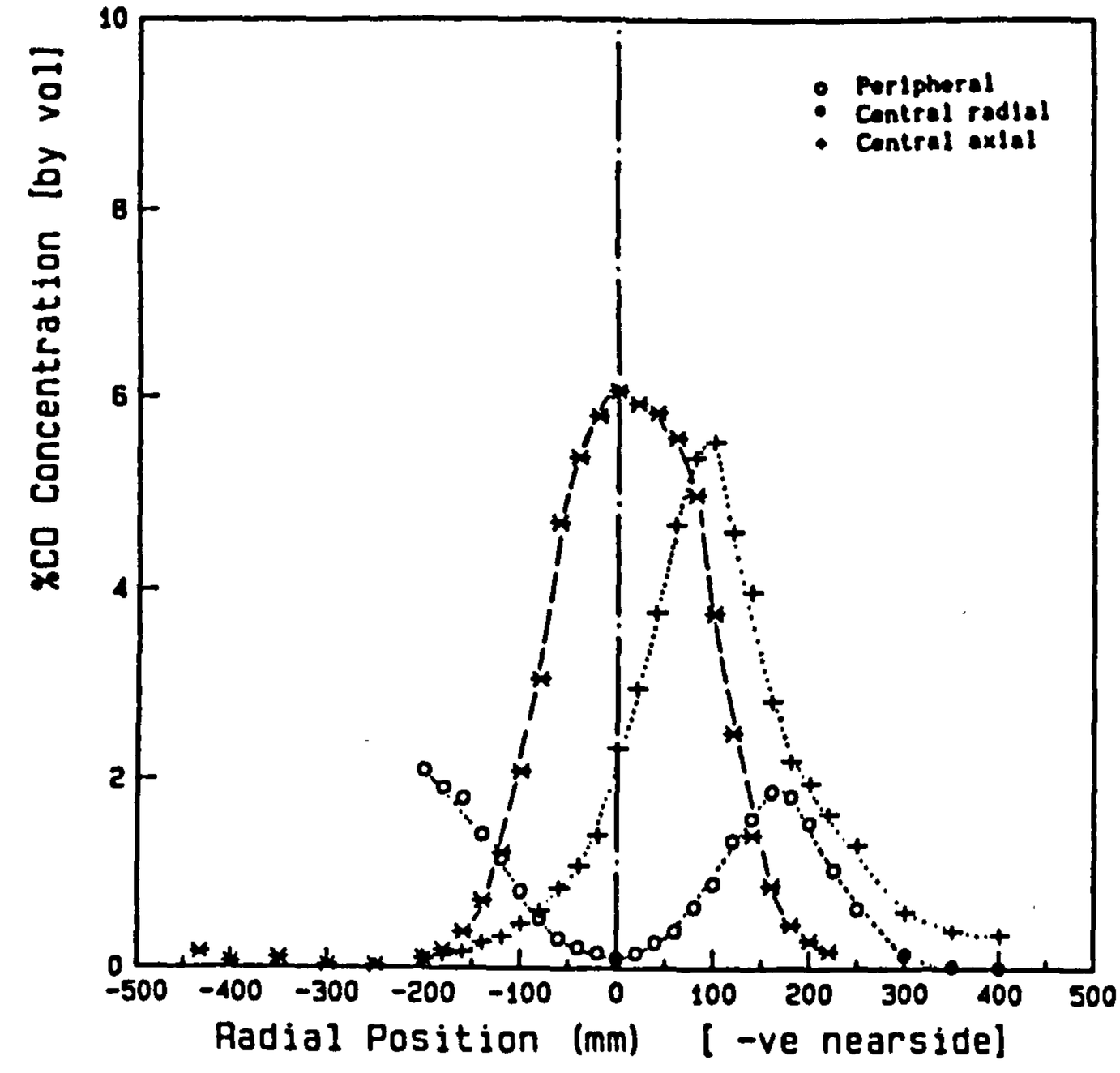

(a) S = 0.90

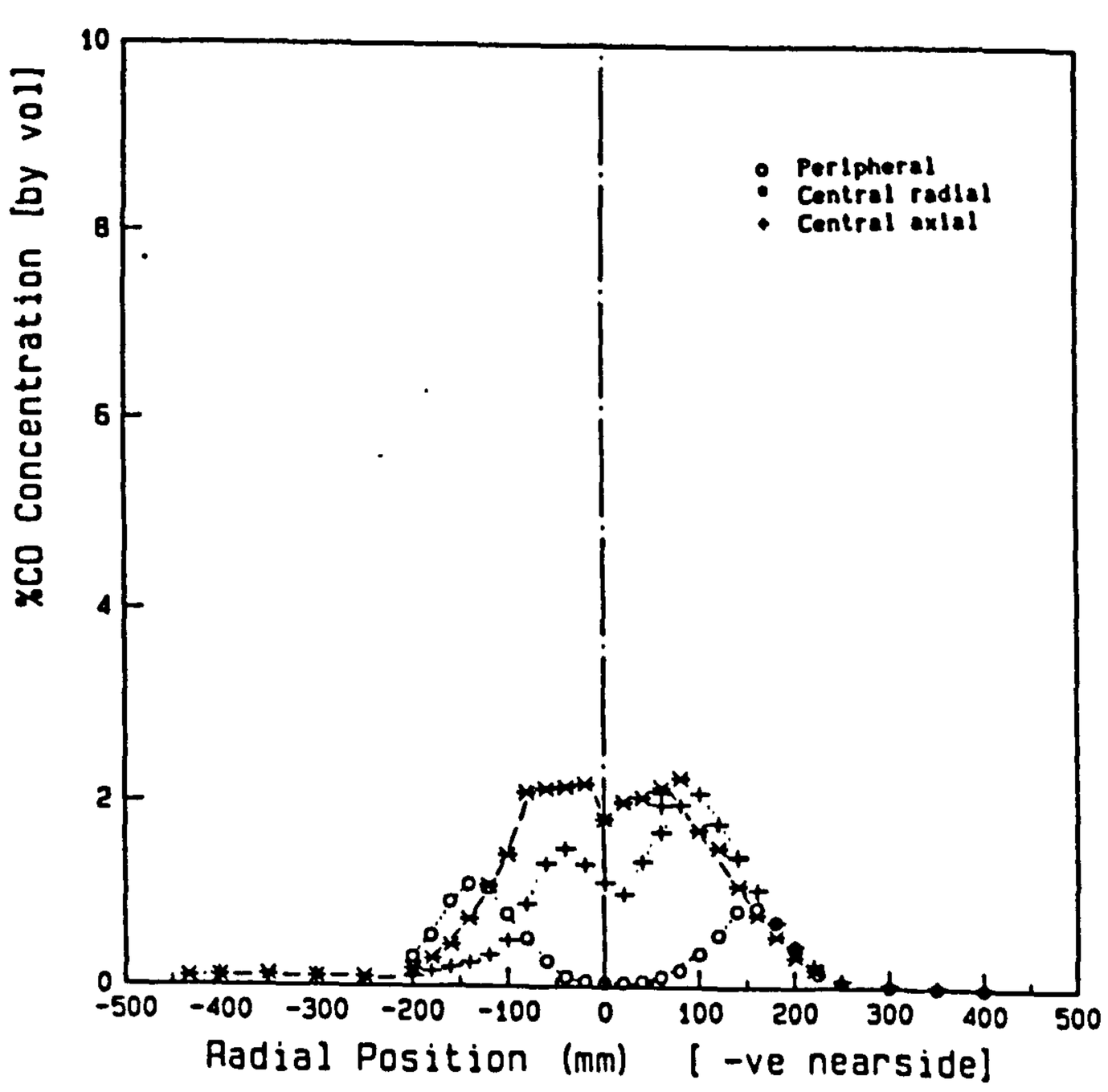

(b) S = 2.25

Fig. 14 Radial CO profiles, x = 200 mm, peripheral, radial and axial fuel injection modes

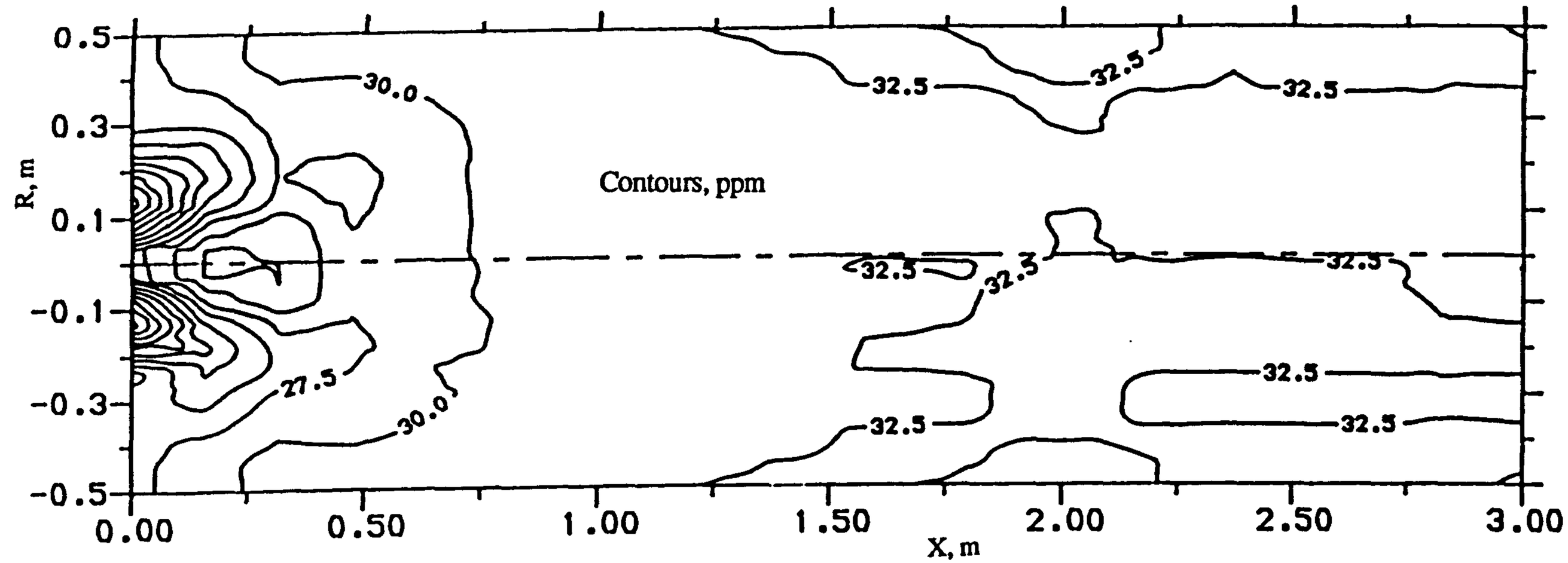

Fig. 15 NO_X contours, peripheral fule injection, Scheme 1

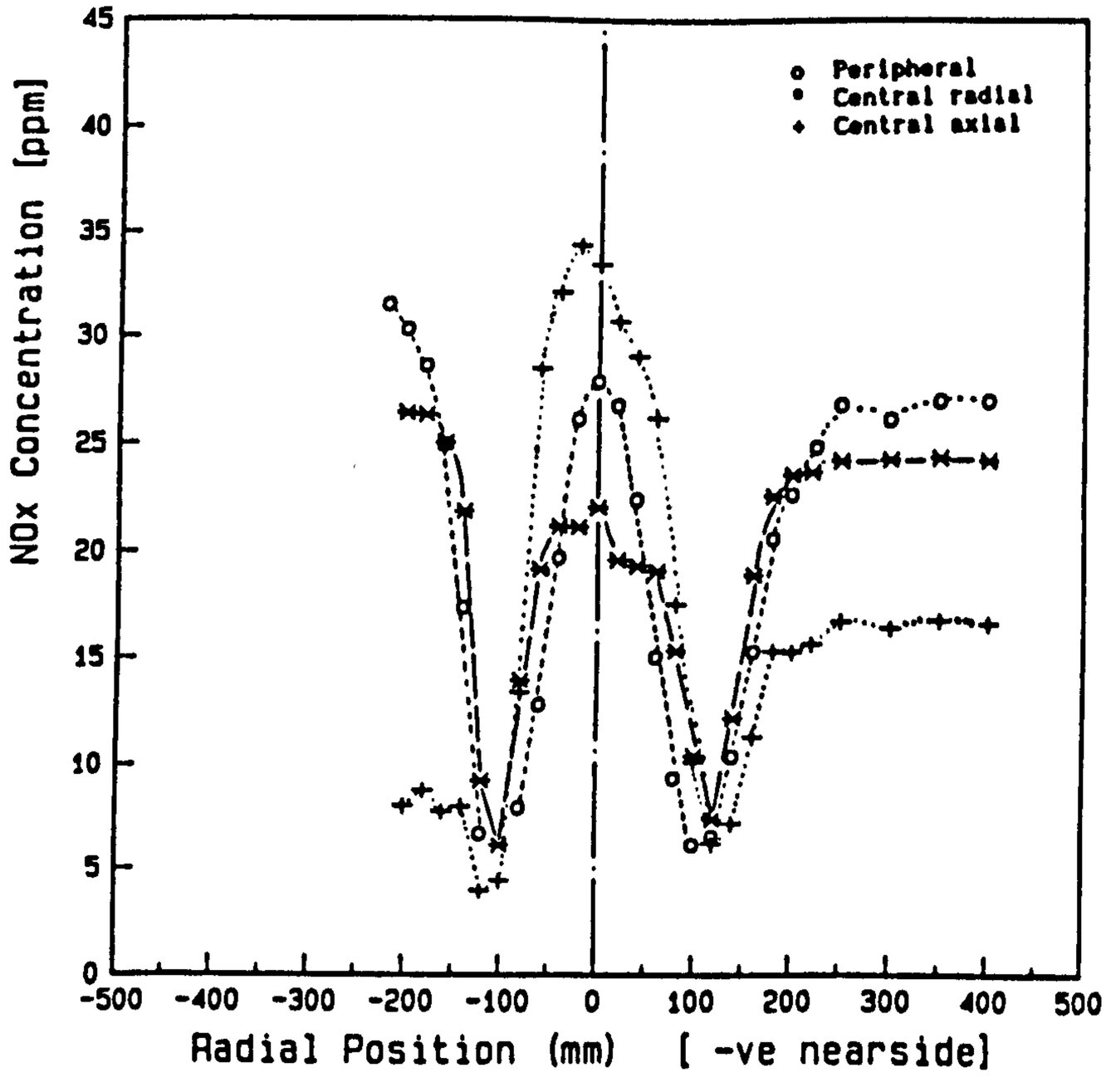

(a) S = 0.90

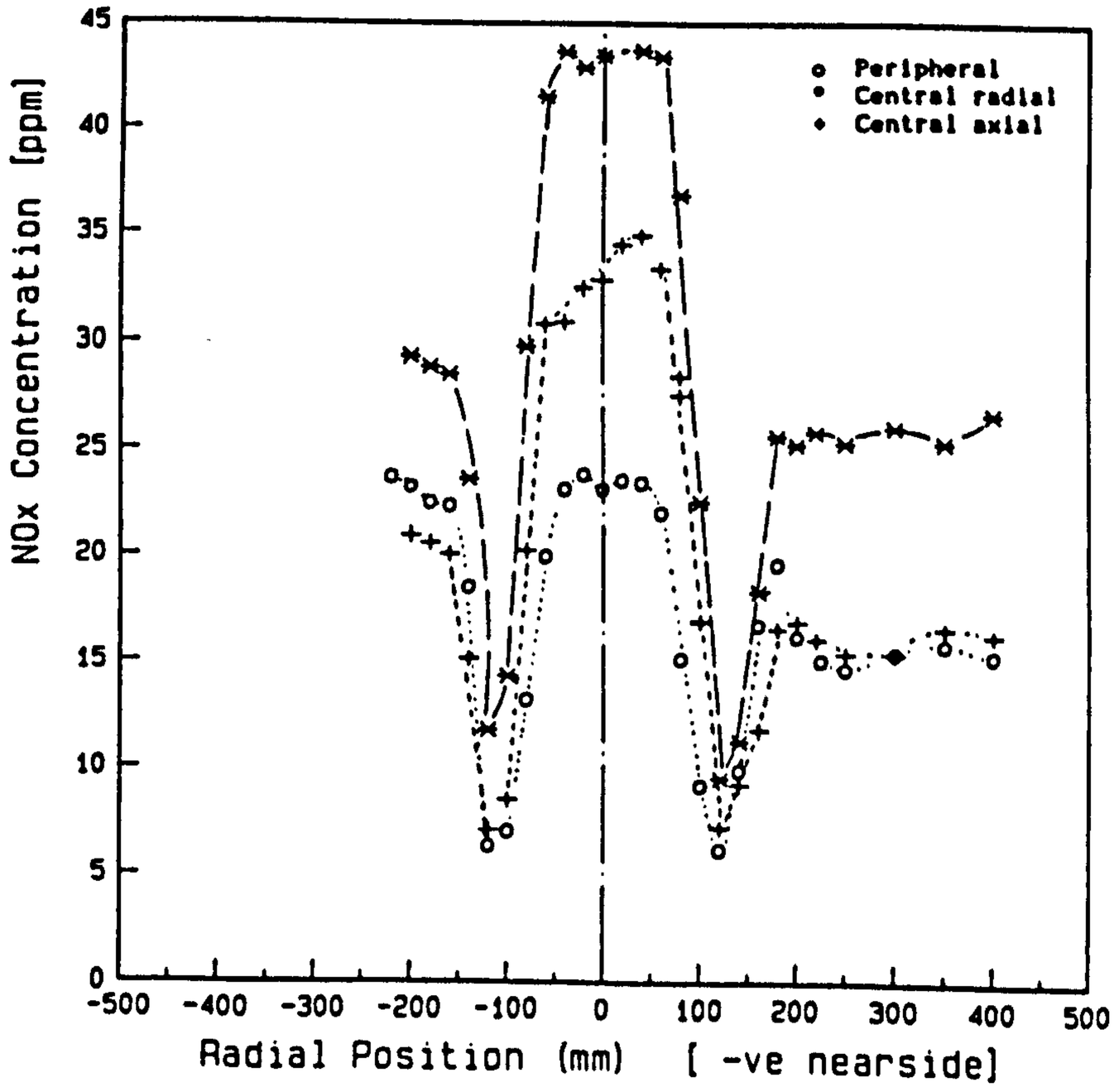

(b) S = 2.25

Fig. 16 Radial NO_X profiles, X - 45 mm, peripheral, radial and axial fuel injection modes

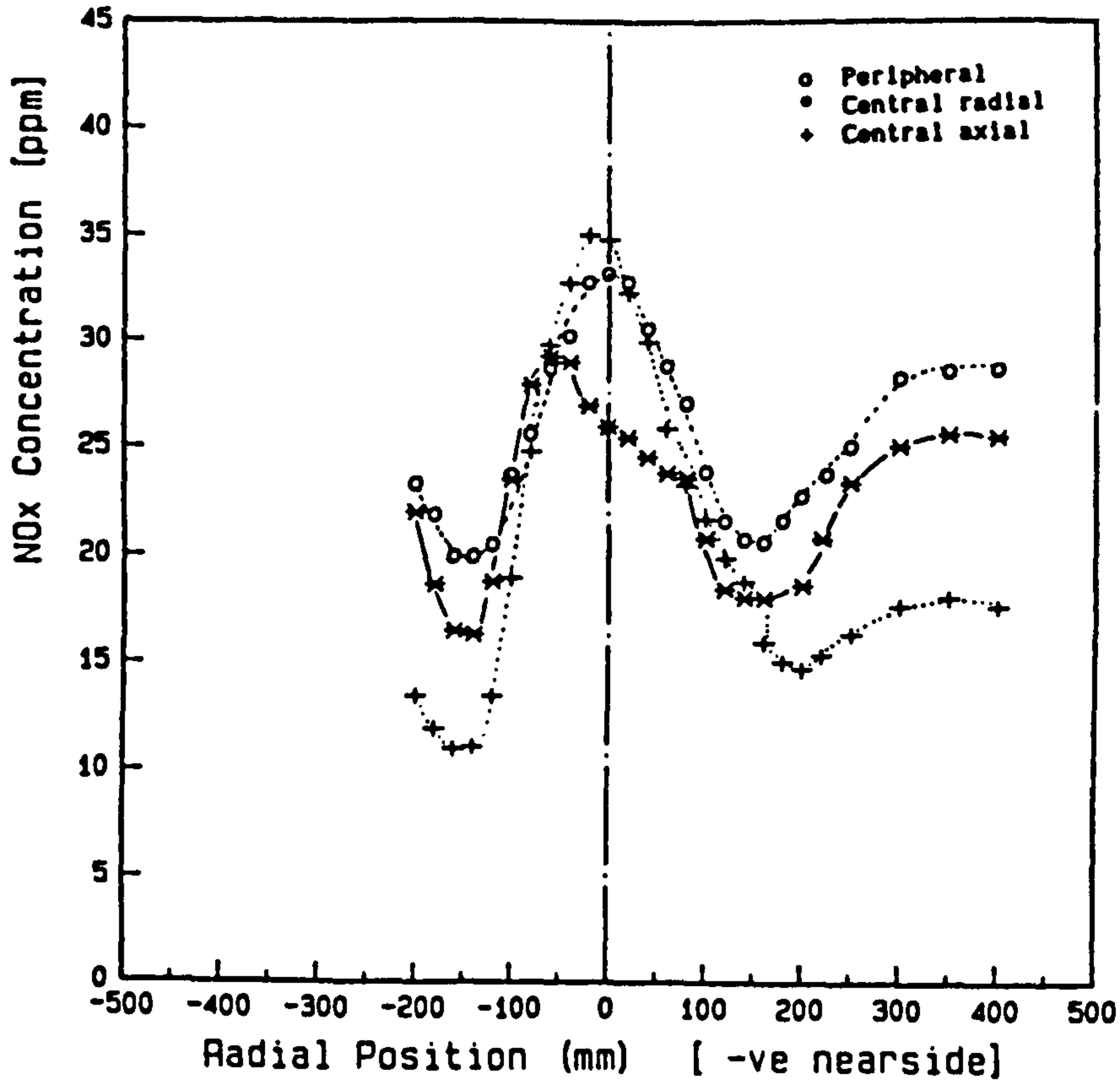

(a) S = 0.90

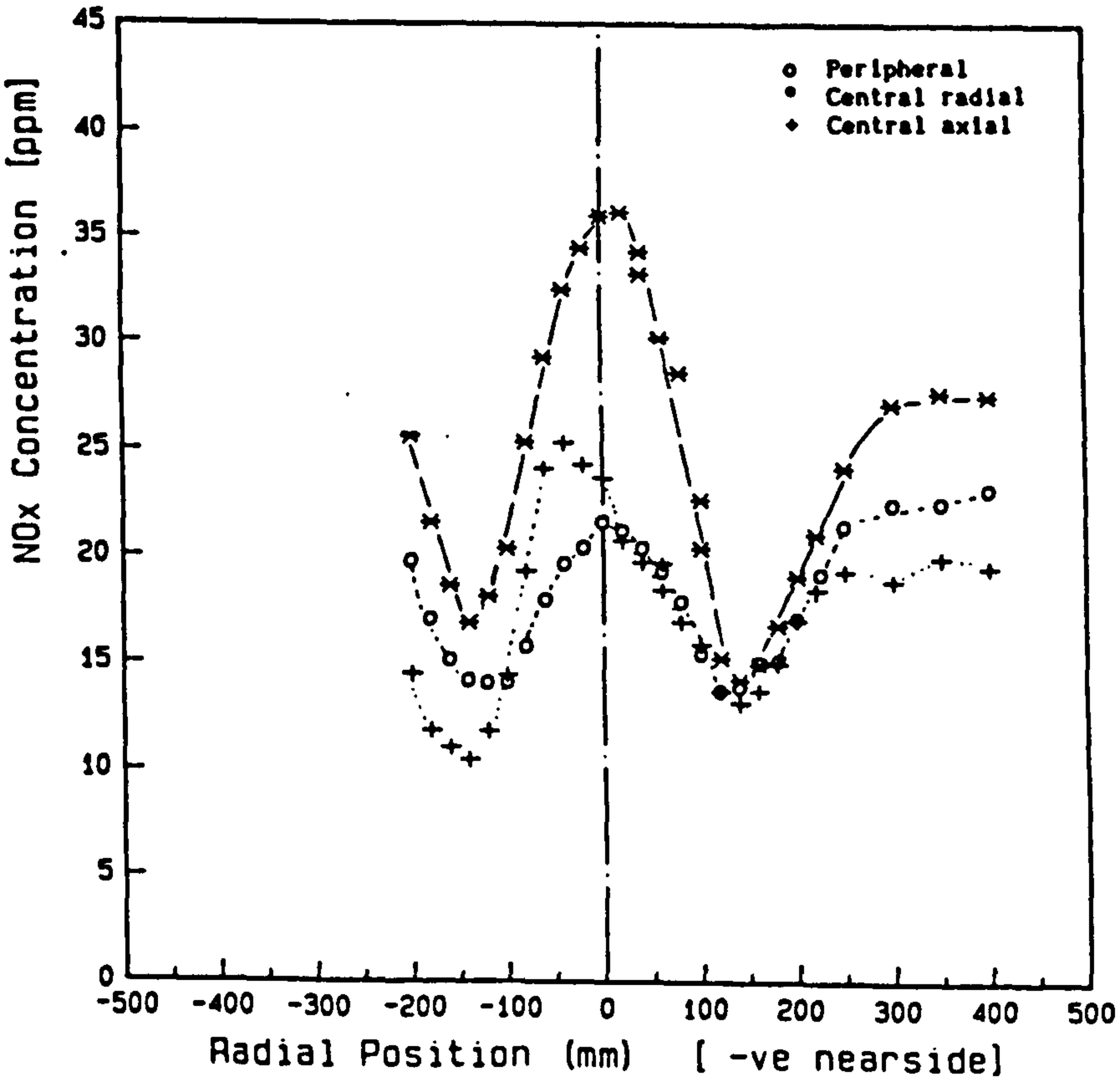

(b) S = 2.25

Fig. 17 Radial NO_x profiles, X = 200 mm, peripheral, radial and axial fuel injection modes

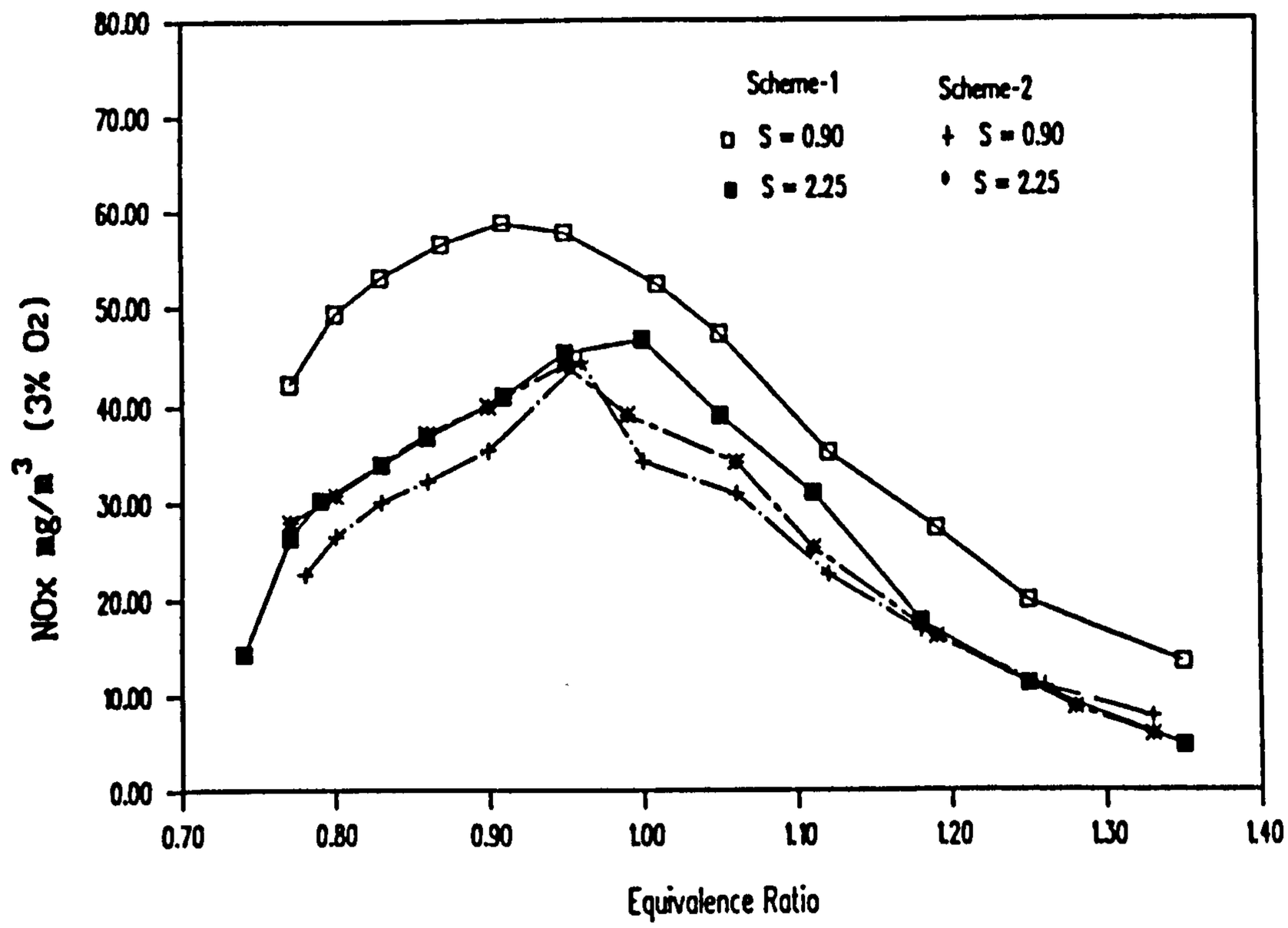

Fig. 18 Overall NO_x concentrations, peripheral fuel injection : Scheme 1 versus Scheme 2

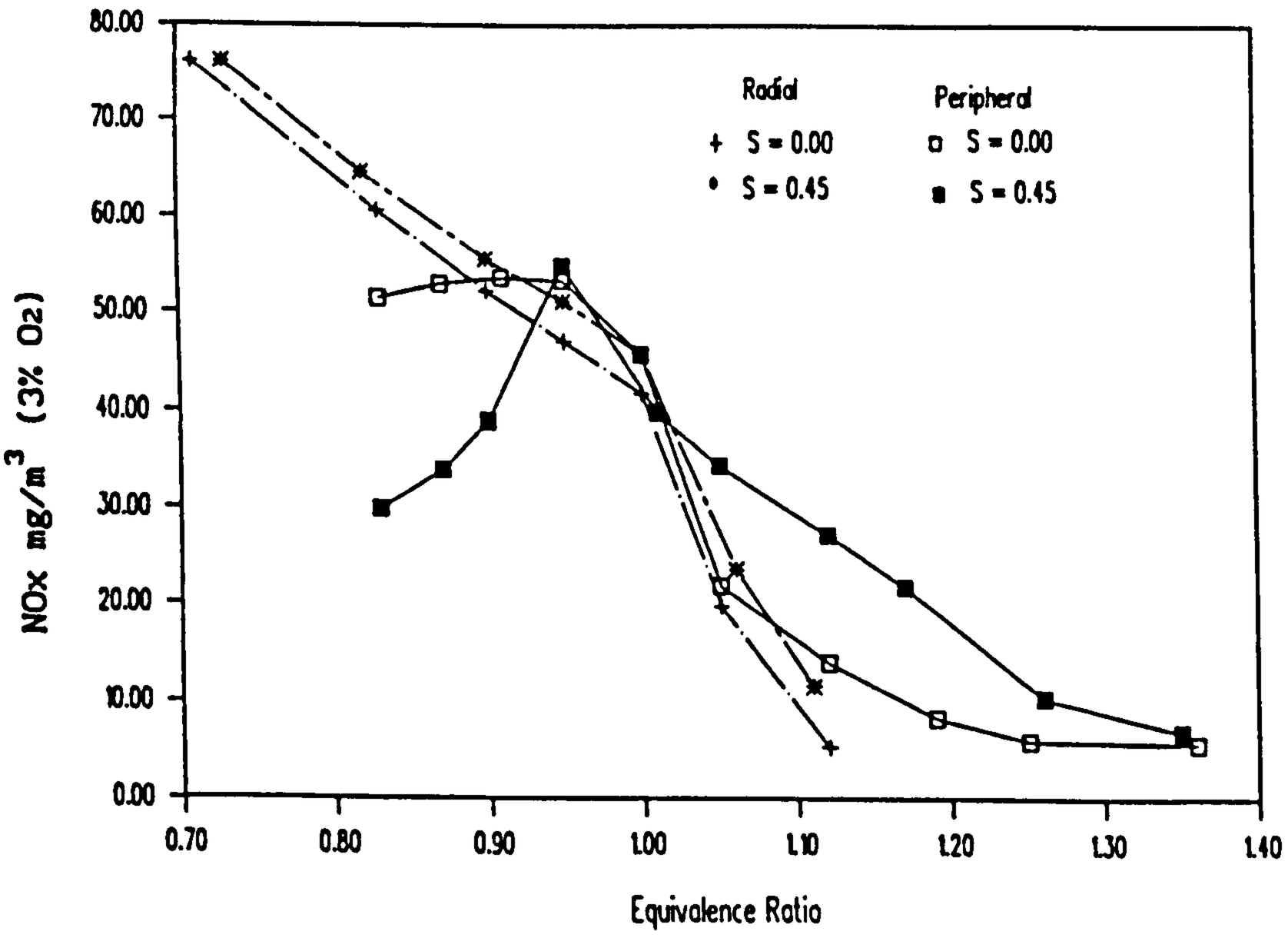

Fig. 19 Overall NO_x concentrations, peripheral (Scheme 2) versus radial fule injection

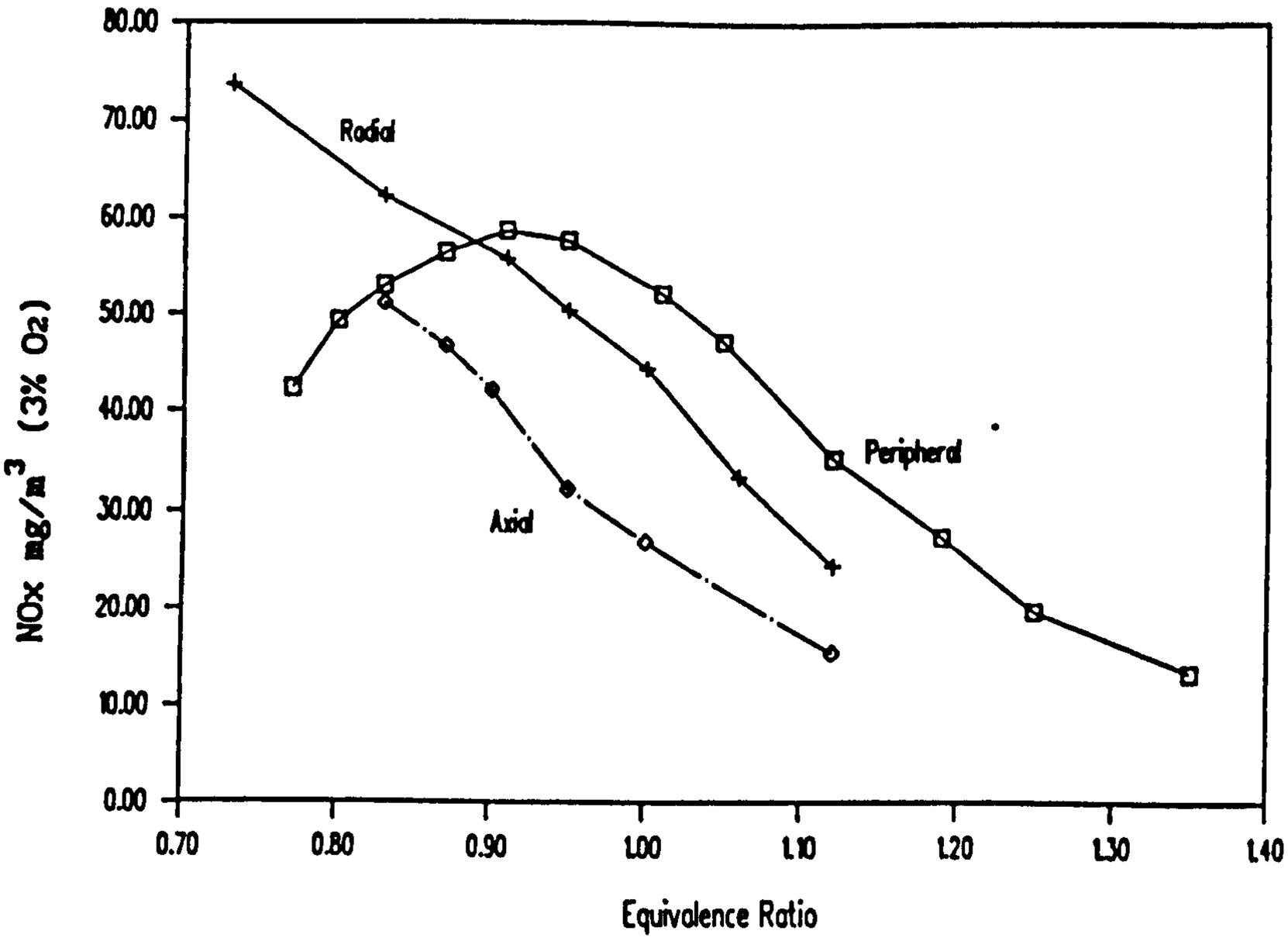

(a) S = 0.90

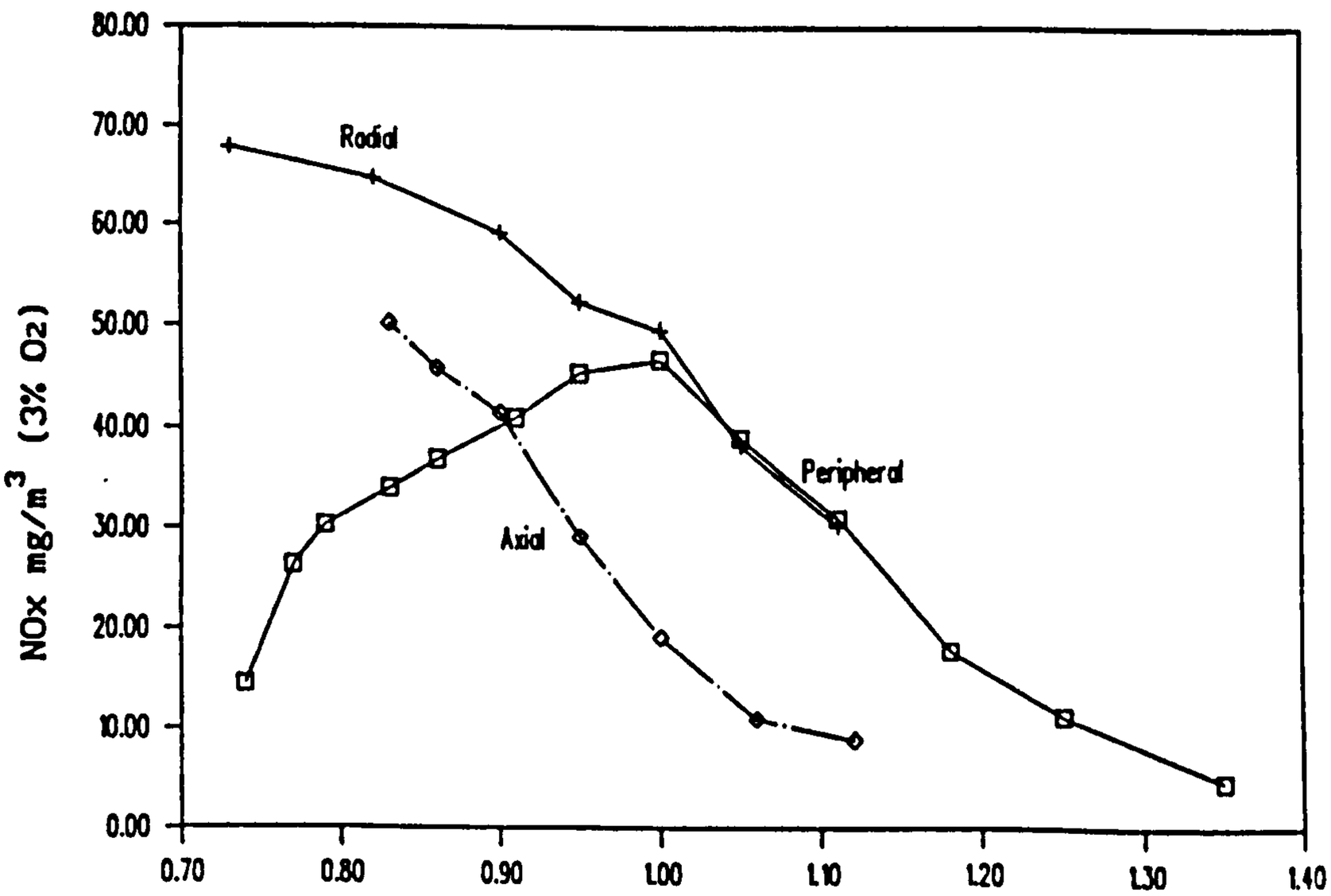

(b) S = 2.25

Fig. 20 Overall NO_x concentrations, peripheral, radial and axial fuel injection modes

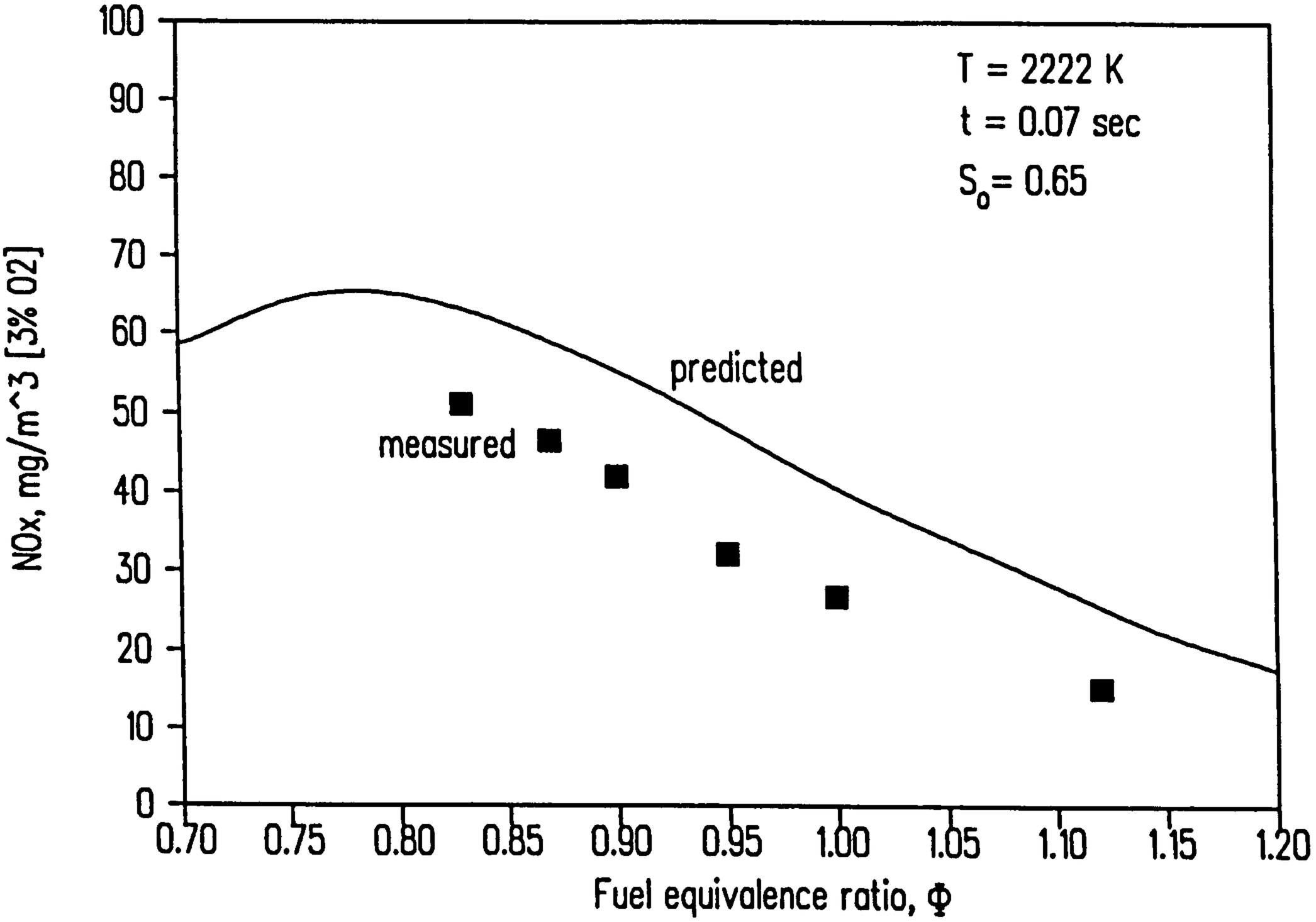

Fig. 21 Predicted and measured NO_x concentrations, central axial fuel injeciton, S = 0.90

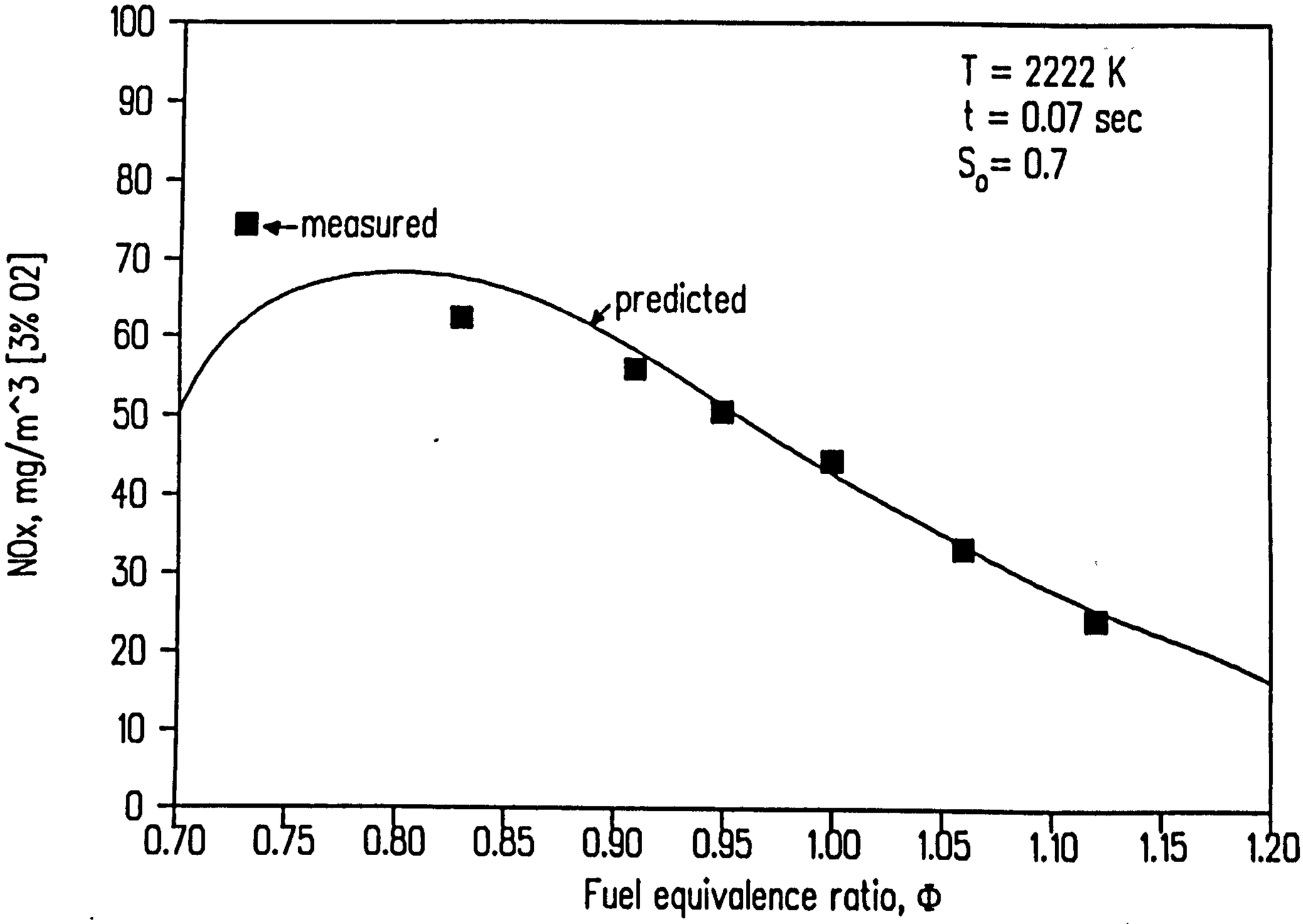

Fig. 22 Predicted and measured NO_x concentrations, radial fuel injection, S = 0.90

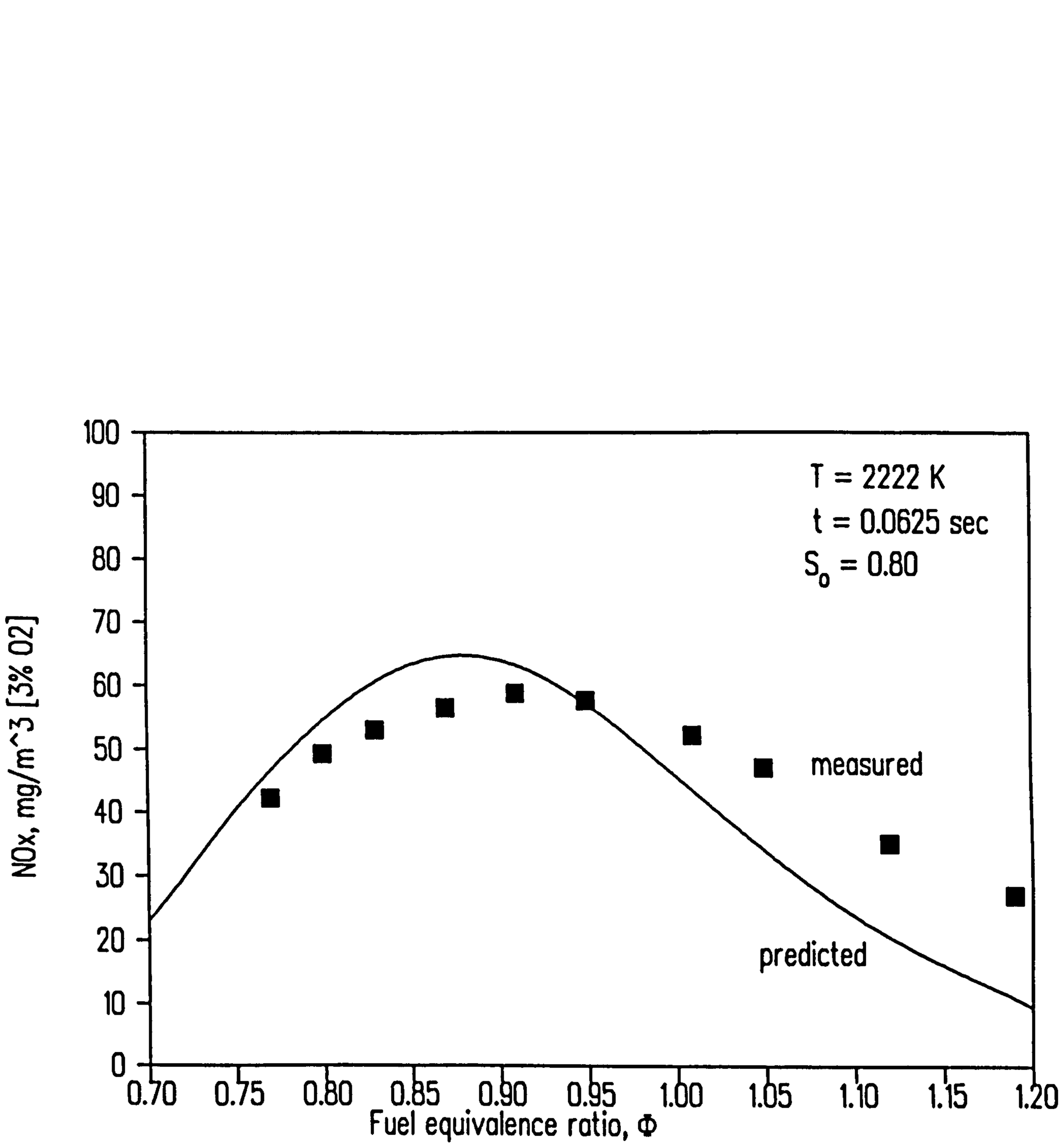

Fig. 23 Predicted and measured NO_x concentrations, peripheral fuel injection, S = 0.90

Publication 63

93-GT-402

A MODEL-BASED APPROACH TO THE CONTROL OF AN AIRCRAFT GAS TURBINE ENGINE

Oliver F. Qi
Department of Electronic Engineering and Applied Physics
University of Aston
Birmingham, United Kingdom

N. R. L. Maccallum
Department of Mechanical Engineering
University of Glasgow
Glasgow, United Kingdom

ABSTRACT

This paper describes a model-based control approach to synthesizing a nonlinear controller for a single-spool gas turbine engine. Since the main control variable, engine thrust, cannot be directly measured, a model-based observer is constructed using a nonlinear model of the engine in order to provide an on-line estimation of the thrust for feedback control. Both proportional and proportional-integral (PI) observers have been used in the model-based observer design. The latter is intended to provide a robust estimation in the event of modeling errors. The controls are the fuel flow and final nozzle area, and the control structure is the PI controller designed using the KQ (K-matrix compensator, Q-desired response) multivariable design technique. A study has been made of the model-based observer control scheme when the engine is subjected to the disturbance of inlet flow distortion. The results are shown to be acceptable in terms of the thrust response and the transient trajectory on the compressor characteristic.

1 INTRODUCTION

One of the main control objectives for a gas turbine engine is to achieve rapidly the required thrust change while ensuring stable operation of the compressor and keeping the turbine inlet temperature below the safety limit. To achieve this performance objective, it is necessary that the engine's thrust, compressor surge margin and turbine inlet temperature be monitored at all instants of time. In practice, however, these performance variables can rarely be directly measured. In this situation, to control these variables, one solution is to use the available measurements from the engine in conjunction with a mathematical model to estimate these unmeasured variables (Weber and Brosilow, 1985). In the present work, the computed thrust from the model of the engine is used for feedback control.

For linear systems, the observer theory has been well established and powerful design methods for observers are now widely available (O'Reilly 1983). However, for nonlinear systems, due to their distinct behaviour, few methods are available with sufficient generality.

Suppose a nonlinear model of a system can be represented by:

$$\dot{x} = f(x, u) \tag{1}$$

$$y = h(x, u) \tag{2}$$

An open-loop observer computes state estimates $\hat{x}(t)$ by solving:

$$\dot{\hat{x}} = f(\hat{x}, u), \quad \hat{x}(0) = \hat{x}_0 \tag{3}$$

when given on-line measurements of u and estimates of the initial states $\hat{x}_0$. For systems with asymptotically stable open-loop dynamics, the open-loop observer given above provides a simple method of reconstructing the states.

For open-loop unstable systems or open-loop stable systems with slow dynamics, a closed-loop observer can be constructed by feeding back the difference between the actual system outputs and the estimated outputs as follows:

$$\dot{\hat{x}} = f(\hat{x}, u) + K_p^*[y - h(\hat{x})] \tag{4}$$

where K_p^* is an observer gain vector. Determination of the observer gain that provides fast convergent estimates is a nontrivial task (Ohtani and Masubuchi, 1991). For systems that operate around a steady state, a popular approach consists of linearizing the nonlinear model around the steady operating point and applying well-known linear observer design methods. Misawa and Hedrick (1989) have given a very comprehensive overview of the different approaches to the nonlinear observer design problem.

2 A SINGLE-SPOOL ENGINE MODEL

The nonlinear thermodynamic model has been developed for this engine by Qi et al. (1992). The engine state variables are compressor discharge pressure P_2, turbine inlet temperature T_3, jet pipe pressure P_4 and shaft speed N. Control inputs are fuel flow and final nozzle area. The equations describing the nonlinear dynamics of the single-spool engine are:

$$\frac{dP_2}{dt} = \frac{RT_2}{v_7}((1-\alpha)\dot{M}_1 - \dot{M}_3) \tag{5}$$

Presented at the International Gas Turbine and Aeroengine Congress and Exposition
Cincinnati, Ohio — May 24–27, 1993

$$\frac{dT_3}{dt} = \gamma((1-\alpha)\dot{M}_1 T_2 + \dot{M}_f T_3 - \dot{M}_3 T_3 + Q + T_3(\dot{M}_1 + \dot{M}_f - \dot{M}_3)) \quad (6)$$

$$\frac{dP_4}{dt} = \frac{RT_4}{v_4}(\dot{M}_3 - \dot{M}_4) \quad (7)$$

$$I\frac{dN}{dt} = \frac{W_{34} - W_{12}}{N} \quad (8)$$

where $\dot{M}_1$, $\dot{M}_3$ and $\dot{M}_4$ are the compressor, turbine and nozzle inlet mass flow rate, respectively. $\dot{M}_f$ is the fuel flow. v_2 and v_4 are the sizes of intercomponent volumes. α is the bleed flow factor. Q is the heat released by burning fuel. T_2 is compressor exit temperature, T_3 and T_4 are the turbine and nozzle inlet temperature, respectively. W_{34} is the power produced by the turbine, and W_{12} is the power consumed by the compressor.

In a gas turbine engine, there are two important classes of outputs. e.g. those that are measurable and those that are not measurable. Measured outputs typically include rotor speeds, temperatures, and pressures throughout the engine gas path. These quantities are often used to model thermodynamic responses and are, therefore, generally state variables . Unmeasured outputs represent engine performance and limiting quantities such as thrust, surge margin, and turbine inlet temperature. These quantities are related to the state variables by thermodynamic equations, such as shown in equation 2.

Disturbances may occur during engine operation. They are primarily caused by control actuator uncertainties or unsteady flow phenomena such as inlet flow distortion. Disturbances may be modeled explicitly for synthesis or, as is common, may be considered qualitatively during the design process in the selection of dynamic design criteria such as weightings and bandwidth. Validation of disturbance rejection and control performance is typically performed on detailed nonlinear simulations of the engine after a design has been completed (DeHoff and Hall, 1979).

3 A MODEL-BASED OBSERVER

The idea of using the model-based observer to synthesize practical nonlinear controllers was first proposed by Gawthrop (1992). The basic philosophy is to run a nonlinear model in parallel with the modeled system. In the present study, parametric uncertainty is assumed, but the model is assumed structurally correct as it is developed from basic thermodynamic principles.

The general scheme of a model-based observer is illustrated in Fig.1. The different aspects of the approach are listed below:

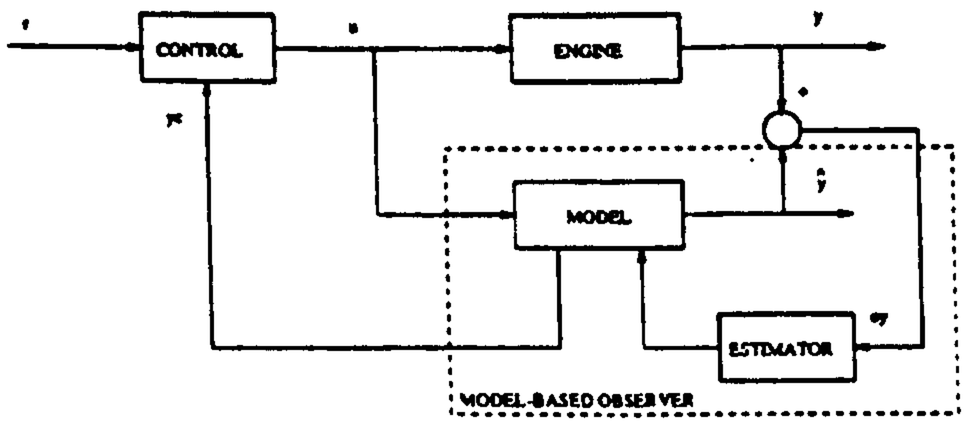

Figure 1: The structure of a model-based observer

- A dynamic simulation model is placed in parallel with the engine to be controlled. This model will usually be nonlinear.
- The measured outputs y of the engine are compared with the corresponding model outputs $\hat{y}$ to create an error e_y.
- The model states have feedback applied to them in such a way as to drive the output error e_y to zero.
- The controller generates the control signal u in terms of any set of variables y_c generated within the model together with the setpoint r.
- If the model-based observer is working well, these variables y_c will be the same as, or close to, the corresponding variables generated within the engine itself.

In Fig.1, the known control inputs which drive the engine are also fed to the mathematical model. The selected measurements from the engine are compared with their corresponding quantities from the model. The differences between them are fed back to the appropriate parts of the model. In this way, the model states will be forced into alignment with their corresponding states of the engine. Therefore, the problem in using a model based observer lies in designing the efficient algorithms for the feedback of e_y to the model such that alignment of the states could be achieved in the shortest possible time while rejecting disturbances and modeling errors.

It should be noted that there are two differences between the engine and the model:

- Corresponding to each of the engine state variables, there is an element in u_r, which can be regarded as an additional imaginary input to the model state, and it will be related to the error e_y. This provides a means of adjusting the model states towards the corresponding engine states.
- All the variables of the model are available for measurement, and the model is implemented an an on-board control computer.

The purpose of the model-based observer is to drive the model states towards the engine states. The purpose of the control is to drive appropriate model variables towards desired setpoints.

3.1 PROPORTIONAL OBSERVER

If we assume that the model is an exact representation of the engine, a proportional observer can be constructed as demonstrated in the present application.

Linearizing the nonlinear model (equation 1 and 2) at the nominal operating point (x_o, u_o), the linear design model is then given as:

$$\delta\dot{x} = A_o\delta x + B_o\delta u \quad (9)$$

$$\delta y = C_o\delta x \quad (10)$$

where A_o, B_o and C_o are matrices of appropriate dimensions. We drop the δ to simplify the exposition, which now follows.

The observer equation is:

$$\dot{\hat{x}} = A_o\hat{x} + B_o u + u_r \quad (11)$$

Here the inputs u_r have the same dimensions as the states. The idea is that if a difference exists between any of the engine outputs and model outputs, the corresponding element of u_r will be used to offset this error by compensating the model states using $K_p e_y$. The model-based observer can be created from the model together with the feedback:

$$u_r = K_p e_y \quad (12)$$

There are many possibilities for designing the observer feedback gains K_p, e.g. Linear Quadratic (LQ) or pole placement method. In the present work, the observer gain K_p is designed using LQ theory based on the linear model corresponding to the engine take-off condition.

It should be noted that although the feedback is linear, the observer itself is nonlinear.

3.2 PROPORTIONAL & INTEGRAL(PI) OBSERVER

If modeling errors exist, or the engine is subjected to unknown disturbances, the engine states and model states will be different in the steady-state. As a result, the corresponding outputs will deviate from each other. In this circumstance, the PI observer is considered to be appropriate (Jones, 1992).

For a linear time-invariant system, the PI observer has been proposed by Mielczarski (1987), and given as:

$$\begin{aligned} \dot{\hat{x}} &= (A_o - LC_o)\hat{x} + B_o u + Ly + K v \\ \dot{v} &= y - C_o \hat{x} \end{aligned} \tag{13}$$

The system defined by equation 13 is said to be a full-order PI observer for the system if and only if:

$$\lim_{t\to\infty} e(t) = 0, \quad \lim_{t\to\infty} v(t) = 0 \tag{14}$$

and all the eigenvalues of the matrix

$$R = \begin{bmatrix} A_o - LC_o & K \\ -C_o & 0 \end{bmatrix} \tag{15}$$

have negative real parts. where $e(t) = \hat{x}(t) - x(t)$,

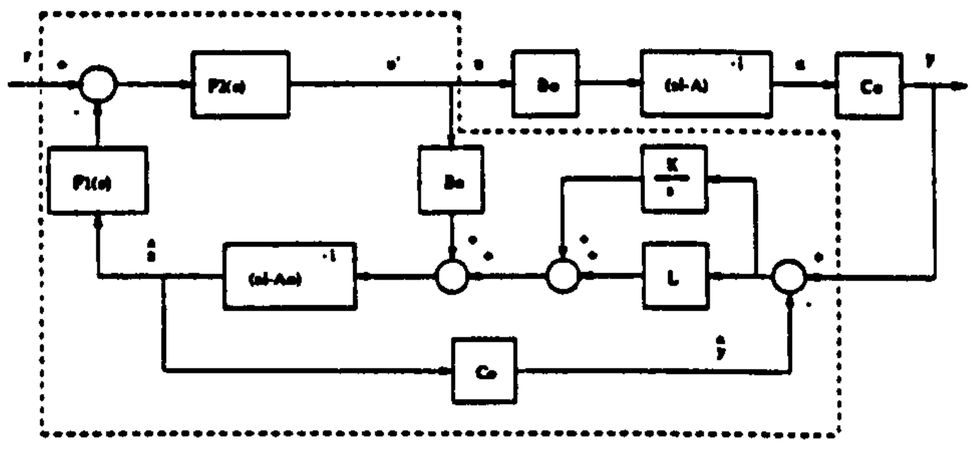

Figure 2: The Structure of a PI Observer

The PI observer structure is shown in Fig.2, from which u_r is related to v as:

$$u_r = Lv + \int K v dt \tag{16}$$

3.3 ROBUST DESIGN OF PI OBSERVER

In this section, a robust design of PI observer is presented. The robustness is considered when facing plant parameter variations, these falling into the category of structured perturbations. In this case, the engine can be modeled as:

$$A = A_o + \Delta A \tag{17}$$

The $n \times n$ matrix ΔA defines the prescribed ranges of variation for the nominal set of plant parameter A_o.

A simple method has been used to determine the PI observer gains following Beale and Shafai (1989). Referring to Fig.2, in ideal case (no observer loop) the transfer function from r to x are given as:

$$x(s) = (sI - (A - B_o F))^{-1} B_o r(s) \tag{18}$$

Hence, the final state is:

$$x(\infty) = -(A - B_o F)^{-1} B_o r(\infty) \tag{19}$$

where $x(\infty) = \lim_{t\to\infty} x(t)$, $r(\infty) = \lim_{t\to\infty} r(t)$. Here A is the true plant matrix as given above and F can be related to the steady-state gains of the controller designed in section 4.

In practice, the transfer functions from r and v to x and $\dot{x}$ are given by:

$$\begin{bmatrix} x(s) \\ \dot{x}(s) \end{bmatrix} = (sI - \Sigma)^{-1} \left\{ \begin{bmatrix} B_o \\ B_o \end{bmatrix} r(s) + \begin{bmatrix} 0 \\ K \end{bmatrix} v(s) \right\} \tag{20}$$

where

$$\Sigma = \begin{bmatrix} A & -B_o F \\ LC_o & A_o - LC_o - B_o F \end{bmatrix} \tag{21}$$

For loop transfer characteristics of the full-state feedback implementation to be recovered at the steady-state in the PI observer-based implementation, it is necessary for $\hat{x}(s)$ and $x(s)$ to be identical at the steady-state. Equating the two, the following condition holds:

$$K v(\infty) = \phi r(\infty) \tag{22}$$

where

$$\phi = \left[(A_o - B_o F)(A - B_o F)^{-1} - I\right] B_o \tag{23}$$

or

$$\phi = -\Delta A (A - B_o F)^{-1} B_o \tag{24}$$

Equation 22 provides a way to tune the PI observer gains K and L. The procedure can be summarized as:

- Set $L = K_p$ (proportional observer) and $K = 0$, find the maximum possible magnitude of $v(\infty)$ by simulations.
- Optimize $J = \|K v(\infty) - \phi r(\infty)\|_2$ in least-square sense to find gain K.
- Further tuning the L and K using the nonlinear simulation.

4 CONTROLLER DESIGN

The KQ (K-matrix compensator, Q-desired response) method has been sucessfully applied to design nonlinear scheduling controllers by Polley et al (1989). The KQ method compensator design methodology is a frequency-domain technique, which uses closed-loop Nyquist and Bode plots. The parameters of the dynamic matrix compensator K are estimated by minimizing the mean square error between the desired closed-loop response Q and the actual closed-loop response. This design, described by Edmunds (1979), consists of the following steps:

- Specification of desired closed-loop transfer function matrix
- Selection of multivariable compensator structure (proportional or proportional/integral, etc.)
- Computation of compensator gains
- Closed-loop performance evaluation.

The performance requirements used for the engine control design may be expressed in terms of requirements for good feedback control, which are:

- Low-frequency command following
- Low-frequency disturbance rejection

- Insensitivity to sensor error
- Robustness to unmodeled high-frequency dynamics
- Insensitivity to low-frequency modeling errors.

These performance requirements are met by using the KQ technique to design the compensator and ensuring that the singular value plots satisfy the required frequency domain constraints. Control of the gas turbine engine specifically requires:

- Fast thrust response without overshoot
- Zero steady-state error.

The fast thrust response requirement is fulfilled by designing to achieve maximum crossover frequencies for the output variables while producing a thrust transient response with no overshoot. The zero steady-state error requirement is met by using a multivariable proportional plus integral (PI) controller (the integrators are added to ensure zero steady-state error). In the present work, the control objective is to drive the engine thrust to the maximum take-off thrust without overshoot, hence the desired closed-loop response is selected as:

$$Q = diag[\frac{a_i}{s + a_i}], \quad i = 1,2 \tag{25}$$

It is noted that although the detuned controller is used, the model-based control scheme (nonlinear model, observer and control) is nonlinear.

5 SIMULATION RESULTS

5.1 OBSERVER PERFORMANCE

The simulations shown in Fig.3 and 4 are based on the assumptions that the model is the exact representation of the engine, i.e. parametrically and structurally correct, but the initial states of the model have been incorrectly guessed, that is the model states are different from the engine states. By subjecting the engine and the model to the same ramp fuel input, from idling to take-off conditions in 4 seconds, the performance of the model-based observer is examined. In Fig.3 and 4, the solid lines are the engine responses and the dashed lines are model responses when setting $K_p = 0$ (open-loop observer). In this case, it is seen that the open-loop dynamics dominate the observer performance. It is also seen that although the engine and model have converged to the same steady-state condition, the rates of convergence (3 seconds) are slow and are considered unsatisfactory in gas turbine application.

Fig. 3 and 4 also show the responses of closed-loop observer (dotted lines). The gain K_p is determined using LQ theory. Comparing with the case of $K_p = 0$, it is seen that due to the feedback action, the errors between the engine and the model have been eliminated quickly, that the closed-loop performance can be guaranteed. It is noted that in Fig.4b, by closing the observer loop ($K_p \neq 0$), the surge of the compressor (dashed line below 0 value) in open loop case ($K_p = 0$) has been avoided.

A convenient way of modeling the turbine in a single-spool gas turbine engine is to use single characteristics as shown by Szuch (1977). These characteristics relate pressure ratio to non-dimensional mass flow and isentropic efficiency in simple manners, which are independent of non-dimensional shaft speed. Mathematically, they can be expressed as:

$$\frac{\dot{m}\sqrt{T_{in}}}{P_{in}} = f_m(\frac{P_{in}}{P_{out}}) \quad \frac{P_{in}}{P_{out}} \leq (\frac{P_{in}}{P_{out}})_{max} \tag{26}$$
$$= (\frac{\dot{m}\sqrt{T_{in}}}{P_{in}})_{max} \quad \frac{P_{in}}{P_{out}} \geq (\frac{P_{in}}{P_{out}})_{max}$$

$$\eta_{is} = f_e(\frac{P_{in}}{P_{out}}) \quad \frac{P_{in}}{P_{out}} \leq (\frac{P_{in}}{P_{out}})_{max} \tag{27}$$
$$= (\eta_{is})_{max} \quad \frac{P_{in}}{P_{out}} \geq (\frac{P_{in}}{P_{out}})_{max}$$

If such a simplification is used, the resultant model will be different from the one used in the present study (using the speed-dependent characteristics), therefore the modeling errors will show up in e_y in steady-state. In this case, the PI observer is used to provide the robust estimations of the steady-state. The simulations are shown in Fig.5 and 6. The use of the PI observer gives the dotted line.It is seen that robust steady-state estimations have been achieved.

5.2 CLOSED-LOOP CONTROL

The simulations of the closed-loop performance are shown in Fig.7 and 9. The linear controller is determined by selecting the desired closed-loop response as shown in equation 25 with $a_i = 4, \ i = 1,2$. The computed thrust and shaft speed from the model are used for feedback control. It is seen that the thrust has been driven to the take-off value in about 4 seconds (Fig.8a). Closed-loop control demonstrates good thrust response and adequate surge margin (Fig.8b). The closed-loop control results in the transient running line following the steady running line (see Fig.9).

5.3 KNOWN DISTURBANCES

Inlet flow distortion can cause the engine inlet pressure and temperature to fluctuate (Goethert and Kimzey, 1968), and these may be treated as disturbances, which tend to cause the compressor to surge. To simulate the effects of disturbances on the current control scheme, the following simple model has been used. Moore (1986) has suggested that a model of the following type might be helpful:

$$\overline{P}_1 = P_1 + A_d P_1 sin(\omega_d t) \tag{28}$$

$\overline{P}_1$ is the perturbed inlet pressure, P_1 nomial inlet pressure. A_d perturbation amplitude, ω_d perturbation frequency. In the present simulation studies, $A_d = 0.1$ and $\omega_d = 10$ are used.

It is noted that this is equivalent to disturbing all the states along the engine gas path as well as shaft speed. The current control scheme was tested by introducing the inlet pressure disturbance at time $t = 6$ *sec.* when the engine was running steadily at maximum speed and thrust after completing the acceleration The simulations are shown in Fig.10 and 11. It is seen that the model follows the engine very well after the disturbance occurred (at t = 6 second). It is noted that when disturbances occur, the compressor surge margin is greatly reduced (Fig. 11b). However, It is also seen that the current control scheme has the ability to bring the magnitude deviation of the surge margin back to that of nomial case (no perturbation).

6 CONCLUSIONS

Direct control of the engine thrust, as computed from the model, avoids the control mode analysis, which otherwise has to be used in engine control design. The latter process requires selection of the mode which best reflects the change of engine thrust. This process can be

very time consuming, but is of critical importance to engine control design as shown in the previous work by Brown and Elgin (1985).

An outline of the model-based observer approach to model-based control has been given. It can be seen that the focus has been on the observer rather than the controller, as control becomes relatively simple when all measurements are available.

It is shown that direct control of engine thrust is possible by using the proposed model-based observer control scheme. The time taken for the model states to converge to the engine states is at most 0.5 second. As the result ,the observers are capable of estimating engine thrust in 0.5 second. In the present work, observer gains are designed on the basis of a linear model. The use of PI observer is shown to provide a robust performance. Further work will use the more advanced control strategies and a critical comparison with other model-based approaches.

7 REFERENCES

Beale, S. and Shafai, B., 1989, "Robust Control System Design with a Proportional Integral Observer", *International Journal of Control* Vol. 50, pp. 97-111.

Brown, H. and Elgin, J.A., 1985 "Aircraft Engine Control Mode Analysis", ASME *Journal of Engineering for Gas Turbines and Power*, Vol. 107, pp. 838-844.

DeHoff, P.J. and Hall, JR. W. E., 1979, "Optimal Control of Turbine Engines", ASME *Journal of Dynamic Systems, Measurements and Control*, Vol. 101, pp. 117-126.

Edmunds, J. M., 1979, "Control System Design and Analysis Using Closed-loop Nyquist and Bode Array", *International Journal of Control* Vol. 30, pp. 773-802.

Gawthrop, P. J., 1992, "Model-Based Observer: An Introduction", Control Group Research Report R-92/7, Department of Mechanical Engineering, University of Glasgow.

Goethert, B. H. and Kimzey, W. F., 1968, "Effect of High-Frequency Fluctuations of Inlet Flow On Compressor Stall" *Proceedings, 32nd Meeting of the Propulsion and Energetics of AGARD*, Toulouse, France.

Hoffman, P. J., Polley, J. A. and Adibhatla, S., 1989, "Multivariable Turbofan Engine Control for Full Flight Envelope", ASME *Journal of Engineering for Gas Turbines and Power*, Vol. 111, pp. 130-137.

Jones, R. W., 1992, "Nonlinear Inferential Control Using Model-Based Observer Control", Control Group Research Report R-92/9, Department of Mechanical Engineering, University of Glasgow.

Mielczarski, W., 1987, "Observing the States of a Synchronous Generator: Part 1, Theory", *International Journal of Control*, Vol. 45, pp. 987-1000.

Misawa, E. A. and Hedrick, J. K., 1989, "Nonlinear Observers: A State-of-the-art Survey", ASME *Journal of Dynamic Systems, Measurements and Control*, Vol. 111, pp. 344-352.

Moore, F. K., 1986, "Stall Transients of Axial Compression Systems with Inlet Distortion", *Journal of Propulsion*, Vol. 2, pp. 552-561.

Ohtani, T. and Masubuchi, M., 1991, "Design Methods of Nonlinear Compensators Based on Canonical Forms", *Proceedings, First IFAC Symposium on Design Methods of Control Systems*, ETH Zurich, Switzerland.

O'Reilly, J., 1983, "Observers for Linear Systems", *Mathematics in Science and Engineering*, Academic Press.

Qi, O. F., Maccallum, N. R. L. and Gawthrop, P. J., 1992, "Improving Dynamic Response of a Single-Spool Gas Turbine Engine Using a Nonlinear Controller", *Proceedings, 37th ASME Gas Turbines and Aeroengine Congress*, Cologne, Germany.

Szuch, 1977, "F-100 Multivariable Control Synthesis: Program Evaluation of a Multivariable Control Using a Real-Time Engine Simulation", NASA TP 1056

Weber, R. and Brosilow, C., 1985, "The Use of Secondary Measurements to Improve Control", *AIChE Journal*, Vol. 18, pp. 107-118.

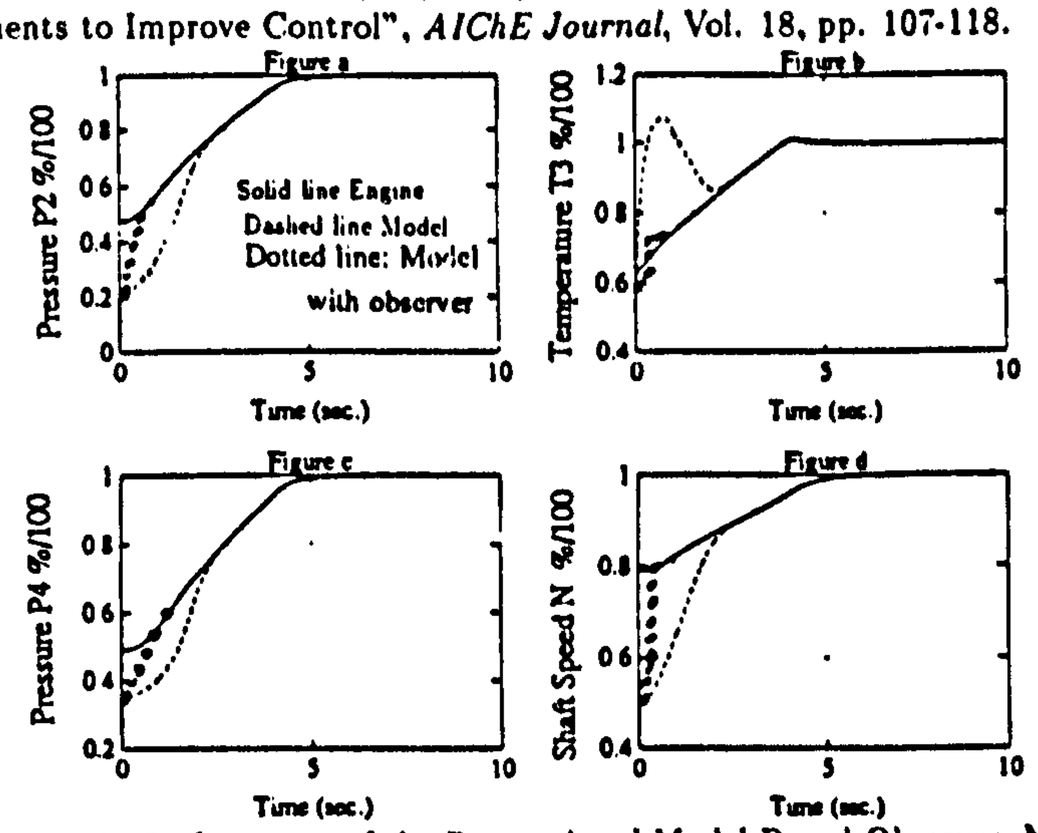

Figure 3: Performance of the Proportional Model-Based Observer, No Closed-loop Control.

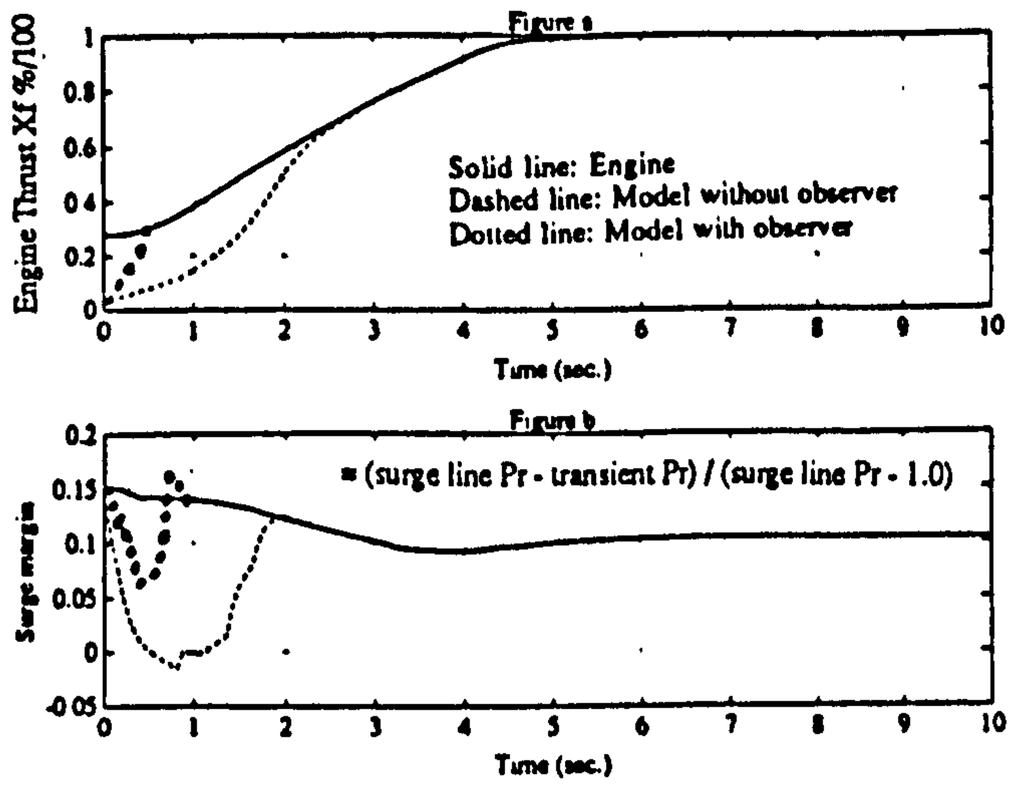

Figure 4: Performance of the Proportional Model-Based Observer, No Closed-loop Control.

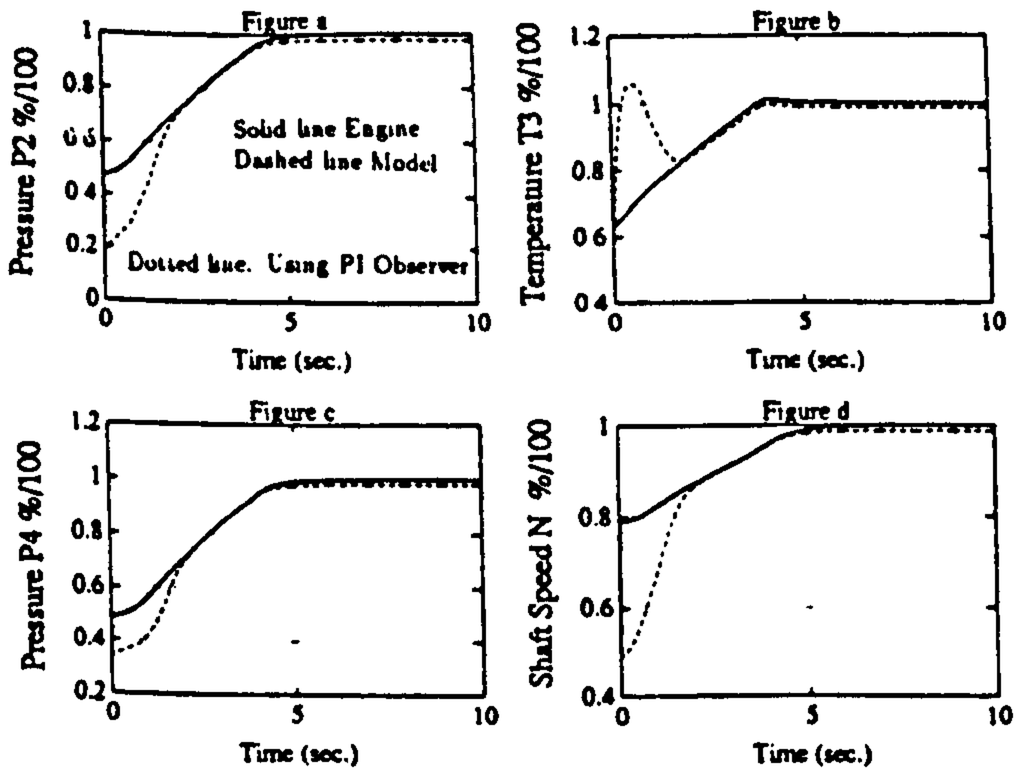

Figure 5: Performance of the PI Model-Based Observer, No Closed-loop Control.

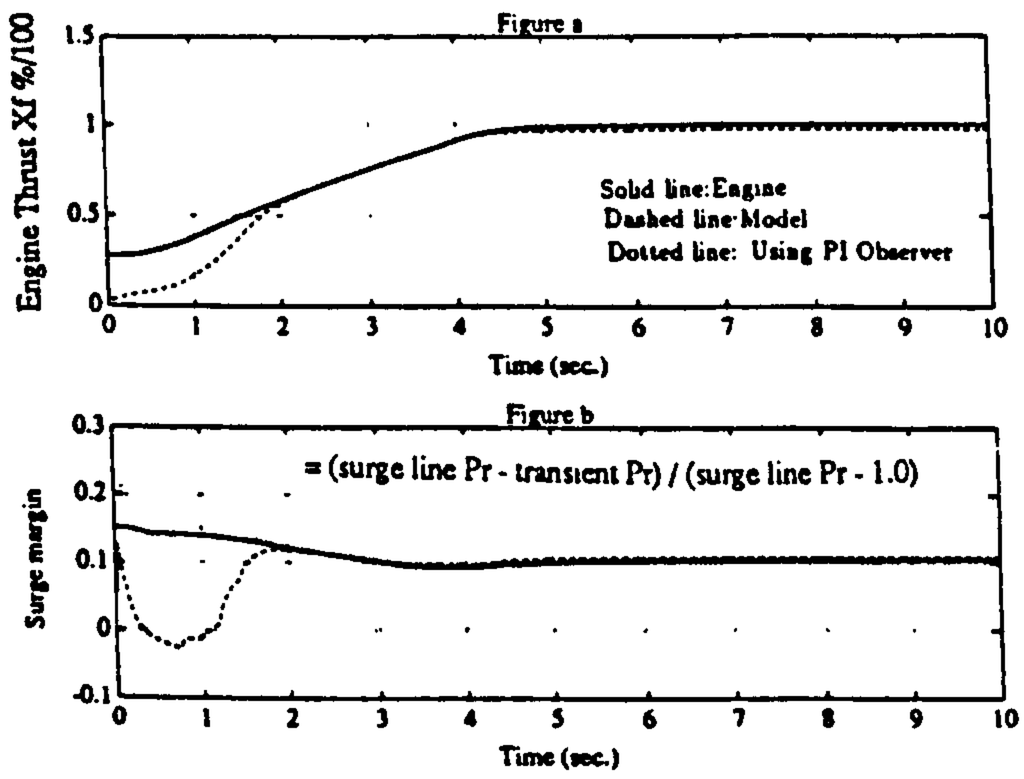

Figure 6: Performance of the PI Model-Based Observer, No Closed-loop Control.

Figure 7: Performance of the Proportional Model-Based Observer Plus Closed-loop Control.

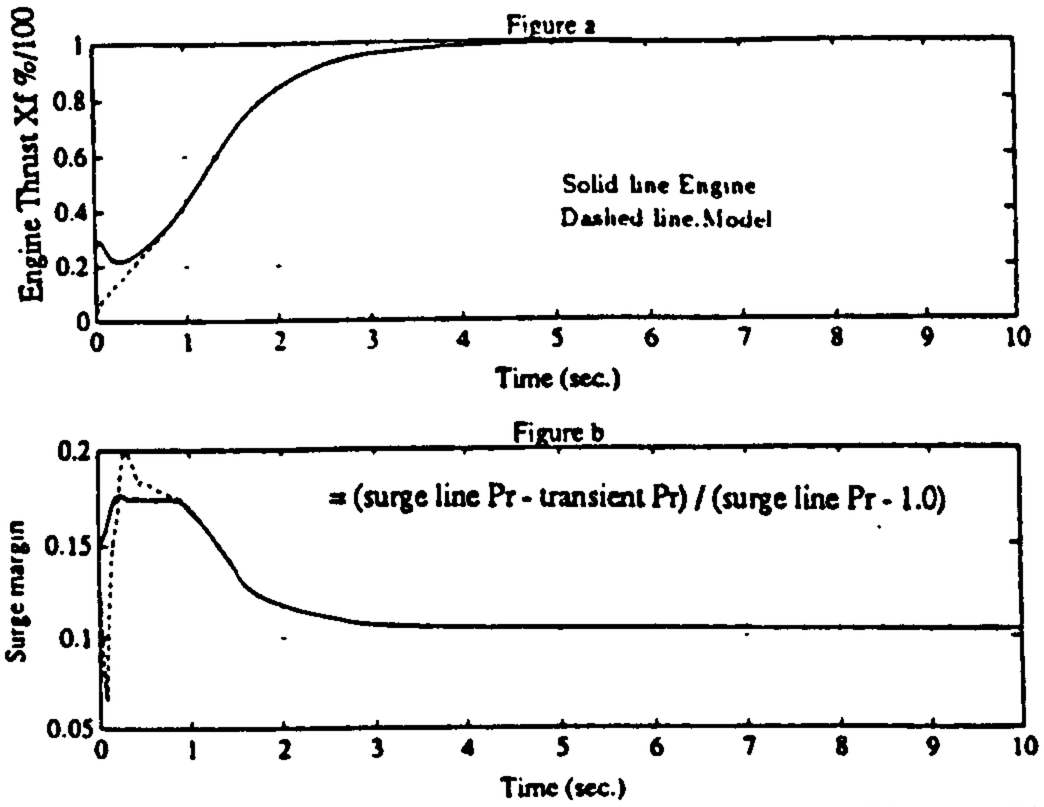

Figure 8: Performance of the Proportional Model-Based Observer Plus Closed-loop Control.

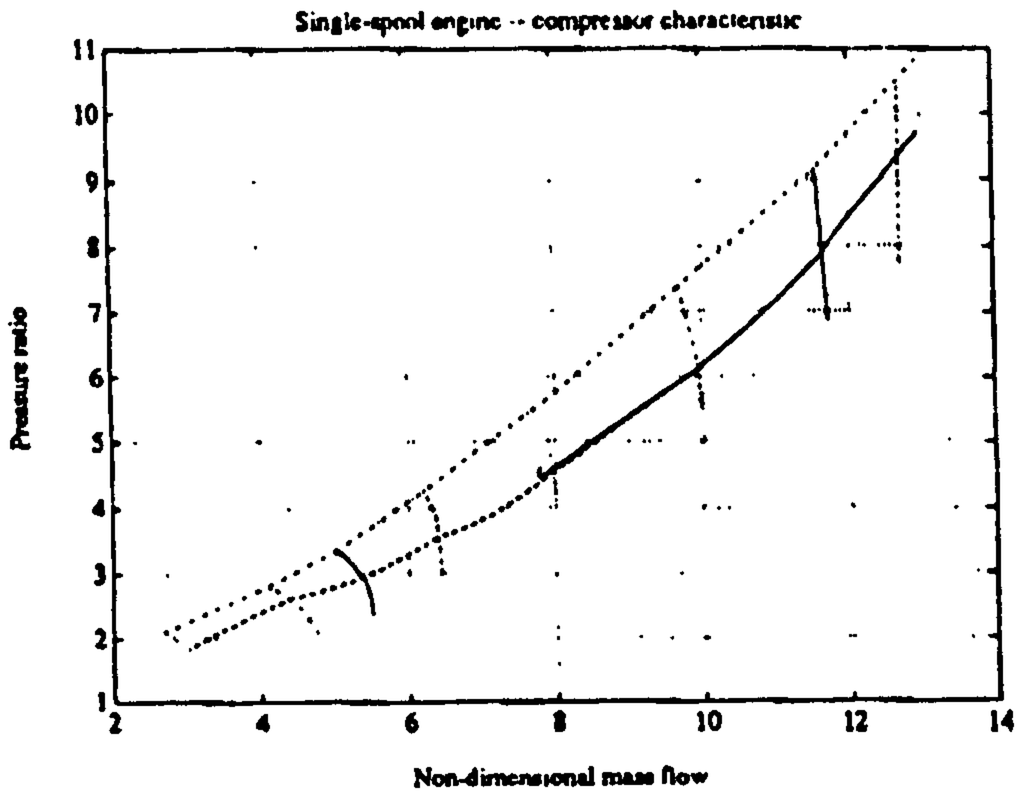

Figure 9: Performance of the Proportional Model-Based Observer Plus Closed-loop Control: Acceleration Trajectory on Compressor Characteristic.

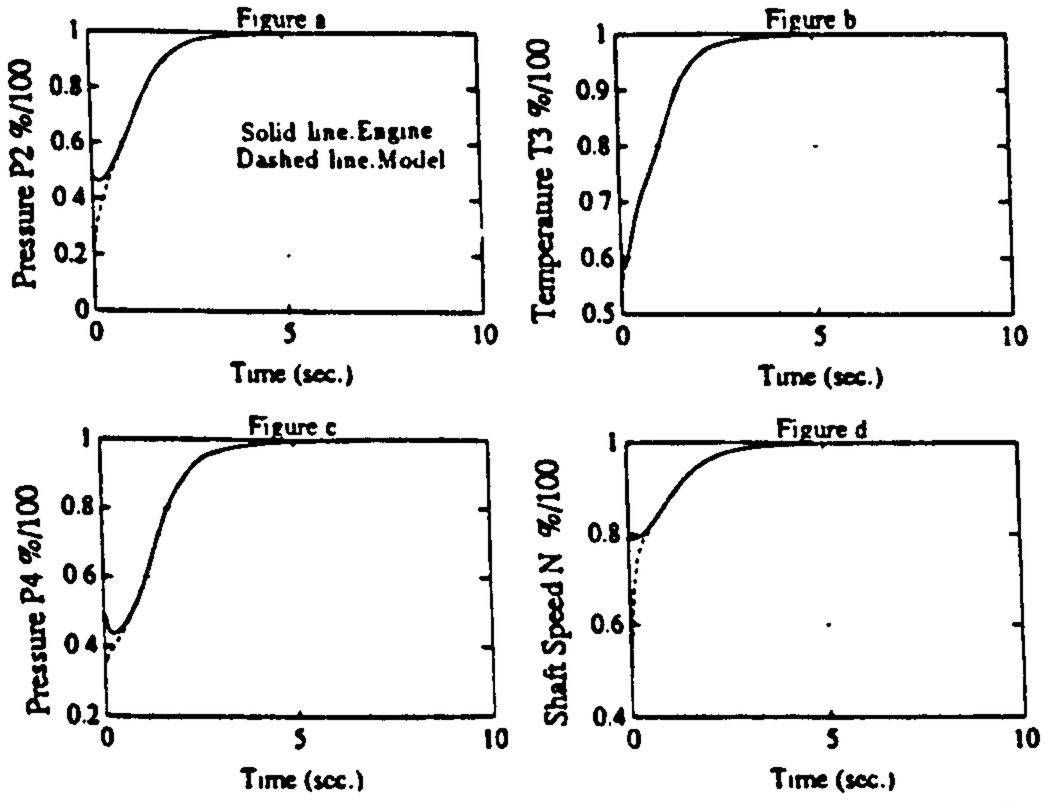

Figure 7: Performance of the Proportional Model-Based Observer Plus Closed-loop Control.

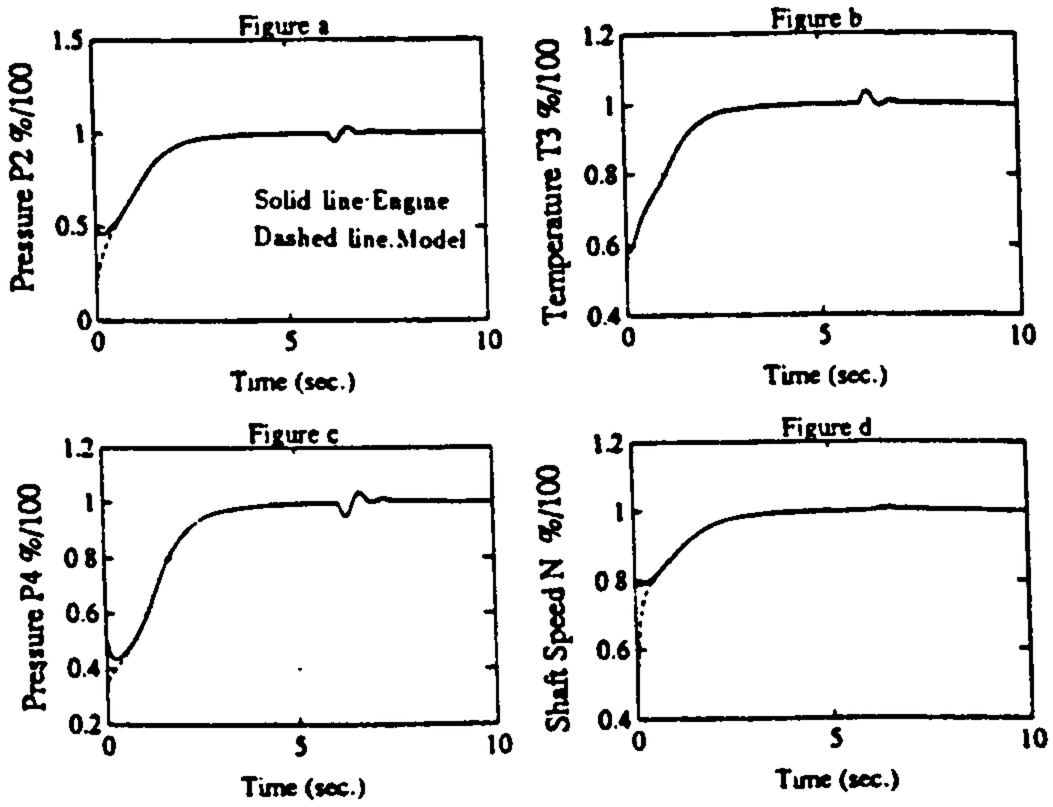

Figure 10: Responses Under the Inlet Pressure Disturbance Using P Model-Based Observer Plus Closed-loop Control.

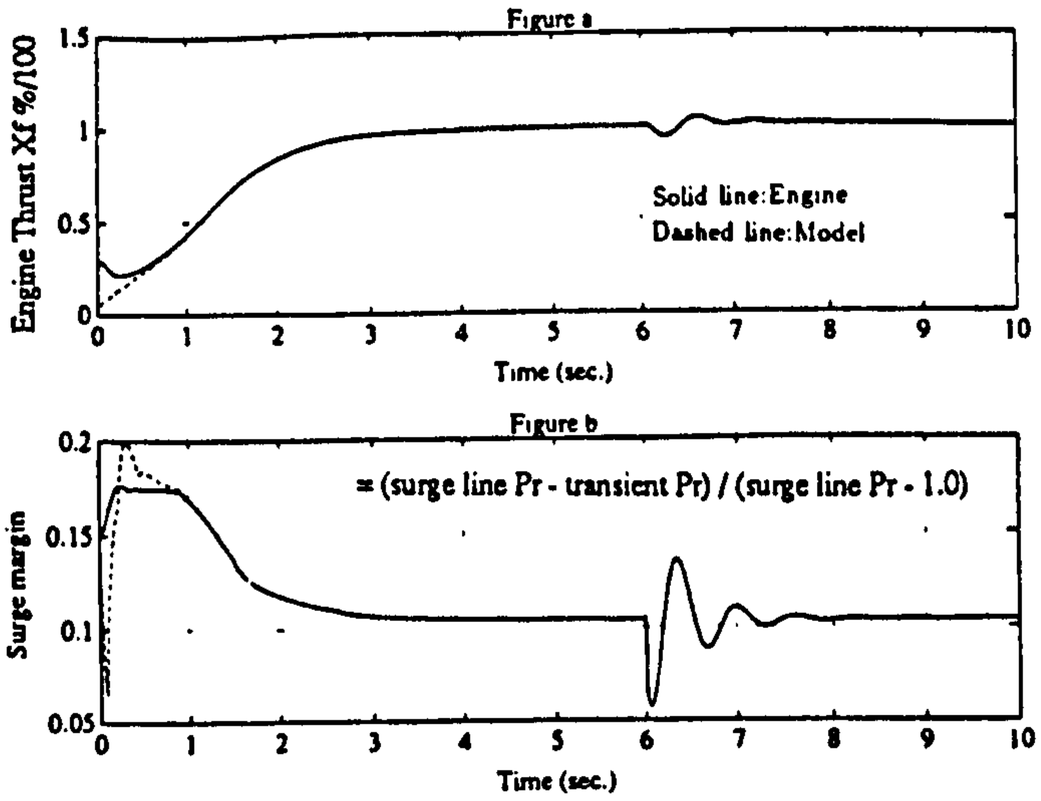

Figure 11: Responses Under the Inlet Pressure Disturbance Using PI Model-Based Observer Plus Closed-loop Control.

PAPER SUBMITTED TO AIAA - MARCH 2000

PRESSURE WAVES IN VOLUME EFFECT IN GAS TURBINE TRANSIENT PERFORMANCE MODELS

Y.G.Li N.R.L.Maccallum P.Pilidis

Abstract

Gas turbine volumes behave like air reservoirs and have an effect on gas turbine transient behavior. The Inter-Component Volume (ICV) method has been widely used in gas turbine transient performance research. It takes into account the volume effect and gives reasonable results in transient performance predictions.

This paper describes the introduction of a pressure waves in volume (PWV) effect based on the physics that the pressure propagation in a volume is the result of pressure wave movement. This effect is introduced in the Inter-Component Volume (ICV) method for gas turbine transient predictions.

This method is applied to a two-spool turbojet engine. The detailed process of propagation of aerodynamic parameters in the engine rear duct during an acceleration is described. Compared with the original inter-component volume method, the transient performance of the engine with the PWV method shows a small but interesting difference.

Nomenclature

A	area
a	speed of sound
ICV	inter-component volume
FN	net thrust
HP	high pressure
LP	low pressure
M	Mach number
$\dot{m}$	mass flow rate
$\dot{m}_f$	fuel flow rate
N	rotational speed
n	polytropic constant
P	pressure
PR	pressure ratio
PWV	pressure wave volume
SHSP	shaft speed
s	entropy
T	temperature
T4	turbine entry temperature
u	velocity
W	turbine work
R	gas constant
γ	ratio of specific heat of gas

η	thermal efficiency
ρ	gas density

Subscripts

0	undisturbed area in front of a pressure wave
1	with ICV method
2	with PWV method
5	LP turbine inlet
6	LP turbine exit
A,B,C,D	either side of a pressure wave
amb	ambient
max	maximum
T	turbine
t	total

1. Introduction

In the prediction of transient behavior of gas turbine engines, two methods are commonly used: the "Continuity of Mass Flow' (CMF) method and the 'Inter-Component Volume' (ICV) method, which were described in detail by Fawke ~~et al~~ and Saravanamuttoo [1]. The former does not take into account the volume effect and it is assumed that at any given instant the mass flow into a component is matched with the mass flow emerging from it.

In the 'Inter-Component Volume' (ICV) method, it is assumed that volumes exist between adjacent components which allow the accumulation or release of air or gas. These volumes are representative of the volume of each component. The ICV method is a more accurate description of transient processes because this procedure includes the local mass accumulation or release in engine components, which is ignored in the CMF method. In practice the CMF method is applicable to cases where large speed transients take place. The ICV method is more general but it has a larger computational cost.

This paper introduces a pressure wave volume (PWV) method to describe the pressure propagation inside a component volume. A comparison between the original ICV method and the PWV method is made with a prediction of the acceleration of a two-spool turbojet engine.

2. ICV and PWV Methods

The current state of the art in the 'Inter-Component Volume' (ICV) method, Fawke and Saravanamuttoo et al.[1], is that the mass flow into a component will not be the same as that out of the component in any transient instant. Engine components have associated volumes, thus air/gas mass will accumulate or diminish and the pressure in that volume will rise or fall at that instant. At the same time, it is assumed that the pressure propagates throughout the volume immediately so the pressure at any place inside the volume is the same at each time interval. This prompt pressure propagation assumption is not accurate and it can alter the transient behavior of the engine, in particular in large volumes.

For example in the volume between the LP turbine and the nozzle of a gas turbine, pressure waves are generated from the turbine when the working conditions of the gas turbine change. The waves move downstream towards the nozzle, are reflected from the nozzle and move upstream. When meeting the turbine the waves are reflected and move downstream again. During the movement, two approaching pressure waves will pass through one another and become two new waves moving in opposite direction. All the pressure waves degrade after they are reflected several times in the duct volume and eventually disappear. As a result of the wave movement, any changes of the aerodynamic parameters, such as pressure, temperature and mass flow rate, from both ends of the duct volume propagate throughout the volume. This physical process is the theoretical basis of the pressure wave volume method.

The pressure wave movement delays the pressure propagation inside the volume and the predicted gas turbine performance response with the PWV method during transient processes will be different when compared to the predictions using the traditional ICV method,

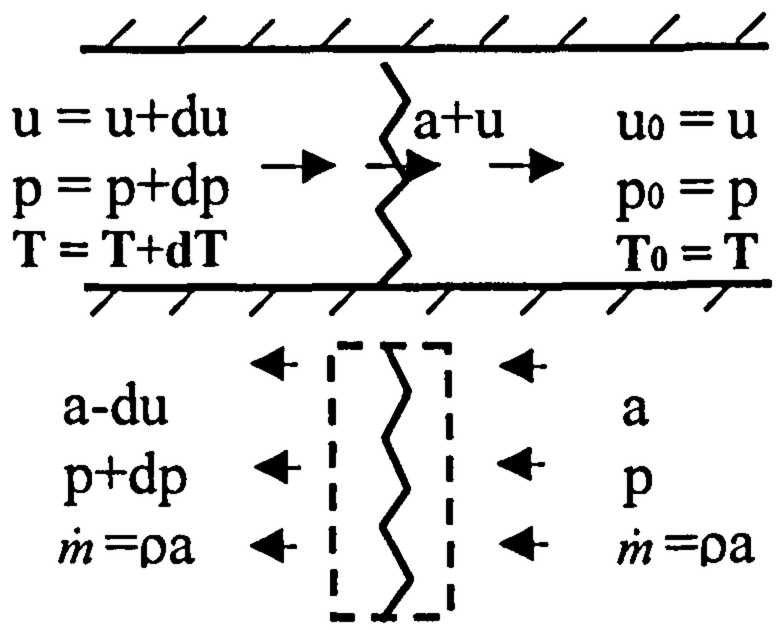

Fig. 1. Control Volume: pressure wave in a Duct

3. Description of PWV Method

The largest volume in a turbojet engine is normally the rear duct behind the turbine. In the present analysis any components inside the engine duct are ignored. The modeling of pressure wave generation, propagation, passing through other pressure waves and reflection from both ends of the duct is described below.

3.1 The Two Sides of a Pressure Wave

When a pressure wave moves inside a duct volume in an axial direction, it is assumed that the gas passes through a pressure wave isentropically and the wave propagates at the speed of sound. Equation (1) can be obtained with the momentum continuity applying to a control volume surrounding a pressure wave in a relative frame of reference, Figure 1.

$$du = \frac{1}{a}\frac{dp}{\rho} \qquad (1)$$

The relationship between the local sonic velocity and the property change rate is:

$$a^2 = \frac{d_P}{d\rho} \qquad (2)$$

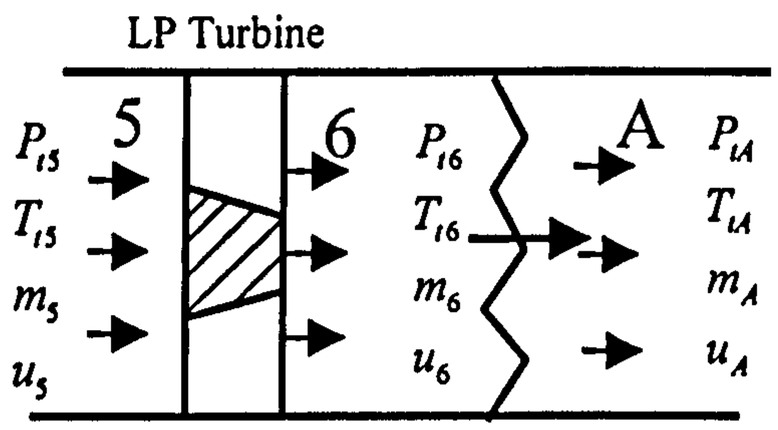

Figure 2. Generation of a Wave

Combining Equations (1) and (2) gives

$$du = a\frac{d_P}{\gamma P} \qquad (3)$$

Then:

$$\frac{a}{a_0} = \left(\frac{T}{T_0}\right)^{\frac{1}{2}} = \left(\frac{P}{P_0}\right)^{\frac{\gamma-1}{2\gamma}} \qquad (4)$$

Integrating Equation (3) and substituting from Equation (4) gives

$$u = u_0 + \frac{2a_0}{\gamma-1}\left[\left(\frac{P}{P_0}\right)^{\frac{\gamma-1}{2\gamma}} - 1\right] \qquad (5)$$

where subscript '0' means undisturbed gas in front of the wave.

3.2 Pressure Wave from the Turbine

During transients, the LP turbine's working point keeps changing and the gas conditions, such as gas temperature, pressure and mass flow rate, change accordingly. In a numerical process it is assumed that a pressure wave is generated from the LP turbine exit in every numerical time step, Figure 2.

With the turbine inlet parameters, the exit total pressure P_{t6} and the efficiency η_T the turbine work W_T can be found. Using the turbine characteristics with $N/\sqrt{T_{t5}}$ and W_T, a new turbine efficiency η_T and mass flow rate $\frac{\dot{m}_T\sqrt{T_{t5}}}{P_{t5}}$ can be obtained. If the calculated mass flow rate is not the same as the inlet value, the turbine exit total pressure p_{t6} needs to be adjusted until both values are in agreement.

It is also assumed that the expansion process in the turbine is a polytropic process. Applying the polytropic relation (6), the mass flow expression (7) and wave Equation (8) into the newly generated pressure wave at the turbine exit, combined with relations between total and static parameters, turbine exit parameters T_{t6}, $\dot{m}_6$ and u_6 can be obtained.

$$\frac{T_{t6}}{T_{t5}} = \left(\frac{P_{t6}}{P_{t5}}\right)^{\frac{n-1}{n}} \qquad \frac{n-1}{n} = \eta_T\frac{\gamma-1}{\gamma} \qquad (6)$$

$$\dot{m}_6 = \frac{P_6 A_6 u_6}{RT_6} \qquad (7)$$

$$u_6 = u_A + \frac{2a_A}{\gamma-1}\left[\left(\frac{P_6}{P_A}\right)^{\frac{\gamma-1}{2\gamma}} - 1\right] \qquad (8)$$

In practice, rater than (6) the appropriate enthalpy-entropy relations would be used. The parameters on both sides of the pressure wave are those at the exit of the turbine in two successive time intervals.

3.3 Pressure Wave Reflection from the Nozzle

The reflection of a pressure wave from a nozzle is illustrated in Figure 3, where (a) shows a pressure wave approaching the nozzle and (b) the wave leaving the nozzle after reflection.

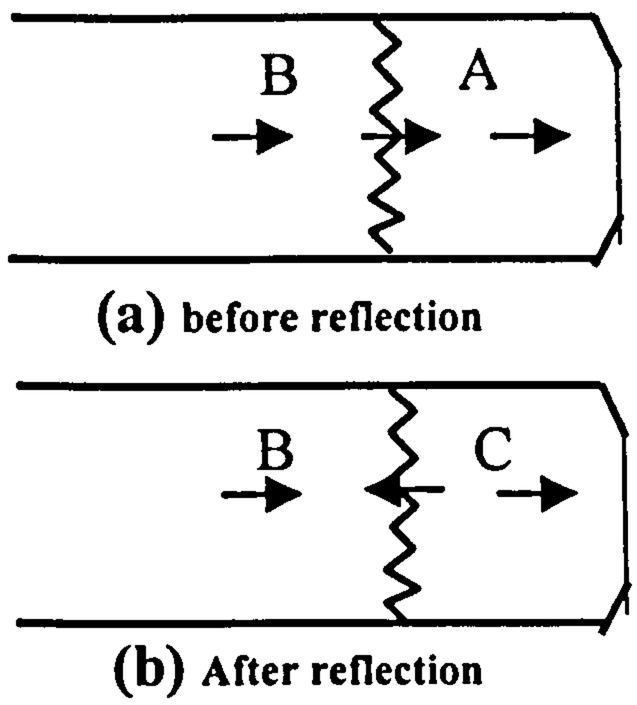

Figure 3. Wave Reflection from Nozzle

The inlet conditions (P_t and T_t), the nozzle area and ambient conditions (P_{amb} and T_{amb}) determine the duct flow. The nozzle may be unchoked or choked. It is assumed that the parameters in zone *A* and *B* are known and the reflection process from *A* to *C* is isentropic. The parameters in zone *C*, in the unchoked case, may be expressed with:

$$P_c = P_{amb}\left[\left(\frac{A_n}{A}\right)^2 \frac{(P_t/P_{amb})^{\frac{r-1}{r}} - 1}{(P_t/P_c)^{\frac{r-1}{r}} - 1}\right]^{\frac{r}{r+1}} \quad (9)$$

$$T_C = T_A\left(\frac{P_C}{P_A}\right)^{\frac{r-1}{r}} \quad (10)$$

$$u_C = u_B - \frac{2a_B}{r-1}\left[\left(\frac{P_C}{P_B}\right)^{\frac{r-1}{2r}} - 1\right] \quad (11)$$

$$\dot{m}_C = \sqrt{\frac{\gamma}{R}}\frac{P_C A}{\sqrt{T_C}} M_C \quad (12)$$

If a pressure wave is reflected from a choked nozzle it is supposed that the effective mass flow rate keeps unchanged and Equation (13) is satisfied.

$$\frac{\dot{m}_A\sqrt{T_{tA}}}{P_{tA}} = \frac{\dot{m}_C\sqrt{T_{tC}}}{P_{tC}} \quad (13)$$

Therefore,

$$M_A = M_C \quad (14)$$

and other parameters in zone C can be obtained with Equations (15) to (17)

$$P_C = \left[\frac{u_B + \frac{2a_B}{\gamma-1}}{u_A\left(\frac{T_B}{T_A}\right)^{\frac{1}{2}} + \frac{2a_B}{\gamma-1}}\right]^{\frac{2\gamma}{\gamma-1}} \bullet P_B \quad (15)$$

$$T_C = T_B\left(\frac{P_C}{P_B}\right)^{\frac{\gamma-1}{\gamma}} \quad (16)$$

$$\dot{m}_C = \frac{P_{tC}A_N}{\sqrt{T_{tC}}}\sqrt{\frac{\gamma}{R}}\left(\frac{2}{\gamma+1}\right)^{\frac{\gamma+1}{2(\gamma-1)}} \quad (17)$$

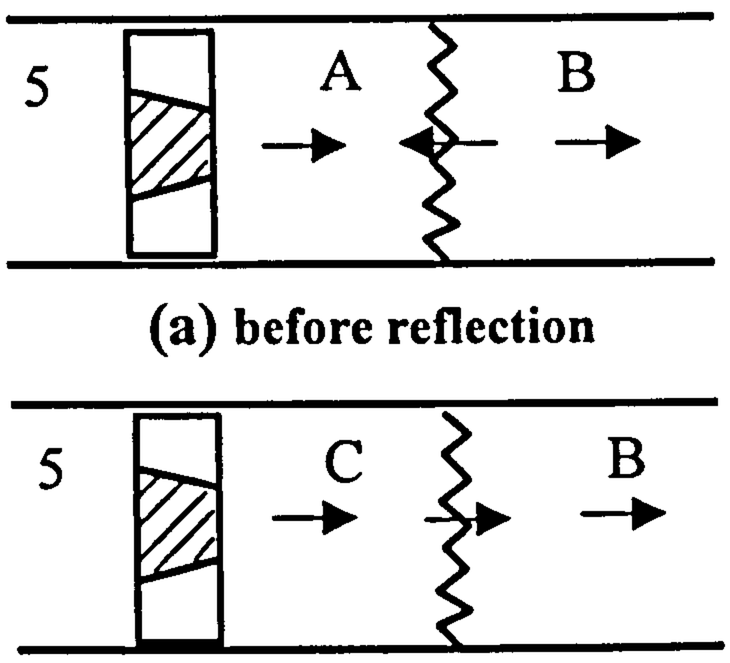

Figure 4. Wave Reflection from Turbine

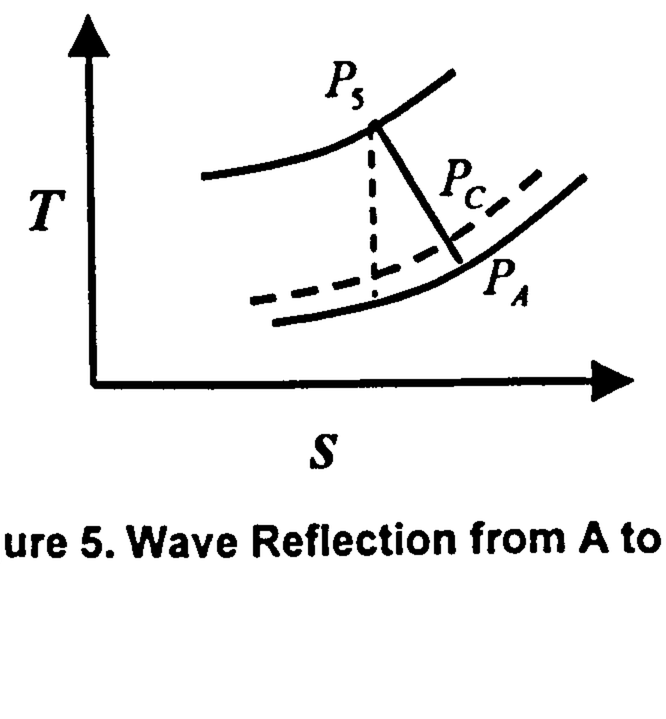

Figure 5. Wave Reflection from A to C

3.3 Pressure Wave Reflection from a Turbine

When a pressure wave moves upstream and approaches the turbine and is reflected (Figure 4) the process from *A* to *C* is assumed to be polytropic and the mass flow rate remains constant. It is also assumed that the parameters in zone *A* and *B* are known and the state of turbine inlet remains unchanged during the reflection process.

The polytropic process of the flow in the turbine is shown in T-s chart in Figure 5. Parameters in zone C can be obtained with a set of Equations (18) to (21).

The polytropic process of the flow in the turbine is shown in T-s chart in Figure 5. Parameters in zone C can be obtained with a set of Equations (18) to (21).

$$\left(\frac{T_C}{T_A}\right)=\left(\frac{P_C}{P_A}\right)^{\frac{n-1}{n}} \qquad \frac{n-1}{n}=\eta_t\frac{r-1}{r} \tag{18}$$

$$\dot{m}_A=\frac{P_A u_A A}{RT_A}=\frac{P_C u_C A}{RT_C}=\dot{m}_C \tag{19}$$

$$u_C-u_B=\frac{2a_B}{r-1}\left[\left(\frac{P_C}{P_B}\right)^{\frac{r-1}{2r}}-1\right] \tag{20}$$

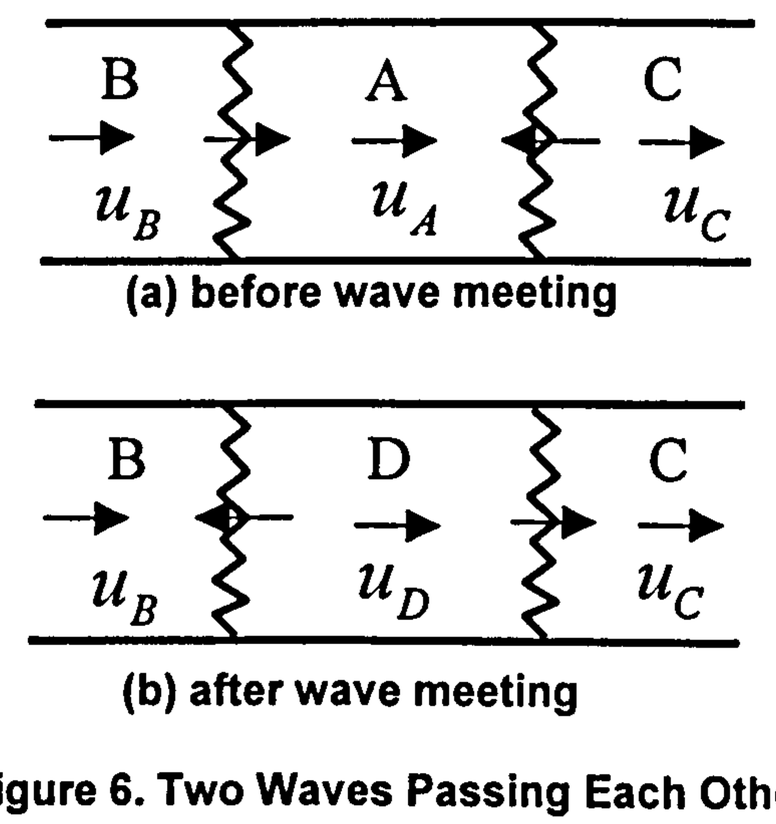

Figure 6. Two Waves Passing Each Other

3.4 Pressure Waves Passing Through One Another

When two pressure waves in a duct approach each other and meet, each wave will go through the other and they will become two new waves moving in opposite directions. This process is assumed to be isentropic and the waves before and after they meet are illustrated in Figure 6. Applying Equation (5) to the pressure waves and combined with isentropic relations, the flow parameters in zone D can be calculated with Equation (21) to (24)

$$u_D=u_B-u_C+u_A \tag{21}$$

$$P_D=P_A\left[\frac{r-1}{2a_A}\left(-u_D+u_B\right)+\left(\frac{P_B}{P_A}\right)^{\frac{r-1}{2r}}\right]^{\frac{2r}{r-1}} \tag{22}$$

$$T_D=T_B\left(\frac{P_D}{P_B}\right)^{\frac{r-1}{r}} \tag{23}$$

$$\dot{m}_D=\frac{P_D A M_D}{\sqrt{T_D}}\sqrt{\frac{\gamma}{R}} \tag{24}$$

3.5 Dissipation of a Pressure Wave

After a pressure wave is reflected in a duct several times, it becomes weaker. A criterion has been set to define the dissipation of a pressure wave. It is assumed that when the pressure difference between both sides of a wave is small enough the wave has disappeared and a set of average values of parameters is used to replace previous parameters on both side of the wave. This criterion is defined in Equation (26)

$$\Delta P<0.001\left(KP_a\right) \tag{26}$$

4. Application to a Turbojet Engine

A two-spool turbojet engine has been used as an example to investigate the difference of the original inter-component volume method and the pressure wave volume method. Both the PWV and the ICV methods were applied to the rear duct behind the turbine where the largest volume is located in the engine.

Two computational cases were carried out and compared with each other, one with the pressure wave volume method and another with the original inter-component volume method. An acceleration process from idle to maximum fuel flow rate with heat transfer is selected for the analysis. A transient performance prediction code with the two volume methods has been developed. Detailed description of the transient prediction method can be found in [2] and [3]. In the two cases, the same fuel schedule was employed, where the non-dimensional fuel flow is a function of HP compressor pressure ratio (equation 27). The

acceleration fuel flow rate shown in Figure 7, the fuel flow is increased to its maximum value in 4.2 seconds and then kept constant until the engine reaches the steady state.

$$\frac{\dot{m}_f}{N_{HP}P_{t2}} = f\left(\frac{P_{t3}}{P_{t2}}\right) \tag{27}$$

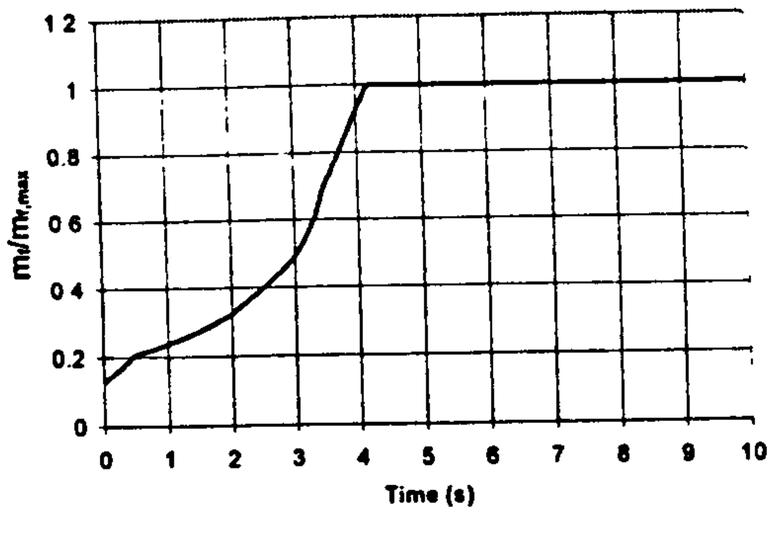

Figure 7. Fuel Flow during theTransient

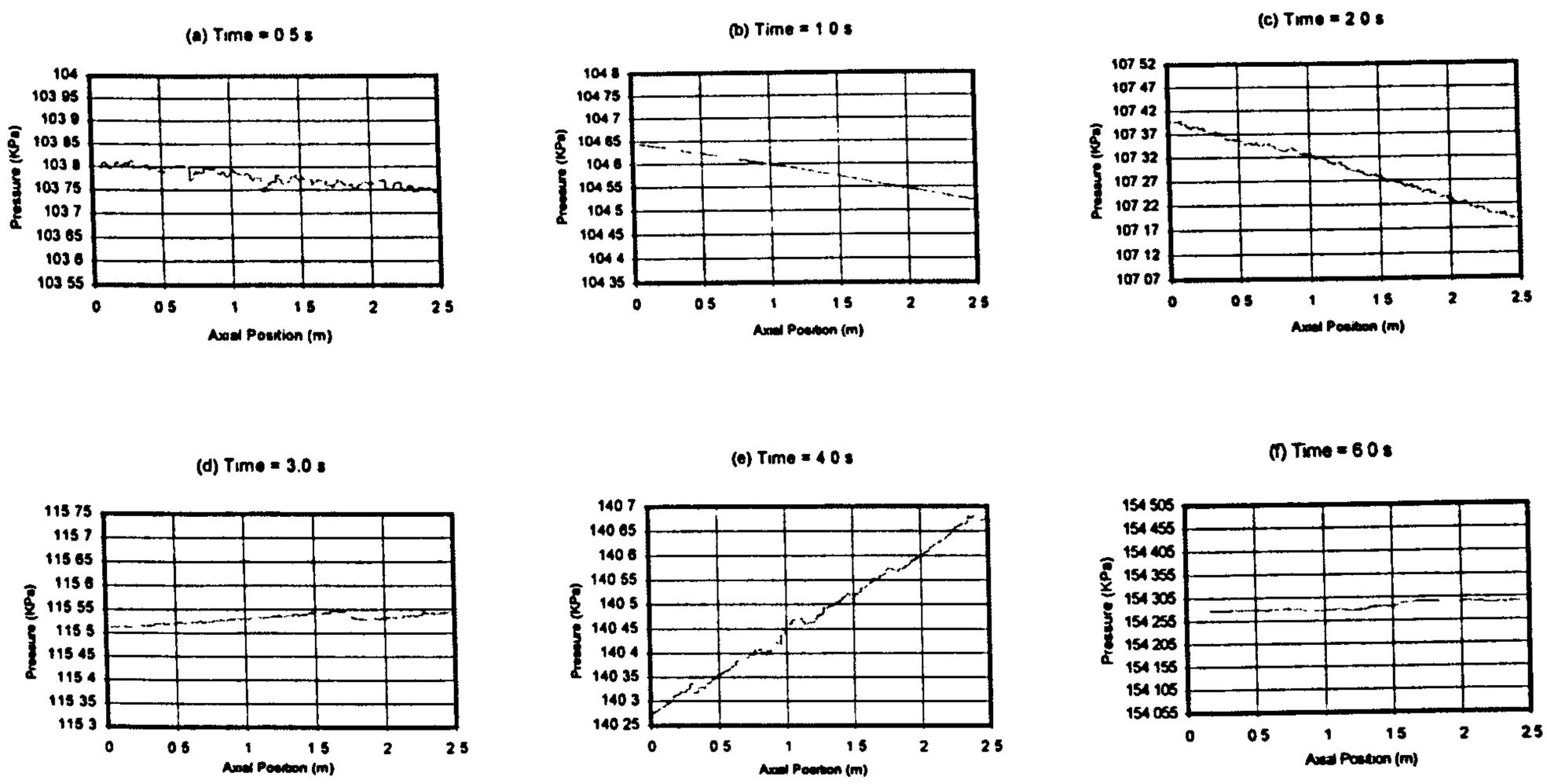

Figure 8. Propagation History of Pressure Waves in the Duct

It has been found that the transient performance difference predicted with the two volume methods is small. So only the difference of the performance parameters during the transient are illustrated

During the acceleration the pressure distributions in the duct at different time instants are illustrated in Figure 8. In the first 2 seconds of the acceleration a large number of compression waves are generated form the LP turbine and the propagation of the pressure change downstream of the turbine exit is delayed due to the movement of the pressure waves. This is shown in Figures 8(a) to (c). The pressure upstream of the duct is higher than that downstream. After 3 seconds the engine nozzle chokes and gas starts to accumulate near it. This causes an increase of the downstream pressure, which is now higher than that upstream. This phenomenon can be seen in Figure 8(d) to (e) until the shaft speeds reach their maximum values at about 4.2 seconds. The engine condition will tend to the steady after the fuel flow rate reaches its maximum value and the pressure difference between upstream and the downstream becomes progressively smaller. This process can be seen in Figure 8(f), this means that the two volume methods give a similar result in that situation.

In the traditional ICV method the pressure inside the duct volume between the upstream and downstream pressure values predicted with the PWV method. The unsteady process of the pressure propagation inside the duct volume shown in Figure 8 determines that the engine experiences an unsteady process oscillating with low frequency around the process predicted with the original inter-component volume

method. This phenomenon is well illustrated with other parameters during the acceleration.

During the first half second of the acceleration the LP turbine pressure ratio predicted with the PWV method (Figure 9) is slightly larger (by about 0.15%) than that obtained with the ICV method. After that they are very similar. After about 2 seconds, the pressure ratio is lower than the value predicted with the ICV method by about 0.15%. After 3 seconds, when the nozzle chokes, the difference reaches a maximum (0.25%). This is maintained for about 2 seconds after the fuel flow reaches its maximum value. The HP turbine pressure ratio shows a similar pattern but with smaller magnitudes because the response is attenuated by the smaller volume of the LP turbine.

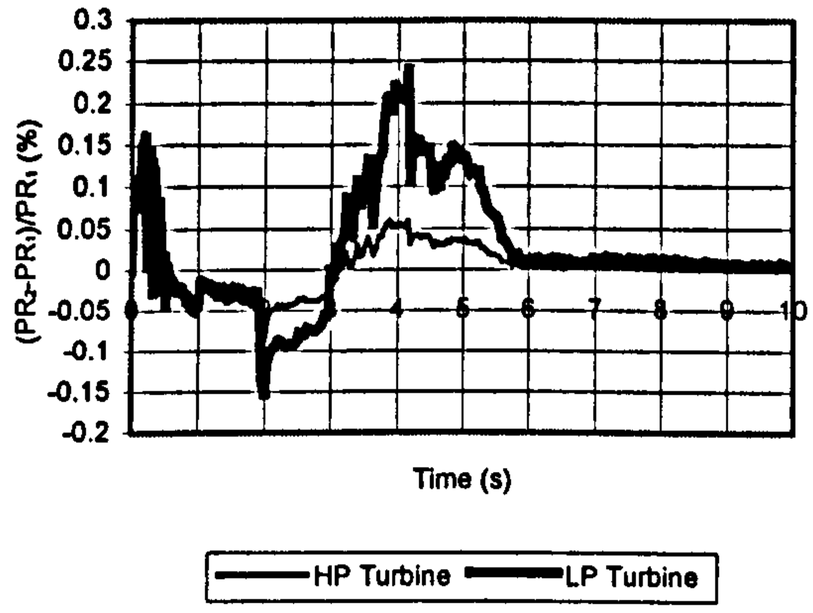

Figure 9 Comparison of Turbine Pressure Ratio

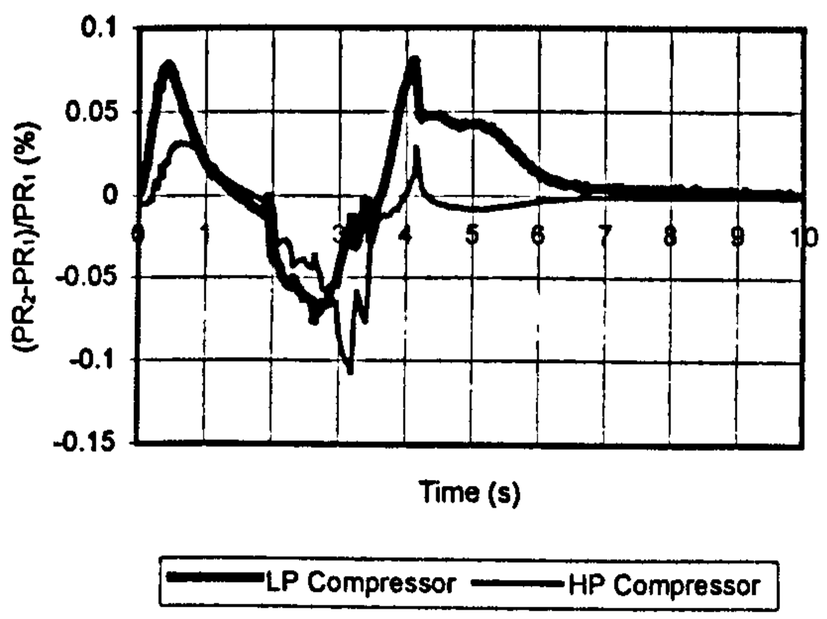

Figure 10. Comparison of Compressor Pressure Ratio

The compressor transient response is similar to that of the turbine (Figure 10). The difference of HP turbine entry temperature between two volume methods during the transient is shown in Figure 11. Although it shows a similar pattern to the pressure ratios, it is clear that the temperature difference is really small in magnitude with maximum difference of about 0.04%, therefore the temperature difference can be neglected.

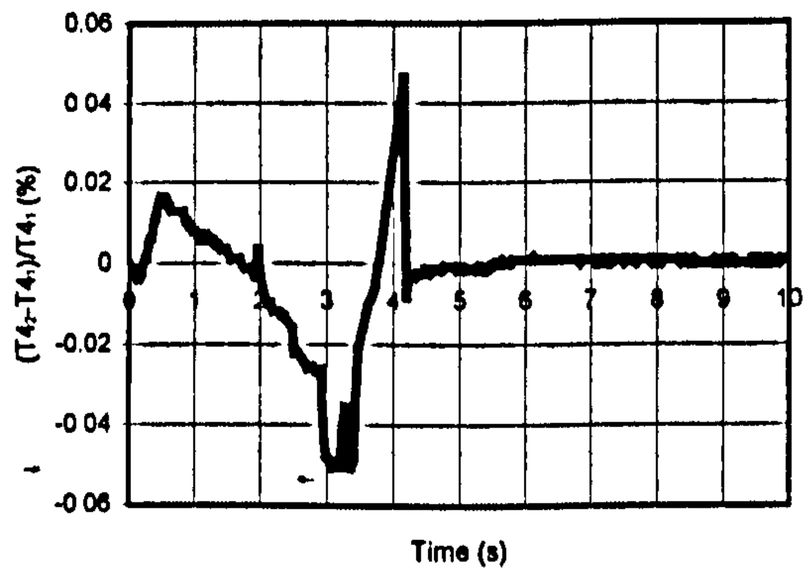

Figure 11. T4 Comparison

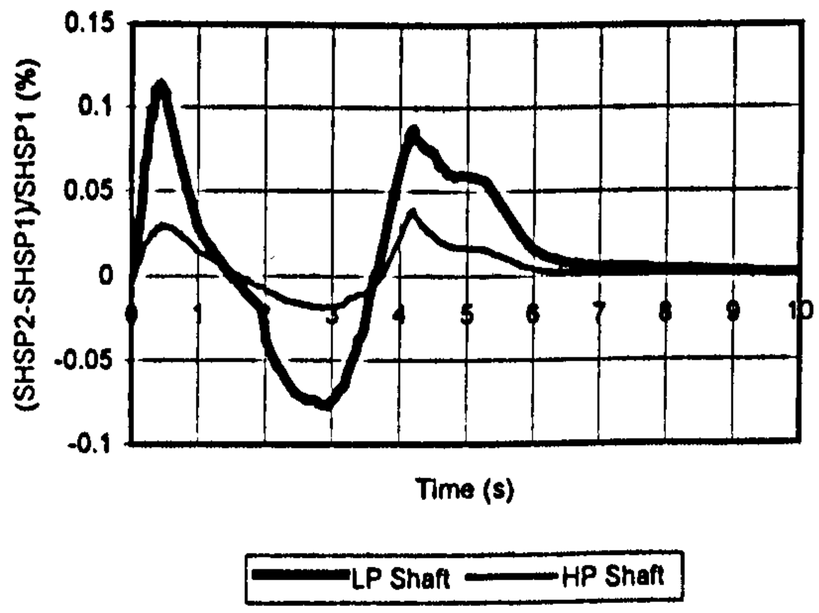

Figure 12. Shaft Speed Comparison

The difference of shaft speeds between the ICV and PWV methods during the transient is shown in Figure 12. In the first 1.5 second, the LP shaft speed predicted with PWV method is higher than that predicted with the ICV method by about 0.11%. In the next 2 seconds it is lower by a maximum of about 0.075%. In the following 2.5 seconds is higher by a maximum of about 0.08% after the nozzle chokes. The HP shaft speed predicted with PWV shows somewhat smaller magnitudes with a maximum difference of about 0.04%.

The thrust difference between the two methods comes from the difference of the parameters at nozzle exit, the pressure and

mass flow rate. Figure 13 shows that in the first 1.5 seconds, the thrust predicted with PWV method is delayed by about 2% in maximum compared with that predicted by ICV method. After about 3 seconds when the nozzle is choked, the thrust with PWV method is delayed again by about 0.08% in maximum to the thrust by ICV method. It can be seen from the above comparison that all the performance parameters of the engine with PWV method oscillate with low frequency around the transient performance predicted with ICV method because of the oscillation of the pressure distribution inside the duct. As expected, volume size has an influence on the oscillation magnitude. When the duct length is halved, the difference between the shaft speeds and thrust predicted with the two methods is reduced (Figures 14 and 15).

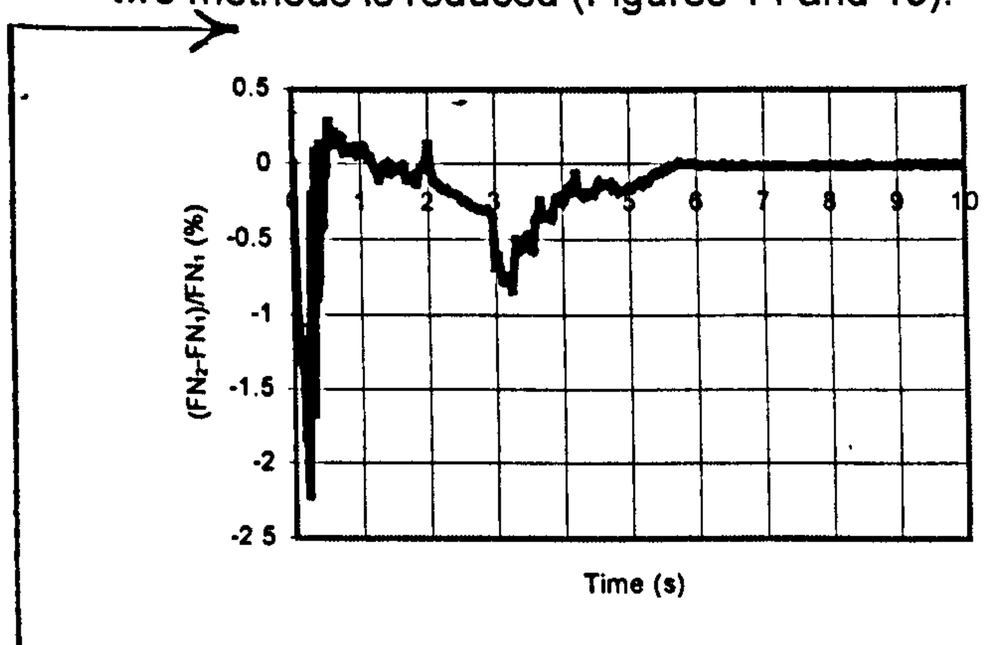

Figure 13. Thrust Comparison

Conclusion

The pressure wave volume (PWV) method described here is a better description of gas turbine transient performance than the original inter-component volume method because it includes the effect of pressure propagation inside the volumes. The predicted transient response of a turbojet engine with PWV method is slightly different from that with original inter-component volume (ICV) method.

The difference predicted here is small, but it may be significant when large volumes such as bypass ducts are considered. Similarly some large industrial gas turbines have very large volumes too.

No experimental verification was carried out, however the authors believe that the inclusion of this effect must be actively pursued because on many occasions the effects could be significant in some critical maneuvers such as altitude relight and reheat lighting in a low-bypass turbofan.

An alternative analysis for the above described high frequency effects has been presented by Merriman [4]. The conclusions reported by the present authors are in general agreement with those of Merriman.

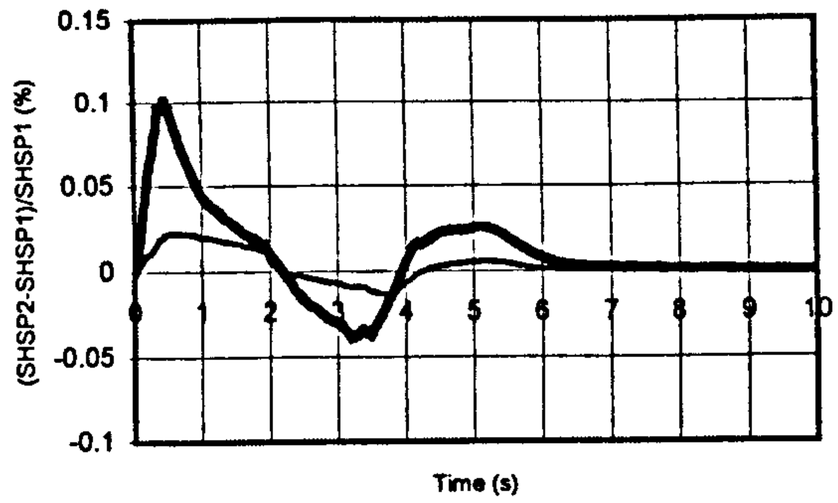

Figure 14. Shaft Speed Comparison (Duct length halved)

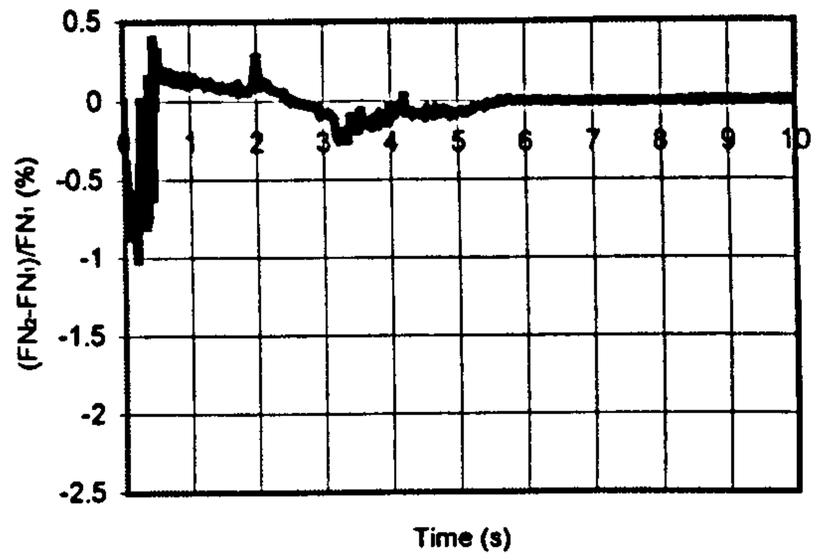

Figure 15. Thrust Comparison (Duct length halved)

References

[1] Fawke, A.J. and Saravanamuttoo, H.I.H., 'Digital Computer Methods for Prediction of Gas Turbine Dynamic Response', SAE Report 710550, 1971.

[2] Maccallum, N.R.L. and Qi, O.F., 'The Transient Behavior of Aircraft Gas Turbines', I.Mech. Seminar on Gas Turbines, London, 1989.

[3] Pilidis, P., 'Digital Simulation of Gas Turbine Performance', PhD Thesis, 1983, University of Glasgow.

[4] Merriman, N.M. 'Simulation of AeroEngine Pre and Post Stall Transient Behaviour', Ph.D. Thesis, 1994, Cranfield University.

GAS TURBINE TRANSIENT PERFORMANCE

Lectures: Cranfield, July 1999

P. Pilidis
N.R.L. Maccallum

TAY H.P. COMPRESSOR

SEA LEVEL MACH 0.2

PREDICTED TRAJECTORIES IN TRANSIENTS - ACCEL & DECEL

MAKING ADIABATIC ASSUMPTIONS

——— BY CMF METHOD

\+ BY ICV METHOD